12422

Oceans'78

"The Ocean Challenge"

Coastal Zone
Information
Center

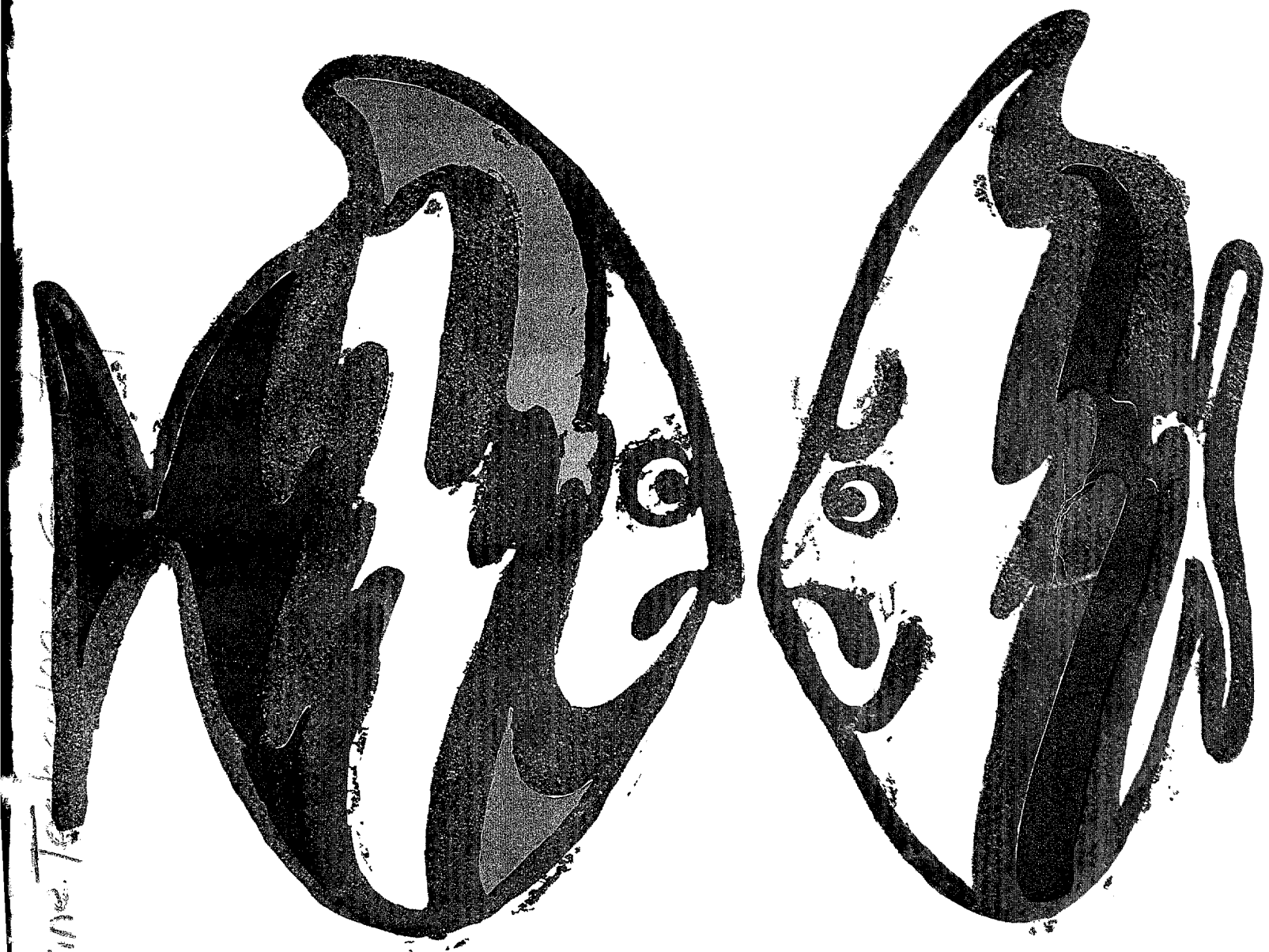

12422

Oceans'78

"The Ocean Challenge"

Fourth Annual Combined Conference
Sponsored by:

The Marine Technology Society and

The Institute of Electrical and Electronics Engineers
- Council on Oceanic Engineering
- Washington Section

September 6-8, 1978
Sheraton-Park Hotel
Washington, D.C.

Participating Organizations
- American Association for the Advancement of Science
- American Geophysical Union
- American Institute of Aeronautics and Astronautics
- American Oceanic Organization
- American Society of Civil Engineers
- American Society of Mechanical Engineers
- American Society of Naval Engineers
- National Association of Corrosion Engineers
- National Ocean Industries Association
- Sea Grant Association
- Society of Naval Architects and Marine Engineers

NOV 9 1978
U.S. DEPARTMENT OF COMMERCE NOAA
COASTAL SERVICES CENTER
2234 SOUTH HOBSON AVENUE
CHARLESTON, SC 29405-2413

Marine Technology Society
TC1505 .03318 1978
4834109 MAY 7 1997

Chairman's Message	iii
Special Activities	v
OCEANS '78 Conference Committee	vi
Plenary and Policy Sessions	vii
Table of Contents	ix
Authors, Chairmen & Panelists	xix
Exhibitors	xxi
Sessions/Papers	Start on page 1

78CH1356-6 OEC

Property of CSC Library

Published by:
The Marine Technology Society, 1730 M Street, N.W., Washington, D.C. 20036 and The Institute of Electrical and Electronics Engineers, Inc., 345 East 47th Street, New York, New York 10017

Responsibility of the contents rests upon the authors, and not upon the MTS, the IEEE, or their members.

Copies of this Record may be purchased from MTS or IEEE.
Reference publication 78 CH 0134-7 OEC
Order from:
MTS: 1730 M Street, N.W., Washington, D.C. 20036
IEEE: 445 Hoes Lane, Piscataway, NJ, 08854

All rights, including translations, are reserved by MTS and IEEE. Abstracting is permitted with mention of source. Request for republication should be addressed to The Marine Technology Society, 1730 M Street, N.W., Washington, D.C. 20036 or the IEEE Editorial Department, 345 East 47th Street, New York, N.Y. 10017.

Copyright © 1978 by The Marine Technology Society.

Library of Congress Card Number 74-76790
IEEE Publication Number 78 CH 0134-7 OEC

Printed in the USA

Property of CSC Library

Chairman's Message

COASTAL ZONE
INFORMATION CENTER

The "challenge" chosen as the theme for the Oceans '78 Conference is to be daring, imaginative, and perseverant—to tap the vast resources of the oceans and to maintain the ocean's ecology for the benefit of mankind.

I am convinced that scientists and engineers and managers can overcome the problems inherent in understanding the behavior of the sea and perfecting the technologies required for its preservation and development The technical papers presented at the Conference are solid evidence of progress. The displayed instruments and systems are further manifestatio that real strides have been made in the last decade in terms of equipment performance, reliability and economy.

Although we have demonstrated our ability to meet distant and difficult goals once we move forward, our capacity to focus on the correct objectives and to commit the necessary resources in the face of competing needs is less clear. This aspect of the challenge is central to the selection of the series of policy discussions presented as part of this year's program. The opportunities for debate and questioning provided by the Conference policy panels will play an important role in advancing the public dialogue on these issues.

The Oceans '78 Conference is the fourth and final in a series sponsored jointly by the Marine Technology Society and the Institute of Electrical and Electronic Engineers. The members of the Conference Committee, assembled from these two technical societies, deserve special appreciation for their dedicated and effective efforts. We also particularly appreciate the help of the firms that joined us to exhibit the latest developments in marine technology. Finally, on behalf of the Conference Committee and the sponsoring organizations, I want to thank those attending the Conference for their active participation.

Richard A. Frank
Administrator
National Oceanic and Atmospheric Administration

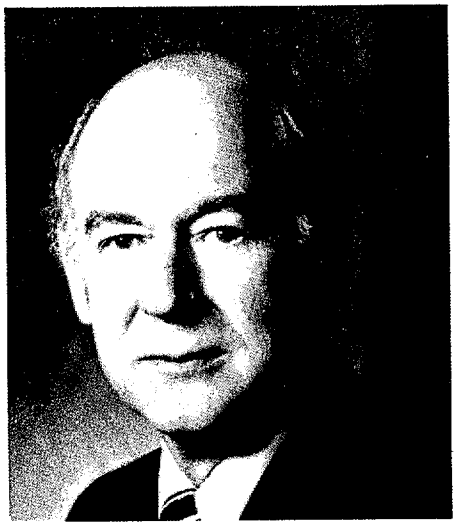

Cecil Andrus
Secretary of the Interior

Juanita Kreps
Secretary of Commerce

Lloyd Maudlin
President
Council on Oceanic Engineering, IEEE

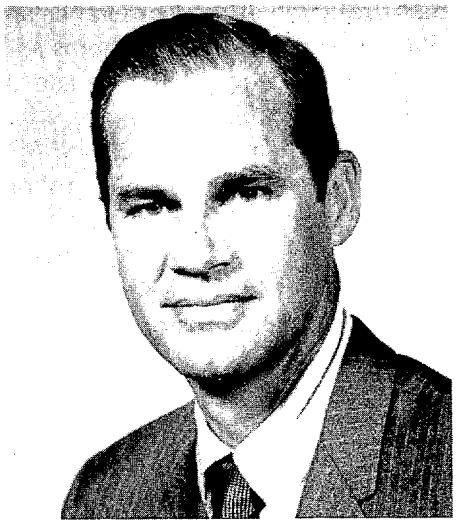

James A. Rickard
President, Marine Technology Society

Richard A. Frank
Administrator, National Oceanic and
Atmospheric Administration

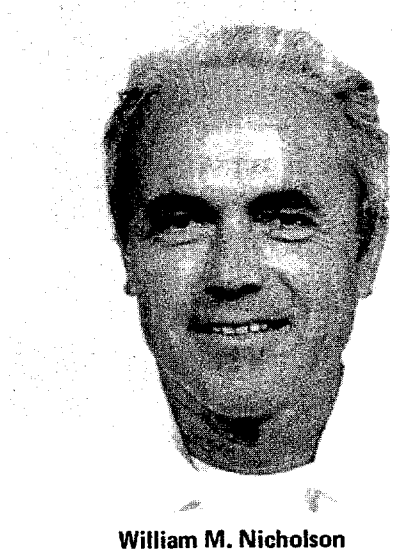

William M. Nicholson
Office of Marine Technology, National
Oceanic and Atmospheric Administration

Special Activities

Plenary Session

The conference opened with a keynote address by Secretary of the Interior Cecil D. Andrus who discussed the benefits and challenges associated with Government-Industry cooperation in ocean development. The more specific issue of Government regulation was then discussed by a panel chaired by Richard A. Frank, Administrator, National Oceanic and Atmospheric Administration. Panel members presented their views of the effectiveness of governmental regulation of ocean industries, whether Government regulates too much or too little, and what the proper role of Government should be so that our Nation's goals for the oceans are best realized.

Policy Program

The Policy Program, an innovation in OCEANS '78, consisted of five separate 2½ to 3 hour discussions and debates on critical oceans issues. Actual and potential policy of the Federal Government was the focus of the discussions for speakers and panels that ran concurrently with the Technical Program. The format consisted of speakers who presented differing points of view followed by a panel discussion and questions from the audience. The five subject areas were:

— Outer Continental Shelf Oil and Gas: The desirable pace of OCS oil and gas development and the desirable degree of government regulation of oil and gas extraction from the Outer Continental Shelf.

— Coastal Zone Management: This panel addressed the problems of consistency between Coastal Zone Management and Federally allowed activities in the oceans, with particular emphasis on the extent and degree of State control beyond the territorial seas. The goals and methods for management of the territorial seas were also discussed.

— Ocean Mining: The developing ocean mining industry may need extensive governmental assistance. Is special assistance appropriate and, if so, what types of assistance, to whom, how much and when are some of the questions which were asked. This session also addressed the question of whether the U.S. should go ahead now with ocean mining or wait for an international treaty.

— Fisheries Policy: This session focused first on issues related to limitations on domestic fishing activity for the purpose of maintaining optimal yield, and second on issues related to joint ventures, import limitations and other aspects of foreign trade.

— Ocean Research & Development: The final Policy Session considered the complex questions involved in how our limited federal resources for scientific programs supporting ocean activities should be allocated. Senator Lowell P. Weicker (R-Conn.) provided a congressional viewpoint.

Early Bird Reception—Richmond Room (Cash Bar); 4:00 p.m. to 8:00 p.m., Tuesday, September 5.

Chairman's Luncheon—No Host Reception 11:45 a.m. to 12:30 p.m., Wednesday, September 6.
Richard A. Frank, Administrator of the National Oceanic and Atmospheric Administration and Chairman of OCEANS 78, will address luncheon attendees. Participants of the Plenary Session are cordially invited to join conference attendees at this luncheon.

Exhibit Hall Cocktail Party—5:00 p.m. to 7:00 p.m., Wednesday, September 6.
Conference participants and exhibitors are invited, at this time, to a free cocktail party.

Ocean Challenge Banquet—No Host Reception 6:15 p.m. to 7:00 p.m., Thursday, September 6.
The banquet will be highlighted by a speech given by the Honorable Juanita Kreps, Secretary of Commerce. Acting as Master of Ceremonies will be Dr. John Craven, University of Hawaii.

Presidents' Award Luncheon—12:30 p.m., Friday, September 8.
At this time, MTS President Dr. James A. Rickard will present four awards on behalf of the Society and IEEE Vice President Mr. Lester Hogan will present three IEEE awards.

Oceans '78 Conference Committee

Chairman
RICHARD A. FRANK
Administrator
National Oceanic and Atmospheric Administration

Vice-Chairman
WILLIAM M. NICHOLSON
Office of Marine Technology
National Ocean Survey
National Oceanic and Atmospheric Administration

Publications
PETER B. MYERS
Magnavox

Exhibits
RICHARD M. SHAMP
Engineering Service Associates

Technical Program
ANTHONY I. ELLER
Naval Research Laboratory

Public Policy Program
HEATHER L. ROSS
Deputy Asst. Secretary—Policy, Budget & Administration
Dept of Interior

RAY KARAM
Dept of Interior

PAUL STANG
Dept of Interior

Finance
RICHARD F. CROSS
R. F. Cross Associates, Ltd.

Publicity
KATHI JENSEN
College of Marine Sciences
University of Delaware

ROLAND D. PAINE
Office of Public Affairs
National Oceanic and Atmospheric Administration

Arrangements
DANIEL J. WEILER
Naval Ship Engineering Center

DONALD CEBULSKI
Naval Ship Engineering Center

Conference Coordinator
JAN BENNETT
JB Inc.

Steering Committee
JOSEPH R. VADUS
Office of Ocean Engineering
National Oceanic and Atmospheric Administration

EDWARD M. MacCUTCHEON

LEONARD T. LYNCH, JR.
B-K Dynamics, Inc.

ROBERT H. CASSIS
U.S. Coast Guard

J. BARRY OAKES
Johns Hopkins Applied Physics Laboratory

ALVIN REINER
Federal Communications Commission

Plenary and Policy Sessions

Session (0) Plenary Session

This opening session of the Conference addressed the broad theme of its public policy program — how can government and industry best play out their respective roles so as to jointly realize for society the greatest possible benefits from the vast ocean resources which surround it. The Keynote Speaker set the stage with a presentation of guiding principles for public resources management policy.

What is the government trying to achieve in its management of ocean resources, and how does it hope to achieve it? The panel followed with discussion of a major management tool which has recently been growing in public use and controversy — government regulation. Is government regulation tuned to realizing the greatest possible social benefits from the oceans? Or has it gone too far? Or not far enough? Widely divergent views were heard from experts from the private and public sectors, with opportunity for questions from the audience.

Session (6) Public Policy Outer Continental Shelf Oil and Gas

The Nation's energy needs require the development of its OCS resources. But how fast should this be done? How can the need for domestic supplies of oil and gas be balanced against the potential costs of development? These costs include possible environmental degradation, conflicts with other ocean activities, and adverse onshore impacts. What pace of leasing is implied by a truly balanced approach? The speakers and panel first explored the pace of leasing questions, and then the statute authorizing regulation of oil and gas extraction. The OCS Lands Act amendments will specify new working relationships between industry, Federal and State Governments and increase the degree of control, reporting and consultation requirements on all who are associated with the offshore oil and gas program. Do the provisions in the law strike a proper balance so that oil and gas development can proceed while affected shorelines are adequately protected, competing users accounted for, and the environment preserved?

Session (12) Public Policy Coastal Zone Management

In this session the controversial effects of the Federal consistency provisions of the coastal zone management program were debated by representatives of industry and State and Federal governments. In the second part of the session two presentations and panel comments focused on the issues related to increasing State and Federal controls on ocean uses nearshore and seaward.

Session (18) Public Policy Deep Ocean Mining

The Ocean mining issues cut across economic, environmental, international and national security concerns. The focus of this session was the economic and international aspects. What are the arguments for and against special public support of ocean mining ventures? If support is warranted, in what form should it be provided? On the international front, are we better off going ahead now with ocean mining activity, or waiting for an international treaty? At what point, in terms of belated timing or adverse content of a treaty, does it make better sense for the U.S. to get out in front alone?

The speakers and panel addressed these issues and answered questions from the floor.

Session (24) Public Policy Debate: Fisheries

The session focused on some of the key policy questions related to commercial fisheries. The first half of the session was devoted to a debate and discussion of the critical issues of limitations on domestic fishing activity for the purpose of maintaining optimum yield. The second half was broader, covering obstacles to growth, market structure, effects of foreign trade barriers and subsidies, joint ventures, appropriate rolls of Federal agencies, incentives needed for development, and other aspects of commercial fisheries management.

Session (30) Public Policy – Ocean Research and Development

One of the great challenges that face this nation in the next decade is how we handle the oceans in terms of its utilization and protection. Increased use of the oceans for such things as food, energy, recreation, and transportation will require larger programs in marine research and development than now exist. Congress must, therefore, shift its attention and push for a National Oceans Policy and a proper organizational structure to administer it. The tremendous job ahead will be expensive however, and require new Federal funding patterns; but perhaps more importantly, new program priorities will be necessary so that Congress can meet its fiscal responsibilities.

Table of Contents

Session 0. Plenary Session

Keynote Speaker:
Honorable Cecil D. Andrus, Secretary of the Interior—"Realizing Our Ocean Riches"

Panel Chairman:
Richard A. Frank, *Administrator, NOAA*

Panelists:
James N. Barnes, *Center for Law and Social Policy*

Charles DiBona, *Executive Vice President, American Petroleum Institute*

William D. Nordhaus, *Member of the President's Council of Economic Advisers*

Session 1. Buoy Technology

Chairman:
Kenneth M. Ferer, *Naval Ocean R&D Activity*

Co-Chairman:
Gene Edgerton, *Western Instrument Corp.*

1A **Evolution of Buoy Electronics and Telemetry,** Jerry C. McCall and Edmund G. Kerut, *NOAA Data Buoy Office;* and George Haas and R. Mueller, *Sperry Support Services* 1

1B **New Mooring Design for a Telemetering Offshore Oceanographic Buoy,** Paul D. Higley and Arthur B. Joyal, *Raytheon Co.* 10

1C **A Successful Meteorological Drifting Buoy** F. A. Reid, *Hermes Electronics Ltd.* 18

1D **An Analog Wave Spectrum Analyzer System for Operational Buoys,** Kenneth E. Steele, *NOAA Data Buoy Office;* and A. S. Hananel, *Sperry Support Services* 22

1E **A GOES Reporting Waverider Buoy,** Louis C. Adamo, *Louis C. Adamo, Inc.,* and Kenneth E. Steel, *NOAA Data Buoy Office;* and Ernest L. Burdette, *Computer Sciences Corp.* 31

1F **Wave Direction Measurement by a Single Wave Follower Buoy,** Wayne I. Sternberger, L. R. LeBlanc and F. H. Middleton, *University of Rhode Island* . . . 37

Session 2. Acoustic Systems

Chairman:
James F. Bartram, *Raytheon Co.*

Co-Chairman:
Salvatore D. Morgera, *Raytheon Co.*

2A **A Digital Survey Fathometer Providing a Chart Display and a Digital Output,** J. Russell Hogan, *Raytheon Co.* 42

2B **A Deterministic and Random Error Model for a Multibeam Hydrographic Sonar,** Dick Angelari, *National Oceanic and Atmospheric Administration* . . 48

2C **Portable Acoustic Tracking Systems (PATS),** Robert W. Gill, *University of Washington;* and William C. Gardner, *Naval Facilities Engineering Command* 54

2D **Swept Carrier Acoustic Underwater Communications,** A. Zielinski and L. Barbour, *Memorial University of Newfoundland* 60

2E **Small Submersible Acoustic Communications System Design,** Salvatore D. Morgera, *Raytheon Co.* . . . 66

2F **Frequency Shift Arrival Time Determination of Acoustic Signals,** Edward W. Early, John E. Ehrenberg and Roundney K. Liem, *University of Washington* 72

Session 3. Ocean Sciences

Chairman:
Walter L. Brundage Jr., *Naval Research Laboratory*

Co-Chairman:
Patrick J. Hannan, *Naval Research Laboratory*

3A **Shipboard Evaluation of Drag Coefficients for the Marine Regime,** C. Fairall, G. Schacker, T. Houlihan and K. Davidson, *Naval Postgraduate School* 76

3B **The Mechanical Properties of Chitosan Membranes,** B. L. Averbach and R. B. Clark, *Massachusetts Institute of Technology* 82

3C **Sediment as a cause of MACROCYSTIS gametophyte Non-Survival,** Louis A. Volse, *U.S. Coast Guard Academy* 87

3D **Navy Research on Marine Borers and the Laboratory Culturing of Limnorians,** Kathleen Parrish and John D. Bultman, *Naval Research Laboratory* 92

3E **The Motility of the Cells and the Extracellular Matrix of Labyrinthula—A Colonial Organism Found on Zastera Marina,** Eugene Bell, Dennis Solomon, and Stephanie Sher, *Massachusetts Institute of Technology* 99

Session 4. Underwater Work Systems & Procedures

Chairman:
W. F. Searle, Jr., *Searle Consultants*

Co-Chairman:
Tom Blockwick, *MAR, Inc.*

4A **A Non-Acoustic Long Distance Underwater Communications System,** R. G. Williscroft, *NOAA Ship Surveyor;* and N. C. McLeod, *TDC Underwater Systems* 105

4B **Lift Line Dynamics: A Technique Tailored for the User,** William S. Pope and Carl S. Albro, *Battelle-Columbus Laboratories* 109

4C **External Work of Breathing of Demand-Air Underwater Breathing Apparatus,** J. J. Grodski, *Defence & Civil Institute of Environmental Medicine, Ontario* 115

4D **Underwater Repair of Nuclear Reactors,** John D. Peters, *System Development Corporation;* and Leon Manry, *The Ocean Corp.* 122

4E **Underwater Stud Welding,** Koichi Masubuchi, Hironori Ozaki, and Jun-ichi Chiba, *Massachusetts Institute of Technology* 125

4F **Development of a Design Baseline for Remotely Controlled Underwater Work Systems,** Robert Lee Wernli, *Naval Ocean Systems Center* 130

Session 5. Economics and Management of Coastal Regions

Chairman:
Milton Steinmueller, *Dept. of Resource Development, Michigan State University*

5A **Coastal Recreation Values and Environmental Perturbations,** Elizabeth A. Wilman, *Resources for the Future, Washington, D.C.* . . . . . .

5B **Coastal Demographic Changes in the U.S. 1950–1974,** Neils West, *University of Rhode Island* 137

5C **Coastal Zone Management—A Decision Process,** Joel M. Goodman, *Frederic R. Harris, Inc.* . . . . . .

5D **Great Lakes Shoreline Erosion—Western Lake Michigan,** J. M. Pezzetta, *Ontario, Canada;* and J. R. Moore, *University of Alaska* 143

5E **Environmental Impact Assessment of Shoreline Bulkheading: A Historical Approach,** Michael E. Penney, *University of Rhode Island* 151

Session 6. Public Policy—Outer Continental Shelf Oil and Gas

Chairman:
Heather L. Ross, *Deputy Assistant Secretary, Department of the Interior*

Speakers:
Frances Beinecke, *Natural Defense Council,* Lloyd Ottman, *Shell Oil Company* and Robert Bybee, *Exxon Company, USA*

Panel:
Lowell D. Evian, *Director, Georgia State Office of Planning and Budget,* Hope M. Babcock, *Deputy Assistant Secretary Dept. of the Interior* and Paul Kelly, *VP. Zapata Corp.*

Session 7. Instrumentation I

Chairman:
Thomas M. Dauphinee, *National Research Council, Canada*

Co-Chairman:
J. Barry Oakes, *Applied Physics Laboratory, Johns Hopkins University*

7A **Drifting Buoys for Ocean Data Collection,** John Garrett, *Institute of Ocean Sciences* 155

7B **A Stable Platform for Micro-Scale Studies of Velocity, Temperature and Conductivity,** Bill P. Johnson, *Scripps Institution of Oceanography* 160

7C **Marine Instrumentation: An Assessement of Technology Versus Needs,** S. H. Koeppen, P. C. Etter, T. H. Hesselbecher and A. L. Inderbitzen, *MAR, Inc.* 164

7D **A Salinity Chain for Estuarine Use,** E. L. Lewis R. B. Sudar and Ron Perkin, *Institute of Ocean Sciences.* . . . . . .

7E **Development of a Small In Situ Conductivity Instrument,** Arthur M. Pederson and Michael C. Gregg, *APL, University of Washington* 173

7F **Evaluation of Metal Film Temperature and Velocity Sensors and the Stability of SPURV for Making Measurements of Ocean Turbulence,** James D. Irish and Wayne E. Nodland, *APL, University of Washington* . . . . . .

Session 8. Fisheries

Chairman:
Fred L. Olson, *National Oceanic and Atmospheric Administration*

Co-Chairman:
Francis M. Schuler, Jr., *National Oceanic and Atmospheric Administration*

8A **Implications of the Japanese Experience in Aquaculture Development for Thirty-Three Food-Short Countries,** Yoshiaki Matsuda, *Woods Hole Oceanographic Institution* 188

8B **Optimal Management of Global Tuna Resources,** Man-Loong Chan, John Buchanan, Wendy Garling, and John Sasser, *Tetra Tech* 199

8C **Acoustic Modeling of the Dolphin-Tuna Associative Behavior,** James W. Fitzgerald and Richard D. Doolittle, *Woodmont Associates, Ltd.;* and Phyllis H. Cahn, *Long Island University* . . . . . .

8D **The Detection of Tuna by Sonar,** Richard D. Doolittle and James W. Fitzgerald, *Woodmont Associates, Ltd.;* and Phyllis H. Cahn, *Long Island University* . . . . . .

8E **A Microcomputer-Based Echo Integration System for Fish Population Assessment,** Raynard Y. Kanemori and John E. Ehrenberg, *University of Washington* 204

8F **Prospects for the Development of a SWATH Fishing Vessel,** Mark S. Rice and J. B. Harmon, *SEACO, Inc.* 208

8G **Developments in the Law — The Fishery Conservation and Management Act of 1976,** Eugene R. Fidell, *LeBoeuf, Lamb, Leiby & MacRae* 214

8H **Input-Output Analysis for Salt Marsh Bioproductivity,** Thomas Leschine and Leah J. Smith, *Woods Hole Oceanographic Institution* 219

Session 9. Unmanned Underwater Vehicles

Chairman:
Norman Doelling, *Massachusetts Institute of Technology*

9A **Undersea Vehicle System Used for Photographic Reconnaissance of the Wreck of the USS Monitor,** Chris Tietze, *Harbor Branch Foundation, Inc.* . . . . .

9C **Trafficability and Performance Analyses for a Deep Ocean Running, Gear Module for an Undersea Vehicle,** Herbert G. Herrmann, *Naval Construction Battalion Center* 723

9D **Underwater Profiling of Icebergs Using Submersibles,** Boris Sukhov, *NORDCO Ltd.* 225

9E **Monitoring System for a New Ocean Cable Plow,** Kazuomi Yamamura, Yoshinao Iwamoto, and Yuichi Shirasaki, *KDD Laboratories* 231

9F **Display Aids for Remote Control of Untethered Undersea Vehicles,** William L. Verplank, *Massachusetts Institute of Technology* 238

Session 10. Law and Policy

Chairman:
John Norton Moore, *Center for Oceans Law & Policy, University of Virginia*

10A **Major Marine Legislative Actions in the 95th Congress,** Alfred W. Anderson, *National Oceanic and Atmospheric Administration* 242

10B **Ocean Area Management—An Emerging Concept,** Joel M. Goodman, *Frederic R. Harris, Inc.* . . . . . .

10C **The Economics & Technology of an Integrated Ocean Surveillance System for Enforcement,** Norman Louis Stone, *Sanders Associates, Inc.* 248

10D **The Marine Sanctuary Program: Implications for Ocean Management,** Carl S. Pavetto, *National Oceanic and Atmospheric Administration* . . . . . .

10E **Cultural Resource Management in the Coastal Zone,** Daniel Koski-Karell, *The Karell Institute* 255

10F **The Impact of the 1978 Geneva Session of UNCLOS III on Ocean Development,** Lewis M. Alexander, Francis X. Cameron, and Dennis Nixon, *University of Rhode Island* 259

10G **International Practice in Implementing 200 Mile Zones,** Myron Nordquist, *Nossaman, Krueger & Marsh* . . . . . .

Session 11. Electromechanical Cables/Connectors and Their Components

Chairman:
G. Rodriguez, *David Taylor Naval Ship R&D Center*

Co-Chairman:
Robert Forbes, *David Taylor Naval Ship R&D Center*

11A **Forced Motions of a Cable Suspended from a Floating Structure,** Raymond I. Bisplinghoff, *Tyce Laboratories;* and David O. Libby, *Simplex Wire & Cable Co.* 263

11B **Effects of Long Term Tension on Kevlar Ropes: Some Preliminary Results,** Thomas P. Bourgault, *Naval Underwater Systems Center* 268

11C **Performance/Failure Analysis of Acoustic Array Connectors and Cables After 6-10 Years of Service,** Colin J. Sandwith, *APL, University of Washington* . . . 273

11D **Flow-Induced Transverse Motions of a Flexible Cable Aligned with the Flow Direction,** R. J. Hansen and C. C. Ni, *Naval Research Laboratory* 287

11E **The State of Technical Data on the Hydrodynamic Characteristics of Moored Array Components,** J. H. Pattison and P. P. Rispin 291

11F **Mooring Component Performance Kevlar Mooring Lines,** G. A. Fowler and R. Reiniger, *Bedford Institute of Oceanography*

11G **Specifying and Using Contra-Helically Armored Cables for Maximum Life and Reliability,** Albert G. Berian, *The Rochester Corp.* 302

Session 12. Public Policy—Coastal Zone Management and Ocean Use

Chairman:
Robert W. Knecht, *Acting Assistant Administrator for Ocean Coastal Zone Management, National Oceanic and Atmospheric Administration*

Part I
Federal Consistency Provisions of the CZM Act

Introduction:
Michael E. Shapiro, *National Oceanic and Atmospheric Administration*

Speakers:
James Ross, *State of Oregon*
Phillip A. Clark, *American Petroleum Institute*

Panelists:
Robert W. Knecht, Michael E. Shapiro, *National Oceanic and Atmospheric Administration,* and Deb Stirling, *Staff, Senate Committee on Commerce, Sciences and Transportation,* G. William Frick, *Van Ness, Feldman & Sutcliffe*

Part II
Comprehensive Coastal Water Management and ocean uses

Speakers:
John Armstrong, *University of Michigan,* and Charles Williams, *C. W. Williams, Inc.*

Panelists:
Robert W. Knecht, Deb Stirling, G. William Frick and Paul Stang, *Dept. of Interior*

Session 13. Instrumentation II

Chairman:
J. Barry Oakes, *Applied Physics Laboratory, Johns Hopkins University*

Co-Chairman:
Thomas M. Dauphinee, *National Research Council, Canada*

13A **The Development and Testing of Current Meters for Long Term Development on the Continental Shelf,** Kenneth I. Heldebrandt, *Texas Instruments;* and Eduardo D. Michelena, *NOAA Data Buoy Office;* and Leslie S. Trest, *Sperry Support Services* 308

13B **Charting of Outer Continental Shelf Surface Currents by Aerial Tracking of Tracers,** Timothy L. Flynn, *Aero-Marine Surveys,* and David O. Cook, *Raytheon Co.* 315

13C **An Automated Tide Gauging Network,** Donald C. Knudsen, *Ocean & Aquatic Sciences* 728

13D **An Underwater Towed Electromagnetic Source for Geophysical Exploration,** Barry E. Tossman, W. A. Swartz, and D. L. Thayer, *Applied Physics Laboratory, Johns Hopkins University* 321

13E **Undersea Stereoscopic Television,** R. B. Fugitt and R. S. Acks, *Remote Ocean Systems, Inc.* 322

13F **The Comparison of Discus Buoy Wave Spectra Produced by Buoy-Fixed and Vertically Stabilized Accelerometers,** Ernest L. Burdette, *Computer Sciences Corp.* 327

Session 14. Acoustic Sources and Sonars

Chairman:
Charles W. Votaw, *Naval Research Laboratory*

14A **A Small, Wide-band, Low-frequency, High-power Sound Source Utilizing the Flextensional Transducer Concept,** J. Pagliarini and R. White, *Sanders Associates, Inc.* 333

14B **An Analysis of the Distribution of Measured Bubble Pulse Periods of Explosive Sources,** Richard J. Hecht and Louis A. Mole, *Underwater Systems, Inc.* 339

14C **Statistical Measures of Beam Output Noise Due to Shipping,** M. Moll, R. M. Zeskind, and W. Scott, *Bolt, Beranek and Newman, Inc.* 345

14D **A Wideband Sonar Equation,** L. W. Brooks, *Binary Systems, Inc.* 350

14E **Synthetic Aperture Imaging Using Acoustical Holography,** Woon Siong Gan, *Acoustical Services Pte, Ltd., Singapore* 355

Session 15. Large-Scale Development of Ocean Energy Resources

Chairman:
Owen M. Griffin, *Naval Research Laboratory*

15A **Environmental Considerations for Siting an Ocean Thermal Energy Conversion Early Ocean Testing Platform at Four Proposed Areas,** M. Dale Sands, *Interstate Electronics Corp.* and Pat Wilde, *Lawrence Berkeley Laboratories* 358

15B **Large Scale Wave Energy—A New Approach,** F. R. Haselton, *Imagineering* . . . . . .

15C **Technology Considerations in the Design of a Commercial Offshore Energy Conversion (OTEC) Plant,** William W. Rogalski, Jr. and Robert J. Scott, *Gibbs and Cox, Inc.;* and Julio G. Giannotti, *Giannotti and Buck Associates* 363

15D **Philosophy of Monitoring, Inspection and Repair for Fixed Offshore Platforms,** Peter W. Marshall, *Shell Oil Company* 369

15E **A Proposal Concerning Total Energy Self-Supply Plan From Ocean Surfaces in Japan,** Yoshiro Kasahara, *Kinki University, Osaka* 377

Session 16. Remote Sensing from Satellites and Aircraft

Chairman:
David E. Weissman, *Hofstra University*

Co-Chairman:
Donald M. Bolle, *Brown University*

16A **Mission Horizons for Oceanic Environmental Monitoring,** S. Walter McCandless Jr., *National Aeronautics and Space Administration*

16B **Oceanographic & Geodetic Surveillance—The Expanding Role of Satellite Radar Altimetry,** Tom Godbey, *General Electric Co.* . . . . . .

16C **SAR Imaging of Waves in Ice,** Byron R. Dawe and Surendra K. Parashar, *Memorial University of Newfoundland* 379

16D **The Comparison Between Synthetic Aperture Radar Imageries and Surface Truth of Ocean Waves,** S. Vincent Hsiao, *Jet Propulsion Laboratory* 385

16E **Laser Bathymetry for Near Shore Charting Application (Preliminary Field Text Results),** Gary C. Guenther, Lowell R. Goodman, and David B. Enabnit, *NOAA/National Ocean Survey;* and Robert N. Swift and Robert W. Thomas, *EG&G* 390

16F **Regional Integration, Validation and Application of SEASAT-A Satellite Scatterometer Data,** Victor E. Delnore, *Rutgers University* 397

Session 17. Institutional Aspects of Ocean Development

Chairman:
Henry H. Esterly, *New York City Community College*

Co-Chairman:
Alexander Bigler, *Environmental Interface*

Discussants:
Kirill Chekotillo, *United Nations*
Arvid Pardo, *University of Southern California*

17A **Regional Aspects of Ocean Management,** Lewis M. Alexander, *University of Rhode Island* 398

17B **The Proposed International Seabed Authority: A Unique Institution,** Samuel R. Levering, *U.S. Committee for the Oceans, Washington, D.C.* and Lee Kimball, *United Methodist LOS Project* 401

17C **Hydrocarbons on the Continental Margins—Some of the Issues Addressed at the Current Law of the Sea Treaty Negotiations,** John N. Garrett, *Gulf Energy & Minerals Co.* . . . . . .

17D **The Impact of UNCLOS III on Marine Scientific Research,** William L. Sullivan, Jr., *U.S. Dept. of State, Office of Marine Science & Technology Affairs* 403

17E **CAESAR, SOSUS and Submarines. Economic and Institutional Implications of ASW Technologies,** Harvey B. Silverstein, *University of South Carolina* . . 406

17F **The Economic Potential of the Oceans and African States,** Penelope Ferreira, *Duquesne University* 411

Session 18. PUBLIC POLICY—Deep Ocean Mining

Chairman:
Charles P. Eddy, *Deputy Assistant Secretary, Department of the Interior*

Speakers:
Leigh S. Ratiner, *Dickstein, Shapiro and Morin*

Helen B. Junz, *Deputy Assistant Secretary of the Treasury*

Samuel R. Levering, *U.S. Committee for the Oceans*

Panel:
Alan Berlind, *Director, Law of the Sea Office, Department of State*

Thomas R. Kitsos, *Staff House Committee on Merchant Marine and Fisheries U.S. House of Representatives*

H. William Menard, Director, *U.S. Geological Survey*

Session 19. Satellite Radiometric & Visible Sensing

Chairman:
James J. Gallagher, *Naval Underwater Systems Center*

19A **Satellite Imagery and the Geomorphology of Bermuda,** Stanley A. Ashmore, *Defense Mapping Agency* 417

19B **Utility of Polarized Visible Radiation in Oceanography,** H. V. Soule, *OAO Corporation* 420

19C **The European Space Agency—Its Ancestry, Objectives and Programs,** W. J. Mellors, *European Space Agency* . . . . . .

19D **Satellite Ocean-Related Imagery Applications Program,** Edward Wedler and Richard D. Worsfold, *Memorial University of Newfoundland* 427

19E **Some Automatic Digital Techniques for Enhancing and Extracting Oceanic Features from Satellite Infra-red Pictures,** D. G. Nichol, *Naval Underwater System Center* 433

19F **Satellite Interferometry for Ocean Surveillance,** Richard S. Orr, *Stanford Communications, Inc.* 437

Session 20. Marine Pollution Analysis & Monitoring

Chairman:
Stanley G. Chamberlain, *Raytheon Co.*

20A **Advancement in Oil Spill Trajectory Modelling,** David R. Garver, *Dow Chemical Co.,* and Glen N. Williams, *Texas A&M University* 441

20B **An Objective Procedure for Evaluating Pollutant Dispersion and Flushing in Tidal Canals and Optimizing Canal System Design,** Frederick W. Morris, IV, *University of Florida* . . . . . .

20C **Marine Pollution in Kuwait,** B. L. Oostdam, *Millersville State College* 445

20D **Stratified Water Circulation Forecasting for Water Quality Management Planning in the Coastal Zone,** Stanley G. Chamberlain, Prekimi V. Tawari, and William J. Comery, *Raytheon Co.* 451

20E **Ocean Disposal in the Mid-Atlantic Bight,** William C. Muir, Gilbert Horwitz, and George D. Pence, Jr., *Environmental Protection Agency* 456

20F **Application of Sonar Techniques to the Surveillance and Enforcement of Dredged Material Disposal Operations,** Gilbert L. Chase, *U.S. Army Corps of Engineers* . . . . . .

20G **Geological Impacts on Sludge Dumping on the Continental Shelf: Estimation by Math Modelling,** David O. Cook, James W. Demenkow, and Priya J. Wickramaratne, *Raytheon Co.* . . . . . .

Session 21. Navigation

Chairman:
Karl R. Schroeder, *U.S. Coast Guard*

Co-Chairman:
B. Harl Romine, *U.S. Coast Guard*

21A **Submersible Acoustic Navigation for Precise Underwater Surveys,** R. C. Abbott, *AMF Sea-Link Systems* 462

21B **Optimal Estimation of Undersea Acoustic Transponder Locations,** David G. Carta, *Jet Propulsion Laboratory* 466

21C **Accurate and Continuous Geophysical Navigation Control with Newly Developed Radio System,** L. E. Ott, *NAV-CON, Inc.* 472

21D **How to Add Satellite Navigational Accuracy and Stability to Existing Offshore NAV Systems,** Phineas J. Icenbice, *JMR Instruments* 478

21E **Performance of a Real World Minimum Variance Integrated Navigation System,** Ronald F. McPherson, *Sperry Marine Systems* 485

21F **A Satellite-Based System for Redundant Maritime Distress Signalling,** Walter C. Scales, *The MITRE Corporation* 490

Session 22. Sea Floor Engineering

Chairman:
Anton L. Inderbitzen, *MAR, Inc.*

Co-Chairman:
Terrence McGuinness, *National Oceans and Atmospheric Administration*

22A **Adhesive Resistance of Underconsolidated Sediments,** T. R. Chari, S. N. Guha, and K. Muthukrishnaiah, *Memorial University of Newfoundland* 497

22B **Submarine Landslides—East Coast Continental Slope and Upper Rise,** Alexander Malahoff and Richard B. Perry, *National Ocean Survey/NOAA;* and Robert W. Embley, *Lamont-Doherty Geological Observatory* . . 503

22C **Design of an Ocean Bottom Seismometer with Response from 25 Hz to 100 Seconds,** Robert G. Bookbinder, Arthur C. Hubbard, William G. McDonald, and Paul W. Pomeroy, *Lamont-Doherty Geological Observatory* 510

22D **Preliminary Results on Sub-Bottom Surveys at Golfo De Campeche Area for Engineering Purposes,** Jose Angle Aguilar-Castro and Pablo E. Torres-Salmeron, *Compania Mexicana Aerofoto, S.A.* . . . . .

22E **A Unique Ocean Test Range,** J. Blaine Davidson, *Florida Atlantic University* 516

22F **Broadband Seismic Data used for Seafloor Sediment Classification,** A. D. Dunsiger, *Memorial University of Newfoundland;* and R. R. MacIsaac, *Acres Consulting Services, Ltd.* 521

Session 23. Information & Data Systems

Chairman:
Salvatore D. Morgera, *Raytheon Co.*

Co-Chairman:
James F. Bartram, *Raytheon Co.*

23A **Microprocessor Acoustic Data Buoy,** Robert C. Spindell, Kenneth R. Peal, and Donald E. Koelsch, *Woods Hole Oceanographic Institution* 527

23B **A Low Power Microprocessor System for Deep-Sea Free Vehicle Applications,** Richard E. Ackermann, C. M. Butler and R. F. Weiss, *Scripps Institution of Oceanography* 532

23C **Real-Time Oceanographic Data from Georges Bank,** Robert N. Lobecker, Earl R. Lind, Gary Milano, and Ronald Franklin, *Raytheon, Co.* 536

23D **Use of Industry Standards for Shipboard Data Systems,** Kenneth R. Peal and Albert M. Bradley, *Woods Hole Oceanographic Institution* 547

23E **A Microcomputer Based Ocean Observation System,** Domingo Munoz, *San Jose State University* 552

23F **Ships Thruster Allocation Logic With Rudder Interaction,** Daniel O. Molnar and M. R. Cramer, *Honeywell* 556

Session 24. PUBLIC POLICY—Fisheries

Chairman:
Terry L. Leitzell, *National Marine Fisheries Service, National Oceanic and Atmospheric Administration*

I. Limited Entry

Speaker:
Virgil J. Norton, *University of Maryland.*

Access Limitations as a Fisheries Management Alternative.

Speaker:
Jacob J. Dykstra, *Point Judith Fishermen's Cooperative*

Limited entry is a regulatory nightmare which places unfair constraints on U.S. fishermen.

Panel:
Terry Leitzell, *National Marine Fisheries Service, National Oceanic and Atmospheric Administration,* Christopher Koch, *Senate Committee on Commerce, Science & Transportation,* Norman C. Venzke, *R. Adm., USCG,* Lee Weddig, *National Fisheries Institute.*

II. U.S. Commercial Fishing Industry

Speaker:
Julio Pontecorvo, *Columbia University*
Current Problems in Fisheries Management

Speaker:
Richard N. Sharoud, *Nat'l Federation of Fisheries*
Constraints on Growth in the U.S. Fishing Industry in the Post 200 Mile Era.

Panel:
Terry L. Leitzell, *National Marine Fisheries Service, National Oceanic and Atmospheric Administration;* Christopher Koch, *Senate Committee on Science, Commerce & Transportation,* Lee Weddig, *National Fisheries Institute;* John D. Negroponte, *Deputy Asst. Secy State for Oceans & Fisheries Affairs*

Session 25. Education & Training for Ocean Involvement

Chairman:
Matilene S. Berryman, *University of the District of Columbia*

25A **The Marine Technologist,** Roger M. Lloyd, Jr., *Florida Junior College* 561

25B **Education—The Bridge to Ocean Exploration,** Matilene S. Berryman, *University of the District of Columbia* 564

25C **Undergraduate Preparation for a Career in Physical Oceanography,** Victor E. Delnore, *Rutgers University* 568

25D **Submarine Radiometry and Physical Environment Monitoring,** Joel Vandenberghe, *Institut Superior D'Electronique du Nord, France;* and Robert Kling, *Universite des Sciences and Techniques, France* 571

25E **Simplified Guidance for Engineers Associates with Design Construction and Certification of Hyperbaric Research Facilities,** Terry Hayes, *Naval Facilities Engineering Command* 575

Session 26. Novel Devices for Extracting Energy from the Ocean

Chairman:
Michael E. McCormick, *U.S. Naval Academy*

26A **Dynamic Dam for Harnessing Ocean and River Currents and Tidal Power,** James T. Yen, *Grumman Aerospace Corp.,* and John Isaacs, *Scripps Institution of Oceanography* 582

26B **A Wave Activated Electric Generator,** Thore Omholt, *SUNY Maritime College* 585

26C **Energy from Sea Waves: System Optimization by Diffraction Theory,** Gaetano Sebastiani, Marco Berta, and A. Blandino, *Technomare, SpA.* 590

26D **A Hydrostatically Actuated Piston and Hydraulic System for Deep-Sea Free Vehicle Applications,** Oskar H. Kirsten and R. F. Weiss, *Scripps Institution of Oceanography* 596

26E **The Use of Ocean Energy In A Hydrostatic Motor,** Stephen Selwyn and F. W. McCoy, *Lamont-Doherty Geological Observatory* 599

Session 27. Deep Sea Mining

Session sponsored by Marine Minerals Committee (MTS) and MS-5 Panel of SNAME

Chairman:
Raymond Kaufman, *Deepsea Ventures, Inc.*

27A **Activities & Economics of Existing Manganese Nodule Mining Consortia,** C. Richard Tinsley, *Continental Bank* 602

27B **A Cost Model for a First Generation Deep Ocean Mining Venture,** G. D. Nyhart, *MIT* 739

27C **Technological Gaps in Deep Ocean Mining,** John B. Herbich and John E. Flipse, *Texas A&M University* . . 606

27D **Utilization of Available Technology to Support Ocean Mining,** Sam Rothman and Robert J. Lynch, Jr., *George Washington University* 611

27E **Coastal Zone Implications of Deep Seabed Mining,** M. Karl Jugel, *NOAA Marine Minerals Division;* and Daniel M. Bragg, *Texas A&M University* 734

Session 28. Wave Direction Measurement Technology

Chairman:
Edward C. Brainard II, *Environmental Devices Corp.*

Co-Chairman:
Marshall D. Earle, *National Oceanic and Atmospheric Administration*

28A **A System for the Routine Measurement of Directional Wave Spectra from Large Discus Buoys,** Kenneth E. Steele, *NOAA Data Buoy Office;* Ernest L. Burdette, *Computer Sciences Corp.;* and Anthony Trampus, *Federal Energy Regulatory Commission, Dept. of Energy* 614

28B **Directional Wave Spectral Data from a Large Discus Buoy,** Ernest L. Burdette, *Computer Science Corp.;* Kenneth E. Steele, *NOAA Data Buoy Office;* and Anthony Trampus, *Federal Energy Regulatory Commission, Dept. of Energy* 622

28C **Directional Wave Spectra Monitoring Horizontal Spar Buoy,** Andrew Van Baird, *Massachusetts Institute of Technology* 629

28D **Measurement of Directional Ocean Wave Spectra from Fixed Platforms,** Leon E. Borgman and Evangelos Yfantis, *University of Wyoming* 634

28E **Ocean Wave Detection and Direction Measurements with Microwave Radars,** Paul G. Teleki, *U.S. Geological Survey;* William McLeish and Duncan Ross, *NOAA Atlantic Oceanographic & Meteorological Laboratories;* Robert A. Shuchman, *Environmental Research Institute of Michigan;* Walter E. Brown, Jr., *Jet Propulsion Laboratory;* and Michael Mattie, *U.S. Army Corps of Engineers* . . . . . .

Session 29. Financing Ocean Development

Chairman:
James J. White, *USNR (Retired)*

Co-Chairman:
George English, *National Oceanic and Atmospheric Administration*

29A **International Programs, Financing the International Seabed Authority,** Hartsell Cash, *International Bank for Reconstruction and Development, Washington, D.C.* . . . . . .

29B **Offshore Petroleum Development Financing,** Arthur Eschenlaur, *Morgan Guaranty Trust Co.* 649

29C **Financial Requirements for Ocean Thermal Energy Conversion,** Frederick E. Naef and R. J. Pont, *Lockheed Corp.* 654

29D **Cost Standards for Ocean Research Vessels,** W. L. Martino, *U.S. General Accounting Office* 655

29E **Deep Sea Mining: Who Should Pay?** Myron Nordquist, *Nossaman, Krueger, and Marsh* . . . . . .

Session 30. Public Policy Ocean Research & Development

Chairman:
Dr. John B. Slaughter, *National Science Foundation, Assistant Director for Astronomical, Atmospheric, Earth, and Ocean Sciences*

Speaker:
Hon. Lowell P. Weicker, *Senator from Connecticut*

Panelists:
Dr. G. Ross Heath, *Dean of the School of Oceanography, Oregon State University, Corvallis, Oregon*
Mr. John R. Botzum, *Editor, Nautilus Press Inc.*
Mr. Marvin Pitkin, *Assistant Administrator for Commercial Development, Maritime Administration*
Mr. Otto Klima, *Vice President and General Manager, Reentry and Environmental Systems Division, General Electric Company*

Poster Sessions

1. A DYNAMIC HYDROTHERMAL EXPERIMENTAL STATION 657
Andrew Gustajtis, Memorial University of Newfoundland

2. DEPLOYMENT OF LONG-TERM SEAFLOOR MINERAL EXPOSURE EXPERIMENTS TO MEASURE CHANGES OF MINERALOGY AND COMPOSITION OF MANGANESE NODULES 662
R. G. Burns, V. M. Burns, H. W. Stockman and C. T. Stockman, MIT, and M. D. Benson, Scripps Institution of Oceanography

3. MOBILE INITIAL CONDITION INDICATOR, A DYNAMIC APPROACH TO MARINE EXPLORATION 668
Lawrence H. Befferman, Em-Log Enterprises

4. COMPREHENSIVE OCEANOGRAPHIC MONITORING PROGRAM IN THE ARABIAN GULF 674
Chung-Sung Ahn, Ebasco Services Inc.

5. A SYSTEMS APPROACH TO UNDERWATER CAMERA DATA CORRELATION AND INTERPRETATION 678
G. G. Hayward and W. D. McElroy, Jr., Benthos, Inc., and D. S. Hosom and W. M. Marquet, Woods Hole Oceanographic Institution

6. ICEBERG ALARM SYSTEM 682
R. Boetes, P. B. Sukhov, R. W. Crocker and W. E. Russell, Nordco, Ltd.

7. USE OF FREE FALL PENETROMETER IN SEAFLOOR ENGINEERING 686
T. R. Chari, W. G. Smith and A. Zielinski, Memorial Universiy of Newfoundland

8. THE DEVELOPMENT OF A SEAFLOOR EARTHQUAKE MEASUREMENT SYSTEM 692
David Ryerson and Eric Reece, Sandia Laboratories

9. MICROWAVE DETECTION OF ADSORPTION AND SPREADING FILMS AT THE AIR-WATER INTERFACE 696
R. Cini, Universita di Firenze and P. P. Lombardini, Universita di Torino

10. ELECTRODEPOSITION OF MINERALS IN SEAWATER 699
Wolf Hilbertz, University of Texas

11. ARCTIC DATA ACQUISITION AND PROCESSING SYSTEM
E. O. Lewis, Canadian Department of Environment

12. JANUS IV CONSTRUCTION DIVING AT 460 M (1509 FT) NEW WORLD RECORD AT 501 M (1644 FT) 707
H. G. DeLauze and J. L. Chasserot, Comex Industries

13. SUBSURFACE LAYERED MEDIA PARAMETER ESTIMATION USING A LINEARIZED MULTIPLE REFLECTION MODEL 712
F. M. El-Hawary and W. J. Vetter, Memorial University of Newfoundland

14. R & D ACTIVITIES OF THE AMERICAN UNDERWATER BAND 718
Richard Bailey

Authors Index

	Page
Abbott, R. C.	462
Ackerman, R. E.	532
Acks, R. S.	322
Adamo, L. C.	31
Ahn, C. S.	674
Albro, C. S.	109
Alexander, L. M.	259, 398
Anderson, A.W.	242
Angelari, R. D.	48
Ashmore, S. A.	417
Averbach, B. L.	82
Bailey, R.	718
Barbour, L.	60
Befferman, L. H.	668
Bell, E.	99
Benson, M. D.	662
Berian, A. G.	302
Berryman, M. S.	564
Berta, M.	590
Bisplinghoff, R. I.	263
Blandino, A.	590
Boetes, R.	682
Bookbinder, R. G.	510
Borgman, L. E.	634
Bourgault, T. P.	268
Bradley, A. M.	547
Bragg, D. M.	734
Brooks, L. W.	350
Brown, W. E., Jr.	639
Buchanan, J. E.	199
Bultman, J. D.	92
Burdette, E. L.	31, 327, 614, 622
Burns, R. G.	662
Burns, V. M.	662
Butler, C. M.	532
Cameron, F. X.	259
Carta, D. G.	466
Chamberlain, S. G.	451
Chan, M. L.	199
Chari, T. R.	497, 686
Chasserot, J. L.	707
Chiba, J. I.	125
Cini, R.	696
Clark, R. B.	82
Comery, W. J.	451
Cook, D. O.	315
Cramer, M. R.	556
Crocker, R. W.	682
Davidson, J. B.	516
Davidson, K. L.	76
Dawe, B. R.	379
DeLauze, H. G.	707
Delnore, V. E.	397, 568
Dunsiger, A. D.	521
Early, E. W.	72
Ehrenberg, J. E.	72, 204
El-Hawary, F. M.	712
Embley, R. W.	503
Enabnit, D. B.	390
Eschenlauer, A.	649
Etter, P. C.	164
Fairall, C.	76
Ferreira, P.	411
Fidell, E. R.	214
Flipse, J. E.	606
Flynn, T. L.	315
Fowler, G. A.	297
Franklin, R.	536
Fugitt, R. B.	322
Gan, W. S.	355
Gardner, W. C.	54
Garling, W.	199
Garrett, J.	155
Garver, D. R.	441
Giannotti, J. G.	363
Gill, R. W.	54
Goodman, L. R.	390
Gregg, M. C.	173
Grodski, J. J.	115
Guenther, G. C.	390
Guha, S. N.	497
Gustajtis, A.	657
Haas, G.	1
Hananel, A. S.	22
Hansen, R. J.	287
Harmon, J. B.	208
Hayes, T.	575
Hayward, G. G.	678
Hecht, R. J.	339
Heldebrandt, K. I.	308
Herbich, J. B.	606
Herrmann, H. G.	723
Hesselbecher, T. H.	164
Higley, P. D.	10
Hilbertz, W. H.	699
Hogan, J. R.	42
Horwitz, G.	456
Hosom, D. S.	678
Houlihan, T.	76
Hsiao, S. V.	385
Hubbard, A. C.	510
Icenbice, P. J.	478
Inderbitzen, A. L.	164
Irish, J. D.	180
Isaacs, J.	582
Iwamoto, K.	231
Johnson, B. P.	160
Joyal, A. B.	10
Jugel, M. K.	734
Kanemori, R. Y.	204
Kasahara, Y.	377
Kerut, E. G.	1
Kimball, L.	401
Kirsten, O. H.	596
Kling, R.	571
Knudsen, D. C.	728
Koelsch, D. E.	527
Koeppen, S. H.	164
Koski-Karell, D.	255
LeBlanc, L. R.	37
Leschine, T.	219
Levering, S. R.	401
Lewis, E. L.	169
Libby, D. O.	263
Liem, R. K. B.	72
Lind, E. R.	536
Lloyd, R. M., Jr.	561
Lobecker, R. N.	536
Lombardini, P. P.	696
Lynch, R. J., Jr.	611
MacIsaac, R. R.	521
Malahoff, A.	503
Manry, L.	122
Marquet, W. M.	678
Marshall, P. W.	369
Martino, W. L.	655
Masubuchi, K.	125
Matsuda, Y.	188
Mattie, M.	639
McCall, J. C.	1
McCoy, F. W.	599
McDonald, W. G.	510
McElroy, W. D., Jr.	678
McLeish, W.	639
McLeod, N. C.	105
McPherson, R. F.	485
Michelena, E. D.	308
Middleton, F. H.	37
Milano, G.	536
Mole, L. A.	339
Moll, M.	345
Molnar, D. O.	556
Moore, J. R.	143
Morgera, S. D.	66
Mueller, R.	1
Muir, W. C.	456
Munoz, D.	552
Muthukrishnaiah, K.	497
Naef, F. E.	654
Ni, C. C.	287
Nichol, D. G.	433
Nixon, D.	259
Nodland, W. E.	180
Nyhart, G. D.	739
Omholt, T.	585
Oostdam, B. L.	445
Orr, R. S.	437
Ott, L. E.	472
Ozaki, H.	125
Pagliarini, J.	333
Parashar, S. K.	379
Parrish, K. M.	92
Pattison, J. H.	291
Peal, K. R.	527, 547
Pederson, A. M.	173
Pence, G. D., Jr.	456
Penney, M. E.	151
Perry, R. B.	503
Peters, J. D.	122
Pezzetta, J. M.	143
Pomeroy, P. W.	510
Pont, R. J.	654
Pope, W. S.	109
Reece, E. W.	692
Reid, F. A.	18
Reiniger, R.	297
Rice, M. S.	208
Rispin, P. P.	291
Rogalski, W. W., Jr.	363
Ross, D.	639
Rothman, S.	611
Russell, W. E.	682
Ryerson, D. E.	692
Sands, M. D.	358
Sandwith, C. J.	273

Sasser, J. 199
Scales, W. C. 490
Schacker, G. 76
Scott, R. J. 363
Scott, W. L. 345
Sebastiani, G. 590
Selwyn, S. 599
Sher, S. 99
Shirasaki, Y. 231
Shuchman, R. A. 639
Silverstein, H. B. 406
Smith, L. J. 219
Smith, W. G. 686
Solomon, D. 99
Soule, H. V. 420
Spindell, R. C. 527
Steele, K. E. 22, 31, 614, 622
Sternberger, W. I. 37
Stockman, C. T. 662
Stockman, H. W. 662
Stone, N. L. 248
Sudar, R. B. 169
Sukhov, B. 225, 682
Sullivan, W. L., Jr. 403
Swartz, W. A. 321
Swift, R. N. 390
Tawari, P. V. 451
Teleki, P. G. 639
Thayer, D. L. 321
Thomas, R. W. 390
Tinsley, C. R. 602
Tossman, B. E. 321
Trampus, A. 614, 622
Trest, L. S. 308
VanBaird, A. 629
Vandenberghe, J. 571
Verplank, W. L. 238
Vetter, W. J. 712
Volse, L. A. 87
Wedler, E. 427
Weiss, R. F. 532, 596
Wernli, R. L. 130
West, N. 137
White, R. P. 333
Wilde, P. 358
Williams, G. N. 441
Williscroft, R. G. 105
Worsfold, R. D. 427
Yamamura, K. 231
Yen, J. T. 582
Yfantis, E. 634
Zeskind, R. M. 345
Zielinski, A. 60, 686

Chairmen, Speakers and Panelists

	Session
Andrus, C. D.	PLENARY
Armstrong, J.	12
Babcock, H. M.	6
Barnes, J. N.	PLENARY
Bartram, J. F.	2, 23
Beinecke, F.	6
Berlind, A.	18
Berryman, M. S.	25
Bigler, A.	17
Blockwick, T.	6
Bolle, D. M.	16
Brainard, E. C., II	28
Brundage, W. L., Jr.	3
Bybee, R. W.	6
Chamberlain, S. G.	20
Clark, P.	12
Cobb, W. R.	6
Dauphinee, T. M.	7, 13
DiBona, C.	PLENARY
Doelling, N.	9
Dykstra, J.	24
Earle, M. D.	28
Eddy, C. P.	18
Edgerton, G.	1
English, G.	29
Esterly, H. H.	17
Evjen, L. D.	6
Ferer, K. M.	1
Forbes, R.	11
Frank, R. A.	PLENARY
Frick, G. W.	12
Gallagher, J. J.	19
Griffin, O. M.	15
Hannan, P. J.	3
Inderbitzen, A. L.	22
Junz, H. B.	18
Kaufman, R.	27
Kelly, P.	6
Kitsos, T. R.	18
Knecht, R.	12
Koch, C.	24
Kreps, J.	BANQUET
Leitzell, T. L.	24
Levering, S. R.	18
Maudlin, L. Z.	LUNCHEON
McCormick, M. E.	26
McGuinness, T.	22
Menard, H. W.	18
Moore, J. N.	10
Morgera, S. D.	2, 23
Negroponte, J.	24
Nordhaus, W. D.	PLENARY
Norton, V.	24
Oakes, J. B.	7,13
Olson, F. L.	8
Otteman, L.	6
Pontecorvo, J.	24
Ratiner, L. S.	18
Rickard, J. A.	LUNCHEON
Rodriguez, G.	11
Romine, B. H.	21
Ross, H. L.	6
Ross, J.	12
Schroeder, K.	21
Schuler, F. M., Jr.	8
Searle, W. F., Jr.	4
Shapiro, M.	12
Stang, P.	12
Steinmueller, M.	5
Stirling, D.	12
Venzke, C.	24
Votaw, C. W.	14
Weddig, L.	24
Weissman, D. E.	16
White, J. J.	29
Williams, C. W.	12

Exhibitors

	BOOTH
AANDERAA INSTRUMENTS, INC.	217
ADVANCED CABLE AND ASSEMBLY	279
AMETEK CORP.	232–33
APPLIED MICROSYSTEMS LIMITED	227
BENTHOS, INC.	319–20
BIRNS AND SAWYER, INC.	230–31
BOOK EXAMINATION CENTER	288
CAYMAN-BELIZE INFORMATION CENTRE	268
COMPASS PUBLICATIONS, INC.	274
CONFERENCE BOOK SERVICE	301
CUBIC WESTERN DATA	277–78
DAMES AND MOORE	244–45
DEFENSE MAPPING AGENCY, WASHINGTON, D.C.	See U.S. Navy
DEL NORTE TECHNOLOGY, INC.	266–67
DIGICOURSE, INC.	269
EASTERN INSTRUMENTATION CORP.	262
ENCYCLOPAEDIA BRITANNICA	302
ENGINEERING SERVICE ASSOCIATES	200–16, 218–224

AMF Sealink
Appleton Machine
D.G. O'Brien, Inc.
Diving Unlimited International
Environmental Devices Corp.
Franklin Electric
Giannini Instruments
Huntec'70, Ltd.
Hydracarta Corp
Hydrobios
J-TEC Associates
Lucker Manufacturing Co.
Nova Scotia Research Foundation
Ocean Applied Research
Philadelphia Resins
Technology Development Corp.
Tension Member Technology
U.S. Phosmarine
Vector Cable Co.
Sabins Corp.

ENVIROMARINE SYSTEMS, INC.	318
ENVIRONMENTAL RESEARCH AND TECHNOLOGY	243
EOTECH	342
GANS AND PUGH ASSOCIATES, INC.	306–08

E.G. & G., Inc.
EPC Labs
Harvey – Lynch
Hydrolab
Memodyne
Rochester Corp.
Subsea Systems, Inc.

GENERAL INSTRUMENT CORP.	256
GEOSERVICES, INC.	246–47
GLENAIR, INC.	258–59
GREAT LAKES ENVIRONMENTAL	228
GUILDLINE INSTRUMENTS, INC.	324

HELLE ENGINEERING, INC. 336
HYDRONAUTICS, INC. 346
INFORMATION HANDLING SERVICES 303
INNERSPACE TECHNOLOGY, INC. 255
INTERNATIONAL UNDERWATER CONTRACTORS 260–61
JMR INSTRUMENTS, INC. 298
KLEIN ASSOCIATES, INC. 253–54
LOCKHEED CORPORATION 249, 250–52
MAGNAVOX GOVERNMENT AND INDUSTRIAL ELECTRONICS CO. 275–76
MAR, INC. 335
MARINE ENGINEERING/LOG 297
MARSH-MCBIRNEY, INC. 312
MCCLELLAND ENGINEERS, INC. 341
MOTOROLA, INC., GOVERNMENT ELECTRONICS DIV. 311
U.S. NAVY 325–8, 331–33, 337–39, 343–44

David Taylor Naval Ship R&D
Naval Ocean Research and Development Activity
Naval Oceanographic Center
Naval Ship Engineering Center
Naval Research Laboratory
Office of Naval Research

NOAA 290–91
NAVIGATION COMMUNICATIONS SYSTEMS 229
OCEAN INSTRUMENTS, INC. 272–73
OCEANIC SERVICES GROUP 239, 240–42

Cortland Line
EMP Industries
General Oceanics
Hydro Search
Loos and Co.
Shape
Telstar Electronics

OIL SPILL INTELLIGENCE REPORT 348
OTIS ENGINEERING CORP. 323
PAROSCIENTIFIC, INC. 257
PERRY OCEANOGRAPHICS, INC. 236
PLESSEY ENVIRONMENTAL SYSTEMS 270–71
PREFORMED LINE PRODUCTS CO. 235
PUBLISHERS FOR CONVENTIONS, INC. 234
RADAR DEVICES, INC. 309
ROCKWELL INTERNATIONAL 225–26
SCHONSTEDT INSTRUMENT CO. 296
SEA DATA CORP. 329
SEA GRANT–MIT 345
SEABOARD INTERNATIONAL EQUIPMENT CO. 263
SIMRAD, INC. 299
SIPPICAN CORP. 304–5
SONATECH, INC. 287
SUB SALVE INDUSTRIES, INC. 248
TA INSTRUMENT CASE CO. 330
TRW SYSTEMS GROUP 264–65
TELEDYNE HASTINGS-RAYDIST 294
TELLUROMETER, USA 300

TETRATECH INC. 317
TRACOR MARINE AND R.F. BUSBY ASSOCIATES 295
UNIVERSITY OF SOUTHERN CALIFORNIA 292
VIKING INDUSTRIES, INC. 237–38
WALL ROPE WORKS 347
WESMAR, OFFSHORE SYSTEMS DIVISION 321
WESTERN GEAR CORP. 282–83
WESTINGHOUSE ELECTRIC CORP. 284–86
ED WINSTON AND CO. 313–15

C.A. Richards and Associates
Edo Western
J.W. Automarine
Kintec, Inc.
Neil Brown Instruments
Sonotech
Varian of Canada

EVOLUTION OF BUOY ELECTRONICS AND TELEMETRY

J. C. McCall, E. G. Kerut - NOAA Data Buoy Office
G. Haas, R. Mueller - Sperry Support Services

National Space Technology Laboratories
NSTL Station, MS 39529

Abstract

In November 1967, the National Data Buoy Development Project was established by the United States Coast Guard. The primary purpose of this organization was to verify and standardize the design and performance of environmental data buoys by establishing an extensive network of sophisticated buoys capable of delivering a wide variety of data, supplemented by smaller buoys of simpler design for special user needs. In 1972, user needs were reevaluated and the program was redirected to be more responsive to these needs. Consequently, the goal of establishing a network of multipurpose buoys was discarded. In January 1973, the project was designated the NOAA Data Buoy Office (NDBO) and was sanctioned by the National Weather Service as a prime user of data.

A major NDBO mission is to develop the technology required to gather and report environmental data from marine areas on an accurate, reliable, and synoptic basis. The provisioning of this data would enable improved weather forecasting, including warnings of impending catastrophies. The essential ingredient in meeting the objective involves the deployment of a number of buoys moored in various gulfs and oceans.

This paper will review the evolution of sensors, electronics, and communication hardware applicable to NDBO programs. We will also present an overview of our major programs so that buoy technology can be better appreciated in terms of the NDBO missions.

1. Background

Since June 1972, NDBO has deployed environmental reporting data buoys in various gulf and ocean regions to provide synoptic data for weather reports and for scientific data archives. As of June 1978, 18 moored buoys have been reporting environmental data on a routine basis. Accurate and reliable buoy sensors, electronics, and communications are required to properly support NDBO's mission of gathering and reporting environmental data from the marine areas of the world. The current complement of buoy electronics was determined by a series of hardware evolutions, which in turn were brought about by our continued quest for the most accurate and reliable equipment that technology could offer. The evolution of the data buoy hardware, together with the availability of microprocessor technology and suitable communication satellites, enables a fully automated and reliable approach for the acquisition of remote marine environmental data on a synoptic basis.

2. Current NDBO Programs

Moored Buoy Payloads

Three types of payloads are currently being maintained and operated by NDBO: the Prototype Environmental Buoy (PEB), and the Phase I and Phase II payloads. Of the 18 deployed systems previously mentioned, 9 are PEBs, 4 are Phase I, and 5 are Phase II Payloads. In addition, development has been completed on a low-cost Continental Shelf Buoy Payload (CSBP) based on advanced technology. Figure 1 shows the current NDBO deployment locations.

A major requirement is the continuous acquisition and telemetry of near-real-time synoptic environmental data to the weather forecasting community, including the National Weather Service (NWS). These data, along with other environmental data, are used for engineering evaluation and analysis and for the generation of monthly inputs to the National Oceanographic Data Center (NODC) and the National Climatic Center (NCC) for archival purposes.

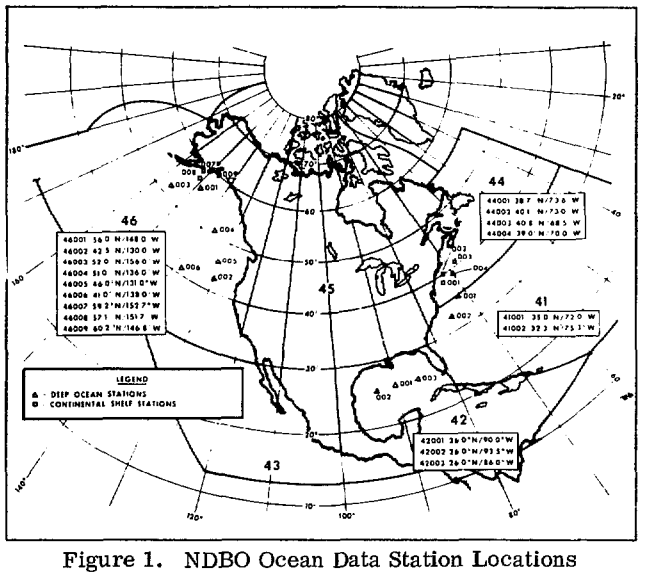

Figure 1. NDBO Ocean Data Station Locations

Prototype Environmental Buoy (PEB) Payload. The Prototype Environmental Buoy (PEB) design was based on concepts proven during initial NDBO programs. Although initially tailored to meet the needs of the weather community, its measurement capability was expanded to encompass surface wave data and subsurface water temperatures down to 300 meters.

Figures 2 and 3 show 10 and 12-meter diameter hulls, respectively. Both types of hull support PEB payloads. Meteorological sensors are located at the 10-meter level. Measured values are telemetered via radio link to shore every 3 hours in a self-initiated, internally programmed mode. For special needs, e.g., during abnormal weather disturbances, the on-board weather data acquisition and reporting can be changed to hourly operation by command from shore to report hourly. Present and previous data frames can also be acquired on demand via radio link. The on-board acquisition and timing is controlled by a special-purpose computer, and batteries provide the power required for up to 3 years of buoy operation. The payload is equipped with a dual HF/UHF communication system.

The redundant rf links were implemented to ensure a reliable and orderly transition from HF to UHF satellite communications. The conversion to UHF communications is occurring as quickly as overall system considerations permit, in order to derive the advantage of this more reliable mode of communications.

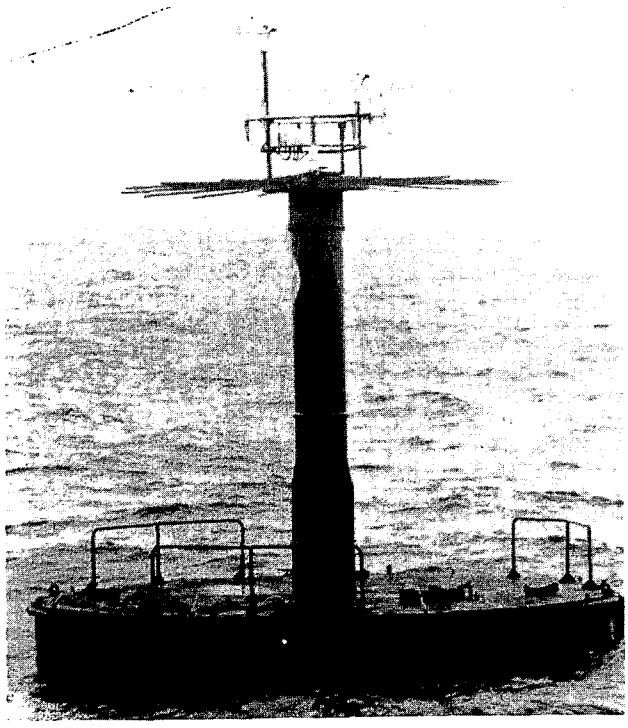

Figure 2. Ten-Meter Discus Head Buoy

PEBs are currently in service in deep ocean areas, including the Gulf of Alaska, North Pacific, and Atlantic.

Phase I and Phase II Payloads - The Phase II Payload program is an outgrowth of the Phase I Payloads for small buoy systems that were developed in the 1972-73 time period. These buoys were configured as spheres and as horizontal and vertical cylinders, with typical diameters ranging between 4-1/2 to 5-1/2 feet. None of the small buoy systems achieved significant success with regard to survivability and operability in the open sea. However, the data acquisition payloads were quite reliable.

The Phase II Payloads are second-generation payloads that evolved from the small buoy technology. These payloads are presently integrated into the 12-meter hull and into an existing intermediate size hull, NOMAD, shown in Figure 4. (The NOMAD hulls were developed in previous U. S. Navy programs.) The Phase II Payload provides meteorological environmental parameters and surface wave data. The on-board data processing and data rf link are very similar to that of the PEB payload, employing nonprogrammable hardware and both HF and UHF satellite communications. Five Phase II Payloads are in service in both deep ocean and continental shelf areas. Additional buoys are operational using the earlier Phase I Payloads.

Continental Shelf Buoy Payload (CSBP) - The CSBP is in production and became operational this summer. The overall system will draw extensively upon proven hardware and system designs. For example, the entire meteorological sensor suite will be identical

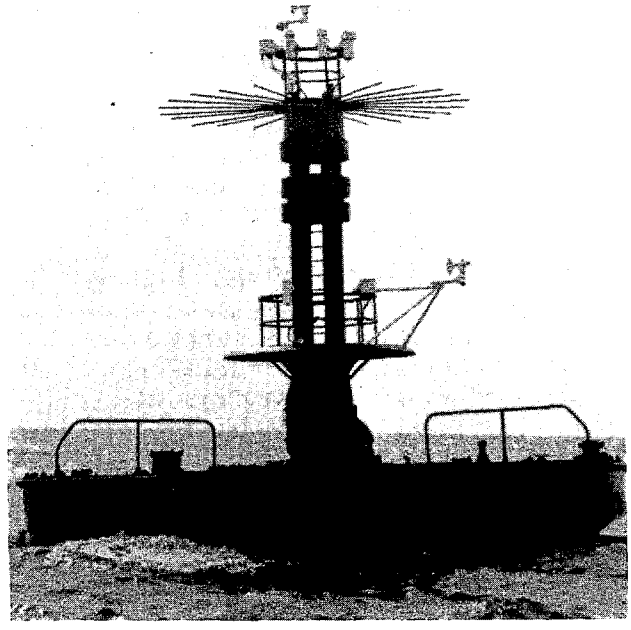

Figure 3. Twelve-Meter Discus Hull Buoy

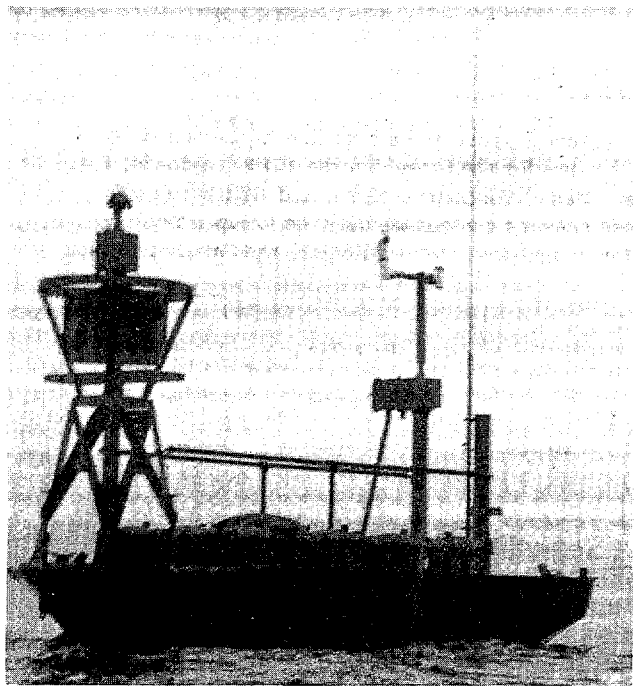

Figure 4. NOMAD Hull

to that used in the Phase II Payload. In addition, data input ports will be provided for future sensor additions, including a wave measurement system and a multi-element thermistor line. The buoy communications will consist of the UHF transmitter and associated electronics similar to that used on Phase II and PEB Payloads.

The CSBP will rely entirely on a UHF-satellite communications relay link, which will eliminate the need for the large buoy antennas required on previous NDBO HF systems. However, the CSBP will feature a program-controlled microprocessor instead of the non-programmable special-purpose computers employed on previous payloads. This element, the Intel 8080 microprocessor, will acquire sensor data and digitally process and format the data. The microprocessor also controls the reception and transmission of data via the UHF radio set. The NOMAD hull, along with other hulls of opportunity, will be used in conjunction with the CSBPs to acquire and report environmental data in various deployment areas.

Twenty-four CSBPs will be procured, with deployment starting in the latter part of 1978 in the continental shelf and deep ocean areas.

Drifting Buoys

Unlike moored buoys, whose prime purpose is the reporting of synoptic data to weather forecasting groups, drifting buoys provide information to the scientific community, usually for nonsynoptic purposes. Occasionally, there is a need for near-real-time receipt of data (e.g., the use of a buoy to track oil spills as was done in the case of the ARGO MERCHANT, which broke up on the Georges Bank just prior to New Year's Day in 1977). Generally, the drifting buoys are used for various scientific investigations, including such projects as arctic ice dynamics, Lagrangian ocean current measurements, and oceanographic and meteorological measurements at sea. These buoys are deployed worldwide.

Ice Drifting Buoys - The ice drifting buoys are capable of monitoring environmental quantities in the deep polar regions to further the understanding of the dynamics and the thermodynamic interaction between the arctic ice and its environment. These buoys are generally equipped with pressure and temperature sensors, and use a UHF orbiting satellite relay data link for telemetry and position fixing. The daily changes in position provide the measurement of ice movements needed to assess the ice dynamics. Figure 5 shows an air-deployable ice buoy.

Lagrangian Drifting Buoys - The primary purpose of this buoy is to achieve Lagrangian tracking of water parcels while simultaneously measuring basic meteorological parameters. Tracking is enhanced by the use of a drogue which couples the surface buoy to a particular water layer depth. The drogue also reduces the wind drift of buoys. The meteorological sensor suite generally measures wind speed, air temperature, and air pressure, and is located less than 2 meters above the design waterline. Communications and position fixing depend upon the operation of a UHF transmitter on the buoy

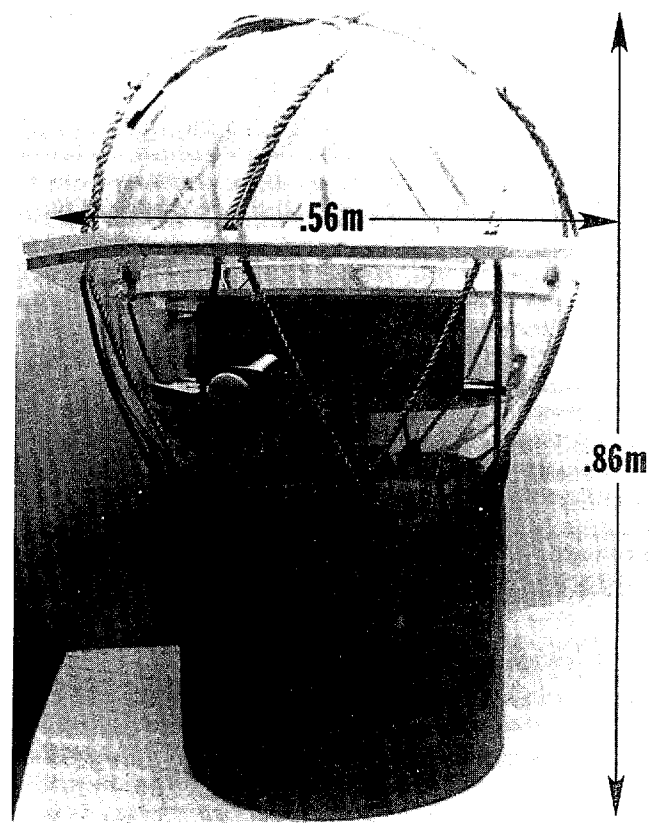

Figure 5. Air Deployable Ice Buoy

which sends data to a specialized electronics package on board a polar-orbiting satellite. The satellite in turn relays the data to a ground station. Relative motion between the satellite and buoy produces a Doppler effect on the frequency of the rf link. This frequency shift is processed along with certain satellite orbital parameters to derive buoy position.

FGGE Participation - NDBO will participate in the First GARP Global Experiment (FGGE) scheduled from June 1 through June 30, 1979. We have developed a TIROS Meteorological Drifting (TMD) buoy for the FGGE application.

The TMD buoy is small, free-drifting buoy capable of measuring barometric pressure and sea-surface temperature in the open-ocean environment. The buoy also monitors its internal temperature and battery voltage. In operational use during the Global Weather Experiment, the TMDs will acquire data on a periodic basis and transmit via a UHF radio frequency up-link to the TIROS-N and NOAA-A polar-orbiting satellites, which are scheduled for launch during 1978.

Figure 6 shows the design configuration of the TMD buoy. The mechanical characteristics are as follows:

Overall Length	10 feet (3.05 m)
Maximum Diameter	27 inches (68.6 cm)
Spar Diameter	8 inches (20.3 cm)
Deployed Weight	204 pounds (92.7 kg)
Total Buoyancy	503 pounds (228.6 kg)

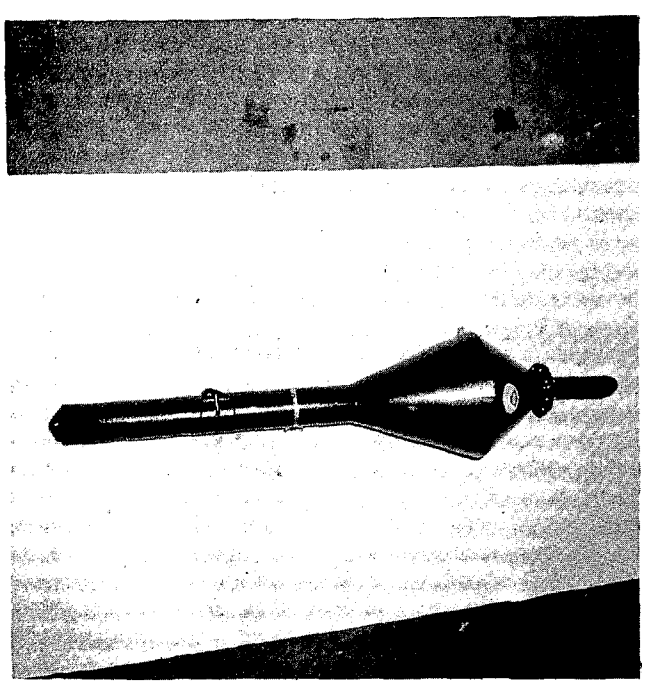

Figure 6. TIROS Meteorological Drifting Buoy

3. Evolution of Hardware

Sensors

Figure 7 presents an overview of the sensor requirements for the three diverse NDBO payloads, i.e., Deep Ocean, Continental Shelf, and Drifting Buoys. These sensors can conveniently be grouped into two major categories: Meteorological and Oceanographic.

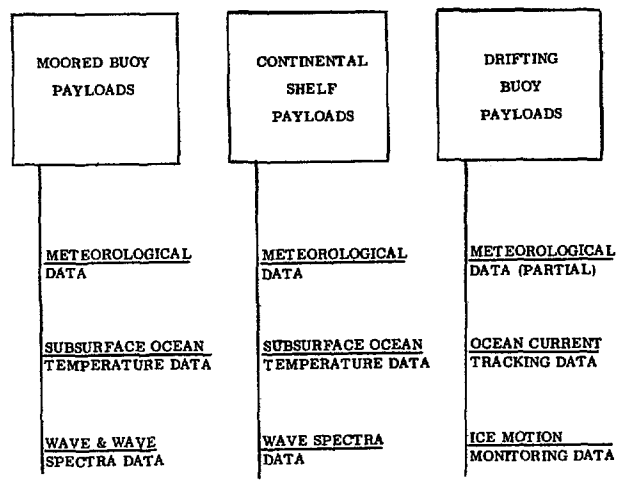

Figure 7. Sensor Requirements Vs. Buoy Payloads

Meteorological Sensors - The meteorological parameters presently measured by the buoys include wind speed and direction, atmospheric pressure, and air temperature. The initial design for wind speed and direction sensors consisted of a vortex-shedding anemometer and a wind vane integral with the anemometer. This device had a fluxgate magnetic compass within the base of the anemometer and provided a direct readout of wind direction with respect to magnetic North. A subsequent configuration consisted of a propeller anemometer and a wind vane integral with the anemometer. This design features an external magnetic compass, and requires an additional stage of wind direction resolution (i.e., from wind direction with respect to the buoy to wind direction with respect to North). Both systems are currently installed on operational buoys.

Air pressure transducers of the variable-capacitance type have been used exclusively by NDBO to measure atmospheric pressure. The pressure-actuated member in these barometers is a diaphragm that deflects in accordance with the applied air pressure. This very small movement causes a change in the capacitance of the sensing capacitor. Although the basic system has remained the same throughout NDBO's various programs, the atmospheric pressure sensors have been improved to provide enhanced long-term stability and less sensitivity to temperature and vibration. These improvements have been brought about by the utilization of more advanced mechanical and electronic

elements and a packaging reconfiguration that isolated the pressure capsule from the transducer electronics.

Both platinum wire elements and thermolinear thermistor elements have been used by NDBO to sense air temperatures. Perhaps the major change for both the platinum and thermistor assemblies has been an improvement in shielding techniques used to reduce the effect of incident and reflected solar and infrared radiation. In addition, wherein previous units were power or fan aspirated, the newer designs are naturally wind aspirated. The air temperature transducer on some buoys is packaged integrally with the wind sensor packages. A separate wind-vaned shield arrangement is used on other buoys.

Sensors for measuring solar and infrared radiation, precipitation, and dew point were developed for the Engineering Experimental Phase (EEP) buoy systems. These sensors are not in use on the present more simplified operational buoys, but a request for these measurements has recently been made to NDBO by the National Weather Service.

The meteorological sensors are installed at the 10-meter level on the large 10- and 12-meter diameter discus hull buoys and at the 5-meter level on the NOMAD buoys. Originally, the EEP discus buoys had meteorological sensors at both the 5- and 10-meter levels, but the lower sensor platform is no longer used.

Subsurface Ocean Sensors - The development of subsurface ocean sensors was perhaps one of NDBO's most ambitious undertakings. The result of this effort was the delivery of several inductively coupled ocean sensors capable of being attached to a combination mooring line/data line. Each sensor was packaged within a cylindrical pressure housing with hemispherical end caps, and each contained individual oceanographic transducers and secondary power cells. The total package was 20-1/2 inches long and 12-1/2 inches in diameter.

In June 1975, NDBO deployed a 12-meter hull buoy in the Gulf of Mexico. In addition to the standard meteorological instrumentation, five inductively coupled ocean sensors attached to a mooring line/data line were included on this buoy. The ocean sensor packages were installed at depths of 50, 100, 200, 350, and 500 meters, to measure conductivity, temperature, pressure, and current direction. The 50- and 100-meter packages were additionally equipped with current transducers to measure current speed.

The buoy was retrieved in late January 1976. Extensive damage was noted on the mooring line/data line at the oceanographic sensor package attachment points. The extent of the damage was such that complete separation of the packages would have occurred in a matter of weeks. Also, it was found that the internal batteries of the ocean sensor packages would neither accept nor retain a charge.

In reviewing the results of this experiment, the following conclusions were drawn:

- The inductive coupling concept is a valid technique for the transmission of information.
- The NDBO-configured ocean sensor system is not operationally feasible due to its high degree of complexity.
- Reliable measurements of current speed and direction cannot be obtained from a surface-moored buoy due to motion of the mooring line and the interference of both the sensor and mooring line.

In view of the limitations associated with the ocean sensor package, NDBO sought alternative solutions. The mooring line/data line sensor package was subsequently replaced by a decoupled configuration in which a subsurface float isolated the ocean sensors from wave action. Currently, the inductively coupled upline telemetry is being replaced by acoustic links. Ocean temperature is the only parameter being measured and reported operational at this time, but developmental efforts are underway on the remaining oceanographic measurands prior to their incorporation as reporting parameters.

Follow-on systems used thermistor strings to measure water temperature. Developed directly by NDBO, the thermistor string is constructed of PVC tubing and nylon tees filled with oil. Individual wires for each thermistor run through the tubing. Breakouts for the thermistor are provided at the tees, and the thermistors are potted and screwed into the tee.

Wave and Wave Spectra Data Sensors - In the area of wave data, NDBO has experienced an orderly transition from simple systems providing only wave height and period, to microprocessor systems providing wave spectrum outputs. The first wave measurement system was essentially a buoy motion measurement device for obtaining experimental data on the severity of the environment within the buoy hull. The measurement device was enclosed in a gyro-stabilized platform from which acceleration and pitch and roll angles were derived. Problems with the stabilized platform led to a strapped-down system. This system consumed considerably less power and was quite reliable, but faltered when it came to producing high-quality data.

Although an improved version of the strapped-down system was on the drawing boards, the requirement for spectral data as well as wave height and period led to the parallel development of two other systems. One of

these systems produces spectra using time-series inputs to generate a covariance function on board a buoy microprocessor. At the shore processing site, the covariances are converted to displacement spectral density by performing the Fourier transform on the covariance function. Integration of the spectra produces the moments from which the wave height and period are calculated. This system produces data of excellent quality.

The other wave measurement system resulted from a requirement for a system that could generate coarse spectral density and reasonable wave height and period data on board a platform without a sophisticated processor. In this system, time-series inputs are derived from a strapped-down accelerometer. Twelve frequency-sensitive analog filter circuits receive the time-series inputs, after which each output is squared and smoothed. At the shore station, the data is processed with a matrix and generates a spectrum for acceleration, velocity, displacement, and estimates of the average value of the displacement spectral density in the band pass of each of the 12 analog channels.

The next area is the development of wave directional spectra. Recent demands by various government agencies for directional spectra has prompted NDBO to pursue this development vigorously. An experimental system has been developed and tested that will provide directional spectra in 15° directional increments. The experimental system calculates auto- and cross-covariances of heave acceleration and wave slope in two orthogonal directions for a number of time displacements. Similar to the routine for nondirectional spectra, these functions are transmitted to shore where the spectra are constructed via the Fourier transform. The output data is three dimensional and includes displacement spectral density, frequency, and direction.

Position-Location Sensors - Position-location sensors are required to track ocean currents, monitor ice motion, and to detect drift of moored buoys. Several approaches have been advanced and implemented to solve the overall position location problem. Initially, a hyperbolic very low frequency Omega system and a satellite position-fixing system were designed and evaluated for determining NDBO buoy position.

The Omega receiver, designed for unattended buoy operation, incorporated several features that were unavailable in general commercial units. Perhaps the most outstanding feature included an automatic synchronizer capable of tracking the shoreline transmitter time-multiplexed sequence. The buoy receives a unique side frequency to synchronize a function generator to the switching sequence of the composite Omega signal. This synchronization is usually performed manually in commercial receivers. Up to four lines of position are digitized by the on-board Omega system and retransmitted digitally to shore.

Special drift tests were conducted to determine the dynamic performance capability of the buoy-Omega system. The results showed that, in processing the digitized data on shore, the computer was unable to maintain correct Omega lane counts. This required manual manipulation of data. An rms error of 5.81 kilometers was determined.

The satellite position scheme used the Navy's Transit system, otherwise termed the Navy Navigational Satellite System (NNSS). The NNSS receiver designed for buoy installation has several important differences from standard commercial units. The two prominent features are automatic operation and low power consumption. The receiver begins a frequency search upon command and locks onto the satellite signal when the satellite rises above the horizon. The Doppler count begins at the appropriate time; at each 2-minute mark thereafter, a Doppler word is completed and loaded into memory and a new Doppler count is started. This sequence continues until the signal is lost or eight Doppler words are obtained. The buoy-NNSS system digitizes the Doppler data and transmits it to shore for processing.

Dynamic tests were performed using drifting platforms and the on-board NNSS system. Only limited ephemeris data were used, with an attendant decrease in position accuracy. In addition, uncompensated buoy motion added to the overall position accuracy error, to yield a total rms error of slightly over 4 kilometers.

The most recent development underway is a standalone NNSS buoy receiver-microprocessor. This system will be capable of extracting ephemeris data directly from the satellite, computing on-board position, and retransmitting processed position data to shore. This will eliminate the need for long-haul wireline ephemeris updates and will reduce the length of the retransmitted message, since processed rather than raw data will be transmitted.

More recently, a Buoy Transmit Terminal (BTT) was designed to operate on small data collection platforms and in concert with the NIMBUS-F satellite Random Access Measurement System (RAMS). In general, RAMS provides the capability for data collection and location determination for a large number of austere platform configurations. The BTT is particularly applicable to scientific programs requiring non-real-time reporting of low volume data from low-cost drifting buoys.

Platform position is derived from the relative motion between the platform and the satellite, which can be measured by Doppler frequency shift patterns. All measurements and processing are centrally located,

either in the satellite itself or at the earth tracking station, thereby enabling the use of relatively simple systems on the small platforms. The location accuracy for buoy applications is specified at 5 kilometer rms, which has been verified by extensive testing and deployments.

The BTT consists of two major functional subsystems: a digital logic section and a solid-state transmitter. The digital section interfaces with the sensor data, converts and formats the data into a proper transmission format, and encodes the data for PSK transmission. The transmitter portion consists of a stable oscillator circuit, a multiplier-phase shift key circuit, and a power amplifier circuit. Prominent BTT characteristics include a power output of 2.4 watts, flexible sensor input interface options, data rates of 100 bits per second, and 300 milliwatts average power. It is packaged to fit within a 4-inch pipe, 21 inches long.

A BTT has also been developed to operate with the TIROS-N and NOAA-A polar orbiters. The prominent performance characteristics are similar to the units developed to operate with NIMBUS, except for changes in bit-rate transmitter frequency and frame-message format. All BTTs developed to date for the TIROS-N will be used in FGGE and are installed in TIROS meteorological drifters. Additional TIROS-N BTTs are scheduled for drift detector application on moored buoys.

Data Processing

The electronics associated with NDBO's first buoys were developed with little experience in advanced state-of-the-art hardware design. Initially, the major requirement was that the buoys have extensive flexibility in order to perform a spectrum of engineering and data acquisition tests necessary for establishing the state of the art of buoy technology. Initially designed to meet what now appears to have been unrealistic data buoy requirements, these complex payloads were expensive and not very reliable. By eliminating some of the excessive processing associated with flexibility and options, and by setting more realistic data accuracy requirements, the cost of the second-generation payloads was about one-third the cost associated with the initial NDBO payloads. In addition, reliability was enhanced by the reduction in system complexity.

The initial buoy payloads had data processing systems constructed around a general purpose minicomputer (NOVA), which acted as a controller and data processor for the overall operation of the entire buoy including sensors, communications, and power systems. However, general data processors of the off-the-shelf variety used in buoy payloads have not performed well. Also, the minicomputers were relatively high average power devices. Some improvement was experienced by the incorporation of permanently programmed read-only memories to correct either programming errors in the digital computer or memory failure or both.

Second-generation systems have had buoy data processors specifically designed for buoys. By simplifying and incorporating data processors of the non-programmable "hard-wired" type, relatively fail-safe systems have been achieved. Greater simplicity has been achieved along with significant reduction in power consumption.

Current and future NDBO payloads will rely on programmable microprocessors for the ultimate in reliability, without the need to set excessive limits for on-board processing.

Communications

There are two general categories of communication requirements for NDBO programs. The first requirement is brought about by the timeliness feature that is required for various weather forecasting groups, including the National Weather Service (NWS). The NDBO weather message is approximately 10 seconds long when transmitted at a 75 bit per second rate, and includes air pressure and temperature, wind speed and direction, sea surface temperature, and wave data. NDBO buoys are deployed in the Atlantic Ocean, Gulf of Mexico, North Pacific, and Gulf of Alaska. These diverse geographic locations require over-the-horizon data links.

The second category of communication requirements is governed by the needs of the scientific community. These applications generally do not require the timeliness feature of the first type, although processed data occasionally is desired in a matter of hours. An important example of user applications would be oceanographers, who have for many years mapped ocean currents through Lagrangian tracking techniques. These oceanographers are interested in obtaining position fixes from drifters that follow ocean currents. The length of the position-fixing message is about 1 second. Another example of scientific users would be investigators concerned with wave data. Fleet Numerical Weather Central (FNWC) currently utilizes NDBO's wave spectral data from moored buoys as calibration points for their formulation of prediction models used to forecast sea states for the entire northern hemisphere. Work is underway to extend the wave measuring capability to drifting buoys. The length of the spectral wave data is approximately 40 seconds. There are other important applications of buoys for scientific uses, including oil spill tracking and the First Worldwide Global Weather Experiment.

The approaches applicable to the NDBO communication requirements are limited because of link range distances, buoy size and power limitations, available frequencies, and the availability of cooperative satellites. The buoy-to-shore ranges are generally beyond the line

of sight. Discounting techniques such as meteor-burst systems and tropospheric scatter, the fulfillment of the over-the-horizon link requirements quickly reduces to either conventional HF or satellite communications.

High Frequency (HF) versus Satellite Communications

HF communication is a mature technology that has been extensively applied in long-range buoy communications. This technology is the mainstay of long-range military, government, international, and amateur operations. However, when theoretically compared to satellite communications, HF has decided disadvantages. Since HF wavelengths are an order of magnitude longer than applicable UHF wavelengths, larger antennas are required for HF. Long-range HF paths are based upon real-time ionospheric support conditions and require optimum frequencies for specific ranges. A reliable HF system entails working in multiple frequency bands to account for the dynamic diurnal/seasonal variations of the ionosphere. Overall, the dependence of HF communications upon good ionospheric support for each buoy-to-shore path establishes an approximate year-round 95-percent upper limit for basic communication reliability.

Satellite communications, employing frequencies above 400 MHz, propagate through the ionosphere and are generally not subject to ionospheric effects. Once established, the satellite link can operate over a dedicated channel. Since satellite communications utilize frequencies possessing one-tenth the length of corresponding HF communications, the antennas can be built to one-tenth the length of corresponding HF antenna elements. The single-band operations at UHF enables these antennas to be naturally tuned, and eliminates the need for frequency-matching networks. This eliminates a mode of failure and also reduces power requirements. Finally, a single ground station can adequately support a synchronous satellite over an earth quadrant, whereas a network of shore stations is required for reliable HF communications support for the same area.

These comparisons were a convincing argument for choosing satellite communications, and formed the basis for NDBO's quest for satellites and associated spectrum resources.

Communications Hardware

HF - The hardware currently used in NDBO buoys belongs to a set of configurations derived by hardware evolution. All configurations are capable of multiple-frequency operation, generally employing three and occasionally four frequencies to obtain optimum frequency utilization for the prevailing ionospheric condition. The configurations use common transmitters and receivers, in conjunction with dynamic switching, to achieve multiple-frequency operation. The first-generation system employed three independent and separate elements throughout the system, including three separate power amplifiers, antenna couplers, and receivers for each frequency of operation. The second-generation systems used common elements coupled with dynamic switching. One-hundred watt amplifiers are employed almost exclusively on all NDBO platforms using HF communications.

The HF antennas are basically variations of vertically polarized dipoles. Where existing masts can be utilized as efficient radiators, they are used as antennas in a disc-stub configuration. Figures 2 and 3 show a model of such an arrangement. On platforms where no suitable masts exist, a vertical whip approximately 21 feet long is used.

UHF - The first-generation NDBO/Geostationary Operational Environmental Satellite (GOES) unit was derived from a land-based design used to provide the communication interface between a remote land-based platform and the geostationary spacecraft. The land-based design was developed from preliminary design tradeoffs with emphasis placed on modulation, modulation rate, and frequency band of operation. The results of this study indicated that the most productive link operation would be from 400 to 500 MHz; and that, with regard to the modulation scheme, differential Phase Shift Keying (PSK) would be moderately superior over other schemes possessing similar cost and complexity of technique. To facilitate timing and to take advantage of the spacecraft's ultra-stable Cesium frequency standard, the earth station unit was designed to track spacecraft signals continuously, thus providing a precise clock reference. The earth station unit can be adapted to receive an entire matrix of commands sent from the GOES spacecraft.

NDBO modified an existing earth station unit to adapt it to buoy use. The major modifications included an increase in output power to compensate for loss of pointed antenna gain, the incorporation of an automatic search and acquisition demodulator, the incorporation of a self-timed-only mode of operation, DC power conversion, and an appropriate mechanical redesign for ocean environment suitability.

HF versus UHF Satellite Performance Comparisons

The subject of HF versus UHF performance comparisons is extensively treated in references 1 and 2. Suffice it to say that, when properly designed and implemented, both HF and UHF can achieve composite link reliabilities in excess of 95%. However, UHF satellite communications does provide a clear advantage over HF. The following is a capsule summary of the comparisons:

- When HF ionospheric conditions are favorable, and for links below the 3000-kilometer range, HF and UHF performances are comparable.

- When HF ionospheric conditions are unfavorable, and for multiple-hop links in excess of 3000-kilometers, UHF performance is superior to that of HF perhaps by a factor as much as 2 to 1.

- UHF link reliability is not affected by message lengths. Under good ionospheric conditions, HF can handle both long, i.e., greater than 30 seconds, and short messages with relative ease. However, as the HF link becomes marginal, reliability of the longer messages decreases considerably.

Evaluation of Performance

Up to this point, we have addressed hardware and system evaluation in our quest for enhanced performance. Actual performance, as measured by system Mean Time Between Failures (MTBF), amount of data acquired and disseminated, and the associated quality of that data have all shown a respectable improvement.

Buoy MTBF

During the 3-year period beginning in July 1972 and ending July 1975, an average of four moored buoys were on station at any one time. During that time period, the composite buoy MTBF was 36 days, calendar 1976 was a transitional year. During calendar year 1977, an average of 15 buoys were on station and the composite buoy MTBF was 150 days.

Quantity of Acquired and Disseminated Data

Between 1972 and 1975, an average of 2200 synoptic weather messages per buoy per year were acquired and delivered to the user community. During 1977, an average of 2550 synoptic weather messages were similarly acquired and disseminated by NDBO moored buoys. In addition to weather messages, a total of approximately 22,000 wave spectra and 8,000 bathymetric reports were acquired and disseminated by our buoys during 1977.

Data Quality

The accuracy of our disseminated data has improved steadily since program inception. Our present buoy requirements are shown on Figure 8. Also shown is our initial buoy quality compared to our present quality performance. By evaluating our on-board buoy systems, we have succeeded in achieving better than one order of magnitude improvement in air temperature and wind speed and better than a two-fold improvement in barometric pressure and wind direction.

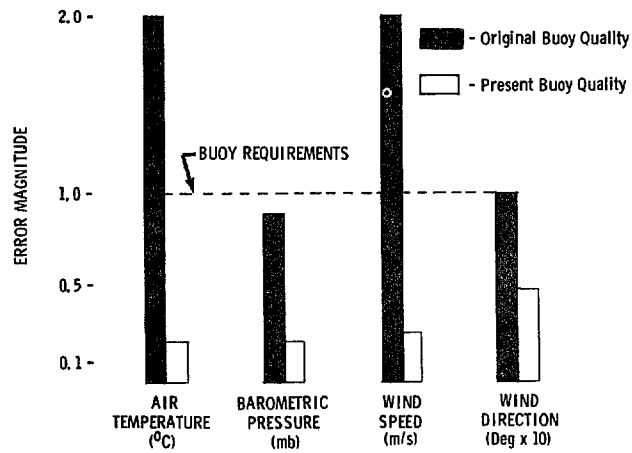

Figure 8. Evolution of Buoy Quality.

4. Conclusion

We believe our successful approach to changing technology and changing requirements has been accomplished by logical and effective evolution of our buoy electronics. It is our goal to further evolve our electronic systems to provide the most productive and reliable vehicle for meeting the needs of our users and potential users.

References

1. Haas, G., T. L. Livingston, R. P., Mueller, R. J. Roten, "Remote ocean engineering environmental data acquisition," presented at the Ocean '77 Conference.

2. Livingston, T. L., G. Haas, R. Mueller, "Data Buoy communications experiences: HF vs. UHF," presented at the 1977 RTCM Assembly.

NEW MOORING DESIGN FOR A TELEMETERING OFFSHORE OCEANOGRAPHIC BUOY

Paul D. Higley and Arthur B. Joyal

Raytheon Environmental and Oceanographic Services
P.O. Box 360, Portsmouth, R.I. 02871
Telephone 401-847-8000

Abstract

A new buoy system has been developed for the U.S. Bureau of Land Management to gather, process, and telemeter oceanographic data from the Georges Bank area of the New England outer continental shelf.

The buoy system incorporates a taut-moored subsurface sphere 6 m below mean water connected to an anchor by an instrument string using an oil-filled synthetic rubber hose as the strength member. Three main sensor packages on the string measure current speed components, magnetic reference heading, conductivity, and temperature. The bottom sensor package is connected to the anchor by an acoustic release.

The anchor consists of a 4500 kg free-flooding storage battery which supplies power to the system for up to four months. The air-sea interface is pierced with a 12.2 m fiberglass mast attached to the subsurface sphere. Mounted on top of the mast is the antenna for transmitting data via the GOES satellite telemetry system. Operational systems were deployed in the fall of 1977.

INTRODUCTION

In 1976, the U.S. Bureau of Land Management initiated a physical oceanographic study as part of the environmental studies program for the New England outer continental shelf. The Georges Bank region of the outer shelf had been delineated as a potential site of petroleum resources. Since a minimum of oceanographic data existed for this area a field program was initiated to obtain necessary data. This data collection program was divided into three parts; surface currents studies by aerial tracking of droques, regional hydrography studies on a series of hydrography cruises, and subsurface current studies using instrumented buoy systems.

Each of these buoy systems was to measure current speed and direction, temperature, and conductivity at three levels. In addition, temperature every 10 meters through the water column and bottom pressure were to be measured. In-situ processing was to include calculations of the salinity, the cross products of current with salinity and temperature, and 30-minute averages of all data. Data was to be stored on-board as well as telemetered to shore. These buoy systems were to be deployed year round in the heavily fished and severe environment of Georges Bank. Water depths for the buoy sites vary from 40 to 200 meters. Frequent storms, high waves, and strong tidal and storm drive currents, characteristic of Georges Bank, necessitated a stable durable mooring mechanical system design with a reliable data link through the air-sea interface. The necessity to pierce this air-sea interface through violent storms, and the need for continuous on-board processing, were two major factors governing the design of the buoy mooring system.

Sensor assemblies selected to be incorporated in these buoy systems include electromagnetic current meters, fluxgate magnetometer compasses, inductive conductivity probes, thermistor temperature probes, and quartz crystal pressure gauges. A microprocessor located within the buoy samples the sensor and controls the magnetic tape data loggers. The telemetry system utilizes the Geostationary Operational Environmental Satellite (GOES). (For description of the instrumentation on this buoy system refer to Real Time Oceanographic Data from Georges Bank by R.N. Lobecker and others in the proceedings of Oceans '78.)[1]

DESIGN CRITERIA

Several platforms have previously been designed to gather oceanographic data from the continental shelf. However, efforts to combine these platforms with a telemetry link to shore have resulted in cumbersome, expensive, or unreliable systems. A new approach to the buoy design was needed to provide a long-life data link through the air-sea interface which could withstand the rigors of the Georges Bank area.

The environmental criteria to be met in the buoy mooring design are called out below:[2, 3, 4, 5]

1. Water depths to vary from 40 to 200 meters.
2. Surface current speeds to range from 1 meter/second at the 40 meter stations to 0.5 meters per second at the 200 meter stations, with bottom speeds 75 percent of these values.
3. The buoy must operate in 6 meter waves and survive 12 meter waves.

4. Systems must operate in 20 m/s wind loading and survive 40 m/s wind loading.

5. System performance should not deteriorate during icing conditions.

These environmental criteria plus the need for a stable instrumentation platform, a reliable telemetry link, and long-term deployments, generate a number of demanding requirements for the buoy mooring design.

1. The data line through the air-sea interface must be secure from the excessive flexing normally encountered in buoy systems utilizing slack moors or surface following buoys.

2. The telemetry antenna must be maintained above the sea surface and must not be deflected by wind and currents such that its performance deteriorates. The antenna beam pattern selected for use with the satellite telemetry system will accommodate a deflection from the vertical of no more than 20°.

3. Sufficient buoyancy must be provided to limit system depression caused by current drag.

4. The drag form of this buoyancy must be as small as possible to limit wave induced motions and the drag form of all major components must be minimized.

5. System resonant frequencies should be out of the wave spectrum and strumming of the mooring line tension member must be minimized when exposed to significant currents.

6. A compliant elastic mooring line to survive storm induced surges loadings during extreme wave conditions is a necessity.

7. Electrical cabling should be mechanically separated from the mooring line strength member to permit energy absorbtion to eliminate detrimental effects on the cabling along with isolating strumming motions from the cabling.

8. Electrical cabling must be protected from sea water intrusion by a double seal.

9. Above water components must resist ice build up.

10. Corrosion protection must be sufficient to prevent deterioration of the system over long-term deployments.

11. Antifouling protection must be sufficient for long-term deployments.

12. A secondary recovery system must be provided to minimize the possibility of loss.

13. The system must be highly visible to the substantial fishing and shipping interests known to traffic the area.

14. The system must be designed to be deployed and retrieved during adverse weather conditions without damage.

SYSTEM DESIGN

Central to the buoy system design is a taut-moored subsurface sphere, nominally 6 meters below the surface and providing a net upthrust of 1100 kg. Mounted atop this sphere is a fiberglass mast piercing the sea surface and serving as a stable platform for the telemetry antenna. The tension member between this subsurface sphere and the anchor is a polyester fiber reinforced rubber hose. This hose is oil-filled and contains electrical conductors to the instruments and the main battery in the anchor. The anchor, which also serves as the power supply, contains lead acid storage cells in an oil-filled, free flooding, steel housing. Figure 1 shows a pictorial view of the system.

The surface piercing mast concept provides a semi-rigid member with a low frontal area and a low drag coefficient. This approach minimizes the transmission of wave-induced motions to the instrument platform and provides a limited flexing conduit for the data cable through the air-sea interface to the telemetry antenna.

The use of a hose system concept satisfies many of the basic mooring design objectives. The large outside diameter produces relatively low strumming frequencies even in high currents. Resonance excursions at these strumming frequencies are prevented by the damping effect of lumped masses (sensor packages and thermistor housing) along the hose mooring line. The hose provides a limited elastic elongation to minimize storm or deployment-induced surge loading while isolating the strength member from the electrical conductors. Extra cabling is coiled into the hoses to accommodate hose stretch. The hose is oil-filled and sealed, and all cabling and connectors are potted to provide two-layer protection from sea water. Throughout the system design, redundant seals were incorporated increase reliability.

The instrument string is attached to the anchor-battery via an acoustic release and a breakaway power cable. This enables separate recovery of the anchor and minimizes the possibility of damage to instrumentation during retrieval. A separate pickup buoy moored to a bottom tether line enables recovery of the anchor-battery, as well as providing a secondary recovery system should the acoustic release fail. In addition to this pickup buoy, three marker buoys are set in the area. All four surface buoys are equipped with zenon strobe lights and radar reflectors to increase visibility to local traffic.

MAST/ANTENNA ASSEMBLY

The antenna/mast assembly provides for the following functions:

- It serves as the antenna platform
- It carries and protects the RF transmission cable
- Most importantly, it penetrates a dynamic ocean surface.

While satisfying these functions stated above, the mast design required the incorporation of the following characteristics:

- Smallest possible profile to minimize the drag effects of current
- Resistance to the long term effects of ultraviolet light
- Resistance to extremes of temperature, air and water
- Watertight
- Sufficient structural stength to withstand the bending moment induced by storm conditions
- Flexibility to crack and flake off ice buildup.

The end result was a mast design having a 14 cm outside diameter at the sphere and a 9 cm outside diameter at the antenna end and a uniform taper over the 12.2 meter mast length. (See Figure 2.) This geometry represents an extreme slenderness ratio, but does in fact satisfy the required design characteristics.

Materials employed for the mast construction consisted of fiberglass cloth and polyester resin wound around a urethane foam core. To minimize the tooling investments, the mas was fabricated in approximately equal segment lengths of 3 meters. This approach resulted in the need for these segments to be joined. A good deal of attention was directed towards developing a joint design which would give an overall greater structural strength than the adjacent mast segments. This objective was achieved by specifying a long taper on adjacent ends, and employing a epoxy/glass system which produced a chemical bond and mechanical interlock of relatively high strength.

The antenna mounting flange has a wave deflection taper to limit wave impact loading. A neoprene gasket seal is used to provide a low pressure watertight seal. The lower mast end has a 316L stainless steel welded fitting, 61 cm long and on which the fiberglass has been wrapped. This fitting serves as a means to rapidly attach the mast to the subsurface sphere and uses an "O" ring to provide a watertight seal at this interface. Central to the mast assembly is a fiberglass conduit through which the RF cable passes. The RF connectors on each end of this cable are sealed to provide a secondary seal in the event the mast seals leak. Following receipt of the mast from the fabricating vendor, each mast is structurally tested by cycling longitudinal axial loads and the application of a number of bending cycles to the designed loads. With the stainless steel end fitting, the completed mast weighs in at 118 kg.

SPHERE ASSEMBLY

The sphere, located 6 meters below the surface to avoid ocean surface dynamic effects, required certain design parameters to be considered:

- Highly reliable penetration seals
- Smallest possible diameter to reduce drag effects from currents
- Corrosion resistance
- Maximum possible net buoyancy
- Sufficient internal volume to contain the system electronics
- Capability of being launched, retrieved and deck handled under poor sea conditions without being damaged
- Should the sphere break the surface under conditions of 12.2 m waves, the sphere structure and attachment areas must have the capability to resist shocks and surges.

The resulting design is a low alloy/low carbon steel sphere weldment fabricated from spherical elements, skin thickness being 0.48 cm. A 46 cm diameter access hatch is provided to install and service the various electronic assemblies. The hatch sealing surfaces have been fabricated from 316 and 316L stainless steel. The hatch flange is welded to the sphere skin with a doubler plate (1 cm thick carbon steel) employed to uniformly redistribute the resulting hydrostatic loads and to minimize the effects of the stress concentration factors resulting from the relatively heavy flange section and light gauge sphere skin.

The net result is a sphere assembly displacing 1814 kg, having a net buoyant force of 1100 kg an air weight of approximately 544 kg.

A 2 meter rigid standpipe is welded to the bottom of the sphere to lower the pivot point to just above the top sensor package. The location of this pivot point combined with the 1100 kg net upthrust provide the righting moment necessary to maintain the mast within the required deflection from the vertical.

Corrosion protection for the sphere assembly consists of standard techniques for undersea equipments. A 316 stainless steel was selected for the unwelded components in order to provide a reasonable resistance to crevice corrosion. In order to avoid sensitizing the stainless steel components which were scheduled to see welding heat, a 316L (L for low carbon) alloy was specified, thus avoiding the formation of carbide precipitates. The carbon steel sphere skin was protected with a multilayer coating system consisting of a primer, zinc rich

layer, epoxy overcoat, and a final anti-fouling paint selected for galvanic compatibility with the alloys employed in fabrication.

Electronic assemblies mounted within the sphere include the following:

- Microprocessor
- Power Distribution Center
- Telemetry Transmitter/Receiver
- Magnetic Tape Recorder
- Three Battery Packs.

All internal assemblies were designed and tested to withstand shock and vibration induced by the rigors of small ship environments, deck handling, launching and retrieval. Figure 3 shows the instrumentation in the sphere. Also, the assemblies were designed to pass through a relatively small hatch and to be rapidly installed or removed for at-sea servicing and maintenance. Humidity control is accomplished by purging the internal volume with a dry nitrogen gas and installing dessicant. Figure 4 shows the sphere and mast ready for deployment.

SENSOR AND MOORING STRING ASSEMBLY

Each mooring string has three sensor assemblies; near the bottom, mid-depth and near the surface. Each sensor assembly measuring temperature, salinity, current speed and direction is mounted in a stainless steel cage. This cage passes mooring tensile loading across the sensor while providing a minimum of current flow disruption. The cage also provides sensor protection during deck handling, launching, and retrieval operations.

Electrical power cabling running from the anchor/power supply to the sphere and instrumentation cabling from the sphere to each sensor assembly and the remote temperature sensors is contained within the rubber hose. A light mineral oil in the hose dampens vibrations and serves to pressure equalize the hose assemblies, thus reducing the possibility and extent of a seawater leak. This oil also has good dielectric properties and further serves to protect the electrical quality of the system.

Each hose is 10 meters long and has terminations of either 316L stainless steel or 5084 aluminum. Aluminum has been used wherever possible to maximize the buoyant force available at the sphere.

The hose has a 7.6 cm outside diameter and a 0.64 cm wall. The hose is constructed with a Nitrile inner core covered by six layers of unidirectional polyester yarns. Four of these yarns are parallel to the axis of the hose and two are laid with opposing bias angles. These yarns are locked onto the metallic termination nipple by a steel wire wrapping. The entire hose has a vulcanized neoprene cover. The final hose design has an actual tested ultimate tensile strength of 8,900 kg.

Mechanical physical properties of the hose assembly were specified as follows:

- Working load—1588 kg
- Ultimate tensile load—6804 kg
- Elongation—0.5% stretch per 454 kg load
- Life expectancy—3 years minimum in operation.

In order to compensate for the hose elongation as the hose is loaded in tension, a method was developed to wind the electrical cables in a helical coil and install them into the hose. Enough extra cable is installed to prevent cable breakage up to the hose elastic limit. A stuffing tube is installed at each hose junction to limit oil migration between sections and strain relieve the cables.

A junction box is used to terminate cables and connect the hoses to the sensor cages. Interruption of the hose at the mid-depth sensor serves to halve the hose length, thus simplifying handling. To be galvanically compatible with the stainless steel sensor cages, the junction boxes have been fabricated from 316L and oil filled for the same reasons metioned for filling the hoses. Pressure-tight electrical bulkhead receptacles are provided on the junction boxes to enable mating of the neoprene molded cable assemblies which bring the cabling past the sensor assemblies. The internal side of the receptacles within the junction boxes are potted with a dielectric urethane potting compound in keeping with the system design philosophy of providing redundant seals.

Dual 1.9 cm diameter pins are employed to couple sensor cages to hose junction boxes, permitting quick shipboard assembly. Cable connectors to junction boxes are threaded to allow connections to be made rapidly. During launching and retrieval, this time is quite critical as the operations must be smooth and continuous to prevent damage to equipment, particularly in heavy seas.

This design provides excellent longevity and survivability in the dynamic ocean environment while maintaining a minimum weight, maximum corrosion resistance, ease of fabrication, and good deck handling characteristics.

ANCHOR/POWER SUPPLY

This assembly serves the dual function of providing electrical power to the system for an uninterrupted period of up to four months as well as serving as the anchor. The anchor-battery consists of two sections of two volt cells. One section provides ±26 volts and the other ±12 volts. The cell used is a photovoltaic stationary cell designed for long-term slow discharge at cold temperatures. This lead-acid cell uses a lead calcium alloy to limit battery gassing and provide a low self discharge. Cell capacity limitation is acid starvation in this application so a 1.300 specific gravity electrolyte is used to increase available power. A glass fiber is wrapped on the plates to improve cell life at this high

specific gravity. Each cell provides 1100 A-hr. at a 2000 hour discharge rate. The 38 series-wired cells are completely filled with electrolyte, capped with a de-entrainment device, and vented to the top of the battery case via a plastic tube. These cells are mounted in the circular steel case pictured in Figure 5. In air weight is less than 4400 kg. while in-water weight is 2585 kg.

As the assembly is lowered, seawater is allowed to enter a built-in compartment to compensate for trapped gas and temperature volumetric changes. Once on the bottom, battery outgassing results in some of this sea water being forced out. Upon raising the unit from the bottom, the trapped gas expands and the remaining seawater is expelled. If the cells have undergone severe deep discharge and excessive gassing occurs, some oil is forced out. The amount of lost oil is limited by internal ducting so that the trapped gas itself is vented. This insures that the battery posts and wiring continue to be protected in oil. For servicing, means were provided to pump out any remaining entrapped sea water and replace it with oil.

The design allows for continuous operation at a tilt angle of 45°, should the container come to rest on an uneven bottom and short-term angular tilts in excess of 90° to allow for handling and retrieval dynamics. Evidence has been observed that during retrieval sufficient drag is produced to, in fact, tilt the container 90°. The container structure is fabricated from a low alloy, low carbon steel protected against seawater and acid corrosion by a multi-coat epoxy system.

ACOUSTIC RELEASE-FLOTATION ASSEMBLY

The instrumented sensor string and hose assemblies are connected to the anchor/power supply via an acoustic release system. During retrieval, activation of the acoustic release results in separation of the sensor hose assembly from the anchor-power supply. A breakaway power cable connector is used to allow electrical separation. Flotation chambers affixed to the acoustic release bring the bottom end to the surface for simplified retrieval of the instrument string. Additional flotation chambers are attached along the string, where necessary, to compensate for the additional weight, and aid in handling during deployment and retrieval operations.

STATIC AND DYNAMIC ANALYSES

A series of static analyses were performed to optimize the instrumented buoy mooring design.[6, 7, 8] The critical parameters of interest included instrument package tilt, hose tension, system depression, horizontal displacement, and antenna angle. Current speeds up to 1.25 m/s and winds up to 40 m/s were inputs to the analyses, as well as hose elasticity, drag coefficients, and system weights and dimensions.

The results of these analyses predicted sensor package tilts ranging from 3° to 7°, hose tensions ranging from 860 to 1100 kg., and buoy depressions ranging from 0.3 to 1.2 meters. A most critical result of this analysis was the forecast of the antenna angular deflection. The antenna beam pattern is omni-directional in the horizontal plane with a 40°-wide beam centered 40° above the horizontal in the vertical plane.

This accommodates a satellite elevation of 40° above the horizon. As a result, the antenna must be held within 20° of the vertical to maintain telemetry communications. The output of the static analysis, combined with the mast flex angle analysis, yields a worst case antenna angle of 18° at the 40-meter station during exposure to 1 m/s currents and 40 m/s winds.

Two types of dynamic models were employed to investigate the response of the instrument mooring system to a matrix of environmental conditions.[9] These models were exercised with various station depths, current profiles and wave spectra. Basic mooring design parameters were varied to optimize buoy mooring design. The first model simulates the torsional characteristics of the mooring system to investigate possible errors induced in current vector calculations due to buoy rotation. The second model investigates heave, surge, and pitch. Both models utilize a finite-element, lumped parameter approach to yield a set of coupled non-linear second order ordinary differential equations. Numerical integration is employed to solve these equation sets for motion response. Forces considered include: hose tension, hydrodynamic drag, inertia, virtual inertia, buoyancy, and weight with dynamic excitation from current and wave effects. Wind drag was inserted as a static input. Current was assumed as a constant for each case and wave conditions inputted as either a regular or an irregular sea. Sea states were inputs as an empirical wave energy spectrum based on the Pierson-Moskowitz model.[10] All wave motion amplitudes were assumed to decay exponentially with depth.

Torsional modeling predicted small mooring displacements with resonant periods varying from 50 to 157 seconds. Heave/surge-pitch modeling predicted no problem motions with the exception of the 40-meter depth station in the regular period survival sea conditions. In this case, hose tensions reached 4500 kg (50% of ultimate strength) and could approach a slack condition. Various inputs were changed and the model rerun. Optimization of this design involved a reduction of the net upthrust of the subsurface sphere to "soften" the buoy response. The modification reduced hose tensions to 2300 kg. and the slack conditions was eliminated.

SYSTEM PERFORMANCE REVIEW

Design of the buoy system was initiated in September 1976, and a prototype mooring was deployed on Nantucket Shoals in March 1977. A full-instrumented engineering model successfully operated off Block Island in September 1977. One buoy system was installed in 84 meters

of water at Georges Bank in November 1977 and retrieved after a one month deployment. A second buoy system was deployed in 84 meters of water at a different site in December 1977 and retrieved after four months operation in April 1978. During this four month deployment, several major storms passed over the buoy site, generating significant wave heights in excess of 7.5 meters and wind speeds over 35 m/s. Following this deployment, the system was extensively inspected for wear and corrosion. Critical wear points, such as the pivot below the sphere, experienced insignificant wear. There was no system deterioration evident from this 4-month deployment. At the time of this writing (June, 1978), three buoy systems are installed and operational on Georges Bank. Two of these buoys are at 84 meter depth stations and one buoy is installed at a 200 meter depth station.

ACKNOWLEDGEMENTS

The buoy systems were developed by the Raytheon Company, Oceanographic & Environmental Services, under contract AA550-CT6-53 with the U.S. Bureau of Land Management. Many individuals, not listed as authors, contributed to the development effort, among them: Robert Lobecker, Ron Franklin, Les Stroup, David Cook, Earl Lind, Gary Milano, Richard Neidich, Robert Day, and Captain Robert Hanson. Dynamic modeling was contributed to by the General Electric Re-entry and Environmental System Division. Technical monitoring of the contract for the Bureau was accomplished by Kenneth Berger and Eiji Imamura.

REFERENCES

1. Lobecker, R.N., Milano, G., Franklin, R. and Lind, E., "Real Time Oceanographic Data From Georges Bank", Proceedings Oceans 1978.

2. Beardsley, R.C. and Butman, B., "Circulation on the New England Continental Shelf; Response to Strong Winter Storm", Department of Meteorology, M.I.T. and Woods Hole Oceanographic Institute, 1974.

3. Bumpus, Dean F., "Review of the Physical Oceanography of Georges Bank", Woods Hole Oceanographic Institute, 1975.

4. Neu, H.A., "Extreme Wave Height Distribution along the Canadian Atlantic Coast", 1972. Ocean Industry.

5. Neu, H.A., "Wave Climate of the Canadian Atlantic Coast and Continental Shelf", 1970, A.O.L. Report 1971-10 December 1971, Bedford Institute.

6. McCormick, M.E. "Ocean Engineering Wave Mechanics", John Wiley and Sons, 1973.

7. Berteaux, H., Buoy Engineering, Wiley Interscience, 1976.

8. Weigel, R.L., "Oceanographic Engineering". Prentice-Hall, Inc., 1964.

9. General Electric, Re-entry and Environmental System Division, Philadelphia, PA.

10. Pierson, W.J., Jr., and Moskowitz, L., "A Proposed Spectral Form for Fully Developed Wind Seas Based on the Similarity theory of S.A. Kitaigorodskii", Journal of Geophysical Research, Vol. 69, No. 24, 1964, pp. 5181-5190.

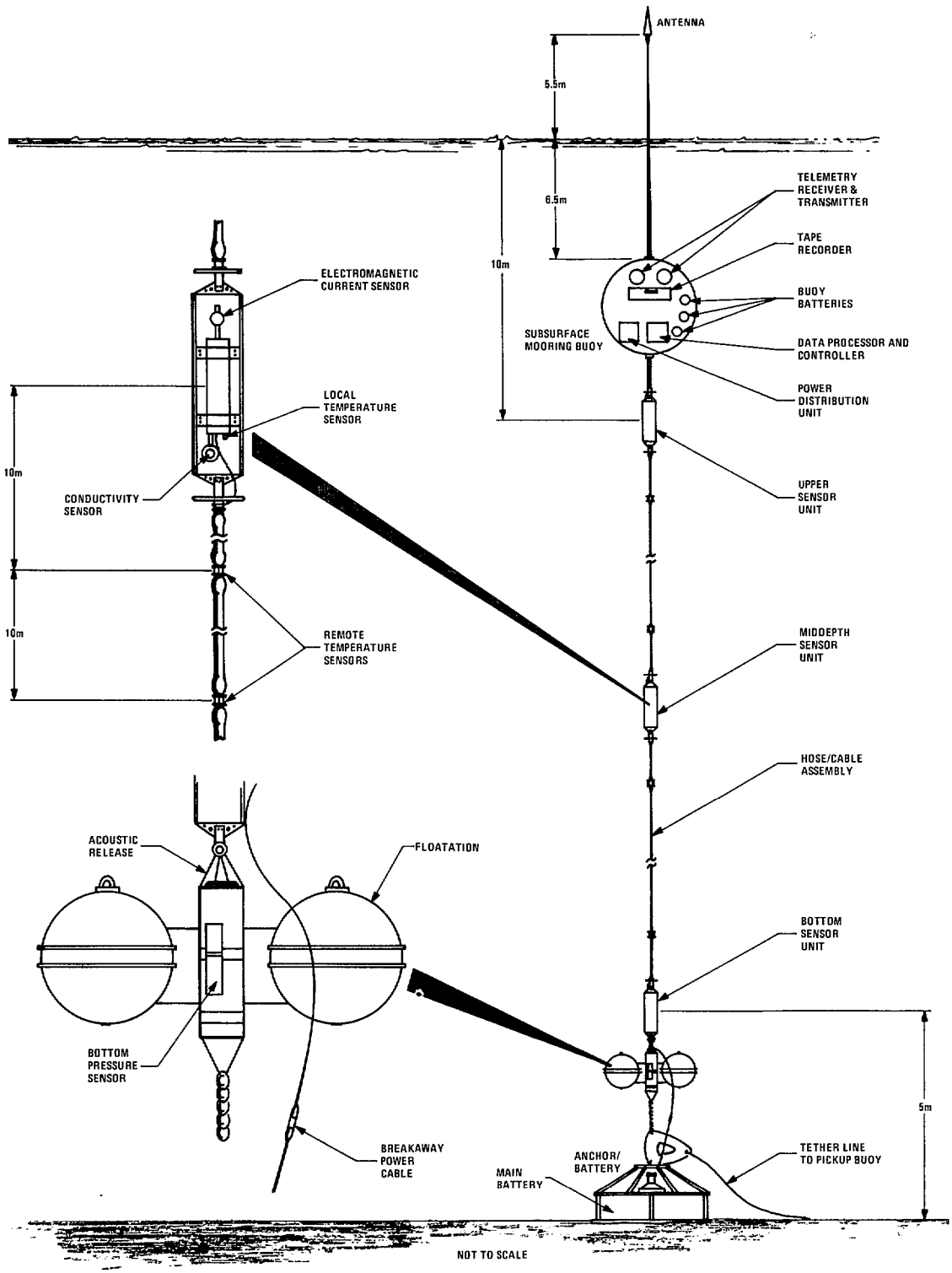

Figure 1. System Configuration

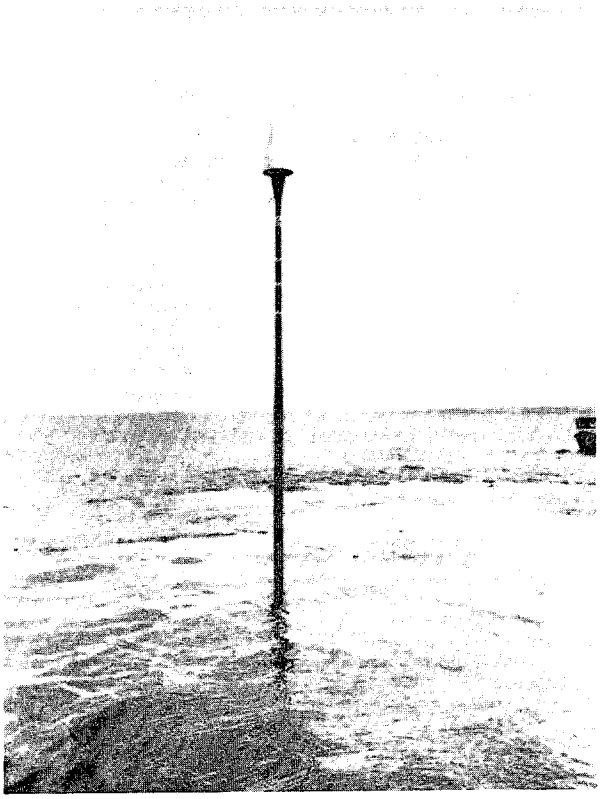

Figure 2. MAST

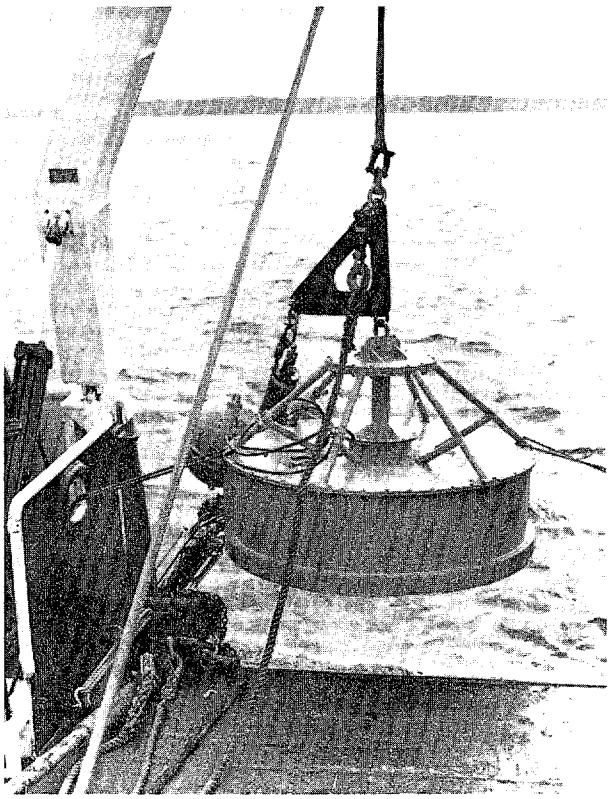

Figure 5. Anchor/Battery

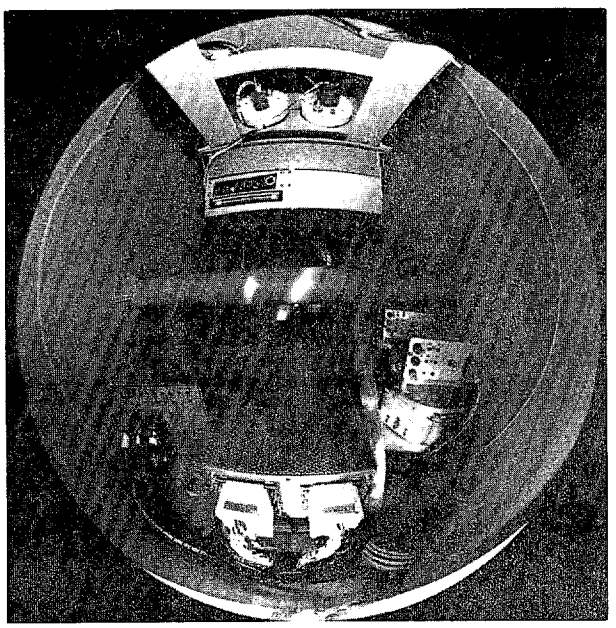

Figure 3. Sphere Electronics

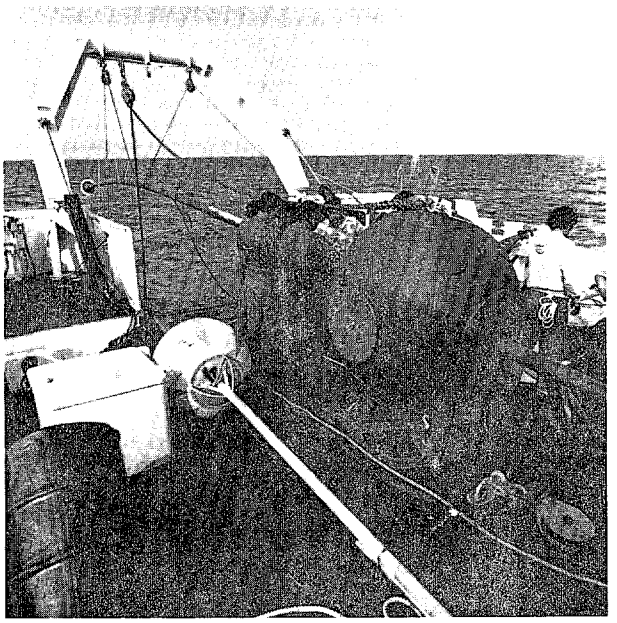

Figure 4. Sphere/MAST Deployment

A SUCCESSFUL METEOROLOGICAL DRIFTING BUOY

F.A. Reid
Senior Engineer
Hermes Electronics Limited
P.O. Box 1005
Dartmouth, Nova Scotia B2Y 4A1

Abstract

The development of a successful meteorological drifting buoy has been undertaken. Buoys which measure sea surface temperature and barometric pressure have been built, tested and successfully deployed. A description of this buoy is given, with details of the sub-systems.

1. Introduction

The development of a successful meteorological drifting buoy was started in 1976 as part of the Canadian Ocean Data System project, a contract held by Hermes Electronics Limited. The buoys were to act as free drifting platforms for the measurement of barometric pressure and sea-surface temperature. The pressure was to be measured to an accuracy of ± 1.0 millibar (mb) (including all sources of error) over the range 900 to 1050 mb. The temperature was to be measured with an accuracy of ± 0.5°C over the range -5°C to +40°C. The buoys were to use the Nimbus-RAMS system for data telemetry and position fixing. The buoy was to last 12 months in 10°C water and 6 months at 0°C.

There are a number of problem areas which had to be thoroughly investigated before a buoy which met the above specifications could be produced. The process has taken two years and has resulted in the production of approximately 100 buoys at Hermes Electronics for use in the First GARP Global Experiment (FGGE).

2. Hull

The earliest prototype hulls were constructed of a fibre reinforced plastic. The two that showed most promise were a 2.0m spar and a 1.6m modified spar, as shown in Figure #1. Several tests including full size tank tests, launch and mooring tests were conconducted with these buoys. The results indicated that, while both types would suit the requirement, the spar was only marginally stable for good communication and the modified spar would be too expensive to produce.

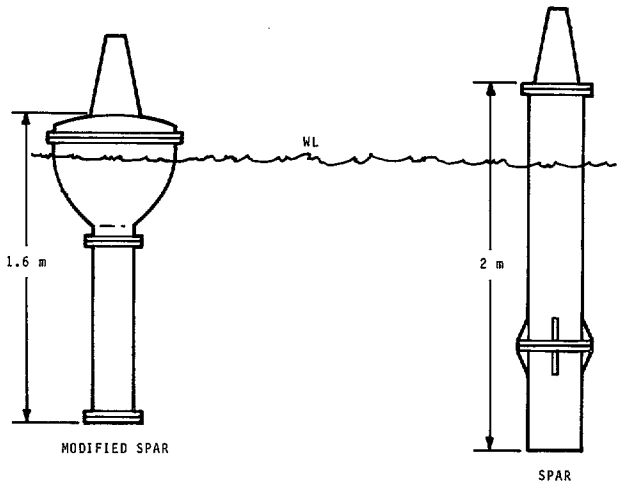

Figure #1. Prototype Hulls

A truncated cone hull shape has characteristics which the above tests proved desirable. The hull material was changed to aluminum for ease of construction, strength and cost considerations. This hull has been tested extensively and has become the basis of several drifting buoy configurations.

As the hull is now made of aluminum, a radio transparent cover must be provided for the antenna. This cover must be extremely robust as it must withstand high impact loading during handling and launch. The antenna cover is constructed of RFP and seals to the aluminum hull via a flat seal above the water line. The antenna cover also forms an integral part of the barometric pressure inlet port which is described below.

3. Electrical System

The electrical system of the drifting buoy has four parts, namely: Battery and switch; Sensors; Data formatter and transmitter; Antenna.

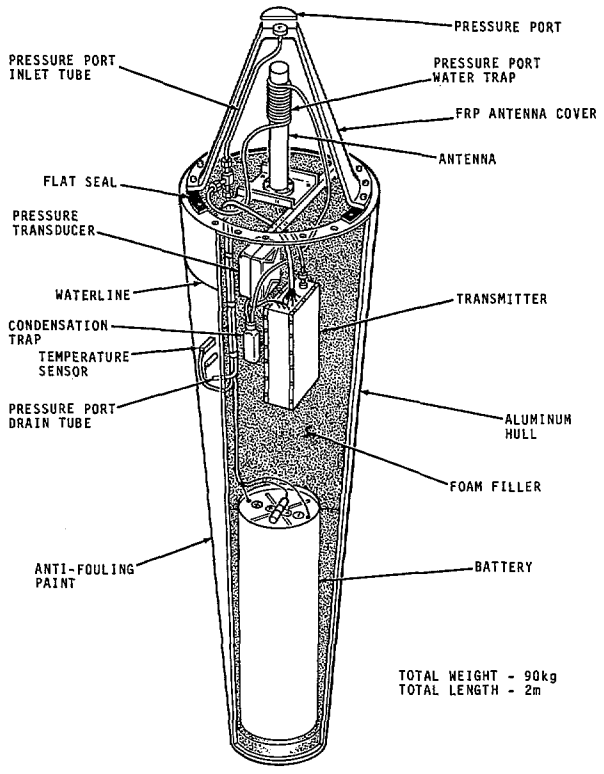

Figure #2. Drifting Buoy

The battery chosen for the drifting buoy was an alkaline dry-cell system with a nominal voltage of 13V and a capacity of 160 Ah. This system was chosen because of its energy-density, low temperature performance and its wide availability. The battery capacity is sufficient to operate the buoys for 1 year at 10°C and 6 months at 0°C. Field tests have shown that the present design meets these requirements.

The switch used for the power supply is magnetically operated, and does not require the integrity of the hull to be broken for actuation. The switch is normally closed and is held open when the magnet is placed in close proximity to it. This allows the buoy to be launched without the necessity of opening the hull to switch on; and more importantly, if the magnet is retained by the packing crate, the buoy cannot be launched in the off state.

The temperature sensor used on the drifting buoy is bonded to the inside of the aluminum hull just below the water line. This allows the measurement of the sea-surface temperature without the problems of sealing the sensor against the sea for one year. The sensor itself, is a linearized thermistor configured in a bridge to give a linear voltage versus temperature characteristic.

The pressure sensor is a Paroscientific Digiquartz pressure transducer model 230A. This unit was chosen for its excellent accuracy and long term stability. The output of the transducer is a square wave with a period proportional to pressure. This output is averaged and linearized over the pressure range to give a count which is linear with pressure.

The data formatter and transmitter is manufactured by Handar. The unit accepts the input data, formats and transmits the data in a form compatible with the Nimbus-RAMS system. The units have proven to be very reliable, with over 18 months of continuous operation in the field.

4. Pressure System

The heart of the meteorological drifting buoy is the accurate measurement of barometric pressure. To make measurements to the accuracy required over 1 year on an inexpensive drifting buoy meant that several novel solutions to the problems of dynamic pressure error, water entrapment, and water vapor inflow had to be found.

The movement of air across the pressure port inlet will give rise to a dynamic pressure which adds to the static pressure and causes an error. The magnitude of this error depends on the velocity of the air and the geometry and attitude of the pressure inlet. The pressure inlet on these drifting buoys is on top of the conical antenna cover. Due to this conical section there is a low pressure area at the apex. The present inlet compensates for this low pressure by causing a dynamic pressure increase. The present port assembly has been tested extensively in the wind tunnel and has given the following results: less than 1 mb dynamic error at all speeds and attitudes up to 30 m/sec, less than 0.3 mb error at speeds of less than 20 m/sec. With the design presently in use no attempt is made to keep water from flowing through the inlet port, as significant pressure gradients could develop across any membrane structure. Instead a drain tube is provided which runs directly from the inlet to an exit below the water line. The pressure for the barometer is tapped off this drain tube, spirals upwards, into a desiccant container and then to the barometer (Figure #3). The purpose of the spiral is to provide a suitable volume of trapped air to allow the buoy to submerge to a depth of 10 metres, without any water reaching the top of the spiral.

The desiccant container is used as a dryer to remove any water vapour present in the system.

5. Testing

The first 30 buoys produced utilizing this design have been the object of extensive testing during the last 18 months.

Twenty of the buoys were deployed in the Atlantic, Pacific, and Indian Oceans. Figure #4 gives a map of their deployments and drifts. Of the twenty buoys only four have had premature electrical or mechanical failure and two have lasted in excess of 18 months. It is very difficult to measure the data quality from the field test buoys but in those instances where a suitable reference existed the data quality was to specifi-

cation.

Further studies were conducted in controlled situations to study the affects of fouling on the buoys and pressure system. The results indicated that there should be no significant fouling of the buoys anywhere in the world's open oceans.

As a design goal the buoys were to be capable of being launched from any type of ship, by an untrained crew without means of a crane or with the ship stopping. To verify this, buoys were dropped from a height of 20m into the water, both horizontally and vertically without damage. The packing crate was designed such that the magnet is retained with the crate when the buoy is unpacked.

A rigourous suite of environmental tests were undertaken to bring to light possible failure modes. No major faults were discovered but a numer of minor modifications were incorporated as a result of these tests.

6. Conclusions

A drifting buoy which meets the design goals set out for has been built and extensively tested. The present design has been used as the basis for the Canadian drifting buoy contribution to FGGE. In addition, in excess of 50 drifting buoys of slightly different configuration but of the same general design have been supplied to various users in the last 12 months.

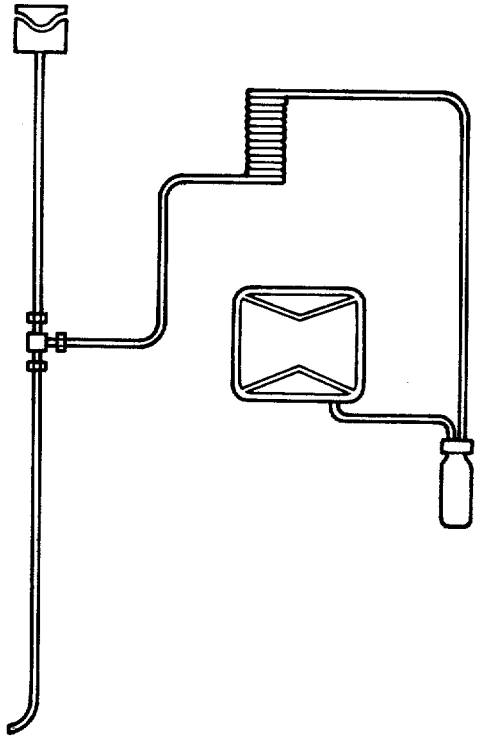

Figure #3. Pressure System

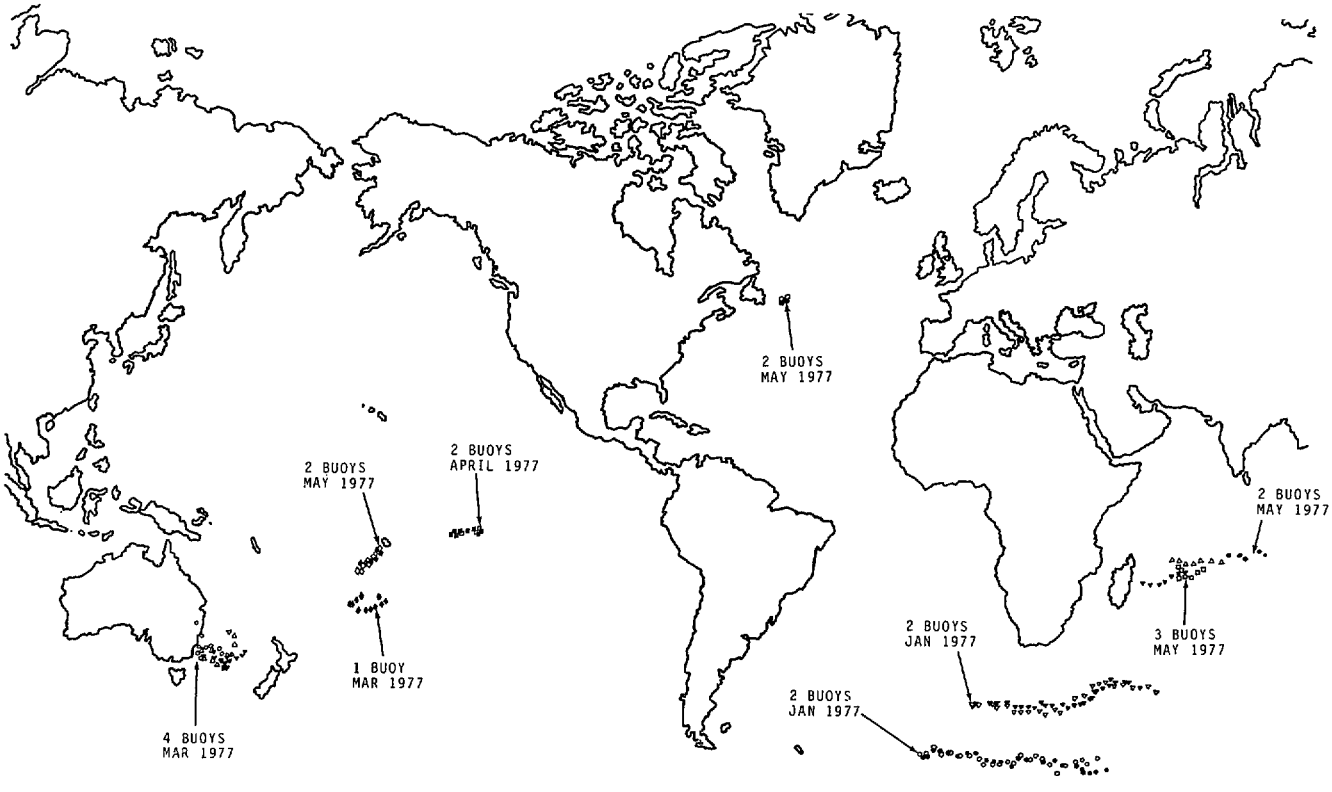

Figure #4. Drifting Buoy Deployments

Acknowledgements

The development of these drifting buoys was undertaken as part of the Canadian Ocean Data System contract # OSZ5-0106 under the supervision of John Brooke. The author would especially like to acknowledge the guidance given by Dr. Jim Elliot, Bedford Institute of Oceanography and Dr. John Garrett, Institute of Ocean Sciences, throughout the entire project.

AN ANALOG WAVE SPECTRUM ANALYZER SYSTEM FOR OPERATIONAL BUOYS

K. E. Steele
NOAA Data Buoy Office
National Space Technology Laboratories
NSTL Station, Mississippi 39529

Dr. A. S. Hananel
Sperry Support Services
National Space Technology Laboratories
NSTL Station, Mississippi 39529

Abstract

In 1975, the NOAA Data Buoy Office (NDBO) began deploying a data acquisition system identified as the Prototype Environmental Buoy (PEB) payload on their operational buoys. This payload could report environmental data from remote ocean areas to shore through radio telemetry, but could only receive data inputs in the form of analog voltages. Digital data could not be accommodated. NDBO subsequently developed a wave measurement system specially designed to interface with the PEB payload. This Wave Spectrum Analyzer (WSA) system consisted of 12 parallel analog filters, each of which produced an output voltage related to the spectral density in the vicinity of the center frequency of the filter. Duplicates of this WSA system have since been deployed on a number of operational deep-ocean buoys and have produced wave data routinely.

1. Introduction

Early in 1973, NDBO initiated an effort to develop an accurate, reliable wave measurement system capable of measuring one-dimensional wave spectra for use on operational buoys. The first step in this effort was the December 1973 deployment of an experimental system in the Atlantic to measure significant wave height and period.[1] Much was learned from this effort, but the data produced was not of good quality.[2] In December 1974, an experimental wave measurement system was deployed which was designed to produce wave spectra data every 3 hours.[3] This system demonstrated the feasibility of the routine acquisition and teletype relay of accurate near-real-time spectral wave data, but unfortunately proved to be unreliable due to a number of design problems, and was thus unsatisfactory as an operational system.

NDBO had planned to use three types of buoy data acquisition and reporting systems, or payloads. Each system needed a reliable spectral wave measurement system. One of these types, the Magnavox Phase II payload[4], was a technically advanced system with digital interfaces for the relay of data from sensor subsystems. A wave data analyzer for this system has been developed and is described elsewhere.[5]

The other two payloads had limited data acquisition capabilities. One was the Magnavox Limited Capability Buoy (LCB) type, which had a digital interface for sensor subsystems.[6] The other type was one that had already been conceived by General Dynamics for the Prototype Environmental Buoy (PEB).[7] The PEB-type payload had analog interfaces and 12 channels available in which to connect the output(s) of a wave measurement system.

NDBO sought to develop a wave measurement system that would take maximum advantage of the 12 channels of the PEB payload, yet at the same time could be used with the Magnavox LCB type. Such a system was developed, and the basic system hardware has been described in detail in another paper.[8] The system consists of 12 parallel analog bandpass filters that are fed by the voltage output of a strapped-down accelerometer as shown in Figure 1.

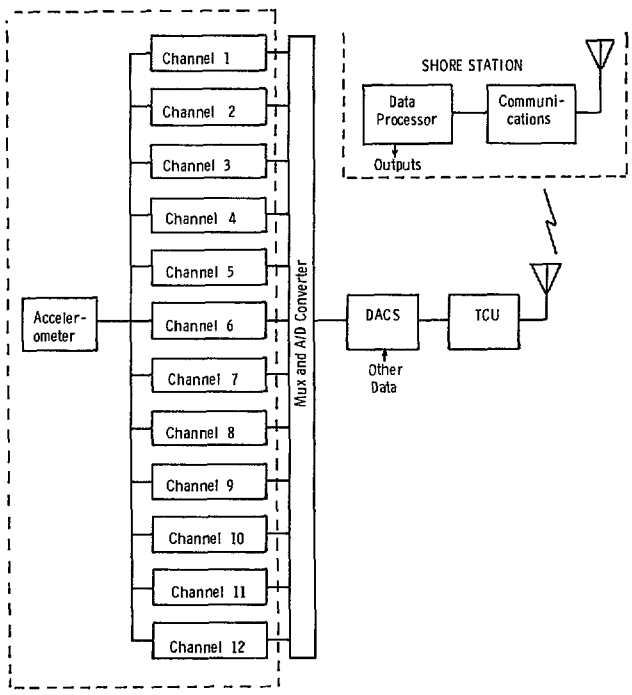

Figure 1. WSA SYSTEM SCHEMATIC

Each filter produces an output voltage dependent on the voltage spectral density of the input in the vicinity of the bandpass of the filter. It has been shown[8] that the weighting factor for the kth of K (normally 12) filters is, in volts/volt^2,

$$g_k(f) = |\overline{G}_k(jf)|^2 = \overline{\overline{g}}\,\overline{\overline{g}}\,\overline{g}_k^2 \frac{(f \cdot \Delta f_k)^2}{\frac{\pi^2}{4}(f^2 - \overline{f}_k^2)^2 + (f \cdot \Delta f_k)^2} \qquad (1)$$

where

$j = \sqrt{-1}$

$\overline{\overline{g}}$ (volts/volt) = gain of the output buffer of the filtering circuit (the same for each filtering circuit, magnitude = 2.0)

$\overline{\overline{g}}$ (volts/volt^2) = gain of the squaring circuit of the filtering circuit (the same for each filtering circuit, magnitude = 0.1)

$\overline{g}_k$(volts/volt) = gain of the kth filter, which is usually different for each filter and is determined by hardware adjustments

f (Hz) = frequency at which the weighting factor is to be computed

$\overline{f}_k$ (Hz) = center frequency of the kth filter, which is usually different for each filter and is determined by hardware adjustments

$\overline{G}_k(jf)$ = modified linear system transfer function, related to the primary system transfer function as follows:

$$\overline{G}_k(jf) = \sqrt{\overline{\overline{g}} \cdot \overline{\overline{g}}}\; G_k(jf)$$

Δf_k (Hz) = noise equivalent bandwidth of the kth filter, which is usually different for each filter and is determined by hardware adjustments

$$= \frac{1}{2\overline{g}_k^2} \int_{-\infty}^{\infty} |G(jf)|^2\, df$$

$$= 1/2 \int_{-\infty}^{\infty} \frac{(f \cdot \Delta f_k)^2}{\frac{\pi^2}{4}(f^2 - \overline{f}_k^2)^2 + (f \cdot \Delta f_k)^2}\, df.$$

Given that eq. (1) is the proper weighting function for the effect of the kth filtering circuit on the input voltage spectrum, it will be shown how the outputs of K separate and independent analog filtering circuits can be used as a system to estimate the original sea heave displacement spectrum. In Section 2, a mathematical expression for the count received at shore from the kth filter is developed. Section 3 shows how the count from a single filter can sometimes be used to estimate the spectral density at the center frequency of that filter. A method for using the set of K counts from the K filters to determine K estimates of the spectral densities at the K center frequency is presented in Section 4. Computations based on the technique of Section 4 are shown in Section 5. Section 6 presents conclusions about the performance of these systems based on operational use. Section 7 acknowledges those who helped in this effort.

2. Mathematical Analysis of the WSA

The objective of the WSA system is to estimate the sea displacement spectrum, $S^{(1)}(f)$ [m^2/Hz], which is usually zero or negligibly small below some lower frequency limit, F_1(Hz); i.e.,

$$S^{(1)}(f) \simeq 0, \qquad f < F_1 \quad . \qquad (2)$$

Estimates of $S^{(1)}(f)$ at particular frequencies are to be made through the use of a number, K, of analog bandpass filters.

The original sea spectrum of displacement, $S^{(1)}(f)$, has an associated sea velocity spectrum, $S^{(2)}(f)$ [(m/sec)^2/Hz], and a sea acceleration spectrum, $S^{(3)}(f)$[(m/sec^2)^2/Hz]. In compact form, the relationship between these three spectra can be written as

$$S^{(r)}(f) = (2\pi f)^{2(r-i)}\, S^{(i)}(f) \qquad (3)$$

where r and i take the values 1 (displacement), 2 (velocity), and 3 (acceleration).

However, the acceleration spectrum seen by the accelerometer on board the buoy, $\overline{S}^{(3)}(f)$, differs from the true sea acceleration spectrum $S^{(3)}(f)$ by the factor of the frequency-dependent hull transfer function, w(f). Thus,

$$\overline{S}^{(3)}(f) = w(f) \,.\, S^{(3)}(f) \qquad (4)$$

There may be a slight difference between the true vertical acceleration of the discus buoy hull and the buoy acceleration vector projected onto the axis of the accelerometer, which has its axis fixed parallel to the mast, but NDBO's experience with other spectral wave measurement systems has shown that $\overline{S}^{(3)}(f)$ in eq. (4) is practically the same as the spectral input to the linear single-axis accelerometer.[9]

The acceleration spectrum is converted by the accelerometer to a voltage spectrum; i.e.,

$$\bar{\bar{S}}^{(3)}(f)[\text{volt}^2/\text{Hz}] = \bar{K}^2[\text{volt}^2/(\text{m/sec}^2)^2] \cdot \bar{S}^{(3)}(f)[(\text{m/sec}^2)^2/\text{Hz}] \qquad (5)$$

where $\bar{K}$ is the slope of the accelerometer linear calibration curve.

If the input voltage to the kth filter, which has a spectral content of $\bar{\bar{S}}^{(3)}(f)$ as given by eq. (5), is identically zero, then the output of the filtering circuit should ideally be zero. Also, when the sea state is stationary with a non-zero $\bar{\bar{S}}^{(3)}(f)$, the output voltage of the filtering circuit should ideally have a steady, constant value. In the actual hardware, however, these ideal performances are not realized. There is usually an offset voltage, $\bar{E}_k$, at the output even when the input is grounded to zero. This offset voltage may be positive, zero, or negative. Thus, the actual performance of the filtering circuit is given by

$$E_k(t) = \bar{E}_k(t) + \int_0^\infty g_k(f) \cdot \bar{\bar{S}}^{(3)}(f) \cdot df \qquad (6)$$

where $g_k(f)$ is given by eq. (1), $\bar{\bar{S}}^{(3)}(f)$ is given by eq. (5), and $\bar{E}_k(t)$ is the time-dependent offset voltage of the kth filter. The time-dependent voltage $E_k(t)$ is input to the analog-to digital (A/D) converter. (See Figure 1.)

When the input to the A/D converter is grounded, the output count of the converter will be $\bar{c}$. This count depends on the type of payload to which the WSA is connected, as described in Table I. The A/D transformation for any WSA system is represented in the following equation:

$$C_{ks}\ [\text{count}] = \bar{c}\ [\text{count}] + B\ [\text{count/volt}] \cdot E_k(t_s)\ [\text{volts}] \qquad (7)$$

except that

$$C_{ks} = 0 \text{ if } \bar{c} + B \cdot E_k(t_s) < 0$$

$$C_{ks} = R \text{ if } \bar{c} + B \cdot E_k(t_s) > R$$

where

C_{ks} = count at the output of the A/D converter from filter k at the time sample number s is taken

$\bar{c}$ = count when zero voltage is input

B = sensitivity of the A/D converter

$E_k(t_s)$ = input voltage to A/D converter from filter k at time t_s

R = upper limit count of the A/D converter

t_s = time at which the sth sample is taken

s = 1, 2, ..., S = the number of samples taken during single data acquisition period

S = total number of samples taken from each filter during a data acquisition period.

Different sets of values for $\bar{c}$, B, R and S correspond to each payload type.

TABLE I. WSA INTERFACE CHARACTERISTICS FOR PEB AND LCB PAYLOADS

A/D CONVERTER CHARACTERISTICS	SYMBOL	UNITS	PAYLOAD: PEB (GENERAL DYNAMICS)	PAYLOAD: LCB (MAGNAVOX)
Min Voltage In / Count Out	— / R or 0	Volts / Count	-10 / 4096	0 / 0
Max Voltage In / Count Out	— / R or 0	Volts / Count	+10 / 0	+10 / 4096
A/D Count for Zero Voltage In (avg)	$\bar{c}$	Count	2047.5	0
A/D Sensitivity (nominal value)	B	Count / Volt	-204.8	409.6
Total Number of Samples Taken	S	Integer	4096	1
Interval Between Samples		Sec	0.125	—
Total Duration of Sampling		Sec	512	—

A number S of samples are taken from the A/D converter and averaged to produce the count sent to shore by the payload; i.e.,

$$C_k\ (\text{count}) = \frac{1}{S} \sum_{s=1}^{S} C_{ks} \quad . \qquad (8)$$

Substituting for C_{ks} from eq. (7) into eq. (8), the count sent to shore can be written as

$$C_k = \bar{c} + B \left\{ \frac{1}{S} \sum_{s=1}^{S} E_k(t_s) \right\} \quad . \qquad (9)$$

Using eq. (6), the average voltage into the A/D converter is given by

$$\frac{1}{S} \sum_{s=1}^{S} E_k(t_s) = \frac{1}{S} \sum_{s=1}^{S} \bar{E}_k(t_s) + \int_0^\infty g_k(f) \cdot \bar{\bar{S}}^{(3)}(f) \cdot df$$

or

$$e_k = \bar{e}_k + \int_0^\infty g_k(f) \cdot \bar{\bar{S}}^{(3)}(f) \cdot df \quad (10)$$

where $e_k = \frac{1}{S} \sum_{s=1}^{S} E_k(t_s)$ is the average actual voltage and

$$\bar{e}_k = \frac{1}{S} \sum_{s=1}^{S} \bar{E}_k(t_s) \quad (11)$$

is the average offset voltage coming out of the kth filter into the A/D converter.

Inserting eq. (10) into eq. (9) yields

$$C_k - (\bar{c} + B\bar{e}_k) = B \int_0^\infty g_k(f) \cdot \bar{\bar{S}}^{(3)}(f) \cdot df \ . \quad (12)$$

If $(\bar{c} + B\bar{e}_k) \geq 0$, then the definition

$$\bar{C}_k = \bar{c} + B\bar{e}_k \quad (13)$$

yields a value $\bar{C}_k$, which is the count received at shore when the accelerometer is not being subjected to any acceleration; i.e., when $\bar{\bar{S}}^{(3)}(f) \equiv 0$ for all f. Thus, $\bar{C}_k$ is measured after the buoy is integrated and is at rest at dockside reporting counts.

If $(\bar{c} + B\bar{e}_k) < 0$, as can occur in the case of the LCB payloads, then $\bar{C}_k$ cannot be measured directly and must be computed from eq. (13) with measured values of $\bar{c}$, B, and $\bar{e}_k$. Also, it must be computed when the system is installed under conditions that preclude having the buoy at rest.

C_k and $\bar{C}_k$ can now be combined into one parameter, as follows:

$$c_k = C_k - \bar{C}_k = B \int_0^\infty g_k(f) \cdot \bar{\bar{S}}^{(3)}(f) \cdot df \ . \quad (14)$$

This c_k value can be computed at shore either from the count C_k sent from the operational buoy and the count $\bar{C}_k$ determined in advance by eq. (13), or by taking direct readings. It will not be necessary to compute c_k, as will be shown.

Substituting in eq. (14) for $g_k(f)$ from eq. (1), and for $\bar{\bar{S}}^{(3)}(f)$ from eqs. (3), (4) and (5), we obtain:

$$c_k = B\, \bar{\bar{\bar{g}}}\, \bar{\bar{g}}\, \bar{K}^2\, \bar{g}_k^2 \int_{F_1}^{F_{k+1}} \frac{(f \cdot \Delta f)^2 \cdot w(f) \cdot (2\pi f)^{2(3-i)}}{\frac{\pi^2}{4}(f^2 - \bar{f}_k^2)^2 + (f \cdot \Delta f)^2} S^{(i)}(f) \cdot df \quad (15)$$

where k = 1, 2, ...,K and i = 1, 2, 3 . The limits of integration have been narrowed due to the negligibility of the product $w(f) \cdot (2\pi f)^{2(3-i)} \cdot S^{(i)}(f)$, when $f < F_1$ and $f > F_{K+1}$. F_{K+1} is that frequency above which there is no significant contribution to the integral, due to either the hull filtering or the absence of wave energy. The significance of the "K+1" subscript will be demonstrated in Section 6.

3. Narrow Band Approximations of Spectral Density

An estimate of spectral density at the center frequency of the kth filter can be made from the output count of the kth filter alone, if the kth filter is very narrow relative to the spectral variation about its central frequency $\bar{f}_k$.

If the assumption is made that the expression $w(f) \cdot (2\pi f)^{2(3-i)} \cdot S^{(i)}(f)$ in the integrand of eq. (15) is slowly varying within the range of non-negligible values of the filtering function $g_k(f)$, then eq. (15) can be approximated as

$$c_k = C_k - \bar{C}_k \simeq B \cdot \bar{\bar{\bar{g}}} \cdot \bar{\bar{g}} \cdot \bar{K}^2 \cdot \bar{g}_k^2 \cdot w(\bar{f}_k) \cdot (2\pi \bar{f}_k)^{2(3-i)} \cdot S^{(i)}(\bar{f}_k) \cdot \Delta f_k \quad (16)$$

in which the definition of the noise equivalent bandwidth given in Section 1 has been invoked. Solving eq. (16) for the spectral density,

$$S^{(i)}(\bar{f}_k) \simeq \frac{(C_k - \bar{C}_k)}{B \cdot \bar{\bar{\bar{g}}} \cdot \bar{g} \cdot \bar{K}^2 \cdot \bar{g}_k^2 \cdot w(\bar{f}_k) \cdot (2\pi \bar{f}_k)^{2(3-i)} \cdot \Delta f_k} \ . \quad (17)$$

This linear relationship between an estimated value for $S^{(i)}(\bar{f}_k)$ and the count C_k sent from the buoy to shore sometimes allows a reasonably accurate determination of spectral density at frequency $\bar{f}_k$ from the kth filter alone, without using all the K filters as a system. The validity of this determination depends on the narrowness of the filters; but making the filters extremely narrow would introduce instabilities into the filters, and would require an impractically large number of filters if no gaps were to be left in the spectrum. Therefore, it is not desirable to make the filters extremely narrow banded, and eq. (17) is only to be used occasionally for quick estimates of spectra.

4. Computation of the Spectral Density Matrix

When the bandwidths of the K filters are not extremely narrow, a considerable contribution to the output of a filter may come from the skirts of the filter due to spectral densities in other parts of the frequency range away from the bandwidth of the filter. Figure 2 shows the 12 filters of the WSA system, spaced in such a way that 12 contiguous bandwidths cover the frequency range from 0.045 to 0.360 Hz. This interaction between filter ranges is derived herein and put into computational form.

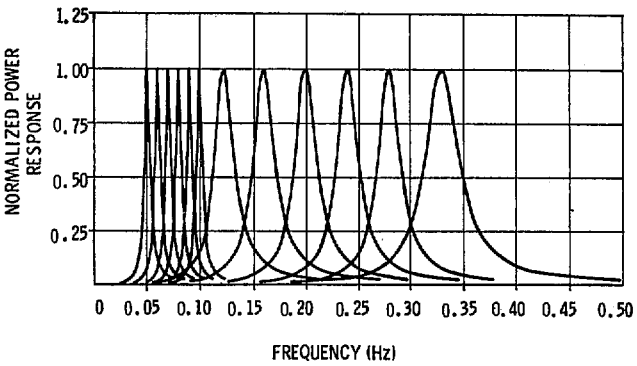

Figure 2. NORMALIZED FILTER RESPONSE CURVES FOR A 12-CHANNEL WSA

Let the total interval $F_1 \leq f \leq F_{k+1}$ (outside of which the integrand of eq. (15) is assumed to be negligible) be divided into K intervals, such that the left-hand boundary of each interval is F_j and the right-hand boundary is F_{j+1}, with j = 1, 2, 3, ..., K. The jth interval has a width of

$$\delta f_j = F_{j+1} - F_j \tag{18}$$

and a center frequency of

$$f_j = (1/2)(F_{j+1} + F_j) \quad . \tag{19}$$

The intervals F_j were chosen so that the widths δf_j are smallest when the integrand is significantly large and varying fast, and largest when the integrand is either small or varying slowly. Furthermore, these intervals were chosen so that $f_j \equiv \overline{f}_j$ for all j; i.e., the center frequency of the interval is identical to the center frequency of the corresponding filter. The total number of intervals must be the same as the total number of filters, for reasons that will be discussed subsequently. Nevertheless, the intervals are distinct from the filters and must be identified by a different subscript.

Table II lists the intervals normally used on all NDBO buoys. The number of filters and intervals is K = 12.

TABLE II. INTERVAL DESCRIPTION

Interval Number j	Interval Boundaries F_j (Hz)	F_{j+1} (Hz)	Interval Width f_j (Hz)	Center Frequency f_j (Hz)
1	0.045	0.055	0.01	0.05
2	0.055	0.065	0.01	0.06
3	0.065	0.075	0.01	0.07
4	0.075	0.085	0.01	0.08
5	0.085	0.095	0.01	0.09
6	0.095	0.105	0.01	0.10
7	0.105	0.14	0.035	0.1225
8	0.14	0.18	0.04	0.16
9	0.18	0.22	0.04	0.20
10	0.22	0.26	0.04	0.24
11	0.26	0.30	0.04	0.28
12	0.30	0.36	0.06	0.33

With the intervals defined in this manner, eq. (15) can be rewritten, with no approximations, as

$$c_k = B \, \overline{\overline{g}} \, \overline{\overline{g}} \, \overline{K}^2 \, \overline{g}_k^2 \sum_{j=1}^{K} \int_{F_j}^{F_{j+1}} \frac{(f \cdot \Delta f_k)^2 \cdot w(f) \cdot (2\pi f)^{2(3-i)}}{\frac{\pi^2}{4}(f^2 - \overline{f}_k^2)^2 + (f \cdot \Delta f)^2} \, S^{(i)}(f) \cdot df \tag{20}$$

If the interval widths, δf_j, are made reasonably small, the function $S^{(i)}(f)$ can be considered, to some degree of approximation, to be a constant within each of the K intervals. Furthermore, the function w(f) can be assumed to behave linearly within each interval, without noticeable loss in accuracy; i.e.,

$$[w(f)]_j = W_j + \overline{W}_j f \quad . \tag{21}$$

The constants W_j and $\overline{W}_j$ are defined as follows:

$$\overline{W}_j = \frac{w_{j+1} - w_j}{\delta f_j} \quad , \quad W_j = w_j - F_j \overline{W}_j \tag{22}$$

where w_j and w_{j+1} are the values of the hull transfer function at the lower and upper bound frequencies of the jth interval.

Thus, using eq. (21) and denoting by $S_j^{(i)} \equiv S^{(i)}(f_j)$, the constant value of the function $S^{(i)}(f)$ within interval j, eq. (20) is transformed into

$$c_k = \sum_{j=1}^{K} \overline{\lambda}_{kj}^{(i)} \cdot S_j^{(i)} \tag{23}$$

where

$$\bar{\lambda}_{kj} = B\,\bar{\bar{\bar{g}}}\,\bar{\bar{g}}\,\bar{K}^2\,\bar{g}_k^2 \int_{F_j}^{F_{j+1}} \frac{(f\cdot\Delta f_k)^2 \cdot (W_j+\bar{W}_j f) \cdot (2\pi f)^{2(3-i)}}{\frac{\pi^2}{4}(f^2-\bar{f}_k^2)^2 + (f\cdot\Delta f_k)^2}\,df \qquad (24)$$

Equation (23) yields K different counts, each of which is generally a function of the K spectral densities. However, each spectral density as a function of the K counts is needed. This is obtained by solving eq. (23) in its matrix form:

$$\left\{ c_k \right\} = \left[\bar{\lambda}_{kj}^{(i)} \right] \cdot \left\{ S_j^{(i)} \right\} . \qquad (25)$$

Solving eq. (25) for the spectral densities yields

$$\left\{ S_j^{(i)} \right\} = \left[\bar{\lambda}_{kj}^{(i)} \right]^{-1} \cdot \left\{ c_k \right\} . \qquad (26)$$

Denoting the inverted matrix of $\bar{\lambda}_{kj}^{(i)}$ by $\lambda_{jk}^{(i)}$, i.e.,

$$\left[\bar{\lambda}_{kj}^{(i)} \right]^{-1} = \left[\lambda_{jk}^{(i)} \right] , \qquad (27)$$

the solution can be written as

$$\left\{ S_j^{(i)} \right\} = \left[\lambda_{jk}^{(i)} \right] \cdot \left\{ c_k \right\} . \qquad (28)$$

It is now obvious why the number of intervals must be the same as the number of filters; eq. (25) can be solved only if the matrix $\bar{\lambda}_{kj}^{(i)}$ is invertible (i.e., only if it is a square matrix in which k and j both take K values).

Using the summation notation, eq. (28) can be written in the fashion of eq. (23):

$$S_j^{(i)} = \sum_{k=1}^{K} \lambda_{jk}^{(i)} \cdot c_k . \qquad (29)$$

Recalling from eq. (14) that $c_k = C_k - \bar{C}_k$, we can further expand eq. (28):

$$S_j^{(i)} = \sum_{k=1}^{K} \lambda_{jk}^{(i)} \cdot C_k - \sum_{k=1}^{K} \lambda_{jk}^{(i)} \cdot \bar{C}_k . \qquad (30)$$

The second term in eq. (30) is the correction to the spectral density calculation based on the total count received at shore. A direct empirical correction, $\Delta S_j^{(i)}$, was added to this correction so that

$$\hat{S}_j^{(i)} = \Delta S_j^{(i)} - \sum_{k=1}^{K} \lambda_{jk}^{(i)} \bar{C}_k . \qquad (31)$$

In principle, there is no need for $\Delta S_j^{(i)}$ to be added, because corrections for all known offsets have already been made. However, we reasoned that, after all known corrections had been made, some residual small random error would still exist in the spectra. If this error were negative, the system would fail to report very small spectral energies which, because they are small, would not be of much interest to users. But, if the error were positive, the system would report small energy spectra that did not exist. $\Delta S_j^{(i)}$ was thus included to desensitize the system. The negative values used to date have been selected by best engineering judgment, but they should ideally be selected by calibration against a satistically valid set of ground-truth spectra.

With eq. (31), the spectral densities in eq. (30) can be redefined to yield

$$S_j^{(i)} = \hat{S}_j^{(i)} + \sum_{k=1}^{K} \lambda_{jk}^{(i)} \cdot C_k . \qquad (32)$$

Using the spectral density values of eq. (32), the spectral moments $M_{2(i-1)}$ are computed as follows:

$$M_{2(i-1)} \cong \sum_{j=1}^{K} S_j^{(i)} \cdot \delta f_j . \qquad (33)$$

The spectral moments M_0 and M_2 are computed in terms of the displacement spectral density by using eq. (3):

$$M_0 \cong \sum_{j=1}^{K} S_j^{(1)} \cdot \delta f_j \qquad (34)$$

$$M_2 \cong \sum_{j=1}^{K} S_j^{(2)} \cdot \delta f_j$$

$$= \sum_{j=1}^{K} (2\pi f_j)^2 \cdot S_j^{(1)} \cdot \delta f_j \qquad (35)$$

These moments are needed for the calculation of the following:

$$H_{1/3} = 4\sqrt{M_0} \qquad (36)$$

$$T_2 = 2\pi\sqrt{M_0/M_2} \qquad (37)$$

where

$H_{1/3}$ = significant wave height = average height of the highest 1/3 of all waves

T_2 = average zero-up-crossing wave period.

5. Computations

The computations leading to the determination of the wave spectra and the spectral moments are summarized in Figure 3. The constants listed in the figure include the following:

$$K = K$$

$$B = B$$

$$G3B = \overline{\overline{g}}$$

$$G2B = \overline{\overline{g}}$$

$$KB = \overline{K}$$

$$CBO = \overline{c}$$

The last printed line in Figure 3 gives the spectral moments, the significant wave height $H_{1/3}$, and the average zero-up-crossing wave period T_2. The displacement spectrum is plotted versus frequency in Figure 4. The noise equivalent spectrum, which is an approximation of the wave spectrum, is plotted in Figure 5.

BUOY = EB03 DATA TIME = 1/28/78 9: 0 LATITUDE = 0.560000E 2 LONGITUDE = 0.147900E 3

NUMBER OF FILTERS (K)	=	12
A-TO-D SENSITIVITY (B)	=	-0.204800E 3
GAIN OF OUTPUT BUFFER (G3B)	=	0.200000E 1
GAIN OF SQUARING CIRCUIT (G2B)	=	0.100000E 0
SLOPE OF ACC. LINEAR CAL. CURVE (KB)	=	0.510000E 0
ZERO VOLTAGE COUNT (CBO)	=	0.204750E 4
GAIN(K) OPTION (1=COMPUTE, 2=INPUT)	=	2
OFFSET OPTION (1=COUNTS, 2=VOLTS)	=	1

* FILTER DATA: $\overline{C}_k = \overline{c} + B\overline{e}_k$ C_k c_k $S^{(i)}(\overline{f}_k)$

FILTER K	CENTER (K)	FREQ.	BAND-WIDTH	G1B GAIN	OFFSET VOLTS	OFFSET COUNTS	MEASURED VOLTS	MEASURED COUNTS	COUNT DIFF.	MAX DISP SPECTRA	NOISE EQUIV. SPECTRAL ACC.	VEL.	DISP.	POTENTIOMETER SETTINGS P1	P2	P3+P4
1	1	0.0500	0.010	196.07	-0.042	2056.0	3.630	1304.0	-752.0	51.334	0.1811	1.8345	18.5877	0.9506	0.0400	0.1047
2	2	0.0600	0.010	69.44	-0.007	2049.0	0.764	1891.0	-158.0	197.372	0.3014	2.1209	14.9230	0.3367	0.0400	0.1257
3	3	0.0700	0.010	52.36	-0.017	2051.0	0.618	1921.0	-130.0	187.378	0.4333	2.2399	11.5792	0.2539	0.0400	0.1466
4	4	0.0800	0.010	52.36	-0.007	2049.0	2.156	1606.0	-443.0	109.838	1.4657	5.8010	22.9595	0.2539	0.0400	0.1676
5	5	0.0900	0.010	52.36	-0.051	2058.0	2.742	1486.0	-572.0	68.571	1.8768	5.8690	18.3536	0.2539	0.0400	0.1885
6	6	0.1000	0.010	52.36	0.012	2045.0	3.103	1412.0	-633.0	44.989	2.0582	5.2136	13.2061	0.2539	0.0400	0.2094
7	7	0.1225	0.035	28.18	0.100	2027.0	3.748	1280.0	-747.0	19.707	2.3423	3.9538	6.6740	0.4782	0.1400	0.2566
8	8	0.1600	0.040	26.18	0.012	2045.0	3.865	1256.0	-789.0	6.865	2.4130	2.3876	2.3624	0.5077	0.1600	0.3351
9	9	0.2000	0.040	26.18	0.012	2045.0	3.792	1271.0	-774.0	2.812	2.3168	1.4671	0.9291	0.5077	0.1600	0.4189
10	10	0.2400	0.040	26.18	-0.027	2053.0	2.932	1447.0	-606.0	1.356	1.9042	0.8374	0.3683	0.5077	0.1600	0.5027
11	11	0.2800	0.040	26.18	0.012	2045.0	2.507	1534.0	-511.0	0.732	1.9898	0.6429	0.2077	0.5077	0.1600	0.5864
12	12	0.3300	0.060	21.37	0.012	2045.0	1.223	1797.0	-248.0	0.380	1.8511	0.4306	0.1001	0.6217	0.2400	0.6912

*INTERVAL DATA:

W_j TRANSFER INTERCEPT	$\overline{W}_j$ TRANSFER SLOPE	w_j LEFT TRANSFER	F_j LEFT FREQ.	j K	f_j CENTER FREQ.	δf_j WIDTH	$\hat{S}_j^{(i)}$ OFFSET ACC.	SPECTRAL VEL.	DENSITY DISP.	$S_j^{(i)}$ MATRIX ACC.	SPECTRAL VEL.	DENSITY DISP.	$\Delta S_j^{(i)}$ EMPIRICAL OFFSETS ACC.	VEL.	DISP.
0.984	0.601	1.0111	0.0450	1	0.0500	0.0100	-1.190	-11.613	-113.926	0.0149	0.1836	0.8185	0.0000	0.0000	-1.2800
0.981	0.657	1.0171	0.0550	2	0.0600	0.0100	3.656	26.230	185.992	0.1441	1.0191	6.5261	0.0000	0.0000	-0.6200
0.978	0.709	1.0237	0.0650	3	0.0700	0.0100	7.761	40.142	206.132	0.0051	0.0929	0.4436	0.0000	0.0000	-0.3300
0.970	0.815	1.0307	0.0750	4	0.0800	0.0100	6.935	27.381	107.449	1.5721	6.2776	24.7491	0.0000	0.0000	-0.2000
0.961	0.919	1.0389	0.0850	5	0.0900	0.0100	6.910	21.591	67.122	1.9371	6.0625	18.7973	0.0000	0.0000	-0.1200
0.955	0.975	1.0481	0.0950	6	0.1000	0.0100	6.753	17.626	45.499	2.0222	5.3360	13.8380	0.0000	0.0000	-0.0800
0.943	1.096	1.0578	0.1050	7	0.1225	0.0350	6.609	11.220	18.612	2.5415	4.3188	7.1460	0.0000	0.0000	-0.0400
0.933	1.164	1.0962	0.1400	8	0.1600	0.0400	6.616	6.487	6.249	2.6583	2.6085	2.5084	0.0000	0.0000	-0.0100
1.133	0.054	1.1428	0.1800	9	0.2000	0.0400	6.425	4.043	2.505	2.6514	1.6633	1.0217	0.0000	0.0000	-0.0100
1.753	-2.765	1.1449	0.2200	10	0.2400	0.0400	6.835	2.995	1.303	2.0040	0.8749	0.3792	0.0000	0.0000	0.0000
3.050	-7.752	1.0343	0.2600	11	0.2800	0.0400	7.738	2.555	0.838	2.2930	0.7432	0.2396	0.0000	0.0000	0.0000
3.377	-8.842	0.7242	0.3000	12	0.3300	0.0600	21.331	5.037	1.177	2.0618	0.4835	0.1121	0.0000	0.0000	0.0000
0.000	0.000	0.1937	0.3600												

MATRIX : M(0)= 1.0745, M(2)= 0.6055, M(4)= 0.6539, HI/3= 4.1464, T= 8.370

Figure 3. SAMPLE WSA PRINTOUT

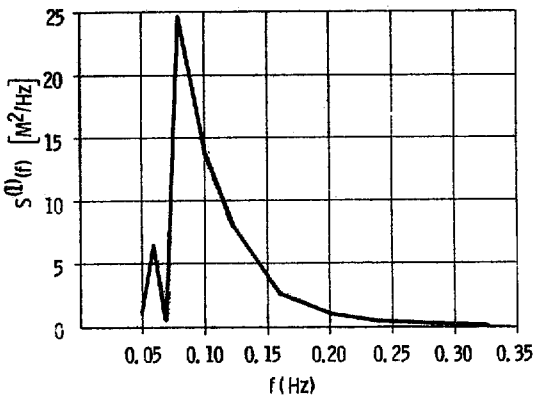

Figure 4. DISPLACEMENT SPECTRUM

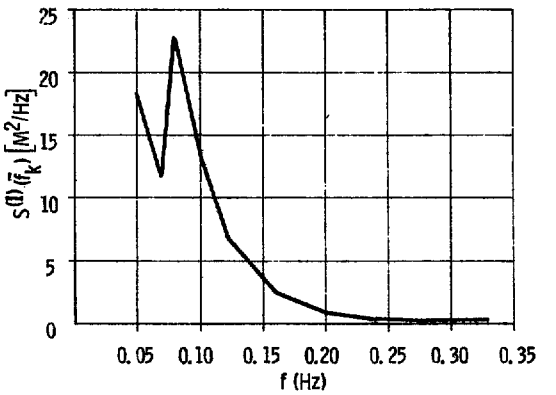

Figure 5. NARROW BAND APPROXIMATION OF THE DISPLACEMENT SPECTRUM

6. Summary and Conclusions

When the work described herein was initiated, a wave measurement system was needed for the PEB-type payloads that were to be produced and used on NDBO's 10-meter discus hull buoys. These payloads were not to have the capability to accept digital inputs, and were not to be programmable internally to perform any function beyond averaging samples. Changing the internal structure or interfaces of these payloads to accommodate digital data was not an option.

NDBO conceived two types of wave measurement systems that could be interfaced to the analog channels of the PEB payload — an analog wave height and period measurement system, and the system described in this paper. We believed that the latter would be considerably better, despite its inferiority to digital sampling systems such as the ones NDBO now has on some of its more advanced buoys. We therefore had the WSA systems designed, fabricated, integrated, and deployed on PEB buoys. Spectra, wave height, and wave period have been generated successfully with computer-produced matrices since 1975.

During the initial deployments of the PEBs, NDBO simultaneously acquired several hours of Waverider spectral data at the deployment sites. The agreement between these two sources of spectra was satisfactory, and as close as could be expected given the design limitations of the WSA.

The remoteness of NDBO's deep ocean sites impedes the acquisition of the large quantities of comparison data needed to establish, with statistical validity, either the hull transfer function or the error bounds of the spectra produced. The main problem is the reluctance of ships to standby for days while data is taken. In the absence of large quantites of comparison data, we have had hindcast evaluations of the WSA data performed by an NDBO contractor.[10,11,12] Those interested are encouraged to read these evaluations, which found the data to be satisfactory as an approximate estimate of spectra.

NDBO plans to perform calibrations and data quality evaluations of the system with the newly available Waverider Analyzer Satellite Communicator (WRANSAC), which circumvents many of the logistical problems we have had with conventional Waveriders.[13] Such calibration would allow the magnitudes of the negative empirical offsets, which we believe to be larger than necessary, to be reduced.

It should be noted that, in the Pacific Ocean, where swells occasionally appear at frequencies below 0.45 Hz, the conditions of the mathematical analysis are violated, and the resulting spectra are distorted.

Since the WSA systems went into service, NDBO has developed a system for the estimation of one-dimensional wave spectra. It is intended to replace the WSA systems as soon as resources allow; however, even with the limitations imposed by budgets and the state of the art of other related systems, the current system has performed its function well. Our experience with this early system is hereby documented for a better understanding of its functions and limitations, and its important contribution to the development of better wave measurement systems.

7. Acknowledgements

Mr. Frank Remond of Sperry Support Services designed and led the development of the WSA hardware which this paper describes mathematically. He provided equation (1) to the authors, and participated in the development of the mathematical description of the system. He also read the final version of this paper for correctness.

Mr. Billy Graham of Sperry programmed the mathematics and was essential to making the calculations work correctly.

Mrs. Deborah Hojem of Sperry edited the paper. The unusually difficult and tedious typing was done by Mrs. Linda Bridges and Ms. Edna Bender, also of Sperry.

References

1. Michelena, E.D., K.E. Steele, C.S. Niederman, and J. H. Hinchman, "A Reliable Wave Measurement System for NOAA Data Buoys," Proceedings of the Tenth Annual Conference of the Marine Technology Society, 1974.

2. Steele, K.E., E.D. Michelena, and J.M. Hall, "Wave Data Available from NDBO — Current and Planned," Proceedings fo the International Symposium on Ocean Wave Measurement and Analysis (WAVES 74), Vol. 1, p. 417, Sept. 1974.

3. Steele, K.E., J.M. Hall, and F.X. Remond, "Routine Measurement of Heave Displacement Spectra from Large Discus Buoys in the Deep Ocean," Proceedings of the First Combined IEEE Conference on Engineering in the Ocean Environment and the Annual Meeting of the Marine Technology Society (OCEANS 75), Sept. 1975.

4. "Equipment Operations Manual for Phase II Payload System," prepared under Contract NAS 13-16 for the NOAA Data Buoy Office by Magnavox Government & Industrial Electronics Company, July 1976.

5. Steele, K.E. P. Wolfgram, A. Trampus, and B.S. Graham, "An Operational High Resolution Wave Spectrum Analyzer System for Buoys," Proceedings of the OCEANS 76 Conference, Washington, D.C., Sept. 13-15, 1976.

6. "Practical Experience with Buoys," NOAA Data Buoy Office, November 1973.

7. "Technical Manual for the Model 313 Data Acquisition and Control System for the Prototype Environmental Buoy," prepared for the NOAA Data Buoy Office by General Dynamics Electronics Division, Report No. TM-75-PEB-3, July 1975.

8. Remond, F.X., "Ocean Spectrum Measurement with Analog Filters," Proceedings of 22nd International Instrumentation Symposium, San Diego, Calif., May 1976.

9. Burdette, E.L., "The Comparison of Discus-Buoy Wave Spectra Produced by Body-fixed and Vertically Stabilized Accelerometers," Proceedings of the MTS-IEEE Conference, The Ocean Challenge (OCEANS 78), Washington, D.C., Sept. 6-8, 1978.

10. Hubert, W.E., "Evaluation of Spectral Wave Data from EB-41," Ocean Data Systems, Inc., Technical Report 6, January 1976.

11. Hubert, W.E., "An Operational Evaluation of PEB Buoy Systems," Ocean Data Systems, Inc., Final Technical Report (Task Order No. Six), December 1976.

12. Hubert, W.E., "Evaluation of Spectral Wave Data Acquired by NOMAD Buoys," Ocean Data Systems, Inc., Final Technical Report (Task Order No. Eight), April 1977.

13. Adamo, L.C., K.E. Steele, and E.L. Burdette "A GOES Reporting Waverider Buoy," Proceedings of the MTS-IEEE Conference, The Ocean Challenge (OCEANS 78), Washington, D.C., Sept. 6-8, 1978.

A GOES-REPORTING WAVERIDER BUOY

L. C. Adamo
Louis C. Adamo, Inc.
P. O. Box "L"
Solana Beach, CA 92075

Kenneth E. Steele
NOAA Data Buoy Office
NSTL Station, MS 39529

Ernest L. Burdette
Computer Sciences Corp.
NSTL Station, MS 39529

ABSTRACT

A NEW INSTRUMENT FOR MEASURING AND REPORTING OCEAN WIND WAVES HAS BEEN CONSTRUCTED, TESTED AT SEA, AND PUT TO USE IN FIELD STUDIES OF THE TRANSFER FUNCTION OF OPERATIONAL WAVE MEASURING SYSTEMS ON LARGE DATA BUOYS. THE PROTOTYPE WRANSAC WAS INTEGRATED FROM AN EXISTING MICRO-COMPUTER, A SATELLITE RADIO TRANSMITTER, AND A WAVERIDER. TWENTY MINUTES OF WAVE DATA ARE PROCESSED AND PRODUCE HOURLY REPORTS OF MEAN WAVE HEIGHT, MAXIMUM CREST, MINIMUM TROUGH, AND 150 LAGS OF THE AUTOCORRELATION FUNCTION. THE INTERNATIONAL NETWORK OF SYNCHRONOUS METEOROLOGICAL SATELLITES PROVIDES A RELAY CAPABILITY PERMITTING WRANSAC TO BE USED ALMOST ANYWHERE IN THE WORLD OCEAN. THE DEVELOPMENT OF THE WRANSAC PROTOTYPE IS DESCRIBED AND DATA FROM THE DECEMBER 1977 DEPLOYMENT IS PRESENTED.

1. INTRODUCTION

THE NOAA DATA BUOY OFFICE (NDBO) HAS BEEN OPERATING SEVERAL DIFFERENT WAVE MEASUREMENT SYSTEMS INSTALLED ON A VARIETY OF DATA BUOY HULLS. FOR THE MOST PART, THESE SYSTEMS REPORT IN REAL-TIME, AND THE REPORTS ARE WIDELY DISSEMINATED BY THE NATIONAL WEATHER SERVICE. NDBO HAS HAD A REQUIREMENT FOR A HIGH-QUALITY WAVE MEASUREMENT SYSTEM TO DETERMINE THE TRANSFER FUNCTION OF EACH OF THE SEVERAL HULL TYPES IN USE, TO VERIFY PROPER OPERATION OF THE WAVE SYSTEMS ON NEWLY DEPLOYED DATA BUOYS, AND TO PROVIDE A REFERENCE MEASUREMENT BY WHICH THE QUALITY OF THE DATA PRODUCED BY THE DIFFERENT TYPES OF HULLS AND MEASUREMENT SYSTEMS CAN BE JUDGED OVER AN EXTENDED PERIOD OF TIME.

BETWEEN 1973 AND 1978, THE WAVERIDER (TRADEMARK OF DATAWELL BV, HAARLEM, THE NETHERLANDS) ACCELEROMETER BUOY WITH ITS OUTPUT RECORDED ON AN INSTRUMENTATION FM MAGNETIC TAPE RECORDER, WAS USED TO MEET THESE REQUIREMENTS. OVERALL, THESE ATTEMPTS WERE NOT SATISFACTORY FOR A NUMBER OF REASONS. THE PRINCIPAL DEFICIENCY STEMS FROM THE COMBINATION OF THE WAVERIDER'S LIMITED TELEMETRY RANGE (50 KM) AND THE HIGH-SEA LOCATIONS OF NEARLY ALL THE OPERATIONAL DATA BUOYS. BASICALLY, TO TAKE THE REQUIRED DATA WITH A WAVERIDER ALONGSIDE AN OPERATIONAL DATA BUOY, REQUIRES THAT A LARGE SHIP STAND BY FOR A RELATIVELY LONG TIME, HOPING FOR A VARIETY OF SEA CONDITIONS, WHILE THE NDBO TECHNICIAN MONITORS DATA BEING ACQUIRED BY THE WAVERIDER. IT APPEARS NOW THAT A MEASUREMENT PERIOD OF AT LEAST ONE WEEK DURATION WOULD BE REQUIRED TO OBTAIN THE TRANSFER FUNCTION OF A DATA BUOY HULL. THIS IS PROHIBITIVELY EXPENSIVE, AND THERE ARE OTHER DIFFICULTIES.

A WAVERIDER EQUIPPED WITH INTERNAL DATA PROCESSING CAPABILITY AND A SATELLITE COMMUNICATIONS LINK COMPARABLE TO THE LONG RANGE LINK ON THE DATA BUOYS WOULD OVERCOME ALL THESE DIFFICULTIES. IN 1976, A FEASIBILITY STUDY (REF. 1) WAS CARRIED OUT TO EXAMINE THIS POSSIBILITY. THE FOLLOWING CONCLUSIONS WERE OBVIOUS IN LATE 1976:

A. A PROTOTYPE WAVERIDER ANALYZER SATELLITE COMMUNICATOR (WRANSAC) COULD BE BUILT MAKING EXTENSIVE USE OF EXISTING HARDWARE AND SOFTWARE WITH A MINIMUM OF DEVELOPMENT;
B. THE PROTOTYPE COULD BE EXPECTED TO PROVIDE ONE-DIMENSIONAL SPECTRAL WAVE DATA IN THE SAME FORMAT AS THE MOST SOPHISTICATED OPERATIONAL DATA BUOYS AND WITH ACCURACIES CLOSE TO THE WAVERIDER'S SPECIFICATIONS;
C. SERVICE LIFE COULD BE EXPECTED TO BE SIX MONTHS WITH HOURLY REPORTS;
D. THE RELIABILITY OF THE COMMUNICATIONS LINK AS A FUNCTION OF ANTENNA PATTERN, TRANSMITTER OUTPUT, SATELLITE ELEVATION AND SEA CONDITONS COULD BE BEST EVALUATED IN THE FIELD.

THE WRANSAC WOULD HAVE OTHER APPLICATIONS. ITS EASE OF DEPLOYMENT WOULD ALLOW ONE OR MORE UNITS TO BE DEPLOYED IN THE PATH OF TROPICAL STORMS FOR SPECIAL STUDIES. IT COULD BE USED AS AN OPERATIONAL SYSTEM FOR OBTAINING WAVE SPECTRA WHERE SHIP TRAFFIC AND VANDALISM WOULD NOT INTERFERE. IT COULD ALSO BE USED AS A BACKUP INSTRUMENT ON THE HIGH-SEAS IN THE EVENT OF THE FAILURE OF AN OPERATIONAL DATA BUOY.

IN MID-1977, NDBO CONTRACTED WITH LOUIS C. ADAMO, INC. TO BUILD A PROTOTYPE (REF. 2). THE PROTOTYPE WAS BUILT, TESTED IN THE LABORATORY, AND TESTED AT SEA IN DECEMBER 1977. ALL TESTS INDICATED IT PERFORMS ACCORDING TO THE EXPECTATIONS OF THE FEASIBILITY STUDY. AVAILABLE EVIDENCE INDICATES THAT COMMUNICATIONS ARE ABSOLUTELY RELIABLE WITH SATELLITE ELEVATIONS ABOVE 40°, ALTHOUGH THE SYSTEM MAY NOT BE OPTIMUM WITH RESPECT TO MINIMIZING POWER CONSUMPTION.

THE FOLLOWING SECTIONS DESCRIBE THE SYSTEM, LABORATORY TESTS, THE SEA TEST, TEST DATA, CONCLUSIONS, AND OPERATIONAL RESULTS TO DATE.

2. SYSTEM DESCRIPTION

THE WRANSAC STRATEGY WAS TO MAINTAIN THE FEATURES INHERENT IN THE WAVERIDER WHILE OVERCOMING ITS TWO LIMITATIONS OF SHORT TELEMETRY RANGE AND NEED FOR A SEPARATE EXTERNAL DATA ACQUISITION SYSTEM; AND TO UTILIZE AVAILABLE HARDWARE AND SOFTWARE. THE RESULTANT PROTOTYPE INSTRUMENT HOPEFULLY WOULD BE CAPABLE OF CARRYING OUT MOST OF THE TASKS ENVISIONED FOR WRANSAC AS WELL AS PROVIDING INFORMATION ON THE RELIABILITY OF THE COMMUNICATION LINK UNDER VARIOUS CONDITIONS. THE WRANSAC PROTOTYPE WAS INTEGRATED FROM THE FOLLOWING MAJOR ELEMENTS:

+WAVERIDER/FL-6900 SERIES; THE 0.9M-DIAMETER BUOY PRODUCED BY DATAWELL;
+WAVE DATA ANALYZER (WDA); A SPECIALIZED MICRO-COMPUTER SYSTEM, DESIGNED BY MAGNAVOX, WHICH SAMPLES AN ANALOG SIGNAL, CALCULATES THE FIRST 150 LAGS OF THE AUTOCORRELATION FUNCTION, AND STORES THE RESULTS IN A RANDOM ACCESS MEMORY;
+GOES DATA TRANSMIT TERMINAL (GDTT); A DATA ACQUISITION SYSTEM AND RADIO TRANSMITTER, DESIGNED BY AMERICAN ELECTRONICS LABORATORY, WHICH SELF-INITIATES REPORTS TO THE SYNCHRONOUS METEOROLOGICAL SATELLITES (AMERICAN, GOES-1, SMS-2; EUROPEAN, METEOSAT; SOVIET, GOMS; JAPANESE, GMS);
+CHU ASSOCIATES INC. MICROWAVE ANTENNA MODEL CA-3140;
+SOFTWARE ON SHORE DESIGNED BY NDBO TO PROCESS THE AUTOCORRELATION FUNCTION OF ACCELERATION OR DISPLACEMENT INTO AN ESTIMATE OF THE SPECTRAL DENSITY FUNCTION OF SEA SURFACE DISPLACEMENT.

A SYSTEM BLOCK DIAGRAM IS PRESENTED IN FIGURE 1.

THE MAIN PROBLEMS SOLVED IN THE COURSE OF INTEGRATION WERE: 1. PROVIDING ENOUGH POWER FOR THE WDA WHICH WAS DESIGNED FOR USE ON MUCH LARGER BUOYS; AND 2. DEVELOPING A DIGITAL INTERFACE BETWEEN THE WDA AND THE GDTT.

THE POWER PROBLEM WAS SOLVED BY SELECTING THE LARGEST LITHIUM CELLS AVAILABLE IN PRODUCTION AS THE POWER SOURCE FOR THE PROTOTYPE. THESE CELLS (POWER CONVERSION INC. MODEL 660-5AS) HAVE AN ENERGY DENSITY OF 300WH PER KG, A NEARLY CONSTANT VOLTAGE, AND CAN TOLERATE SURGES DURING DISCHARGE. THE DIGITAL INTERFACE WAS DESIGNED AND FABRICATED BY DATA/WARE DEVELOPMENT, INC. UNDER SUBCONTRACT. THEIR DESIGN IS IMPLEMENTED WITH CURRENT C/MOS TECHNOLOGY. A CASSETTE TAPE RECORDER WAS INCLUDED IN ORDER TO EXPEDITE CHECKOUT AND TO PROVIDE THE CAPABILITY FOR RECORDING COMPLETE SAMPLES AND CALCULATED RESULTS FOR ABOUT 100 RECORDS, FOR THOSE APPLICATIONS IN WHICH THE AUTOCORRELATION FUNCTION IS INSUFFICIENT.

THE WDA WAS DESIGNED FOR THE LARGER NDBO BUOYS, AND HAS BEEN RELIABLY FUNCTIONING ABOARD VARIOUS OF THEM SINCE OCTOBER 1976. IT WAS DESCRIBED BY STEELE, ET AL (REF. 3).

THE WDA WAS DESIGNED TO ACCEPT AN ANALOG VOLTAGE FROM EITHER AN ACCELERATION OR DISPLACEMENT TRANSDUCER. ALTHOUGH ACCELERATION TRANDUCERS HAVE BEEN EMPLOYED ON VIRTUALLY ALL NDBO BUOYS, THIS DISPLACEMENT OPTION WAS INCLUDED SO THAT THE WDA COULD BE USED WITH THE OUTPUT OF A DATAWELL HEAVE SENSOR, A WAVERIDER, OR A WAVE STAFF, WITHOUT REDESIGN.

AN AMPLIFIER IS INCLUDED AT THE WDA INPUT TO OPTIMIZE THE TRANSDUCER SIGNAL LEVEL AT THE ANALOG-TO-DIGITAL CONVERTOR. THE SIGNAL PASSES THROUGH A SIX-POLE BUTTERWORTH LOW-PASS FILTER WITH HALF-POWER FREQUENCY AT 0.5HZ. THE FILTER OUTPUT IS SAMPLED AT A RATE OF 1.5 HZ TO PRODUCE 8-BIT COUNTS. RELATIVE TO THE UNITY GAIN AT VERY LOW FREQUENCIES, THE GAIN OF THE FILTER AT 1.0HZ IS 0.000244. THUS, THE ALIASING ALLOWED BY THE WDA AT THE HIGHEST FREQUENCY OF INTEREST, 0.5 HZ, IS INSIGNIFICANT.

A MICRO-PROCESSOR IN THE WDA FORMS THE EQUIVALENT OF AUTOCOVARIANCES FROM THE RAW SAMPLES. THE COMPLETE RECORD IS NEVER STORED. THE SUMS NEEDED FOR AUTOCOVARIANCES ARE FORMED DURING THE 2/3-S BETWEEN SAMPLES. SAMPLING CONTINUES FOR TWENTY MINUTES, FOR A TOTAL OF 1800 SAMPLES. THESE SUMS AND OTHER WAVE DATA ARE FORMATTED INTO 155, 16-BIT WORDS AND STORED IN A BUFFER IN THE WDA. FROM THE BUFFER, THE INTERFACE TO THE GDTT RELAYS THE WORDS UPON REQUEST BY THE GDTT, TO THE GDTT. THE GDTT TRANSMITS THE DATA VIA THE SATELLITE TO WALLOPS ISLAND AND THEN TO THE NATIONAL SPACE TECHNOLOGY LABORATORIES (NSTL).

RAW DISPLACEMENT SPECTRA, $S_d(K)$, ARE CONSTRUCTED AT NSTL FOR FREQUENCIES $F = K \times \Delta F$, K EQUALS 0, 1, 2, ... M, IN WHICH $\Delta F = 0.005$HZ AND $\overline{M} = 150$. THESE DISPLACEMENT SPECTRA ARE CONSTRUCTED IN THE SAME MANNER AS FOR THE LARGE NDBO BUOYS, EXCEPT THAT NO MULTIPLICATION BY FREQUENCY-TO-THE-MINUS-FOURTH-POWER IS NECESSARY TO TRANSLATE ACCELERATION SPECTRA TO DISPLACEMENT SPECTRA. A SMOOTH ESTIMATE OF BUOY DISPLACEMENT POWER SPECTRAL DENSITY IS OBTAINED BY HANNING:

$$S_d(1) = 0.5\,\overline{S}_d(1) + 0.25\,\overline{S}_d(2)$$

$$S_d(K) = 0.25\,\overline{S}_d(K-1) + 0.5\,\overline{S}_d(K) + 0.25\,\overline{S}_d(K+1),$$

$$K = 2, 3, \ldots (\overline{M}-1)$$

$$S_d(\overline{M}) = 0.5\,\overline{S}_d(\overline{M}-1) + 0.5\,\overline{S}_d(\overline{M})$$

THROUGH THE APPLICATION OF A SYSTEM POWER TRANSFER FUNCTION B(K) AND A NOISE CORRECTION FUNCTION N(K), AN ESTIMATE OF WAVE DISPLACEMENT POWER SPECTRAL DENSITY W(K) IS PRODUCED:

$$W(K) = (S_d(K) - N(K))/B(K), \quad K = 1,2, \ldots \overline{M}.$$

THE WRANSAC IS SO QUIET THAT N (K) IS SET TO 0. CALCULATION OF MOMENTS M_i AND PERIOD T ARE ALSO MADE. (REF. 4)

$$M_i = \sum_{k=1}^{\overline{M}} (2\pi K\Delta F)^i \, W(K) \, \Delta F \qquad i = 0, 2$$

$$H_{1/3} = 4 \, M_o^{1/2}$$

$$T = 2\pi \left(\frac{M_o}{M_2}\right)^{1/2}$$

THE SYSTEM POWER TRANSFER FUNCTION COMPRISES THE EFFECT OF THE WAVERIDER HULL TRANSFER FUNCTION, THE WAVERIDER DOUBLE-INTEGRATOR FILTERING FUNCTION, AND THE BUTTERWORTH FILTER IN THE WDA.

THE PRINCIPAL SPECIFICATIONS OF THE WRANSAC PROTOTYPE ARE GIVEN BELOW.

* * *

PHYSICAL
- 170KG
- 0.9M DIAMETER
- 1.5M/S MAXIMUM OPERATING SURFACE CURRENT
- 4300 REPORTS AT HOURLY INTERVALS

SENSOR
- WAVE HEIGHT
  - MINIMUM: P-P NOISE (1HZ BANDWIDTH EQUIVALENT TO 2CM)
  - MAXIMUM: 40M
  - ACCURACY: +/- 4% BETWEN 0.035HZ AND 0.5HZ
- ACCELEROMETER LINEARITY
  - NON-LINEARITY RECTIFICATION: <0.002M/S/S FOR 6M/S/S AMPLITUDE
- HORIZONTAL SENSITIVITY
  - <3% OF VERTICAL SENSITIVITY

MICRO-COMPUTER
- INPUT BANDWIDTH: 0 TO 0.5HZ
- DIGITIZATION: 8 BITS
- OUTPUT: 155 WORDS, EACH 15 DATA BITS INCLUDING, MEAN, MAX CREST, MIN TROUGH, 150 LAGS
- SAMPLING: 1.5HZ FOR 20 MINUTES/RECORD

RECORDER CAPACITY
- 104 RECORDS, EACH COMPRISED OF 1800 SAMPLES AND 155 WORDS OF CALCULATED RESULTS

GDTT
- RADIATED POWER: 40W @ 400MHZ
- REPORT INTERVAL: JUMPER PROGRAMMABLE FOR 1-12HRS IN 1-HR INCREMENTS
- OUTPUTS: ASCII ENCODED, 100 BITS/S

* * *

3. LABORATORY TESTS

THE LABORATORY TESTS WERE CONDUCTED IN TWO PARTS: FIRST, A CHECKOUT OF THE WDA, INTERFACE, GDTT, TAPE RECORDER AND SATELLITE COMMUNICATIONS; SECOND, A COMPLETE SYSTEM TEST INCLUDING THE WAVERIDER. TO ACCOMPLISH THE FIRST CHECK TWO SPECIAL PROGRAMS WERE WRITTEN AND LOADED INTO THE WDA'S PROGRAMMABLE READ-ONLY MEMORY. THESE PROGRAMS CAUSED THE WDA TO LOAD PARTICULAR PATTERNS OF NUMBERS INTO ITS RAM TO BE READ VIA THE INTERFACE TO THE CASSETTE, RECORDED, AND THEN TRANSMITTED. COMPARISON OF THE DATA RECORDED AND RECEIVED VIA THE SATELLITE LINK VERIFIED CORRECT OPERATION OF THE INTERFACE. WITH THE NORMAL PROGRAM INSTALLED IN THE WDA, SINUSOIDAL INPUTS FROM A SIGNAL GENERATOR WERE INPUT TO THE WDA, PROCESSED AND STORED ON THE MAGNETIC TAPE. THE MAGNETIC TAPE RESULTS WERE COMPARED WITH THE CHARACTERISTCS OF THE INPUT WAVE TO VERIFY THE OPERATION OF THE MICRO-COMPUTER AND ITS SOFTWARE.

FINALLY, THE AUXILIARY HARDWARE WAS INSTALLED IN THE WAVERIDER AND AN END-TO-END SYSTEM TEST WAS RUN. THIS INCLUDED THE STANDARD TEST FOR ATTITUDE OF THE WAVERIDER PLATFORM, AND THE TEST OF VERTICAL SENSITIVITY PERFORMED ON A VERTICAL TEST STAND WHICH RAISES AND LOWERS THE WAVERIDER WITH A NEARLY SINUSOIDAL MOTION OF APPROXIMATELY 3-S PERIOD AND 40-CM AMPLITUDE. A COMPUTER PROGRAM WAS WRITTEN TO SIMULATE THE WDA SOFTWARE ON A GENERAL PURPOSE COMPUTER. THIS PROGRAM WAS USED TO PROCESS THE DIGITAL DATA RECORDED ON THE CASSETTE TAPE.

THE RESULTS WERE COMPARED WITH THE RESULTS OF THE WDA'S CALCULATIONS, ALSO STORED ON THE TAPE, AND THOSE SAME RESULTS RECEIVED AT NSTL AFTER TRANSMISSION THROUGH THE GOES. EXACT AGREEMENT WAS FOUND. THE SENSITIVITY OF THE SYSTEM AS CONFIGURED FOR INITIAL DEPLOYMENT IS 12.25 DIGITAL COUNTS PER METER VERTICAL DISPLACEMENT. FULL RANGE IS 256 COUNTS OR APPROXIMATELY PLUS/MINUS 10 METERS.

4. SEA TEST

AFTER COMPLETION OF THE LABORATORY TESTS, WRANSAC WAS DEPLOYED TOGETHER WITH A STANDARD WAVERIDER OFF LA JOLLA, CALIFORNIA, ON 7 DECEMBER 1977. THE LOCATION WAS 32° 51.8'N, 117°15.9'W IN 18M DEPTH OF WATER. THE TWO BUOYS WERE 150M APART. DEPLOYMENT WAS ACCOMPLISHED FROM A SMALL BOAT LOWERED FROM SCRIPPS PIER WITH THE COOPERATION OF THE SHORE PROCESSES GROUP AT SCRIPPS INSTITUTION OF OCEANOGRAPHY. ACTUAL DEPLOYMENT INCLUDING TIME SPENT IN A QUICK SURVEY OF THE BOTTOM IN THE DEPLOYMENT AREA WAS ABOUT THREE HOURS. THE BUOYS WERE RETRIEVED ON 5 JANUARY 1978.

DURING THIS TEST, UNUSUAL WEATHER CONDITIONS OCCURRED IN THE SAN DIEGO AREA, INCLUDING THE ABSENCE OF NORMAL WINTER STORMS, AND THE OCCURRENCE OF UNUSUAL CALMS AND STRONG EASTERLY WINDS. AS A RESULT, THE TWO BUOYS DID NOT EXPERIENCE A WIDE RANGE OF WAVES APPROACHING FROM SEAWARD, AND THERE WAS ONLY A SHORT FETCH SHOREWARD OF THE BUOYS. THE DIFFERENCE IN LOCATION OF THE BUOYS AND THE PRESENCE OF LA JOLLA SUBMARINE CANYON COULD BE EXPECTED TO INTRODUCE SIGNIFICANT DIFFERENCES IN WAVES AT THE TWO LOCATIONS OVER SOME OF THE WIND CONDITIONS THAT OCCURRED. DURING THE DEPLOYMENT AN ARRAY OF PRESSURE SENSORS, PART OF THE CALIFORNIA COASTAL ENGINEERING DATA NETWORK, WAS OPERATING OFF THE END OF SCRIPPS PIER. DUE TO THE COMPLICATED TOPOGRAPHY IN THE AREA, DIRECT COMPARISON BETWEEN THE TWO SYSTEMS IS NOT STRAIGHTFORWARD. THE SHOALING COEFFICIENT FOR DEEPWATER WAVES OF 2.8 SECONDS PERIOD IS ALREADY REDUCED TO 0.95 AT THE DEPTH OF THE BUOY INSTALLATION. THERE ARE NO WIND DATA NOR WIND OBSERVATIONS AVAILABLE AT SCRIPPS PIER DURING THE TEST. THE STANDARD WAVERIDER DATA WAS RECORDED IN OUR OFFICES USING A DATAWELL WAREP AND AN INSTRUMENTATION FM TAPE RECORDER. THE WAREP AUTOMATICALLY CONTROLLED THE INTERVAL AND DURATION OF THE RECORDINGS TO SYNCHRONIZE WITH THE WRANSAC'S SAMPLE PERIOD. DUE TO THE RUGGED OVERLAND TRANSMISSION PATH, THE TELEMETRY SYSTEM WAS OPERATING NEAR ITS LIMIT. AS A RESULT, RECORDS MADE DURING REGULAR BUSINESS HOURS WERE OFTEN INTERRUPTED BY A NEARBY POWERFUL TRANSMITTER.

THE FM TAPES WERE ANALYZED AT NSTL. SPECTRA WERE CALCULATED FROM ABOUT 1000, 1HZ SAMPLES WITH A RESOLUTION OF 0.01HZ (50 LAGS). DISPLACEMENT RESOLUTION WAS 205 COUNTS PER METER. THESE SPECTRAL ESTIMATES HAVE AT LEAST 36 EQUIVALENT NUMBER OF DEGREES OF FREEDOM. NO ANTI-ALIASING FILTER WAS USED DURING DIGITIZATION OF THESE TAPES AND THE RESULTING NOISE IS VARIABLE FROM RECORD-TO-RECORD AND REEL-TO-REEL. NO NOISE CORRECTION HAS BEEN APPLIED TO DATA PRESENTED HEREIN, EXCEPT TO IGNORE ESTIMATES AT 0.01 AND 0.02HZ.

FOR THE COMPARISON PLOTS SHOWN HEREIN, SPECTRA BASED ON THE WRANSAC REPORTS WERE CALCULATED USING ONLY 75 LAGS; THUS IN THE COMPARISONS THESE SPECTRA HAVE 48 DEGREES OF FREEDOM. PRESENTATIONS OF WRANSAC DATA EXCLUSIVELY ARE BASED ON 150 LAGS AND HAVE 24 DEGREES OF FREEDOM.

5. SEA TEST DATA

THE AVAILABLE DATA INCLUDE 30 DAYS OF HOURLY REPORTS FROM WRANSAC, THE COMPLETE RECORD OF SAMPLES FOR THE FIRST 104 REPORTS, FM RECORDINGS OF THE WAVERIDER RECORDS MADE AT EITHER 2- OR 4-HR INTERVALS THROUGHOUT THE PERIOD, AND CORRESPONDING STRIP-CHART RECORDS FOR MOST OF THE FM RECORDINGS. ONLY A FEW SAMPLES OF THESE DATA ARE PRESENTED HEREIN.

THE FM RECORDINGS ENCOUNTERED A TYPICAL SAMPLE OF PROBLEMS. AS MENTIONED ABOVE, A NEARBY TRANSMITTER CAUSED RADIO INTERFERENCE DURING BUSINESS HOURS. THIS IS SIMILAR TO THE INTERFERENCE FROM A VESSEL'S COMMUNICATION TRANSMITTER WHEN THE WAREP IS USED AT SEA. THE STRONG EAST WINDS FILLED OUR OFFICES WITH SAND AND DUST, CONTAMINATING THE RECORDER AND TAPES.

THE RECORDS SELECTED FOR COMPARISON WITH WRANSAC WERE TAKEN DURING THE HOLIDAY WEEK 27-31 DECEMBER, AT 2-HR INTERVALS, WHEN INTERFERENCE WAS AT A MINIMUM. THE TIME HISTORIES OF THE SURFACE SYSTEMS AND THE NEARBY PRESSURE ARRAY ARE SHOWN IN FIGURE 2. (REF. 5) A SAMPLE OF THE SPECTRA FROM WRANSAC (W) AND THE WAVERIDER (E) IS SHOWN IN FIGURE 3. THESE SPECTRA, TAKEN AT A TIME OF RELATIVELY RAPID CHANGE IN TOTAL ENERGY, ILLUSTRATE THE CLOSE CORRESPONDENCE AT FREQUENCIES BELOW 0.15HZ, AND THE GENERALLY ELEVATED VALUES OF THE WAVERIDER AT HIGHER FREQUENCIES. THE WRANSAC PLOT BEGINS AT 0.02HZ, WHILE THE WAVERIDER PLOT BEGINS AT 0.03HZ. THE LOW FREQUENCY DISCREPANCIES ARE WELL-WITHIN THE 80% CONFIDENCE LIMITS ESTIMATED FROM A CHI-SQUARE DISTRIBUTION, USING THE DEGREES OF FREEDOM MENTIONED ABOVE.

FIGURE 4 PRESENTS THE TIME HISTORY OF A SINGLE SPECTRAL ESTIMATE (0.13HZ) FROM THE WRANSAC AND WAVERIDER.

LINEAR REGRESSIONS WERE COMPUTED FOR FIVE PAIRS OF SERIES, INCLUDING THOSE PLOTTED IN FIGURES 2 AND 4, PLUS SPECTRAL ENERGY DENSITIES AT THREE OTHER FREQUENCIES. THE REGRESSIONS WERE NOT FORCED THROUGH THE ORIGIN. THE RESULTS ARE PRESENTED IN THE FOLLOWING TABLE.

* * *

REGRESSIONS: 27 DECEMBER - 31 DECEMBER 1977

PARAM	SERIES	NBR	RANGE	SLOPE	INTRCPT	CORREL COEFF
SIG HT [CM]	E VS W	38	55-85	0.80	10.65	0.89
SIG HT [CM]	E VS P	8	35-83	0.53	7.39	0.80
ENERGY DENSITY [CMCM/HZ]						
0.05HZ	E VS W	40	50-700	1.04	16.36	0.87
0.09HZ	E VS W	40	200-3000	0.90	132.82	0.93
0.13HZ	E VS W	40	600-6300	0.85	130.00	0.93
0.17HZ	E VS W	40	300-3000	0.60	343.48	0.81

NOTES: E DESIGNATES WAVERIDER; W, WRANSAC;
P, PRESSURE ARRAY.

* * *

CONSIDERING THE SMALL RANGE OF SEA STATES AND ENERGY DENSITIES REPRESENTED IN THE DATA, AND THE PROBLEMS WITH THE FM RECORDINGS, THE CORRELATIONS BETWEEN THE TWO INSTRUMENTS ARE QUITE HIGH.

THE HIGH DENSITY OF THE WRANSAC DATA IN THE FREQUENCY VS. TIME PLANE PROVIDES UNUSUAL DETAIL

AS SHOWN IN FIGURES 5 AND 6. THE DATA PRESENTED IN FIGURE 5 WERE OBSERVED DURING THE PERIOD OF RECORD-BREAKING SANTANA WINDS. THESE ARE SOUTHERN CALIFORNIA'S FÖHN WINDS WHICH ARE GENERALLY NORTHEAST, BUT STRONGLY INFLUENCED BY LOCAL TOPOGRAPHY. THESE WINDS REACHED THEIR PEAK DURING THE PERIOD INCLUDED IN FIGURE 5, DYING AWAY TO A CALM AT THE END OF THAT PERIOD. WITH THE INSTRUMENTS ONLY ABOUT 1000M FROM SHORE, NO LOCAL WAVES WERE GENERATED, YET THOSE APPROACHING FROM SEAWARD WERE STRONGLY ATTENUATED. FIGURE 6 PRESENTS DATA OF A MORE TYPICAL NATURE FOR DECEMBER. THE HIGHER FREQUENCY MAXIMUM RESULTS FROM THE TYPICAL LAND BREEZE, SEA BREEZE REGIME. THE TWO LOW FREQUENCY RIDGES AT 0.12HZ AND 0.05HZ ARE SWELL FROM DISTANT STORMS. THE FORMER IS ASSOCIATED WITH A GULF OF ALASKA SYSTEM, WHILE THE LATTER APPEARS TO HAVE A SOURCE IN THE NORTHWEST PACIFIC. MOST OF THE FEATURES IN FIGURE 6 WOULD BE VERY POORLY REPRESENTED WITH SAMPLING LESS DENSE THAN WRANSAC PROVIDED.

6. CONCLUSIONS AND RECENT RESULTS

THE CONCLUSIONS OF THE FEASIBILITY STUDY OF THE WRANSAC CONCEPT HAVE BEEN PUT TO THE TEST BY CONSTRUCTING, TESTING, AND USING A PROTOTYPE WRANSAC INSTRUMENT. THE RESULTS HAVE BEEN EXTRAORDINARILY SATISFYING WITH THE PROTOTYPE OPERATING AS EXPECTED IN EVERY WAY. CONCERNS ABOUT RELIABLE COMMUNICATIONS FROM A SMALL BUOY ARE DIMINISHING. WHILE NO SPECIFIC TESTS HAVE BEEN CONDUCTED, 1700 TRANSMISSIONS OF ABOUT 4.2 MILLION BITS HAVE BEEN COMPLETED, WITH SEAS UP TO 3M SIGNIFICANT HEIGHT FROM 30°N LAT. ONE THOUSAND FIFTY-THREE REPORTS WERE EXAMINED, INCLUDING THE HIGHEST SEA STATES, AND FIVE REPORTS WERE FOUND TO CONTAIN TRANSMISSION PARITY ERRORS, WHILE 13 REPORTS WERE MISSING DUE TO GROUND STATION PROBLEMS. THIS IS GOOD EVIDENCE THAT THE PROTOTYPE IS PROBABLY OVER-POWERED.

SINCE COMPLETION OF THE DECEMBER 1977 TEST, WRANSAC HAS BEEN USED TO ESTABLISH THE HULL POWER TRANSFER FUNCTION OF TWO OPERATIONAL NDBO BUOYS. IN MARCH 1978 IT WAS TETHERED TO A 12-METER DIAMETER DISCUS HULL LOCATED AT SITE 42002 (26N LAT, 93.5W LONG) IN THE GULF OF MEXICO. AS A SHIP STOOD BY, 43 HOURLY REPORTS FROM WRANSAC WERE RECEIVED AT SHORE ALONG WITH THE SPECTRAL WAVE DATA FROM THE DISCUS. THESE REPORTS LED TO THE FIRST HULL TRANSFER FUNCTION BASED ON SYSTEMATIC AT-SEA MEASUREMENTS. THIS CALIBRATION OPERATION HAS UNDOUBTEDLY IMPROVED THE QUALITY OF DATA FROM NDBO'S 12-METER DISCUS HULLS. THE SHIP STOOD BY AT SITE 42002 TO PROTECT AGAINST THE LOSS OF NDBO'S ONLY WRANSAC. BUT THIS USE OF WRANSAC SHOWED THAT 43 REPORTS ARE NOT REALLY ADEQUATE TO ACCOMPLISH A SATISFACTORY CALIBRATION, PARTICULARLY WHEN THE SEA STATE IS UNCHANGING OR QUIET.

WRANSAC WAS LEFT UNATTENDED, TETHERED TO THE NOMAD-HULL BUOY AT SITE 42003 (26N LAT, 86W LONG) IN APRIL 1978. HIGH SEAS INTERFERED WITH THE SCHEDULED RECOVERY, RESULTING IN A SIX-WEEK TEST. A RELIABLE HULL TRANSFER FUNCTION FOR THE NOMAD AT THIS SITE HAS BEEN PRODUCED WITH THE EXCELLENT WRANSAC DATA ACQUIRED.

THIS LONG TEST SHOWED THAT, IN THE ABSENCE OF HIGH OR VARIABLE SEA STATES, MANY DAYS OF HOURLY DATA ARE REQUIRED TO PRODUCE A STATISTICALLY RELIABLE HULL TRANSFER FUNCTION. JUST EXACTLY HOW MANY DAYS ARE NEEDED IS A MATTER OF JUDGEMENT, BUT TWO IS TOO FEW AND FORTY-TWO IS MORE THAN NECESSARY. AT EITHER EXTREME THE DURATION IS LONGER THAN IS CONVENIENT FOR A SHIP TO STAND BY. IT IS THIS FACT THAT MAKES THE WRANSAC SO VALUABLE TO NDBO IN ITS OPERATIONS.

AS SHOWN IN REFERENCE 1, THERE IS ROOM FOR IMPROVEMENT IN THE PROTOTYPE: THE COMPUTER AND GDTT CAN BE SIMPLIFIED, POWER CONSUMPTION CAN BE REDUCED, AND MORE FLEXIBILITY CAN BE INTRODUCED INTO THE DATA PROCESSING. SUCH CHANGES SHOULD RESULT IN A LESS EXPENSIVE, MORE RELIABLE INSTRUMENT, SUITABLE FOR WIDE APPLICATION.

ACKNOWLEDGMENTS

THE WORK DESCRIBED HEREIN WAS PERFORMED UNDER NDBO CONTRACT NO. 03-7-038-720 AND COMPUTER SCIENCES CORP. P.O. NO. A-016. THE AUTHORS WERE ASSISTED BY MR. FRANK REMOND OF SPERRY SUPPORT SERVICES. A MAJORITY OF THE CREDIT FOR THE SMOOTH TECHNICAL PROGRESS OF THIS WORK IS DUE TO MR. RICHARD KEELE, OF DATA/WARE DEVELOPMENT, INC., WHO WAS RESPONSIBLE FOR THE DIGITAL INTERFACE. DATAWELL, BV PROVIDED INVALUABLE TECHNICAL INFORMATION ON THE WAVERIDER AS WELL AS THE MODIFIED TOP HATCH TO MATE WITH THE MICROWAVE ANTENNA. DEPLOYMENT FROM SCRIPPS PIER WAS MADE POSSIBLE THROUGH THE COOPERATION OF THE SHORE PROCESSES GROUP AT SCRIPPS INSTITUTION OF OCEANOGRAPHY. THE PREPARATION OF THIS PAPER WAS SUPPORTED BY THE AUTHORS' RESPECTIVE ORGANIZATIONS.

REFERENCES

1. ADAMO, L. C., "AN EVALUATION OF THE FEASIBILITY OF INTEGRATING THE WAVE DATA ANALYZER AND GOES DATA TRANSMIT TERMINAL WITH THE WAVERIDER BUOY SYSTEM TO REPORT THROUGH THE GOES DATA NETWORK." NDBO CONTRACT 01-6-038-901, APRIL 1977. (UNPUBLISHED)

2. ADAMO, L.C., "FINAL REPORT OF THE DEVELOPMENT TESTING, AND DELIVERY OF A PROTOTYPE GOES-REPORTING WAVE MEASUREMENT SYSTEM KNOWN AS WRANSAC." NDBO CONTRACT 03-7-038-720, FEBRUARY 1978. (UNPUBLISHED)

3. STEELE, K. E., A. TRAMPUS, P. A. WOLFGRAM, B. S. GRAHAM, "AN OPERATIONAL HIGH RESOLUTION WAVE DATA ANALYZER SYSTEM FOR BUOYS." PUBLISHED IN THE PROCEEDINGS OF OCEANS '76. (CORRECTED 9 DECEMBER 1976)

4. GODA, YOSHIMI, "ESTIMATION OF WAVE STATISTICS FROM SPECTRAL INFORMATION." WAVES '74. AMER. SOC. OF CIVIL ENG., NY 1974.

5. CALIFORNIA COASTAL ENGINEERING DATA NETWORK MONTHLY SUMMARY REPORT NO. 25, CALIFORNIA DEPARTMENT OF NAVIGATION AND OCEAN DEVELOPMENT AND USA CORPS OF ENGINEERS. DECEMBER 1977. (UNPUBLISHED)

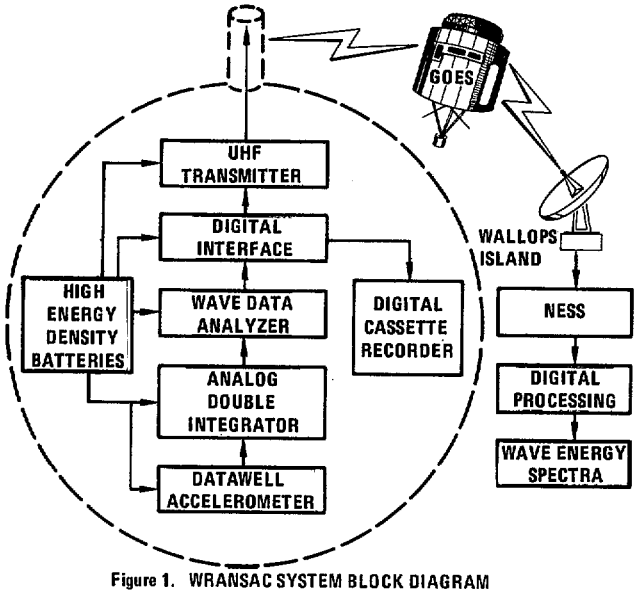

Figure 1. WRANSAC SYSTEM BLOCK DIAGRAM

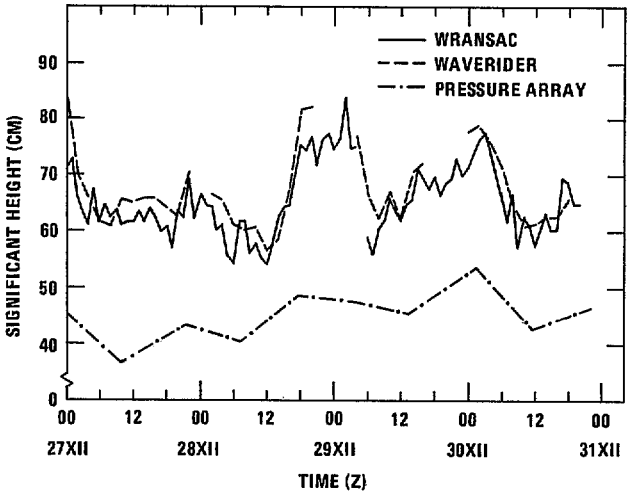

Figure 2. TIME HISTORIES OF SIGNIFICANT HEIGHT

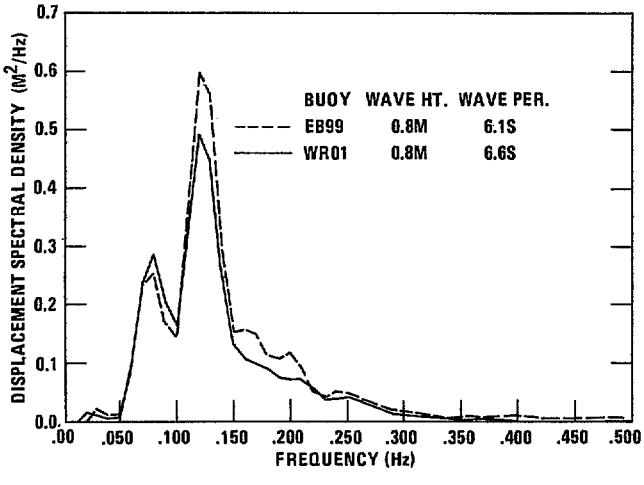

Figure 3. WAVE SPECTRAL PLOTS WR01-EB99 SDR ±2059

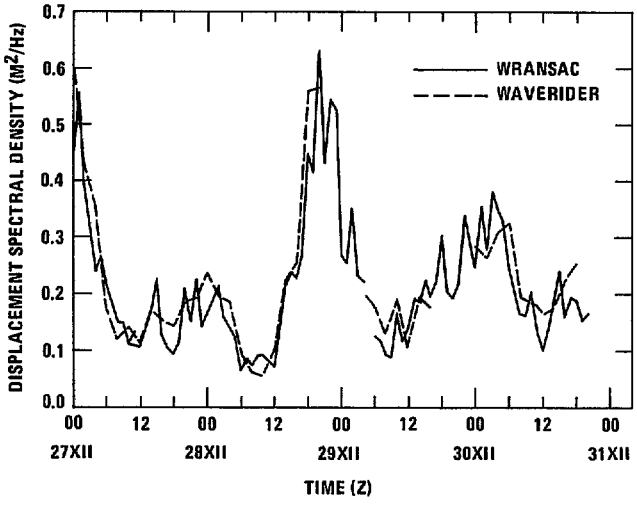

Figure 4. TIME HISTORIES OF SPECTRAL DENSITY (0.13 Hz)

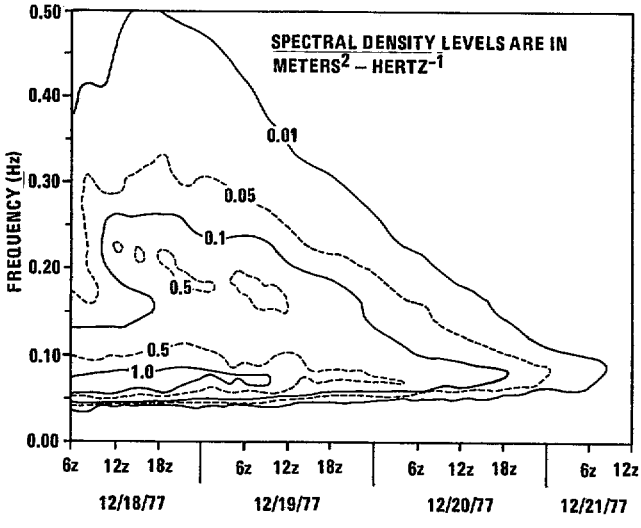

Figure 5. CONTOURS OF EQUAL SPECTRAL DENSITY FROM WRANSAC

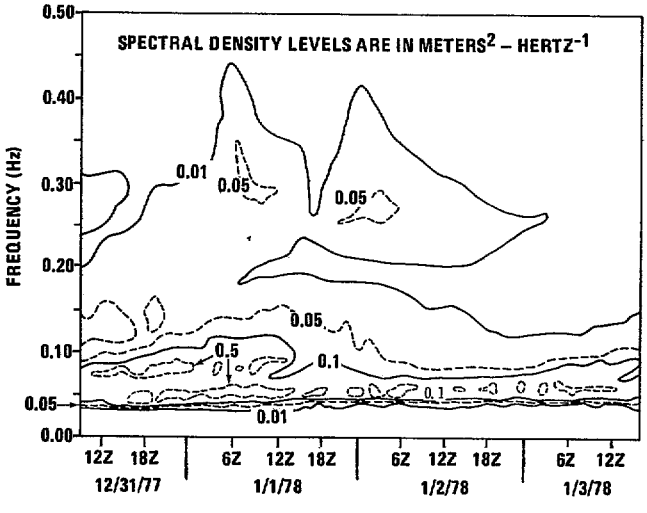

Figure 6. CONTOURS OF EQUAL SPECTRAL DENSITY FROM WRANSAC

WAVE DIRECTION MEASUREMENT BY A SINGLE WAVE FOLLOWER BUOY

W. I. Sternberger, L. R. LeBlanc, F. H. Middleton
Department of Ocean Engineering
University of Rhode Island
Narragansett Bay Campus
Narragansett, Rhode Island 02882

Abstract

This paper describes a system for measuring the direction of ocean wave propagation, as well as wave height and period. The system employs a conventional wave follower buoy, modified so as to provide compass, pitch and roll signals in addition to the vertical component of buoy acceleration. The modifications are indicated in the paper, and the buoy was tested in two sea state conditions in Narragansett Bay. The pitch, roll, compass, and heave acceleration signals were all processed on the computer in the laboratory to provide a variety of results. One test condition was ideal in that the wind and wave conditions were changing steadily throughout the data recording process. The second test was exactly opposite, with small waves and a consistent wind direction. The results presented in the paper include the wave height power spectral density, a polar tilt histogram for the buoy motion, and a family of polar plots of the average tilt angle in each 5° sector of azimuth of the buoy pitch/roll.

1. Introduction

This paper is one of a series of papers on the subject of the development of wave follower buoys. The series commenced in 1975 with OTC paper 2424 on the mathematical analysis of wave data making optimum use of fast computer techniques. Next, was OTC paper 2597 in 1976 devoted to the problem of spectral compensation of acceleration data in order to produce a true wave height power spectral density (PSD). Finally, a preliminary set of results, of wave direction measurements, was presented in 1978 in OTC paper 3180. It is the purpose of the present paper to elaborate upon the measurement of the direction of propagation of wave mode(s) present in an open-sea field.

In many important ocean operations, either on the open sea or near shore, the direction of propagation is often of more importance than the significant wave height, or the power spectrum. This is clearly the case, for instance, for storm waves striking a beach, a harbor channel, a breakwater or any sort of offshore structure. Up to the present time, anyone needing wave incidence direction data has been forced to deploy complex, complicated, and expensive spatially distributed arrays of wave measurement devices. Using wave staffs on a structure requires spatial separation on the order of the wave length of interest in order to obtain reliable results.

The buoy used in this study was a Model WF-100 Wave Follower Buoy manufactured by Coastal Data Service, Inc., (licensed to Hydro Products, San Diego), on loan to the University of Rhode Island for purposes of the present development. It was necessary for Coastal Data Service to modify their standard buoy, by the addition of tilt and compass sensors, to make it possible to measure propagation direction. Some internal modifications were required to provide space for the necessary additional sensors.

This paper will describe these modifications, explain the operation, and show at-sea test results from a particular wave field. The results will include the usual power spectral density plots and the directional pattern of the dominant wave frequency bands that were present at the time and place of the experiment.

2. Theory

The wave follower buoy which was used in this study is designed so that it acts as an inverted pendulum. It is the small pitching and rolling of the buoy which makes it possible to sense the propagation direction of the various dominant wave frequency bands. The primary hydrodynamic features of the WF-100 buoy assembly were given in detail in the 1976 OTC paper mentioned earlier. The most important feature for the present discussion is the "inverted pendulum" configuration wherein the center of horizontal drag is located near the bottom of the assembly.

With this arrangement, when a wave passes by the free-floating buoy, the wave surface slope presents a pitch/roll driving moment to the buoy assembly. Since the buoy is axisymmetric, pitch and roll really apply to orthogonal tilt angles relative to an arbitrary fore-and-aft direction of the buoy. The only sensors required in addition to the high sensitivity accelerometer are two good inclinometers and a magnetic compass fixed to the buoy hull. The tilt angle magnitude and its magnetic heading are correlated with the slope of a

---

Illustrations at end of paper

wave and its direction of propagation.

There is rarely interest in individual wave slope characteristics. The data user is much more interested in wave direction statistics, because this is more relative to wave forces on structures, or slamming effects on beaches and breakwaters. Since there is no apparent standard method for displaying directional spectra, the tilt data from the experiment are displayed in different ways.

In an ideal model instance, with sinusoidal waves passing a buoy, the magnitude of the wave slope on the front (before a crest) of a wave would be the same as on the back (after a crest) of a wave. In the real world, with non-symmetric waves, the magnitude of the slope is higher and the duration of the slope shorter on the front of an individual wave. Another source of roll asymmetry is the relatively steady roll force applied to the exposed portion of the buoy in an actual wind driven wave field. For these reasons it is not simple to predict the roll behavior of a given buoy on an open water wave situation. In fact, the one safe prediction is that tilting in the direction of propagation on the front of a wave, as well as the reverse tilt on the back side of the wave will occur with most small surface buoys.

This sort of rocking behavior, enhanced somewhat by the roll resonance of the buoy would at first appear to present a 180° ambiguity problem. In most wave measurement operations, the local geography, wind data, and other conditions make it quite simple to eliminate the ambiguity if the wave direction display fails to do so itself.

3. Equipment and Processes

As indicated earlier, the buoy used in this study is a Coastal Data Service Model WF-100 modified to incorporate two inclinometers and a magnetic compass. The WF-100 is thoroughly described and shown in photos in the 1976 OTC paper. The hull shape has changed to more of an ellipsoid of revolution than the spherical shape shown in the paper.

The inclinometers first used were commercial units that proved to be unsuitable for two reasons. They displayed resonant behavior and were sensitive to inclination at right angles to their normal response axes. For this reason, the two orthogonal inclinometers were unavoidably cross-coupled, so that another solution had to be found. The solution came from a special inclinometer design which provided two analog output signals (DC voltage) almost linearly proportional to the pitch and roll angles. (Figure 1). Pitch is defined as a tilt in the direction of the arbitrarily established lubber line on the buoy.

Calibration of the tilt sensor is performed in the lab with the aid of a tilt jig. Static tilts of known magnitude, along each of the orthogonal planes, are correlated to the D.C. output of the unit under test.

The commercial magnetic compass performed satisfactorily and it provided an analog output voltage produced by a low-torque pot connected to the compass card. Finally, the output signals from the complete buoy system included four analog voltages -- buoy vertical acceleration, pitch, roll, and magnetic heading of the lubber line.

To make use of these four analog signals for this experiment they were delivered by a tether wire to the small surface vessel which carried the tape recorders and other support equipment. The four signals were each applied to an individual FM magnetic tape channel on the same recorder so the signals were synchronized.

Since the end result of this study was to be wave propagation direction, there was no specific need to generate an accurate wave height PSD. Instead, the acceleration PSD was transformed by dividing through by ω^4 which was an easy way to produce a crude PSD for wave height which was valid for most of the energetic wave frequency band.

This wave height PSD was then used as a guide for processing the tilt data. The data will be shown later, but for the present discussion, there are many processes that might be of some use with the tilt data. For example, to a first approximation, the two tilt signals constitute a Cartesian form of displacement from the vertical. One can readily convert this to a polar form, with the magnitude corresponding to the tilt angle and the polar angle giving the direction of the tilt relative to magnetic North.

4. Results and Data

There were several ideas for ways to handle the tilt and bearing data to get the most out of it. One was to generate a polar histogram (1° intervals) of events which corresponded to the magnitude of the tilt exceeding some arbitrary threshold angle. The purpose of the threshold is to simply remove a great deal of the purely random tilting motion that any surface buoy encounters in surface waves. A sample polar histogram produced on the computer for the total 15-minute data set is shown in Figure 2 simply because it is interesting. In this case, an event was defined as a tilt exceeding an arbitrary threshold value, within a 1° azimuth bin and the radial scale is arbitrary corresponding to the number of events.

For comparison's sake, a polar histogram for the data corresponding to the calm sea conditions is presented as Figure 3. Both figures are plotted versus the same scales with thresholds of 1σ. Because of the apparent lack of activity in the calm sea case, it was decided that further analysis be limited to the rough sea condition data.

What is interesting to note about the histograms is the fact that more occurances of large tilt happen into the wind rather than with the wind. It is hypothesized that this occurs as a

result of the extended duration of the back of the wave. When data sampling occurs at a fixed rate, an extended tilt duration results in a proportionally larger incidence count.

This discussion will be limited to one field operation in Narragansett Bay, under rough storm conditions (see Figure 4). The locations marked 1, 2, and 3 correspond to the beginning of each of three continuous five-minute data recording intervals. The test site was selected because it was obvious that the support vessel would drift roughly North by Northwest in the wind, and drift would be out of the lee of Prudence Island. This seemed ideal because the combination of the steady waves plus those refracted by Prudence Island would be changing as time progressed. In addition, the wind was not steady from one direction and the result was a highly confused sea, as far as observers were concerned.

All of the data was brought back to the computer lab for processing, first for the PSD of wave height which is plotted in Figure 5. This is the PSD for the entire 15-minute data run and was produced by the ω^{-4} transfer function mentioned earlier. This rough PSD plot is sufficient to show the maximum wave height power point at about 0.43 Hz. The corresponding period is about 2.32 seconds which appeared consistent with visual observations at the time. The lower local peak in the PSD at about 0.725 Hz. is known to be related to the 1-1/3 second natural heave frequency of the buoy. Compensation for this non-wave feature is thoroughly discussed in the 1976 paper, and it is of minor importance in the present study.

Figures 6 - 9 are polar plots of the average magnitude of the tilt angle within each 5° azimuth interval after removing the purely random component of tilt. This random component is the tilt of the particular 5° interval which has the smallest average tilt.

The question naturally arises as to which dominant wave bands are influencing this polar plot the most. The processing was set up to perform a numerical filtering process on the wave data at the dominant frequency 0.425 Hz $\pm$ 0.05 Hz at the 3 db down points. The objective was to isolate this dominant mode to determine its own propagation direction. Figures 6, 7, and 8 are respectively the 1st, 2nd, and 3rd five-minute segments, while Figure 9 is the entire 15-minute data interval.

5. Interpretation of Data

Figure 4 shows the sites marked 1, 2, and 3 corresponding to the three sequential five-minute data intervals. They are situated some 1500 and 2000 feet apart, indicating a wind (and tidal current) drift on the order of five to seven feet per second (3 knots) roughly in the direction of the wind. Each time interval finds the vessel and buoy further out of the lee of Prudence Island and in a different position relative to the waves being refracted by the island. Observers on the vessel agreed that refracted waves could be seen by the eye, the wind was mainly out of the heading 165° and shifting back and forth to a considerable extent. The sea was quite mixed also, and occasional large troughs came at the vessel from unexpected directions. The reason for picking this position near Prudence was that we would have an opportunity to expose the buoy to quite different sea conditions.

It is interesting to compare the "event" pattern of Figure 2 with the tilt angle magnitude pattern of Figure 9. Both were produced from the same collection of data -- the total 15-minute run. In the former case, there is no averaging across adjacent bins, which process would have produced a smoother pattern. In such a case, relatively small rocking components of tilt produce the large number of counts in the 1° bins and the corresponding large spikes in the polar pattern.

Now referring to Figure 9, the number of tilt events in a given polar interval (here 5° of azimuth) is given no weight at all. A single large buoy roll in a particular 5° sector will cause a large average value of tilt angle or a large radius in this figure. The asymmetric character of surface waves is important here. Because the slope is greater on the front of the wave than it is on the back, the pattern of Figure 9 indicates a large average tilt tendency of the buoy in the direction of propagation.

These differences discussed relative to the tilt count and the tilt magnitude do not constitute any sort of problem with the data, but rather they display a useful range of information that can be extracted from the same data. Since the accelerometer output signal is always available, it is a trivial matter to detect whether a particular tilt of the buoy is associated with the front or the back of an individual wave crest by the polarity of the accelerometer signal.

6. Conclusions and Suggestions

The application of a single wave follower buoy to determine both the PSD of a wave field and the direction of propagation of dominant wave modes was successfully demonstrated. No attempt was made to exhaustively treat the data gathered in the experiment, but rather to show in simple ways that the data is good. The proposition that a single buoy having the proper pitch-roll-heave properties can be so effective in observing essential wave characteristics has been proven.

The buoy can actually be handled by two men without the aid of lifting gear on the vessel. It can just as well be launched from a small dinghy because of its light weight. The data in this experiment was transferred from the buoy to the recorder on the support vessel by means of an electrical cable containing a wire for each of the four analog signals. There is some extra power required to energize the compass and the two tilt sensors, but there is no reason to prohibit telemetering the data to shore to avoid the need for a support vessel.

As mentioned in the introduction, this paper is the third in a series dated back to the 1975 OTC meeting. The developmental process is continuing, and present efforts are maintaining the focus on buoy deployment during extreme sea events (storms). A control clock has been used which can detect the onset of a storm and adjust the data sample length and period to suit the user. An on-board microprocessor is being designed which can easily pick out such wave parameters as a significant wave height, wave period, etc., to be updated and delivered over the telemeter link. Such features as these can be selected, changed, improved, etc., by simple program changes in the microprocessor. Remote command of an unattended buoy, well off shore, is well within the realm of possibility in the near future.

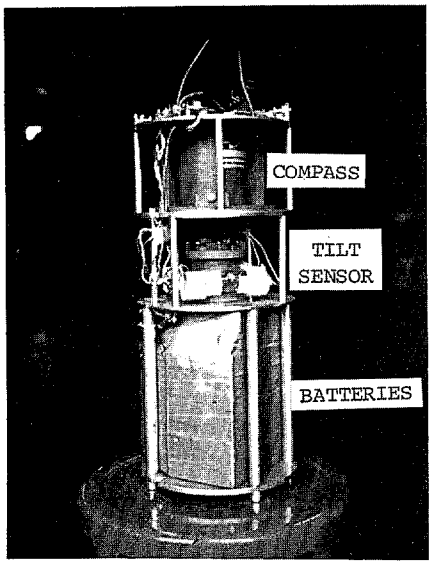

Fig. 1 Buoy Instrument Package

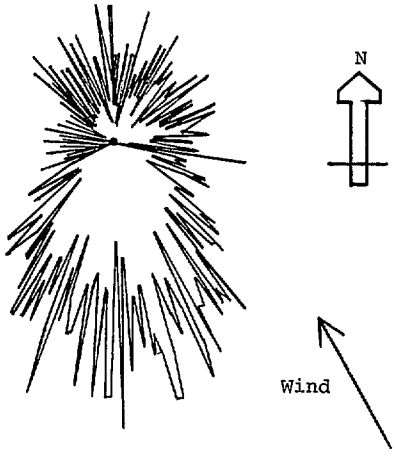

Fig. 2 Polar Histogram Test 1, 1° bins.

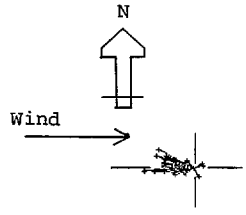

Fig. 3 Polar Histogram Test 2, 1° bins

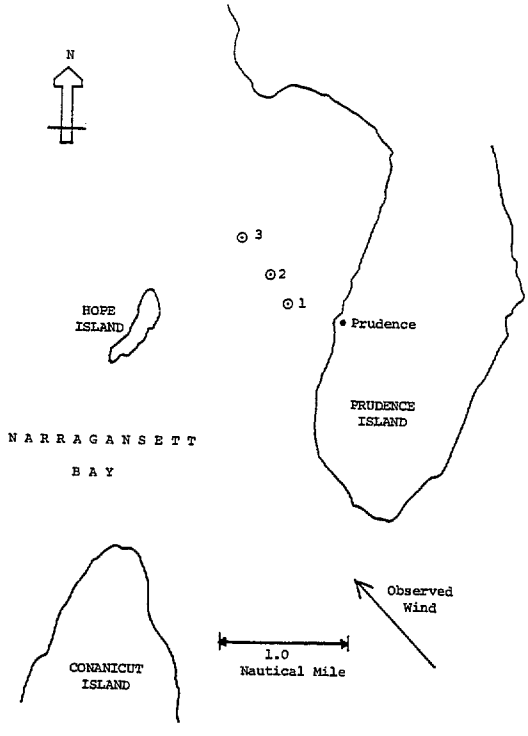

Fig. 4 Test Site

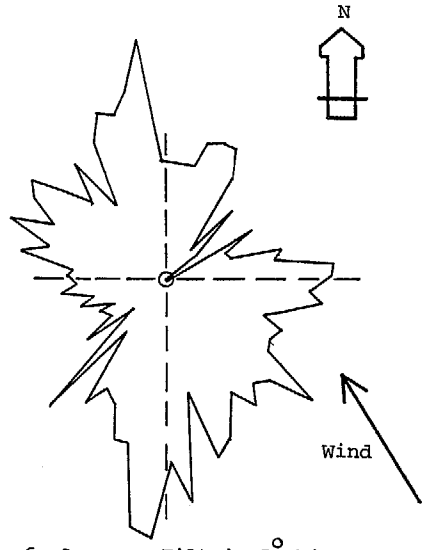

Fig. 6 Average Tilt in 5° bins
1st 5-minute filtered

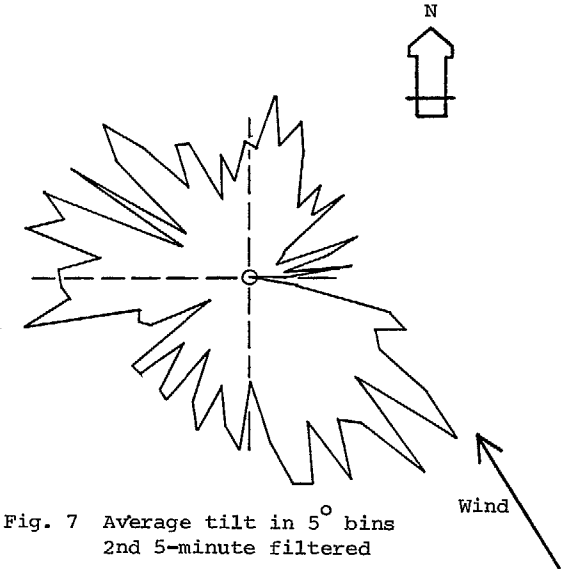

Fig. 7 Average tilt in 5° bins
2nd 5-minute filtered

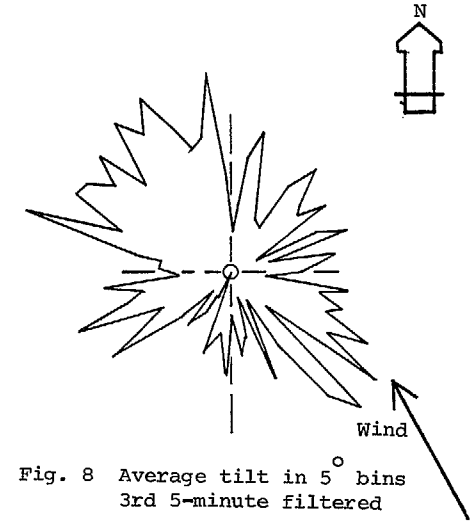

Fig. 8 Average tilt in 5° bins
3rd 5-minute filtered

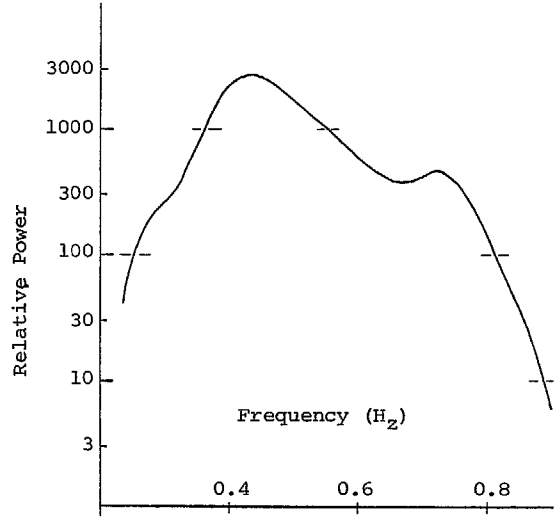

Fig. 5 Wave Height PSD

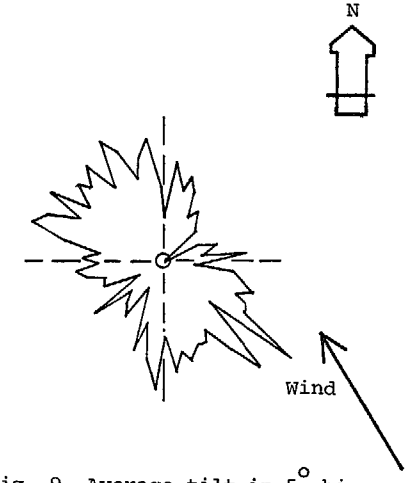

Fig. 9 Average tilt in 5° bins
Total 15-minutes filtered

A DIGITAL SURVEY FATHOMETER® PROVIDING A CHART DISPLAY AND DIGITAL OUTPUT

Mr. J. Russell Hogan
Raytheon Company
P. O. Box 360
Portsmouth, Rhode Island 02871

Abstract

The Digital Survey Fathometer® (DSF-600) is a portable, dual frequency recording depth sounder with a permanent chart display, digital output, and features automatic phase changing of the chart display. Operating at frequencies of 40kHz and 200kHz (frequency switch selected), the DSF-600 provides high resolution, quality bathymetric profiles in water depths to 310 fathoms. By interconnecting it with position finding equipment and a suitable digital tape recorder or data logger, depth and position data is generated in permanent digital form for precision bathymetric survey operations. The DSF-600 system is offered with several options, allowing the user to choose the combination that best meets his surveying needs.

1. Introduction

The DSF-600 Digital Survey Fathometer® is a highly accurate, medium water recording depth sounder with a digital display, specifically designed for precision bathymetric survey operations. Tide, draft, sound speed and depth information can be stored in permanent digital form by interconnection with a digital tape recorder or data logger. A choice of high or low frequencies is available, as well as a combination of the two. Also available are a narrow beam transducer for increased bottom definition, a DC inverter for portable operation and a remote digital depth display for ease of navigation by the boat operator.

The DSF-600 has several features that make it unique in depth sounding equipment:

- TVG Circuitry
- Bottom Acquisition Gating
- Automatic Phasing Mode
- Test Mode

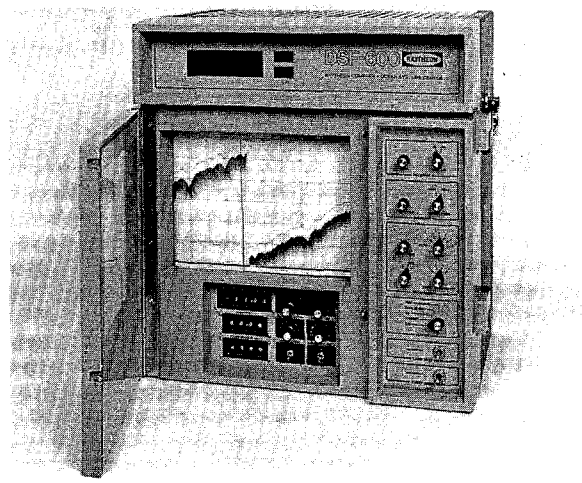

The DSF-600, consisting of an analog chart display and a visual digital display, is capable of highly accurate measurement of water depths up to 310 fathoms or 620 meters, depending upon the model utilized. Raytheon manufactures two versions of the DSF-600, one measuring the depth in feet or fathoms dependent upon a switch position selection, or the other version measuring depths in meters.

The unit operates with a 40kHz or 200kHz transducer depending upon the desired depth and its resolution. The 200kHz transducer operation is limited to 50 fathoms or 100 meters in depth.

Depth information is continuously updated at a maximum rate of 600 soundings/minute and permanently recorded on electrosensitive chart paper. Pulses of acoustic energy are transmitted into the water and depth measurements are based upon the propagation time of the return echoes.

In order to visually and permanently store depth measurements, electrosensitive paper is passed beneath an electrical pen that marks the paper only when electrical energy from the transducer is present. The recorder's electrical marking pen is time synchronized with the pulses of transmitted acoustic energy and with the digital processing circuitry so that return echoes printed on the paper correspond to a specific digitized depth measurement.

The system is fully automatic. The receiver incorporates time varying gain and very little manual gain and threshold adjustments are required after initial set-up. With the phase select switch in the automatic position, phase selection is automatically changed with varying depths. The depths are divided into 6 different range phases for purposes of recording upon the chart display. A range phase is divided into 60 foot or 60 fathom increments. This is delineated later in the paper.

The scale switch selects "feet" or "fathoms" for the depth scale, and also selects the transmitted pulse width. A pulse width of 0.1 millisecond (ms) is used for 0-310 foot depths, while a 1ms pulse width is used for 0-310 fathom range. Probing of deeper depths require more acoustical energy be transmitted, thus a longer pulse is needed.

A detection mode switch selects either the first or peak return echo within an automatically set bottom acquisition gate. The first return (digital) signal is generated at the beginning of the return echo (analog) signal, whereas the peak return signal (digital) is generated when the return echo has reached its maximum signal level. The threshold is adjusted for minimum signal strength required for digital processing.

Other information, such as tide, draft and speed of sound values can be entered digitally via thumbwheel switches so that the depth can be accurately computed for visual and chart display.

Another feature is the shallow water limit setting. Any depth measurement less than the value set for the shallow water limit, will cause an audible alarm to be sounded and the digital display to read zero.

2. System Description

The system is synchronized and initiated from the key pulse signal. This signal is an electrical pulse generated once every revolution of the stylus belt. See Block Diagram, Figure 1. The belt contains a slotted hole, and when it aligns with the keying light and phototransistor, the light signal, converted to current, is amplified and sent to the main electronics card cage to reset the necessary circuitry to initialize operation of the system.

The digital electronics generates all of the vital timing signals essential for proper system performance. A KEY signal initiates operation and time synchronizes the recorder's printing stylus to the system electronics. A start of line pulse, "T_o", is produced from the KEY signal. This signal, which changes its time relation to KEY in accordance with the phase selected, is used to reset the depth counter circuitry. The timing relationship between the KEY and T_o signals are automatically compensated for depending upon the depth range. For example, if the depth being recorded is increasing beyond the limit of the phase that it is printing within, the electronics automatically select the next deeper phase, by generating the transmit pulse earlier with respect to the KEY pulse. See Figure 2, Key Pulse and Phase Timing.

Automatic phasing, as it is called, is discussed later in the paper. The transmit signal, generated from "T_o", is applied to the transmitter card which pulses the transducer causing a burst of acoustic energy to be sent through the water. The transmit pulse will occur simultaneously with "T_o" if both the tide and draft thumbwheels are set at zero. Any tide or draft settings other than zero will cause "T_o" and transmit to occur at different times. If this condition exists, the depth shown in the digital display will indicate the depth beneath the transducers, plus any adjustments made by the tide or draft settings. See Figure 3, Example of the Tide/Draft Adjustment Feature.

Return signals are sensed by the transducer, amplified in the 200/40 TVG receiver, and passed to both filter receiver cards. The frequency in use determines which filter card will amplify. The filtered signal is then amplified in the Post Detection receiver which, effectively, is a low pass filter, rectified to a DC level, and passed to the digital electronics to be digitized and processed. The received signal is also applied to a high voltage print amplifier which boosts the signal up to a level to energize the stylus and print through the chart paper. This event pulse samples a highly accurate depth counter and stores the processed depth information into memory latches.

This depth information is then sent along the data bus to the digital depth display, computer I/O and remote display connectors. Other digital inputs transmitted along the data bus are Draft, Tide and Speed of Sound information. All data is time multiplexed and presented in parallel in BCD format on the bus.

3. TVG Circuit

A unique feature employed is the time varying gain (TVG) circuit. As the name implies, the output gain of receiver circuit is proportional to the elapsed time between the transmitted pulse and return echo signal. The farther the transmitted signal travels in water and, consequently, the return echo signal, the more the echo signal is attenuated. It is known as transmission loss. As distance travelled is directly proportional to the elapsed time, the echo attenuation increases with time. Thus, the TVG circuit compensates for the return echo signal strength.

The transmission loss[1] may be considered as a sum of a loss due to spreading and a loss due to attenuation. The spreading loss varies with range according to the logarithm of range and is expressed in db per distance doubled. Attenuation loss, on the other hand, varies linearly with range and is expressed as db per unit distance.

Knowing the speed of sound in water, the transmission loss in db can be expressed as a function of time as opposed to that of range or distance. Thus, the time differential between the transmitted signal and the return signal corresponds to a specific transmission loss (db). This loss (db) is compensated for in the TVG circuitry by adding the appropriate gain to the input amplifier so that its output signal is at the same level for any depth. For example, a transmitted sound signal takes 100 milliseconds (ms) round-trip to reach a depth of 240 feet (assume 4800 ft/sec speed of sound) and it is assumed the attenuation loss is 65db/kyd, the total propagation loss is 54db. Therefore, the amplifier gain would be set for +54db so as to obtain a 0db output signal.

4. Bottom Acquisition Gate

An automatic bottom acquisition gate is generated from the depth information. This gate is used to lock around and track the depth. Any return signals that fall outside this gate are ignored by the digitizer. If three consecutive transmit signals occur and the depth information received falls outside the auto bottom acquisition gate, the system enters an "alarm" mode which fully opens the gate, allowing for any analog return signal to be processed. The alarm warning buzzer will sound, the selected scale indicator will flash, and the digital depth display will read zero.

During this alarm mode, a bottom acquisition gate will be generated only after three consecutive return signals have been detected and digitized. The width of this gate is determined by the actual depth measurement of the third return signal and the scale and phase selected. Either the first or peak return echo that falls within this gate can be processed.

A bottom reference mark is printed on the chart at a fixed distance above the bottom. It is printed at the lead edge of the tracker gate. The distance mark varies as a function of depth. As the depth increases, the tracker gate becomes wider proportionally.

The phasing can be accomplished manually or automatically. The manual selection of Phase 1 through 6 can be thought of as a back-up operation to the automatic phase mode.

5. Automatic Phasing Mode

Another feature in the unit is the automatic phasing mode. This allows the DSF-600 to operate in a "hands-off" mode and does not require operator assistance after initial equipment turn-on and receive sensitivity adjustment.

The recording chart is divided into six different phases (depth ranges) for purposes of condensing the depth recordings, so that the depth range from 0 to 310 fathoms can be printed. The phase and corresponding depth ranges are tabulated below:

Phase	Depth
1	0 - 60 ft/fms
2	50 - 110 ft/fms
3	100 - 160 ft/fms
4	150 - 210 ft/fms
5	200 - 260 ft/fms
6	250 - 310 ft/fms

Note: (1) Each phase has 10 feet/fathoms of overlap.

(2) Phase and Range are automatically printed on the record.

Each phase has a maximum depth capability. When this maximum value is approached, the depth value will be printing near the bottom portion of the chart paper. If this maximum is exceeded, the system will change phase and the depth value will print near the upper of the chart. The maximum (analog) depth recording of the system is 310 fathoms. See Figure 4, Chart Recording.

As previously discussed in the System Description, the KEY pulse signal synchronizes the printing stylus to the electronics. As the depth range increases or decreases by 60 feet or fathoms, depending upon the position of the scale switch, the phases will change. It is accomplished by generating the transmitting phase pulse early (20ms which corresponds to 50 feet in depth) with respect to the next lower adjacent phase number pulse. See Figure 5, Automatic Phase Timing.

Phase 1 pulse is delayed from the KEY pulse depending upon the setting of a chart zero potentiometer, located on the front panel. In order to compensate for stylus wear, this potentiometer enables the operator to adjust the calibration marks to agree with the preprinted scale marks on the chart paper.

The KEY pulse is generated approximately every 100ms (feet-scale position) or every 600ms (fathom-scale position). For this explanation, "feet" position will be used.

The DSF-600 would be limited to four (4) phases without special circuitry, as Phase 5 transmit pulse would occur close to the previous KEY pulse and sometimes coincident due to the asynchronous condition between KEY and Phase pulses. Phase 5 and Phase 6 pulses are made coincident with Phase 1 and 2, respectively so that the depth range could be expanded. In these two phases (5 and 6), the next KEY pulse is ignored or gated out of the circuits so that the echo return from 310 foot depth (corresponding to 130ms in time from transmit pulse to return echo) can be printed upon the chart display in proper depth position. Note that the Range depth is automatically printed on the record.

6. Display Only Mode

In the event that the water depths exceed the value of 310 fathoms, it becomes necessary to operate the unit in the DISPLAY ONLY mode. This mode is selected when the DSF-600 is to be used just as a digitizer or when depth information exceeds 310 fathoms. The unit has satisfactorily digitized depths in excess of 600 fathoms.

7. Test Mode

The test mode allows the operator to self-test the operation of the digitizer. In this mode, the operator checks the printed calibration marks on the chart paper. Correct operation of all controls can also be verified.

As the phase switch is changed from one phase to another (i.e., Phase 1 to Phase 2 to Phase 3, etc.), preselected depths will be displayed and printed upon the recorder for each of the six phases.

The automatic phasing has a testing procedure also. The AUTO TEST DEPTH potentiometer is turned slowly and depths from 0 to 310 fathoms (feet) can be tested and printed upon the recorder.

8. Performance Capability

The DSF-600 has been building a reputation in the hydrographic survey community for performance. Proof was given during field demonstrations, with conditions established and performance observed by potential users of the equipment.

Those who have observed the DSF in operation include representatives of the Bedford Institute of Oceanography, the Canadian Coast Guard, the U.S. Army Corps of Engineers, Texas Instruments, Inc., the N.O.A.A., and the U.S. Naval Oceanographic Office.

Tests by Bedford Institute were conducted on board one of the "Baffin's" launches. Primary interest was in reliable operation at 40kHz in deep water with vessel speeds of up to 12 knots.

The Canadian Coast Guard's test platform was a 55-foot shallow draft survey boat, and interest is in shallow water channel depth verification at 200kHz. Very fast changes in depth are encountered at the channel's edge, and a prime requirement is that the digitizer should track these slopes accurately. Results of the demonstration showed that the DSF's performance was superior to that of other digital sounders under test.

9. Summary and Conclusions

The DSF-600 has many unique features that other similar equipments do not offer:

- Automatic Phasing
- Bottom Acquisition Gating
- TVG Circuitry
- Self Test Mode
- Reliable operation with a MTBF which can be in excess of 1200 hours.
- Constructed for environmental conditions on ocean-going vessels and open launches (qualified to MIL Spec shock, vibration, temperature and humidity).
- Provisions made for bulkhead, rack or table mounting.
- Housed in one-piece lightweight aluminum cabinet.

Reference

1. Urick, Robert J., "Principles of Underwater Sound", pp. 94.

FIGURE 1. DSF-600 BLOCK DIAGRAM

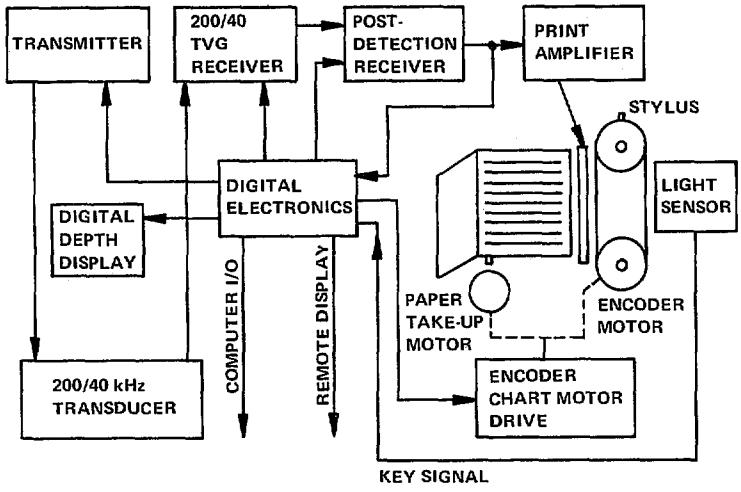

FIGURE 2. KEY PULSE AND PHASE TIMING

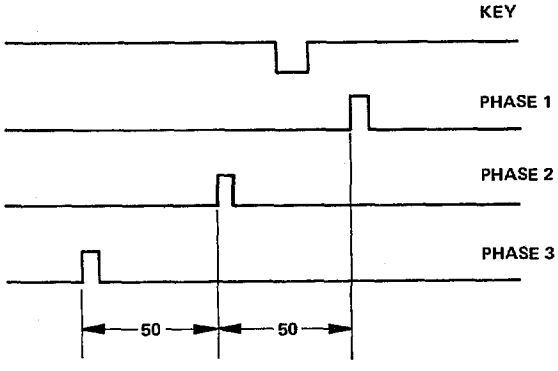

FIGURE 3. EXAMPLE OF TIDE/DRAFT ADJUSTMENT FEATURE

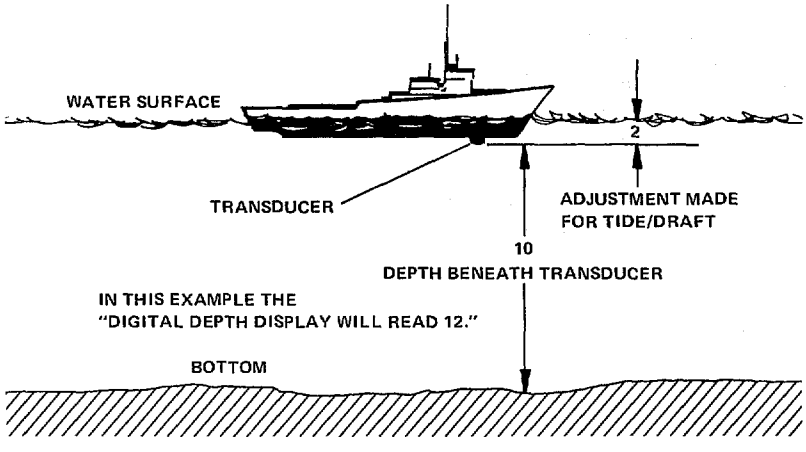

FIGURE 4. CHART RECORDING

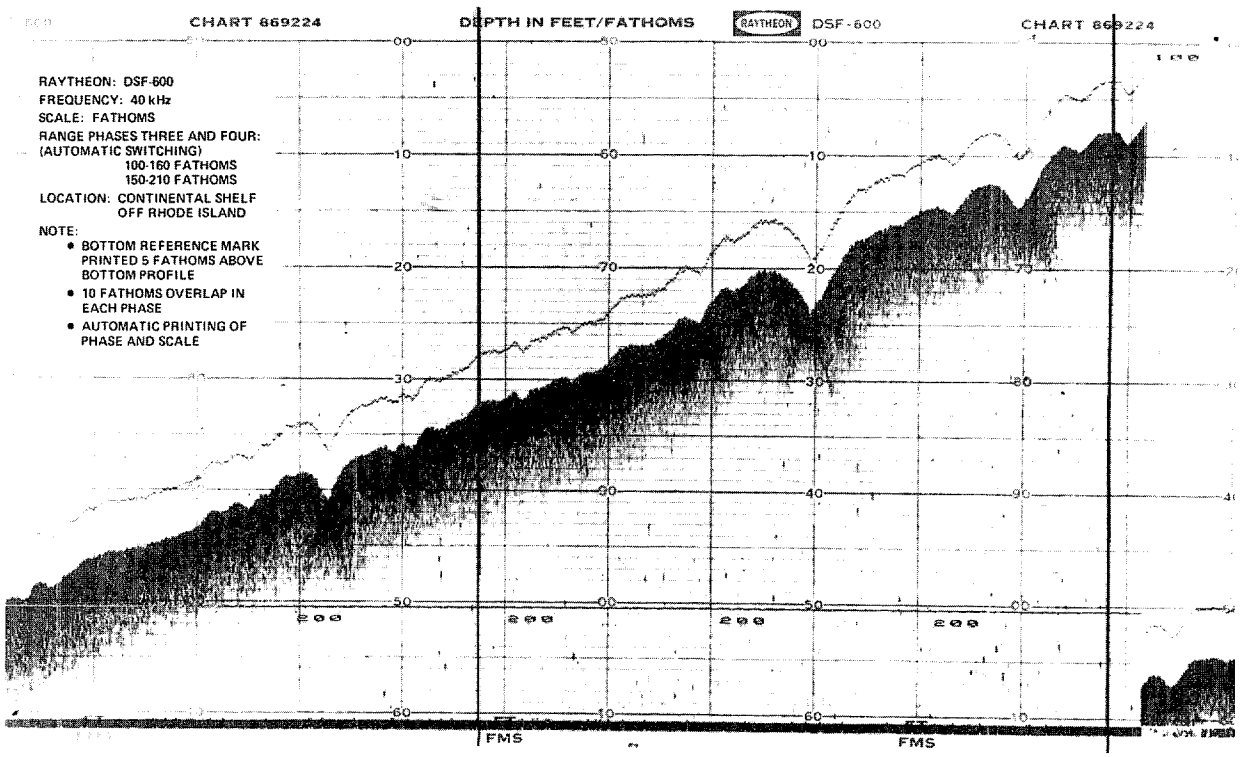

FIGURE 5. AUTOMATIC PHASE TIMING

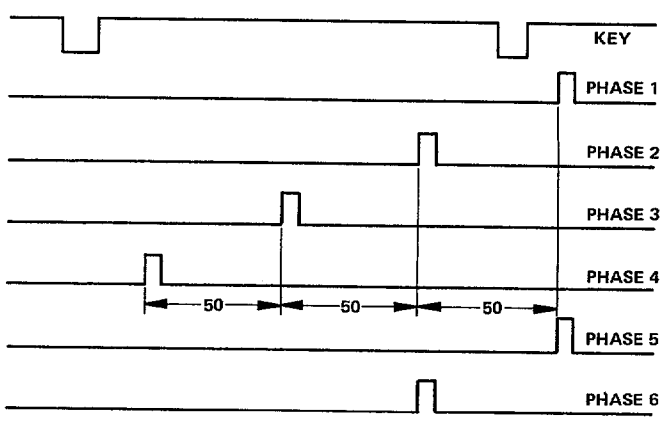

A DETERMINISTIC AND RANDOM ERROR MODEL FOR A MULTIBEAM HYDROGRAPHIC SONAR SYSTEM

Richard D. Angelari, PhD

National Oceanic and Atmospheric Administration
National Ocean Survey C651
Test and Evaluation Laboratory
Sensor Test Branch
Rockville, Maryland 20852

Abstract

The expanding and increasing affluent world population has brought about a growing need for commodities and energy on a global scale. Two major marine activities affected by this are shipping and mining. The shipping industry, because of its up to 30 meter draft superships, and the mining industry (particularly the hydrocarbon sector), both require timely and accurate bathymetric charts for safe and economical operation. To meet these needs the Bathymetric Swath Survey System (BS^3) is being developed. The BS^3 is a 21 beam mapping sonar designed to accurately and efficiently portray the seabed directly beneath and to the port and starboard side of an underway hydrographic ship. This paper examines the effects of four major inherent error sources on system accuracy. These sources are uncompensated ship roll, sound velocity errors, pulse stretching and noise.

1. Introduction

The BS^3 is a 21-beam sonar system designed to measure a swath of ocean bathymetry during hydrographic missions. Figure 1 depicts the swath geometry. Basically, the system operates in two modes, the transmit mode and the receive mode. During one transmit mode, the portside bottom is insonified by an acoustic pulse, followed by a portside receive mode. The receive mode utilizes 11 contiguously directed 5° beams, one vertical beam, and 10 portside beams. The portside operation therefore consists of a total swath coverage of 55°. These operating modes are then repeated for the starboard side. Depth sensed by each beam is determined by measuring the go-return time of the acoustic pulses and transforming this time interval to slant ranges to the bottom. These slant ranges in turn are then translated to depths by a simple trigonometric operation. Errors due to ship's motion and environmental factors are for the most part sensed by the BS^3 signal processing subsystems and corrected for, however, limitations of the sensing elements, electronics, and noise may contribute errors. The establishment of the error bounds due to these sources is the objective of this study.

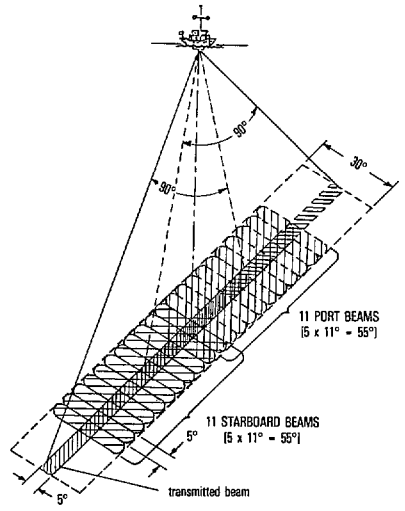

Figure 1. Bathymetric Swath Survey System (BS^3)

2. Error Sources

Error sources will be designated as follows:

Type I error (uncompensated roll error) is that portion of ship roll not sensed by the ship roll sensor (due to its inherent limitations) and therefore uncompensated by the BS^3 processing system. This error will be symbolized by $\Delta\theta_p$.

Type II error (sound speed error) is error resulting from less than perfect estimates of sound speed in water. This error is expressed as a ratio of the measured velocity to true velocity $= C^* = \frac{C \text{ measured}}{C \text{ true}}$.

Type III error (pulse stretching error)

It will be demonstrated in the discussion to follow, although the return echo is time delayed and attenuated, it is not a replica of the idealized pulse, i.e., having infinite slope at its leading and trailing edges. It is, in fact, attenuated and in addition, it is rounded and stretched. This distortion results in delaying the indicated time of arrival of the return echo and is therefore an error source.

U.S. Government work not protected by U.S. copyright.

Type IV error (noise related error) error is similar in effect to pulse stretching error since it causes premature indication (instead of delayed as for pulse stretching) of the pulse arrival time and is therefore considered an error of the same rank. Figure 2a shows a ship's hull together with the necessary geometry to establish the error model. Figure 2b depicts the pulse stretching effect. The inner beam (vertical beam) receives a relatively narrow pulse with relatively straight edges. The outer beam return pulse is much more rounded and stretched. The slope of the leading edge decreases as the pulse width increases. This becomes apparent by the following argument. Consider a beam pointing at an angle θp degrees from the vertical as indicated. θ_{BW} is the beam width angle. The center of the beam strikes the bottom at D, the inner edge at A, the outer edge at C. AB represents a wave front. The inner edge arrives at the bottom first whereas the outer edge does so at some time later equal to the time of propagation along X*. Thus points A&B on the incoming wave front which traveled together at launch time arrive back at the receiver separated from each other by the propagation time to traverse distance 2X. The pulse has therefore been stretched. This stretching decreases the edge slopes of the return pulse.

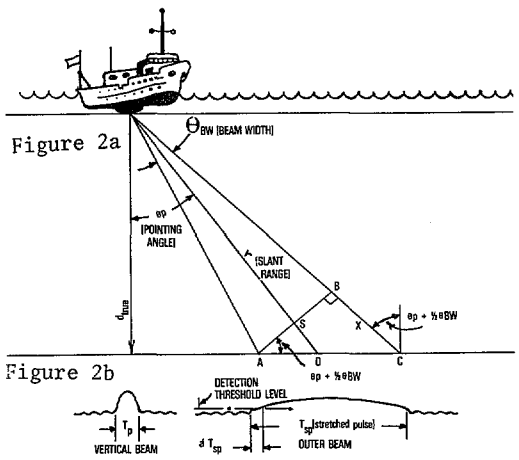

Since the detection threshold level is fixed, pulse detection time will vary as the pulse stretches. As a first approximation, it will be assumed that the error is proportional to the stretched pulse (T_{sp}), i.e., detection time error is ϕT_{sp} where ϕ is a positive fractional number less than 1 and is hereon designated as the timing error coefficient. ϕ can also take on negative values; this follows since the stretched pulse is in a noisy environment and premature triggering can occur if noise peaks exceed the threshold level for any appreciable time prior to the true arrival time of the return echo.

*X represents the distance BC.

3. Mathematical Error Model

Type I, II, III, IV Error Model - Depth error can be expressed as a % quantity as follows:

$$\mathcal{E}\% = \frac{\text{True Depth- Measured Depth}}{\text{True Depth}} \times 100\% \qquad (1)$$

where $\mathcal{E}\%$ is the error in % relative to the true depth.

To establish the contribution to depth error due to error sources, a functional relationship between these sources and depth error in % is desired, that is:

$$\mathcal{E}\% = F\{\Delta\theta_p, C^*, \phi\} \qquad (2)$$

This relationship is: (Angelari [1])

$$\mathcal{E}\% = \left[1 - C^*\left\{\frac{\cos\theta_p}{\cos[\theta_p+\Delta\theta_p]} + \phi\theta_{BW}\frac{\cos\theta_p \tan[\theta_p+\Delta\theta_p+\theta_{BW}/2]}{\cos[\theta_p+\Delta\theta_p-\theta_{BW}/2]}\right\}\right] \times 100\% \qquad (3)$$

Equation (3) is the mathematical error model for the BS^3 system having Type I, II, III, and IV. error sources.

4. Error Analysis

Deterministic versus Random Error Sources:

Central to the analysis are the concepts of deterministic phenomena and random phenomena. Deterministic phenomena are those that can be described by an explicit mathematical relationship. Random phenomena are those that can be described only in terms of probability statements and statistical averages.

The error model, Equation (3), may represent either deterministic or random system error depending on the nature of the error sources. If the error sources $\Delta\theta_p$ C^*, and ϕ are deterministic then this equation is the BS^3 Deterministic Error Model (DEM). If the sources are random then this equation represents the Random Error Model (REM). Both types may exist simultaneously, for this reason both will be considered in this study.

Estimates of the expected ranges of error sources are:

$\Delta\theta_p = \pm 1°$ to $\pm 3°$

$\phi = \pm 0.1$ to ± 0.3

$C^* = 1 \pm .01$ to $1 \pm .02$

These will be denoted as the specified error sources (SES) and will be designated as follows:

$\Delta\theta p = \pm 1°$, $\phi = \pm 0.1$ and $C^* = 1 \pm .01$ "1o error" SES

$\theta p = \pm 3°$, $\phi = \pm 0.3$ and $C^* = \pm 1.02$ "hi error" SES

The SES will first be considered as deterministic errors and will be used in the DEM analysis to follow. For the REM analysis "lo error" (i,e., $\Delta\theta p = \pm 1°$, $\phi = \pm 0.1$ and $C^* = 1.01$) will be specified as the statistical descriptors and represent the 1σ values for the uncompensated roll, sound velocity, pulse stretching and noise error sources.

5. Deterministic Error Model

Plots of the error model (eq 3) for ranges of error source magnitudes will be informative. To decrease the number of plots the outer beam $\theta_\psi = 50°$ and the inner beam $\theta_\psi = 0°$ only will be plotted and only the maximum roll specified for the BS^3 (20°) will be treated. Thus a total of four pointing angles will be considered. These are shown in Table I.

Table I

POINTING ANGLES EVALUATED IN THIS STUDY

1. $\theta p = 0°$ vertical beam
2. $\theta p = 20°$ (vertical beam + 20° roll)
3. $\theta p = 50°$ outer beam
4. $\theta p = 70°$ (outer beam + 20° roll)

Plots of the BS^3 system model error due to the SES are shown in Figures 3 through 8, $\mathcal{E}\%$ is plotted along the ordinate, $\Delta\theta p$ along the abscissa, ϕ as a parameter and for fixed values of C^*. The rhomboids in these figures delimit the error bounds for "lo error" (mnop) and "hi error" (rstu) sources.

6. Discussion of Error Curves

Case 1. The 50° beam with + 20° roll, ($\theta p = 70°$.) $C^* = 1.00$ (Figure 3)

Figure 3 is the error diagram for the outermost beam ($\theta_\psi = 50°$) with a positive 20° roll, i.e., $\theta p = 70°$. In addition, it is assumed here that the sound speed has been correctly estimated, i.e. $C^* = 1.00$. The rhomboid mnop represents the operating error region for "lo error", i.e., for $\Delta\theta p = \pm 1°$ and $\phi \pm 0.1$. From this diagram it is concluded that the measured depth error will not be greater than between 6.7% positive (point n) or 7.8% negative (point p) for "lo" excursions. Thus a true depth of 100 feet would be indicated as being anywhere between 93.3 feet and 107.8 feet. For "hi error," $\theta p = \pm 3°$, $\phi = \pm 0.3$, the range of error is between 17.9% (s) and approximately -30% (u). For this case the true depth would be indicated as being anywhere between 82.1 feet to 130 feet. Clearly the more serious errors are the ones having the greatest negative magnitudes since hazards at the true depth could be indicated to be deeper than they are, i.e., 100 feet true depth may be indicated to be 130 feet deep. The diagram also shows that for 50% of the time the excursion is in the negative regions (3rd and 4th quadrants) meaning that the more serious type error is as probable as the less serious (positive regions) error. Point q is the quiescent operating point and represents a bias due to error in estimating sound velocity with no other sources present. In this case, since the estimate of sound speed was correct, the static system bias error is zero.*

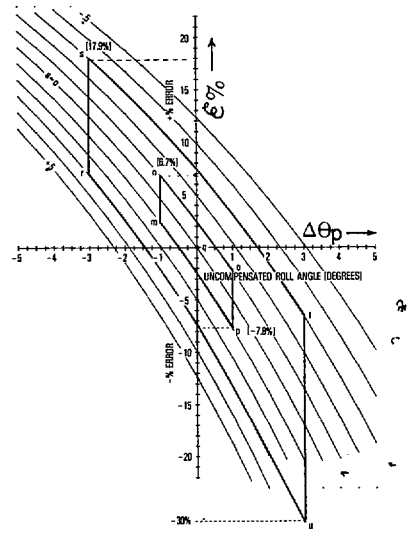

Figure 3 $\theta p = 70°$, $C^* = 1.00$

Case 2. The Vertical Beam with 0° Roll, $\theta p = 0$, $C^* = 1$ (Figure 4)

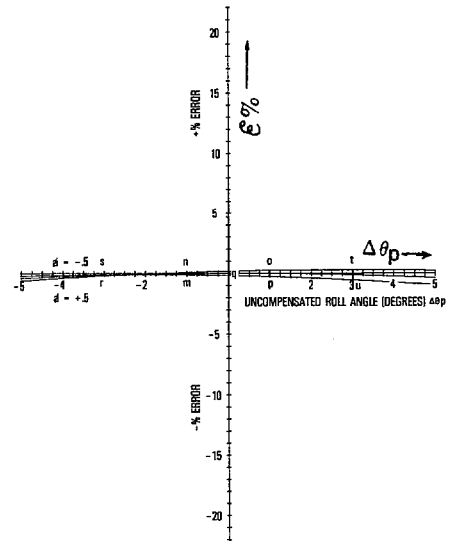

Figure 4 $\theta p = 0$, $C^* = 1.00$

θ_ψ is the fixed array beam angle, θp is the pointing angle

* It is not meant here that the BS^3 error is zero when $C^* = 1$ but rather the MODEL bias error is zero. It is expected that an overall system bias error exists and will show itself when the BS^3 field tests are completed.

The rhomboid area has diminished greatly indicating a greatly reduced error mode of operation. This is to be expected since the return echo in the vertical beam experiences the least pulse stretching (see Figure 2b). Note that for this case the system error is almost independent of the magnitude of $\not{d}$. The maximum error, (for "hi error") is less than +0.5%. The rhomboid degenerates to a point (the q point) for $\not{d}$=0 and $\Delta\theta p$=o and since C*=1 (for this case) $\mathcal{E}$% is zero, i.e., an errorless system.

Case 3. The vertical beam with 20° roll i.e., θp= 0° C*=1.00 (Figure 5).

The rhomboid area has increased such that "lo error" and "hi error" are approximately ±1% and ±2% respectively.

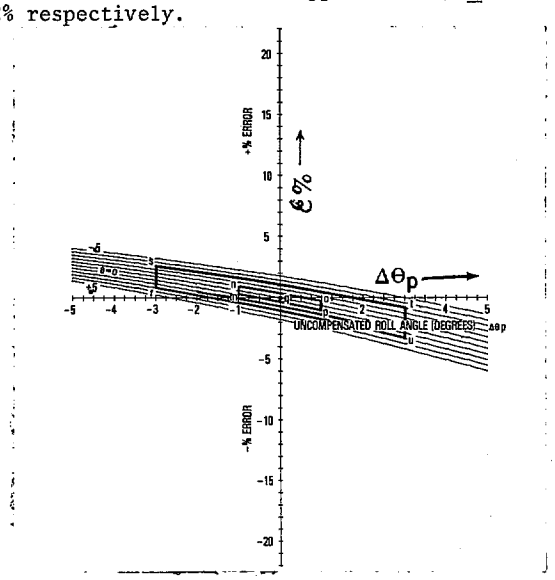

Figure 5 θp=20°, C*=1.00

Case 4. The 50° beam with 0° roll i.e., θp=50°, C*=1.02 (Figure 6).

This figure depicts system error with 0° roll and an overestimation of sound speed of +2%. The quiescent point has shifted negatively by 2% this is a systematic error. The "lo" rhomboid is now almost entirely in the negative quadrants, this is the most undesirable error since this would indicate a potential hazard to be deeper than its true depth.

Case 4. The vertical beam with 0° roll, C*=1.02 (Figure 7).

The rhomboid are significantly decreased, the quiescent point is again at -2%. Uncompensated rolls of magnitude up to 3° contribute little error, here again this is due to the near negligible effect on the vertical beam of pulse stretching as previously discussed (Fig. 2b). Figure 7b shows the biasing effect in the vertical due to error in estimating sound speed by ±5% (C*=1±.05). The case for 0% error (C*=1.00) is included for emphasis.

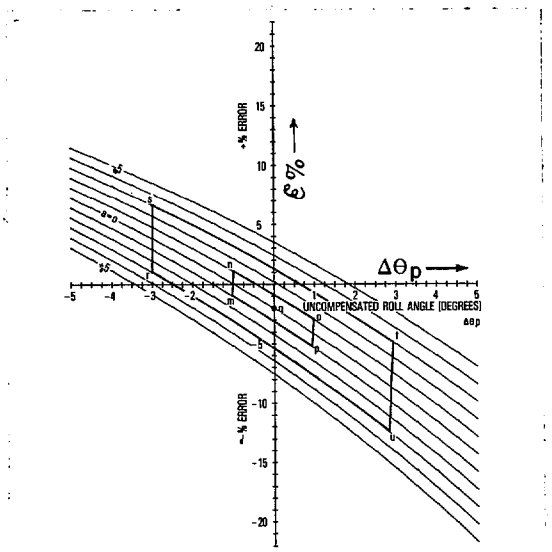

Figure 6 θp=50°, C*=1.02

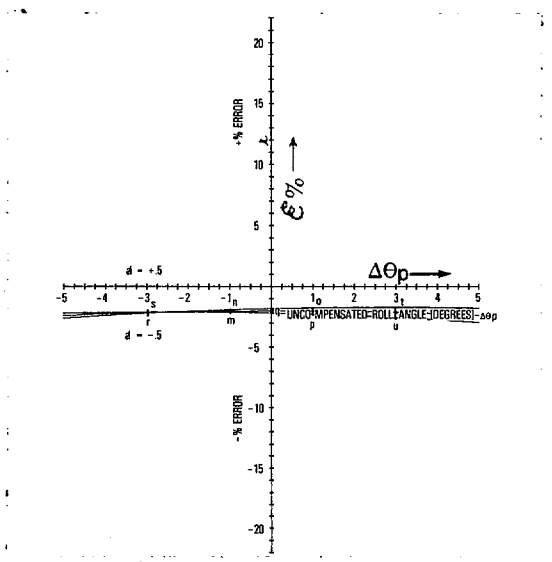

Figure 7a θp=0°, C*=1.02

A passing note is made to indicate the role played by the beam-width angle Θ_{BW} As can be verified by reference to equation (3), a reduction of beam-width from the present 5° to 1° will reduce sensitivity to $\not{d}$ (pulse stretching and noise effect). This in effect would have a marked improvement on system performance. Since decreased beam-width requires larger transducer elements, among other factors, a trade-off study would be necessary should such an improvement be sought. The highlighted rhomboid (Figure 8) represents "lo error" region for the outer beam with 20° roll (θp=70°) C*=1 00 and θ_{BW} =1°. This figure represents the same magnitude error sources of figure 3 but with a 5 to 1 reduction in beam-width (i.e. from 5° to 1°).

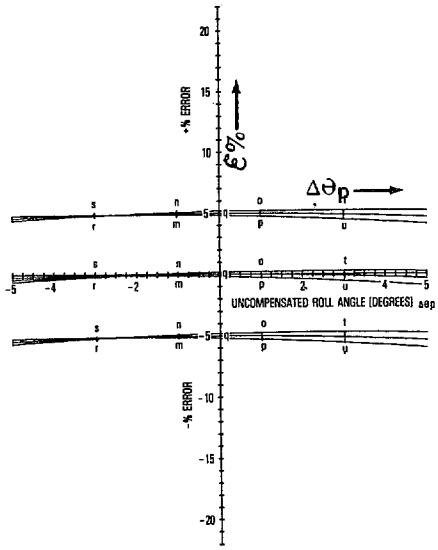

Figure 7b θp =0°, C*-1.00, 1.05 and 0.95

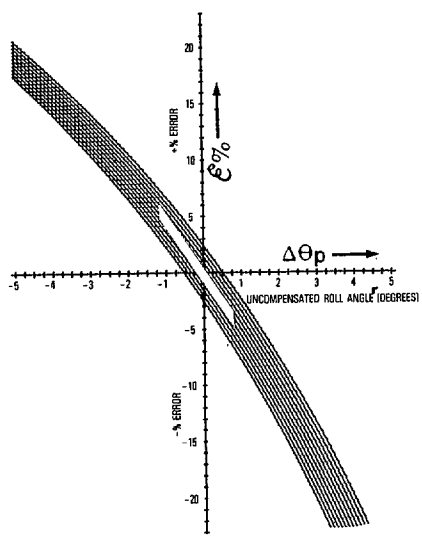

Figure 8 Effect of decreasing beamwidth from 5° to 1° for the outermost beam with θp =70°, C* =1.00 (compare with Figure 3)

Figure 9 is a graphical display (in bar-line graph form) summarizing the salient information of this study. This figure displays the following information for θp=70°, 50°, 20°, and 0° for C*=1.02, 1.01, 1.0, 0.99, and 0.98.

1. The location of the operating point q (dot)

2. The error in % of true depth due to a variation in $\not{a}$ and θp, for "lo error" (bar ends)

3. The error in % of true depth to a variation in $\not{a}$ and θp, for "hi error" (line ends)

4. The operating area in the upper (clear areas) and lower (shaded areas) regions.

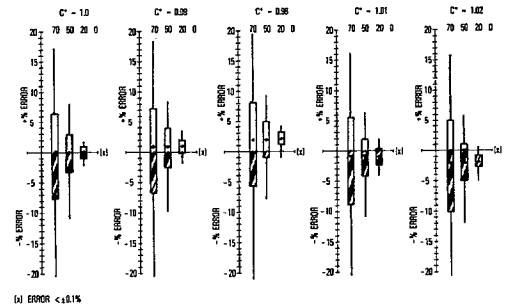

Figure 9 Bar-line graph summarizing "lo","hi" error ranges . The dot represents the quiescent operating point (q point)

V. Random Error Model

For this model the error sources $\Delta\theta p$, $\not{a}$ and C* will be considered random variables normally distributed with zero mean and standard deviations equal to the SES "lo" error values. Formally stated this becomes:

$$\Delta\tilde{\theta}p = N[0, \sigma^2_{\Delta\theta p}] = N[0, (1^\circ)^2]$$
$$\tilde{\not{a}} = N[0, \sigma^2_{\not{a}}] = N[0, (0.1)^2]$$
$$\tilde{C}^* = N[0, \rho^2_{C^*}] = N[0, (1)^2]$$

(where a tilda (~) indicates a random variable) Equation 3 may now be replaced by the corresponding random error model.

$$\mathcal{E}\% = \left[1 - \tilde{C}^* \left\{ \frac{\cos\theta p}{\cos[\theta_p + \Delta\tilde{\theta}_p]} + \frac{\tilde{\not{a}}\,\theta_{Bw}\cos\theta p \,\mathrm{TAN}[\theta_p + \Delta\tilde{\theta}_p + \theta_{Bw}/2]}{\cos[\theta_p + \Delta\tilde{\theta}_p - \theta_{Bw}/2]} \right\}\right] \times 100\% \quad (4)$$

The probability density function (pdf) $f_{\mathcal{E}}(\mathcal{E})$ corresponding to 4, once found will completely describe the REM. Unfortunately, the density function may be very difficult or even impossible to determine directly from Equation 4. Equation 4 will be expanded about the zero point as a truncated Taylor series, a more tractable expression results, for small error excursions this becomes

$$\varepsilon\,(\Delta\tilde{\theta}p, \tilde{\not{a}}, \tilde{c}^*) = p\Delta\tilde{\theta}p + q\tilde{\not{a}} + r\tilde{c}^* \quad (5)$$

where now θp, $\not{a}$ and C* are realizations of the rvs and represent small excursions and

$$p = \frac{\partial\varepsilon}{\partial\Delta\theta p}^{@} \quad (5a)$$

$$q = \frac{\partial\varepsilon}{\partial\not{a}} \quad (5b)$$

$$r = \frac{\partial\varepsilon}{\partial c^*} \quad (5c)$$

are partial derivatives and for small excursions

@ the tilda (~) will be omitted it is understood we are dealing with random variables (rvs)

are essentially constant. These partials are derived directly from Equation 4. A tabulation of p, q, and r for each of the 11 pointing angles is given in Table II.

Table II

$\theta p°$	p	q	r
0	0	-0.38	-1.00
5	-0.15	-1.15	-1.00
10	-0.31	-1.92	-1.00
15	-0.47	-2.72	-1.00
20	-0.64	-3.56	-1.00
25	-0.81	-4.46	-1.00
30	-1.01	-5.43	-1.00
35	-1.22	-6.50	-1.00
40	-1.46	-7.72	-1.00
45	-1.75	-9.13	-1.00
50	-2.08	-10.82	-1.00

Since a linear combination of Gaussian terms is itself Gaussian,

$$\varepsilon(\%) = N\left[\mu_{\varepsilon}(\%), \sigma^2_{\varepsilon}(\%)\right] \tag{6}$$

where $\mu_{\varepsilon}(\%) = 0$ (7a)

$$\sigma^2_{\varepsilon}(\%) = p^2\,\sigma^2_{\Delta\theta p} + q^2\,\sigma^2_{\phi} + r^2\sigma^2_{c*} \tag{7b}$$

The two descriptive parameters $\mu_{\varepsilon}(\%)$ and $\sigma^2_{\varepsilon}(\%)$ completely define the REM. Thus, probability of the BS^3 error being between $\pm\delta$ is:

$$P\left[-\delta(\%) \le \varepsilon(\%) \le \delta(\%)\right] = \frac{1}{2\pi\sigma_{\varepsilon}(\%)}\int_{-\delta(\%)}^{+\delta(\%)} \exp\left[-\frac{\varepsilon^2(\%)}{2\sigma^2_{\varepsilon}(\%)}\right] d\varepsilon(\%)$$

Integral (8) is a well tabulated function and may readily be evaluated. However, a more convenient method is to evaluate it graphically using normal probability paper. As an example consider the error predicted by the REM when the outermost beam angle is pointing at 50°, i.e. $\theta p = 50°$. From Table II:

$$p = -2.08$$
$$q = -10.82$$
$$r = -1.00$$

Substituting into Equation 7b

$$\sigma^2_{\varepsilon}(\%) = (-2.08)^2[\,1°\,]^2 + (-10.82)^2\,[0.1\,]^2 + (-1)^2\,[\,1\,]^2$$

(the quantities in the square [ ] brackets are the "1σ" SES)

from which $\sigma^2_{\varepsilon}(\%) = 6.59$

or $\sigma_{\varepsilon}(\%) = 2.75$ I

also $\mu_{\varepsilon}(\%) = 0$ II

Figure 10 is a plot of the REM (equation 4), it is seen that the 50° beam when pointing at 50° may be in error by up to ±5.2% of depth at 95% CL. Similarly, the vertical beam, $\theta p = 0°$, may be in error by ±1.9% of the true depth at the 95% CL. $\theta p = 10°$, 20°, and 30° plots are also shown. Intermediate pointing angle error plots may be established by calculating ε% using Equation 7b and values of p, q, and r for the desired θp. The plots also indicate the 1σ error values.

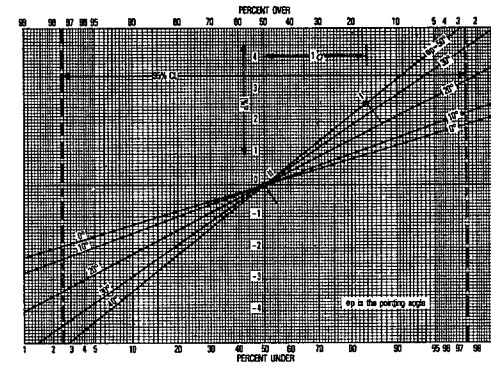

Figure 10 Plot of the REM on probability paper

8. Conclusions and Recommendations

Two error models for the BS^3 have been developed. Either one or both may apply depending on whether the error sources are primarily deterministic or random or both. If the sources are deterministic then the accuracy and precision of the BS^3 may be markedly improved through calibration and corrective processes. If the sources are random then only statistical bounds may be defined for the system i.e., accuracy may be specified at any desired confidence level.

It should be borne in mind that, although four error sources considered in this study are major sources, other sources are present and can only serve to further degenerate system performance. These other sources are believed to be minor so that their contributions are believed to be small. Since the specified error sources (SES) magnitudes given in Section 4 are estimates, laboratory/field measurement experiments designed to establish the ranges/statistics of the error sources are recommended.

Acknowledgement

The author would like to thank Mr. Richard Ribe of NOAA's Test and Evaluation Laboratory for evaluating the partials p, q, and r (eq 5a, 5b, 5c) and for generating Table II.

References

[1] Angelari, Richard D. (National Ocean Survey, National Oceanic and Atmospheric Administration, U.S. Department of Commerce, Rockville M.D.) 1978 "System Error Model of the Bathymetric Swath Survey System (BS^3)" 77pp (unpublished manuscript)

PORTABLE ACOUSTIC TRACKING SYSTEM (PATS)

Robert W. Gill
Applied Physics Laboratory
University of Washington
1013 N.E. 40th Street, Seattle, WA 98105

William C. Gardner
Naval Facilities Engineering Command
Chesapeake Division
Washington Navy Yard, Washington, D.C. 20390

Abstract

A portable acoustic tracking system has been developed for the Navy to track underwater construction teams in water depths to 300 ft. The tracking system can be deployed and operated by the divers and is intended for use in remote areas and for nearshore survey, maintenance, and construction work. A self-calibrating system provides a geographically justified track for up to eight divers. Diver position coordinates are computed from acoustic measurements at periodic intervals and displayed for control purposes. The positions are also recorded for future reference.

System Requirements

The basic requirements governing the design and construction of PATS were that the system be portable and readily usable at remote field sites by Navy underwater construction teams. Specifically, PATS was designed:

(a) to be deployable from boats as small as 20 ft in length

(b) to be capable of continuously tracking up to eight targets simultaneously

(c) to contain no single subassembly with a weight greater than 60 lb

(d) to be suitable for operation in water depths of up to 200 ft

(e) to be suitable for use in a relatively noisy nearshore environment

(f) to have a range of approximately 1 mi

(g) to have a circular probable error of 5 ft

(h) to include plotting equipment to provide a permanent record of target track

(i) to be suitable for immersion periods of 60 days on station

(j) to include a radio frequency link which would permit monitoring, plotting, and controlling the system at points up to 5 mi from the tracked object

(k) to include nonmagnetic, diver-carried acoustic transponders.

Operation

The deployment and utilization of the PATS, as conceived, will generally proceed as follows. The PATS, along with the members of the underwater construction team, will be deployed to the work site where the system will be removed from portable shipping containers. The PATS receiving/plotting modules will be set up either on the beach or aboard a diver-support platform. The portable tracking array, complete with cable and surface buoy, will be loaded aboard a small, maneuverable boat such as a Zodiac or Boston whaler, and taken to the deployment site. The array will then be lowered to the sea floor by its own electromechanical umbilical cable. After the array has been implanted on the sea floor and a surface buoy with a radio frequency transmitter has been deployed, the small boat, with a pinger attached, will traverse over the array while being tracked from shore by either a radio frequency positioning system or theodolites. Once the array's center and orientation have been established with respect to geodetic bench marks or major landmarks, the divers can begin work. Each diver will carry a synchronous pinger attached to a backpack (see Figure 1).

Suppose that the divers are searching for a cable, pipeline, or other object. They will be continuously tracked, and the track will be plotted in X-Y coordinates as well as depth. Once the object has been located, the divers will toggle a "mark" switch on the pinger assembly which will cause the plotter to annotate the recording. As the divers follow the contour of the object, they will continue to toggle the "mark" switch at each significant feature. In this way, the path or contour of the object will be mapped. The scale on the X-Y plotter can be selected to match the scale of charts or maps of the area so that the completed recording can be overlayed directly on the chart.

Figure 1. Diver with backpack unit.

In situations where a buried cable is being tracked, the divers will use PATS in conjunction with underwater magnetometers. PATS will contain chargeable batteries which can be changed on site to accommodate lengthy operations. Upon completion of the underwater task, two people aboard a small boat will retrieve the surface buoy and array for replacement in the transportable shipping containers.

System Description

The PATS system allows the positions of up to eight divers to be accurately determined at intervals as short as 1 s. The Cartesian X,Y,Z coordinates are listed on a line printer, and the positions are displayed on an analog plotter and on a liquid-crystal display; this display can also show the positions in polar coordinates (range and bearing) for guiding the divers within the tracking volume.

The system employs synchronous tracking. In such a system, a tracking projector emits a pulse at a precisely known time. If the sound velocity in the medium is known, measurement of the acoustic transit time to receiving transducers in a tracking array allows an accurate determination of range. These transit times will be referred to as timing numbers. If the locations of the receiving transducers are known in some coordinate system, the position of the tracking projector can be determined in that coordinate system. This requires measurement of the time (range) from the tracking projector to three or more separated transducers. Three transducers can determine the position except for the image ambiguity (i.e., the location above or below the plane of the transducers); addition of a fourth transducer resolves that ambiguity.

The PATS system accomplishes its objectives through the interaction of three major subsystems (see Figure 2):

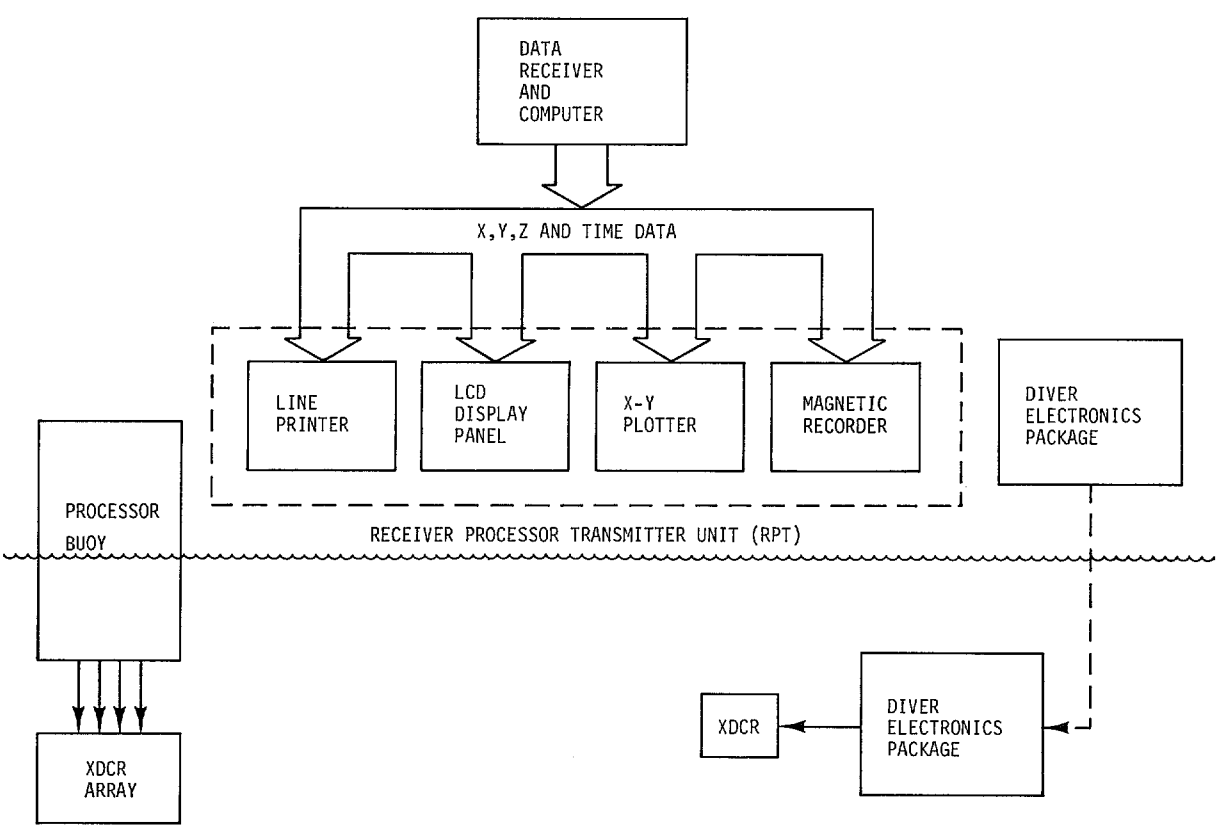

Figure 2. Block diagram of underwater electronics.

(a) a tracking array containing a microprocessor and acoustic and radio telemetry systems

(b) a receiver-processor-transmitter (RPT) unit containing synchronizing, display, and computation systems

(c) diver units containing synchronous acoustic transmitters.

Each of these systems is operated by detachable, rechargeable batteries. Time for array deployment or retrieval is about 1 h. Battery power is sufficient for about 24 h of continuous operation of the RPT unit and the tracking array, and 8-h operation of the diver unit. An external battery can be used to extend the operation of the tracking array.

The underwater tracking portion of PATS (Figure 3) consists of two bottom reference transducers and a floating tracking array of four buoyant, subsurface transducers deployed in the form of a square with 250-ft sides. The two transducers on opposite corners of the square are about 40 ft higher than the others, forming four "tilted" triangles. This configuration allows the resolution of the image ambiguity. The two reference transducers on the bottom are about 750 ft apart, one on each side of the square.

The PATS tracking cycle consists of 10 subcycles, each approximately 1 s (1.048576) in length. During the first subcycle, 250-kHz "survey" pulses are transmitted, in turn, from each tracking transducer. In this way, the shifting positions of the buoyant tracking transducers are updated every 10 s. The next eight periods are reserved for transmissions from the diver units. A different diver unit may transmit in each period, the same unit in all periods, or any other combination; the diver units must be preset to these conditions before water entry. The last period contains sequential transmissions from both ground reference transducers.

The diver units transmit at 31.25 kHz. The transmissions consist of a 1.024-ms pulse for tracking purposes followed by a pulse that is delayed in proportion to the output of a depth transducer. This allows an accurate depth measurement at extreme ranges where the normal depth calculation would be degraded due to multipath propagation. To mark a specific spot on his track, the diver depresses a switch that elongates the tracking pulse to 4.096 ms. Emergency conditions are indicated by locking this switch down, which elongates both the tracking pulse and the depth pulse.

The acoustic receivers incorporate automatic gain control (AGC) so that the receiver gain is always the maximum possible in the particular noise environment, and a time-varied gain so that transmissions from divers slightly beyond the 1.048576-s period will not affect the following period. The PATS design goal was a signal-to-noise ratio of 26 dB at the receiver. The transmitting level of the diver unit is 190 dB re 1 μPa at 1 m. At 2000 yd, for example, the approximate transmission losses would be 11 dB for absorption and 66 dB for spreading; the signal level at the tracking transducer would thus be 113 dB re 1 μPa. This means that the level of the background noise within the bandwidth of the receiver must be less than 87 dB re 1 μPa. Some representative ambient source levels within the 2-kHz bandwidth of the tracking transducers are:[1]

Beaufort wind-force 4.....30 dB
Sea state 3.....41 dB
Moderate precipitation.....76 dB

A "moderately moving" small boat emits about 67 dB; therefore, the support boat can be as close as 300 yd from the tracking transducer, even when the divers are at maximum range.

It was assumed that the divers would operate, at most, 1 h after synchronization; therefore the oscillator stability requirement is ±3 parts in 10^7. The azimuthal error depends on the frequency and the baseline of the tracking transducers. At 31.25 kHz, a baseline of, say, 167 ft would result in an error of 5 ft at 5000 ft from the transducer. Because of acoustic considerations, it was decided to use buoyant transducers located at mid-depth. The use of buoyant transducers necessitated the continuously updated calibration survey.

Diver Unit

To allow divers to swim over cables with an operational metal detector (such as the Mk 14 ordnance locator), the diver unit had to be as nonmagnetic as possible. Therefore, plastic encapsulated transistors, a plastic-encased oscillator, air-core transformers, and gel-cell batteries were used. The unit weighs 12 lb in air, and is 2 lb negatively buoyant, 26 in. long, and 4 in. in diameter. Although the "mark" switch requires pressing, it is on a cord at the diver's wrist so that the diver is essentially hands free.

The battery provides about 8 h of operation and is detachable to allow charging. The diver unit must be connected to the RPT unit to be turned on or off or synchronized. To protect the pinger, the diver assembly contains a pressure transducer that reduces the power when the water depth is less than 6 ft. The diver unit is housed in a clear, plastic (Lexan) cylinder to allow monitoring of the switches that control the transmission period, a neon light that indicates the transmitter is transmitting, and a liquid-crystal display of a number of internal parameters.

In normal operation, the array and RPT would be activated approximately 1/2 h before the dive. At this time, the RPT is synchronized to the array and the diver units turned on and synchronized to the RPT. Feedback from the diver unit allows monitoring of synchronization drift. The diver unit can be hung from the side of the boat for a position check. System operation is now fully automatic.

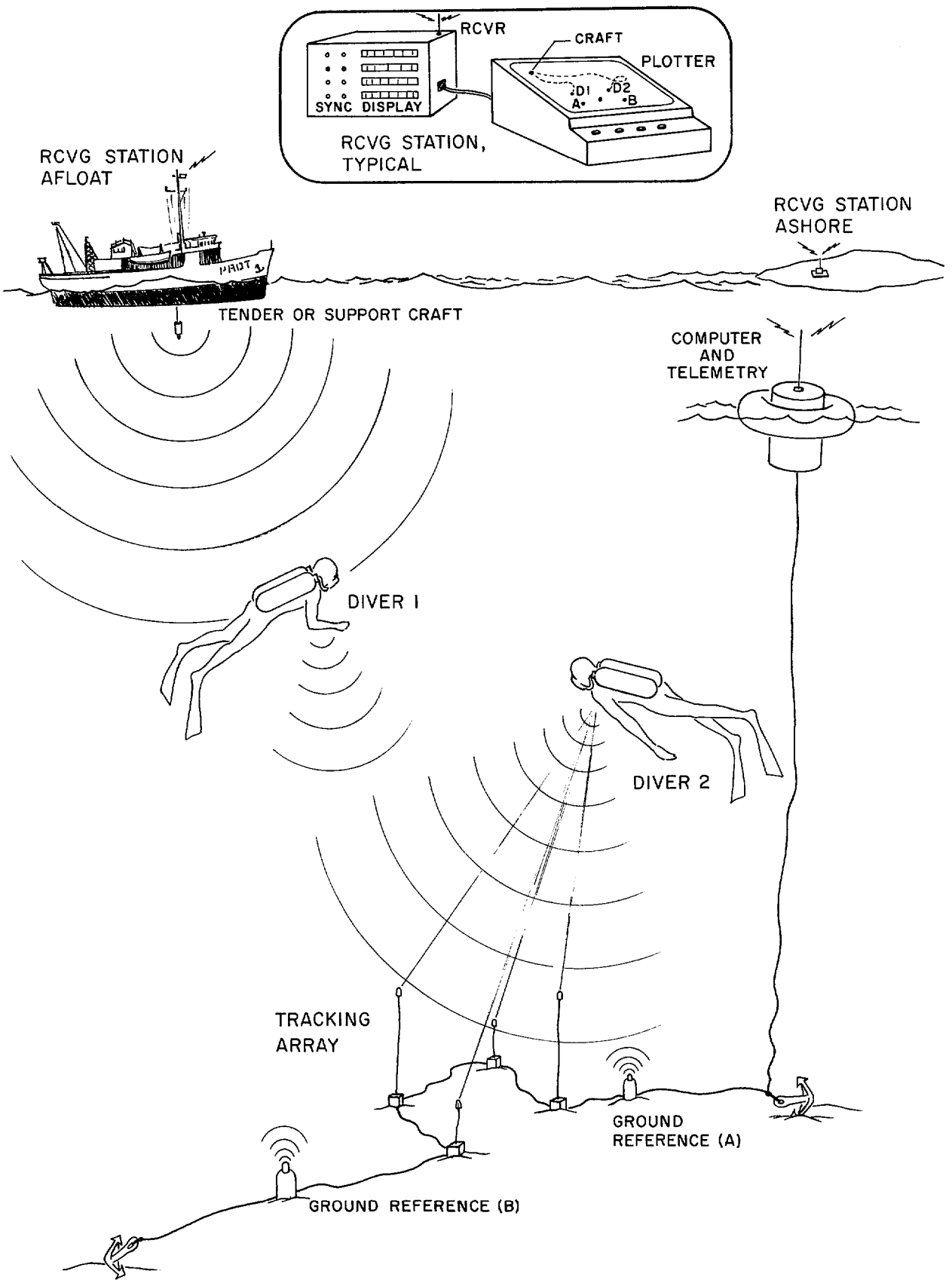

Figure 3. Artist's sketch of system.

Tracking Array

The original concept was that almost all of the computational ability would be located in the tracking array. However, the size of the survey and tracking programs became larger than expected, increasing the current drain because of the added programmable read-only memories (PROMs). Further, it was thought that, at least in the first version, the more complex parts of the system should be easily accessible. Therefore, the survey and tracking programs were moved to the RPT unit. The recent availability of low-drain PROMs and microprocessors will allow a return to the original concept when the system no longer requires modification.

The microprocessor portion of the array electronics is based on the Intel 8080.[2] This is an eight-bit parallel processor with instruction times between 4 and 20 μs at our clock rate of 1 MHz. The microprocessor can run at a clock rate of 2 MHz, but a slower rate allows the use of CMOS gating and logic, which reduces the current drain. The limiting factor for the current drain now is the RF transmitter which draws 4 W and has a 50% duty cycle.

A precision, 4-MHz, temperature-compensated oscillator provides the drive for a binary timing chain. The resulting period is 1.048576 s. Some thought was given to using decade counters so that the period would be exactly 1 s and could be synchronized with WWV of the National Bureau of Standards. It was decided, however, that the storage of the additional data would overburden the system. The period is divided into 65,536 parts by representing the timing number with a 16-bit digital number. The resolution of the timing number is thus about 16 μs, or 2 in. in water, so that the system resolution is limited by the acoustic jitter. Data are strobed from the timing chain into holding latches since the Intel 8080 is not capable of servicing three interrupts in 16 μs. The timing chain, through gating, also provides the drive for the four survey transmitters and the two ground reference transmitters, the drive for the RF transmitters, and, with a PROM, the TVG-AGC curve for the acoustic receivers.

The radio telemetry link between the array and the RPT unit is a 4-W, 139.55-MHz radio with a 3-kHz bandpass. While only one frequency is now in use, two may be required if two systems are used within 5 mi of each other.

The telemetry transmission consists of the data gathered in the previous ten 1-s periods and is 180 eight-bit bytes. Transmission is asynchronous and is modulated at a rate of 500 Hz. The beginning of the data burst occurs precisely at the beginning of the 10-s period to allow synchroization of other units to the array. One hundred seventy-six bytes represent timing numbers; two bytes contain mark and emergency information, and two bytes contain system status information (buoy moisture alarm and battery low voltage alarm). The array transmits about one-half of the 10-s period and then switches to receive to conserve power and allow radio control of the array. Currently, the only function implemented is the power on/off control. To do this, a small part of the circuit must be active at all times.

The acoustic tracking frequency is 31.25 kHz to achieve long range and the signals are amplitude modulated and frequency shift-keyed. Since a shorter distance is involved, the survey frequency is higher (250 kHz) to provide better resolution; the survey frequency is amplitude modulated.

The array is designed to withstand the impact of a small boat. The flotation collar that houses the radio antenna is highly visible to assist in location. Short-time operation (1 day) is provided by an internal battery and extended operation by an external, field-replaceable battery.

Receiver-Processor-Transmitter

The RPT unit can be operated on the beach, on board the divers' boat, or at the site of a more powerful computer where the RPT data can be subjected to more sophisticated processing. The RPT unit itself is battery-operated; a small, battery-driven inverter is used for the auxiliary printer and plotter which are powered by alternating current. Since current drain is not as severe a problem in the RPT as it is in the tracking array, the processor is an Intel SBC 80/10 single-board computer.[3]

The RPT, in addition to transforming the timing numbers into X,Y,Z coordinate positions, can provide information to the following detachable devices: (a) an analog plotter, (b) a more powerful computer, and (c) a line printer. The internal liquid-crystal display can show coordinate information for a selected diver or, alternatively, the range and bearing of a diver to any other diver or the ground reference points, so that divers can be easily vectored to other points on the range. The original timing numbers are retained on a tape cassette so that a permanent record is available for replay. Replay is accomplished on the RPT unit by changing one switch, and transferring the data cassette from the tape writer to the tape reader.

Software

The tracking array program gathers timing numbers for 10 s and determines whether a valid (three receiving transducers out of four) mark/emergency pulse has been transmitted by a diver. This information, along with the system status, is reformatted and sent to the radio transmitter. The program requires 1250 bytes of memory.

A test unit has been designed and constructed that uses data from an externally-generated tape cassette to simulate the acoustic pulses that would be received during a diver operation. In this way, the entire processor, software and hardware, was extensively tested before actual data were available.

The survey and tracking programs for the RPT unit were written in FORTRAN on a minicomputer and were thoroughly tested before being transferred to the microcomputer. These tests involved a simulated track with 100,000 points. No errors were found when signals from all four tracking transducers were received; the maximum error was 1% when one transducer was allowed to drop out randomly. First, the survey program is initialized and performs a survey (i.e., constructs the matrices for transforming the timing numbers into coordinate positions, using the spacings between the buoys and from the buoys to the surface). Six valid surveys are required before proceeding to the tracking portion of the program. To be valid, the surveys must contain no missing spacings and the redundant spacing must agree with the calculated distance. Depths are averaged to compensate for wave action. The first survey requires about 1.8 s, and subsequent surveys take about 1.3 s. Next, the tracking program starts. The initial tracking computation requires reception of signals from all four transducers; the first three timing numbers are used in one computation and the last three in another. These values are then compared to resolve the image ambiguity, and the correct two are averaged. After the initial computation, computations with only three transducers may be made based on previous coordinate data. The entire tracking computation for all 10 periods requires about 5 s. Total memory requirements for the survey and tracking programs are about 10,000 bytes.

Other Uses

Although the PATS will initially be used by the Naval Facilities Engineering Command, other uses are possible. For example, operations involving underwater oil platforms require precise information about the location of structural imperfections. Inquiries have been made concerning the use of PATS to study the habits of sharks. In this case, placement of the "diver" unit on the shark would clearly be the responsibility of the user.

Acknowledgments

This work was supported by the Naval Facilities Engineering Command under Contracts N62477-75-C-0364 and N00017-74-C-1208.

References

1. G.M. Wenz, "Acoustic ambient noise in the ocean: spectra and sources," J. Acoust. Soc. Am. 34: 1936-62, December 1962.

2. Data Catalog 1977, Intel Corporation, pp. 10-28 to 10-32.

3. T. Rolander, "SBC 80/10 - System 80/10 Single Board Computer Applications," Intel Corporation Application Note AP-26, 1977.

SWEPT CARRIER ACOUSTIC UNDERWATER COMMUNICATIONS

A. Zielinski
Faculty of Engineering and Applied Science
Memorial University of Newfoundland
St. John's, Nfld., A1B 3X5
CANADA

L. Barbour, Graduate Student
Faculty of Engineering and Applied Science
Memorial University of Newfoundland
St. John's, Nfld., A1B 3X5
CANADA

Abstract

This paper describes a novel idea of reducing multipath interference in underwater acoustic communication systems. The proposed idea is based on the observation that the time separation between direct and multipath waveforms can be utilized to suppress the multipath interference. A proposed system employs a carrier with instanteous frequency swept periodically in time over a broad frequency range. This frequency range is much larger than the bandwidth occupied by a message signal. On the other hand the reciprocal of sweeping rate is much smaller compared to the message bandwidth. The carrier is modulated by a message resulting in a time varying instantaneous narrow-band spectrum of the transmitted signal. The received signal is demodulated by a band-pass tracking receiver and suppression of the out-of-band multipath spectrum is accomplished. A simple model for the multipath channel has been proposed and related to the system operation and performance. Some results and conclusions from tests performed on the prototype are presented.

1. Introduction

In line with increasing interest in ocean research and industrial offshore development there is a growing demand for an efficient, reliable and high speed underwater sonic communication system. Speech communication between divers, remote control and telemetry for underwater operations, diverse oceanographic measurements are but some examples of data to be transmitted.

Underwater communication by means of the acoustic waveform encounters however several problems related to the characteristics of the underwater channel [1]. With sufficient transmit power for an adequate received signal level, the principal obstacle against reliable transmission is believed to be the multipath interference [2].

The physical phenomina responsible for multipath are primarily:

- multiple acoustic paths resulting from surface and bottom reflections
- Ray bending due to water temperature variation.

Both factors are time dependent, resulting in a complex, randomly time varying communication channel. The transmitted acoustic signal is also attenuated due to spreading and absorbtion of the acoustic energy by water.

2. A Model for Underwater Acoustic Communication Channel

It is assumed, that in addition to multipath, there exist a direct acoustic path between transmitter (T) and receiver (R) as shown schematically in Fig. 1.

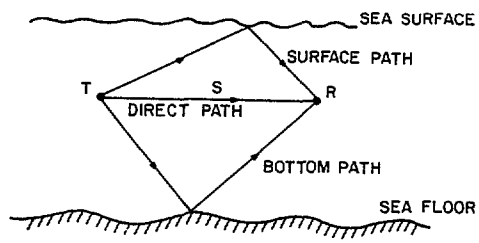

FIG.1 MULTIPLE UNDERWATER ACOUSTIC LINK

A complete underwater communication system can be represented by a model shown in Fig. 2.

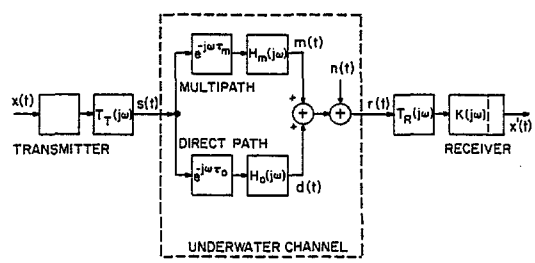

FIG. 2 AN UNDERWATER COMMUNICATION SYSTEM MODEL

In the transmitter, a message signal, x(t), is transferred by a suitable modulation into a desired frequency range. The electric signal is then converted into an acoustic signal by a transmitting transducer represented by a filter $T_T(j\omega)$. The acoustic signal, s(t), is transmitted through an

underwater channel, converted back into an electric signal by a receiving transducer, $T_R(j\omega)$, and applied to a receiver front filter, $K(j\omega)$, which is followed by a demodulator. $x'(t)$ represents the demodulated message signal. The underwater channel is simulated by a parallel connection of the direct and indirect path. A time delay τ_o in the direct path is represented by filter $e^{-j\omega\tau_o}$ and is related to the geometrical distance S between the transmitter and the receiver and to the sound velocity c.

$$\tau_o = \frac{S}{c} \tag{1}$$

The filter, $H_o(j\omega)$, represents attenuation and absorbtion of the acoustic energy in the water and is assumed to have a real transfer function, i.e.

$$H_o(j\omega) = H_o(\omega)$$

Based on emperical data [4] and assuming spherical spreading one can conservatively approximate $H_o(\omega)$ by:

$$H_o(2\pi f)_{dB} = -(20 \log S + 36.4 \times 10^{-5} fS) \tag{2}$$

$$\text{for } 20\text{kHz} \leq f \leq 100 \text{ kHz}$$

where

$H_o(2\pi f)_{dB}$ is expressed in dB refering to 1μbar

S is the distance between transmitter and receiver in meters

f is the frequency of the transmitted signal in kHz.

Clearly, $H_o(\omega)$ is the transfer function of a low pass filter.

A time delay, τ_m, in the indirect path of Fig. 2 is related to the shortest multipath distance between transmitter and receiver and it is assumed that

$$\tau_m > \tau_o \tag{3}$$

A filter $H_m(j\omega)$ represents the combined effect of all multipath signals. It is basically a low pass filter due to the similar considerations as for $H_o(j\omega)$ filter. Longer distances for multipath imply higher attenuation and therefore a smaller bandwidth of $H_m(j\omega)$ compared to $H_o(j\omega)$ should be expected.

The random and time varying nature of multipath suggests that the modelling filter, $H_m(j\omega)$, should be a time variant, random filter described in probabilistic terms rather the deterministic transfer function $H_m(j\omega)$.

With this approach, the time dependance can be explicitly indicated by writing

$$H_m(j\omega) = H_m(\omega,t)\, e^{j\psi(\omega,t)} \tag{4a}$$

where $$H_m(\omega,t) = |\, H_m(j\omega)\, | \tag{4b}$$

and $$\psi_m(\omega,t) = \angle\, H_m(j\omega) \tag{4c}$$

whereas the random character of $H_m(j\omega)$ can be introduced by considering $H_m(\omega,t)$ and $\psi_m(\omega,t)$ as random processes for any particular ω.

A simplified probabilistic model for multipath which assumes an infinite number of scatterers with random and uniform phase gives a Rayleigh probability density function (pdf) for $H_m(\omega,t)$ and uniform pdf for $\psi_m(\omega,t)$ [5].

Attempts have been made to obtain a more adequate model for $H_m(j\omega)$ by relating statistical properties of the modeling filter to the actual physical conditions. Venetsanopoulos [3] developed, for example, a statistical model related to surface roughness.

Finally, n(t) in Fig. 2 represents an additive ambient noise which will not be considered in this paper.

When the delta pulse is applied at the input of the underwater channel model, i.e. $s(t) = \delta(t)$ then the received signal r(t) will be as shown schematically in Fig. 3.

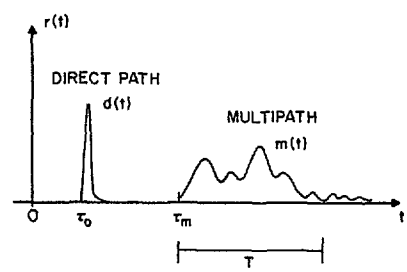

FIG. 3. IMPULSE RESPONSE OF THE UNDERWATER CHANNEL MODEL.

The direct path impulse response, d(t), has a finite width due to the low-pass nature of the filter $H_o(j\omega)$. The multipath signal, m(t), is the impulse response of the time varying random filter $H_m(j\omega)$. Because of the finite energy carried by the multipath signal

$$\lim_{t \to \infty} E\{m(t)\} = 0$$

where $E\{\cdot\}$ denotes expected value.
The multipath duration time, T, can be arbitarily defined as the value of t for which $E\{m(t)\}$ is neglegible (assuming time origin at τ_m). Physically $\tau_m + T$ is the time limit for the meaningful multipath signal.

When a harmonic signal (carrier)

$$s(t) = A\cos \omega_c t = \text{Re}\{Ae^{j\omega_c t}\};\ -\infty \leq t \leq \infty \tag{5}$$

is applied at the input of the underwater channel model, then the output signal is given by:

$$\begin{aligned} r(t) &= \text{Re}\{ Ae^{j\omega_c t} [e^{-j\omega_c \tau_m} H_m(j\omega_c) + e^{-j\omega_c \tau_o} H_o(j\omega_c)] \} \\ &= \text{Re}\{ M(t) e^{j(\omega_c t + \alpha(t))} + De^{j(\omega_c t + \beta)} \} \end{aligned} \tag{6}$$

where $M(t) = A\, H_m(\omega_c, t)$ (7a)

$$\alpha(t) = -\omega_o \tau_m + \psi_m(\omega_c, t) \quad (7b)$$

$$D = A\, H_o(\omega_c) \quad (7c)$$

$$\beta = -\omega_c \tau_o \quad (7d)$$

In the phasor notation, a phasor, $M(t)e^{j\alpha(t)}$, represents the time varying multipath signal, m(t), while phasor, $De^{j\beta}$, corresponds to the direct signal, d(t).

A phasor, $R(t)e^{j\gamma(t)}$, representing the received signal, r(t), is a geometrical sum of the others as shown in Fig. 4, where

$$R(t)\, e^{j\gamma(t)} = M(t)e^{j\alpha(t)} + De^{j\beta} \quad (8)$$

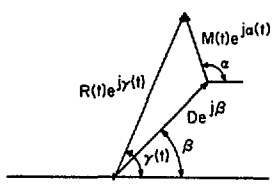

FIG. 4 PHASOR REPRESENTATION FOR THE DIRECT AND MULTIPATH SIGNALS.

For constant values of D and β, the direct signal, d(t), has only one frequency component, ω_c. On the other hand the multipath signal which is both amplitude and angle modulated: i.e.

$$m(t) = M(t) \cos [\omega_c t + \alpha(t)] \quad (9)$$

occupies a finite frequency band. Because M(t) and α(t) are in practice slow varying functions of time, the frequency band occupied by m(t) is narrow and centered at ω_c. Similarly, the received signal, r(t), is both amplitude and frequency modulated:

$$r(t) = R(t) \cos [\omega_c t + \gamma(t)] \quad (10)$$

The instantaneous frequency of the received signal is:

$$\omega_i(t) = \frac{d\gamma}{dt} + \omega_c \quad (11)$$

The presence of interfering amplitude and angle modulation of the received carrier reflects difficulties encountered in underwater communication.

3. Swept Carrier Communication Concept

A situation is considered in which the carrier of eq. (5) is transmitted through the channel model of Fig. 2.

It is assumed that the receiving transducer characteristic $T_R(j\omega)$ is constant over a broad frequency range, i.e.

$$T_R(j\omega) = 1 \quad \text{for} \quad \omega_{min} < \omega < \omega_{max} \quad (12)$$

The receiver front filter $K(j\omega)$ is assumed to have a band-pass frequency characteristic, centered at the carrier frequency ω_c, bandwidth ΔB and impulse response duration b.

In sequel we introduce a instantaneous and possibly a time varying spectrum, $F(\omega, t)$, as determined by a finite observation window b.

In particular the instantaneous spectra of the direct signal, d(t) and multipath signal, m(t), are denoted by $F_d(\omega, t)$ and $F_m(\omega, t)$ respectively.

For a sufficiently high carrier frequency i.e., for

$$\frac{2\pi}{\omega_c} << b \quad (13)$$

the instantaneous spectra, $F_d(\omega, t)$ and $F_m(\omega, t)$ are narrowband and essentially time independent as shown schematically in Fig. 5a, where $F_d(\omega, t)$ is in fact a single frequency component ω_c.

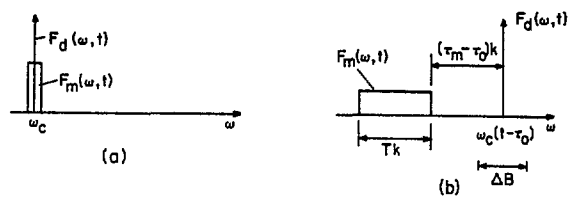

FIG. 5 INSTANTANEOUS SPECTRA OF THE DIRECT AND MULTIPATH SIGNALS

Suppose now that the carrier frequency, ω_c, is changing linearly in time, i.e.

$$\omega_c(t) = kt, \quad -\infty \leq t \leq \infty \quad (14)$$

where k is a proportionality constant.

The change in carrier frequency is followed by changes of the instantaneous spectra, $F_d(\omega, t)$ and $F_m(\omega, t)$.

If the rate of change is slow enough, $F_d(\omega, t)$ will remain approximately a single frequency component located at $\omega_c(t - \tau_o)$. The spectrum, $F_m(\omega, t)$, due to the time delay, $\tau_m > \tau_o$, is lagging $F_d(\omega, t)$, and due to multipath duration T, is broadened proportionally to T as shown in Fig. 5b. Clearly, if the receiver band-pass filter with bandwidth ΔB could track a slow change in the carrier frequency $\omega_c(t)$, then the multipath signal spectrum would be outside of the filter bandwidth resulting in principle, in a complete rejection of the multipath signal.

Any narrowband modulation of the carrier by a message signal would broaden both $F_d(\omega, t)$ and $F_m(\omega, t)$ spectra but with a proper choice of a system parameters the frequency separation between $F_d(\omega, t)$ and $F_m(\omega, t)$ could be maintained. The main practical problem in the implementation of this idea arises from the limited frequency range over which the carrier frequency can be swept.

Water attenuation and transducer characteristics confines the sweeping range to a certain limit

$$\omega_{min} \leq \omega_c(t) \leq \omega_{max} \tag{15}$$

For continuous operation therefore, $\omega_c(t)$ has to be a periodic function of time, with a period T_s

$$\omega_c(t) = f(t) = f(t - T_s) \tag{16}$$

Because f(t) can always be represented by a Fourier Series we limit our attention to the harmonic frequency sweep:

$$\omega_c(t) = \omega_o + B \cos \omega_s t \tag{17}$$

where ω_o - central frequency

$\omega_s = \frac{2\pi}{T_s}$ - low sweeping frequency

and $\omega_o - B = \omega_{min}$

$\omega_o + B = \omega_{max}$

The time-frequency relationship for the instantaneous spectra, $F_d(\omega, t)$ and $F_m(\omega, t)$ are now more complex then that shown previously in Fig. 5 for the linear sweep. To show this relationship it is convenient to write the departure of the instantaneous carrier frequency, $\omega_c(t)$, from the central frequency, ω_o, as:

$$\omega_c(t) - \omega_o = B \cos \omega_s(t) = \mathrm{Re}\,\{Be^{j\omega_s t}\} \tag{18}$$

The projection of the rotating phasor, $Be^{j\omega_s t}$, onto the real axis therefore indicates the transmitted carrier instantaneous frequency.

Similarly, the instantaneous frequency location of the direct signal is given by:

$$\mathrm{Re}\,\{ Be^{j\omega_s(t - \tau_o)} \}$$

The instantaneous frequencies of the earliest and latest multipath signals are represented by phasors $Be^{j\omega_s(t - \tau_m)}$ and $Be^{j\omega_s(t - \tau_m - T)}$ respectively. The location of the instantaneous spectrum of the multipath signal lies then between the projections of the above phasors as shown in Fig. 6.

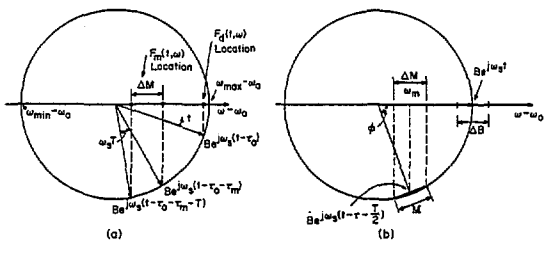

FIG. 6 PHASOR REPRESENTATION FOR $F_d(\omega,t)$ AND $F_m(\omega,t)$

As can be seen from Fig. 6a, the multipath spectrum, $F_m(t, \omega)$, changes both its position and width, ΔM, as a periodic function of time. A more convenient geometrical model for finding the locations of $F_d(t, \omega)$ and $F_m(t, \omega)$ can be derived from Fig. 6a and is shown in Fig. 6b. Here the time origin is assumed to be: $-\tau_o$. The multipath spectrum width and its location are obtained as the projection of a segment:

$$M = \left| 2B \sin \frac{\omega_s T}{2} \right| \tag{19}$$

which is rigidly attached to the rotating phasor

$$Be^{j\omega_s(t - \tau - \frac{T}{2})} \tag{20}$$

where $\tau = \tau_m - \tau_o$

From geometrical consideration the multipath spectrum central frequency ω_m is given by

$$\omega_m = \omega_o + B \cos (\omega_s t - \omega_s \tau - \frac{\omega_s T}{2}) \tag{21}$$

and bandwidth, ΔM by:

$$\Delta M = \left| 2B \sin (\omega_s t - \omega_s \tau - \frac{\omega_s T}{2}) \sin \frac{\omega_s T}{2} \right| \tag{22}$$

The receiver's tracking filter of bandwidth ΔB follows the location of the instantaneous frequency of the direct signal, $\omega_c(t)$. As seen from Fig. 6b, the direct and multipath signal spectra move along the frequency axis periodically in time. The multipath spectrum, $F_m(\omega, t)$, falls periodically within the tracking filter bandwidth ΔB. The multipath signal supression results as an effect of two mechanisms:

- for periods of time in which ΔB and ΔM do not overlap, $F_m(\omega, t)$ is outside of the receiver filter bandwidth and ideally is completely rejected by the filter.
- for periods of time in which ΔB and ΔM overlap, multipath supression is still possible, if

  $$\Delta M > \Delta B$$

  In this situation only a portion of the multipath energy falls within the receiving filter bandwidth.

Any narrowband modulation of the swept carrier by a message signal will not appreciably alter the geometrical model shown in Fig. 6b. If modulation is applied, the instantaneous spectrum of the direct signal will occupy a finite frequency band, and the multipath spectrum will be broader than that without modulation.

4. System Parameter Considerations

The swept carrier communication concept described earlier is applicable to any narrowband modulation applied for a message transmission. The most obvious and simple choice would be either the narrowband frequency or amplitude modulation. The message signal, x(t), could be either an analog or digital signal of a limited spectrum. Without these specific assignments it is difficult to propose a system performance criterion for parameter optimization.

Certain general observations can be made however at this point. Considering the geometrical model of Fig. 6 it seems obvious that increasing the sweeping frequency range $\omega_{max} - \omega_{min}$ will allow better separation between the direct and multipath spectra and therefore will result in better multipath supression. However, the maximum sweeping range is limited by the characteristics of the transmitting and receiving transducers and by water attenuation.

Parameters, τ and T, are determined by a particular transmission situation and by multipath duration. The possibility of optimization lies in the proper choice of a sweeping function, f(t) shown in eq. (16) or, if sweeping is harmonic, by the proper choice of a sweeping frequency ω_s.

If, for example, it is required that

$$\Delta M < \omega_{max} - \omega_{min} \quad \text{for all } t \tag{24}$$

then the sweeping frequency must satisfy

$$M = \left| 2B \sin \frac{\omega_s T}{2} \right| < 2B$$

or

$$\omega_s T < \pi \tag{25}$$

For the maximum frequency separation between direct and multipath spectra, the angle ϕ in Fig. 6b should be:

$$\phi = \omega_s \tau + \frac{\omega_s T}{2} = \pi \tag{26}$$

Both conditions (25) and (26) can be satisfied only if

$$T < 2\tau \tag{27}$$

and the optimum sweeping frequency in this case is:

$$\omega_s = \frac{\pi}{\tau + \frac{T}{2}} \tag{28}$$

For large T, the multipath spectrum will occupy the entire bandwidth (ω_{min}, ω_{max}) and the system performance can be improved by narrowing the tracking filter bandwidth.

5. Receiver Structure and Experimental Results

The block diagram of a possible receiver configuration is shown in Fig. 7.

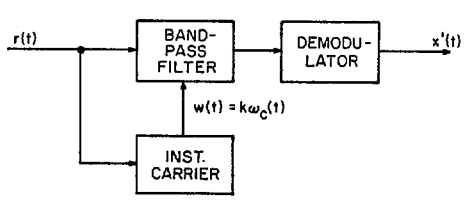

FIG. 7 BLOCK DIAGRAM OF A RECEIVER

The slowly varying instantaneous carrier frequency is recognized by the functional block "Inst. carrier". The output signal of which

$$w(t) = k\omega_c(t)$$

is then used to tune the central frequency of the band-pass tracking filter. The output of the tracking filter is passed through a demodulator, the output of which represents the transmitted message signal x'(t).

An experimental system has been designed and tested. Narrowband frequency modulation was chosen for message transmission.

The prototype has the following parameters:

- frequency sweep range ($f_{min} \div f_{max}$)	:	65kHz - 95kHz
- central frequency, f_o	:	80kHz
- sweeping frequency, f_s - variable	:	5Hz < f_s < 50Hz
- Message signal frequency, f_m	:	300Hz < f_m<1800Hz
- Receiving filter bandwidth, ΔB	:	4kHz

Back to back tests of the system were conducted and excellent results were obtained for the designed parameters' range.

To assess the system performance in a multipath situation a harmonic interfering signal has been added to the unmodulated transmitted swept carrier. The signal w(t), proportional to the instantaneous carrier frequency is shown in Fig. 8.

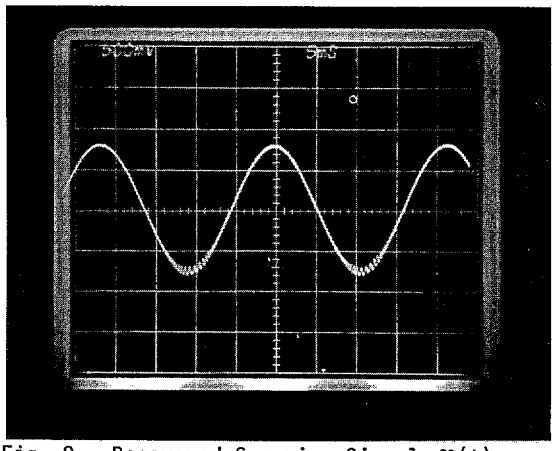

Fig. 8 - Recovered Sweeping Signal, W(t)

The maximum and minimum values of w(t) correspond to the carrier frequencies of 65kHz and 95kHz respectively. The interfering tone has a frequency of 80kHz and small distortion can be observed in the corresponding level of w(t).

A similar test has been conducted for modulated carrier. Fig. 9 shows a transmitted and

demodulated message signal, x(t) (upper trace) and x'(t) (lower trace) respectively. The periodical distortion seen is again caused by an interfering tone of frequency 80kHz.

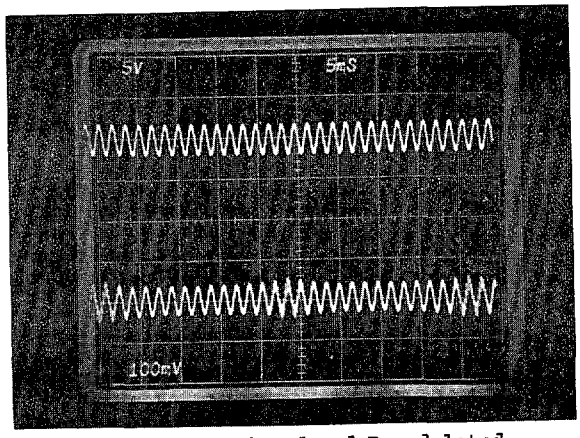

Fig. 9 - Transmitted and Demodulated Message Signal

Limited tests have also been carried out in a small water tank. Due to the dimensions of the tank, very strong and long lasting multipath was encountered. Fig. 10 shows the received signal structure (lower trace) for the transmitted harmonic burst (upper trace).

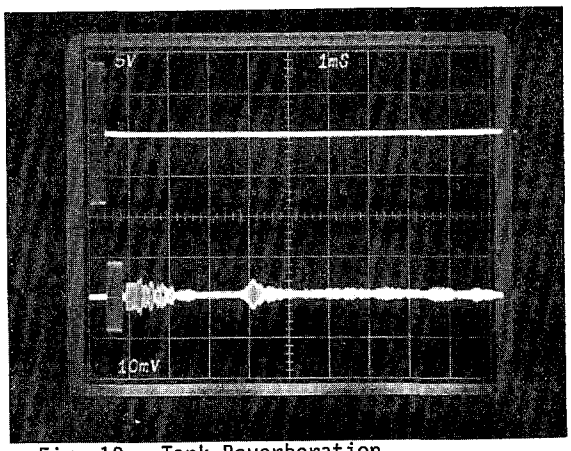

Fig. 10 - Tank Reverberation

Even under this severe condition, the tracking signal w(t) was well defined as shown in Fig. 11.

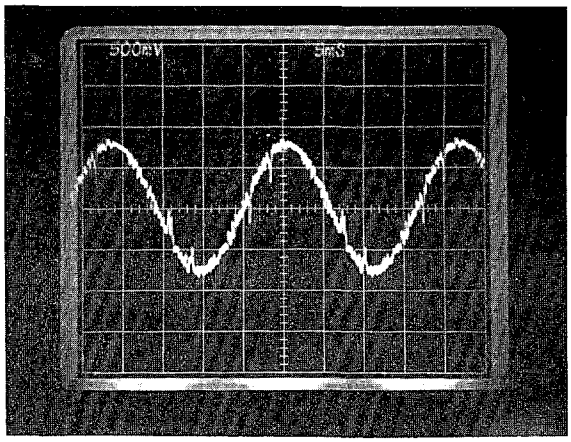

Fig. 11 - Recovered Sweeping Signal, w(t)

More extensive full scale ocean tests are to be carried out in the near future.

Conclusions

Based on limited experimental results the proposed swept carrier communication coccept seems to be a promising way of message transmission in a multipath situation. The generality of the concept allows different modulation - demodulation schemes to be considered for further investigation. Full evaluation of the swept carrier communications concept shall be possible only after extensive ocean tests.

Summary

A model for multipath communication is described. Based on this model, a novel swept carrier communication concept has been proposed and discussed. Several observations concerning system parameters have been made. Some experimental results from tests carried out on the system prototype are presented.

References

1. Lytle, D.W.: "Characteristic Problems of the Underwater Channel", IEEE International Conference on Communications, Seattle, Washington 1973, V2 pp. 38/1-3.

2. Chauncey, S. Miller; Bohman, Carl E: "An Experiment in High Speed Underwater Telemetry", IEEE Int. Conference on Engineering in the Ocean Environment, New Port, R.I. 1972, pp. 34-38.

3. Venetsanopoulos, A.N.: "Stochastic Filter Modeling for the Sea-Surface Scattering Channel", J. Acoust. Soc. Amer., V. 49, N 4, PI 1, April 1971, pp. 1100-7.

4. Urick, R.J.: "Principle of Underwater Sound for Engineers", McGraw-Hill Book Co., 1975.

5. Schwartz, M.: "Information transmission, modulation, and noise", McGraw-Hill Book Co., 1970.

SMALL SUBMERSIBLE ACOUSTIC COMMUNICATIONS SYSTEM DESIGN

Salvatore D. Morgera

Raytheon Company
Submarine Signal Division
Portsmouth, RI 02871

Abstract

A design is presented for a system providing highly reliable command and control acoustic communications between a mother ship and a number of small, fast submersibles. The small submersibles may be employed for underwater mining, exploration, bottom mapping, or military surveillance. Modulation and coding design is presented; the techniques discussed provide multiple protection against multipath and fading, high reliability, acceptable transmitted signal total time duration, simplicity, and economy. The required decision point signal-to-noise ratio (SNR) for Rayleigh fading conditions is derived for the modulation and coding design. Particular attention is paid in the receive signal processing to the initial doppler and message doppler variation problems inherent in a scenario with mobile end points. A Figure-of-Merit calculation is provided for typical geometrical and environmental parameters. It is shown for a realistic source level that the required SNR can be achieved at long range with extreme end point motion.

1. Introduction

The explosive growth of undersea vehicles, which followed development of North Sea oil and gas discoveries of the late sixties and early seventies, continues. While the diver still dominates commercial underwater activities, the role of manned submersibles and remotely controlled vehicles progressively increases. The largest US submersible commitments at present are in the academic and military communities. The Navy has a total of seven manned submersibles and seven unmanned vehicles in operating condition at the moment. They are based on both coasts and in Washington, DC; their largest concentration is in the San Diego area.

Most of the Navy vehicles have a capability for TV viewing and video taping. Most have a manipulator and are constructed to carry 35 mm or 70 mm still cameras with a light strobe. Configuration, dimensions, weight, complexity, and depth capabilities vary from vehicle to vehicle, as does work instrumentation and vehicle attitude monitoring instrumentation. At present, Navy vehicles operate within a relatively confined radius of the mother ship and up to depths of about 20 kft. It is desirable for future Navy oceanographic and military operations to equip the submersibles with sophisticated active and passive sonar equipment and have it operate at ranges up to 100 nmi from the mother ship and at speeds of up to 10 kn.

Figure 1 illustrates the scenario of interest. A surface ship with an acoustic transmit array, generally at a shallow-to-intermediate depth, communicates with a submersible equipped with an acoustic receive array, generally at an intermediate-to-deep depth, the objective being to provide command and control information to the submersible. The acoustic information transfer is treated here as strictly being from ship-to-submersible and the amount of message information that must be transmitted is small. We assume that any data gathered by the submersible can be retrieved at a later time, either physically or via EM means, although a submersible-to-ship communications link utilizing data compression is possible. Since there may be more than one submersible, the message must contain destination information as well as the actual command and control information. It is anticipated that the above message information can be conveyed by an 8-bit block.

The minimum operational range is established as 100 nmi. This operational range capability permits a substantial operating radius about the surface ship. The reliability of the communications system is described by two (conditional) error probabilities:
1) $\Pr\{M_i \neq m_i \mid m_i\}$, the probability that a message m_i destined for the ith submersible is not received and

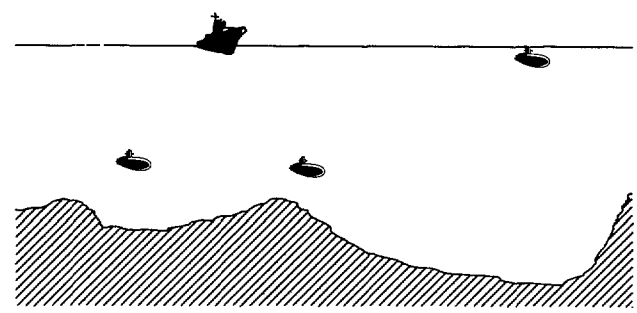

Figure 1. Small Submersible Scenario

decoded correctly as M_i, and 2) $\Pr\{M_j = m_j \mid m_i; i \neq j\}$, the probability that a message m_i is received and decoded as a valid message by the (incorrect) j^{th} submersible. The communications system is designed to conform to the following error probabilities per message,

$$\Pr\{M_i \neq m_i \mid m_i\} = 10^{-6} \tag{1}$$

$$\Pr\{M_j = m_j \mid m_i; i \neq j\} = 10^{-12} \quad i, j = 1,2,\ldots,N_s \tag{2}$$

where

$$N_s + N_T \leqslant 2^8$$

The quantity N_s is the number of submersibles within operational range and N_T is the command and control information.

2. Modulation and Coding Design

The modulation and coding design proposed here provides the following features:

- Multiple protection against multipath and fading
- Low (conditional) error probabilities [cf. Equations (1) and (2)]
- Acceptable transmitted signal total time duration
- Simplicity
- Economy.

The last point above is a matter of extreme practical importance; the proposed modulation and coding design can be easily implemented utilizing existing communications system technology.

Several considerations, foremost among them being the capability of existing communications system hardware, the minimum operational range requirement of 100 nmi and associated standard path loss to the receiver, and the relative absence of commercial and military traffic lines, have led to a signaling center frequency f_c in the range [175, 225] Hz and a signaling bandwidth W of 50 Hz, as shown in Figure 2a. The geometry of surface ship and (any one) submersible, depicted in Figure 1, allows multiple reflections, caustics (surface ship projector in surface duct), and ray path refraction. The severity of these effects depends (environmentally) on the ocean depth, season, nature of the boundary inhomogeneities, and vertical and horizontal sound velocity gradients. In general, there will be degradations suffered by the transmitted signal, due to multipath cancellation and fading; the source of these degradations is conveniently described by the medium time dispersion L and frequency dispersion B. NISSM II and other theoretical models were utilized with a surface ship projector (source) depth S = 30 ft (9.1 m), receiver array depths R = 300 ft (91.4 m) and R = 1000 ft (304.8 m), and frequency f_c = 200 Hz to obtain the following interval estimates for L and B,†

$$L \approx [0.5,\ 2.4]\ \text{s} \tag{3}$$

$$B \approx [.02,\ 0.2]\ \text{Hz}. \tag{4}$$

The lower limit on L is valid for the important range increment 100 - 200 nmi; the upper limit on L obtains only at the shorter ranges on the order of 10 nmi. The lower limit on B applies to volume dispersion (i.e., purely refracted propagation paths) and an end point relative motion of 30 kt at a range of 100 nmi; the upper limit on B includes the effects of surface and bottom scattering with the standard deviation of the boundary undulations assumed to be 1.4 m (SS3) and 0.2 m, respectively. The upper limit on B is believed to be quite pessimistic.

The communications system's basic design philosophy is to use minimum signaling elements well suited to the acoustic communication channel and any existing equipment, further improve the bit error rate performance by diversity to achieve a moderately low bit error rate, and employ error correcting coding to obtain the final error rates. The proposed callup communications system employs 4-ARY FSK (M = 4), a simple modulation technique which is efficient in terms of the available bandwidth W, facilitates recognition of fades and receiver AGC adjustments, and allows an acceptable transmitted signal time duration. Multiple protection against multipath and fading is provided, first, by use of a long-time duration T for the minimum signaling element (tonal or chip), i.e., we choose,

$$T = 16\text{s} \gg L \tag{5}$$

and second, by the redundancy offered by 5-fold frequency diversity with the diversity-to-diversity channel tonal spacing much greater than the fading correlation width of 1/L. The transmitted tonal frequency width is approximately 1/T; whereas, the receive frequency resolution Δf is equal to

$$\Delta f \cong \frac{2}{T} = .125\ \text{Hz} \geqslant B \tag{6}$$

These selections leave sufficient unused bandwidth to accommodate realistic doppler shifts associated with the down-link end point relative motion. The long tonal time duration and the redundancy act to increase the SNR at the decision point for the transmission bits. The modulation and diversity design parameters are depicted in Figure 2b.

† Bottom class and sound velocity profile (SVP) employed were those associated with the acoustic province MGS3(57N, 40W) and the summer season.

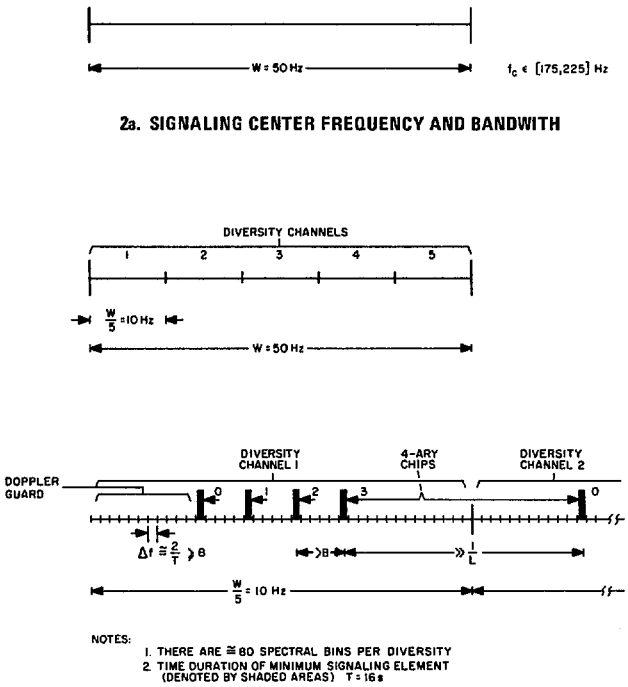

Figure 2. Modulation and Diversity Design

The low (conditional) error probabilities of Equations (1) and (2) may be met by an encoded message format consisting of two codewords, each carrying the eight information bits. Upon reception, the codewords are decoded separately and the eight information bits accepted as valid only if both codewords decode identically. Mathematically, we may express the ith encoded message x_i in the following manner,

$$x_i \triangleq [f_1(m_i), f_2(m_i)] = (c_{1i}, c_{2i}) \tag{7}$$

where $f_1(\cdot)$, $f_2(\cdot)$ denote linear transformations on the message m_i and (c_{1i}, c_{2i}) are the two aforementioned codewords concatenated. The probability of message error may be written as,†

$$\begin{aligned} \Pr\{M_i \neq m_i \mid m_i\} &= 2\Pr\{M_{\ell i} \neq m_i \mid m_i\} \\ &\quad - \Pr\{M_{\ell i} \neq m_i \mid m_i\}^2 \\ &\cong 2\Pr\{M_{\ell i} \neq m_i \mid m_i\} \quad \ell = 1,2 \end{aligned} \tag{8}$$

where M_{1i} and M_{2i} represent the received and decoded messages associated with the codewords c_{1i} and c_{2i}, respectively. Since the probability of message error is to be maintained at 10^{-6} [cf. Equation (1)], the probability of a codeword error, from Equation (8), must be held to,

$$\Pr\{M_{\ell i} \neq m_i \mid m_i\} \cong 5 \times 10^{-7} \quad \ell = 1,2 \tag{9}$$

The false message error probability of Equation (2) is related to the probability that both codewords (c_{1i}, c_{2i}) contain the same error, i.e.,

$$\begin{aligned} \Pr\{M_j = m_j \mid m_i; i \neq j\} &= \Pr\{M_{1j} = m_j \mid m_i; i \neq j\} \cdot \\ &\quad \Pr\{M_{2j} = m_j \mid m_i; i \neq j\} \\ &\leq \left(\frac{1}{N}\right)\left[1 - \Pr\{M_{\ell j} = m_i \mid m_i; \right. \\ &\quad \left. i \neq j\}\right]^2 \quad \ell = 1,2 \end{aligned} \tag{10}$$

The upper bound is obtained by assuming that each codeword has N nearest neighbors†† which are equally likely to decode in error. The bracketed complementary probability is numerically equal to that of Equation (9). For a particular 8-bit block of information bits, there are eight nearest neighbors; thus, N = 8 and,

$$\Pr\{M_j = m_j \mid m_i; i \neq j\} \leq 3.1 \times 10^{-14} \tag{11}$$

which is substantially less than the error probability requirement of Equation (2). An upper bound on the probability that any one or more vessels have a false message is given by,

$$1 - [1 - \Pr\{M_j = m_j \mid m_i; i \neq j\}]^{N_s} \leq N_s \cdot \Pr\{M_j = m_j \mid m_i; i \neq j\} \leq 1.0 \times 10^{-12}$$

by invoking the Union bound and assuming that N = 32.

We now turn to the detailed code structure. The code must be capable of correcting at least two errors so that received bits of moderate quality will not affect proper response, and must admit economical and simple encoding and decoding. The latter requirement demands that the codeword length be as short as possible. The number of linear code alternatives that satisfy the practical requirements is small; namely, we have the (21, 11; 2, 6) difference-set code and the (24, 12; 3, 7) (overall parity check) extended Golay code [1]. The difference-set code corrects up to two errors in the 21-bit codeword and is relatively simple to decode; the fact that it is a Projective Geometry cyclic code also guarantees that it can be (1-step) majority-logic decoded. The Golay code corrects up to three errors and is capable of detecting the existence of a fourth error in the 24-bit codeword. The Golay code is moderately hard to decode; however, much recent work on efficient implementation and block synchronization techniques make it the more desirable choice. To use

† We assume that the occurrences of codeword errors are statistically independent, justified by the fact that the codewords will be separated in time by greater than the average fade duration 1/B.

†† In the Hamming metric sense.

the Golay code, we shorten it to a (20, 8; 3, 7) code in order to accommodate the eight information bits. Note that the shortened code retains the same distance and error correcting features of the original code [2].

Assuming the codeword error of Equation (9), we may compute the error rate per coded bit for the shortened Golay code, and then the required SNR per tone at the decision point. The interleaving and unanimity count on the transmission bits acts to guarantee the statistical independence of coded bit errors; therefore, the coded bit error rate P may be found from the expression,

$$\Pr\left\{M_{\ell i} \neq m_i \mid m_i\right\} = 5 \times 10^{-7}$$

$$= \sum_{n=4}^{20} \binom{20}{n} P^n (1-P)^{20-n}$$

$$\cong \binom{20}{4} P^4 \quad \ell = 1, 2 \qquad (12)$$

and

$$P \cong 3.2 \times 10^{-3} \qquad (13)$$

The transmission bit error rate p may be determined from the expression,

$$P = p^3 + 3p^2 (1-p)$$

$$\cong 3.2 \times 10^{-3} \qquad (14)$$

and

$$p \cong 3.3 \times 10^{-2} \qquad (15)$$

Finally, the transmission character error rate P_e for M = 4 FSK signaling is related to the bit error rate of Equation (15) by,

$$P_e = \frac{2(M-1)}{M} p$$

$$\cong 5.0 \times 10^{-2} \qquad (16)$$

The character error rate is directly related to the required SNR at the decision point. For M = 4 FSK signaling, ideal detection, and 5-fold frequency diversity, the shortened Golay coding scheme requires the following SNR value per tone for (Rayleigh) fading conditions [3],

$$\frac{S}{N} = 4.5 \text{ dB} \qquad (17)$$

The total required SNR is, of course, 11.5 dB. Under fading conditions, an additional allowance of 2.0 dB is necessary to allow for non-ideal filters, timing error, waveform distortion in the medium, and AGC and noise shifts in the receiver. The required $\frac{S}{N}$ per tone is then 6.5 dB to meet the (conditional) error probabilities; this is a most reasonable figure for the operational range requirement, as shown in Section 4.

In concluding the modulation and coding design, we must mention the total transmitted signal time duration. We transmit two codewords for a total of 40 bits with the time duration of a minimum signaling element equal to 16s; thus, the total time duration is 10.7 min. We must also allow, at most, 1.0 min for a preamble segment to alert the receiver and provide real time bit synchronization and 2.0 min propagation time for a 100 nmi range.

3. Receive Signal Processing

The receive signal processing is that commonly associated with M-ARY FSK supplemented by doppler processing to accommodate the down-link end point relative motion. It is required that the initial doppler be estimated and that any doppler variations be estimated throughout the transmitted signal time duration of approximately 10.7 min.

To aid in the initial doppler estimation, a two-phase preamble is proposed. Each phase would consist of a predefined burst of no more than five tonals with time duration T = 16s; thus, the entire preamble time duration is a mere 2T = 32s. The preamble and (encoded and modulated) message time allocations are shown in Figure 3. The preamble tonals for each phase are located utilizing the processing shown in Figure 4; tonal detection/location unanimity is required for the two phases.† The initial doppler estimate so obtained is then employed to assign a total of 20 phase-difference frequency trackers to the anticipated message spectral bins (four per diversity, 5-fold diversity). Shortly after the transmitted signal onset, 15 of the trackers may be disabled, with the remaining five tracking the encoded and modulated message bits.

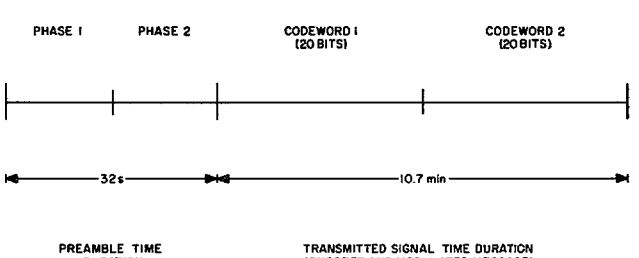

Figure 3. Preamble and Message Time Allocations

† The same reliability philosophy is employed here as is in using two codewords to transmit the message and requiring that both be identically decoded.

As shown in Figure 4, the tracked encoded and modulated message bits are diversity combined, Golay decoded, and thresholded, resulting in the desired 8-bit block of information bits. A matter of concern is the capability of the frequency trackers to deal with the expected frequency slew rate. Exceedingly worst-case CPA dynamics calculations indicate that the slew rate s is bounded as follows.

$$s \leqslant 1.7 \times 10^{-3} \text{ Hz/s} \tag{18}$$

The slew rate of Equation (18) is computed using a relative end point range rate of 30 kn, a closest point of approach of 10 nmi, and a frequency of 200 Hz. The simple phase-difference tracker algorithm envisioned for the receive signal processing is capable of a slew rate of 3.1×10^{-3} Hz/s at a SNR of 3 dB per spectral bin (a spectral bin $\Delta f = .125$ Hz; cf. Figure 2). We note that this SNR figure is less than the 4.5 dB of Equation (17), required for acceptable (ideal) detection/decoding. No problem is then anticipated with tonal tracking during the transmitted signal time duration.

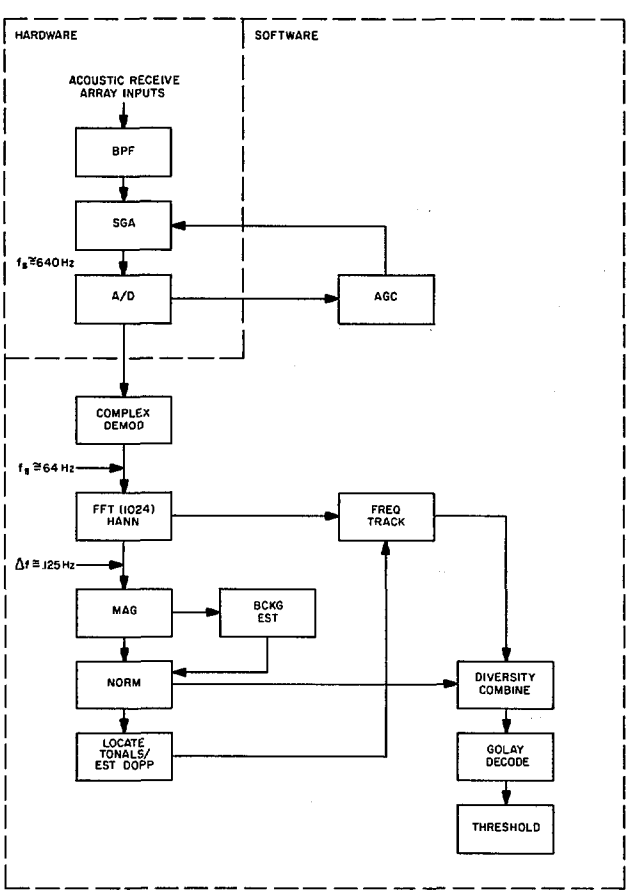

Figure 4. Receive Signal Processing Functional Diagram

4. Performance Prediction

The Figure of Merit (FOM) is given by,

$$\text{FOM} = L_S - \{[L_A - (DI - DA)] \oplus [L_{SN} - (L_{SNR} - D_N)]\} - (DT + DS) \tag{19}$$

where L_A is the ambient noise spectrum level, DA is the degradation to the theoretical acoustic receive array directivity index DI, L_{SN} is the self noise level, L_{SNR} is the theoretical acoustic array discrimination against self noise, D_N is the degradation to the L_{SNR}, DT is the detection threshold, and DS is the processing system loss. The symbol $\oplus$ denotes power level addition.

The total background noise spectral level L_N (bracketed term of Equation (19)) has been measured at the broadside beam output of a representative receive array for several speeds and a frequency of 200 Hz.† The values obtained are shown in Table 1.

Table 1. Total Background Noise Spectral Level for Several Speeds, 200 Hz

Speed (kn)	L_N $\left(\text{dB}/\!/1\mu\text{Pa}/\sqrt{\text{Hz}}\right)$
3	57.0
6	58.8
8	62.0
10	68.0
15	79.1

The transmitted source level per tone is taken to be,

$$L_S = 188.0 \text{ dB}/\!/1\mu\text{Pa} \cdot \text{m} \tag{20}$$

implicitly assuming an omnidirectional projector. The value of Equation (20) is also selected as a value achievable by existing equipments.†† The detection threshold per tonal may be calculated from the relation,

$$DT = MDL + 10 \log (\Delta f) - RG \tag{21}$$

where $\Delta f = 0.125$ Hz is the receive frequency resolution, MDL is the minimum detectable level per tonal, and RG is the redundancy gain. The MDL is obtained from Equation (17) plus 2.0 dB to account for non-ideal detection; thus, the MDL = 6.5 dB per tone. We assume RG = 1.0 dB, nominally associated with a redundancy factor of from 2 to 4. Inserting the above values into Equation (21), we obtain,

$$DT = -3.5 \text{ dB} \tag{22}$$

† The ambient noise spectral level included in the total background noise spectral level is consistent with that of the acoustic province MGS 3 (57N, 40W), S=30 ft (9.1m), R=300 ft (91.4m), and the summer season.

†† More precisely, the total required source level $L_S + 10 \log M$ is achievable by existing equipments.

Contribution to the factor DS principally arises from operator loss. We assume the operator loss is zero; accordingly, we set DS = 0 dB in the ensuing calculations.

Based on the above discussion and the data presented in the form of Table 1 and Equations (20) and (22), we compute the FOM values of Table 2.

Table 2. FOM and Signal Excess at 100 nmi for Several Speeds, 200 Hz

Speed (kn)	FOM (dB)	SE (dB), 100 nmi
3	134.5	15.5
6	132.7	13.7
8	129.5	10.5
10	123.5	4.5
15	112.4	- 6.6

To complete the picture, transmission loss calculations have been made utilizing the FACT and NISSM II models with coherent multipath combination and the geometrical and environmental parameters previously mentioned. The peak transmission loss in a 50 nmi window centered about 100 nmi was computed as approximately 119 dB. The signal excess SE at 100 nmi is also shown in Table 2. We see that it appears possible to provide reliable command and control capability out to the desired range of 100 nmi for submersible speeds up to approximately 10 kn.

5. Conclusions

A design has been presented for command and control acoustic communications between a surface ship and a number of small fast submersibles. The design offers a reliable command and control capability out to the desired range of 100 nmi for submersible speeds up to 10 kn, in addition to a simplicity and economy of implementation. It is felt that the results presented here will prove useful to the command and control of commercial submersibles devoted to mining, exploration, and bathymetry tasks and to military submersibles dedicated to coastal protection and enemy surveillance activities.

References

[1] Peterson, Wesley W. and E.J. Weldon, Jr., Error-Correcting Codes, The MIT Press, Cambridge (1972).

[2] Berlekamp, Elwyn R., Algebraic Coding Theory, McGraw-Hill, New York (1968).

[3] Nuttall, Albert H., "Error Probability Characteristics for Orthogonal Multiple Alternative Communication With D-Fold Diversity," NUSC/NL TR 4769, 19 June 1974.

FREQUENCY SHIFT ARRIVAL TIME DETERMINATION OF ACOUSTIC SIGNALS

by

Edward W. Early
John E. Ehrenberg
Roundney K.B. Liem

Applied Physics Laboratory, University of Washington
1013 N.E. 40th Street, Seattle, Washington 98105

Abstract

In the demodulation of underwater acoustic signals, timing determination is usually based on the leading edge of a pulse, and is therefore subject to errors that are functions of pulse rise time and signal level. This paper describes a system using a phase-locked loop demodulator to determine the time of arrival of a frequency-shifted pulse. In this system, timing is shown to be essentially independent of signal strength, and timing jitter is shown to be low.

Introduction

Many underwater acoustic systems use pulse modulation techniques in which detection occurs at the leading edge of the pulse. This method leads to timing errors that are functions of the pulse rise time and the received signal level, in addition to timing perturbations due to a low signal-to-noise ratio. In a system developed by the Applied Physics Laboratory to track Navy divers, the total error had to be kept within ±5 ft even though the signal strength might vary widely. Because it was recognized that the medium itself might introduce considerable errors, it was sought to keep receiver timing errors to a minimum.

The acoustic system developed to fulfill that requirement uses a pulse in which the carrier frequency is shifted several kilohertz midway through its length. At the receiver, the signal is amplified and presented to a phase-locked loop (PLL) which detects the frequency transition. By proper choice of bandwidth and pulse length, the midpoint of this shift can be made relatively independent of signal strength. The remaining timing perturbations are then a function of signal-to-noise ratio only.

The Receiver

A functional block diagram of the receiver is shown in Figure 1. An acoustic pulse in the water is picked up by the receiver hydrophone and amplified together with the in-band noise. The noise component is then integrated and used to adjust the gain of the receiver to the maximum possible under the particular ambient noise condition without saturating the receiver. Since the receiver is used in a synchronized system, a time-varied gain is incorporated to compensate for the decreased signal level as the distance increases.

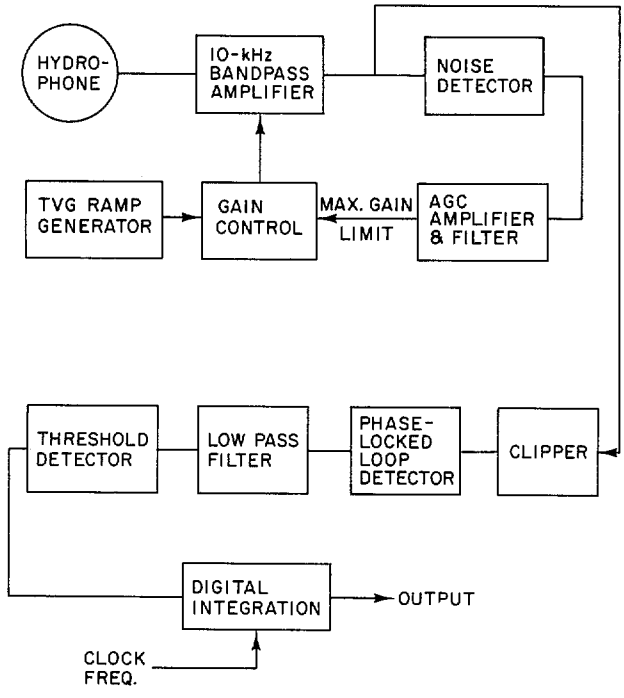

Figure 1. Functional block diagram of receiver.

The amplified signal is passed to the detector channel where the timing information is deciphered. A clipper removes the lower amplitude noise. The signal is then band-limited in the phase-locked loop and the transition edge is determined. The output of the PLL is then low-pass filtered. Two criteria are imposed on the pulse after this step. It must meet threshold and minimum pulse width requirements. The latter is determined by digital integration.

The in-band noise that is not removed by the clipper is generally of shorter duration than the pulse and would be removed by the minimum pulse-width requirement.

Receiver Application of the PLL

In the receiver just described, a phase-locked loop is employed to detect a 1-ms frequency-shifted pulse centered at 31.25 kHz. The pulse is transmitted at 34.48 kHz for twenty cycles and switched to 28.57 kHz for twelve cycles, which completes the 1-ms period.

The phase-locked loop is tuned to a free-running frequency of f_0 = 31.25 kHz, and the capture range is set to include the high and low frequency extremes of the pulse. During the reception of a frequency-shifted pulse, the PLL locks onto the high-frequency portion within a few cycles. At the frequency transition, the PLL follows the frequency shift almost instantaneously. This results in a negative ramp in the output of the phase detector. In the presence of noise and reverberation, this frequency transition is the most stable timing edge of the signal. Note that the PLL is always locked during the frequency transition.

Timing Error Due to Noise

The phase-locked loop functions as an FM discriminator. The output of the low-pass filter following the loop can be written as

$$Y(t) = s(t) + n(t) \ , \qquad (1)$$

where s(t) is the noiseless output and n(t) is additive noise. The additive noise at the output of the discriminator can be attributed to two effects. When the signal-to-noise ratio is high, the additive noise causes fluctuations in the envelope of the input signal. These fluctuations in turn result in noise at the output of the discriminator. Secondly, the input noise can also result in some spurious zero crossings in the input signal. The spurious zero crossings primarily occur when the signal-to-noise ratio is low, and cause noise spikes at the output of the discriminator. An expression for the variance of the output noise that accounts for both effects is[1]

$$\sigma_n^2 = \frac{W^2}{3BR} + 2Wf_\Delta \exp[-R] \ , \qquad (2)$$

where f_Δ is the magnitude of the frequency step, R is the signal-to-noise power ratio out of the bandpass filter, and B and W are the bandwidths of the bandpass and low-pass filters, respectively.

The effect of noise on the output of the FM discriminator is shown in Figure 2. The additive noise causes an amplitude error ε_n which in turn results in a timing error ε_t. If the signal-to-noise ratio is large, the following approximations can be used:

$$\varepsilon_t \frac{dy(t)}{dt} = \varepsilon_n \qquad (3)$$

or

$$\varepsilon_t = \frac{\varepsilon_n}{\frac{dy(t)}{dt}} \ . \qquad (4)$$

The slope of the output is approximately equal to the size of the frequency step f_Δ divided by the rise time t_r. Therefore

$$\varepsilon_t = \frac{\varepsilon_n t_r}{f_\Delta} \simeq \frac{\varepsilon_n}{2Wf_\Delta} \ . \qquad (5)$$

The variance of the timing error is

$$\sigma_t^2 = \frac{1}{4W^2 f_\Delta^2} \sigma_n^2 \ , \qquad (6)$$

where σ_n^2 is given by Eq. 2. The standard deviation of the resultant timing error is

$$\sigma_t = \frac{1}{2Wf_\Delta} \sqrt{\frac{W^3}{3BR} + 2Wf_\Delta \exp[-R]} \ . \qquad (7)$$

For the system being considered here, W = 3.3 kHz, B = 10 kHz, and f_Δ = 6 kHz.

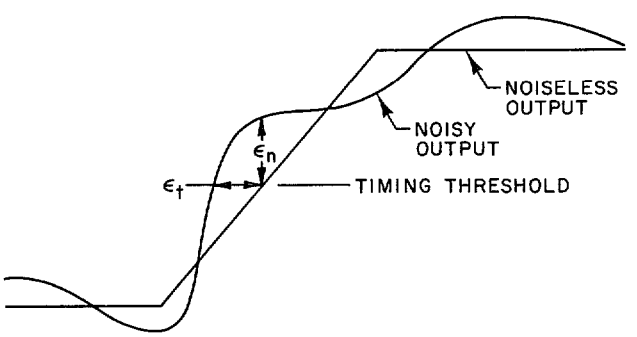

Figure 2. Effect of noise on the output of the FM discriminator.

Experimental Analysis of the Receiver

In determining the timing errors of the receiver, we used the experimental setup shown in Figure 3. The sync pulse triggered a frequency-shifted pulse and, at the same time, started the time interval counter. The receiver processed the pulse and generated a digital signal to stop the counter. In order to compare the frequency-shift method of time determination and the leading-edge method, the PLL was temporarily converted to an amplitude detector for another series of timing error tests.

The results of the tests using the frequency-shifted pulse and the PLL detector are tabulated

in Table I and the results using a single frequency burst and an amplitude detector are tabulated in Table II.

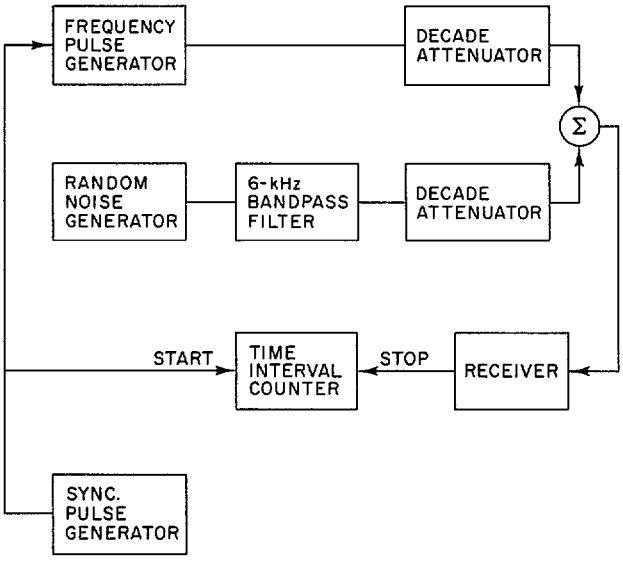

Figure 3. Experimental setup for determination of timing errors.

Table I. Frequency-shift detection.

S/N Ratio (dB)	$\bar{\chi}$ (μs)	σ (μs)
10	942	18
13	933	4
16	929	6
20	927	3
30	934	1
40	934	1
50	933	1

Table II. Leading-edge (amplitude) detection.

S/N Ratio (dB)	$\bar{\chi}$ (μs)	σ (μs)
10	672	47
13	589	38
16	491	25
20	410	20
30	367	17
40	346	11
50	336	6

The average time from the trigger pulse to the arrival time $\bar{\chi}$ for these two situations is plotted in Figure 4. These data show a significant minimization of the timing error when the frequency-shift detection method is used. With the leading-edge detection method, the timing error is 336 μs over the 40-dB range of S/N ratios shown whereas with the frequency-shift method it is 10 μs (see Tables I and II). In theory, $\bar{\chi}$ is constant as a function of the S/N ratio for the frequency-shift method. When timing errors are important and the dynamic range of the received signal is large, the improvement shown by use of the frequency-shift method would be very significant. The difference between the leading-edge average timing and the frequency-shift average timing is due to the fact that the frequency-shift detection point comes at approximately 600 μs whereas leading-edge detection occurs at the start of the pulse.

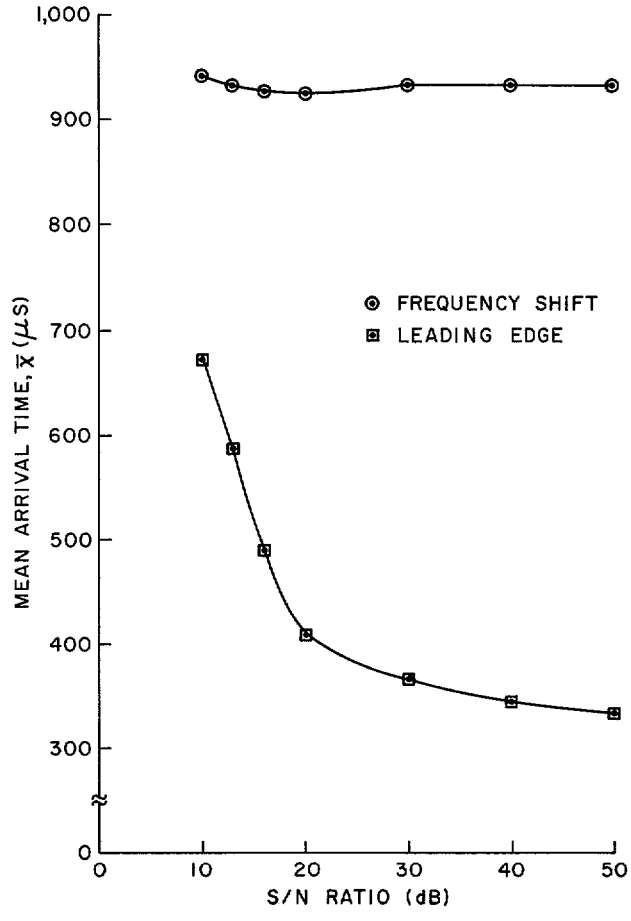

Figure 4. Mean arrival time.

Figure 5 plots the standard deviations of the timing errors with the two methods. There is good agreement between the frequency-shifted experimental data and theory except at the higher S/N levels where the receiver has become saturated. It should be noted that a 1-μs standard deviation is insignificant in most underwater acoustic systems. The leading-edge data show a considerably greater timing deviation.

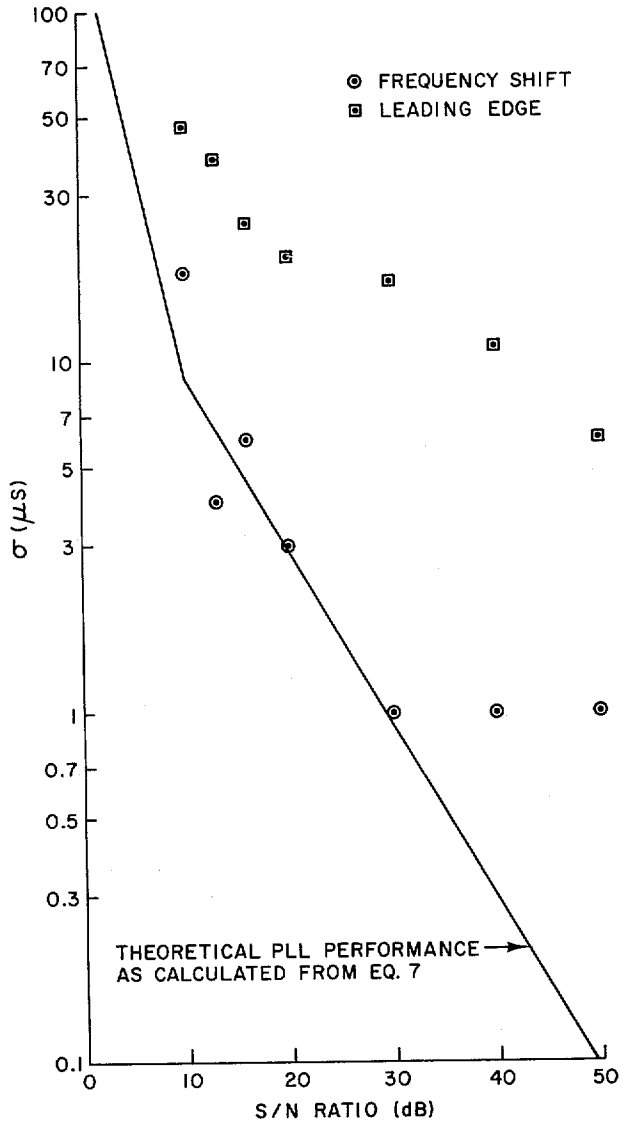

Figure 5. Standard deviation of timing errors.

The foregoing presentation has shown the decided improvement of the PLL detector over the leading-edge detector--both in the reduction of mean timing error and in the reduction of timing deviations (jitter).

Acknowledgment

This work was supported by the Naval Facilities Engineering Command under Contracts N62477-75-C-0364 and N00017-74-C-1208.

Reference

1. R.E. Ziemer and W.H. Tranter, Principles of Communications, Houghton-Mifflin Co., 1976.

SHIPBOARD EVALUATIONS OF DRAG COEFFICIENTS FOR THE MARINE REGIME

C. W. Fairall, G. E. Schacher,
K. L. Davidson, T. M. Houlihan

Environmental Physics Group
Naval Postgraduate School
Monterey, California 93940

Abstract

A considerable amount of overwater dissipation and wind profile data obtained from shipboard measurements were interpreted relative to the representation of the drag coefficient. Drag coefficients were interpreted relative to wind speed, wave and hydrostatic stability influence. It was noted that at all wind speeds and particularly at low wind speeds, drag coefficient values are larger when large waves are present. Likewise, it was noted that in unstable conditions drag coefficient values increase as neutral conditions are approached.

1. Introduction

Drag coefficient is one of the important quantities for characterizing the air-sea interaction. A number of calculations of drag coefficient were made from values of the rate of turbulence dissipation, ε, measured during research programs on optical propagation, fog, and turbulent transport over the ocean. The data was taken during shipboard operations in the Pacific and Atlantic oceans and the Mediterranean Sea. The bulk of the data is from two cruises: The first was the "Cooperative Experiment in West Coast Oceanography and Meterology, 1976" (designated CEWCOM 76) aboard the RV Acania, primarily a marine fog investigation off southern California. CEWCOM 76 was organized by the Naval Postgraduate School and the Naval Ocean Systems Center. The second cruise was aboard the USNS HAYES (designated HAYES 77), organized by Naval Research Laboratory to study aerosols and turbulence in the Atlantic and Mediterranean. A small amount of data taken at anchor in Monterey Bay from the RV Acania using a bow-tethered buoy (designated BUOY 77) that permitted measurements closer (~ 1 meter) to the sea surface is also included in this report.

Atmospheric turbulence and the air-sea interaction have been under investigation for a number of years. Wu (1968) has compiled drag coefficient data from investigations back to 1876 and compared them to laboratory work. He found the oceanic ten meter drag coefficient (C_{10}) to increase with increasing wind velocity up to about U_{10} = 15 m/sec, and to remain constant at higher velocities. Cardone (1970) has proposed a velocity dependence of C_{10} based on Wu's work and Charnock's (1955) relation for aerodynamically rough flow. Cardone proposes that a minimum in C_{10} occurs at wind velocity $U_{10} \simeq 6$ m/sec due to the transition from smooth to rough flow. The velocity at which this minimum occurs is related to the minimum free surface ocean wave phase velocity. On the otherhand, Kraus (1972) lists five investigations that showed no significant velocity dependence for C_{10}. In addition, Cardone showed that C_{10} should be larger for unstable conditions than for stable conditions. This is in agreement with the data of DeLeonibus (1966) and Hasse (1968) but contrary to the results of Smith (1970). This paper will examine both of these issues. Since it is difficult to see how drag coefficient could be a strong function of sea state and also be, on the average, independent of wind velocity (in other words, a lack of dependence on wind velocity implies a lack of dependence on sea state), an examination of wave height effects on drag coefficient is also presented.

2. Theory

A thorough treatment of the boundary layer equations exists in Lumley and Panofsky (1964), Businger (1971) or Kraus (1972). The Reynolds stress, τ, is represented by

$$\tau/\rho = -\langle u'w' \rangle = U_*^2 , \qquad (1)$$

where u' is the fluctuating horizontal wind velocity, w' is the fluctuating vertical wind velocity, U_* is the friction velocity and ρ is the density of air. The height dependence of the mean horizontal wind velocity U and the rate of turbulent energy dissipation ε are

$$\frac{KZ}{U_*}\frac{\partial U}{\partial z} = f_m(R_i), \qquad (2)$$

$$\frac{KZ\varepsilon}{U_*^3} = f_\varepsilon(R_i),$$

where K = .35 is the Von Karman constant. Z is the height above the surface, R_i is the Richardson number, and f_m and f_ε are stability

corrections, equal to 1 in neutral conditions. The Richardson number describes the atmospheric stability in terms of temperature and velocity gradients,

$$R_i = \frac{g}{T} \frac{(\partial\theta_v/\partial Z)}{(\partial U/\partial Z)^2} , \quad (4)$$

where g is the acceleration of gravity, T is the absolute temperature, and θ_v is the virtual potential temperature. In near neutral conditions

$$U_* = (KZ\varepsilon)^{1/3} , \quad (5)$$

and the drag coefficient at height Z is

$$C_z = (U_*/U_z)^2 , \quad (6)$$

and is normally taken at a reference height of 10 meters. Calculations of C_{10} reported herein are based on determination of U_* from ε using the Kolmogorov representation of the one dimensional velocity power spectral density $\phi_u(k)$,

$$\phi_u(k) = \alpha\varepsilon^{2/3} k^{-5/3} \quad (7)$$

where α = .52 and k is the wave number. This is an indirect method of obtaining drag coefficient and several authors have found that it gives 20% to 40% higher results for C_{10} than those from flux or direct stress measurements. This discrepancy is attributed to a breakdown of the "local isotropy" assumption inherent in Equation 7. Unfortunately, small ships are non-stable platforms and a high frequency velocity fluctuation determination of ε (via Eqn. 7) is the only practical method of avoiding the platform motion problem.

3. Instrumentation

The velocity fluctuations were measured with cylindrical hot film sensors using a Thermo-Systems type 1054 constant temperature amemometer. The velocity signal was amplified, filtered, and recorded on FM tape. On the HAYES 77 cruise the data was real-time analyzed in a manner described in Section 4. Mean temperature was measured with an HP model 2850 B quartz thermometer, accurate to .01°C. The relative humidity was measured with Hygrodynamics hygrosensors (Dunmore type lithium chloride), accurate to about 3% RH. Mean winds were measured using Thornthwaite cup anemometer units, accurate to about 4%. One of each of the instruments was operated at each level, with an additional quartz thermometer for sea surface temperature. The measurement heights for the three cruise were as follows:

	Height in Meters			
CRUISE	LEVEL I	LEVEL II	LEVEL III	LEVEL IV
CEWCOM 76	4.2	6.6	11.3	17.5
BUOY 77	1.0	3.0	6.6	
HAYES 77	10.5	21		

The mean data from all levels were logged with a mini-computer data acquisition system. Averaging times were usually 20 to 30 minutes. In addition, routine weather observations were made including estimations of wave height.

4. Data Analysis

Velocity fluctuation data from the FM tape was evaluated using a fourier spectrum analyzer. Assuming k = $2\pi f/U$, Equations 4 and 7 yield

$$U_* = (2\pi Kz/U)^{1/3} (f\phi_u(f)/\alpha)^{1/2}, \quad (8)$$

where f is the frequency in Hertz. A real-time analysis during the HAYES 77 cruise was obtained by measuring the RMS value of the velocity fluctuations in a frequency band specified by a lower frequency limit, f_ℓ, and an upper frequency limit, f_u. This can be related to the spectral density by

$$\int_0^\infty \phi_u(k)\, dk = \langle u'^2 \rangle. \quad (9)$$

Since we are measuring the RMS of u' between frequency limits, we must evaluate the integral between these same limits,

$$\int_{k_\ell}^{k_u} \phi_u(k)\, dk = \langle u'^2 \rangle_{measured}. \quad (10)$$

Again using k = $(2\pi f/U)$ we can write the friction velocity as

$$U_* = (2\pi KZ/U)^{1/3} \left[\frac{\pi/(3\alpha)}{f_\ell^{-2/3} - f_u^{-2/3}}\right]^{1/2} u'_{RMS}. \quad (11)$$

Equation 8 is referred to as the spectral method and Equation 11 as the RMS method. During HAYES 77 an f_ℓ = 2 HZ and f_u = 200 HZ were selected. A comparison of the two techniques for the HAYES 77 data is given in Fig. 1.

Since the HAYES 77 and CEWCOM 76 cruises were moving ship operations, U_{10} was not measured directly. For CEWCOM 76 periodic true wind measurements made with the ship stopped (Fig. 2 is an example) were used and interpolations between measurements were effected. For HAYES 77, U_{10} was calculated from the relative wind speed and direction and the ship's speed (hand recorded from a convenient readout). Both methods lead to considerable errors in U_{10}. The BOUY 77 data is much more accurate since the system is not moving and the sensors are closer to the surface where the turbulence and gradients are greater. Fig. 3 shows the single measurement standard deviation, σ , for C_{10} (calculated from U_* averaged over all levels) from the BUOY 77 data and the combined HAYES 77 and CEWCOM 76 data. It is interesting that for the BUOY 77 data, the ε based values for U_* are lower than the profile values (Fig. 4). Except for Fig. 4, corrections for stability were

not made since data occurs predominately for neutral conditions. Fig. 5 shows the probability distribution of the Richardson number (at Z = 10 meters) for 523 values obtained over the three cruises.

5. Results

Average values of C_{10} for the three data sets are shown as a function of wind velocity in Fig. 6 and are combined in Fig. 7 to compare with Cardone's curve. The error bars represent the expected error for the average ($\pm \sigma/\sqrt{N}$, N = number of points). The minimum value of C_{10} occurs at $U_{10} \simeq 5.5$ m/sec in good agreement with Cardone's proposed minimum of 6 m/sec. The average for all 445 data values is $C_{10} = 1.55 \times 10^{-3}$ and $\sigma/\sqrt{N} = .05 \times 10^{-3}$.

A part of the normal operation weather observations were "visual" estimates of predominate wave height categories and the C_{10} vs U_{10} analysis (Fig. 8) was repeated. Kraus (1972) argues that there should be little, if any, sea state effect on C_{10} on the grounds that the wind interacts primarily with the high frequency part of the spectrum. The measured rapid increase of C_{10} for decreasing velocity with larger waves is definitely statistically significant, although it could be due to increasing violation of the local isotropy assumption.

One of the more interesting results of this data is the shift of the C_{10} vs U_{10} curve with stability. Despite theoretical predictions, lower values of C_{10} were found for unstable conditions (Fig. 9). In this graph, U_* elements used to determine C_{10} were corrected for stability using $f_\varepsilon(R_i)$ from Champagne et al (1977).

This unexpected result in relative magnitudes of neutral and unstable C_{10} values also occurred in a considerable number of overwater data described by Deleonibus (1971). He argued convincingly that differences from predictions were due to wave influence.

6. Summary and Conclusions

A considerable amount of overwater dissipation (ε) and wind profile data obtained from shipboard measurements were interpreted relative to the representation of the drag coefficient. Analyses procedures used were those which are practical in view of inherent difficulties in shipboard measurements of both fluctuating and mean parameter. Drag coefficients were interpreted relative to wind speed, wave and hydrostatic stability influence. The small scale velocity fluctuation data used to define ε was not considered to be influenced by ship motion. Reasonable definitions of hydrostatic stability as well as visual estimates of wave conditions were used in the interpretations.

Drag coefficient (C_{10}) versus wind speed (U_{10}) results are in agreement with representation which characterize a smooth flow regime, C_{10} decreasing with increasing U, at low wind speeds and rough flow regime, C_{10} increasing with increasing U_{10}, at higher wind speeds. The minimum C_{10} value was near 5.5 m sec^{-1} and the distribution agreed reasonably well with a representation by Cardone (1969).

A C_{10} versus U_{10} representation in which C_{10} values were grouped in three wave height categories indicated that at all wind speeds and particularly at low wind speeds the C_{10} values are larger when larger waves were present.

A C_{10} versus V_{10} representation in which C_{10} were grouped in two stability categories indicated that in unstable conditions, C_{10} values increase as neutral conditions are approached.

Acknowledgements

The authors wish to recognize the technical and operational contributions of Jim Corbin and Lyn May. This work is supported by NAVSEA PMS 405 and NAVAIR.

References

1. Brocks, K. and Krugermeyer, L., 1970: The Hydrodynamic Roughness of Sea Surface. Institute for Radiometeorologie and Maritime Meteorologie Report No. 14, Hamburg University.

2. Businger, J. A., Wyngaard, J. C., Izumi, Y. and Bradley, E. F., 1971: Flux-Profile Relationships in the Atmospheric Surface Layer. J. Atmos. Sci. 28, 181-9.

3. Cardone, J. J., 1969: Specifications of the Wind Distribution in the Marine Boundary Layer for Wave Forecasting. New York University, Scientific Report GSL-TR69-1, University Heights, New York.

4. Champagne, F. H., Friehe, C. A., LaRue, J. C., 1977: Flux Measurements, Flux Estimation Techniques and Fine Scale Turbulence Measurements in the Surface Layer Over Land. J. Atmos. Sci. 34, 515-530.

5. Charnock, H., 1955: Wind Stress on a Water Surface. Quart. J. Roy. Meteorol. Soc. 81, 639.

6. DeLeonibus, P. S., 1966: Momentum Flux Observations from an Ocean Tower. U. S. Naval Oceanographic Office (Unpublished) Washington, D.C.

7. Hasse, L., 1968: On the Determination of the Vertical Transports of Momentum and Heat in the Atmospheric Boundary Layer at Sea. Hamburg Geophysikalishe Einzelschrifen, Heft II.

8. Kraus, E. B., 1972: Atmosphere - Ocean Interaction. Oxford, Clarendon Press.

9. Lumley, J. L. and Panofsky, H. A., 1964: The Structure of Atmospheric Turbulence, New York, Inter-Science.

10. Smith, S. D., 1970: Thrust-Anemometer Measurements of Wind Turbulence, Reynolds, Stress and Drag Coefficient over the Sea. J. Geophys. Res. 75 (33), 6758-70.

11. Wu, Jim, 1969: Froude number Scaling of Wind-Stress Coefficients. J. Atmos. Sci., 26, 408-13.

12. DeLeonibus, P. S., 1971: Momentum Flux and Wave Spectra Observations from an Ocean Tower, J. Geophys. Res., 76, 6506-27.

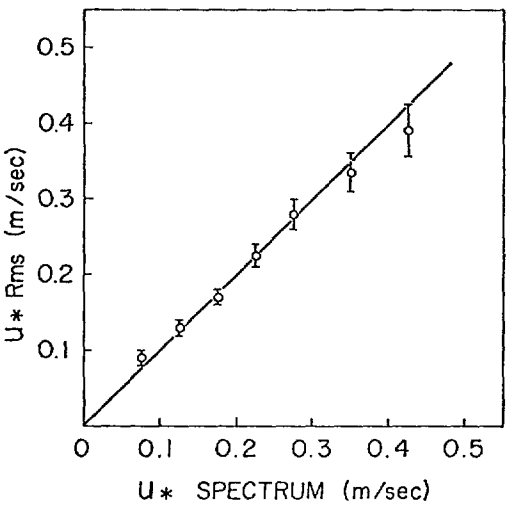

Figure 1. A comparison of the RMS vs the SPECTRUM method for measuring U_* during HAYES 77. The error bars represent $\pm \sigma/\sqrt{N}$.

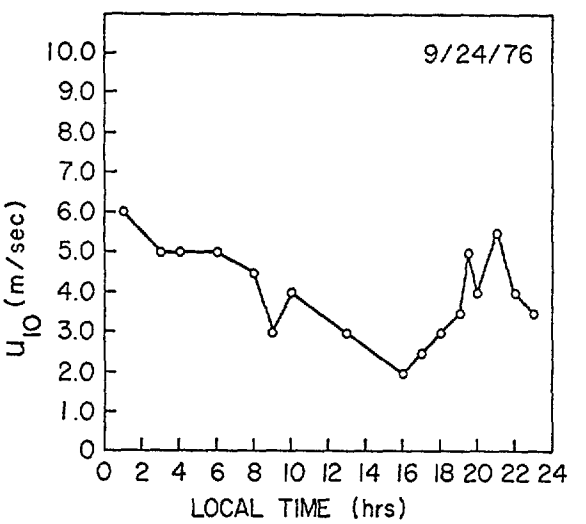

Figure 2. Mean wind velocity at Z = 10 meters vs local time for the day 9/24/76 during CEWCOM 76.

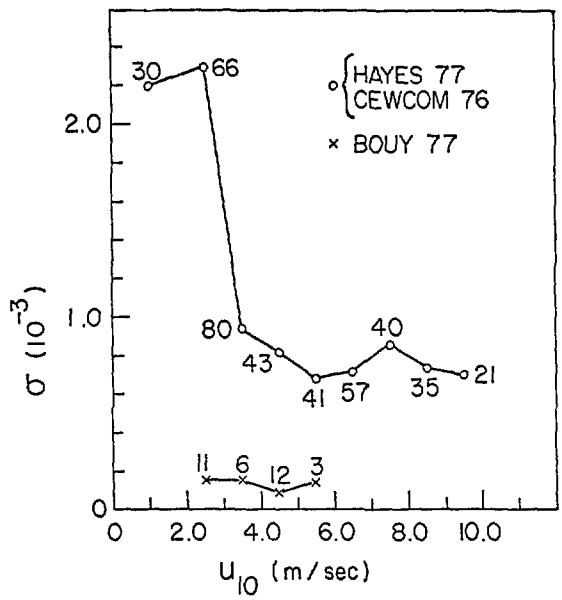

Figure 3. Standard deviation, σ , vs U_{10}. The number of values averaged are shown for each point.

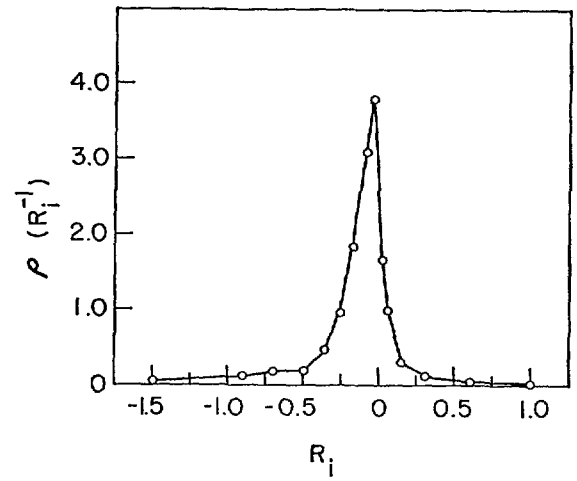

Figure 5. The probability density of occurrence of Richardson number, $\rho(Ri)$ vs R_i, all data combined.

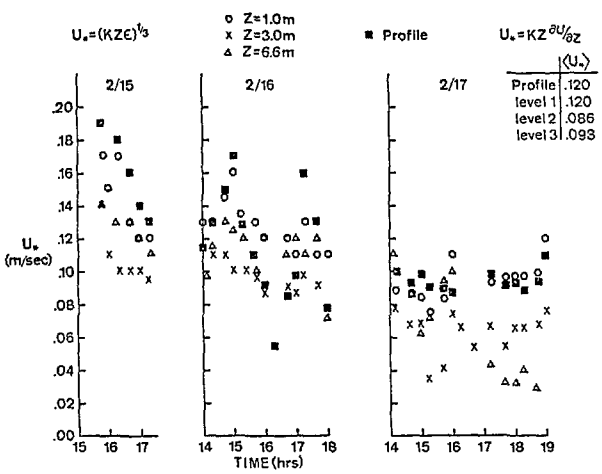

Figure 4. Friction velocity, U_*, vs local time for BUOY 77.

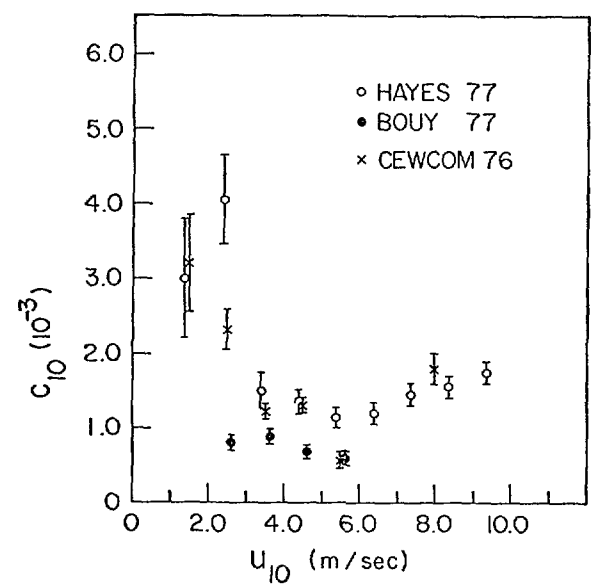

Figure 6. Drag coefficient vs wind velocity for each data set. The error bars represent $\pm\ \sigma/\sqrt{N}$.

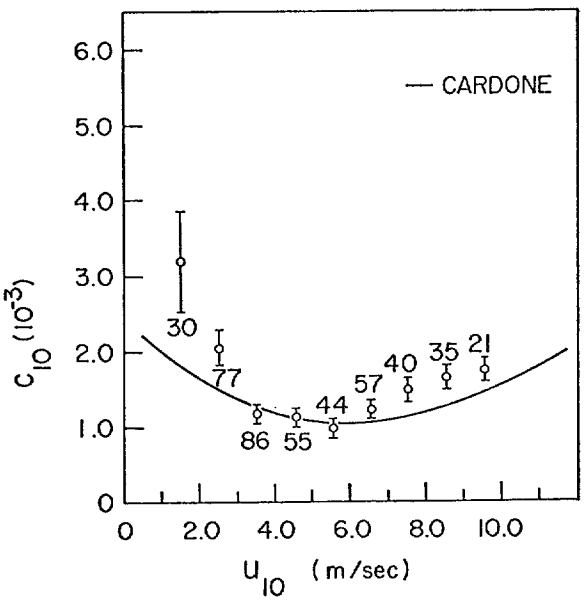

Figure 7. Drag coefficient vs wind velocity, all data. The error bars represent $\pm\ \sigma/\sqrt{N}$. The number of values averaged are shown for each point.

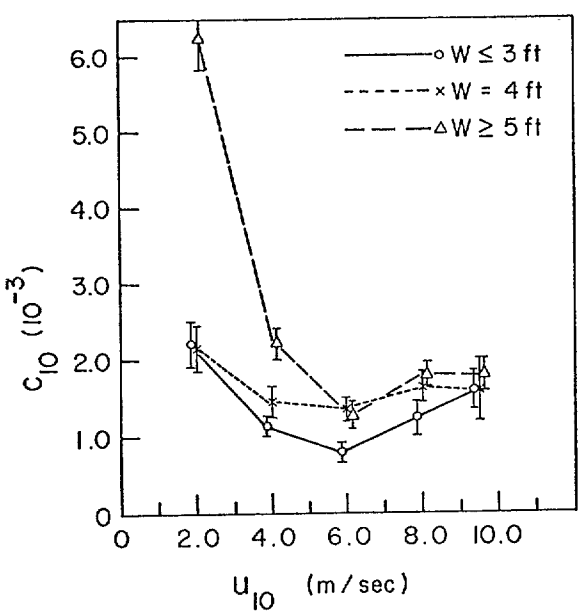

Figure 8. Drag coefficient vs wind velocity for different categories of wave height, W. The error bars represent $\pm\ \sigma/\sqrt{N}$.

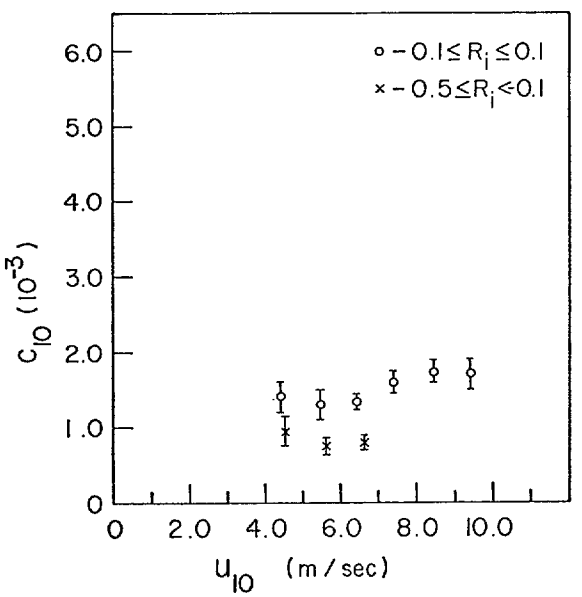

Figure 9. Drag coefficient vs wind velocity for different categories of atmospheric stability.

THE MECHANICAL PROPERTIES OF CHITOSAN MEMBRANES

R. B. Clark
Graduate Research Assistant
Department of Materials Science and Engineering
Massachusetts Institute of Technology
Cambridge, Massachusetts 02139

B. L. Averbach
Professor of Materials Science
Department of Materials Science and Engineering
Massachusetts Institute of Technology
Cambridge, Massachusetts 02139

ABSTRACT

The mechanical properties of chitosan membranes have been investigated as a function of several processing variables. Chitosan, the deacetylated derivative of chitin (N-acetyl-D-glucosamine), was processed from blue crab shells from Virginia. Various chitosans, which had been deacetylated under different conditions, were dissolved in weak acetic acid and then cast into clear, flexible membranes about 50 μm thick. The stress-elongation curves exhibited a fairly constant elastic modulus, a yield point, and a high tensile strength (avg. 135 MPa). The mechanical properties were not greatly affected by the deacetylation procedures investigated here, although a small decrease in yield strength and an increase in elongation were observed at the highest temperature used (100°C).

1. INTRODUCTION

Chitin is the structural component in the shells of crustaceans. Chitosan is formed by the deacetylation of chitin, but chitosan is not a unique product because of variations in the raw materials and in the processing procedures. Chitin itself varies from one crustacean species to another and even from part to part in the same animal. Also, the literature indicates a wide variety of processing procedures, and these variations result in chitosans with different properties. In the present work we utilized only the bottom shell of the blue crab from Virginia. Each phase of the processing was carefully controlled. First, the crushed shells were soaked in dilute HCl to remove minerals, primarily calcium carbonate. Next, a weak NaOH solution was used to remove the intrinsic protein. The resulting chitin was deacetylated in strong NaOH solutions at elevated temperatures. This last step, deacetylation, is the most difficult. If the conditions are too mild, the product is insoluble, due to residual chitin. If the conditions are too severe, the chitosan polymer chains are degraded. This work addresses the effects of such degradation on some of the properties of chitosan.

Chitosan is an excellent film former. We have cast membranes from various chitosans dissolved in weak acetic acid and have investigated the effects of the deacetylation variables on the mechanical properties of the resulting films. Although the properties of chitin membranes have been studied, there has been very little research on the mechanical properties of chitosan films. Chitosan membranes are potentially useful as a wrapping material, and these data on the mechanical properties may serve as basic information for such applications.

2. RAW MATERIAL

Nine samples of chitosan were produced from the bottom shell of blue crabs by Mr. Peter Perceval at the Hunt Crabmeal Company of Hampton, Virginia. Samples A through F were demineralized in 5% HCl for 16 hours at room temperature and deproteinated in 2% NaOH for 2 hours at 85°C. For samples G, H, and J, the time of demineralization was reduced to 5 hours, and the temperature of deproteination was lowered to 65°C. There were no significant differences in properties due to these changes.

Table I shows the variations in deacetylation parameters among the samples. Samples A, B, and C were made from the same batch of chitin and were identical except for the time of deacetylation. Samples D, E, and F were processed to check the effects of NaOH concentration. The last three, G, H, and J, differed mainly in the temperature of deacetylation. The chitosans used in this study were low in impurity content. Calcium averaged 0.02% (by weight) and never exceeded 0.06%. Residual ash values ranged from 0.02% to 0.17% and averaged 0.1%.

3. EXPERIMENTAL PROCEDURE

Eight grams of chitosan were mixed with 784 grams of distilled water. After the addition of 16.00 grams of acetic acid, the solution was stirred for 10 minutes and allowed to stand for at least 12 hours. Large insoluble particles were filtered out with nickel mesh (#40). The solution was maintained at 20°C, and viscosity measurements were made using spindle #1 of a Brookfield LV viscometer. The solution was then centrifuged through a TFE filter having 30-60 μm

TABLE I

CHITOSAN SAMPLES

Sample	Deacetylation procedure	Viscosity* ($N \cdot s/m^2$)	Mw+ (10^6)
A	50% NaOH, 2 hrs., 100°C	.652	1.012
B	50% NaOH, 3 hrs., 100°C	.476	.997
C	50% NaOH, 4 hrs., 100°C	.297	.732
D	41% NaOH, 4 hrs., 100°C	.148	.634
E	45% NaOH, 3 hrs., 100°C	.142	.635
F	50% NaOH, 3 hrs., 100°C	.332	.886
G	50% NaOH, 4 hrs., 75°C	2.070	1.298
H	50% NaOH, 3 hrs., 90°C	1.010	1.094
J	50% NaOH, 3 hrs., 100°C	.354	.887

* Solution containing 8 gms chitosan, 16 gms acetic acid, and 784 gms of water.

\+ Weight average of the molecular weight.

pores. (Sample D had so many insoluble particles that this step was omitted.) After a thorough stirring, the solution was poured into a level glass tray (29 cm square) and dried with forced air. When the film was dry (approximately 40 hours later), it was soaked in 1 M NaOH and then rinsed with distilled water to neutrality. The wet membrane was placed on a celluloid sheet and dried with forced air. The result was a clear, flexible membrane about 50 μm thick.

The mechanical testing procedure closely followed ASTM Method D882. The films were conditions at 23° ± 3.0°C in 30-50% relative humidity for at least 40 hours prior to testing. Test strips 1.27 cm in width and about 16 cm in length were cut with a razor blade. 223 specimens were obtained from 23 films. The thicknesses were measured to ± 1 μm with a dial micrometer, and the minima were marked with a felt-tip pen. (Due to the presence of insoluble particles, sample D had to be measured optically in a microscope, resulting in a loss of accuracy.) The strips were examined for flaws and then placed in rubber-faced grips with a 10 cm length between grips. Tensile tests were made at a strain rate of 0.5 per min. at room temperature in 30-50% relative humidity. The films were observed during testing to see if yield and failure occurred at the minima and if flaws influenced the results.

4. RESULTS AND DISCUSSION

Figure 1 shows the characteristic shape of the stress-elongation curve of thin chitosan films. The two almost linear regions were also noted by Joffe and Hepburn for aged regenerated chitin films (1). The sharpness of the yield point seemed to improve with the uniformity of film thickness. Some of the thinner films also exhibited a slight yield drop just past the yield point, as shown in Figure 1.

The modulus of elasticity was difficult to determine accurately because of the relatively high strain rate employed. 194 strips had an average value of 6300 MPa with a standard deviation of 710 MPa (based on minimum rather than average areas). Joffe and Hepburn reported values close to 2000 MPa; Yaku and Yamashita obtained moduli near 1200 MPa for acetylated chitosan films (2).

The tensile strength varied widely from strip to strip but showed no significant differences among the batches. The average value, 135 MPa (standard deviation: 18 MPa), was based only on the 166 samples that broke at or near their marked minima. This result compares favorably with the value of Muzzarelli et al of 69 MPa for chitosan films (3). One of us (B.L.A.) earlier reported a tensile strength of 152 MPa for a chitosan film prepared in a manner similar to the present method (4). However, these values are all below the 590 MPa reported for horseshoe crab chitin by Rutherford and Austin (5).

Figure 1. Stress-elongation curve characteristic of chitosan membranes (strain rate: 0.5 per min.).

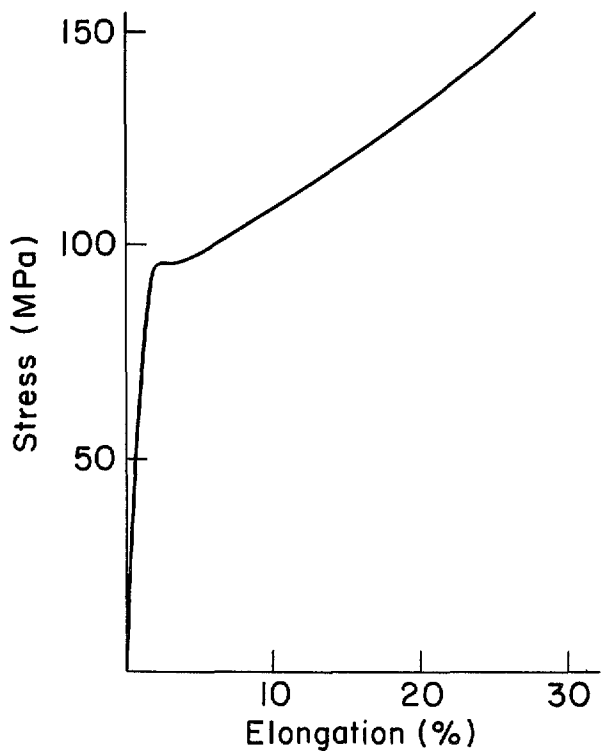

Table II lists the yield strengths of the samples. Examination of the results for samples A - C reveals no clear trend of yield strength with respect to deacetylation time. Thus, polymer degradation, as judged by viscosity and molecular weight (Table I), had no effect on the yield strength of samples varying in time of deacetylation. For samples deacetylated with varying NaOH concentrations (D - F), no trend could be established since the high yield stress of D was probably due to the inaccurate thickness measurements.

On the other hand, temperature variations appeared to have a slight effect on the yield strength. This is shown graphically in Figure 2. The yield strength remains constant for the lower temperatures but drops between 90° and 100°C. This slight trend however is not comparable to the large shift in molecular weight illustrated in Figure 3.

The total elongation of the chitosan strips is shown in Table III. Samples A, B, and C again show the ambiguous effect of deacetylation time. More study will be required to confirm an increased elongation for chitosan deacetylated for 3 hours (sample B). The apparent trend due to NaOH variation (samples D - F) should be viewed with caution since the insoluble particles in D probably caused premature fracture. It is felt that the 8.2% elongation of sample D is not characteristic of the material.

TABLE II

YIELD STRENGTHS OF CHITOSANS

Sample	Number of usable test strips*	Average yield strength (MPa)	Standard deviation (MPa)
A	13	96.4	6.5
B	20	93.5	4.0
C	18	102	3.5
D	25	116	7.7
E	30	98.4	6.7
F	23	95.0	5.1
G	25	103	6.7
H	31	104	4.0
J	27	97.0	5.3

* Includes only strips that yielded near measured minima.

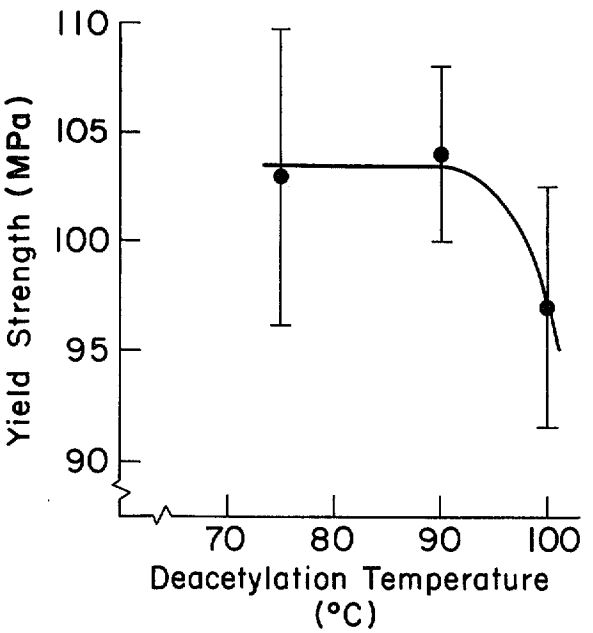

Figure 2. The effect of deacetylation temperature on the yield strength of chitosan membranes.

Samples G, H, and J indicate that increased deacetylation temperatures caused larger elongations. This trend is graphically depicted in Figure 4. The reason for increases in elongation with lower molecular weights is unclear. Microstructural analysis of these samples should aid in intrepreting these data.

The NaOH concentration during deacetylation appeared to be critical for the solubility of the resulting chitosan. For the blue crab chitosan, 45% NaOH was the minimum solution strength required.

1. CONCLUSIONS

The deacetylation variables studied had little effect on the mechanical properties of blue crab chitosan membranes. However these same variables caused substantial changes in viscosity and molecular weight. It therefore appears that variations in viscosity and molecular weight do not greatly affect the mechanical properties of chitosan films. It should be noted that these conclusions only apply to the rather narrow range of deacetylation variables studied here.

6. ACKNOWLEDGEMENTS

This work is a result of research sponsored by the MIT Sea Grant Program, supported by NOAA's Office of Sea Grant, U.S. Department of Commerce, under grant number 04-7-158-44079. The U.S. government is authorized to produce and distribute reprints for governmental purposes notwithstanding any copyright notation that may appear hereon.

The authors wish to thank Mr. Peter Perceval, and Mr. William P. Hunt of the Hunt Crabmeal Company, for their close cooperation in the processing of the chitosan. Thanks are also due Dr. Wayne Bough and Dr. Arnold Wu of the Marine Extension Service, University of Georgia, for the molecular weight data and for advice on the techniques of viscosity measurements.

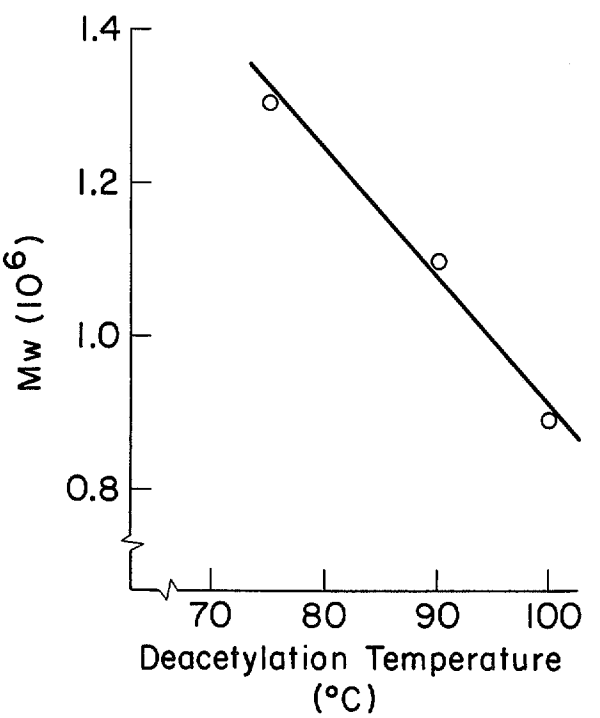

Figure 3. The effect of deacetylation temperature on the molecular weight of blue crab chitosan.

TABLE III

ELONGATION OF CHITOSAN STRIPS

Sample	Number of usable test strips*	Average elongation to fracture (%)	Standard deviation (%)
A	12	15	6.4
B	18	25	7.5
C	18	14	7.2
D	28	8.2	4.2
E	23	19	8.4
F	21	24	7.4
G	28	9.1	5.8
H	30	19	9.4
J	27	25	9.6

* Excludes strips that broke at flaws.

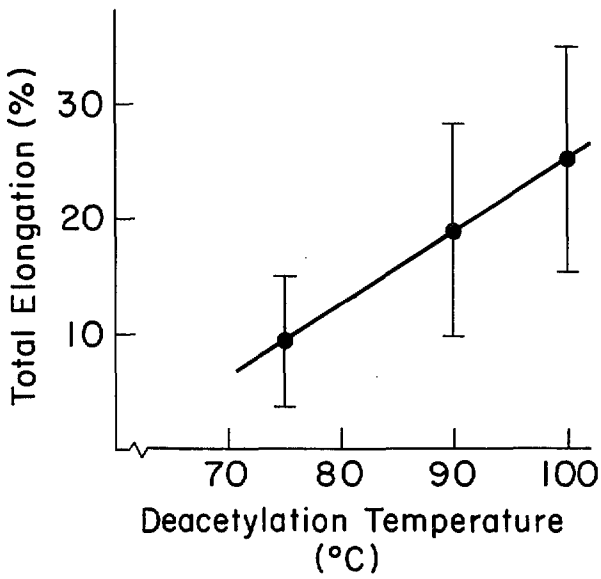

Figure 4. The effect of deacetylation temperature on the elongation at break of chitosan membranes.

7. REFERENCES

1. I. Joffe and H. R. Hepburn, Observations on Regenerated Chitin Films, Journal of Materials Science, 8 (1973), p. 1751.

2. F. Yaku and K. Yamashita, A Method for the Production of Chitin Film, Japanese Patent No. 48-19213, June 12, 1973.

3. R. A. A. Muzzarelli, A. Isolati, and A. Ferrero, Chitosan Membranes, Ion Exchange and Membranes, 1 (1974), p. 193.

4. B. L. Averbach, Film Forming Capability of Chitosan, Proceedings of the First International Conference on Chitin and Chitosan, (to be published).

5. F. A. Rutherford and P. R. Austin, Marine Chitin Properties and Solvents, Proceedings of the First International Conference on Chitin and Chitosan, (to be published).

SEDIMENT AS A CAUSE OF MACROCYSTIS GAMETOPHYTE NON-SURVIVAL

L. A. Volse, Associate Professor
Department of Applied Science and Engineering
U.S. Coast Guard Academy
New London, Connecticut 06320

Abstract

Survival of Macrocystis spp. gametophytes is a function of sediment depth on the surface to which they attach. Relative survival varies as an exponential function of calculated mean depth in all cases. If spores attach to a surface prior to sediment settlement, no survival is noted after four days at depths above 500 microns. If spore inoculation occurs after settlement, no survival is noted for calculated mean depths above 40 microns. Microscopic examination of silt dispersal patterns showed that below 40 micron depths the percentage of non-occluded surface was also an inverse exponential function of mean sediment depth. We infer that motile zoospores cannot pass through even the finest silt particles. Comparatively better survival is noted with attachment prior to deposition.

1. Introduction

Considerable concern over the disappearance and fluctuation in density of giant kelp (Macrocystis spp.) beds along the southern California coastline has been shown recently. Fisherpersons (sic), sports divers, environmentalists and others value this algae as a vital part of the complex marine ecosystem.

Commercially, the giant kelp plant is a principal source of algin, a highly efficient thickening and gelling agent. Kelp is also a good source of potash and other useful chemicals (Limbaugh, 1955). More recently, concerns over limitations of food and energy resources have pointed towards kelp as a promising panacaea, owing to it's rapid growth characteristic. The former Energy Research and Development Administration's Ocean Farm Project is an example of one of these later schemes.

Giant kelp beds apparently have diminshed both in size and density as the human population of the coast of west America has grown. Although evidence is confusing and difficult to evaluate, North (1970-74) and others contend that Macrocystis tends to flourish along coastlines with less dense populations, compared with it's growth off heavily populated regions such as the Los Angeles basin.

Many hypotheses have been formulated to explain the alleged kelp bed diminishment. They include sea urchin proliferation at sewage outfalls (North, 1970-74), near-extinction of the sea otter (Estes, 1974), increased water turbidity near sewage outfalls (Neushal, 1976), presence of toxic chemicals or pesticides (Barilotti, 1976), and sediment settlement on rock substrate (Devinny, 1977).

The purpose of this paper is to outline certain experiments conducted to test the latter hypothesis that sediment deposits (whatever their origins) might be a direct cause of Macrocystis spp non-survival (Volse, 1977). The studies described herein deal only with the effects of varying the sediment depths under laboratory conditions. Timing of spore inoculations (i.e. whether spores were inoculated prior to or after sediment settlement) proved to be a most important parameter in all of the experiments conducted.

2. Experimental Methods

Procedures for Macrocystis spp. laboratory culture have been developed by Neushal (1963), North (1970) and others. By modifying existing techniques, a standard procedure was developed by the author to provide for statistical analysis throughout the course of his experiments. Zoospores from Macrocystis spp. sporophylls, through chilled seawater temperature shock, were released to form a spore solution. These spores were incubated under controlled conditions of temperature and lighting for a standard period of four days. Various combinations of sediment with and without spore solution went into an array of petri dishes, each containing a microscope slide in conjunction with an appropriate amount of nutrient-rich seawater. Temperature was kept at 80°C throughout all experiments. Four days after inoculation of zoospore solution, slides were removed. sediment washed clean, and a slide cover put in place. Under a light microscope of appropriate power to insure statistical significance, counts of surviving gametophytes were made. A typical appearance of these germlings after four days incubation is shown in the microphotograph of figure 1.

U.S. Government work not protected by U.S. copyright.

Figure 1. Macrocystis pyrifera germlings four days after spore inoculation. Note original 5 micron dia. spore with 30 micron long germ tube offshoot.

To measure a particular inoculation of spores' ability to attach to substrate and survive conditions imposed experimentally, a measure, called gametophyte survival index (GSI) was devised. One petri dish of each experimental array was designated as a "control" dish, with no sediment to be introduced therein. Four days following inoculations, germling counts were made on both control and experimental slides. GSI is defined as the ratio of a field count for an experimental sedimentary slide to a field count for the control slide without sediment. Setting control slide GSI at 100, GSI on a scale from 0 through 100 becomes a relative measure of gametophyte survival under each of the imposed invironmental conditions.

Amounts of sediment calculated to settle compactly at its specific gravity were weighed into plastic bottles along with volumetric measurement of sea water media (enough for duplicate samples). In cases where sediment was added concurrently with spore inoculation (providing opportunity for sediment to settle prior to spore attachment), each dish received 30-ml of well-shaken media-spore-sediment suspension. In cases where sediment was added 24 h later, only 20 ml of media-spore solution first went into dish. The following day an additional 10 ml suspension of media and sediment followed.

Source of Macrocystis spp. zoospores was from sporophylls obtained from the base of plant growing in the vicinity. When immersed in chilled seawater media at 80°C, temperature shock released spores giving a golden-brown color to the solution. A one-ml amount of spore solution went into the sediment-media bottles, and after careful shaking, inoculation into petri dishes was then carried out volumetrically.

To guard against mistakes and to provide a better statistical basis, each of the experiments was run in duplicate. Germlings were counted in the field of either a 500x or 125x light microscope, depending upon the quantities to be visually counted. Nine random counts were made on each experimental slide. Data was compiled and is shown in Tables 1, 2, and 3. Regression analysis is the basis of all statistical testing. Empirical equations fit data selected by the method of least squares. Curves of the types $y = a + mx$, $y = e^{mx}$, and $y = mx^a$ were investigated and the type selected which showed the best correlation coefficient, even when significant fits with lesser correlation might be found.

3. Gametophyte Survival as a Function of Sediment Depth

The totality of experiments established a relationship between GSI and mean calculated sediment depth. Best fit for all data proved to be given by an equation of exponential type, plotting on semi-logarithmic paper as a negatively sloped straight line. Using statistical tables based on quantity of data and correlation coefficients obtained, indicates 99+ percent probability of such data relationship being valid.

Consolidated data from Tables 1 and 2 gave the best equation for the case where spore solution was introduced simultaneously with or prior to sediment placement as

$$GSI = 34.3\, e^{-0.088d}, \qquad \text{Eq. 1}$$

where GSI is in percent and sediment depth, d, is in microns. For 37 data pairs, correlation coefficient is -0.777.

In cases where spores were allowed to attach to slide prior to sediment introduction, the empirical equation is of the same type as Eq. 1 but the exponential coefficient is 1/200th that of Eq. 1 With data from 23 observations (Table 3), best equation is

$$GSI = 54.4\, e^{-0.0044d}, \qquad \text{Eq. 2}$$

with a correlation coefficient of 0.792. Plot of these data along with corresponding empirical equations are shown in Figure 2.

4. Partial Slide Occulsion by Thin Sediment Layers

An examination of several slides before sediment had been washed off prior to germling counts revealed that, owing to gradation of particle sizes (i.e. according to Figure 3, less than 10 percent are smaller than 10 micron diameter) slides with calculated mean depths of up to 20 microns were not fully occluded by sediment. Table 4 indicates the observed relationship between calculated mean sediment depth and the observed percentage of field which appeared as sediment-free. A plot of these data is given in Figure 3, for which the empirical equation

$$PSF = 103\, e^{-0.127d} \qquad \text{Eq. 3}$$

was obtained. PSF is the observed percentage of field that was sediment-free and d is the calculated mean sediment depth (up to about 40 microns). With data from 24 observations during one experiment, a regression coefficient of r= -0.966. This is far greater than r(crit. 1%) = -0.462, showing an extremely high statistical significance. At mean calculated sediment depth of 40 microns or greater,

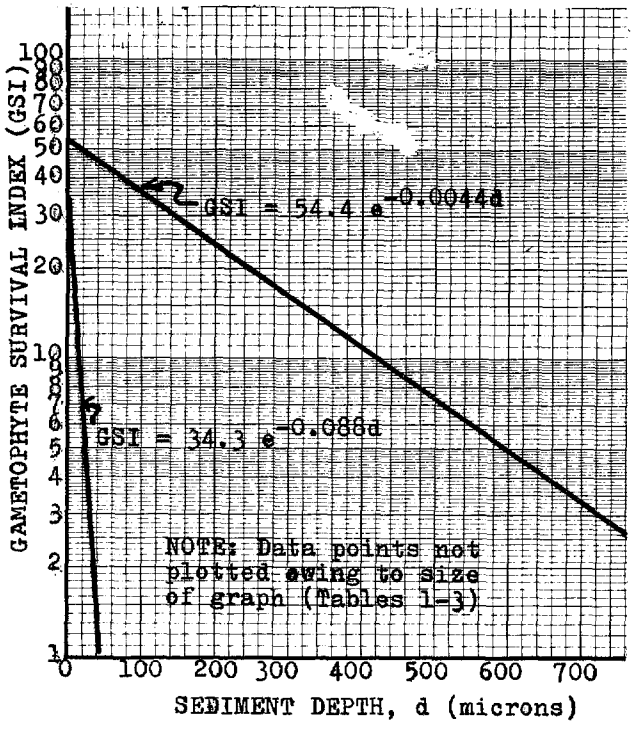

Figure 2. Effects of sediment on survival of Macrocystis pyrifera gametophytes, including effect of timing of spore inoculations. Data taken from Tables 1-3.

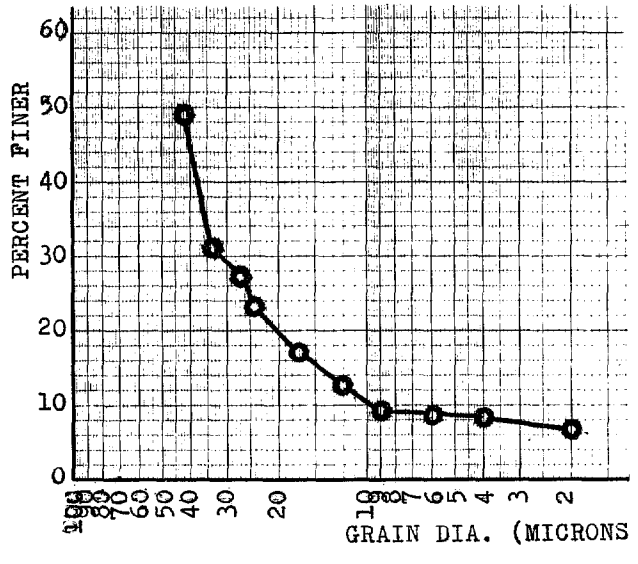

Figure 3. Sediment grain size based on hydrometer analysis of sediments. All particles are smaller than 74 micron diameter.

sediment coverage proved to be complete in all cases viewed. The prime factor involved here seems to be particle occlusion of a surface. Long (1976) remarked that germlings have been observed to attach themselves to small particles and continue their growth under laboratory conditions. Such attachment, although possible, would seem to provide an uncertain fate for the gametophyte, being subject to whatever water currents nature provided. It seems apparent that such attachment to fine particles would prove futile insofar as ultimate sporophyte survival is concerned.

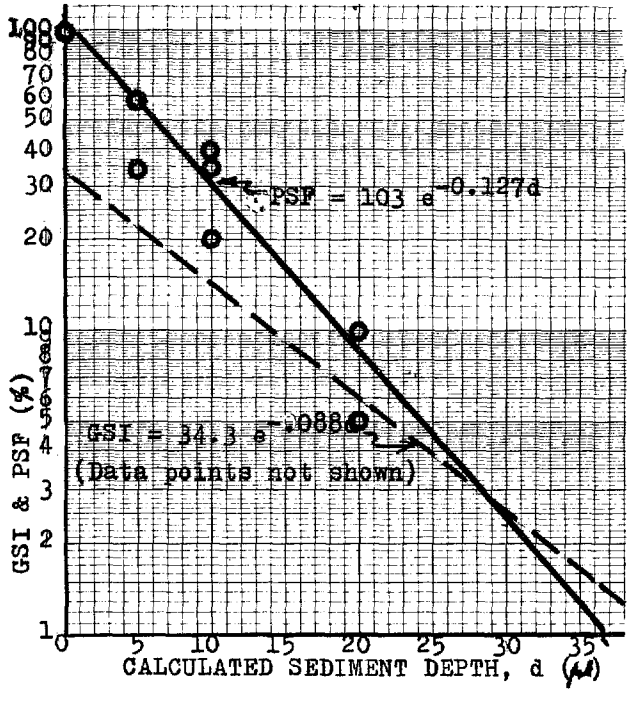

Figure 4. Relationship between calculated mean sediment depth and percentage of field observed as sediment-free. Note the similarity of relationships between GSI and PSF vs. d.

We note from Equation 3 that the percentage of field sediment-free (PSF) is an inverse exponential function of sediment depth, d, as is the gametophyte survival index (GSI) of Equation 1. While the equations are not identical, comparisons over much of the range examined (Figure 3) are consistant with a simple explanation: the spore produces a germling attached to the slide only if it falls on exposed glass. If the spore falls on sediment particles, it either fails to develop or is lost when the slide is rinsed. Because a spore attached to sediment is unlikely to survive under natural conditions, experimental survival rates probably are similar to those under appropriate circumstances in the ocean.

5. Summary and Conclusions

Macrocystis pyrifera gametophyte survival is inversely related to sediment depth. In cases of sediment introduction either before or along with zoospore inoculation, the best empirical equation

corresponding to 37 data pairs (Fig. 2) is

$$GSI = 34.3\ e^{-0.088d}, \qquad \text{Eq. 1}$$

where GSI is gametophyte survival index in percent and d is mean sediment depth in microns. In cases where spore inoculation occurred 24 hours prior to sediment placement, the best empirical equation corresponding to 23 data pairs (Fig. 2) is

$$GSI = 54.4\ e^{-0.0044d}. \qquad \text{Eq. 2}$$

Excellent statistical correlation exists for both equations showing the relationship between variables to be highly significant.

Examination of slides made prior to counting procedures revealed that field coverage by particles is variable, increasing with sediment depth. According to a plot of twenty data pairs (Fig. 4), the best empirical equation is

$$PSF = 103\ e^{-0.127d}, \qquad \text{Eq. 3}$$

where PSF is percentage of surface sediment-free and d is sediment depth in microns. We can conclude that although Equation 3 is not identical with Equation 1, comparison over most of the range examined is consistent with the explanation that a spore produces a germling attached to a slide only if it falls on exposed glass.

By comparison of Equation 1 and Equation 3, and by rounding off the exponential exponent to 0.1 in both cases, we can conclude that an arrpoximate linear relationship exists between GSI and PSF, up to a calculated sediment depth of some 40 microns. It appears that the diameter of particles at these low depths does not control the relationship, but rather the degree of distribution of these particles in occluding the slide. When sediment is in place prior to zoospore arrival, presence of any sized particle is sufficient to impede attachment of zoospore to substrate. Even though spores may manage to attach themselves to loose sediment particles, the ultimate instability of the particle seems to preclude gametophyte survival.

Whenever spores attach themselves to a surface prior to sediment introduction, gametophyte survival chances are greatly increased. We infer that the effect of sediment in this case lies not in interfering with the germling's continued attachment, but rather in preventing nutrients or oxygen from being absorbed by the attached gametophyte.

TABLE 1 -- EFFECT OF VARYING DEPTH OF CONSTRUCTION SAND SEDIMENT ON GAMETOPHYTE SURVIVAL (SEDIMENT IN PLACE PRIOR TO SPORE INOCULATION)

Date of count	Mean sediment depth, d (microns)	No. of counts/ observ.	Mean germling count per field	Std. dev. of mean count	Gametophyte survival index, GSI (percent)
11/12/76	0	18	5.54	2.75	100
	19	9	1.56	0.68	28.2
	19	9	1.11	0.93	20.0
	92	9	0.11	0.33	2.0
	92	9	0.89	0.96	16.1
12/7/76	0	18	348	25.0	100
	5	9	87	6.07	25.0
	5	9	91.4	7.54	26.3
	10	9	12.4	2.14	3.6
	10	9	30.0	2.28	8.6
	20	9	7.00	5.88	1.7
	20	9	5.44	2.07	1.6
	40	9	1.78	1.30	0.5
12/8/76	0	18	300	17.8	100
	5	9	147	12.7	34.4
	5	9	50.5	10.6	16.8
	10	9	50.5	10.6	16.8
	10	9	50.5	10.6	16.8
	20	9	3.22	2.86	1.1
	20	9	5.67	6.28	1.9

Notes: (1) Tabulation consists of compilation of data from two separate experiments, each having a four day culture period.
(2) Sediment particles are less than 74 micron dia.

TABLE 2 -- EFFECT OF VARYING DEPTH OF CONSTRUCTION SAND SEDIMENT ON GAMETOPHYTE SURVIVAL (SEDIMENT AND SPORES MIXED AT TIME OF INOCULATION)

Date of count	Mean sediment depth, d (microns)	No. of counts/ observ.	Mean germling count per field	Std. dev. of mean count	Gametophyte survival index, GSI (percent)
12/15/76	0	36	40.0	10.3	100
	5	9	7.80	3.90	15.9
	5	9	3.00	2.00	6.1
	10	9	5.11	2.20	10.4
	10	9	6.33	2.12	12.9
	20	9	2.40	1.01	4.9
	20	9	2.11	1.27	4.3
1/3/77	0	9	11.56	4.56	100
	5	9	3.00	0.87	26.0
	10	9	3.89	1.76	33.7
	20	9	1.78	1.30	15.4
	30	9	0.33	0.50	2.9
	40	9	0.11	0.33	1.0
1/12/77	0	9	5.56	2.65	100
	5	9	1.56	1.33	28.1
	10	9	0.67	0.50	12.1
	20	9	0.44	0.53	7.9
	30	9	0.44	0.73	7.9
1/23/77	0	9	43.0	9.06	100
	5	9	10.22	3.56	23.8
	10	9	5.67	2.45	13.2
	20	9	2.11	1.05	4.9
	30	9	1.44	1.33	3.3
	40	9	1.11	1.36	2.6

Notes: (1) Tabulation consists of compilation of data from four experiments, each with a four day culture period.
(2) Sediment particles are less than 74 micron dia.

TABLE 3 -- EFFECT OF VARYING DEPTH OF CONSTRUCTION SAND SEDIMENT ON GAMETOPHYTE SURVIVAL (SEDIMENT INTRODUCED ONE DAY AFTER SPORE INOCULATION)

Date of count	Mean sediment depth, d (microns)	No. of counts/ observ.	Mean germling count per field	Std. dev. of mean count	Gametophyte survival index, GSI (percent)
11/12/76	0	18	5.54	2.75	100
	19	9	2.78	1.64	50.2
	19	9	2.22	1.19	40.1
	92	9	4.78	2.17	86.3
	92	9	1.67	1.41	30.1
	456	9	0.67	0.71	12.1
	456	9	0.67	0.67	12.1
12/1/76	0	36	9.00	4.81	100
	19	9	2.56	1.68	28.4
	19	9	7.78	2.39	86.4
	19	9	6.00	3.57	66.7
	19	9	6.22	2.77	69.1
	92	9	4.67	3.08	51.9
	92	9	5.89	2.32	65.4
	92	9	3.56	2.13	39.6
	456	9	1.44	2.13	16.0
	456	9	0.11	0.33	1.2
	456	9	0.44	0.68	4.9
12/15/76	0	36	49.0	10.3	100
	5	9	16.0	6.12	32.7
	5	9	23.7	5.43	48.3
	10	9	17.6	10.5	35.9
	10	9	14.6	5.34	29.7
	20	9	11.3	4.06	23.1
	20	9	21.1	5.18	43.1

Notes: (1) Tabulation consists of compilation of data from three experiments, each with a four day culture period.
(2) Sediment particles are less than 74 micron dia.

TABLE 4 -- RELATIONSHIP BETWEEN CALCULATED MEAN SEDIMENT DEPTH AND PERCENTAGE OF FIELD CLEAR OF SEDIMENT

Calculated mean sediment depth, (d)	Percentage of field observed sediment-free, (PSF)
0	100
0	100
0	100
0	100
0	100
0	100
5	60
5	60
5	60
5	60
5	60
5	35
10	40
10	40
10	40
10	35
10	20
10	20
20	10
20	10
20	10
20	10
20	5
20	5

Notes: (1) Observations made during experiment of 12/8/76.
(2) Construction and sand sediment with particle diameter less than 74 microns.

References

1. Barilotti, D. Craig, "An overview of kelp forest biology," paper presented at environmental symposium for teachers. University of California, La Jolla, California, 2 April, 1976.

2. Devinny, Joseph S., personal communication, University of Southern California, Environmental Engineering Department, Los Angeles, California, 1977.

3. Estes, James A. and Plmifano, John, "Sea otters: their role in sea urchin nearshore communities," Science, 1974: 1058-1060.

4. Limbaugh, Conrad, Fish Life in the Kelp Beds and the Effects of Kelp Harvesting, La Jolla: University of California Institute of Marine Resources, IMR Ref. 55-59, 1955.

5. Long, Ann, personal communication, California Institute of Technology, Marine Laboratory, Corona del Mar. 1976.

6. Neushul, M. and Haxo, Frana T. "Studies on the giant kelp Macrocystis i., growth of young plants," American Journal of Botany 50, 4 (1963):349-353.

7. Neushul, Michael, personal communication, University of California, Santa Barbara, California, December, 1976.

8. North, Wheeler J., Kelp Habitat Improvement Project, Annual Report, 1969-1974, 5 vols., Pasadena, California. Institute of Technology, 1970-1974.

9. Volse, Louis A., Effects of Sediments on Macrocystis pyrifera Gametophytes, doctoral dissertation, University of Southern California, Los Angeles, California, June 1977.

NAVY RESEARCH ON MARINE BORERS AND THE LABORATORY CULTURING OF LIMNORIANS

Kathleen M. Parrish and John D. Bultman

Naval Research Laboratory
Washington, D.C. 20375

ABSTRACT

The Naval Research Laboratory's investigation of the protection of wood in marine service which began with an in depth study of creosote, is now concentrating on a study of the active antiborer constituents of naturally bioresistant woods. This work is now focussing on woods which are resistant to limnorians, marine crustacean isopods, because most current protective measures are inadequate against these pests. In order to study the effect of the natural wood extractives on the physiology of these marine borers under controlled conditions, a laboratory culture of Limnoria tripunctata has been established using a closed recirculating aquarium system. The usual invertebrate closed aquarium culture techniques have been modified to fit our needs. This includes the redesign of the biological filter bed, and its location outside each aquarium. A full description of our closed recirculating aquarium system and the procedures for its maintenance are given.

INTRODUCTION

The ravages of wood-destroying organisms have been known to man since the time of Aristotle. The Greeks and the Romans mention wood-borers in their writings, and according to a German biologist, the Bible refers to borers in the passage, "As the worm the wood, so an ugly wife destroyeth her husband". The Phoenecians and the Vikings and others charred the hulls of their ships and smeared them with a mixture of arsenic, sulfur, pitch, and animal fat to prevent borer attacks. The galleys of Troy were similarly sheathed with lead, and in the 16th century preventive measures were needed when the wooden dikes of Holland were being destroyed.

Today, wooden-hulled ships are no longer important militarily or in world commerce so for them borer damage is no longer a pressing economic problem. However, man is still plagued by the depredation of fixed harbor installations by marine boring organisms and also by fungal infection. Figure 1 shows the extreme damage wrought by these animals in the San Francisco Bay area around 1920 (1).

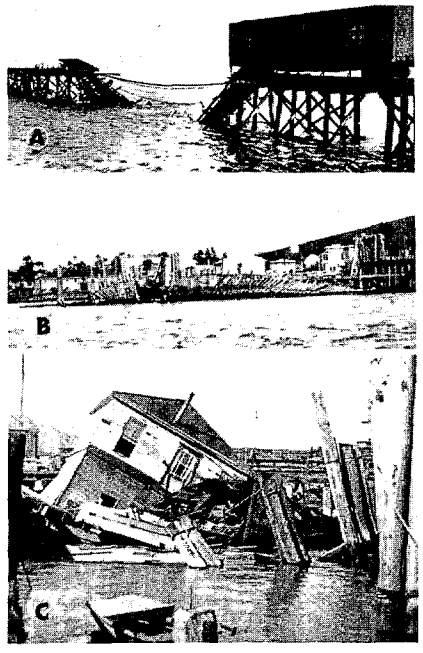

Fig. 1 Wooden structures in San Francisco Bay destroyed by marine boring organisms: A - railroad trestle, B - ferry slip, and C - municiple warf and pier (1). Photo courtesy of the American Wood-Preservers Assn.

Figure 2 shows the typical hour-glass effect caused by limnorians as they damaged piling supporting a pier, and Fig. 3 shows a fender timber thoroughly infested by teredinids. The outer surface of the wood gives little indication of the extent of the internal damage. Although it is difficult to assess the annual expenditure by the Navy for repair or replacement of biodamaged wood, the most recent estimate (2) places the cost at $200 million.

NAVY INTEREST IN WOOD PROTECTION

Navy use of Wood

Wood is our only renewable natural resource available as a construction material. Also, wood is still the cheapest, and frequently the most suitable construction material for many purposes because of its unique physical properties such as strength-to-weight ratio and resiliency. Because

U.S. Government work not protected by U.S. copyright.

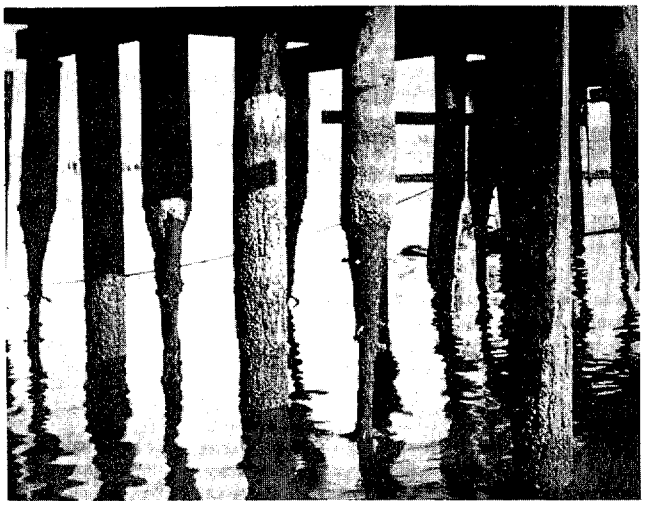

Fig. 2 Limnorian-damaged piling showing the characteristic damage pattern produced by these organisms in the inter-tidal zone (1). Photo courtesy of the American Wood-Preservers Assn.

Fig. 3 Fender timber thoroughly infested by marine borers. The outer surface gives little indication of the extent of internal damage.

of these attributes the Navy uses large quantities of wood. It has in service about 1.5 million utility poles, over 6 million crossties, innumerable dolphins and camels, 1000 piers and wharves, and over 180 miles of fender system constructed of this material (3). Since all of this wood must be treated to protect it from biodeterioration, the Navy has a vested interest in wood preservatives and preservation techniques.

Shortcomings of Present Preservatives

The Navy is interested in wood treatments because current preservatives for wood in marine service are not entirely effective. The most widely used preservative treatment is pressure impregnation with whole creosote or creosote/coal tar, but in tropical and subtropical waters creosoted timbers are often destroyed in a few years by the gribble *Limnoria tripunctata*. Also, creosote can be metabolized by the bacterium *Pseudomonas creosotensis* (4). This microbe degrades the creosote, thus making the wood vulnerable to marine borers. Other treatments with mixtures of copper, chromium, and arsenic (CCA, ACA), with or without subsequent pressure impregnation with creosote, are very effective against borers but the treating process embrittles the wood (5) which breaks upon impact.

Environmental Pollution

The potential for environmental pollution has become a vital consideration in the use of wood preservatives. Creosote and other wood protectants are becoming increasingly suspect, and they are scheduled for review by the Environmental Protection Agency (EPA) as materials possibly hazardous to the environment. Also, creosote is classified as an oil by EPA and its use is subject to the same stringent environmental regulations as other oils. In addition, current attitudes toward copper, chromium, or arsenic in natural situations may prevent their use as wood protectants in the future, even if the treatment technique is improved to prevent embrittlement.

Because of its large investment in wood, the need for more effective treatments, and the potential environmental problems associated with the current wood preservatives, it is important to the Navy to seek new wood protectants which will eliminate these problems and also reduce the annual maintenance costs associated with wooden marine structures.

MARINE BORER RESEARCH

The Naval Research Laboratory (NRL) has been engaged for many years in research on materials protection in the natural environment. Early work by Sweeney and Price (6,7) on wood-preservation involved an exhaustive study of creosote as a marine wood preservative. Currently, research on wood protection is based on a study of naturally bioresistant woods. This includes the isolation of their active constituents, a determination of the effects of these compounds on the physiology of the target organisms, and a determination of the feasibility of using these compounds directly as wood protectants or models from which to develop new protectants. A search for such woods in the Panamanian forest and elsewhere culminated in the evaluation of a large

number of woods for their inherent resistance to wood-destroying organisms (8,9). The most resistant wood in all environments to all wood-destroyers evaluated (marine borers, termites, fungi) was Dalbergia retusa (cocobolo). A phytochemical examination of the heartwood was performed to isolate and characterize the antiborer constituent, subsequently identified as obtusaquinone (10). This compound was active against teredinids but not pholads or limnorians. Research (11) showed that obtusaquinone interfered with the normal formation of shell by metamorphosing teredinid larvae. This is accomplished by disrupting the formation of the tanned protein matrix, the conchiolin network, upon which mineralization takes place.

The ineffectiveness of obtusaquinone toward pholads and limnorians and the prohibitive cost of its commercial production led to a manipulation of the molecular structure of obtusaquinone to see if a better compound could be synthesized. The extensive alteration of the obtusaquinone molecule produced a series of benzylphenols, one of which was found to be very active against the molluscan borers (teredinids, pholads). Susceptible wood treated with this compound was free of damage by teredinids and only very lightly attacked by pholads (Fig. 4). Preliminary studies indicate that this dibutylbenzylphenol will also be an anti-termitic. Its effectiveness against molluscan borers and its easy, economical synthesis on a commercial basis, make this compound a good candidate as a wood protectant for marine service at least for these organisms, and steps will be taken to obtain its certification for this use.

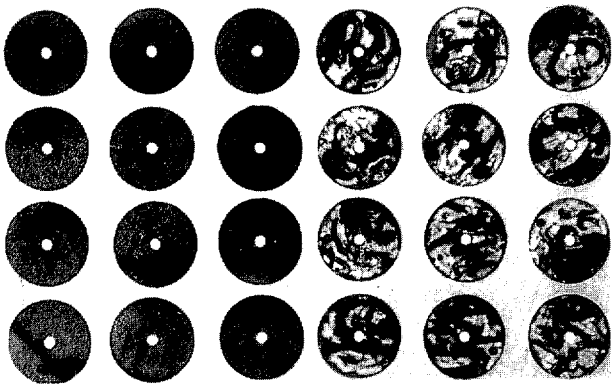

Fig. 4 X-ray photograph of pine sapwood disks. Those of the left contain 0.9% dibutylbenzylphenol, those on the right are untreated controls. The damage was caused predominantly by teredinids.

However, the problem of inadequate protection against wood damage by limnorians remains, and will remain even if creosote continues to be used as a wood preservative. Consequently future work at NRL will be more strongly oriented toward an investigation of those woods which were particularly resistant to attack by limnorians (8). If an economically favorable anti-limnorian could be isolated from one of these woods, it might be possible to incorporate it into creosote, or use it in conjunction with the dibutylbenzylphenol to provide complete borer protection. To study the effects of extractives from these limnorian-resistant woods on the physiology of limnorians we have established a laboratory colony of Limnoria tripunctata to provide the necessary experimental animals.

BIOLOGY OF LIMNORIANS

Limnorians, or gribbles as they are commonly called, are small isopods belonging to the class Crustacea. They average about 0.5 mm in diameter x 3 mm, the male being slightly smaller than the female. The body (Fig. 5) can be divided into three main segments which are the head, thorax, and abdomen. The head possesses six sets of appendages. These include the mandibles and first pair of maxillae which are equipped with sharpened, chitinized tips and strong muscles for chewing. The thorax contains seven pairs of walking legs ending in claws which are used to grasp the wood. During the breeding season a brood pouch develops between the second and fifth swimming legs. Fertilized eggs are deposited here and develop into embryos and larvae; young adults immediately begin boring at right angles to the parental burrow. The abdomen bears six pairs of legs called pleopods. These pleopods are equipped with gills which are constantly in motion, causing a circulation or water within the burrow. This water is enriched with oxygen which is adsorbed and used by the animals for metabolism.

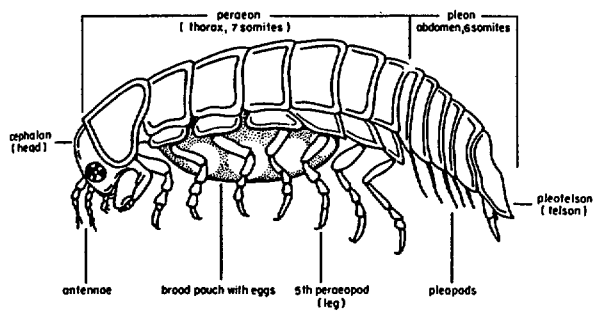

Fig. 5 Morphological representation of a limnorian, showing the whole animal, lateral view. (From Marine Boring and Fouling Organisms, D.L. Ray (Ed.); with permission of the University of Washington Press. 1959).

Limnorians are continually active and once a new burrow is begun, the animals are usually enclosed within the wood in 4-6 days. The burrows, which are just beneath and parallel to the wood surface, are marked at regular intervals by small breathing holes not large enough for the animals to pass through. These holes serve as passages

for oxygen-containing water which is circulated through the burrows by the beating action of the pleopods.

No wood debris accumulates at the anterior end of a burrow, and all wood fragments scraped away are ingested and pass through the alimentary canal (12). Limnorians were once thought to burrow into wood solely for protection, however subsequent studies have indicated that they are capable of utilizing the wood scrapings as food. The wood is hydrolyzed by a cellulase which is produced by the borers (13) rather than by cellulase-producing microbial symbionts in the gut. In fact, Ray (14) showed that no microorganisms are present in the alimentary tract of these animals. Scanning electron microscope studies by Sleeter, et al (15) have confirmed these observations. They also showed that there are no microorganisms at the anterior ends of the burrows where the boring activity of the animals is apparently rapid enough to prevent the colonization of the newly-formed wood surface. Limnorians require nitrogen for amino acid and protein synthesis, and wood is low in this element. Thus if limnorians utilize wood as a food, their nitrogen requirement must be satisfied from another source. Marine fungi have been considered because these nitrogen-rich microorganisms are so ubiquitous; another suggested source is the pool of dissolved nitrogenous compounds (ammonia, nitrites, nitrates) in the water (16).

Lignicoulous marine fungi (or bacteria) may have some relationship to limnorians other than nutritional. It has been hypothesized that before marine borers can penetrate a wood surface it must be softened by fungal activity, and it has been reported that limnorians are unable to attack wood in the absence of marine fungi (17), however it was demonstrated subsequently that limnorians are capable of growing in fungus-free wood (18,19). The consensus is that marine fungi are not necessary for limnorian attack on wood, although a fungal-softened wood surface would certainly increase the rate of attack.

LABORATORY CULTURING OF LIMNORIANS

Laboratory culturing of experimental animals is desirable if controlled research is to be conducted because culturing allows the researcher ready access to a population of animals with a known history. The organisms can be watched closely, under conditions most like those encountered in nature, and their patterns of growth and reproduction can be observed to determine if laboratory inbreeding is causing adverse genetic effects.

Open Seawater Aquarium Systems

Culturing of marine crustaceans and bivalves is not new. In 1927 Wells (20) reared the American oyster Crasseostrea virginica from artificially fertilized eggs to the settlement and shell-building stage. However as late as the 1950's culturing depended upon using planktonic larvae instead of obtaining them from fertilized eggs under controlled laboratory conditions. Most recently, Loosanoff and Davis (21), and Walne (22) employed techniques which enables them to culture successfully the larvae of bivalves. However, their laboratories were located at the seashore and their culture systems utilized running seawater. Turner, a leading authority on the laboratory culture of limnorians and teredinids, also uses natural seawater in her system (23). The advantage of open culture systems is that the animals are supplied with a continuous flow of fresh seawater and the used water containing the waste products of their metabolism, mostly toxic nitrogeneous organic compounds, returns to the sea.

There are also disadvantages associated with open systems. These include problems with the mechanics of the system, corrosion of pipes with concomittant release of undesirable metallic components, fluctuations in salinity and temperature of the water, and clogging of filters by storm-generated silt.

Closed Recirculating Aquaria

Laboratories not located near the seashore must use closed aquarium systems which are more complex to maintain. These systems, however, offer advantages such as ease and convenience of monitoring and sampling, continuous visual observation, freedom from severe variations in salinity and temperature, preferential selection of biota cultured without danger of contamination by planktonic forms, and independence from such natural effects as algal blooms and increasing levels of pollution encountered in the near-shore environment.

Many laboratories and commercial aquaria use recirculating tanks for culture and display purposes. The design parameters for monitoring these tanks have been presented by several investigators (24-26). Some of the standard techniques were modified and unique features were incorporated to accommodate the special problems encountered in culturing our limnorians.

Aquarium System at NRL

Limnoria tripunctata are maintained in five 30-gallon, all-glass aquaria; tight-fitting lucite covers minimize evaporation. Artificial seawater is made up according to Kester, et al (27) in 45-liter batches. Each batch of water is adjusted to a final salinity of 30.0$^{o}/_{oo}$ with distilled water, aerated until the pH is steady at approximately 8.2, and stored at 3°C without filtering. Figure 6 presents a schematic of the recirculating culture system and Fig. 7. shows three tanks containing limnorian-infested pine panels. A small magnetic-drive centrifugal pump circulates water from the tank via 3/4 inch polyethylene tubing through an in-line filter then to the base of the biological filter bed (BFB). The water passes upward through the filter and back to the tank. The flow rate ranges from 12 to 60 liters/hr depending on the buildup of detritus within the BFB. Three air

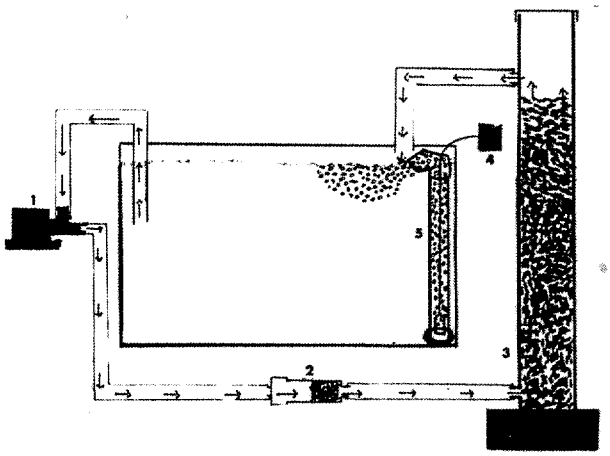

Fig. 6 Schematic view of our closed-system aquaria for maintaining limnorian cultures. Water from the tank is moved by an all-plastic centrifugal pump (1) through an in-line filter containing charcoal and plastic wool (2) which removed larger particulate matter, to the bottom of the vertical biological filter bed (3) of crushed oyster shells, and then back into the tank. The water is oxygenated and the intra-tank circulation improved by air from an air pump (4) which is routed through an air-lift tube (5).

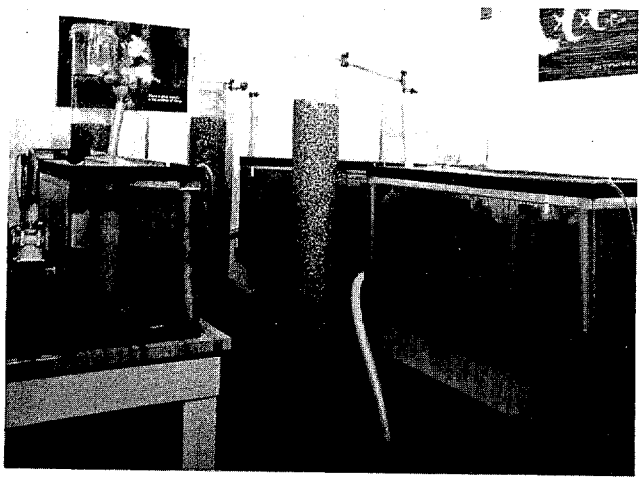

Fig. 7 Three laboratory culture tanks containing limnorian-infested pine panels suspended by glass hooks from horizontal support rods. The vertical columns are the biological filter beds containing the crushed oyster shell.

pump-operated airlift tubes located at the corners of each tank provide adequate intratank water circulation and keep the water saturated with oxygen. The in-line filter which prevents large particles from reaching the BFB, consists of a plexiglass cylinder containing activated charcoal with plastic filter fiber on the upstream side. The BFB consists of a plexiglass cylinder about 6 feet tall and 6 in. in diameter, filled with 40 pounds of crushed oyster shells. The shells are supported off the bottom of the cylinder by a perforated plexiglass plate. The usual BFB for closed water aquaria is normally contained inside the tank and is used in conjunction with a subgravel filter/airlift system. This system could not be used in our laboratory because the boring activity of the limnorians produces frass (a combination of powered wood and fecal material) at a rate of about 1 inch/month.

If the filter bed were contained inside the aquarium, the frass would clog the interstices between the oyster shells, preventing efficient water flow. The resulting stagnation would upset the efficient biological filtration of the water and could eventually lead to the death of the animals. Wood panels used for culturing the borers are suspended in the tank (see Fig. 7) from glass hooks inserted into one end and hung from a plexiglass framework which rests on the bottom of the aquarium. These panels are riddled with burrows in about 6 months' time as is shown in Fig. 8. A control pine panel is also shown at lower right.

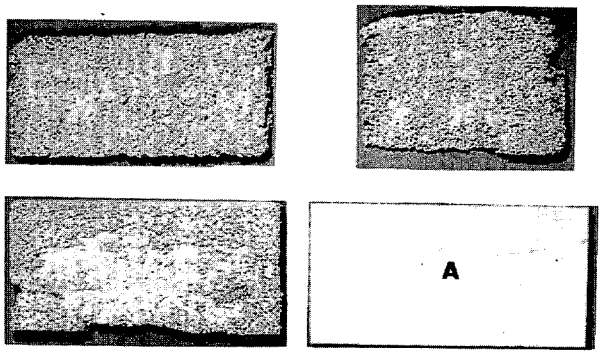

Fig. 8 Attacked from both sides, these pine panels were reduced from sound wood (A) to spongy masses after 6 months' exposure in our laboratory colony of Limnoria tripunctata.

Water Conditioning

A newly established aquarium goes through a conditioning period of about 1 month before the culture animals are introduced. During this time the new filter system is exposed to the excretory products, e.g. urea, of hardy marine organisms such as hermit crabs, brittle stars, urchins, or small fish. The conditioning process is accelerated by the addition of some bacterial-contaminated oyster shells from an operating aquarium. The oyster shell inoculum provides the beginning of a rapidly increasing population of heterotrophic bacteria which became suspended in the water column and attached to the shell surfaces in the BFB. The organic nitrogenous compounds (urea) produced by the 'conditioning' animals is rapidly converted by these bacteria into ammonia which reaches a high concentration in the water shortly after the animals are introduced into the system.

This mineralization reaction is the first stage in the biological removal of toxic metabolites (Fig. 9).

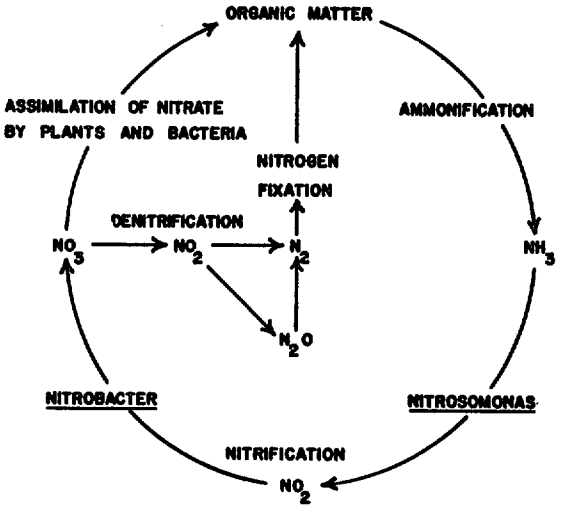

Fig. 9 Scheme for biological removal of harmful nitrogenous metabolites which accumulate in the water. (From Spotte, S.H. 1970. Fish and Invertebrate Culture. John Wiley and Sons, Inc.).

The high concentration of ammonia stimulates a rapid increase in the number of the supplied nitrifying autotrophic bacteria Nitrosomonas sp. and Nitrobacter sp. which perform the oxidation of ammonia to nitrite and nitrite to nitrate, respectively. The oxidation of ammonia to nitrate is the second step in the biological filtration of the water. The final stage in this process is the reduction of nitrate to nitrous oxide or elemental nitrogen. This denitrification step can be carried out by autotrophic or heterotrophic bacteria and can occur aerobically or anaerobically.

Within 2 weeks to a month the system is conditioned and the concentrations of ammonia, nitrite, and nitrate have stabilized; there is no longer a lag time between successive steps in the nitrogen conversion process because all the nitrogen intermediates are being processed simultaneously, and the bacterial colony is in equilibrium with the system. At this time the limnorians can be introduced.

The buildup of toxic products (ammonia, nitrite, nitrate), oxygen concentration, pH, and salinity are monitored weekly. The concentration of toxic substances is controlled further by the monthly replacement of 25% of the water in the tanks with fresh salt water. The in-line filters are cleaned twice weekly, and the tank bottoms are vacummed monthly. Also, the BFB is dismantled and cleaned with salt water bimonthly.

FUTURE RESEARCH

To reiterate, dibutylbenzylphenol holds promise as a preservative against the molluscan borers which makes it a candidate as a creosote replacement should the continued use of creosote be banned. However, this benzylphenol is not effective against limnorians. To provide this missing protection, future work at NRL will be more strongly oriented toward an investigation of those woods from the earlier study (8) which were particularly resistant toward limnorians; the interest in teredinids will be maintained. Cocobolo (Dalbergia retusa), guayacan (Tabebuia guayacan), and cedro espino (Bombacopsis quinata) are already being examined for their anti-limnorian heartwood component; lignum vitae (Guajacum officinale), zaragosa (Conocarpus erectus), and quirá (Platymiscium pinnatum) will be added to the list. The extractives from these woods will be evaluated as anti-limnorians, and a study of the effects of the active compounds upon limnorian physiology will be made to determine which biochemical systems are being disrupted; relationships between chemical structure and biological activity will be sought. Animals from our laboratory culture will be used for this purpose.

REFERENCES

1. Hill, C.L. and C.H. Kofoid. (Eds.). 1927. Marine borers and their relation to marine construction on the Pacific coast. Final report of the San Francisco Bay marine piling committee. National Research Council/American Wood-Preservers Assn. San Francisco, CA.
2. Fischer, E.C., L.S. Birnbaum, J. DePalma, J.S. Muraoka, H. Dear, and F.G. Wood. 1975. Survey report: Navy biological fouling and biodeterioration. Report NUC TP 456. Naval Undersea Center, San Diego, CA.
3. Page, R.Z. 1972. Federal Committee on Wood Protection, Minutes of the 8th. Meeting, June 6-7. Naval Facilities Engineering Command, Washington, D.C.
4. O'Neill, T.B., R.W. Drisko, and H. Hochman. 1961. Pseudomonas creosotensis sp., a creosote-tolerant marine bacterium. Appl. Microbiol. 9: 472-474.
5. Eaton, M.L., J.A. Erelicharz, and T. Roe. Mechanical properties of pressure-treated marine piles - Results of limited full-scale testing. Naval Civil Engineering Laboratory Technical Report (in press).
6. Sweeney, T.R., T.R. Price, and S.M. Miller. 1958. Coal tar creosote studies. Part 2 - An evaluation of certain fractions for their resistance to marine borer attack. Corrosion 14: 62-64.
7. Price, T.R. and T.R. Sweeney. 1956. Marine borer control. Part VII - Evaluation of petroleum-ether-soluble fractions and distillation fractions of creosote. Formal Report 4851. Naval Research Laboratory, Washington, D.C.

8. Southwell, C.R. and J.D. Bultman. 1971. Marine borer resistance of untreated woods over long periods of immersion in tropical waters. Biotropica 3(1) 81-107.

9. Bultman, J.D. and C.R. Southwell. 1976. Natural resistance of tropical woods to terrestrial wood-destroying organisms. Biotropica 8(2): 71-95.

10. Jurd, L., K. Stevens, and G. Manners. 1972. Quinoid constituents of Dalbergia retusa heartwood. Phytochemistry 11: 3287-3292.

11. Waite, J.H. and K.M. Wilbur. 1976. Dalbergia polyphenols and shell formation in mollusks: Preliminary results. In, J.D. Bultman (Ed.). Proceedings of a Workshop on the Biodeterioration of Tropical Woods: Chemical Basis for Natural Resistance. Naval Research Laboratory, Washington, D. C.

12. Oliver, A.C. 1962. An account of the biology of Limnoria. J. Inst. Wood Sci. 9:32-91.

13. Ray, D.L. and J.R. Julian. 1952. Occurrence of cellulase in Limnoria. Nature 169: 32.

14. Ray, D.L. 1959. Nutritional physiology of Limnoria. In, D.L. Ray (Ed.). Proceedings of the Friday Harbor Symposium on Marine Boring and Fouling Organisms. pp 46-60. University of Washington Press.

15. Sleeter, T.D., P.J. Boyle, A.M. Cundell, and R. Mitchell. 1978. Relationships between marine microorganisms and the wood-boring isopod Limnoria tripunctata. Mar. Biol. 45: 329-336.

16. Ray, D.L. 1959. Marine fungi and wood borer attack. Proceedings of the American Wood-Preservers Assn. 55: 147-154.

17. Schafer. R.D. and C.E. Lane. 1957. Some preliminary observations bearing on the nutrition of Limnoria. Bull. Mar. Sci. Gulf Carib. 7: 289-296.

18. Kohlmeyer, J., G. Becker, and W.D. Kampf. 1959. Versuche zur kenntnis der ernahrung der holzbohrassel Limnoria tripunctata und ihre beziehung zu holzzerstorenden pilzen. Z. angew. Zool 46: 457-489.

19. Ray, D.L. and D.E. Stuntz. 1959. Possible relation between marine fungi and Limnoria attack on submerged wood. Science 129: 93-94.

20. Wells, W.F. 1927. Report of the experimental shellfish station. Rep. N.Y. St. Conserv. Dep. No. 16, 1-22.

21. Loosanoff, V.L. and H.S. Davis. 1963. Rearing of bivalve molluscs. In, F.S. Russel (Ed.). Advances in Marine Biology, Vol. I, pp 1-136. Academic Press, New York, N.Y.

22. Walne, P.R. 1964. The culture of marine bivalve larvae. In, K.M. Wilbur and C.M. Yonge (Eds.). Physiology of Mollusca, Vol. I, pp 197-210. Academic Press, New York, N.Y.

23. Culliney, J.L., P.J. Boyle, and R.D. Turner, 1975. New approaches and techniques for studying bivalve larvae. In, W.L. Smith and M.H. Chanley (Eds.). Culture of Marine Invertebrate Animals. pp 257-271. Plenum Press, New York, N.Y.

24. Saeki, A. 1958. Studies on fish culture in filtered closed-circulation aquaria. Bull. Japanese Soc. Sci. Fisheries 23(11): 684-695.

25. Kelley, E.E. Ideal configurations for semi-closed circulating aquarium systems. American Society of Ichthyologists and Herpetologists, 50th Meeting.

26. Goldizen, V.C. 1970. Management of closed-system marine aquariums. Helgolanderwiss Meersunters 20: 637-641.

27. Kester, D.R., I.W. Duedall, D.N. Connors, and R.M. Pytkowicz. 1967. Preparation of artificial seawater. Limnol. Oceanog. 12 (1) 176-179.

THE MOTILTIY OF THE CELLS AND THE EXTRACELLULAR MATRIX OF LABYRINTHULA -- A COLONIAL ORGANISM FOUND ON ZOSTERA MARINA

D. Solomon, S. Sher and E. Bell
Room 16-820A
Department of Biology
Massachusetts Institute of Technology
Cambridge, Massachusetts 02139

ABSTRACT

Labyrinthula is a saprophytic colonial marine protist found on Zostera marina. It consists of cells which move only within an elastic matrix thought to be synthesized and secreted by the cells themselves. Although they have no visible means of locomotion, that is, no cilia, flagella or podia, the cells exhibit movements at velocities up to 200 μ/min. The extracellular matrix also exhibits motility. We have found, with the help of time lapse cinemicropraphy, lamellipodia-like extracellular processes which exhibit rapid translocation and appear to form the extracellular corridors within which the cells move. Indirect antibody staining shows antimyosin specific rails extending through the extracellular corridors and branching into the lamellipodia-like processes. The rails appear to correspond to regions of birefringence observed with polarized light. Our observations have led us to construct a model which attempts to explain Labyrinthula motility.

INTRODUCTION

Labyrinthula is a eukaryotic colonial protist suspected of being the etiological agent of the wasting disease of Zostera Marina, reported to have occurred in temperate waters of the Atlantic from 1930-34 (15). Out of convenience it has been classified phylogenically as a marine slime mold although it has no true affinity with the Mycetozoa (13,19). In its vegetative state, an extracellular, anastomosing, network of unit-membrane-bound corridors encloses fusiform cells 10-15 microns long (5,11,12).

The vegetative cells may have as many as 15-20 electron-dense invaginations on the cell surface. These are called "bothrosomes" and are thought to be membrane synthesizing centers, but a role for the "bothrosome" in membrane synthesis, matrix production, nutrition, locomotion or intercellular communication is still undemonstrated (11).

Cells move within the matrix corridors at speeds up to 200 μ per minute (7,19). Cells have no visible means of locomotion, i.e. no cilia, flagella or podia (11). Cells without matrix are stationary. Changes of direction with or without reversal of cell polarity and movements past stationary cells have been documented by time lapse microcinematography using phase-contrast and Normaski illumination. The decomposition of food organisms such as yeast, bacteria, and diatoms occurs extracellularly but only when the matrix is in direct contact with food (11, 19). The lytic enzymes capable of such activity are presumed to be localized in the matrix which in addition to acting as a conduit for a vegetative cell also may serve as a nutrient reservoir. The matrix does not appear to be a site of protein synthetic activity (16, 19). New branches of the matrix in the form of fine filaments have been observed forming and fusing at distances of 200 microns from a vegetative cell (2).

METHODS AND MATERIALS

A. Culture of Labyrinthula

Labyrinthula was isolated from free-floating strands of Zostera marina gathered in shallow water in Sippiwisset, Mass. during late May of 1977. The strands were transported to M.I.T. in local sea water and refrigerated at 4°C for 48 hours before plating. Thirty-six segments (3 cm. in length) were plated on 1% SSA (11) medium containing the following antibiotics: 0.25 grams/liter of streptomycin sulfate and 0.25 grams/liter penicillin G sodium salt (ICN Pharmaceuticals, Inc.). The agar-sea water solution was autoclaved and cooled to 50°C before adding horse serum and antibiotics. Labyrinthula growth was observed after 48 hours, extending an average of 3 mm from each of two segments. Colonies were excised with a micropipette and plated on fresh 1% SSA with antibiotics. This procedure was repeated twice before plating on 1% without antibiotics. Since then, labyrinthula cultures have been maintained at room temperature by transferring every two weeks 1 cm blocks excised from 1% SSA which include the leading edge of a colony.

A marine yeast, Rhodotorula sp., was isolated from Zostera marina gathered from the same source. Twelve segments of Zostera (3 cm. in length) were plated on MV (14) medium. Cubes (0.5 cm.) of agar medium containing Rhodotorula sp. and other organisms were transferred to YM (14) acid medium, pH 3.5, which selects for Rhodotorula. They were then incubated at room temperature for 14 days and transferred by pasteur pipette to YPGS (14), a maximum growth medium. Rhodotorula cells were grown by inoculating YPGS medium and incubating at room temperature for 4 days with gentle, sterile aeration (1 liter air/min./liter of medium). The culture was subsequently centrifuged at 300xg for 15 minutes at 4°C, decanted and resuspended in 3.3% saline, pH 7.4, and autoclaved for 20 minutes. Cell counts were made with a hemacytometer.

We found that the addition of 10 (5) autoclaved Rhodotorula sp. in 0.1 mm saline solution layered on the petri plate (100 mm.) prevented the encystment of Labyrinthula.

B. Microcinematography

Time-lapse films of moving cells and matrix were taken with a 16 mm. Arriflex camera modified for time-lapse sequencing. Exposures of 1/2 sec. at intervals ranging from 1/2 to 5 seconds were made on Kodak Plus-X Reversal film. A Zeiss standard microscope was used with a 5X Zeiss ocular and 20X and 40X Zeiss phase contrast #2 objectives. Colonies were prepared by inoculating a Sykes-Moore chamber filled with a solution of 1% horse serum in 0.2 mμ. millipore-filtered, autoclaved sea water with 100 microliters of a 0.1% Labyrinthula culture.

C. Polarization Microscopy

Polarization photomicrography was carried out with a Zeiss Universal microscope fitted with Zeiss polarizer and analyser, 10X Zeiss ocular, 20X and 100X oil Nikon HI rectified objectives, and a 0.00006mm mica compensator. Photographs were taken with a Zeiss 35mm leaf-shutter microscope camera on Tri-X film pushed to 1600 ASA with Dynafine. Specimens were prepared by culturing colonies on 25 mm diameter A.H. Thomas Co. cover slips following the protocol described under antibody staining. Cover slips were mounted inverted in a Sykes-Moore chamber.

D. Antibody Staining

Cover slip cultures of Labyrinthula were prepared by inoculating 12 mm diameter, #1 cover slips with 0.01 ml of 0.1% SSA medium drawn from the leading edge of a colony between two and six days old. Inoculated cover slips were placed on an open-cell urethane spacer in an 100 mm petri dish with approximately 10 ml of double-distilled water.

0.05 ml of 1% horse serum-sea water was added to each cover slip. The dish was covered and incubated from 8-48 hours before fixation in order to permit the colony to extend beyond the aggregation of agar. Cover slips were then gently rinsed in 3.3% saline, pH 7.4, and fixed in 10% Formalin phosphate-buffer saline (PBS) for 5 min. Fixed cover slips were immersed for 5 minutes in the following solutions; PBS, 50% acetone-water, 100% acetone, 50% acetone-water, and PBS. The coverslips were incubated with ten lambda of rabbit antimyosin antibody at 37°C for 60 minutes. The cover slips were rinsed and incubated with twenty lambda of goat antirabbit antibody (GAR) conjugated with fluorescein isothiocyanate for 60 minutes at 37°C. Cover slips were rinsed in PBS and mounted inverted on glass slides with a non-fluorescent mounting medium (Aqua-Mount™, Lerner Laboratories). Examination was with a Zeiss incident-fluorescence microscope. Microphotographs were taken with a Zeiss 35 mm leaf-shutter camera.

RESULTS

A. Culture of Labyrinthula

The species of Labyrinthula isolated from Sippiwissett resembled type LX reported by Watson in cell size, cell form, cell division and colony morphology. Growth varied considerably despite attempts to establish uniform conditions. "Slime-way" width and cell concentration were related to colony age and moisture content of the medium as others have previously reported.

Maximum growth occurred in colonies inoculated with 10^4 cells of live Rhodotorula sp. From a 2 mm. diameter inoculum, colony growth could cover a 100 mm petri plate in 85 hours at 25°C -- a radial increase averaging 0.56 mm. per hour and an increase in area of 2500 fold.

Autoclaved Rhodotorula sp. induced growth in colonies which had aggregated but which had not undergone a noticable change in cell morphology by forming encystment structures. Two months after the addition of autoclaved yeast in these colonies growth was retarded or ceased completely. However, the further addition of 10^4 cells of live, as distinguished from autoclaved, Rhodotorula sp. induced growth approaching the maximum obtainable in our cultures.

Colony morphology varied in relation to the agar (Bacteriological Grade AgarAgar, Fisher Laboratories) or agarose (Agarose Powder, Bio-Rad) concentrations. In 1% agar or agarose colony growth was three-dimensional from the start.

B. Matrix and Cell Motility

Time-lapse films of expanding vegetative colonies revealed the presence of lamellipodia-like extracellular processes not previously reported. The lamellipodia exhibited cell-independent motility. They were observed to extend perpendicularly from existing "slimeways", with a sheet-like form varying from 10 to 70 microns in width and 5 to 90 microns in length (Fig. 1). As the lamellipodium advanced (Fig. 2) vegetative cells were observed to travel into its distal portion only, but not into the fan-like process itself (Fig. 3). Frequently, such cells were observed to enter the new "slimeway", stop 15 to 60 seconds, and without turning around, reverse direction and exit. Using the distal region of the lamellipodium as the beginning of a new "slimeway", the presence or absence of vegetative cells appeared to have no effect on the developing morphology or motility of the lamellipodia.

When the lamellipodium reached an existing "slimeway", fusion was observed to occur. On fusion the lamellipodium, with its wide fair like leading edge, formed a concave triangular "slimeway" junction (Fig. 4), and vegetative cells were observed to travel through the junction into other regions of the colony.

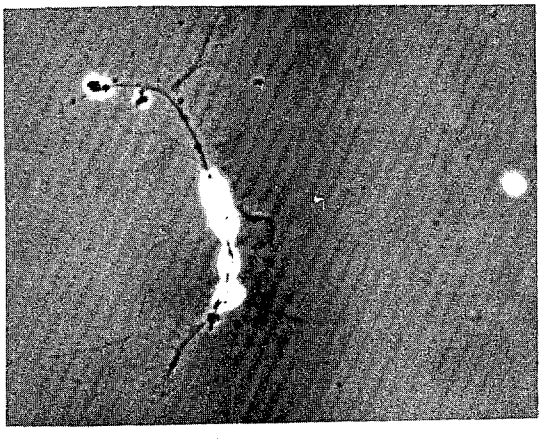

Fig. 1. Phase contrast micrograph of Labyrinthula vegetative cells and extracellular matrix. Lamellipodium extending to the right of the "slimeway." Bar equals 10 μm —

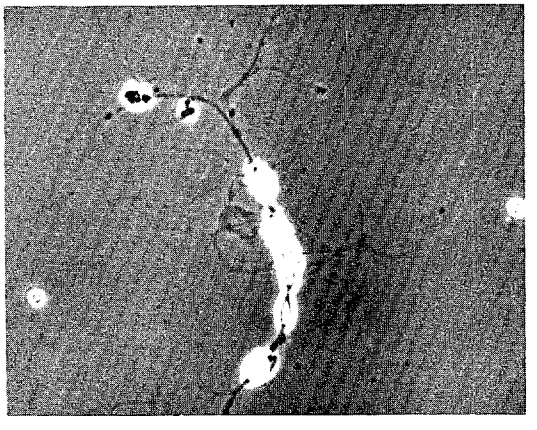

Fig. 2. Sequence of lamellipodia morphogenesis. Formation of anastomosed lameelipodium on the right.

Fig 3. Expansion of lamellipodium to the left of the "slimeway."

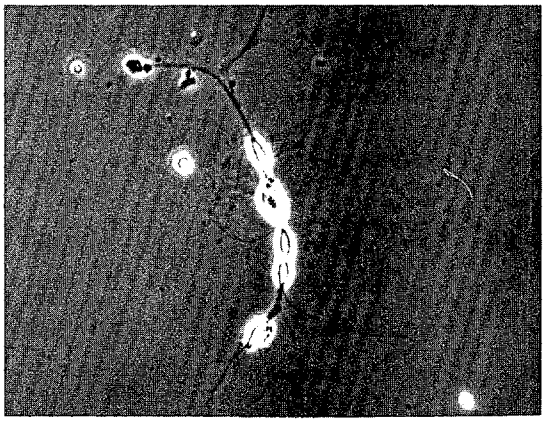

Fig. 4. Formation of a new "slimeway" in the left lamellipodium.

C. Antibody Staining of Labyrinthula Colonies

Indirect fluorescent antibody staining of formalin-fixed colonies by rabbit antimyosin antibody, specifically stained a branched network of extracellular cables extending throughout the extracellular matrix (Fig. 5). These cables correspond, in part, to the phase-contrast observed "slimeways" along which the vegetative cells move (Fig. 6). Cables were also observed throughout regions of the extracellular matrix where phase-contrast or Nomarski images of "slimeways" were hardly visible. These thin cables were observed in high concentrations at "slimeway" junctions and in regions of the leading edge of the extracellular matrix of the colony. Within the lamellipodia, the stained cables are fan-like and are observed to converge as the ribs of a fan in a direction opposite to the leading edge of the lamellipodium.

In some slimeways the antibody staining was observed to be in the form of two lateral rails which diverged to follow the perimeter of a cell and either converge or closely approach each other after passing the cell. Between some cells separated by less than 30 micron the separation between rails was uniform.

A double-blind evaluation of the antimyosin staining and (Table 1) suggests that the stained structures contain myosin.

TABLE I. DOUBLE-BLIND EVALUATION OF INDIRECT ANTIBODY STAINING AND CONTROLS (n=4).

INHIBITOR	1st STAIN	2nd STAIN	AVE. INTENSITY
PBS	RAM	GAR	+ + +
Myosin	RAM	GAR	+
Myosin	RAM	GAR	+ +
PBS	Myosin	GAR	-
Myosin	NRS	GAR	-
PBS	PBS	GAR	-
PBS	NRS	GAR	-
PBS	NRS	GAR	-
PBS	PBS	GAR	-

GAR = Goat Antirabbit; NRS = Normal Rabbit Serum
PBS = Phosphate buffer Saline; RAM = Rabbit Antimyosin

[1]Myosin and rabbit antimyosin antibody were pre-incubated at 37°C for 30 minutes.

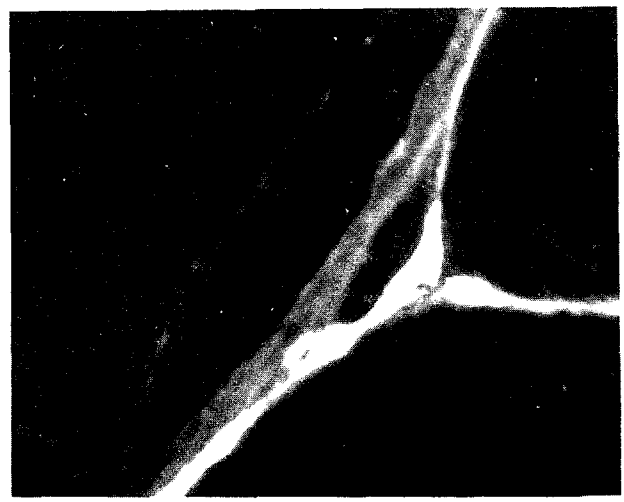

Fig. 5. Antimyosin antibody stained Labyrinthula cells and matrix. Bright fusiform shapes are vegetative cells. Bar equals 10 μm ——

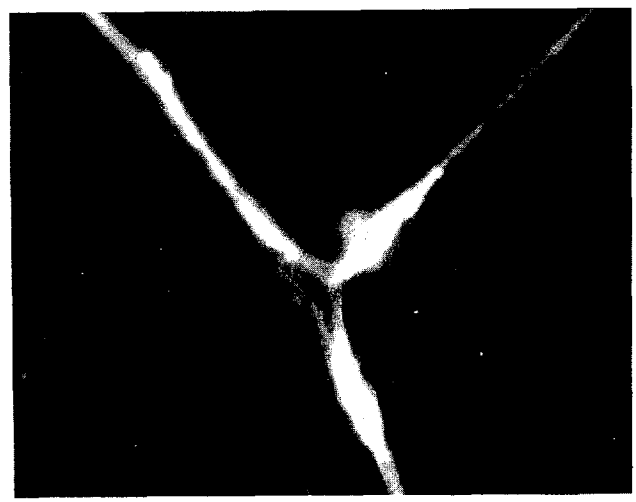

Fig. 7. Antimyosin antibody stained "slimeway" junction. Note seperate cables extending from the cell on the right.

D. Polarization Microscopy

Observations with rectified polarization optics revealed the presence of birefringence within the "slimeways" as identified by phase contrast microscopy, and within regions of lamellipodia seen poorly with phase-contrast microscopy. Figures 8 and 9 show the bifringence of slimeways were taken on the + and - side of extinction. The pattern of birefringence appears to correspond to that of the antimyosin antibody cabling reported in this paper. Rapid changes (1-2 seconds) in sign and intensity of birefringence were observed in conjunction with and independent of cell movement. Certain birefringent cables have been observed to diverge as they approach vegetative cells, and converge behind the cells like the antimyosin stained cables. In addition birefringent zones, 3-4 microns in length, have been observed to travel along the length of the "slimeway" without apparent relation to the translocation of cells. As yet we have no evidence of what is responsible for the phenomena.

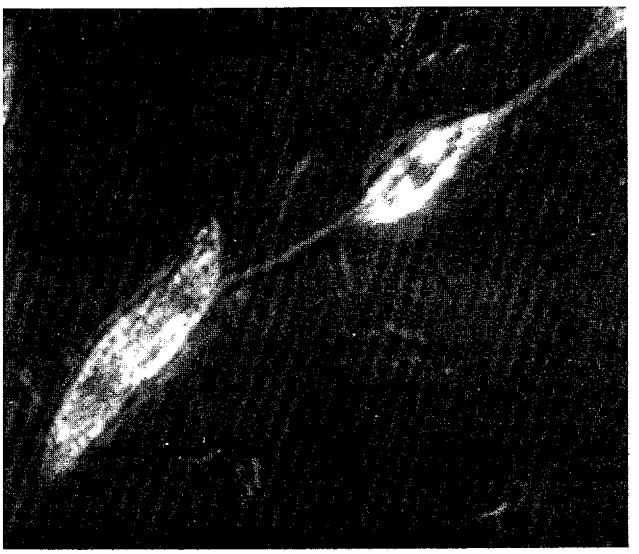

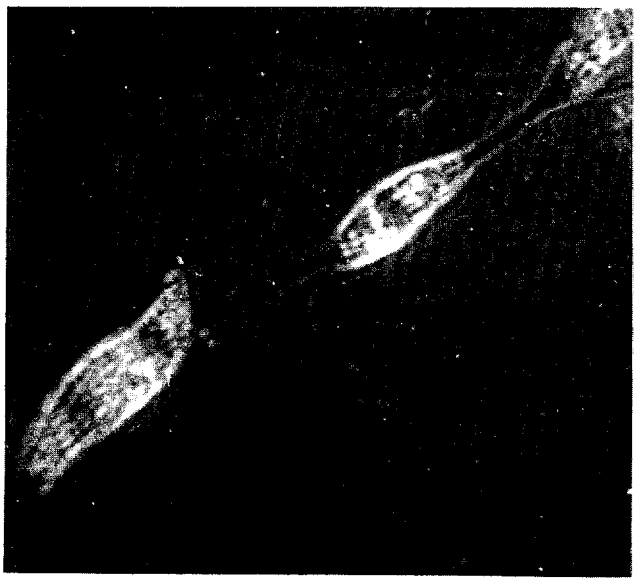

Figs. 8 & 9. Polarization micrograph of living cells and matrix on the + & - sides of extinction. Matrix exhibits distinct birefringance. Bar equals 10 μm

DISCUSSION

We have reported the existence in Labyrinthula of highly motile extracellular lamellipodia and a network of extracellular cables or rails which stain with antimyosin antibody. The presence of lamellipodia at the leading edge of a colony as well as at points within the colony suggest that they play an important role in colony expansion and intracolonial slimeway development. The lamellipodium appears to be homologous with the leading edge of the animal tissue cell which extends on a substrate in advance of the cell during translocation. The putative presence of a network of fine myosin cables in the lamellipodium is suggestive that the contractile protein is implicated in the movement of the organism.

Similarly the presence of putative myosin cabling in the slimeways suggests a mechanism for the motility of labyrinthula cells which possess no visible means of locomotion. Although we suspect the presence of myosin in Labyrinthula by demonstrating a protein band from colony extracts which comigrates with chicken gizzard myosin during thin layer acrylamide gel electrophoresis, we have not yet been able to show the presence of actin. Nonetheless we speculate that active filaments on the surface of the cell interacting with myosin cables of the slimeway could constitute the driving force needed for cell movement. Equally fascinating in the interaction between cells and extracellular matrix are the signals and controls needed to establish direction and speed of cell movement. Understanding the basis for Labyrinthula motility, both cellular and extracellular, may have important ecological significance. If Labyrinthula is the agent responsible for periodic eel grass decline we may discover factors which permit it to overun a host with which it is normally in balance.

ACKNOWLEDGMENTS

The authors thank Peter Yanover and Dr. L. Marek for their help in time lapse microcinematography and, Charlotte Merrill for her technical assistance. Support for this project was provided in part by the M.I.T. - U.R.O.P. fund.

REFERENCES

1. Amon, T.P. and Perkins, F.P. 1968. Structure of Labyrinthula Sp. Zoospores. J. Protozool. 15(3):543-546.

2. Bell, E. 1969. Labyrinthula, a E.D.C. film with D. Porter as consultant.

3. Bonner, J.T. 1967. The Cellular Slime Molds (2nd ed.) Princeton Univ. Press, Princeton, 205 pp.

4. Hofer, H.W., Pette, D., Schwab-Stay, H. and Schwab D. 1972. Enzyme Acitivty Patterns and Mitochondria - cytoplasmic Relations in Protozoa. Comparative Study of Tetrahymena pyriformis, Allogromia laticollaria, and Labyrinthula coenocytis. J. Protozool. 19(3): 532-537.

5. Hohl, H.R. 1966. The Fine Structure of the Slimeways in Lab. J. Protozool., 13:41-43.

6. Hollande, A. and M. Enjumet. 1955. Sur l'evolution at La Systematique des Labyrinthula Algeriensis nov. sp. Am. Sci. Nat. Zool. 17:357-368.

7. Quick, J.A. 1974. A New Marine Labyrinthula with Unusual Locomotion. Trans. Amer. Micros. Soc. 93(1):52-61.

8. Perkins, F.O. 1970. Formation of Centriole and centriole-like structures during meiosis and mitosis in labyrinthula sp. J. Cell Sci. 6:629-653.

9. Perkins, F.O. and Amon, J.P. 1969. Zoosporulation in Labyrinthula; an electron microscope study. J. Protozool. 16:253-256.

10. Perkins, F.O. 1972. The ulstrastructure of holdfast, "rhizoids" and "slimetracks" in thraustochy-triaceous fungi and Lab spp. Arch. Mikrobiol. 84:95-118.

11. Porter, D. 1969. Ultrastructure of Labyrinthula. Protoplasma 67:1:19.

12. Porter, D. 1972. Cell division in the marine slime mold, Labyrinthula sp. and the role of bothrosome in extracellular membrane production. Protoplasma 74:427-448.

13. Porter, D. 1974. Phylogenic considerations of the Thraustochytriaceae and Labyrinthulacalae. Veroff. Inst. Meeresforsch. Bremerh. Suppl. 5:19-44.

14. Porter, D. Unpublished methods and materials of Labyrinthula and Marine Yeast culture.

15. Renn, C.E. 1935. A Mycetozoan Parasite or Zostera Marina Nature. April 6, 1935: 544-543.

16. Solomon, D.J. 1977. Personal films on abyrinthula motility.

17. Sykes, E.E. and D. Porter 1973. Nutritional Studies of Labyrinthula Sp. Mycologia. Vol. LXV, No. 6, pp. 1302-1311.

18. Watson, S.W. 1957. Techniques for the isol ation of Labyrinthula and Thraustochytrium in pure culture. J. Bact. 73:368-377.

19. Watson, S.W. 1957. Cultural and Cytological Studies on Species of Labyrinthula. Ph.D. thesis, Univ. of Wisconsin. 164 pp.

20. Young, E.L. 1943. Studies on Labyrinthula; the etiological agent of the wasting disease of eel grass. Amer. J. Bot. 30:586-593.

A NON-ACOUSTIC LONG DISTANCE UNDERWATER COMMUNICATIONS SYSTEM

Lt. R. G. Williscroft
National Oceanic and Atmospheric Administration
NOAA Ship Surveyor S-132
1801 Fairview Avenue East
Seattle, Washington 98102

N. C. MacLeod
Technology Development Corporation
Underwater Systems
155 Moffett Park Drive, Bldg. C
Sunnyvale, California 94086

Abstract

An underwater communications system is described which utilizes Technology Development Corporation's (TDC) Hydrocom coupled to a Radio Retransmission Buoy. Hydrocom is nonacoustic, utilizing instead an electric current field which is not adversely affected by thermoclines, reverberation, or interferometer effects. It can be operated in noisy and confined environments where acoustic systems are severely degraded and even when objects, such as reefs or man-made structures, lie between the communicators. The Radio Retransmission Buoy enables telephone clarity communications to exist between divers or a submerged vehicle and a ship several miles distant. Suitable radio patch or satellite relay will extend the communications link to any place on Earth, enabling real-time laboratory overview of distant onsite underwater inspection or data gathering.

1. Introduction

The history of underwater communications has been dominated by hardwire systems for the tethered diver and by acoustic systems for the free-swimming diver (Shilling, Werts, Schandalmeier, 1976). A hardwire system is comparable to a telephone, including a transducer at both ends, amplification methods, and transmission line. It will not be further discussed here. Acoustic systems fall into two categories: direct and modulated.

The simplest acoustic system is direct projection in which the voice is projected into the water using an "underwater loudspeaker" and is usually received by the diver without any special processing. The simplest of these is a waterproof diaphragm through which the diver speaks. More complicated versions employ simple amplification devices at the transmitting, and sometimes even the receiving, end. All direct projection acoustic systems are severely limited by waterborne noise (Shilling, Werts, Schandalmeier, 1976).

The most common acoustic system uses a modulated carrier frequency between 8 kHz and 50 kHz in a single side band (SSB) suppressed carrier mode (Martin and Adams, 1970). Amplitude modulation (AM) systems are possible, but half the output energy is lost to the carrier. Frequency modulation (FM) systems, while producing excellent results, are practical only over very short distances because the broad-band carrier frequency deviation requirements necessitate the use of ultrasonic frequencies which are quickly absorbed in sea water (Shilling, Werts, Schandalmeier,1976). SSB system at the low frequency end of the spectrum are characterized by relatively long range (900 to 1,000 meters) and high noise, while those at the high end of the spectrum experience comparatively little noise but have one-fifth the range for the same output power (Martin and Adams, 1970).

All acoustic systems are subject to masking by waterborne noise and suffer from transmission losses due to absorption, scattering, refraction, and multiple-path transmission. According to Woods and Lythgoe (1971), absorption, which increases exponentially with frequency in sea water, sets a practical limit of about 0.5 MHz to low power transmission. Scattering is most serious in turbid water or in the presence of large concentrations of fish, with the greatest losses occuring when the deep scattering layer (DSL) rises near the surface at night time. For divers, communication along nearly horizontal paths is most seriously affected by refraction. A temperature gradient of 0.07 degrees Celsius per meter is sufficient to counter the effect of pressure on the speed of sound in sea water (Woods and Lythgoe, 1971). Thus, normal near-surface temperature variations can strongly affect acoustic communication ranges. Multiple

reflections off the sea surface, rocky bottom, and interposing natural structures, such as reefs and plants, and man-made structures lead to signal distortion and fading.

The current state of underwater communications is aptly summed up by Penzias and Goodman (1973): "None of these (current underwater communication systems) is satisfactory ... ."

The system discussed in this paper is nonacoustic and is unaffected by the losses described above. In fidelity it exceeds acoustic systems and possesses a nominal line-of-sight range to the horizon which can be extended to any place on Earth with off-the-shelf equipment.

2. Electric Current Field

An electric current field (ECF) is generated when an electric potential is applied across two electrodes immersed in a conducting medium. In normal sea water (salinity near 33 o/oo), this field propagates at a speed of approximately $3x10^6$ meters per second. The ECF spreads in a pattern similar to the magnetic field surrounding a magnet and produces a voltage gradient which is directly proportional to the amount of current. A second pair of electrodes introduced into the ECF, as shown in Figure 1, will have a voltage induced across them. The voltage varies as the cosine of the angle formed by the baselines of the two sets of electrodes. Thus, a second pair of electrodes oriented in the ECF, as shown in Figure 2, will experience essentially no induced voltage.

In a communication system using ECF, a voice signal is impressed across the transmitting electrodes, and a suitable means of detecting and amplifying the received signal is connected to the receiving electrodes. For a given angular orientation of the transmitting and receiving electrode pairs (antennas), the voltage at the receiving electrodes is directly proportional to:

(a) The output power (amount of current put into the field;
(b) The length of the transmitting baseline (distance between transmitting electrodes); and
(c) The length of the receiving baseline (distance between the receiving electrodes).

and is inversely proportional to:

(a) Water conductivity; and
(b) The cube of the range between transmitting and receiving antennas.

The quality of a signal transmitted via ECF is subject to the limitations of the equipment being used instead of environmental considerations. The result is a near-telephone clarity and intelligibility which surpasses any acoustic system.

3. System Description

General. The Hydrocom Retransmission System (HRS) consists of two primary components. The first is a standard Hydrocom Diver Unit, which provides voice communication between divers and which allows them to locate each other using the directional characteristics of the ECF. The second is a small surface buoy which couples Hydrocom Diver Unit electronics to a Motorola HT-220 Handi-Talki UHF transceiver.

Diver Unit. The HRS-1 Diver Unit consists of a main housing which contains the electronics and batteries, a microphone and bone conduction earphone, ankle electrode, and connecting wire. The housing is constructed of 16-inch long, 3-inch diameter stainless steel tubing, capped with Delrin plastic end caps sealed with O-rings. It is rated to 300 feet.

The top cap contains the microphone-earphone connector, electrode connector, charge plug receptacle, and power/sensitivity switch. The internal electronics and power chassis are connected to the top cap.

The bottom cap contains the ground electrode and a large screw which holds the unit together.

The microphone and earphone are connected to the main housing with a single waterproof connector. The microphone is protected with a special micropore bladder which allows it to equalize to 300 feet, and it can be installed in almost any full or half face mask. The earphone is a rubber-covered bone conduction unit. Bone conduction is used to eliminate the distortion problems caused by the water-tympanic membrane interface.

The ankle electrode is attached to the ankle with a Velcro fastener and is connected to the top cap by a simple insulated wire.

The entire unit is provided with a bracket for mounting to a standard SCUBA backpack (see Figure 3).

Retransmission Buoy. The HRS-1 Retransmission Buoy consists of a 24-inch long, 5-inch diameter stainless steel tube with Delrin plastic end caps sealed with O-rings, an electrode with 150 feet of connecting wire, a 39-inch antenna, and a float collar (see Figure 4). The internal electronics couple a standard HRS-1 Diver Unit transceiver to a Motorola HT-220 Handi-Talki UHF transceiver in a bi-directional simplex arrangement. The buoy automatically receives any Hydrocom signal within its effective range and retransmits it on whatever UHF channel the internal Handi-Talki is set; and it also automatically retransmits underwater any signal it receives on the UHF receiver.

Electronics. HRS-1 electronics consist of a transmitter, receiver, and voice-operated transmitter (VOX) circuits. The 30-watt transmitter is powered by a 24-volt nickel cadmium battery pack. The receiver incorporates automatic gain control (AGC) circuitry, which maintains nearly constant volume in the diver's ear. The VOX circuit is a two-stage, two-level device. An initial "throwaway" word, such as "Hi," is used to trigger the first stage. The first stage threshold is set high enough so that hard breathing noises or bubbles do not trigger the transmitter. Once the first stage VOX trips, the voice may be returned to a normal speaking level. The second stage VOX then takes over and continues transmission until the diver stops speaking or breathing for approximately one second.

The system is normally in the receive mode. When the VOX circuit is triggered by the diver's voice, the receiver is disabled and the transmitter activated.

In the HRS-1 Retransmission Buoy, the receiving Handi-Talki squelch circuit activates the VOX circuits, and the received UHF signal is coupled to the Hydrocom transmitter. When the buoy receives an underwater signal, that signal activates the Handi-Talki transmitter and is then broadcast on the selected UHF channel. (The HRS-2 Retransmission Buoy incorporates a tone generator in the interface to effect more positive control over the switching process.)

4. System Operation

The HRS operates in four modes. D-mode (diver to diver) is the basic Hydrocom in action and preceded HRS. DRS-mode (diver retransmit short range) is the principal HRS mode. DR-mode (diver to diver retransmit) and DRL-mode (diver retransmit long range) are special applications of the DRS-mode.

D-Mode. In the D-mode, two or more divers are equipped with HRS Diver Units. Communication range is generally less than 400 feet and is optimum between divers who have the same general orientation to the water column, i.e., both horizontal or vertical. A diver wishing to communicate uses a "throwaway" word to activate his VOX and then speaks normally. The other divers will hear him speak. To shorten the transmission range (to avoid interference with a nearby group, for instance), the ankle electrode need only be moved nearer the backpack. To enable all other divers to home in on one diver under low visibility conditions, that diver activates his transmitter and talks continuously, i.e., counting, while holding himself horizontally oriented. The other divers place themselves horizontally and rotate through the azimuth until they detect a transmission null. They then swim towards the null.

DRS-Mode. In the DRS-mode, the HRS Retransmission Buoy is placed in the water near the divers. The divers still communicate among themselves in the D-mode, but all transmissions are simultaneously retransmitted by the buoy on the selected UHF channel for surface reception by any portable or fixed radio capable of receiving on that channel. Surface transmission to the divers is usually made with a hand-held or other portable unit. The communication range between surface unit and divers is limited to the normal range of UHF units (usually line of sight to the horizon). Homing on the buoy can be effected in a similar manner to D-mode homing.

DR-Mode. In the DR-mode, two HRS Retransmission Buoys are used. Each buoy is associated with a group of divers. Although the two groups of divers can be widely separated, a diver from one group can communicate with a diver from the second group so long as the buoys are within radio range of each other. This mode is a logical extension of the DRS-mode, wherein a surface unit is controlling two sets of divers on a coordinated underwater project.

DRL-Mode. The DRL-mode is another extension of the DRS-mode in which the surface unit is patched by some suitable means to a very distant receiver. The two-way communication link can be effected by a standard radio patch or even by satellite relay. The essential innovation here is that the signal from the diver arriving at the surface unit is already in electromagnetic form and requires no further processing for relay.

5. System Potential

The Hydrocom Retransmission System utilization potential falls into three main areas: communication, monitoring, and control. Communication is primary and has been discussed in some detail already. Beyond the obvious appeal of enhanced local communications lies the possibility of direct laboratory control of distant instrument emplacement and maintenance. The value of real-time system feedback can never be overestimated, and the HRS brings this benefit to the field of diver-emplaced instrumentation.

ECF has been shown to be responsive to objects placed within the field (U.S. Navy, 1972). This principle of "electric anomaly detection" has applications ranging beyond submarine and swimmer intrusion detection for the military. Applications range from remote fish counting for a marine biologist to a relatively inexpensive system for the marine traffic manager who continuously monitors shipping location and flow within his area.

In June 1977, TDC Underwater Systems personnel demonstrated the feasibility of telemetry transmission utilizing ECF. Applying this capability to HRS results in the unique ability to apply real-time sophisticated computer analysis to distant underwater events. A pilot study has also shown that ECF techniques can effectively be applied to acoustic net and to azimuth-dip-range planimetric survey methods. Due to its greater in-water velocity and its freedom from environmental degrading, a survey technique based upon ECF is inherently more accurate than acoustic methods, and its design simplicity results in considerably lower manufacturing costs.

HRS bidirectionality is an additional factor. Any underwater system which would benefit from direct or feedback control is a potential area for HRS application. The automatic positioning of a floating platform over a submerged reference point has been demonstrated at TDC using scale models. The marine traffic monitoring system discussed above could be expanded to include a passive navigating system with shipboard readouts, enabling bridge personnel to monitor the vessel's channel position. An automatic pilot could be incorporated into such a system. With suitable shipboard alarms, bridge pylons and submerged obstructions could be marked with an ECF for an effective anti-collision system.

6. Summary

Diving operations require a speech communication system that can be carried by the diver without hampering mobility and safety; can provide easy two-way intelligible speech; is reliable, effective, efficient, flexible, and simple to operate; and has a reasonable signal propagation range. The Hydrocom Retransmission System (HRS) meets these requirements and, in areas of intelligibility and range, far exceeds anything available today. HRS provides near-telephone clarity communications over unlimited range. It also provides the diver with a simple-to-operate homing system.

HRS can be adapted for applications in remote surfaced and submerged traffic monitoring and control, accurate, inexpensive underwater object location and planimetric survey, real-time telemetric and feedback analysis of remote underwater data, and various anti-collision devices.

7. References

Martin, W. R. and R. L. Adams, "Physiologic Factors in the Design of Underwater Communication," Marine Technology Society Journal, 4:55-58 (May-June 1970).

Penzias, W. and M. W. Goodman, Man Beneath the Sea, p. 332, Wiley-Interscience, New York (1973).

Shilling, I. W., M. F. Werts, N. R. Schandalmeier, "Underwater Communications," in I. W. Shilling, M. F. Werts, N. R. Schandalmeier, eds., The Underwater Handbook, Plenum Press, New York (1976).

U.S. Navy, Phase I Final Report, Bridge Defense System Feasability Model, Contract N61339-71-C-0230 (Confidential) (February 1972).

Woods, J. D. and J. N. Lythgoe, "Apparatus and Methods for the Diving Scientist," in J. D. Woods and J. N. Lythgoe, eds., Underwater Science, pp. 1-31, Oxford University Press, London (1973).

LIFT LINE DYNAMICS - A TECHNIQUE TAILORED FOR THE USER

W. S. Pope
Principal Research Engineer
Battelle, Columbus Laboratories
505 King Avenue
Columbus, Ohio 43201

C. S. Albro
Research Engineer
Battelle, Columbus Laboratories
505 King Avenue
Columbus, Ohio 43201

Abstract

A technique is proposed as an aid to the marine salvage master at sea and the ocean engineer. The aid may be used to find line size, factors of safety, maximum operating conditions, salvage object parameters and other useful information relating to the lifting or lowering of heavy objects at sea. A computer program based on Arthur D. Little, Inc. equations for maximum dynamic line force is used to generate a number of parametric curves for a specific ship lift point and line type which are then collapsed into one simple equation--the key formula--for dynamic factor of safety. This is combined with the easily obtained static factor of safety, and the results displayed on a set of nomographs and charts.

The paper explains the need for such a scheme, what the basic equations mean, their limitations, and how the charts and nomographs are used.

1. Introduction

The lifting or lowering of objects at sea from a floating platform has always been a risky and expensive business. There seems to be no widely accepted design method for selection of line and figuring safety factors. Instead a wide variety of rules of thumb, manufacturers' recommendations and computer programs are employed. This paper illustrates an approach to simplifying the problem of matching the characteristics of the line, platform, and lifted object.

In this paper we have proposed a straightforward, rational technique for line selection based on best engineering information and analysis, which avoids ad hoc computer solutions for each and every lift situation. The results are presented in such a way that they may be used by the salvage master at sea, as well as the ocean engineer in the design office.

2. The Problem Facing the Salvor

After analyzing a number of specific lift cases, and looking at various aspects of the problem, we became concerned that the mariner who would have to use a previously selected line, and possibly make some on-site decision based on changing circumstances, was not being considered.

Suppose, for instance, that a line has been selected for a specific lift task; e.g., lift a specific object from a specific ship in a maximum depth and sea state. Further suppose that when the expedition arrives on station: the object has tipped over and filled with mud, or slid into deeper water, or the seas are higher than anticipated, or the primary line is damaged and a backup employed, or any of a host of occurrences which could change the parameters of the lift. The salvage master would then have to decide whether to proceed, abort, or change the situation enough to proceed. The proposed method will help in making that decision, and many others, concerning the selection, use and limitations of lifting lines.

3. How the Technical Aid is Used

The salvor would have in front of him a set of charts and nomographs which would relate the lift parameters. His job would be to determine the numbers for the parameters for which values are available or can be estimated, enter the charts and determine the remaining unknown factor for the lift. All of the heavy analytical work has been "front end loaded" by the engineers preparing the charts, so that the effort in actually using them is brought to a minimum number of steps.

Each set of charts is prepared for:

- o A specific ship and lift point (e.g., a stern "A" frame on an offshore supply boat, as in our example)
- o A specific type of line (e.g., Samson 2-in-1 Power Braid, also used in our example).

Thus each set becomes part of the ship's equipment, usable indefinitely, as long as the hydrodynamic characteristics of the ship are not altered.

4. Preparation of the Charts

The information needed to prepare the charts consists of:

Fixed for one set of charts:

- o Ship Response Characteristics - response amplitude operator (RAO) is used in this analysis
- o Sea State Formulation - the Bretschneider sea state spectrum was chosen for our example, for Sea States 3, 4, and 5
- o Line Characteristics - modulus (average value at 20% of breaking strength), density

Variables:

- o Generalized Salvage Object Characteristics - size, shape, weight, density
- o Lift Operation Characteristics - line diameter and maximum length.

This information is input to a computer program, which increments the variables so as to map regions of maximum line load for the expected ranges of all variables.

The output is then plotted parametrically and examined for best fit to simple power function relationships. The result is a relatively simple formula for total dynamic safety factor as a function of three parameters: a "nominal" dynamic safety factor, a sea state parameter, and an object parameter. Finally, the static and dynamic safety factors are combined into a total safety factor. All parameters are displayed in nomograph form for ease of manipulation.

5. The Dynamic Model

The mathematical model used to compute dynamic stresses was the Arthur D. Little, Inc.[1,2] boundary value equation, derived from the basic equation of motion of a line segment. The following limitations apply to its use.

1. A single, constant diameter cable
2. Constant cable modulus of elasticity
3. Cable hangs vertically under lift point
4. Ship exciting force is sinusoidal, or can be represented as a sum of sine waves
5. Damping on the cable is neglected
6. Rate of raising or lowering is small relative to the exciting velocity
7. Sea state is statistically stationary and ergodic
8. The ship RAO function remains unchanged over time
9. The damping force on the object is linearized.

In Ref. 1, the sensitivity of the solutions for dynamic stress to the degree of compliance with some of the above assumptions was examined. Liu[3] looked at the sensitivity of the solution to varying values of each independent variable, and in Ref. 4 reported on an actual at-sea test conducted by Muga to verify analytical predictions based on these equations.

In general, the limitations are reasonably well met in normal practice, with certain specific exceptions, in which case caution must be exercised in interpreting the stress results. In particular, the non-linearities involved in the line modulus, object damping and hoisting speed have more pronounced effects on stress near resonance, when the drag to inertia affects ratio is either very low or very high.

The Arthur D. Little equation can be expressed as follows:

$$|\Sigma_o'|^2 = (\omega')^2 (U_1')^2 [1 + 2 \tan \phi \cos^2 \omega' (\tan \psi + \tan \omega')]$$

where ω' is the dimensionless frequency

U_1' is the dimensionless load displacement

Σ_o' is the dimensionless tension of the top end of line

and ω', U', ϕ and ψ are functions of the line and load properties and/or surface displacement, U.

This, and a companion equation, which calculates the maximum tension anywhere in the line, can be rearranged to provide a response function,

$$R_\omega = \left| \frac{D}{U_o} \right|$$

which represents the maximum line tension, D, wherever it occurs in a given line, divided by the excitation amplitude, U_o, as a function of frequency. Figure 1 is a series of power spectral density plots which illustrate the following sequence of steps used to arrive at the values for significant dynamic tension.

1. The <u>amplitude</u> of response of the lift point on the ship to unit wave <u>height</u> is determined; this is the RAO.
2. A sea way power spectral density is constructed for the sea state of interest. This is $S_{(H,\omega)}$; the area of this curve represents significant wave height $H_{1/3}$ (average of 1/3 highest waves).
3. The lift point excitation spectrum $U^2_{(H,\omega)}$ will be the product of the RAO^2 spectrum and the sea state

FIGURE 1

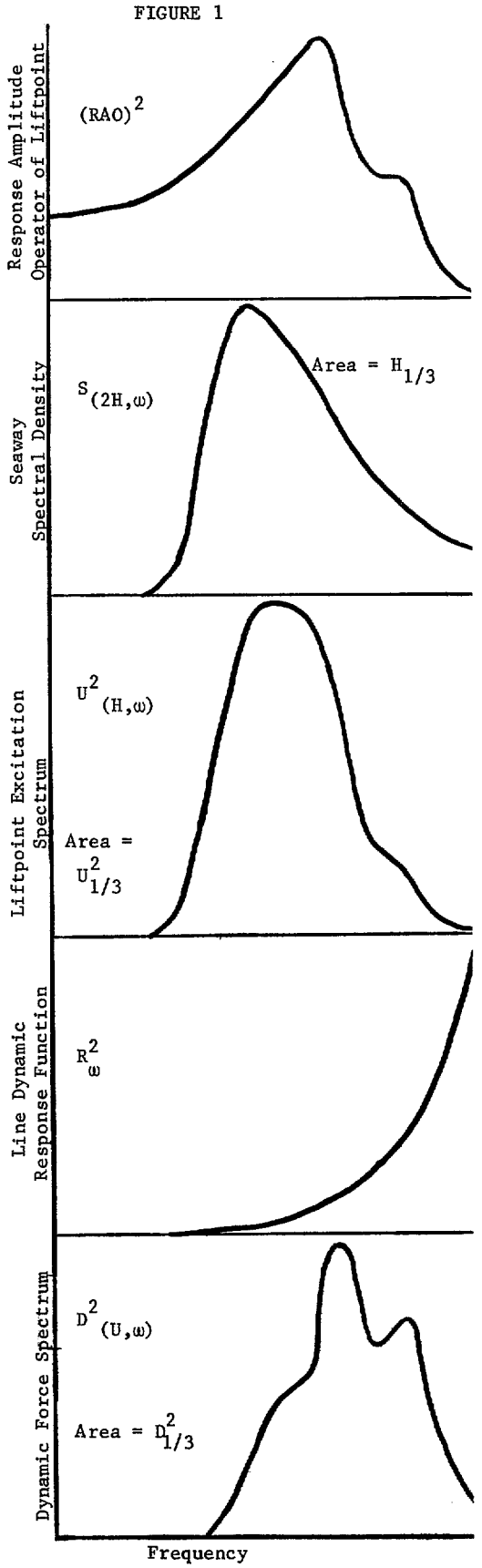

spectrum. (As noted, the area under the $U^2_{(H,\omega)}$ curve is the square of the significant excitation, $U^2_{1/3}$. (The response equation for dynamic force involves a linearization of the normal "velocity squared" drag term in the equation of motion of the load. $U_{1/3}\omega$ becomes a synthetic velocity, used in the response equation, to represent the same energy dissipation as the velocity squared term in the equations of motion.)

4. Finally, the product of the lift point excitation spectrum $U^2_{1/3(H,\omega)}$ and the line dynamic response function R^2_ω is the Dynamic Force Spectrum $D^2_{(U,\omega)}$, the square root of whose area is the significant line tension, $D_{1/3}$.

A calculation is made for dynamic force for incremental values of line length from 0 to 20,000 ft. Each answer is compared to the one in memory and replaces it if the new answer is higher. Thus, each combination of lift parameters (ship characteristics, sea state, object parameters and lift line parameters), produces one answer which represents the highest value of significant dynamic force encountered in the line, at a length not specified, during a transit between surface and 20,000 ft.

These results may also be presented in terms of a probability to exceed a set point dynamic load in a given time. However, it was felt that the approach of presenting simple forces and factors of safety has more universal appeal.

6. Results and Discussion

For each support platform, the total factor of safety can be expressed as:

$$f_T = \frac{1}{\frac{1}{f_s} + \frac{1}{f_D}} = \frac{B}{W_o + D} \text{ and } f_s = \frac{B}{W_o},\ f_D = \frac{B}{D}$$

where B = breaking strength of line, lb
W_o = wet weight of object (dry weight minus buoyancy)
D = dynamic line force, lb

Our curve fitting exercise resulted in the following equation for f_D:

$$f_D = K[\frac{1}{U_o\omega_o}]^a[K_Z Z]^b[f_d]$$

where, K = constant

$U_o\omega_o$ = significant excitation amplitude times frequency of highest energy input

a,b = exponents, derived from curve fitting

$f_d = \frac{B}{W_D}$, nominal dynamic safety factor

with, W_D = dynamic weight, a factor accounting for wet weight plus added mass effects due to entrained and entrapped water, around and inside the object.

This derived equation could in fact be used by the salvors and engineers*, however, we felt that a nomograph presentation would be more accessible and also allow easier manipulation to find answers other than f_T.

A worked example is shown in Figure 2 along with the nomographs and chart required; additional information, which would be included to help in estimating values for C_D and C_M, has been omitted for brevity.

Four points are worth noting:

- The salvor need not be concerned with critical length. This is so because computations for stress are made at all lengths, but only the greatest stress is retained. For neutrally buoyant nylon line (our test case) the critical length usually occurs within about 1200 feet of the surface, so that even much deeper lifts will still be governed by the higher loads as the object passes through this critical region.

- "Wet" weight (weight in air minus weight of displaced water) and enclosed volume of object are the key parameters used in the nomographs and they are most readily estimated by the salvor.

- It is not necessary to make an estimate of E, the line modulus, as this has been done in the initial calculations. Breaking strength is needed, but is a much more readily available number. Noteworthy in this regard is that the differences in max. load between nylon and power braid are very small over wide ranges of parameters, so that both may be used on these graphs, if the appropriate breaking strength tables are consulted.

- The particular relations derived here were for nearly buoyant synthetic line; the basic dynamic equations would still be valid for metal or Kevlar lines, but more curve fitting would be needed to accommodate a more marked dependence of the dynamic load on line weight.

7. Technical Aid Example (See Figure 2)

To illustrate the use of the charts and nomographs, take the following situation:

Given:
- Synthetic line, breaking strength B = 100,000 lb
- Spherical Salvage Object -
  Wet weight, W_o = 15,000 lb
  Mass coefficient, C_M = 1.5 = 1 + added mass coeff
  Total volume, V = 310 cf
  Drag Product, C_DA = 22 sq.ft.

Find: what is highest sea state which can be tolerated for a total factor of safety of 3?

<u>Nomograph A (line (1))</u>

1. Connect V and C_M; read added weight W_A = 30,000 lb
2. Dynamic weight $W_D = W_o + W_A$ = 15,000 lb + 30,000 lb = 45,000 lb

<u>Nomograph B (line (2))</u>

3. Connect B and f_T, extend to read total line force, $D + W_o$ = 34,000 lb
4. Dynamic force $D = (D + W_o) - W_o$ = 34,000 lb - 15,000 lb = 19,000 lb

<u>Nomograph C</u>

5. Connect W_D and D, extend to find W_D/D = 2.37 (line (3))
6. Extend line at W_D/D = 2.37 to the right, parallel to Z-axis (line (4))
7. Connect W_D and C_DA, find Z = 4.8 (line (5))
8. Go to sea state chart, intersection of W_D/D= 2.37 and Z = 4.8 (line (6)) gives max operating sea state = 3

---

* A computer run was made as a check in which the dynamic and total safety factors were calculated from the A. D. Little equation and the derived equation. For the 270 distinct data points, the standard deviation between the two was 5.2% for f_D and 2.7% for f_T.

Optional Iteration

1. Salvor adds a light disk 5.3 ft in diameter a distance above object; this provides additional added weight effect (line (7), nomograph A) in the amount of 5000 lb (the disk acts as if it were a sphere of water of the same diameter whose volume is 80 cf).

2. The effective drag-area will be doubled.

3. In nomograph C, connect new W_D = 50,000 lb with new C_DA product = 44 to find new Z = 9.0 (line (8)).

4. Connect new W_D with previous D (unchanged from requirements imposed in Nomograph B) extend to find W_D/D = 2.63, line (9).

5. Intersect new Z and new W_D/D to find increased max sea state >4.

In addition to the examples cited here, any of the other parameters besides sea state may be treated as unknowns and solved for by use of the nomographs, as long as the remaining factors are known or can be estimated.

References

1. Arthur D. Little Inc., Tech Report No. 1370863, Stress Analysis of Ship-Suspended Heavily Loaded Cables for Deep Underwater Emplacements, Cambridge, Mass, August 1963.

2. Arthur D. Little, Inc., Memorandum Report No. 3030365, Some Design Considerations for Deep Water Suspension Lines, Cambridge, Mass, March 1965.

3. Dynamic Tension Analysis of a Simple Lift System - a Computer Method, by C. L. Liu, Naval Civil Engineering Laboratory, Port Hueneme, California, ASME Paper No. 71-UnT-7, 1971.

4. Naval Civil Engineering Laboratory, Technical Report No. R703, "Dynamic Stress Response of Lifting Lines for Oceanic Operations", Port Hueneme, California, 1970.

5. Computation of Relative Motion Effects in Offshore Supply Operations, by J. R. Paulling, P. D. Wood, University of California, OTC Paper No. 2634, 1976.

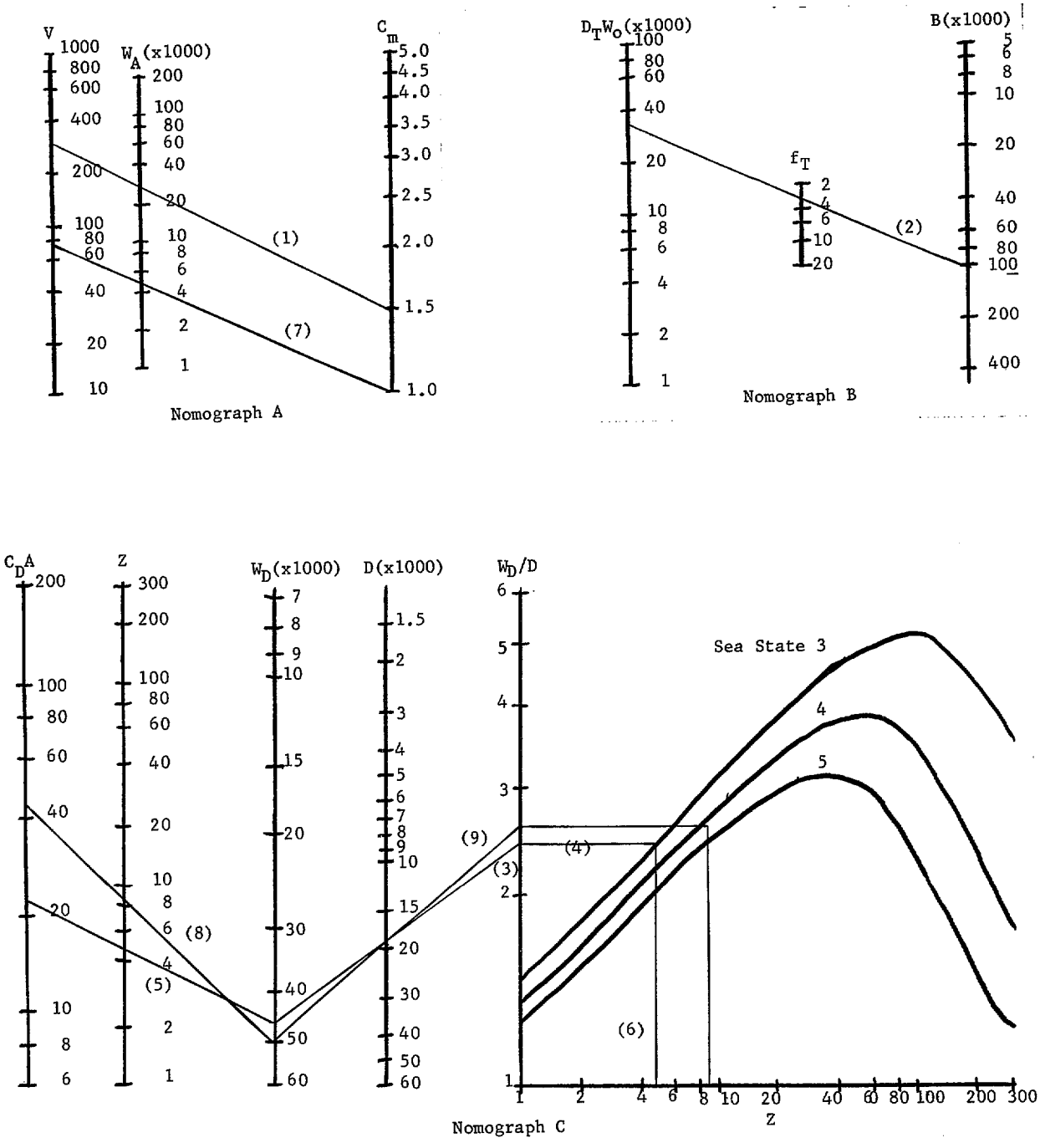
V
1000
800
600
400
200
100
80
60
40
20
10
W_A(x1000)
200
100
80
60
40
20
10
8
6
4
2
1
C_m
5.0
4.5
4.0
3.5
3.0
2.5
2.0
1.5
1.0
(1)
(7)
Nomograph A
D_TW_o(x1000)
100
80
60
40
20
10
8
6
4
2
1
f_T
2
4
6
10
20
(2)
B(x1000)
5
6
8
10
20
40
60
80
100
200
400
Nomograph B
C_DA
200
100
80
60
40
20
10
8
6
Z
300
200
100
80
60
40
20
10
8
6
4
2
1
(8)
(5)
W_D(x1000)
7
8
9
10
15
20
30
40
50
60
D(x1000)
1.5
2
3
4
5
6
7
8
9
10
15
20
30
40
50
60
(9)
W_D/D
6
5
4
3
2
1
Sea State 3
4
5
(4)
(3)
(6)
1
2
4
6
8
10
20
40
60
80
100
200
300
Z
Nomograph C

FIGURE 2

EXTERNAL WORK OF BREATHING OF DEMAND-AIR UNDERWATER BREATHING APPARATUS*

J.J. Grodski

Defence and Civil Institute of Environmental Medicine
1133 Sheppard Avenue West
P.O. Box 2000
Downsview, Ontario, M3M 3B9
Canada

Abstract

Underwater breathing apparatus can be effectively evaluated by measuring the external work of breathing. This paper reviews the existing and the proposed standards for demand-air breathing apparatus and recommends improvements to the Bentley-Reimers criterion. An automated method of collecting data on the external work of breathing is also described along with test results of various demand-air breathing apparatus. The test and evaluation data in this paper support the proposed, modified Bentley-Reimers criterion.

1. Introduction

The life support systems designer is continuously attempting to provide divers with low breathing-resistance life support equipment. The ultimate goal, of course, is to reduce the external work of breathing to zero. Numerous investigators have attempted to define acceptable external respiratory workload standards for men wearing respiratory apparatus. Silverman et al.[1] conducted the first comprehensive study of the physiological effects of resistive breathing at atmospheric pressures. Cooper[2] reviewed the work of Silverman and co-workers and recommended standards for maximum permitted total rate of respiratory work done on a breathing apparatus. More recently, Bentley et al.[3] investigated the tolerance to the external respiratory work of miners at atmospheric pressures. They proposed that the standard should use the level of the total external respiratory work per unit ventilation at which 90 percent of the tested population does not experience respiratory discomfort. Their experimental data showed that the level corresponded to 0.17 kg.m/liter of air breathed. Others proposed either higher or lower acceptance criteria. Reimers[4] summarized these proposals and suggested that Bentley's criterion should be adopted for testing underwater breathing apparatus and that this criterion should remain unaltered for pressures (depths) up to 1000 feet of seawater (fsw). This Bentley-Reimers limit of 0.17 kg.m/liter of ventilation has been used in recent underwater breathing apparatus evaluations at the Defence and Civil Institute of Environmental Medicine (DCIEM) (unpublished) and the U.S. Navy Experimental Diving Unit[5] (NEDU).

The purpose of this paper is to show how practical, automated calculations of the external work of breathing can be obtained. Additionally, performance of various demand-air underwater breathing apparatus is examined by relating the experimentally determined external work of breathing to the Bentley-Reimers limit. A modification of the Bentley-Reimers criterion, consistent with the U.S. Military Specifications[6,7] (Mil-Specs) and the current technology, is proposed for the shallow end of the depth scale.

2. The External Work of Breathing

The cumulative product of the pressure and the volume of air moved at each instant is equal to work:

$$\text{work} = \int p.dV \qquad (1)$$

Fig. 1 shows the pressure-volume (p-V) loop of a breathing cycle. The area within a p-V loop is proportional to the respiratory work, which can be determined by simultaneous plotting of the variables p and V in appropriate units and measuring the resulting area. The measurement is often performed manually but such a procedure is laborious. The same may be accomplished quickly and with a high degree of accuracy by performing a programmed, numerical integration using a suitable calculator.

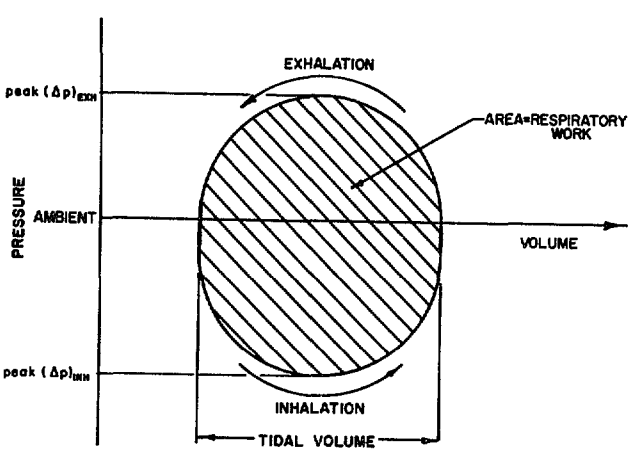

Figure 1. Pressure-volume loop of a breathing cycle and its features

* DCIEM Publication No. 78X18

This latter approach was used in this work.

The total respiratory work (internal plus external, if any) is calculated from measurements of the differential pressure between the thoracic cavity and the external ambient pressure. The external work of breathing for demand-type of underwater breathing apparatus is determined from the pressure differences between the airway (mouth) pressure and the hydrostatic reference pressure at the level of the centre line of the second stage diaphragm. In dry testing, the ambient pressure is used as the reference. Wet testing of other than the demand type of apparatus involves a different approach[4]. The meaning and significance of the external respiratory work of breathing is recognized by both engineers and physiologists.

3. Respiratory Impedance Standards

Mil-Specs[6,7] for demand-air, double hose and single hose SCUBA regulators in depths from the surface to 200 fsw provide the single, presently accepted breathing impedance standard. The mechanical inhalation and exhalation peak pressure limits specified by the Mil-Specs may be described by the following equations:

$$(\Delta p)_{EXH}[\text{cm } H_2O] = 5.0 + 0.075 \times (\text{depth}[\text{fsw}]) \quad (2)$$

$$(\Delta p)_{INH}[\text{cm } H_2O] = 6.5 + 0.0675 \times (\text{depth}[\text{fsw}]) \quad (3)$$

The peak pressures are readily measured and hence the standard has been used in numerous equipment evaluations. In fact, because of the lack of general standards, the Mil-Specs were applied to other types of underwater breathing apparatus for which they were neither intended nor well suited. Moreover, the physiological significance of the peak pressures is obscure and the need to tighten the standard is well known[8]. The Reimers proposal[4] eliminates these difficulties and provides a standard, acceptable in both physiological and engineering terms. It is, therefore, interesting to make a comparison of the Mil-Specs standard to the Bentley-Reimers criterion.

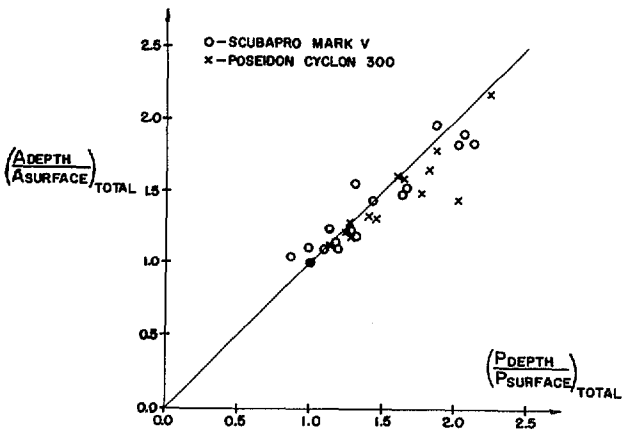

Figure 2. Normalized total external respiratory work vs normalized sum of mechanical peak pressures

Addition of equations (2) and (3) yields an equation for the peak total pressure difference:

$$(\Delta p)_{TOT}[\text{cm } H_2O] = 11.5 + 0.1425 \times (\text{depth}[\text{fsw}]) \quad (4)$$

It can be readily shown that under steady flow conditions, the sum of the volume-average respiratory and expiratory pressure difference equivalent to the Bentley-Reimers limit of 0.17 kg.m of work per liter of ventilation is 17 cm H_2O. Bentley et al.[3] discuss implications of the various waveforms on this conversion. A set of breathing simulator tests conducted at DCIEM on two different single-hose regulators provided a direct measurement of the relationship between the sum of the peak inspiratory and expiratory pressures and the external work of breathing. Fig. 2 shows the spread of the data with both parameters normalized to the zero depth (surface). The slope of an equivalent dimensional relationship was found to be constant, approximately .009 [(kg.m/ℓ)/cm H_2O]. Therefore, the Bentley-Reimers limit is equivalent to the sum of the peak inspiratory and expiratory pressures of 18.9 cm H_2O and the pressure dependence of the combined specifications shown in equation (4) has an equivalent form involving the external respiratory work per unit ventilation:

$$\text{work}[\text{kg.m}/\ell] = 0.1035 + 0.00128 \times (\text{depth}[\text{fsw}]) \quad (5)$$

or in metric units,

$$\text{work}[\text{kg.m}/\ell] = 0.1035 + 0.0042 \times (\text{depth}[\text{msw}]) \quad (6)$$

The line representing this equation intercepts the Bentley-Reimers limit at the pressure equivalent to 51.93 fsw or 15.83 meters of seawater (msw) as shown in Fig. 3. At the shallow depths, the Mil-Specs standard is more severe than the Bentley-Reimers proposal. Moreover, recent material and technological improvements incorporated into the

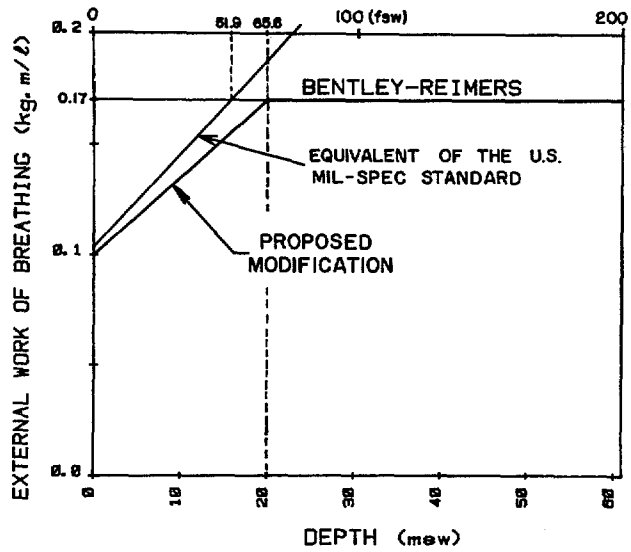

Figure 3. Bentley-Reimers acceptance criterion and its proposed modification

equipment warrant a tightening of the Mil-Specs standard. It is therefore proposed that the Reimers proposal[4] be modified for demand-air breathing apparatus, within the depth range of 0 to 20 msw (65.6 fsw), to include a change (Fig. 3) described by the following equation:

$$\text{work}[\text{kg.m}/\ell] = 0.1 + 0.0035 \times (\text{depth}[\text{msw}]) \qquad (7)$$

This modification is not significantly more restrictive than the corresponding range of the Mil-Specs standard, and further diminution of the limit is possible. It should be recognized that the provision of optimal breathing conditions in this shallow range is particularly important because it affects the largest diving population.

4. The Experimental System

The hyperbaric unmanned respiratory testing facility (HURTF) at DCIEM has been used for the measurement of external work of breathing on underwater breathing apparatus. The facility includes a hyperbaric chamber, a breathing simulator system[8] schematically shown in Fig. 4, and analytical instrumentation interfaced to a fast data acquisition system, schematically shown in Fig. 5. The breathing machine uses the reciprocating action of a piston moving within a cylinder to simulate the ventilatory action of the human lungs.

During the experiments, the momentary piston position and the pressure difference between the mannequin mouth pressure and the reference pressure were measured concurrently. The resulting piston position and the piston velocity waveforms, with the velocity of the driving motor preset to a constant value throughout the cycle, are shown in Fig. 6. The waveform of the flow at the mouthpiece, affecting the pressure difference, is related to the piston velocity waveform. The discontinuity in the sinusoidal pattern of the piston velocity waveform is due to the backlash existing in the drive linkage. A linear transducer (SCR Division of Moxon Inc., Model D1110) and a pressure transducer (Validyne Eng., Model DP15), equipped with a diaphragm rated at 1 psi, were used to measure respectively the piston position and the pressure difference (Fig. 5). The

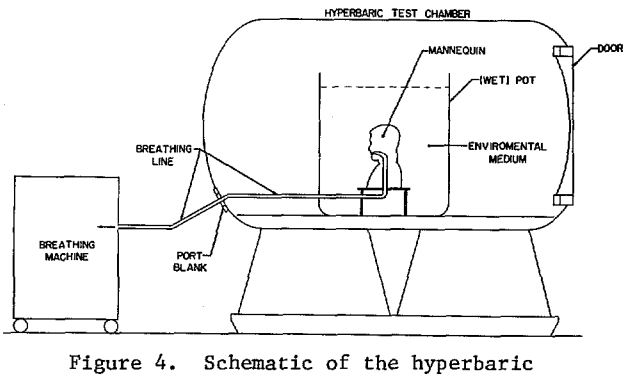

Figure 4. Schematic of the hyperbaric chamber-breathing simulator configuration

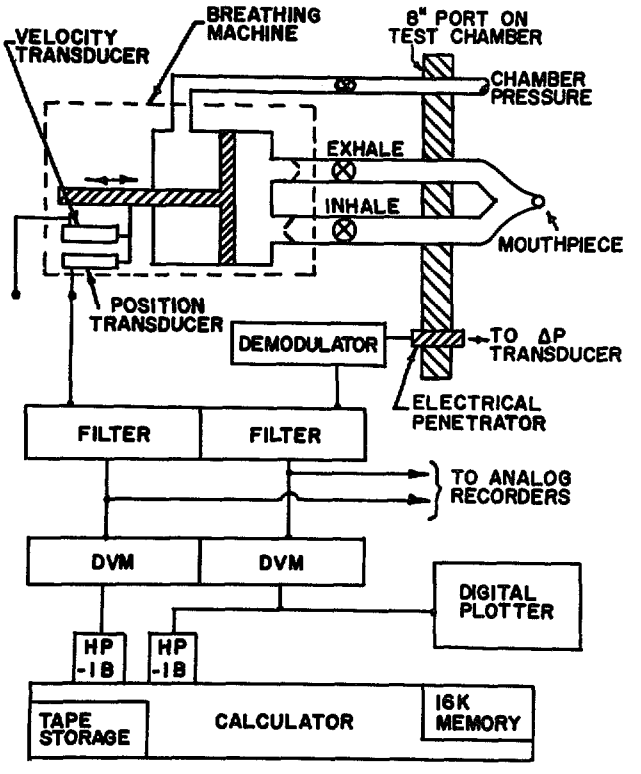

Figure 5. Schematic of the fast data acquisition system

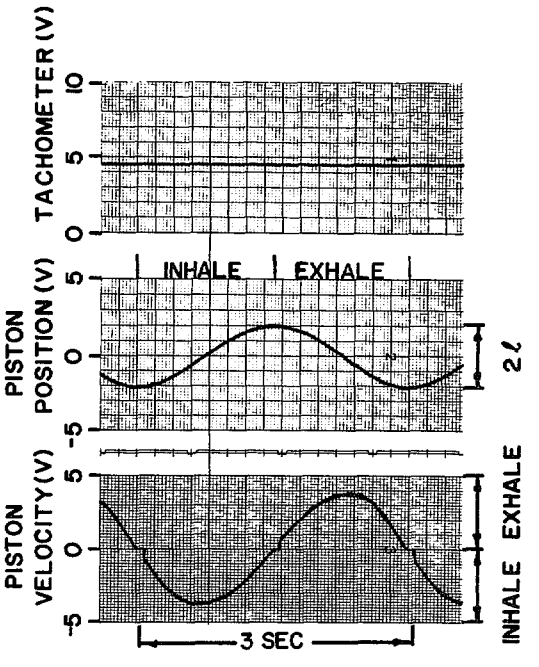

Figure 6. Velocity of the driving motor, piston position, and piston velocity waveforms of DCIEM breathing machine

transducer was powered from a carrier demodulator (Validyne, Model CD19). Routing of the measured signals through low-pass filters (Krohn Hite, Model 3342) elimintated noise from the signals before they were fed to analog recorders or to the digital data acquisition system. The latter consisted of two fast digital voltmeters (HP-3437A) controlled from a calculator (HP-9825A) with a 16K memory and equipped with a string - advanced programming and a plotter - general I/O - extended I/O ROMs. This two channel system acquired data at a rate of up to 100 data pairs per second when the voltmeters were interfaced to the calculator using a single HP-IB interface. The use of two HP-IB interfaces increased the acquisition rate to a maximum of 500 data pairs per second with the total capacity of 1750 data pairs. The acquired data was stored on a magnetic tape for subsequent analyses and management. In the analysis, a complete inhalation/exhalation cycle was selected from the recording and the integration was performed using the digital data. A digital plotter (HP-9872A)was used for the graphical display of the resulting diagrams.

5. Experimental Data

The combined experimental and data acquisition systems were used to obtain data on the external work of breathing of a variety of underwater breathing apparatus for pressures up to the maximum depth of 60 msw (197 fsw). The tested equipment was dry throughout the tests.

Fig. 7 shows examples of p-V diagrams obtained with a single hose regulator at three different test conditions. Two diagrams were obtained respectively at atmospheric pressure and 60 msw (197 fsw), with the breathing machine creating a sinusoidal demand of 40ℓ respiratory minute volume (RMV), corresponding to the respiratory demands[10] of an average man performing heavy work at surface atmospheric pressures. This RMV was attained by selecting the tidal volume (V_{TV}) of 2ℓ and the respiratory rate of 20 breaths per minute (bpm). This combination of V_{TV} and the respiratory rate was specified as the test condition in the Mil-Specs standards; it also corresponds to the second of three test conditions recommended by Reimers[4]. The third p-V diagram, enclosing the largest area, was obtained at the pressure equivalent to 40 msw and 62.5ℓ RMV, corresponding to the human respiratory demands[10] at the onset of the severe work level. This RMV setting, attained at 25 bpm is the highest demand setting recommended by Reimers[4].

The external work of breathing was calculated from these and additional p-V traces. Fig. 8 shows the effects of pressure and the simulated level of RMV on the work per unit ventilation. The inhalation and exhalation components of the external work of breathing for 40ℓ RMV are also shown. The external respiratory work per unit ventilation at this ventilation level is well below the Bentley-Reimers standard; however, at 62.5ℓ RMV, it crosses the standard in the vicinity of 37 msw (121 fsw). This is in agreement with expectations expressed by Reimers[4]: "most open circuit SCUBA regulators will not support a 62.5ℓ/min minute volume except at very shallow depths". It is interesting to identify and correlate the particular total, inhalation, and exhalation data points in Fig. 8 with the corresponding p-V loops in Fig. 7.

Fig. 9 shows examples of p-V diagrams obtained with a double hose regulator using experimental conditions similar to those described earlier. A comparison with Fig. 7 indicates that the peak pressures and corresponding work of breathing associated with the double hose regulator are larger than with the single hose regulator. This is in agreement with the well known facts, further confirmed by a comparison of data shown in Fig. 8 and Fig. 10. A summary of the external work of breathing data for the double hose regulator for depths up to 60 msw is contained in Fig. 10. The portion of the work associated with inhalation is high at the

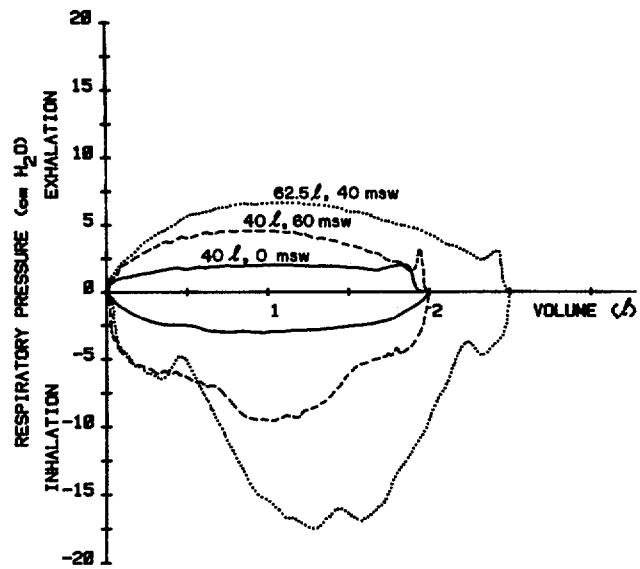

Figure 7. Examples of p-V diagrams obtained with a single hose regulator

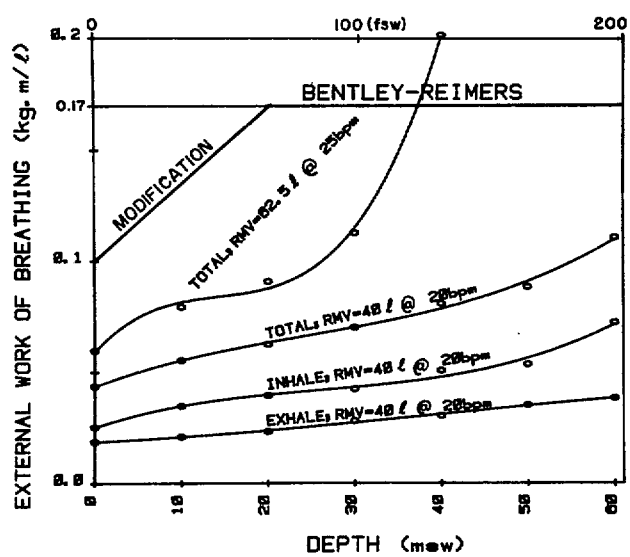

Figure 8. External work of breathing data for a single hose regulator

surface and varies little with the depth, while the work of exhalation is initially low but markedly increases with the depth. The total work of breathing at 40ℓ RMV is relatively high and it intercepts the Bentley-Reimers limit in the vicinity of 50 msw (164 fsw). The 60ℓ RMV curve (obtained at 30 bpm and V_{TV} of 2ℓ) shows that the larger respiratory demands are associated with an unacceptably high level of respiratory work.

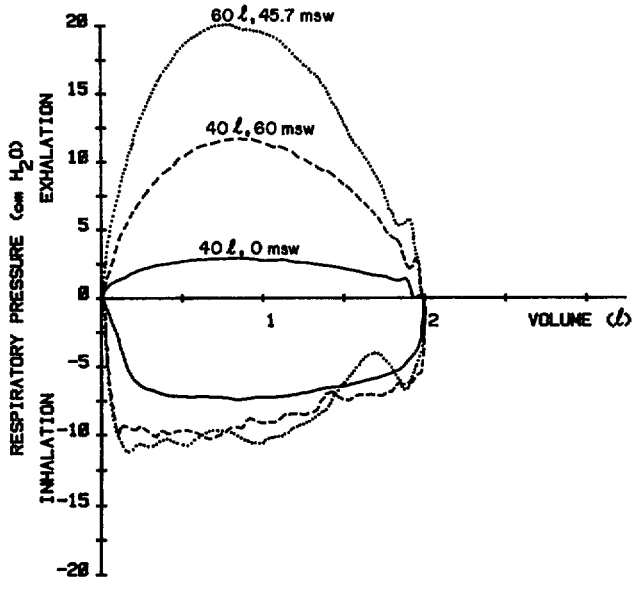

Figure 9. Examples of p-V diagrams obtained with a double hose regulator

Tests conducted on a Band Mask, operated with a 3/8" I.D., 300 ft long umbilical and supplied with air at 150 psi over the bottom pressure (psiob), resulted in p-V diagrams and the external work of breathing data shown respectively in Fig. 11 and Fig. 12. The work of breathing associated with the use of the Band Mask is relatively low. However, at 62.5ℓ RMV, the work deviates significantly from the 60ℓ RMV results at depths greater than about 25 msw (82 fsw), and becomes excessive around 50 msw (164 fsw).

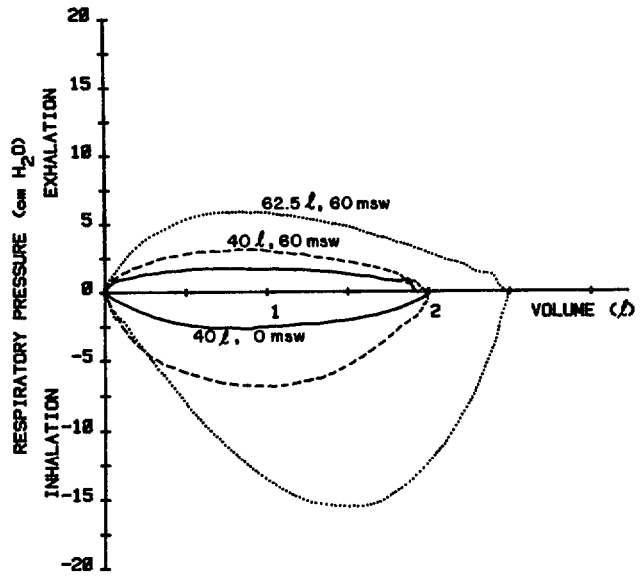

Figure 11. Examples of p-V diagrams obtained with a Band Mask

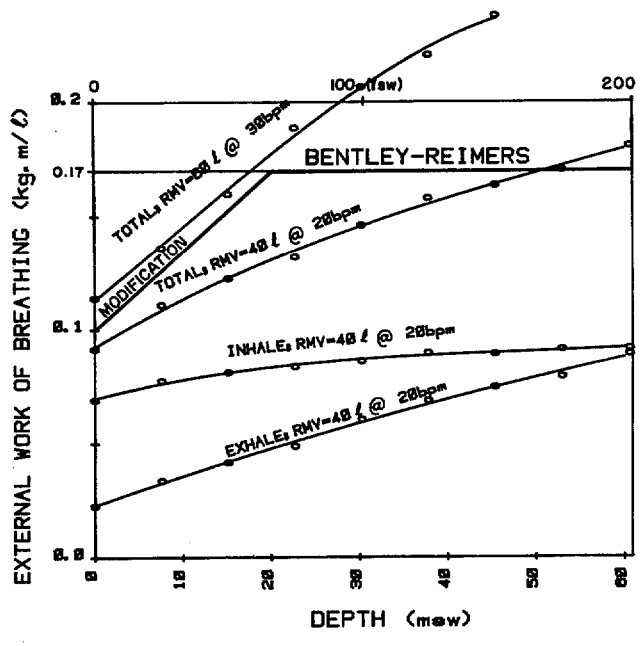

Figure 10. External work of breathing data for a double hose regulator

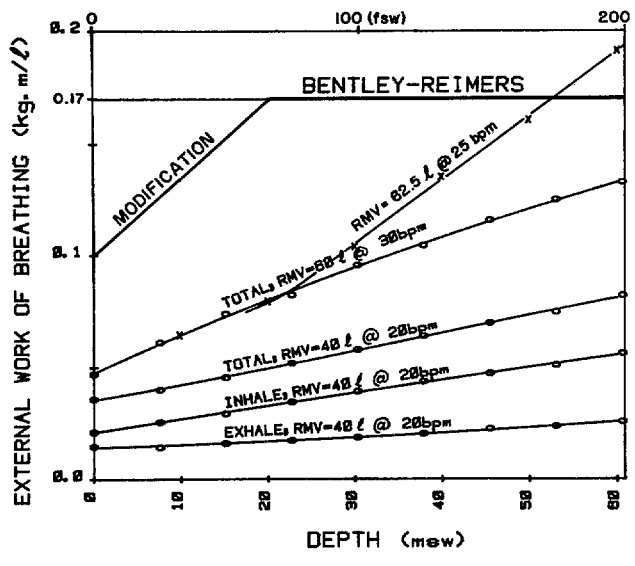

Figure 12. External work of breathing data for a Band Mask

Results of tests conducted with a helmet, capable of operating in the demand mode, are shown in Fig. 13 and Fig. 14. The helmet was supplied with air at 170 psiob, using the same umbilical which was used in the Band Mask tests. The regulator stage at the mouthpiece of the helmet was equipped with a venturi assist. Effects of this feature are readily discernible in the inspiration half of the p-V diagrams shown in Fig. 13. They indicate that at depth, the system provides a positive pressure in the mouthpiece once an initial demand is created and a continuous gas flow condition exists. This effective assistance yields a negative external work of inhalation at depths greater than about 9 msw (30 fsw) and reduces the total external respiratory work below the exhalation external work of breathing (Fig. 14). The positive pressure during the inhalation also reduces the internal work of inhalation. This contribution is not identified in the data presented in Fig. 14. However, its effect would reduce the combined internal and external (total) work of breathing.

None of the tested equipment was subjected to 22.5ℓ RMV, the lowest respiratory demand level recommended by Reimers[4]. However, it is expected that at such a low respiratory demand level, all tested apparatus would readily satisfy the modified Bentley-Reimers standard.

An examination of figures showing the external work of breathing per unit ventilation for the four types of demand-air breathing apparatus tested, shows that the modified Bentley-Reimers criterion is a suitable standard within the range of pressures tested using 40ℓ RMV (20 bmp and 2ℓ V_{TV}). Interestingly, the older technology double hose regulator failed to satisfy the modified Bentley-Reimers criterion at depths greater than 50 msw (164 fsw).

When the greatest recommended demand[4] of 62.5ℓ RMV was used, the Bentley-Reimers criterion was not satisfied at the various depth ranges. The available physiological data does not clearly provide the probabilities for occurrence of such demands at depth. Therefore, further investigation of the statistical aspects of divers' physiological demands and external work of breathing limits at high demand rates should be conducted.

It is proposed that the modified Bentley-Reimers criterion be adopted by researchers in this field as the external work of breathing standard to evaluate demand-air breathing apparatus. Secondly, it is suggested that the conditions and requirements associated with the maximal ventilation of divers are further investigated.

Summary

In conclusion, the following points are submitted:

a. a suitable method of evaluating underwater breathing apparatus is to measure the external work of breathing;

b. an automated method of collecting data on the external work of breathing has been described;

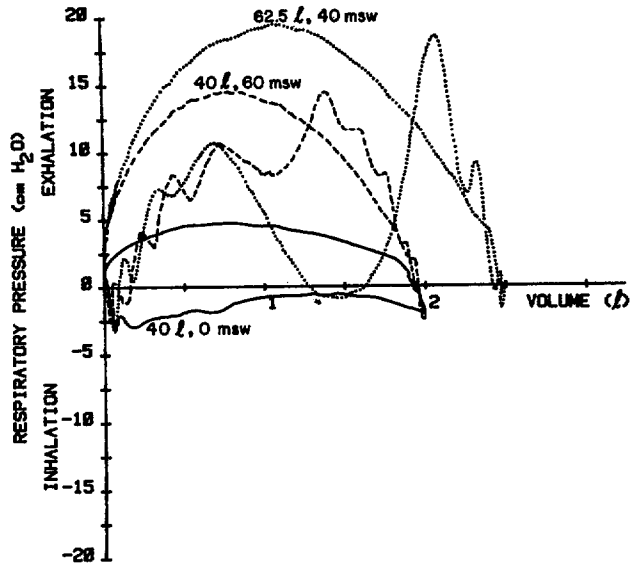

Figure 13. Examples of p-V diagrams obtained with a helmet operating in the air demand mode

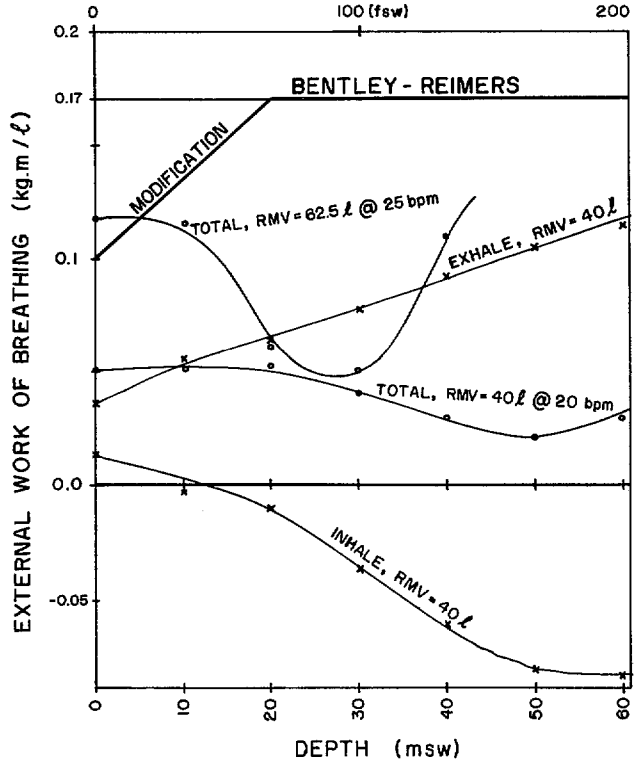

Figure 14. External work of breathing data for a helmet operating in the air demand mode

c. the modified Bentley-Reimers criterion represents a suitable standard to evaluate all types of demand-air breathing apparatus in the 0-60 msw range, using an RMV of 40ℓ; and,

d. the upper limit RMV for demand-air breathing apparatus and its suitability to the modified Bentley-Reimers criterion requires further investigation.

Acknowledgements

Encouragement from LCdr B.A. Ridgewell, experimental contributions of Mr. R.E. Clark, P. Eng. and Mr. R.S. MacLean, and programming efforts of Sgt D.J. Stewart, Mr. P.K. Tam and Miss S.M. Brennan are gratefully acknowledged.

References

1. Silverman, L., et al. Arch Ind. Hyg. and Occ. Med. 3, 461 (1951)

2. Cooper, E.A., J. Appl. Physiol. 15, 1053 (1960)

3. R.A. Bentley, et al., Proceedings, Second Conference on Portable Life Support Systems, held at Ames Research Centre, Moffett Field, California, May 11-13, pp. 295-303, (1971), NASA SP-302

4. Reimers, S.D., Report 19-73, Navy Experimental Diving Unit, U.S. Navy (30 Jan 74)

5. Middleton, J.R., Report No. 9-77, Navy Experimental Diving Unit, U.S. Navy (May 77)

6. U.S. Military Specifications: Regulator, Air, Demand, Diver's; MIL-R-19558 (SHIPS), 14 Aug 56, superceded by MIL-R-19558A (SHIPS), 17 May 60.

7. U.S. Military Specification: Regulator, Air, Demand, Single Hose, Non-Magnetic, Diver's; MIL-R-24169 (SHIPS), 3 Dec 65, superceded by MIL-R-24159A (SHIPS), 22 Mar 67.

8. The Second Undersea Medical Society Workshop, Respiratory Limitations of Underwater Breathing Equipment, held at Harvard School of Public Health, 14-15 Mar 73.

9. Grodski, J.J., The Breathing Simulator System at DCIEM, DCIEM Technical Report, DCIEM, Toronto, Canada, Jul 78.

10. Kao, F.F., An Experimental Study of the Pathways Involved in Exercise Hypernoea Employing Cross Circulation Techniques. The Regulation of Human Respiration, (Eds. Cunningham, D.J.C. and Lloyd, B.B.), Blackwell, Oxford, (1963)

UNDERWATER REPAIR OF NUCLEAR REACTORS

Mr. Leon V. Manry
The Ocean Corporation
7929 Glenmont
Houston, Texas 77036

Dr. John D. Peters
Energy and Resources Department
System Development Corporation
7929 Westpark Drive
McLean, Virginia 22102

Abstract

An innovative approach to maintenance and repair inside reactor vessels without dewatering has been accomplished by the utilization of underwater technicians. The presence of water provides shielding to the workers thereby reducing both the radiation dosage and the dose rate and permits much longer stay time in the repair area. This provides several distinct benefits: (1) the number of people exposed to radiation during a repair operation is reduced by an order of magnitude or more; (2) the overall duration of the repair operation is usually shortened drastically; (3) quality standards are more easy to maintain; and (4) the individual radiation dosage is reduced to unprecedented levels for repair operations. Present experience with underwater technicians indicates clearly that virtually all kinds of jobs can be accomplished under water. This includes determination of the problem, repair, and quality assurance check up which are all done with greater safety because of the shielding effect of the coolant.

Introduction

Repairs on nuclear reactors and their associated equipment customarily have been done either with remotely manipulated tools or by men working in radioactive areas for short periods of time. Both procedures have disadvantages.

Exposure is less when remotely operated tools are used, but the methods are so specialized that existing tools have to be modified, or new ones fabricated each time. While these tools are highly maneuverable, repair work using them tends to be less efficient than when a worker is at the spot where he can use a variety of tools, take measurements, make observations, and take instructions from support personnel.

Traditional practice has been to dewater the reactor vessel when workers have to go inside for the repair operation, or for inspections. A new practice is to use underwater techniques without dewatering the vessel. This provides decisive advantages in safety, time, and cost. Most important is the reduction in radiation exposure because the water attenuates the radiation emanating from the vessel itself.

A man in a dry reactor vessel is exposed to radiation from the full 360 deg. of the vessel wall. A worker under water receives only a small dose of radiation, coming primarily from the wall nearest to him.

The rate of radiation falls off dramatically as the diver backs away from the wall. Measurements taken before the underwater technician enters the vessel can establish how far he must stay away from the working area to receive the minimum practical dose of radiation for a given time period. (See Table 1).

RADIATION PROFILE SURVEY OF REACTOR VESSEL

DEPTH	DISTANCE FROM VESSEL WALL	NORTH SIDE	WEST SIDE	SOUTH SIDE	EAST SIDE
0′	Reactor Flange	200	250	100	60
0′	1′	60	90	30	25
	2′	10	50	10	-
	3′	5	10	10	-
5′	1′	90	150	30	250
	2′	50	40	10	-
	3′	30	20	5	-
10′	1′	100	200	150	400
	2′	50	150	30	-
	3′	30	40	10	-
15′	1′	4500	10000	6000	10000
	2′	2500	8000	2000	-
	3′	1000	2000	500	-
20′	1′	6000	10000	6000	12000
	2′	4000	10000	3000	-
	3′	900	3500	1000	-
Snubber Level	Contact	1500	Northwest 1500	1500	-
	1′	500	-	500	-
	2′	100	-	100	-
	3′	10	-	30	-
25′	1′	900	1000	1000	1000
	2′	200	500	200	-
	3′	100	150	100	-

Survey Instrument:
Rad Gun: underwater probe.

Table 1

Data collected to date show radiation doses received by underwater technicians doing inspection and maintenance inside reactor vessels have been kept one or two orders of magnitude below what individuals would obtain in a dewatered vessel. This is in spite of the fact that underwater technicians spend 10 to 15 times as much time inside the reactor vessel; in fact, the underwater technicians pick up less radiation than surface support workers.

Nuclear Underwater Services

Complete underwater nuclear service can be provided in different ways. One example is the collaboration between The Ocean Corp. of Houston, Texas and System Development Corporation (SDC) with offices in McLean, Virginia. SDC provides the engineering design capability needed to replace inoperative mechanical systems inside reactor vessels. This includes the design and manufacture of tools that can be used efficiently while the diver remains at a safe distance from vessel walls, and the running of engineering analyses on parts that are excessively worn or damaged. Ocean Corporation has extensive experience in nuclear reactor maintenance. Their divers have a total of 3475 minutes at work inside reactor vessels.

The divers used as nuclear underwater technicians are college-trained, have extensive diving experience, understand engineering terminology, and can manipulate engineering measuring devices and equipment. They are especially trained for the work inside reactor vessels.

Nuclear underwater technicians inspect, repair, or replace parts inside the reactor vessels. They are used for reconfiguring spent fuel storage racks, repairing fuel transfer equipment, repairing leaks in fuel storage pool liners, and for almost any conceivable operation that has to be performed in a radioactive environment where water can be used for shielding.

The First Job

Technicians from Ocean Corp. conducted their first dives in a commercial nuclear reactor during the period of December 1973 through March 1974. The major work required was replacement of the shims on six snubbers near the bottom of the nuclear vessel, a region of high radioactivity.

At a preliminary meeting between the prime contractor and the owner, it was agreed that scientifically trained divers, capable of operating with scientists and engineers and understanding precision operations, were desired for this job. The primary coolant inside the vessel was water which contained 1900 ppm of boron with a pH factor of 4.8. This coolant was not expected to present any difficulty, but to avoid any possibility of radioactive contamination or of ingestion of the coolant, the divers were required to have total water-tight integrity. Therefore, the suits and helmets they wore had to be totally dry. To eliminate any possibility of backflow of coolant into the helmet, the helmet exhaust was not allowed to go into the water but was diverted to the surface through a return air hose. This also alleviated any possibility of exhaust bubbles contaminating the air.

This was the crew's first nuclear diving operation, and they received two weeks of training for the job. Three days on location were spent in planning, preparation, and gaining familiarity with the procedures for getting into and out of the vessel. Concurrently, procedures were developed for doing the work. Diving operations began on the fourth day and continued over the next several weeks without incident or difficulty.

A total of 18 diving days were spent on this job and the underwater working time was 55 hours and 4 minutes. Thirty hours and 30 minutes of this diving time was used for the actual removal, replacement, torquing, and quality inspection of the shims. The remaining time was used for subsidiary operations, such as grinding, removal of debris, setting and removing dummy shims, vacuuming, alignment, quality control, and inspection of other parts of the vessel.

It had been estimated that the job (performed in the usual manner) would take three or four months and use as many as 200 to 300 boilermakers. Although any such estimate is open to speculation, there undoubtedly was dramatic saving in time, personnel, and cost by use of underwater technicians.

Health Physics Aspects

A major concern was the radiation dosage to which the diving personnel might be exposed. Health physics personnel supervised all operations, and a number of detectors of different types were used on the divers, both in and out of the water. During the diving operations, the divers received less radiation dosage than the workers on the surface. No diver received a radiation dose even approaching the three-month limit of 2500 millirem set by the contractor. (See Table 2).

These underwater technicians have worked at several nuclear power plants, the latest being the Three Mile Island Plant near Harrisburg, Pennsylvania. Here they entered the reactor vessel to replace a pintal pin pusher tool which was stuck. Attempts at repair using remote tools and other methods had been unsuccessful. The underwater technicians did the job in 2 hours and 54 minutes.

DOSE SUMMARY

Diver's - Ocean Corporation

DIVER	TIME UNDERWATER	DOSE - QTR	ALLOWABLE	REMAINING
1	227 minutes	560	2500	1940
2	263 "	862	"	1638
3	269 "	892	"	1608
4	347 "	784	"	1716
5	50 "	351	"	2149
6	27 "	909	"	1591
7	454 "	681	"	1819
8 *	0 "	97	"	2403
9	169 "	967	"	1533
10	359 "	823	"	1677
11 *	0 "	181	"	2319
12	359 "	909	"	1591
13	275 "	679	"	1821
14	288 "	741	"	1759
15	217 "	1211	"	1289
Total	3304 minutes			

* These two gentlemen spent no time underwater, but were on the surface at all times.

NOTE: All of the divers spent time on the surface in addition to their diving time.

Table 2

The diver who spent the longest time (1 hour and 54 minutes) in the vessel received a total full body count of approximately 75 millirem for that entire period of time. The other diver, who had been down for a period of one hour, took a whole body dose of only 54 millirem. These values are so low it is hard to justify other methods for such repairs. The radiation hazard is almost completely eliminated if tools are devised that permit the diver to maintain a reasonable distance from the vessel wall.

Time is Vital

Experience has shown that when a utility needs divers for emergency repairs or inspection, time is vital. This makes it important that divers are prepared to initiate diving operations as rapidly as safety permits. Divers must be accustomed to working inside the tanks that approximate the configuration, depth, and diameter of a reactor vessel. In addition, diving gear modified for nuclear operations must be kept ready for use.

Underwater operations have proved to be a practical way to reduce radiation hazards for maintenance and repair personnel in nuclear power plants. In addition, repair and inspection times are shorter, which leads to lower costs.

UNDERWATER STUD WELDING

Professor Koichi Masubuchi
Department of Ocean Engineering
Massachusetts Institute of Technology
Cambridge, Massachusetts 02139

Dr. Hironori Ozaki
Kawasaki Heavy Industries Co., Ltd.
Kobe, Japan

Mr. Jun-ichi Chiba
Mitsui Engineering and Shipbuilding Co., Ltd.
Tokyo, Japan

Abstract

Stud welding is a simple process which requires no skill of the operator. Experiments were conducted to determine whether underwater stud welding could be made. Most experiments were made with mild-steel studs 3/4 inch in diameter. Base plates used were mild steel and HY-80 steel, 1/2 and 1 inch (6.4 and 25.4 mm) thick. It was found that stud welding could be made successfully under water. In the mechanical and metallurgical examinations, including tensile tests, bend tests, examinations of macro-structures, and micro-hardness tests, underwater welded specimens exhibited properties comparable to those of welds made in air.

An effort is being made to develop an integrated stud welding unit which can be used for various applications in underwater fabrication and repair.

1. Introduction

During the last several years researchers at the Massachusetts Institute of Technology have conducted an extensive study on underwater welding. The research effort was supported by the National Sea Grant Office of the National Oceanic and Atmospheric Administration, Department of Commerce. The study covered various welding processes including shielded metal arc, gas metal-arc, flux-shielded metal arc as well as stud welding which is discussed in this paper. Several reports, theses, and papers have been published.[1,2]

Stud welding is an arc welding process in which a metal stud (or a similar part) and a work piece are heated and melted by an electric arc drawn between them. Then the two pieces are brought together rapidly under pressure to form a welded joint. Although stud welding is widely used in various construction work in air; there have been no, or a very few if any, published articles reporting the use of underwater stud welding.

During the course of the systematic research on underwater welding M.I.T. researchers noticed that stud welding has a great potential for underwater use. Stud welding is a simple process which requires no skill of the operator. The welding unit can be installed in a water-tight enclosure and the welding gun can be remotely activated to complete welding. An initial work was conducted during the 1974/75 academic year. A U.S. patent on underwater stud welding gun(#3,989,920) was granted in November, 1977.[3]

During the 1976/77 academic year further experiments were conducted on underwater stud welding. Most experiments were made with mild-steel studs 3/4 inch in diameter. Base plates used were mild steel and HY-80 steel, which is a low-alloy, quenched-and-tempered steel with a minimum specified yield strength of 80,000 psi (56 Kg/mm^2). HY-80 steel is widely used for submarine hulls and other structures.

This study was conducted at the Massachusetts Institute of Technology under the direction of Professor K. Masubuchi. Dr. H. Ozaki, who was a research associate at M.I.T., is a research engineer, Welding Research Laboratory, Kobe Works, Kawasaki Heavy Industries Co., Ltd., Kobe, Japan. Mr. J. Chiba, who was a graduate student at M.I.T., is an engineer, Mitsui Engineering and Shipbuilding Co., Ltd., Tokyo, Japan.

2. General Description of Stud Welding

Stud welding is an arc welding, in which the stud serves as the electrode and a "stud welding gun" as the electrode holder. The heat for welding the stud is developed by passage of current through an arc from the stud to the workpiece.

There are two basic types of stud welding; arc stud welding and capacitor discharge stud welding, that differ mainly in the method of power supply. For arc stud welding a d-c power source (a motor generator, a transformer-rectifier, or a storage battery) is used. The power supply for capacitor discharge stud welding is a low-voltage, electrostatic storage system usually charged by a-c current.

Of the fifty or so years that stud welding has been around, only in the last 15 has there been an upsurge in the variety of applications of this welding process. Capacitor discharge stud welding is the fast production process used in thin-gage metal fabrication. It is suitable for welding studs approximately 1/4 to 1/2 inch (6.4 to 12.5 mm) in diameter to a base plate up to approximately 0.4 inch(10 mm) thick. Arc stud welding can be used for broader applications. Some

of the fields that utilize stud welding include appliances, automotive, construction, industrial equipment, and shipbuilding.

3. Welding Experiments

In the study conducted during the 1974/75 academic year, experiments were conducted using a capacity discharge type stud welding equipment available at M.I.T. at that time. Underwater welds were successfully made using small studs 1/8 inch (3.2 mm) diameter. Results were reported in a thesis by Zanca.[4]

During the 1976/77 academic year, attempts were made to weld larger studs up to 3/4 inch(19mm) in diameter. The KSM Fastening Division of Omark Industries was kind enough to loan, at no cost to M.I.T., a complete set of arc stud welding equipment. This paper presents results obtained in experiments using this equipment. Further details are given in a thesis by Chiba.[5]

Figure 1 shows schematically the experimental set-up.

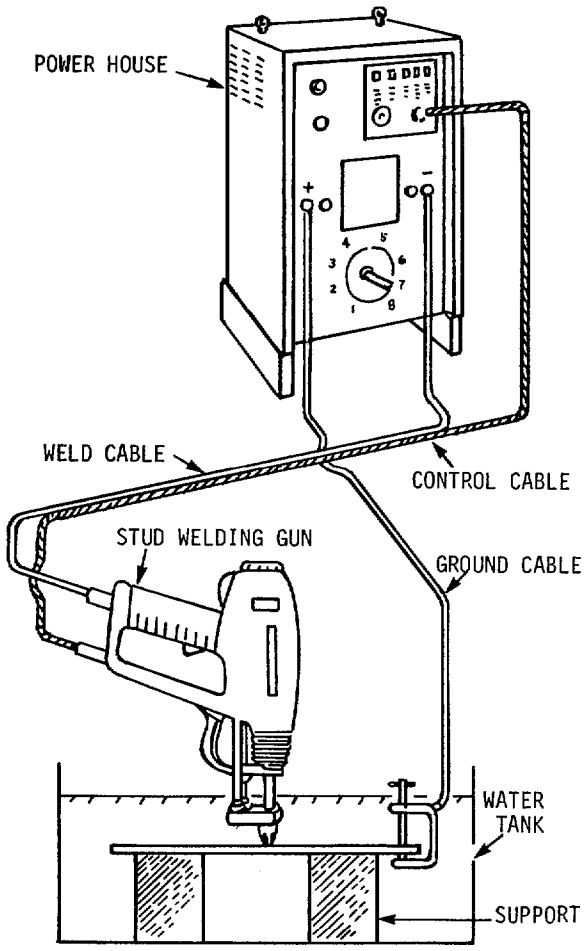

FIGURE 1 ARC STUD WELDING SET-UP

The power house, or stud welding machine, is a transformer-rectifier type welding power supply which can be used for both stud welding and ordinary shielded metal arc using covered electrodes.

An arc stud welding gun designed for air use was used in the experiment. Since the gun was not made water tight, the gun was not immersed in water.*

In conducting a welding experiment under water, the specimen was placed in a tank containing tap water. Limited experiments using actual sea water revealed little difference in weld appearance from that made using tap water.

Mild steel studs were used for both mild-steel and HY-80 steel base plates 1/2 inch and 1 inch (12.5 and 25.4 mm) thick. The stud diameter was 3/4 inch (19 mm), and the weld base diameter was 0.684 inch (17.4 mm). The stud was 2.75 inch (70 mm) long before welding, and 2.5 inch (64 mm) after welded.

Welds were made under three conditions:

1. Air welding with dry surface
2. Air welding with wet surface
3. Underwater welding (1 inch(25.4 mm) deep).

In an initial study, it was found that arc initiation under water was practically impossible. Even in welding on a wet surface it was found to be more difficult to initiate the arc than welding on a dry surface.

An effort was made toward finding ways of initiating a stable arc under water. A stable arc could be effectively initiated when a small amount of steel wool or aluminum foil was placed between the tip of the stud and the workpiece. Steel wool was used throughout the experiment. Studs could be successfully welded in sea water. It was found that successful welds could be made in water 4 inches (100 mm) deep.

The optimum welding time for an air weld and a wet surface weld were experimentally found to be 0.6 to 0.9 second. For underwater welding (1 inch (25.4mm) deep) it was 0.7 to 0.85 second. In both cases, the welding current was set to 1750 amperes, which was recommended by the manufacturer for air welding. When the welding time was too short (0.5 sec.), an extremely "cold" was the result. A welding time of 0.9 second gave an excessively "hot" weld. The welding time had a significant influence on the weld quality. For each welding condition, the welding machine was set to produce optimum results. Test specimens were taken from welds made under optimum conditions.

4. Mechanical and Metallurgical Tests

4.1 Tensile Tests

Tensile specimens were prepared by welding

* Currently an effort is being made to develop a water tight stud welding gun which can be used completely immersed in water.

studs on both sides of the plate. The specimen was set between the threaded chucks of a Baldwin hydraulic testing machine, which provided a slow, steady tensile force to the test specimen. The test on each specimen was run until either stud fractured, giving the ultimate strength of the weld, or the weld fractures, indicating an insufficient fusion in the weld joint.

Table 1 gives the tensile test results of the welded stud specimens. Two specimens were prepared from both air welding and wet-surface welding. Three specimens were prepared for underwater welding (1 inch (25.4 mm) deep). All of these specimens were welded under optimum conditions.

All of the specimens, except #3 (wet-surface weld) fractured at the threaded portion of the studs, giving the ultimate strength of the stud. Specimen #3 fractured in the stud along the heat-affected zone of the weld. The fractured surface revealed insufficient fusion.

TABLE 1 TENSILE TEST RESULTS OF STUD WELDED SPECIMENS

SPECIMEN	CONDITION	MAXIMUM LOAD lbs per stud (metric ton)	TENSILE STRENGTH ksi (kg/mm^2)
1	AIR WELD	2.82×10^4 (12.79)	76.74 (53.97)
2	AIR WELD	2.65×10^4 (12.02)	72.12 (50..72)
3	WET SURFACE WELD	*2.58×10^4 (11.68)	70.08 (49.29)
4	WET SURFACE	2.72×10^4 (12.34)	74.02 (52.07)
5	UNDERWATER 1 in. DEPTH	2.70×10^4 (12.25)	73.48 (51.69)
6	UNDERWATER 1 in. DEPTH	2.70×10^4 (12.25)	73.48 (51.69)
7	UNDERWATER 1 in. DEPTH	2.72×10^4 (12.34)	74.02 (52.07)

* -- HAZ portion of the stud side fractured

From the tensile test results, it was found that underwater stud welding with the quality of an air weld could be achieved by carefully applying a steel wool arc initiator. A 3/4 (19 mm) diameter stud can hold a load of approximately 10 to 12 tons.

4.2 Bend Tests

A simple bend test was devised to provide information about weld quality. A steel pipe four feet long was used for bending studs. Although no bending load was recorded, this simple bend test was adequate in that the soundness of the welded joint could be quickly examined. Studs that fractured in the weld metal or the heat-affected zone were considered unsuitable for usage. This type of test is easily carried out at the job site by an operator, and can be used to test weld studs when any change of welding conditions is made.

Figure 2 shows an example of a specimen subjected to the bend test. The specimen fractured along a thread of the stud. The bend test results showed that welds were sufficiently strong.

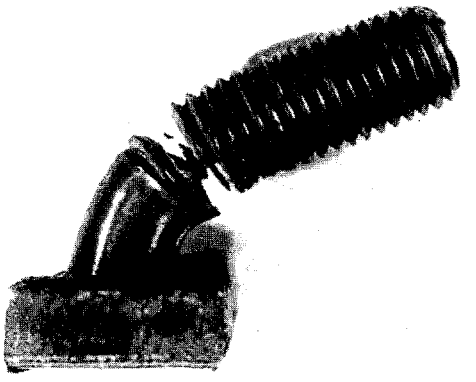

FIGURE 2 APPEARANCE OF BEND TEST RESULT

UNDERWATER 1 in. DEPTH--- MILD STEEL BASE PLATE

4.3. Macroscopic Examinations

Macroscopic examinations were made of sections prepared from some welded samples to study how welds were made. As an example, Figure 3 shows the cross section of an underwater stud weld made on a mild-steel plate. The width of the welded zone was about the same for both underwater and air welds. This was rather surprising, because a smaller weld zone was expected for underwater welds due to the quenching effect.

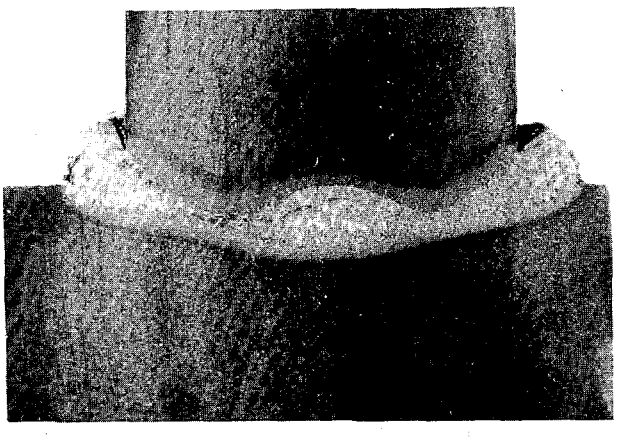

FIGURE 3 CROSS SECTION OF WELDED STUD

UNDERWATER 1 in. DEPTH---MILD STEEL BASE PLATE (X3.7, 1% NITAL ETCH)

Even under careful examinations, no voids, cracks or slag inclusions were found in weld areas of all the specimens examined. Fused metals apparently solidified with no visible defects. We concluded that studs can be successfully welded to both mild-steel and HY-80 steel plates

4.4 Microstructures and Microhardness

Examinations of microstructures were made of some specimens after the macroscopic examinations. Details are described in Chiba's thesis.

Examinations of microstructures were carried out by employing magnifications of x100 to x1000. No cracks were found in the welded specimens made either in air or under water.

The welded specimens were subjected to micro-hardness surveys using a Wilson Tukon Tester. A vertical traverse was made along the center of the weld. A 500 gram load was used to relate the Knoop hardness number (KHN) to the Vickers hardness number. The maximum hardness numbers at the heat-affected zone were as follows:

	Maximum Hardness, Vickers
Mild steel	
Air	325
Underwater	340
HY-80 Steel	
Air	380
Underwater	400

5. Conclusions and Possible Applications

The purpose of this research project was to develop a method of joining a large diameter stud to a metal object under water. Major conclusions drawn in the research are as follows:

(1) The arc stud welding system can be easily used under water provided that a proper arc initiator, such as steel wool or aluminum foil, is used.

(2) No sophisticated system, such as a dry chamber for water evacuation from the welding site or gas shielding equipment, is needed in order to obtain a weld with good quality.

(3) In the mechanical and metallurgical examinations, including tensile tests, bend tests, examinations of macrostructures and microstructures, and micro-hardness tests, underwater welded specimens exhibited properties comparable to those of welds made in air.

(4) An HY-80 steel plate can be successfully stud welded using a mild-steel stud. Neither Neither cracks nor significant porosity, which are responsible for the loss of mechanical properties, were found in the weld area.

On the basis of the results obtained in this research we believe that the arc stud welding can be used successfully for a variety of underwater applications.

For example, it is technically possible to develop an integrated stud welding system which has the following features:

1. Remote control
2. Automatic stud feeding
3. Multiple stud heads
4. Waterproofed

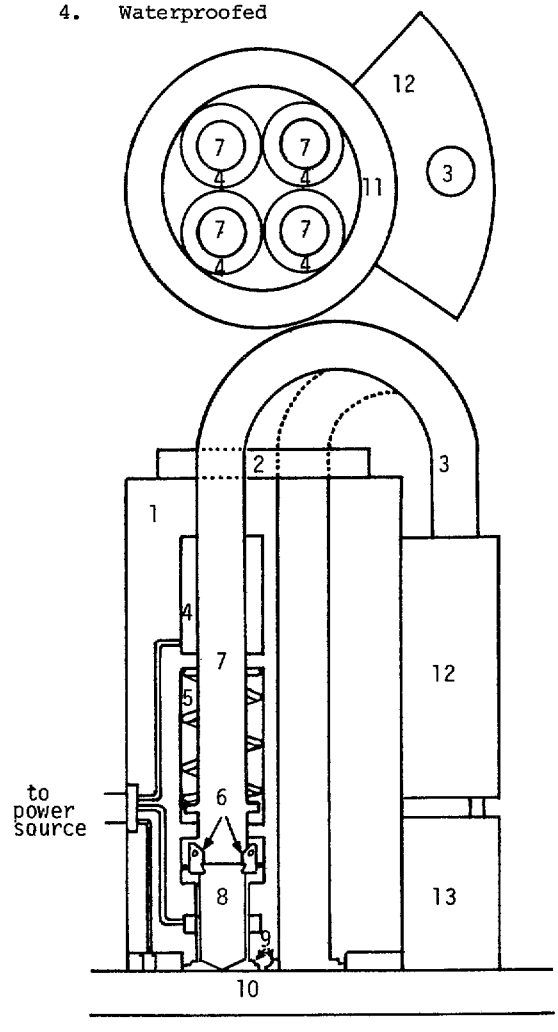

ITEM

1.	Bushing	7.	Spindle
2.	Stud distributor	8.	Stud
3.	Feeding pipe	9.	Ferrule
4.	Solenoid	10.	Workpiece
5.	Spring	11.	Magnet
6.	Hook	12.	Stud feeder
		13.	Water pump

FIGURE 4 INTEGRATED UW STUD WELDING UNIT

Figure 4 shows the comceptual design of an integrated stud welding unit. The unit has four stud heads and can attach four studs to the workpiece in a consecutive order within two seconds. Each stud (3/4 inch (19 mm) diameter mild steel, for example) can hold a load of 8 tons, thus a 32-ton capacity can be achieved with this four-head unit.

In welding operation, stud welding unit can be held in position by electric magnets. The unit is energized by pressing a button either by a diver on site or by remote control switches. New studs can be fed automatically through a stud feeder after each welding is completed. A water pump may be used to create a dry welding environment in the arc zone to ensure weld quality in some critical operations.

One example of many expected applications of such a development is to lift a sunken ship in ocean salvage operations. Figure 5 shows a schematic presentation of such operations. The welding unit can even be operated by a special rescue submersible.

It is hoped that such an integrated system can be developed in the near future

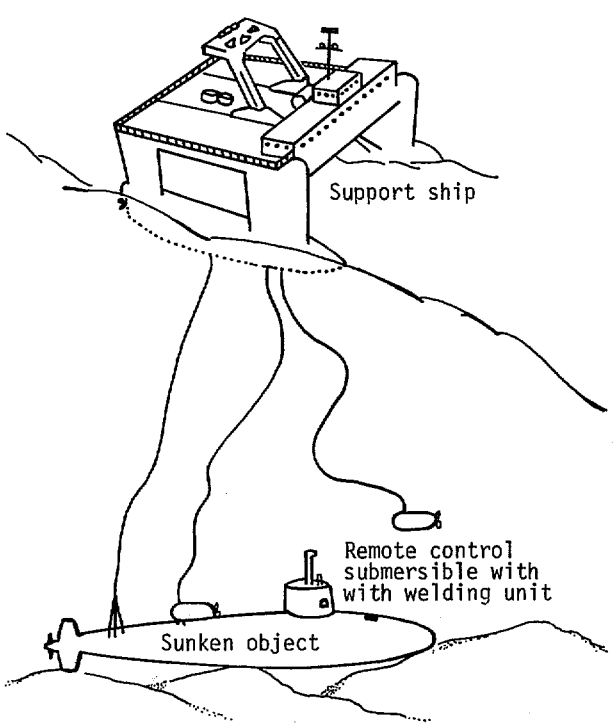

FIGURE 5 APPLICATION OF INTEGRATED WELDING SYSTEM FOR OCEAN SALVAGE OPERATION

References

1. Brown, A. J., Brown, R. T., Tsai, C. L., and Masubuchi, K., Report on "Fundamental Research on Underwater Welding", Report No. MITSG 74-29, M.I.T. Sea Grant Program, September, 1974.

2. Tsai, C. L., Ozaki, H., Moore, A. P., Zanka, L. M., Prasad, S., and Masubuchi, K., "Development of New Improved Techniques for Underwater Welding", Report No. MITSG 77-9, M.I.T. Sea Grant Program, April 1977.

3. Masubuchi, K., and Kutsuna, M., "Underwater Welding Gun", U.S. Patent No. 3,989,920, November 2, 1976.

4. Zanca, L. M., "Underwater Stud Welding", M.S. Thesis, M.I.T., September, 1975.

5. Chiba, J., "Fundamental Study of Underwater Arc Stud Welding", M.S. Thesis, M.I.T., May, 1977.

DEVELOPMENT OF A DESIGN BASELINE FOR REMOTELY CONTROLLED UNDERWATER WORK SYSTEMS

Robert L. Wernli

NAVAL OCEAN SYSTEMS CENTER
San Diego, California 92152

Abstract

The Work Systems Package (WSP), following two years of at-sea testing and evaluation, has completed an extensive laboratory time-motion analysis. This analysis, designed to simulate remote operation, provided a controlled evaluation of the system.

Instrumentation was installed to provide time-motion and power consumption data on system components. The work tasks were divided into numerous subtasks and behavior motions which would be representative of the WSP's diverse capabilities. A computer analysis was performed on the data to provide a quantitative description of the WSP, its capabilities and the parameters effecting them. Thus, the effect of system modifications on mission time and power requirements can be easily simulated to assist the designer in system optimization.

The operational evaluation of the WSP has, for the first time, provided a quantitative data base on which to base future underwater work system designs.

1. Background

The Work Systems Package (WSP), under the direction of the Naval Sea Systems Command, was designed, fabricated and is undergoing operational testing at the Naval Ocean Systems Center (NOSC) in San Diego. As part of the Deep Ocean Technology (DOT) project, the WSP program was initiated in February of fiscal year 1972, by NOSC working in conjunction with Battelle Institute, Civil Engineering Laboratory and the David Taylor Naval Ship Research and Development Center/Annapolis. The Work Systems Package (WSP) is designed to provide a versatile work capability when mounted as a unit on the Navy's Cable Controlled Underwater Recovery Vehicle (CURV III) or the Remote Unmanned Work System (RUWS) unmanned cable controlled submersible vehicles, and the ALVIN, SEACLIFF, and TURTLE manned vehicles. In addition, it can be positioned and controlled by divers or operated independently from a surface support ship for operations at shallow depths without the need for a submersible.

The system was designed to accomplish a complete work task on the ocean floor without the necessity of resurfacing for tool interchange. Potential tasks include salvage, recovery, installation and repair operations. Basic components of the work package (Fig. 1) include two simple outer manipulator arms without elbow functions that act as "grabbers" or restraining/holding arms to steady the vehicle or hold small work pieces.

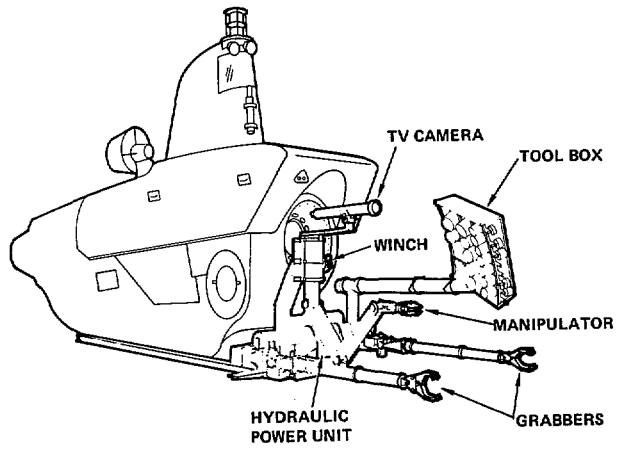

Figure 1. WSP as it would appear mounted to the manned submersible ALVIN.

A centrally located seven-function manipulator arm can select, interchange and operate a variety of hydraulically-powered, explosively-actuated or electrically-actuated tools. Included in the tool storage box are tools to perform cable cutting, synthetic line cutting, nut torquing, jacking, prying, wire brushing, sawing, grinding, drilling, tapping, chipping and stud driving. An electrically-driven hydraulic pump unit supplies the power to most tools. Electric power is supplied to the system from a self-contained battery package. Control of all operations and functions is provided through a multi-plexed telemetry circuit from the vehicle. Pressure tolerant electronic and hydraulic components operate at full ambient pressure in oil filled, pressure compensated enclosures.

Upon completion of assembly, checkout and preliminary tests, the WSP was mated to the CURV III for its first major in-water test. The WSP underwent

U.S. Government work not protected by U.S. copyright.

six weeks of operational testing at the Navy's San Clemente Island test facility in fiscal year 1976. Such tests as underwater docking with a submerged test fixture, tool exchanges and operation, object identification and recovery, and a simulated flight recorder recovery were successfully completed.

The superior operability of the system, the short-time (2 to 2-1/2 minutes) required for remote tool exchanges underwater and the successful performance of a complicated recovery sequence requiring exchange and operation of nine different tools and bits in 2-1/2 hours, achieved, and in many cases, surpassed original design goals.

Following the successes at San Clemente Island, the WSP was flown to NOSC's Hawaii Laboratory for interface and testing with the Remote Unmanned Work System (RUWS). The WSP and RUWS were mated and operated in the RUWS test pool in preparation for support of the Large Object Salvage System (LOSS) operational demonstration at the Naval Coastal Systems Laboratory (NCSL) during the fiscal years 1976 and 1977. The WSP/RUWS was flown to Panama City, Florida, where it successfully completed support of the LOSS operations. The systems easily performed such tasks as midwater docking, cable cutting, stud driving, messenger line attachment, and air hose attachment using quick-disconnects.

The WSP was then returned to San Diego where it was prepared for an extensive laboratory evaluation of the operating characteristics of the system. This laboratory evaluation is the subject of this report.

2. Test Description

Test Setup

The WSP was set up in the laboratory at NOSC, San Diego. A frontal work plane test fixture, the primary work area for which the WSP was designed, was set up exactly as the test fixture used during the San Clemente Island tests with CURV III (reference (1)). This would allow comparison of lab tests results to those acquired at sea.

To simulate at-sea conditions, the operator was isolated from viewing the work area directly. Viewing was provided by the two low-light level TV cameras and the two monitors located on the WSP control console. The two cameras, one located approximately in the center of the system and the other on the upper right side above the manipulator, provided the dual perspective necessary for the performance of tool exchanges and work operations. Both cameras could be remotely moved in pan and tilt from the control console by means of position control joysticks.

The manipulator is a seven degrees-of-freedom, rate-controlled, hydraulic manipulator, which is controlled through the activation of discrete action joystick (toggle) switches. Through utilization of a special chain drive within the manipulator, the plane of the wrist joint remains constant in reference to the horizontal, irrespective of the operation of either the shoulder pivot or elbow joints. Simultaneous activation of both joints results in a linear motion of the wrist pivot axis along a line passing through the intersection of the shoulder rotate and pivot axes. The combination of the chain drive and linear extend features provides a linear feed capability for the operation and interchange of tools and bits.

Each tool of the WSP is stored in its assigned location in an extendable tool box. Stiff nylon brushes provide the restraint required for retention and the compliance necessary for tool exchanges. Hose reels are eliminated from the system by running hydraulic lines down the manipulator, through a hydraulic slip ring in the hand to two quick-disconnect fittings designed to mate underwater with each tool. Mechanical guides along both the tools and the manipulator hand ensure proper alignment, while interlocking notches on the tool secure it in the hand when gripped. Through the linear extend feature of the manipulator, tools can be gripped easily and extracted from the tool box for work operations.

Tools which require bits, such as drills, taps, sockets and saw blades, are equipped with a special quick-disconnect chuck assembly. Bits are obtained by deflecting this chuck against the bit holder on the tool box, moving the tool forward until the bit is fully inserted, and pulling the bit laterally out of its clip. This last action releases pressure on the tool chuck, thus locking the bit in the tool. Bits are replaced by following the reverse procedure. Figure 2 illustrates an acquired saw bit just after it has been pulled laterally out of its clip.

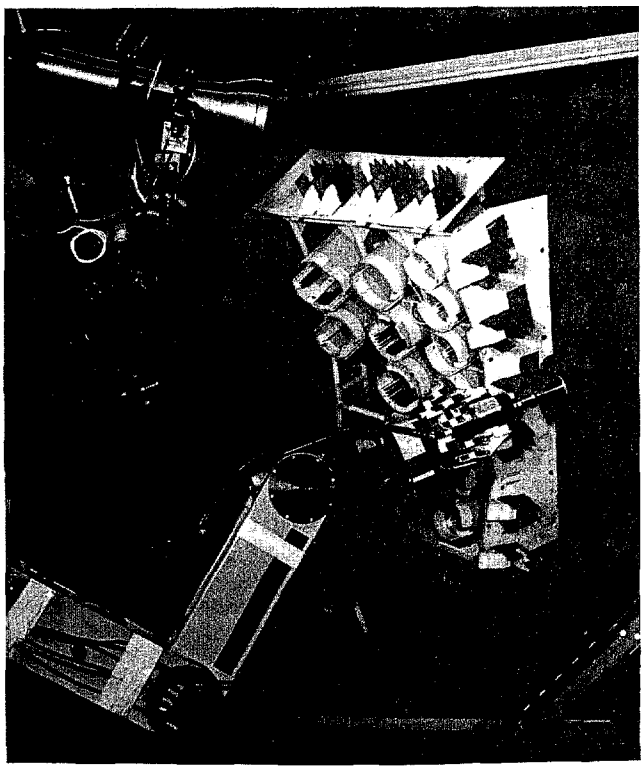

Figure 2. WSP manipulator extracting cutoff wheel from the tool box. Two TV cameras and winch are visible in the upper left of the photo.

The primary analysis of the tests was directed towards a description of the manipulator, tools, control functions and their interactions.

Task Requirements

The objective of the laboratory testing was to obtain sufficient data to permit accurate prediction of work completion time and power consumption for typical WSP salvage missions. Through applications of this data base, subsystems which would receive the greatest benefit through a design modification would be identified and more advanced work systems could be reliably designed.

To achieve this goal, the tasks performed in the laboratory had to be representative of those performed at sea during the San Clemente Island and LOSS operations. This would allow verification of the laboratory data in salvage mission projections. The tasks would also be representative of those performed at Electric Boat (References 2, 3 and 4) which would be used in future time-motion analysis.

The resultant Laboratory Test Plan consisted of 14 tasks that collectively utilized a representative sample of all tool types and their various precision requirements.

The 14 tasks selected for evaluation in the laboratory included the following:

1.	Sample retrieval	8.	Brushing
2.	Acquire tool	9.	Hooking
3.	Replace tool	10.	Valve turning
4.	Acquire bit	11.	Unbolting
5.	Replace bit	12.	Sawing
6.	Cut rope sample	13.	Drilling
7.	Cut cable sample	14.	Tapping

Data Requirements

To provide accurate projections of salvage missions, the data taken must be subdivided into subtasks small enough to be representative of all system operations. Therefore, each of the 14 tasks was subdivided into four subtasks, or Behavior Elements, which consisted of various combinations of the basic actions (travel, tool use and alignment) required to perform the task. All work and tool capabilities required on realistic WSP salvage missions can be represented by sequentially performing a series of these tasks and subtasks. Each of the categories of travel, alignment and tool use were subdivided by the requirement for force control, high or low precision and specific tool function.

In addition, data were taken on the amount of time the manipulator operated or was idle and the amount of time the TV pan and tilts were utilized. This would provide a more accurate time motion analysis of the operator's workload.

Data were taken also on the power consumption of the system during the performance of each of the subtasks. This was of primary importance since the WSP is designed for installation on battery operated manned boats with limited dive times. When the 30 VDC and 60 VDC power consumption of the WSP is known, it is possible to determine the impact on these vehicles and the dive time or number of dives required to perform a given salvage mission.

Test Subjects

The subject pool consisted of four operators one with 100 hours experience in operating the WSP during previous testing and major WSP sea trials, and the others with only limited experience (less than 10 hours each) in operating either laboratory or operational manipulator systems. Data obtained from the experienced subject were utilized to validate the laboratory test data as a representative performance of the WSP in underwater conditions. Data collected on the four operators were evaluated and their performance with the WSP was averaged to provide realistic estimates of time and power parameters. The operators performed each of the 14 tasks repeatedly for 10 trials to ensure the existence of an adequate data base free of significant learning effects. Data representative of learning were eliminated from the final data pool to represent performance by experienced operators as nearly as possible.

3. Test Results

Operator Workload Allocation

The first task of the data analysis was to identify and eliminate learning effects from the data base. During projection of slavage scenarios, elimination of the learning effects will provide more reliable results.

Figure 3 shows the learning curves resulting through 10 trials of tool acquisition. It can be seen that the naive subjects approached the proficiency of the experienced operator during the testing period. Since these data points were taken throughout the entire test period (as opposed to sequential operation of primary tasks), the effect of total system learning can be indicated.

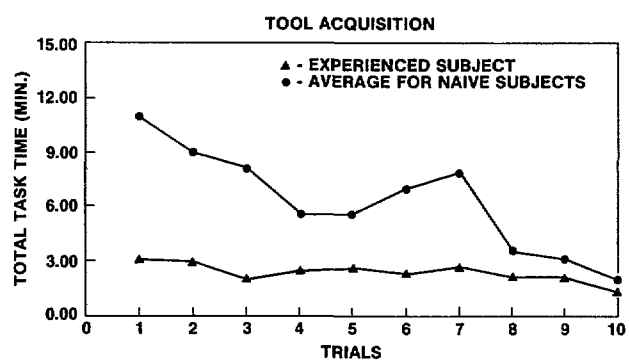

Figure 3. Subject learning curves for tool acquisition.

Since erratic behavior is expected when learning is occurring, a good measure of learning is the variability of variance associated with each task

mean. If no learning occurs, the operator's performance would be relatively stable. Figure 4 is a comparison of the total variance occurring in trials four through 10 with the overall variance occurring in trials one through 10. A 40 percent reduction in variance is found for all subjects and all tasks for trials four through 10, thus substantiating the assumption that task learning occurs in trials one through three. The analysis, therefore, was focused on mean task time for trials four through 10.

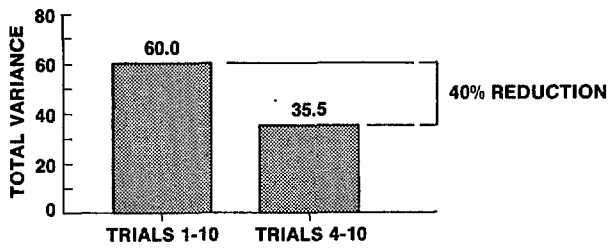

Figure 4. Comparison of total variance for all tasks - all subjects.

The resultant task performance times averaged across subjects appear in Table 1.

	TOTAL TIME (MIN.)	STD. DEVIATION (MIN.)	VEHICLE* 30 VDC POWER WATT-HR	VEHICLE** 60 VDC POWER WATT-HR
1. SAMPLE RETRIEVAL	1.58	.27	5.5	84
2. ACQUIRE TOOL	4.32	2.95	13.4	191
3. REPLACE TOOL	2.74	1.83	8.3	112
4. ACQUIRE BIT	2.58	1.43	12.1	117
5. REPLACE BIT	2.93	1.90	9.0	127
6. CUT ROPE	2.02	.30	6.6	125
7. CUT CABLE	1.30	.42	4.3	66
8. BRUSH	2.39	.59	8.2	155
9. WINCH HOOK	5.45	2.17	17.2	239
10. VALVE OPEN	1.03	.26	3.3	51
11. UNBOLT	1.66	.89	5.4	79
12. SAW ALUMINUM	7.61	3.12	26.0	542
13. DRILL HOLE	2.25	.63	7.6	118
14. TAP HOLE	2.50	1.15	8.2	119

* ASSUMES THE UTILIZATION OF ONLY ONE TV MONITOR

** ASSUMES THE UTILIZATION OF 750 WATTS FOR UNDERWATER LIGHTING: ONE 250 WATT LIGHT ON THE TV BRACKET AND ONE 500 WATT SIDE LIGHT

Table 1. Summary of WSP laboratory results for total task time and power consumption.

Table 2 gives a breakdown of the operator's time based on the data taken. Two of the most striking results indicated by Table 2 show the amount of time the operator spends contemplating the situation or problem and the amount of time spent operating the TV pan and tilts. Efforts to reduce these times would have considerable impact, possibly without complicated or expensive system modifications. In comparison, the first area usually addressed for modifications is the manipulator, which could result in a more expensive, complicated, less reliable system, although it may do the job faster and more accurately. But, according to the data, this decrease in time will apply primarily to manipulator operation, 33 percent of the time spent and not necessarily across the time of the entire mission by that same amount. Since several areas are interrelated, adjustments to the data, based upon subtask modifications, will allow a more accurate evaluation of potential system modifications and concentration on areas where maximum benefit will be realized.

OPERATION WITHOUT TOOLS (%)	OPERATOR DECISION	MANIPULATOR OPERATION	CAMERA PAN AND TILT OPERATION	TOOL OPERATION	LIGHT OPERATION (1)
AVERAGE OPERATION TIME	50	33	17		100
LOW SPEED PUMP IDLE TIME (2)	50				
LOW SPEED PUMP DUTY TIME (3)		33	17		
TOTAL POWER CONSUMPTION	32	27	14		27

OPERATION WITH TOOLS (%)					
AVERAGE OPERATION TIME	37	30	11	22	100
LOW SPEED PUMP IDLE TIME	37			(22)*	
LOW SPEED PUMP DUTY TIME		30	11		
HIGH SPEED PUMP DUTY TIME (4)				22	
TOTAL POWER CONSUMPTION	17	18	6	(10) 26	23

(1) LIGHTING = 0.75 KW
(2) LOW SPEED PUMP IDLE = 1.55 KW
(3) LOW SPEED PUMP DUTY = 2.00 KW
(4) HIGH SPEED PUMP DUTY = 3.97 KW (ON-OFF ONLY)

*IT IS ASSUMED THE MANIPULATOR IS NOT BEING MOVED DURING TOOL ACTIVATION.

Table 2. Operational time distribution (percent).

Power Allocation

The power analysis on the system was broken into two sections. The first was the 30 VDC power required by the Command/Control electronics; the second was the 60 VDC power required by the lights and hydraulics. The WSP runs on 60 VDC batteries, either its own or those of a manned submersible. Therefore, the impact of the task or mission to be performed on the battery supply of the vehicle is important. Also, in the case of a manned boat, the 30 VDC power is provided by the life support system power of the vehicle. Therefore, adequate data in this area are also required. Table 1 provides the power data required for the performance of any of

the tasks. The power data have been derived to represent operation on a manned vehicle with one TV camera and a lighting load of 750 watts.

Table 2 shows the allocation of this power to the system. It was found that the overall power consumption was directly proportional to the task times and that the manipulator and tool operation used 75 percent of the power, while the lighting accounted for 25 percent of the power consumption. By utilizing the data of Table 2, areas of high power consumption can be identified and reduced. For example, the time spent by the hydraulic system idling accounts for 32 percent of the power consumption. The power loss in this area could be reduced by increasing the efficiency of the hydraulic system during idle or by reducing the operator decision time.

Data Validation

Utilization of the laboratory data to predict salvage scenarios for WSP in an ocean environment requires that proof be developed to show that the laboratory and at-sea performances are equivalent. Development of such proof is possible via comparison of the data base collected in the laboratory and the data collected during the San Clemente Island and LOSS support operations and sea trials. Since the experienced subject is common to all the test series, direct comparison of his data provides the required validation.

Comparison of the data bases may occur at two levels: (1) comparison of the performance of specific tasks and (2) comparison of the completion times for entire salvage scenarios.

Two specific tasks were replicated in the laboratory and the at-sea data bases. These are tool acquisition and tool replacement. Data indicate the average performance times and standard deviations recorded are statistically identical at a 99 percent level.

The completion of three major salvage scenarios during WSP sea trials allows comparison of the predicted completion time with that actually recorded at sea. Two scenarios were completed during the San Clemente Island sea trials: salvage of a simulated flight recorder (Figure 5) and recovery of a test box. One scenario was completed during the LOSS support operations: connection of an air hose and messenger line. Completion time for these three scenarios was predicted by sequentially adding appropriate task and subtask data recorded in the laboratory.

The data indicate that the actual scenario times are accurate to within the standard deviation calculated.

Therefore, the laboratory task and subtask data effectively represent the general performance capabilities of the WSP system at sea. Further, the prediction of large salvage scenarios (in excess of 30 minutes) with laboratory data provides an accurate prediction of work completion times for actual undersea missions.

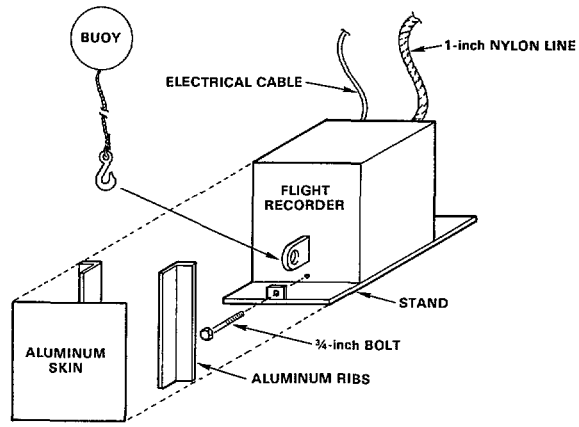

SEQUENCE OF OPERATION

1. EXTRACT THE DRILL MOTOR AND A 1-INCH DRILL BIT
2. DRILL ACCESS HOLES IN THE ALUMINUM COVER TO ALLOW SPREADER INSERTION
3. EXTRACT THE SPREADER, INSERT INTO THE ALUMINUM SKIN AND OPEN THE SKIN TO ALLOW INSERTION OF THE JACK
4. REPOSITION THE VEHICLE TO ALLOW USE OF THE JACK
5. EXTRACT THE JACK, INSERT, AND SPREAD APART THE ALUMINUM RIBS ALLOWING REMOVAL OF THE "FLIGHT RECORDER"
6. EXTRACT THE IMPACT WRENCH AND SOCKET AND REMOVE THE ¾-INCH BOLT FROM THE "FLIGHT RECORDER"
7. ATTACH A BUOY-LINE TO THE "FLIGHT RECORDER" AND REMOVE IT FROM THE TEST FIXTURE USING THE MANIPULATOR
8. EXTRACT THE CABLE-CUTTER AND CUT THE ELECTRICAL CABLE ATTACHED TO THE "FLIGHT RECORDER"
9. EXTRACT THE SYNTHETIC LINE-CUTTER AND CUT THE 1-INCH NYLON LINE ATTACHED TO THE "FLIGHT RECORDER" RELEASING IT TO FLOAT TO THE SURFACE

Figure 5. Simulated "flight recorder" recovery scenario.

Predicted Salvage Missions

With the validation of the data base, it can now be used to predict salvage mission time and power requirements. With this in mind, ten different work scenarios were evaluated to demonstrate the WSP's salvage capability. A list of the scenarios and their respective time and power requirements are shown in Table 3.

SCENARIO DESCRIPTION	TOTAL WORK TIME (min)	STANDARD DEVIATION (min)	30 VDC VEHICLE POWER (KwHr/Watt-Hr)	60 VDC VEHICLE POWER (KwHr/Watt-Hr)
1. CUT OPENING, THIN METAL	216	17	0.70	12.3
2. CUT OPENING, THICK METAL	265	17	0.89	16.3
3. REMOVE ELECTRONICS	110	11	0.35	5.3
4. PADEYE DRILL/TAP FASTENERS	29	6	0.09	1.2
5. PADEYE CONVENTIONAL FASTENERS	122	12	0.40	5.6
6. RIG CABLES	65	6	0.21	3.2
7. OPERATE SEA VALVES	46	5	0.14	2.0
8. LOSS SUPPORT OPERATIONS	10	3	0.03	0.4
9. SCI FLIGHT RECORDER	79	10	0.25	3.6
10. SCI TEST BOX RECOVERY	38	7	0.12	1.7

Table 3. Estimated work time and power consumption for ten salvage scenarios.

A detailed description of the tasks and their analysis can be found in Reference 5. For simplicity, only one task is shown here. That task, the "simulated flight recorder recovery," which was performed at SCI, is shown in Figure 5. Performance time predicted for this scenario was 89 minutes (maximum) compared to 91 minutes recorded at-sea, which substantiates this technique.

System Modification Studies

Controller Evaluations

One of the applications of the WSP data base is the capability to evaluate modifications to critical subsystems. One such area is the manipulator controller.

Control options include pushbutton fixed rate (WSP current design), pushbutton variable rate, joystick fixed and variable rate, discrete position control, and harness (master-slave) position control. Experimental data collected at Electric Boat Division, (References 2, 3 and 4) were used in the projections.

The pushbutton fixed rate controller is taken as the baseline data since its operation was similar to the controller used on the WSP. The resultant increase or decrease in subtask completion time for other control options is indicated relative to the baseline data. Adjustments to the baseline for the ten salvage scenarios is presented in Table 4. Projection of the effectiveness of each of the control options listed in Table 4 is made by adjusting the subtasks of individual tasks by the Electric Boat Data.

	PRESENT WSP BASELINE	PUSH VARIABLE RATE	JOYSTICK FIXED RATE	JOYSTICK VARIABLE RATE	DISCRETE POSITION CONTROL	HARNESS POSITION CONTROL
1. CUT OPENING, THIN METAL	1	.93	1.34	1.18	1.53	.93
2. CUT OPENING, THICK METAL	1	.94	1.48	1.28	2.43	.99
3. REMOVE ELECTRONICS	1	1	1.29	1.13	1.88	.77
4. PADEYE DRILL/TAP FASTENERS	1	.97	1.24	1.07	1.69	.66
5. PADEYE CONVENTIONAL FASTENERS	1	.96	1.27	1.11	1.72	.70
6. RIG CABLES	1	.91	1.08	.97	1.37	.55
7. OPERATE SEA VALVES	1	1.02	1.26	1.11	1.98	.74
8. LOSS SUPPORT OPERATIONS	1	.90	1.10	1.00	1.40	.50
9. SCI FLIGHT RECORDER	1	.94	1.16	1.04	1.56	.61
10. SCI TEST BOX RECOVERY	1	.92	1.15	1.03	1.53	.58
	1.0	.95	1.24	1.09	1.71	.70

Table 4. Normalized scenario completion times utilizing various control types.

Depending on the type of work to be performed, the benefit of the different controllers can be easily seen. Results indicate a potential savings of 30 percent of salvage time through the use of the harness position controller. The savings in power may not be quite as high since, although the time required to complete the task is less, the power consumed per unit time will be higher. One must also consider the working environment of the operator when considering control devices. It is not an easy task to use a position controller when viewing through a manned vehicle viewport as opposed to a more spacious control room topside in a tethered vehicle configuration. The designer is now given an indication of the proper design path in achieving an efficient work system. This path could be easily verified through hands-on testing of the most probable modification candidate without the need of testing all of the other options.

Automatic Manipulator Control

The use of minicomputer programmed control of manipulators and robots in industry has increased rapidly. Such automation has increased accuracy and decreased work time in the performance of repetitive tasks. Therefore, it becomes a viable area for application to the WSP. In an effort to determine its benefit, a series of tests was performed using a microprocessor controller for the WSP manipulator. The controller was programmed to go through a series of tool and bit exchanges which it accomplished with excellent time reductions and near perfect alignment and target location. The time reductions, Table 5, are shown as compared to both experienced and inexperienced operators. Preliminary adjustments to the data base were performed using only the experienced operator times of Table 5 and resulted in an 18 percent time reduction. It can be concluded that the data acquired with the programmer tests will yield even more dramatic results.

TASK	OPERATORS INEXP.	OPERATORS EXP.	PRO-GRAMMER	REDUCTION INEXP.	REDUCTION EXP.
ACQUIRE TOOL	5.18	2.12	0.90	82%	57%
REPLACE TOOL	3.24	1.42	1.31	59%	8%
ACQUIRE BIT	3.02	1.23	1.00	33%	17%
REPLACE BIT	3.56	1.30	0.74	79%	43%

Table 5. Comparison of WSP task times (minutes) under direct operator control and computer control.

Automatic Camera Control

With the inclusion of position feedback sensors on the manipulator, the possibility of automatic camera positioning exists. Microprocessor control could be easily applied to have the pans and tilts move the cameras so that they will follow the manipulator hand exactly. This would enable the operator to concentrate on the task and not have to stop work operations to move or adjust the cameras.

Calculating the reduction in salvage scenario completion times is straightforward. If it is assumed that all present camera control times will

be eliminated by automatic positioning, completion times may be calculated by subtracting the predicted camera operation time from the predicted scenario completion time.

The resultant data indicate that an average 8 percent reduction is achieved across all the salvage scenarios.

4. Conclusions

It has been shown that the data base which has been generated for the WSP will be a valuable tool to those individuals working on advancing the state-of-the-art in undersea work systems. The system designer now has an indication of the areas where he should concentrate and the potential benefits achievable. The laboratory tests performed with the WSP have also yielded a great deal of practical data on performing remote work in the areas of viewing, sensors, tool and control requirements and much more. For a more detailed discussion of the actual work tasks and recommendations, the reader is referred to the laboratory test report, Reference 5. The testing also has shown areas where more research is required to answer the question of how man is to work remotely in the sea. Hopefully, these and other studies will continue the quest for that answer.

References

1. Wernli, R. W., WSP/CURV III Operational Testing at San Clemente Island - 1975 Work Systems Package (WSP) Program, Naval Undersea Center, NUC TN 1699, July 1976.

2. Pesch, A. J., G. R. Simoneau and R. G. Hill, Final Report: Operator Performance in Undersea Manipulator Systems, Electric Boat Division, General Dynamics, Groton, Connecticut, 1972.

3. Pesch, A. J., R. G. Hill and W. F. Klepser, Capabilities of Operators as Divers Versus Submersible Manipulator Controllers in Undersea Tasks, Electric Boat Division, General Dynamics, Groton, Connecticut, June 1970.

4. Pesch, A. J., W. F. Klepser, R. G. Hill and G. R. Simoneau, Operator Performance with Alternate Forms of Unilateral Position Control for Undersea Manipulators, Electric Boat Division, General Dynamics, Groton, Connecticut, September 1972.

5. Bertsche, W. R., K. P. Logan, A. J. Pesch, R. L. Wernli (Principal Investigator), Evaluation of the Design and Undersea Work Capability of the Work Systems Package, Final Report, Naval Ocean Systems Center, NOSC TR 214, 1 April 1978.

COASTAL DEMOGRAPHIC CHANGES IN THE UNITED STATES, 1950-1974

Niels West

Department of Geography and Marine Affairs
University of Rhode Island
Kingston, RI 02881

Abstract

The present paper compares the demographic developments which have characterized the coastal zone in conterminous United States. The population changes in the coastal counties are analyzed for the two census periods 1950-1960 and 1960-1970, and population estimates made in 1974. The coastal counties are grouped into three classes: coastal urban, non coastal urban, which are part of coastal SMSAs and coastal rural. Three objectives are sought. The first describes the demographic changes which have taken place nationally during the past 24 years. The second objective analyzes the demographic differences in the three types of settlements discussed above. The final objective compares regional, urban/exurban differences in the demography within the coastal zone. The findings of these are discussed in light of the urban/suburban migration and competing uses for the nation's shoreline.

1. Introduction

Considering the recent legislative emphasis on economic, environmental, and social problems occurring in the coastal zone, it is surprising that the vast majority of papers concerning this region have dealt with either the physical impacts of proposed coastal modifications or the legal and institutional interpretations of the C.Z.M.A. of 1972.

This paper is descriptive in the sense that it traces the demographic changes which have taken place in the coastal zone during the past quarter century. The coastal zone, as defined here, consists of 286 counties which border on the coast, estuaries, or tidewaters of conterminous United States. Thus, neither Alaska nor Hawaii have been included in this analysis. Nor have the 85 counties surrounding the Great Lakes been included.

The 286 counties have been divided into three groups. The first group consists of 116 counties located on the shore, and is part of Standard Metropolitan Statistical Areas (SMSA). The second group consists of 37 counties, which are part of coastal SMSAs but do not actually border on the shoreline. The third group consists of 133 counties which are both coastal and rural (i.e., not located within coastal SMSAs). This approach differs from that used by Spangler[1], who looked at coastal demographic changes but based his analysis on U.S. Coast Guard regions.

Two objectives are sought in this paper. The first seeks to describe the demographic changes between urban and rural counties from a functional approach. The rationale for this line of inquiry parallels recent research in the suburbanization process, which attempts to account for the increases that suburban counties have experienced and which are often directly related to the decline of many central cities. The second objective documents regional changes within the coastal environment. This line of inquiry parallels non-coastal demographic research, which has analyzed the higher growth rates in the so-called sunbelt states compared to changes occurring in the rest of the United States.[2]

The coastal zone, as presently defined, covers 209,167 square miles, or 7 percent of the 48 contiguous states. In 1950, this area had a population of slightly less than 30 per cent of the national population, a proportion which grew moderately during the 1950 and 1960 decades.

The United States population grew by 18.4 per cent during the 1950-60 decade, a rate which declined significantly during the following census period which continued into the 1970's. Assuming similar trends between 1974 and 1980 to those prevailing during the first four years of the decade, it is estimated that the national population will grow by approximately 10 per cent during the present decade.

The demographic changes in the coastal zone stabilized during the early 1970's. Slightly more than one-third the total national (conterminous) population now reside in this area. This trend parallels the national growth, except the changes which occurred in the coastal zone were more varied. During the 1950's, the coastal population grew by more than 29 per cent compared to 18 per cent for the nation as a whole. This development continued during the 1960's, although at a much reduced rate and converged with the national demographic development in the early 1970's. In 1974, the population growth in the coastal zone had actually dropped to below the national rate (3.4 and 3.9 per cent respectively). The comparative density figure for the coastal zone was about four times higher than the national average, although it should be recognized that great variances in county densities exist within both the coastal zone and the nation.

2. Functional Analysis

The importance of the coastal zone for urban and marine transportation is reflected in the proportion of the total coastal zone area classified rural,

SUMMARY STATISTICS FOR CONTERMINOUS AND COASTAL UNITED STATES 1950 - 1974

YEAR	TOTAL CONTERMINOUS U.S. POPULATION	PERCENT CHANGE	DENSITY	TOTAL COASTAL U.S. POPULATION	PER CENT OF TOTAL U.S. POPULATION	PER CENT CHANGE	DENSITY
1950	150.697.361		50.6	44.434.425	29.5		212.4
1960	178.464.236	18.4	59.9	57.065.131	31.9	28.4	272.8
1970	202.143.083	13.2	67.9	68.089.035	33.6	19.3	325.5
1974	210.196.000	3.9*	70.7	70.433.000	33.5**	3.4	336.7

* Projected population growth rate estimated at 9.9 per cent assuming similar trends between 1974/80 as prevailed between 1970/74.

** Projected population growth rate estimated at 8.6 per cent assuming similar trends between 1974/80 as prevailed between 1970/74.

Table I

coastal urban, and inland urban. Nearly half the coastal zone of 209,228 square miles (48 per cent) (Table II) is classified non-urban, a significant portion of which is used for private (primary and secondary) residences. Kimmelman et.al., in a separate study, concluded that 32 per cent of the shoreline is residential, while another 59 per cent is undeveloped. The balance of 9 per cent is in public recreational usage.[3]

The next largest group consists of the coastal urban counties which comprise approximately 42 per cent of the total area. In reflecting upon these figures, it should of course be noted that not all areas classified as urban coastal necessarily are urban from a functional point of view. Much of the New York waterfront, from a functional point of view, is coastal rural because of the extensive areas included as part of the Gateway National Park, yet all five Boroughs have been classified coastal urban. The inland urban counties, which are part of coastal SMSAs, made up the balance comprising about 9 per cent of the total coastal zone.

Of the three functional groups, the inland urban counties experienced the most rapid growth during the 1950's and 1960's with declining rates in the early 1970's. Assuming similar trends during the latter part of the present decade, overall growth in the inland urban counties is likely to fall from nearly 36 per cent during the 1960's to little more than 11 per cent for the present decade.

In light of the attractiveness of the coastal zone in terms of private residences and businesses, it is interesting that the category classified as urban coastal grew at a rate significantly lower than either inland urban or coastal rural. Two possible explanations may account for these developments and are briefly outlined below. The first is related to the suburbanization process and concurrent stabilization or even stagnation of the central business districts (CBD) of many older cities. The CBD of most North American coastal cities is located close to the waterfront, which reflects the important functional ties between the port facility and the rest of the city. With increasing emphasis on industrial and business developments in the suburbs, it is clear that counties located at some distance from the CBD and the water would benefit relatively more from immigration than the central city counties and counties with large urban port facilities. The urban planning and urban geographical literature is replete with examples documenting population changes between suburban counties and inner cities, although empirical studies emphasising coastal demographic changes are very few.

There is at least one additional notion which may contribute to our understanding of the comparatively lower growth rates which coastal urban counties have experienced. This relates to the dramatic changes which most North American waterfronts have undergone. Because of containerization and the vastly increased demand for space required for marshalling yards, much of the traditional waterfront is now vacant and awaiting urban renewal developments.[4] In cities with former active urban port facilities, only a few of the previously busy piers have been retained and in some instances refurbished for use by a growing cruise industry. The vast majority of urban piers are now often abandoned. Warehousing and manufacturing which used to occupy much of the inner city waterfront have most often moved with the shipping lines and freight forwarders to the larger fully integrated container facilities, most of which are located peripherally to the CBD. It is suggested that these factors have contributed significantly to the somewhat lower growth rates which coastal urban counties have experienced. Because of rapid changes along the urban waterfronts, it is expected that much of the abandoned real estate will become the focus for urban renewal efforts. In fact, some very interesting urban waterfront renewals are currently underway or have been completed in Boston, Baltimore, Seattle, and New Orleans.

COMPARATIVE DEMOGRAPHIC ANALYSIS OF COASTAL URBAN, INLAND URBAN, AND COASTAL RURAL COUNTIES 1950 - 1974

		1950	1960	1970	1974
Total Urb. Coastal Pop.		37.446.298	47.812.621	56.539.285	58.068.900
Per cent of Total Coastal Population	Population	84.3	83.8	83.0	82.4
	Land		42.5		
Per Cent Change			27.6	18.3	2.7*
Density		420.6	537.1	635.2	652.3
Total Urb. Inland Pop.		3.803.404	5.155.803	6.553.340	6.863.800
Per Cent of Total Coastal Population	Population	8.6	9.0	9.6	9.8
	Land		9.2		
Per Cent Change			35.6	27.1	4.7**
Density		198.3	268.8	341.6	357.8
Total Rural Coastal Pop.		3.184.723	4.096.707	4.996.410	5.500.300
Per Cent of Total Coastal Population	Population	7.1	7.2	7.3	7.8
	Land		48.3		
Per Cent Change			28.6	21.9	10.1***
Density		30.5	40.6	49.5	54.4

* Projected 1970/80 growth rate assuming similar trends for balance of decade = 6.8 per cent
** Projected 1970/80 growth rate assuming similar trends for balance of dacade = 11.8 per cent
*** Projected 1970/80 growth rate assuming similar trends for balance of decade = 25.2 per cent

Table II

In some respects, the coastal rural counties provided the real surprise. As a group, these counties grew slightly faster than the coastal urban counties during the 1950's and increased their rates during the 1960's. Of even greater interest, however, has been the ability of these counties to continue to grow during the early 1970's at rates two to three times those of the two urban classes. In fact, if the rates prevailing between 1970 and 1974 continue during the rest of the decade, these counties will grow twice as fast as the inland urban counties and nearly four times the rate of the coastal urban counties. While it is still too early to formulate and test hypotheses related to this phenomenon, Barry, a few years ago, suggested that "inter-urban peripheral" growth may be a result of the movement of businesses from the core of cities to exurban areas located in relatively close proximity to the urban centers. The advantage of this strategy is to be located close enough to the services (airports, stock exchange, etc.) available in large metropolitan areas and yet far enough away to obtain real and relative environmental amenities available in rural or exurban counties located peripherally to the larger metropolitan areas.[5]

In this context, it should be noted that the population density in the coastal zone is significantly below those of both the coastal urban and inland urban counties as well as below the mean density values for the county as a whole. (Tables 1 and 2.)

Several generalized conclusions can be drawn from the analysis of the three functional groupings identified in this part of the analysis. Not surprisingly, the rate of growth in the coastal zone followed the overall slowdown which has been observed for the rest of the country, i.e. a much more rapid dempgraphic growth during the 1950's which continued into the 1960's and has tended to converge with the national rates in the 1970's.

The second conclusion concerns the temporal changes which have occurred within each of the groups. Surprisingly, the non-coastal counties located within coastal SMSAs grew significantly faster in the early part of the study period, but also showed the fastest

relative slowdown in growth. The urban coastal counties also grew, although not as rapidly as the non-coastal urban counties. Several notions were advanced relating urban overall changes to the specific case of coastal urban counties which should be looked at in greater detail than has been possible here.

In some ways, the most surprising group was the rural coastal counties which exhibited growth rates similar to the urban coastal group, except that rural coastal counties have been projected to grow in the short term (to the end of the 1970 decade) by 25 per cent.

3. Regional Coastal Analysis

The previous analysis compared coastal population by county with comparable sets on the national level. The ensuing analysis divides the coastal zone into six sub-regions. Regional and functional differences will be noted. Finally, some of the key demographic variables will be tested for purposes of detecting statistically significant differences among the six regions.

The 286 counties were divided into six regions defined arbitrarily as New England, Mid-Atlantic, Southeast, Gulf, Southwest and Northwest. Each region was defined on the basis of state boundaries. The regions and states included appear in Table 3.

U.S. COASTAL DEMOGRAPHIC REGIONS

Regions	Nos. of Counties	States
New Engl.	28	Maine, New Hampshire, Massachusetts, Rhode Island and Connecticut
Mid-Atl.	54	New York, New Jersey, Maryland, Delaware, Pennsylvania and Washington, D.C.
Southeast	109*	Virginia, North Carolina, South Carolina, Georgia, Florida
Gulf	48	Alabama, Louisiana, Texas
Southwest	19	California
Northwest	28	Oregon, Washington

* The number of counties included in this region varies from 107 to 109 as Virginia Beach was not created until the mid-fifties and Chesapeake until 1963. Furthermore, Nansemond was deleted as a county following the 1970 Census. All changes occurred in Virginia.

Table III

Regionalizing a given area represents an attempt to spatially classify the coastal zone. Since all classification is intended to minimize differences within each class (region) while maximizing differences between classes, a chi square test was performed on the six regions and the three types of counties tabulated (coastal urban, coastal rural and inland urban). The chi square is a non-parametric statistic, testing for differences between two or more variables. The observations are cast in a contingency table or matrix where one axis represents the value of the observation (county) on one variable, while the other axis represents the value of the county on the remaining variable. The higher the chi square statistic, the lower the probability that the differences between the two variables would have occurred by chance. In the social sciences, levels of confidence of .05 or .01 are the usual accepted probabilities.

The 286 counties were classified by region (as predetermined) and the coastal urban, inland urban, and coastal rural trichtomy. The test statistics proved to be highly significant (alpha = .0001), which suggests that the six regions as defined are valid.

The six regions vary in size from approximately 60,000 square miles (Southwest) to less than 16,000 square miles (New England). Not surprisingly, the population density is almost perfectly inversely correlated with the size.

The temporal changes in the population showed interesting shifts, which again reflects at least some of the changes in the settlement patterns which have characterized the nation during the third quarter of the 20th century.

The gross population changes suggest a regrouping of the six regions for purposes of analyzing regional population shifts between 1950 and 1974. The smallest region, comprising the Pacific Northwest, neither increased or decreased its share of the total coastal population. (Table IV).

REGIONAL POPULATION SHIFTS

1950 - 1974

REGIONS	1950	1960	1970	1974
New England	13.7	12.1	11.4	11.3
Mid-Atlantic	45.1	41.3	39.0	37.7
Southeast	9.7	12.3	13.9	15.1
Gulf	7.9	8.4	8.5	8.8
Southwest	17.8	20.4	21.5	21.5
Northwest	5.8	5.5	5.7	5.6

Table IV

The remaining five sub-regions can be assembled into two, those which reduced their share and those which increased their share of the coastal zone population. Both the New England and Mid-Atlantic regions reduced their shares considerably during

the past 24 years. For New England, the reduction was less than half of that which the Mid-Atlantic experienced. The latter region maintained a 45 per cent share of the total coastal population in 1950 which dropped to less than 38 per cent by 1974.

Of the three remaining regions, the Southeast increased its share by more than 5 per cent -- from slightly less than 10 percent in 1950 to more than 15 per cent by 1974. The Southwest followed with a 3.7 per cent advance from 17.8 per cent to 21.5 per cent. The net increase for the Gulf region's share of the coastal population was minor, slightly less than one per cent, and could as easily have been discussed together with the Northwest.

It is clear that the migration to the sunbelt states, which has been in evidence for some time, is reflected in the coastal migration pattern as well. The two regions which lost in their share of the coastal population (New England and Mid-Atlantic) also are the most densely populated sections of the coast. Conversely, the three southern regions which gained were characterized by significantly lower densities. The scale of the present analysis is too coarse to determine the maximum number of people a given area can support, but it is possible that the declining shares of the New England and Mid-Atlantic regions may be affected by the relative scarcity or cost of land in close proximity to the shore. This would appear to be particularly relevant in the case of the Mid-Atlantic region. Newling, in working with population projections for New Jersey's municipalities, suggested that the "filling in" process of a given region would follow the logistic curve. The shape of the curve would be contingent upon the size of the initial population, density, and the area available (zoned) for residential growth.[6]

Assuming the validity of the Newling model and applying it not in the context of forecasting, but merely to account for past growth, it is suggested that the Mid-Atlantic Region may be approaching the upper asymptote of the logistic curve. In this context future increases are likely to be a result of a "filling in" process of existing empty areas. Additional growth may occur as a result of changes in local zoning ordinances from a relatively low density of one, half and quarter acre zoning, (R-40, R-20, or R-10) to significantly higher densities, possibly available under PUD or other multi-family zoning.

In order to test this notion, it would be necessary to analyze municipal population changes within each of the 286 counties included in the analysis. Because of the magnitude of the data required, it was not possible to provide answers to these important questions in the present paper.

A regional demographic breakdown of the three classes of counties was made for the four periods 1950-1974. (Table V). While significant variations exist in the urban coastal/urban inland/rural divisions, further inspection of the table suggests that the proportion of total population classified remained remarkably stable throughout the 24 years. Both the Northwest and Southeast had significantly fewer people classified as urban coastal in 1950 compared to any of the four remaining regions. On the opposite scale, the vast majority of the people in the Mid - Atlantic and Southwest were classified urbanin both 1950 and 1974. These figures suggest relatively few changes in the proportion of coastal urban population to the total regional population. Both the Gulf and Northwest regions remained remarkably stable as the urban coastal population only varied between 68 and 78 percent.

The rural coastal population in the sunbelt states declined or remained stable, whereas the comparable figures for the New England and Mid-Atlantic regions experienced slight increases between 1950 and 1974. The decline in coastal rural populations for the three southern regions is related to the overall growth which these regions have experienced, most of which appears to have occurred in urban counties. Of potentially greater interest, however, are the increases in the rural coastal population which the Mid-Atlantic region has experienced and which may well be related to the population increase of rural counties at the expense of population losses in urban counties. If the equalization process between urban and rural counties can be further verified, it would appear to lend further support to Berry's notion of "inter-urban peripheral growth" as applied to the coastal zone, which was discussed briefly above. It should, of course, be borne in mind that population density is only one --albeit an important -- consideration influencing regional growth. Other factors may be of even greater importance which should be investigated, if further attempts are to be made to identify regional growth.

The chi square test was used to test if the population densities for the four time periods were statistically significant. All counties were cast in four 2 x 6 contingency tables where the density variable for each of the four time periods was nominalized. Counties with mean densities below the overall coastal zone mean were separated from the counties above the coastal zone mean. Four sets of contingency tables were cast, one for 1950, 1960, 1970 and 1974 and all proved to be highly statistically significant. The chi square verifies the qualitative conclusions which have been discussed above.

4. Summary

This paper has addressed the demographic changes occurring in the coastal zones of the 48 contiguous states. Significant differences exist between the growth and development of coastal zone and the nation. It was found that the population in the coastal counties grew at significantly higher rates during the 1950's and 1960's, Three different types of counties were recongized, coastal urban, inland urban and coastal rural. Again demographic differences were observed. Inland urban counties were found to grow at rates faster than both coastal urban and coastal rural counties. Unable to test statistically, a few hypotheses were advanced which relate coastal demographic developments to the urban/suburban changes characterizing much of the eastern older cities. To test regional differences, the coastal zone was divided into six regions. Temporal and functional differences were noted among the six subcoastal regions. On the basis of temporal and functional demographic

REGIONAL, FUNCTIONAL AND TEMPERAL DEMOGRAPHIC PER CENT CHANGES 1950 - 1974

		1950	1960	1970	1974
New Eng.	Coastal Urban	95.7	95.7	95.6	95.1
	Inland Urban				
	Rural	4.3	4.3	4.4	4.9
Mid-Atl.	Coastal Urban	84.5	81.6	79.3	78.4
	Inland Urban	13.6	16.2	18.1	18.6
	Rural	1.9	2.2	2.6	3.0
S. east	Coastal Urban	56.7	65.5	67.7	68.9
	Inland Urban	14.0	10.3	9.4	8.8
	Rural	29.3	24.2	22.9	23.3
Gulf	Coastal Urban	77.6	78.4	78.1	77.6
	Inland Urban	8.9	8.7	9.1	9.8
	Rural	13.5	13.0	12.8	12.6
S. west	Coastal Urban	97.9	97.8	98.2	98.0
	Inland Urban				
	Rural	2.1	2.2	1.8	2.0
N. west	Coastal Urban	70.0	70.9	70.8	68.5
	Inland Urban	5.8	6.6	8.5	9.7
	Rural	24.2	22.4	18.7	21.8

Table V

developments occurring, three coastal geographic trends were recognized. The Northeast, comprising New England and the Mid-Atlantic regions, was losing its proportionate share of the total coastal population. Urban populations were not growing at nearly the same rate as the coastal rural areas, which appears to increase at a faster rate than in any of the remaining four subregions.

The sunbelt regions proportionately grew the fastest reflecting the overall regional migration pattern which has been in evidence for some years. The coastal rural areas tend to decline, probably in response to the rapid urban demographic development which has occurred in this region. The third development consists of the Northwest, which is the most stable in demographic terms. While population growth has been experienced in this region, it has maintained its overall relative share of the coastal zone population as well as its share of functional land-uses.

References

1. Spangler, M.B. "Projections of Socio-economic Trends in the Coastal Zone," Marine Techn. Soc. Jour. (July/Aug., 1972), 6,4,21-24.

2. Borchert, D.J. and J.D. Fitzsimmons, "Population Redistribution in the United States, 1950-1975," paper presented at the annual meeting of the Assoc. of Amer. Geographers, New Orleans, LA., April 10, 1978.

3. Kimmelman, B. (et.al.), Studies in Environment Vol. 5 - Outdoor Recreation and the Environment, Office of Research and Development, E.P.A., Washington, D.C., 1974.

4. Moss, M.L. "The Challenge of Urban Waterfront Revitilization," paper presented at the Princeton University Conf. on the Urban Coast and Energy Alternatives, May 17-18, 1978.

5. Barry, B.J.L. "The Geography of the United States in the Year 2000," Ekistics, (1970), 29, 341-345. See also his Growth Centers in the American Urban Systems, Vol. 1, Ballinger Publishing Co., Cambridge, MA., 1973.

6. Newling, B. "Population Projections for New Jersey to 2000," City College Publications, New York, 1968.

GREAT LAKES SHORELINE EROSION - WESTERN LAKE MICHIGAN

J. M. Pezzetta
University of Petroleum and Minerals
Dhahran, Saudi Arabia

J. Robert Moore
Institute of Marine Science
University of Alaska
Fairbanks, Alaska 99701

Abstract

Three coastal sites of varying topographic and geologic characteristics were selected along the Wisconsin shoreline of Lake Michigan for monitoring the processes and rates of shoreland erosion. Periodic (seasonal) plane surveys revealed that the mean recession rates varied from 0.05 ft (0.015 m)/TDM (thirty-day month) to 2.7 ft (0.082 m)/TDM, the latter having occurred during the fall/winter of 1975/76 along a high, steep, clayey bluff near Port Washington. A sinuosity factor S, invoked as a quantitative measure of the planimetric geometry of the bluff crest, provided an indirect evaluation of the compositional uniformity or variability of the bluff deposits. While high lake levels have accelerated the processes which induce failure and slumping, particularly along those shoreline segments having narrow beaches, the entire mechanism of bluff undermining and collapse depends largely on the direct and indirect effects of precipitation including rainfall, sheet & channelled runoff, water table fluctuations, frost action & shore ice.

1. Introduction

A pervasive water resource problem in the Great Lakes basin which has received considerable attention in recent years is the extensive erosion of the coastlines. Shoreland segments that are particularly vulnerable to the forces of erosion tend to suffer severe and rapid slumping during periods of high lake elevations. By eliminating the protection afforded by a wide beach face, high lake levels enable the erosive activity to be focussed directly at the toes of the bluffs, terraces, or dunes. As a consequence, wave-induced undermining and bank failure are substantially accelerated during such times. However, field observations have demonstrated quite clearly that bluff erosion and recession are not entirely a function of lake level fluctuations and that other, sometimes subtle, environmental phenomena play a very significant, often dominant role in this complex process.

Several interrelated factors, both natural and man-made, which merit consideration in evaluating the nature and degree of coastal erosion are:
(1) the natural geometry of the shoreline and its orientation to prevailing wind-induced waves;
(2) the morphology, geology and competency of the shorelands and inshore zone;
(3) nearshore hydrodynamics, particularly waves and alongshore currents;
(4) meteorological effects, especially wind fields, storm tracks, and their frequency, intensity and duration;
(5) the effects of the freeze-thaw process and shore ice on the shoreland materials;
(6) the influence of artificial protective structures on nearshore processes and shoreline configuration.

The development of emergency as well as long term coastal zone management programs should be structured, therefore, in a manner which seeks to address these specific factors. Shoreland zoning and setback allowances must be developed within the context of well-defined regulations that consider not only the rates of bluff recession but also the mechanics and variability of erosive processes in the coastal environment. In addition, the effectiveness of different types of erosion control measures must be evaluated in terms of both engineering/economic considerations and land use management practices. Historical evidence has shown that a piecemeal approach to shoreline protection, more often than not, serves only to enhance rather than ameliorate the problem. Innovative plans of an integrative nature that maximize the protection at a reasonable cost must be explored and developed (cf. Brater, et al, 1975).

A necessary part of any program which seeks to optimize the effectiveness of any plan of shoreline protection must rely on a substantial and adequate data base derived from a critical examination and evaluation of the physical characteristics and dynamic processes of the coastal environment, particularly along shoreline reaches that are rapidly succumbing to erosive activity.

Available information on the erosional characteristics of the western coast of Lake Michigan generally has been of a qualitative nature (e.g. Striegel, 1968; U.S. Army Corps of Engineers, 1971). Striegel's work is especially detailed in its description of the lakeshore and includes one of the few quantitative assessments of bluff recession for Lake Michigan. For the period 1874 to 1946, he calculated the recession rate in Racine County to be approximately 1.2 ft (36.6 cm)/year or 0.099 ft (3.02 cm) per thirty-day month (TDM).

The principal purpose of this study is to establish rates of shoreline recession along select segments of the western coastline of Lake Michigan and to evaluate the sediment distribution patterns in the immediate offshore waters adjacent to the onshore monitoring sites.

This initial report addresses primarily the

bank recession problem and to a lesser extent the relationship between nearshore hydrodynamics and sediment dispersal in the littoral zone.

2. Description of the Study Area

Excluding the shores of Green Bay, the Wisconsin section of the Lake Michigan coastline is approximately 288 statute miles (463 km) in length and extends from Rock Island just off the tip of Door County peninsula to the Illinois state line (Fig. 1).

The entire coastal environment falls within a physiographic region of the state known as the Eastern Ridges and Lowlands (Fig. 2), the topographic features of which were shaped by Pleistocene glaciers. The relief of the coastal bluffs ranges from a few feet above the lake surface near the southern limits of the survey to a maximum of 164 ft (50 m) above the lake (744 ft or 227 m above mean sea level) just north of Milwaukee. The shorelands fall away to the north and south of this regional high.

Except for the rocky northern portions of Door County, the lakeshore consists essentially of till deposits in the form of end and ground moraines and to a lesser extent of ancient lake basin deposits the latter which have been reworked into dunes and low terraces of fine to medium grade sand (Thwaites, 1956 and Thwaites and Bertrand, 1957).

Beneath the cover of glacial drift the western coastline of Lake Michigan is underlain almost entirely by sedimentary rocks of Silurian age, principally the mid-Silurian Niagaran dolomites which dip at a low angle (approximately 1°) eastward beneath Lake Michigan. A narrow subcrop of Upper Devonian shale and dolomite is found in the area between the cities of Sheboygan and Milwaukee. The principal surface exposures of bedrocks occur along the shoreline north of Jacksonport and extend across the straits to Washington and Rock Islands. There in the immediate offshore region are rocky ledges and platforms often strewn with glacially derived boulders and cobbles.

Ten principal streams drain the watershed of this coastal environment (Fig. 2). Although the landscape through which these short rivers and creeks flow is generally rolling to quite subdued, some streams enter the lake through channels which have deeply incised the coastal bluffs. A hydrological study conducted on three creeks near one of the monitoring stations (M-7) indicates that the sediment load contributed to the lake by fluvial discharge may be quite low (Pezzetta, 1974). Therefore, the modern nearshore lacustrine deposits are derived principally through the erosion of the till banks of which the shorelands are composed.

3. Field and Laboratory Methods

During the summer of 1974 a reconnaissance survey was undertaken of the entire coastline to identify a tractable program of study that would include some of the more problematic sections of the shoreline. Seventy-six coastal sites were visited on that survey of which 15 were selected as warranting detailed monitoring, both onshore and offshore. Of those 15 stations, the three discussed in this report were chosen to provide specific examples of erosional characteristics of shoreline segments showing varying geological properties and susceptibilities to bank undermining as well as to demonstrate actual or potential hazards to riparian owners.

The general locations of these sites are shown in Fig. 2. These three principal stations are described as follows: M-2 in Sevastopol Town Park, northeast of Sturgeon Bay; M-7 in Sandy Bay, southern Kewaunee County; and M-11 in Lake Park, Port Washington.

At each site a steel rod or 'pin', 1/2" OD by 50" long (1.27 cm x 127 cm), was driven into the ground until some seven or eight inches (18 to 20 cm) were left protruding above the surface. These pins served as bench marks from which the departures to the bluff edge were measured. The actual spot on the ground where the pin was driven was chosen on the basis of the field of view offered the transit operator, the scope of the bluff crest that could be measured from the pin and possible hazards arising from loss of the marker by bank slumping. Generally the pins were set at some convenient distance back from the crest edge but in positions that provided good bearings along approximately 100 to 300 ft (30 to 91 m) of the shore bluff. At some sites good setback was not possible due to the proximity of the highway which is located within 15 ft (4.6 m) of the bluff scarp. In such cases the marker was 'tied in' to other permanent structures nearby, e.g. utility poles, buildings, etc.

The number of bearings and distances to the crest edge that were measured as well as the spread of the sight lines were determined largely on the basis of the crest geometry. An irregular configuration generally required a greater 'spray' of bearings than one with a smoother outline.

Samples of the bluff materials were obtained along the faces of the banks. In addition beach sediments were collected near the toe of the bluff at locations directly in line with the survey pin. Bottom sediments were obtained from the nearshore zone in the vicinity of the shore stations. The textural properties of the field samples were determined by means of standard sedimentological techniques.

Each of the three sites was surveyed a minimum of three times, with each survey coinciding approximately with a change in season. A fourth survey was conducted at Station M-11, Lake Park because the rapid rate of bank failure there warranted further observation.

The recession rates calculated for each site are mean values of several measurements scaled from data plotted on accurate base maps. Using the total elapsed time in days between surveys the rates of bank recession were evaluated in terms of a thirty-day month (TDM).

A sinuosity factor was invoked as a measure of the changes in crestline geometry. This factor is defined as $S = L_{bc}/L_{sl}$, where S is the ratio between the actual length of the bluff crest (L_{bc}) and the length of a straight line (L_{sl}) which joins the distal points of the surveyed section. The sinuosity thus offers a numerical means for repre-

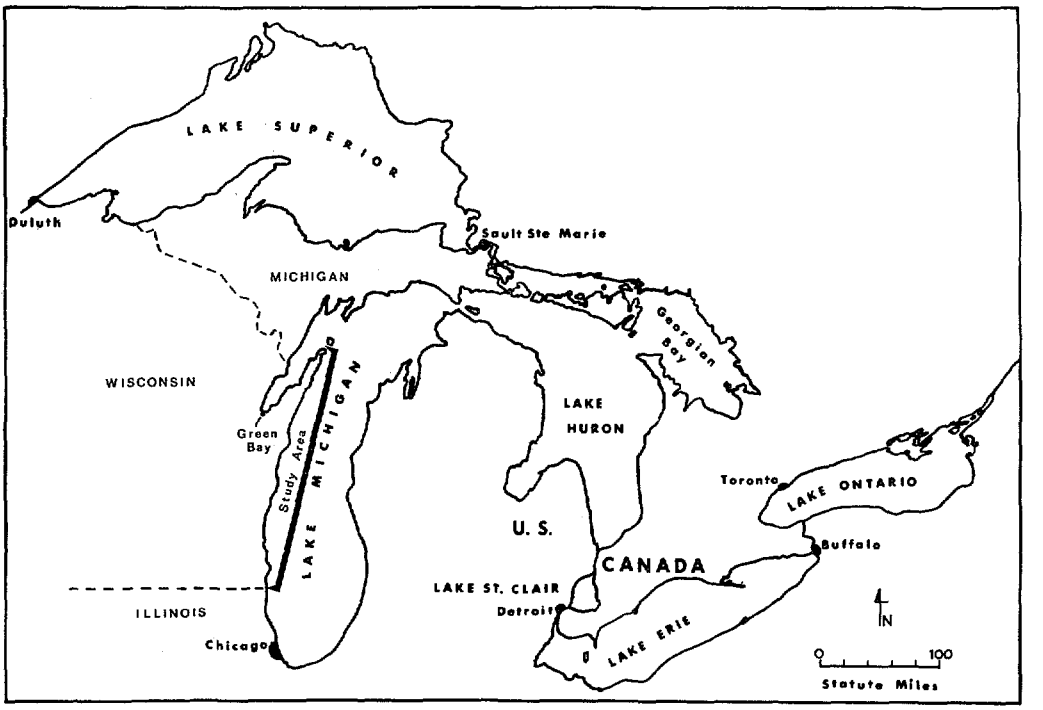

Figure 1. The Great Lakes showing study area.

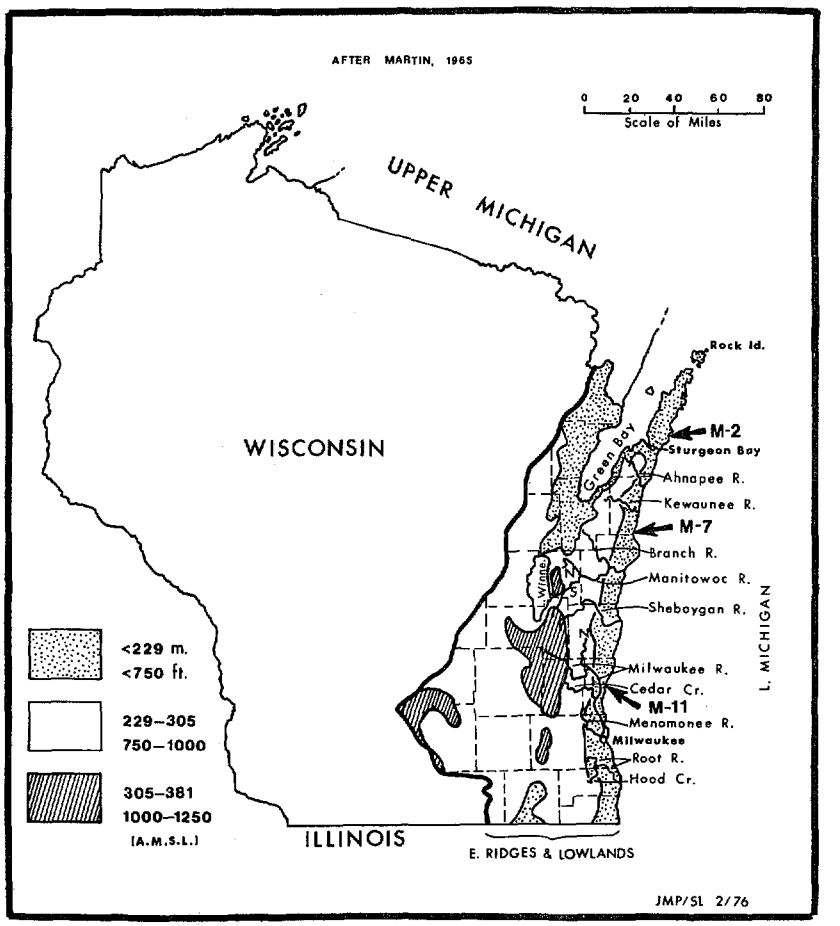

Figure 2. Map showing locations of stations M-2, M-7 and M-11 along the Wisconsin shoreline.

senting the general configuration of the bluff crest with time. Therefore, S indicates the degree of irregularity or smoothness of the crestline after each survey. The limiting value for S is unity, in which case the sinuosity, and hence, the shape of the bluff edge is reduced to a straight line. It should be noted that the sinuosity of the bluff crest is not to be equated with the actual shoreline configuration at the water's edge except in the case of vertical cliff shorelines. Field observations have shown that a smooth and regular shoreline is often found adjacent to an irregular, receding bluff crest.

The sinuosity also provides an indirect means for assessing the nature and intensity of the erosional processes and the changes in composition of the shoreland materials as the banks recede. A highly irregular crestline ($S \gg 1$) indicates that the processes of bank erosion operate in such a manner as to accelerate the development of landward-directed cusps or hollows while lakeward protruding elements or promontories recede at a lesser rate. In this study it has been observed that cusp formation tends to occur in slumping bluffs of highly variable composition and texture, e.g. coarse, very poorly sorted glacial till.

4. Observations at Stations M-2, M-7, and M-11

(i) Sevastopol Town Park, Door County (M-2): This site is located in a sand dune environment immediately south of Cave Point, a rocky bluff northeast of Sturgeon Bay. The survey pin was set next to the forest cover some 74 ft (22.6 m) from the dune crest (Fig. 3). The crestline of the shorelands at this location was more difficult to delineate than the bluff edges of sites composed of clayey till deposits. A distinctive change in slope along the lakeward side of the dunes is not generally present because the wind rounds off the tops of the dunes. However, at the base of the sand bluffs, where wave action had removed part of the dune face, a well-developed, steeply-dipping scarp was observed (see profiles in Fig. 3). The dune face above the scarp dips lakeward at about 35°, the maximum angle of repose of loose sand. However, from the dune crest back towards the survey pin the dune surface dips lakeward at much shallower angles that ranged from 7° to $11\text{-}1/2^{o}$.

The seasonal mean bluff recession rate at this site was remarkably uniform with values of 0.61 ft (0.19 m)/TDM for late fall, 1975 and 0.57 ft (0.17 m)/TDM for late spring, 1976. After the first survey, the sinuosity of the dune crest decreased from 1.176 to 1.118. Hence the processes of erosion had partially straightened out the crest edge. Between the second and third surveys the bluff continued to recede at approximately the same rate with no perceptible change in sinuosity. The textural uniformity of the dune sediments (Mn = 2.22ϕ, 0.22 mm; σ_ϕ = 0.44) is an important factor which contributes to this regular type of bluff recession.

Stabilization of the dune sands was only partially developed between the crest edge and the forest cover immediately to the west of the survey monument through plant overgrowth. Along the bluff crest vegetation ranged from sparse to absent. It should be noted here that a critical examination of the nature and rate of plant succession over sand dunes would be of particular interest to coastal zone planners and managers, especially if an effective yet natural process of shoreline stabilization is desired within this type of shoreline environment.

The texture of the nearby littoral deposits (Mn = 2.52ϕ, 0.18 mm) is quite similar to that of the dune sands. These fine sands which comprise the principal offshore sediment facies grade eastward (i.e. lakeward) into slightly coarser fractions. Therefore, the fine clastics derived from the coastal dunes tend to blanket the inshore zone proximate to the monitoring site. Subsequent dispersal of the sediments is effected by coastal lake currents which transfer the deposits both north and south of this location.

(ii) Sandy Bay, Kewaunee County (M-7): This station is located along a moderately high, steeply-dipping bluff whose crest lies about 25 to 40 ft (7.6 to 12.2 m) above the lake surface.(Fig. 4).

Between the first and second surveys the mean recession rate for the entire site was determined to be 0.05 ft (0.015 m)/TDM. After the third survey it was observed that the rate had increased by a factor of two, i.e. up to 0.10 ft (0.03 m)/TDM. Concommitant with the change in recession rate, the sinuosity had decreased from 1.135 to 1.099. However the greatest amount of slumping (2 to 4 ft., 0.6 to 1.2 m) had taken place near the distal ends of the survey line where the bluff is characterized by cusps and promontories. In the intervening, straighter segment only minor erosion had taken place, generally less than 1 ft (0.03 m). Hence, the rapid slumping of the promontories in effect had gradually reduced the irregularities of the crestline toward a smoother configuration.

Where the crestline is cuspate in form the deposits tend to be comprised of poorly sorted layers of variegated sand and silt with numerous stringers and lenses of gravel scattered throughout. The straighter part of the bluff was somewhat more uniform in composition with higher proportions of finer clastics. The overall texture of the bluff deposits ranged from 0.18ϕ (0.88 mm) to 6.20ϕ (0.014 mm).

Sampling of the bottom sediments in the immediate offshore zone was rendered quite difficult by the presence of a shallow platform of bedrock and indurated glaciolacustrine clays which extends out into the lake at this location. Waves sweeping over this shelf-like part of the lake floor preclude the retention of unconsolidated sediments along this surface. The littoral zone, however, was characterized by a narrow band of well-sorted, fine to medium sand (2.30ϕ, 0.20 mm to 1.92ϕ, 0.26 mm) derived from the coastal slump blocks by the sorting action of waves. Lag deposits of coarse textured, fairly well-rounded gravels comprise the blanket sediments of the beach face.

(iii) Lake Park, Port Washington (M-11): The survey bench mark for this monitoring site consists of a fiducial mark impressed into the concrete base of a light stand located in a small urban park at the north side of the city of Port Washington (Fig. 5). The surface of the bluff near the survey area is smooth and even with a slight rise to the north. The mean elevation of the bluff crest ranges from 82 to 97 ft (25 to 30 m) above the elevation of the

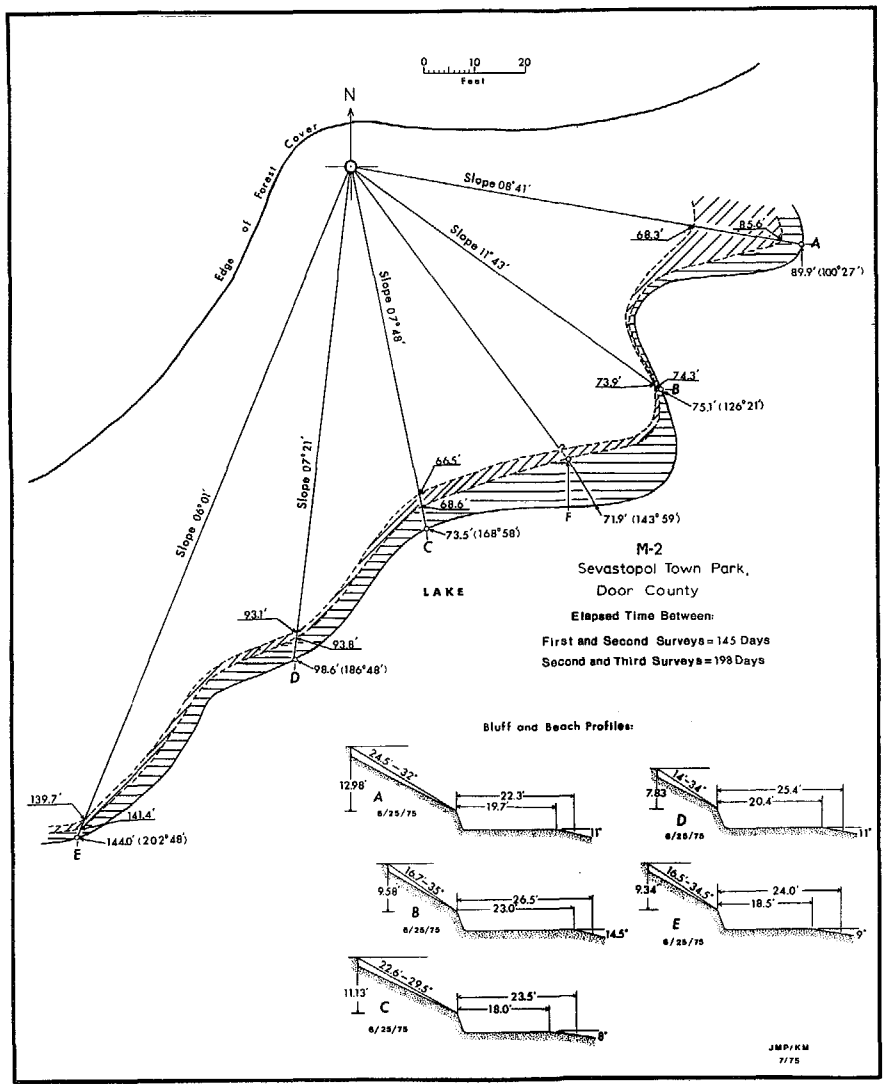

Figure 3. Station M-2, Sevastopol Town Park, Door County.

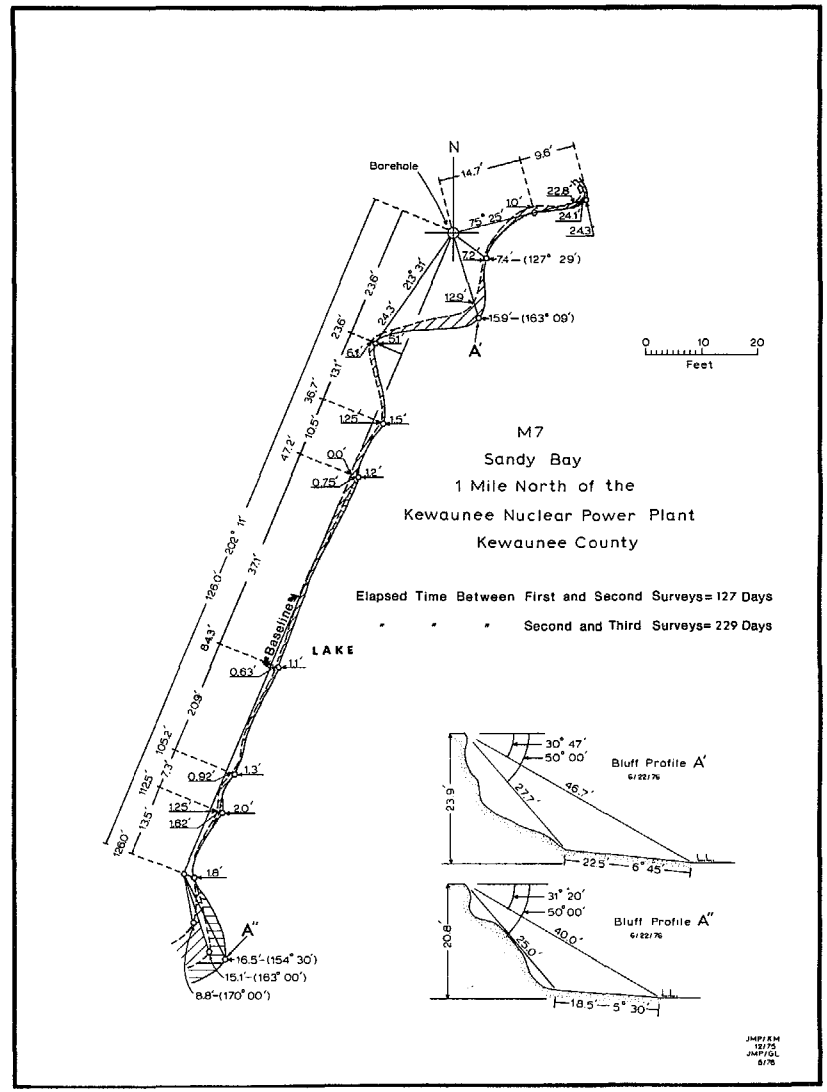

Figure 4. Station M-7, Sandy Bay, Kewaunne County.

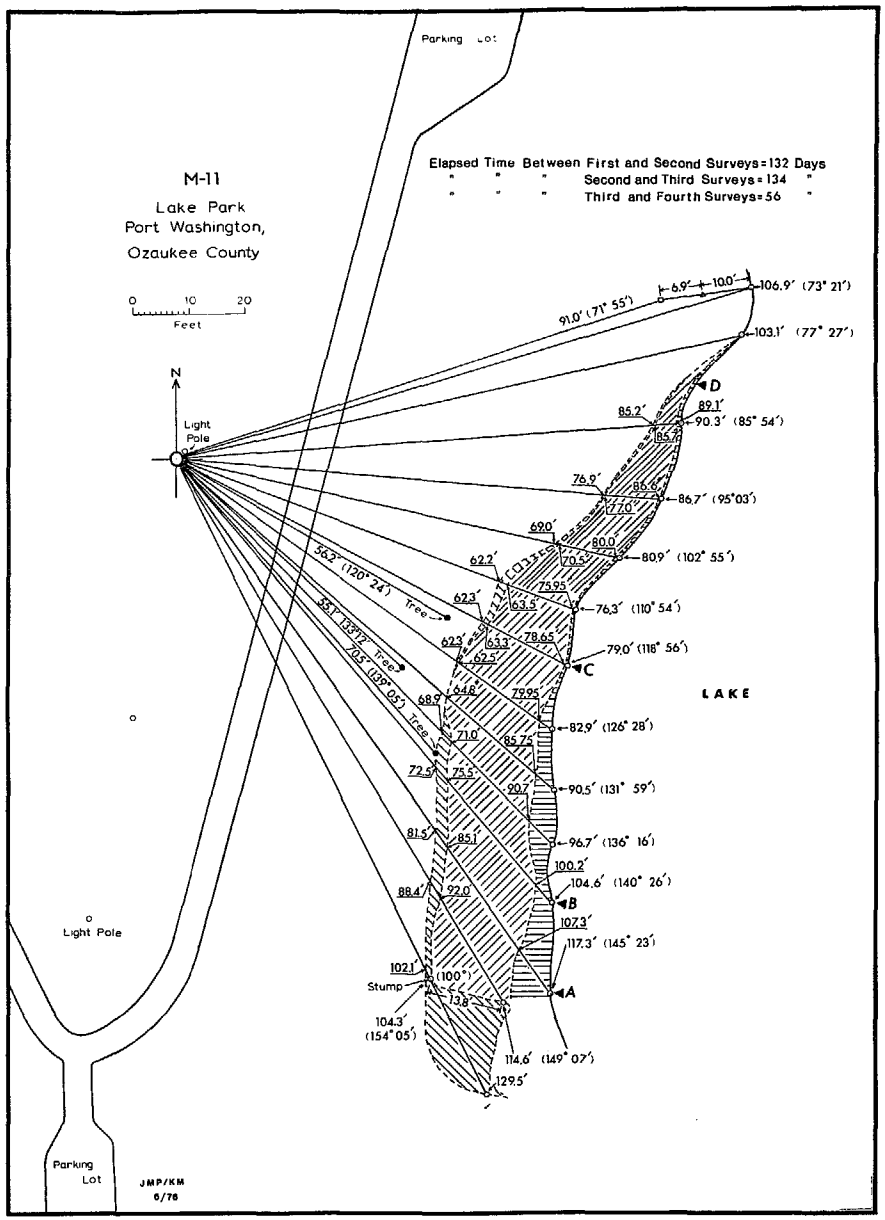

Figure 5. Station M-11, Lake Park in Port Washington, Ozaukee County.

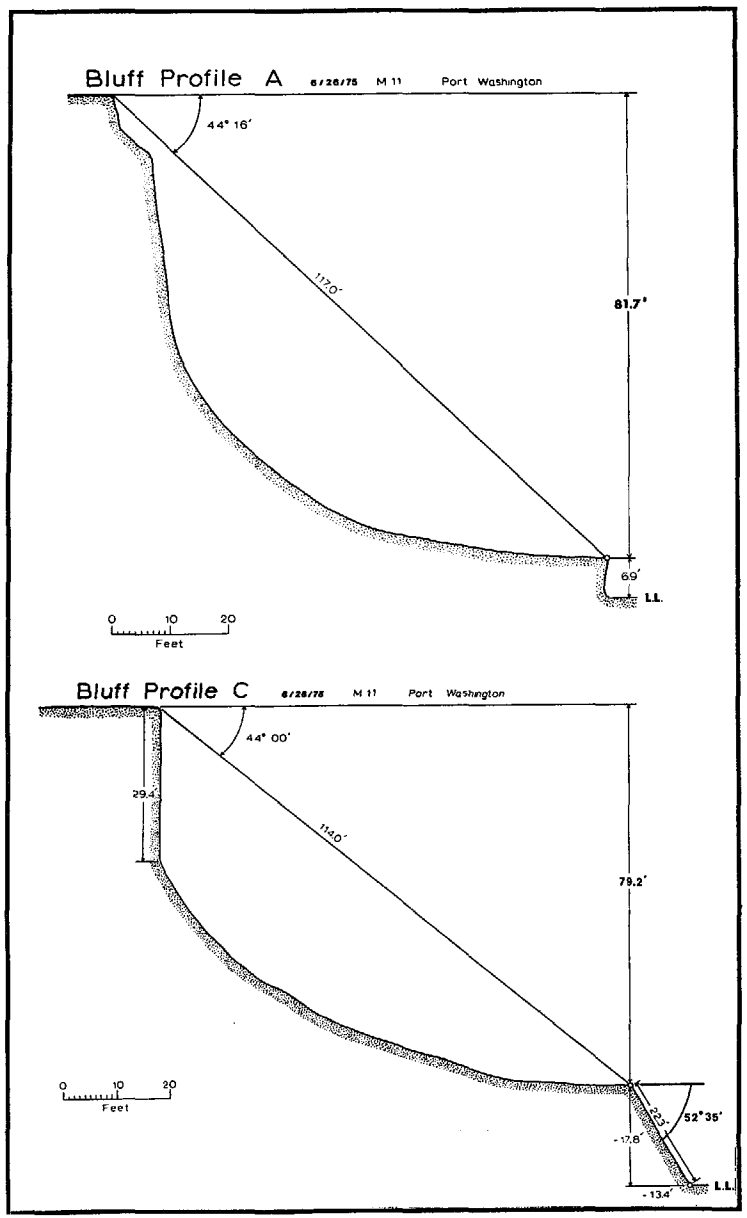

Figure 6. Bluff profiles A and C, Station M-11.

lake (Fig. 6). At the time of the survey the projected horizontal distance between the crest edge and the waterline ranged from 82 ft (25 m) at point C to 95.5 ft (29 m) at point D. The upper 25 to 40 ft (7.6 to 12.2 m) of this bluff is an extremely steep to vertical face. The surface of the slumped debris which accumulates at the base of the bluff, however, assumes more moderate slope angles (see profiles A and C).

The inherant danger which such a steep bluff poses to park visitors prompted the City Park Commission to install a snow fence along the crest as a precautionary measure. The site, therefore, offers a dramatic example of a serious environmental hazard which has arisen from rapid erosion of a coastal bluff within an urban setting.

The seasonal variation in the sinuosity of the bluff crest is given as follows:

S = 1.038, summer of 1975
1.029, fall of 1975
1.168, winter of 1976
1.138, spring of 1976

The mean rate at which the bluff edge receded between the first and second surveys was 0.40 ft (0.12 m)/TDM. During the same period slumping had resulted in a minor adjustment in the crestline geometry toward a slightly straighter configuration (S decreased from 1.038 to 1.029). The amount of material dislodged during that interval, however, was not uniformly distributed along the bluff. Rather, the largest segment with a maximum surface thickness of approximately 7 ft (2 m) broke away from the face at point A within the southern end of the section while the least amount of erosion occurred at point D near the northern end where only one-half to one foot (0.15 to 0.30 m) of mass movement had taken place.

During the late fall of 1975 and the winter of 1976 a very remarkable change occurred at this site when a large slice of the bluff some 17 ft (5.2 m) thick slipped down the sheer face of the bluff. The mean recession rate for that interval of time was determined to be 2.7 ft (0.82 m)/TDM, or 6.75 times the mean rate calculated for the previous summer. At the same time the sinuosity increased very markedly from 1.029 to 1.168. This event left behind at the southern end of the survey section a large, projecting element or promontory which subsequently slumped down the bluff during the late winter and early spring of 1976. In so doing, the sinuosity decreased somewhat to a value of 1.138.

The thick glacial deposit of which this bluff is composed consists mostly of very poorly sorted, fine to very fine clayey sand with mean grain sizes that range from 2.62ϕ (0.16 mm) to 3.85ϕ (0.066 mm). The southern segment tends to contain a higher proportion of clayey sediments which may account for its somewhat greater resistance to slumping. However, eventual failure does take place in this material due to the oversteepening effect produced by undermining.

The inference to be drawn here is that while changes in the rates of bluff recession reflect variations in the intensity of erosional processes, the geometric response (i.e. sinuosity) of the receding crestline apparently is controlled largely by the textural composition of the bluff materials.

The offshore deposits adjacent to this site consist of two distinctive facies, one of silt distributed close to shore, and the other of sand dispersed in somewhat deeper water. This pattern of sedimentation implies that the inshore zone tends to be flooded by a preponderance of fine clastic debris derived principally from the nearby clayey till bluffs by rapid erosion of the banks.

5. General Observations and Conclusions

Careful field observations have established that shoreline erosion involves a complex interaction of a number of interrelated and sometimes subtle environmental factors. While no single cause has been identified in this study, meteorological effects must play a significant role in the overall process. In particular, precipitation and wide ranging temperature fluctuations act upon the bluff materials to alter substantially their cohesive properties and thereby induce instability of the banks. Eventual failure of the bluffs stems from oversteepening which, in turn, is related to the manner in which the bluffs respond to erosional processes.

Slumping of large segments of clayey till, in particular, is generally preceded by the development of vertical cracks which gradually widen and cause 'peeling away' of slices of the bluff face. These openings usually persist over a period of several seasons. In summer, rain and runoff which enters the fissures saturates the deeper porous layers, weakens the cohesiveness of the clays, and in some cases causes washout of sand lenses. These processes, operating individually or collectively, serve to undermine and oversteepen the banks to such an extent that often overhangs of matted, root-filled soil layers 6 to 12 in. thick (15 to 30 cm) develop at the crest edge. In winter, the freezing of pore water and its accompanying expansion causes further enlargement of the cracks and fissures. This process of seasonal dilation thus facilitates the further entry of rain and meltwater into the banks.

When bank failure occurs, the oversteepened segments either slide or cascade down the bluff face and accumulate at the base in the form of moderately steep surfaces, somewhat akin to mountain talus slopes. If further movement of the dislodged debris does not take place, grass sod carried down with the slump may continue to grow in place and help to stabilize temporarily the loosened mass. In some places, however, water seeping out of the bluff face may offset the stabilizing effect of plant growth by keeping the slump soft and plastic and, hence, susceptible to further rapid movement.

As noted above, slump block separation first occurs in the form of vertical fractures near the tops of the bluffs. The development of curved slip surfaces is more complicated and arises from a subsequent accretionary process in which the dislodged and slumped debris plays an important part. If a sufficient mass of sediment accumulates at the base of the bluff, it acts as a sort of pedestal the top of which temporarily supports the base of a newly developing slice in the upper part of the bluff. As the toe of the block which has already slumped is carried away, either through wave action or by

sheet and rill wash, its supportive effect is substantially diminished. This then permits another segment to break away completely from the top of the bluff and to slide down over the remaining part of the previous one. The process eventually results in the accumulation of a series of imbricated slump blocks whose repose angles rapidly decrease in a lakeward direction. In time erosion smooths over the irregularities and the surface so formed assumes a concave curvature over which subsequent slumps can slide.

It is apparent that if the toe of the slumping bluff exists at or very close to the waterline, the undermining effects of wave action, particularly storm waves, will be considerable. However, if the beach face is quite wide, the wave energy will be dissipated before impingement at the base of the bluff can occur. In the latter case, it is evident that the processes which induce erosion of the bluffs are quite independent of lake level fluctuations.

The significance of variations in lake levels insofar as erosion of the shorelines is concerned lies, therefore, in the fact that higher or lower lake stages reflect corresponding changes in the amount of precipitation which falls over the Great Lakes basin. Above-normal precipitation not only fills the lake basins above their long term mean levels, and thereby reduces the width of the protective beach faces, but it also has a more pervasive effect on the land surface. Under such circumstances the bluff materials acquire a greater amount of moisture than they would under conditions of normal precipitation either through direct absorption of rain and meltwater or as a consequence of upward migration of the local watertable. The excess moisture reduces the cohesive properties of the bank deposits and thus renders them more susceptible to failure.

The efficacy of this process was demonstrated quite convincingly in a similar type of study conducted along the south shore of Lake Superior (Edil, et al, 1975). There severe erosion of the steep banks of red glacial till had been observed in locations quite removed from the influence of the lake even given the highest recorded changes in the elevation of the lake surface. In one locale considerable bank failure had taken place some 60 ft (18.3 m) upstream from the mouth of a deep, dry gully that dissects the high, abrupt shorelands in that area. Instability of these bluffs had developed, therefore, principally through moisture seepage which was manifest high within the upper faces of the gully walls where prominent scars revealed the effects of massive slumping.

The climatic extremes which characterize the Great Lakes region also contribute to the processes of shoreline erosion. Winter observations have shown that in spite of freezing air temperatures, sufficient radiant energy from the sun is absorbed by the dark-colored, eastward to southeastward facing banks to cause melting of a thin (1/8 to 1/4 in; 0.3 to 0.6 cm) surface layer of the frozen bluff face sediments. Hence, around midday mud slurries would begin to flow down the bank slopes and often run out across the beach face to the waterline. The quantity of sediment transferred from the bluffs to the lake in this manner is usually quite small. However, the mechanism effectively mixes fine, clayey sediments derived from the banks with the coarser components of the beach. Wave action subsequently restores the equilibrium texture of the beach deposits by winnowing out the finer fractions.

The degree to which lake ice causes damage to the shoreline has not been fully established along this part of Lake Michigan. Depending on the severity of the winter season, it has been noticed that a well-developed ice foot as much as 80 to 90 ft (24 to 27 m) wide may form along parts of the lakeshore, particularly in bays and coves where protection from the wind mitigates the movement of the water. As long as the ice remains fast to the offshore bar, it acts as a sturdy barrier in shielding the beach zone from the pounding action of waves. However, during spring breakup, and especially with the onset of strong onshore winds, the dislodged ice floes can inflict considerable damage to vulnerable segments of the shoreline.

In conclusion, caution should be exercised in directly relating changes in shoreline recession rates to lake level fluctuations alone. Rather, the perspective should be one which includes a consideration of the total spectrum of geological, meteorological, and nearshore lacustrine phenomena which influence the coastal regions of the Great Lakes.

Acknowledgments

This project was funded (in part) by the Office of Sea Grant, NOAA, U.S. Department of Commerce, through an institutional grant awarded to the University of Wisconsin, Madison, Wisconsin.

References

Brater, E., Armstrong, J.M. and McGill, M. (1975). Michigan's Demonstration Erosion Control Program, Update Evaluation Report, Michigan Department of Natural Resources, Lansing, Michigan, 53 pp.

Edil, T.B., Pezzetta, J.M. and Wolfe, P.R. (1975). Sediment and Erosion Control in the 'Red Clay' Area of Western Lake Superior Basin, A Demonstration Project. Interim Report submitted to the Ashland County Soil and Water Conservation District, 65 pp.

Pezzetta, J.M. (1974). Sedimentation Off the Kewaunee Nuclear Power Plant, University of Wisconsin Sea Grant College Program, TR No. 221, 59 pp.

Striegl, A.R. (1968). Shoreland and Floodplain Zoning along the Wisconsin Shore of Lake Michigan, Wisconsin Department of Natural Resources, Division of Environmental Protection, 50 pp.

Thwaites, F.T. (1956). Wisconsin Glacial Deposits-Map. Wisconsin Geological and Natural History Survey, Madison, Wisconsin.

Thwaites, F.T. and Bertrand, H. (1957). Pleistocene Geology of the Door Peninsula, Wisconsin, G.S.A. Bull., Vol. 68, pp. 831-879.

U.S. Army Corps of Engineers (1971). Great Lakes Region Inventory Report, National Shoreline Study, U.S. Army Corps of Engineers, North Central District, Chicago, Illinois, 221 pp.

ENVIRONMENTAL IMPACT ASSESSMENT OF SHORELINE BULKHEADING: A HISTORICAL APPROACH

Michael E. Penney
Department of Marine Affairs-Geography
University of Rhode Island
Kingston, Rhode Island 02880

Abstract

One limitation to the environmental impact assessment of incremental developments, such as private bulkhead-fill projects, is the lack of historical data on the rate and extent of development. Analysis of a historical series of aerial photographs provided a baseline for demonstrating the need for and effectiveness of regulation of shoreline bulkheading. Projections of pre-regulation bulkheading rates into the regulatory period make wetlands regulation seem highly effective in reducing the overall rate of bulkheading in a Virginia county. However, this bulkheading appears to be spatially contagious and it is suggested that the causes of this contagion need to be carefully examined by decision-makers unless lowering the rate of activity is the only objective.

1. Introduction

Analysis of a historical series of aerial photographs can reveal the rate and spatial arrangement of many coastal activities. For privately constructed shoreline bulkheading, such information can be used to construct a with and without regulation scenario. The scenario for a Tidewater Virginia county is interesting in light of the established state and federal guidelines for making regulatory decisions about wetlands alterations. Knowledge of the historic rate of bulkheading allows projection of amounts of bulkheading into the period of regulation. These projections are useful in constructing several measures of regulatory effectiveness. Determination of the spatial distribution of bulkheading channelward of and along the shoreline allows inferences about the amounts of wetlands destroyed. These estimates are also useful in constructing measures of regulatory effectiveness. Finally, private bulkheading is spatially contagious, and it can be inferred that case by case regulation of this type of activity can never be completely effective. It should be emphasized that the type of analysis used here is applicable in other geographic areas and for other types of activities, but the specific results are not.

The Commonwealth of Virginia passed a Wetlands Act in 1972 and promulgated guidelines for making regulatory decisions in 1974. The act has a preservationist tone that is modified by acknowledging a need to "accommodate necessary economic development" (1, p. 13). Counties, cities, and towns may adopt a wetlands zoning ordinance under provisions of the act and administer it through an appointed wetlands board. The board is charged with determining its jurisdiction over specific development sites and with conducting a balancing test of the "anticipated public and private benefit" and detriment of the proposed activity. If the benefits outweigh the detriments and the activity does not "violate or tend to violate the purpose and intent" of the act, a permit can be granted (1, p. 20).

The guidelines are to assist the boards in making correct decisions. They assign a system of relative values to various wetland communities and detail development criteria tending to preserve the intent of the act. The valuation scheme recognizes the importance of wetland productivity and habitat and the functions of erosion control, flood buffering, and water quality control. Development criteria include establishing a need for the wetland alteration for purposes of protecting existing property or gaining water access when other alternatives are not available and when the environmental value of the specific site is low.

In many respects, the Virginia guidelines are similar to those developed for Corps of Engineers "Section 404" regulatory programs. Of central importance to this study are the concepts of cumulative impacts and "anticipated" structures in the Corps guidelines. In making regulatory decisions, consideration should be given to

> the probable impact of each proposal in relation to the cumulative effect created by other existing and anticipated structures or work within the general area. [3, 320.4(a)(2)(iv)]

"Probable impact" seems to refer to the uncertain nature of the assessment process; "cumulative effect" to the total effect of many activities or alterations; and "anticipated structures or work" to projections or predictions of alteration levels. These factors suggest three overlapping measures of regulatory effectiveness. One would be based on whether regulation considered environmental and developmental values in proper balance. Another might consider whether regulation slowed

the rate of development and detrimental impacts to some specified levels. A third might be to compare patterns and levels of development before and after regulation. The final two measures can be approached with the type of analysis presented in this paper. The first involves definitions of environmental and developmental values, a controversial subject only touched on here.

The environmental valuation and impact assessment literature is voluminous, and much of the most controversial work is oriented toward valuation of wetlands. The literature also reflects a growing controversy over the balancing methodology used in regulatory decision making. Wetland "preservationists" cite the need for regulation in face of rapid disappearance of wetlands in many areas. Those oriented toward "balanced" development cite familiar property values for filled wetlands. But neither side has expended much effort in even describing the typical development. An excellent overview of this controversy is available through reference to Gosselink, Odum, and Pope (4); Pope and Gosselink (5); and Odum and Skej (6) on the "preservationist" side. Walker (7 and 8) and Shabman and Batie (9) present views that seem oriented toward "balanced" development. Lynne (10) and Huettner (11) review valuation methodology from an economic standpoint. The problematic nature of regulatory decisions is implicit in all of these references, but none of them deal explicitly with the problems associated with slow, incremental alterations perpetrated by private landowners. Many of these developments are for purposes of erosion control, land acquisition, and aesthetic enhancement and the developmental values may be as difficult to determine as wetlands values are. In some areas, incremental developments may account for a large percentage of regulatory decisions. This paper describes one type of incremental development, bulkheading, in one area.

2. Method

A linear grid, scaled to 500 feet, was registered on aerial photographs from 1937, 1952, 1963, and 1974 of York County, Virginia. Grid cells were also located and numbered on a large scale master map and on data sheets. Locations of houses within 500 feet of the shoreline were interpretively transferred to the master map for each year of photography, and then counted. Interval scale measurements of bulkheads were made on each set of photographs and the data recorded on the sheets. The mean distance of the bulkheads from the toe of the upland bank was about 15 feet and highly skewed to smaller distances. Due to gaps in the photographic record, measurements and counts were limited to about 80% of the shoreline.

Of the studied shoreline of 815 grid cells only, two short sections are in nonresidential usage. One 1500 to 2000 foot, 3 to 4 cell, section contains an oil refinery embedded in residential shoreline. Another 2000 foot section contains a Coast Guard training center similarly surrounded by residential housing. One 6 to 8 cell section, with one bulkhead and five houses in 1974, is eroding at over 3 feet per year. The remaining shoreline is eroding at an average of less than 3 feet per year. Independently repeated house counts and bulkhead measurements differed by less than 15%.

An existing wetlands inventory of the county was examined (12). Of the total 6,991 acres present, only 1,163 were adjacent to the studied shoreline. The individual wetland units were highly skewed toward small fringe or pocket marshes with an average size of approximately 8 acres. The small size and proximity to developed areas of these wetlands would seem to have made them candidates for fill over this historical period.

3. Results

House counts and bulkhead measurements were analyzed to determine general bulkhead construction trends and spatial distribution on this shoreline. General trends were determined using standard least square techniques for bulkheads and houses over time. The spatial arrangement was analyzed using the Wald-Wolfowitz runs test. Results of both efforts are only summarized here, but details are available on request.

Summary data for bulkhead measurements and house counts are presented for the 815 cell shoreline in Table 1. Simple exponential curves fit house and bulkhead data well (r larger than .99) with acceptable levels of significance (p less than 5%). Estimates of the amount of bulkheading added between 1972 and 1974 were obtained using the fitted exponential curve and a straight line interpolation between 1963 and 1974. These estimates are 14,382 and 5,371 feet added for the exponential and straight line approximations, respectively. The reason for obtaining these very different estimates is for later comparison to estimates of the amount of bulkheading actually added between 1972 and 1974 under the Virginia Wetlands Act as reported in Jones (13).

Table 1

Summary House and Bulkhead Data

	1937	1953	1963	1974
Total bulkhead length in feet	720	5750	24005	53545
Total number of houses	209	367	688	1171

Detection of spatial patterning of bulkheading was essential to this study, but the approach was kept simple. If the spatial distribution on the developed shoreline for each year is random, the implication would be that each grid cell is equally likely to contain a bulkhead. If the spatial distribution is nonrandom or clustered, the implication would be that some grid cells are more likely to contain a bulkhead than others.

Similarly, the spatial distribution of developments on the entire shoreline is significant to this study.

A set of Wald-Wolfowitz runs tests were made of the hypothesis that bulkheading is randomly distributed on the developed shoreline, and that developments are randomly distributed on the entire shoreline. For this test, runs were defined as adjacent grid cells of identical, say house presence, elements. Runs of each element could be any number of grid cells long. Runs of one element are separated by runs of a different element, say cells with no houses. The runs test allows calculation of the expected number of runs and the variance under the hypothesis of randomness, knowing only the total number of runs actually present and the number of cells containing each type of element. The results of the test show that the developed shoreline was clustered along the entire 815 cell shoreline with a probability of less than .00003 of incorrectly rejecting the hypothesis of random spatial distribution for both 1963 and 1974.

Runs tests for the spatial distribution of bulkheads on the developed shoreline are more central to this study and are presented in Table 2. The results show that bulkheads are nonrandomly distributed on the 1963 and the 1974 shorelines (no tests were performed for the 1937 and 1952 data).

Table 2

Bulkhead Runs Test Results

	1963	1963*	1974
Number of Cells			
Bulkheaded	69	87	189
Unbulkheaded	276	290	290
Number of Runs			
Predicted	111.4	134.9	226.7
Actual	74	102	173
Run Length			
Predicted	1.2	1.3	1.7
Actual	1.9	1.7	2.2
Actual/ Predicted	1.6	1.3	1.3

*Additions of bulkheading to 1963 shoreline.

Also, bulkhead additions, which have an average length of less than 250 feet, are nonrandomly distributed on the space available for bulkheading. For each test, the probability of incorrectly rejecting the hypothesis of randomness is less than .00003. The table also illustrates that the actual average bulkhead run length is longer than the predicted average run length.

4. Discussion

Jones states that rough statewide estimates of yearly amounts of wetlands destroyed before the Virginia Wetlands Act (app. 450 acre/year) and after (app. 25 acre/year) make regulation under the act appear to be very effective in that wetlands destruction was reduced to 5.5% of the original value (13, p. 50). Pre- and postact estimates of amounts of bulkheading added and wetlands destroyed from analysis of aerial photographs provide an interesting contrast.

Linear (5,371 foot) and exponential (14,382 foot) estimates of the amount of bulkheading that would have been added between 1972 and 1974 with no regulation are contrasted with Jones's estimates of 1,300 to 1,400 feet from permit data after regulation began. These contrasts suggest that actual amounts of bulkheading added under regulation were from 7.5% to 26% of the amounts expected (for the exponential and linear estimates, respectively) had the historical trends continued. Neither of these estimates make regulatory effectiveness appear quite as high for bulkheading in this county as the measure suggested by Jones for amounts of wetlands destroyed statewide.

The amount of wetlands destroyed in York County can also be estimated, assuming that the 53,545 feet of bulkheading present in 1974 was installed 15 feet from the toe of the upland bank (the average value) in a continuous fringe marsh at least 15 feet wide. With these assumptions, the amount destroyed would be about 22.4 acres. Considering that 1,163 acres remain on this segment of shoreline, the amount destroyed is about 1.9% of that originally present. Since 56% of the bulkheading present was added between 1963 and 1974, approximately 12.5 acres were destroyed during that period, or about 1.1 acres/year. Jones estimates that .14 acres/year were destroyed in this county during the first two years of regulation (13, p. 20). The implication is that regulation reduced wetlands loss to about 12.7% of the amount expected had historical trends continued. But the model used to estimate wetlands losses in this study is unrealistic. Since wetlands are not a continuous fringe in this county and bulkhead to bank distances are skewed to smaller than 15 feet, the estimate of 1.1 acres/year is probably large and actual/expected loss of 12.7% too small.

Whatever estimate is chosen, regulation appears to have been very effective in reducing the historic rate of bulkheading and wetlands loss. If historic bulkheading practices had continued (keeping the assumption about a continuous wetland fringe), approximately 12% of the current wetlands acreage present would have been destroyed with complete bulkheading. If regulation is <u>just</u> a rate-controlling process, it is

likely that bulkheading will still become complete at a later date. If regulation is to be more than a rate-controlling process, some attention would have to be given to the spatial pattern of bulkheading in the regulatory decision-making process.

Over the historical period covered by this study, most bulkheads have not only been installed close to the bank but closer to each other than random placement would lead us to expect. The implication of this spatial clustering is that the decisions of private homeowners to install a bulkhead have somehow been influenced by the previous decisions of their neighbors. Three common reasons for bulkheading are erosion control, land acquisition, and aesthetic improvement. And it is easy to see how any one of these might be contagious in a neighborhood on a short stretch of shoreline. For instance, erosion might be naturally high or exacerbated by existing bulkheads. Or the change in appearance and increase in amount of property from one bulkhead might be attractive to a neighboring homeowner. However, current state and federal guidelines make it clear that proposed alterations must fulfill some real need and/or result in minimal environmental damage. In many situations, the individual need may be unclear and the incremental damage seem minimal; but as this study shows, there can be a natural tendency for bulkheads to be contagious. Detection of contagious activities in specific areas could lead regulatory agencies to a closer examination of the cause of these activities.

This study has used historical bulkheading data to make inferences about regulatory effectiveness in one locality in Virginia. By all the measures used, regulation seems to have reduced bulkheading and fill activity to small percentages of what projections of historical trends would lead us to expect. But these levels of regulation may not satisfy everyone. For those who feel regulatory decisions should be more closely examined, discovery of spatial clustering of bulkheads, or other activities, could lead to closer examination of the reasons for private bulkheading. Although the results of this study are applicable only to one area, the method could be used with photographic and other historical data to develop careful estimates of regulatory effectiveness.

References

1. Laws of Virginia Relating to Wetlands and Subaqueous Lands. (Issued by the Marine Resources Commission, Newport News, Virginia.) Charlottesville, Virginia: The Michie Company, 1975.

2. Wetlands Guidelines. (Issued by the Marine Resources Commission, Newport News, Virginia, 1974.)

3. Regulatory Program of the Corps of Engineers. 42 FR 37122-37164. July 19, 1977.

4. Gosselink, J. G., Odum, E. P., and Pope, R. M. The Value of the Tidal Marsh. Pub. No. LSU-SG-74-03, Center for Wetland Resources, Louisiana State University, Baton Rouge, 1974.

5. Pope, R. M., and Gosselink, J. G. A Tool for Use in Making Land Management Decisions Involving Tidal Marshland. Coastal Zone Management Journal, 1973, 1, 65-74.

6. Odum, E. P., and Skej, S. S. The Issue of Wetlands Preservation and Management: A Second View. Coastal Zone Management Journal, 1974, 1, 151-163.

7. Walker, R. A. Wetlands Preservation and Management on Chesapeake Bay: The Role of Science in Natural Resource Policy. Coastal Zone Management Journal, 1974, 1, 75-101.

8. Walker, R. A. Wetlands Preservation and Management: A Rejoinder--Economics, Science, and Beyond. Coastal Zone Management Journal, 1974, 1, 227-233.

9. Shabman, L. A., and Batie, S. S. Estimating the Economic Value of Natural Coastal Wetlands: A Cautionary Note. Research Report AE 30, August 1977. Department of Agricultural Economics, VPI, Blacksburg, Virginia.

10. Lynne, G. D. Incommensurables and Tradeoffs in Water Resources Planning. Water Resources Bulletin, 1977, 13, 93-105.

11. Huettner, D. A. Net Energy Analysis: An Economic Assessment. Science, 1976, 192, 101-104.

12. Silberhorn, G. M. York County and Town of Poquoson Tidal Marsh Inventory. Special Report No. 53 in Applied Marine Science and Ocean Engineering, Virginia Institute of Marine Science. Gloucester Point, Virginia, 1974.

13. Jones, J. C. Local Environmental Management--A Case Study: The Virginia Wetlands Acts, 1972-1974. Unpublished masters thesis, College of William and Mary, Williamsburg, Virginia, 1976.

DRIFTING BUOYS FOR OCEAN DATA COLLECTION

Dr. John Garrett
Institute of Ocean Sciences
P.O. Box 6000
Sidney, B.C. V8L 4B2
Canada

Abstract

Development of low cost drifting buoys is now to the point where they may be considered a proven tool for ocean data collection. Recent experiments in preparation for the First GARP Global Experiment have demonstrated lifetimes in excess of a year. An operational data processing and dissemination service will soon be available. Although collection of ocean current data continues to be of interest, buoys intended for other purposes are discussed, using examples from experiments conducted by the Canadian Ocean Data Systems project.

1. Introduction

Techniques for locating and recovering data from remote platforms using polar orbiting satellites have matured to the point where they may be considered operational rather than experimental. Although they depend on the complexity of the sensor system the total costs for each day of operation of simple meteorological buoys are comparable to the cost of a radiosonde or an XBT. Thus buoys of this type can be expected to receive increasing use for routine data collection from presently data sparse areas of the ocean.

The common elements to all such systems are the satellite equipment and ground data processing and dissemination system, and the platform transmitters. The sensors, hull characteristics and use of data will be different from system to system depending on the objectives involved.

2. Satellite Data Location and Retrieval System

Although several experimental systems have been used up to now, such as IRLS, Eole, and Nimbus-6 RAMS, an operational system is planned for the period 1979-1985. The Argos system, as it is called, will be carried aboard a series of operational meteorological satellites beginning with Tiros N, and followed by NOAA-A through NOAA-G. This system will be supported by a data processing and dissemination service called Service Argos, which plans to have observations available within 6 hours after the time they are transmitted. This service is operated by the Centre National d'Etudes Spatiales of France on a cost recovery basis. The following is a summary of information available from Service Argos.

Two polar orbiting satellites carrying the Argos equipment are planned to be in operation at the same time, so that observations can be obtained from any point at least four times per day. However the satellite orbits are not separated by 90° so that these observations will not be equally spaced in time. Also because of the low altitude (830 km) of the orbits data will only be received from a band approximately 5000 km wide centred on the satellite sub track. Hence the age of the most recent data available at any given instant will vary considerably depending on the location of the platform involved relative to the current location of the satellite. As an example of this, the age of the data expected to be available up to a transmission time of 0100 GMT, for the Southern Hemisphere, is shown in Figure 1. The number of passes per day permitting determination of locations depends on the latitude of the platform and

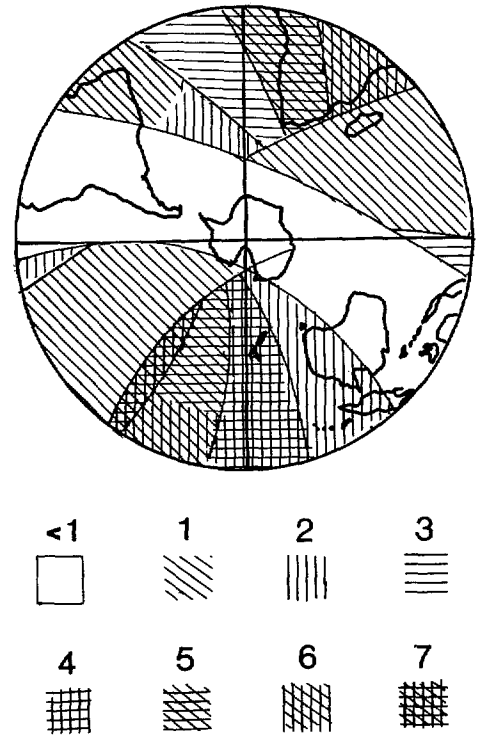

Figure 1. Age of latest data for transmissions up to 0100 hours GMT, in hours.

varies from 6 at the equator to 10 to 12 at ±60° and 26-27 at ±90°. The location accuracy will be better than ±5 km.

The data transmitted from the buoy or platform are stored on the satellite until the satellite passes over one of three ground stations, where it is transmitted to the ground and sent to NOAA in Suitland, Maryland, U.S.A. There the Argos data is separated from the data from other experiments on the satellite, and is relayed to the Service Argos Centre at Toulouse, France. In Toulouse the platform locations are calculated, the telemetry data translated to physical values as requested by the user, and the data is stored or disseminated as requested by the user. The data is available in a variety of forms such as telex, magnetic tape, direct line computer to computer transfer, or mailed listings.

In order to operate with the satellite each buoy or platform must have a suitable transmitter. To insure against disruption of the whole system by poorly designed or constructed transmitters the transmitters must undergo an acceptance and certification process administered by Service Argos. The transmitters already accepted and certified typically weigh 1 kg and have an average power consumption of 60 to 100 mw, including transmissions. The total power requirement for a given platform will of course depend on the requirements of the sensors and signal conditioning.

At the same time that the data received aboard the satellite is being stored in the on board memory it is rebroadcast on the satellite VHF beacon. With a suitable receiver it is possible to receive this data directly and to extract the sensor messages and convert them to physical values. This will minimize the time delay in acquiring the data, but data can only be acquired from those platforms which are in view of the satellite while the ground station is also in view of the satellite. This limits the effective radius of reception of such a station to less than 4000 km. Also determination of the location of platforms requires independent knowledge of the satellite orbit.

3. Reliability and Costs

The costs of obtaining data in this way involve capital costs for the buoy or platform plus operating costs associated with the data processing and dissemination. In order to estimate the cost-effectiveness it is often interesting to estimate the capital cost per unit time or observation by dividing the capital costs for a platform by the time the platform can be expected to serve or the number of data points it can be expected to provide. For many drifting buoy applications the buoys are considered expendable so that the amortization period depends on the reliability of the buoys.

A recent experiment provides an indication of the reliability presently achievable. Twenty drifting buoys measuring sea surface temperature temperature and barometric temperature were constructed for a pre FGGE test as part of the Canadian Ocean Data Systems programme, by Hermes Electronics Ltd. of Dartmouth, Nova Scotia. These buoys were designed to be launched from ships of any type without use of cranes or without the ship stopping, i.e. they were to be simply dropped into the water from deck level. The battery life was to be 6 months in water temperatures of 0°C and one year in water temperatures of 10°C. Eighteen of the buoys were deployed in the Southern Hemisphere and two in the North Atlantic between January and May 1977.

The life histories to present are shown in Figure 2. Half of the buoys had ceased to transmit after 366 days of operation. Of these, two had been deliberately turned off, two had exhausted their batteries after nearly a year, two had failed after being washed ashore and four were premature electronical or mechanical failures. Another buoy has since exhausted its battery after 394 days, while the 9 still transmitting have been transmitting for an average of 450 days (to June 1, 1978). If the two buoys which were switched off are excluded we are left with a population of 18 buoys of which the ninth failed after 394 days. Eleven of the 20 have never gone ashore: the fifth failure among those occurred after 366 days and the sixth after 390 days. It is somewhat difficult to apply classical failure analysis techniques to this sample to estimate Mean Time Before Failures because of the question of how to treat buoys which have gone aground. It seems clear that at least half of the buoys can be expected to be transmitting at the end of a year, which might thus be taken as an upper limit to the time over which their cost can be amortized.

For many buoy applications the buoy will be considered to have gone out of service when it runs aground. The rate at which this occurs will depend on the locations at which the buoys are launched. The 20 FGGE prototypes were generally launched in mid ocean regions and thus might provide an estimate of the grounding rate to be expected from a network covering the whole ocean. It is in fact a conservative estimate since the replenishment of such an array would usually take place on the upstream edges, so that the buoys used for replenishment could expect much longer than average lifetimes. Ten out of the twenty prototypes had either failed or gone aground after 213 days, which might be used as an estimate of the minimum time over which the cost can be amortized.

At the present time the simplest transmitters cost less than $2,000, complete with antenna, while complete FGGE type buoys with barometric pressure and temperature sensors, cost less than $10,000. Thus the average capital cost per day for such a buoy is less than $50 per day and probably less than $30 per day. To this must be added the cost of data location and retrieval. Service Argos estimated that to recover their costs they would have to charge a maximum of $20 per day for calculating the buoy location and converting the telemetry values to physical

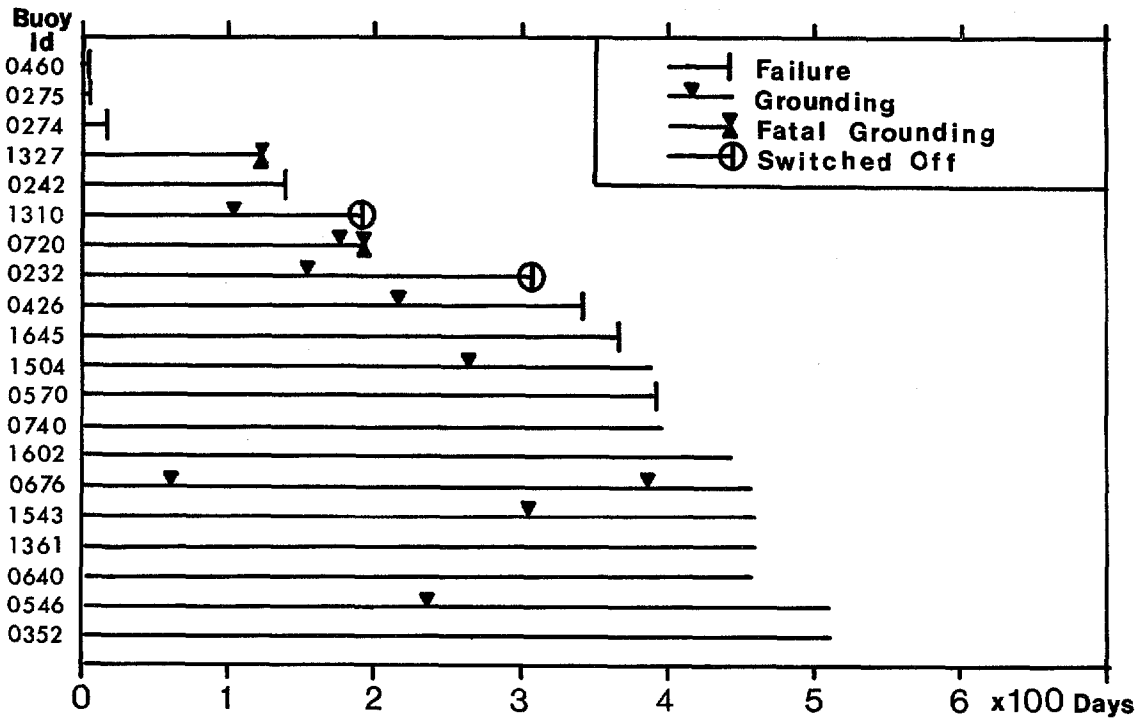

Figure 2. Histories of FGGE Prototypes to June 1, 1978.

parameters. However this figure was based on an estimate of the minimum number of platforms which would be operating so that if more platforms are operating the cost will come down. There will be a cost associated with getting the data from Toulouse to the user, but in any case the maximum total cost is $70 per buoy day, with the probable cost more in the range of $40 to $50 per buoy day. This is of course comparable to the cost of an XBT or a radiosonde.

4. Measurements

To date the principal use of satellite tracked drifting buoys has been to measure ocean currents or the motion of pack ice or icebergs. Results of such investigations have been presented by Cresswell (1978), Kirwan, McNally, Reyna and Mervell (1978) and Martin and Gillespie (1976).

Elementary calculations of the probable effects of wind drag and current shear between the surface and the depth of the drogue, if any, suggest that errors of several centimeters per second should be expected. More complex calculations including wave effects are even less reassuring (Nath, 1977a). A few careful model experiments (Nath 1977b, Vachon 1977) and a few careful full scale tests (Saunders 1976, Vachon 1977) tend to support them. The effects of vector errors of this magnitude could be serious as pointed out in Kirwan, McNally, Chang and Molinari (1975).

However, field data from actual buoys seem to be much more useful and interesting than might be expected. For a typical spar buoy drogued at 20 m or 30 m it is very difficult to determine from the track when or whether the drogue has failed (Kirwan, 1978). The average speeds are entirely consistent with those to be expected from currents.

The Hermes FGGE prototype buoys mentioned earlier carried barometric pressure transducers. For several periods during the experiment three or more buoys were distributed in such a way that the pressure measurements could be used to make an estimate of the vector geostrophic wind. The fluctuations in the north and east components of the wind could be correlated with the fluctuations in the north and east components of the buoy velocities. In 19 out of 24 records of between 36 days and 201 days in length the correlation between the wind component and the buoy velocity component parallel to it was higher than would be significant at the 95% level. Only 7 out of 24 correlations between the wind component and the velocity component directed at 90° to the left of the wind were significant at this level, although it should be noted that all but 5 of the 24 were positive, indicating a tendency to the left of the wind. (These buoys were in the Southern Hemisphere.) The correlation coefficients were typically 0.25 to 0.50, i.e. the fluctuations in the wind explained 25% to 50% of the fluctuations in the buoy motion. The interesting feature is that the regression coefficients for the significant correlations ranged between 0.01 and 0.02, i.e. the buoy speed was between 1% and 2% of the geostrophic wind speed.

This is surprisingly low for a buoy which is undrogued and which has nearly half of its cross sectional area above the water, with a total length of less than 2 meters. The motion also includes not only the buoy response but the response of the surface layer of the ocean in which the buoy is imbedded. On the other hand the geostrophic wind probably overestimates the surface wind so that the response to the surface wind could be higher. The only conclusion that can be drawn is that during periods of light winds even an undrogued buoy provides reasonably good measurements of water velocities.

Whatever the credibility of drifters as indicators of water motion, they can also be used as reliable inexpensive platforms to obtain other types of information. The first large scale example of this will be provided during the First GARP Global Experiment, when an array of 300 drifting buoys provided by 8 different countries will provide barometric pressure and sea surface temperature measurements from the oceans of the Southern Hemisphere. This array will be deployed by the cooperating ships of a number of countries between October 1978 and June 1979.

Other possible surface level sensors would be wind speed and direction and air-sea temperature difference, which would then permit an estimate of the air-sea heat exchange. Also useful and practical would be a wave gauge of some type, with processing circuits on the buoy to reduce the data to a few statistical values for transmission as described by Clayson (1975). This could be combined with satellite remote sensing of wave direction to reduce some of the ambiguities and uncertainties of the satellite measurements.

Oceanographers of course are interested in subsurface data. Many thousands of XBTs are dropped annually to try to monitor just the thermal structure. One obvious alternative is drifting buoys equipped with thermistor chains. Here a choice presents itself. If the buoy does not move with respect to the water column the changes recorded in the temperature structure will reflect change in the structure of the water column, which might be due to internal waves, to heating and cooling or to a variety of other causes. If the ocean temperature field has significant variability on space scales of 100 km a buoy array with a resolution of 100 km will be required to delineate this field, i.e. 100 buoys in an area 1000 km square. The other alternative is to deliberately make the buoy move with respect to the water, so that the thermistor chain provides a transect or a section. Then the number of buoys required to resolve the temperature field depends on the time scale as well. If the time scale of ocean temperature variability is a month, and if the buoys move 300 km in a month, only one third as many buoys would be required as for buoys fixed relative to the water.

To examine the feasibility of this idea at the same time as conducting reliability tests of a new type of thermistor string a few prototypes have been constructed, again as part of the Canadian Ocean Data Systems Project at Hermes Electronics. These buoys, shown in Figure 3, are designed to be blown along by the action of the wind, and hence have a maximum surface area. They will be deployed in the North Pacific during the summer of 1978.

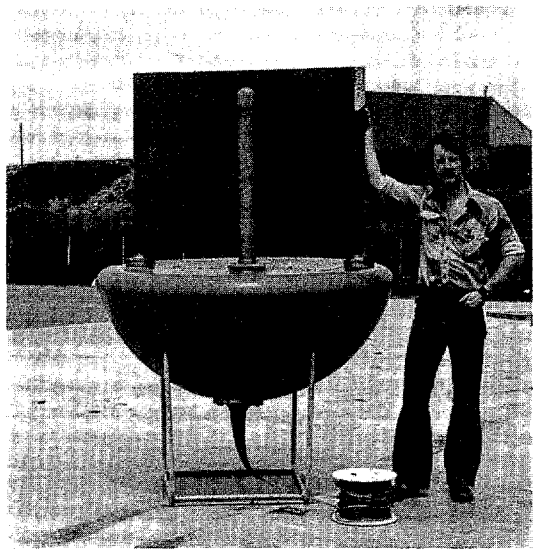

Figure 3. Prototype "Fast Drifter" for thermal structure transect measurements using thermistor chain.

5. Conclusions

The operational use of satellite tracked drifting buoys will be possible with the advent of an operational data processing and dissemination service. Expendable buoys can be cost effective as their reliability permits amortization of their capital cost over periods of 200 to 300 days. A variety of measurement capabilities have already been demonstrated for such buoys and more will be developed soon. Thus we should expect expendable drifting buoys to become an increasingly common tool for various measurements from ocean areas.

Acknowledgements

The buoys described were constructed as part of the Canadian Ocean Data System project which has been managed by John Brooke and Jim Elliott at the Bedford Institute of Oceanography and Graham Smith at Hermes Electronics Ltd. Andy Reid of Hermes Electronics was primarily responsible for the drift buoys. The data were obtained using the RAMS on the Nimbus 6 satellite with the help and cooperation of the NASA Nimbus-6 team.

References

Clayson, C.H. (1975) Wave Data Telemetry via the Nimbus-F Satellite; Proceedings of Conference on Instrumentation in Oceanography held at University College of North Wales, Bangor, 23-26 September 1975.

Cresswell, G.R. (1976) A Drifting Buoy Tracked by Satellite in the Tasman Sea; Aust. J. Mar. Freshwater Res., 27, 251-62.

Cresswell, G.R. (1978) The Trapping of Two Drifting Buoys by an Ocean Eddy., Deep Sea Research (in press).

Kirwan, A.D., G.J. McNally, E. Reyna, W.J. Merrell (1978) The Near Surface Circulation of the North Pacific: J. Phys. Oceanog. (in press).

Kirwan, A.D., G. McNally, M.S. Chang, R. Molinari (1975) The Effect of Wind and Surface Currents on Drifters, J. Phys. Oceanog., 5, No. 2, pp. 361-368.

Martin, Pat, C.R Gillespie (1976) Arctic Odyssey - Five Years of Data Buoys in AIDJEX: Proc. Symposium on Meteorological Observations from Space June 1976, Philadelphia Pennsylvania. COSPAR, IAMAP/IUGG, WMO, AMS.

Nath, J.H., (1977a) Laboratory Validation of Numerical Model Drifting Buoy-Tether-Drogue Systems, Final Report to NOAA Data Buoy Office on Contract 03-6-038-128.

Nath, J.H., (1977b) Laboratory Model Tests of Drifting Buoy and Drogue, Engineering Report for NOAA Data Buoy Office on contract 03-6-038-711.

Saunders, P.M. (1976) Drifting Buoy Lagrangian Test, Final Report of Woods Hole Contract NAS 13-5 with NOAA Data Buoy Office.

Vachon, W.A. (1977) Current Measurements by Lagrangian Drifting Buoys - Problems and Potential : Proc. IEEE Oceans '77, pp. 46 B1 - 46 B7.

A STABLE PLATFORM FOR MICROSCALE STUDIES OF VELOCITY, TEMPERATURE AND CONDUCTIVITY

Bill P. Johnson

Scripps Institution of Oceanography
La Jolla, California 92093

Abstract

In the past ten years, several investigators have constructed instruments to measure small scale processes in the oceans. In attempting to describe these processes, insufficient attention has been given to the problem of the sensors or the recording of body motion relative to the media which is being measured. Many investigators chose to limit their studies to scales which are unaffected by sensor motion or to make certain assumptions about frequencies and amplitudes of the sources of noise. When attempting to resolve microscale phenomena, these problems become acute if not absolutely limiting. An instrument was developed at Scripps Institution of Oceanography in 1974 to attempt to advance the state-of-the-art in ability to accurately resolve these small scale processes. It has at its heart a free falling body which employs a large overmass and uniform drag characteristics to stabilize its motion during data acquisition. In addition, several body motion parameters are carefully recorded. The sensors are selected for optimum resolution in time and space and very careful examination of sampling techniques were undertaken.

HISTORY - VELOCITY MICROSTRUCTURE RECORDER (VMSR)

In 1973 development was begun on a new device which capitalized on the experience gained at SIO with microstructure recorders. While temperature and conductivity micro and fine scale experiments had been done by several researchers (Gregg and Cox, 1971), small scale velocity measurements had not been previously carried out. It was obvious that in order to measure water velocity independent of body motion, a very stable platform would be required. A large spar type apparatus was chosen so that a large overmass and vertical righting moment could be employed. A 25 cm outside diameter 7075-T6 aluminum tube with 1.4 cm wall thickness was fitted with hemispherical end caps to achieve a high ratio of displacement to weight. For descent rate control, the tube was fitted with light weight carbon fiber reinforced "wings" which could be retained alongside of the tube during free fall to the desired depth and then deployed in a horizontal mode. This configuration allowed the fitting of a heavy 26 kg lead weight as low as possible on the instrument to provide a very stable fall characteristic. It was hoped that this configuration would yield the least perturbation in the presence of velocity shear layers as the instrument descended in the ocean.

To verify the behavior of the instrument body, vertical and horizontal accelerometers were fitted to measure any residual motions. These devices are balance beam type accelerometers and thus are also useful for tilt measurements. In order to relate these measured motions with the rotation of the instrument, due to the autorotation of the wing assembly, a magnetometer of the flux-gate type was also installed. This device measures rotational displacement relative to the earth's magnetic field. Wing pitch was selected such that the instrument would have a fall rate of from 5 to 15 cm/sec. Later, computer modeling by Mortensen and Lange (1977) confirmed the applicability of the design approach and experimentally determined data agreed favorably with the computer model. The development of the VMSR occurred at approximately the same time as the Osborn velocity shear probe (Osborn, 1974) which employs the airfoil probe developed by Siddon (1974). The Osborn instrument is more closely tailored to cross flow velocity shear measurements while the VMSR measures finer scale turbulent rates of strain.

Early prototyping of the VMSR employed an FM data acquisition which was selected because of its compatibility with an existing data transcription system. Several test cruises were conducted in the San Diego Trough and the instrument was used on its first cruise in the Gulfo expedition in the Gulf of California in 1974. Prior to the Mixed Layer Experiment (MILE)(August, 1977) in the Gulf of Alaska, a digital data acquisition system was installed which stores data on a cassette recorder. The MILE requirement of working in the surface wave field led to the installation of an hydraulic wing deployment system to positively lock the wings in position. Since horizontal velocity fluctuations are sensed on one of the wing tips, any "flopping" of the wings would introduce spurious velocity signals. This system was removed in preparation for the POLYMODE Local Dynamics Experiment. A conductivity cell and platinum resistance thermometer were then added. The instrument is shown in Figure 1.

THE SENSORS

The method used on the VMSR for velocity measurement is the classic "hot wire anamometry". During the development of this instrument, several types of thermistors were evaluated. Cox et al. (1969) used several glass thermistors in parallel for obtaining temperature measurements. However, the unbacked "flake" was later thought to be

capable of faster response times. The flake consists of thermistor material with leads attached and coated with a thin plastic dialectric material. These flakes were used also as early velocity sensors. Sizes ranging from 20 x 20 x 2 mills to 100 x 200 x 4 mills were used with coatings ranging from .2 to 1 mill. Response characteristics of some of these thermistors were reported by Mortensen (1976). All of the flake variations were extremely fragile and the thin plastic coating was easily destroyed by impact with oceanic biota. An additional problem of the flakes was the relatively high noise level assumed to be associated with the method of lead attachment. The recent availability of substrate backed flakes led to the use of BeO backed flakes for fast temperature measurements and alumina backed flakes for velocity measurements. These units use a gold masking process which seems to reduce the noise problem considerably. We are currently evaluating these units with a thin glass coating on the thermistor material with an uncoated reverse side. These units are very rugged, can be made very small (50 x 50 x 10 mills) and show some promise.

Passive unheated thermistors are used for temperature gradient measurements with one located on a nose cone at the lowest point on the bottom of the instrument and 1 located on a wing tip. Thermistors heated to 40°C above water temperature with a constant current are located 1 cm distant from the temperature measuring thermistor for the velocity gradient measurement. An additional velocity sensor is mounted on a 2nd wingtip.

A 3000 psi digiquartz pressure transducer is mounted on the lower end cap. This device has a nominal 40 kHz output which is period counted (4096 periods of a 2.09 MHz clock) to allow an 8 cm resolution in 2000 m of water. An NBIS Inc. 3 cm conductivity cell is used along with a platinum resistance thermometer (PRT) mounted on a separate pressure case on the lower end cap. The conductivity cell and PRT are mounted in the same horizontal plane 3 cm apart. Response time of the PRT is 300 ms while the conductivity cell has a 3 cm length. At a fall rate of 10 cm/sec these time constants are approximately matched.

The circuit used for the conductivity cell (Fig. 3) is transformerless and thus avoids many of the problems usually encountered with conductivity measurements. A 100 kHz signal is divided by 10 and used to excite two of the four electrodes with a precision constant square wave current. A track and hold amplifier samples the voltage present on the remaining two electrodes at a point 40% and 80% on the square wave excitation wave form. This scheme does not require any correction for the reactance of the cell. The plus and minus voltage is rectified and fed to an optically coupled amplifier and the low impedance signal is then fed to the main pressure case and hence to the data acquisition system. The disadvantage of this circuit is that it requires considerable power (0.8 watt) and is relatively expensive to construct.

In addition to the differentiated velocity and temperature gradients, 3 axis accelerometers, conductivity, platinum resistance temperature, magnetometer and pressure, several engineering parameters are sampled. These include supply voltages, reference voltages and wing deployment verification. The parameters and their resolution and accuracies are shown in Table 1.

DATA COLLECTING SYSTEM

The electronics package located in the large tube is preprogrammed to sample the pressure gauge frequency until the instrument has descended to the desired depth. When trigger depth is reached the wings are deployed into the horizontal position and recording is commenced.

The velocity and temperature signals from the thermistors are actively filtered at 25 Hz, the Nyquist frequency (sample frequency/2) with an 18 db per-octave roll-off and appropriately scaled for a ± 10 volt range. The remaining signals are sampled with a 2.5 Hz sample frequency and under programming control are multiplexed to a 12 bit analog to digital converter.

Six channels are sampled at a 50 sample per second rate with one of the 6 channels subcommutated so that 10 parameters are sampled at 50 samples per second. The serial bit stream thus emanating from the analog to digital converter is passed in alternate seconds of time to 1 of 2 3600 bit memory banks. At the end of 1 second of data collection, data storage is switched from one memory bank to the other and the cassette tape recorder is started and then receives the previous 1 second's 3600 bits of data. The writing on tape requires about 1/4 of a second so that the tape deck is idle 75% of the time. In order that start-stop transients of thetape recorder do not induce noise in the high gain gradient circuits, all signals are passed to and from the tape via optically isolated electronics and the tape recorder has its own battery pack.

At the end of a predetermined elapsed time the recording process is stopped, the ballast weight is jettisoned via an explosive squib and the instrument becomes positively buoyant and ascends to the surface. A leak detector in the lower end cap can terminate the recording process and jettison the ballast also. Hydrostatic backup release systems are fitted to protect against electronic system failures.

We have been able to successfully use entertainment quality cassettes with this recorder and thus are able to record greater than 10 mega bits of data on a 120 minute cassette. At the sample rate of 6 channels x 50 samples per second or 300 x 12 bits per second, we sample 2700 seconds. At a fall rate of 12 cm/sec, we sample 325 meters of water column. The data acquisition system is shown in block form in Figure 2.

DATA RECOVERY

The development of the micro-computer within the last five years has had as great an impact on

oceanography as the development of the transistor in the late 1940's. Fully operational computers can now be hand-carried aboard ship. We use the Tektronics 4051 Graphic Display unit as the basis of our data handling system. This unit has interfaced to it a cassette reader, line printer, hard copy unit and also is interfaced to an IBM computer when used on land. This unit uses a higher level language (Basic) so that sophisticated programming can be accomplished in 10-20% of the time that would be required for a mini-computer system. The entire system costs less than $15,000 and maintenance costs have been less than $1,000/year.

With the Tektronics system we are able to play our recorded cassettes into the graphic unit displaying analog and/or spectral plots and numeric variance data all within minutes after the instrument has been recovered from a launch. The simplicity and versatility of this system has allowed greater attention to the VMSR itself.

SOME COMPARATIVE DATA

Figures 4 and 5 show data taken on a pre-Polymode shakedown cruise and on the MILE experiment respectively. The MILE launch was a near surface deployment and clearly shows the effects of the surface wave field on the motional behavior of the instrument. Any attempt to resolve the measured velocity fluctuations without complete understanding of the motions would obviously be futile.

The San Diego Trough data shows the instrument's response to a velocity shear layer. The fluctuations of vertical velocity measured at the lowest point on the instrument are encountered 1.2 rotational periods later by the wings at the highest point on the instrument and where virtually all of the drag or lift exists. This introduces a perturbation in the fall rate and in the instrument tilt (inserts). The instrument falling at 12 cm/sec with a spatial separation between nose sensor and wing of 250 cm and rotating at 18 seconds per rotation will encounter the shear layer 250/12 = 31.3 seconds or 1.15 rotational periods later. This motional behavior is used to correct the velocity and temperature data recorded.

CONCLUSIONS

The Velocity Microstructure Recorder is a useful tool for accurately describing the velocity and temperature microstructure fields in the ocean. To date more than 100 launches have been made with this instrument. The single most perplexing problem remains the ability to manufacture reliable temperature and velocity sensing probes whose response characteristics are both fast enough and adequately understood. Additional work on this problem is underway.

ACKNOWLEDGEMENTS

My thanks to Dr. R.E. Lange for his guidance on this project. William Fleck, Helmut Moeller and Jack Lucas have given diligent laboratory and at sea support. This work was supported by the Office of Naval Research under Contract N00014-75 C-0152.

REFERENCES

Cox, C. S., P. W. Hacker, B. P. Johnson and T. R. Osborn, 1969, 1969, Finescale of temperature gradient. Marine Temperature Measurements Symp., Trans. Mar. Tech. Soc., June, 95-104.

Gregg, M. C. and C. S. Cox, 1971, Measurements of oceanic microstructure of temperature and electrical conductivity. Deep-Sea Res., 18, 925-934.

Mortensen, A. C., 1976, Optimized system for high resolution measurements of oceanoc temperature and velocity. PhD Thesis, Univ. of Ca., San Diego, 168 pages.

Mortensen, A. C. and R. E. Lange, 1977, Design criteria for wing-stabilized free-fall vehicles. Deep-Sea Res., 23(12),1231-1240.

Osborn, T. R., 1974, Vertical profiling of velocity microstructure. J. Phys. Oceanogr., 4, 109-115.

Table 1

Parameters	Sample Interval	Resolution	Accuracy
Δ V vert.	.02 sec	.1 mm/sec/sec	2 mm/sec/sec
Δ V horiz.	.02 sec	.2 mm/sec/sec	1 mm/sec/sec
Δ T vert.	.02 sec	10 μ°C	NA
Δ T horiz.	.02 sec	20 μ°C	NA
Z acc.	.02 sec	100 μ G	100 μ G
x acc.	.02 sec	1 m° tilt	1 m° tilt
y acc.	.02 sec	1 m° tilt	1 m° tilt
PRT	.2 sec	.04°C	.04°C
Cond.	.2 sec	5 μ U	uk
Rot.	.2 sec	.8°	.8°
Press.	.2 sec	8 cm	20 cm
Eng.	.2 sec	1/4096	

Laboratory calibrations for absolute conductivity are very difficult. Oceanic calibrations are used and are dependent upon the quality of the standards.

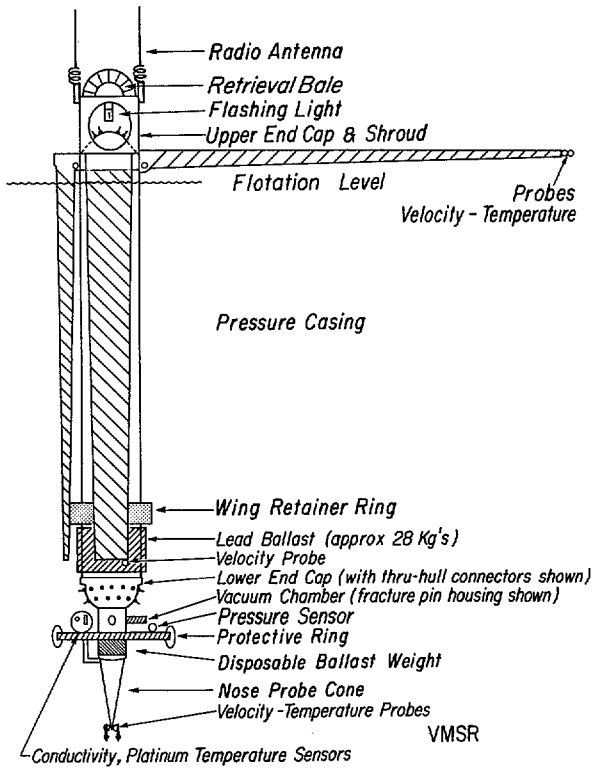

Figure 1

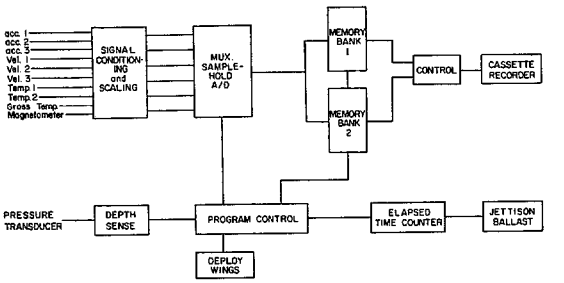

Data Acquisition System

Figure 2

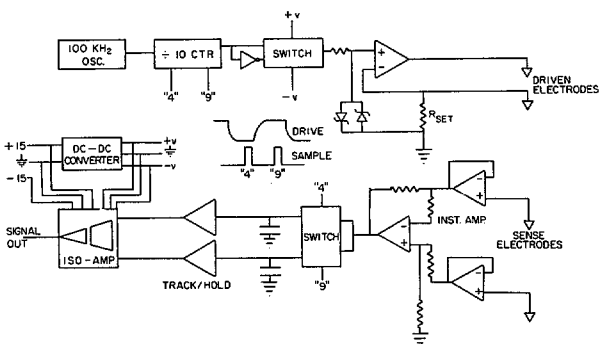

Conductivity Circuit

Figure 3

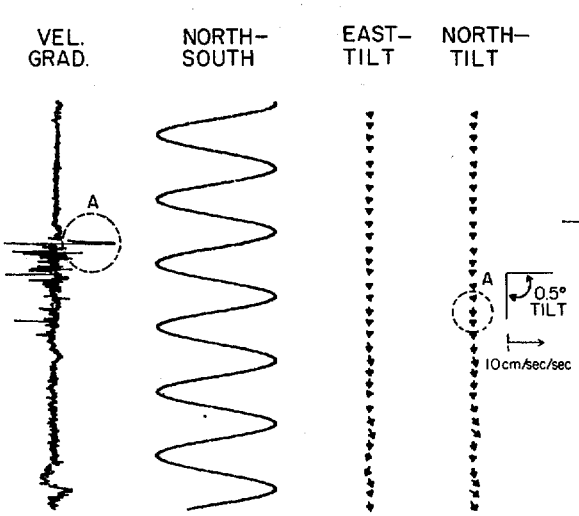

Figure 4

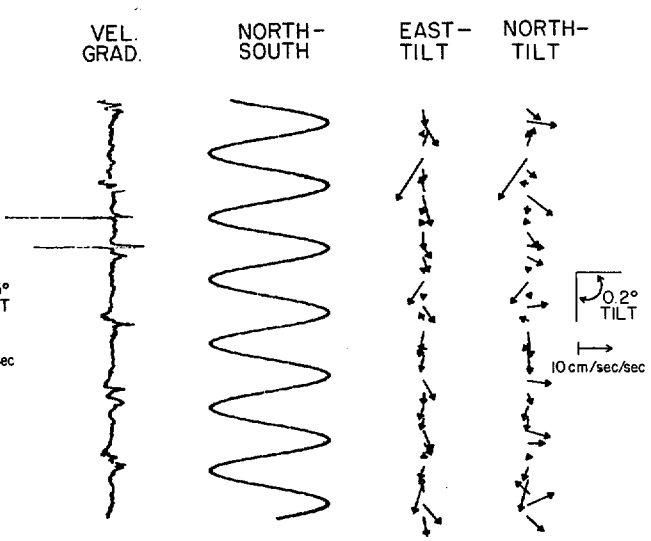

Figure 5

MARINE INSTRUMENTATION: AN ASSESSMENT OF TECHNOLOGY VERSUS NEEDS

Stephen H. Koeppen, Paul C. Etter
Thomas H. Hesselbacher, Anton L. Inderbitzen
MAR, Incorporated
1335 Rockville Pike
Rockville, Maryland 20852

Abstract

This paper summarizes a recently completed study undertaken to provide NOAA's Office of Ocean Engineering with an up-to-date information base on: (1) the needs of government, academia, and industry for marine environmental data, and (2) the state-of-the-art of oceanographic instrumentation in support of these identified data needs. This information was ultimately used to assess the present state of oceanographic sensor technology.

1. Introduction

One of the functions of NOAA's Office of Ocean Engineering is the assessment of the technology and programs related to ocean data acquisition systems and instrumentation. In order to carry out this assessment effectively, it is necessary for OOE to be aware of: (1) the needs of government, academia, and industry for marine environmental data and (2) the state-of-the-art of marine sensors and instrumentation. It was the objective of the present study to provide OOE with a documented, up-to-date information base in these two areas and assess the present state of marine instrument technology based on this information.

The study consisted of three parts. The first part was a review and analysis of previous studies of marine data needs completed over approximately the past 10 years. No new survey was undertaken as it was felt necessary to first summarize and document what had been done to date. A ranking system was developed and applied to these results to arrive at the twenty most importtant marine parameters. The second part was a questionnaire survey of instrument production and development organizations to obtain an up-to-date summary of the state-of-the-art in instrumentation for measuring these twenty parameters. The third part was an identification of deficiencies in marine instrumentation with recommendations for correcting them.

The following two sections discuss the approach, the results, and the conclusions drawn with regard to data needs information, instrument technology, and deficiencies. Section 4 presents recommendations based on these conclusions.

2. Approach

Marine Environmental Data Needs

As mentioned in the Introduction, the scope of ascertaining the needs for marine environmental data was limited to a review and analysis of data needs studies conducted over the previous ten years and documented in report form. The reasons for limiting the scope in this manner were to avoid needless duplication, to identify areas where data needs information is lacking, and to identify problems and pitfalls encountered in conducting data needs surveys.

The approach to the needs part of the study consisted of a number of well-defined, though interrelated tasks. First, a literature search for data needs reports was conducted via telephone calls to cognizant individuals in the marine community combined with a computer search on the NOAA OASIS system of the Oceanic Abstract and NTIS data bases. Reports which were the results of actual surveys as well as other reports documenting data needs of various users were considered. Telephone calls were attempted to one hundred ninety-four individuals resulting in successful contact with one hundred sixty-one. The names of the individuals contacted are listed in Ref. 1 by organization. As a result of these calls, over one hundred documents were received of which forty-six were found to be applicable to data needs. The computer search turned up an additional seven documents. A cursory analysis of these fifty-three reports identified thirteen which contained quantitative information worthy of a detailed analysis. A closer analysis resulted in two of these reports being ruled out as "representative" of marine data needs. The eleven reports used in the detailed analysis are listed as Refs. 2-12.

Based on the cursory analysis of the reports, a classification scheme was developed to classify marine environmental data needs as a framework for the detailed analysis. The classification scheme was developed with the goal in mind of ultimately comparing data requirements with

instrument characteristics to determine deficiencies in the present state-of-the-art. Consequently, the approach taken was to choose classification categories which would lend themselves to a direct comparison with instrument design specifications. The result was a scheme containing six major categories of characteristics:

- Marine Parameter
- Application
- User
- Geographic Area
- Data Specifications
- Operational Considerations

The rationale for this choice of major categories is that the first four categories should tend to determine the requirements in the last two categories, which contain the characteristics directly related to instrument design.

These categories were further broken down as shown in Table 1. The data specifications are the characteristics usually associated with "data needs". Although the operational considerations are extraneous to pure "data needs", it is these types of needs which are quite often expressed in a survey intended to identify instrument deficiencies.

In order to prioritize data needs, a weighting scheme was developed with which to compute an importance score for each marine parameter encountered in the reports. Four assessment criteria were chosen: application, user, volume of data needed and number of requests for data on a given parameter. Within the application category, the first four applications listed in Table 1 were favored over the last two because benefits from their use of ocean data are more immediate. Within the user category, Government was favored over the other users since Government formulates the legislative mandates to which the other users respond. A discussion of the detailed weighting scheme for each of the four assessment criteria may be found in Ref. 1.

State-of-the-Art of Instrument Technology

For the state-of-the-art survey of the twenty top ranking parameters, a two-page questionnaire

Table 1

Breakdown of Six Major Categories of Marine Environmental Data Needs Characteristics

MARINE PARAMETER	USER	DATA SPECIFICATIONS	OPERATIONAL CONSIDERATIONS
• Physical • Chemical • Biological • Geological • Meteorological	• Government • Industry • Academia	• Range • Accuracy • Resolution • Temporal - Sampling Interval - Averaging Period - Experiment Duration • Spatial - Sampling Interval • Vertical • Horizontal - Resolution • Vertical • Horizontal - Measurement Extent • Vertical • Horizontal	• Measurement Technique - Remote - In-Situ - Field - Lab • Physical - Size - Weight • Electrical - Power Requirements • Support - Deployment Platform - Data Recording and Processing - Auxiliary Equipment • Limitations - Temperature - Shock - Pressure - Tow Speed - Other
APPLICATION	GEOGRAPHIC AREA		
• Operational • Forecasting • Regulatory • Monitoring • Baseline • Research	• Deep Ocean • Continental Shelf • Estuary • Lake • River • Arctic/ Antarctic		

was designed. Accompanying this questionnaire was a stamped, return-addressed postcard to obtain a quick indication of who planned on responding and how many questionnaires we would receive. A list of production and development sources was prepared for three categories: federal laboratories, academic/research institutes, and industrial manufacturers. Names for the list were obtained through contacts made during the data needs study, the Sea Technology Buyers Guide/ Directory 1977-78, and personal knowledge. The final mailing list consisted of six federal laboratories, eighteen academic/research institutions, and one hundred sixty-four industrial manufacturers for a total of one hundred eighty-eight potential sources.

3. Results and Conclusions

Marine Environmental Data Needs

The eleven data needs reports analyzed contained information on ninety-seven different marine parameters. The top twenty, resulting from the assessment scheme, are listed in Table 2 in order of descending score. The list includes eight physical parameters, seven chemical parameters and five meteorological parameters. No biological or geological parameters made the top twenty (the top biological parameter, coliform, ranked twenty-fifth and the top geological parameter, bottom geomorphology, ranked fortieth). These rankings tend to indicate either: (1) that within the overall marine community these two categories are not very important, or (2) the published reports do not adequately represent the entire marine community. The latter conclusion is the most probable.

Table 2

Top Twenty Marine Parameters

Temperature	Wave Direction
Salinity	Wave Height
Depth	Tides
Barometric Pressure	Nitrate
Wave Period	Nitrite
Current Velocity	Silicate
Air Temperature	Phosphate
Water Surface Temperature	Humidity
	pH
Wind Velocity	Low Molecular Weight Hydrocarbons
Dissolved O_2	

State-of-the-Art Survey

Of the one hundred ninety-one queries sent out (three sources were sent two questionnaires):

- Ninety-one parties did not respond at all.
- Fifty-one parties returned the postcard saying they had no relevant information.
- Twenty-four parties sent brochures and/ or specification sheets from which sixty-nine questionnaires were filled out by MAR.
- Forty-one questionnaires were filled out and returned by the remaining twenty-five parties (five questionnaires were not applicable).
- More than thirty-three additional questionnaires were promised (as per postcard) but never received.
- Thirty-eight organizations were contacted by phone as a follow-up to the mailing. Some of these responded with questionnaires or literature, others promised to but didn't.

The response of each organization that a questionnaire was sent to is given in Ref. 1. One hundred and five questionnaires thus formed the data base for the state-of-the-art assessment.

Technology Assessment

In the technology assessment phase of the study, the documented marine environmental data needs were compared with the results of the instrumentation state-of-the-art (SOTA) survey. It must be stressed that this comparison suffered from two major limitations which may have a significant impact on the credibility of the results (it was beyond the scope of the effort to assess the degree of credibility afforded by the study; rather, only an attempt to point out potential shortcomings in the analysis was made). These two limitations are as follows:

The first involves the nature of the data needs expressed by the users. Specifically, it must be recognized that there are inherent problems in precisely specifying data requirements, as discussed in some detail in Ref. 1, and that there is no assurance that these stated needs do not reflect the more commonly-measured, and thus familiar, parameters rather than those which actually may be required. The second limitation concerns the instrument capabilities based on manufacturer's specifications. Since there are no universally accepted procedures or techniques available for instrument calibration and intercomparison, no attempt was made to validate manufacturer's stated instrument capabilities.

In spite of these limitations, it was possible to make a number of recommendations regarding marine data requirements, state-of-the-art analysis procedures and instrument development. The detailed conclusions supporting these recommendations may be found in Ref. 1.

4. Recommendations

- Although our SOTA survey indicated that instrumentation to measure the parameters listed below were acceptable to meet the stated needs, follow-up discussions indicate there are problems in the area of reliability and dynamic performance. Therefore, it is recommended that more performance information be sought for these areas before any definitive direction is taken toward new development.

  - temperature
  - salinity
  - depth
  - barometric pressure
  - wave period
  - wave height
  - humidity
  - current velocity
  - air temperature
  - water surface temperature
  - wind velocity
  - wave direction
  - tides

- Those requirements exceeding state-of-the-art capability for the above parameters should be examined in greater detail to determine their validity.

- Instrumentation development should be considered for in-situ or field measurements of the following parameters:

  - dissolved oxygen
  - nitrate
  - nitrite
  - phosphate
  - pH
  - low molecular weight hydrocarbons

- Developmental emphasis in dissolved oxygen sensors should be directed at improving reliability.

- Developmental emphasis in sensors to measure the nutrients (nitrate, nitrite, silicate, phosphate) should be placed on reliable, automated in-situ capabilities. Present measurement techniques involve wet-chemical methods in the laboratory, either afloat or ashore.

- Sensors for in-situ or field measurements of pH need improvements in reliability.

- Further definition of hydrocarbon measurement requirements, in general, is required before any specific assessment of low molecular weight hydrocarbon data requirements can be made.

- Efforts should be made to establish uniform performance criteria, perhaps through standardized performance specifications, for each suite of sensors used in the measurement of any of the twenty parameters identified in this study. Standard specifications should be developed and matched against test results sought from sources other than manufacturers.

- It is recommended that a centralized information system be established in OOE listing all commercially available instruments and ongoing development projects. The system also should include a reference file of performance test data.

- It is recommended that no additional data needs surveys be conducted until the SOTA analysis procedure can be more firmly established and made more credible. A well defined and comprehensive classification scheme for marine instrumentation and means of verifying instrument performance relative to standardized performance criteria must be included in any future SOTA analysis procedure to make it credible and worthwhile.

Acknowledgements

The authors would like to acknowledge the cooperation and assistance of the many individuals contacted during the literature search portion of this study. In addition, we would like to thank the organizations responding to the instrument state-of-the-art survey for taking the time to do so.

References

1. Koeppen, S.H., P.C. Etter, T.H. Hesselbacher and A.L. Inderbitzen, "Marine Instrumentation: An Assessment of Technology Versus Needs", MAR TR No. 207, Final Report, NOAA Contract No. 7-35281, May 1978.

2. Eskite, W.H., Jr., and R. DeRyche, 1977, "Requirements for Marine-Related Data which may be obtained by Satellite Remote Sensing in the Period 1980-1985 and Beyond" (draft). U.S. Department of Commerce, NOAA. Unpublished Manuscript.

3. Haugen, Dean, P., 1972. "Survey of Operational and Research Requirements for Arctic Data". Prepared for National Data Buoy Center, NOAA, under Contract NAS 8-26886. University of Washington, Applied Physics Laboratory, APL-UW 7225, November 1972.

4. Intergovernmental Oceanographic Commission and World Meteorological Organization, 1977. "Integrated Global Ocean Station System, General Plan and Implementation Programme, 1977-1982". IOC Technical Series 16, WMO No. 466. World Meteorological Organization, 37 pp.

5. National Aeronautics and Space Administration, 1977. "Proposed NASA Contribution to the Climate Program", November 1977 Goddard Space Flight Center.

6. Rose, F.W., 1977, "Determination of Design and Operational Criteria for Offshore Facilities", in Satellite Applications to Marine

Technology, Conference Proceedings, November 15-17, 1977, New Orleans, Louisiana, AIAA.

7. U.S. Department of Commerce, NOAA, 1976. "Measurement Requirements for Marine Water Quality Data", a collection of survey responses on file at the Office of Ocean Engineering.

8. U.S. Department of Commerce, NOAA, 1974. "Ocean Instrumentation". Prepared for the Interagency Committee on Marine Science and Engineering, Federal Council for Science and Technology in response to the National Ocean Policy Study, U.S. Senate, November 1974.

9. U.S. Department of Commerce, NOAA, Data Buoy Office, 1976. "Proceedings of the Ocean Profiling Workshop", Bay St. Louis, Mississippi, June 2-4, 1976. National Technical Information Service, Springfield, Virginia, 182 pp.

10. U.S. Department of Commerce, NOAA, National Weather Service, 1977. "Shipboard Environmental Data Acquisition System" (draft), NWS Headquarters (W16), Silver Spring, Maryland.

11. U.S. Department of the Navy, Office of Naval Research, 1969. "National Data Program for the Marine Environment", Volume I, July 31, 1969. Prepared by System Development Corporation under Contract No. N00014-67-C-0559.

12. U.S. Department of the Navy, Naval Oceanographic Office, Marine Sciences Department, 1964. "Table of Proposed Oceanographic Measurement Requirements". Informal Manuscript Report No. 0-15-64, 16 pp.

A SALINITY CHAIN FOR ESTUARINE USE

E.L. Lewis
Frozen Sea Research Group
P.O. Box 6000
9860 West Saanich Road
Sidney, B.C. V8L 4B2

R.B. Sudar
Frozen Sea Research Group
P.O. Box 6000
9860 West Saanich Road
Sidney, B.C. V8L 4B2

Abstract

Preliminary results are presented for sensors with good long-term stability allowing salinity determination from measurements of electrical conductivity and temperature.

A chain of these sensors, multiplexed onto a single electronic driving board within the recorder unit, allows time series measurement of salinity/temperature profiles to within ± 0.02° °/₀₀ and ± 0.01° C over a period of a month. The length of the chain is not limited by any electrical considerations.

For a long time there has been a requirement for a moorable sensor chain to record salinity and temperature values in coastal regions. A major limitation in past attempts to fill this need has been lack of stability in the conductivity sensor cell constant caused by biological activity, dimensional changes, or corrosion. Another problem in chain construction was that most conductivity sensors employed an inductive principle which made it difficult to place them more than a few feet from their associated electronics. Thus a chain would be assembled from a number of individual sensors complete with electronics rather than permitting them to be multiplexed onto a single electronics board, a much cheaper construction. In contrast the four electrode method of measuring conductivity, such has been utilized in the Guildline CTD system and the Neil Brown microprofiler, typically operates at frequencies where the inductive effects associated with long lines separating sensor and electronics no longer are significant.

My modifying electrode design it is possible to minimize the consequences of corrosion or dimensional changes in the immediate vicinity of the electrodes themselves. In the four electrode system described by Dauphinee (1968) two "voltage" electrodes sense a potential difference between fixed points along a current path between two "current" electrodes, the current being varied to keep this voltage constant. The current then provides a measure of the cell conductance. Changes in current flow path due to corrosion etc. will effect the sensed voltage

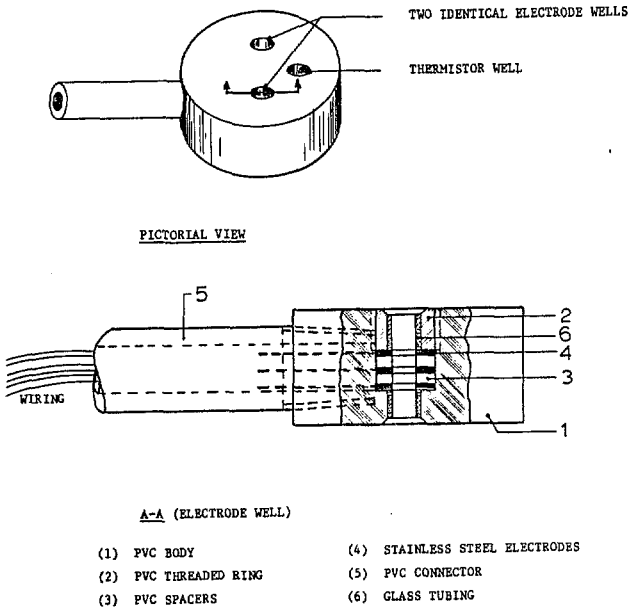

FIG.1 Physical Construction of C-T sensor

particularly if the electrodes carry any current due either to the finite input impedance of the amplifier or because they partially shunt the seawater circuit. A very high input impedance is offered by Dauphinee's circuit and the voltage electrodes are recessed to stay out of the current path. Nevertheless variations in current density over the current electrodes as a result of changing metal/sea water interface conditions can alter the sensed voltage difference. A development of this system used for the Guildline Bench salinometer is described by Dauphinee and Klein (1975). All four electrodes are placed in side arms away from the main current path so that current flow along the path interval containing the voltage electrodes is almost independent of local changes at the electrode surface. Another factor in cell design has been the need to obtain a high enough cell impedance in typical sea water to allow use of easily obtainable electronic circuit components within their normal operating range. This has usually required considerable physical constrictions in current flow which in turn have created a problem in

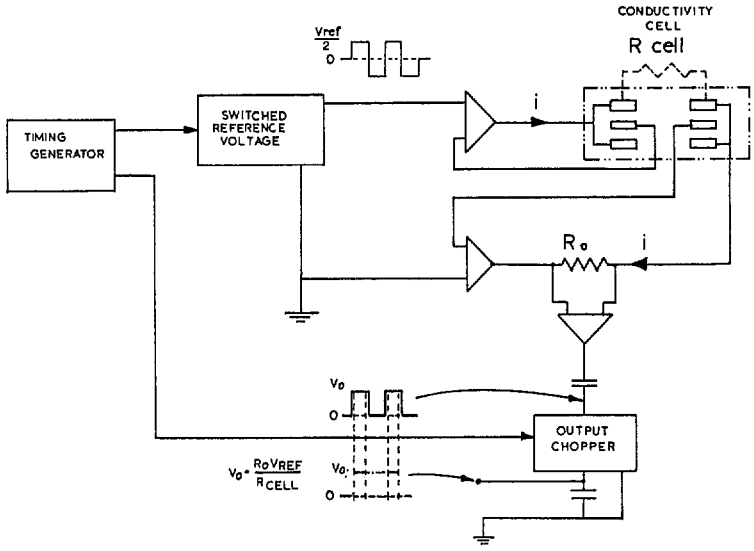

FIG.2 Conductivity Circuit (Schematic)

cell flushing as different water masses move past the sensor in the chain.

A design to minimize these problems is shown in Figure (1) and comprises two electrode wells each containing three electrodes in the form of washers. The two outer current electrodes in each well are short-circuited to give an approximation to a field free space between them and the voltage electrode is placed therein centrally. This ensures no current flow through the voltage electrode and the cell impedance is insensitive to variations in the interelectrode spacing. In one constructional form the main body of the cell is made of PVC plastic and the washer electrodes with appropriate PVC spacers are dropped into cylindrical holes machined in its surface. The spacer/electrode assembly is then set up with an epoxy bond while being compressed by a PVC threaded bushing. Dimensions outside the electrode assembly are critical and two small glass tubes are inserted in each well to be coaxial with the electrode rings; the glass to PVC bond is made with silicon rubber. The impedance of the sea water circuit appears to have only minor dependence on current electrode corrosion, a fact attributable to the symmetry of the thin disc geometry. A third well contains a thermistor that is used in a conventional Wheatstone bridge to determine resistance and hence temperature.

The electronics to drive the conductivity sensors is contained on one 5 x 13 cm printed circuit board and has a component cost of about $50.00. It is shown schematically in Figure (2). The circuit is a variation of that described by Dauphinee (1968). A timing generator produces switching pulses for a reference voltage and output sampling. The reference voltage is applied to an operational amplifier which drives an alternating current between the two pairs of current electrodes through the external sea water so that the potential sensed by the voltage electrodes is forced to be equal to half the reference voltage. The current required to do this is measured across the series resistance R_o and the output chopper times the sampling of this voltage so that transients associated with the square wave current drive through the sea water have decayed away. A typical operational frequency for this system is 250 Hz. Power consumption is approximately 7 milliamps from a 12 volt DC (± 6 volt DC nominal) single unregulated source. Readings can be taken after 5 seconds following application of power. The DC output voltage is directly proportional to the conductance of the cell in the range 0 to 20 mmhos. The constant of proportionality is normally determined by substituting standard resistors in place of the cell and the repeatability of such calibration is within ± 1 μmhos or ± 0.004 mmhos/cm equivalent for the cells used. A limitation of this system is that both the power source and the circuitry must float electrically, being "grounded" to the sea through the conductivity cell electrodes only. Any leakage resistance must exceed a minimum of 100K ohms.

It was considered that results from tests on one cell alone would be of questionable value as variations in calibration might be discovered due to individual mechanical problems, electrical malfunctions etc. In addition if readings from three systems were to change simultaneously, this probably would indicate a variation in the environment rather than in the cells themselves. Thus three lots of electronics were connected to three cells and tests made by interchanging them so that each cell would read the same with any set of electronics and that each set of electronics would produce the same value for a standard resistor. Once this

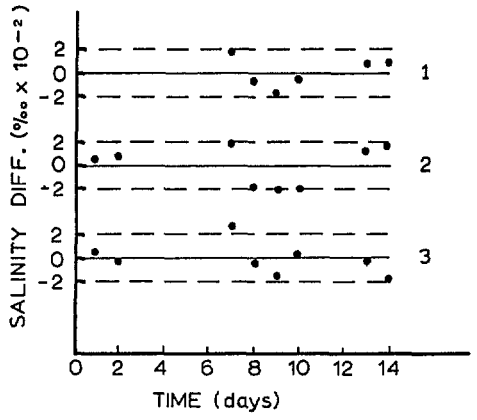

FIG.3 Difference between salinity readings from conductivity - temperature systems and bath salinity determined by bottle samples.

had been done the three cells were placed in an insulated tank of sea water which was being continually mixed by a magnetic stirrer. Samples were withdrawn from this bath at weekly intervals for analysis in a bench salinometer when it was found that the salinity was changing very slowly due to evaporation. At the beginning and end of every test period a standard resistor was used as a check of the entire measurement and recording system. Figure (3) shows results from a typical calibration test in the laboratory.

The sea water in the laboratory tank was sterilized to prevent biological growth . When the cells were placed in the sea they were fitted with a light shield and a pad containing an antifoulant containing tributyl tin. Previous laboratory experiments had shown that this compound in sea water does not contribute to conductivity values at the level of interest. This confirms the results of Waff et al (1975).

Figure (4) section 1, shows a histogram of the salinity values obtained from one of the three cells after four weeks of an eight week period of continual immersion in the sea. A wide spread of values is noticeable. At this stage a diver went to inspect the installation which was in 6 meters of water near the pier off shore from this institute. Although the cells were not taken from the water, his replacement of the antifoulant pads with a more permeable version was sufficient to improve cell flushing which was the cause of the spread in readings. The results just after his visit are shown in section (2) of Figure (4). Subsequently a storm churned up the sediment surrounding the pier and the values of salinity varied widely from one cell to the other. At this stage the instrument was recovered, still keeping the cells beneath sea water in a bucket, and was transported back to the laboratory. After a simple flushing with fresh water all cells and gave values in a range of ± 0.02 °/₀₀, Figure 4 (section 3),

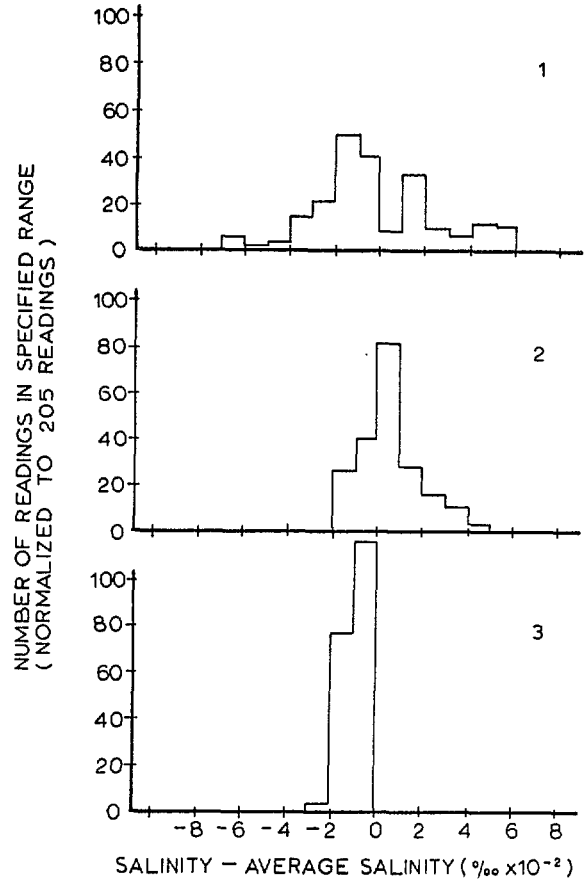

FIG.4 Histograms of the salinity of one cell minus the average salinity of three cells all measuring the same water mass. The three cases shown correspond to; 1. poor flushing due to fouling of the entrance port, 2. improved flushing due to widened entrance ports, 3. perfect flushing in a laboratory stirred bath. All readings were taken at 30 minute intervals.

which contained the measured salinity of bottle samples from the tank.

Following the success of these near shore tests a chain was manufactured consisting of five cells which was deployed from a buoy offshore. For test purposes the chain was wound into a circle of approximately 1m diameter so that the five cells protruded radially inwards and should be in the same water mass. As a result of an accident, the entire assembly dropped from the buoy and fell to the seabed at a depth of 186 meters. The initial results had appeared good but, upon recovery, it was noted that a shift in calibration of approximately 0.08 °/₀₀ salinity had occured in four of the five cells. This shift appears to be permanent and is probably associated with small dimensional changes, perhaps movement of the glass tube in the rubber as a result of the pressure. Tests were started on the effects of pressure on

the cell constant using a pressure vessel but at present are inconclusive in that at 300 psi an instability was introduced in the cell almost certainly the result of water penetration between some components of the assembly. This cell eventually recovered, presumably after the injected water emerged. At the time of writing, June 1978, the chain is back in the sea and results taken over a period of one week are encouraging.

Work is proceeding making cells of the same basic design using different constructional techniques with a view to eliminating the pressure sensitivity. Data from the chain will be collected over longest periods. Hopefully results can be reported during the verbal presentation of these studies at the conference.

References

1. Dauphinee T.M. "Some applications of D.C. and square wave A.C. techniques to undersea measurements". Paper #68-635 Instrument Society of America Annual Conference 1968.

2. Dauphinee T.M. and H.P. Klein "A new automated laboratory Salinometer" Sea Technology 16 1975 pp 23-25.

3. Waff W.B., Wolfgram P.A., and J.P. Rohling "Development of a water quality instrumentation package for long term operation from buoys and other unattended marine platforms. Paper #OT C 2299 Seventh Annual Offshore Technology Conference Dallas Texas 1975 pp 529 - 533.

DEVELOPMENT OF A SMALL IN-SITU CONDUCTIVITY INSTRUMENT

A.M. Pederson
Applied Physics Laboratory
University of Washington and
Sea-Bird Electronics
4735 W. Mercer Way
Mercer Island, Washington 98040

M.C. Gregg
Applied Physics Laboratory and
Department of Oceanography
University of Washington
Seattle, Washington 98195

Abstract

The initial development and testing of a small in-situ conductivity instrument was reported at OCEAN 73.[1] Since then, extensive operational experience has been obtained with a number of these instruments on moorings and on free and tethered platforms that move vertically and horizontally. This experience is reported here, as well as design improvements, and calibration and maintenance procedures. Also discussed are cell flushing characteristics and the problems of matching conductivity measurements spatially and temporally to temperature measurements.

1. Introduction

For details of instrument theory of operation and construction the reader is referred to Refs. 1 and 2. Briefly, the instrument's sensing element is a three-electrode (platinum) flow-through type cell used as a two-terminal device by holding the outer electrodes at the same potential. The cell resistance R_2 between the center electrode and the outer pair is used as one of the bridge components in a patented high quality Wien bridge type oscillator, whose frequency of oscillation is given by the familiar relationship

$$\omega^2 = \frac{1}{R_1 R_2 C_1 C_2} . \qquad (1)$$

R_1, C_1 and C_2 are fixed stable bridge components, and $R_2 = K/\sigma$; σ is the electrical conductivity of the fluid within the cell in Siemens per meter,* and K is the cell constant (determined by cell geometry). Thus,

$$\sigma = R_1 K\, C_1 C_2\, \omega^2 = k_1 f^2 . \qquad (2)$$

Nominal parameter values are $R_1 = 450\ \Omega$, $K = 2000$, and $C_1 = C_2 = 0.033\ \mu F$, resulting in $k_1 \simeq 4 \times 10^{-8}$.

*Multiply S/m by 10 to obtain mmho/cm.

The instrument was originally developed by the Applied Physics Laboratory, University of Washington,† and is now commercially available from Sea-Bird Electronics (under license from the University of Washington) as Model SBE-4 (Figure 1).

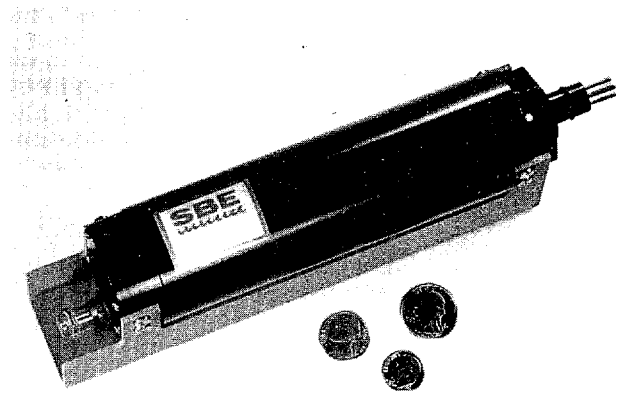

Figure 1. Conductivity meter, SBE Model 4-01.

2. Platinization

A spongy coating of platinum black is deposited on the cell electrodes by electrolysis, using a solution of platinum chloride and lead acetate in hydrochloric acid. The process is called platinization, and results in greatly reduced electrode impedance due to the increased effective surface area.

The cell used in the instrument is purchased from Beckman Instruments with platinization of about 7 coulombs per cm^2 of electrode area. According to Ref. 3, this should be sufficient to ensure low electrode resistance R_s, and high electrode capacitance C_s (hence minimum Z_s). However, Beckman uses a much higher current density while platinizing than is recommended in ASTM Standard

†Partially supported by the Office of Naval Research and the National Science Foundation.

D1125-64 (reapproved 1971). We have experimented with platinizing cells at the lower ASTM current density (1 to 4 mA per cm^2 of electrode area), and have found no significant difference in performance compared with cells platinized at higher currents. We do, however, routinely add another 3 coulombs/cm^2 to all new cells at the ASTM current density, reversing the polarity on the electrodes every 10 to 20 s to minimize hydrogen formation.

3. Static Calibration and Curve Fitting

All SBE-4 conductivity instruments are calibrated at the Northwest Regional Calibration Center (NRCC), operated under the direction of the National Oceanographic Instrumentation Center (NOIC), a NOAA organization. Methods of calibration used by NRCC are described in Ref. 2. The absolute accuracy of the calibration bath is better than 0.01‰ (corresponding to ≈ 0.001 S/m), with long term stability and repeatability probably on the order of ±0.003‰. Calibrations are done over a temperature range of 0 to 30°C at two different salinities to reveal any temperature effects of the instruments.

In the following discussion we will be speaking of residuals ($\Delta\sigma$).

$$\Delta\sigma = \sigma_C - \sigma \ , \tag{3}$$

where σ_C is the measured conductivity of the calibration bath and σ is the conductivity indicated by the SBE-4 instrument. If the simple theoretical relationship $\sigma = k_1 f^2$ is used, we find $\Delta\sigma$ as shown in Figure 2a. Note the relatively poor fit, particularly at higher conductivities. This was the method reported in Ref. 1. It can be shown that most of the positive slope of the curves is caused by the fact that the RC oscillator deviates slightly from the theoretical relationship $\omega^2 = 1/(R_1R_2C_1C_2)$ due to parasitic capacitances in the circuitry. If the oscillator conformed perfectly to the theoretical relationship, the instrument residuals would be as shown in Figure 2b. We see that there is still a concave upward curvature, as well as an apparent temperature effect (at 4.3 S/m there is about 15°C difference in bath temperature between the 24.7‰ and 35.0‰ baths). Some of the temperature effect could be due to temperature sensitivity of the RC oscillator ($\leq$ ±1 Hz over 0°C to 20°C, corresponding to ±0.0008 S/m at σ = 4.3 S/m). However, this is not large enough to account for the observed effect, and it could be in the wrong direction (all instruments show similar characteristics, with the low salinity residuals positive with respect to the high salinity residuals).

In Ref. 4, Jones and Christian showed that electrode polarization impedance is essentially a small resistance (R_s) in series with a large capacitance (C_s), that R_s is inversely proportional to $f^{1/2}$, C_s is approximately inversely proportional to $f^{0.4}$,* and that R_s and C_s are temperature dependent at about -1% per °C and +1% per °C, respectively. The magnitudes of R_s and C_s were found to be dependent on the electrode material, as well as on the chemical composition of the electrolyte. None of the work reported in Refs. 3 and 4 used salt water as the electrolyte--hence the results cannot be applied directly to electrodes used for the measurement of ocean conductivity. There is some evidence that R_s is an order of magnitude larger[5] and that C_s is somewhat smaller for platinum electrodes in salt water than in potassium chloride (potassium chloride was used for much of the work in Refs. 3 and 4). For well-platinized electrodes of the size used in SBE-4 (100 mm^2), it is estimated that R_s is a few tenths of an ohm and C_s is a few hundred microfarads.

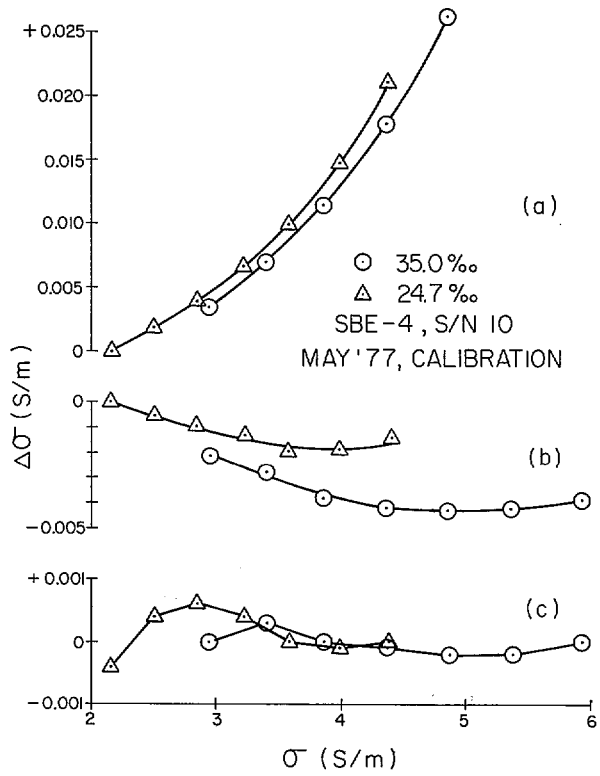

Figure 2. Conductivity residuals for (a) $\sigma = k_1 f^2$; (b) $\sigma = k_2 f^2$, oscillator frequency adjusted to theoretical; and (c) $\sigma = f^2/(a - bf^n)^2 + cT^2$.

If we now assume that R_s and C_s are the same for each of the three electrodes, we can compute the frequency of oscillation to be

$$\omega^2 = \frac{1 - 1.5 \dfrac{R_1 C}{(\frac{K}{\sigma} + 1.5\, R_s)C_s}\left(1 + 1.5 \dfrac{C}{C_s}\right)}{R_1 \left(\frac{K}{\sigma} + 1.5\, R_s\right)C^2} \ , \tag{4}$$

where $C_1 = C_2 = C$. Equation 4 can be solved for σ to yield

*Work reported in Ref. 3 showed that C_s is very nearly independent of frequency for well-platinized electrodes.

$$\sigma \simeq K\omega^2 R_1 C^2 \; (1 + 3R_s\omega^2 R_1 C^2) \left\{ 1 + 1.5\omega^2 R_1 C^2 \; (1 + 6R_s\omega^2 R_1 C^2) \left[\frac{R_1 C}{C_s} - R_s \; (1 - 1.5R_s\omega^2 R_1 C^2) \right] \right\} . \quad (5)$$

Since $R_s\omega^2 R_1 C^2 << 1$, it can be shown that

$$\frac{\delta\sigma}{\delta R_s} \simeq 1.5 \frac{\delta\sigma}{\delta R_2} = -1.5 \frac{\sigma^2}{K} , \quad (6)$$

and

$$\frac{\delta\sigma}{\delta C_s} \simeq \frac{1.5 R_1 C \sigma^2}{K C_s^{\;2}} . \quad (7)$$

It can also be shown that the effects of R_s and C_s, considering their temperature and frequency dependence, are sufficient to approximately explain the shape of Figure 2b.

The observed effects of electrode impedance and oscillator deviations from theoretical are relatively small, and can be eliminated from the static calibration data by an equation of the form:

$$\sigma = \frac{f^2}{(a - bf^n)^2} + cT^2 , \quad (8)$$

where T is in °C and the constants a, b, c, and n are obtained by solving to fit the equation to the calibration data. A program for the HP97 has been written to do this--at least four calibration points are required with one of the points at a different salinity than the other three. The relationship of the empirically derived equation 8 to equation 2 can best be seen by using the binomial expansion on equation 8 to obtain

$$\sigma = \frac{f^2}{a^2} \left[1 + 2\frac{b}{a} f^n + 3\left(\frac{b}{a} f^n\right)^2 + \ldots \right] + cT^2 . \quad (9)$$

All terms are small with respect to f^2/a^2 (the term expected from the theoretical relationship depicted by equation 2). The expansion terms beyond those listed are insignificant. The f^n and f^{2n} terms correct for the nonperfect performance of the oscillator and the additional curvature, while the cT^2 term brings the curves for the two different salinities into alignment. Figure 2c shows the quality of fit typically obtained by this method. The fit is clearly within the limits of accuracy and repeatability of the NRCC facility.

4. Dynamic Calibrations

The above procedure produces an equation that adequately relates instrument output frequency to conductivity under static conditions; i.e., when the instrument has come to equilibrium with the environmental parameters of interest (conductivity, temperature, and pressure). In order to be of practical use, it must be possible to compute salinity and density from a conductivity-temperature-pressure data set under nonstatic conditions. This requires that the frequency response functions of the sensors be known. Pressure sensors essentially respond instantaneously to pressure changes, and cause no difficulties. The response of temperature sensors to a change in ambient temperature is limited by the time required for diffusion through the thermal boundary layer around the probe, the insulating coating or protective sheath, and through the temperature sensitive material. The response of conductivity sensors is generally limited by the flushing time of the cell, although the thermal mass of the cell body can also cause an effective lag due to transfer of heat between the cell body and the sample volume of water within the cell. In some applications on slowly moving vehicles, a pump has been used with the SBE-4 instrument to give a flushing time of 130 ms. Laboratory measurements and computations indicate that for speeds through the water > 1 m/s the free-flow flushing time (in seconds) is 0.25/speed, where speed is in m/s. There is an additional delay time of 0.23/speed due to the cell volume that precedes the first electrode.

For probes moving in linear gradients, the effect of the lag of the probes is to produce a constant offset in the measurements. For up and down casts of a CTD,* or a cycling towed body, the offsets are in opposite directions, and produce a separation of the two temperature-salinity (TS) diagrams.

Due to the existence of finestructure in the profiles, which is defined as changes in the gradients over scales from about 0.5 m to tens of meters, simple lag corrections are not adequate to reconstruct the true profile from the data. This is illustrated by considering a linear gradient with a step change superimposed. The difference in the phase and amplitude response of the temperature and conductivity sensors to this transient produces a salinity spike, which is not removed by a lag correction. To correct for transients such as this, digital filters based on accurate determinations of the frequency response functions of both temperature and conductivity sensors must be used to deconvolve the data. To date, this has not been done, although the problem is being worked on. The principal difficulty has been obtaining the transfer functions of the sensors. The values published by many manufacturers are not adequate since they were obtained by plunging the probes from air into water and thus do not simulate the boundary layers present on probes as used in the ocean.

The problem of salinity spiking can be illustrated with a section of MSR† data from the MILE** cruise. Figure 3 shows the vertical profile of measured temperature, with salinity and density computed from conductivity, temperature and pressure

---

* Conductivity-temperature-depth instrument.

† Microstructure recorder--a free-falling CTD slowed by helicopter-like rotors to a descent rate of about 80 mm/s.

**Mixed Layer Experiment

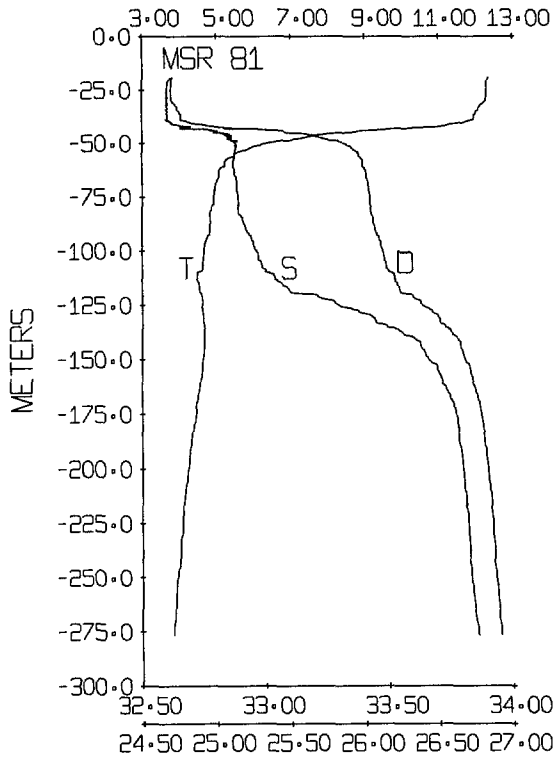

Figure 3. Temperature, salinity and density profile from MSR drop 81.

for water with only a moderate amount of high wavenumber activity (a well-mixed surface layer with a smooth transition into the thermocline). Figure 4 is an expanded section of Figure 3, where a salinity spike can now be seen in an area of sharp temperature gradient. For stormy sea conditions with violent overturning at the base of the mixed layer,

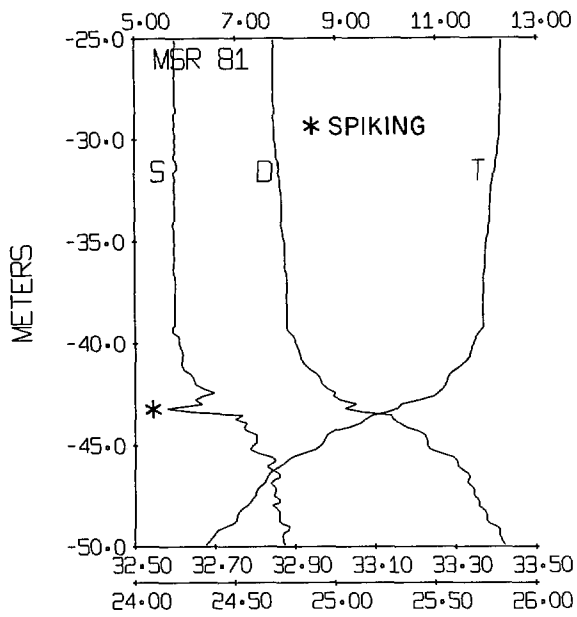

Figure 4. Expanded section of data from MSR drop 81.

the spiking problem is much worse. It is interesting to note that data taken during MILE with other CTD systems also exhibit spiking of several tenths of ‰, even though some of the conductivity cells are much smaller than the SBE-4 cell.

5. Cell Maintenance

Since the SBE conductivity instrument output frequency is determined by the cell resistance, it is important that the electrodes be kept clean. Cell electrodes contaminated with oil, biological growth, or other foreign material will cause the instrument to indicate a water conductivity lower than it really is. As with other types of conductivity cells (including inductively coupled types), fouling within the cell can reduce the effective cross-section area, resulting in the same effect.

If the cell is allowed to dry between usage, salt crystals may form on (and in) the platinized surface of the electrodes. The next time the instrument is used, it will take some time before these crystals are dissolved--in the meantime, electrode impedances may be affected. We therefore keep the cells filled with distilled water between use; this is easily done with a length of Tygon tubing looped between the ends of the cell. An additional important benefit of keeping the cell ends closed is that airborne contamination (of which there is an abundance on most research vessels) can not enter the cell. For long-term storage, we have recently begun using a special storing solution (MT-A-10*) designed to prevent the growth of micro-organisms, a possible source of cell contamination.

For applications where it is not convenient to keep the cells filled with water, such as work in the polar regions, we recommend flushing the cells with distilled water after each use.

6. Cell Cleaning

When checks against water samples or other evidence indicates that a cell needs cleaning, we fill the cell with a 4% solution of MT-6* and let soak for 30 min, then flush with warm fresh water for 1 min.

If severe fouling has occurred (visible deposits on the inside of the cell walls), we fill the cell with a 4% solution of MT-6 and place the entire instrument in an ultrasonic bath for 15 min, then flush for 5 min with warm fresh water.

We tried a number of different cleaning techniques on several conductivity instruments in December 1977, using a calibration bath to carefully determine the effects of each cleaning process on the instruments. Unfortunately, we had no badly

---

*Available from General Chemical Corporation, 4710 S Street N.E., Kenilworth, Washington, D.C. 20027.

contaminated cells to work with, so our test results were more an indication of whether the cleaning process itself would adversely affect the instrument calibration. The tests indicated that either MT-6 or a non-ionic detergent such as Triton X-100 is a satisfactory cleaning agent, the residual chemicals being easily flushed away with a small amount of water. In fact, little or no adverse effects were observed when there was no flushing after cleaning other than that due to normal bath stirring.

7. Resolution and Noise Level

To obtain maximum resolution, some form of period counting should be used. In a typical application, the time interval generated by 1408 periods of the SBE-4 signal is measured by a 5-mHz clock. A 5-Hz sample rate is used, since the count is completed in less than 0.2 s. The resolution (least count) varies from 5.6×10^{-6} S/m at $\sigma = 2.5$ S/m to 1.6×10^{-5} S/m at $\sigma = 5.0$ S/m.

In Figure 5 the noise level of the instrument is shown by the spectrum of a quiet section of MSR data taken in a fjord. The spectral level of the noise is about 5×10^{-11} $(S/m)^2/Hz$, corresponding to an rms value of 1.1×10^{-5} S/m over a 2.5-Hz bandwidth. For period counting, the theoretical spectral level due to the least count is given by $(\text{least count})^2/6$ (see Ref. 6). Because the least count value for these data is 8.6×10^{-6} S/m, the corresponding spectral level due to quantization only is 1.2×10^{-11} $(S/m)^2/Hz$, or 5.5×10^{-6} S/m rms over a 2.5-Hz bandwidth. Since this is considerably less than the observed noise level, Figure 5 represents the inherent noise of the instrument.

How well salinity can be resolved is of ultimate interest to the oceanographer. The system noise in the conductivity, temperature, and pressure channels limits the sensitivity of the salinity data, and that of other derived parameters such as N^2 (the stability frequency) and the gradient Richardson number.[7] The variance of the salinity noise, Var_S, is given by

$$Var_S = \left(\frac{\partial S}{\partial T}\right)^2 Var_T + \left(\frac{\partial S}{\partial \sigma}\right)^2 Var_\sigma + \left(\frac{\partial S}{\partial P}\right)^2 Var_P \ . \quad (10)$$

The partial derivatives are the sensitivities of salinity to temperature ($\delta S/\delta T \simeq 0.8$), conductivity ($\delta S/\delta\sigma \simeq 10$), and pressure ($\delta S/\delta P \simeq 4.2 \times 10^{-8}$). The variance of conductivity, Var_σ, is just the square of the rms noise computed from Figure 5 ($Var_\sigma = (1.1 \times 10^{-5}\ S/m)^2$). The variance of temperature, Var_T, is derived from Figure 6, a plot of the spectral level of the companion SBE temperature sensor from the same MSR drop from which Figure 5 was obtained. The temperature spectral noise level is $\simeq 6 \times 10^{-9}$ $°C^2/Hz$, or 1.2×10^{-4} °C rms over a 2.5-Hz bandwidth. Thus $Var_T = (1.2 \times 10^{-4}\ °C)^2$. Similar data are used to compute $Var_P \simeq (27\ \text{pascals})^2$. When these values are used in equation 10, we find

$$Var_S = \underbrace{9.2 \times 10^{-9}}_{T} + \underbrace{1.2 \times 10^{-8}}_{\sigma} + \underbrace{1.3 \times 10^{-12}}_{P} \ . \quad (11)$$

$$= 2.12 \times 10^{-8} \ .$$

The rms noise level in salinity is therefore $(2.12 \times 10^{-8})^{1/2}$, or 1.5×10^{-4}‰.

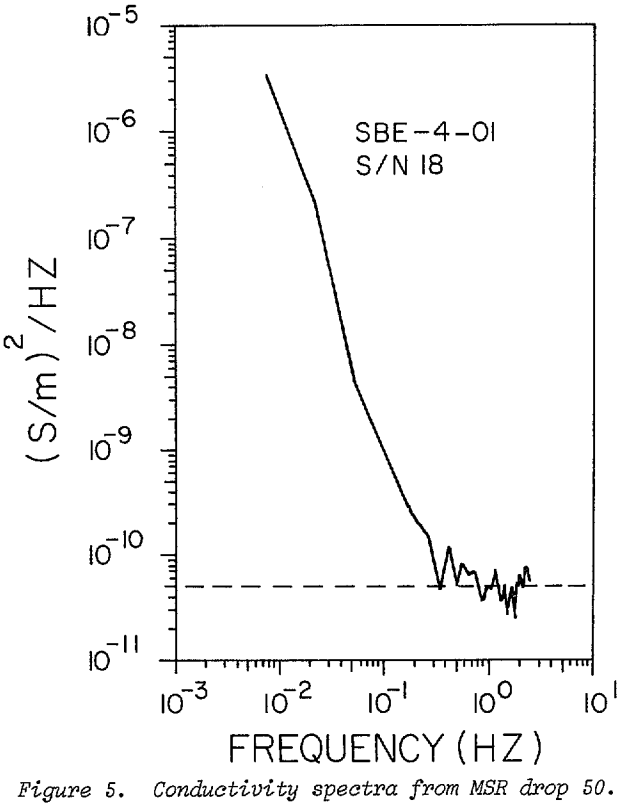

Figure 5. Conductivity spectra from MSR drop 50.

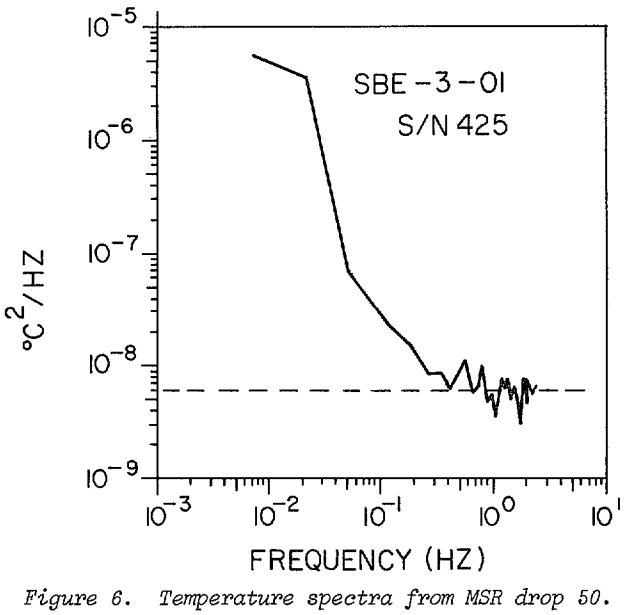

Figure 6. Temperature spectra from MSR drop 50.

8. Circuit Modifications

Our first two conductivity instruments were built for use with SPURV* in 1973,[8] and since that time about 30 more have been built for a number of different organizations in a variety of applications. Initially, we had some problems with long-term stability due to galvanic currents flowing between the instrument case and the cell electrodes, and because of improper cell cleaning procedures. In the spring of 1977 we devised a method of isolating the electrodes from the rest of the circuitry with large capacitors, thus eliminating the galvanic current problem. The modification causes a small shift in the instrument calibration constants, primarily because of a 1-megohm resistor in parallel with the cell resistance now required to bias the input stage FET. However, the effects on instrument calibration due to temperature coefficients or aging of the isolation capacitors are negligible.

Galvanic currents through the electrodes are now believed to be the cause of the -0.002 S/m drift observed in the 87-h bath test reported in Ref. 1. A similar bath test performed in December 1977 after dc isolation of the electrodes showed almost no detectable drift during an 89-h test of two instruments (+0.0001 and -0.0001 S/m).

The galvanic current problem first arose when it was found necessary to hard-wire the instrument case to electronic ground in certain RF-noisy environments to prevent spurious modulation of the output frequency. Recently, we have added RF chokes inside the instrument in the power, ground, and signal lines, as well as additional filtering on the internal regulated supply voltage. These changes have made the circuit immune to stray RF fields, and it may no longer be necessary to hard-wire the cases to electronic ground in noisy environments. However, to be on the safe side, we still recommend case grounding unless there are compelling reasons for having the whole instrument floating electrically.

9. User Experience

Our best results have been obtained during the past year, after dc isolation of the electrodes. We had a conductivity meter on each of two moorings at 1100 m depth for 25 and 8 days, respectively, during MATE.† Calibrations at NRCC before and after the MATE cruise showed drifts in $\Delta\sigma$ of +0.001 and -0.0005 S/m for the 2-1/2 month period between calibrations. When a single point calibration check was made 5 months later, additional drifts of +0.0005 and -0.0005 S/m were observed. These results were obtained with no cleaning, but with the cells kept filled with distilled water between use.

A third SBE-4 instrument was used on SPURV during about 20 h of operation at depths to 1500 m during MATE. Before and after calibrations for this instrument showed a drift in $\Delta\sigma$ of -0.0007 S/m, with a subsequent drift of +0.0005 S/m during 5 months of non-use. Again, no cleaning was performed and the cell was kept filled with distilled water between use.

Four SBE-4 instruments were used on a towed CTD system in tests in Puget Sound and during the MILE cruise, again without cleaning. For reliability, the towed system had two pairs of temperature and conductivity instruments. Calibrations for the two conductivity instruments used in the Puget Sound tests showed drifts in $\Delta\sigma$ of -0.0005 and +0.0005 S/m during the 2-1/2 month period. Another calibration 5 months later showed additional drifts of -0.0005 and +0.001 S/m. Before and after calibrations for the two conductivity instruments used during about 140 h of towing during MILE showed drifts in $\Delta\sigma$ of +0.001 and -0.01 S/m. The excessive drift in the one instrument apparently occurred catastrophically prior to cruise operations, since the offset between the two instruments was relatively constant throughout the cruise. The drift was caused by an electronic failure rather than by electrode contamination.

Five SBE-4 instruments were used during the summer of 1977 on a 9-m vertical array which was towed in near-surface estuarian waters of Puget Sound.[9] Calibrations by NRCC showed drifts in $\Delta\sigma$ of less than ±0.002 S/m for all instruments during the 6-month period between calibrations. The cells were kept filled with distilled water during periods of non-use.

In yet another application, an SBE-4 instrument was used in Puget Sound tests and during MILE on the MSR system. Calibrations at NRCC before and after these experiments showed a drift in $\Delta\sigma$ of about -0.002 S/m during the 4-month period. A single point calibration 3 months later showed an additional drift of -0.002 S/m.

Note that, due to the form of equation 3, only positive changes in $\Delta\sigma$ can be attributed to electrode contamination. Since a number of drift trends in $\Delta\sigma$ were negative, we tend to believe that instrument drift is dominated by electronic drift rather than cell contamination. There are exceptions, of course. Several years ago an SBE-4 instrument was used on a near-surface mooring for 30 days off the mouth of the Columbia River. After that period of time, visible organic growth had contaminated the interior of the cell, the instrument output was noisy, and $\Delta\sigma$ had shifted by about +0.03 S/m.

10. Summary

Since first reported,[1] extensive operational experience has been obtained with about 30 of the instruments on moorings and on free and tethered platforms moving both vertically and horizontally through the water. This experience has shown typical long-term stabilities of ±0.0003 S/m per month. While fouling remains a potential problem, evidence suggests that it is not a serious problem except in near-surface moorings or in heavily polluted waters.

---

*Self-Propelled Underwater Research Vehicle.

†Mid-ocean Acoustic Transmission Experiment.

Dynamic calibration, including flushing characteristics, is an area that needs further work to reduce salinity "spiking." This is a problem common to all conductivity sensors. In this instrument, flushing time can be controlled with an external pump--not a viable technique with some types of cells.

Since the instrument output is an FM signal, resolution is dependent on the counting method used. In a typical application, resolution is 1 x 10^{-5} S/m at five samples per second, and the spectral level of instrument noise is 5 x 10^{-11} $(S/m)^2/Hz$, corresponding to an rms noise level of 1 x 10^{-5} S/m over a 2.5-Hz bandwidth.

Acknowledgments

The preparation of this paper was partially supported by the Office of Naval Research (by the oceanography section of ONR through the Oceanic Microstructure Program, and by the acoustic section of ONR through the MATE program). We are indebted to Larry Murdock of NRCC for consistently good calibrations, to Eric Aagaard (APL-UW) for instrument mechanical design and flushing characteristic computations, and to Bob Francois (APL-UW) for measurements of cell flushing characteristics.

References

1. A.M. Pederson, "A small in-situ conductivity instrument," Proceedings of OCEAN 73, IEEE International Conference on Engineering in the Ocean, pp. 68-75, September 1973.

2. M.C. Gregg and A.M. Pederson, "High resolution salinity measurements," Instruments and Methods in Air-Sea Interaction (Text from NATO Advanced Study Institute), Ustaoset, Norway, April 1978 (in press).

3. G. Jones and D.M. Bollinger, "The measurement of the conductance of electrolytes," Journal of the American Chemical Society, Vol. 57, pp. 280-284, February 1935.

4. G. Jones and S.M. Christian, "The measurement of the conductance of electrolytes," Journal of the American Chemical Society, Vol. 57, pp. 272-280, February 1935.

5. R.G. Paquette, "A modification of the Wenner-Smith-Soule salinity bridge for the determination of salinity in sea water," University of Washington Oceanography Department, Technical Report No. 61, Ref. 58-14, August 1958.

6. J.D. Irish and M.D. Levine, "Digitizing error from period and frequency counting techniques," Deep Sea Research, Vol. 25, pp. 211-219.

7. M.C. Gregg, "The effect of bias errors and system noise on parameters computed from T, C, P and V profilers," submitted to Journal of Physical Oceanography.

8. H.R. Widditsch, "SPURV--The First Decade," Applied Physics Laboratory, University of Washington, APL-UW 7215, October 1973.

9. G.B. Gardner and J.D. Smith, "Turbulent mixing in a salt wedge estuary," Hydrodynamics of Estuaries and Fjords, Elsevier Scientific Publishing Co., Amsterdam, 1978.

EVALUATION OF METAL-FILM TEMPERATURE AND VELOCITY SENSORS AND THE STABILITY OF A SELF-PROPELLED RESEARCH VEHICLE FOR MAKING MEASUREMENTS OF OCEAN TURBULENCE

James D. Irish and Wayne E. Nodland

Applied Physics Laboratory
University of Washington
1013 N.E. 40th, Seattle, WA 98105

Abstract

Metal-film temperature and velocity sensors are being added to the Applied Physics Laboratory's Self-Propelled Underwater Research Vehicle (SPURV) to extend its measurement capability to turbulence scales. Before making field measurements, the sensors are being evaluated in the laboratory and the vibration level of SPURV is being measured to evaluate its stability as a platform from which to make turbulence measurements. The vibration is measured along the three major vehicle axes (vertical, horizontal, and longitudinal) using accelerometers. Field measurements were made with the accelerometers and the records integrated to obtain velocity spectra which are compared with typical measurements of ocean turbulence. The vehicle's motion is below the turbulence spectra when ocean turbulence dissipation is above 10^{-4} ergs/cm^3/s, except at a multiple of the motor rotation frequency where the vibration appears as a strong peak.

Electronics for remote operation of the metal-film temperature and velocity sensors were developed. To evaluate the sensors and electronics, test facilities were built for both static and dynamic calibrations. A temperature-controlled bath is used for static temperature calibrations. A submerged jet mounted within the temperature bath is used for static velocity calibrations. A thermal plume tank is used for dynamic temperature response calibrations of both the temperature and velocity sensors. The dynamic velocity calibration is made by oscillating the sensor within the static jet with a shaker pot.

Results of these tests show that the sensor frequency response can be adequately determined, and that it extends to high enough frequencies to resolve turbulence fluctuations. The temperature sensor's noise and drift are low enough that good temperature measurements to turbulence scales can be made. However, poor stability and high noise in the velocity sensor make the measurements unreliable, and more work is being done in an attempt to improve the sensor.

Introduction

In experimental oceanographic research, many different types of measurements and techniques are required to sample properly the physical processes occurring in the ocean. Measurements are required as a function of both time and space. The Applied Physics Laboratory (APL) of the University of Washington has developed and utilized unmanned, free-swimming submersible vehicles to make horizontal spatial measurements. These vehicles have been given the acronym SPURV for Self-Propelled Underwater Research Vehicle. Development began in 1958; since that time, the navigation and data-collection systems in the prototype and later vehicles have been modified to meet different needs. These needs include studies of thermal structure (McKean and Ewart, 1974; Ewart, 1976a) and dye diffusion (Ewart and Bendiner, 1974a) and support of acoustic measurements (Ewart, 1976b; Ewart, Irish and Olson, 1977).

The two current versions of SPURV are designated SPURV I and SPURV II. Further information on the SPURV I vehicles can be found in a report by Widditsch (1973). The lower-frequency temperature and conductivity sensors carried on the SPURVs were developed at APL and are described by Pederson (1969 and 1973). A fluorometer for diffusion measurements was also developed at APL for SPURV, and its use is described by Ewart and Bendiner (1974b). We are currently increasing the measurement capability of SPURV II to include water temperature and water velocity sensors with a sufficiently high frequency response to resolve turbulence and dissipation scales. While developing the new sensor package, we are also investigating the stability of SPURV II as a platform for making the high-frequency measurements, studying the behavior of the individual sensors, and comparing the results with expected signal levels in the ocean.

Vehicle Motion Compared with Expected Turbulence Levels

Knowledge of the vehicle's motion (vibration) is critical for interpreting the high-frequency velocity and temperature measurements. It is impossible to differentiate a true high-frequency velocity signal from a high-frequency vibration

that moves the sensor. Also, vertical motion of the temperature sensor in a temperature gradient will produce a false temperature signal.

To measure the vehicle motion, a three-axis complement of force-balanced accelerometers (Sundstrand, Model QA-1100-T2) was mounted as far forward as possible in the new SPURV II configuration (see Figure 1). The accelerometers were individually calibrated on a shaker table at the University of Washington. Also a self-calibration was done by injecting a signal into the accelerometers' self-test input according to the manufacturer's specifications. The results of the two methods agreed.

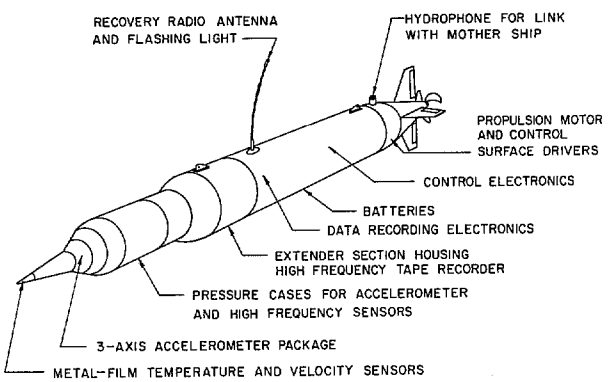

Figure 1. The SPURV II vehicle for turbulence measurement.

Accelerometer measurements were made during the summer of 1977 to evaluate the new vehicle configuration and to compare the results with expected turbulence signals. The signals from the accelerometers were passed through a bandpass filter (8 Hz to 1400 Hz) before recording. All resulting spectra were corrected for the sensor and filter responses.

Figure 2 shows three acceleration spectra with SPURV II traveling at 3.5 m/s. The longitudinal vibration was less than the vertical motion or horizontal cross-axis motion. Several single and multiple peaks are seen in the record which are due to natural vehicle vibration modes and to forced oscillations induced by the propulsion motor. The largest amplitude peak occurs at 547 Hz, and is related to the motor speed. The motor commutator slot frequency is 28 times the motor frequency, or about 1130 Hz, which is double the frequency at which this peak occurs. It is not clear why a large vibrational peak should appear at a sub-harmonic of the commutator slot frequency. It probably is not an electrically induced signal because it does not immediately disappear when power to the motor is shut down, but decays rather slowly as the vehicle slows down.

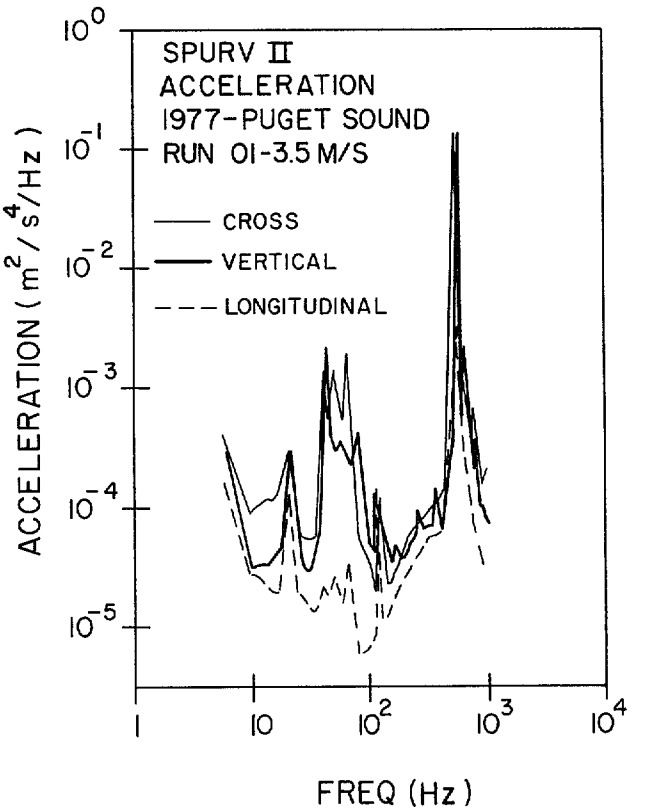

Figure 2. Acceleration spectra from three-axis accelerometer.

Another series of measurements was made with SPURV II traveling at four different speeds between 3.5 m/s and 1.6 m/s. The acceleration spectra were integrated to obtain velocity spectra for comparison with measurements of oceanic turbulence. The results for the vertical axis are plotted for all speeds in Figure 3. The overall vibration decreases as vehicle speed decreases. The peaks labeled 1, 2, 3, and 4 are due to forced oscillations. The peaks labeled 2 occur at the basic motor rotational frequency of 41 Hz at the highest speed and decrease to 22 Hz at the lowest speed. The peaks labeled 1 are at half the motor frequency, decreasing from 21 to 11 Hz. The peaks labeled 4 (not completely resolved in frequency) occur at the commutator slot frequency, and the peaks at 3 are at one-half the slot frequency. The peaks at 3 are the major contamination in our turbulence measurements. The peaks labeled A through F do not change frequency with motor speed, and are natural frequencies in the vehicle itself.

Since the total vibrational energy decreases with velocity, the vehicle would provide the best background for the high-frequency measurements when traveling at the slowest velocity for which it is stable (about 2 m/s). To provide a worst-case estimate, we will use the 3.5 m/s spectra for comparison with expected levels of oceanic turbulence.

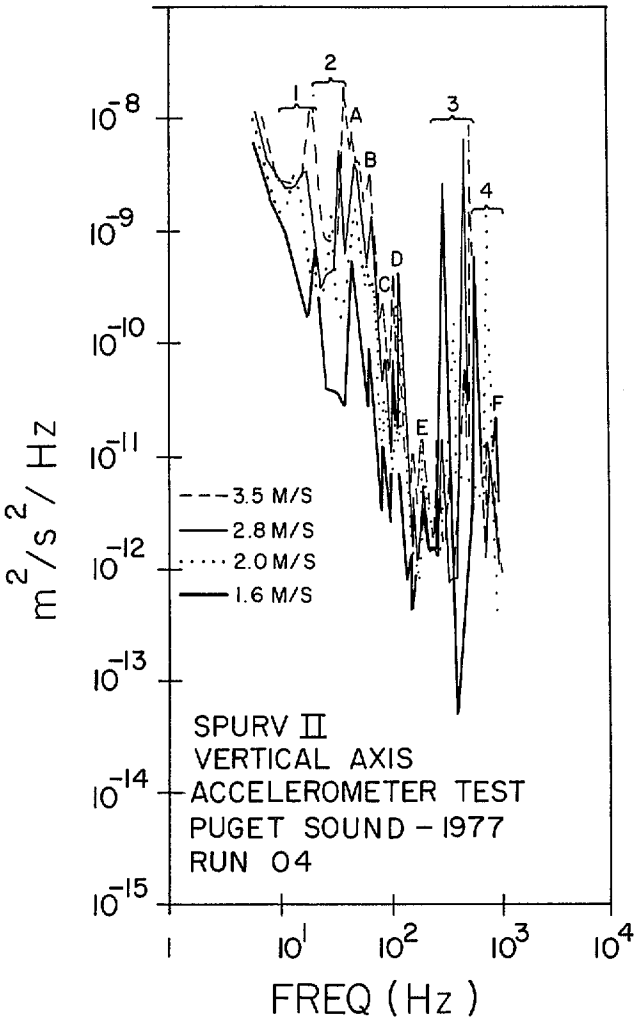

Figure 3. Velocity spectra from vertical accelerometer at four vehicle speeds. Peaks 1 through 4 are due to forced multiples of the propulsion motor frequency. Peaks A through F are natural vehicle vibrations.

Vertical motion of the temperature sensor in a vertical temperature gradient will contaminate the temperature measurements. The amount of contamination was estimated by integrating the vertical velocity spectrum to get displacement, and then multiplying by the vertical temperature gradient to get an equivalent temperature spectrum. Since theory assumes turbulence on these scales is isotropic, vertical and horizontal measurements should be equal. Our vibrational contamination is more than 40 dB below the vertical temperature-gradient spectra taken by Gregg (1977) in the North Pacific thermocline, and more than 50 dB below his measurements beneath the equatorial undercurrent (Gregg, 1976). Our estimated contamination is more than 60 dB below horizontal spectra taken by Nasmyth (1970) beneath the thermocline off Vancouver Island. Therefore, we do not expect that vibrational effects will be observable in our temperature measurements.

The metal-film velocity sensor is sensitive to longitudinal motions of the vehicle and fairly insensitive to vertical and cross vibrations. The apparent velocity vector (mean vehicle velocity plus turbulent fluctuations) is very close to the longitudinal axis. We will use the longitudinal spectrum at 3.5 m/s for comparison with expected turbulence levels.

Turbulence theory predicts that at high wavenumbers the energy density depends only on the kinematic viscosity ν and the rate of energy dissipation ε. With this assumption, dimensional arguments lead to a so-called Universal Turbulence Spectrum. Assuming $\nu = 0.015$ cm^2/s (which is typical of sea water at 8°C), we used the method of Stewart and Grant (1962) to graph a family of curves for different dissipation rates. Figure 4 shows these universal spectral curves for dissipation rates between 10^{-4} and 10 ergs/cm^3/s.

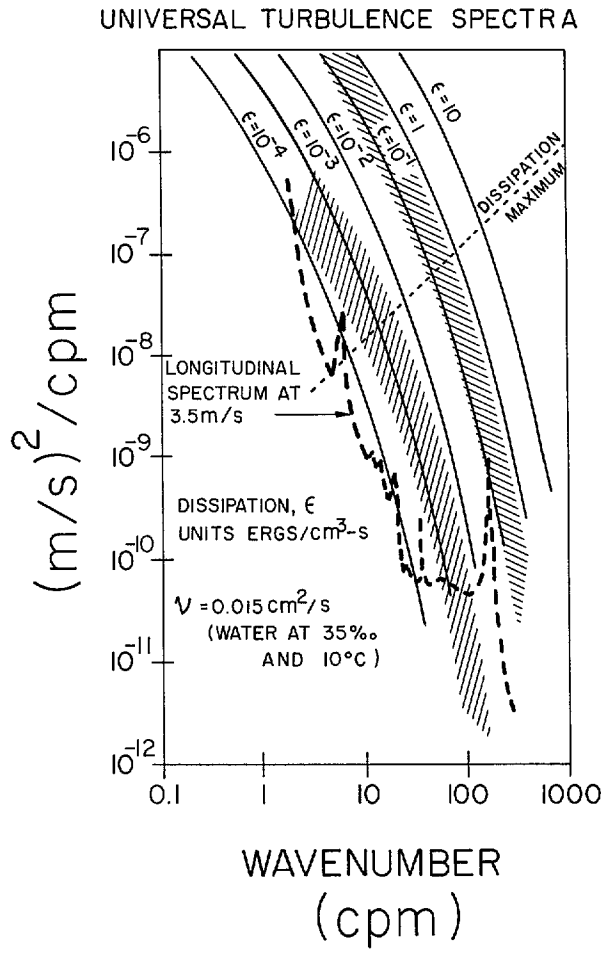

Figure 4. Comparison of SPURV vibrations with theoretical dissipation rates between 10^{-4} and 10 ergs/cm^3/s and rates measured by Nasmyth (1970) and Grant, Stewart and Moilliet (1962). The light dashed line is the locus of points at which the maximum dissipation exists. ▨ represents the measurements by Nasmyth; ▧ represents the measurements by Grant, et al.

Values of ε between 2×10^{-4} and 3×10^{-3} ergs/cm^3/s were found by Nasmyth (1970) in the Pacific Ocean off Vancouver Island at depths between 60 and 200 m (lower shaded region). Grant, Stewart and Moilliet (1962) made measurements in a tidal channel with high Reynolds flow and found values of ε between 0.1 and 0.6 ergs/cm^3/s (upper shaded region). Values of ε in the ocean are expected to be around 10^{-4} to 10^{-3} ergs/cm^3/s, with energetic regions approaching an ε of 1 erg/cm^3/s.

When compared with the longitudinal vibration spectrum at 3.5 m/s, turbulent signals with ε down to 10^{-4} ergs/cm^3/s are for the most part above the level of the vibration-induced velocity. The vibration peak at one-half the commutator slot frequency affects the results only at a specific frequency. The effects of this peak on estimates of dissipation can be eliminated by the technique described by Stewart and Grant (1962) to fit measurements to the Universal Turbulence Spectrum. Also, cross-spectral techniques using the simultaneous accelerometer measurements could be used to subtract the coherent vibrational effects from the measurements (Bendat and Piersol, 1971). We are continuing to investigate these forced vibrational peaks and trying to reduce their effects.

A comparison of the measured turbulence spectra and vibrational spectra taken concurrently will give signal-to-noise ratios from which confidence estimates can be calculated. The lack of an error estimate is a deficiency found in much of the turbulence work published to date.

Hot-Film Velocity Measurements

In order to resolve the velocity spectra for dissipation rates up to 1 erg/cm^3/s, at vehicle speeds of 3.5 m/s, the frequency response of the velocity sensor must extend to beyond 500 Hz. To obtain a better than 10-dB signal-to-noise ratio out past the maximum in the dissipation spectrum, the sensor noise should be below 10^{-9} (m/s)^2/cpm. Metal-film velocity sensors such as used by Grant, Stewart, and Moilliet (1962) have the required frequency response. For our study we used Thermo Systems Incorporated type 1230 NACL, conical platinum-film sensors. These sensors consist of a 1.5-mm diameter quartz rod whose end has been ground to a 40° cone. A band of platinum is plated around the end of the cone, and is the resistance element. The resistance is typically 5 to 6 Ω with a temperature sensitivity of about 8 to 9×10^{-3} Ω/°C. The sensors are coated with a thin quartz coating to insulate the film from salt water.

The sensor electronics were built by APL and the sensor is contained in one leg of a dc bridge. The bridge is remotely balanced at operating depth to the ambient water temperature using a low-voltage bridge excitation. The circuit is then switched to the feedback configuration typically used for constant-temperature hot-film anemometry (Weidman and Browand, 1975; Fremuth, 1977). A probe overheat of approximately 44°C is used. The electronics maintain the sensor at constant temperature; the bridge voltage required to do this is related to velocity by the so-called King's Law:

$$E^2 = [A + B(\rho u)^n](t_s - t_e) , \qquad (1)$$

where A, B, and n are constants, ρ is the fluid density, u is its velocity, t_s is the sensor operating temperature, and t_e is the ocean background temperature. Since ρ, u, and t_e vary with time, the velocity sensor actually measures density fluctuations, velocity fluctuations, and environmental temperature fluctuations.

To calibrate the velocity sensor, we constructed a flow tunnel in the APL temperature calibration bath so that the ambient temperature can be controlled during calibration runs. A typical static calibration at four different overheat settings is shown in Figure 5. A reasonable fit to these curves is given by

$$E^2 = [-8\times10^{-2} + 0.32(\rho u)^{0.26}] \times (T_o + t_i - t_e) , \qquad (2)$$

where t_i is the initial temperature when the bridge is balanced and T_o is the overheat temperature of the sensor.

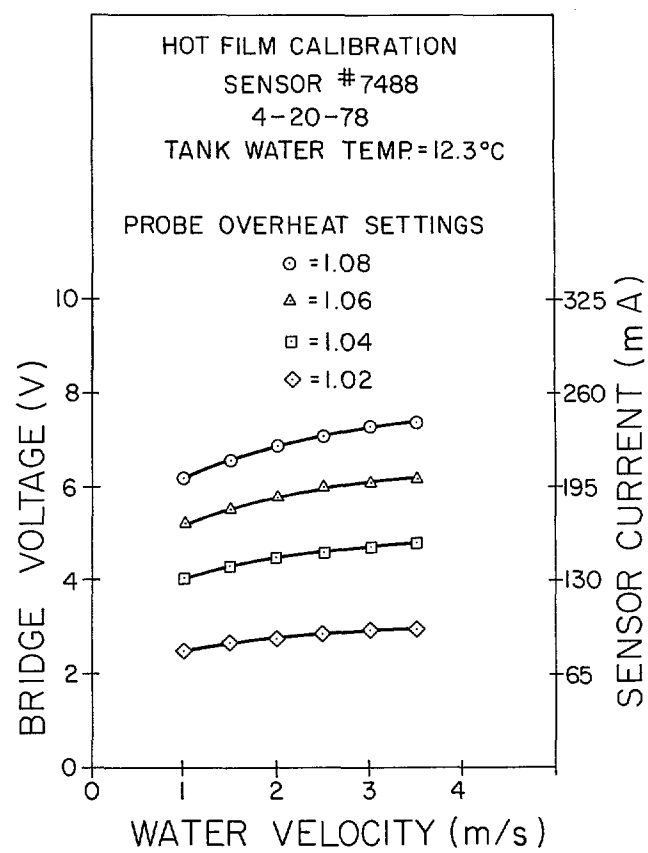

Figure 5. Static calibration of hot-film velocity sensor at four overheat settings.

Because the gain of the feedback amplifier in the constant-temperature anemometer circuit is limited by circuit stability requirements, the bridge operates off-balance, with the amount of off-balance dependent on the output bridge voltage. To obtain the true sensor overheat, the overheat settings must be corrected by the amount of the bridge unbalance.

Equation 2 was used to estimate the effects on the velocity measurement of typical variations in fluid density and temperature encountered in the ocean environment. For the North Pacific thermocline at constant depth, typical density variations would produce an output signal equivalent to a velocity variation of about 10^{-3} m/s, which is considered insignificant for the purposes of our measurements. However, the effects of temperature variations in the medium are much more severe; a 0.1°C rms variation in temperature (which is typical of internal wave effects) would produce an equivalent velocity signal of approximately 3×10^{-2} m/s rms and could be a significant part of the sensor output.

The typical sensitivity to velocity at a mean speed of 3.5 m/s is 0.3 V/m/s. Because of the nonlinear relationship between bridge output and velocity, this sensitivity increases with decreasing velocity (at 2 m/s, $\partial E/\partial u = 0.5$ V/m/s). Thus, to achieve maximum sensitivity, it would be best to operate at the slowest vehicle velocity. The estimated sensor noise level at 3.5 m/s is 2×10^{-9} $(m/s)^2$/cpm, which is barely good enough to resolve the dissipation peak at $\varepsilon = 10^{-4}$ ergs/cm^3/s. At lower vehicle velocities the signal-to-noise ratio would improve since the sensitivity to velocity fluctuations would increase.

Dynamic calibration is accomplished by oscillating the hot-film sensor in the mean flow with a shaker pot. We have not made this measurement as yet, but similar measurements by others indicate that sensor response is fairly flat past 500 Hz, so we are not concerned about frequency response limitations. We are concerned about the dynamic response of the velocity sensor to turbulent temperature fluctuations. To evaluate this effect, measurements will be made in the plume tank described in the following section.

The major problem with these sensors is stability. Several of them have developed pinhole leaks, or the quartz coating over the thin film has flaked off. Also any "goop" such as oil or living organisms in the water can coat or stick to the sensor. Any change in the boundary layer around the sensor will drastically affect the calibration.

We are considering using an acoustic velocity meter to obtain measurements with the required low frequency and dc stability. This meter would also enable in-situ calibrations of the thin-film sensor in the region of spectral overlap. Our experience to date with hot-film sensors does not make us confident that we can make accurate measurements of turbulent velocity fluctuations without the acoustic current meter.

Metal-Film Temperature Measurement

To resolve the dissipation scales of temperature (which are on the order of 1 cm) at a maximum vehicle speed of 3.5 m/s, a sensor is required that responds to frequencies of several hundred hertz. Lueck, Hertzman and Osborn (1977) have measured the response of a number of thermistors made for use in the ocean. They find that thermistors do not meet this high-frequency requirement. The problem is the slow response time of the insulating coating required to isolate the element electrically from salt water. Metal-film sensors exhibit a higher frequency response than thermistors and appear to be the best solution. We use the same type of conical sensor for temperature measurements as for the velocity measurements.

The sensor electronics were designed and built by APL for utilization in SPURV. The sensor is in one leg of an ac bridge operated at 6 kHz and balanced close to the mean ocean temperature during the operation. Temperature changes at the sensor produce a corresponding resistance change in the metal film and a change in the unbalanced output from the bridge. This output is amplified, bandpass filtered, and synchronously detected. In SPURV, the signal is digitized to 14 bits at a sampling rate of 900 Hz. Sensitivity is about 1×10^{-3}°C temperature change per bit. The SPURV circuitry is self-ranging in two bands spanning 0° to 29°C. The electronics also have self-test features to check their operation before launch.

Static calibration of the metal-film temperature sensors is done in the APL temperature-controlled bath. The temperature of the bath is measured with a platinum resistance thermometer and a Mueller bridge. The thermometer is standardized in a triple-point cell. Comparisons show that calibrations made in our tank are within 2×10^{-3}°C of calibrations done by the Northwest Regional Calibration Center under the direction of the National Oceanographic Instrumentation Center. The static calibration measurements are made at various bridge currents, and the measured sensor resistance is extrapolated back to a zero-current resistance. The extrapolated resistances are fit with a second-order polynomial. A typical calibration is

$$R(\Omega) = 5.492854\ \Omega + 8.8468 \times 10^{-3}\ \Omega/°C \cdot T - 3.7 \times 10^{-6}\ \Omega/°C^2 \cdot T^2 , \quad (3)$$

where T is temperature in degrees Celsius. The resistance change as a result of bridge current is typically 2×10^{-6} Ω/mA^2. The current in the bridge circuit creates a small amount of self-heating which makes the sensor slightly velocity sensitive, but the effects are negligible. Probe resistances have tended to increase about 0.02 Ω during the past year, which is about a 2°C drift in calibration. Minor variations in resistance have been observed between weekly calibrations which are probably due to changes in the contact resistance when the sensors are disconnected and reconnected. This low-frequency drift is not detrimental, since the low-frequency and mean temperature will be measured with a thermistor-controlled Wien bridge

oscillator (Pederson, 1969) which has good low-frequency stability. The two sensors will overlap one decade in frequency to aid in intercalibration.

Dynamic calibrations to obtain the frequency response of the metal-film sensor to temperature are done in our plume tank. A thermal plume acts as a thermal impulse when a sensor is moved horizontally through it. The response function is determined from the sensor's output as it passes through this impulse. For this measurement, the sensor and electronics are evaluated as one unit.

The plume (Figure 6) is generated by heating five Manginin resistance wires spaced 3 mm apart. About 100 W are dissipated in the wires, generating a plume with a 4°C rise in temperature and a width of 0.25 to 0.5 cm.

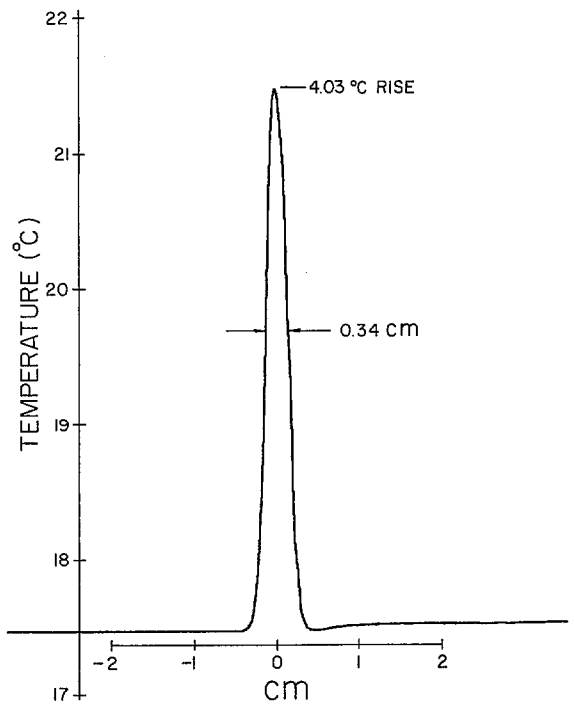

Figure 6. Spatial plot of temperature through thermal plume.

The metal-film sensor is mounted on the end of a pneumatic piston and rammed horizontally through the plume at speeds between 1 and 3.5 m/s. The speed is measured over a 10 cm distance by two photo-transistor/LED pairs (the plume being centered between the pairs).

The output of the metal-film sensor's electronics is recorded on SPURV's high-frequency recorder. For this measurement, the signal is digitized to 8 bits at a sample rate of 10,800 Hz. A plot of the digitized output is shown in Figure 7. The frequency response function is the transform of the high-frequency sensor response divided by the transform of the plume.

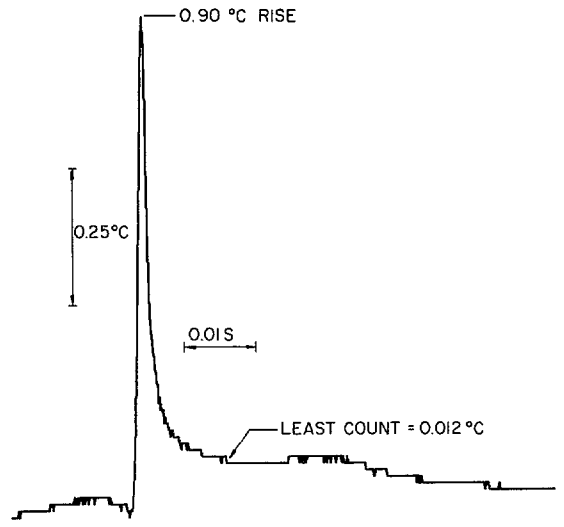

Figure 7. Response of metal-film sensor when shot through plume at 3.3 m/s.

Fabula (1968) studied the response of metal-film temperature sensors, and determined that the frequency response can be modeled by

$$H(f) = \mathrm{Exp}[-\Delta(\pi f/D)^{1/2}] \ , \qquad (4)$$

where f is the frequency, D is the thermal diffusivity of the fluid, and Δ is a length scale related to the thickness of the boundary layer over the metal film which, in turn, is a function of velocity. The faster the sensor speed, the smaller Δ becomes and the higher the sensor frequency response extends. Figure 8 shows a plot of the measured response at 3.3 m/s and the theoretical curve. Hughes (1968) measured the response at slower speeds and his response is also shown. When the sensor is operating on SPURV, the temperature signal is band-limited to frequencies below our 450-Hz Nyquist frequency. Figure 8 indicates the response at the Nyquist frequency would be about 16 dB down from its response at low frequencies (i.e., below 10 Hz). This is the best response obtainable with the present state of sensor development. The response of the metal-film sensors begins to roll off at lower frequencies than the response of coated thermistors. However, the response of the metal-film sensor decreases at a slower rate so as to be better at high frequencies. Because of this low-frequency attenuation, response corrections must be made over all frequencies.

Figure 9 compares the noise of our metal-film temperature sensor with some typical horizontal temperature spectra. The SPURV measurements were taken in the North Pacific (Ewart, 1976a) and are averages over long horizontal transects regardless of energy level in each block. A single energetic patch is thus averaged out. The Grant et al. (1962) data are from selected patches of high-turbulence regimes, and hence are higher than the SPURV results. The two Nasmyth (1970) curves are also patches selected for high energy.

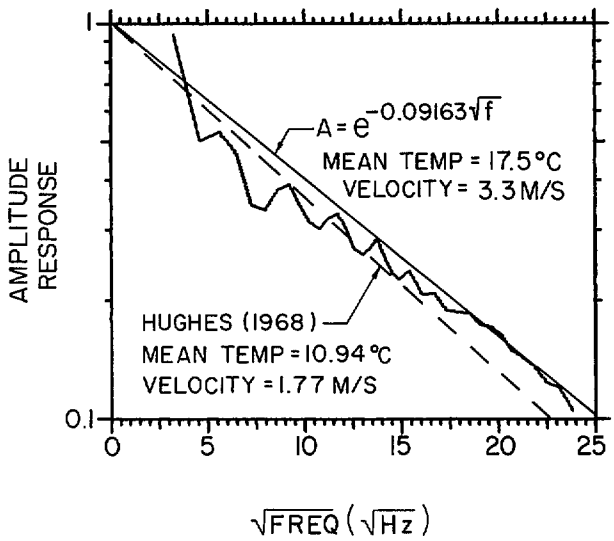

Figure 8. Frequency response for metal-film temperature sensor.

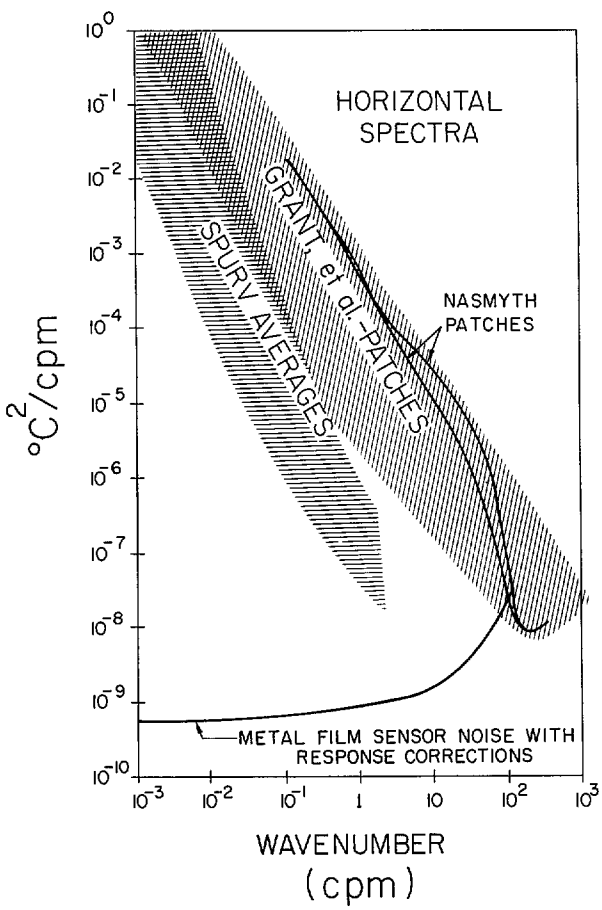

Figure 9. Comparison of metal-film thermometer noise level with measurements of temperature in the ocean.

The electronic and sensor noise is nearly white, and its spectral level is 6.8 x 10^{-10} °C^2/Hz. When this level is divided by the frequency response function of the sensor shown in Figure 8, it forms a lower bound on the measurements of environmental temperature fluctuations (see Figure 9). In the more energetic regions shown, we will be noise limited only at the highest frequencies.

Therefore, in turbulent patches where the signal levels are high, good spectra can be measured, but at the speeds of SPURV the extended frequency response of the metal-film sensors is required. There will also be quiet regions that have energy levels much below the sensor noise levels, and these will not be resolved. Again, as with the accelerometer results, there is a window in which good estimates of temperature spectra can be made. Knowing our noise level and the sensor response will allow us to eliminate those measurements that are sensor limited, and determine a confidence level for the rest.

References

Bendat, J.S., and A.G. Piersol, 1971. Random Data: Analysis and Measurement Procedures, Wiley-Interscience.

Ewart, T.E., 1976a. Observations from straight isobaric runs of SPURV, Preliminary report for the IAPSO/IAMAP PS11 Poster Session of the JOA in Edinburgh.

Ewart, T.E., 1976b. Acoustic fluctuations in the open ocean--a measurement using a fixed path, J. Acoust. Soc. Am., 60(1): 46-59.

Ewart, T.E., and W.P. Bendiner, 1974a. Dye diffusion in the deep ocean, Transactions of the 55th Annual Meeting of the AGU, 55(4): 316.

Ewart, T.E., and W.P. Bendiner, 1974b. Techniques for estuarine and open ocean dye dispersal measurement, Rapp. P.-v. Reun. Cons. int. Explor. Mer., 167: 201-212.

Ewart, T.E., J.D. Irish, and L.O. Olson, 1977. The MATE Experiment, A Preliminary Report, Applied Physics Laboratory, University of Washington.

Fabula, A.G., 1968. The dynamic response of towed thermometers, J. Fluid Mech., 34(3): 449-464.

Fremuth, P., 1977. Frequency response and electronic testing for constant-temperature hot-wire anemometers, J. Phys. E. Sci. Instrum., 10: 705-710.

Grant, H.L., R.W. Stewart, and A. Moilliet, 1962. Turbulence spectra from a tidal channel, J. Fluid Mech., 12(2): 241-268.

Gregg, M.C., 1976. Temperature and salinity microstructure in the Pacific equatorial undercurrent, J. Geophys. Res., 81(6): 1180-1196.

Gregg, M.C., 1977. A comparison of finestructure spectra from the main thermocline, J. Phys. Oceanog., 7(1): 33-40.

Hughes, B.A., 1968. Appendix to Fabula, 1968.

Lueck, R.G., O. Hertzman, and T.R. Osborn, 1977. The spectral response of thermistors, Deep Sea Res., 24: 951-970.

McKean, R.S., and T.E. Ewart, 1974. Temperature spectra in the deep ocean off Hawaii, J. Phys. Oceanog., 4(2): 191-199.

Nasmyth, P.W., 1970. Oceanic Turbulence, Ph.D. Dissertation, University of British Columbia.

Pederson, A.M., 1969. An accurate low cost temperature sensor, Transactions of Marine Technology Society Temperature Measurements Symposium.

Pederson, A.M., 1973. A small in-situ conductivity instrument, Proceedings IEEE Intern. Conf. Engineering in the Ocean Environment, pp. 68-75.

Stewart, R.W. and H.L. Grant, 1962. Determination of the rate of dissipation of turbulent energy near the sea surface in the presence of waves, J. Geophys. Res., 67(8): 3177-3180.

Weidman, P.D. and Browand, F.K., 1975. Analysis of a simple circuit for constant temperature anemometry, J. Phys. E. Sci. Instrum., 8: 553-560.

Widditsch, H.R., 1973. SPURV--The First Decade, APL-UW 7215, Applied Physics Laboratory, University of Washington.

IMPLICATIONS OF THE JAPANESE EXPERIENCE IN AQUACULTURE DEVELOPMENT FOR THIRTY-THREE FOOD-SHORT COUNTRIES *

Yoshiaki Matsuda
Woods Hole Oceanographic Institution
Woods Hole, Massachusetts 02543

Abstract

Aquaculture development in Japan has been limited by the following factors: supply and demand, environmental suitability, technical capability, legality, experience, infrastructure, existence of leadership, economic feasibility and social welfare incentives. Similar limiting factors were examined for thirty-three food-short countries. Fifty-five aquaculture variables were tested using multiple regression analysis combined with Pearson correlation analysis. Results imply that aquaculture development in these countries are affected by the same limiting factors as in Japan. These findings are the basis for a two-dimensional aquaculture development model which may be helpful in coping with future technology transfer problems.

1. Introduction

This study is designed to devise an effective aquaculture development strategy for developing countries where there are food shortages.

The rapidly increasing popularity of aquaculture and the debates which issue from the world-wide aquaculture development scene necessitate a re-evaluation of present schemes to transfer technology related to aquaculture (13). Aquaculture has the potential for developing into an important vehicle for solving some of the employment, income, and nutrition problems in food-short countries. FAO and other UN agencies, the World Bank, the Asian Development Bank, Southeast Asian Fisheries Development Center (SEAFDC), International Center for Living Aquaculture Resource Management (ICLARM), USAID, U.S. Peace Corps, OXFAM (England), International Development Research Center in Canada (IDRC), International Foundation for Science in Sweden (ISF), Japan International Cooperation Agency (JICA), and German Volunteers are some of the organizations promoting aquaculture in developing countries (11). In addition, national development plans for aquaculture have been proposed in many developing countries (4, 6,7). However, strategies now in use are inflexible and show a bias toward technological aspects.

The purpose of this paper is to suggest a flexible model for revitalizing aquaculture development strategies, emphasing the 33 food-short countries in 1973 (1). Assuming that experience in developed countries has some applications to developing countries, the history of aquaculture in Japan is reviewed. The limiting factors for aquaculture development in Japan are then tested for the 33 food-short countries. Finally, a two-dimensional aquaculture development model is developed as a key to cope with technology transfer problems.

2. Methodology

The methodology used in this study is based primarily on a combination of descriptive, correlation and multiple regression analyses. Aquaculture development in Japan is described first in order to explore limiting factors in aquaculture development and the growth pattern. The hypothesis that aquaculture activities in the 33 food-short countries are not limited by these factors described for Japan is tested using Pearson correlation and multiple regression analyses. Based on these findings, an aquaculture development model is suggested.

(1) Study area. The countries considered were Japan and the 33 food-short countries reported in 1973 (1). These include Algeria, Angola, Bangladesh, Bolivia, Cameroon, Central African Republic, Chad, Ecuador, El Salvador, Ethiopia, Gambia, Guinea, Guyana, Haiti, India, Indonesia, Iran, Iraq, Kenya, Mali, Mauritania, Niger, Nigeria, Philippines, Saudi Arabia, Senegal, Syrian Arab Republic, Tanzania, Uganda, Upper Volta, Yemen Arab Republic, Yemen Democratic, and Zaire.

(2) Data. There is an abundance of literature on Japanese aquaculture. The most useful data are Drew 1951 (2), Inaba 1964 (9), Japanese Federation of Laver and Shell Fisheries Cooperatives (IFLSFC) 1969 (10), Matsuda 1977 (12), Miyaji 1974 (15), Oshima 1973 (16) and Suisansha Fisheries Yearbook (20).

Aquaculture data for the 33 food-short countries were compiled from Bell and Canterbery 1976 (1); FAO 1974 (2); FAOa,b,c, and d, 1975 (4,5,6,7),

*Prepared with funds from the Pew Memorial Trust and by the Department of Commerce, NOAA Office of Sea Grant under Grant #04-7-158-44104, and the Marine Policy and Ocean Management Program of the Woods Hole Oceanographic Institution.

Pillay 1972 (17); 1973 (18) and 1976 (19) and information from the World Bank, SEAFDC, USAID, U.S. Peace Corps, OXFAM, and JICA (11).

Selected variables are summarized in Appendix Tables 1-2. Included were 1 dependent and 54 independent variables. Per capita aquaculture production in 1975 (kg) was selected as the dependent variable because most of these countries have few imports or exports of these products and this reflects consumption as well as production. The total aquaculture production in 1975, based on Pillay 1976 (19), was divided by population estimates for 1975 in the UN Demographic Yearbook 1975 (4).

Eleven basic variables are chosen as independent variables. It should be noted that data from private sectors were not readily available; thus this analysis is biased toward government activities. These 11 variables include consumer acceptability, environmental suitability, amount of papers presented at any one of the 3 FAO Symposia on Aquaculture, experience, degree of international relations, degree of political activities, average rates of return on investment (%), average rates of return on operating costs (%), and average rates of return on gross income (%).

A preliminary analysis suggested that the last three economic variables had no significant correlation with dependent variables at the 0.05 level mainly due to insufficient data (Table 1). Therefore, we deleted these three variables from further analysis. In addition, there were interactions and overlapping among the rest of the 8 independent variables (Table 2). Thus, twenty-eight two-way interactions of these 8 variables and 15 three-way interactions were added as independent variables (Appendix Table 1).

Consumer acceptability was taken to represent the equilibrium of present supply and demand although the data in this category is insufficient. Consumer acceptability scores were adopted from Bell and Canterbery. Total scores for each country are the sum of consumer acceptability scores of 14 aquaculture species (Indian carp, channel catfish, tilapia, eel, rainbow trout, mullet, milkfish, yellowtail, Panaeus shrimp, oyster, mussels, walking catfish, macrobrachium, and blue-green algae) measured by a 4-point scale (0: unacceptable; 1: poor potential acceptance; 2: satisfactory potential acceptance; and 3: already cultured).

For the environmental suitability variable, environmental acceptability scores were adopted from Bell and Canterbery. Each country's total score consists of the sum of environmental acceptability scores of the 14 species measured by a 1.2-point scale (0: no environmental acceptability, and 1.2: the highest environmental acceptability).

For technical capability, three variables were used: amount of international assistance, number of research units, and number of papers presented at any one of the 3 FAO Symposia on Aquaculture. International assistance is an external factor affecting technical capability, while research units are an internal factor. The number of papers reflects, at least roughly, the degree of research activity. International assistance to aquaculture is measured by a score of 1 if exist, 0 otherwise for each variable: aquaculture joint ventures, technical assistance to aquaculture from UN, related agencies, and so forth, during the 1967-1973 period. The number of research units is the total number of research institutions presenting papers to any one of the 3 FAO Symposia on aquaculture in Asia (17), Latin America (3) and Africa (5). Another variable is the total number of papers presented at any one of the 3 FAO Symposia. The use of numbers for these activities may not reflect the true relative importance because one project might be much larger than others. However, in this instance each project is weighted equally because sufficient data is not now available to provide a better indicator.

The degree of political activities (which represent legal structure, infrastructure and social welfare programs)takes account of government subsidies, research institutions, extension service, cooperatives, joint ventures, government farms, stocking and conservation practices, and international assistance to aquaculture.

International assistance to aquaculture, fisheries trade (imports and exports) data for 1975 with FAO Yearbook of Fisheries Statistics 1975 (8), presentation of papers at any one of the 3 FAO Regional Workshops on Aquaculture Planning in Africa (4), Asia (6) and Latin America (7) in

1975, and participation (1 if participated, 0 otherwise) to any one of the 3 FAO Symposia on Aquaculture were used to indicate interest on the part of the countries' leaders in aquaculture ("Leadership").

Experience may not be a product of long history; it may be a function of learning during a relatively short period. However, data is limited on such short-term experience. Therefore, we used historical records as a proxy for experience (1: old practice - before 1900; 2: moderately old practice - 1900-1945; 3: recent practice - after World War II; and 4: negligible practice).

Profits are a measure of economic feasibility as an incentive for the private sector. Economic feasibility is represented by average rates of return on investment (%), on operating costs (%) and on gross income (%). However, data were available for only six of the 33 countries (Central African Republic, India, Indonesia, Nigeria, Philippines and Senegal). These data were a mixture of survey results and proposed budgets, so an average of such rates of return was figured for each of these six countries.

(3) Techniques. Techniques employed are a combination of Pearson correlation, and multiple regression analyses using the SPSS system at the Woods Hole Oceanographic Computer Center. One of the serious problems of the regression analysis is multicollinearity, which means that some or all of the independent variables are very highly intercorrelated, resulting in a reduced reliability in the relative importance indicated by the partial regression coefficients. In order to eliminate the effects of multicollinearity, Pearson correlation and multiple regression analyses were combined in such a way that one selected the most important independent variable from the Pearson correlation analysis, checked the correlation coefficients between the most important variable and the rest of independent variables through Pearson correlation analysis, selected variables of low correlation coefficient ($r < .5$) with the most important variable, and analyzed a set of the most important variable and its low-correlated independent variables with the dependent variable through multiple regression analysis. If more than two independent variables were ranked as most important, the same procedure was repeated until the analysis was completed. This method was adopted as it gaves the most reliable results.

3. History of Aquaculture in Japan

Japanese history reflects chronological phases in the history of aquaculture: precondition (before Edo era), phase I (Edo era: 1600-1868), phase II (1868-1945), and phase III (after World War II) (12). During the precondition period, common carp (Cyprimus carpio L.) was first raised and became popular among the nobles. During the phase I period, oyster (Osterea gigas T.), laver (Porphyra tenera k.), fancy carp (Cyprinus carpio L.) and goldfish (Carassius auratus L.) appeared as aquaculture species. During the phase II period, salmon (Onkorhynchus spp.) and trout (Salmo gairdnerii irideus G.), eel (Anguilla japonica T. et S.), pearl (Pinctada martensii D.), "Ayu" fish (Plecoglossus altivelis T. et S.), and yellowtail (Seriola quinqueradiata T. et S.) were added. All other aquaculture species were introduced during the phase III period.

Some knowledge of methods of raising carp in ponds was apparently introduced from China by 100 A.D. (2). In 724 the Emperor Shomu emphasized the Buddisht precept against killing and changed Japanese eating habits for the next five centuries until Shinran, a new Buddism leader in the 13th century, advocated that people might eat fish because eating fish was beyond the Buddhist precept against killing (16). During the 9th and 10th centuries, common carp were raised as pet fish among the nobles and developed as moving treasures in landscape gardening.

Despite the early introduction of fish culture into Japan, the rearing of fish was of relatively little importance and its development was modest before 1600. This is attributable to limited supply and demand, quasi-legal prohibition of eating fish, and the lack of strong interest among the countries' leaders in aquaculture development, in addition to a lack of infrastructure and experience.

During the phase I period (1600-1868), aquaculture was regarded as a potential local industry by some local lords, and they attempted to transplant various species in various parts of Japan. After much trial and error, a common carp culture settled in Niigata and Nagano prefectures, oyster at Hiroshima Bay, laver and clams (Corbi-

cula leana P.) in Tokyo Bay, and goldfish at Yama-to-kooriyama. Despite the favorable climate, the development of aquaculture as a whole was slow during this period because of limited infrastructure, experience and technical capability, and a relatively low demand for the cultured species.

During the phase II period (1868-1945) the country, after long isolation, adopted some aspects of modern Western civilization with energy and enthusiasm. The government dispatched people to America and Germany to learn techniques pertaining to aquaculture (16). Salmon and trout hatcheries were built, a Fishery Section was established in 1881, many laws concerning aquaculture were legislated, and numerous related educational and research institutions were established. Corresponding to government efforts, commercial aquaculture developed among private sectors. (9,15 and 16). Eel, pearl, Ayu, and yellowtails were added as aquaculture species, due mainly to the enthusiasm of individuals.

Aquaculture production in Japan during the 1912-1975 period is shown in Figure 1. The first national aquaculture conference was held in 1913, and subsidies for aquaculture became available in 1918. Raft culture of oysters developed in 1924. The Perfectural Experiment Station Act was legislated in 1929.

A high quality of leadership toward aquaculture development in both public and private sectors played an important role. Increased experience and technical capability, as well as a favorable legal environment, encouraged the growth of aquaculture. Further more, the demand for aquaculture products increased due to rapid population growth and urbanization and to efforts to expand markets (9,16), particularly in the eel and pearl industries. By 1930 all the basic conditions for a large expansion of aquaculture had developed, and an infrastructure existed which would lead to economically sound aquaculture.

This growth was curtailed by Japan's involvement in international wars during the 1930's and 1940's. Pearls and eels were regarded as luxury goods, and were prohibited. Carp, laver and some other aquaculture species were also treated in the same way, with the exception of grass carp (Ctenopharyngodon idellus C. et V.) and silver carp (Hypophthalnlchthye moritrix C. et V.) which constituted most of the relatively high aquaculture production during the 1941-1945 period. This is a clear example of a government's ability, through its legal powers, to wipe out all past efforts toward aquaculture development, as well as to promote its development.

Immediately after the war the aquaculture industry entered a period of recovery during the general reconstruction, and began phase III. Owing to General MacArthur's intervention, the pearl and oyster industries recovered quickly (16), and the Fisheries Agency Act was passed in 1948. Again the legal climate became favorable for aquaculture development, and the infrastructure recovered quickly. By 1960 the experience of aquaculture workers had been restored and technical capability increased rapidly. Fixed net culture developed in 1952, and artificial seedlings for laver became possible in 1958 (JFLSFC 1969). The demand for aquaculture species was also high, resulting in good profit potential. The following decades, which were characterized by economic growth, resulted in the rise of living standards and increased demand for aquaculture products, except for pearls and oysters. In 1962 the Inland Sea Fish Farming Center was established and floating net culture developed for laver, a popular magazine "Fish Culture" was first published in 1964, and a low temperature seed storing net for laver was developed in 1965.

However, the aquaculture industry has encountered environmental problems due to urbanization and water pollution as well as natural catastrophe. Abnormally warm weather (laver), typhoon, diseases (laver, goldfish, eel, yellowtail and scallops), shortage of fingerlings (yellowtail and eel), red tide (yellowtail, pearl, oyster), declines of demand (pearl and oyster) and reclamation (laver) have been some of the limiting factors for aquaculture development following the war. Thus, Japanese aquaculture production as a whole does not show a smooth growth curve; instead, it follows a modified combination of the Sigmoid curve and the J-shaped growth curve.

In 1973, the Japanese Diet dealt with issues pertaining to pollution and on July 1, 1977, the Japanese government declared a 200-mile economic zone. There now exists a new climate favorable for aquaculture.

In summary, throughout the history of Japan, aquaculture development has been limited by supply and demand, environmental suitability, technical capability, legality, experience, infrastructure, existence of leadership, economic feasibility and social welfare incentives. Aquaculture has not followed a smooth growth curve.

4. Analysis of the Material for the 33 Food-Short Countries

(1) Preliminary Results

Pearson correlation analysis with per capita aquaculture production in 1975 reveals several significantly correlated independent variables ($S = 0.001$): consumer acceptability, amount of international assistance, number of research units, number of papers, degree of international relations, degree of political activities, and experience; and one less significant variable ($S = 0.033$), environmental suitability (Table 1). The high correlation among these independent variables results in multicollinearity problems (Table 2).

Among these independent variables, consumer acceptability is the only one subject to changes in demand. Although the data include species which are not now consumed in the 33 food-short countries, consumer acceptability is highly correlated with per capita production. Consumer acceptability is likely to reflect present consumption patterns in such a way that the higher the present per capita consumption, the larger the consumer acceptability. Because external trade is negligible at present, per capita consumption and per capita production can be interchanged. Further, consumer acceptability is significantly correlated with 7 other independent variables ($r > .7$): international assistance, number of research units, degree of political activities, and experience. Since international assistance, number of research units, and degree of political activities are highly production oriented variables, it is possible that effects of these variables on production are transformed into effects on consumer acceptability. Experience, or a past history in aquaculture, certainly effects consumer acceptability because consumer taste and preference are products of their past.

Despite the importance of environmental suitability for aquaculture production in general, it was not highly correlated with per capita production. This might result from inadequate data. In fact, most of the selected species for the environmental suitability contribute neither to present aquaculture production nor to consumption. Although, environmental suitability value is positively correlated with the values for consumer acceptability, international assistance, and degree of international relations there is no obvious explanation for this. It maybe that an environment suitable for selected species maybe of a general enough type to attract the interest of international agencies. Nevertheless, improvement of data on environmental suitability is essential for future analysis.

Among technical capability variables, the amount of international assistance has the highest correlation with per capita production. International assistance is intended to provide technology for these countries to increase per capita production in response to critical nutrition problems. The largest recipient of international assistance to aquaculture during the 1967-1973 period was the Philippines, which recorded the highest per capita aquaculture production in 1975 (2.94 kg). Further, the amount of international assistance is correlated with all other seven independent variables. In particular, high correlations are observed with the number of research units, degree of international relations, degree of political activities, and experience. High correlation with experience is explained by the fact that one main purpose of technical assistance projects has been to improve existing aquaculture management. Therefore, most international assistance has been practiced in Bangladesh, India, Indonesia and the Philippines where aquaculture is an ancient practice. Thus, all these high correlations are reasonable.

The next highest correlation with per capita production was .7864 with the number of research units. This high correlation is partly attributable to one inclusion of the Philippines where there are seven research units (the highest) and the highest per capita production. Although most of these research units have been supported by international assistance, internal activities are partially also important for production. Internal research activities provide fingerlings where they

are not easily available, advice, better aquaculture management, and support through extension services. Research activities might affect total production directly and per capita production indirectly. For example, in India where total aquaculture production, supported by the same number of research units as in the Philippines, is the highest (494,000t), per capita production in 1975 was relatively small (.825Kg) because of India's huge population. Further, the number of research units is highly correlated with number of papers, degree of international relations, degree of political activities and experience. The direct correlations among these variables are obvious. However, these correlations could be directly or indirectly affected by the following logic: the longer the experience, the higher the consumer acceptability, which in turn leads to larger total production, and more active political and research activities. As political and research activities increase, international relations become more important.

Number of papers presented at international meetings had the least correlation with per capita production because of its indirect effects. Number of papers has a high correlation with degree of political activities. The logic behind this is that the more active the political activities, the more active the research activities, which in turn leads to larger number of papers.

Degree of international relations is correlated with per capita production, but only a little. The high correlation with degree of political activities is because external incentives have enhanced internal activities.

Degree of political activities and experience are also correlated with per capita production. High correlation between degree of political activities and experience is reasonable because historical experience has influenced aquaculture activities internally.

Despite the fact that most data on independent variables is limited to government activities, significant correlations with the dependent variable, per capita production, imply that the role of government in per capita aquaculture production is important.

(2) Results

Results from the multiple regression analysis, combined with Pearson correlation analysis, are summarized in Table 3.

After eliminating multicollinearity problems, the final results indicate that a three-way interaction of the consumer acceptability, amount of international assistance, and the number of papers presented at any one of the 3 FAO Symposia on Aquaculture has the most significant relationship to per capita aquaculture production in 1975. The square of multiple correlation (R^2) is .85794 which implies that the result is highly reliable. The regression coefficient is large (B = 2443) so that the impact of the interaction of these three limiting factors on per capita aquaculture production would be large.

Despite relatively high correlations with per capita production, the final result does not include any direct effect of the 8 basic independent variables, because of high interactions and/or overlap among these. Since the result is mechanically determined by regression analysis, assuming linearity, we could not simply say that other variables are insignificant. Instead, if this interaction variable is deleted from the data, we could expect a completely different second best answer which might be some other combination.

In summary, per capita aquaculture production in these 33 food-short countries is limited by consumer acceptability, environmental suitability, amount of international assistance, number of research units, number of papers presented to any one of the 3 FAO Symposia on aquaculture, degree of international relations, degree of political activities, and experience. These limiting factors interact with and/or overlap each other and can explain per capita aquaculture production up to the point that the square of multiple correlation (R^2) reaches .85794, based on our present data. These results for the 33 food-short countries imply that aquaculture development is also limited by one or a combination of the same factors as prevail in Japan.

5. Discussion

The evaluation of economic feasibility for the thirty-three food-short countries has suffered from insufficient and/or inadequate data for economic variables in these countries. There

is much room for the improvement of data. Nevertheless, economic feasibility seems to be critical in these countries. According to FAO (4), failures of some of the ill-conceived programs in the past have continued to remain a major constraint in convincing farmers and investors of the economic viability of aquaculture. There are indeed problems of increasing input costs, exploitation of middlemen, perishable products and remoteness of production areas from the market, which directly affect the economic feasibility.

Based on the previous analyses, together with the importance of economic feasibility, we could assume that aquaculture development measured by per capita production in these food-short countries is limited by one or combinations of nine factors in any given circumstance: supply and demand, environmental suitability, technical capability, legality, experience, existence of leadership, infrastructure, economic feasibility and social welfare incentives which interact with one another. Assuming that the Japanese experience is also applicable to a growth model in these countries, a hypothetical aquaculture development model could be posited. The model consists of functional and growth dimensions.

The functional dimension emphasizes the importance of the existence of leadership as a lubrication function, infrastructure as a transportation function, social welfare as an incentive for the public sector, and of economic feasibility as an incentive for the private sector. Supply and demand, environmental suitability, technical capability, legality and experience become crucial as basic limiting factors for aquaculture development only when leadership exists, and infrastructure, economic feasibility and social welfare incentives are sound and adequate.

The growth dimension is regarded as a combination of the Sigmoid shaped growth curve in the long run and the J-shaped growth curve in the short run which occurred in aquaculture development in Japan. If each limiting factor is removed, the growth curve should be a perfect combination of these two curves. However, each limiting factor may become so critical that despite increasing efforts the growth curve would stagnate as in India or decline as in Indonesia (18 and 19). Aquaculture could even be eliminated. For example, regardless of an early introduction of aquacultural methods, aquaculture activity is negligible in Guyana, Iran, Iraq, Niger, Saudi Arabia, Syrian Arab Republic, and Upper Volta (3 and 5). Another classic example is the abandoned ponds built by colonial governments in many parts of Africa (5). Modern versions of this disintegration could result from disease and competition, urbanization and pollution, as occurs in Japan (12).

6. Summary and Conclusions

In any given circumstance, aquaculture development in Japan has been limited by one or a combination of the following factors: supply and demand, environmental suitability, technical capability, legality, experience, infrastructure, existence of leadership, economic feasibility and social welfare incentives. The results for the 33 food-short countries indicate that present per capita aquaculture production as an indicator for aquaculture development is a function of an interaction of the consumer acceptability, amount of international assistance and the number of papers presented at any one of the FAO Symposia on aquaculture; and all the other basic independent variables could also be used, with a declining degree of correlation. These results imply that aquaculture development in these countries is also limited by one or a combination of the same sort of factors as prevail in Japan. One possible development from our analyses could be a hypothetical aquaculture development model to cope with technology transfer problems in these food short-countries. This model would imply the following:

i) Until industry reaches the "take off" stage, the growth of aquaculture is a slow, step-by-step process.

ii) The elimination of any one of the limiting factors will contribute to the growth of aquaculture, but not much.

iii) Nevertheless, the best way to develop aquaculture is to eliminate the limiting factors one by one.

Although further research is needed for the improvement of data, economic feasibility, experience, social welfare, links among limiting factors and methodology, the proposed two-dimensional aquaculture development model -- function and growth -- is likely to be adequate to predict when, how, and why aquaculture can develop in any given circumstance or place.

Acknowledgment

The author wishes to acknowledge Mr. M.N. Mistakido at FAO and his colleagues for providing me the variable information; Drs. Paul M. Fye, H. Burr Steinbach, Kenneth O. Emery, Robert W. Morse, Susan B. Peterson, Leah J. Smith and Woollcott Smith, at the Woods Hole Oceanographic Institution for constructive criticism of the manuscript. Acknowledgment is also extended to Mrs. Yoko Matsuda, Kaleroy L. Hatzikon, Ann Martin and Lynda E. Davis for their kind cooperation and assistance. I would like to thank the Institution's Marine Policy and Ocean Management Program which made this study possible.

References

(1) Bell, F.W. and E.R. Canterbery, Aquaculture for the Developing Countries: A Feasibility Study. Ballinger Publishing Company. Cambridge, Massachusetts, 1976, pp. 266.

(2) Drews, R.H., "The Cultivation of Food Fish in China and Japan: A Study Disclosing, Contrasting National Patterns for Rearing Fish Consistent with the Differing Cultural Histories of China and Japan," Ph.D. Dissertation, University of Michigan, 1951, pp. 250.

(3) FAO, Working Papers on Symposium on Aquaculture in Latin America, Montevideo, Uruguay, 26 November - 2 December 1974.

(4) FAOa, Aquaculture Planning in Africa. Report of the First Regional Workshop on Aquaculture Planning in Africa, Accra, Ghana, 2-17, July 1975. ADCP/REP/75/1, pp. 114.

(5) FAOb, Working Papers on Symposium on Aquaculture in Africa, Accra, Ghana, 30 September - 6 October 1975.

(6) FAOc, Aquaculture Planning in Asia. Report of the Regional Workshop on Aquaculture Planning in Asia, Bangkok, Thailand, 1-17 October 1975. ADCP/REP/75/2, pp. 154.

(7) FAOd, Aquaculture Planning in Latin America. Report of the Regional Workshop on Aquaculture Planning in Latin America, Caracas, Venezuella, 24 November - 10 December 1975. ADCP/REP/76/3, pp. 173.

(8) FAO, Yearbook of Fisheries Statistics 1975, Vols. 40-41, 1976.

(9) Inaba, S., Practical Eel Culture, Midori Shobo, Tokyo, 1959, pp. 281 (in Japanese).

(10) Japanese Federation of Laver and Shell Fisheries Cooperatives, "The First Twenty Years of Japanese Federation of Laver and Shell Fisheries Cooperatives," 1969, pp. 8 (in Japanese).

(11) Matsuda, Y., "International Assistance on Aquaculture in Developing Countries," Unpublished paper, Woods Hole Oceanographic Institution, 1977, pp. 28.

(12) Matsuda, Y., "History of Aquaculture in Japan," Woods Hole Oceanographic Institution. Unpublished paper, 1977, pp. 56.

(13) Matsuda, Y., "The Growth of Aquaculture in Developing Countries: Potentials, Patterns, and Pitfalls," Fisheries, 1978, in press.

(14) Ministry of Agriculture and Forestry, Fisheries Statistics of Japan 1975, 1977, pp. 77.

(15) Miyaji, D., A Story of Ayu, Iwanami-shinsho 386, Iwanami-shoten, Tokyo 1974, pp. 227 (in Japanese).

(16) Oshima, J., A Geographical Study of Aquaculture in Japan, University of Tokyo Press, Tokyo, 1973, pp. 455 (in Japanese).

(17) Pillay, T.V.R., ed., Coastal Aquaculture in the Indo-Pacific Region, Fishing News (Books) Ltd., London, 1972, pp. 497.

(18) Pillay, T.V.R., "The Role of Aquaculture in Fisheries Development and Management," J. Fish. Res. Board Can., 1972, 30(12): 2202-2217.

(19) Pillay, T.V.R., "Overview of Aquaculture Development During the Last Ten Years," FAO Technical Conference on Aquaculture, Kyoto, Japan, 26 May - 2 June, 1976.

(20) Suisansha, Fisheries Yearbook 1968, Tokyo 1968; 1971, 1971; and 1976, 1976 (in Japanese).

(21) United Nations, U.N. Demographic Yearbook 1976, 1977.

Figure 1. Aquaculture Production in Japan during the 1912-1975 Period (Unit: 1,000t)

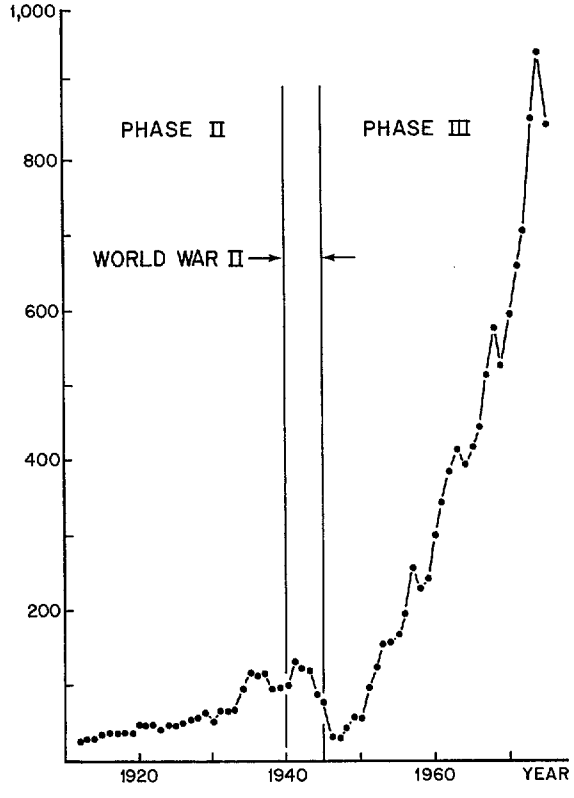

Sources: Ministry of Agriculture and Forestry, Fisheries Statistics of Japan 1975, 1977(14) and Suisansha, Fisheries Yearbook 1968, 1968; 1971, 1971; and 1976, 1976(20).

Table 1. Pearson Correlation with Per Capita Aquaculture Production in 1975 for the Thirty-Three Food-Shortages Countries

Categories	Independent Aquaculture Variables (Indicators)	Correlation Coefficient (r)	Cases	Significance
Supply and Demand	1. Consumer acceptability scores	.7653	27	.001
Environmental Suitability	2. Environmental suitability scores	.3965	29	.033
Technical capability	3. Amount of international assistance	.7881	33	.001
	4. Number of research units	.7864	33	.001
	5. Number of papers	.5540	33	.001
Existence of leadership	6. Degree of international relations	.5550	33	.001
Legality-infrastructure-social welfare	7. Degree of political activities	.6172	33	.001
Experience	8. Experience	-.6553	33	.001
Economic feasibility	9. Average rates of return on investment	.6762	6	.140
	10. Average rates of return on op. costs.	-.4594	6	.359
	11. Average rates of return on gross income	-.4849	6	.326

Table 2. Correlation Matrix for the Eight Basic Independent Variables

	CA	ES	IA	RU	P	DIR	DPA	E
Consumer acceptability (CA)	1.0	.52	.76	.80	.60	.68	.80	-.74
Environmental suitability (ES)	.52	1.0	.55	.47	.42	.61	.47	-.40
Amount of international assistance (IA)	.76	.55	1.0	.80	.65	.73	.76	-.78
Number of research units (RU)	.80	.46	.80	1.0	.88	.70	.85	-.73
Number of papers (P)	.60	.42	.65	.88	1.0	.61	.76	-.59
Degree of international relations (DIR)	.68	.61	.73	.70	.61	1.0	.75	-.72
Degree of political activities (DPA)	.80	.47	.75	.85	.76	.75	1.0	-.80
Experience (E)	-.74	-.40	-.78	-.73	-.59	-.72	-.80	1.0

Table 3 Emperical Results

** Significant at the 0.01 level

$$Y' = 3.812 \times 10^{-2} + 2443\ X_1X_2X_3$$

where Y' is an estimated per capita aquaculture production in 1975 (kg), X_1 is the consumer acceptability, X_2 is the amount of international assistance, X_3 is the number of papers; Pearson correlation coefficient between Y (per capita aquaculture production in 1975) and $X_1X_2X_3$ is .92625 in which 33 countries are included; F value for regression coefficient (B) is 187.2187**; multiple correlation coefficient (R) is .92625; R^2 is .85794; and F value for multiple correlation coefficient (R) is 187.2187.**

Apendix Table 1: Aquaculture Variables Used

Item	Variables
1	Consumer acceptability*
2	Environmental suitability*
3	Amount of international assistance on aquaculture: 1967-73*
4	Number of research units concerning aquaculture in 1975*
5	Number of papers presented at the 3FAO Symposia on Aquaculture in Asia, Africa and Latin America*
6	Degree of international relations on aquaculture*
7	Degree of political activities*
8	Aquaculture experience*
9	Average rates of return on investment (%)*
10	Average rates of return on operating costs (%)*
11	Average rates of return on gross income (%)*
12	Item 1 x Item 2
13	Item 1 x Item 3
14	Item 1 x Item 4
15	Item 1 x Item 5
16	Item 1 x Item 6
17	Item 1 x Item 7
18	Item 1 x Item 8
19	Item 2 x Item 3
20	Item 2 x Item 4
21	Item 2 x Item 5
22	Item 2 x Item 6
23	Item 2 x Item 7
24	Item 2 x Item 8
25	Item 3 x Item 4
26	Item 3 x Item 5
27	Item 3 x Item 6
28	Item 3 x Item 7
29	Item 3 x Item 8
30	Item 4 x Item 5
31	Item 4 x Item 6
32	Item 4 x Item 7
33	Item 4 x Item 8
34	Item 5 x Item 6
35	Item 5 x Item 7
36	Item 5 x Item 8
37	Item 6 x Item 7
38	Item 6 x Item 8
39	Item 7 x Item 8
40	Item 1 x Item 3 x Item 4
41	Item 1 x Item 3 x Item 5
42	Item 1 x Item 3 x Item 6
43	Item 1 x Item 3 x Item 7
44	Item 1 x Item 3 x Item 8
45	Item 3 x Item 4 x Item 5
46	Item 3 x Item 4 x Item 6
47	Item 3 x Item 4 x Item 7
48	Item 3 x Item 4 x Item 8
49	Item 4 x Item 5 x Item 6
50	Item 4 x Item 5 x Item 7
51	Item 4 x Item 5 x Item 8
52	Item 5 x Item 6 x Item 7
53	Item 5 x Item 6 x Item 8
54	Item 6 x Item 7 x Item 8
55	Per capita aquaculture production in 1975 (Kg)**

* Basic independent variables.

** Dependent variables.

Appendix Table 2: Data Matrix for the Thirty-Three Food-Short Countries

	Consumer Acceptability*	Environmental Suitability*	Amount of Int. assistance: 1967-73*	No. of research units in 1975*	No. of Papers	Degree of international relations*	Degree of Political Activities	Experience*	Ave. rate of return on investment(%)*	Ave. rate of return on operating costs (%)*	Ave. rate of return on investment (%)*	Per capita aqua-culture production in 1975 (Kg)**
Algeria	9	8.0	0	0	0	0.0	0	4	n.a.	n.a.	n.a.	0
Angola	16	10.2	0	0	0	0.0	0	4	n.a.	n.a.	n.a.	0
Bangladesh	31	11.8	4	1	0	2.0	3	1	n.a.	n.a.	n.a.	0.995
Bolivia	23	4.4	0	1	1	0.0	2	2	n.a.	n.a.	n.a.	0.248
Cameroon	23	12.8	4	1	1	1.0	4	3	n.a.	n.a.	n.a.	0.007
Central Afr.Rep.	n.a.	5.0	2	2	5	3.0	3	2	174.7	196.8	58.8	0.023
Chad	17	5.0	0	0	0	1.0	0	4	n.a.	n.a.	n.a.	0
Ecuador	22	13.2	2	2	4	3.5	4	2	n.a.	n.a.	n.a.	0.147
El Salvador	27	13.5	1	2	2	3.0	5	3	n.a.	n.a.	n.a.	0.301
Ethiopia	17	11.3	0	1	1	1.0	3	4	n.a.	n.a.	n.a.	0
Gambia	n.a.	n.a.	0	0	0	1.5	0	4	n.a.	n.a.	n.a.	0
Guinea	16	13.0	0	0	0	0.0	0	4	n.a.	n.a.	n.a.	0
Guyana	n.a.	n.a.	1	0	0	2.0	1	3	n.a.	n.a.	n.a.	0
Haiti	18	12.1	0	0	0	0.0	0	4	n.a.	n.a.	n.a.	0
India	33	13.0	5	7	11	3.0	7	1	20.8	152.6	49.3	0.825
Indonesia	35	12.0	4	3	1	4.0	4	1	35.7	93.2	45.0	1.101
Iran	9	10.9	2	0	0	1.0	0	3	n.a.	n.a.	n.a.	0
Iraq	10	7.0	2	0	0	1.0	0	3	n.a.	n.a.	n.a.	0
Kenya	16	13.8	2	1	0	3.0	3	2	n.a.	n.a.	n.a.	0.029
Mali	16	5.0	0	0	0	1.5	0	4	n.a.	n.a.	n.a.	0
Mauritania	n.a.	n.a.	0	0	0	0.0	0	4	n.a.	n.a.	n.a.	0
Niger	16	7.0	1	0	0	1.0	2	3	n.a.	n.a.	n.a.	0
Nigeria	22	13.0	3	2	6	3.0	4	2	7.7	22.0	18.0	1.191
Philippines	37	13.0	7	7	6	4.0	7	1	371.6	149.8	46.3	2.940
Saudi Arabia	11	4.8	0	0	0	0.0	0	3	n.a.	n.a.	n.a.	0
Senegal	n.a.	n.a.	2	1	1	2.0	5	3	14.9	1650.0	93.0	0.046
Syrian Arab Rep.	10	6.0	0	0	0	0.0	1	3	n.a.	n.a.	n.a.	0
Tanzania	18	13.0	2	2	3	4.0	4	2	n.a.	n.a.	n.a.	0.098
Uganda	17	5.0	2	1	2	2.0	4	3	n.a.	n.a.	n.a.	0.060
Upper Volta	17	5.0	0	1	1	0.0	0	3	n.a.	n.a.	n.a.	0
Yemen Arab Rep.	9	4.8	0	0	0	0.0	0	4	n.a.	n.a.	n.a.	0
Yemen Dem.	n.a.	4.8	0	0	0	0.0	1	4	n.a.	n.a.	n.a.	0
Zaire	17	5.0	1	1	1	1.0	4	2	n.a.	n.a.	n.a.	0.201

*Basic independent variables

**Dependent variables

OPTIMAL MANAGEMENT OF GLOBAL TUNA RESOURCES

Man-Loong Chan, Ph.D.*
Tetra Tech, Inc.
3700 Mt. Diablo Blvd.
Lafayette, CA 94549
*currently affiliated with Systems Control, Inc.,
1801 Page Mill Road, Palo Alto, CA 94304

J.E. Buchanan W. Garling J. Sasser, Jr.
Tetra Tech, Inc.
1911 Ft. Meyer Drive
Arlington, Virginia 22209

Abstract

A global bionomic model capable of evaluating management policies for the world tuna resources is developed. The model integrates the biological and economic forces into an analysis framework. It is made up of two major modules: a Population Dynamics Module (PDM) and an Economic Module (EM). The model has been coded and tested on a computer. The PDM tracks the variations in the populations of the different tuna stocks throughout the world. The EM computes the profit-maximizing fishing efforts of the various countries at different fishing grounds, given the available standing crops and a world ex-vessel price of tuna. This computation of fishing efforts is accomplished using a linear programming model. The model as currently formulated is particularly useful for evaluating the various tuna management alternatives. It is useful as a screening tool to reduce the numerous tuna management alternatives (and their combinations) into a smaller set of options for more detailed assessment.

1. Introduction

This paper describes a global bionomic model for evaluating management policies for the world tuna resources. It highlights the functions and operating characteristics of the model, its uses and limitations, and the attendant data needs.

The model, entitled the Global Tuna System Model, has been developed to achieve several goals. It should be capable of delineating the interplays between biology and economics. This is accomplished by simulating the biological dynamics of the different tuna stocks in the world, and representing the economic forces governing the different tuna fisheries throughout the world. It should also be able to evaluate tuna population dynamics models as management tools. The model should also serve as a framework for organizing data bases to be used in the evaluation of tuna management alternatives.

To accomplish these goals, the model has been developed and coded in modular forms to accomodate modifications in the future. It is conceptually correct but has not yet been fully verified. However, as more data become available and a better understanding of dynamics is gained, the model can easily be modified. The model includes five versions, each of which incorporates a different version of the Population Dynamics Module.

The remaining portion of this paper consists of two sections. Section 2 presents a description of the model and its uses and limitations. Section 3 describes the input requirements and the output generated by the model.

2. Description of the Model

General Description of the Model

The Global Tuna Systems Model is made up of two major modules: a Population Dynamics Module (PDM) and an Economics Module (EM). The PDM tracks the variations in the populations of the different tuna stocks throughout the world. These variations are due to reproduction, natural mortality, recruitment, fishing mortality, and migration.

The Economics Module (EM) computes the profit-maximizing fishing efforts of the various countries at different fishing grounds, given the available standing crops and a world ex-vessel price of tuna. This amount of fishing effort is then translated into landings, the sum of which comprises the world supply tuna. The demand for tuna by various consuming nations is next computed. If the supply matches the demand at the ex-vessel price, then this price and quantity will constitute the equilibrium quantities; otherwise, the above computations are repeated with a different ex-vessel price until approximate equality is achieved between supply and demand quantities.

The interrelationship between the PDM and the EM is illustrated in Figure 1. As indicated in the figure there are five versions of the Population Dynamics Module: Generalized Production Model, Cohort Model, Schaefer's Model, Leslie Matrix Model, and the Birth-Death Process Model. Since the Shaefer's Model is a special case of the Generalized Production Model, in essence there are only four versions. Each of these four versions is integrated into a specific version of the Economics Module.

Formulations of the Model

The mathematical formulations of the model are summarized below. It should be noted that the population dynamics are formulated in terms of bionumbers. Translating these into units of biomass

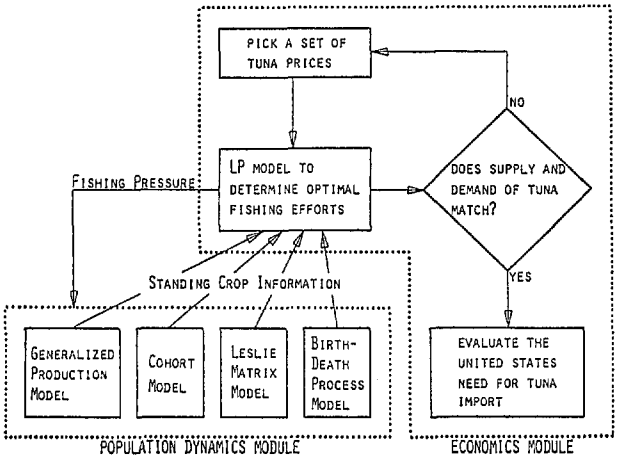

FIGURE 1 INTERRELATIONSHIP BETWEEN POPULATION DYNAMICS MODULE AND ECONOMICS MODULE

can be easily accomplished by multiplying with the appropriate average biomass per fish.

Population Dynamics Module

a. Generalized Production Model

The generalized production model is a variation of the Bernoulli's equation (Chapman, 1967; Pella and Tomlinson, 1969). In particular, it also includes the effects of fishing mortality and migration.

$$\frac{dP_{j\ell}(t)}{dt} = H_{j\ell}\, P_{j\ell}^{m_{j\ell}}(t) - K_{j\ell}\, P_{j\ell}(t) - q_{j\ell} \sum_{i,k} V_{ik\ell} \frac{f_{ijk\ell}(t)}{T_{ijk\ell}} P_{j\ell}(t) + \sum_{m\neq\ell} \beta_{jm\ell}\, P_{j\ell}(t-\Delta_{n\ell}) - \beta_{j\ell\ell}\, P_{j\ell}(t)$$

where t = time in half years

$P_{j\ell}(t)$ = bionumber of species j at fishing ground ℓ at time t

$H_{j\ell}, K_{j\ell}, m$ = constants

$V_{ik\ell}$ = number of fishing vessels of type i in the fleet of country k at fishing ground ℓ

$f_{ijk\ell}(t)$ = fishing effort in fishing days of boat type i, country k, catching species j at fishing ground ℓ at time t

$q_{j\ell}$ = catchability coefficient

$T_{ijk\ell}$ = conversion factors that translate fishing efforts into units of fishing days with respect to a standard size vessel and type

$\beta_{jm\ell}$ = migration mortality coefficient of species j transferring from fishing ground n to ℓ

$\Delta_{n\ell}$ = transit time to migrate from fishing ground n to ℓ

It should be noted that Schaefer's Model is a special case of this model, with $m_{j\ell}$ being set equal to two (Schaefer, 1954; 1957).

b. Cohort Model

This is an age-specific population dynamics model with the capability of accommodating up to ten age classes. It is a variation of the Murphy catch equation (Tomlinson, 1970; Murphy, 1965; 1966). Migration and fishing mortality are also incorporated into the model.

$$\frac{dN_{j\ell}^{(m)}(t)}{dt} = \begin{cases} -M_{j\ell}^{(m)} N_{j\ell}^{(m)}(t) - \beta_{j\ell\ell} N_{j\ell}^{(m)}(t); & t_{j\ell}^{r} \leq m < t_{j\ell}^{c} \\ \sum_{n\neq\ell} \beta_{jn\ell} N_{jn}^{(m)}(t) - \beta_{j\ell\ell} N_{j\ell}^{(m)}(t) - \left[M_{j\ell}^{(m)} + q_{j\ell}^{(m)} \sum_{i,k} V_{ik\ell} \frac{f_{ijk\ell}^{(t)} F_{j\ell}^{(m)}}{T_{ijk\ell}} \right] N_{j\ell}^{(m)}(t); & m \geq t_{j\ell}^{c} \end{cases}$$

with $N_{j\ell}^{(1)}(0) = g\left(\sum_{m=2}^{M} N_{j\ell}^{(m)}(t)\right)$, spawner-recruit relationship

and $N_{j\ell}^{(m)}(t_+) = N_{j\ell}^{(m-1)}(t_-)$

where

$N_{j\ell}^{(m)}(t)$ = population size (in bionumber) of age class m of species j at fishing ground ℓ at time t

$M_{j\ell}^{(m)}$ = natural mortality coefficient

$F_{j\ell}^{(m)}$ = fraction of fishing effort applied to age class m

$g(\cdot)$ = spawner-recruit relationship, giving the number of recruits

$t_{j\ell}^{r}$ = age of recruitment, i.e., age at which the fish first become catchable

t_+ = beginning of year t

t_- = end of the year (t-1)

c. Leslie Matrix Model

The Leslie Matrix Model (Leslie, 1945) is a vector difference equation with a ten-dimensional vector, accommodating ten different age classes. The Leslie matrix relates the population size of the

stock at one time period to the next time period as shown below:

$$\underline{N}\ (t+1) = \underline{A}\ (t)\ \underline{N}\ (t)$$

where

t = time
$N\ (t)$ = vector of population size in bionumber of different age classes at time t
$\underline{A}\ (t)$ = Leslie matrix (10x10)

$$= \begin{bmatrix} 0 & f_1 & f_2 & f_3 & \cdots & f_9 \\ p_0 & 0 & 0 & 0 & \cdots & 0 \\ 0 & p_1 & 0 & 0 & \cdots & 0 \\ & & \vdots & & & \\ 0 & 0 & 0 & \cdots & p_8 & 0 \end{bmatrix}$$

f_i = fecundity rate of age class i

p_i = probability of a fish of age i surviving to the age (i+1)

$$= 1 - 0.5\left(M_{j\ell}^{(i)} + q_{j\ell}^{(i)} \sum_{i,k} V_{ik\ell} \frac{f_{ijk\ell}(t)}{T_{ijk\ell}} F_{j\ell}^{(i)}\right)$$

d. Birth-Death Process Model

The Birth-Death Process Model is a variation of the stochastic process formulation used in epidemilogic research (Karlin, 1969). The state of the stochastic process $N_{j\ell}(t)$ represents the number of individuals in a stock j at fishing ground ℓ. Its transition from one state to another, representing the population size fluctuation, is governed by probability measures related to a Poisson process (Papoulis, 1965). Then the expected population size $M_{j\ell}^{(i)}(t)$ at time t, given an initial mean population size of i, is described by the following differential equation:

$$\frac{dM_{j\ell}^{(i)}(t)}{dt} \cong \left(a_{j\ell} - b_{j\ell}\right) + \left(\lambda_{j\ell} - \mu_{j\ell}\right) M_{j\ell}^{(i)}(t)$$

with $M_{j\ell}^{(i)}(0) = i$

where

$$M_{j\ell}^{(i)}(t) = E\left[N_{j\ell}(t) \middle| N_{j\ell}(0) = i\right] = \sum_{k=0}^{\infty} P_{ik}^{j\ell}(t)$$

$$P_{ik}^{j\ell}(t) = Pr\left\{N_{j\ell}(t) = k \middle| N_{j\ell}(0) = i\right\}$$

$N_{j\ell}(t) = \{0, 1, 2, \ldots\}$; bionumber of stock j at the ℓth fishing ground

$$Pr\left\{N_{j\ell}(t+h) = i+1 \middle| N_{j\ell}(t) = i\right\} = \left(a_{j\ell} + i\lambda_{j\ell}\right) h + \theta(h)$$

$$Pr\left\{N_{j\ell}(t+h) = i-1 \middle| N_{j\ell}(t) = i\right\} = \left(b_{j\ell} + i\mu_{j\ell}\right) h + \theta(h)$$

$$Pr\left\{N_{j\ell}(t+h) = i \middle| N_{j\ell}(t) = i\right\} = 1 - \left[a_{j\ell} + b_{j\ell} + i\left(\lambda_{j\ell} + \mu_{j\ell}\right)\right] h + \theta(h)$$

with $\lim_{h \to 0} \theta(h) \to 0$

h = very small time increment

$a_{j\ell}$ = immigration rate

$\lambda_{j\ell}$ = fecundity rate per spawner

$b_{j\ell}$ = emigration rate

$$\mu_{j\ell} = M_{j\ell} + q_{j\ell} \sum_{i,k} V_{ik\ell} \frac{f_{ijk\ell}}{T_{ijk\ell}}$$

Economics Module

To determine the profit-maximizing fishing efforts the following linear programming (LP) model is used:

maximize

$$\sum_{i,j,k} \left(P_j\ q_{jl}\ V_{ikl}\ P_{jl} - b_{ik}\right) \frac{f_{ijk\ell}}{T_{ijk\ell}} - F_{ik}$$

subject to

$$\sum_{i,k} q_{j\ell}\ V_{ik\ell} \frac{f_{ijk\ell}}{T_{ijk\ell}}\ P_{j\ell} \leq \min\left\{B_{j\ell}, Q_{j\ell}\right\}$$

$$\sum_{j} q_{j\ell}\ V_{ik\ell} \frac{f_{ijk\ell}}{T_{ijk\ell}}\ P_{j\ell} \leq C_{ik\ell}$$

$f_{ijk\ell} \geq 0$ for all i,j,k,ℓ

where

P_j = ex-vessel price per ton of tuna species j

b_{ik} = variable cost per ton of tuna landing by country k of boat type i

F_{ik} = fixed cost per vessel

$B_{j\ell}$ = standing crop of species j at fishing ground ℓ
$Q_{j\ell}$ = catch quota for species j at fishing ground ℓ
$C_{ik\ell}$ = fleet capacity of boat type i, country k, at fishing ground
$V_{ik\ell}$ = fleet size of boat type i, counting k at fishing ground

This LP model is solved for a different fishing ground each time, assuming the fleet sizes $V_{ik\ell}$'s are dispatched to each region based on an investment function. Summing up the landings from each fishing ground gives the world's supply of tuna for a given set of ex-vessel prices P_j's.

The following investment function is based on research conducted by Huppert (1976):

For the first five years:

$$V(t+1) = V(t) + C(t) \qquad t = 1, 2, 3, 4$$

where

$V(t)$ = number of vessels in the fleet at time t
$C(t)$ = change in the number of vessels for the time period t

After five years,

$$V(t+1) = \begin{cases} V(t) + 20 & \text{if } A(t) \geq 0.2 \\ V(t) + 100A(t) & \text{if } 0 \leq A(t) < 0.2 \\ 0.95\ V(t) & \text{if } -0.1 \leq A(t) < 0 \\ 0.75\ V(t) & \text{if } -0.2 \leq A(t) < -0.1 \\ 0.5\ V(t) & \text{if } A(t) < -0.2 \end{cases}$$

where

$$A(t) = \sum_{i=2}^{5} \frac{\pi\ (t-i)}{3\ V(t-i)}$$

$\pi(t)$ = profit for year t

For this study, the following demand function is based on the research of Bell (1969).

$$\ell n\ D = \alpha - \beta\ \ell n\ p + \gamma\ \ell n\ I$$

where ℓn D is the natural logarithm of tuna demand by a country, ℓn p the natural logarithm of tuna price, ℓn I the natural logarithm of per capita disposable personal income in a country, and α, β, γ are constants.

Uses of the Model

This Global Tuna System Model is useful for evaluating the following management alternatives: setting of total catch quota on different species at the various fishing grounds; setting of different countries' landing quota at various fishing grounds; regulations on fleet capacity expansions; policy affecting the tuna demand; tuna fleet investment policies; and regulations on uses of fishing gears.

The current model as formulated is also capable of considering the management alternative of adopting 200-mile fishing zones, except that the memory core and computer time requirements are prohibitive. The equivalent number of fishing grounds must be doubled, and the complete model run using at least monthly time intervals instead of the current semi-annual intervals. Moreover, the cost functions must be modified for each month.

The model also has other uses. It serves as a framework to guide the data collection procedure needed for evaluating management strategies. It specifies data requirements, and thus data collection schemes can be designed to minimize extraneous efforts.

The model can also serve as a screening tool to reduce the numerous management alternatives (and their combinations) into a smaller set of options. This smaller set of options can next be evaluated in detail, taking into account political, institutional and other considerations. However, the model should not be construed as the ultimate only authority on what the optimal management policy should be.

Limitations of the Model

The current formulation does not give a truly optimal solution. The assignment of fleet sizes to various fishing grounds is pre-specified at the beginning of the season. Ideally this should be part of the optimization problem and should be computed concurrently with the fishing effort optimization.

The current formulation is not truly optimal for another reason: The LP model is run for one region at a time. The mathematical formulation, of course, is set up to provide the global optimum. Unfortunately the large computer core size requirement forces the adoption of suboptimal solutions.

The current model also has other limitations. On the biological side, the catchability coefficient does not take the density-dependency into account. As a result the landing value may be inaccurately estimated.

The unit stock also need to be properly defined. The constants cited in the literature for the different population dynamics models may not always be appropriate if the unit stock does not correspond to the geographical specifications of the model.

An added dimension to the unit stock concept is the migration effect. The incorporation of migration may influence the constants used in defining the population dynamics. Consequently, a new estimation scheme may be in order to properly discern the interaction between unit stock and migration.

The other major limitation associated with the biological aspect of the model is that many of the required parameters are age-specific.

Obtaining the data to estimate these parameters may be difficult.

Another major limitation related to the biological aspect of the model is the lack of reliable estimates of the fishing power conversion factors. Such estimates should be able to take into account the catchability of different stocks by the various types of fishing gear.

On the economical side, one major limitation of the model is that perfect competition has been assumed in the model. But the real world is an imperfect competition market. A handful of tuna-consuming or -producing nations can affect the market drastically. Consequently, the Economics Module should be modified in the future to accommodate this consideration.

This model also assumes that the objective of all the producing nations is to maximize the total profits. But each nation may have different objectives (e.g., equity, employment, foreign exchange), so that the objective in this model may need to be modified for the proper management of the fishery.

The adoption of this objective also has the implicit assumption that an international tuna management council exists which has jurisdiction over all the global tuna resources. In this case the "council" decides that profit maximization is the best for all nations involved. In reality such a "council" does not truly exist. Consequently, the Economics Module may benefit from a modified formulation.

The model also utilizes a relatively primitive formulation of the demand function. Interactions among the demands for other tuna species have not been fully taken into account. Other important considerations like the price of substitutes have not been incorporated. Moreover, the demands of nations other than those of the United States cannot be accurately estimated due to the lack of supporting data bases. These demands were rather crudely extrapolated from the United States demand in this project. Future refinement of this demand formulation is in order.

3. Input and Output

There are two major groups of input data: fishery and population dynamics related. The fishery related inputs include: number of boat types, species, tuna-producing nations and fishing grounds; definition of boat types, species, tuna-producing nations and fishing grounds; fishing fleet size; variable and fixed costs associated with each type of fishing vessel; changes in fleet sizes; and management alternatives (e.g., catch quota, legal size limitations, fishing gear limitations).

The population dynamics related inputs include the following categories of information (Age-specific data may be required for some versions of the model.): Initial population size; natural mortality rate; constants for the von Bertalanffy growth equation (1938) and the weight-length relationship; mortlaity rates associates with migration; spatial distribution of tuna species; catchability coefficient; fishing power conversion factors; spawner-recruit relationships; and fecundity rates.

The output consists of two groups of information. The first group pertains to the standing crop. It shows the biomass and bionumbers of different tuna stocks at various fishing grounds.

The other group of output is related to the catches. A tabular output summarizing the tuna catches by various types of boats owned by different producing nations is given for each fishing ground at each half of a year. At the end of all these tabular outputs is a summary of the world's tuna market indicating the total catches in metric tons segregated by species, countries, and types of fishing vessel.

References

Chapman, D.G., 1967. "Statistical Problems in the Optimum Utilization of Fisheries Resources", Int. Stat. Inst. Bull., Vol. 42, No. 1, pp. 268-290.

Huppert, D., 1976. Personal communication.

Karlin, S., 1921. A First Course in Stochastic Processes, Academic Press, 4th ed.

Leslie, P.H., 1945. "On the Use of Matrices in Certain Population Mathematics", Biometrika, Vol. XXXIII, Part III, November, pp. 183-212.

Murphy, G.I., 1965. "A Solution of the Catch Equation", J. Fish Res. Board of Canada, Vol. 22, pp. 191-202.

Murphy, G.I., 1966. "Population Biology of the Pacific Sardine (Sardinops Caevulea)", Proc. Calif. Acad. Science, Vol. 34, p. 84.

Papoulis, A., 1965. "Probability, Random Variables and Stochastic Processes", McGraw-Hill.

Pella, J.J. and P.K. Tomlinson, 1969. "A Generalized Stock Production", Inter-Am. Trop. Tuna Comm. Bulletin, Vol. 13, pp. 419-496.

Tomlinson, P.K., 1970. "A Generalization of the Murphy Catch Equation", J. Fish. Res. Board of Canada, Vol. 27, pp. 821-825.

von Bertalanffy, L., 1938. "A Quantitative Theory of the Organic Growth", Human Biology, Vol. 10, pp. 181-213.

A MICROCOMPUTER-BASED ECHO-INTEGRATION SYSTEM FOR FISH POPULATION ASSESSMENT

Raynard Y. Kanemori and John E. Ehrenberg

Applied Physics Laboratory
University of Washington
1013 N.E. 40th, Seattle, WA 98105

ABSTRACT

Abundance estimates obtained with acoustic echo-sounding equipment play an important role in the management of fish stocks. The common technique presently used is to process the signal from the echo sounder with a digital computer or to record the analog signal for later processing.

A microcomputer-based echo-integration system has been developed for fish population assessment. It is a relatively inexpensive, field-oriented, portable instrument that can process data in real time from any existing echo sounder. The signal from the echo sounder is detected, digitized, squared, and averaged for various depth ranges. The averaged squared echo level is then scaled to provide a measure of the density of the fish school at the selected depth ranges. The system automatically tracks the bottom depth and prevents integration of the return from the bottom.

1. INTRODUCTION

Recently, there has been an increase in the use of acoustic techniques for fish population assessment. The two common acoustic techniques used to estimate fish abundance are echo counting and echo integration. In echo counting, the density is obtained from the acoustic return by a processor that counts the number of fish echoes. Echo counting provides a good abundance estimate for low-density fish populations. However, it can not be used for high-density fish populations because the echoes from the individual fish overlap. The echo-integration method does not have this limitation. The basic principle behind echo integration is that the echoes from individual fish add incoherently.[1] In other words, the average value of the squared signal scattered from a fish school is proportional to the number of fish. An echo-integration system calculates the average squared echo sounder output for various depth layers. The averages are then scaled to provide estimates of the fish density.

A number of different echo-integration systems have been developed.[2-5] Analog echo-integration systems have been found to be inaccurate, and they have inadequate dynamic range compared with digital echo-integration systems. Some digital echo-integration systems have been implemented using minicomputers.[3,4] Although minicomputer-based systems have great storage and processing power, they are very expensive and normally data can not be processed in real time because of their size. A tape recorder is used to collect the fish data in the field and the data are then processed on the minicomputer-based echo-integration system at the laboratory.

With the advent of microprocessor technology, an echo-integration system can be built that has the same processing power as a minicomputer-based system. A microcomputer-based echo-integration system with limited capabilities has previously been developed by Wiebe and Stevens.[5] The system discussed here is an extension of past work on echo-integration systems done at the University of Washington. The system calculates the averaged squared echo voltage levels for up to ten different depth ranges. The digital integrator output for a given depth range, R1 to R2, is

$$I_{R1,R2} = \sum_{i=1}^{N} V_i^2/N ,$$

where V_i^2 is the squared sample values of the detected echo signal and N is the number of samples processed for the depth layer. The output is later scaled to provide an estimate of the density of the fish school at the selected depth ranges. The scale factor relating the integrator output to fish density, λ, is split into two parts. That is,

$$\lambda = A \cdot B \cdot I_{R1,R2} ,$$

where A is a constant that depends on parameters that are not depth dependent, B is a constant that depends on the time-varied gain characteristics of the sounder and the depth range being processed, and $I_{R1,R2}$ is the digital integrator output for the depth range from R1 to R2.

2. HARDWARE DESIGN

A block diagram of the hardware for the microcomputer-based echo-integration system is shown in Figure 1. The analog signal-processing hardware includes an amplifier which increases the amplitude of the input signal from the echo sounder, and an envelope detector which consists of a rectifier and a low-pass filter. These circuits were implemented with operational amplifiers.

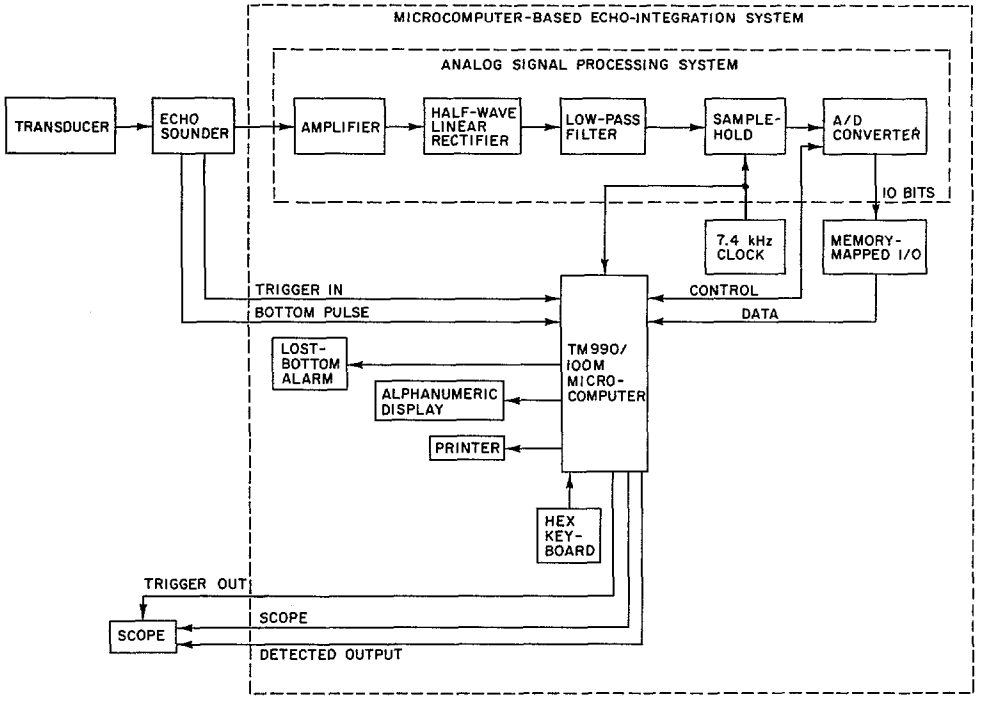

Figure 1. Block diagram of the microcomputer-based echo-integration system hardware.

The signal from the analog signal-processing hardware is digitized by a sample-hold integrated circuit and a 12-bit analog-to-digital converter. The signal is sampled at a rate of 7.4 kHz by an asynchronous clock. The converter has a short-cycled conversion time of 6 μs because only 10-bits are being used. This leaves about 129 μs for the real-time integration process.

The microcomputer used in the present system is a TM 990/100M, which is a single-board computer based on the 16-bit TMS 9900 microprocessor. The board has a maximum of 512 words of Random Access Memory and 4000 words of Erasable Programmable Read-Only Memory as well as programmable serial and parallel input/output interfaces. If more capability is needed, the memories and I/O can be expanded. The TM 990/100M runs at a clock rate of 3 MHz. There are 15 external maskable interrupts. The board also has hardware multiply and divide.

The input devices consist of a keyboard to input the parameters for the integration program and a number of switches that interrupt the computer to perform various tasks required by the user. These parameters and tasks are discussed in the software section of this paper.

The output devices consist of a portable printer which lists the parameters and final integration results and a 16-character, alphanumeric, light-emitting diode display which is used for the same purpose. An oscilloscope displays the signal that is being integrated and the depth ranges that are being processed. The bottom depth is tracked automatically by the microcomputer software so that the echo return from the bottom is not integrated. A bottom alarm is set off when the bottom pulse is lost.

3. SOFTWARE DESIGN

A block diagram of the software for the microcomputer-based echo-integration system is shown in Figure 2. The initialization of the software starts the interactive parameter-entry program. This program asks the user to input the parameters for the integration program through the keyboard. The questions include (1) the duration of the run, which is set by the number of pings; (2) the normalizing constant, which converts the final integrated value to fish density (this constant depends on the target strength and acoustic system parameters such as source level, gain, transducer directivity, and receiving response); (3) the threshold to eliminate unwanted noise; (4) the depth intervals; and (5) the time-varied gain corrections. Up to 10 depth intervals can be processed with this system. The integration program begins when the last parameter is entered. This program strobes the sample-hold to begin the data acquisition process. It then checks the A/D converter to see if the sample has been converted. Digitization takes 6 μs. After the sample has been digitized, the data are transferred to the microcomputer. The sample is squared and accumulated. The accumulation is done using 32-bit double-precision addition. The depth of the acoustic return is determined by keeping track of the number of samples processed following the trigger pulse. The number of samples is directly proportional to the depth. For a 7.4-kHz sampling rate, a depth interval of 1 m contains 10 samples.

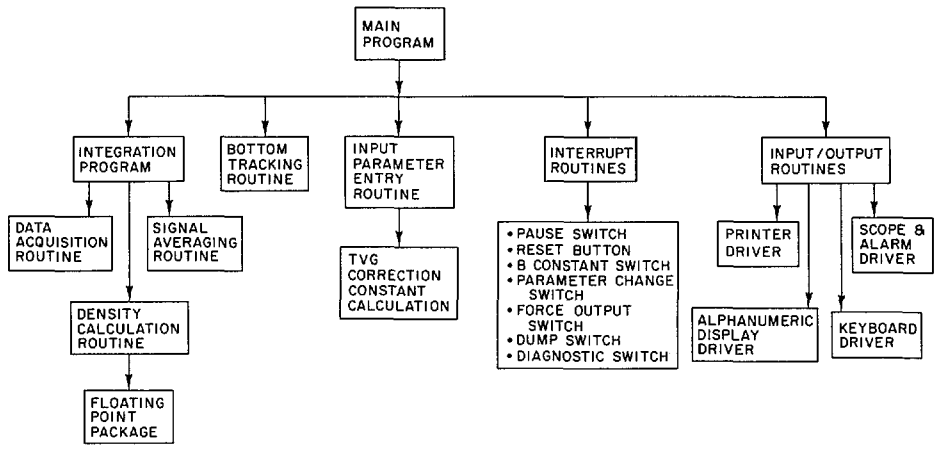

Figure 2. Block diagram of the microcomputer-based echo-integration system software.

The bottom is tracked automatically by the microcomputer. A bottom pulse from the echo sounder sends an interrupt signal to the microcomputer to begin the bottom-tracking routine. A time window is created around the interrupt signal, and the next bottom pulse is checked to see if it is within the time window. If it is, the window is centered about the present bottom pulse. If a bottom pulse falls outside the window, the integration process stops and the microcomputer waits for the next trigger pulse. If the bottom pulse is outside the window again, an alarm is sounded.

After all the samples are accumulated, the average value is calculated for each depth range by dividing the accumulated totals by the number of samples. The results are then scaled to provide a measure of the density of the fish school.

Each switch on the front panel has a task. If a switch is turned on, it will send an interrupt to the microcomputer. The microcomputer will go to the routine selected by the switch and perform the task. A pause switch is used to stop the integration temporarily. The diagnostic switch is used to check the functioning of the keyboard, printer, display, and memory. The force output switch is used to stop the integration at any time and print the results. The parameter change switch is used to change parameter values in the integration program. The dump switch is used to reset the accumulators for each depth layer to zero.

4. CONCLUSIONS

A prototype unit has been constructed, and is shown in Figure 3. The unit is currently being tested in the laboratory with tape-recorded data. As soon as the laboratory testing is completed, the unit will be ready for field testing.

Several improvements can be made in the future to increase the capabilities of this system. One improvement might be to provide a method

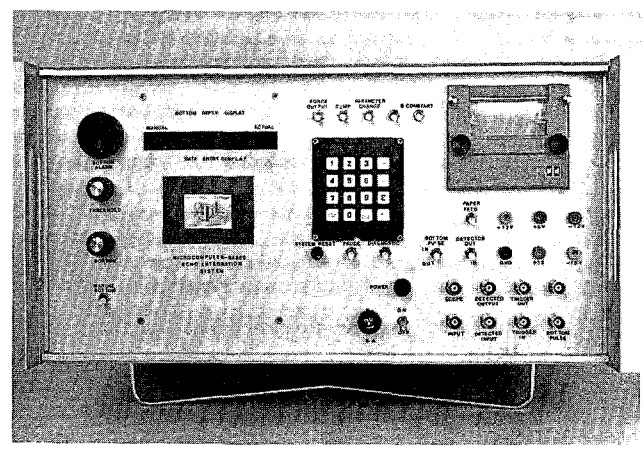

Figure 3. The prototype unit.

for mass storage of the digital data for later processing. Floppy disk systems, cassette tape recorders, and bubble memory boards are some of the alternative storage devices. Another future improvement will be to calculate the time-varied gain constant and the final density in real time. This could be done by hardware built around an integrated-circuit floating-point processor, or by software written in FORTRAN and using the stand-alone FORTRAN library. If the software approach is chosen, additional memory must be incorporated into the present prototype.

The microcomputer-based echo-integration system appears to have much potential. This system should provide an accurate, inexpensive, and portable method for the real-time estimation of fish stock size.

5. ACKNOWLEDGMENTS

The research described in this paper was sponsored in part by the Washington Sea Grant program under National Oceanic and Atmospheric Administration Grant 04-7-158-44021. The authors would like to thank Dr. Gregory Zick of the University of Washington Department of Electrical Engineering for the use of his microprocessor development system during the software development.

REFERENCES

1. J. Ehrenberg and D. Lytle, "Acoustic Techniques for Estimating Fish Abundance," IEEE Trans., Vol. GE-10, pp. 138-145, 1972.

2. H.W. Lahore and D.W. Lytle, "An Echo Integrator for Use in the Estimation of Fish Populations," Washington Sea Grant Publ. (70-1), 1970.

3. R.E. Thorne, "A New Digital Hydroacoustic Data Processor and Some Observations on Herring in Alaska," J. Fish. Res. Board Can., 34:2288-2294, 1977.

4. P.H. Moose, J.E. Ehrenberg and J.H. Green, "Electronic System and Data Processing Techniques for Estimating Fish Abundance," Proc. IEEE Conf. on Eng. in the Ocean, Vol. 1, pp. 33-36, 1971.

5. A.J. Wiebe and D. Stevens, "Digital Integrator Enhances Echo Sounder's Accuracy" in Applying Microprocessors, L. Altman and S. Scrupski, eds., McGraw-Hill, pp. 145-146, 1976.

PROSPECTS FOR THE DEVELOPMENT OF A SWATH FISHING VESSEL

Mark S. Rice
Advanced Design Staff
SEACO, Incorporated
Kailua, Hawaii 96734

Jack Harmon
Systems Engineering and Analysis
SEACO, Incorporated
Kailua, Hawaii 96734

ABSTRACT

The modern fishing fleet has adopted multiple fishing techniques for survival. A single vessel is equipped to deep trawl, shallow trawl, long-line and even set pots for lobster and crabs. In this way, today's fisherman is no longer restricted to the fortunes of the traditional one-technique fishing boat. Data are presented on the variable requirements for the Central Pacific industry and the type of vessel that is needed.

The introduction into modern ship design of the Navy's SWATH* concept provides the industry with an advanced craft that has a wide expanse of usable deck and work spaces and extraordinary stability for safer, more effective deployment of equipment. The numerous features of the SWATH design are discussed, and a specific, though necessarily preliminary, design is presented for an advanced Semi-submerged Fishing Vessel (SSFV) that will be constructed in the early 1980's.

INTRODUCTION

SEACO, Incorporated has initiated a program in Hawaii that will culminate in the construction of a Semi-submerged Fishing Vessel (SSFV). The program calls for the cooperation of several state, federal and commercial concerns in developing and building a vessel that can economically fish the Central Pacific. The program is unprecedented in that it involves a cooperative government/commercial effort to match an advanced technology to present fishing needs.

The present schedule calls for design of the SSFV to be completed in 1979. Construction of the first of five initial vessels is to begin in early 1980. Construction will commence on subsequent vessels at four to six-month intervals. Inquiries have been received from both scientific and industrial organizations that are interested in the unusual advantages of this type of vessel.

The SSFV is an outstanding example of the military technology transfer to the civilian sector. The SEACO advanced fishing concept, Figure 1, is a close relative to the Navy's Stable Semi-submerged Platform (SSP) *KAIMALINO*; its introduction into other industries is long overdue. The benefits to be derived from such a vessel are discussed in numerous Navy publications and are summarized in this report as they pertain to the fishing industry.

*Small Waterplane Area Twin Hull

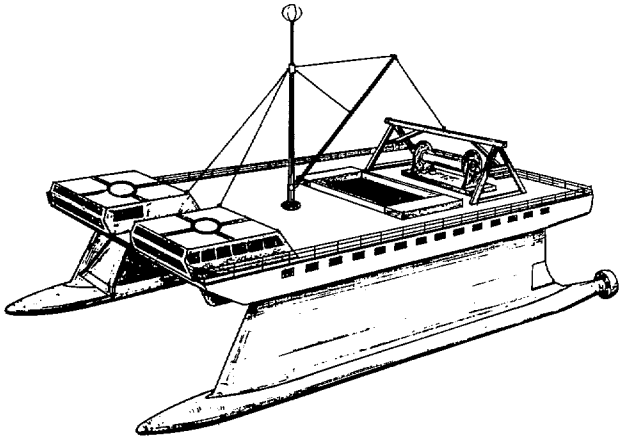

FIGURE 1. SEACO's SSFV Concept

REQUIREMENTS FOR MULTI-SPECIES FISHING VESSELS

In seeking a profitable return on investment, the modern fisherman faces both economic and legislative restrictions. The economic restrictions are generated by the market via the influence of intermediates in the marketing structure; the modern fisherman can do little to influence either the intermediates or the consumer. Furthermore, he has limited control over legislative restrictions since they often stem from environmental limitations or international political pressures. To remain profitable in the face of these variable restrictions, the modern fishing vessel must be VERSATILE--the vessel's return on investment can no longer depend on a single species of fish or a single fishing technique. As noted by Blount and Schaefers (Reference 1) more than a decade ago:

> "There is a growing trend in the USA for combination-type fishing vessels to be built in areas other than the Pacific coast. This trend has been brought about by the realization that by building combination-type vessels, fishermen are able to harvest several types of fish, each of which may require a different type of gear. This provides for year-round use of vessels and removes the risk that one-purpose boats always face, dependence on a single type of fish, the abundance and availability of which may fluctuate greatly."

Since the Blount and Schaefers article, the availability of many commercially important species has declined and today the economic pressures in many fisheries are more severe than at any time in the past. In contrast, recent legislative action has given the U.S. fisherman an unparalleled opportunity to compete with foreign boats in U.S. coastal waters via the

recently enacted 200-mile territorial limit. The result of the relaxation in foreign competition is manifest in several present conditions, namely:

- Increased speculative capital for new vessel design and construction
- Increasing competition among U.S. vessels, and
- Growth of larger conglomerate fishing organizations

Thus, there are two sources of pressure in today's U.S. commercial fishing industry, both of which suggest that technological advances are imminent, namely:

- Increased economic pressure promoting versatility
- Increased potential profits resulting from 200-mile restrictions

The Central Pacific fishery represents a special case of the general U.S. fishing industry. That is, the 200-mile territorial limit, when applied to the Hawaiian chain alone, results in more than 800,000 square miles of rich fishing grounds that are now under U.S. jurisdiction. Although the region is in a temporate climate, sea conditions are generally bad throughout the year. The fishing within this region is characteristic of deep open-ocean fishing. Species sought commercially within this region range from crustacea to pelagic. Fishing in the vicinity of shoals and reefs is commonplace while the long-line is a principle technique in open-ocean work. A general summary of species sought and landed in Hawaii is given in Figure 2. This total is estimated to be a very small percentage of the landings that the region could ecologically support (Reference 2). Furthermore, this list of fish that are presently sought on a commercial scale by U.S. vessels does not include significant pelagic catches. The exploitation of open-ocean catches is currently being carried out only by foreign vessels that are operating under quotas established by the U.S. The U.S. vessels capable of the extended open-ocean fishing simply do not exist. Rather, the Hawaiian fishing fleet consists of a myriad of old designs that are interspersed with a handful of more modern vessels, all of which are under 125 feet in length.

Based on a knowledge of the resource, the shortcomings of existing fishing vessels, and the current economic situation, one is able to project a conceptually optimum vessel for work in the Central Pacific. The major characteristics of such a vessel are discussed below.

1. Range

The principal fishing port in the Central Pacific is Honolulu. From this port, a vessel may transit 1500 miles to the N.W. to the nearest refueling port, Midway Island. To the southwest. American Samoa represents the closest island of commercial significance at a range of more than 2200 miles. To the west, Guam and the scattered islands of the Pacific Trust Territory are all more than 1500 mile from Honolulu. Since the straight-line transits to these ports exceed, in all cases, 1500 miles, the working range of vessels fishing in these areas should be at least 4000 miles at design speed or 2000 miles at design speed with an additional range of 4000 miles at fishing speeds. Corresponding to these distances are deployment durations that range from three weeks to two months, depending upon fishing techniques and the catch found.

2. Displacement Tonnage

Displacement tonnage can be roughly correlated with overall vessel dimensions. The optimum dimensions for a multi-species, Central Pacific fishing vessel will be related to the economics of the vessel and its catch. It will be necessary to have a vessel of some minimum size to weather the sea conditions that will be encountered. Similarly, the vessel must have a catch holding capacity to make a 3,000 to 4,000 mile voyage profitable unless a mother ship is to be used for the transport of fuel, stores, crew, etc. The upper limit to vessel size will be governed both by the density of the species sought (operating costs per unit time must be well below the wholesale value of the catch brought on board per unit time) and by the capital available for vessel construction. Thus, an upper and lower limit to vessel size may be defined with relative ease while optimum size remains a function of numerous economic and ecological considerations.

ISLAND AND SPECIES	POUNDS CAUGHT	VALUE (DOLLARS)
Total landings	11,891,275	7,503,964
ISLAND		
Hawaii	2,361,850	1,754,979
Maui	750,414	277,209
Lanai	6,990	3,178
Molokai	35,761	27,175
Oahu	8,388,893	5,255,543
Kauai	347,367	185,880
SPECIES		
Sea catch, total[2]	11,871,076	7,486,272
Aku (Skipjack)	6,891,039	2,911,061
Ahi (Yellowfin)	1,723,128	1,463,376
Akule (Bigeye Scad)	746,857	442,211
Ahi (Bigeye)	425,537	845,188
Opelu (Mackerel Scad)	291,337	231,236
Striped Marlin	230,412	113,243
Opakapaka (Snapper)	147,505	165,195
Ono (Wahoo)	132,105	90,448
Mahimahi (Dolphin)	119,332	145,010
Ahipalaha (Albacore)	104,942	93,311
Ulua (Jack)	93,771	74,542
Ulaula Koae (Onaga)	80,543	162,219
Pacific Blue Marlin	73,582	22,108
Uku (Snapper Family)	69,832	68,321
Kawakawa (Bonito)	66,669	18,215
Limu	62,211	36,873
Hapuupuu (Grouper)	57,478	66,920
Kahala (Amberjack)	40,434	21,822
Weke (Goldfish)	37,086	21,673
Ulaula (Ehu) (Snapper)	34,310	58,411
Crab (Kona)	26,577	55,900
Pond Catch, total	20,199	17,692

[1]Shown separately for all species over 35,000 pounds or $50,000.

[2]Includes species not shown separately.

Source: Hawaii State Department of Land and Natural Resources, Division of Fish and Game, Commercial Fish Landings for Fiscal Year July 1975 through June 1976 (October 1976).

FIGURE 2: Commercial Fish Landings by Species and Island: Year Ended June 30, 1976, reproduced from the Hawaii State Data Book - 1977.

3. Speed

The optimum average speed for a Central Pacific fishing vessel is a function of five basic competing variables as shown in

Figure 3. It is apparent that drag will escalate as a function of the velocity squared via the basic equations for vessel drag and propulsive power:

$$D = C_d \tfrac{1}{2} \rho V^2 A$$

where: D = total drag

C_d = total drag coefficient

ρ = the mass density of sea water

V = velocity

A = characteristic area of the vessel

$$P = (DV)/\eta$$

where: P = power

η = propulsive efficiency

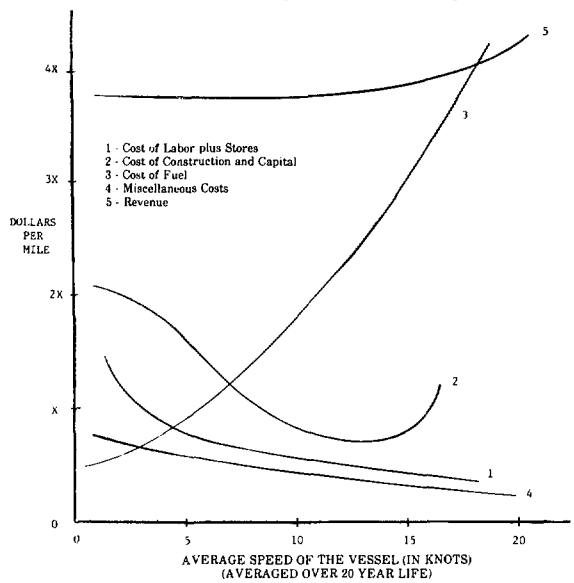

FIGURE 3. Semi-Qualitative Illustration of Fishing Vessel Revenue to Cost Ratio

The labor costs, expressed in terms of dollars per mile, will decrease as the average speed of the vessel increases. Similarly, the initial capital cost of the vessel amortized over the life of the vessel will decrease with increasing speed to the point where it costs proportionately larger amounts of initial capital to achieve the higher average speeds. The revenue (or value of catch) per mile will be relatively independent of speed except as increased speed may lead to increased fishing efficiency (as in the case of trawling for fish that can escape the trawl). The curves shown in Figure 3 are qualitative and thus represent only the general trends for each variable. The specific analysis for an individual vessel will be a function of many variables that characterize the vessel and its operation; however, these curves do illustrate the need for an iterative approach in determining fishing vessel revenue to cost ratios.

Although there are many other variables to consider in optimizing a Central Pacific fishing vessel, they may all be considered subordinate to the three principle variables: speed, displacement and range. Secondary variables include considerations such as: crew size, propulsion type, storage method, etc. However, the discussion to this point has assumed a standard hull configuration. Such assumptions are routinely made since basic hull shape/design has been standardized through many years of convergent design practices. Although size may vary from region to region, the basic design shapes of fishing hulls are remarkably similar throughout the United States. To some extent, the catamaran hull was a new approach to hull design for fishing vessels. Unfortunately, the catamaran has three basic characteristics that have limited its acceptance as a commercial fishing vessel, namely:

- The increased capabilities do not offset increased costs
- The concept's sharp motions make deck work hazardous
- It suffers from structural problems that result from wave-impact loading

In this paper, a radically different but already proven design is discussed with respect to its applicability as a fishing vessel.

THE SMALL WATERPLANE AREA TWIN HULL (SWATH) CONCEPT

The predecessors of the modern SWATH concept were early platforms designed without propulsion for stability where men worked in waves. From this initial concept, the idea evolved in two directions, the large drilling platform and higher-speed vessels such as the *DUPLUS* (Netherlands), the *KAIMALINO* (U. S. Navy), and the recent Mitsui vessel, *MARINE ACE* (Japan). These vessels may take various forms as shown in Figures 4 and 5.

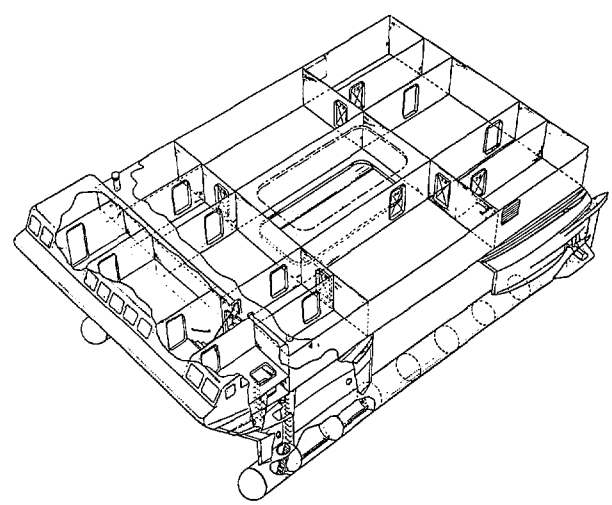

FIGURE 4. SSP *KAIMALINO* U. S. Navy Prototype SWATH Ship

The U.S. Navy's introduction to the semi-submerged ship concept came from Dr. Thomas Lang of the Naval Ocean Systems Center (NOSC). The concept combines two torpedo-shaped lower hulls and a box-like upper hull using four streamlined struts for support. The vessel was designed by the NOSC Hawaii Laboratory and is currently home-ported in Kaneohe, Hawaii. Although this vessel was designed for military use and does not have many design features that would make it suitable as a fishing vessel, it does have certain basic characteristics (Reference 3) that are representative of a SWATH fishing vessel as is discussed in the following paragraphs.

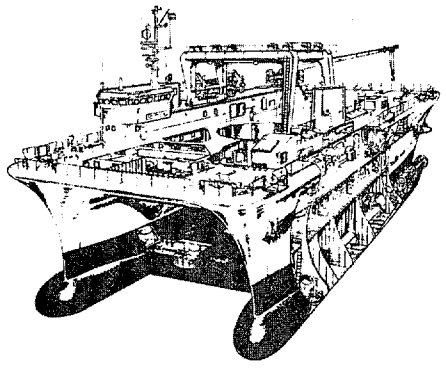

FIGURE 5. Trident "DUPLUS" Ship Concept

1. Stability and Seaworthiness

Perhaps the greatest advantage offered by the SWATH concept is its seaworthiness and stability under all weather, speed and heading combinations. As with a monohull, the natural period of the vessel in a given seaway will depend upon its external loading from deck gear, over-the-side loads, etc. However, it may be stated without exception that the natural periods of SWATH vessels in roll, pitch and heave are much longer than corresponding quantities for similar monohull vessels. Furthermore, the motions are highly regular with near-critical damping. Thus, the motions of a SWATH vessel in a seaway are in complete contrast to the motions of a catamaran which experiences short-period, sharply-damped motions.

2. Static Stability

When Dead-In-the-Water (DIW), a SWATH vessel has the stability attributes that have made the semi-submerged drilling platform a success. Waves pass between the upper and lower hulls with little change in the vessel's displacement. The beam of the SWATH vessel is not tied to overall displacement as in a monohull; thus, the beam may be a large fraction of the length, giving the vessel similar response to head and beam seas.

The lower hulls and control surfaces provide large drag in vertical motions. This drag is the source of damping that makes SWATH motions gentle. Upper hull sections may be faired to dissipate the energy of wave impact should amplitudes exceed the critical clearance between the design waterline and the upper hull. When DIW, the SWATH ship will turn broadside to wind and/or waves in a manner similar to that experienced by a monohull. Due to the large beam and characteristics of the hulls, the broaching problems of a SWATH ship are much less severe than those of a monohull of equivalent displacement.

3. Dynamic Stability

The stability of a SWATH vessel when underway in a seaway is a function of both the basic semi-submerged hull design and the control that may be imparted by submerged control surfaces. Such control surfaces are hydraulically actuated and may be controlled manually or by electrical signals generated by simple heave, pitch and/or roll gyros. Although not necessary for moderate speeds, these surfaces improve the vessel's response beyond that attained by the hull configuration alone.

4. Internal Load

The SWATH concept has been criticized as one that is load limited; in fact, if high operating speeds are required, then any design becomes load limited due to sustained limitations on the practical size of power plants that may be utilized. However, drilling platforms are not considered to be load-constrained vessels and moderate-speed SWATH vessel designs share this attribute. If, for example, we consider the displacement of two cylinders with a radius of 6.5 feet and a length of 80 feet as compared with two cylinders with a radius of 8.5 feet and a length of 104.6 feet, one sees a displacement change of 211 short tons (171 short tons as compared with 381 short tons) or 123 percent. Thus, a very large change in displacement is characteristic of relatively small changes in lower hull dimensions. For moderate speed vessels, the additional power required is a function of increases in the projected frontal area of the vessel. The drag penalty is not a strong function of displacement, and, as a result, moderate-speed SWATH vessels are not payload constrained from a design standpoint.

As the price of petroleum fuels increases, it is increasingly critical that the energy expended be minimized. Along these lines, the SWATH vessel may be conceptualized to tailor the hull geometry to the load onboard. For instance, flexible boundaries may allow fuel compartments to be used for catch storage, or collapsible appendages to the hull may further increase the storage capability (at a corresponding penalty in drag). In this manner, the hull retains its minimal drag characteristics under all loading conditions. Some interesting alternatives include towing devices of minimum drag shapes such as a semi-submersible barge or devices that can be stowed onboard when not in use. Still other alternatives include the Soviet's factory ship concept or some form of transport/mother vessel which will allow the SWATH vessel to remain on-station.

5. External Loading

The SWATH concept has the capability to compensate for list created by off-axis external loads. This is accomplished with integral ballast tanks in each submerged hull. These compartments may contain fuel in appropriate bladders, refrigerated cargo or ballast air/water. By employing a *KAIMALINO* style ballast system, the entire vessel may be raised and lowered in the water to meet specific freeboard requirements. If, for instance, a stern trawl is to be brought onboard, the vessel may be deballasted to ensure that the cod end does not rupture during recovery.

Due to the spacing of the lower hulls, a moon pool or open well is easily incorporated in the SWATH design. Such a pool can be located at the intersection of the fore-and-aft and side-to-side axes of motion. It may be used in recovering objects and/or fishing equipment when seas are rough and relative motion between the SWATH and incoming objects must be minimized.

6. Survivability

The SWATH concept entails a relatively large number of integral compartments. In the event of hull rupture, it is unlikely that a significant loss of buoyancy would result. If both lower hulls should flood, the vessel will be supported by the upper hull. Given a SWATH vessel of 100-125 feet in length, it is anticipated that a vessel so damaged still could survive in sea state 7.

7. Maneuverability

The characteristically large beam of SWATH vessels allows a wide propeller spacing. This results in the potential for large turning moments due to the application of differential

thrust between propellers. A SWATH vessel can easily pivot on its own axis or, while underway, can be maneuvered by propellers alone. When turning at high speeds the SWATH vessel exhibits a natural tendency to bank into turns in contrast to the motion of turning monohulls. These phenomena make work on deck relatively safe at any speed or sea state.

8. Speed and Powering

The drag on a SWATH hull is similar to that on a monohull of similar displacement until the vessels are compared in a strong seaway. The small waterplane area has the advantage of reduced drag in large seas. The extent of this drag reduction relative to a monohull is not well documented for actual SWATH vessels although a large amount of model data exists (Reference 4).

Propulsion on existing SWATH vessels includes gas turbines and diesels. Propellers are located at the aft end of the lower hulls, thus providing a very favorable cavitation number. The propulsive efficiency is further increased by the symmetric boundary layer that is drawn into the propeller. Under average sea states SWATH propeller efficiencies will be 5% to 10% better than monohull propeller efficiencies. An indirect benefit of SWATH powering in a seaway is the capability of maintaining design speed in high sea states. Monohull vessels thus have three basic problems in a seaway with regard to speed and powering, namely:

(1) The propeller efficiency decays as sea states rise due to the entrained air that is drawn into the propeller.

(2) The overall drag of the vessel increases significantly as the wave loading on the hull increases.

(3) Severe heave, pitch and/or roll motions may force a reduction in speed since the wave-induced loads on the hull could cause structural failure.

A SWATH ship is relatively immune from these problems. The depth of the propeller centerline is deeper than on a conventional vessel of equal displacement; this produces a more favorable cavitation number. In addition, the lower propeller centerline and the reduced vessel motions greatly reduce the risk of the propeller emerging from the water. The drag of the SWATH ship is not a strong function of sea state; rather it is a direct consequence of the small waterplane area of the struts. Reduced motions and initial structural design characteristics make speed reductions in most sea states unnecessary. Only extremely large or steep waves might impose a speed reduction and even then, adjusting the attitude by shifting ballast can compensate for the condition without slowing.

Thus, SWATH vessel offers little improvement in drag displacement relative to a monohull on a flat sea although it does exhibit superior drag/displacement characteristics in a seaway.

9. Habitability

The habitability of a SWATH vessel is superior to any monohull of equivalent displacement or even several times larger. This characteristic is a result, in part, of the reduced magnitude and longer period of roll, pitch and heave motions. Comparative studies between several monohulls and a SWATH vessel have demonstrated a significant reduction in seasickness of personnel on SWATH vessels (Reference 3). The geometry of the upper hull provides an increase in the usable space, a reduction in the ambient humidity, and does not have multiple decks nor a large sheer in the deck. There is a large deck area that provides more open space for crew members on extended voyages. Since the enclosed area of the upper hull is large and free of equipment/machinery, there is ample area for recreation.

10. Deck Versatility

The box-shape upper hull structure of the *KAIMALINO* is conducive to a wide variety of deck configurations. Since there is no sheer in the deck, cables and lines may be buried in the deck to prevent injury from line parting. Deck equipment may be mounted on semi-permanent mounts, rails, or may be fixed to the deck. The large open deck area makes fairleading much easier. Trawl drums and net handling gear may be located a safe distance from the ramp (where surges have taken the lives of many fishermen). Cranes, catheads, winches and miscellaneous deck hardware may be mounted on pallets that interface directly with the ship. In this manner, a vessel may come alongside and change her entire fishing configuration in a short period. Similarly, entire container modules may be "plugged" into the deck. Such modules could fit within the upper hull or could rest on deck. As demonstrated by the U.S. Navy's SWATH vessel, the concept also provides an excellent helicopter platform at sea, a useful tool for modern fish spotting.

AN SSFV DESIGN FOR THE CENTRAL PACIFIC

Through studies of the literature and discussions with fishing interests in Hawaii, a program to determine specific design is being formulated for a Central Pacific SSFV. Final conceptualizations of candidate SSFV vessels will be dependent on the outcome of the design studies; however, specifications for two preliminary concepts are shown in Figure 6. The 300 ton concept has been illustrated in Figure 7. This design has been generated around the 15 knot design speed that is presently considered to be economically optimum for many Central Pacific fishing vessels. Also shown in Figure 6 are the anticipated costs to build and operate both the 300 and 450 ton vessels. The costs have been expressed in terms of dollars per mile such that they may be compared with the generalized argument shown in Figure 2. Although this method of estimating operating economics has a number of inaccuracies, it provides a conceptually straightforward estimate of the breakeven point for the vessel. This projection for a 450 ton SSFV yields a breakeven point of 18¢/lb. of catch while the projection for the 300 ton SSFV yields an estimate of 12¢/lb. It is evident that these estimates are a strong function of the initial assumptions. Thus, the analysis of the economic viability is subject to revision as these initial assumptions become established fact.

As a vessel ages, the fuel, labor and miscellaneous costs will increase with inflation. However, the construction and capital costs have been amortized over the vessel's life. If the retail cost of fish follows inflationary trends, then the overall ratio of revenue to cost will improve with vessel age since the initial construction/capital cost remains constant.

ECONOMIC CONSIDERATIONS

A rule of historic inflation dictates that no new design can be as inexpensive as one that currently exists. And, this is true except in those rare cases involving a breakthrough in technology or an inordinate saving through a value engineering achievement. And while the SSFV indeed represents a breakthrough in technology, it undoubtedly is going to suffer from the inflationary cost of tooling up for a new design.

Informal discussions with some of the European Shipyards indicate that they believe the cost of a semi-

submersible design to be in the same ballpark with that of a similar-sized monohull. This is possible when one considers the design economies of the easy-to-fabricate shapes (round lower hulls and box-shaped upper hull) with the complex monohull components. It is highly likely that a production line of semi-submersible vessels will enjoy additional economies over a similar line of monohulls; obviously the lower hulls and struts lend themselves to certain mass production techniques.

There are additional economies (operational) due to the small number of crewmen. The semi-submersible vessel, with its single operator concept, can be operated at-sea with a much smaller crew than its monohull counterpart.

The major economies of the SSFV, however, are most likely to be found in its greater operational effectiveness. This vessel will put to sea under conditions where other vessels cannot leave port. More important, when it reaches the operating site, the SSFV will be able to go into an operational state, despite most weather conditions that it might encounter. Most of the present Hawaiian fleet puts to sea about 80% of the time (during the summer, perhaps 99%), but often circles the operating area waiting for the environment to improve. It has been roughly estimated that the overall operating time at the site is in the order of 50%.

SPECIFICATION	300 TON CONCEPT	450 TON CONCEPT
Displacement Tonnage	300 long tons	450 long tons
Payload	140 long tons	220 long tons
Range	2000 nmi @ 14 kts.	4000 nmi @ 15 kts.
Design Speed	16 knots	17 knots
Length Overall	96 feet	112 feet
Beam	52 feet	62 feet
Crew	8	12
Fuel Cost per Mile [1]	$4.80/nmi	$5.56/nmi
Labor Cost per Mile [2]	$4.20/nmi	$5.60/nmi
Const. & Outftg. Cost [3]	$2.5 million	$4.0 million
Amort. Cost per Mile [4]	$5.56/nmi	$13.88/nmi
Misc. Cost per Mile [5]	$4.00/nmi	$5.00/nmi
Total Cost per Mile	$18.56/nmi	$30.04/nmi

[1] This estimate is based upon a shaft horsepower of 2500, a fuel consumption of 0.4 lbs/hp-hr, a speed of 15 knots and a fuel cost of $0.55/gallon.

$$\text{i.e. } 2500 \text{ hp} \times \frac{0.40 \text{ lb}}{\text{hp-hr}} \times \frac{1 \text{ gal}}{6.6 \text{ lb}} \times \frac{\$0.55}{\text{gallon}} \times \frac{1 \text{ hr}}{15 \text{ mi}} = \frac{\$5.55}{\text{mile}}$$

[2] Labor estimates are based on: 12 crew members, an average 8-hr working day, an average rate of pay of $7.00/hr, and an average speed of 15 knots (this speed covers in-port time as well).

$$\text{thus: } 12 \text{ men} \times \frac{8 \text{ hrs}}{\text{man-day}} \times \frac{\$7.00}{\text{hr}} \times \frac{1 \text{ day}}{120 \text{ mi}} = \frac{\$5.60}{\text{mile}}$$

[3] Total vessel cost estimate is based on a bare hull cost of $3.6 million ($4.00/lb of displacement) and an outfitting cost of $1.4 million.

[4] The amortization is based on an initial cost of $5,000,000 on a 9 percent loan over 20 years with a resulting finance charge of $4,725,000. The average life span speed of the vessel is assumed to be 4.0 knots.

$$\text{i.e. } \frac{\$9{,}725{,}000}{20 \text{ years}} \times \frac{1 \text{ hr}}{4.0 \text{ kts}} \times \frac{1 \text{ day}}{24 \text{ hrs}} \times \frac{1 \text{ year}}{365 \text{ days}} = \frac{\$13.88}{\text{mile}}$$

[5] This estimate includes insurance and drydocking costs as well as miscellaneous berthing feets, etc.

FIGURE 6. Specifications for Two SSFV Concepts

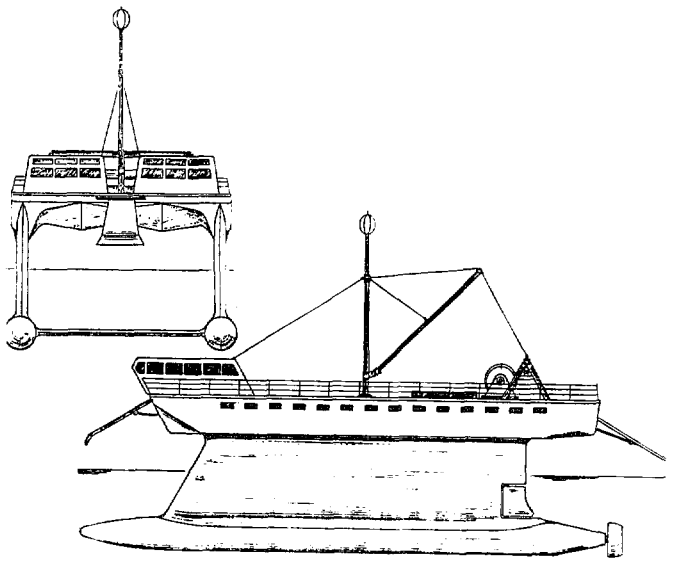

FIGURE 7. A 300-Ton SSFV

In contrast, the SSFV should be able to put to sea 99% of the time, year-round, and begin operations immediately upon arrival at the operating site. These factors are admittedly crude but provide some insight into the anticipated improvements in operational economies. More exact relationships will result from the economic studies soon to be carried out in conjunction with the University of Hawaii Sea Grant Office.

SUMMARY

This paper has addressed briefly the dilemma faced by the modern fisherman in the United States. The specific situation in the Central Pacific has been expressed. SWATH technology provides an exciting solution to most of the problems that exist. A specific design for this region has been shown with detailed substantiations for its effectiveness. Plans are underway for construction of five SSFV's. Since this paper has been written as plans are in the formative stages, the descriptions are somewhat general. However, studies are presently underway to examine specific technical, economic and operational alternatives. The results of these studies will be presented in future reports to preserve the cooperative and open nature of the SSFV program.

REFERENCES

1. Blount, L. H. and E. A. Schaefers, "Recent U. S. Combination Fishing Vessels," in Fishing Boats of the World:3, Jan-Olof Traung (editor), Fishing News (Books), Limited, London, England, 1967.
2. Comitini, S., "An Economic Analysis of the State of the Hawaiian Skipjack Tuna Fishery," Univ. of Hawaii Sea Grant Program, UNIHI-SEAGRANT-TR-76-01, Nov. 1977.
3. Hightower, J. D. and R. L. Seiple, "Operational Experiences with the SWATH Ship SSP *KAIMALINO*," presented at AIAA/SNAME, Advanced Marine Vehicle Conference, April 1978.
4. Lamb, R. G., "The SWATH Concept: Designing Superior Operability into a Surface Displacement Ship," David Taylor Naval Research and Development Center, Report No. 4570, Dec. 1975.

DEVELOPMENTS IN THE LAW: THE FISHERY CONSERVATION AND MANAGEMENT ACT OF 1976

Eugene R. Fidell
LeBoeuf, Lamb, Leiby & MacRae
1757 N Street, N.W.
Washington, D.C. 20036

Abstract

The Fishery Conservation and Management Act of 1976 has now been in effect for over 1-1/2 years, and has been the subject of attention and action by the Congress, the Executive Branch and the Federal Courts. A summary of the legal concerns that have arisen and that merit further attention is presented.

Introduction

The Fishery Conservation and Management Act of 1976 was signed into law by President Ford on April 13, 1976, although its important substantive provisions did not go into effect until March 1, 1977.(1) As a result, we currently have only about eighteen months of practical experience under this legislation. Nevertheless, there have already been many significant legal developments with respect to the FCMA, and my purpose today will be to describe these. I shall organize these observations in the following categories: (1) legislative developments; (2) litigation; (3) administrative aspects. Because there is more to tell than time permits, much of this treatment will necessarily be rather summary, but I shall be happy to entertain questions afterwards.

1. Legislative Developments

Changes in the FCMA have been proposed for a variety of reasons. Perhaps the most important is the recognition that the statute as originally enacted failed to make adequate provision for the possible loopholes in the area of foreign investment and joint ventures. This subject received a considerable amount of attention both on the Hill(2) and within NOAA,(3) and I assume that most of this audience is aware of the present legislative situation on this point. An effort has been made to tidy things up with respect to the treatment of foreign fish processing vessels,(4) although we should not underestimate the creativity of businessmen in seeking new ways to do business in light of changing legislative mandates.

Legislative action was also required in connection with the Governing International Fishery Agreements (or GIFAs)(5) since it became clear early on that certain of the procedural steps necessary for the issuance of foreign fishing permits could not be completed in time for the onset of the new regulatory regime under the FCMA.(6) It was unfortunate that all the pieces of the puzzle could not be in place at the appointed hour, but Congress ultimately did, in approving the first round of GIFAs, make allowance for the unusual situation, and granted relief from these procedural niceties (which included the requirements that license fees be paid in advance, that permits be on board the vessel, and that certain waiting periods be observed by the Regional Fishery Management Councils before permit issuance).(7) Congress also gave express recognition to the special circumstances of the Reciprocal Fisheries Agreement with Canada,(8) a matter that has since been the source of some international friction and even litigation, as I will shortly note. Here Congress was faced with a departure from the framework of the statute, since the Canadian agreement was deemed not to be a GIFA.(9) A special act was felt to be necessary because the agreement had provisions that were not consistent with the FCMA. (10)

Congress has not, however, felt moved yet to address some of the thorny technical issues that inhere in the statute. These issues have to do with such matters as the jurisdiction of the federal courts to provide judicial review of NOAA actions under the FCMA, elements of proof in a forfeiture action, and the scope of reserved state powers in light of the extremely confused provisions of § 306 of the law.(11) For its part, NOAA has expressed interest in fine-tuning on some of these items,(12) but the idea has failed to catch fire on the Hill, even though other measures have received detailed attention, including hearings. Happily, the Congress has taken steps to alter the statutory requirement that all applications for foreign fishing permits be reproduced in their entirety in the Federal Register.(13) Perhaps Congress' reluctance is due to the fact that there are few votes to be gained by such legislative action, but it is to be hoped that the 96th Congress will do better than its predecessor in addressing the technical legal issues, rather than leaving them to the courts for resolution.

I might perhaps close this legislative overview with the observation that the FCMA has had some unusual impacts on other legislation, both foreign and domestic. Domestically, you may be aware that the 1977 amendments to the Clean Water Act extended certain United States marine pollution controls to the area covered by the FCMA.(14) Note, incidentally, that those amendments do not simply push the pollution controls out to a 200-mile limit; they actually extend the Clean Water Act further to the extent that the FCMA covers marine resources beyond 200 miles. Thus, because the FCMA protects anadromous fishes of United States origin beyond the Fishery Conservation Zone, or living resources of the continental shelf where the shelf extends beyond the FCZ,(15) the Clean Water Act, too, has a broader sweep.

On the foreign legislative front, Canada has amended its Fisheries Act to provide for issuance of summonses in lieu of arrest for minor offenses.(16) Quite plainly this was inspired by the streamlined "parking ticket" concept found in § 311(c) of the FCMA, and shows quite nicely how one nation may learn from another in the development of laws.

2. Litigation

Fishermen have been suing one another for centuries over the damnedest things. They are probably as litigious as any group in American society, but nonetheless, there has been surprisingly little litigation to date under the FCMA. Only a few cases have reached the Courts of Appeals, and no case directly involving the FCMA has yet come to the Supreme Court. Domestically, the paucity of cases may be because the industry does not have a deep-seated tradition of doing things together, whether nationwide, regional, or even between neighboring ports. On the foreign front, fishing industries in other countries have failed to assert legal rights in our courts, presumably because they continue to rely upon the Department of State and their own governments as their spokesmen in dealings with the regulators. Finally, because the FCMA provides for administratively-assessed civil penalties as an alternative to immediate recourse to the federal district courts(17)--and because NOAA has been slow in developing the civil penalty cases to the point where litigation might ensue --the structure of the Act and the nature of its implementation have both served to reduce the flow of litigation--at least for the moment.

As of June 1978 there had been only a handful of court cases under the Act. Only three of these were criminal prosecutions, and in fact one of the three cases had little to do with fishing. Rather, it was a prosecution in the United States District Court for the District of Rhode Island on a charge of assaulting a boarding officer.(18) A special agent of NMFS was assaulted while trying to perform a routine dockside boarding of a United States vessel. Despite a contention that the boarding was unconstitutional because there was no probable cause, the defendant was convicted and fined $200. The other criminal prosecution involved the masters of a Mexican fishing vessel seized by the Coast Guard off Texas(19) and a Soviet vessel seized off Massachusetts.(20) The Mexican master pleaded guilty and was given a suspended prison term of three months, while the Soviet skipper was given a suspended nine-month sentence.

There have been a number of judicial proceedings to forfeit foreign fishing vessels. These have included the Soviet vessel Taras Shevchenko,(21) the Mexican vessel Adriana,(22) the Taiwanese vessel Highly No. 301,(23) the Japanese vessel Sachi Maru No. 22,(24) and the Spanish vessel Costa de Noruega.(25) In addition, part of the catch of another Soviet fishing vessel was seized shortly after the FCMA took effect.(26)

More interesting and more important than these isolated fishing violation cases are the cases in which litigants have sought to obtain direct judicial review of administrative actions under the FCMA.

The first such action was brought by Maine to obtain review of the 1977 herring quotas. Basically, the state alleged that these quotas were a rerun of the earlier ICNAF quotas, and that the Commerce Department had taken improper factors into consideration when developing the quotas under the FCMA. The case was at first remanded to the trial court by the First Circuit Court of Appeals, with instructions to require Secretary Kreps to state the reasons for her decision with respect to the quota.(27). Thereafter, Maine appealed again, and on the second appeal the Court of Appeals in Boston sustained the district court's approval of the Secretary's action.(28) The Court's opinions are important because they show that the Commerce Department may take into account relations with foreign countries even though the "cardinal aim" of the statute is to help "the development of a United States' controlled fishing conservation and management program designed to prevent overfishing and to rebuild depleted stocks...."(29) The Court went out of its way to underscore the breadth of the Secretary's discretion in setting quotas.

Other litigation has been directed at a variety of NOAA and NMFS actions under the new law. For example, two civil actions were filed to challange the policy announced by NOAA with respect to foreign fish processing ventures within the FCZ. One such case was filed in the district court in Washington, D.C., by a variety of West Coast fishing companies, (30) while the other case was commenced in the district court in Seattle by a different group of firms.(31) Both actions seek to invalidate the NOAA policy under which fish caught by U.S. vessels, but processed by foreign vessels, are treated as part of the U.S. share, rather than deducted from the total allowable level of foreign fishing.(32) Both cases also raise questions as to whether NOAA properly complied with the Administrative Procedure Act in adopting the policy statements on this issue.

Beyond this recent activity, cases have been filed in the district court in New Jersey regarding the validity of the Fishery Management Plan for surf clams and ocean quahogs;(33) in the district court for Massachusetts regarding the validity of the Fishery Management Plan for Atlantic groundfish;(34) in the Western District of Washington regarding the continuation of Canadian fishing for salmon prior to Congressional approval of the appropriate international agreement;(35) and in the same district court with respect to the validity of the Fishery Management Plan for salmon.(36) Maine has also sued to challenge the structure and operation of the Regional Councils.(37)

Little purpose would be served by going through the details of each of these cases. It is perhaps more important to identify the main themes that are being struck in the various lawsuits. These are: has there been compliance with the Administrative Procedure Act with regard to rulemaking, and to what extent does that law apply to particular agency actions under the FCMA? Has a proper Environmental Impact Statement been issued? Have the proper factors established in the FCMA for management decisions been taken into account and the analysis spread upon the record? To the extent that statutory obligations exist with respect to enforcement, have these been observed? If emergency action is taken, was it necessary?

Obviously, this list is not exhaustive, and as further litigation arises, entirely new theories will be advanced. One issue which I expect will be the basis for much litigation is the basic one of whether the biological/scientific data base actually supports the management decisions that have been made. Congressman Ruppe, for example, has stated that "[t]he available biological data on which to base fishery management plans is inadequate and the development of a sufficient data base will require an extensive research program."(38) Unless there is a sound, articulable basis for the management plans, they will be subject to question and judicial invalidation. For this reason it is critical that NOAA's research efforts be directly linked to the FMP-development process, and that plans disclose, in intelligible terms, the scientific basis upon which they are founded.

Other judicial actions should perhaps also be mentioned. The Supreme Court has been quite active in the natural resources field of late, including the fisheries law area in particular. In Massachusetts v. Westcott,(39) the Court held that Massachusetts could not bar a U.S.-documented fishing vessel from fishing in waters of Massachusetts even though the vessel was homeported in Rhode Island. Similarly, in Douglas v. Seacoast Products, Inc.,(40) the Court struck down Virginia's efforts to establish its own citizenship requirement for vessels seeking to fish in its waters; the Court held that the Enrollment and Licensing Act of 1793, which had previously been applied to defeat New York's efforts to control U.S.-documented steamboats in the landmark case of Gibbons v. Ogden,(41) was also applicable to vessels licensed for the fisheries. More recently, however, the court took a step backward in holding that Montana could have big-game license fees that discriminated against nonresidents,(42) despite a rather long line of cases that had seemed to cast doubt on such measures. Whether the doctrine will have an impact on the administration of the FCMA remains to be seen.

3. Administrative Aspects

Turning to the Executive Branch role in administration of the FCMA, it must be said that things have gotten off to rather a slow start. Hundreds of notices of violation have been given out by NOAA and the Coast Guard, but the process of bringing these cases to fruition has been exceedingly slow. This is perhaps the most severe shortcoming in the administration of the Act, for the lack of enforcement teeth can bring the entire regulatory effort into disrepute.

More broadly, question may be raised as to whether administration of the Act is being conducted evenhandedly as between foreign and domestic vessels. As Senator Magnuson has observed, "[c]onservation is not a one-sided affair, and foreign and domestic fishermen must be subject to the same enforcement rules. To create a double standard for speculative 'foreign policy' reasons will undermine our entire conservation effort."(43) I confess that I have in the past more or less assumed that there might be some discrimination against foreign fishing vessels given the fact that the FCMA built upon a statutory scheme that essentially barred the door to foreign fishing. I am happy to report that the statistics to date do not appear to bear out such a supposition. The figures for the period ending December 31, 1977 are inconclusive, although they can be read as suggesting that foreign fishing vessels tend to get off more easily in the enforcement process. However, this may also be because there are in fact fewer foreign violations. In any case, during that period there were 225 reports of serious domestic violations, and only 133 reports of serious foreign violations. Domestic vessels were given citations for minor offenses 129 times, and foreign vessels received 329 such citations.(44) These data would have to be analyzed to determine whether foreign or domestic vessels were boarded disproportionately to their numbers.

Administrative action of an important kind occurred last Spring in the context of the ongoing negotiations with Canada. After the negotiations seemed to be falling apart, a decision was made to bar Canadian fishing from United States waters, including Canadian recreational fishing on the seacoasts and recreational and commercial fishing on the Great Lakes.(45) Despite the fact that the FCMA's predecessor, the Bartlett Act, had been construed to apply to the Great Lakes,(46) the Administration concluded that the Great Lakes were not covered by the FCMA's prohibition on foreign fishing on the ground that the term

"fishing" in the statute must be read in light of the definition of "fish", which in turn may be read as limited to marine fishes.(47) The result was that Canadian recreational fishing was permitted to go forward on the Lakes.(48) Whether the decision is right or wrong, it shows quite eloquently how much discretion is vested in the administrative agencies concerned with implementation of the new law.

Another administrative aspect has to do with the flow of information, such as the rendering of interpretations like the one just mentioned. I am very pleased to state that NOAA has, at my urging, adopted a liberal policy with respect to the public availability of its General Counsel's opinions. Without these opinions, many observers of the fishing scene have had to rely on rumor and guesswork to learn the details of the Government's legal position on important questions. With the opinions, all affected parties will be able to guide their actions with a far better understanding of Government policy than was available in the past. NOAA is to be applauded for this welcome change.

Which leads me to my concluding observation. The lack of regular access to agency General Counsel opinions is only a small part of a larger problem. Information flow as a whole under the FCMA has, in my view, been haphazard at best, and this void has not been properly filled by the trade press. What is badly needed is a regular information and document service that will present important textual materials of general interest to the fisheries industry, recreationists, environmental groups and government officials, in a convenient form with a minimum of delay and expense. It is my hope that industry will support development of such a service at an early time, both in its own interest and as a public service.

Conclusion

There have been major legal developments on every front since the Fishery Conservation and Management Act took effect last year. The pace of these developments will accelerate in the next year or two, as the shakedown period under this important legislation continues. While specific predictions can be hazardous, one can at least suggest that important changes could come about as a result of President Carter's ongoing interest in government reorganization, whether that interest manifests itself as a Department of Oceans, an overall Department of Environment, or as part of the new approaches being taken with respect to protection of our borders. Other changes can be anticipated as the law in general continues to evolve. For example, the Supreme Court's recent decision with respect to administrative inspections(49) could have an impact on enforcement of the Act, as could a possible future decision by the Court on the question whether lethal force may be used in pursuing a nonviolent fleeing criminal.(50) In any event, the opportunities for change, whether on the administrative, judicial or legislative side, are manifold. It will be a test of the wisdom and skill of the drafters of the FCMA to see how well their brainchild withstands these changes.

References

1. 16 U.S.C. §§ 1801 et seq. (1976) ("FCMA"); see FCMA §§ 201(a), 204(a).
2. See, e.g., 200-Mile Fishery Oversight--Joint Ventures, Hearings on Joint Ventures: H.R. 2564, H.R. 4165 and H.R. 4166 Before the Subcomm. on Fisheries and Wildlife Conservation and the Environment of the House Comm. on Merchant Marine and Fisheries, 95th Cong., 1st Sess., ser. no. 95-19 (1977) ("Joint Ventures Hearings").
3. See NOAA Proposed Interim Policy, 43 Fed. Reg. 5398 (1978); NOAA Policy Statement, U.S./Foreign Fishing Ventures Within Fishery Conservation Zone, 43 Fed. Reg. 20532 (1978).
4. See Fishery Conservation and Management Act Amendments, S. Rep. No. 95-935, 95th Cong., 2d Sess. (1978).
5. FCMA § 201(c).
6. See generally International Fishery Agreements: Hearings on H.J.Res. 240, H.R. 2081, H.R. 3753 and H.R. 4954 Before the Subcomm. on Fisheries and Wildlife Conservation and the Environment of the House Comm. on Merchant Marine and Fisheries, 95th Cong., 1st Sess., ser. no. 95-1 (1977).
7. Fishery Conservation Zone Transition Act § 3(1), 16 U.S.C. § 1826 (1976).
8. H. Doc. No. 95-90, 95th Cong., 1st Sess. (1977); Pub. L. No. 95-73, 91 Stat. 283.
9. See, e.g., H.R. Rep. No. 95-783, 95th Cong., 1st Sess. 4 (1977).
10. See Letter of Transmittal from the President to the Congress, Feb. 28, 1977, in H. Doc. No. 95-90, supra note 8.
11. See Memorandum of the author on Technical Amendments to Fishery Conservation and Management Act of 1976, in Joint Ventures Hearings, supra note 3, at 281-82.
12. Letter from Dr. Robert M. White, Adm'r, NOAA, to Rep. Robert L. Leggett, Mar. 21, 1977.
13. See FCMA § 204(b)(4).
14. See Clean Water Act § 311(b), 33 U.S.C.A. § 1321(b) (West Supp. 1978).
15. FCMA § 102.
16. See 25-26 Eliz. 2 ch. 35, § 18 (Can. July 14, 1977), amending Fisheries Act § 61 (Can.).
17. FCMA § 308; see generally Fidell, Enforcement of the Fishery Conservation and Management Act of 1976: The Policeman's Lot, 52 Wash. L. Rev. 513, 546-50 (1977).
18. United States v. Champlin, Crim. No. 77-67 (D.R.I. Nov. 21, 1977).
19. United States v. Hernandez-Lopez, Crim. No. B-77-302 (S.D.Tex. Aug. 8, 1977). The indication in [1977] NOAA Annual Report, Fishery Conservation and Management Act of 1976, at 22 (1978), that a six-month sentence was imposed appears to be erroneous.

20. [1977] NOAA Annual Report, supra note 19, at 22; N.Y. Times, May 3, 1977, at 20, col. 4.
21. United States v. Russian F/V Taras Shevchenko, Civil No. 77-1086-M (D.Mass., filed Apr. 21, 1977).
22. United States v. F/V Adriana, Civil No. B-77-179 (S.D.Tex., filed July 29, 1977).
23. United States v. F/V Highly No. 301, Civil No. A77-181 (D. Alas., filed Sept. 2, 1977).
24. United States v. F/V Sachi Maru No. 22, Civil No. A78-34 (D. Alas., filed Feb. 24, 1978).
25. United States v. Spanish F/V Costa de Noruega, Civil No. 78-762 (D.N.J., filed Apr. 12, 1978).
26. United States v. 17.56 Metric Tons, More or Less, of Fish, Civil No. 77-1086-M (D.Mass., filed Apr. 21, 1977).
27. Maine v. Kreps, 563 F.2d 1043 (1st Cir. 1977).
28. Maine v. Kreps, 563 F.2d 1052 (1st Cir. 1977).
29. 563 F.2d at 1049.
30. Tom Lazzio Fish Co. v. Kreps, Civil No. 78- (D.D.C., filed May 1978).
31. Pacific Seafood Processors Ass'n v. Kreps, Civil No. C78-313S (W.D. Wash., filed May 23, 1978).
32. Cited supra note 3.
33. Sea Harvest, Inc. v. Kreps, Civil No. 78-514 (D.N.J., filed Mar. 15, 1978).
34. Ferrara v. United States, Civil No. 78-420-G (D.Mass., filed Feb. 21, 1978).
35. Washington Trollers Ass'n v. Vance, Civil No. C78-248V (W.D. Wash., filed Apr. 24, 1978).
36. Nevaril v. Kreps, Civil No. C77-358S (W.D. Wash., filed May 13, 1977).
37. Maine v. Kreps, Civil No. 77-176-SD (D.Me., filed Aug. 3, 1977).
38. 124 Cong. Rec. H2629 (daily ed., Apr. 10, 1978) (remarks of Mr. Ruppe).
39. 431 U.S. 322 (1977).
40. 431 U.S. 265 (1977).
41. 9 Wheat. 1 (1824).
42. Baldwin v. Fish and Game Comm'n of Montana, 46 U.S.L.W. 4501 (U.S. May 23, 1978).
43. Sen. Comm. on Commerce, News Release No. 95-52 (Apr. 13, 1977).
44. [1977] NOAA Annual Report, supra note 19, at 18-19.
45. See N.Y. Times, June 6, 1978, at 1, col. 1; 124 Cong. Rec. H4928 (daily ed. June 5, 1978) (remarks of Mr. Latta).
46. See Fidell, Ten Years Under the Bartlett Act: A Status Report on the Prohibition on Foreign Fishing, 54 B.U.L. Rev. 703, 716-17 (1974).
47. See FCMA §§ 3(8), 3(10), 307(2).
48. Washington Post, June 11, 1978, at A21, col. 1.
49. See Marshall v. Barlow's, Inc., 46 U.S.L.W. 4483 (U.S. May 23, 1978).
50. See N.Y. Times, June 1, 1978, at A19, col. 1 (reporting 8th Cir. decision sustaining damage action by parent of fleeing nonviolent felony suspect killed by police gunfire).

INPUT-OUTPUT ANALYSIS FOR SALT MARSH BIOPRODUCTIVITY *

Thomas M. Leschine
Woods Hole Oceanographic Institution
Woods Hole, Massachusetts 02543

Leah J. Smith
Woods Hole Oceanographic Institution
Woods Hole, Massachusetts 02543

Abstract

Input-output analysis is applied to a salt marsh system to describe possible bio-economic effects of adding nitrogen fertilizer. A simple model is developed to trace exchanges of nitrogen among five compartments of the marsh model: sediments, Spartina root/rhizome biomass, Spartina aboveground biomass, tidal water and shellfish. The resulting matrix can be used to show relationships in the system among controllable inputs and outputs with potential economic value. Some costs of fertilizing an experimental plot are given, but no direct comparison can yet be made between costs and likely economic benefits.

1. Introduction

Recent research on salt marshes at Woods Hole has emphasized both qualitative and quantitative aspects of the flow and interconversion of nitrogen as it passes among the various biological compartments of salt marsh systems. It has been established that the artificial addition of nitrogen-based fertilizer can enhance the productivity of biological systems within such salt marshes (10), although the possible bio-economic benefits of salt marsh fertilization - enhanced fish and shellfish production - are relatively far removed from initial perturbations on the system such as fertilization. The structure of this small-scale bio-economic system is in many ways similar to that of economic systems which have been described with input-output analysis. Other economic approaches have been used to describe production in manufacturing or agricultural systems. Production functions of various kinds either describe such systems in engineering terms or make assumptions about the contribution and substitutability of various factors of production (principally labor and capital). Most of these systems, however, assume a high degree of control over all inputs and outputs. In a salt marsh used as a site for enhanced productivity, many of the assumptions underlying standard economic production functions do not hold. In addition, the complex and vital roles of biological interactions require different treatment than a standard manufacturing system. The input-output approach enables us to combine some of the important biological interactions with the total input requirements and potential economic outputs of the system.

In a sense, nitrogen is the "currency" being passed back and forth among tidal water, grasses, herbivores and other compartments in the marsh as biological activity takes place. Much ecosystem analysis over the past 20 years has focused on the flow of energy and nutrients through similar biological systems (among frequently cited energy flow models are H.T. Odum (6) and J.M. Teal (9)). Several recent authors have noted the similarity of these flows to the flow of money through a national economy, and a mathematical theory of flows in ecosystems equivalent to the economic input-output analysis of W. Leontief (5) has been developed (Hannon (3) and Finn(1)). Gosselink et al (2) have used this analogy directly in placing a dollar value on an acre of salt marsh, determined by measuring annual net primary productivity, a proxy for annual energy flow, and converting energy units to dollars. Our goal is to link the costs of marsh fertilization to the potential harvest of fish and shellfish relatively far removed in position in the food web from these initial nutrient inputs, and it is natural for us to use an input-output format.

Productivity of the grasses which comprise the major component of the tidally borne detritus in these marshes, mainly two species of Spartina, is enhanced by fertilization. This detritus in turn is the basic food source for the marsh's food webs. Primary production both in salt marshes (10) and in coastal waters (7) is nitrogen limited. A good deal of research on the flow of nitrogen through marsh food webs has been done in Great Sippewissett Marsh of Falmouth, Massachusetts, and in Buzzard's Bay, with which the marsh has tidal exchange. A complete annual budget of nitrogen inputs and outputs to and from Great Sippewissett has been prepared (10).

*Prepared with funds from the Pew Memorial Trust and by the Department of Commerce, NOAA Office of Sea Grant under Grant #04-7-158-44104, and the Marine Policy and Ocean Management Program of the Woods Hole Oceanographic Institution.

The salt marsh performs an important "conversion" activity on the nitrogen which enters it. The marsh intercepts a flow of ground water rich in dissolved nitrates, its principal natural nutrient source, and converts it to a mixture of particulate nitrogen and disssolved organic and inorganic nitrogen compounds, comprising a net annual export to the Bay. The particulate nitrogen is mostly grass detritus while a large portion of the dissolved nitrogen export is ammonium. The effect of the marsh is thus to manufacture particulate nitrogen food for harvestable shellfish which is then available to man, and for small mollusks and other benthic creatures available in turn to commercially valuable fish. All are dependent on the tidally innundated habitat the marsh provides. Were the marsh not there, the impact of the nitrogen from the groundwater would be primarily on the phytoplankton in the Bay, and through them on the grazing food webs less directly tied to resources harvestable by man.

The effects of nitrogen-based fertilizer applications on the biomass yield of Spartina alterniflora, the dominant grass in the marsh, can be dramatic: an application of 8.4 g/m^2/week, done biweekly over a seven month period, was shown to double net annual aboveground production of S. alterniflora in experimental plots, while an application of 25.2 g/m^2/week resulted in a near tripling of biomass yield (11). Thus, the simple application of fertilizer can increase the food supply for marine organisms, making it tempting to regard fertilized salt marshes as open aquaculture systems and to view salt marsh fertilization in economic terms.

It is unlikely that commercial aquaculture based on salt marsh fertilization would be practical, since little control can be exerted over the natural biological processes in a marsh. On the other hand, lack of controllability is a virtue in that the costs incurred in maintaining a salt marsh as an open aquaculture system are low. This is especially true if we adopt the viewpoint that fertilization, if it proves practical, should be conducted locally by towns for the benefit of local residents and in-shore fishermen who harvest marsh-dependent fish and shellfish. The explicit costs are thus limited to maintenance of the fertilization program if harvesting is assumed free. It is possible that secondarily treated sewage effluent could be used as fertilizer in some areas, reducing costs even further and providing an additional tertiary sewage treatment benefit (8). Though the market value of the potential increase in harvest may be small, an important component of its total value is recreational and difficult to quantify.

We will show how "biomass flow" through the marsh can be indirectly charted by an analysis of the flows of nitrogen which result as initial nitrogen inputs are converted biologically into higher organisms. In the sections that follow we describe our input-output methodology in more detail and develop some cost estimates for marsh fertilization. We show how it is possible by "back calculation" through a flow model to estimate the nitrogen requirements of meeting a desired level of demand for marsh outputs expressed in terms of biomass output of fish or shellfish. This gives a way of estimating the feasibility of marsh fertilization for the purpose of enhancing bioproduction as well as the probable costs of fertilization. The method is general and can be applied in any situation in which an appropriate flow model is available.

2. A Linear Model for Bioproduction

If a national or regional economy is composed of n sectors $i = 1,\ldots,n$, then the total cash flow through sector j (i.e. the value of j's total production) can be expressed as the sum of the cash flows to all other sectors from j (the value of sales made by j to other sectors for the purposes of their production) and the value of sales to consumers by j (final demand). Letting x_j be the value of j's total production, x_{ij} be the value of sales to i by j for production by i, and y_j be the final demand for j's production, we can express this formally as

$$(1) \quad x_j = \sum_i x_{ij} + y_j.$$

If we assume further that x_{ij} is proportional to x_i, then Equation (1) can be written

$$(2) \quad X_j = \sum_i a_{ij} x_i + y_j, \text{ or}$$

$$(3) \quad \overline{X} = \overline{X}A + \overline{Y}$$

in vector notation, where $\overline{X}$ and $\overline{Y}$ are n dimensional row vectors and A is an nxn matrix of coefficients.

The equations above are derived from the usual assumptions of economic input-output analysis. Replacement of the economic sectors with compartments in an ecosystem model and the cash flows with flows of energy or nutrients generates the equivalent interpretations of Hannon (3) and Finn (1). In the specific example we will present below, Equation (1) will be interpretable as a statement that the total nitrogen flow through compartment j is equal to the sum of the direct flows from j to all other compartments and the flow from j out of the system, after Finn. It is not necessary to assume that the system modeled is conservative (i.e. that the inputs balance the outputs for each compartment), though in a technical sense the computations require that inputs and outputs do balance. It is easy enough, however, to balance the flows artificially by the addition of sources and sinks without changing the nature of the basic result. It should also be noted that the substitution used to derive Equation (2) assumes that a change in total compartment flow leads to proportional changes in the flows which enter that compartment from other compartments. Were the methods of Isard (4) to be cast in this framework, then the flows could be thought of as flows of goods or

materials directly, rather than of the nutrients or energy stored in such materials.

The model described by Equation (3) has two simple equivalent forms of interest:

(4) $\overline{X}(I-A) = \overline{Y}$, and

(5) $\overline{X} = \overline{Y}(I-A)^{-1}$,

where Equation (5) is understood to mean the equality holds given that $(I-A)^{-1}$ exists. The first form expresses the outflow from the various compartments in terms of the total flow through them, while the second makes it possible to solve for the total flow necessary for the system to produce an outflow of a given intensity. This latter interpretation is the one of greatest interest to us and also the formulation of greatest use in input-output economics. In our system we will consider marsh shellfish production (measured as nitrogen content in average annual mussel growth) as an outflow from the model's shellfish compartment. By expressing the total nitrogen flow through the compartment to which fertilizer is an input (marsh sediments) as a function of its nitrogen input, we can then estimate the increase required in nitrogen inflow (and hence the required fertilization rate) to support an increase of a given size in shellfish production.

In the economic literature the quantity $(I-A)^{-1}$ is called the Leontief inverse of the matrix A. In a sense, it expresses the multiplier effect that a change in final demand for one sector's goods will have on the other sectors, as a result of the direct and indirect cash flows which that sector's changed production will induce throughout the economy. This is easy to see in the simple one-dimensional case: If we replace Y by $Y + \Delta Y$ in Equation (5) and solve for the new level of total cash flow X' which will result, we find

$$X' = (Y+\Delta Y)(1-A)^{-1} = Y(1-A)^{-1} + \Delta Y(1-A)^{-1} =$$

$$X + \Delta Y(1-A)^{-1}$$

In the special case in which $\Delta Y = \$1$, $X' = X + (1-A)^{-1}$, so that $(1-A)^{-1}$ represents exactly the total new cash flows required to sustain the new level of production. In the nitrogen flow model elements of the nxn matrix $(1-A)^{-1}$ essentially total the direct and indirect outflows coupling the compartments at the row and column headings which result when a unit change is made in the outflow from the compartment at the row heading. Specifically, the element in the (i,j) position represents the portion of outflow from i which has been through j.

3. A Flow Model for the Great Sippewissett Marsh

Figure 1 below illustrates a hypothetical three-compartment ecosystem with intercompartmental flows, inflows and outflows of specified magnitude. Note that the flow in the figure is

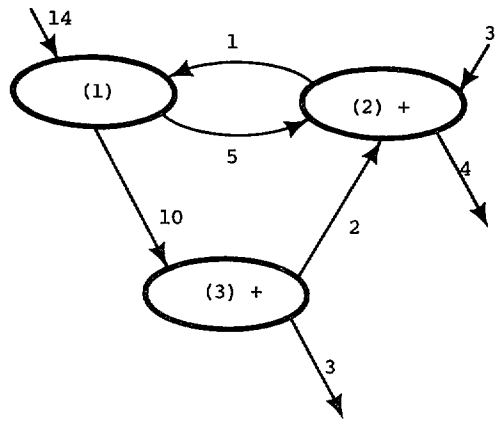

Figure 1

A three compartment ecosystem with flows. Plus signs indicate compartments which are accumulating excess flow.

unbalanced and that compartments two and three are each accumulating an excess of five units of flow. The system's flows are summarized in input-output form in Table 1. Here each column represents the outflows from the compartment at its heading, both to the compartments at the row headings and out of the system completely. Sinks are added to the appropriate columns so that total inflows and outflows balance. Rows provide similar information with respect to inflows for compartments at their headings.

	(1)	(2)	(3)	Sources	Inflows	Total
(1)	0	1	0	0	14	15
(2)	5	0	2	0	3	10
(3)	10	0	0	0	0	10
Sinks	0	5	5		0	
Outflows	0	4	3	10		
Total	15	10	10	10		

Table 1

Flows matrix for the system in Figure 1.

The 4x4 matrix A, consisting of the intercompartmental and balancing flows of Table 1 after division by the row totals, is shown in Figure 2, along with the corresponding $(I-A)^{-1}$ matrix. Direct calculation via Equation (5) shows that if the outflows vector $\overline{Y}$ is replaced by $\overline{Y}' = (0,4,6,10)$, in which the outflow from compartment 3 is doubled, a total flow requirement from compartment 1 of about 18 units results, a 20% increase in the 15 units total flow it supplies to the rest of the system in Figure 1. If

intercompartmental flows in the system are proportional to flows into the donor compartments, then an appropriate manipulation of the magnitude 14 inflow to compartment 1 could produce the desired total requirement from that compartment.

$$A: \begin{bmatrix} 0 & .07 & 0 & 0 \\ .5 & 0 & .2 & 0 \\ 1 & .0 & 0 & 0 \\ 0 & .5 & .5 & 0 \end{bmatrix}$$

$$(I-A)^{-1}: \begin{bmatrix} 1.05 & .0736 & .0147 & 0 \\ .735 & 1.06 & .210 & 0 \\ 1.05 & .0736 & 1.015 & 0 \\ .893 & .563 & .612 & 1 \end{bmatrix}$$

Figure 2.
Normalized matrix of flows A and corresponding matrix $(I-A)^{-1}$ for the system of Figure 1.

The detailed marsh model, together with its application to the problem of linking shellfish production to marsh grass fertilization, is quite similar to the example above. The model traces the annual exchanges of nitrogen (in units of kg N yr^{-1}) among five compartments in a schematic flow model of the marsh. The compartments are (1) Sediments, (2) Spartina root/rhizome biomass, (3) Spartina aboveground biomass, (4) Tidal water, and (5) Shellfish. The path of a nitrogen input via fertilization would be roughly through the five compartments in the order listed, though there is a fair amount of internal cycling and flow to and from the outside environment in the model. The nitrogen in all major forms of nitrogen found in the marsh (particulate organic, dissolved organic, dissolved inorganic) is included. Inputs to the system from outside include the nitrogen in groundwater, precipitation and tidal inflow, and bacterial, algal and rhizomal fixation. Outputs include the nitrogen in tidal outflow, denitrification, volatilization, and losses to deep sediments. All are summed over a year. In most cases data used are averages of several years. Details of how various values were calculated are omitted here, but are available upon request.

Fertilization, the nitrogen in groundwater and precipitation and that fixed by surface bacteria and algae are lumped into a single exogenous inflow to compartment 1. The inflow value used in the model excludes fertilization values, however, so that the model actually describes the marsh in its natural state. Fertilization is thus viewed as a manipulation of this inflow similar to that described for the input to compartment 1 in the hypothetical system. Likewise, the nitrogen in net annual average growth of shellfish, as estimated for the marsh's natural population of ribbed mussels (Modiolus demissus), is listed as the sole exogenous output from compartment 5. This is done in an attempt to approximate a potential sustained yield harvest. This figure, 70 kg N yr^{-1}, corresponds to roughly 8500 kg mussel meat production, wet weight. Flows in the marsh are summarized in Table 2 below, in the format used for Table 1. The flow diagram is omitted, but it can be easily drawn from the information in the table.

	(1)	(2)	(3)	(4)	(5)	In-flows
(1)	0	4200	0	490	470	5970
(2)	6990	0	0	0	0	1270
(3)	0	1210	0	0	0	0
(4)	1270	0	1160	0	70	26250
(5)	0	0	0	730	0	0
Out-flows	2870	0	0	31600	70	

Table 2

Annual nitrogen flows for Great Sippewissett Marsh in kg N yr^{-1}, summed over the nitrogen in all major forms found in the marsh. Balancing flows are omitted. Compartments are: (1) Sediments, (2) Belowground biomass (3) Aboveground biomass (4) Tidal water (5) Shellfish.

The central portion of the matrix $(I-A)^{-1}$ is presented in Figure 3 below. As explained above, the elements of this matrix summarize the intercompartmental transfers which lead to the various outflows from the system. This kind of information can provide important clues about the specific relationships between flows in the system. With respect to the problem we have posed, the element in the (5,1) position is especially significant. It tells us that, given an outflow of a specified magnitude from compartment 5, only about 10% of that outflow has been through compartment 1. This stands in marked contrast to the situation in our hypothetical example, in which no flow could enter compartment 3 without first passing through compartment 1 (See Figure 1). Thus, based on the model, it would be difficult, for example, to double shellfish production in the marsh (outflow from compartment 5) by fertilization alone (i.e. by increasing the magnitude of the inflow to compartment 1).

	(1)	(2)	(3)	(4)	(5)
(1)	1.48	.564	.005	.128	.063
(2)	1.25	1.48	.004	.108	.053
(3)	1.25	1.48	1.00	.108	.053
(4)	.102	.074	.036	1.01	.006
(5)	.102	.074	.036	1.01	1.01

Figure 3

The central portion of the matrix $(I-A)^{-1}$, as computed for Great Sippewissett Marsh nitrogen flows.

This result is not surprising in terms of the nitrogen flow model we have presented. Inspection of Table 2 shows, for example, that no flow can enter the shellfish compartment without first passing through compartment 4, tidal water. This compartment in turn is strongly driven by the large annual tidal exchanges it has with nearby coastal waters, signified by the large inflows and outflows shown for this compartment in the table. A related factor which must be considered is the fact that dissolved organic nitrogen (DON), whose function is not well understood in the marsh, makes up a significant portion of the inflows and outflows in our model. In fact DON makes up 62% of tidal inflows, 58% of tidal outflows, 45% of groundwater flow, and more than half of the total inputs and outputs to and from the marsh (10). DON apparently plays no role in shellfish feeding and in fact may pass through the marsh with very little interconversion, since total inputs and outputs of this species very nearly balance (10). The model presented here must be regarded as a first pass attempt at analytical assessment of the potential for enhanced shellfish production via marsh fertilization. A fairer test would probably involve a model in which all DON is subtracted from the flows. Final judgement on the ultimate practicability of marsh fertilization must thus be withheld until further analysis is made.

4. Costs of Fertilization

Estimating the cost of nitrogen fertilization of a salt marsh is difficult because the equipment for applying the fertilizer is not standard. Rather than provide engineering cost estimates of large - scale systems, we will indicate the approximate cost of the system now used to fertilize a 2 to 3 ha section of marsh. This system pumps the fertilizer through spray irrigation pipes to all sections of the plot. The capital cost of the system is approximately $29,000, excluding design costs. Depending on remoteness, type of foundation required and other site - specific factors, this cost could be reduced by $5,000 or more. Vandalism has been a problem in maintaining the equipment, so a ten-year life is estimated. Assuming that the operator of the system can check it during periodic visits to the marsh for other purposes, and that approximately the present level of vandalism continues, annual maintenance cost is estimated to be $3,000 per year or less.[1] The operating costs are then labor and fertilizer. If fertilizer is applied for six months of the year, labor requirement will be about one-half time during that six months ($3,000 if annual full-time salary rate is $12,000) to apply fertilizer daily and check the equipment. Commercial fertilizer containing 45% nitrogen is estimated to cost $1,000 per year(25kg N/ha/week for 25 weeks = 650 kg of nitrogen in fertilizer). This is the high-level application rate; researchers feel most of the increase in growth of Spartina could be obtained with only one-third as much fertilizer[2]. This would decrease fertilizer cost but not labor and capital upkeep costs.

The alternative of obtaining nitrogen from secondarily treated sewage effluent would depend on acceptance by the local community as well as on the presence of a nearby sewage treatment plant. Under these circumstances, the nitrogen itself could be provided free of charge to the marsh, but the labor and capital costs would be higher to handle the greater volume required. In contrast to the 45% nitrogen content of some commercial fertilizers, secondarily sewage effluent has only about 15 parts per million of nitrogen, and an application rate comparable in nitrogen content would be 1.25 million liters per week per hectare (instead of 25 kg N/ha/week of commercial fertilizer). The feasibility of using this source of nitrogen is clearly very dependent on particular characteristics of the site.

5. Summary and Conclusions

Input-output analysis can be a useful tool for assessing the economic potential of biological systems over which man can exert little control. It makes possible the linkage of controllable inputs to outputs of potential economic value, while allowing for explicit consideration of the complex biological processes which ultimately govern the system's output of such commodities. This seems particularly true of salt marshes, where research has shown that fertilization can lead to dramatically increased yields of marsh grass biomass, and hence grass detritus which is potential food for shellfish.

We have used an input-output format to describe nitrogen flow through a New England salt marsh which has been intensively studied by biologists over the past few years. While much has been written about the use of input-output analysis to integrate environmental and economic concerns, attempts to do so are often limited by the lack of a detailed data base for the analysis. We believe the problem of linking a marsh's biomass yield of fish and shellfish to fertilization presents a valuable opportunity to test in detail this extended input-output methodology in a setting in which all links in the system being considered are under active study.

The input-output model presented here represents a distillation of data collected in field and laboratory studies. While the present model is far from definitive in answering the questions we have presented, it illustrates a method which can be used to examine other similar ecological-economic interactions. Future work should lead to detailed analysis of the fate of the various flows in the marsh system and provide some strong indications of the extent to which similar systems lend themselves to this type of analysis.

Acknowledgements

Several people must be acknowledged for helpful criticisms and access to unpublished data used in the preparation of this paper. These include Ivan Valiela and Thomas Jordan of the Boston University Marine Program, Jim Morris of the Marine Biological Laboratory Ecosystems Center, John Teal and Peter Kallio of Woods Hole Oceanographic Institution. Special thanks go to Jack Finn of the MBL Ecosystems Center for his assistance in the computer analysis of our results.

---

[1]Peter Kallio, personal communication, June 1978.

[2]John Teal, personal communication, June 1978.

References

1. Finn, J.T., "Measures of ecosystem structure and function derived from analysis of flows," The Journal of Theoretical Biology, Vol. 56, 1976, pp. 363-380.

2. Gosselink, J.G., E.P. Odum and R.M. Pope, "The value of the tidal marsh," The Center for Wetland Resources, La. State University, Baton Rouge, 1973, SG-74-03.

3. Hannon, B., "The structure of ecosystems," The Journal of Theoretical Biology, Vol. 41, 1973, pp. 535-546.

4. Isard, W., Ecologic-Economic Analysis for Regional Development, The Free Press, New York, 1972.

5. Leontief, W., "Quantitative input-output relations in the economic system of the United States," The Review of Economics and Statistics, Vol. 18, 1936. pp. 105-125.

6. Odum, H.T., "Trophic structure and productivity of Silver Springs, Florida", Ecological Monographs, Vol. 27, 1957, pp. 55-112.

7. Ryther, J.H. and W.M. Dunstan, "Nitrogen, phosphorus, and eutrophication in the coastal marine environment," Science, Vol. 171, pp. 1003-1013.

8. Smith, L.J. and J.E. Huguenin, "The economics of waste water - aquaculture systems," IEEE OCEAN '75 Proceedings, 1975, pp. 285-293.

9. Teal, J.M., "Energy flow in the salt marsh ecosystem of Georgia," Ecology, Vol. 43, 1962, pp. 614-624.

10. Valiela, I. and J.M. Teal, "Inputs, outputs and interconversions of nitrogen in a salt marsh ecosystem," Paper presented at the First European Ecological Symposium, Ecological Processes in Coastal Environments, Norwich, U.K., 1977.

11. Valiela, I., J.M. Teal and W. Sass, "Production and dynamics of salt marsh vegetation and the effects of experimental treatment with sewage sludge," The Journal of Applied Ecology, Vol. 12, 1975, pp. 973-982.

UNDERWATER PROFILING OF ICEBERGS USING SUBMERSIBLES

B.P. Sukhov

NORDCO Limited
P.O. Box 8833
St. John's, Newfoundland, Canada A1B 3T2

Abstract

A new method is proposed for iceberg draft measurement and profiling using an unmanned, tethered submersible as an underwater platform equipped with a depth meter, an up-looking echo sounder or an up-looking scanning sonar. Block diagrams and instrumentation for measurement and processing of data are presented. Basic measurement equations and accuracy of measurement are analyzed by two methods which give comparable results.

1. Introduction

Icebergs transported by the Labrador Current from the northern Baffin Sea are a great danger for oil well heads and other equipment installed on the sea bottom such as pipes and cables. Since icebergs may ground and destroy equipment installed on the bottom, the offshore oil industry requires statistical iceberg draft data which can be used to estimate the probability of a break or disaster. Iceberg draft is also of interest for shipping and other marine activities and the effect it may have on drift, groundings and deterioration.

The measurement of the physical properties of icebergs is also of great interest in connection with their use as a source of fresh water and energy. Projects for utilizing icebergs are very dependent upon the success of long distance towing operations. Knowledge of the iceberg's draft, underwater profile, volume and mass is of great fundamental importance to such operations.

Regarding the iceberg draft measurement problem, there are three methods which have been used with varying degrees of success.

1. Measuring the water depth close to a grounded iceberg. It was first done by H. Rodman in 1890 [1] and later by W.B. Dowson in 1907 in the Strait of Belle Isle [2].

2. Dragging a cable with a depth sensor attached underneath the iceberg by means of two ships passing on either side of the berg [3].

3. Using a side scan sonar operating in a vertical mode. This technique was used with success by R.Q. Robe in 1974 [4]. An attempt to map the underside of Arctic sea ice using back scattered acoustical waves and a scanning sonar is also worth mentioning here [5,6]. Both a side scan sonar and a scanning sonar were also used for underwater profiling of either icebergs [7] or pack ice [8]. The accuracy of the above methods proved to be very low. Therefore, there is a need to propose new techniques.

2. Basic Principle of Iceberg Draft Measurement and Underwater Profiling

A. Echo Sounder Mode of Operation

An underwater platform is equipped with a depth sensor, up-looking and down-looking echo sounders and moves under the iceberg (Fig. 1 and 2). The down-looking echo sounder measures a distance from the platform to bottom, CD = h_3. The depth sensor measures a platform's depth h_2, i.e. a distance AC, an up-looking echo sounder measures a vertical distance from platform up to the iceberg, i.e. distance CB. Iceberg draft, d, in point B immediately above the platform could be calculated as $d = h_2 - h_1$. Measurement of these parameters during a platform movement gives a cross-section profile of an iceberg's underwater

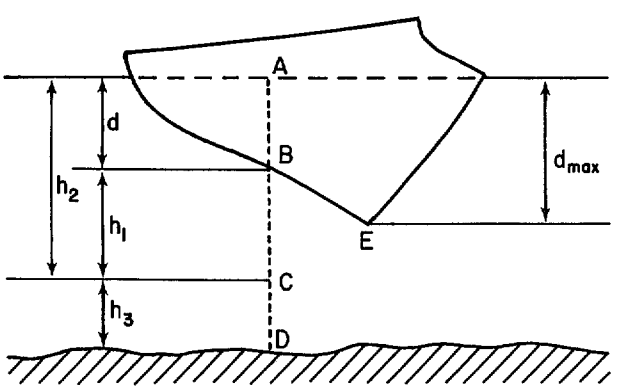

Fig. 1 BASIC PRINCIPLE OF MEASUREMENT

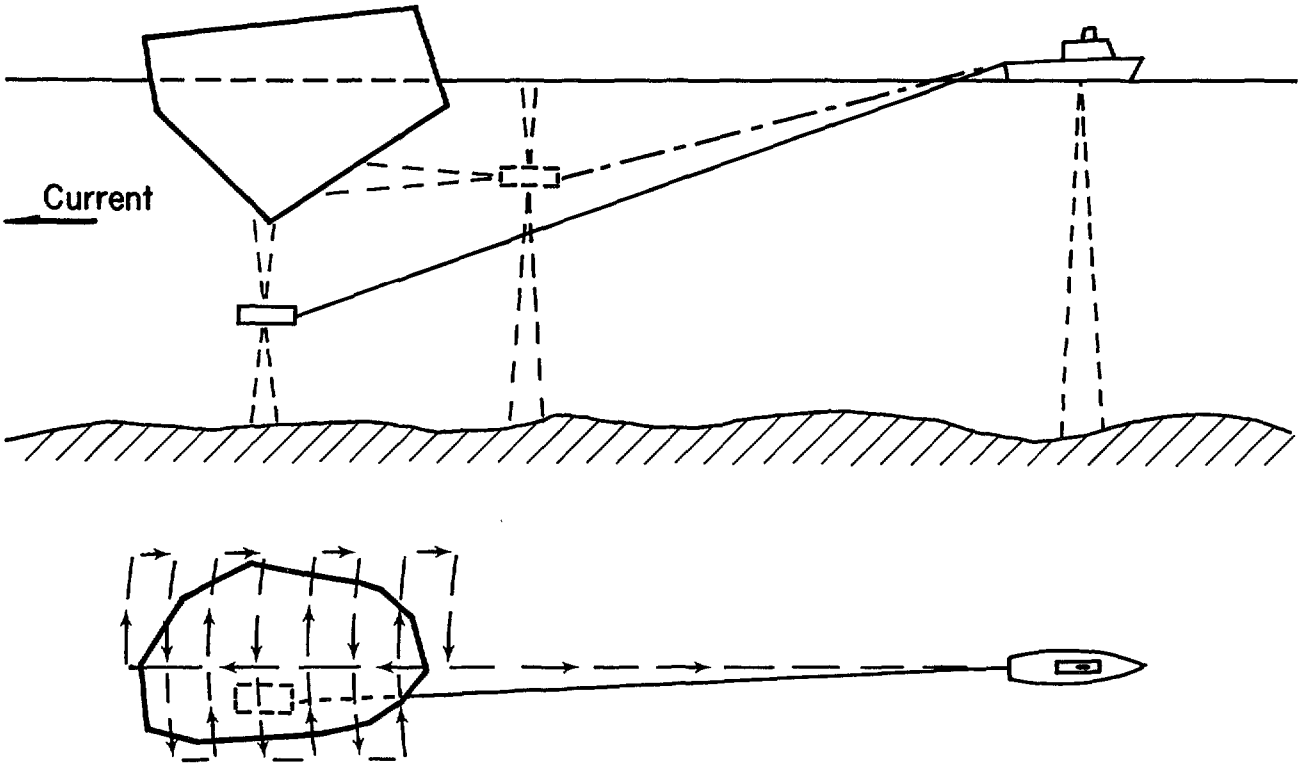

Fig. 2 ECHO SOUNDER MODE OF OPERATION

part. Maximal measured difference, $d_{max} = h_2 - h_1$, is determined as d for the lowest point E, i.e. an iceberg draft.

B. Sonar Mode of Operation

An underwater platform is equipped with a depth sensor and an up-looking sonar scanning in a plane perpendicular to the direction of platform movement (Fig. 3). Here the platform is in point C, and it moves in a direction perpendicular to the plane of the drawing. Scanning angle sensor gives the angle α between a vertical line AD and a sonar beam CF. ρ is the distance between the platform and the iceberg measured by sonar. Thus, the iceberg draft in point F can be calculated as:

$$d = h_2 - h_1 = h_2 - \rho \cos \alpha$$

Every sonar scan gives a cross-section semi-profile, i.e. a profile up to the deepest point. For full profile, we need a second run at the other side of the deepest point E. Again a measurement for the deepest point represents an iceberg draft d_{max}.

For in situ measurements, instruments and sensors should be delivered under the iceberg. There are various ways in which this could be accomplished:

1. a scuba diver
2. a towed body
3. a manned submersible
4. a military submarine
5. an unmanned submersible, tethered or untethered.

Analysis with all pros and cons has been given in a previous paper with the conclusion that a most suitable platform for iceberg measurements is an unmanned, tethered submersible (Fig. 2). Mode of operation for both the manned and unmanned submersible has been described as well [9].

3. Instrumentation

A block diagram of the system suitable for the echo sounder mode of operation is shown in Fig. 4. The wide view recorder sends a trigger signal to the clock and generators of both the up and down-looking echo sounders. The clock starts to measure time. Echo signals from both the iceberg and bottom stop the clock and as a result, its output is h_1 - the distance from the submersible to the iceberg and h_3 - the distance from the submersible to the bottom. Data from the sound velocity sensor is used for distance measurement corrections. The sign invertor changes the parameter h_1 into $-h_1$ and puts it in the operational amplifier-summator. The second input of the operational amplifier is the submersible depth h_2, i.e. the distance from the submersible to the surface. Its output is $h_2 + (-h_1) = d$, the iceberg draft at the point immediately above the submersible. So three parameters, d, h_3 and h_2

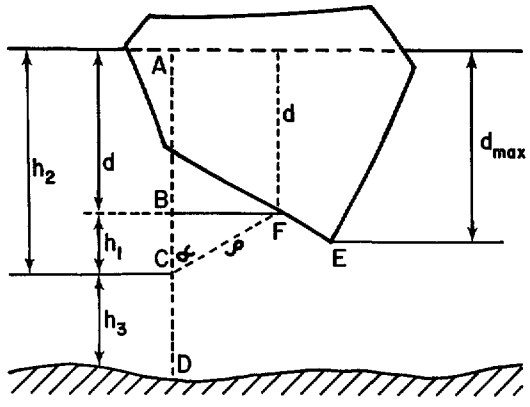

Fig. 3 SONAR MODE OF OPERATION

go into the processor which inputs them into a side view recorder. Both the recorder and the processor work in the following sequence:

1. A trigger signal forces the recorder's pen to place a mark on the paper strip which represents the surface. The same signal is inserted in the processor.

2. After a certain time proportional to the local iceberg draft, the processor sends a signal to the recorder and the pen makes a second mark which represents a profile line of the underwater part of the iceberg.

3. After a time proportional to h_2, the distance between the surface and the submersible, the processor sends another signal to the recorder. Its pen makes a third mark which represents the track of the submersible.

4. After a time proportional to h_3, the distance from the submersible to the bottom, the pen makes a fourth mark.

As a result, we have on the recorder diagram a series of underwater profiles and the track of the submersible between the iceberg and the bottom (Fig. 5).

The processor calculates the form, volume and mass of the underwater part of the iceberg. Besides this, with the help of a keyboard on the ship, data concerning the above water portion of the iceberg (width and height) can be inputed to the processor. It then calculates a volume and mass of the entire iceberg and constructs on the CRT screen and top view plotter the underwater profile of the iceberg consisting of isodepth lines or isodepth planes. The position of both the ship and submersible relative to the iceberg could be represented on both the CRT screen and top view recorder using data from a positioning system.

A block diagram for the sonar mode of operation is shown in Fig. 6. A continuously rotating transducer is installed on a tilting mechanism which can be in either of two positions. In the vertical position, I, the transducer rotates in the horizontal plane and looks forward. This mode of operation is used in approaching the iceberg for a rough estimation of the iceberg draft and underwater profile. After lowering the submersible to its working depth with sufficient clearance below the iceberg the pilot rotates the tilt mechanism to the horizontal position, II, so that the transducer scans in a vertical plane perpendicular to the movement direction of the submersible.

The following data is fed into the processor; the distance to the iceberg, ρ, from a transducer, an angle, α, from an angle sensor and the submersible position relative to the surface, the depth h_2, from the depth sensor. It calculates the draft, volume and mass of the iceberg as in the previous case. A top view plotter gives an iceberg's profile in the form of isoplanes or isolines of equal depth.

4. Accuracy Analysis

Let us now investigate the accuracy and possible errors of the proposed modes of operation. This is a typical case of indirect measurement; that is, iceberg draft cannot be measured directly but is calculated after the other two or three parameters have been measured.

Basically, the accuracy of the echo sounder mode depends on accuracy of the depth meter and the echo sounder to be used.

Total error of method might be found from the following simple calculation:

$$d = (h_2 \pm \Delta h_2) - (h_1 \pm \Delta h_1) =$$

$$h_2 \pm \Delta h_2 - h_1 \pm \Delta h_1 =$$

$$h_2 - h_1 \pm \Delta h_2 \pm \Delta h_1 =$$

$$h_2 - h_1 \pm (\Delta h_2 + \Delta h_1) =$$

$$h_2 - h_1 \pm \Delta d$$

$$|\Delta d| = |\Delta h_2| + |\Delta h_1|$$

where Δh_2 - absolute error of depth meter

Δh_1 - absolute error of echo sounder

Δd - absolute error of a measured berg's draft

Practically, Δd is equal to the sum of $\Delta h_1 + \Delta h_2$.

Now let us discuss an error of the second mode of operation, i.e. a submersible equipped with a scanning sonar. The problem could be approached by two methods - an analytical method and a direct method.

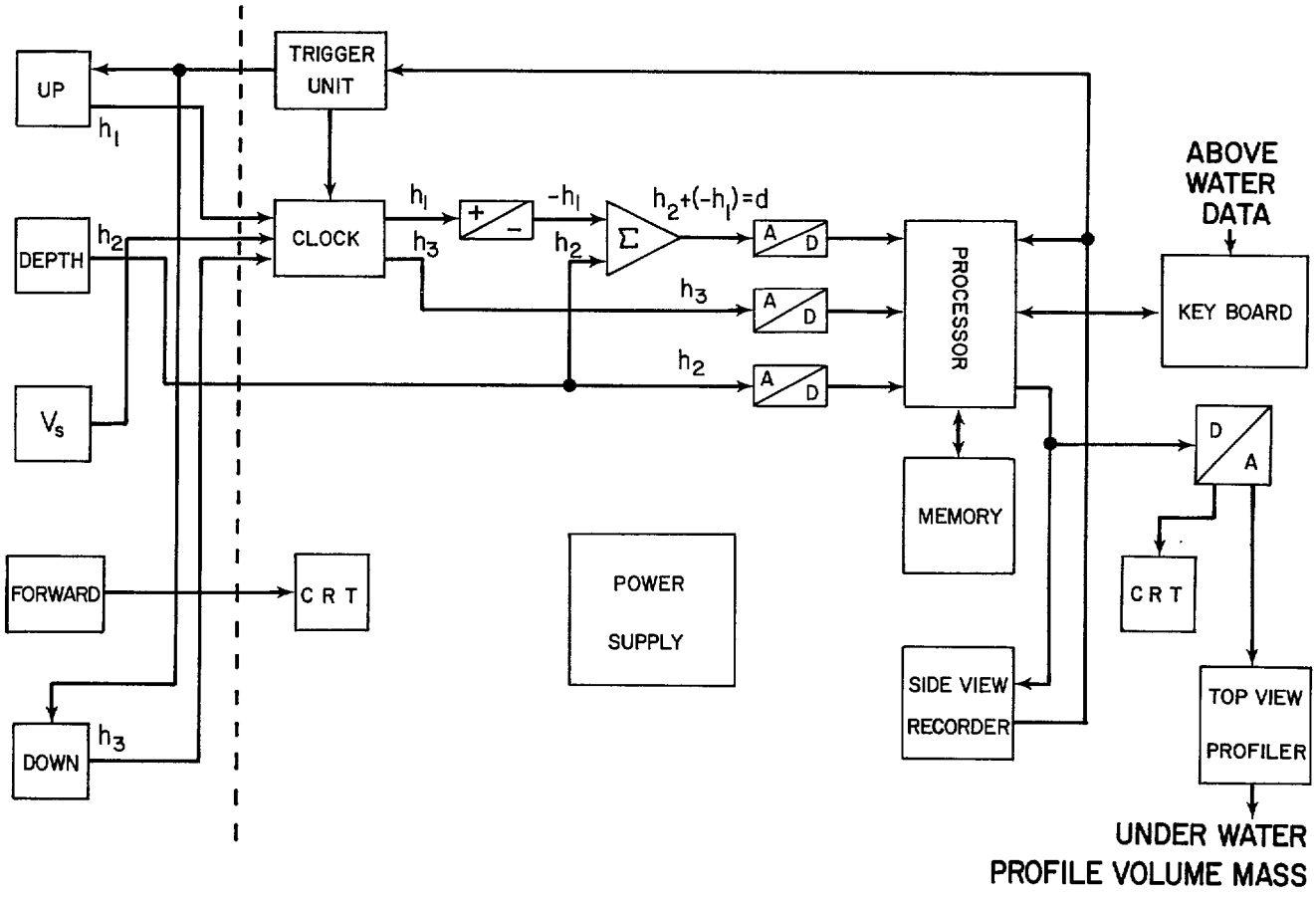

Fig. 4 BLOCK DIAGRAM FOR THE ECHO SOUNDER MODE

A. Analytical Method

Let us consider the basic equation

$$d = h_2 - \rho \cos \alpha$$

$$d \pm \Delta d = h_2 \pm \Delta h_2 - (\rho \pm \Delta \rho) \cos (a \pm \Delta \alpha)$$

This can be represented in the following form

$$A = B - CD \qquad \text{or}$$

$$A \pm \Delta A = B \pm \Delta B - (C \pm \Delta C)(D \pm \Delta D)$$

This last term can have four possible forms

$$(C + \Delta C)(D + \Delta D) = CD + \Delta CD + \Delta DC + \Delta C\Delta D$$

$$(C + \Delta C)(D - \Delta D) = CD + \Delta CD - \Delta DC - \Delta C\Delta D$$

$$(C - \Delta C)(D + \Delta D) = CD - \Delta CD + \Delta DC - \Delta C\Delta D$$

$$(C - \Delta C)(D - \Delta D) = CD - \Delta CD - \Delta DC + \Delta C\Delta D$$

Therefore

$$A \pm \Delta A = B \pm \Delta B - [CD \pm \Delta(CD)]$$

$$\Delta(CD)_{max} = \Delta CD + \Delta DC + \Delta C\Delta D$$

$$|\Delta A| = |\Delta B| + |\Delta CD| + |\Delta DC| + |\Delta C\Delta D|$$

Remember: $\Delta C = \Delta\rho$

$C = \rho$

$D = \cos \alpha$

$\Delta D = \Delta(\cos \alpha)$

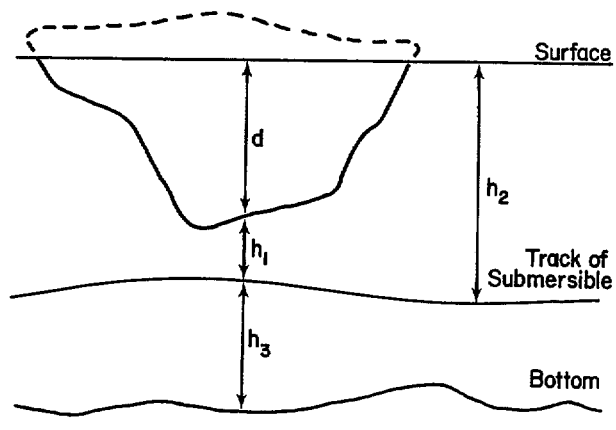

Fig. 5 RECORDER DIAGRAM FOR THE ECHO SOUNDER MODE

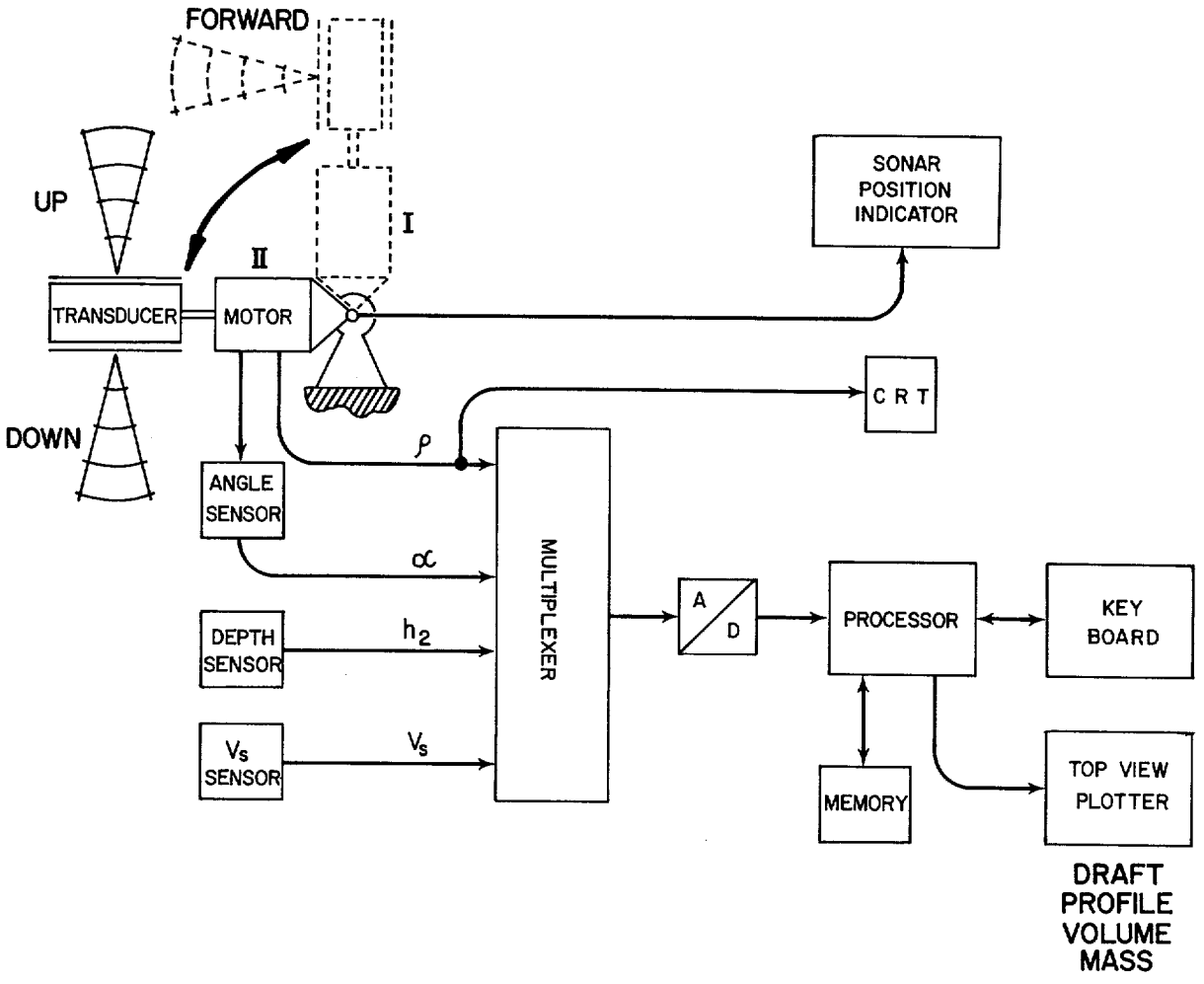

Fig. 6 BLOCK DIAGRAM FOR THE SONAR MODE

We need to find $\Delta(\cos\alpha)$. So $\cos(\alpha \pm \Delta\alpha) = \cos\Delta\alpha \mp \sin\alpha \sin\Delta\alpha$. But $\cos\Delta\alpha \simeq 1$, because $\Delta\alpha \simeq 0$ and $\cos(\alpha \pm \Delta\alpha) = \cos\alpha \mp \sin\alpha \sin\Delta\alpha$. So that $|\sin\alpha \sin\Delta\alpha|$ is the modulus of absolute error of $\cos\alpha$ and the equation for $|\Delta A|$ becomes:

$$|\Delta d| = \Delta h_2 + \Delta\rho \cos\alpha + \rho \sin\alpha \sin\Delta\alpha + \Delta\rho \sin\alpha \sin\Delta\alpha$$

A relative error is equal to

$$\gamma_d = \pm \frac{\Delta d}{d} \times 100\%$$

B. Direct Method

According to the basic equation, $d = h_2 - \rho \cos\alpha$, the error for an iceberg draft is a function:

$$\Delta d = f(\Delta h_2, \Delta\rho, \Delta\alpha)$$

Let us find Δd as a difference between the measured and true values of draft.

$$+\Delta d = d_{meas} - d_{true}$$

$$-\Delta d = d_{true} - d_{meas}$$

A positive error $+\Delta d$ reaches a maximum when h_2 is maximum and $\rho \cos\alpha$ is minimum, i.e. $h_2 + \Delta h_2$ and $(\rho - \Delta\rho) \cos(\alpha + \alpha\Delta)$ correspondingly.

A negative error $-\Delta d$ reaches a maximum when h_2 is minimum and $\rho \cos\alpha$ is maximum, i.e. $h_2 - \Delta h_2$ and $(\rho + \Delta\rho) \cos(\alpha - \Delta\alpha)$ correspondingly. So therefore we have:

$$+\Delta d_{max} = [(h_2 + \Delta h_2) - (\rho - \Delta\rho) \cos(\alpha + \Delta\alpha)] - [h_2 - \rho \cos\alpha]$$

$$-\Delta d_{max} = [h_2 - \rho \cos\alpha] - [(h_2 - \Delta h_2) - (\rho + \Delta\rho) \cos(\alpha - \Delta\alpha)]$$

5. Conclusion

Calculations have been taken using real parameters of modern depth meters, echo sounders and sonars available on market. These calculations show that both methods give results which are in good agreement and the accuracy of iceberg draft measurement and profiling using a submersible in both modes of operation would be approximately ± 1%.

References

1. H. Rodman, "Report of Ice and Ice Movements in North Atlantic Ocean", U.S. Navy Hydrographic Office, 1890, No. 93

2. W.B. Dawson, "The Currents in Belle Isle Strait", Department of Marine and Fisheries, Ottawa, 1907.

3. E.H. Smith, "International Ice Patrol", The Meteorological Magazine, The Meteorological Office, Air Ministry, 1925, Vol. 60, No. 718, pp. 229 - 236.

4. R.Q. Robe, "Height to Draft Ratios of Icebergs", POAC '75, Third International Conference on Port and Ocean Engineering under Arctic Conditions, 1975, Vol. 1, pp. 407 - 415.

5. J.M. Berkson, E.S. Clay, T.K. Kan, "Mapping the Underside of Arctic Sea Ice by Backscattered Sound", Journal of the Acoustical Society of America, 1973, Vol. 53, pp. 777 -781.

6. T.K. Kan, C.S. Clay, J.M. Berkson, "Sonar Mapping of the Underside of Pack Ice", Journal of Geophysical Research, 1974, Vol. 79, No. 3, pp. 483 - 488.

7. C.P. Benedict, "Underwater Profiling of Icebergs", POAC '73, Second International Conference on Port and Ocean Engineering Under Arctic Conditions, 1973, pp. 601 - 607.

8. T. Pousi, M. Luukkala, "A Narrow Beam Sonar to Measure the Submarine Profile of an Ice Ridge", POAC '75, Third International Conference on Port and Ocean Engineering Under Arctic Conditions, 1975, Vol. 1, pp. 389 - 406.

9. B.P. Sukhov, "Measurement of Iceberg Draft", First International Conference on Iceberg Utilization, Ames, Iowa, 1977.

MONITORING SYSTEM FOR A NEW OCEAN CABLE PLOW

K. Yamamura
Research & Development Laboratories
Kokusai Denshin Denwa Co., Ltd. (KDD)
1-23, 2-chome, Nakameguro, Meguro-ku, Tokyo, Japan

Y. Iwamoto
Research & Development Laboratories
Kokusai Denshin Denwa Co., Ltd. (KDD)
1-23, 2-chome, Nakameguro, Meguro-ku, Tokyo, Japan

Y. Shirasaki
Research & Development Laboratories
Kokusai Denshin Denwa Co., Ltd. (KDD)
1-23, 2-chome, Nakameguro, Meguro-ku, Tokyo, Japan

Abstract

On the continental shelves, it is desirable to bury ocean cables under the sea bottom from the point of view of coexisting with fishing activities. A new type of cable plow with seven blades developed by KDD is designed to have a capability of burying the cable to a depth of 70 cm under the sea bottom at a towing speed up to about 3 knots. Since the plow is equipped with no power mechanism and is relatively small in size and light in weight, the effective burying works are achieved by adequate operation of the cable ship. This paper describes the cable plow monitoring system for obtaining enough information for the operation of the cable ship. A new ocean telephone cable system was constructed between Japan and China in 1976. KDD succeeded in burying the cable about 700 km across the continental shelf.

1. Introduction

The ocean telephone cable system plays an important role in international telecommunication network together with the satellite communication system.

Five international cable systems are now working in Japan, among which Japan-China Cable System[1,2,3] was constructed in summer 1976. Since the cable route crossed the vast continental shelf in the East China Sea, the cable of about 700 km which corresponded to about 80% of the total cable length was buried successfully under the sea bottom.

The continental shelf abounds in fishing resources, where fishing activities are carried out extensively. Most of cable troubles which have occurred on the continental shelf area in the past were caused by fishing activities, especially trawling[4].

To protect the cable against the damage the following two methods have been adopted:

(1) protecting the cable by armor wire
(2) burying the cable under the sea bottom

In the area where the latter method is applicable, it is more desirable to bury the ocean cable under the sea bottom from the point of view of coexisting with fishing activities and cable system construction cost. Because the buried cable will be protected against damage caused by fishing gear, and also will not interfere with fishing activities and moreover the cable to be buried will be fairly cheaper than the armored cable.

KDD has conducted investigations into a cable burying plow[3] since 1962, because the plow would be indispensable for constructing cable systems on the vast continental shelves around Japan and Southeast Asia.

The cable burying system is composed of a cable plow and a cable ship, so that the cable plow must be designed to be suitable for the performance of the cable ship. The new cable plow developed by KDD was designed to adapt the cable ship KDD-Maru (4300 tons).

As shown in Figure 1, the cable burying plow with seven blades is relatively small in size (7 m length) and light in weight (6.5 tons).

The plow is composed of a balancing wing and a digging blades. The balancing wing is for stabilizing the plow attitude, and the digging blades is for digging a trench in the sea bottom.

The pin-joint coupling of the balancing wing with the digging blades enables the plow to get over small obstacles on the sea bottom and to be towed stably even at sandwave area.

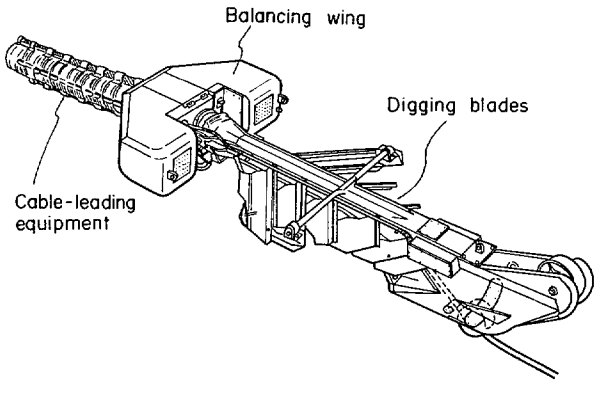

Figure 1 Cable plow

The plow towed by the cable ship is designed to bury several hundred kilometers of the cable to a depth of 70 cm under the sea bottom at a speed up to about 3 knots. The cable and repeaters are smoothly guided to the plow through the lots of guiding rings which form a path from the ship to the plow, and are laid on the bottom of the trench dug by the plow. Figure 2 shows the operating configuration of the cable burying works. As the cable is fed from the ship to the plow through the guiding rings which are supported by the main towing rope and auxiliary rope, a complicated control system for feeding the cable is unnecessary.

The cable burying system developed by KDD is relatively simple, but has sufficient function for burying the cable and repeaters. But the plow does not have any active mechanism such as an attitude stabilizer and a plowshare suspension, accordingly, the effective burying works are achieved by adequate operation of the cable ship, for example, towing speed, towing rope length.

The important information required for adequate operation of the cable ship and the plow has to be given from the plow monitoring system. But the plow structure is not suitable for equipping the sensors to monitor the condition of the plow. In the plow the space for the sensors and the type of the sensors are subject to restriction, because the sensors which may restrict the plow handling on board or the plow lowering and recovery will degrade the work efficiency excessively.

Within these constraints, the cable plow monitoring system was satisfactorily developed to obtain enough information as to the plow on the sea bottom for carrying out the burying works.

To avoid an interruption of the burying works due to a trouble of the monitoring system, high reliability and long life are attained by adopting the following basic principles: minimum interdependence of one functional element upon another, use of reliable components supplied on the market, minimization of the number of components, duplication as much as possible, and simplicity in mechanical configuration.

2. Monitoring System

Configuration of monitoring system

The cable plow monitoring system is mainly consists of the following: (1) sensors on the plow, (2) multiconductor cable, and (3) monitoring equipment on board as shown in Figure 3.

The sensors on the plow are designed for 300 m of water depth, because the operating depth is less than 200 m. Most of the sensors are installed in the balancing wing of the plow to be protected against various hazard on board or on the sea bottom, which consequently does not impose any restrictions on the handling of the plow.

Each signal detected by each sensor is transmitted to the monitoring equipment on board through the multiconductor cable. Multiplex transmission technique which is usually adopted for transmitting the lots of signals is not adopted in this system, because simplification of the monitoring system, facilitation of the system check, and reduction of the influence of a partial trouble of transmission cable such as broken wire are thought more important.

The monitoring equipment on board displays several kinds of information as to the plow on the panel-meters, pen recorders and also displays the plow working on the sea bottom on a model plow simulator, by processing the signals transmitted from the sensors.

Monitoring items

The number of monitoring items as to the plow is ten as follows, which is decided in consideration of the structure of the plow and its working conditions on the sea bottom.

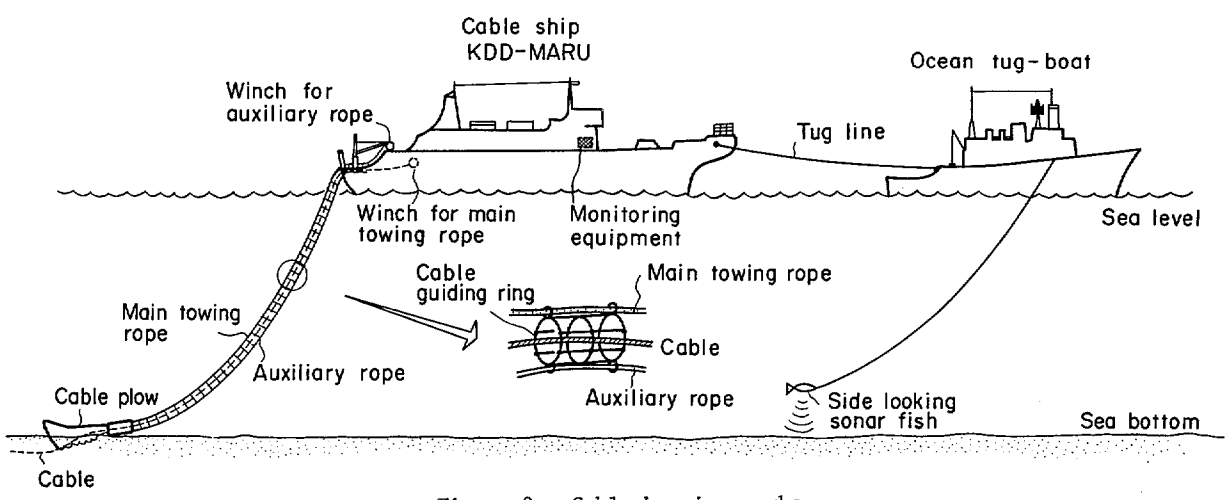

Figure 2 Cable burying works

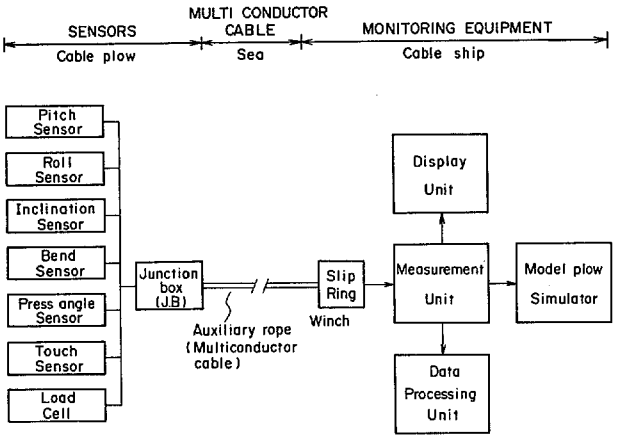

Figure 3 Configuration of monitoring system

(1) pitch angle of the balancing wing (pitch angle)
(2) roll angle of the plow (roll angle)
(3) pitch angle of the digging blades of the plow (inclination angle)
(4) bend angle between the balancing wing and the digging blades (bend angle)
(5) operating press angle of the cable press roller (press angle)
(6) information whether the balancing wing touches the surface of the sea bottom or not (touch bottom)
(7) information whether the plow is set on the sea bottom correctly or upside down (correct setting)
(8) towing rope tension
(9) dug trench depth
(10) cable burial depth

In addition to the items mentioned above, the following items as to the ship board facilities are also monitored:

(11) tension, speed, and length of the cable to be buried
(12) tension of main towing rope
(13) tension of auxiliary rope

On the other hand, an ocean tug-boat which keeps the cable ship on the cable laying course tows a side-looking sonar fish for surveying obstacles such as rock, sunken ship.

The plow attitude is monitored in items (1), (2), and (3) mentioned above which monitor the inclination angle of the plow to a horizontal plane, because stable attitude of the cable plow is necessary to dig trench in the sea bottom efficiently.

Item (4) is not only useful to grasp the plow attitude intuitively, but also is used to compute the dug trench depth and the cable burial depth.

The operation of the cable press roller which presses the cable into the trench bottom is monitored in item (5). This item is also used to compute the cable burial depth and moreover it gives the information whether the repeater passes through the plow smoothly.

Whether the balancing wing touches the surface of the sea bottom or not is monitored in item (6).

Whether the plow is set on the sea bottom correctly or upside down is monitored in item (7). This information is especially important at the beginning of the cable burying works when the plow is hanged down by the main towing rope and set on the sea bottom. The plow is designed to be set on the sea bottom correctly, it is apprehended, however, that the plow is set upside down where the sea bottom is muddy or when tide runs very strong.

Tension required to dig trench is monitored in item (8). On the other hand, item (12) shows the tension which is sum of item (8), weight of guiding rings, fluid resistance to cable and guiding rings, and frictional force caused between the main towing rope and the stern chute of the cable ship. Accordingly, the results obtained from items (8) and (12) are sometimes much different.

The depth of the trench dug by the plow and the cable burial depth are shown in item (9) and item (10) respectively, which are computed

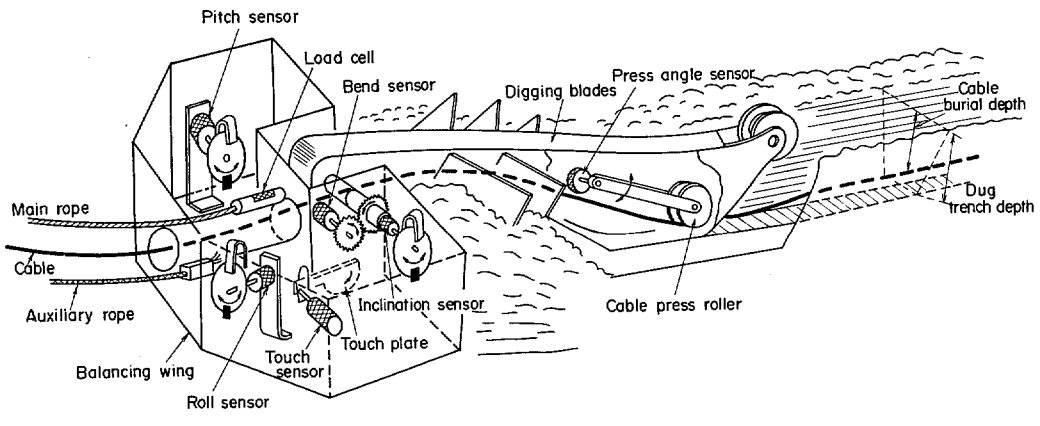

Figure 4 Appearance of the sensors on the plow

from the results obtained from items (1), (2), (3), (4) and (5).

3. Sensors on the Plow

Figure 4 shows an appearance of the sensors on the plow. A pendulum method is adopted in the sensors that detect pitch angle, roll angle, and inclination angle. To obtain high confidence of the monitoring system, the check and calibration of it are carried out thoroughly on board before the plow is hanged down to the sea bottom. But the plow is placed upside down on the deck for reasons of its handling, accordingly, these sensors should be applicable throughout 360°.

The sensor is composed of a synchros, an aluminum thin circular plate which has an adequate small weight on one point of its edge, and a magnet as shown in Figure 5. Since the mechanical torque of the synchros is small, the required length of the pendulum, that is, the radius of the circular plate, is short for obtaining required accuracy, accordingly the sensors are composed small in size. Figure 6 shows an equivalent circuit of synchros. When ac voltage is applied to the rotor winds, the voltage across the external stator legs are expressed by the following function of rotor shaft angle β

$$E_{bc} = E_b - E_c = -\sqrt{3}\, E_m \sin\beta \qquad (1)$$

where E_m is the maximum rms voltage that is induced from the stator neutral to any of the external connections. As the sensor is placed horizontally and is set to make the angle β of equation (1) zero, the voltage E_{bc} therefore corresponds to the inclination angle of the sensor to a horizontal plane. But, because of a relation of sinusoidal function between the synchros output E_{bc} and the angle β, the average output $\bar{E}_{bc}$ measured by electric circuits does not agree with the true mean angle $\bar{\beta}$ when the swing amplitude of the pendulum is large. Figure 7 shows the error computed theoretically, where $\Delta\beta$ is the error, $\bar{\beta}$

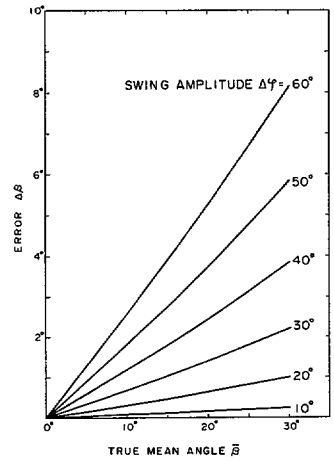

Figure 7 Error for swing amplitude of pendulum

is true mean angle, and $\Delta\varphi$ is swing amplitude of the pendulum. The error due to such input-output non-linearity of synchros is decreased by adopting a magnetic damping which damps the swing amplitude of the pendulum by eddy-current effect on the aluminum plate. The accuracy of the sensor is designed better than ±0.5°.

The digging blades has no space for the sensor of inclination angle in it, then the sensor is installed in the balancing wing. Figure 8 shows the sketch of the sensor. As shown in the figure, the axis of rotation of the digging blades is combined with the case of synchros (stator) through a shaft A, therefore the pitch of the digging blades is transferred to the synchros. The spur gear A attached to the shaft A turns the spur gear B attached to the axis of the potentiometer. As the case of the potentiometer is fixed at the sensor housing,

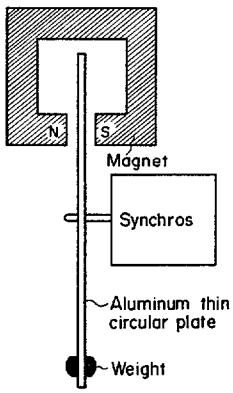

Figure 5 Sensor for pitch angle

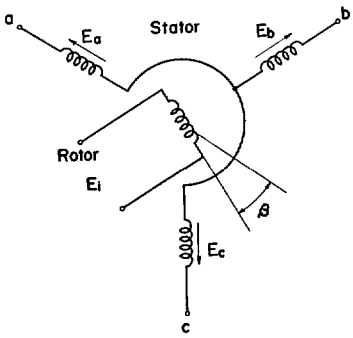

Figure 6 Equivalent circuit of synchros

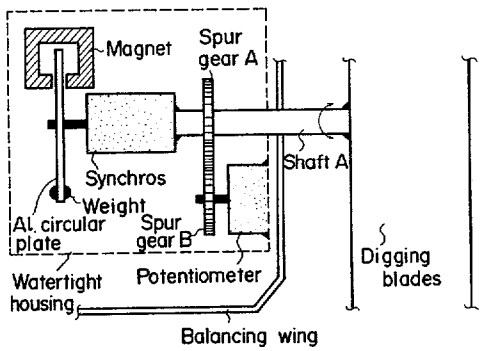

Figure 8 Inclination and bend sensor

that is, the balancing wing, the potentiometer can detect the bending angle between the balancing wing and the digging blades. This potentiometer is required to have such characteristics as long rotational life and high resolution.

A potentiometer is also used in the sensor of the cable press roller for detection of an operating angle of the cable press roller. As the sensor can be composed small in size, it is installed near the axis of rotation of the press roller.

To detect whether the balancing wing touches the surface of the sea bottom, it is advisable for the sensor to be non-touch type from the point of view of handling and reliability. But it is very difficult for our plow to install such non-touch type sensor as an ultrasonic or optical sensor. Therefore a following touch-type sensor is developed as shown in Photo. 1. The sensor is composed of a touch-plate mechanism and a potentiometer, the former touches the sea bottom and the latter detects the rotational movement of its plate. In order to protect the sensor against various damages caused by bump, and to compose duplication, two touch-plates with enough flexibility are installed in each narrow space between the balancing wing and the digging blades.

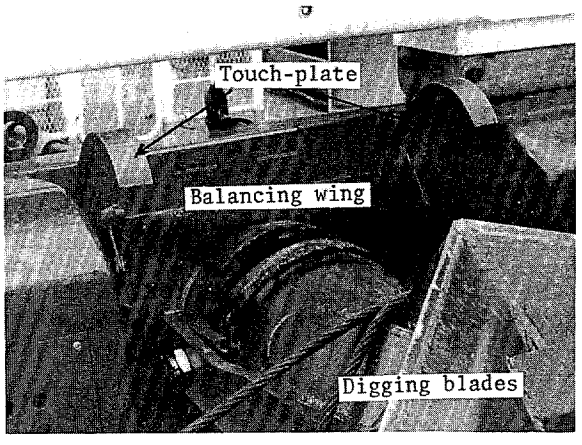

Photo. 1 Touch sensor

The information whether the plow is set on the sea bottom correctly is obtained from a part of signal of the pitch or roll angle sensor. In Figure 6, another voltage across the external stator legs is expressed by the following function

$$E_{ca} = E_c - E_a = \sqrt{3}\, E_m \sin(\beta - 60°) \qquad (2)$$

where

$E_{ca} < 0$; $-120° < \beta < 60°$

$E_{ca} > 0$; $60° < \beta < 240°$

When the plow is set on the sea bottom correctly, the angle β is generally in the range from -30° to +30°, therefore the voltage E_{ca} is negative. On the other hand, when the plow is set upside down on the sea bottom, the voltage E_{ca} is positive. Consequently the information whether the plow is set on the sea bottom correctly is obtained by monitoring the polarity of the voltage E_{ca}.

The towing rope tension is detected by a watertight load cell (max. 30 tons).

The dug trench depth and cable burial depth are computed with the above-mentioned various angles. These depths are able to be computed by two methods, which are intended to increase the reliability in monitoring the depth. The fundamentals of the measurement is shown in Figure 9. The following relationship is established among pitch angle θ_1, bend angle θ_2, and inclination angle θ,

$$\theta = \theta_2 - \theta_1 \qquad (3)$$

In Figure 9, point A shows a jointing point between the balancing wing and the digging blades, point B shows the axis of rotation of the cable press roller, point C shows the top of the seventh plow-blade, and point G shows the point where the balancing wing touches the surface of the sea bottom. The dug trench depth D_1 is given by;

$$D_1 = L_2 \cos\theta - L_1 \sin\theta - L_3 \qquad (4)$$

where $\overline{AB} = L_1$, $\overline{BC} = L_2$, $\overline{AG} = L_3$, and $\overline{AB} \perp \overline{BC}$. Using the relationship of equation (3), D_1 is given by;

$$D_1 = L_2\cos(\theta_2-\theta_1) - L_1\sin(\theta_2-\theta_1) - L_3 \qquad (4)'$$

On the other hand, the cable burial depth D_2 is given by;

$$D_2 = L_4\cos(\theta+\alpha) - L_1 \sin\theta + L_5 - L_3 \qquad (5)$$

or

$$D_2 = L_4\cos(\theta_2-\theta_1+\alpha) - L_1\sin(\theta_2-\theta_1) + L_5 - L_3 \qquad (5)'$$

where $\overline{BE} = L_4$, L_5 is radius of the cable press roller and α is operating angle of the cable press roller ($\angle CBE = \alpha$). As mentioned above, D_1 and D_2 are computed from θ, α or θ_1, θ_2, α. The measurement error of D_1, D_2 is less than ±2 cm, the main cause of this error is due to a little looseness of the joint between the balancing wing and the digging blades.

As the parts on the market which are mass produced are adopted in the sensors, the cost of the sensors is low. The detecting mechanism is simplified to decrease the parts which have possibility of trouble.

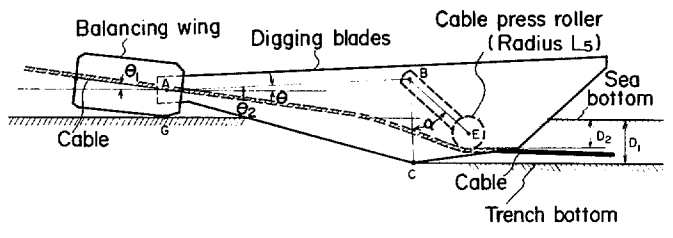

Figure 9 Fundamentals of the depth measurement

4. Multiconductor Cable

The multiconductor cable is used to transmit the monitoring signals from the cable plow to the monitoring equipment on board, on the other hand, it plays a part in supporting the cable guiding rings together with the main towing rope as shown in Figure 2. Consequently the cable suffers a stretching and bending force repeatedly at the stern chute of the cable ship and the cable-leading equipments of the plow. Figure 10 shows the armored multiconductor cable. A breakdown tension of the cable is about 15 tons. The cable is designed torsionless structure and contains thirty-five conductors. The cable tension usually is kept less than 2 tons to prevent breaking down of the conductors.

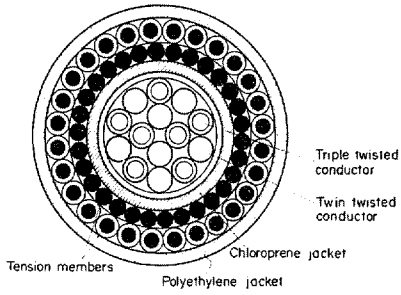

Figure 10 Multiconductor cable

5. Monitoring Equipment on Board

The monitoring equipment on board which is mainly composed of measurement unit, display unit, data processing unit and model plow simulator, is designed for easy operation and high reliability. Photo. 2 shows this equipment.

The basic functions of the measurement unit are to receive the signals transmitted from the sensors on the plow, to process the received signal so as to show the working conditions of the plow on the sea bottom, to transmit the processed signals to the display unit and model plow simulator, and to check and calibrate throughout the monitoring circuits.

The dug trench depth and the cable burial depth are computed by analog computing circuits equipped in this unit, which are mainly composed of several operational amplifiers. The formulas (4) and (5) are expressed in following formulas (6) and (7) respectively when the angles θ, α are less than 10° which is true in the real case.

$$D_1 \cong L_2 - L_1\theta - L_3 \qquad (6)$$

$$D_2 \cong L_4 + L_5 - L_1\theta - L_3 \qquad (7)$$

The computing circuits are designed to suit the approximate formulas (6) and (7) respectively in order to simplify the circuits. The computation error is, however, less than a few percentage which is not a serious problem practically.

Under normal conditions, the frequency of troubles of monitoring circuits is very low. It is important, however, that the monitoring circuits function properly under the very severe conditions for a long time while the burying works are carried out successively. Therefore, additional circuits for check and calibration of the monitoring circuits are provided on this unit in order to obtain high confidence by carrying in-service testing periodically.

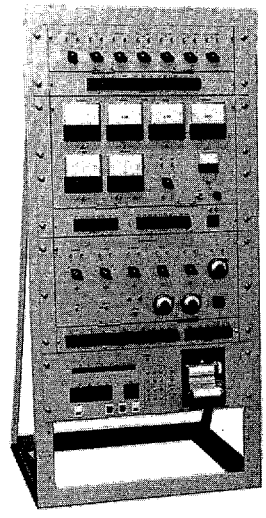

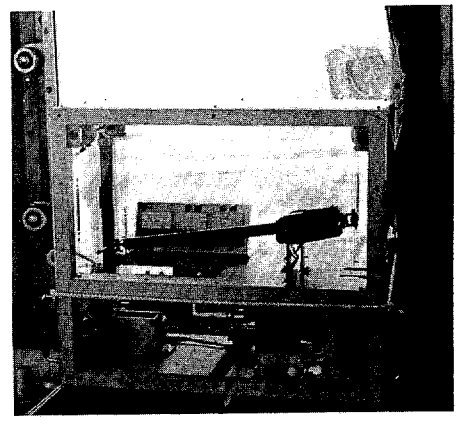

Model plow simulator (Bridge)

Photo 2. Monitoring equipment on board

At the display unit, the panel-meters indicate important information such as pitch angle, roll angle, bend angle, trench depth, burial depth, and towing rope tension. The operation of the touch sensor and information of correct setting are displayed on indication lamps.

The signals of pitch, roll and bend angle are transferred to the model plow simulator unit, in which the model plow is actuated to simulate precisely the plow attitude, in servo mechanism. The steering and speed control of the cable ship and adjusting of the towing rope length will be carried out adequately by referring the model attitude. Displaying with such model is much helpful for the ship operator to grasp the plow attitude than with meters or two dimensional display unit such as CRT.

A microcomputer is equipped in the data processing unit to process the information which is important as a cable laying work record. In this unit, average value, maximum value, and minimum value of the data detected by sensors are computed and printed out periodically. Automatic data correction which decreases the error caused by drifts of characteristics of measurement circuits is adopted in this unit.

6. Cable Laying Works

Japan-China Cable System was constructed in summer 1976. This cable system was designed to have a capacity of 480 voice-grade circuits by employing CS-5M submarine cable system which had been developed in Japan.

Since the cable route crossed the vast continental shelf in the East China Sea, special countermeasures were taken to solve problems arising from cable laying in shallow water over long distance. Their major points were adoption of temperature controlled variable-gain repeaters and cable burying under the sea bottom.

The cable laying works were carried out dividing into four times. In second works which succeeded first works carried out at the offshore area of China, the cable of about 500 km including 40 repeaters and equalizers was buried satisfactorily under the sea bottom day and night for six days successively.

In this area, water depth changed from 40 m to 140 m gradually. The cable burying speed was average 2.0 knots (max. 4.2 kt, min. 0.4 kt), and the cable burial depth was from 50 cm to 130 cm.

The plow monitoring system which was adopted in this works worked perfectly during all construction works without any troubles.

By virtue of burying the cable, no trouble has ever occurred since the system was constructed.

7. Conclusion

This paper describes the plow monitoring system for the new ocean cable plow developed by KDD.

The monitoring system is designed to provide enough information for the effective cable burying works.

The sensors on the plow are designed to have enough reliability against the hazards of the ocean and severe working conditions on board or on the sea bottom.

The construction of Japan-China Cable System in which the cable of about 500 km was buried successively has been the first of its kind in the world.

8. Acknowledgement

The authors would like to thank Dr. S. Shimura, Dr. Y. Nakagome, Dr. H. Kaji, and Dr. H. Yokoi for their guidance and encouragement. They also wish to thank Dr. T. Ezoe, Mr. K. Kobayashi, Mr. H. Sugimoto, and Mr. K. Shirai, for their helpful cooperation, who worked on the development of the cable plow and the auxiliary rope. Appreciation is also expressed to Mr. M. Yamashita for his helpful cooperation in the work which is closely relating to the contents of this paper.

References

1. M. Itano, "Burying Work of the Japan-China Submarine Cable," ITU Telecommunication Journal, Vol. 44, No. 7, 1977.

2. S. Shimura, O. Kameda, "Japan-China Submarine Cable," Journal of IECE of Japan, Vol. 61, No. 5, 1978.

3. K. Suzuki, F. Kinoshita, "New Submarine Cable Burying System," Journal of IECE of Japan, Vol. 61, No. 5, 1978.

4. H. A. Baxter, R. E. Mueser, "The Development of Ocean Cable Plows," IEEE Trans. on Communication Technology, Vol. COM-19, No. 6, 1971.

DISPLAY AIDS FOR REMOTE CONTROL OF UNTETHERED UNDERSEA VEHICLES*

W. L. Verplank

Man-Machine Systems Laboratory
Department of Mechanical Engineering
Massachusetts Institute of Technology
Cambridge, Massachusetts 02139

Abstract

A "predictor" display superimposed on slow-scan video or sonar data is proposed as a method to allow better remote manual control of an untethered submersible. Simulation experiments show good control under circumstances which otherwise make control practically impossible.

1. Introduction

Untethered, unmanned submersibles have been limited to automatic control on simple pre-programmed or target-seeking trajectories. More precise navigation and obstacle avoidance will require increasingly sophisticated automatic control and/or direct control from the surface. Direct human control through a sonic communication channel will be difficult because of the low bandwidth and the signal travel time. Probably the most productive approach will be a combination of elementary automatic control such as is possible with some present-day tethered submersibles (e.g., altitude or depth and heading control) plus display aids which make control easier for the operator. This paper proposes a display aid which is particularly applicable to the problems of time-delay and slow frame-rate.

2. The Problem

For remote control, there are two sources of difficulty with sonar communications: time-delay and slow-frame-rate. Round trip time-delay is the time for a command to travel to the vehicle and the first indication of response to travel back. At a minimum this will be two times the distance divided by the speed of propagation, 2T. For example, T = 1 second at about 5,000 feet.

Pictorial information from television camera or obstacle avoidance sonar will be further delayed because of limited channel capacity. Assuming a low resolution picture of 80 K bits and a channel capacity of 10K bits/sec., there would be at most, one picture every 8 seconds (S = 8 seconds).

The effects of trying to navigate with just this pictorial information are illustrated in Figure 1.

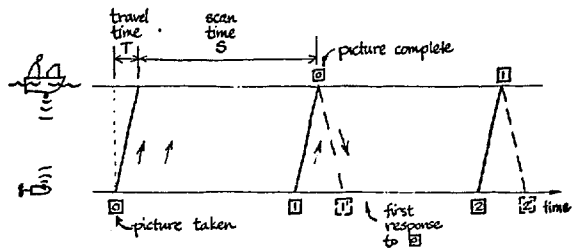

Figure 1a. Effect of delays from transport time (T) and scan time (S).

The picture from ⊡ is received T + S seconds after it is taken; the first operator response is received by the vehicle at least T seconds later, for a total delay of 2T + S seconds. While the operator is looking at the still picture from ⊡ the commands he is sending are actually moving the vehicle from 1' to 2', as illustrated in Figure 1b.

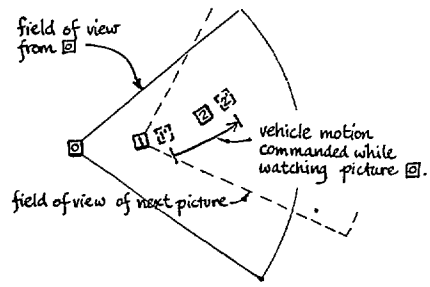

Figure 1b. Positions of vehicle at times in Fig. 1a.

* This work was supported in part by ONR Contract N00014-77-C-0256. The untethered vehicle control problem was suggested in discussions with the Harbor Branch Foundation and the M.I.T. Office of Sea Grant.

3. Predictor Display

Predictor displays were first used for submarine control (Kelley, 1968). NASA considered predictor dispalys for remote control of unmanned lunar roving vehicles, (Arnold, 1963) but sent men instead.

The predictor display proposed here presents a symbol superimposed on the slow-frame-rate and time-delayed picture from the vehicle's television camera. The symbol responds instantaneously and continuously to the operator's commands predicting "future" positions of the vehicle. For example, refering to Figure 1b, when [0] is complete the predictor symbol would show the position 1' . Before the next picture from [1] arrives, the symbol will be moved, in response to the operator's commands, to position 2'

The position of the vehicle is computed from a local model of the vehicle responses and the operator's commands u(t), as shown in Figure 2.

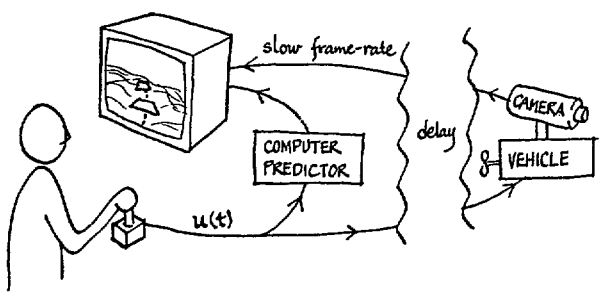

Figure 2. Predictor display superimposed on pictorial data

Pictorial or Map Displays

The predictor symbol may prove useful both on pictorial displays (superimposed on television or obstacle-avoidance sonar) and on map-like position diaplays. Map displays would avoid one difficulty of pictorial displays,which is loosing the predictor symbol when it moves out of the field of view of the camera (for example, moving sideways or backward).

Auxiliary Position Data

If position data is available from transponders or locator beacons, it could be used to update the vehicle model. With just the pictorial data, the open-loop prediction would have to span an interval of (at least) 2T + S to (at most) 2T + 2S seconds. With auxiliary feedback the open loop estimate will only need to span the delay of that auxiliary data (at minimum 2T). The signals and corresponding delays are shown in Figure 3. (u(·), command vector; x(·), vehicle location data).

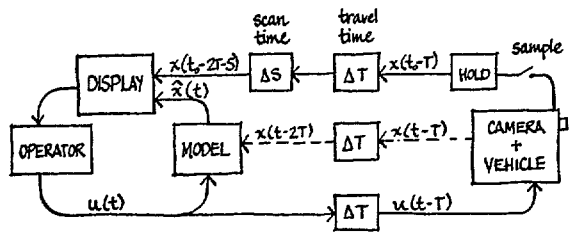

Figure 3. Delays associated with predictor calculation

Adaptive Estimation

Another feature that could be built into the local model of the vehicle is some estimate of the disturbances (such as current). The current model as well as the vehicle model could be updated on the basis of the mismatch between predicted and measured vehicle position.

4. A Dmonstration Experiment

In order to explore the effects of the predictor display, an interactive simulation was written on an Interdata 70 computer and Imlac graphic display. A random terrain was generated and displayed in perspective, updated every 8 seconds, to simulate the pictorial information. A moving predictor symbol was generated respresentin the vehicle as a square in perspective. Two straight ridges were added to the random terrain to serve as a test course. (Figure 4).

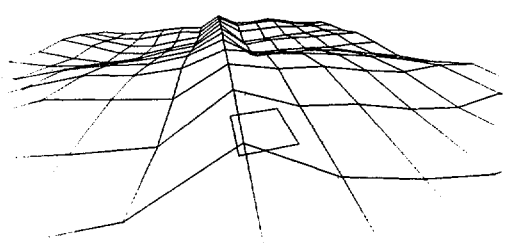

Figure 4. Computer-generated terrain with predictor symbol

The simulated vehicle was controlled by the operator with a spring-centered 2-degrees-of-freedom joystick. The dynamic response of the vehicle was simple integration with forward speed proportional to forward-back position of the stick and turn-rate proportional to left-right position of the stick. The vehicle was always the same height above the terrain (simulating automatic altitude hold). No disturbances such as currents were simulated. Also, it was found important to

have a good detent and dead-zone on the stick to avoid inadvertant commands.

A stationary "table" was drawn to indicate where the next picture was to come from while the "real-time" predictor continued to move in response to the operator's commands (Figure 5). Dotted lines were added to this table to indicate the field of view. This reduced the considerable confusion about how the picture was expected to change, and served as a guide for keeping the vehicle within its own field of view, which is the best strategy for using this kind of predictor on the pictorial display.

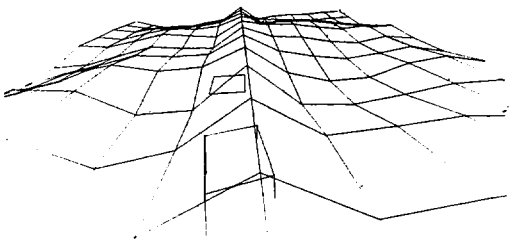

Figure 5. Predictor plus "table" showing from where next picture will come

Results

A typical path, without the predictor, is shown in Figure 6. The dotted lines represent ± 1 terrain-unit from the ridge. The circles represent the vehicle's position every 2 seconds. V's represent the field of view of each picture sent. Quite often there is no movement between successive dots (2 sec.) or successive pictures (8 seconds).

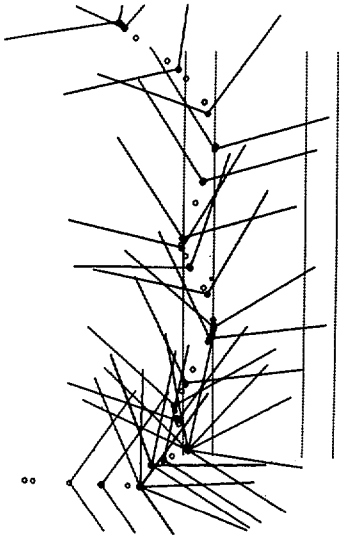

Figure 6. Typical path with no predictor

Only with extremely slow speed was it possible to keep track of the ridge. Approximately five minutes and 40 pictures were required to traverse just one of the ridges (half the course). This is shown in Figure 7.

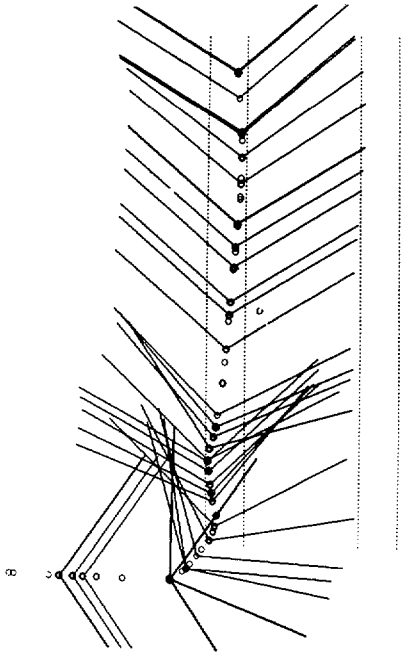

Figure 7. Success at slow speed with no predictor

With the predictor symbol, practically continuous motion was possible. A typical path is shown in Figure 8. The course was completed in 3 minutes and 23 pictures.

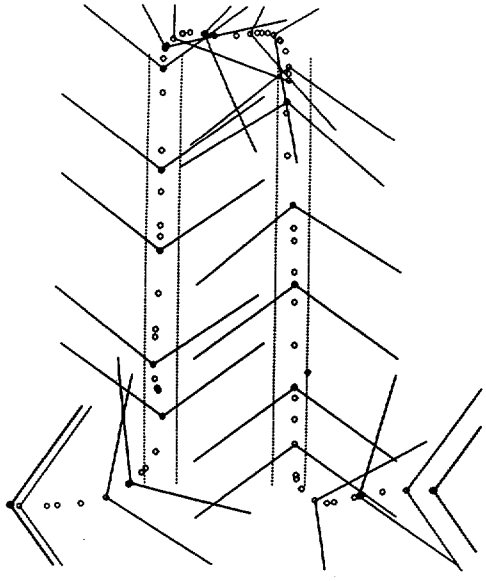

Figure 8. Path with predictor display

Request Mode

One unexpected finding from these experiments was that rather than sending the picture periodically every eight seconds, sending the picture only upon the operator's request reduces the total number of pictures necessary, and encourages a "move and wait" strategy which avoids confusion. The difference is illustrated in Figure 9.

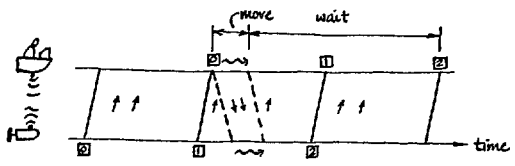

Figure 9a. New picture every 8 seconds: "periodic mode"

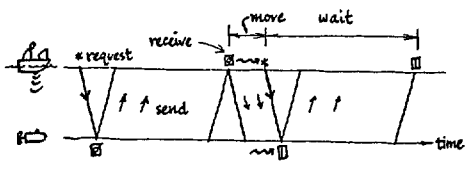

Figure 9b. New picture upon request: "request mode"

In the periodic mode (Figure 9a) a short move starting with the receipt of picture 0 will not be reflected in the next picture, 1 , as the operator might expect; instead he has to wait for 2 . In request mode (Figure 9b), the wait for pictorial confirmation is minimized.

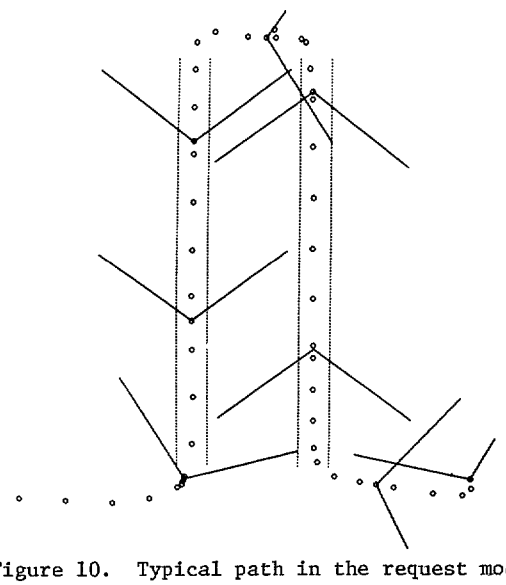

Figure 10. Typical path in the request mode

A typical path in request mode (using the predictor) is shown in Figure 10. Compared to periodic mode, the time is about the same but the number of pictures used is one-half to one-third; velocities are higher but there is a wait for 10 seconds as each picture is taken and sent.

On an actual vehicle, probably both modes should be available with the request mode used when move-and-wait strategy is appropriate (for precise positioning based on pictorial feed-back, and when environmental disturbances are small). Periodic mode is probably more appropriate for less precise navigation and continuous motion when the predictor symbol can be relied upon.

Another trade-off that should probably be built into the pictorial feedback is variable frame-rate/resolution. In a more dynamic and uncertain environment (i.e., larger bandwidth disturbances or target motion) sampling rate will want to be higher at the expense of resolution.

6. Conclusions and Recommendations

For the conditions studied (T = 1 sec., S = 8 sec.) manual control is not feasible without display aids such as the predictor symbol. The request mode is preferred as it seems to avoid confusion and reduce the number of pictures necessary.

The present results are at best preliminary. We studied only very simple vehicle dynamics and only one set of delay conditions. Further study with laboratory simulation can investigate:

1) more realistic vehicle dynamics,

2) environmental uncertainties such as drift,

3) a broader range of delay conditions and

4) various degrees of partial automation.

Also, the predictor displays (both pictorial and map) could be used on existing tethered vehicles to simulate untethered operation and evaluate the potential for untethered operation.

References

Kelley, C. R., Manual and Automatic Control, Wiley, New York, 1968

Arnold, J. E., and Braisted, P. W., Design and Evaluation of a Predictor for Remote Control Systems Operating with Signal Transmission Delays. NASA TN D2229, 1963.

MAJOR MARINE LEGISLATIVE ACTIONS IN THE 95TH CONGRESS

Alfred W. Anderson*
Office of General Counsel
National Oceanic and Atmospheric Administration
6001 Executive Boulevard
Rockville, MD 20852

Abstract

The legislative process provides safeguards for the American democratic system. It provides a method whereby the people can govern themselves and direct their destiny and, to an extent, determine their fate. In marine, as in other affairs, the U.S. has been far from perfect, but we have the chance each year to legislatively reconsider our marine problems.

1. Introduction

The legislative process was designed to be a practical safeguard of the American democratic system. The fact that a proposal cannot become law without approval of both houses of Congress and consideration by the President is a tremendous safeguard.

Traditionally, legislation originates with a Member of Congress. Yet, constituents (either as individuals or corporate entities or other associations) transmit proposals for legislation to Congressmen who may introduce them as they see fit. Many laws originate this way.

Executive communications from a Cabinet member or the President transmitting draft bills to the Speaker of the House and the President of the Senate are significant sources of legislation. An executive draft bill is referred to the standing committee(s) having jurisdiction over the subject matter, and the Chairman(men) usually introduce the bill in the form it was received.

Proposed legislation with the most significant effect upon the general population are the "Bills" and the "Joint Resolutions." The bills initiating in the House carry the prefix "H.R." while bills originating in the Senate carry the prefix "S."

Joint resolutions may originate in the House or in the Senate--not jointly. There is very little difference between a bill and a joint resolution. A joint resolution from the House is labeled "H.J. Res." A joint resolution from the Senate is labeled "S.J. Res."

Concurrent and simple resolutions are matters affecting the operations of the House and Senate.

Bills introduced in the House are placed in the "hopper." Bills introduced in the Senate are introduced on the floor and may or may not be read for the Members. Once introduced, a bill is referred to the appropriate committee/subcommittee for hearings and study. If it meets the approval of the subcommittee/committee, it is reported to the floor of the respective house. Once a bill passes in one house, it moves to the other house and goes through the same process. If differences arise, a bill goes to a Conference Committee where, hopefully, the differences are eliminated or one of the two houses must accept the other's version. Once differences are resolved, the compromise bill must then be passed on the floor of the House and the Senate. Upon passage by both houses, the bill is checked for accuracy, printed, and signed by the Speaker of the House and the President of the Senate. The bill is then delivered to the President for action.

If the President approves, he signs the bill and it becomes law. By constitutional provision, a bill may become law without the President's signature. If the President objects to a bill, he must return it to Congress with his objection within 10 days (Sundays excepted) after it has been presented to him. If he does not return it and both houses are still in session, the bill automatically becomes law. If Congress has adjourned, and the President does not act, the bill does not become law; thus, the "pocket veto." If Congress is in session and the President vetoes a bill, it is returned with his objections to the house in which it originated. The House and the Senate may then pass the bill with two-thirds of the Members present and override the President's veto. If the bill is initially approved by the President or if the bill becomes the law of the land over the objections of the President, it is ready for enrollment and publication as a binding statute.

An enacted bill is sent to the Administrator of the General Services Administration for assignment of a Public Law (P.L.) number, paginated

---

* This paper represents remarks to be made at the September 1978 Meeting of the Marine Technology Society. The views expressed are personal and do not necessarily represent the views or position of the U.S. Government.

for the Statutes at Large covering that session of Congress, and published as a "slip law."

After printing by the Government Printing Office (GPO), the slip laws are available to officials and the public immediately. They may be obtained by annual subscription or individual purchase from the Superintendent of Documents, GPO. They are printed in sequence in the Statutes at Large and later appear in the United States Code.

2. Summary of Significant Legislation

P.L. 95-6, February 21, 1977, the Fishery Conservation Zone Transition Act, gave congressional approval to certain international fishery agreements negotiated in accordance with the Fishery Conservation and Management Act of 1976. The Act officially approved the international fishery agreements between the United States and Bulgaria, Rumania, the Republic of China, German Democratic Republic, the Union of Soviet Socialist Republics, and the Polish People's Republic, all concerning fisheries off the coast of the United States.

Appropriate amendments were made to the Fishery Conservation and Management Act of 1976 concerning the definition of the term "governing international fishery agreement," action by the Councils, permits, and permit fees. In addition, it repeals the Northwest Atlantic Fisheries Act of 1950.

Several other laws approved other U.S. fishery agreements as follows: P.L. 95-8, March 3, 1977, European Economic Community, Japan, Republic of Korea, and Spain; P.L. 95-73, July 26, 1977, Canada; and P.L. 95-219, December 28, 1977, Mexico.

P.L. 95-26, May 4, 1977, made supplemental appropriations for the fiscal year ending September 30, 1977, to the United States Fish and Wildlife Service and the National Oceanic and Atmospheric Administration (NOAA) for operations, research, and facilities as well as for coastal zone management and for the Coastal Energy Impact Fund. The Coast Guard also received supplemental appropriations for the Pollution Fund.

P.L. 95-33, May 26, 1977, authorized appropriations for fiscal years 1978-80, to carry out the Atlantic Tunas Convention Act of 1975. The Act of 1975 was amended to define the term "fisheries zone" as the waters included within a zone contiguous to the territorial sea of the United States, in which the inner boundary is a line coterminous with the seaward boundary of each coastal State, and the outer boundary is a line drawn in such a manner that each point on it is two hundred nautical miles from the baseline from which the territorial sea is measured; or similar zones established by other parties to the Convention to the extent that such zones are recognized by the United States.

P.L. 95-36, June 1, 1977, authorized appropriations thru September 1980 for the administration of the Deepwater Port Act of 1974.

P.L. 95-53, June 22, 1977, authorized appropriations for fiscal years 1978-80, to carry out the Commercial Fisheries Research and Development Act of 1964. Funds were provided the Department of Commerce (NOAA) for apportionment to the States to carry out the purposes of the 1964 Act, and additional funds were authorized to be available to States where there was a commercial fishery failure or serious disruption affecting future production due to a resource disaster arising from natural or undetermined causes. In addition, the Secretary of Commerce was authorized funds for use by States to develop new commercial fisheries.

P.L. 95-58, June 29, 1977, authorized appropriations for the National Sea Grant Program for the fiscal year 1978.

P.L. 95-63, June 5, 1977, the National Advisory Committee on Oceans and Atmosphere Act, established qualifications for individuals appointed to the National Advisory Committee on Oceans and Atmosphere (NACOA) and authorized appropriations for the Committee for fiscal year 1978. The Act established a committee of 18 members. Section 3 defined membership qualifications, terms, and duties. This section also provided that the President designate one of the members as Chairman and one as Vice Chairman. The Act required the Committee to undertake the continuing review of the national ocean policy, coastal zone management, and the status of the marine and atmospheric science and service programs of the United States, and advise the Secretary of Commerce with respect to the carrying out of the programs administered by NOAA. The Act provided for an annual report, compensation and travel expenses, interagency cooperation and assistance, and repealed the Act of August 16, 1971, which established the original advisory committee. Section 8 authorized appropriations in the amount of $520,000 for the fiscal year ending September 30, 1978.

P.L. 95-85, August 2, 1977, authorized appropriations for the Department of Transportation. Included are funds for U.S. Coast Guard operations, construction, improvements, and R&D among other activities.

P.L. 95-86, August 2, 1977, appropriated funds for the Departments of State, Justice, Commerce, and the Judiciary for the year ending September 30, 1978. The Act appropriated more than $600 million for operations, research, and facilities of NOAA; more than $50 million for the Coastal Zone Management Fund; and $115 million for the Coastal Energy Impact Fund. In addition, the Act appropriated funds for expenses of the Marine Mammal Commission, as authorized by Title II of P.L. 92-522.

P.L. 95-86 also appropriated funds for the

Maritime Administration for, among other activities, ship construction, research and development, operations, and training.

P.L. 95-91, August 4, 1977, the Department of Energy Organization Act, established a Department of Energy with, among other things, an Assistant Secretary with environmental responsibilities.

P.L. 95-99, August 15, 1977, authorized appropriations for activities of the National Science Foundation. Among the funds authorized for fiscal year 1978, slightly more than $210 million were for Astronomical, Atmospheric, Earth, and Ocean Sciences.

P.L. 95-113, September 29, 1977, the Food and Agriculture Act of 1977, provided price and income protection for farmers and assured consumers an abundance of food and fiber at reasonable prices. Title XIV contained declarations of needs in agricultural research and extension. Although the Act is primarily designed for fresh water systems, it has possible application for coastal areas. In section 1403, the Department of Agriculture is designated as the lead agency for food and agricultural sciences, and in section 1404, Congress defined aquaculture as an agricultural science. Section 1414 authorized appropriations.

P.L. 95-136, October 18, 1977, authorized appropriations for fiscal year 1978 for the Departments of Commerce and the Interior; and for fiscal years 1978-83 for the Marine Mammal Commission to carry out the Marine Mammal Protection Act of 1972. In addition, it amended the Act of 1972 to make it unlawful for any person or vessel or other conveyance to take any species of whale incident to commercial whaling in waters subject to the jurisdiction of the United States.

In addition, Congress declared: (1) the navigable waters of Puget Sound to be fragile; (2) that Puget Sound and the shore areas are threatened by domestic and international traffic of tankers carrying crude oil; and (3) that it is necessary to restrict such tanker traffic in the Sound in order to protect the navigable waters, the natural resources, and the shore area immediately adjacent thereto from environmental harm. The law prohibits any officer, employee, or other official of the Federal Government from issuing, renewing, granting, or approving any permit, license, or other authority for constructing, renovating, or modifying a terminal, dock, or other facility affecting the waters of Puget Sound, which may result in any increase in the volume of crude oil capable of being handled by any such facility (measured as of October 18, 1977,) other than oil to be used in the State of Washington.

P.L. 95-153, November 4, 1977, amended the Marine Protection, Research, and Sanctuaries Act of 1972 to authorize appropriations to carry out the provisions of such Act for fiscal year 1978. The Act provided authorizations for Titles I, II, and III. In addition, it required the Environmental Protection Agency to end the dumping of sewage sludge into the oceans or into waters described in section 101(b) of P.L. 92-532 as soon as possible after November 4, 1977, but in no case may the Administrator issue any permit or any renewal thereof after December 31, 1981. In effect, this ends dumping of sewage waste after December 31, 1981. The Act defined the term "sewage sludge" as any solid, semisolid, or liquid waste generated by a municipal waste-water treatment plant the ocean dumping of which may unreasonably degrade or endanger human health, welfare, amenities, or the marine environment, ecological system, or economic potentialities.

P.L. 95-194, November 18, 1977, extended the provisions of the Fishermen's Protective Act of 1967 relating to the reimbursement of seized commercial fishermen until October 1, 1978. It also authorized the Secretary of Commerce in a new section of the Act to make loans to the owners or operators of U.S. vessels for damage or fishing gear loss valued at $2,000 or more which the Secretary has determined was caused by a vessel of a foreign nation operating within the fishery conservation zone established by the Fishery Conservation and Management Act of 1976. It directed the Secretary to investigate each incident of loss for which a loan was made under this section. If the Secretary determines that the owner or operator who received the loan was not at fault, the Secretary may cancel repayment of such loan and refund to such owner or operator any principal and interest pryments made prior to the date of such cancellation. If the owner or operator was at fault, the loan shall be repaid within a reasonable time as determined by the Secretary. The law authorized the Secretary, with the assistance of the Attorney General and the Secretary of State, to take appropriate action to collect for loss of funds under this Act.

P.L. 95-212, December 19, 1977, amended the Endangered Species Act of 1973 (P.L. 93-205) and authorized appropriations of $10 million for section 6 of the Act for fiscal year 1977 and a sum not to exceed $16 million for the period October 1, 1977, thru September 30, 1981. The authorization is to be shared by the Department of the Interior and the Department of Commerce. The funds are to be used by the States for an active program for the conservation of endangered or threatened species.

P.L. 95-217, the Clean Water Act of 1977, December 27, 1977, amended the Federal Water Pollution Control Act of 1972. More than 45 pages of amendments were made to the original Act. Many amendments concerned authorization approval and authorization extensions. Some concerned State Jurisdiction (Water Rights), a Clearinghouse for Alternative Treatment Information, and Training Grants to name a few. Others concerned an accelerated program of estuarine studies, oil spill liability out to 200 miles, marine sanitation devices, aquaculture, dredge and fill permit hearings, and sludge disposal. It has a requirement for a study to be completed

by January 1, 1979, on the effects of seafood processing which disposes of untreated natural wastes in marine waters.

P.L. 95-219, December 28, 1977, approved the fisheries agreement with Mexico. It also amended section 2 of Reorganization Plan No. 4 of 1970 (relating to NOAA) to provide a General Counsel and five Assistant Administrators, one of whom shall be for Coastal Zone Management and one of whom shall be for Fisheries.

P.L. 95-257, April 7, 1978, amended title XI, section 1104, of the Merchant Marine Act of 1936 to permit the guarantee of obligations for financing fishing vessels in an amount not to exceed 87-1/2 percentum of the actual or depreciated actual cost of each vessel.

P.L. 95-263, April 17, 1978, authorized the President to issue a proclamation designating the week of April 16-22, 1978, as "National Oceans Week." The President urged all Americans to become aware of the oceans and to learn about their proper use.

P.L. 95-269, April 26, 1978, the Rivers and Harbors Improvements Act, amends the Acts of August 11, 1888, and March 2, 1919, pertaining to projects for the improvement of harbors and rivers by contract. The 1978 Act authorizes private contract for dredging if the Secretary of the Army determines that private industry has the capability to carry out the work at reasonable prices. The federally owned fleet for dredging and related work may be reduced in an orderly manner to a point where only emergency and national defense work can be accomplished "in house" if private industry demonstrates the capability to carry out the required projects.

A two-year study is to be conducted to determine the necessary size of the federally owned fleet. The cost of private contract for subject work may not exceed 25 percent of the cost of Government work on the same project.

P.L. 95-273, May 8, 1978, the National Ocean Pollution Research and Development and Monitoring Act, established a program of ocean pollution research, development, and monitoring. It directed the Administrator of NOAA, in consultation with the Director of the Office of Science and Technology Policy and other Federal officials, to prepare a comprehensive 5-year Plan for the overall Federal effort in ocean pollution research and development and monitoring.

The Administrator is further directed to establish a comprehensive coordinated and effective ocean pollution research and development and monitoring program.

The Administrator is authorized to provide financial assistance in the form of grants or contracts for research and development and monitoring projects or activities which are needed to meet the priorities set forth in the Plan.

The results, findings, and information regarding ocean pollution research and development and monitoring programs conducted by the Federal Government are to be disseminated to other Federal departments and agencies and to other interested persons by the Administrator.

Appropriations not to exceed $5 million for fiscal year 1979 are authorized.

3. Pending Legislation

The 95th Congress could have another four to five months to act at the time this paper goes to press. As a result, it is impossible to accurately list all of the legislation passed and signed into law for the 95th Congress. Consequently, it is worth while to list a few of the bills pending at this time and later at the MTS Meeting indicate their progress as of that date. The following are some of the important bills listed by title, number and description:

Deep Seabed Mining - H.R. 3350 and S. 2053, to promote the orderly development of hard mineral resources in the deep seabed, pending adoption of an international regime relating thereto.

Superfund - Oil Spill Liability - H.R. 6803, S. 2083, and S. 2900, to provide a comprehensive system of liability and compensation for oil spill damage and removal costs.

NOAA Organic Act - H.R. 9708 and S. 2224, to establish a national ocean policy and set forth the missions of NOAA.

Sea Grant Authorization - H.R. 10822 and H.R. 10623, to authorize appropriations to carry out such programs for FY 79-80.

Marine Protection, Research, and Sanctuaries Act - H.R. 10661 and S. 2767, to authorize appropriations for FY 79-80.

NACOA Authorization - H.R. 10823, to authorize appropriations for FY 79-80.

Fishery Conservation and Management Act Authorization - H.R. 10732, to authorize appropriations for FY 79-80.

Endangered Species Authorization - H.R. 10883 and S. 2899, to authorize appropriations to carry out the Endangered Species Act of 1973 during FY 79, 80, and 81.

Marine Mammal Protection Act Authorization - H.R. 10730, extends appropriations for FY 79-81.

Fishermen's Protective Act Authorization - H.R. 10878, would : (1) amend section 7(e) of the Fishermen's Protective Act of 1967 relating to the reimbursement of seized commercial fishermen; and (2) amend section 10 of the Act dealing with compensation for vessel or gear loss due to foreign fishing activities.

Aquaculture - S. 1043, S. 2218, and H.R. 9370, to provide for the development of aquaculture in the U.S.

Polar Living Marine Resources Conservation Act of 1978 (Krill bill), H.R. 12668, to provide funds for the construction of a research vessel for the Arctic and Southern Oceans.

Tanker Safety - S. 682, to amend the Ports and Waterways Safety Act of 1972.

Liquid Natural Gas (LNG) Terminal Siting and Safety Act - S. 2273, would confer on the Secretary of Energy jurisdiction over construction permits and operating licenses for LNG facilities.

Shoreline Erosion bills - H.R. 10015, H.R. 3775, H.R. 10825, and S. 2514, to authorize the Secretary of Commerce to make annual grants to assist States in carrying out public shoreline erosion management measures in the Great Lakes region.

National Weather Service Act - H.R. 8763, to require the improvement of weather programs of NOAA and affirm Federal responsibility for the provision of effective weather and related services to assure, to the maximum extent possible, that all available Federal resources are utilized in a coordinated manner for weather related research, development, and technology.

National Climate Program Act - S. 1980, S. 2092, and H.R. 6669, to establish a national climate program.

National Manned Undersea Science and Technology Act - S. 2285, would establish a program for the enhancement of the U.S. capability in manned undersea science and technology.

Fishery Conservation and Management Act Amendments - S. 3050, would authorize the Secretary of Commerce to issue permits under certain conditions to allow American-caught fish to be sold to foreign fish processing vessels if such catches exceed the American processing capability.

Navigation Development Act - H.R. 8302, would: (1) impose a fuel tax on inland waterway barges; (2) authorize approximately $2.4 billion for harbor and waterway development; and (3) establish an international commission for further study of the feasibility of a sea-level canal in Panama.

4. Prospective Legislation

As of May 20, 1978, there are other legislative topics that are likely to be formalized as bills and considered in the 95th Congress. An example is the Anadromous Fish Conservation Act authorization . There are obviously others that will be introduced prior to the presentation of this paper before MTS in September. The more important of these will be described at that time.

5. Summary and Conclusions

The 95th Congress, 1st and 2nd Sessions, produced 278 public laws from January 1, 1977, thru May 21, 1978. More than 20 were marine or ocean oriented. Undoubtedly, additional laws affecting the oceans will be enacted prior to the end of the 2nd Session.

Other than the appropriations Acts, there are several that deserve special consideration. For example, the July 1977 National Advisory Committee on Oceans and Atmosphere Act (P.L. 96-63) restructured and redirected the Federal Advisory Committee considering marine and atmospheric affairs. The members were not confirmed until January 1978, and it is likely that significant studies and/or recommendations of the Committee will not be issued before the latter part of 1978.

The Food and Agriculture Act of 1977 (P.L. 95-113) is interesting. Section 1404 defined aquaculture as an agricultural science. This appears, at first glance, to be in conflict with Federal freshwater and marine fisheries policies. However, from analysis of the intent of Congress and interdepartmental arrangements, the authorities in aquaculture of the Department of the Interior and of the Department of Commerce have not been altered.

Public Law 95-153, amended the Marine Protection, Research, and Sanctuaries Act of 1972 and provided more than authorizations. Importantly, it directed the Administrator of EPA to cease issuing or renewing permits for dumping of sewage sludge into ocean waters and defined the term "sewage sludge." This Act could be the beginning of the end of ocean dumping of harmful sludge.

The Rivers and Harbors Improvements Act of 1978 (P.L. 95-269) has a potential for directing additional funds to qualified private contractors for carrying out projects for improvement of rivers and harbors (other than surveying, estimating, and gagings). In addition, it may reduce the Army Engineer's fleet but, at the same time, ensure its modern and technical ability. The reduction may create a need for additional contract services in the field and contracts for more modern equipment.

Another Act with potential impact is the National Ocean Pollution Research and Development and Monitoring Act (P.L. 95-273). It formally establishes a program of ocean pollution research, development, and monitoring. The Administrator of NOAA, in consultation with the Director of the Office of Science and Technology Policy in the Executive Office of the President, is designated as the leading Administrator for pollution research. The Administrator is directed to seek and accept assistance provided by other Federal agencies engaged in pollution research. Section 6 provides for grants and contracts for research and

development and monitoring projects needed to support the objectives of the Act. This appears to be a major move ahead in R&D.

The major effect of these marine oriented laws will be seen in 1979 and ensuing years, first in the budget process, next in the work load, and hopefully, in environmental and natural resource protection. Therefore, the results of the 95th Congress probably will not be fully appreciated for several years.

References

1. Anderson, Alfred W., Unpublished Manuscript, "Legislative and Other Authorities for Marine Affairs," January 1978.

2. Johnson, Frances, Unpublished Print, "Chronological List of Legislative Authorities" (NOAA 1977).

3. Public Laws 95-1, January 19, 1977, thru 95-284, May 21, 1978, Government Printing Office, Washington, D.C.

4. Zinn, Dr. Charles J., Revised and Updated by Willett, E. F., "How Our Laws Are Made," Document No. 93-377, U.S. Government Printing Office, Washington, D.C., 1974.

THE ECONOMICS AND TECHNOLOGY OF AN INTEGRATED OCEAN SURVEILLANCE SYSTEM FOR CIVIL ENFORCEMENT

Norman L. Stone

Ocean Systems Division
Sanders Associates, Inc.
95 Canal Street
Nashua, New Hampshire 03060

Abstract

Ocean surface surveillance for civil enforcement is more complex in some respects than military surveillance because of the requirement for very detailed information on what the ship is doing and has done and because of the legal requirement for hard evidence of any violation. The partnership between patrol aircraft and surface ships will probably continue to be the keystone but unmanned platforms such as anchored buoys can help. Sensors such as high resolution radar, IR/UV, LLTV and ESM combined with on-board data retrieval and storage and real time data communications can aid the task by helping to optimize resource allocations. A command and control scheme using tight data links and interactive displays can provide timely all-source information. Costs can be quite reasonable compared to the economic benefits. The man is still indispensable, and in the case of on-board observers on foreign vessels competitive with standoff methods.

1. Introduction

Surveillance for enforcement in the new 200 mile economic zone and in the territorial and contiguous zones is in many ways more complex and difficult than military ocean surveillance. About 2 million square miles are included within the US 200 mile economic zone, over half of which are off Alaska and Hawaii.

Until some new breakthrough comes, the word "enforcement" when it comes to a surveillance system must be understood in the sense that electronics can't enforce anything. The man on the scene - from a ship in most cases - is the one who finally does "enforcement." What maritime surveillance technology can do is locate potential violators with more or less accuracy, classify them by type and even by name and perhaps indicate something about what the suspect ship is doing or intends to do. The technical tools we have to work with include the surveillance platform, sensors, and interpretation and data storage devices and the command and control and communication links that interconnect them.

Each of the combinations of platform, sensor and communications has its strengths and weaknesses - all weather ability, resolution, range, revisit time, endurance or time on station to name a few. None can tell precisely what type of fish is in a hold from a distance.

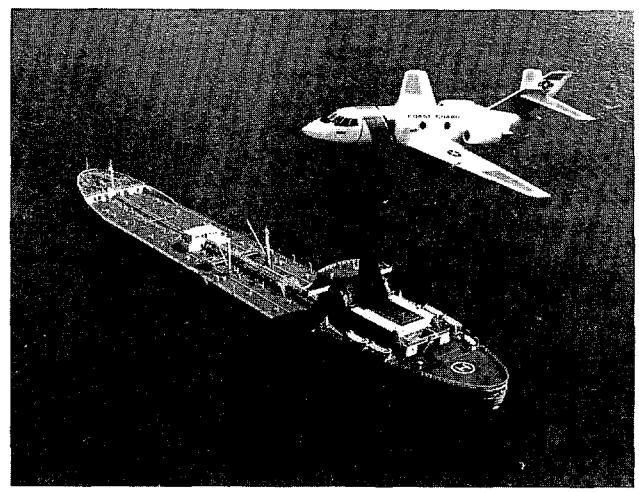

Figure 1 - The Falcon Guardian in its US Coast Guard Surveillance Role (Photograph Falcon Jet)

Generally speaking, the high altitude platforms have the advantages of wide area coverage and synoptic viewing. Today's enforcement systems include combinations of surface ship and aircraft patrol together with inputs from military agencies. Domestic vessels operating in the vicinity of foreign ships have a vested interest in enforcement and are also a source of surveillance information.

Automatic tracking from shore is possible by means of automatic encoding and transponder retransmission of LORAN location. The requirement for detailed analysis of the cargo and even, in the case of fisheries enforcement, of fishing gear, records, and even fishing techniques goes far beyond what standoff sensors can do from a distance in today's art. Retention of hard evidence, mostly

photographic is a necessary requirement for prosecution of violators.

	NOM SEARCH AREA COVERAGE NM2/HR	TOTAL OPERATION COSTS/NM2/YEAR	INITIAL COST/UNIT $	REVISIT TIME	NOTES
AIRCRAFT (MANNED)	10^5	3.50	6×10^6	1/DAY	
HELICOPTER	2×10^4	7-	2×10^6	1/DAY	
SHIP (DISPLACEMENT HULL)	3×10^2	1000	2×10^7	DAYS	
RADAR SATELLITE (MULTIPLE LOW ORBIT)	3×10^7	2800	5×10^7	4 HRS	
ANCHORED BUOY	3×12^2	60	10^4	CONSTANT	FIXED AREA
SHORE STATION (OTH, DF, HF LORAN TRANSPONDER)	2×10^4	250	5×10^6	CONSTANT	FIXED AREA

*ONE COAST GUARD ESTIMATE FOR PRESENT COSTS AVERAGE $25/NM^2/YEAR.

Figure 2 - Surveillance Platform Comparison

The chief method of surveillance will doubtless continue to be a partnership between patrol aircraft and surface ships, with the bulk of the stand-off large area search capability in the aircraft. Equipped with high resolution radar, infra-red or low light level TV for night viewing, microwave radiometry, photography and means of electronic intercept, and the dual advantages of speed and altitude, the wide area covered by an aircraft is the key to efficient enforcement. Anchored buoys can provide early alerting information for drug law enforcement. Satellites and shore stations have potential roles, but cost or lack of all-weather imaging with high resolution in the first case and short seaward range except for HF DF or OTH radar in the second case leaves air search as today's primary wide area surveillance tool with radar as the key long range sensor. Typical airborne surface search radars have a 50 nm detection range on a 100 m^2 trawler target in sea state 4-5.

2. The Type of Enforcement Affects Surveillance

Several of the world's coastal nations have already established a 200 mile economic zones with primary emphasis on fisheries. The U.N. Conferences on Law of the Sea will probably result in a world wide agreement on establishment of such zones.

The traditional interests of coastal nations also remain. These include controlling customs and drug traffic, ocean bottom mineral exploitation, search and rescue, weather and ice patrol, and environmental or pollution control of oil spills, hazardous chemicals and wastewater and dumping.

The underlying reasons for civil enforcement are economic or protection of life. The cost of surveillance and enforcement must bear some relationship to the gains the enforcing country obtains by so doing. Fisheries enforcement, for instance, is intended to prevent overfishing beyond the optimum harvest - an economic benefit to all countries. It also provides priority to the fishing fleet of the sovereign country.

Military budgets for Ocean Surveillance usually exceed civil budgets and some quite complex ocean surveillance systems have evolved. Many of the sensors, and particularly the data handling, display and communications and command and control techniques developed for the military have important civil applications. This paper describes a "integrated" system.

3. How the Particular Need Affects the Surveillance System

3.1 Fisheries Enforcement

Fisheries enforcement is in many ways more complex and difficult than ASW because of the need to make detailed examination of the catch including species and the date caught. No remote sensor or surveillance can provide complete information, but combinations of sensors used synergistically with a modern data link and command and control can make the job easier - more thorough and more cost effective.

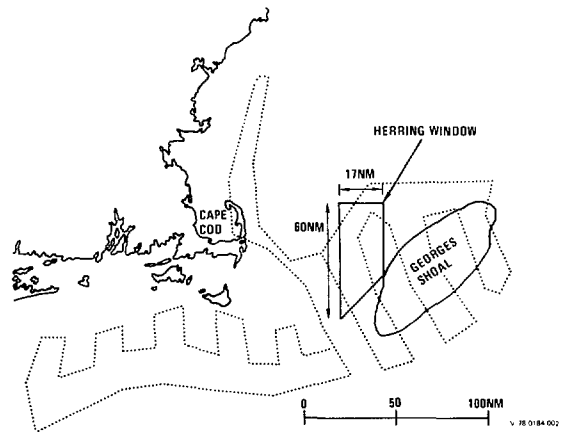

Figure 3 - Potential Patrol Aircraft Route Covering Herring Window in Sub Area 5 - New England

Much more than observation from a distance is required to answer many fisheries enforcement related questions.

Is there a valid permit? Is the catch proper in terms of species, quota and minimum size? Is the authorized fishing gear being used and including trawl or seine type and net mesh size, and is it being employed as authorized (bottom or midwater trawl)? Is there an excessive incidental catch of other species aboard? Shelf bottom fish? Has the vessel kept proper navigation and operations records?

Other questions fortunately can often be answered to some degree by remote observation.

What is the identity and nationality of the ship? Is or was there a conflict with fixed gear?

Modern technology offers much, but it is clear that stand-off sensor cannot tell a red hake from a silver hake or a 520 mm haddock from a 520 mm cod in the fish hold or reefer of a ship. Last year US and foreign fishermen took more than 5 million metric tons in the coastal zone.

Figure 4 - The Taras Shevchenko Being Boarded in March 1977 (UPI Photo)

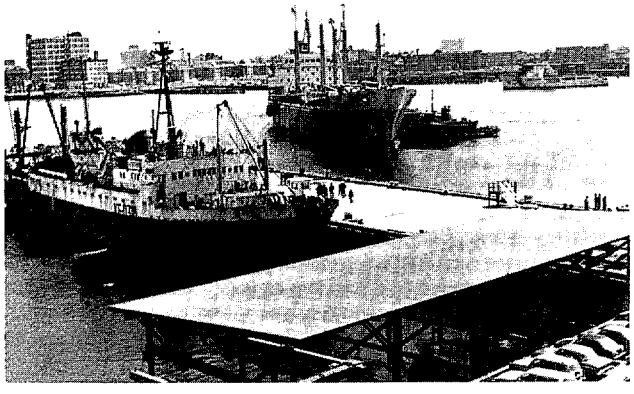

Figure 5 - The Taras Shevchenko was Stopped Again and Seized in April 1977 for Fisheries Violations and Brought to Boston (USCG)

Fishing fleets of a given nation usually follow traditional patterns of fishing as to time and location and type of fish. They are often grouped fairly closely in the area where the fish are. They often exchange catch information by radio, usually VHF. These characteristics at least tend to bound the search area. Typical numbers of foreign fishing vessels in the US Northwest Atlantic fisheries in 1977 were 50-90 in groups of 10 to 30, often grouped by nationality. Alaska reached a peak of nearly 700 foreign fishing vessels in June 1977. US Coast Guard guidelines require boarding by a party that often includes a fisheries inspector at the start and end of the permit period, and random boardings during the fishing period resulting in perhaps 2 or more boardings per ship in 1-3 months or a minimum of once per quarter. One Coast Guard officer estimates that a single ship can conduct 2 thorough boardings and inspections per day. Given the number of US Coast Guard ships available for fisheries duty, (about 45 high and medium endurance cutters plus 70 smaller ships), a limit of several hundred ships could be handled in a month if that was all they had to do which is <u>not</u> the case. Last year the US Coast Guard conducted about 1500 fisheries enforcement boardings. Long range surveillance can give clues as to activity and location, and what to look for so as to optimize the use of ship time. In the New England/mid Atlantic area in 1978 US Coast Guard expects that 1400 aircraft flight hours and 900 ship days would fulfill sighting and boarding standards in areas 1-5 and other potential violation zones. US and Canadian officials report that ships of some countries, particularly the USSR, are usually very cooperative.

3.2 Customs and Smuggling

The requirement here centers on the drug traffic. Quite large quantities of drugs such as marijuana are imported to the US from South America and other areas by ship. Marijuana by nature is bulky, easing the search, but hard drugs such as cocaine or heroin are easily concealed and present a most difficult ship search problem. An estimated $5 billion worth of drugs at street value came into the US by ship in 1976. The patterns of operation of the boats, areas and time of operation, routes followed and advance information from informants are important clues for surveillance. A history of offense by a given ship as is also the case in fisheries enforcement, is an important enforcement clue. For this reason, the ease of access to historical records that modern digital data storage and retrieval techniques can supply is important. Drug traffickers may rendezvous with smaller vessels to transfer cargo for the run into shore, providing another clue to activity by their pattern of operations. Radio intercept may be of value in some cases, but aircraft radar, direct visula observation, informants, and possibly anchored deep water buoys are the surveillance tools. The US enforces customs requirements only to 12 miles, but information obtained hundreds of miles away in the passages between the Carribean Islands or off the North Coast of South America and the Yucatan Channel may be vital to the close-in task. Cooperation by the trafficker cannot be expected and they routinely monitor US Coast Guard frequencies for advance warning of intercept.

The ships often simulate flaglessness and conceal or mislead as to their identity. Night surveillance or boardings are virtually not conducted with the advantage going to the trafficker. Anchored buoys with recorders aboard and HF or VHF transmitters may be of value in certain areas to extend the time and area of surveillance at moderate cost.

The US emphasis on fisheries enforcement as compared to drug law enforcement is about 4 to 1 in resources and time in favor of fisheries. Foreign fishing vessels receive the bulk of

attention but the emphasis on drug enforcement is increasing. In 1977 there were about 8200 fisheries related flight hours compared to about 1700 general law enforcement flight hours and about 30 vessel seizures for all causes.

3.3 Other Surveillance Objectives

Search and rescue, pollution control, mineral exploitation, weather and ice patrol and general law enforcement remain important civil surveillance objectives.

All of their ends must be served by a surveillance system. SAR will often be a cooperative matter using radio distress signals such as the US Coast Guard Distress Alerting Location System or emergency beacons. As with fisheries and customs, environmental standoff surveillance techniques must be supplemented with physical presence. For instance, an oil spill may be pinned to the offending ship by photography of the slick, but if time has passed a physical sample must be obtained for fingerprinting. In 1977 there were about 1200 aerial oil pollution patrols and 800 ocean dumping surveillance missions conducted by the US Coast Guard.

4. Sensors

	TYPICAL FREQUENCY RANGES	DETECTION RANGE (NM)	USEFUL FOR CLASSIFICATION	USEFUL FOR IDENTIFICATION	PROVIDE OPERATIONS INFORMATION	ALL WEATHER	RESOLUTION
RADAR	EFI BAND	50–200	NO	NO	NO	YES	10–20'
LLTV	0.4–0.7μM	1–5	YES	YES	YES	NO	1–2'
FLIR	3–20μM	1–5	YES	YES	YES	NO	1–2'
ACOUSTICS	20HZ–20KHZ	5+	YES	PARTIAL	SOME	YES	N/A
ESM/DF							
MICROWAVE	2-12 GHZ	50–200	YES	PARTIAL	NO	YES	N/A
HF, VHF, UHF	COMMS 2–500MHZ	50–200+	YES	PARTIAL	SOME	YES	N/A
MICROWAVE RADIOMETER	36 GHZ	1–2	–	NO	NO	NO	10–20'
PHOTO	0.2–30μM	1–20	YES	YES	YES	NO	0.5"
VISUAL	0.4–0.7μM	1–20	YES	YES	YES	NO	0.5"
TRANSPONDERS	D OR I BAND	50–200	YES	YES	NO	YES	N/A

V-78-0184-005

Figure 6 - Typical Airborne Standoff Sensor Characteristics

4.1 Radar

The primary wide area search sensor will probably continue to be aircraft radar. I-band search radars or SLAR's are usually a part of any airborne sensor suite. With a 100-200 Kw peak power, a typical radar will weigh about 300 pounds and have a range of 40-50 miles on a 10-50 m^2 fishing boat and 100 miles or more on a 10^3 m^2 freighter in sea state 4/5. Range is reduced as sea state increases due to background sea clutter. Maximum ranges in low sea states require high flight which is inconsistent with detailed contact investigation which requires low attitudes. As satellite and active OTH radar techniques become economical, they may play a part.

Figure 7 - AIL AN/APS-128 Airborne Surveillance Radar

4.2 Electro-Optical and Visual

Photo, visual and LLTV/IR/UF techniques in clear weather provide the best resolution of all the sensors. Oil spill detection by multispectral sensors is possible and night detection and classification means are an essential part of a comprehensive surveillance system. Photographs or stored IR/UV images together with superimposed location data are often key evidence in fisheries violations and oil spill or dumping cases. A drawback in all of these cases is their reduced effectiveness in bad weather such as heavy fog or low cloud cover. Passive microwave radiometry may help supplement these sensors at close ranges.

4.3 Electronic Signal Intercept (ESM)

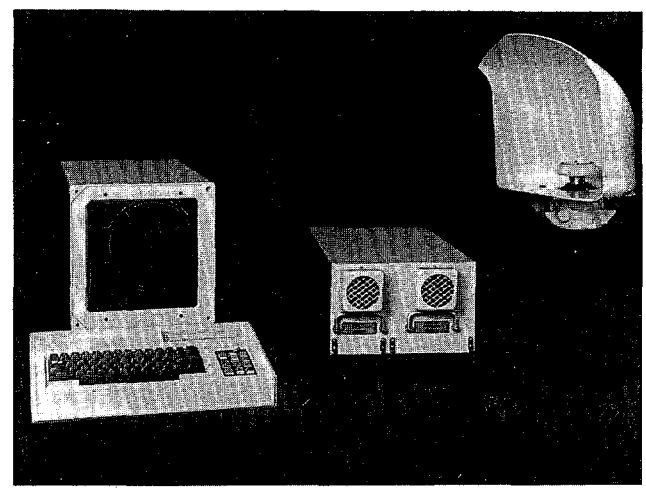

Figure 8 - Sanders' SR-200 Low Cost ESM System Covers 2-18 GHz

Using scanning or wideband receivers from patrol aircraft, direction, and sometimes identity or intention can be determined depending on

intercept equipment and the sophistication of the target vessel. In some cases, it may be possible to determine ship name from signal externals alone much as an expert manual telegrapher could recognize frequent contacts by their fist. The use of ESM depends on the fishing vessel using its radar (if any) and ship to ship communications. Radio and radar silence can reduce the usefulness of these too but it remains an important part of total surveillance.

4.4 Acoustics

Air dropped free floating sonobuoys or permanently stationed deep water anchored buoys can provide additional clues as to identity, location, and possibly type of activity. Engine acoustics transmitted through the water and depth sounder or fish finder emissions can be interpreted in some cases to tell the number and type of engines, possibly size and speed, and country of origin. A library of past contacts is necessary for best use of this method. In some areas, the sound of a trawl drogue against the bottom will give evidence of illegal methods or depth of catch. Anchored buoys appear applicable to drug traffic detection in distant straits and passages and possibly at egress from point of origin.

4.5 Transponders or IFF

A possible identity sorting method is to issue a low cost portable transponder with each fishing permit. At VHF or microwave upon aircraft interrogation this would be coded to provide ship identity, permit number, and location on the aircraft CRT graphic display superimposed on the target skin return. It is a relatively inexpensive means of sorting.

5. Evasion and Countermeasures

Active enforcement may lead to active opposition or inverse surveillance.

Among the more obvious techniques are use of false or unclear identities, radio and radar silence, misleading communications, and deception as to intent. Radio and radar silence on the part of violators would eliminate radio intercept or ESM effectiveness. Installation of radar detection equipment on the suspect ship will warn of the coming approach of a search aircraft at 200 mile ranges and more - time enough to change course, enter or leave an area, cease an illegal fishing procedure, or conceal or dump contraband overboard. One remedy is sparing use of the airborne search radar. Enforcement communications may likewise be intercepted and narcotics smugglers sometimes use the technique by monitoring Coast Guard frequencies. Very little can be done to minimize radar cross-section of larger steel ships, but the deliberate use of ships made of low reflection materials can reduce radar visibility. This is more applicable to the drug trade. It is unlikely that active countermeasures such as radar or communications jamming would be employed, particularly in fisheries where continuity of the right to use the area is of great importance to the foreign ship and where deliberate interference with enforcement carries a heavy penalty.

Today's civil surveillance equipment is not usually built with countermeasures in mind. Those techniques employed by the military would have to be used should active resistance to surveillance become a problem. Low probability of intercept radar using coded pulse wide band transmissions and ESM and direction finding with high speed set on and analysis capability are two approaches. These techniques will add considerably to the cost of surveillance equipment.

6. Description of an Integrated System

The system uses the patrol aircraft with all-weather and night imaging equipment as the basic sensor platform. Examples of suitable patrol aircraft are the Lockheed P-3, CP-140 & S-3, the Fokker F-27 Maritime, the Falcon-Jet Guardian, and the Hawker-Siddeley Nimrod and 748 Coastguarder. Tightly knit and reliable communication links to shore and to the enforcing surface ships are combined with automatic data storage, analysis and retrieval.

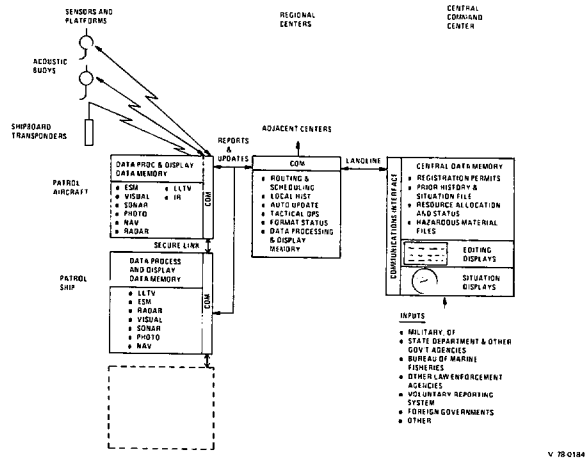

Figure 9 - Enforcement System Functional Diagram

The surveillance sensor suite on the aircraft consists of microwave surface search radar, IFF interrogation, an electronic intercept and HF VHF/UHF DF equipment from 2-500 MHz and ESM such as the Sanders SR-200, Figure 8 covering 2-18 GHz, night vision devices, and photography with superimposed date, location and intercept identity information tied into the aircraft omega navigation system. An inexpensive floppy disk storage system working with an alphanumeric CRT and keyboard permits the aircraft surveillance operator to retrieve and store timely information on registration permits, prior records, such as previous inspections or offenses. A modem connected to an HF or VHF digital data link feeds the floppy disk and CRT display so that the aircraft stored record can be updated remotely from shore (to enter or modify new permits in flight) or the aircraft operator can enter new data into the system on shore. One current problem is maintaining timely registration

permit data during extended patrols.

Because the aircraft works closely with surface patrol ships, a two way digital data exchange over a data link to identical ship-board storage and retrieval equipment is part of the system. Single sideband secure HF and VHF voice is also included.

As might be expected, the major delay times in timely enforcement actions requiring command decisions are not primarily in the data link, but in the decision making process ashore. For instance, on the high seas where no offense has been committed as in drug or fisheries cases involving highly migratory species where there is no right to board, cooperation of the suspect ship's country of registry may be required and the decision chain may be quite lengthy before receiving a statement of "no objection" through the Coast Guard Commandant. Some fishing enforcement actions may require US Statement Department consultation. According to Gerry Studds, a Massachusetts Congressman, the National Security Council became involved in a seizure last April, refusing permission to seize an obvious violator.

Anchored deep water buoys such as used in synoptic oceanographic data collection have a potential role in customs enforcement by providing early detection and location of ships using remote channels between islands. For instance, logical installations of such buoys might be made in the Florida Straits and Windward Passage between Cuba and Haiti, and in the Nova Passage, Yucatan Straits and waters around Puerto Rico. Equipped with tape recorders the anchored buoys can be read out upon interrogation from aircraft, ship or shore or even self initiated upon the triggering of an acoustic threshold. Abbreviated data are transmitted over an HF link frequency selected for current RF propagation conditions.

Two way data from local area command centers and the central command and control location would be combined with military and other types of sailing reports. Voluntary reports, however, are not particularly useful for exact location. Except in selected high density harbor areas we have not begun to approach the tight positional control attained by airways systems.

At the central command and control information on location and readiness status of surveillance forces, operations in progress, records of recent past history, links with other civil agencies and military will be maintained. Graphic CRT displays such as those depicted in Figure 10 are used to display wide area data or to zoom in on a particular situation. For instance, computer retrieved data on fishing permits on a given date in a particular area might be spotlighted in response to a real time query from a surveillance aircraft upon spotting a vessel displaying an unfamiliar permit number. Chemical Hazard Information can also be accessed.

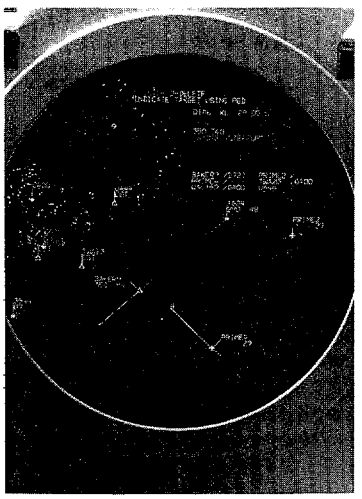

Figure 10 - This Typical Sanders Editing Graphic Display Used in the AN/FYK-14 System is Appropriate for Enforcement Command Centers

The data would be automatically stored and retrieved in a disk file. An operator can automatically transmit edited or updated data to any desired area center or ship or aircraft at sea so that the corresponding display can appear on both the on-site aircraft or ship and the area center. By this means data time late, particularly on routine matters such as permit initiation or modification will be minimized. Fortunately, most enforcement matters do not require the instant response times that some military situations do. Slower speed often permits economy of equipment.

It is estimated that a moderate size low cost computer of the PDP-11 type with a 30 megabit disc memory and editing graphic displays similar to those shown in Figure 10 could amply handle all enforcement requirements for data storage and retrieval for an area such as the US East Coast. A smaller duplicate of the central setup would be installed at each of the local area or regional headquarters.

7. The Dollar Value of Coastal Surveillance and Enforcement

Enforcement only has a point if it has some economic or other value translatable into a benefit. As one measure of value some percentage of the value of the products obtained from and carried over the coastal areas could be used using the assumption that enforcement prevents or reduces economic damage in some relation to the total cargo value. Such measures may apply to minerals obtained (oil, etc) and fisheries products. Other measures are the value of the customs tariff income on shipped products, areas kept unpolluted (fisheries and recreational income preserved), and the value of keeping shipboard undesirable imports (such as illegal drugs) out of the USA.

In 1977 the Coast Guard seized 24 ships and about 900,000 pounds of marijuana with a retail

value of nearly $300 million. Experienced Coast Guard officers estimate that about 10 times that amount escapes them.

The 1975 US fisheries catch of 2.2 million metric tons had an estimated landed value of $971 million dollars. Foreign ships in US waters landed more than the US catch.

Oil spill surveillance and fingerprinting as a minimum could lead to financial recovery of cleanup costs from the offenders and is a most effective deterrent against deliberate infractions based on some Coast Guard experiences.

It would take a very detailed knowledge of the relationship between the intensity of enforcement and the reduction of violations and the optimum fisheries harvest to draw a specific conclusion about the value of enforcement. The sheer dollar size of the fishing and drug traffic and the number of violators caught suggest that the economics will probably support enforcement at or above present levels.

Lest we get too fond of technological solutions keep in mind that a shipboard observer program which could cost about $5 million megs for a 100 man program would put an observer on nearly every foreign fishing boat off New England. Compared to the initial cost of a single surveillance aircraft ($5 meg or more), to which operating costs must be added, this does not sound like a bad return.

8. Summary and Conclusions

Aircraft with an integrated surveillance suite and in a partnership with surface patrol ships will continue to be the primary enforcement means. Technology has not developed approaches that give enough detail to eliminate the requirement for boarding and close-up inspection but it can provide valuable resource allocation information. Modern data processing and command links will permit even better resource allocation. Enforcement surveillance costs are probably more than justified by the economic benefits obtained, but a more rigorous estimate of the relationship between enforcement, surveillance and economic return needs to be made.

Acknowledgements

The kind help of CDRS Streeper and Crowell of the US Coast Guard Headquarters in providing information on Enforcement Operations and Plans is gratefully acknowledged.

CULTURAL RESOURCE MANAGEMENT IN THE COASTAL ZONE

Daniel Koski-Karell
The Karell Institute
P.O. Box 1616
Arlington, Virginia 22210

Abstract

This paper discusses cultural resources in the coastal zone, touching upon their definition and character. It also cites several legislative authorities relating to their protection and management. Lastly, a possible means to integrate cultural resource management into the coastal zone program is suggested.

1. Introduction

The cultural resources of the coastal zone represent a significant aspect of our country's heritage and national patrimony. Because of their location, and the fact that they are a non-renewable resource, it is apparent that a managerial concern under the Coastal Zone Management program is required. However, cultural resources on land and underwater normally do not have a political constituency, and are often ignored even though their protection is mandated under various Federal and State laws.

This paper discusses several aspects of cultural resource management in the coastal zone. One of these is an introduction to its cultural history ranging from Pleistocene times to the recent past. Particular emphasis is given to the maritime aspect--especially shipwrecks from 1500 to the present. Attention is also called to the studies seeking to identify sensitivity areas and known locations of ship losses since the time of European contact.

A review of applicable Federal and various State laws will follow. The National Environmental Policy Act and the Archeological and Historic Preservation Act will be discussed as they relate to cultural resources in the coastal zone. Several states also have laws which mandate the protection of such resources located on State-owned submerged lands.

Suggestions on how to effectively manage these resources as part of existing Coastal Zone Management programs will also be made. It appears that integration into the planning process is the best recourse. This would prevent the possible delay of a project during its construction phase, for if it is discovered that construction threatens a significant cultural resource, work may be halted. Case studies will be used as examples to illustrate how cultural resources can be integrated into the planning process, and, conversely, what can and has resulted should they be ignored.

2. Cultural Resources

Perhaps a definition of the term "cultural resource" is in order. Essentially, it means an object or assemblage of them (which may include people) that can provide a society with information relating to its origins and development. As human beings are both immersed in, and tireless producers of cultural resources, one can understand that the total sum of these objects and assemblages is immense. However, cultural resources vary in significance, and it is this key concept--"significance"--that usually determines their disposition if a decision must be made. Of course, the significance of a cultural resource is often a subjective decision, one that is sometimes tempered by economic and political considerations. Significance is very often related to, and a result of, the input received from interested people or groups.

The earliest cultural resources in the United States for which there is firm evidence date from the Ice Ages of the Pleistocene. It appears that

big-game hunting peoples crossed the land bridge linking northeastern Asia with Alaska, and populated the New World. At that time the sea level was much lower than today. It is likely that these peoples lived on lands now submerged, in addition to the uplands where evidence from their culture is normally found today. As the millenia passed, and the glaciers melted, these prehistoric Americans shifted their areas of habitation as the coastal zone was displaced by the rising sea level.

The European colonization of the New World, which began in earnest after the year 1500, was marked by a concentration of activity along the coastal zones of the hemisphere. Settlements and farms were established there. Shipping soon became the preeeminent means of commercial transport and communications. In the course of time, a tremendous number of vessels were lost due to storms, warfare, and navigational errors. Study of their distribution reveals that the greatest number met their fate less than a mile (1.6 km) from shore. Their remains rest there to this day, with exact locations being largely unknown. Many of the early settlements and farms were ultimately abandanoned, also. These cultural resources are now being rediscovered during archeological survey activities, and sometimes during the construction of a coastal facility.

Currently the Bureau of Land Management of the U.S. Department of the Interior is conducting under contract two intensive cultural resource studies of the Atlantic Continental Shelf. The goal is to develop a management tool to utilize in conjunction with OCS development efforts. When complete, they will both assist in managing submerged cultural resources and in developmental planning to predict which areas are likely to contain those of significance.

3. Legislation

There is a long history of Federal legislation relating to cultural resources. For example, the 1906 Antiquities Act provides protection for cultural resources over a certain age on Federally-owned lands. Also, the National Environmental Policy Act specifically includes important historic and cultural aspects of our national heritage. The 1974 Archeological and Historical Preservation Act directs that in any Federally-licensed activity or program or Federal construction project, archeological and historical data and resources must be preserved or have any unavoidable impact mitigated through scientific excavation or recording. The Coastal Zone Management Act reinforces this legal tradition by including cultural, historic, and esthetic values.

Several States also have laws protecting cultural resources. Some examples are Virginia, South Carolina, Florida, and California. In such cases, the State usually claims title to material of archeological and historical value located on State-owned lands, including submerged lands. In such cases, unauthorized disturbance of such material is prohibited. Delaware is one example of a State which even seeks to protect archeological resources on privately-owned lands.

Over the past few years there has been developing an effort to incorporate the protection and enhancement of cultural resources into development projects, both on land and underwater. This has resulted both from the legislated requirements, and from unfortunate project delays resulting from inadequate measures to determine the presence or absence of cultural resources before construction. An example of this latter case involved a sewage treatment plant which was scheduled to be built in Virginia in 1975. Construction had almost begun when it was determined that the facility would destroy the site of an Indian village dating from 1200 A.D. The significance of this site was such that the start of construction was delayed and an emergency salvage excavation conducted. If the project managers had not decided to sponsor this excavation, the project would have been halted during construction by court order, resulting in considerable delays and additional expense.

A more practical approach is being taken by the Army Corps of Engineers in their project to improve the shipping channel from Baltimore to the entrance to the Chesapeake Bay. Already a preliminary cultural resources reconnaissance has been conducted to determine if there is evidence to warrant an archeological survey of the several areas to be affected. If that survey discovers significant cultural resources, there is adequate time to make minor modifications of the project design or to conduct emergency archeological excavations to mitigate any adverse impact.

4. Planning

To some managers involved in the coastal zone, cultural resources may be viewed as a low priority problem among many others. However, a more efficient approach is to view these particular resources as one of the irreplacable elements of the coastal zone, one to be managed as well as possible within the overall program. The optimum way to deal with this particular aspect is to integrate it into the planning process. No reasonable person wishes to see a needed project delayed on account of cultural resources. However, such delays have happened in the past, and could very well occur in the future. It is much better to determine if any significant resources are present in a project area long before the construction phase is scheduled to begin.

For coastal zone managers, the chief point of contact concerning cultural resources is the State Historic Preservation Officer in each state or territory. By coordinating with his office, as well as with the state archeologist, the best recourse concerning a planned project can be determined. There are currently on-going survey and planning activities within most state historic preservation programs. They can often provide prompt answers to questions involving areas of the coastal zone. To date, most inventories have been oriented towards cultural resources on dry land. If a project is to affect submerged lands it is likely to be necessary to enter into a program of area-specific background studies and survey.

There are three general phases involving a determination of whether significant cultural resources are located within a given area. The first of these is background study and reconnaissance. The second is intensive survey and evaluation. Third, if necessary, is an emergency excavation and recording effort to mitigate any adverse impact upon the resources in the project area. Evidence from each phase is used to determine the necessity for conducting the following one. If properly implemented early in the planning process, these studies will provide guidance for any necessary design modifications or management decisions. If not implemented, the unwelcome possibility of delays, litigation, and restraining orders could adversely affect the progress of a coastal zone project.

5. Conclusion

The goal of cultural resource management in the coastal zone is to both protect and enhance the cultural patrimony of our nation and to avoid ununecessary delays in development projects. The optimum approach for project managers is to prevent problems from developing by doing what is necessary, correctly, the first time around.

The ownership of cultural resources is diffused throughout our society. They constitute a part of the cultural patrimony that we all share. For this reason their protection has been mandated by several Federal and State laws. This protection must be weighed, however, against the needs of our present and future society, and decisions as to disposition made accordingly. If threatened, significant cultural resources can still be removed and recorded to preserve their inherent data. By working in concert with cultural resource managers, the managers of the coastal zone can both protect the heritage of our nation and facilitate coastal zone development efforts.

References

1. Act for the Preservation of American Antiquities, 1906; (PL 59-209; 34 Stat. 225; 16 U.S.C. 431).

2. Archeological and Historical Preservation Act, 1974; (PL 93-291; 88 Stat. 174; 16 U.S.C. 469A).

3. Coastal Environments, Inc., Cultural Resources Evaluation of the Northern Gulf of Mexico Continental Shelf; Interagency Archeological Services, Department of the Interior; Washington, D.C.; 1977.

4. Ditton, Robert B., John L. Seymour, and Gerald C. Swanson, Coastal Resources Management, Beyond Bureaucracy and the Market; Lexington Books; Lexington, MA; 1977.

5. Iroquois Research Institute, Archeological and Historical Investigations for Energy Facilities: A State of the Art Report; Office of Energy Systems, Federal Power Commission; Washington, D.C., 1977.

6. Koski-Karell, Daniel, "Underwater Archeological Surveys and the Proton Magnetometer," Quarterly Bulletin, Archeological Society of Virginia 30(4):192-193; June 1976.

7. Koski-Karell, Daniel, Cultural Resources Reconnaissance for the Baltimore Harbor and Channels Advanced Engineering and Design Study; Baltimore District, U.S. Army Corps of Engineers; Baltimore, MD; 1978.

8. National Environmental Policy Act, 1969; (PL 91-190; 91 Stat. 852; 42 U.S.C. 4321-4347).

THE IMPACT OF THE 1978 GENEVA SESSION OF UNCLOS III ON OCEAN DEVELOPMENT

Lewis Alexander
Francis Cameron
Dennis Nixon

Marine Affairs Program
Washburn Hall
University of Rhode Island
Kingston, RI 02881

Abstract

After four and a half years of effort, the third United Nations Law of the Sea Conference has still not produced a draft treaty that could be open for signature. The Spring 1978 Geneva session brought a new will to negotiate on critical areas of the text, and made significant progress towards consensus. However, the result of the many compromises necessary to reach this agreement may tamper its acceptance by the world community.

The Seventh Session of the Third U. N. Conference on the Law of the Sea (UNCLOS III) met in Geneva, Switzerland from 28 March through 19 May, 1978 with 142 delegations in attendance. The first two weeks of the Session were taken up in deciding the designation of a President. Hamilton Shirley Amerasinghe of Sri Lanka had served as Conference President since the beginning of UNCLOS III in 1973, as well as heading the Sri Lanka delegation to the U. N. But between the Sixth and Seventh sessions of UNCLOS III there was a change of government in Sri Lanka, and Ambassador Amerasinghe was subsequently removed from that country's delegation. So the question arose, could a person not accredited by his own country to the United Nations serve as President of a major U. N. Conference? Ultimately, it was voted by the delegates to the seventh session that Mr. Amerasinghe should continue in the Presidency, but by this point one-quarter of the time allotted for the seventh session had gone by. And with the Presidency issue settled, a third week was taken up in deciding on the organization of work for the session, leaving only five weeks for serious negotiations.

The work of the session was ultimately entrusted to seven negotiating groups (NGs) on outstanding hard-core issues. The first three of these concerned Part XI of the Informal Composite Negotiating Text (ICNT) on deep seabed mining. The United States and other industrialized countries had objected strenuously to Part XI, as it emerged after the sixth session in New York City during the summer of 1977. It was claimed that the text leaned far too much toward the positions advocated by the Group of 77, representing the developing states, and that unless Part XI were amended the developed countries would be unable to accept a new oceans treaty. The other four negotiating groups addressed non-mining issues. The subject matters of the seven NGs were as follows:

NG - 1 -- System of exploration and exploitation of deep seabed minerals

NG - 2 -- Financial arrangements for deep seabed mining

NG - 3 -- Composition and voting of the Council of the Seabed Authority

NG - 4 -- Access of landlocked and geographically disadvantaged states to fisheries within the economic zones of other states in the same region or subregion

NG - 5 -- Settlement of disputes relating to the exercise of the sovereign rights of coastal states in the exclusive economic zone

NG - 6 -- Definition of the outer limits of the continental shelf, and the question of revenue sharing

NG - 7 -- Delimitation of maritime boundaries between adjacent and opposite states and the settlement of disputes thereon.

In addition, Committees II and III worked during the last five weeks of the session to try and identify other parts of the ICNT text in which proposed revisions might receive substantial support. In the work both of the Committees and of the NGs, they were bound by Paragraph 10 of the document adopted on 13 April, 1978 concerning organization of work. The paragraph reads in part "Any modifications or revisions to be made in the Informal Composite Negotiating Text should emerge from the negotiations themselves...(and should not be adopted) unless presented to the Plenary and found, from the widespread and substantial support prevailing in Plenary, to offer a substantially improved prospect of a consensus."

1. Suggested Revisions of the ICNT

Negotiating Group I issued a report recommending changes or additions affecting eight articles

of Part XI of the ICNT, as well as two paragraphs of Annex II. The changes are generally favorable to the positions of the United States and other industrialized countries. These texts do not represent a consensus, and were not discussed either by Committee I or the Conference Plenary, but they are thought to offer a substantially improved prospect of achieving a consensus at some subsequent session of UNCLOS III. One important feature of the proposed changes is that transfer of technology would no longer be a condition of obtaining a contract from the Seabed Authority. However, new language in the text, requiring transfer of technology in certain cases, is strongly opposed by U. S. ocean mining interests.

Negotiating Group 2 made progress on the question of financial arrangements, a topic which had not been negotiated previously. There was some redrafting of Articles 170 through 175 of the ICNT, as well as of paragraph 7 of Annex II and of paragraphs 9 and 10 or Annex III. The result was that the new texts are considerably clearer than was that of the ICNT on complex financial matters, although the revised texts offer little in the way of specific figures and percentages. Many consider detailed financial planning for the Seabed Authority too speculative without more data regarding the anticipated profits from seabed mining activities. Like the report of NG-1, this report also was not considered by Committee 1 or by the Plenary.

Negotiating Group 3 debated strenuously the question of the composition of and voting procedures of the Council, but no consensus was reached on these issues.

Negotiating Group 4 issued a report amending paragraph 2 of Article 62 of the ICNT, and substantially modifying Articles 69 and 70. In the case of the latter article it was suggested that the term "geographically disadvantaged state" be replaced by "states with special geographical characteristics". The Article then goes on to spell out the criteria for being so designated. Although there appeared to be strong support for the revised text of NG-4, during discussions in the Plenary, it became apparent that the issues of the land-locked/gds were becoming bound up with that of the outer limits of the continental shelf and the procedures for revenue sharing with respect to continental margin exploitation beyond 200 miles from shore.

Negotiating Group 5 issued a text amending Article 296 of the ICNT, and added a new article, as well as a general provision in the Convention on abuse of rights. The basic concept that NG-6 agreed upon was compulsory conciliation with respect to various types of fisheries disputes within the economic zone, particularly on the allocation of surplus stocks to foreign nations. The text is seen as a considerable improvement over dispute settlement provisions in the ICNT, and should form a basis for serious negotiations at subsequent UNCLOS III sessions.

Negotiating Group 6 was unable to reach a consensus on defining the outer limits of continental shelf jurisdiction, due largely to a new proposal put forward by the Soviet Union that there be a distance limit of 300 nautical miles on national rights to seabed resources. Since, as noted earlier, the continental shelf issue may be part of a general "package" involving also the rights of land-locked and geographically-disadvantaged states, the failure to reach consensus within NG-6 is quite unfortunate.

There was also no agreement in Negotiating Group 7 on the wording of Articles 74 and 83, concerning the delimitation of maritime boundaries between opposite and/or adjacent states. Clearly, this is a major problem for a large number of countries, and its resolution will impact fisheries and mineral production problems. A good example is the existing disagreement between the United States and Canada with respect to lateral maritime boundaries. Tentative progress was, however, made on the question of the extent, if any, of the third party settlement procedures for boundary delimitation disputes.

Most of the changes that occurred at the last negotiating session concern procedural matters or recommendations for change, rather than revisions based on a consensus of the countries represented. Therefore, much of the substantive material in the text remains the same. The only major revisions have resulted from a reaction to external events such as the grounding of the Amoco Cadiz, illustrating that the major catalyst for agreement will be similar "crisis" situations, or unilateral responses to perceived "crisis" situations, such as the establishment of exclusive fishery zones.

The Amoco Cadiz incident led the United States and France to reopen the draft treaty text on marine pollution even in the face of fears that this would eventually undermine the consensus already reached, and actually could weaken the text. However, the French specifically called for changes in the Text which would allow coastal states to intervene at the early stages in tanker casualties and to strictly regulate vessels entering their coastal waters. The United States generally stated the need to clarify the provisions on a coastal state's right to protect itself against pollution in the territorial sea, and to strengthen enforcement in the economic zone.

The existing text established a combination of port state, coastal state, and flag state jurisdiction over marine pollution. The proposed revisions to the Text generally strengthen the rights of coastal states to prevent vessel source pollution in their waters. There was broad agreement on a revision that would allow coastal states to employ special measures to protect rare or fragile ecosystems as well as habitats of depleted, threatened, or endangered species of marine life. Consensus was also reached on the promotion of IMCO's recommended ship routing systems designed to minimize the threats of tanker casualties, and on the adoption of international rules and standards on prompt notification to coastal states of maritime accidents. There was less agreement on the more controversial issue of the coastal state's right to adopt discharge standards that are stricter than the international standards for vessels passing through their territorial sea.

Also in Committee III the United States and several other countries sought in vain to bring about some amendments of the ICNT articles on marine scientific research, but the only "improve-

ments"obtained were small changes in the provisions on scientific research with respect to deep seabed mining. From the viewpoint of the United States Scientific Community, substantial restrictions still exist on oceanic research.

The fisheries provisions of the text remain basically unchanged, and most of the unilateral fishery management declarations, such as the Fishery Conservation and Management Act, corresponds substantially with the UNCLOS III text. This neglects the fact that the Law of the Sea negotiations were largely responsible for shaping national legislation. However, while there is widespread agreement on the basic right of the coastal state to manage fisheries within the economic zone, there is still no better understanding of the fishery management concepts to be used within that zone. The concept of optimum yield is still being defined in the United States' Exclusive Fisheries Zone, as well as what the harvesting capacity of the coastal state is and thus of the surplus available for allocation to foreign nations. These problems obviously are the same for similar provisions in the ICNT. Although these concepts are still in the process of definition, there was agreement at the Geneva session on dispute settlement mechanisms for dealing with the problems of coastal state conservation obligations, as well as allocation of surplus fishery resources.

An additional problem presented in the ICNT is the question of what fishing rights land-locked and geographically disadvantaged states have in the exclusive economic zones of their coastal neighbors. There is agreement on the fact that these "disadvantaged" states should have some type of preferential rights, but disagreement on the nature and extent of these rights. Little has changed in regard to highly migratory species, such as tuna, or in regard to anadromous species, such as salmon. However, the primary right of the state of origin in regulating and harvesting salmon was strengthened in the latest Geneva session. The trend set in establishing unilateral fisheries management schemes will continue whether or not a successful treaty emerges from the Law of the Sea Conference. However, the tuna and salmon fisheries, as well as other stocks that cross between different management jurisdictions, indicate that bilateral and multilateral agreements will be critical for future fisheries management.

Did the Geneva session bring us any closer to a Law of the Sea treaty? Negotiations, after the initial procedural problems had been overcome, were intense. The difficult issue of how to manage the revisions of the ICNT was solved by the adoption of the "collegial"system, which gave the President and the Chairmen of the main committees, acting together as a team, collective responsibility for the revisions. Serious discussions on the Preamble and Final Clauses were begun. The issue of reservations received serious consideration as well.

The net result is that the Geneva negotiations did bring us closer to a treaty -- but in a form that is unlikely to be favorably received by the United States Senate. Ambassador Richardson reported that the deliberations produced a text "sufficiently improved over (last year's) Informal Composite Negotiating Text" so as to "substantially enhance the prospect of consensus." Yet Marne Dubs, of the Kennecott ocean mining consortium, has stated emphatically that the new articles and the revised old ones are "worse than they were before." Dubs has charged that the Carter administration is attempting "to establish a new adult partnership with the third world by simply acceding to its demands. . ."

What will be the cost of consensus for U.S. ocean interests? The discussions which took place concerning the Preamble and Final Clauses indicate the potential difficulties ahead. Many states expressed the view that even after four years of negotiations, discussion of the clauses was still premature. However, others argued on behalf of an extended preamble incorporating the Common Heritage concept and endorsing the New International Economic Order along with related "guiding principles." Although a consensus of delegates may approve of the New International Economic Order, the United States Senate is unlikely to be as sympathetic. This reflects the disenchantment of United States ocean development interests with the deep seabed mining provisions of the text, as well as the general frustration felt by other United States ocean interests with the evolution of the UNCLOS III.

One possible "safety valve" for the United States, if the treaty ever reaches the ratification stage, is the use of reservations. However, there was only limited support for a liberal reservations policy at the Geneva session. The Philippines and Syria supported the concept because in their view, it would encourage nations to sign which might otherwise not do so. Peru, Chile, and Uruguay argued that reservations should be restricted to "non-fundamental" provisions of the convention; this proposal creates the obvious problem of gaining consensus on which articles are "fundamental" or "non-fundamental". Japan spoke out most strongly against reservations stating that it would destroy the "package deal" concept which has served as the foundation for the UNCLOS negotiations.

The necessity of permitting reservations in a massive endeavor such as UNCLOS must be realized. The permissive use of reservations would encourage adherence to the treaty and bring us as close to universal adherence as could be reasonably expected.

An adverse effect, of course, is that reservations will confuse the legal relationships among the parties which ratify the treaty. The problem at this point, however, is salvaging something worthwhile from all the effort that has been devoted to UNCLOS III. Without the use of reservations, legal relationships will become even more confusing some nations will be forced to renounce the entire treaty over only a few issues. Would it not be more advisable to have as many nations as possible agree to the treaty provisions which are compatible with their national goals, and at least provide a common basis upon which individual negotiations can begin?

The impacts of the Geneva session of UNCLOS III are several: first, the delegates were able to reach consensus on a number of articles in the negotiating text; second, a serious effort to

work out the final details was agreed to take place in New York from August 21 to September 8; third, the text produced has created enough irreconcilable differences that a policy on reservations must be approved before the treaty is open to signatures. A liberal reservations policy may be the only means by which the treaty can achieve some measure of the significance its drafters had hoped for.

U. S. interests might be served by reservations in at least three cited areas: (1) transfer of technology in seabed mining; (2) revenue sharing in the proceeds of exploitation of the resources of the continental margin beyond 200 miles; and (3) marine scientific research within the extended econimic zone. Since there is a substantial possibility that the provisions of the treaty concerning these areas would not receive the advice and consent of the U. S. Senate, it is incumbent upon the U. S. negotiators to ensure that reservations to the treaty will be specifically provided for in the final clauses.

If the final draft of the treaty specifically forbids the use of reservations, U. S. interests, and those of many other states, might be better served through the development of customary law. UNCLOS has had a tremendous educational influence in the world community. However, it remains highly unlikely that one comprehensive document could be signed and ratified by all members of the community of nations without reservations. In areas where consensus was truly reached, the revised ICNT will provide a valuable starting point in deliniating accepted bounds for state practice in the oceans.

FORCED MOTIONS OF A CABLE SUSPENDED FROM A FLOATING STRUCTURE

Raymond L. Bisplinghoff
Tyco Laboratories, Inc.
Tyco Park
Exeter, New Hampshire 03833

David O. Libby
Simplex Wire and Cable Company
P.O. Box 479
Portsmouth, New Hampshire 03801

Abstract

Recent and proposed applications for power cables in the ocean require that the cable be suspended from floating structures which move due to the wave action. Tension changes in the cable due to these motions may be a substantial percentage of the static tension under some conditions. Limiting values of the tension are necessary for proper design of cable strength members to withstand simultaneous flexing and tensioning.

A method is described for calculating these tensions. In-plane and out-of-plane motions of the cable are analyzed separately. The basic equations of motion of the cable are developed and lowest-mode solutions are derived.

1. Introduction

Power cables for OTEC plants and other recent applications in the ocean environment[1] require that long lengths of cable be suspended from floating structures to the ocean floor. This is an unusual operating condition for a power cable because it is simultaneously subject to a relatively high tension, a variety of possible motions, and substantial electrical stresses. In order to properly design a power cable for this environment, it is necessary to estimate the loads on the cable and the amount of bending to which it might be subjected.

In order to suitably limit tension and control bending, while accommodating a maximum of movement of the structure, an intermediate support system was chosen. A schematic of it is shown in figure 1. A buoy supports the cable at a distance from the structure somewhat greater than the water depth. This distance and the length of cable are adjusted to avoid either over-tensioning the cable or depositing part of the cable on the ocean bottom during movement of the structure. The buoy is placed deep enough to avoid most wave action, and its anchoring system is designed to limit its movements to negligible amounts. The attachment of the cable to the structure is assumed to be at approximately the same depth as the buoy.

Figure 1
Cable Support System

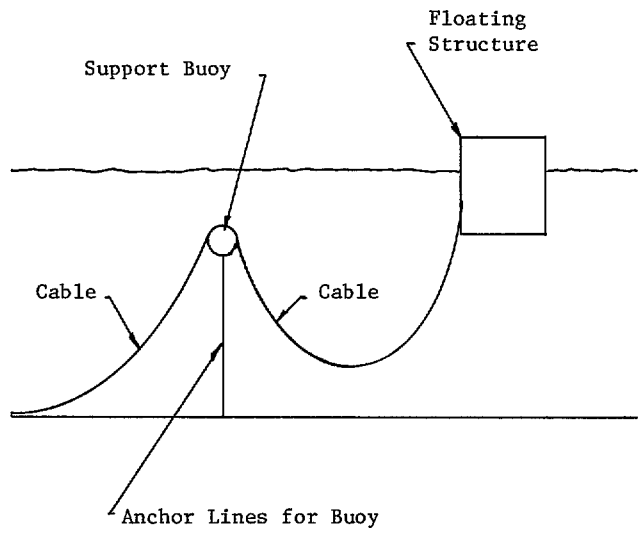

Four kinds of loading were identified which might have significant effects on tension and/or bending:

1) static tension, 2) current drag, 3) strumming effects, and 4) forced motions.

For cable design purposes, relatively simple calculations of the static configuration, and the effects of current drag seemed adequate. Estimates of the relative effects of strumming were made by judicious application of techniques such as those described in Ref. (2). Although these techniques are not yet developed for catenary cables with substantial sag, some approximations using the basic methods led to an estimate of

maximum strumming amplitude and resulting drag increase. Existing work on forced motion of slack cables did not seem to go far enough or lend itself to routine use for estimation of cable motion and increased tension due to that motion. It was therefore necessary to develop an approximation technique for estimating maximum values of the cable tension and movement resulting from forced motions of one end.

2. Defining the Problem

A cable suspended from a floating structure is forced into motion when the structure moves in response to waves. For structures large enough to require a large power cable, it can be initially assumed that the cable has a negligible effect upon the motion of the structure. As a first approximation, the motions of the structure will be assumed to cause simple harmonic movements of the end of the cable. Frequency and amplitude will be specified to be consistent with the motions of the structure in a given sea condition.

Only the lowest modes of motion of the cable will be considered unless the excitation frequency is substantially different from the frequency of the lowest mode. This simplified analysis allows calculation of cable loads and motions accurately enough to establish bounds on the loads for cable design.

3. Formulation in Terms of Normal Coordinates

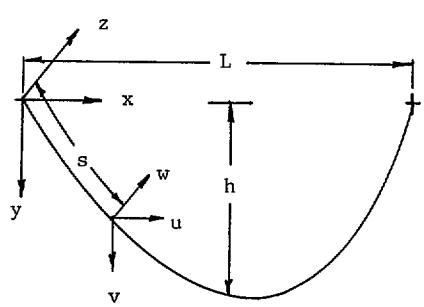

Figure 2
Cable in Static Configuration

Referring to the coordinate system exhibited in Fig. 2, small vibratory displacement of the cable during forced motion may be expressed in terms of the normal modes of vibration, as follows:

$$u(x,y,t) = \sum_{i=1}^{n} \phi_{xi}(x,y)\,\xi_i(t) \tag{1}$$

$$v(x,y,t) = \sum_{i=1}^{n} \phi_{yi}(x,y)\,\xi_i(t) \tag{2}$$

$$w(x,y,t) = \sum_{i=1}^{n} \phi_{zi}(x,y)\,\xi_i(t) \tag{3}$$

Where $\xi_i(t)$ are normal coordinates and ϕ_{xi}, ϕ_{yi}, and ϕ_{zi} are the x, y and z components, respectively, of the i-th normalized eigenfunction or mode shape of the cable in water. The latter satisfy the orthagonality property

$$\int_0^s (\phi_{xi}\phi_{xj} + \phi_{yi}\phi_{yj} + \phi_{zi}\phi_{zj})\, m\, ds = 0 \quad \text{for } i \neq j \tag{4}$$

where

s = length of cable

m = mass per unit length of cable including the virtual mass of water

The normal coordinates $\xi_i(t)$ are computed by solving the differential equation

$$M_j \ddot{\xi}_j + M_j \omega_j^2 \xi_j = \overset{\vdash\!\dashv}{H}{}^{D}_{j} + \overset{\vdash\!\dashv}{H}{}^{M}_{j} \quad (j=1,2\ldots n) \tag{5}$$

where

ω_j = frequency of j-th natural frequency

$M_j = \int_0^s (\phi_{xj}^2 + \phi_{yj}^2 + \phi_{zi}^2)\, m\, ds$ = generalized mass of j-th natural mode

and where

$$\overset{\vdash\!\dashv}{H}{}^{D}_{j} = \int_0^s (F_x^D \phi_{xj} + F_y^D \phi_{yj} + F_z^D \phi_{zj})\, ds$$

$$\overset{\vdash\!\dashv}{H}{}^{M}_{j} = \int_0^s (F_x^M \phi_{xj} + F_y^M \phi_{yj} + F_z^M \phi_{zj})\, ds$$

are generalized forces in the j-th natural mode. The latter are formulated as prescribed forces derived from external disturbances designated by superscript D and forces arising from the motion of the cable designated by superscript M. F_x^D, F_y^D and F_z^D are force components per unit length of cable due to prescribed disturbances and F_x^M, F_y^M and F_z^M are force components per unit length resulting from the motion.

In the following sections of the paper, it is assumed that the in-plane and out-of-plane motions of the cable are uncoupled and can be treated separately.

4. Out of Plane Forced Motion

If it is assumed that the in-plane and out-of-plane motions of the cable are uncoupled, we may express the out-of-plane motion by:

$$w(x,y,t) = \sum_{i=1}^{n} \phi_{zi}(x,y)\,\xi_i(t) \qquad (6)$$

Where $\xi_i(t)$ are defined by Eq (5) in which:

$$M_j = \int_0^s \phi_{zj}\, m\, ds \qquad (7)$$

$$\overset{\vdash\!\dashv}{H}{}^{D}_{j} = \int_0^s F_z^{D}\, \phi_{zj}\, ds \qquad (8)$$

$$\overset{\vdash\!\dashv}{H}{}^{M}_{j} = \int_0^s F_z^{M}\, \phi_{zj}\, ds \qquad (9)$$

The natural frequencies ω_j and corresponding mode shapes ϕ_{zj} for the out-of-plane motions are defined by the homogeneous integral equation

$$\phi_z(s) = \omega^2 \int_0^s C^{zz}(s,\eta)\,\phi_z(\eta)\, m(\eta)\, d\eta \qquad (10)$$

Where $C^{zz}(s,\eta)$ is an influence function. In practice, the eigenfunctions and eigenvalues are obtained from a lumped parameter approximation of Eq (10) expressed as

$$\phi_{zi} = \omega^2 \sum_{j=1}^{n} C_{ij}^{zz}\, m_j\, \phi_{zj} \qquad (11)$$

Or in matrix form

$$\{\phi_z\} = \omega^2 \left[C^{zz}\right][m]\{\phi_z\} \qquad (12)$$

Where is an n x n matrix of influence coeffecients and is a diagonal matrix of lumped masses.

In the present analysis, an engineering approximation is obtained by taking the lowest mode of out-of-plane motion. This is a pendulous motion in which the cable swings laterally in the manner of a "jump rope".

The cable end defined by the coordinates (L, 0, 0) is attached to the floating structure and is assumed to be displaced harmonically in the z direction according to

$$w(L,0,t) = A \sin \alpha t$$

Where α is the frequency and A is the amplitude of motion of the floating structure.

The terms of Eq (5) may be reduced with appropriate simplifications to

$$M_1 = \frac{64}{15} m h \qquad \omega^2 = \frac{5}{4}\frac{g}{h} \qquad \phi_1 = y/h$$

$$\overset{\vdash\!\dashv}{H}{}^{D}_{1} = \frac{8}{3} m \alpha^2 A \sin \alpha t \qquad \overset{\vdash\!\dashv}{H}{}^{M}_{1} = -\frac{64}{15} h C_f \dot{\xi}_1$$

Where C_f is a viscous damping coefficient defined by

$$C_f = 2.25\, \pi \rho D \sqrt{\nu \alpha}$$

and where

ρ = density of sea water
D = cable diameter
ν = kinematic viscosity of sea water

The differential equation defining the displacement of the first mode of out-of-plane motion becomes:

$$\ddot{\xi}_1 + 2n\dot{\xi}_1 + \omega_1^2 \xi_1 = \frac{5}{8}\frac{\alpha^2}{h} A \sin \alpha t \qquad (14)$$

where

$$2n = 2.25\, \pi \frac{\rho D h}{m} \sqrt{\nu \alpha}$$

In Eq (14), the normal coordinate ξ_1 represents physically the angular motion of the swinging cable in its first mode. The soluction of Eq (14) may be written as

$$\xi_1 = \xi_{max} \sin(\alpha t - \beta) \qquad (15)$$

Where the maximum angular excursion of the cable in the "jump-rope" mode is

$$\xi_{max} = \frac{5\alpha^2 A}{8 h \omega_1^2} \frac{1}{\sqrt{(1-\alpha^2/\omega_1^2)^2 + (4n^2\alpha^2)/\omega^4}}$$

The additional dynamic cable tension induced by the swinging motion is computed from the maximum inertial load per unit length,

$$p = m y \xi_{max}^2 \alpha^2 \qquad (16)$$

Eq (16) may be substituted into the catenary equations to compute the added cable tension.

Recently, this method was applied[1] to a cable approximately 600 feet (180 m) long, 6 inches (150 mm) in diameter, and weighing 16 pounds (7.3 kg) per foot in water. The analysis showed that static tension in the cable was approximately 10,000 pounds (4500 kg). When the end was forced into harmonic motion at a period of about 14 seconds and an amplitude of 20 feet, (6 m) the additional tension in the cable was less than 1000 pounds. At shorter periods the tension was less.

5. In-Plane Forced Motion

The displacements u and v of in-place forced motion, assumed to be uncoupled from lateral motion, are defined by

$$u(x,y,t) = \sum_{i=1}^{n} \phi_{xi}(x,y)\,\xi_i(t) \qquad (17)$$

$$v(x,y,t) = \sum_{i=1}^{n} \phi_{yi}(x,y)\,\xi_i(t) \qquad (18)$$

Where $\xi_i(t)$ are defined as before by Eq (5) in which

$$M_j = \int_0^s (\phi_{xj}^2 + \phi_{yj}^2)\, m\, ds \qquad (19)$$

$$\overset{\vdash\!\dashv}{H}{}^{D}_{j} = \int_0^s (F_x^{D}\phi_{xj} + F_y^{D}\phi_{yj})\, ds, \qquad \overset{\vdash\!\dashv}{H}{}^{M}_{j} = \int_0^s (F_x^{M}\phi_{xj} + F_y^{M}\phi_{yj})\, ds$$

The natural frequencies, ω_j and the corresponding mode shapes defined by ϕ_{xj}, ϕ_{yj} are computed from the coupled integral equations

$$\phi_x(s) = \omega^2 \int_0^s \left[C^{xx}(s,\eta)\phi_x(\eta) + C^{xy}(s,\eta)\phi_y(\eta)\right] m(\eta)\, d\eta \qquad (22)$$

$$\phi_y(s) = \omega^2 \int_0^s \left[C^{yx}(s,\eta)\phi_x(\eta) + C^{yy}(s,\eta)\phi_y(\eta)\right] m(\eta)\, d\eta$$

Which may be reduced through finite difference approximations to the lumped parameter form

$$\begin{Bmatrix}\{\phi_x\}\\ \{\phi_y\}\end{Bmatrix} = \omega^2 \begin{bmatrix}[C^{xx}] & [C^{xy}]\\ [C^{yx}] & [C^{yy}]\end{bmatrix}[m]\begin{Bmatrix}\{\phi_x\}\\ \{\phi_y\}\end{Bmatrix}$$

The influence coefficient matrix in Eq (23) may be calculated numerically by techniques such as those described in Ref. (3).

In the present analysis, an engineering approximation is obtained by taking only the lowest mode of in-plane motion. This mode is computed by representing the cable by a three mass system with mass matrix

$$[m] = \begin{bmatrix} m_1 & 0 & 0\\ 0 & m_2 & 0\\ 0 & 0 & m_3\end{bmatrix}$$

As in the out-of-plane analysis, the cable end, defined by the coordinates (L, 0, 0), is attached to the floating structure and is assumed to be displaced harmonically in the X direction according to

$$u(L,0,t) = B\sin\alpha t$$

Where α is the frequency and B the amplitude of motion of the floating structure.

The appropriate terms in Eq (5) are computed from

$$M_1 = \sum_{i=1}^{3}\left(\overline{\phi_{xi}^{(1)}}^2 + \overline{\phi_{yi}^{(1)}}^2\right) m_i$$

$$\overline{H}_1^{D} = \frac{B}{L}\left[\sum_{i=1}^{3}\phi_{xi}^{(1)} x_i m_i\right]\alpha^2 \sin\alpha t$$

$$\overline{H}_1^{M} = -c_f\left\{\sum_{i=1}^{3}\left[\phi_{xi}^{(1)}\left(\frac{dy}{ds}\right)_i - \phi_{yi}^{(1)}\left(\frac{dx}{ds}\right)_i\right]^2 \Delta L_i\right\}\dot{\xi}_1$$

Where ΔL_i is a segment of cable associated with the i-th mass for purposes of computing the force due to damping and $\left(\frac{dy}{ds}\right)_i$ and $\left(\frac{dx}{ds}\right)_i$ are computed at the location of the i-th mass.

The appropriate differential equation defining the first mode of in-plane motion is

$$\ddot{\xi}_1 + 2n\dot{\xi}_1 + \omega_1^2\xi_1 = \frac{B/L\left[\sum_{i=1}^{3}\phi_{xi}^{(1)} x_i m_i\right]\alpha^2 \sin\alpha t}{\sum_{i=1}^{3}\left(\overline{\phi_{xi}^{(1)}}^2 + \overline{\phi_{yi}^{(1)}}^2\right) m_i} \qquad (27)$$

Where

$$2n = \frac{c_f\left\{\sum_{i=1}^{3}\left[\phi_{xi}^{(1)}\left(\frac{dy}{ds}\right)_i - \phi_{yi}^{(1)}\left(\frac{dx}{ds}\right)_i\right]^2 \Delta L_i\right\}}{\sum_{i=1}^{3}\left(\overline{\phi_{xi}^{(1)}}^2 + \overline{\phi_{yi}^{(1)}}^2\right) m_i}$$

The solution of Eq (27) is expressible as

$$\xi_1 = \xi_{max}\sin(\alpha t - \beta) \qquad (28)$$

$$\xi_{1max} = \frac{B/L\left[\sum_{i=1}^{3}\phi_{xi}^{(1)} x_i m_i\right]\alpha^2}{\sum_{i=1}^{3}\left(\overline{\phi_{xi}^{(1)}}^2 + \overline{\phi_{yi}^{(1)}}^2\right) m_i\ \omega_1^2\sqrt{\left(1-\frac{\alpha^2}{\omega_1^2}\right)^2 + \frac{4n^2\alpha^2}{\omega_1^4}}}$$

The additional cable loads induced by the first in-plane mode of motion are computed from the inertial loads on each mass by means of the formulas,

$$F_{xj} = m_j\phi_{xj}^{(1)}\omega_1^2\xi_{max}$$

$$F_{yj} = m_j\phi_{yj}^{(1)}\omega_1^2\xi_{max}$$

The same cable described in the previous section can be characterized for in-plane motions by a mass matrix:

$$[m] = \begin{bmatrix} 351 & 0 & 0\\ 0 & 234 & 0\\ 0 & 0 & 351\end{bmatrix}$$

Where the units are slugs. The lumped masses, which include the entrained mass of water, are equally spaced 195 feet apart. When the support points of the cable are 500 feet apart in the static condition, the frequency of the first mode of in-plane motion is

$$\omega_1 = 0.29 \text{ rad./sec.}$$

and the normalized mode shape is

$$\{\phi_x^{(1)}\} = \begin{bmatrix}1.00\\ 0.601\\ 0.801\end{bmatrix} \qquad \{\phi_y^{(1)}\} = \begin{bmatrix}0.505\\ -0.101\\ -0.404\end{bmatrix}$$

The additional tensions induced by a motion of the end of the cable at a period of 14 seconds and an amplitude of 20 feet (6 m) are less than 1500 pounds (680 kg). Analysis of behavior at shorter periods has been limited but tensions appear to be lower.

6. Recommended Additional Effort

Two particular assumptions used in simplifying the above analysis are subject to review and further development. The present model assumes a linear drag term at the outset of the analysis. An initial assumption of a drag term proportional to velocity squared, followed by a linearization at a later stage of mathematical development might provide a more accurate picture of cable motions, but the present analysis probably produces conservative results. The assumption that one end of the cable remains fixed may not be an accurate one for some applications. Significantly more work is necessary to accurately analyze motions of a second, movable end.

7. Conclusions

The analysis of forced-end motion of a suspended cable provides an estimate of motions and tensions in the cable. For many cables, the accuracy of this analysis will be sufficient for design purposes because substantial safety factors in strength will be utilized. In addition, the limits of motion are often of more interest than the details of that motion.

Limited experience in the application of this method indicates that a multiplier of 1.5 to 2 should be applied to the static tension to allow for these dynamic effects before a safety factor is applied to cable strength. This figure may not apply to cables of much different sizes, however.

No attempt has yet been made to analyze the phasing of the two motions. An in-plane addition of the two tensions was sufficient for previous work. Incorporation of the two motions into one analytical model may be necessary if detailed analysis of the combination of the two motions is desired.

References

1. Pieroni, C. A., B. S. Clark, and D. O. Libby, "A High Voltage Power Cable Installation Concept between Offshore Structures," Proceedings of the 10th Offshore Technology Conference, Paper Number 3325, May 1978.

2. Skop, R. D., O. M. Griffin, and S. E. Ramberg, "Seacon II Strumming Predictions," Naval Research Laboratory Memorandum Report 3383, October 1976.

3. Dominguez, R. F., and C. E. Smith, "Dynamic Analysis of Cable Systems," Journal of the Structural Division, American Society of Civil Engineers, Vol. ST8, August 1972.

EFFECTS OF LONG TERM TENSION ON KEVLAR ROPES: SOME PRELIMINARY RESULTS

Thomas P. Bourgault

NAVAL UNDERWATER SYSTEMS CENTER
NEWPORT, RI 02840

Abstract

This paper is a summary of the preliminary results obtained thus far in the NUSC Kevlar Test Program. The purpose of the program is to investigate the documented strength reduction of a number of Kevlar ropes when subjected to a variety of loads in the ocean environment.

Long term tests, both in-air and in-sea water were initiated with periodic residual testing to establish the effects of load, time and environment on over 400 rope samples.

Final and more conclusive results will be available upon completion of the 12 month test period in November 1978.

Introduction

At the Oceans 76 Conference, the Naval Underwater Systems Center presented data showing extensive strength loss of Kevlar after four months in an ocean mooring system.[1] At about this same time, the Woods Hole Oceanographic Institution produced data supporting these findings which together posed serious questions as to the lifetime and reliability of using Kevlar in the ocean environment.[2]

Prior to these reports, all documented testing done by DuPont and others on the basic Kevlar fiber showed no significant strength loss when subjected to various load levels both in air and in water. Therefore in an effort to resolve this dilemma, the Naval Underwater Systems Center acquired funding to initiate a comprehensive test program to investigate this phenomena.

This report describes the test program conducted and some preliminary results that indicate no "significant" loss in strength of Kevlar ropes after both the three and six month test periods.

Test Program

After researching all existing information along with the results of various test programs, it was found that the majority of documented data was based on the testing of individual Kevlar fibers and not from finished rope samples. Another discrepancy in the available data was the lack of actual environmental testing, and before the NUSC and WHOI data became available, there was essentially no at-sea test results. Therefore, in order to undertake a program which was both realistic of actual usage and at the same time controlled for variable isolation, NUSC consulted with DuPont and the rope manufacturers to lay out the entire test plan.[3] From these meetings, the following six categories were identified as being the most important considerations in an effort to determine the effects of long term tension on Kevlar ropes.

These considerations include:

1) fiber to be used to build the samples,
2) rope constructions to be tested,
3) duration of the test,
4) static load levels,
5) environment, and
6) terminations to be used.

All Kevlar rope samples acquired for the test program use Kevlar 29 as the basic building component. This fiber was specially fabricated by DuPont for the test program and fully characterized by them prior to shipment to the manufacturers. This not only assured the quality of the fiber to be used in the test program but also established a basis for comparison should the results indicate a basic fiber problem.

Both the NUSC and WHOI data was comparable although the rope constructions (and manufacturers) tested by each were different. Therefore, an effort was made to include in the sample group as many different constructions as was economically feasible. The actual sample groups and rope constructions selected are discussed later in this report.

The duration of the test program is one year with the initial control testing being followed by residual testing at three, six and twelve months. In this way, the time history effect of load on the various samples could be determined.

The static load levels selected were 0, 1200, 2100 and 3000 lbf. All samples were specified at 6000 lbf so that these load levels would correspond to 0, 20, 35 and 50% of the rated breaking strength. In this way, the effect of increasing loads would be

U.S. Government work not protected by U.S. copyright.

determined along with any aging problem when considering the zero load samples.

The environment itself was an important consideration since most of the fiber testing had been done in air and the NUSC and WHOI data followed extensive exposure at sea. Therefore, to determine any environmental effects, analogous in-air and in-sea water testing was done.

Finally, since general usage ropes are supplied with manufacturers terminations, it was decided to acquire all samples pre-terminated utilizing each manufacturers most effective method. In this way, the cutting and reterminating of long samples which could possibly affect the data during residual testing was eliminated.

Test Samples

The five sample groups included in the test program are defined below:

A. U.S. Steel: 3 x 19 construction, torque balanced oceanographic wire rope with a polyethelene jacket and terminated at both ends with swaged sockets.

B. Philadelphia Resins Corp.: 1500 denier braided construction with a polyester jacket and terminated at both ends with epoxy filled wire rope sockets.

C. Wall Rope Works: 1500 denier uniline (parallel) construction with a polyester jacket and spliced terminations at both ends with heavy thimbles.

D. Cortland Line Co.: 15000 denier counter/helical construction with a polyester jacket and spliced terminations at both ends with thimbles.

E. Cortland Line Co.: 15000 denier braided construction with a polyester jacket and spliced terminations at both ends with thimbles.

The U.S. Steel wire rope samples were included in the test program as an additional control and also as an up-to-date comparison of steel versus Kevlar in similar applications.

The total number of test samples, 400 (80 per sample group) is significant since this translates into 800 individual terminations. Therefore, due to the large number of terminations, the test program becomes an investigation of not only the effects of load etc. on Kevlar but also the reliability of terminations and the ability of the manufacturers to apply them. The breakdown of the 400 samples and the entire test program is given in figure 1.

LOAD HISTORY \ EXPOSURE TIME	MONTHS 0 (10/77)	3 (1/78)	6 (4/78)	12 (10/78)	TOTAL NO. OF SAMPLES
0 LOAD					
-AIR	5	3	3	3	14
-SEA WATER	–	3	3	3	9
1200 lbf					
-AIR	–	3	3	3	9
-SEA WATER	–	3	3	3	9
2100 lbf					
-AIR	–	3	3	3	9
-SEA WATER	–	3	3	3	9
3000 lbf					
-AIR	–	3	3	3	9
-SEA WATER	–	3	3	3	9
					77 + 3 SPARES
					80

Figure 1. Test Program and Sample Breakdown

Test Set-Up

Subjecting 400 samples to four separate loads in two different environments was accomplished by attaching the various samples of each group in series for each particular load and exposure time.

In air, the sample lengths were suspended horizontally (anchored at one end) and tensioned by a snatch block arrangement with the prescribed weight.

For the in-water test, steel buoys were fabricated (with the buoyancy of the floats being equal to the required tensions) and used in subsurface mooring systems in Narragansett Bay. The big advantage of implementing the test in this way is that, at the conclusion of each exposure period complete systems could be recovered and tested without interrupting any other test apparatus.

Test Results

The environmental testing was initiated in October 1977. At the time of this writing, both the three month and six month test periods have been completed with only the twelve month data left to finish the test program.

All the sample testing throughout the program took place at the U.S. Coast Guard R&D Center at Avery Point in Groton, CT. The testing was done by the author and Mr. Carl Jones of DuPont so that any discrepancies or unexpected phenomena could be analyzed when they occurred.

All samples from the various manufacturers were specified at 6000 lbf breaking strength. However the delivered samples ranged from 5000 to 10,500 lbf. Because of this, the expected loading

percentages of 20, 35 and 50% were variable depending upon the sample group.

The tensile testing procedure for all the samples is identical. Each one is exercised from 0 to approximately 1500 lbf ten times prior to destruction. The cross head speed is held constant at 12 in/min. Finally, it should be noted that a 5% change in strength is attributed to scatter which is based on the evaluated standard deviations of all the samples.

The results obtained thus far in the test program are presented in figures 2 thru 6. They are given individually by sample group to avoid confusion when comparing results.

All of the 3000 lbf in-water moorings failed early in the test due to premature sample termination failures. Because of this, and the lack of spare samples, this portion of the program has been deleted.

The steel wire rope, as expected, has lost none of its strength at this point in the program. The lack of in-water data is a result of corrosion which developed due to a galvanic couple between the galvanized terminations and the large bare steel buoys. These samples are being reterminated and the data will be published when available.

ENVIRONMENT	TEST PERIOD (MONTHS)	STATIC LOAD (lbf)	AVERAGE STRENGTH (lbf)	CHANGE IN STRENGTH (%)
AIR	0	0	6926	–
	3	0	7170	+3.5
	6	0	7253	+4.7
	3	1200	7347	+6.1
	6	1200	7293	+5.3
	3	2100	6868	-0.8
	6	2100	7613	+9.9
	3	3000	*	
	6	3000	7387	+6.7
SEA WATER	3	0	7413	+7.0
	6	0	7107	+2.6
	3	1200	*	
	6	1200	*	
	3	2100	*	
	6	2100	*	

* data not yet available

Figure 2. U.S. Steel Wire Rope Results

ENVIRONMENT	TEST PERIOD (MONTHS)	STATIC LOAD (lbf)	AVERAGE STRENGTH (lbf)	CHANGE IN STRENGTH (%)
AIR	0	0	6276	–
	3	0	6293	+0.3
	6	0	6053	-3.6
	3	1200	6347	+1.1
	6	1200	5650	-10.0
	3	2100	5800	-7.6
	6	2100	5867	-6.5
	3	3000	*	–
	6	3000	6047	-3.6
SEA WATER	3	0	5733	-8.7
	6	0	5593	-10.9
	3	1200	6060	-3.4
	6	1200	5367	-14.5
	3	2100	5500	-12.4
	6	2100	*	

* data not yet available

Figure 3. Philadelphia Resins Braid Results

The Philadelphia Resins 1500 denier braided Kevlar shows a reduction in strength in virtually all of the tests. However, the tendency of the in-air tests is for the reduction to decrease with increasing load. A possible explanation is that elongation, alignment and load sharing of the fibers is accomplished more efficiently at the higher loads. This argument does not hold true however, for the in-water samples and the absolute numbers are significantly higher which possibly indicates that sea water does contribute to overall strength reduction.

Initially in the test there was some problems with the Philadelphia Resins potted terminations. After some investigation, it was found that the solvent used to clean the Kevlar had not been given sufficient time to evaporate thereby causing inefficient bonding between the fiber and epoxy. (Note: Philadelphia Resins had, for safety purposes changed solvents from MEK to less volatile Xylene. However, because of this problem, they have returned to using MEK exclusively.)

The Wall Rope uniline construction showed much scatter in the data and at this point in the program, no definite trends can be established. The data from the final test period will hopefully yield more insight into this construction.

One very important characteristic was noted however, with the uniline in the 3000 lbf in-air (3 month) set-up. Shortly after this test was initiated, a Philadelphia Resins sample failed (due to the termination/bonding problem noted above) causing all the samples in this string to go slack. The sample was replaced and the weight reapplied but within two days a uniline sample failed midspan. Again the sample was replaced and the test continued. However, this phenomena

occurred four more times and it is now believed that the uniline construction is susceptible to shock damage caused by the instantaneous release of tension. This finding is important when considering a mooring system under load that is recovered by the actuation of an acoustic release which in effect would subject the rope to the same shock release damage as that observed in the test set-up. If this is the case, then reusing the rope could be catastrophic even after extremely short exposure periods.

ENVIRONMENT	TEST PERIOD (MONTHS)	STATIC LOAD (lbf)	AVERAGE STRENGTH (lbf)	CHANGE IN STRENGTH (%)
AIR	0	0	4946	–
	3	0	5193	+5.0
	6	0	5340	+8.0
	3	1200	4733	-4.3
	6	1200	4993	+1.0
	3	2100	4693	-5.1
	6	2100	4560	-7.8
	3	3000	*	–
	6	3000	4400	-10.2
SEA WATER	3	0	5140	+3.9
	6	0	5400	+9.2
	3	1200	5173	+4.6
	6	1200	4780	-3.4
	3	2100	4625	-6.5
	6	2100	*	–

* data not yet available

Figure 4. Wall Rope Uniline Results

Cortland Line supplied two different constructions to be evaluated in the test program. The 15000 denier counter helix construction has showed a similar tendency as the Philadelphia Resins data, that being in this case, a decrease in the strength reduction with time under load. Also similar is the greater strength loss observed in sea water for this construction.

As noted previously, the Wall Rope uniline showed no indication of sea water being detrimental. This data reaffirms the fact that sea water does not affect the strength of the Kevlar fiber.[4, 5] However, this does not exclude the possibility that in some constructions, sea water does have a detrimental effect due to increased fiber abrasion etc. when wet.

ENVIRONMENT	TEST PERIOD (MONTHS)	STATIC LOAD (lbf)	AVERAGE STRENGTH (lbf)	CHANGE IN STRENGTH (%)
AIR	0	0	7358	–
	3	0	7680	+4.4
	6	0	7710	+4.8
	3	1200	7360	0.0
	6	1200	7385	+0.3
	3	2100	6760	-8.1
	6	2100	7260	-1.3
	3	3000	*	–
	6	3000	7380	+0.3
SEA WATER	3	0	6987	-5.0
	6	0	6547	-11.0
	3	1200	6680	-9.2
	6	1200	7380	+0.3
	3	2100	6708	-8.8
	6	2100	*	–

* data not yet available

Figure 5. Cortland Counter/Helix Results

The Cortland 15000 denier braid tested performed extremely well in the program with no system failures caused by premature sample or termination problems. However, very little data, as shown in figure 6, could be used to evaluate the overall performance of this rope. The reason for this was that almost all samples failed "within" the termination during residual testing. Therefore, this data did not reflect the actual rope strength and was not accepted as being valid.

ENVIRONMENT	TEST PERIOD (MONTHS)	STATIC LOAD (lbf)	AVERAGE STRENGTH (lbf)	CHANGE IN STRENGTH (%)
AIR	0	0	10666	–
	3	0	**	–
	6	0	**	–
	3	1200	**	–
	6	1200	**	–
	3	2100	**	–
	6	2100	10380	-2.7
	3	3000	*	–
	6	3000	10190	-4.5
SEA WATER	3	0	10240	-4.0
	6	0	9660	-9.4
	3	1200	**	–
	6	1200	**	–
	3	2100	**	–
	6	2100	*	–

* data not yet available
** termination failures

Figure 6. Cortland Braid Results

Conclusions

The preliminary results obtained thus far in the test program have provided no definitive trends attributable to all Kevlar ropes. The environmental testing in sea water has been conclusive in that it appears that this medium has little, if any, affect on the basic Kevlar fiber. The effects of load and exposure time have also varied throughout the sample groups which indicates that a major variable affecting residual strength is rope construction. Based on the data generated thus far, this does not appear to be a major factor, however, the final results from the 12 month test period should provide additional insight into the extent of this problem.

The test program has reaffirmed the need for additional termination research and has also uncovered a load release problem with the parallel construction.

References

1. Bourgault, T. P., "Design and Performance of a Two-Stage Mooring for Near Surface Measurements," Proceedings of the Marine Technology Society Oceans 76 Conference, Marine Technology Society, Washington, DC, 1976.

2. Walden, R. G., "Tests of Kevlar as a New Mooring Material," Polymode News, No. 15, 17 September 1976.

3. Bourgault, T. P., "The Kevlar Cable Test Program," NUSC TM No. 77-2004, NUSC, Newport, RI, 18 January 1977.

4. Swenson, R. C., and Ferer, K. M., "Aramid Fiber for Use as Oceanographic Strength Members," NRL Report 8040, NRL, Washington, DC, 5 November 1976.

5. Ferer, K. M., "Effects of Long Term Tension on Kevlar Aramid Fiber," NORDA Technical Note 8, Naval Ocean Research and Development Activity, National Space Technology Laboratories Station, MS, May 1977.

PERFORMANCE/FAILURE ANALYSIS OF ACOUSTIC ARRAY CONNECTORS AND CABLES AFTER 6-10 YEARS OF SERVICE

Colin J. Sandwith

Applied Physics Laboratory
University of Washington
1013 N.E. 40th Seattle, WA 98105

Abstract

A performance/failure analysis was conducted on three acoustic arrays recovered from a depth of 3300 ft at a naval tracking range off St. Croix in the Virgin Islands. The analysis included bench tests of electronic components and examination of connectors, cables, seals, and housings with electron microscopes, X-ray diffraction, and optical microscopes to determine the effectiveness of design features and materials. One array had been submerged for about 10 years, the others for 6 years.

Cables with polyethylene jackets performed satisfactorily whereas cables with polyurethane jackets exhibited leaks and visible circumferential cracks approximately 1/4 in. long. Of 42 double O-rings examined, 8 of the first O-rings leaked; half of these were on one array. The second O-ring on all seals was effective. Arcing, apparently due to lightning, produced a low resistance in one of the Morrison connector seals by creating a carbon path of charred teflon. Certain packing seal glands and backup washers in the Morrison seals of one array sustained permanent deformation because of improper assembly.

Introduction

The Applied Physics Laboratory of the University of Washington (APL-UW) conducted a performance/failure analysis on three acoustic tracking arrays for the Naval Facilities Engineering Command (NAVFAC). This analysis was part of an effort to document the effects of long-term deep submergence on seals, electrical cables, and housings.[1] The results will be used to increase array life by improving design. In addition, reduced data will be incorporated into an APL reference manual on seals and connectors.[2]

A primary objective of the analyses was to locate all failures--including those in the electronic systems--and determine the cause of each failure. This paper will be limited to tests on the cables, seals, and housings and their results. The extensive tests conducted on the electrical-acoustical system will be the subject of another paper.

One of the arrays, Array 8, was a buoyant type such as that shown in Figure 1; the other two, Arrays 9 and 6, were rigid types. The major difference between these arrays is the foundation of the structure (rigid vs buoyant). The major differences between the electrical-acoustical systems (hereafter referred to as the harnesses) are the diameter of the cable seals and the materials used in the cable jackets. Array 8 had been in service for 10 years and Arrays 9 and 6 for 6-1/4 years. A complete performance/failure analysis was conducted on Array 8 whereas a less rigorous analysis was conducted on Arrays 9 and 6 because they had been in service for a shorter period. All the arrays had been installed at 3300-ft depth on the ocean bottom a few miles off St. Croix in the Virgin Islands. The water at this site has an average oxygen content of 4 ml/l, a salinity of 35.00 ‰, and a temperature of 5.6°C.[3]

A performance/failure analysis uses all background information on design, fabrication, testing, implantment, operation, recovery, and shipping to explain the results observed and determine the cause or causes of failures. Since a number of contractors and agencies were involved to varying degrees in each one of these tasks, the background information was somewhat fragmented. For example, the performance of the systems just before recovery is uncertain, and there are conflicting reports on the coating systems, if any, used on the housings.

General Procedure

NAVFAC and subcontractors recovered the arrays in the fall of 1976, detached the harnesses from the superstructures, and packed and shipped them to APL. The packed harnesses were stored in the shipping crates in a dry, cool place for approximately 6 mo. awaiting approval for the analysis. On approval, the components of all three arrays were unpacked and identified. Identification was facilitated by the color-coded vinyl tape that had been used to designate the position of the hydrophones during assembly and implantment. The components were then tagged to maintain identity and their as-received condition was documented with photographs and notes.

The following is a synoptic description of the examination program carried out on Array 8, which was subjected to a complete performance/failure analysis.

First, the corrosion and other damage on housings, cable clamps, fasteners, transducer caps, and strain-relief components was noted visually and recorded. Observations included the type of corrosion damage (uniform, pitting, crevice or leaching) and a description of its extent (deposit thickness, depth of penetration, shape of the deposit, distribution of products, color of deposit, and structure of deposit). The corrosion mechanism, such as galvanic coupling, crevices, concentration cells, fretting, coating failure, and selective leaching, was also identified if meaningful and possible. Little attempt was made to evaluate the corrosion damage in terms of reduced strength or increased friction, or to identify the corrosion product.

Interconnecting cables between transducers and junction chambers were disconnected by pushing the Morrison-type cable seals[2] out of the junction chamber and separating the cable from the hydrophone housing at the double O-ring joint at the Morrison seal housing. Hydrostatic tests, resistivity tests, visual examinations, and dimensional checks were carried out on the cable and seal assemblies to find leaks and determine the effect of pressure on resistivity in the cable jacket and Morrison cable seals. If defects were found, further tests with a scanning electron microscope were conducted to determine the cause. The resistance of each cable and seal assembly was systematically measured with a megohmmeter (General Radio Co., Type No. 1862-B) both in air and in water after approximately 1 day at 1500 psig to test for changes caused by time and exposure. Where megohmmeter readings were not possible because of low resistance paths due to voltage breakdown, the resistances were measured with an ohmmeter.

After the Morrison seals were pushed out, the seal housings were examined to determine the depth of water penetration and the type and extent of corrosion damage to the housing surface. In certain uses, the housings were also sectioned for the examination.

Each cable seal that exhibited low resistivity was then systematically disassembled to locate the low resistance paths and determine their cause. The size, condition (distorted, stained and/or cut) and resistivity of the seal glands and backup washers were measured. Evidence of leaks such as corrosion products and water penetration was recorded and the cause was determined if possible.

Each hydrophone assembly was disassembled further to perform an analysis on the housings, seals and electronic-acoustical systems. The conditions of the boot and the O-ring seal were documented.

Results

Array 8

Array 8 was planted in December 1966 and recovered in September 1976. The specific reasons for recovery, other than general malfunction, are not known by the author. However, a tracking range status report dated 9 December 1973 shows the following entry: "Y hydrophone bad (?) on Array 8."

The packing of the Array 8 harness was the best of the three harnesses received and probably produced the least shipping damage. Array 8 was the only array that had styrofoam in front of its hydrophones to protect them from shipping damage. The most notable packing damage was to the interconnection cables and cable clamps, and was caused by the low bending radius of the cables. The extent of the damage could not be quantified.

The design and the material specifications for Array 8 were extracted from engineering files. Material specifications are summarized in Table I. No documentation was found on painting or other protective coatings.

Table I. Array 8 Material Specifications

Description	Material	Plating
Housing, Seal (Preamp)	Steel AISI C1010-1020	Zinc, 0.0005-in. thick,* QQ-Z-325 Class 2, Type 2
Housing, Junction Chamber	Steel AISI C1015	Same as above
Housing, Preamp	Steel AISI C1010-1020	Same as above
Caps, End, Junction Chamber	Steel AISI C1010-1020	Same as above
Packing Gland	Commercial Neoprene Non-Conductive, 40 ± 5 duro	N/A*
Washer Backup	Commercial Neoprene Non-Conductive, 80 ± 5 duro	N/A
Insulator	Laminated Nylon, Fabric Base, Phenolic Resin	N/A
Washer, Thrust	Plastic Sheet, Glass Fabric Base, Epoxy Resin	N/A
Cable, Coaxial Interconnecting	Polyurethane Jacket 0.25 in. O.D.	N/A
Cable, Coaxial Signal	Polyethylene Jacket 1.0 in. O.D.	N/A

*No additional coatings specified.

External Condition

Junction Chamber: The corrosion and calcareous deposits were thinner (1/16 in. to 3/16 in.) on the signal cable end plate of the junction chamber than on the interconnecting cable end plate (3/4 in.) of the junction chamber. At the O-ring points on the junction chamber, the deposit was approximately 1/4 in. thick. Light scraping with a screwdriver exposed bare metal on the side of the housing, where a 3/8-in. thick deposit was found. The scraped surface had wide shallow pits no deeper than 1/16 in.

Hydrophone Assembly: Corrosion and calcareous deposits on the hydrophone housings were thinner and more tenacious than those on the junction box (1/16 in. thick or less). The hydrophone housings were made of a slightly different alloy than the housing on the junction chamber, and may have been painted.

The stainless-steel cap screws used on both the junction chamber and the hydrophone housings performed perfectly. Upon drying, the corrosion and calcareous products on the sides and the bottom of the hydrophone housings had become powdery and easy to remove compared to the crusted products on the junction chamber. However, the corrosion and calcareous deposits on the metal top of the hydrophone housing were much harder and tenacious like those on the junction chamber.

Transducer Boots and Retaining Wires: The transducers' rubber boots and retaining wires performed exceptionally well in this environment. They were practically free of marine growth and corrosion products, except for slime and microfouling.

Fasteners: The stainless-steel, cap-screw type fasteners used on Array 8 were more resistant to corrosion damage than the fasteners used on either of the other two arrays. The low-carbon steel structures in Array 8 apparently were sacrifically corroded to protect the stainless-steel fasteners, which were used in all cases except on the cable clamps. The fasteners used on the cable clamps were made of carbon steel and had deteriorated beyond use.

Main Cable Strain-Relief and Hose Clamps: The strain relief had reached the end of its useful life. The metal and nonmetal components used to attach the cable to the housing had failed because of corrosion. The tightening bolts in the two stainless-steel hose clamps, used to compress a sleeve around the cable, failed completely. This type of failure would be expected of stainless-steel hose clamps exposed to such extended marine service. The bolt is often made of 400 series stainless steel, the threaded portion of the clamp constitutes a crevice, and the clamp strap is usually made of 300 series stainless steel. Therefore, the bolt and threaded portion are anodic, and are sacrificed by galvanic corrosion to protect the large, cathodic clamp strap.

The stainless-steel hose clamps behaved most satisfactorily when they were covered with vinyl electrical tape. Electrical tape was used in numerous places around the housings, cables, and structures and performed well.

Heavy encrustations ($\leq$1/4 in. thick) of a combination of calcareous deposits and hydrated forms of iron-oxide compounds were attached to the strain-relief housing. Penetration of corrosion into the low-carbon steel was estimated to be 1/16 in.

Cables: The condition of the interconnecting cables appeared to be good on first visual examination. Subsequent electrical and hydrostatic tests, which are discussed later, revealed several defects.

Internal Condition

System Operation: Performance tests were made on each hydrophone assembly. During these tests, the power to the hydrophone and the hydrophone output signal were routed through the main signal cable. By starting with the main signal cable and systematically making electronic and acoustic measurements through to the acoustic transducer, defects and malfunctions could be identified and located, and the performance of working components could be evaluated. Selected results from these tests are given in Table II and described in the following paragraphs.

The main signal cable could not be used to power the hydrophones because of a discontinuity in the conductive shield. Examination indicated that the shield had parted because of thinning induced by plastic straining. The shield was apparently continuous (at least intermittently) at the time of recovery because that conductive shield was used to fire an explosive bolt.

The junction chamber was opened at the main signal cable end in order to power the hydrophones through the junction chamber electronics. By powering each hydrophone through internal junction chamber leads, it was determined that hydrophones C, X and X-Y were operational and that hydrophones Y and Z were dead. The finding that hydrophone Y was dead agrees with the 1973 tracking range report.

The problem in the Y hydrophone was traced to the preamplifier. The housing of the Y preamplifier was opened like a clam shell by milling lengthwise on both sides so that the electronics could be examined. Figure 2 shows the sectioned housing, the potted preamplifier, and the hydrophone assembly less the cable assembly. The staining in the center of the housing is due to welding and the staining on the ends is probably due to corrosion produced by sealed-in volatile matter.

Close examination indicated that the cable for the Z hydrophone was stretched at the point where it entered the hydrophone housing. Tests on the cable indicated that the stretching had parted both the center conductor and the shield. The Z hydrophone was found to be operational when power was applied beyond the damaged cable section.

Table II. Summary of Performance/Failure Analysis on Array 8

	Hydrophone						
	C	X	Y	Z	X-Y	Tilt	Ex. Bolt
Morrison Cable Seals							
Corrosion Depth (Hydrophone End)	0.80	0.80	0.80	0.80	0.80	1.15	1.40
Cause	Deform[a]	Deform	Deform	Deform	Deform	Deform	Cable[b]
Corrosion Depth (Junction Chamber End)	0.80	0.97	0.79	0.76	0.91	1.07	0.86
Cause	Deform	Deform	Deform	Deform	Deform	Deform	Deform
Cable, Interconnect (RG 58)							
Condition	---	---	---	Cut	---	Cut	Cut
Damage	2 leaks	---	---	Separation	2 leaks	---	---
Cause	Aging (Leaching)	---	---	Stretch	Cracks	---	---
Seals, O-Ring							
Hydro Transducer	OK	OK	OK	OK	OK	OK	NO
Hydro Cable	OK	OK	OK	OK	OK	1st Leak	Cuts
Junction Chamber, Main Cable End (1st OK, 2nd backup cut)							
Junction Chamber, Hydro End (1st OK, 2nd OK)							
Transducer							
Impedance	OK	OK	OK	OK	OK	---	---
Corrosion	ND	ND	ND	ND	ND	None	---
Boot	OK	OK	OK	OK	OK	---	---

[a]1st seal glands deformed by incorrectly installed cable clamp sleeve and excess of metal shims

[b]Leak in polyurethane jacket

O-Ring Seals: The O-ring seals in both junction chamber end plates were well lubricated and not leaking even though a defect existed. The O-ring backup gland of the second (inboard) O-ring on the signal cable end of the junction chamber had been cut (sheared) as the end cap was pushed into the cylinder. (See Figure 3.) The cutoff section (about 3/4 in. long and 1/16 in. deep) of the O-ring backup had then been pushed into the first (outboard) O-ring groove. This defect did not affect the successful operation of the first O-ring.

The double O-ring piston seal on the bottom plate of the tilt sensor housing worked perfectly. The surfaces on the piston part of the seal were very clean and excess lubricant was evident. However, the cable seal housing assembly had to be pressed out of the bottom plate because the first O-ring had leaked. The decrease in the inside diameter of the housing due to corrosion products caused interference between the piston and the housing wall. Dense, tenacious and hard corrosion products had collected from the seawater side all the way up to the second O-ring. The cause of leakage could be a defective O-ring or lack of sufficient squeeze on the O-ring.

Cables and Cable Seals: The depth that sea water and corrosion products had penetrated the Morrison cable seals was measured on the seal housings. The results are shown in Table II. The Morrison seal housings on the junction chamber, which were made by boring holes through the end plate, were sectioned to illustrate the distribution and nature of corrosion products. The sectioned junction chamber end plate shown in Figure 4 graphically illustrates the depth of seawater penetration.

The sectioned Morrison seal housing with the double O-ring joint to the tilt mechanism housing is shown in Figure 5. The distribution and location of corrosion products and knowledge about Morrison seal design lead to the conclusion that a leak in the cable jacket allowed seawater to surround the seaward backup washer, but that the seal glands on either side blocked further leaking.

Electrical and mechanical tests were conducted to detect leaks in the cables or seal assemblies and to measure the seal resistivity. The procedure was to disconnect each interconnecting cable, with its seal assemblies intact, from the array harness. The section tested included the Morrison seal from the junction chamber end, the interconnecting cable, and the Morrison seal with its housing from the hydrophone assembly. A typical interconnecting Morrison cable seal assembly is shown in Figure 6. The test setup is shown in Figure 7.

Insulation breakdown megohmmeter measurements were made between all connector pin and housing combinations, first in air and then in water at 0, 500, 1000, and 1500 psi; pressure was maintained at 1500 psi for approximately 24 hours and the measurements repeated, both at 1500 psi and after reducing the pressure back to zero. The results are given in Table III.

Table III. Megohmmeter and Resistivity Values: Typical or Representative Values for Array 8 Interconnecting Cables and Cable Seal Assemblies

	Hydrophone						Explosive Bolt	
	C	X	Y	Z	X-Y	Tilt	J.C. End	Bolt End
Air								
Hydro (end)								
C-S[a]	17[b]	24	ND	---	9	---	---	0.4
C-H	17	24	ND	---	9	---	---	0.45
S-H	120k/0[c]	200k/0	ND	---	80k/0	---	---	180k/0
Junction Chamber (end)								
C-S	17	24	40	72	9	37	60	---
C-H	13	24	ND	58	9	37	60	---
S-H	100k/0	80k/0	ND	200k/0	50k/0	40k/0	90k/0	---
Water								
P=0, t=0[d]								
C-S	17	28	40	82	18	40	50	0.60
C-H	17	28	40	130	18	40	50	0.60
S-H	120k/0	200k/0	200k/0	1	18k/0	100k/0	90k/0	180k/0
P=1500, t=0								
C-S	33	35	50	140	22	ND	ND	0.45
C-H	33	35	45	170	22	ND	ND	0.50
S-H	2k/0	220k/0	200k/0	1	50k/0	ND	ND	140k/0

[a]C = center conductor; S = shield, H = housing.

[b]If a megohmmeter reading could not be made because of breakdown at the 500 Vdc megohmmeter setting, the voltage was reduced until a satisfactory reading could be obtained. When it was necessary to use a voltage other than 500, the megohmmeter or resistance reading and the voltage are indicated as follows: reading/voltage.

[c]All readings are 1000 MΩ unless otherwise indicated. The letter k indicates 1000 Ω.

[d]P = pressure; t = time (hours).

Leaks in the interconnecting cables were often detected by measuring a low resistance between the shield and the water in the test chamber shown in Figure 7. The location of the leak was determined by one or both of two methods: (1) injecting air into the cable jacket and observing bubbles emitting from the leak, or (2) withdrawing the cable slowly from the water and detecting a change in the measured resistance between the shield and the water. Several leaks were located by these methods.

Figure 8 shows an example of typical cracks through the urethane cable jacket. Figures 9a and 9b are a series of photomicrographs taken with a scanning electron microscope to determine the material microstructure and deduce the probable failure mechanism. Figure 9b shows extensive microcracking. The cable jacket material was badly deteriorated and embrittled probably because of leaching of binder or resin.

Cable Seal Packing Glands and Backup Washers: Each Morrison seal assembly was completely disassembled, and the size of each individual packing gland and backup washer was measured to determine the amount of dimensional change (creep) that had taken place under service conditions. The hardness, voltage breakdown resistance, and appearance of each item were also determined. The results are shown in Table IV and discussed briefly here.

All of the interconnecting cable sleeves on Array 8 were installed backward. The typical interconnecting cable clamp, cable sleeve, metal shims, and Morrison seal assembly in Figure 6 show the distortion and gap produced by the improperly installed cable sleeves.

All of the seaward backup washers showed substantial reductions (by factors of 10^4 to 10^6) in voltage breakdown resistance, except for the seal at the sensor end of the explosive bolt cable. The low resistance of the backup washers was probably caused by adsorption of corrosion products and the absorption of seawater admitted, in part, by the improperly installed cable sleeves. The absorption was symptomatized by swelling. The diameter of the seaward backup washers increased by 1.2% and the thickness by as much as 32%. The diameter of the other backup washers tested increased by 1.2% and the thickness by about 11%.

The seal glands in the Morrison seals showed a dimensional change due to creep and a substantial reduction in hardness. The diameter of the seals decreased by 1.4% and the thickness increased by 2%. The measured hardness was consistently 15% below the mean hardness specified in the design drawings.

Table IV. Cable Seal Packing Gland and Backup Washer Properties

	Cable Seal Components						Design	
	← (Inboard)				(Seawater) →			
	Backup Washer	Seal	Backup Washer	Seal	Backup Washer	Seal	Backup Washer	Seal
Hydrophone End:								
Diameter (in.)							0.761 ± 0.005	0.781 ± 0.005
Avg[a]	0.768	0.769	0.769	0.770	0.769	---[c]		
Max[a]	0.772	0.770	0.776	0.772	0.772	---[c]		
Min[a]	0.768	0.767	0.767	0.768	0.763	---[c]		
Thickness (in.)							0.094 ± 0.005	0.250 ± 0.005
Avg	0.104	0.225	0.103	0.257	0.123	---[c]		
Max	0.107	0.258	0.108	0.260	0.125	---[c]		
Min	0.098	0.250	0.099	0.255	0.120	---[c]		
Hardness							80 ± 5	40 ± 5
Avg (duro)	68	38	68	38	64	39		
Max	70	40	70	40	70	40		
Min	65	35	66	35	60	37		
Voltage Breakdown Resistance[b]							None	None
Avg	432	170	29	34	10^{-3}	172		
Max	800	250	40	800	7	200		
Min	240	120	12	180	10^{-5}[d]	5		
Junction Chamber End:								
Diameter							0.761 ± 0.005	0.781 ± 0.005
Avg	0.769	0.770	0.770	0.770	0.771	0.769		
Max	0.768	0.772	0.772	0.772	0.775	---[c]		
Min	0.770	0.769	0.768	0.769	0.765	0.769		
Thickness							0.094 ± 0.005	0.250 ± 0.005
Avg	0.104	0.255	0.104	0.255	0.125	---[c]		
Max	0.110	0.257	0.109	0.260	0.130	---[c]		
Min	0.100	0.252	0.100	0.252	0.120	---[c]		
Hardness							80 ± 5	40 ± 5
Avg	70	40	69	40	67	41		
Max	72	43	70	42	70	42		
Min	65	39	65	40	65	39		
Voltage Breakdown Resistance[b]							None	None
Avg	380	174	260	258	1×10^{-3}	500		
Max	800	240	700	300	17×10^{-3}	900		
Min	160	140	52	170	6×10^{-3}	220		

[a]Average for all (7) identical cable seal components

[b]Megohmmeter readings taken across seal or washer with clamp contacts touching both faces and separated by approximately one-third the seal diameter. Megohmmeter voltage was 500 Vdc unless otherwise indicated. All readings are 1000 megohms.

[c]Deformed

[d]@ 50 Vdc

Array 9

The analysis performed on the harnesses from Arrays 9 and 6 was less extensive than that performed on Array 8. No hydrostatic tests were performed on the cable and seal assemblies and only defective seals were completely disassembled and analyzed.

Array 9 was a rigid design planted in June 1970 and recovered in September 1976. The array was recovered because of malfunction, but the specific defects are not known by the author. The tracking range status report indicated that hydrophones C and Z were bad. The material specifications for Array 9 are summarized in Table V.

The crating procedures and the shipping damage received by Array 6 and Array 9 appeared to be equal. Because neither had styrofoam in front of the acoustic transducer, some of the observed transducer damage may have been produced during shipping. In Array 9, two transducers (C and Z) were exposed because of cuts on the boots. It is unlikely that the cuts in the boots were solely the

Table V. Material Specifications for Arrays 9 and 6

Description	Material	Plating
Housing Seal (Preamp)	Steel, AISI, C1010-1020 Cold Finish	Zinc,* Electrodeposited QQ-Z-325, Class 2, Type II
Housing, Junction Chamber	Carbon Steel, AISI MT 1015	Same as above
Housing, Preamp, Cap, End	Steel AISI, C1010-1020	Same as above
Junction Chamber	Steel AISI, C1010-1020	Same as above
Cap, End (Seal Junction Chamber)	Steel, Cold Finish AISI, C1018 or leaded C1018	Same as above
Pin, Connector	Brazz or Bronze	Nickel Plate QQ-N-290,* Class 2, Type V
Packing, Gland	Butyl, Chloriniated 30 ± 5 duro	N/A*
Washer, Backup	Teflon	N/A
Insulator	Teflon	N/A
Washer, Thrust	Plastic Sheet NEMA G 10	N/A
Cable, Coaxial	Polyethylene Jacket 0.3 in O.D.	N/A
Cable, Coaxial Signal	Polyethylene Jacket 1.0 in O.D.	N/A

*No additional coatings specified

results of shipping. However, at least one transducer of Array 9 appeared to have been jammed into the side of the crate. None of the hydrophones on any of the arrays had transducer cap protection.

External Condition

The UQC interconnecting cable was severed about 20 ft from the hydrophone.

The corrosion and calcareous deposits on the junction chamber and housings of Array 9 were substantially less and their distribution was more uniform than those on Array 8.

No indications of paint were found.

Internal Condition

Cables and Seals: The resistivity of the interconnecting cables and seal assemblies for hydrophones C, Y and Z and the UQC was measured in air before the Morrison seals were pushed out of the junction chamber end-plate. Because many of the cables were parted or cut, each cable and cable seal assembly was measured individually. The results of these tests are shown in Table VI. The Morrison seals in the hydrophones exhibited higher resistance readings than those in the junction chamber. Some factors that may have contributed to the noted difference in behavior are the attitude (gravity effects) of the seal during service, the seal-to-housing diametral interference, and the electrical potential (grounding and stray current) of the housings.

The results of the resistivity tests indicate that the cable seal assemblies in Array 9 performed better than those in Array 8. However, this conclusion is qualified by differences in seal material, period of service, cable performance, and assembly errors.

Cable Seal Packing Glands and Backup Washers: Megohmmeter measurements of the Morrison seal assembly for the Z hydrophone, as received in the junction-chamber end of the interconnecting cable, showed a low (160 kΩ) resistance between the center conductor and the shield conductor. The 160-kΩ path became intermittent after the seal assembly was pushed out of the junction chamber housing. Slight flexing of the cable seal assembly produced erratic changes in resistance readings, which varied between 16 kΩ and 50 MΩ at 500 Vdc. Disassembly, inspection, and examination with a scanning electron microscope revealed that the low resistance path was through a black residue on two adjacent teflon washers in the Morrison seal. The resistance of the black residue between the hole for the center conductor and the hole for the shield conductor was 350 kΩ on both of the two adjacent insulating washers. At the site of the

Table. VI. Summary of Performance/Failure Analysis on Array 9

	C	X	Y	Z	X-Y	UQC
Seals, O-Ring						
Hydro Trans	OK	OK	OK	OK	OK	OK
Hydro Cable	OK	OK	OK	1st Leak	OK	1st Leak
JC Hydrophone	---	---	---	---	---	---
JC Main Cable	OK	---	---	---	---	OK
Seals, Morrison[a]						
Hydrophone (end)	---	---	---	---	---	---
CS	∞	---	∞	∞	---	50 kM
CH	∞	---	∞	∞	---	20 kM
SH	30 M	---	10 M	3 M	---	13 M
Junction Chamber (end)	---	---	---	Lightning	---	---
CS	40 kM	---	40 kM	160 k	---	50 kM
CH	40 kM	---	40 kM	5 M	---	18 kM
SH	10 M	---	3 M	5 M	---	8 M
Failure	---	---	---	JCCS Arcing Lightning	---	---
Corrosion Depth						
Hydrophone	---	---	1.4 in.	0.85 in.	---	---
Cause	---	---	Crevice-Corrosion		---	---
JC	---	---	1.4 in.	1.4 in.	---	---
Cause			Crevice-Corrosion			
Cable, Interconnector: (RG 58)						
Condition	Cut	Intact	OK	Good	Intact	Intact
Damages	---	---	---	Cut	---	---
Cause	---	---	---	?	---	---
Transducer						
Impedance Plot	Exposed, Cocked	OK	OK	Exposed, Straight	OK	OK
Corrosion	ND	ND	ND	ND	ND	ND
Boot	Cut	OK	OK	Cut	OK	OK
Fasteners: Severe corrosion damage						
Housings: Hydrophone, Poor; JC, ND; Morrison Main, OK						
Clamps: Severe corrosion damage						

[a]Voltage breakdown and resistance measurements: megohmmeter measurements with 500 Vdc indicated by km = 10^9 Ω; M = 10^6 Ω @ 50 Vdc; VOM measurements with 3 Vdc indicated by k = 10^3 Ω.

black residue, the center conductor pin and the shield pin were coated by a thin layer of black liquid. The liquid was not identified.

Figures 10a and 10b show SEM photomicrographs of the residue and damaged teflon between the two conductor holes on the teflon washer. The residue appears to be charred teflon created by lightning or arcing. The damage occurred at the point of closest approach between the center conductor and the shield.

The post-service properties of the Morrison seal packing glands can be summarized as follows: avg. diameter = 1.034 in.; avg. thickness = 0.375 in.; avg. hardness = 32 durometers; voltage breakdown resistance = →∞ (i.e., exceeds capacity of instrument); and appearance, good. The design diameter, thickness, and hardness are 1.040 ± 0.005 in., 0.374 ± 0.005 in. and 30 ± 50 durometer, respectively.

The post-service properties of the packing seal glands of Array 9 indicate that the chlorinated butyl performed better than the commercial neoprene used on Array 8. However, this conclusion is qualified by the fact that the service period for Array 8 was ten years whereas that for Array 9 was six years, and the fact that the reversed cable sleeves in Array 8 produced substantial seal distortion and increased the susceptibility to leaking.

Array 6

Array 6, a rigid design, was planted in June 1970 and recovered in September 1976. The specific reasons for recovery are not known to the author. The range status report of 9 December 1973 lists the following entry for Array 6: "Z bad."

Examination of Array 6 was limited to evaluating the external corrosion and mechanical damage, determining the acoustical and electrical performance of individual hydrophones, and recording the general condition of the interconnecting cables and the seals.

Some damage could be observed to the transducers as the hydrophone assemblies sat in the cradles in the shipping crates. The X-Y transducer was missing. The only part remaining was the base of the boot under the stainless wire. The Z transducer was still in the boot, but crushed. The Y transducer was also in the rubber boot, but the boot was almost completely severed and the element was crushed.

The corrosion and calcareous deposits on the housing of the hydrophone were not as extensive nor as deep as those on the other two arrays.

The results of the tests conducted on the Array 6 are summarized in Table VII.

Table VII. Summary of Performance/Failure on Array 6

	C	X	Y	Z	X-Y	UQC
Seals, O-Ring						
Hydro Trans	OK	OK	OK	OK	OK	OK
Hydro Cable	OK	1st Leak	1st Leak	1st miss.(1)	1st	1st leak
JC Hydro	OK			2nd OK	leak	
JC Shore	OK					
Seals, Morrison	ND	ND	ND	ND	ND	ND
Cable Interconnect (RG 58)						
Condition	Cut	Intact	Intact	Cut	Intact	Intact
Corrosion	ND	ND	ND	ND	ND	ND
Cause	ND	ND	ND	ND	ND	ND
Transducer						
Impedance	OK	OK	Crush	Crush	Gone	OK
Corrosion	ND	ND	ND	ND	ND	ND
Boot	OK	OK	Crush	Cut	Gone	OK
			Cut	Base	Cut	
Fasteners: Corrosion; Heavy						
Housings: (Hydrophones and JC uniform light)						
Clamps	Torn Sleeve					Torn Sleeve

(1) 1st O-Ring missing

Observations

1. Interconnecting cables with polyurethane jackets exhibited visible circumferential cracks about 1/4 in. long at several places. These cables exhibited many additional leaks which were easily located by checking the electrical conductivity to seawater and by observing bubble escapement.

2. Arcing, probably due to lightning, occurred at the closest approach (approximately 1/16 in.) between the center conductor and the shield in the rigid teflon washers of the Morrison seal in the junction chamber of Array 9. This arcing produced a low-resistance path of what appeared to be charred teflon.

3. The cable sleeves under the cable clamps for the interconnecting cables on Array 8 were installed backward. This error produced some of the gland deformation that led to leakage past the first gland on many of the Morrison seals.

4. A small piece of the backup O-ring in the end-plate seal on the main cable end of the junction chamber on Array 9 had been cut off during assembly and become lodged in the first (seaward) O-ring groove. The first O-ring was effective.

5. The first, or seaward, O-ring was missing from the interconnecting cable seal housing on hydrophone Z of Array 6. The second inboard O-ring was effective.

6. Of 42 double O-ring seals examined, 8, or approximately 20%, of the first O-rings leaked. Four of the six first O-rings in the cable seal housings on the hydrophones of Array 6 leaked. The second O-ring on all these seals was effective.

7. The deepest penetration of corrosion products (yellow and black deposits) in the Morrison seals was 1.4 in. This corrosion was due to an interaction between seawater, the lubricant, the housing, and the gland materials.

8. The first gland of all the Morrison seals on Array 8 was adversely affected by deformation due to installing the cable sleeves backward, and to the use of too many shims; i.e., overcompression of the Morrison seals.

9. It is not always possible to differentiate between damage sustained during use and physical damage sustained during recovery, packing, and shipping.

10. Especially in Morrison seals, dark to black stains and corrosion products were found in the vicinity of large solder joints in the center conductor and the shielding. The color, location, and distribution of the products suggest they were caused by incomplete removal of the solder flux.

11. Analysis of test data from Array 8 did not indicate that the high pressure on the Morrison seals glands produced any significant decrease in the resistance between the conductors and the housings.

12. All seaward backup washers in the Morrison seals on Array 8 showed substantial reductions (by factors of 10^4 to 10^6) in resistivity, except for the seal at the sensor end of the explosive bolt. The low resistivity was caused primarily by deformation which contributed to the absorption of seawater and corrosion products.

13. The backup washers in the Morrison seals on Array 8 increased in volume. The diameter of the seaward washers increased by 1.2% and the thickness by 32%. The diameter of the other backup washers tested increased by 1.2% and the thickness by 11%.

14. The packing seal glands in the Morrison seals on Array 8 showed a dimensional change due to creep, and a reduction in hardness. The diameter of the seals decreased by 1.4% and the thickness increased by 2%. The measured hardness was consistently 15% below the mean hardness specified in the design drawings.

Recommendations

1. A comprehensive performance/failure analysis program for acoustic arrays should be instituted. Each recovered array should be analyzed to determine why it failed and what improvements should be made.

2. The value of performance/failure analyses on arrays, as with any instrument system, can be significantly increased by maintaining a complete record on design, fabrication, initial performance, installation, operation, recovery, handling, and storage.

3. On recovery of all arrays, either an expert in performance/failure analysis should be on hand or a procedure should be prescribed and followed during the recovery, packaging and shipping to verify the as-recovered condition of all arrays.

4. Continuous or regular monitoring of the shield-to-seawater resistance and center conductor-to-seawater resistance should be made at the range. Failures or changes in array behavior could then be traced either to climatological conditions such as lightning storms or to operational conditions such as voltage or current overloads.

5. Stricter quality control measures should be instituted for the assembly and installation of Morrison seals, solder joints within the seals, cable clamps, and sleeves.

6. There should be greater insulation capacity and greater separation between the center conductor and the shield than is presently provided in the Morrison seal designs used in Arrays 9 and 6.

7. All O-rings should be heavily coated with O-ring lubricant and all O-ring grooves and spaces of the O-ring seals should be filled with lubricant at the time of installation.

8. Double O-ring or even triple O-ring seals should be used where a long-term (several years or more) O-ring seal between seawater and electronics is required.

9. Quality control measures during installation and assembly of O-rings should be improved. To prevent cutting and shearing of O-rings during assembly, more alignment fixtures or alignment procedures should be adopted.

10. A test and evaluation study should be conducted on elected and candidate materials for Morrison seals, spacers, and washers to identify the materials that have the best resistivity, dimensional stability, and corrosion resistance.

11. A cathodic protection system for the array harnesses should be designed and used.

12. Protective hoods should be put over all hydrophones immediately after recovery to prevent further damage.

Acknowledgment

This work was supported by the Naval Facilities Engineering Command, Chesapeake Division, Washington Navy Yard, Washington, D.C., under Contract N00017-74-C-1208.

References

1. NAVTORPSTA Report 1332, "Analysis of Array Components Recovered at St. Croix, VI," by M.M. Abo, Naval Torpedo Station, Keyport, Washington, May 1977.

2. Reference Manual on Interference Seals and Connectors for Undersea Electrical Applications, prepared by the Applied Physics Laboratory of the University of Washington for the Naval Facilities Engineering Command, Chesapeake Division (available from NTIS, 5285 Port Royal Road, Springfield, Virginia 22161; ref. Publ. ADA 036841), June 1976.

3. Technical Note 1424, "Inspection of Objects Retrieved from the Deep Ocean - AUTEC Acoustic Array," by J.F. Jenkins, Civil Engineering Laboratory, Port Hueneme, California, DN 487017, February 1976.

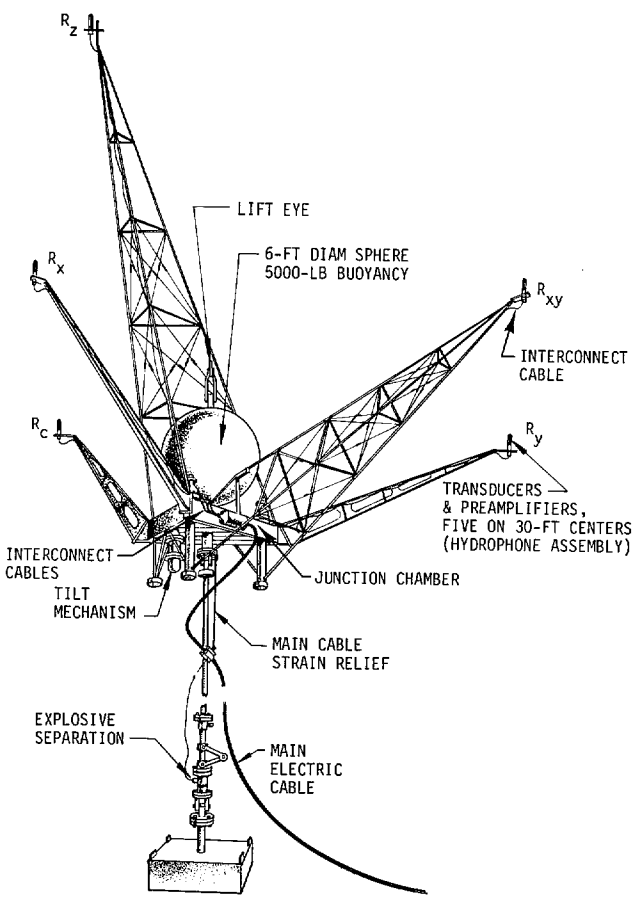

Figure 1. Buoyant array, St. Croix

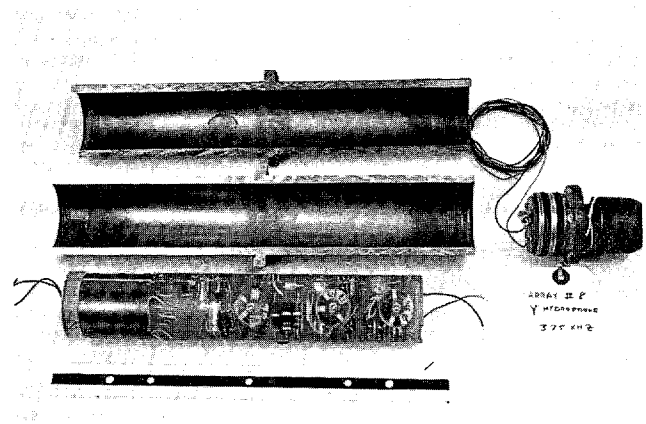

Figure 2. Sectioned hydrophone housing, potted preamplifier and acoustic transducer assembly

Figure 3. Double O-ring seal of main signal cable end of junction chamber, showing cut piece of O-ring backup gland as it was deposited in the 1st O-ring groove

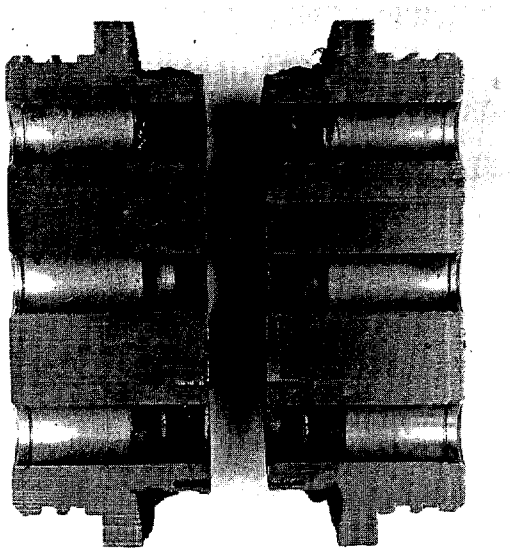

Figure 4. Seawater corrosion products in (left to right) X hydrophone, explosive bolt and tilt cable seal housings

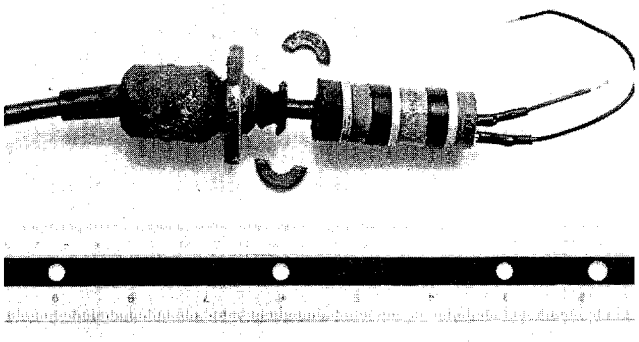

Figure 6. Typical interconnecting-cable seal assembly, Array 8

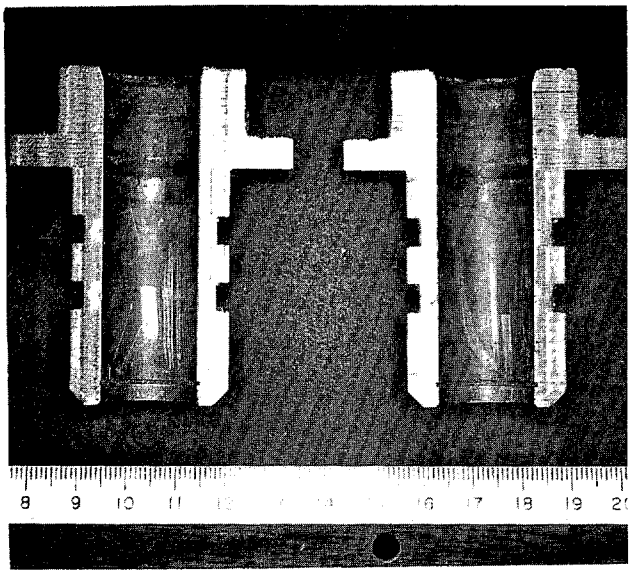

Figure 5. Sectioned Morrison seal housing from the tilt mechanism housing

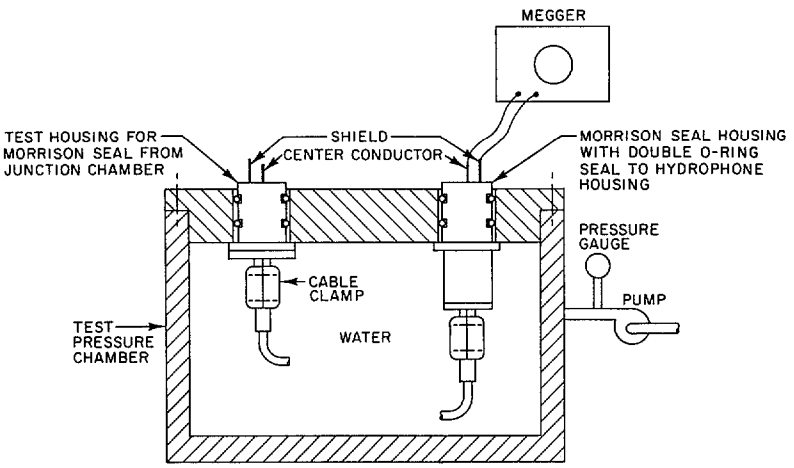

Figure 7. Hydrostatic test apparatus

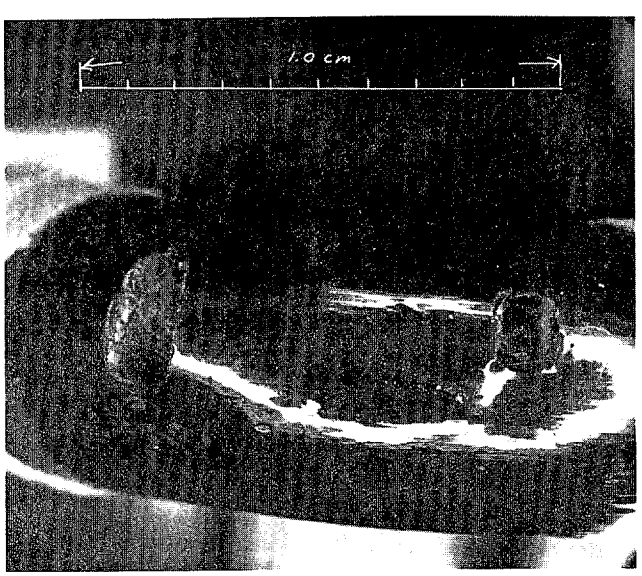

Figure 8. Cracks in urethane jacket opened by bending the cable

Figure 9a. Circumferential cracks through urethane cable jacket, SEM (76X)

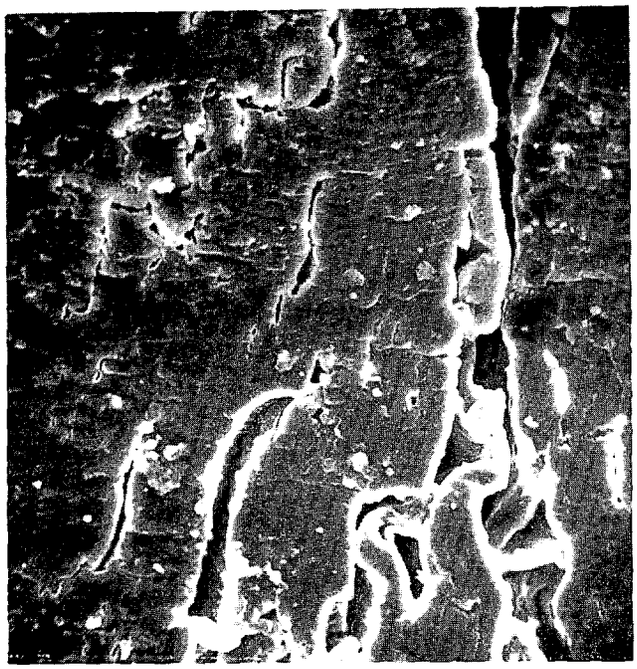

Figure 9b. Magnification of a region in Figure 9a showing microcracks in deteriorated urethane cable jacket, SEM (1,500X)

Figure 10b. Magnification of Figure 10a, SEM (50X)

Figure 10a. Arcing damage between conductor holes in teflon washer in Morrison seal, Array 9, SEM (20X)

FLOW-INDUCED TRANSVERSE MOTIONS OF A FLEXIBLE CABLE ALIGNED WITH THE FLOW DIRECTION

R. J. Hansen
Naval Research Laboratory
Washington, DC 20375

C. C. Ni
Naval Research Laboratory
Washington, DC 20375

Abstract

Experimental studies of the motions induced in a long, flexible cable by axial flows have been conducted in a large,blowdown water channel. A cable with a diameter of 1.59cm and a length of 9m was employed. Experiments were conducted over a fluid velocity range of 4.6 to 9.1 m/s. Both free and fixed downstream terminations of the cable were utilized, the former simulating a towed cable and the latter a mooring cable. Measurements of the drag coefficient of the cable were also made and compared with previously made predictions.

1. Introduction

Flexible cables aligned with the flow are present in a variety of systems used in the ocean environment, including mooring lines aligned with the current and tow cables aligned with the tow direction. The present paper describes a laboratory-scale experimental study of the flow-induced transverse motions of such cables. Experimental results are presented for a 1.59cm diameter braided polypropylene cable having a length of approximately 9m. Results are reported for a cable fixed at both ends (simulating a mooring line) and for a cable which is free at the downstream end (as is a towed cable.)

2. Experimental Facility and Procedures

The experiments were conducted in a large, blowdown water channel. The facility is described in detail elsewhere (1, 2.) It was designed to subject the flexible cable to a fully-developed turbulent, annular flow of constant velocity. The facility consists of upstream and downstream liquid reservoirs, an air tank for pressurization of the upstream liquid reservoir, and a 15.5m long, 19.1cm diameter transparent test section. A constant flow velocity through the test section was realized by holding the total head (pressure plus gravity) constant at the bottom of the upstream reservoir. A 1.59cm diameter rigid rod was mounted on the centerline of the first 4m of the test section to produce a fully-developed turbulent, annular flow in the test section. The downstream end of the rigid rod was attached to the upstream end of the flexible cable. The downstream end of the cable was either free or fixed on the test section centerline. The flexible cable was terminated a minimum of 2m from the downstream end of the test section to avoid any flow irregularities caused by the exit of the flow into the downstream liquid reservoir. The dynamic behavior of the cable was monitored photographically by three motorized 35mm cameras. One was focused on the entire flexible member, the second on an approximately 2m segment near the middle of the member, and the third on a similar length of cable near its downstream extremity.

Because of the horizontal orientation of the test section, a nearly neutrally buoyant test cable was employed. It consisted of a braided polypropylene rope (1.59cm diameter) through which a 6.4mm diameter water-filled Tygon tube had been threaded. The experimentally determined relationship between force and elongation for this composite test piece is shown in Figure 1.

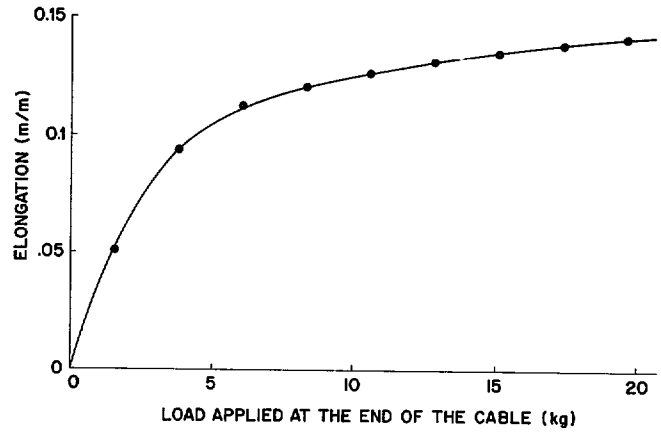

Figure 1: Tension - elongation relationship for the cable

When the downstream end of the cable was free, it had a hemispherically shaped downstream termination in the present work. Previous experimental studies have shown that the flow-induced motions of flexible cylinders with length-to-diameter ratios on the order of 50 or less are affected by the shape of this downstream extremity (3), whereas more recent work with much larger length-to-diameter ratios show no

U.S. Government work not protected by U.S. copyright.

significant dependence on this parameter (1). The flow-induced motions with a fixed downstream termination were studied in the present work by attaching this end to a rigid rod in much the same way as at the upstream end.

3. Experimental Results

A. Free downstream end

Typical photographs of the center region of the cable with a free downstream end at a bulk flow velocity of 7.52 m/sec and of the downstream region over the bulk velocity range of 4.60 to 7.52 m/s are shown in Figure 2.

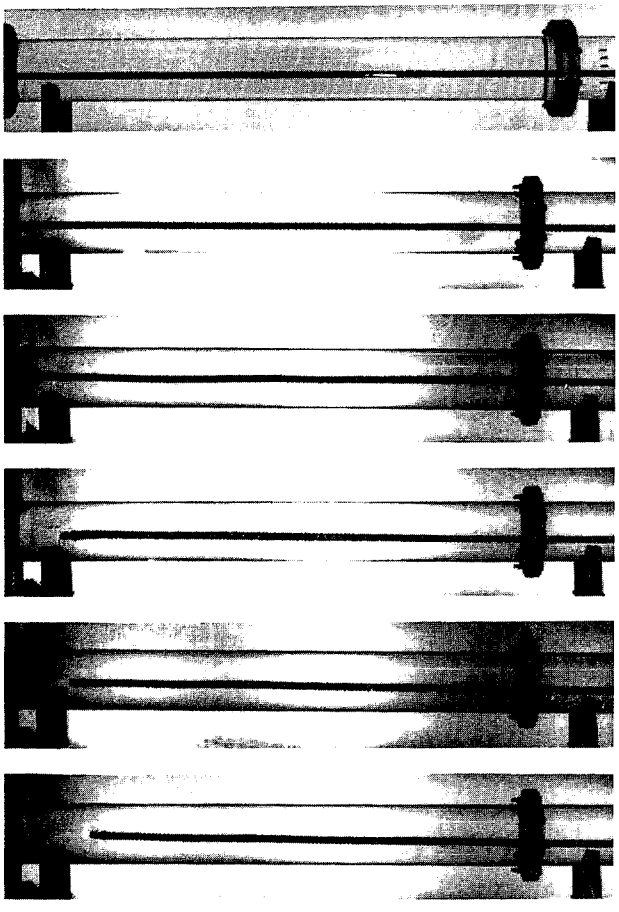

Figure 2: Photographs of the cable with a free end (from top to bottom the center region of the cable at a bulk fluid velocity of 7.52 m/s and the downstream end region at 7.52, 6.70, 5.85 5.09, and 4.60 m/sec).

The flow is from right to left, and the bulk flow velocity in the test section, hereafter denoted by V, is approximately 0.88 times the maximum value, U. The actual displacements are 0.75 times those recorded by the cameras because of the curvature of the pipe wall. Transverse motions are readily apparent, as well as a change in cable length with flow velocity.

The change in length of the cable produced by the flow was used along with the results of Figure 1 to obtain the drag coefficient on the cable. The assumption was made in the calculation that the flow exerts a uniform shear stress over the entire length of the cable. Thus, the tensile force, F_o, on the upstream extremity of the cable is twice the value obtained from Figure 1 as the force corresponding to the total elongation caused by the flow. The drag coefficient, C_D, defined by the following equation, is shown in Figure 3.

$$C_D = \frac{F_o}{\rho U^2 \pi a L} \qquad (1)$$

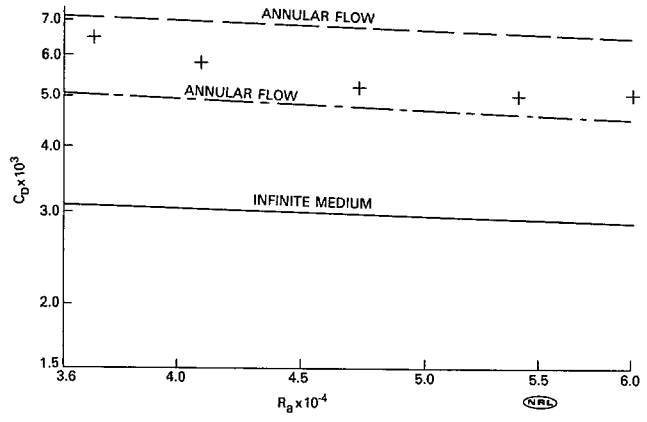

Figure 3: Measured drag coefficient of the cable and theoretically predicted drag coefficients of cylinders with smooth surfaces in annular flow and in an infinite medium.

Here ρ denotes liquid density and a and L the cable radius and length, respectively. Also shown in Figure 3 are two analytical predictions for the drag coefficient of a smooth cylinder in annular flow (4) and one for a smooth cylinder in an infinite medium (5).

The mean positions of the cable with a free downstream end at four of the five bulk flow velocities at which extensive data was taken are shown in Figure 4. The vertical scale is

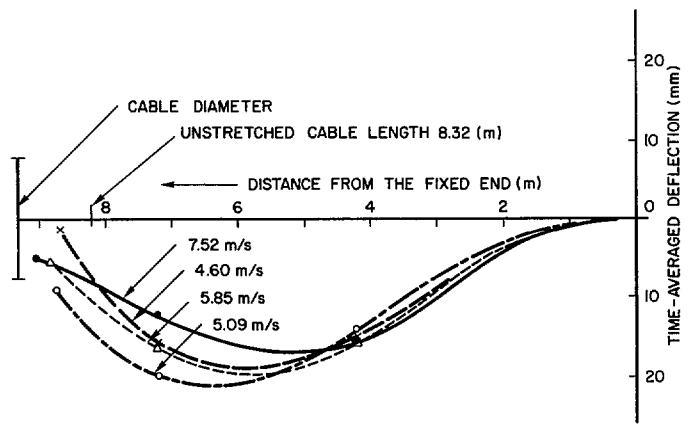

Figure 4: Mean position of the cable with a free downstream end (relative to the test section centerline).

magnified 120 times compared to the horizontal scale for the sake of clarity. The displacements of the mean positions of the cable from the test section centerline are due to slight deviations from neutral buoyancy. These displacements and the associated angles of the cable to the mean flow are very small, so their effect upon the flow-induced motions of the cable are thought to be negligible.

The rms deviation of the cable position from the mean, σ, is a measure of the magnitude of the flow-induced motions in the cable. Figure 5

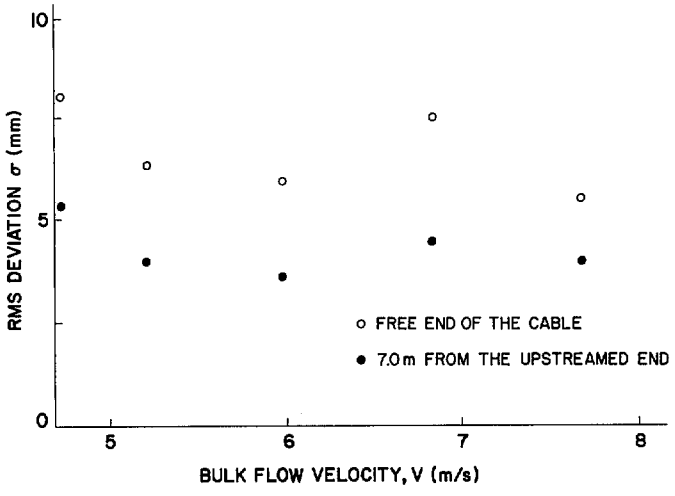

Figure 5: RMS deviation of the cable with a free end from the mean location.

shows σ over the range of bulk flow velocities studied and at two axial locations: the free end and 7.0m from the fixed upstream end. An average of 30 measurements of cable position were used to obtain each data point. The amplitude of the flow-induced motions is weakly dependent on the flow velocity. Larger values at 4.60 and 6.71 m/s are probably attributable to the existence of in-phase motions of the dominant frequency components at these velocities. At all velocities the values of σ decrease with increasing distance from the free end. This trend is apparent in Figure 5.

The frequency content of the flow induced motions of the cable with a free end could not be determined quantitatively from the photographic records. The frame rate of the cameras (3 per second) was too low to preserve frequency information according to the Nyquist criterion. Visual observation suggested that these motions were of predominantly low frequency (on the order of 10 Hz or less), however. Subsequent studies of the transverse motions of large L/D, smooth-surfaced cylinders in axial flow have shown a continuous spectrum of vibration frequencies, with the spectral intensity largest in the 3-10 Hz range (1).

B. Fixed downstream end

When the downstream end of a cable in axial flow is fixed in space, three distinct conditions can exist with increasing flow velocity: (a) the entire cable is in tension, the tensile force varying monotonically from a maximum at the upstream end to a minimum at the downstream end; (b) a zero-tension condition exists at the downstream end; (c) the zero-tension condition is between the two ends of the cable, with observable slack downstream of this point. This range of conditions may be anticipated from a force balance on the cable, which takes the form

$$F(x) = F_s + 2\,\pi\,a\,\tau_w\left(\frac{L}{2} - x\right). \qquad (2)$$

Here F(x) denotes the force in the cable at a distance x from the upstream end, F_s the tensile force in the cable in the absence of flow, τ_w the wall shear stress exerted by the flow on the cable exterior, and L the cable length. Also the assumption is made in deriving equation 2 that F(x) is greater than or equal to zero in the whole cable or if not that the cable can support compressive as well as tensile forces. Since the first of these assumptions is satisfied when the tension is zero at the downstream extremity of the cable, equation 2 may be used to obtain the following relationship between F_s and other parameters at this critical condition:

$$F_s = \left(\tfrac{1}{2}\,\rho\,U^2\right)\left(C_D\right)\left(\pi\,a\,L\right). \qquad (3)$$

Experiments were conducted at bulk fluid velocitites of 4.60, 5.64, and 5.97 m/s to realize the range of conditions which has been identified. The mean position of the cable in the test section at these velocities is shown in Figure 6.

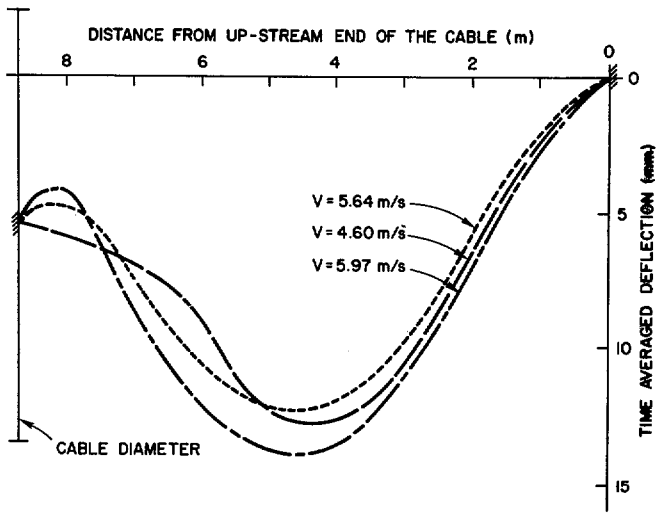

Figure 6: Mean position of the cable with a fixed downstream end (relative to the test section centerline).

The zero tension condition at the downstream end occurred at a bulk velocity of approximatedly 5.2 m/s, corresponding to a value of F_s from equation 3 of approximately 4.2 kg. Slack in the downstream region of the cable is apparent at higher velocities.

The value of σ at three axial locations is shown in Figure 7 for the three fluid velocities.

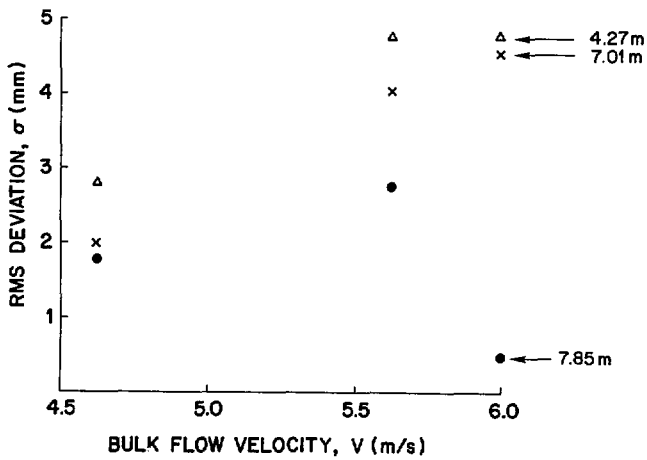

Figure 7: RMS deviation of the cable with a fixed downstream end from the mean position at the three distances from the upstream end indicated.

A trend of increasing amplitude of the flow-induced motions with fluid velocity is observed. As in the free downstream end configuration the motions appeared to be of predominantly low frequency, but the frame rate of the cameras was too low to make a quantitative determination of frequency spectrum as a function of fluid velocity and axial position.

4. Discussion

The results reported herein show that axial flows can excite transverse motions of towed and moored cables. These motions are largest in conditions of low cable tension, such as near the downstream extremity of a cable with a free end or, if both ends are fixed, a cable with small tension in the absence of flow. Even in these circumstances the motions are of the order of a cable diameter or less over the range of parameters considered in the present work. Moreover, the motions appear to be of predominantly low frequency. Thus, the transverse motions induced by axial flows should in general be of engineering significance only for cables or cable systems used in conjunction with instrumentation packages or other equipment which is sensitive to low-frequency, small-amplitude vibrations.

A number of distinctions exist between the flow-induced motions of the large L/D cables studied in the present work and those reported previously for flexible cylinders with smooth exterior surfaces. Static divergence (a stationary bending deformation) is not present in the fixed or free downstream end cables over the range of parameters studied. Static divergence is present above a critical flow velocity near the free downstream end of a large L/D cylinder with a smooth exterior surface (1). It is also evident above a critical flow velocity in flexible cylinders having relatively small L/D ratios of 50 or less (3). As flow velocity is increased adjacent to such small L/D cylinders, static divergence is replaced by progressively higher oscillatory modes. No circumstances similarly dominated by a single mode of deformation could be identified for the large L/D flexible cable.

Further experimental studies would be helpful in more completely characterizing the flow-induced motions of long, flexible cables and identifying the dominant mechanisms by which they are generated. Measurements of the transverse motions should be made which allow determination of their frequency content at selected locations along the cable. Companion two-point measurements should be conducted to ascertain the dominant propagation velocities and directions of transverse disturbances as a function of frequency. The optical displacement sensor technique utilized in recent flexible cylinder studies (1) would be well suited for such experiments.

5. Conclusions

Transverse oscillations are excited in long cables by axial flows. These motions are largest near the downstream end when this end is free. For the fixed end case the motions are a function of the tension in the cable in the absence of flow. These motions should be of importance in towed or moored systems with components sensitive to low-frequency and small-amplitude oscillations.

Acknowledgement: This work was supported jointly by the Office of Naval Research (Code 222) and the Naval Research Laboratory.

References

1. Ni, C.C. and R.J. Hansen, "An experimental study of the flow-induced motions of a flexible cylinder in axial flow," (in preparation, 1978).

2. Hansen, R.J. and C.C. Ni, "An experimental study of flow-induced motions of flexible cables and cylinders aligned with the flow direction," ASME Preprint 76-WA/FE-15, 1976.

3. Paidoussis, M.P., "Dynamics of flexible slender cylinders in axial flow; part II: experiments," Journal of Fluid Mechanics, Vol. 26, 1966, pp. 737-751.

4. Knudsen, J.N. and D.L. Katz, Fluid Dynamics and Heat Transfer, McGraw Hill Book Co., Inc., New York, 1958.

5. White, F.M., "An analysis of axisymmetric turbulent flow past a long cylinder," ASME Transactions: Journal of Basic Engineering, Vol. 94, 1972, pp. 200-206.

THE STATE OF TECHNICAL DATA ON THE HYDRODYNAMIC CHARACTERISTICS OF MOORED ARRAY COMPONENTS

J. H. Pattison
David W. Taylor Naval Ship
Research and Development Center
Bethesda, Maryland 20084

P. R. Rispin
David W. Taylor Naval Ship
Research and Development Center
Bethesda, Maryland 20084

Abstract

A survey is presented of the available hydrodynamic data on components of suspended-array mooring systems. The data are used by the system designer in calculating the forces and motions induced in the system by the dynamic ocean environment. The components include a variety of shapes of packages which contain oceanographic sensors and other moored array components. The data include hydrodynamic load coefficients, added mass and damping coefficients, and strumming effects which result from surface waves and subsurface currents. The various components are catalogued according to types and shapes of components. Types include sensor and array elements, mooring lines, and buoys. The quality and quantity of data are assessed. Suggestions are given for research to improve the quality and quantity of certain data.

1. Introduction

Various organizations involved in ocean research develop suspended array systems for such applications as the measurement of environmental parameters, weather prediction, and the tracking of military and commercial shipping. Designers of the moorings for these systems require a knowledge of the hydrodynamic environment, including surface wave spectra and subsurface currents to be expected at the site of interest. They also need to know the responses of the system's components. When the environment is known many of these responses may be determined from the hydrodynamic characteristics of the various components. This paper explores the state of technical data on the hydrodynamic characteristics of oceanographic sensors and mooring components and indicates their use in determining the responses of such systems.

In an investigation for the Naval Facilities Engineering Command, the published and unpublished literature was searched to establish the present level of technical knowledge of experimental and analytical procedures and of data on the hydrodynamics of components of moored arrays and similar systems. Data from selected sources were extracted and arranged according to component shape and major grouping of hydrodynamic characteristics, including hydrodynamic load coefficients, added mass and damping coefficients, strumming, and responses in waves.

As to the state of the data, complete data were found for components with simple geometric shapes, such as cylinders and spheres. However, data for more complex shapes were incomplete. In the sections which follow, the quality and quantity of data are assessed. Suggestions are given for research to improve the quality and quantity of certain data.

2. Hydrodynamic Parameters

In the ocean environment, moored array components are acted upon by different forces, including gravity, tensions from the mooring lines, hydrostatic forces, and steady and unsteady hydrodynamic forces. All the forces affect the responses of moored array components to the environment. This paper concentrates on the hydrodynamic forces.

As discussed by Morgan (Reference 1), steady hydrodynamic forces induced by a steady current on a body may include both friction and gravity components and are relatable to the inertia of the moving fluid by the following Newtonian force coefficients:

Drag coefficient $$C_D = \frac{D}{(1/2)\rho U^2 A_D}, \quad (1)$$

Lift coefficient $$C_L = \frac{L}{(1/2)\rho U^2 A_L}, \text{ and} \quad (2)$$

Moment coefficient $$C_M = \frac{M}{(1/2)\rho U^2 \ell A_L} \quad (3)$$

where A_D and A_L are the characteristic areas for drag and lift (such as frontal area and planform area), D and L are drag and lift forces, ℓ is a characteristic length of the body, M is pitching moment, U is flow velocity, and ρ is water density. These coefficients typically depend on angle of attack and on the Froude number, $F_n = U/\sqrt{g\ell}$ and Reynolds number, $R_n = U\ell/\nu$ where ν is the kine-

U.S. Government work not protected by U.S. copyright.

matic viscosity and g is the acceleration due to gravity.

The typical case of a sensor or array component oscillating in pure translation, as shown in Figure 1 may be used to illustrate unsteady forces. In this case, the unsteady forces can be described by an equation of motion of the form:

$$m'\ddot{z} + c\dot{z} + kz = F(t) \qquad (4)$$

where c is the damping factor, k is the spring constant provided by the mooring lines, m' is the virtual mass (mass of the body m plus the added mass of water m_a), z is the displacement of the component from an equilibrium position, and the dots represent time derivatives. Similar equations exist for other translational and rotational modes of motion. Added mass and damping data are often presented as functions of amplitude and frequency of motion. Also, spring constants are functions of the configurations in which the components are moored. The above oscillating system has a natural frequency given by:

$$f_o = \frac{1}{2\pi}\sqrt{\frac{k}{m'}} \quad . \qquad (5)$$

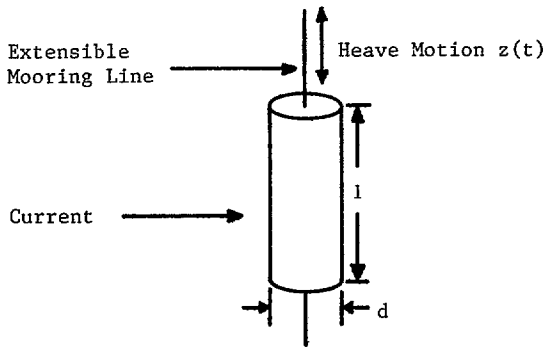

Figure 1 - Cylindrical Component Subject to Typical Flow and Motions

In a steady current, cylinders, spheres and other shapes often are subjected to transverse or lift forces due to vortex shedding at a frequency defined by:

$$f_s = \frac{US_n}{\ell} \qquad (6)$$

where S_n is the Strouhal number, which is a function of Reynolds number. When the frequency f_s approaches f_o, vortex shedding excites the component into resonance. This phenomenon, called strumming, can lead to structural failure or sensor overload.

The wave effects on moored components also must be considered. The motion of the water particles generated by waves is at its maximum at the surface and diminishes below the surface. When water particles move less than a significant length of the moored component, the effect of waves can be neglected. The relationship between the amplitude of water particle motion in deep water and the surface wave amplitude is shown in the following equation:

$$A(h) = A_o \exp(-\omega^2 h/g) \qquad (7)$$

where A(h) and A_o are single amplitudes of the water particle and waves respectively, h is the depth of submergence and ω is the wave frequency in rad/sec.

One empirical formulation of surface wave amplitude is that of Bretschneider, (Reference 2)

$$A_o = \frac{32.4\ H_s}{T_s^2\ \omega^3} \exp\left(-\frac{525}{T_s^4\ \omega^4}\right) \text{ feet} \qquad (8)$$

where H_s is the significant wave height in feet and T_s is the average period of the wave in seconds.

It follows from the above discussions that the sources of some hydrodynamic forces on mooring components depend on the depth at which the components are submerged. When a component is on or near the surface, surface waves are the primary source of hydrodynamic loading. When the component is submerged, current is usually the main source of hydrodynamic loading. Changes of water depth also affect hydrodynamic characteristics. When a component is submerged in intermediate or shallow water where the speed of the current is high, the strumming force induced by the shedding or vortices is important. It is not an important factor, however, when the component is deeply submerged and the speed of the current is low.

Thus, the nature of the hydrodynamic characteristics of a mooring system is related to the location of the array and to the depth of submergence of each of its components. The importance of the depth of submergence on the hydrodynamic characteristics of the types of component considered here is indicated in Table 1.

With the above considerations, the designer may use hydrodynamic data summarized below in various mathematical models to predict the performance of a moored system in the ocean environment. Details on various models are given in References 3, 4 and 5.

3. Survey of Data Available

For convenience in the assessment of hydrodynamic data, moored array components may be divided into three general groups according to component shape. The first group contains basic shapes of packages and housings which enclose oceanographic sensors and other subsurface components. A second group contains basic shapes of various mooring lines. A third group contains various shapes of surface and subsurface buoys.

TABLE 1. IMPORTANCE OF VARIOUS HYDRODYNAMIC CHARACTERISTICS

Depth of Submergence \ Hydrodynamic Characteristics	Steady Forces (drag, lift)	Added Mass	Damping	Strumming	R_n	F_n	S_n
Great depth of submergence in deep sea where low current exists	A	C	C	C	A	C	C
Intermediate and shallow submergence where higher current exists	A	B	C	A	A	A	A
Shallow submergence and surface where wave effects exist	B	A	A	A	B	A	A

where

A: Predominant parameter

B: Important parameter

C: Nonimportant parameter

R_n: Reynolds Number; the ratio of inertia to viscous forces

F_n: Froude Number; the ratio of inertia to gravity forces

S_n: Strouhal Number; the period parameter of vortex shedding

For the three groups, the availability of the data is summarized in a matrix form in Table 2. The letter symbols indicate whether the available data are ample, adequate, or inadequate for each combination of parameter and type of component. Ample indicates that many sources of data are available to characterize the parameter in question. Adequate indicates that enough sources are available to choose from. Inadequate indicates that either too few sources or no sources are available.

TABLE 2. AVAILABILITY OF HYDRODYNAMIC DATA

Type of Components	Range of Parameters	Flow Forces: Normal	Flow Forces: Axial	Flow Forces: Moment	Added Mass and: Normal	Added Mass and: Axial	Added Mass and: Moment	Dynamic Responses
Packages and Housings	Cylinders	B	C	B	B	B	C	C
	Spheres	A	A	*	A	A	*	B
	Spheroids	A	B	B	B	B	B	C
	Ellipsoids	C	C	C	B	B	B	C
	Other Streamline Shapes	B	A	B	B	B	B	C
Mooring Lines	Rigid Cylinders	A	A	A	A	A		A
	Bare Cable	A	A	A	A	B		B
	Chain	A	C	C	C	C		C
	Cable Fairings:							
	Fringe & Ribbon	B	B	C	C	C		B to C
	Streamlined	A	B	C	C	C		C
	Other	A	B	C	C	C		C
Buoys		Combined			Combined			
	General Floating Bodies	A			B			B
	Specific Surface Buoys	A			A			B
	Submerged Buoys	A			B			C
	Buoy Appendages	A			C			C

A Ample B Adequate C Inadequate * not applicable

Basic Shapes for Packages and Housings

The basic shapes include the following generic shapes: circular cylinders with flat, hemispherical, and conical ends; spheres; oblate and prolate spheroids; and general streamlined shapes such as torpedo shapes.

Of all the shapes considered, the hydrodynamic characteristics of prolate spheroids and torpedo-shaped bodies have been most extensively investigated. Thus, data for these bodies are the most reliable for ocean engineering applications.

The existing data for finite length cylindrical bodies tend to be sketchy and piecemeal. A measure of engineering judgment is recommended in selecting the hydrodynamic data for these components.

However, finite length cylinders are often used to house oceanographic sensors. In a typical situation, as shown in Figure 1 these sensors are subjected to current normal to the cylinder and to mooring line induced motion along the cylinder. The current induces a normal drag on the cylinder which may be determined from a plot of drag proportionality $C_D/C_{D\infty}$ shown in Figure 2 as a function of fineness ratio ℓ/d. Equation (1) gives the form for the drag coefficients C_D and $C_{D\infty}$ where the area $A_D = d\ell$ and d is the diameter and ℓ is the length of the cylinder. Typically, $C_{D\infty} = 1.2$ for the nonvibrating cylinder. As to the forces experienced in the heave motion, added mass is one input to the equation, Equation (4). It is shown as a function of fineness ratio and an acceleration modulus in Figure 3, from Reference 6. The added mass is given as a ratio to the mass of the displaced water

$$m_d = \frac{\pi}{4} \rho d^2 \ell. \qquad (9)$$

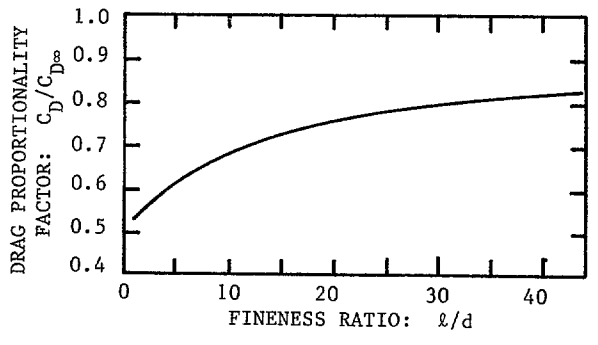

Figure 2 - Drag Coefficients on Cylindrical Bodies in Normal Flow

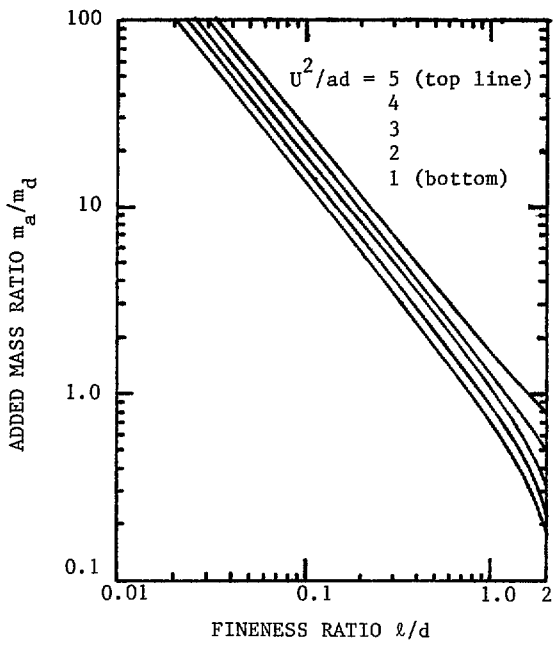

Figure 3 - Added Mass on Circular Cylinders in Axial Motion as a Function of Fineness Ratio ℓ/d and Acceleration Modulus U^2/ad

The acceleration modulus is defined as U^2/ad where a is the half amplitude of a sinusoidal acceleration. In the absence of data on damping on cylinders in axial motion, damping forces are assumed to be quasi steady functions of the drag computed at any instant of time from

$$D(t) = 1/2\rho z^2(t) \frac{\pi}{4} d^2 C_{D\cdot} \qquad (10)$$

where for a blunt cylinder $C_{D\cdot} = 0.83$.

Except for surface buoy applications, which are treated in a later subsection, the typical component sensors usually are located in intermediate and/or great depths of submergence. As shown in Table 1, the dominant hydrodynamic characteristics for this range of depth are the steady force, added mass, and strumming force. Since the strumming force is not considered important in the case of streamlined bodies, ample data exist on the steady forces and added mass for sensor and array components in deep and intermediate submergence. Only limited data are applicable to the case of shallow submergence where the strumming and wave effects are important.

Basic Shapes for Mooring Lines

Typical shapes for mooring lines include bare, smooth jacketed, and faired cable and chain. The cable includes wire rope and other constructions, such as electromechanical cable.

Of all the shapes considered, the most data are available for rigid circular cylinders which are considered simulations of flexible cables. Adequate data are available on bare cables of circular cross-section. There is a need, however, to determine the hydrodynamic characteristics of chains and fairings. Particularly, the added mass and damping coefficients for chains and fairings are needed for the design and dynamic analysis of moored systems.

Bare cables are often used in mooring and towing applications. The hydrodynamic characteristics of cables are quite different from those of cylinders of infinite length. One reason is that cables are flexible. A long cable may respond to a flow in many different modes of vibration, depending on the tension and flow speed. For example, the drag coefficient of a bare cable in a flow speed of 2 knots may differ from that of a smaller bare cable in a flow speed of 3 knots, even if the Reynolds numbers are the same for both cases. The tension, mass, and length of the cable must be considered in determining the proper drag coefficient for the cable in the flow.

Skop, Griffin and Ramberg (Reference 7) have developed a mathematical model which accounts for the interdependence between tension, mass, and length of cable and drag on the cable. In many cases, the model yields drag coefficients which are too high. For example, on a long cable the vibration induced by vortex shedding does not lock on to one distinct mode. A better fit to sea trial data is obtained if the maximum amplitude distribution in the model is reduced to 15 to 25 percent of its computed value, and this reduced amplitude is used in the remainder of the computations. Average drag coefficients of 1.7 and 1.9 are obtained on bare cable at sea.

Published data are available for other mooring line shapes. See Reference 8.

Various Shapes for Buoys

Buoys are considered to include floating bodies, surface and submerged buoys, and appendages of buoys. As components of moored systems, the buoys experience wave, current, and wind loads. The important hydrodynamic characteristics are the damping, drag, and added mass of the buoys, and the response of buoys in waves. Strumming is not an important factor because the drag and wave forces are larger than the strumming force induced by current.

Data available on basic shapes discussed in the last two sections are general enough to be applied to wide ranges of sizes and shapes of moored array components and mooring lines. By contrast, the data available on buoys apply to specific shapes and sizes of buoys and may not be easily generalized.

As a sample of data on buoys, Figure 4 compares the drag characteristics in smooth water of various buoy shapes and sizes listed in Table 3. Here, for the same buoyancy (payload carrying capability) hemispheres and disks have lower drag than do spheres. As another sample, Figure 5 shows the heave response of a spar buoy whose

characteristics are given in Table 4. See also Reference 9.

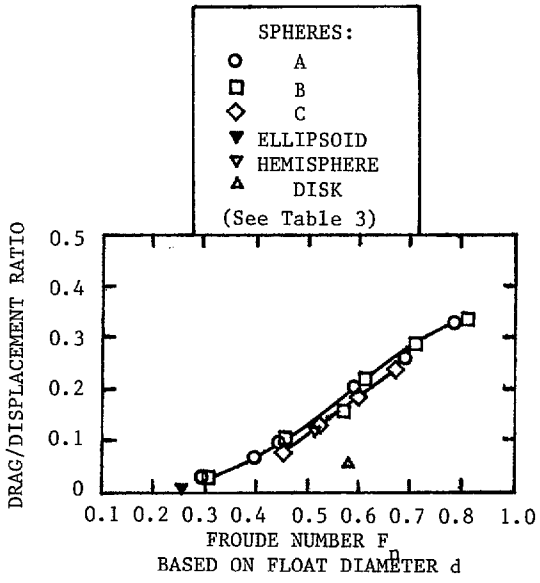

EQUATION: $F_n = U/\sqrt{gd}$

Figure 4 - Drag Characteristics of Spheres and Other Shapes at a Vertical Force to Displacement Ratio of 0.75

TABLE 3. PHYSICAL CHARACTERISTICS OF SURFACE FLOATS SHOWN IN FIGURE 4

Model	Diameter		Weight in Air		Displacement		Note
	in.	cm	lb	N	lb	N	
Sphere A	27.75	70.5	69.1	307	409.1	1820	Aluminum
Sphere B	26.00	66.0	17.5	78	335.3	1492	Rubber
Sphere C	12.00	30.5	14.2	63	32.7	145	Laminated Wood
Ellipsoid	9.50	24.1	17.8	79	32.4	144	Laminated Wood, 19-inch long
Hemisphere	20.60	52.3	10.3	46	75.6	336	Laminated Wood, 9.5-inch high
Disk	18.50	47.0	16.0	71	58.2	259	Laminated Wood, 6-inch high

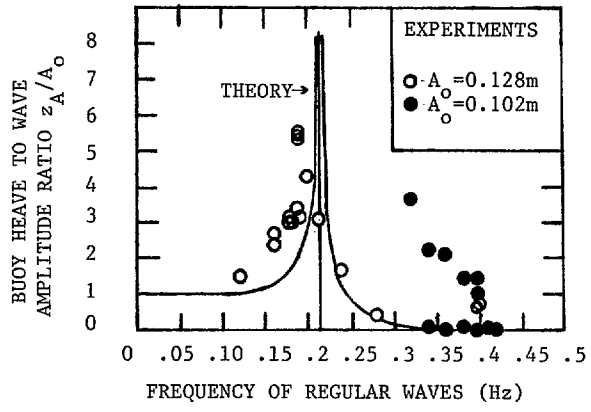

Figure 5 - Heave Response of Spar Buoy Described in Table 4

TABLE 4. FULL-SCALE CHARACTERISTICS OF SPAR BUOY FOR WAVE RESPONSES SHOWN IN FIGURE 5

Buoy Radius	0.2667	m
Overall Length	5.600	m
Mass	1182	kgm
Draft	5.155	m
Fineness Ratio	19.34	
Position of G above Baseline	1.735	m
Position of B above Baseline	2.578	m
$\overline{BG}$	0.843	m
Moment of Inertia	0.304	

G = Center of gravity B = Center of buoyancy

5. Summary and Conclusions

The hydrodynamic characteristics of moored array components such as buoys, cables, fairings, and sensors are available in published and unpublished literature. These data are presented in tables and figures on basic component shapes, on basic mooring line shapes, and on buoys and are presented in terms of hydrodynamic coefficients, added mass and damping, strumming, and wave force and response of buoys.

For the basic component shapes, there are adequate data for the steady flow forces on the shapes either in the submerged or floating condition. Adequate inertia and damping coefficients also can be found or calculated with existing methods. Inadequate data exist for strumming forces, body responses to strumming excitation, and the effects of interference from appendages, attachments to mooring lines, or other nearby components on the hydrodynamic characteristics of the basic component shapes.

For the basic mooring line shapes, there are adequate data on the drag and strumming forces but inadequate data on the inertia and damping characteristics. In addition, the hydrodynamic data on chains are inadequate. It should be noted that the data for cables are either obtained from rigid cylinders or from short cables. The hydrodynamic characteristics of long mooring cables in water are being investigated as parts of ongoing research programs.

For the available buoys, there are adequate data sources for the flow forces and the inertia and damping coefficients. Data are inadequate on the effects of appendages on the hydrodynamic characteristics of buoys.

A systematic evaluation of the literature on basic shapes of moored array components indicates a lack of data on the effects of vibration on their hydrodynamic characteristics. A component, being a part of a moored system, is always in a state of motion. As a result, the flow forces of drag and lift, and the inertia coefficients on a vibrating body are different from those on a body stationary in the flow. An experimental program is needed to evaluate the effects of vibration on the hydrodynamic characteristics of streamlined bodies.

The effect of the length of a flexible cable on the hydrodynamic characteristics of cables and cable fairings is not fully resolved. Analytical and experimental studies are necessary to investigate the responses of moored systems to various environmental conditions.

The effects of the interference of other components on the hydrodynamic characteristics of moored array components are not yet known. An experimental program is suggested to study these effects.

References

1. Morgan, W. B., "Testing of Hydrofoils and Propellers for Fully Cavitating or Ventilated Operation," 11th International Towing Tank Conference, 1966.

2. Berteaux, H. O., BUOY ENGINEERING, John Wiley & Sons, Inc., New York, 1976.

3. Albertson, N. D., "A Survey of Techniques for the Analysis and Design of Submerged Mooring Systems," U.S. Naval Civil Engineering Laboratory, Technical Report R-815, August 1974.

4. Dillon, D. B., "An Inventory of Current Mathematical Models of Scientific Data-Gathering Moors," Hydrospace-Challenger, Inc., Report TR 4450 0001, February 1973.

5. Berteaux, H. O. and N. K. Chhabra, "Computer Programs for the Static Analysis of Single Point Moored Surface and Subsurface Buoy Systems," Woods Hole Oceanographic Institution, Technical Report WHOI-73-22, March 1973.

6. Holler, R., "Hydrodynamic Effect of Harmonic Acceleration," Naval Air Development Center Report AESMTM-29-71, 1971.

7. Skop, R. A., O. M. Griffin and S. E. Ramberg, "Seacon II Strumming Predictions," Naval Research Laboratory Memorandum Report 3383, October 1976.

8. Folb, R., "Experimental Determination of Hydrodynamic Loading for Ten Cable Fairing Models," David W. Taylor Naval Ship Research and Development Center, Report 4610, November 1975.

9. Dern, J. C., "Unstable Motion of a Spar Buoy," 9th Symposium of Naval Hydrodynamics, ONR, 1972.

MOORING COMPONENT PERFORMANCE KEVLAR MOORING LINES

G.A. Fowler
Atlantic Oceanographic Laboratory
Bedford Institute of Oceanography
Dartmouth, Nova Scotia
Canada B3L 4A2

R. Reiniger
Atlantic Oceanography Laboratory
Bedford Institute of Oceanography
Dartmouth, Nova Scotia
Canada B3L 4A2

Abstract

Kevlar[R] ropes used as oceanographic mooring lines potentially offer the advantages of corrosion resistance, low stretch combined with high strength and low specific gravity. Tests completed at sea to date on a variety of line constructions to evaluate the performance of the material in the ocean environment, have resulted in ambiguous but dissapointing results. Strength degradations have been noted that reduce its desirability as a long term mooring line material. More testing must therefore be completed to determine the reasons for the noted strength reductions so that methods or eliminating the problem may be found.

1. Introduction

The scientific use of data obtained from oceanographic moorings is influenced by overall mooring configuration which in turn depends upon the performance of its individual components. In particular the choice of line material plays a key role in the determination of the maximum mooring length and operational life of the system. Kevlar mooring lines offer definite advantages such as high strength, low stretch corrosion resistance and low specific gravity over metallic lines as described by Swenson (1975) and Ferer and Swenson (1976).

This paper describes some of the work that has been conducted at the Bedford Institute of Oceanography to evaluate Kevlar 29 as a potential mooring material so that moorings could be set without restriction of location for extended periods of time. The mooring line sought was a direct replacement for the 3 x 19, 5 mm (3/16" nominal) stainless steel wire presently used in the Institute's field programs. The wire is prepared by hand-splicing terminations, which are potted in zinc for cathodic protection and, typically, experience 6-month exposure on taut-line subsurface buoy moorings. It was anticipated that the use of Kevlar would extend operational life to 12 months or more and allow current meter data to be collected throughout a 5000 m water column.

2. Test Program

Extensive work has been carried out in laboratory conditions to evaluate the performance of Kevlar as a mooring material (Horn et al., 1977). However, before it can be considered as an operational mooring material information on its performance at sea must be collected. Therefore, a program to assess Kevlar under typical environmental and operational conditions was initiated.

In addition to assessing material performance it was important to learn methods of handling the material and adapting it for use in on-going field programs. Termination techniques which would give good strength conversion results while being quickly and reliably completed by field personnel were thus accorded prime importance in the study.

Because of the nature of the tests run, two restrictions on the results obtained must be mentioned. Firstly, Kevlar samples or longer lines were placed in moorings with loading factors determined by the scientific program. No attempt was made to include or assess the effect of transient forces such as those encountered in the anchor last setting technique employed or experienced during recovery. Secondly, the number of samples, was small so that some concern with statistical significance exists.

As is the case with conventional materials the construction of the strength member is of major importance. For Kevlar it is even more critical in that it determines, in large measure, the type of termination that should be employed. However, concern over the type of termination to be used played no part in the initial purchase of material. Four Kevlar rope constructions with breaking strengths in the desired order of 2000 kg (4400 lb) have been acquired during the past two years for evaluation in operational use as summarized in Table 1.

Rope samples were first terminated and tested in the laboratory to establish a tested rating

---

R Kevlar is the registered trade mark of EI duPont de Nemours and Co.

Table 1. Types of Kevlar Mooring Lines Evaluated

Type	Construction	Impregnation	Diameter (mm)	Jacket
A	1 x 19	Polyurethane	5.2 (0.205")	Extended polyurethane
B	3-layer braid	Polyurethane	6.1 (0.240")	Braided dacron
C	7 x 7	Polyurethane	5.3 (0.210")	Braided bonded nylon
D	Single braid	Wax	6.4 (0.250")	Braided nylon

NOTE: In addition to the rope types outlined above two other samples, of parallel construction, were acquired but never used at sea because of very light or nonexistent impregnation and very loose jackets.

rather than the manufacturer's listed breaking strength. Test lengths were then subjected to limited exposure on an uninstrumented mooring before inclusion on an operational system. However, before this stage was accomplished it was necessary to achieve a measure of competence in the termination of each rope type. Originally mechanical terminations as recommended by the manufacturer were tried but were discarded in favour of splicing techniques. For field work where the rope must be wound on winch drums and passed over sheaves the mechanical terminations were felt to be too rigid while splicing was more attuned to the material. Similarly, potted terminations were not used operationally because of inflexibility, erratic results obtained and the fact that they were not considered to be field installable.

Kevlar lines constructed in the same manner as conventional wire rope (Types A and C) a simple "liverpool" (or long splice) with a minimum of 10 tucks and covered with a mastic adhesive lined heat shrinkable tubing was found to produce a quick and robust termination. However, initial tests with this termination gave results with wide scatter. Various methods of completing the splice including varying the number of tucks, up to 15, and varying the tension in the rope being spliced were tried with no observed improvement. A very compact tight splice is obtained if each strand of the bitter end is given a full 10 tucks around a standing strand rather than to tuck each bitter end strand once in sequence, but scatter improvement was minimal. The braided ropes do not lend themselves to conventional splicing techniques but a method described by the Wall Rope Co. involving the weaving of a grip was used with good results. In the case of the three-layer braid rope, a time of close to two hours was required to complete each termination. For our operations this is excessive.

With a bonded braided jacket one of the most time-consuming parts of the termination procedure is the jacket removal in the area to be terminated. A soldering iron with a 370°C (700°F) fine tip makes this job easier and also reduces the possibility of damage to the strength member.

Several moorings (Table 2) were set at different loading factors (fraction of breaking strength) the exposure periods were dependant primarily on the scientific operation and therefore left in place for periods ranging from 3 to

Table 2. Kevlar Moorings and Duration

Type	Depth (m)	Mooring Length (m)	Exposure (month)	Loading Factor (%)
A	240	200	2½	12.5
B	240	200	3	12.5
	170	130	3	12.5
	5180	1180	6	19
	60	30	14	12.5
C	60	30	3	12.5
	170	130	3	12.5
	5400	1400	6	25
	5400	1400	6	25*
D	60	30	3	12.5

* This mooring includes a 750 m length which had experienced a previous 6-month exposure.

14 months. Figure 1 shows a typical deep water mooring on which Kevlar materials have been exposed. Current meter records on these deep water moorings have shown mean currents of 4 to 10 cm/s; however, maximum speeds were in general between 30 to 40 cm/s. Also, the records have shown occasional peaks as high as 60 cm/s over a time period of 1 to 2 months.

After the moorings were recovered samples were cut from the line to produce terminated specimens 1.5 m long. Exposed terminations were cut so as to produce suitable test specimens thereby allowing comparison between material with an exposed termination and material taken from the body of the rope. Samples were taken from unabraded sections of the rope and terminations which showed obvious damage were not included in the test results.

3. Mooring Line Test Results

Tests of the 1 x 19 construction rope (Type A) were discontinued after one trial at sea since it exhibited excessive torque imbalance. It was also found that the polyurethane jacket was extremely prone to damage which made the choice of test samples difficult and produced questionable test results.

The three-layer braid rope (Type B) stood up well at sea, in part because of the durability of the braided dacron jacket. Although the dacron jackets are tough they do add to the diameter of the assembly, 28% as opposed to 12% for braided nylon jackets in the rope size tested. However, its use was also discontinued when strength losses in the terminations reached the unacceptable levels shown in Table 3. Breaks were mostly located right at the end of the exposed terminations. However, when companed with the results later obtained with other rope types these strength losses were not significantly higher. The long term mooring (14 months) was placed before tests on the Type B material was completed and when it was recovered test results contradicted the results previously obtained. The variability of test values constitutes a major difficulty in the evaluation of the material. It should be noted that the latter mooring was set and recovered in an inshore area without the need for spooling the rope on a winch either during setting or recovery.

The 7 x 7 construction (Type C) has the advantage of almost zero torque imbalance and can be easily terminated with conventional techniques but with the reservation of erratic results noted above. Break strength data shown in Table 3 indicate that degradation can be appreciable. The 12-month data is obtained from so few samples that it must be considered with caution, also the noted degradation in the rope of 18% on the 3-month mooring is questionable since the four tests were split with two very high and two very low breaks. These comments aside, there is evidence of a negative effect of exposure which is not

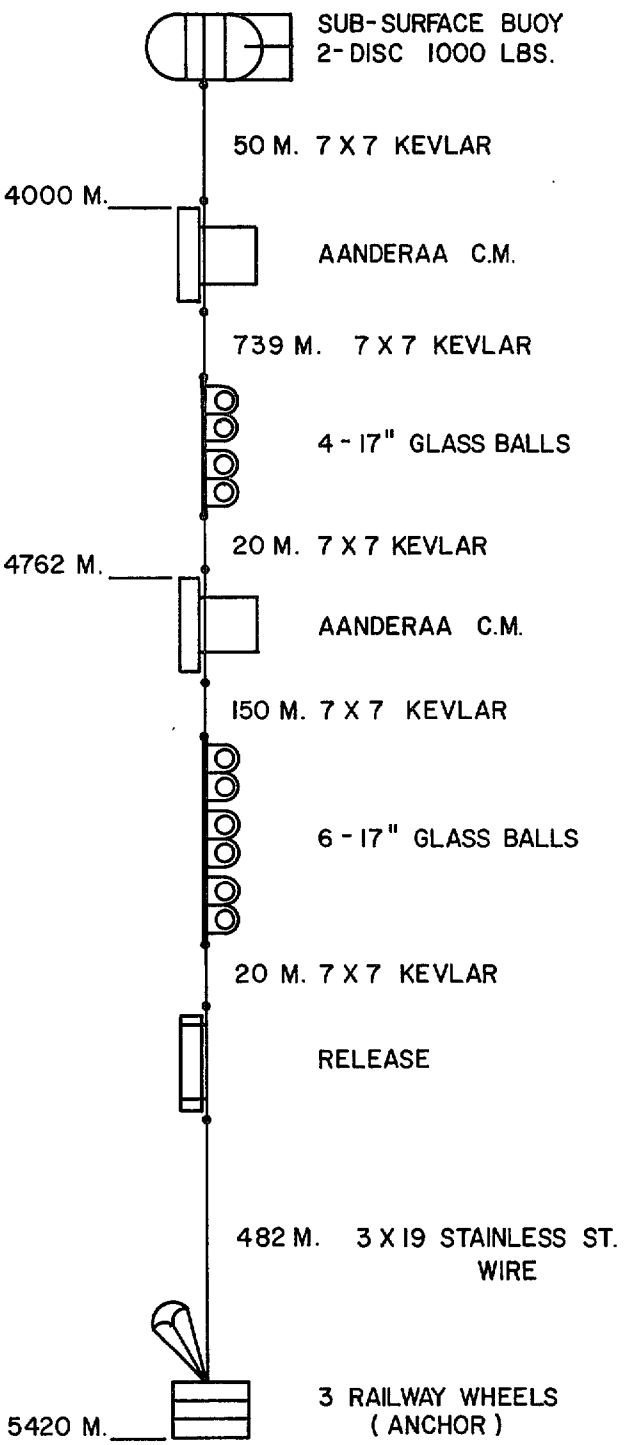

Figure 1. Typical Deep Water Oceanographic Mooring.

Table 3. Strength Degradation of Kevlar Rope and Terminations after Mooring Explosure

Type	Tested Break Strength kg	Exposure month	No. of Samples	Strength Reduction % (Deviation as % of Sample Means) Rope	Termination
B	1910 (4200)	3	4 16	9	19(10)
		6	4 6	9(2)	29(17)
		14	2 5	20(4)	14(7)
C	1920 (4230)	3	4 5	18(12)	13(12)
		6	21 13	9(7)	18(8)
		12	2 1	20(0.5)	23
D	2430 (5350)	3	2 4	6(3)	20(9)

readily explained. The nylon jacket used on this rope abraded much more readily than the dacron jacket employed in Type B. In addition, the latex material which bonds the jacket to the strength member softened after submergence and may affect the re-use of this material.

The results from one shallow mooring trial only are available on the single braid rope (Type D) but it appears to be following the same trend as the three-layer braid (Type B) with excessive strength losses at the end of the terminations. Further tests at the 6- and 12-month time periods will have to be completed before any conclusion can be reached on the usability of this material/termination combination.

4. Operations at Sea

Kevlar mooring lines are well adapted to use at sea with the material's lightness, flexibility and resistance to twist being the salient 'deck' advantages. Extra care, however, must be taken to avoid abrasion of the material or jacket particularly during the recovery of a mooring where the potential for fouling is extreme. Redesign of some mooring components, back-up buoyancy packages for example, will have to be carried out to eliminate sharp edges which contribute to mooring line abrasion. Slight modification of the anchor last mooring technique is required in that the ship must be slowed from the speed normally used when deploying an all metallic mooring. The lighter Kevlar lines do not form a catenary to the same extent as the wire with the result that greater snap loading can develop.

5. Conclusion

Of the Kevlar mooring lines which have been examined for possible use as an operational material in direct replacement of metallic lines, none can be judged as offering the desired quality of assured extended operational life.

The testing procedure employed, that of placing the material in the ocean environment complete with all the shipborne hazards, may have caused the contrast with results obtained in the laboratory. But since the material must eventually be used in that role it is essential that confidence in its performance at sea be gained.

The engineering and scientific benefits which would accrue from the use of Kevlar in oceanographic moorings certainly justify further experimentation. However, at present there is no economic justification for use of the material, considering the price differential over metallic lines, can be made.

References

1. Swenson, R.C., "The cable development programs for suspended sensor applications," Naval Underwater Systems Center, New

London, CT, 22 September 1975, NUSC Technical Report 4915.

2. Ferer, K.M. and R.C. Swenson, "Aramid fibre for use as oceanographic strength members," Naval Research Laboratory, Washington, D.C., November 5, 1976, NRL Report 8040.

3. Horne, M.H., P.G. Riewald and C.H. Zweben, "Strength and durability characteristics of ropes and cables from Kevlar Aramid fibres," MTS-IEEE Ocean '77, pp. 24E-1 to 24E-12.

4. Walden, R., "Tests of Kevlar as a new mooring material," Polymode News No. 15, September 1976.

5. Ferer, K.M., "Effects of long term tension on Kevlar Aramid fibre," Naval Ocean Research and Development Activity, May 1977, NORDA Technical Note 8.

SPECIFYING AND USING CONTRA-HELICALLY ARMORED CABLES FOR MAXIMUM LIFE AND RELIABILITY

ALBERT G. BERIAN

THE ROCHESTER CORPORATION

Abstract

The importance of complete information regarding system parameters in the specification of a cable is discussed. System parameters to be covered include cable performance and mission profile, environmental consideration, verification testing, the cable handling system and connection features. The impact of these parameters on the material and construction features of the cable is discussed in terms on the effect on life and reliability.

The mechanical effect of various cable handling operations are related to life and reliability. Successfully used spooling procedures, the trade-offs for zero rotation torque balance in and the major factors affecting flexure fatigue life are studied. The effects of corrosion in a salt water environment together with successful techniques currently being used to minimize this corrosion are also studied.

1. Introduction

The major limiting factors for contra-helically (C-H) armored cables used in the marine environment are:

- misapplication
- mishandling
- corrosion

in order of importance. The bases for misapplication of a cable include: (1) incomplete specification, including a description of the mission and ancillary cable handling system and (2) compromizes in cable design due to late consideration in the system design. Misapplication, therefore, is primarily due to lack of an information exchange between the systems designer and E-M cable designer or applications engineer.

A cable which is properly designed for a system can be damaged by mishandling such as:

- using improper spooling techniques
- using an incorrect sheave groove and/or pitch diameter
    - overrunning
    - overloading

Some of this mishandling is negligence but many cable failures have been attributed to a misunderstanding of E-M cable characteristics and limitations. This constitutes another communication gap between the cable handling personnel and the cable manufacturer. Another possible reason for mishandling is lack of knowledge of the interaction between the cable and handling system components.

The corrosion effect of salt water on the material of the strength member and the associated returement criteria should be evaluated in establishing the mission objective of the cable. Although the diameter reduction of isolated steel wires in stagnant and flowing salt water have been test determined, the application to the E-M cable composite is very difficult. The effects of current flow in metallic strength members has been observed but not quantitively established. Cathodic protection of exposed metallic strength members is being successfully used for large metal masses, but it has not been studied as a corrosion preventative technique for steel contrahelically armored cables.

The importance of communicating a thorough desciption of the performance, environment, handling system and connections to the C-H cable supplier is shown to be necessary in order to obtain the optimized design.

2. The Contra-Helically Armored Cable Specification

Specification Structure and Coverage

Information necessary for the proper specification of E-M cables includes:

- desired electrical and mechanical performance and their interaction during the objective cable mission life including storage, shipment and operations.
- life cycle objective
- environmental impact including pressure, temperature, temperature shock, fluids (salt water, oils, etc.), mechanical (strumming, vibration)
- type of system and major mechanical loading characteristics (Ref. 1)
- characteristics of the E-M cable handling

and deployment system
- electrical and mechanical terminations
- test verification of the design

Performance vs. Construction Specification

In many applications the systems designer becomes inclined to specify the major construction characteristics of the desired E-M cable. The primary motivation for this approach is usually timesaving because the use of a construction specification can shorten the initial procurement cycle. The disadvantage of this approach is firming of the specification before the cable manufacturer has an opportunity to incorporate experience relative to appropriate materials and constructions for meeting the specification elements as discussed in Ref. 2.

The by-passing of the performance specification also avoids the opportunity for an effective trade-off study wherein reliability and life are evaluated for various costs, diameters and weights of the E-M cable. The several types of available strength member designs, as discussed in Ref. 3, encompass a variety of configurations and metal and coating techniques, providing wide latitude of selection for the cable designer.

Test Verification of Performance Capabilities

The strength member properties of major concern are usually breaking strength and flexure fatigue life over sheaves. Other characteristics which are important to determining usage limits include stress-strain and load-rotation.

Whenever possible the test procedure should include comparative testing of the new cable or construction with one previously tested in the same equipment using the same procedures to permit correlation of the new cable performance with that of a cable having some operational history.

Conditioning of the cable specimen is an essential part of a test specification to insure that the strength member elements have their proper stable relative relationship for maximum mutual support. This condition can be verified by the specimen exhibiting a repeatable stress-strain characteristic. A typical decline in the constructional stretch, or that which is non-repeatable, is illustrated in Exhibit 1.

Handling System

A major function of the strength member of E-M cables is mechanical protection of the electrical components. As discussed in Ref. 2 the outer metal strength member types provide the best protection while the synthetic fibers and center strength member designs offer minimum protection. The limits of this mechanical protection can be exceeded by improper design of handling equipment or by use of improper procedures.

Major characteristics of the handling system of importance to the cable specification are bend diameters (winch drums and sheaves), reverse bends such as in some load measuring heads and type of traction winch or capstan. When the system is committed to the use of particular equipment some compatability provisions can sometimes be made in the cable design.

Terminations

Compatability of potting and molding materials with cable insulations and jacket compounds should be considered. The use of polyurethane as a molding and potting compound has become very popular becuase of its versatility. However, a bond of polyurethane to some commonly used insulating compounds such as polyethylene and polypropylene is difficult.

To obtain the multiple pressure carriers which may, as discussed in Ref. 4, include sealing of the conductor insulation, cable jacket and connector body to the potting/molding compound, those materials having proven bonding properties should be specified and selected.

Armor terminations can usually be adapted to any strength member design. The desire for field repairability has encouraged the use of epoxy potted or locking cone assemblages.

3. Cable Handling

The life and reliability of a C-H armored cable can be adversely affected by the handling secnario which encompasses all facets of equipment selection and use.

Spooling Tension: This is the operation of transferring cable from a reel which may be the shipping reel to a tension drum. As discussed in Ref. 5 the geometric objective of proper spooling onto a tension winch drum is to uniformly wind the cable so that maximum diametral support is provided to all turns. Contrahelically armored cable has a greater crushing resistance when all components are tightly held in a stable, mutually supportive position such as occurs when the cable is under tension. The problem of proper spooling onto a storage drum whereby the load tensions of the cable are assumed by a traction winch or capstan is relatively noncritical. In the many systems using tensioning winches, however, proper spooling technique is mandatory in order to avoid cable damage. When several layers are spooled onto a winch drum under tension the drum and inner cable layers can be damaged under the high compressive force. A proper spooling procedure will provide for sufficient spooling tension to insure a uniformly firm, crush-resistant cross-section but not high enough to impose a crushing load on the winch drum.

This idealized tension will vary from a maximum at the layers near the drum to a minimum on the outer layers. The maximum tension will generally not exceed 50% of the cable breaking strength. As a generally applied rule, the spooling tension should equal expected service tension profile which will include the sum of loads due to buoyed cable weight, payload and friction or drag forces.

A spooling tension schedule which applies to a vertical cable deployment is illustrated in Exhibit 4. Note that the approximate slope of 1½% of cable breaking strength per 1000 ft. of cable deployed can also be expressed as about 90% of the cable weight per 1000 ft. in air. A procedure which has proven satisfactory is to reduce the tension by ½ the slope value every 500 ft.

Grooved Sheaves

The use of these sleeves has been successful because they provide:

- correct cable spacing on the first and successful layers to form the basis for spooling with a double break; i.e. two one-half pitch offset movements per drum revolution.
- support for the bed (inner) layer by increasing the bearing surface area and therefore reducing the bearing pressure, P_B, expressed as:

$$P_B = \frac{2T}{Dd}$$

P_B = bearing pressure, lb./sq.in.
T = cable tension, lb.
D = groove pitch diameter, in.
d = cable diameter, in.

Spooling with a Double Break on an Ungrooved Drum

To achieve the two ½ pitch offset movement per drum rotation, two filler strips are needed. Their length should be ½ the drum circumference and the diameter, or thickness, should be about 0.54 times the cable diameter being spooled.

As shown in Exhibit 5 the drum is layed out by scribing a line across the drum at 90 degrees to the flange at a point about 2 in. behind the cable entry hole.

The cable is started onto the drum against the flange and one spacer is inserted after a 180 degree rotation. The spooling is continued with the coils tight so that the ½ breaks start at the scribed lines.

At the opposite flange the second spacer is located 180 degrees from the first. The last cable coil should fit snugly against the drum flange and filler. As spooling continues the cable will enter the valley formed by the bed layer and proceed in the opposite direction.

Sheave and Drum Diameters

A rule of thumb for establishing the minimum pitch diameter is to multiply the diameter of the largest wire by 400. A cable having the largest wire of 0.030" dia. in the armor would have, by this rule, a minimum bend diameter of 12 inches. The consequence of bending over a smaller diameter is a reduced flexure fatigue life.

Comparative tests on wire rope has shown a 2.5-3.5 times increase in fatigue life as the sheave to cable diameter ratio (D/d) was increased from 15 to 25 times. The relative service life for various D/d = T ratios can be approximated by:

$$\frac{T_2^2}{T_1^2}$$

When T is increased from 12 to 25 the service life would be increased by:

$$\frac{625}{225} = 2.78 \text{ times}$$

The similarily of wire rope and C-H armor constructions suggests that these relationships may also apply to C-H armored cables. Insufficient data are available at this time to verify this assumption.

Torque Balance

The generic term "torque balance" is an incomplete description of a cable characteristic. Additional information required is the tolerance in terms of the amount of rotation at a tensile load and is expressed in degrees per foot.

The construction effect of decreasing the rotation characteristic of a C-H armored cable is illustrated in Exhibit 6. In this example, different armor assemblies were applied over the identical core. The armor construction of Cable B is a standard 24 x 24 wire which is used on many logging cables. To improve the torque ratio, R_T, from 2.00 to 1.04, the metal ratio of the outer and inner armor layers had to be reduced from 1.6075 to 0.9683 and it was accomplished by an increase in the inner armor wire diameter and decrease in the outer armor wire diameter. The resultant rotation decrease from 18.28 degrees per foot to 0.67 degrees per foot was obtained by trading off other advantages, such as:

- the larger outer armor wires of cable B are more resistant to snagging and wear
- the larger cable B outer armor wires have a greater preform spring constant and will therefore tend to be more stable and remain tightly wrapped over a longer service life.

The advantage of near zero rotation balance is greater kink resistance and elimination of the damaging consequences. The mechanism of kink formation is initiated when a large amount of torsional energy, developed by the rotation and unbalanced torque, is suddenly released by a step decrease in tension. This condition can occur when a load is allowed to strike a fixed surface (a condition termed over-running) or the tension is suddenly released at the support end.

When the load is slowly released from an unbalanced cable the slow counter-rotation will permit the torque in the armor wires to overcome the high inter-armor friction and initiate a return rotation to the original angular position.

The sudden load decrease prohibits initiation of this return process and loops form in the cable-the reverse process of coiling a cable. There is

a tendency of developing one loop or coil per rotation of the cable. If the cable is allowed to remain unloaded or the load was reapplied very slowly, the normal return rotation could occur. However, upon a sudden reapplication of tension the diameter of these coils or loops decrease to the point where the armor wires are permanently deformed. In extreme cases the very tight inner armor can form a separate loop which emerges between the outer armor wires.

Fatigue Life over Sheaves

When C-H armored cable is flexed, either over sheaves or other handling equipment, the armor wires experience high rubbing contact forces. Evidence of wires becoming repositioned is in the crackling sound heard when these cables are winched at high tension. Operational conditions which increase the amplitude of this relative armor wire motion, the bearing pressures and the friction all tend to increase wear and shorten the flexure fatigue life.

The major factors which contribute to this increased armor wire wear include:

- diameter of sheaves and drums; the smaller diameters increase the motion amplitude and bearing pressure.
- winching under a high load; the bearing pressure between armor wires increases with increased cable tension.
- lubrication; as for any rubbing metals, good lubrication will decrease friction and reduce wear.
- contamination; mud, sand, rust or other abrasive materials trapped between armor wires will increase wear.
- winching speed; the higher speeds will accelerate the effect of other wear-inducing conditions. In extreme cases, individual armor wires may yield because of having insufficient time to relocate to a stable position in the armor assembly.

4. Corrosion

The most commonly used armoring material is galvanized improved plow steel which is usually coated with a corrosion preventive compound. This compound can be flushed from the cable after a short service life, leaving the galvanized coating unprotected. By corrosion and abrasion, the galvanized coating, in turn, may be removed and corrosion of the basis steel is initiated.

To avoid the source of much corrosion, the salt water trapped between armor layers, flushing with fresh water or spraying with a lubricant/inhibitor will greatly extend the cable life.

Additional protection for GIPS can be obtained by jacketing overall. This technique protects the armor even if punctured. It appears that the water which accumulates under the jacket becomes saturated with zinc ions and therefore becomes neutral with respect to the steel. Over a long time period, however, these ions will tend to dissipate and leave a normal salt water corrosion condition.

The sea water corrosion of unprotected steel has been measured as a surface reduction of:

- .003" to .008" during the first year
- .001" to .005" thereafter

Alternate materials to GIPS for corrosion resistance include stainless steel, Inconel and beryllium copper. The stainless steels have proven somewhat disappointing; for example, the following are data for tunnel attack on samples of stainless steels are 2340 feet depth in a North Atlantic harbor.

AISI	Length of Tunnel Attack
302	6 inch
304	2 inch
306	0.5 inch

Some cable users have reported that crevice corrosion of stainless steels can be greatly reduced by using zinc anodes and some others report success with mild steel anodes.

The high cost of Inconel and other highly corrosion resistant materials has prevented their broad use.

5. Conclusions

The reliability and life cycle cost of oceanographic systems using contra-helically armored cables can be greatly improved by considering cable and connection requirements during system design. The cable and connector specification should include all operational, environmental and handling system information to permit selection of optimum materials and concepts.

The selection of handling system components should be made with consideration of the effects on the mechanical action of armor wires. The internal armor friction and wear will increase with larger and faster movements within the armor and with decreased lubrication. Bend diameters, winching speeds, contamination and lubrication are major points of consideration in maximizing reliability after the optimum design has been selected.

6. References

1. Stange, Wm. F., "New Synthetic Cables and Terminations for Underwater Instrumentation Systems", ISA, 1977 Annual Conference.

2. Berian, Albert G. and Felkel, Edward M., "Armor Designs Offer a Wide Range of E-M Cable Properties", Oceans 75 IEEE/MTS Annual Conference.

3. Berian, Albert G., "Specifying Electro-Mechanical Cables", Sea Technology, pp. 21-22, July 1975.

4. Berian, Albert G., "Compatability of Underwater Cables and Connectors", Oceans 76 IEEE/MTS Annual Conference.

5. Berian, Albert G., "Design and Handling Factors in the Reliability and Life of Electrical Wirelines", Inter-Ocean '76, June 1976, Dusseldorf, West Germany.

6. Lilly, Joseph C., "The Mathematical Relationship Between the Bending Radius of a Cable and the Length of Cable Lay"

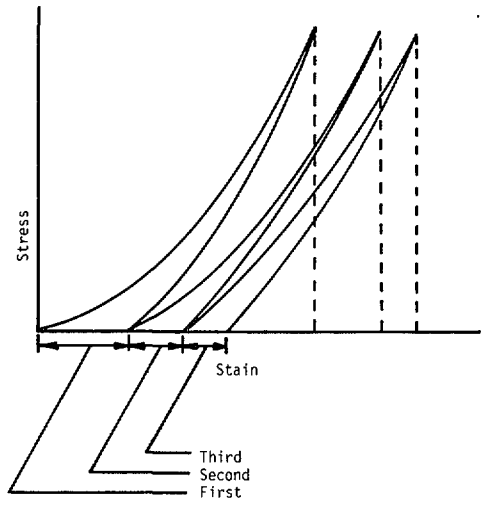

EXHIBIT 1

TYPICAL DECREASING CONSTRUCTION STRAIN OF E-M CABLES

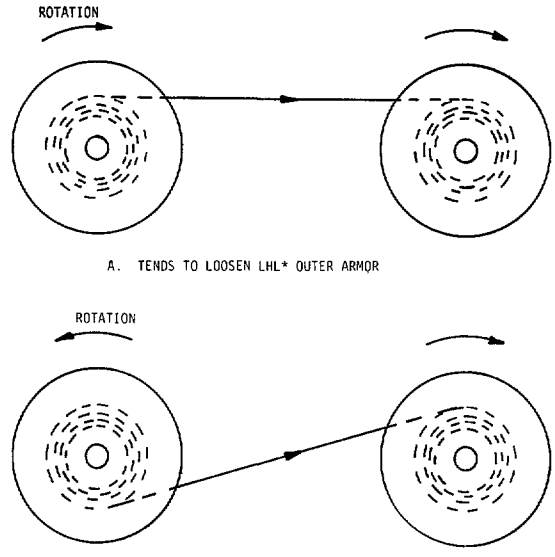

*Left Hand Lay

EXHIBIT 2

EFFECT OF SPOOLING ARRANGEMENT ON C+H ARMOR

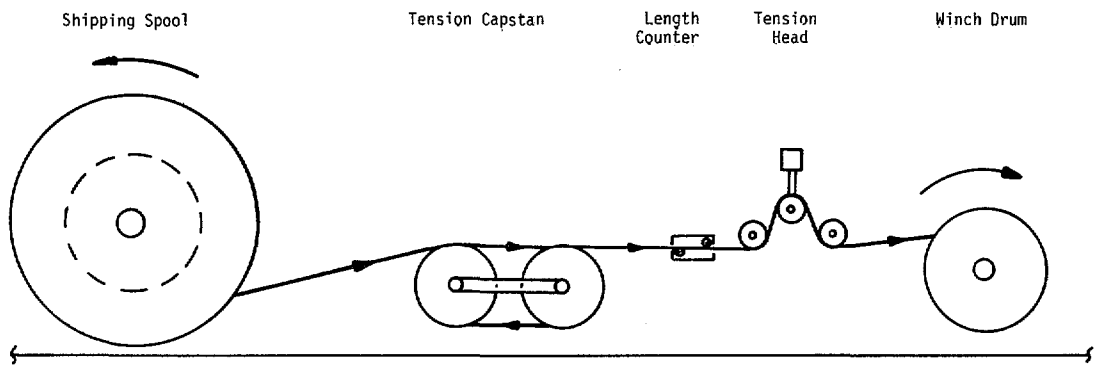

EXHIBIT 3

TYPICAL E-M CABLE SPOOLING SET-UP

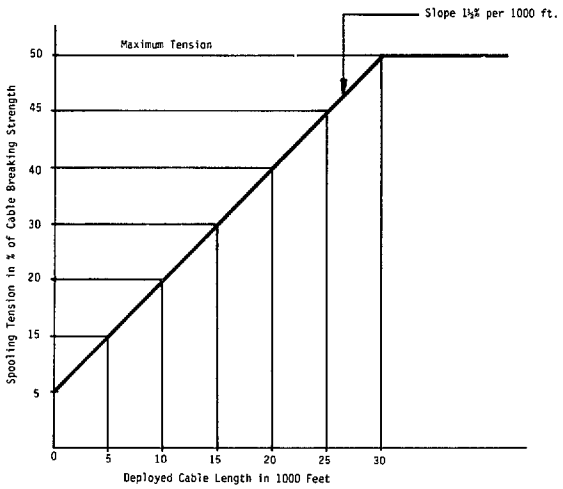

EXHIBIT 4

SPOOLING TENSIONS FOR A TENSION WINCH

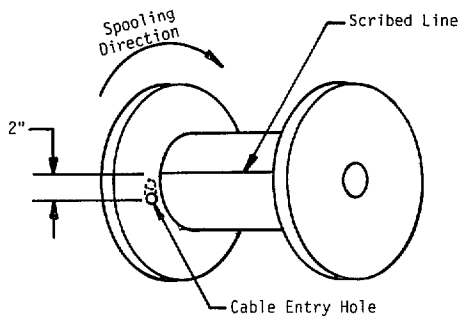

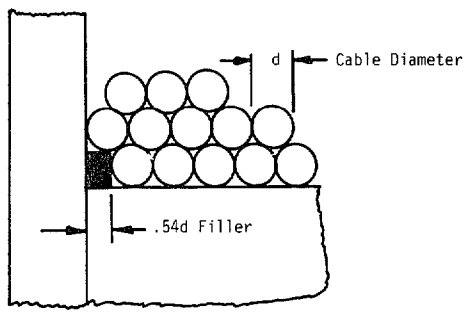

EXHIBIT 5

SPACER AND DRUM LAYOUT FOR DOUBLE-BREAK SPOOLING

EXHIBIT 6

COMPARISON OF CONSTRUCTIONS WITH DIFFERENT TORQUE RATIOS, R_T

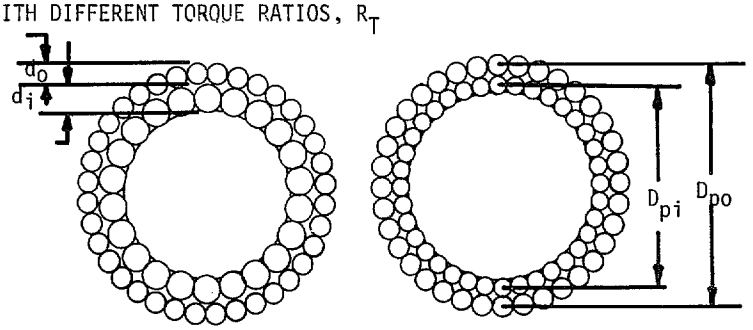

	CABLE A	CABLE B
O.D.	.680"	.675"
Outer Armor $N_o d_o$	36 wires .050" dia.	24 wires .071" dia.
Inner Armor $N_i d_i$	22 wires .065" dia.	24 wires .056" dia.
Pitch diameter, outer, D_{po} In.	.630"	.604"
Pitch diameter, Inner, D_{pi} In.	.515"	.471"
Wire diameter, outer, d_o	25.00×10^{-4}	50.41×10^{-4}
Wire diameter, inner, d_i	42.25×10^{-4}	31.36×10^{-4}
Metal ratio: $\frac{N_o d_o^2}{N_i d_o^2}$	0.9683	1.6075
Torque ratio: $R_1 = \frac{N_o d_o^2 D_o \sin \theta_o}{N_i d_i^2 D_i \sin \theta_i}$	1.04	2.00
Ultimate Tensile Strength, UTS, lb.	31,450	34,300
Rotation at 16,000 lb. deg/ft.	0.67	18.28
ϵ at 16,000 lb. in/in.	0.82	0.93
Weight in air, W_a, lb./1000'	675	665
Weight in water, W_w, lb./1000'	518	512
$\frac{UTS}{W_w}$ (ft.)	64,710	65,960

THE DEVELOPMENT AND TESTING OF CURRENT METERS FOR LONG-TERM DEPLOYMENT ON THE CONTINENTAL SHELF

K. E. Heldebrandt
Texas Instruments, Inc.
P. O. Box 6015
Dallas, Texas 75222

L. S. Trest
Sperry Support Services
National Space Technology Laboratories
NSTL Station, Mississippi 39529

E. D. Michelena
NOAA Data Buoy Office
National Space Technology Laboratories
NSTL Station, Mississippi 39529

Abstract

Measurements of ocean currents to support U.S. continental shelf construction and environmental projects have been established as a major user need.[1,2] Regimes of interest range from the surface to 300 meters and from concentrated, short-term measurements to sparse, long-term measurements of up to 3 years. The timeliness, reliability, and availability of the data are frequently more important to the user than absolute data accuracy. One of the more critical needs of the offshore industries is for measurements of current during design events, such as severe storms. Near-real-time data is also highly desirable during quieter periods to aid on-site construction and to permit timely environmental monitoring in coastal and estuary regions. The NOAA Data Buoy Office (NDBO) has initiated a development and test program to provide current measurement systems to meet these needs. NDBO's objective is to develop this capability using existing state-of-the-art current sensors and data buoys. A parallel effort is also underway to develop an underwater acoustic data link for long-term at-sea testing and operation of the current sensors. This paper presents an overview of the NDBO current meter development and test program, including the implementation plan, significant features of the hardware design, and the results of testing conducted to date.

1. Introduction

A detailed study in 1975 by the Current Meter Review Panel within the NOAA Office of Marine Technology (OMT) established the urgent need for measurement of currents in the mixed layers of the ocean and on the continental shelf, to support marine surveying and offshore construction projects. Major obstacles to satisfying this need were the inability of available current measurement systems to operate reliably and to deliver accurate measurements under the influence of the dynamic ocean environment within these regions. The Working Conference on Current Meters held at the University of Delaware in January 1978, confirmed many of the findings of the 1975 study; the conference also found that neither the need for ocean current data nor the number of associated problems seemed to have diminished.

In 1976, NDBO initiated a current meter development and test program to satisfy many of the established user needs for ocean current measurements. NDBO's objective was to develop current measurement systems for direct applications in the mixed layer and high survivability situation along the continental shelf. Accomplishment of the program objective was based on the judicious selection of the more promising state-of-the-art current sensors, and on a coordinated plan of laboratory testing, field testing, and improvements.

2. NDBO Current Meter Test Plan

Major elements of the NDBO plan for on-going testing and development of a current measurement capability are as follows:

- Selection, procurement, and laboratory test of current sensors that have previously shown good promise in tests or actual use.
- Modification and adaptation of current sensors to facilitate at-sea testing on a subsurface array designed to decouple the sensors from the effect of surface waves.
- Addition of a remote capability to control and monitor the status of current measurement subsystems (CMSSs) from the surface during short-term at-sea testing.
- Short-term at-sea testing to identify defects in design and operational performance.
- Correction of defects, retesting, and modification of CMSSs for near-real-time data transmission to facilitate long-term at-sea testing.
- Addition of full capability for control and near-real-time transmission of current test data to shore.
- Long-term at-sea testing to evaluate reliability and determine operational degradation.
- Post-deployment calibration of CMSSs in the laboratory, correction of defects, and retesting.

3. Test Implementation

Selection, Procurement, and Laboratory Tests of Current Meters. Three ocean current sensors were initially selected for test — the Cushing Engineering, Inc. (CEI) electromagnetic current meter, the Marsh-McBirney, Inc. (MMB) electromagnetic

current meter, and the Neil Brown Instrument System, Inc. (NBIS) acoustic current meter.

Each type employs a different technique to sense and measure current velocity. The CEI and MMB sensors use the electromagnetic principle with orthogonal electric probes, a concept that has been in use for several years. However, the techniques of application are different. The CEI uses a large 7-inch cylindrical flow transducer, whereas the MMB uses a 4-inch spherical transducer. The NBIS type uses an acoustic path-length concept in which the relative time of travel of two simultaneous signals is used to determine current velocity. The basic considerations in the selection of these models over other available designs were their lack of moving parts in the sensor, their potential for accurate measurements in the mixed layer, potential for high reliability and survivability in extreme environmental conditions, and the favorable early test results of the transducer concepts.

Three of each type of current meter were procured by NDBO for testing. The original design of each was modified to meet a common electrical and mechanical interface specification and to provide a capability to respond to data rate and status request commands from external controls.

Each CMSS measures and records mean values of east and north ocean current vectors, as well as the time the mean was taken and the operational status of the CMSS at that time. Data is sampled at a 1 Hz rate, and a 5-minute mean is computed either every 5 minutes or every 3 hours, depending on the external data rate command. Other sampling and data rates are available by adjustment of internal controls. The cassette tape recorder is standard in all CMSSs, and the recording format has been standardized. Each type has an internal data recording capacity of over 1 year at normal data rates, and is designed to operate to a depth of 300 meters and with a mooring line tension of up to 10,000 pounds.

The CEI CMSS (designated Model LCD 612 In Situ Velmeter[3]) is shown in Figure 1. The pressure housing is 64 inches long, with an outside diameter of 7 inches; the total length is 89.5 inches. It weighs 95 pounds in air. This design has a cylindrical flow sensor large enough to house all subsystems. The sensor incorporates an alternating electromagnet and two orthogonal pairs of flow detection electrodes located near the center of the housing and attached flush with the outside container. Figure 2 is a functional block diagram of the basic unit.

Each pair of electrodes senses a voltage proportional to the component of velocity perpendicular to the plane determined by the axis of the electrode pair and the sensor longitudinal axis of symmetry. These voltages are conditioned and resolved into east and north components of current by a vector rotator using the output of a fluxgate compass which is proportional to the angle of the electrode pair relative to magnetic north. The current components are then processed into mean values and recorded incrementally on magnetic tape.

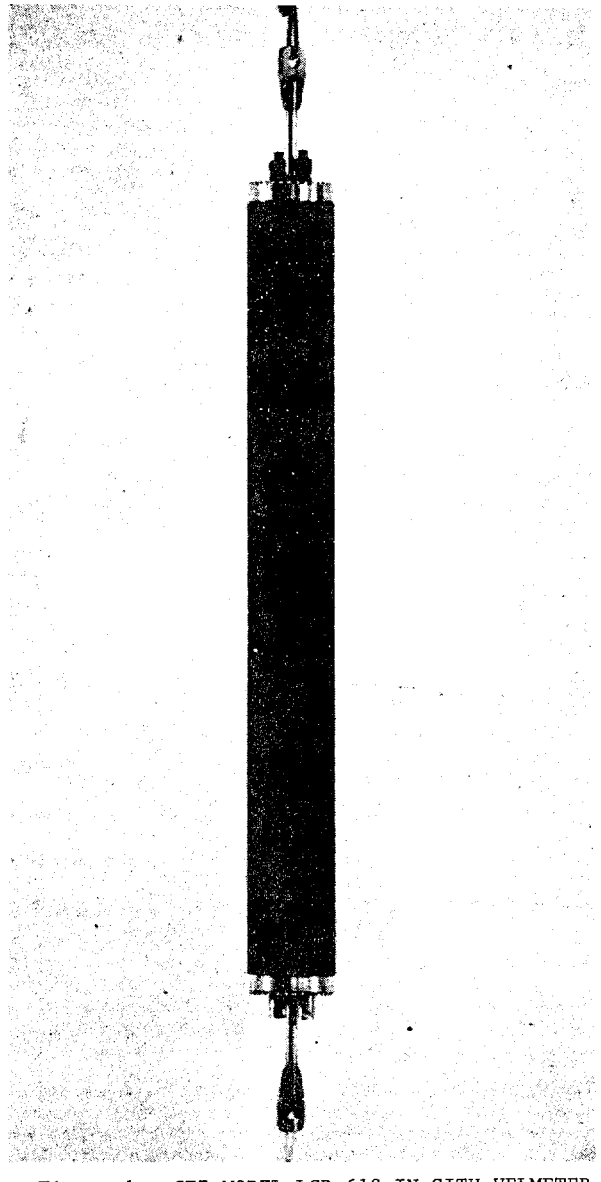

Figure 1. CEI MODEL LCD 612 IN-SITU VELMETER

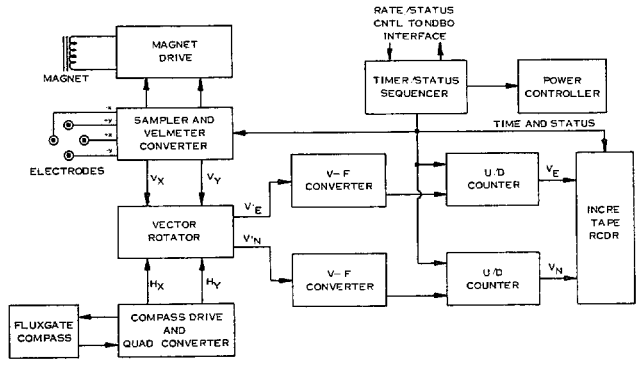

Figure 2. BLOCK DIAGRAM, CUSHING ENGINEERING, INC., IN-SITU VELMETER

Figure 3 shows the MMB CMSS (designated Model 585 Adaptive Recording Current Meter[4]). The pressure housing is 42 inches long, with an outside diameter of 7 inches; the total length is 60 inches. It weighs 95 pounds in air. This sensor has a spherical electromagnetic water velocity sensor with two orthogonal pairs of flow detection electrodes. A digital geomagnetic compass measures the orientation of the current meter with respect to the magnetic meridian. A microprocessor-based data acquisition system resolves the current vectors into east and north components of current, computes the means of these components, and transfers the mean values to an incremental tape unit for recording. A functional block diagram of the system is shown in Figure 4.

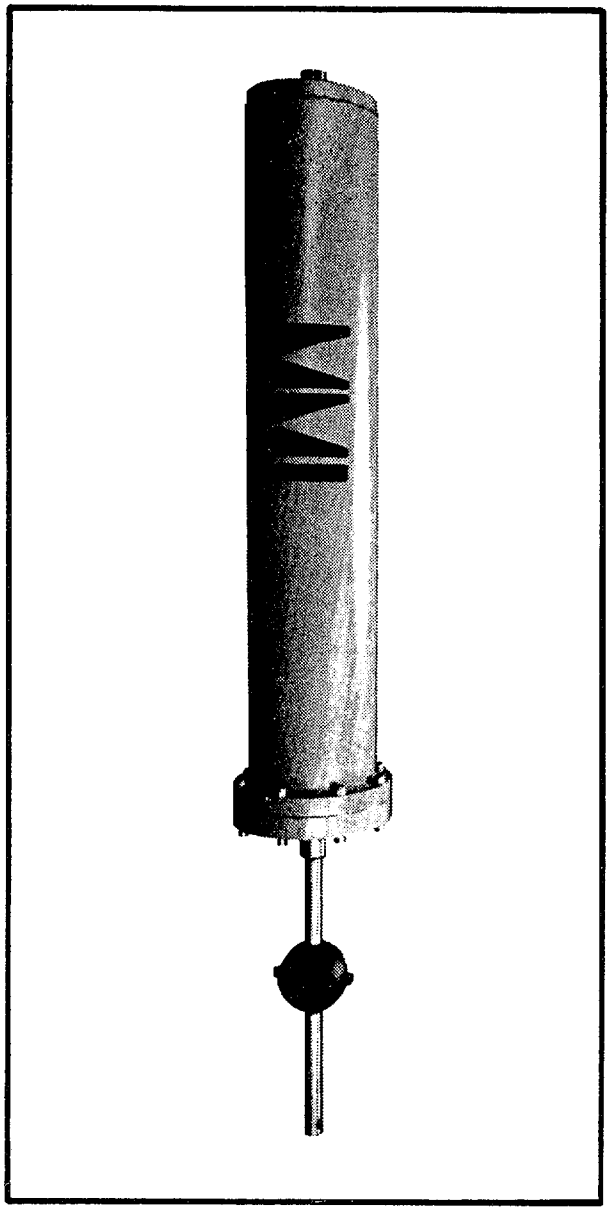

Figure 3. MMB MODEL 585 ADAPTIVE RECORDING CURRENT METER

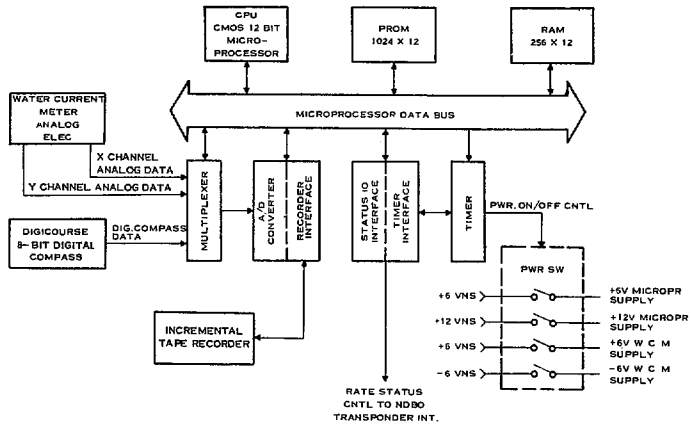

Figure 4. BLOCK DIAGRAM MARSH-McBIRNEY, INC., MODEL 585 ADAPTIVE RECORDING CURRENT METERS

The NBIS CMSS (designated ACM-1 Vector-Averaging Acoustic Current Meter[5]) is shown in Figure 5. Its pressure housing measures 32 inches long, with an 8-inch outside diameter; the total length is 48 inches. It weighs 75 pounds in air. This design employs an acoustic phase shift detection scheme for correlating the time of travel of two acoustic beams to the velocity of the fluid medium along the beam path. Two pairs of orthogonal transducers measure velocity components relative to the instrument. The transmitted acoustic beams are focused on a reflecting plate, which then returns the signals to the receiving transducer. A functional block diagram of this system is shown in Figure 6. Voltages proportional to the current velocity components are resolved by a trigonometric resolver using the output of a magnetometer compass. The compass output is proportional to the angle between the instrument housing and magnetic north. These current components are averaged and recorded incrementally on magnetic tape.

A series of investigative tests of elements of the CMSS were planned and implemented prior to delivery of the completed units to NDBO. The three types of current velocity transducers were flow tested to determine their characteristics. The CEI transducer was tested by NDBO in the U.S. Geological Survey Flow Facility at the National Space Technology Laboratories (NSTL). The MMB and NBIS trans-transducers were tested for NDBO in the Naval Ship Research and Development Center flow basin by the NOAA Test and Evaluation Laboratory (T&EL).

The initial NDBO test plan specified that all CMSS types would undergo the same test sequence; however, a delay in the delivery of the CEI units, caused by technical difficulties during factory testing, necessitated a revision in the plan whereby only the MMB and NBIS CMSSs would undergo this test sequence. Upon completion of assembly and subsequent testing by the manufacturers, the MMB and NBIS units were transferred to the NOAA T&EL for a series of evaluation tests to determine the performance and suitability of the instruments for field deployment and testing. Laboratory tests

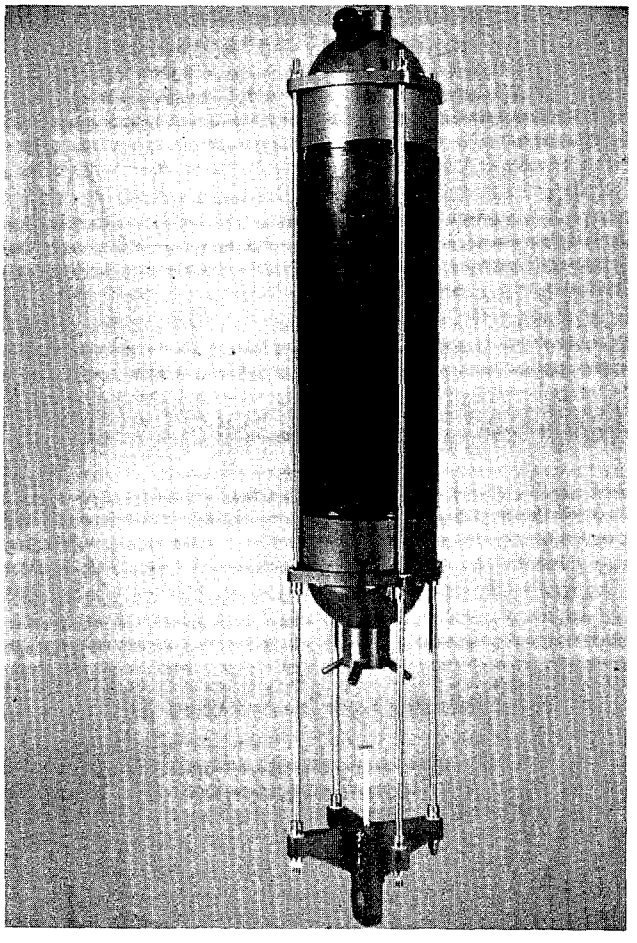

Figure 5. NBIS MODEL ACM-1 VECTOR AVERAGING ACOUSTIC CURRENT METER

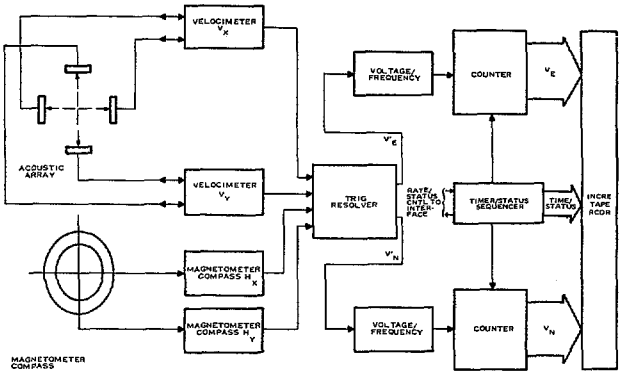

Figure 6. BLOCK DIAGRAM, NBIS, INC. VECTOR AVERAGING ACOUSTIC CURRENT METER

were conducted, as well as water flow tests using the Naval Ship Research and Development Center flow basin.[6,7]

The evaluation included steady flow calibrations on the four cardinal headings, directivity response tests in both the horizontal and vertical planes, and compass calibrations. Environmental tests were performed on selected CMSSs. Vibration testing was conducted in accordance with MIL-STD-167B and temperature testing was in accordance with MIL-STD-801C. The NBIS CMSS was also subjected to a combined pressure-tension test at maximum specified hydrostatic pressure and tension. No leakage or observable defects occurred as a result of any of the environmental tests. The results of these tests indicated that the CMSSs were capable of operating within the requirements of the NDBO performance specification under these controlled conditions, and that they should be suitable for field deployment and testing. The six CMSSs were subsequently shipped to Texas Instruments, Inc. (TI), for implementation of the current meter field test program.

Control and Status Monitoring to Facilitate Testing. In order to enable long-term at-sea testing of current meters, NDBO began a parallel effort in 1976 to develop a method to remotely control and monitor the status of current meters under test. This was the first step toward the ultimate goal of transferring test and operational data in near real time from a subsurface current meter to a surface platform where the data could be retransmitted to shore by UHF satellite link.

An at-sea test of an underwater acoustic communication system to control and monitor from the surface the status of deployed current meters began in December 1976 off Jacksonville, Florida. Frequent boat trips to the site were required to execute the test. Difficulties in obtaining ship support and weather-related delays impacted schedules during the test. Part of the equipment was lost while attempting to recover the test hardware for removal of recorded test data. However, the test met the objective, and reliable performance was achieved under a wide variety of test conditions during the 10-month test period.[8]

During this test period, the Applied Physics Laboratory of the University of Washington conducted a current measurement system concept study for NDBO to define the preliminary requirements for current measurements in an operational scenario. This study indicated the feasibility of a Current Measurement System (CMS) similar in concept to that being tested by TI, but with an acoustic telemetry subsystem that could transmit data to the surface in near real time.[9] Beyond the potential increase in value to users of operational data received in near real time, the data could have great value during the current meter testing. Access to data before retrieval of the cassette tapes from the CMSSs could prevent loss of recorded date in case of catastrophic loss of the CMSSs. It could also eliminate the need for frequent sea trips to monitor status during testing. Frequent retrieval of the moored CMS array to recover the test data was costly and had been difficult in the past.

NDBO evaluated both concepts in reference to the immediate requirements for testing the current measurement subsystems, and to meeting future operational goals. It was concluded that the TI concept, with the addition of a near-real-time data capability, would provide the best technical approach in the near term. TI was subsequently

contracted by NDBO to integrate, test, and evaluate a prototype CMS, including CMSSs selected from the current meter test program and a TI-developed real-time acoustic telemetry subsystem. The tasks to be accomplished by TI include the preparation and field testing of CMSSs, a parallel effort to design and test the acoustic telemetry subsystem, integration of these subsystems with a subsurface mooring and buoy data system, and installation and testing of the complete system on a data buoy for approximately 1 year in the Gulf of Mexico.

Field Testing of CMSSs. In preparing the three MMB and three NBIS CMSSs for field testing, functional testing and inspection were conducted to verify that NDBO performance and interface requirements were being met. Electrical interfaces, including status request, status reply, high data rate on, and high data rate off, were checked for proper operation with a test set that simulated an acoustic telemetry unit. Operational procedures were developed and performed on each CMSS. Execution of these procedures resulted in the isolation of several front end problems, particularly on the MMB units, which had not been identified during previous testing. All identified problems that were expected to impact field testing were corrected prior to entering the next test sequence.

The first planned at-sea test phase of the CMSSs program has been underway at the Naval Coastal Systems Center (NCSC) in Panama City, Florida, since April 1978. Tests accomplished to date have included a 2-week preliminary at-sea test to establish functional operation, followed by a 3-month extended test to evaluate short-term performance.

The CMSSs were installed at the NCSC Stage 1 deep-water tower, which is located 12 miles offshore. Figure 7 shows the test setup. Each CMSS was hardwired to an acoustic telemetry interface simulator to provide interface characteristics identical to the actual acoustic telemetry. This permitted the data rates to be changed during testing and accommodated the linkage of the status monitor through the NCSC tower-to-shore telemetry system for routine monitoring of the CMSSs at the NCSC shore station. The compasses in each of the CMSSs were caged prior to deployment to eliminate the effects of local electromagnetic disturbances. The CMSSs were carefully aligned with the known direction of the tower, so that current directions could be measured. An MMB cylindrical, electromagnetic current sensor was installed at each test level on the tower subsequent to the 2-week test, to provide reference current data. No suitable reference was available for the 2-week test.

Upon recovery of the units following the 2-week test, several equipment anomalies were noted. The MMB units failed to record data during the entire test, but all NBIS units measured and recorded data throughout. The severe environment under the tower had resulted in the beginning of fouling on all unprotected surfaces of the MMB

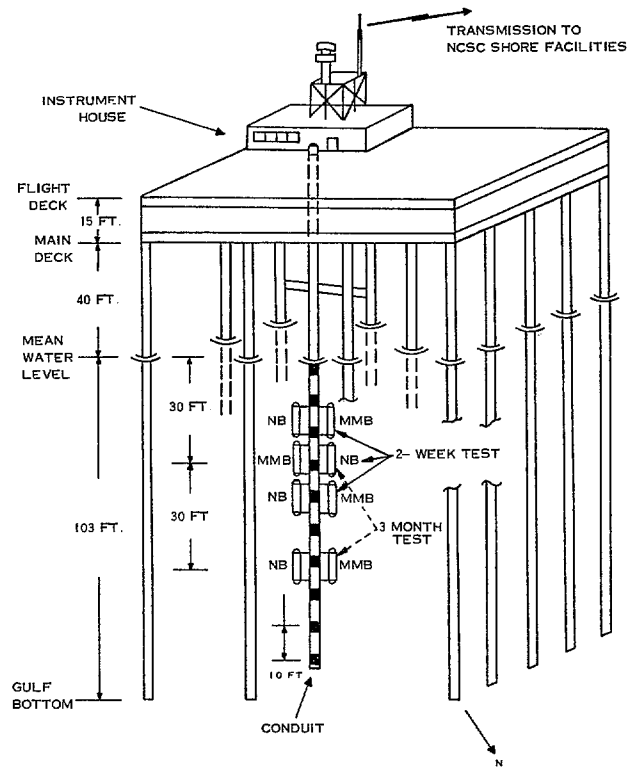

Figure 7. TEST SETUP AT DEEP TOWER

units, as shown in Figure 8. Severe crevice corrosion was observed between one of the titanium rods and the lower aluminum casting on one of the NBIS units (Figure 9). A plot of the measured current magnitudes by the NBIS units is shown in Figure 10, which shows good correlation between the three CMSSs. Directional correlation was also good.

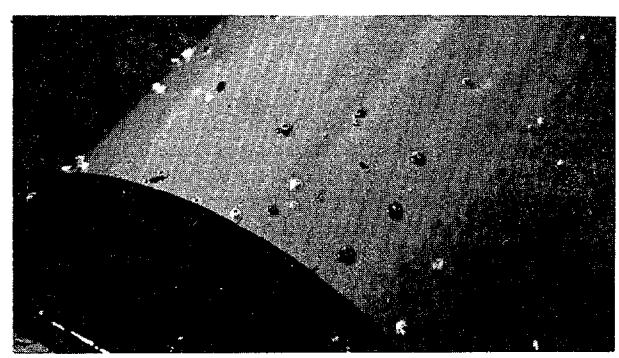

Figure 8. FOULING OF MARSH-McBIRNEY CMSS

The failure of the MMB units was traced to a subtle error in the software which was manifested by the zeroing (caging) of the compasses. Bench tests were ineffective in uncovering the problem before deployment. This problem was corrected and the three MMB units were reinstalled on the tower, along with two NBIS units, for a 1-week retest. The crevice corrosion on the NBIS unit

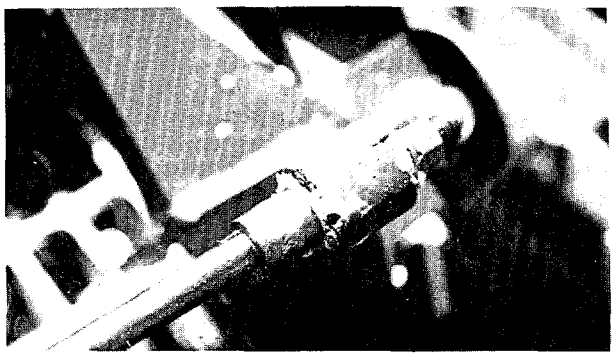

Figure 9. CORROSION OF NEIL BROWN CMSS

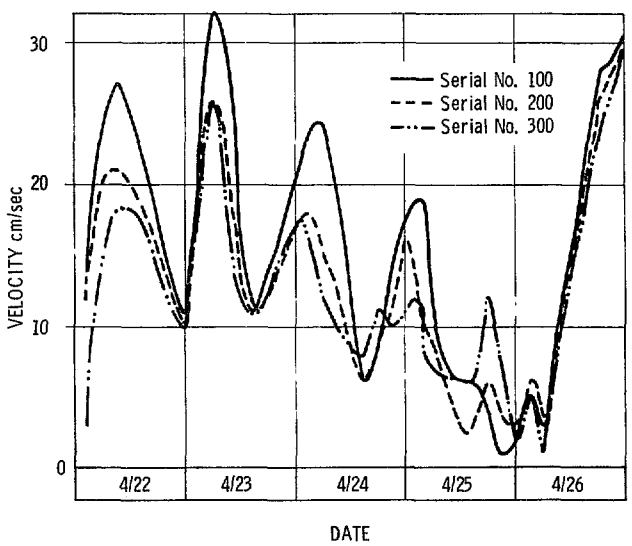

Figure 10. CURRENT MAGNITUDE - NBIS CMSS DURING 2-WEEK NCSC TOWER TEST

was found to be caused by direct contact between the titanium rod and the aluminum base. This was corrected by installing the proper insulator.

Upon recovery of CMSSs after the retest, the following was observed. All MMB units had successfully recorded data, but the magnitudes of the measurements were grossly in error. The acoustic reflecting plates from both NBIS units were found to be missing. However, the units had recorded data, although erroneous. At this time, these failures are still under investigation. We believe that their origins can be found quickly and corrected.

Following correction of the problems discovered during the preliminary tests, two of each CMSS type will be installed as shown in Figure 7 for a 3-month extended test. In addition to the periodic monitoring of CMSS status during this test, observations of fouling, corrosion, and general appearance of the CMSSs will be made. At the conclusion of the 3-month tower test, the performance of all CMSSs will be evaluated, and units with adequate performance potential will be modified for real-time data transfer and integration into the long-term current measurement system test.

Acoustic Monitoring Reporting Capability. The acoustic telemetry subsystem that is now under development by TI will be used to facilitate long-term testing of the CMSSs. It consists of an Underwater Acoustic Subsystem (UASS) that interfaces directly with the CMSS, and a Surface Monitoring Reporting Subsystem (SMRS) that interfaces directly with the digital data processor of the buoy data system. A functional diagram of the acoustic subsystem and its interfaces is shown in Figure 11. Each CMSS will be connected to a UASS to provide for control and real-time data transfer to the surface. Each SMRS will be capable of communicating with up to 16 UASSs within a radius of at least 1 nautical mile.

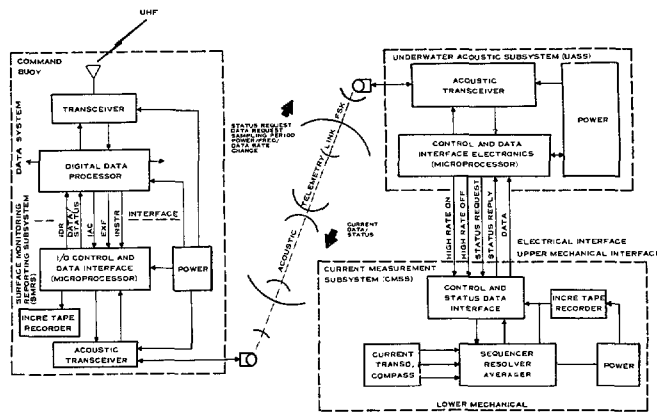

Figure 11. FUNCTIONAL DIAGRAM OF CMSS AND ACOUSTIC TELEMETRY SUBSYSTEM SHOWING THEIR INTERFACES

Long-Term Test of Current Measurement System. Preparations for the long-term at-sea testing of the modified CMSSs are underway, with deployment scheduled for February 1979. The subsurface mooring that will support the CMSSs and interconnected UASSs is planned to be deployed in the northern Gulf of Mexico approximately 10 miles from South Pass at the mouth of the Mississippi River. A 20-foot NOMAD boat-shaped buoy, containing the SMRS and a standard NDBO Data System, will be moored nearby. The water depth at this location is 600 feet. This site was chosen for relative ease of logistics and access.

TI will coordinate all aspects of the long-term test, including the planning, integration, and testing of all subsystems, deployment and recovery operations, maintenance and servicing, and data reduction and analyses. Figure 12 illustrates the data flow during the long-term test.

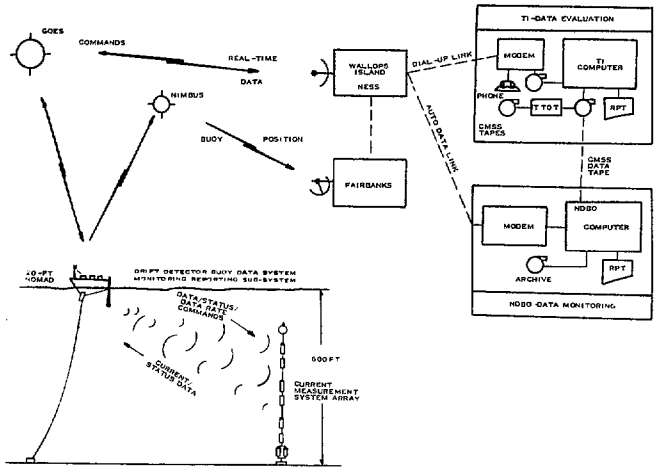

Figure 12. CURRENT MEASUREMENT SYSTEM AT-SEA TEST-DATA FLOW

4. Conclusions

The development of an ocean current measurement capability for the mixed layer and continental shelf regions of the oceans is not a straightforward endeavor, and requires considerable resources and a great deal of patience. The success of the program requires a good technical plan and strict adherence to sound technical disciplines and a methodical approach. Experience has shown that there are no shortcuts to an operational ocean current measurement capability.

NDBO's approach to development testing and refining state-of-the-art current sensors, and to adapting them for system operation in the actual environment, together with the application of the principles stated herein, should accomplish the desired objective. This development approach is expected to provide reliable current sensors to measure and internally record ocean currents in a conventional manner; to provide reliable current sensors interfaced to a standard buoy data subsystem to deliver ocean current data via satellite to users in near real time; and to provide this information over an extended (relative to present systems) period of time.

References

1. NOAA Office of Marine Technology, unpublished report of the Current Meter Review Panel, 1975.

2. NOAA Office of Ocean Engineering, "Minutes of the Working Conference on Current Measurements," Sponsored by NOAA OOE and the Delaware Sea Grant College Program, University of Delaware, Newark, 1978.

3. Cushing, V., "Electromagnetic Current Meter," Proceedings of the OCEANS 76 Conference, Washington, D.C., Sept. 13-15, 1976, pp. 25C-1 - 25C-17.

4. Marsh-McBirney, Inc., Technical Manual for ARC 585 Adaptive Recording Current Meter, 1978.

5. Lawson, K. D., N. L. Brown, D. H. Johnson, and R. A. Mattey, "A Three-Axis Acoustic Current Meter for Small Scale Turbulence," ISA, 1976, pp. 501-508.

6. Appell, G. F., "Performance Assessment of Advanced Ocean Current Sensors," NOAA T&EL unpublished presentation of the OCEANS 77 Conference, Los Angeles, California, 1977.

7. Appell, G. F., "A Review of the Performance of an Acoustic Current Meter," NOAA T&EL summary of laboratory tests on NBIS current meters, 1977.

8. Texas Instruments, Inc., "Long Term Testing of Acoustic Telemetry System, Test Report", May 15, 1978, NASA Contract NAS 13-25.

9. Okerlund, J. H., "Operational Current Measurement System, Final Report", June 20, 1977, Applied Physics Laboratory, University of Washington, NOAA Data Buoy Office Contract 03-6-038-732.

CHARTING OF OUTER CONTINENTAL SHELF SURFACE CURRENTS BY AERIAL TRACKING OF TRACERS

Timothy L. Flynn
Aero-Marine Surveys
P.O. Drawer 1230
New London, CT 06320

David O. Cook
Raytheon Company, Oceanographic & Environmental Services
P.O. Box 360
Portsmouth, RI 02871

Abstract

As part of a physical oceanographic study of the New England OCS sponsored by the U.S. Bureau of Land Management, techniques have been developed for acquisition of synoptic surface currents data over large areas. Dye-emitting Lagrangian tracers, equipped with radio location beacons, are seeded in patterns and tracked by aircraft for several days.

The aircraft-deployed tracers consist of 132 cm-long cylinders, containing a fluorescent dye mixture, which are weighted to float vertically. Four color coded arms joined to the cylinder near its top provide for unique visual identification, and frequency-audio coded VHF radio location beacons are mounted in the top of selected tracers.

Tracer tracking is accomplished with a Cessna Skymaster aircraft with VHF homing equipment, vertically mounted Hasselblad cameras, a radiometer, and an advanced Loran C unit. The photographic tracer data is subsequently digitized in the lab and computer-processed into tabular and graphical displays.

In a typical study, between 60 and 180 tracers are deployed in several patterns dispersed over an area of approximately 25,000 km^2. A cargo aircraft such as a Beechcraft G-18 is used for tracer deployment, and relocation of tracers takes place with the Skymaster for several days thereafter. Results to date have yielded interesting data on regional circulation, diffusion, and circulation within a warm-core eddy.

1. Introduction

A knowledge of surface currents is critical to predicting potential environmental impacts from offshore activities such as oil development and waste disposal. Floatable wastes and most spilled oil remain at the water surface where their transport is controlled by surface currents and direct wind stress. Eulerian data can not be readily extrapolated to the surface because flow at these two levels is frequently decoupled. Lagrangian methods represent the only viable method for measuring currents in the upper few meters of the water column.

Several Lagrangian techniques are available for studying surface currents. Drift bottles/cards represent the simplest approach, but provide only indirect data on flow trajectories. Shallow-drogued buoys have traditionally been tracked by ship[1] and more recently by satellite. Logistics and expense tend to limit the number of buoys which can be simultaneously tracked.

Aerial photography has provided a means of tracking large numbers of surface current markers concurrently in estuaries and the nearshore area. Several investigators[2,3,4,5] have used time-lapse photography to document the motion of drogues or other surface current followers in relation to fixed references such as the shoreline or moored buoys. This method was extended offshore using a vessel with known position as a reference[6]. Another aerial technique involves stereo photography of floating targets to measure instantaneous surface current velocities[7,8]. These previously-employed aerial tracking techniques have had limited offshore application because of the lack of fixed reference points. Also, relocation difficulties caused by drogue or target dispersion have limited the duration of aerial Lagrangian studies to a tidal cycle.

This paper describes a new approach to aerial measurement of Lagrangian currents in the offshore region. Development of this approach was prompted by the U.S. Bureau of Land Management's need to acquire data on surface currents on the New England outer continental shelf in connection with potential oil and gas development there. The study area, Georges Bank, encompasses over 50,000 km^2. Synoptic surface current data within this area were required over a period of several days in each season; spatial scales of interest were regional (several hundred km), local (20 to 50 km), and small scale (2 to 5 km). Special interest was directed at frontal zones on the northern and particularly the southern flanks of Georges Bank.

To meet this requirement, a new surface current tracer was developed and a Cessna skymaster aircraft was outfitted with an advanced Loran C unit for positioning, aerial cameras, a radiometer, and recording equipment. Up to 180 tracers have been deployed over the study area with tracking continuing for several days. Relocation of the dye-emitting tracers is facilitated by equipping selected units with radio beacons. Data is processed using specially-developed computer software.

This new approach to the measurement of surface currents is described from the standpoints of tracer design, survey aircraft, field logistics, and data reduction in the remainder of this paper.

2. Tracer Design

The Lagrangian surface current tracers required for aerial tracking on the outer continental shelf had to satisfy the following criteria:

(1) They must respond to water motion in the surface layer, as defined physically and biologically, and have minimal exposure to the wind.

(2) They have to be visible and uniquely identifiable in aerial photographs taken from altitudes of 150 to 600 m.

(3) They must be relocatable after intervals of 1 to 3 days.

(4) They have to be air-deployable, and sufficiently rugged to remain intact in the water for at least two weeks.

Existing Lagrangian devices did not meet all of the above criteria, and this led to development of a new tracer. The development work was undertaken in conjunction with Eotech Corp. (Ft. Lauderdale, Florida) and involved several increments of field testing off Florida and in New England waters.

The first consideration in the design process was definition of the surface layer. Physical oceanographers often consider surface waters to lie above the thermocline. The surface layer can be more strictly defined as the upper few meters of the water column which is susceptible to wind forcing and diurnal heating and cooling. However, recent field studies[9] have demonstrated the existence of intense shear in the upper meter of the water column which affects oil and other pollutants borne at the water surface. These studies identify the surface layer as a three-dimensional body whose thickness ranges from centimeters to meters depending on environmental conditions. This thickness decreases with increasing stability of the water column; conversely, the thickness increases with homogenization of temperature and salinity by mixing.

From a biological standpoint, the upper few cm to 1 m of the water column corresponds to the neustonic layer. This zone of intense sunlight is selectively inhabited by various species, such as meroplankton, at certain stages of their life cycles and by zooplankters on a diurnal basis.

In view of these physical and biological considerations, it was decided that the Lagrangian tracer should respond to currents in the upper meter of the water column.

The tracer developed for the surface current study (Figure 1) consists of a 132 cm long, 9 cm diameter polyethylene tube with a flotation collar near the top with four radiating flat polyethylene arms. The tube is ballasted to float vertically similar to a spar buoy, with the upper 20 cm exposed above the water surface. The four arms serve as a rotochute during air deployment and are color-coded to provide for unique visual tracer identification in the water. These arms, which are 20 cm wide and 60 cm long, lie a few cm below the water surface after the tracer is deployed.

Within the outer tube is an inner tube filled with a mixture of fluorescein dye, polyethylene glycol, and oleic acid. Wave-induced vertical motion of the tracer and a check valve at the tube bottom cause water to be forced upward in the space between the inner and outer tubes. Rising water entrains the fluorescein dye through holes in the inner tube, and this bright green dye is discharged through vent holes near the water surface. With moderate sea conditions, the dye supply will last three days. To achieve a uniform rate of dye dissolution, the ratio of dye to oleic acid must be adjusted for seasonally-varying water temperatures. The purpose of the green fluorescein dye is to assist in visual relocation of the tracers.

A VHF homing beacon placed within the exposed portion of the tube in selected units is the most important aid to tracer relocation. These beacons are similar to those which serve as downed aircraft locators, and for this study we have been assigned six frequencies each of which have up to six audio codes. Depending on battery type, the beacons will operate up to 2 weeks and can be aerially-detected from 30 to 80 km distance.

Susceptibility of the tracers to transport by wind acting directly on the portion exposed to air was investigated in a series of field tests. In each test, displacement of a tracer from a "zero leeway marker"—a dye-emitting device floating in the upper 30 cm of the water column with minimal exposure at the surface—was documented as a function of time by aerial photography. The rate of displacement varied from 2 to 4 cm/s with a wind speed varying between 5 and 8 m/s. This downwind motion relative to the U.S. Coast Guard "zero leeway marker" was less than one percent of the wind speed.

During the Georges Bank studies, it has been observed that the tracers move downwind faster than dye patches diffused in the upper few meters of the water column but slower than aluminum powder at the water surface. These observations coupled with test results lead us to conclude that the tracers effectively reflect motion of the upper meter of the water column, as intended.

3. Data Collection Platform

Aircraft

The aircraft used for tracking and relocating surface current tracers is a Cessna Skymaster model 337-G (Figure 2). It is a high wing monoplane with one 210 hp Continental engine on the forward end of the fuselage and another on the aft end. The tail is a twin boom type with dual rudders connected by a single horizontal stabilizer and elevator.

The aircraft is the civilian equivalent of the military 02 observation and light attack aircraft. It has a gross weight of 2100 kg, a cruise speed of 313 km/h and a range of approximately 2224 km with reserves. It is equipped with full civilian instrumentation for instrument flight in bad weather including dual VHF communications, dual VOR navigation receivers, distance measuring equipment, a marker beacon receiver, an ILS receiver, a radar altimeter, multi-mode radar, a flight director, a horizontal situation indicator, and a fully coupled autopilot. It also has dual head automatic direction finders, and for tracer homing, it has VHF direction finder units.

The main camera hatch is located under the right forward seat and contains two 70 mm cameras and a radiometer. Aft on the port side is a periscope which affords forward as well as vertical visibility for the photo-operator. A strip chart recorder for radiometric data is located amidships. Behind the seats in the aft end of the cabin are a photo data panel, life raft, survival kit, and life preservers.

The aircraft has accommodations for a crew of three or four, depending on the season, in the survey configuration. Normal crew would be a pilot and navigator in the front and a photo-operator and scientist-observer (during colder months) in the rear. Due to the engine and wing configuration, each crew position has excellent visibility to the sides and downward.

Navigation System

The offshore positioning system is a critical element to the experimental design of the surface currents program and much effort has been devoted to obtaining the best possible performance. During the first year program, a Simrad Model 123 Loran C system specially programmed for airborne use was utilized. This unit tracks up to four rates concurrently and provides a visual update once per second of any two of these rates. A coordinate convertor displays and updates the equivalent latitude and longitude.

The first year program had numerous instances of temporary Loran C outages either due to weather or precipitation static build-up on the aircraft. Occasional 10 microsecond jumps have also occurred when the aircraft is maneuvering; if properly documented, these can be corrected. Much of this problem relates to the poor existing Loran C coverage of the Georges Banks area, a situation which will improve considerably this summer when a new East Coast net goes into operation. In the absence of outages of jumps, accuracy of the Loran C positions is rated at ± 100 m which is considerably better than Loran A or Omega.

Aerial Cameras

Hasselblad MK-70 photogrammetric cameras are used to determine tracer positions. These 70 mm format cameras were originally developed for NASA for the Apollo series of manned space flights. The MK-70 has a 70 mm distortion-free lens and a reseau plate with a 5x5 grid calibrated to within several microns. Bulk film magazines have been fitted to the cameras to allow loading a standard 30 m roll of uncut film. This provides up to 500 exposures without reloading.

Radiometer

A Barnes PRT-5S radiometer is employed to sense sea surface temperature beneath the aircraft. Incoming infrared radiation in the 9.5 to 11.5 micron range is compared with an internal reference of known temperature, yielding an output of surface water temperature versus time. Data has been logged on a strip chart recorder annotated with position information.

Data Panel

Flight data has, for the first year of the program, been recorded on a photographic data panel originally built for Dr. W. Richardson at Nova University. The panel resembles an aircraft instrument panel and contains a gyro-horizon for vertical reference, a direction gyro, a wet compass, a magnesyn compass, a pressure altimeter, a dual Loran C display, a 24 hour sweep second hand clock, and a digital second counter. Dial faces are photographed by a standard Hasselblad 500-EL camera mounted in the unit and synchronized with the two vertical Hasselblad MK-70 cameras. The data panel is currently being replaced with a digital data logger which will also accept the radiometer input and record all data on magnetic tape cassettes.

4. Logistics

Study Design

The surface current field studies have been executed in two modes relating to the time scales of the transports under investigation. Of primary interest is the regional circulation pattern of the overall study area. Because the scale of non-tidal motion, such as wind drift, is usually greater than that of tidal motion, establishing the positions of Lagrangian tracers once a day is generally sufficient to resolve regional circulation over periods of several days. By contrast, small scale circulation in the vicinity of frontal zones requires higher frequency sampling of tracer movement. In the present study area, such processes as convergence, shearing, and Langmuir circulation require observations of tracer locations at 15 to 30 minute intervals.

Regional circulation has been addressed with large scale surface current studies. These involve seeding large numbers of tracers-between 60 and 180 have been used—along a series of patterns distributed around Georges Bank. A total of 10 to 12 line and occasionally "L" shaped patterns, lying mostly at the margins of the Bank and normal to isobaths, have been used to investigate the seasonal surface currents climatology. The

patterns are 20 to 30 km long and have tracers spaced every few km. Occasional closely-spaced "clusters" of tracers are deployed along key lines to study dispersion. During a season, the patterns are occupied in two groups in back-to-back large scale studies focusing on the eastern and western halves of the Bank. A typical season's deployment scheme is shown on Figure 3. Tracking of the deployed tracers then takes place daily for several days. These large scale studies constitute the core of the program.

Small scale studies completed in a single day have been used to examine local circulation near shear zones, irregular topography, and other areas of interest. One to two short lines 2 to 4 km long are seeded with tracers, dye, and aluminum powder every 100 to 300 m. Positions of these Lagrangian devices are monitored every 15 to 30 minutes.

Methodology

Deployment of tracers during the large scale studies involves two aircraft: the Skymaster survey airplane which navigates to the proper locations and obtains initial positions for tracers, and a larger cargo aircraft which actually deploys tracers. A Beechcraft Model G-18 cargo aircraft has been used quite successfully for deployments—it can accommodate large numbers of tracers, has a speed and maneuverability compatible with the Skymaster, and has the necessary range to complete the usual 1100 to 1300 km deployment track. Once the two aircraft navigate to the start of a deployment pattern, they fly down the line in formation with the Beechcraft at 225 m and the Skymaster following at 380 m. The Skymaster directs the Beechcraft to deploy tracers when critical Loran C intercepts are reached. The physical act of tracer deployment is performed by two technicians stationed at the open rear door of the Beechcraft. Tracer "clusters" were initially deployed by throwing out nine tracers in rapid succession; the present approach is to wrap these in bundles of four and five using water soluble polyvinyl alcohol so the subgroups begin dispersing from point sources. The Skymaster following the Beechcraft obtains initial positions on the deployed tracers and observes that radio beacons are performing properly.

Tracer relocation overflights are normally scheduled for days 2, 3, 5, 7 or days 2, 4, 6, 8 of a large scale study, weather permitting. The program has evolved away from large numbers of unbeaconed tracers, which are increasingly difficult to relocate as time passes and originally-straight lines become distorted, towards fewer numbers of beaconed tracers. Logistics are constrained by available daylight and fuel reserves, and time is simply not available for extensive visual searching. The radio beacons can be sensed from 30 to 80 km away depending on aircraft altitude and, with practice, the pilot can navigate the aircraft directly over them. At present, unbeaconed tracers are reserved for the clusters.

A time budget is established prior to each day of tracer relocating which allows all patterns to be visited. The time at each pattern is then used to navigate from radio beacon to radio beacon, with visual searching confined to the cluster locations. Excessive dispersion normally results in abandonment of cluster searching after the third day. The relocation rate for beaconed clusters is quite high—80 to 90 percent—on the first two days of relocating, and then begins to drop off as the beacons weaken and tracers disperse. The tracer location overflights are long, with individual flights running 7 to 9 hours.

The field operations are scheduled for fair weather periods, although weather encountered over Georges Bank has included squalls, rain, snow, and high wind. Poor weather in the form of precipitation or low clouds is unfavorable to a mission from several standpoints. Radiometry and photography are precluded, the Loran C signal may be degraded, and the flight schedule must be more conservative because of safety factors. Operating experience has led to fairly accurate forecasting of weather over the study area and aborted missions have been kept to a minimum.

5. Data Processing

Following the field data acquisition phase of a surface currents study, films from the data camera and aerial cameras are developed. Aircraft flight tracks are plotted for each day of operation, and any necessary corrections to the Loran C rates are implemented. Loran C positions associated with each tracer sighting are then plotted and converted to latitude-longitude coordinates. These coordinates correspond to a point on the aerial photographs whose precise position depends upon aircraft tilt and other factors. Tracers appearing on each frame of aerial film are digitized with respect to selected reseau marks, and these digitized locations along with tracer identification, aircraft orientation (roll, pitch, heading, altitude), time, and latitude-longitude coordinates for each frame are placed on punched paper tape.

The tape is processed on a CDC CYBER 174 computer which uses photogrammetric equations to calculate the latitude and longitude of each tracer photographed. The accuracy of the calculated tracer positions relates to several potential error sources. These sources, along with the uncertainty in tracer position associated with them, include the following: 1) resolution of aircraft tilt indicator ±13 m; 2) resolution of aircraft altitude indicator, ±15 m; 3) camera film distortion, ±3 m; 4) lack of synchronization between triggering of the cameras and Loran C updating, ±26 m; and 5) Loran C accuracy, ±100 m. The total error[10] of ±105 m is dominated by accuracy of the Loran C navigation system. This degree of accuracy is acceptable in view of the

normal 5 to 30 km transport exhibited by tracers between daily sightings.

Outputs of the computer processing include the following data products: 1) a listing of tracer identification, position, time, date, photographic frame, and extrapolated speed since the last sighting of the tracer in question; 2) a map showing successive tracer locations connected by straight lines and annotated with data on tracer identification, time, date and extrapolated speed; and 3) a map showing the area encompassed within each aerial photograph to aid in constructing photomosaics (applicable where individual photographs are overlapping).

The radiometer data is digitized and computer-processed separately, producing a listing of time and temperature and a map showing the aircraft track line annotated with observed water temperatures.

The type of surface current data which can be acquired by aerial tracking of the Lagrangian tracers is illustrated on Figures 4 and 5. Figure 4 shows observed tracer transport in the Georges Bank vicinity during companion studies in the winter of 1978. The first study, covering the eastern half of the Bank, extended from Jan. 31 to Feb. 3; the second study which concentrated on the western half lasted from Feb. 20 to 25. Successive positions of individual tracers are connected with straight lines.

This figure illustrates the substantial area which can be synoptically studied using the methods described in this paper. The tracer transport reflects two factors: a wind-induced surface current caused by moderate west to northwest winds occuring during both studies which is superimposed upon a topographically-controlled subsurface circulation pattern. The subsurface circulation is directed clockwise around the north, east and southern flanks of Georges Bank. Tracer paths which are in apparent conflict in the southwestern portion of the Bank actually reflect the presence of a warm water filament. This filament was observed both by aerial radiometry and by hydrographic measurements from a concurrent cruise.

Figure 5 illustrates the Lagrangian transport observed during November 15 to 20, 1977 when a warm core Gulf Stream eddy was impinging on the southern flank of Georges Bank. Note the marked clockwise rotation of tracers within the eddy; these moved as much as 90 km in a single day. Those tracers at the eddy margin and beyond exhibited much lower rates of transport. The airborne radiometry measurements made in conjunction with the tracer tracking provided valuable information on daily changes in eddy position.

The surface current data exemplified by Figures 4 and 5 has obvious implications from a scientific standpoint as well as for the prediction of the transport of spilled oil and other pollutants.

6. Conclusions

Techniques have been developed to enable collection of synoptic data on surface currents in offshore regions having areas of many thousand square kilometers. These techniques include use of a new Lagrangian tracer and of specialized aerial deployment and tracking methodologies. Results can be used to define a seasonal surface current climatology and investigate transport processes in eddies. The surface current capability constitutes a significant tool for assessing potential impacts of offshore activities such as oil development and ocean dumping.

Acknowledgements

The surface current technology described in this paper was developed under U.S. Bureau of Land Management contract AA550-CT6-53 with the Raytheon Company. The field program is being executed by Aero-Marine Surveys, subcontractor to Raytheon. The LaGrangian tracers were developed in conjunction with Eotech Inc., who then fabricated production units. Many persons contributed to the surface current program, and in particular, we acknowledge the efforts of Kenneth Berger (BLM), Ted Crosby, Gary Davis, Dan Frye, Barbara (Grube) Flynn, William Kielhorn, John McMicken, James Richardson, Harry Williams, and Priya Wickramaratne.

References

1. Cromwell, T., Montgomery, R., and Stroup, E., "Equatorial undercurrent in Pacific Ocean revealed by new methods", Science, Vol. 119, 1954, pp. 648-649.

2. Duxbury, A.C., "Currents at the mouth of the Columbia River", Photogrammetric Engineering, Vol. 33, 1967, pp. 305-311.

3. Cook, D.O., "Evaluation of estuarine circulation by aerial photography of current drogues", Preprints, 7th Annual Marine Technology Society Conference, 1971, pp. 663-670.

4. Assaf, G., Gerard, R., and Gordon, A.L., "Some mechanisms of oceanic mixing revealed in aerial photographs", Journal of Geophysical Research, Vol. 76, 1971, pp. 6550-6572.

5. Klemas, V., Davis, G., and Wang, H., "A cost-effective satellite-aircraft-drogue approach for studying estuarine circulation and shelf waste dispersion", IEEE Ocean '75 Conference Proceedings, 1975, pp. 751-760.

6. Ramey, E.H., "Measurement of ocean currents by photogrammetric methods", U.S. Coast and Geodetic Survey Technical Memorandum 5, 1968, 18 pp.

7. Cameron, H. L., "The measurement of water current velocities by parallax methods", Photogrammetric Engineering, Vol. 18, 1952, pp. 99-104.

8. Keller, M., "Tidal current surveys by photogrammetric methods", U.S. Coast and Geodetic Survey Technical Bulletin 22, 1963, 20 pp.

9. Gordon, A. L. and Gerard, R. D., "Wind drift surface currents and spread of contaminants in shelf waters", U.S. Coast Guard Office of Research and Development Center, Report No. CG-D-5-75, 1973, 64 pp.

10. Fisher, A., "The Mathematical theory of probabilities", McMillan Co., New York, Vol. 1, 1915, p. 106.

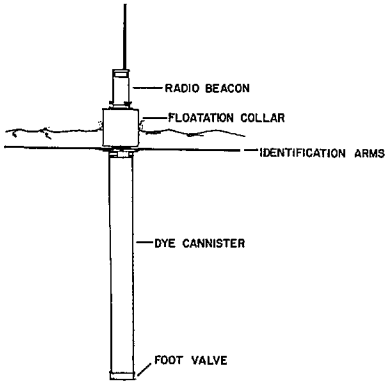

Figure 1. a - side view of the Lagrangian tracer;

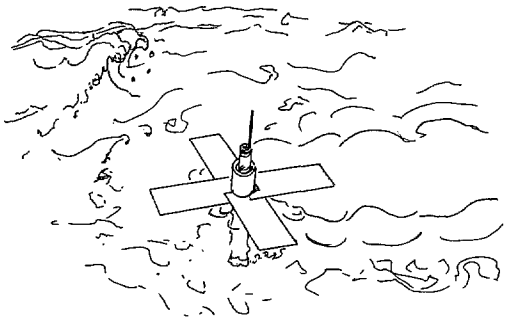

b - appearance of the tracer after deployment.

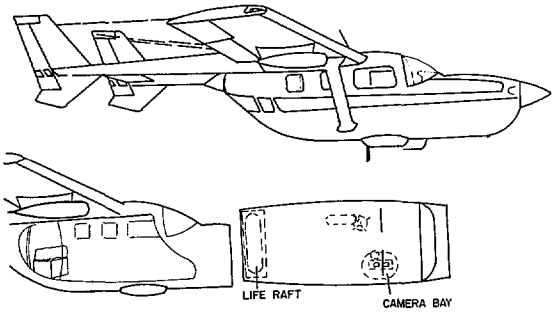

Figure 2. The Cessna Skymaster C-337 survey aircraft, N700AM, owned by Aero-Marine Surveys, Inc.

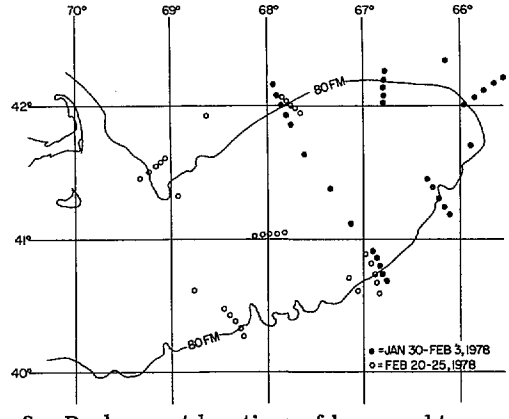

Figure 3. Deployment locations of beaconed tracers in the Georges Bank study area during the winter 1978 large scale surface current studies. Not shown are clusters of eight unbeaconed tracers deployed around four of the beaconed units during each study.

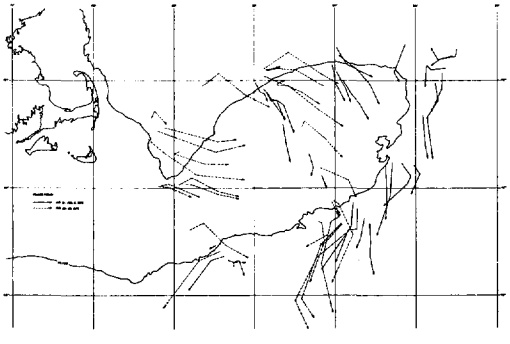

Figure 4. Observed motion of surface current tracers during the winter 1978 large scale studies. Positions where tracers were observed are connected by straight lines.

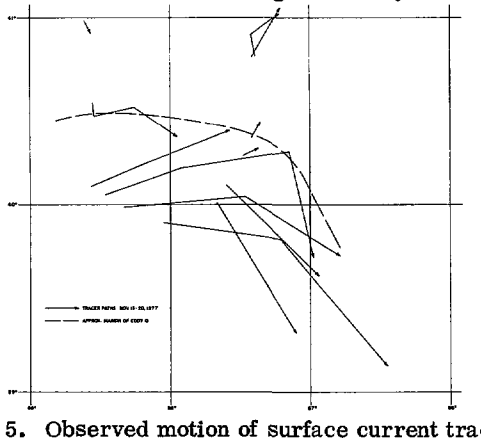

Figure 5. Observed motion of surface current tracers in the vicinity of warm core eddy Q during the November 1977 large scale study. Observed tracer positions are connected by straight lines.

AN UNDERWATER TOWED ELECTROMAGNETIC SOURCE FOR GEOPHYSICAL EXPLORATION

B. E. Tossman
The Johns Hopkins University
Applied Physics Laboratory
Johns Hopkins Road
Laurel, Maryland 20810

D. L. Thayer
The Johns Hopkins University
Applied Physics Laboratory
Johns Hopkins Road
Laurel, Maryland 20810

W. A. Swartz
The Johns Hopkins University
Applied Physics Laboratory
Johns Hopkins Road
Laurel, Maryland 20810

Abstract

Low frequency electromagnetic methods are used in geophysical exploration by detecting the magnetic field distortion between a transmitter and receiver produced by locally conductive bodies. Both ground and airborne systems are in current use. One airborne multi-coil aerial electromagnetic prospecting system houses the transmitter and receiver in a 30 ft bird while another reduces the system to an impedance measurement using a single superconducting coil.

It is possible to extend low frequency airborne geologic prospecting techniques into the ocean environment by employing an underwater towed source of electromagnetic radiation and a receiving magnetic or electric field detector. The receiver can be simultaneously towed on an auxiliary cable, boom mounted on the towing platform (surface or subsurface), or land or underwater based.

An underwater towed body suitable for geophysical exploration applications has been constructed and employed in underwater propagation studies of low frequency electromagnetic fields. Called the Underwater Calibrated Source (UCS), it is 13 ft long weighing 840 pounds in air with a capability of producing magnetic dipoles in vertical and horizontal directions, and a horizontal electric dipole. Powered by a current feedback controlled high-power modified sonar amplifier, the UCS can produce 9700 amp-turn-meter^2 of magnetic dipole or 200 amp-meters of electric dipole at 50 amps at frequencies up to 200 Hz without significant attenuation from coil inductance.

The magnetic dipoles are produced by 6 ft diameter multi-turn loops built into aft vertical and horizontal stabilizing surfaces. The electric dipole is produced by driving nose and tail electrodes with low frequency current. The UCS also contains an instrumentation cylinder which includes vehicle altitude and depth sensors, tracking transducer, and relays for directing the input power to either the magnetic or electric dipoles or a high-power dissipation non-field producing dummy load.

Hydrodynamic towing requirements for this electromagnetic source were that it be stable in roll, pitch, and yaw to better than ±5 degrees oscillatory motion with average values within 5 degrees of straight and level flight. Position was to be stable to within ±5 ft in both horizontal and vertical directions. These hydrodynamic characteristics were achieved passively with the body being towed at depths up to 500 ft and speeds of 5 to 7 knots. In addition, the body was to be constructed of mostly nonmetallic and nonmagnetic components.

This paper concentrates on the design details of the UCS including its mechanical, hydrodynamic, and magnetic design characteristics and the electrical system consisting of the high current drive power system and shipboard monitoring system for attitude and depth detectors.

UNDERSEA STEREOSCOPIC TELEVISION

R. B. Fugitt and R. S. Acks

REMOTE OCEAN SYSTEMS, INC.
P.O. Box 26626
San Diego, California 92126

Abstract

The enhanced visual depth perception provided by stereoscopic television offers improved efficiency for many undersea tasks involving inspection, positioning, manipulation, or remote vehicle control. Several techniques exist for implementation of stereoscopic television. A two-camera system with a polarization coded display has been developed for undersea use. A video multiplexing technique is employed allowing signal transmission on a single coaxial cable and stereo documentation using a standard single-channel video recorder. Tests of the undersea stereoscopic system have demonstrated its effectiveness in providing accurate, realistic depth perception and a sense of spatial awareness not possible with conventional closed circuit undersea television systems.

1. Introduction

One of the primary limitations of presently available undersea television systems is lack of display realism. Experienced operators of manned submersibles almost invariably prefer direct vision through viewports to the use of closed circuit television. This preference exists because underwater television systems generally provide no color information, they often suffer from poor contrast and resolution and they provide little or no visual depth perception and orientation information.

The technology exists to alleviate these shortcomings, but it has been applied only to a limited extent, partly due to cost and system complexity. Backscatter reduction techniques exist for improving underwater visibility, and the use of head-coupled stereoscopic television has been demonstrated in the laboratory and on remotely controlled undersea vehicles (Ref 1, 2, 3). At present, color television is available for undersea use and is being utilized in an increasing number of applications. Although desirable for any application from a human factors standpoint, the greater realism and resultant sense of "operator presence" provided by such improvements will be particularly helpful when used with remotely operated manipulators or other related work systems (Ref 4, 5), and for greater control during precise maneuvering of undersea vehicles. Extensive testing performed at the Naval Ocean Systems Center has shown significant improvement in terms of accuracy and reduced task times when stereo television was used for control of underwater manipulators (Ref 6, 7).

The purpose of this report is to discuss the theory and alternative implementations of stereoscopic television and to describe a system which has been developed for offshore applications.

2. Methods of Depth Perception

There are many mechanisms by which visual "depth" or object distance can be perceived when using only one eye or camera. The most important of these are:

1. Occlusion of objects by those located nearer to the observer.
2. Subtended angle of objects of known size.
3. Relative sizes of objects of known size.
4. Nearness to the horizon of objects, e.g., an airplane in the sky or boat on the ocean.
5. Position with respect to objects of known location, e.g., a book located on top of a desk.
6. Focusing of the eye or camera.
7. Apparent motion of stationary objects with respect to a moving observer.
8. Color degradation and loss of resolution with distance.
9. Shadow relationships with respect to artificial lighting.
10. Rate of angular displacement of objects with known velocity.
11. Loss of perspective with distance.

Unfortunately, when working in the underwater environment most of these depth cues are lost. The distance at which objects can be seen is severely restricted, and no horizon is apparent. In general, the operator of a sub-

mersible vehicle or work system will be dealing with objects that are unfamiliar in size and perspective. In most cases, therefore, the only available single-eye or single-camera cues will be occlusion, focus, color degradation, shadow relationships and apparent motion. In many cases, some or all of these remaining cues may also be absent or may be too subtle to be of any use.

Stereoscopy is one of the most powerful depth cues, but it requires the use of two eyes or two camera images. This mechanism of depth perception is discussed in greater detail in the following section.

3. The Mechanism of Stereoscopy

Because our left and right eyes are spaced approximately 2-1/2 inches apart, each receives a slightly different image. The amount by which the optical axes of the eyes of any observer converge to superpose the right and left images of any object is a function of the distance from the observer to that object. Parallax between objects at different distances is instinctively interpreted as an indication of their relative distances. This is the mechanism of stereoscopic vision which literally interpreted means "seeing solid."

Stereoscopy is the technique or art of creating an illusion of stereoscopic presence by means of a stereogram, which is actually a set of two images, one provided for each of the observer's eyes. Every artist and photographer knows a painting or picture has a particular "station point" from which it should be observed. In a stereogram, two such station points must be simulated.

To faithfully conserve the stereoscopic illusion requires attention to the following geometric considerations.

1. Each image must be properly oriented about the optical axis of the observer's eye so horizontal lines appear to be horizontal.
2. The vertical position of both images must be identical, e.g., the horizon images should superpose in the eyes of the observer.
3. Each object in each view must subtend the same angle to the observer's eye as it would if viewed from the appropriate station point.
4. The horizontal spacing of the two images of a distant object should be such that an eye convergence angle of 0 degrees is required to superpose them, i.e., infinity should appear at infinity.
5. Station point or camera separation should be about 2-1/2 inches to approximate the average interocular spacing.
6. The camera's optical axes should converge to a distance closer than the nearest object of interest and, in general, at an angle between 6 and 12 degrees.

These rules in effect state that the geometry of the cameras and the viewer should be such that the observer has the illusion of actually being present at the camera location. Rules 1 and 2 are absolutely necessary for superposition of the two images. Rules 3 and 4 can be varied under certain conditions to enhance the stereoscopic illustion by distorting the scene's dimensions.

Variation from rule 5 results only in an apparent scale change which is equal for height, width and depth dimensions. Consider, for example, a situation in which two large sharks are being observed at 30 and 40 feet, respectively. If the station points are separated by the standard 2-1/2 inches, very little parallax between the sharks will be noted. If, however, the stereogram is based on a 25-inch effective interocular spacing, the visual angle subtended by each shark will be unchanged; however, parallax will be greatly increased, allowing the relative distances to be judged more easily. The pair of sharks in effect appears stereoscopically to be at a distance of 3 and 4 feet, respectively, and reduced to 1/10 actual size. This technique is often used with long-range, aerial, stereoscopic photography for enhancement of terrain features.

The intersection of the camera axes is necessary to create the illusion that the scene is being viewed through a window or frame located between the observer and the scene. Just as every two-dimensional photograph, painting or television image has a border, so must a stereogram. This effect is very noticeable in Viewmaster stereoscopic slides. The border actually has a depth effect and seems to float in space a few feet before the observer's eyes. The frame contributes nothing to the illusion of depth, but does make it easier to rationalize the stereoscopic illusion with the limited field-of-view. The stereoscopic frame, if the illusion is properly handled, becomes an immediate reference when an observer first looks into the viewer and helps him focus on the scene. If handled improperly, however, the stereoscopic distance to this illusionary window is greater than that to the observed objects. This is a disturbing illusion, and it is difficult to rationalize why objects disappear from view when they cross the border of the frame. Since the borders of the separate images are used to form the stereoscopic frame, the amount of eye convergence necessary to superpose the borders should be equal to the convergence angle of the camera's axes. With a 2-1/2-inch camera separation, the apparent distance from the observer to this frame would then be equal to the distance from the cameras to the intersection point of their axes. In practice, an apparent distance of 12 to 24 inches to the stereoscopic frame is both comfortable to the observer and is usually within the range of the nearest objects to be observed. This requires a camera convergence angle between 6 and 12 degrees. The set of rules proposed in this section describe how the

mechanism of stereoscopy is most effectively reproduced in artificial form. This can be summarized by the following statement: The geometry of the camera(s) and viewer should provide the observer with an undistorted illusion of stereoscopic presence at the camera's location.

4. Implementation of Stereoscopic Television

The general principles discussed in the previous section can be employed in a wide variety of stereoscopic television systems, each with its own applications, advantages, and disadvantages. Several different techniques can be used for separation of the stereoscopic images. Among them are sequential switching (electronically or mechanically) between views, color filter and polarization techniques, and optical separation and superposition using lenses, prisms, and mirrors.

A simple approach which requires only one camera and one monitor is shown in Figure 1.

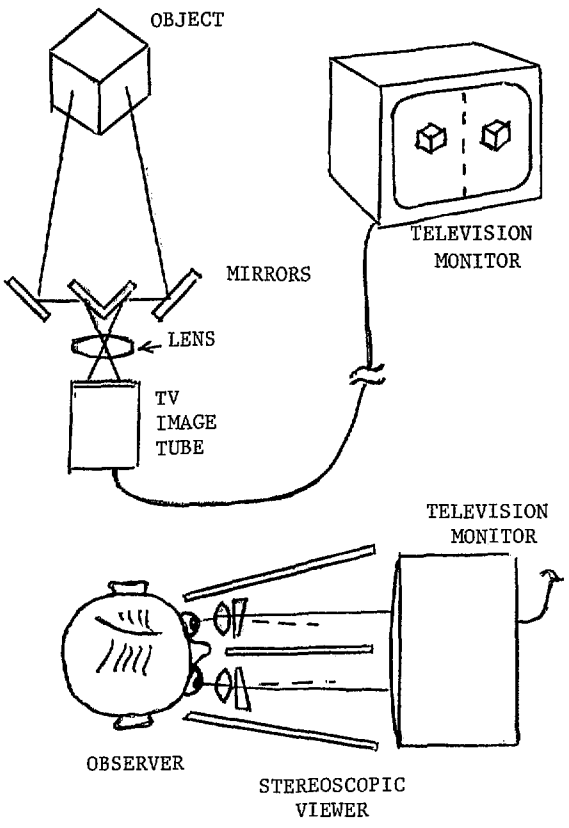

Figure 1. Single Camera Stereoscopic Television

A system of mirrors placed in front of an undersea camera form a side by side stereoscopic image pair on the television monitor. This image pair is then viewed with an optical system which presents the appropriate image to each eye of the observer. Lenses and mirrors (or prisms) are used to superimpose the views and form the image at a comfortable viewing distance from the observer.

A single camera underwater system of this type is described more fully in Reference 8. Although underwater tests showed significant reduction in task time and operator errors, the system suffered from off-axis image distortion and a narrow horizontal field of view (17 degrees).

An alternative approach is to use two cameras which readily provide larger fields of view and higher resolution. Figure 2 shows a display technique using two side-by-side television monitors. A preferable approach which allows freedom of operator movement is shown in Figure 3. Since no viewing hood or electrical connections to the glasses are required, the observer can easily divert his attention to other controls or displays, and can move freely about when required. An undersea stereoscopic television system based on this technique has been developed, and is described more completely in the following section.

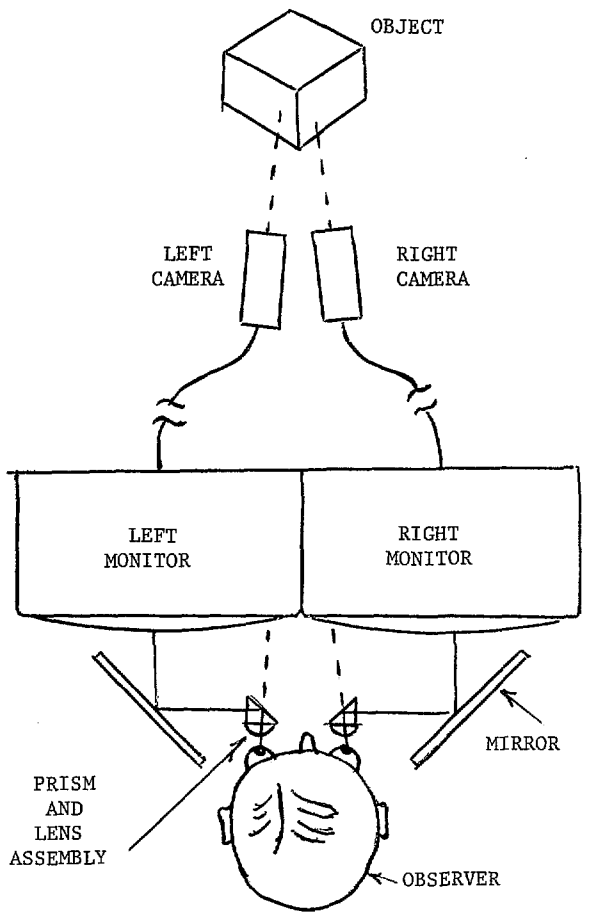

Figure 2. Two Monitor Periscope Display

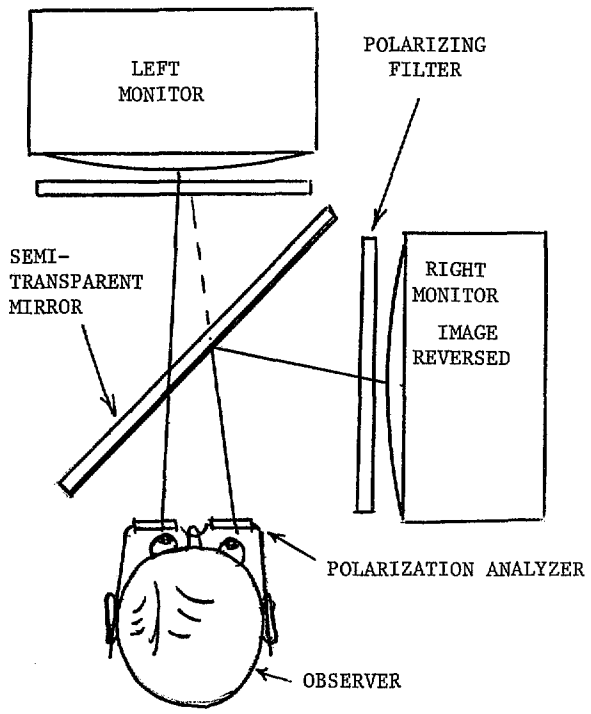

Figure 3. Polarization Coded Stereoscopic Display

5. Undersea Stereoscopic Television System

The basic stereoscopic television system consists of two underwater television cameras, a camera mounting fixture, the stereo display and viewing glasses.

For most applications the cameras are separated by approximately 2-1/2 inches to provide realistic depth perception. With appropriate selection of the camera and monitor fields of view, no camera convergence or separation adjustment is required to view objects ranging in distance from approximately one foot away to infinity. For other special applications such as long range object detection, sea floor stereo mapping or drill pipe re-entry, an appropriate wide baseline between cameras can be used for exaggerated depth perception.

The stereoscopic display utilizes a geometry similar to that shown in Figure 3. The images are linearly polarized and superimposed using a semi-transparent mirror. An angle-dependent light attenuating film placed in front of the side monitor allows the observer to see only the superimposed stereo pair. The observation glasses use polarization filters oriented such that the appropriate image is presented to each eye of the observer.

Since separate monitors are used for each camera, differences in the camera images (size, distortion, position, etc.) can be adjusted at the monitors to provide a matched, undistorted stereo image pair.

For stereoscopic documentation, video multiplexing circuitry was developed which allows both right and left camera signals to be recorded on a standard single-channel video tape recorder. To re-construct the stereo image, the signal is re-played and viewed using the stereoscopic display.

To accomodate stereo television on systems presently limited to one camera due to cable, penetrator, or data channel constraints, an undersea power and video multiplexing unit was also developed. With the addition, both video channels are sent over a single coaxial cable or data channel. The undersea multiplex unit is small in size (2-3/4 inches OD by 9-1/2 inches long) and can easily be used by divers or on small undersea vehicles.

6. Applications

Many undersea and offshore applications of conventional closed circuit television could benefit from the depth perception and sense of spatial awareness which is obtained with stereoscopic television. These include:

1. Positioning tasks using manipulators or other work systems.
2. Precise control of remotely manned vehicles.
3. Inspection and video tape documentation (diver or vehicle).
4. Enhanced optical search and detection.
5. Real time and recorded stereoscopic bottom mapping and site surveys.
6. Subsea equipment positioning in drilling and production operations.
7. Mating of structures in offshore construction
8. Internal pipeline inspection.
9. Shipboard or platform monitoring tasks (reels, etc.)

Figure 4 illustrates the display for a two-camera stereoscopic system manufactured by Sub Sea Systems, Inc. This system has been

Figure 4. Stereoscopic Display

successfully employed for many of the above applications. At present, it is being used in a diver-held version and on the remotely controlled vehicles TELESUB 1000 (Remote Ocean Systems Inc.) (Fig. 5) and Seabug I (UDI Operations, Ltd.) for pipeline inspection in the Gulf of Mexico.

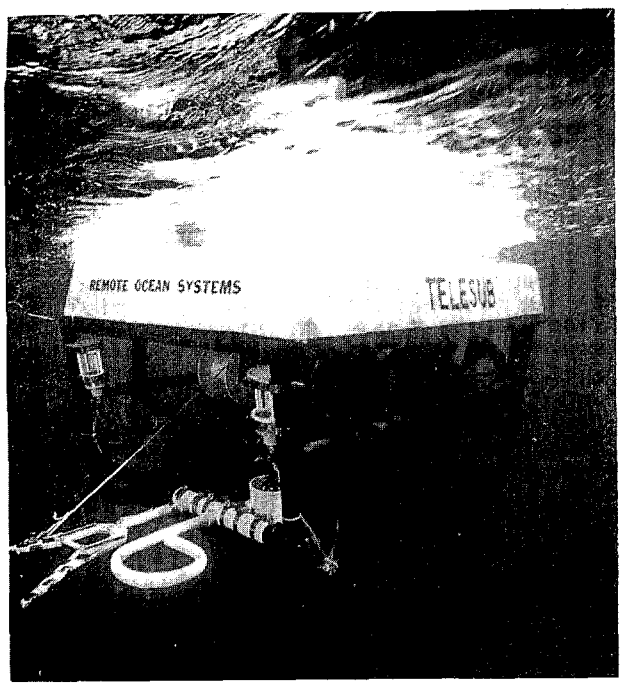

Figure 5. TELESUB 1000 Remotely Controlled Vehicle

7. Conclusions

Many present and future undersea vehicles and work systems do or will depend on closed circuit television to provide visual feedback. Improved display realism through the use of stereoscopic television can significantly improve system effectiveness by providing operators with an accurate sense of depth perception. This three dimensional awareness of objects and their positions relative to the remote cameras is particularly useful in situations where accurate manipulation or precise vehicle control is required.

References

1. Fugitt, R. Bruce, "Advanced Television Systems for Undersea Use," 1971 IEEE Conference on Engineering in the Ocean Environment, Sept 1971.
2. Fugitt, R. Bruce, "Small Remotely-Manned Vehicles," 1973 IEEE International Conference on Engineering in the Ocean Environment, Sept 1973.
3. Fugitt, R. Bruce, "Design and Operation of Two Remotely Manned Undersea Vehicles," IEEE and Marine Technology Society Converence on Engineering in the Ocean Environment, Sept 1975.
4. Uhrich, Richard W., "Terminus Controlled Deep Ocean Manipulator," 1973 IEEE Conference on Engineering in the Ocean Environment, Sept 1973.
5. Uhrich, Richard W., "Manipulator Development at the Naval Undersea Center," Naval Undersea Center, San Diego, CA, NUC TP 553, January 1977.
6. Pepper, Ross L., Robert E. Cole and David C. Smith, "Operator Performance Using Conventional or Stereo Video Displays," 1977 Proceedings of the Society of Photo-Optical Instrumentation Engineers, August 1977.
7. Uhrich, R. W. and R. Bruce Fugitt, "Investigation of Control and Viewing Techniques for use with Remote Undersea Manipulators," Naval Ocean Systems Center, San Diego, CA NOSC TR 233, 1 May 1978.
8. Fugitt, R. Bruce and Richard W. Uhrich, "Underwater Stereoscopic Television and Display Realism," Naval Undersea Center, San Diego, CA, NUC TP 358, July 1973.

THE COMPARISON OF DISCUS BUOY WAVE SPECTRA PRODUCED BY BUOY-FIXED AND VERTICALLY STABILIZED ACCELEROMETERS

E. L. Burdette
Computer Sciences Corporation
National Space Technology Laboratories
NSTL Station, Mississippi 39529

Abstract

A 12-meter discus buoy was instrumented to measure wave spectra by the NOAA Data Buoy Office (NDBO) with both buoy-fixed and vertically stabilized accelerometers feeding a data acquisition system which, on a 3-hour cycle, acquired and stored a 15-minute time series of the two sensor outputs. The buoy was deployed and operated in the Atlantic Ocean for several months, and produced wave data over a range of conditions. This paper describes the sensors and data acquisition system. The data are compared on the basis of their acceleration spectra; phase and coherence functions for the two time series are also examined. Results are presented which indicate that, for frequencies where significant wave energy is measured by the buoy, the output of the buoy-fixed accelerometer can be used to replace that of the vertically stabilized accelerometer.

1. Introduction

The measurement of the acceleration of a floating surface platform has been used as a technique for obtaining wave data for over 20 years. Time series of buoy acceleration may be processed to obtain wave displacement spectra in either of two ways:

- Analog or digital double integration of the acceleration time series into a displacement time series from which a spectral estimate is obtained directly
- Transformation of an estimate of the acceleration spectrum into displacement by dividing each spectral density value by the corresponding factor of angular frequency to the fourth power.

Early experiments obtained acceleration data from a single-axis accelerometer mounted on a short-period spherical pendulum[1] or mounted rigidly parallel to the symmetry axis of a surface following buoy.[2] Either approach results in the measurement of the vector sum, or resultant, of gravitational and wave accelerations (including horizontal components). Tucker[3] has shown that use of the resultant acceleration can cause reduced sensitivity in the displacement spectrum to low-frequency waves, as compared to systems that measure true vertical acceleration of a float. The error was shown to increase with sea state number.

True vertical acceleration may be measured by a vertically stabilized gimballed accelerometer. Vertical stabilization has been achieved by gyroscopic means[4] and by an inertial system equivalent to a long-period pendulum. The latter approach is employed by Datawell in the widely used Waverider buoy.[5] The acceleration sensor from this buoy, with analog double integration circuitry, is marketed as a separate item, the Datawell Heave Sensor.

NDBO operates buoys in the Atlantic and Pacific Oceans, and Gulfs of Alaska and Mexico. Buoys moored at these stations have on-board data acquisition and reporting systems, commonly referred to as payloads. A payload comprises meteorological and oceanographic sensors, electronics for the acquisition, processing, and formatting of data from these sensors, and a communication system to relay the formatted data to shore on a 3-hour synoptic cycle. Each operational buoy is normally equipped with a wave measurement subsystem, which provides a displacement spectral estimate for inclusion in the synoptic report. Two types of wave systems[6,7] are used by NDBO, each of which has a buoy-fixed, single-axis accelerometer mounted parallel to the buoy mast as a motion sensor.

The decision to use a buoy-fixed rather than vertically stabilized sensor was based on an NDBO in-house theoretical analysis, which indicated that such a sensor mounted on a discus buoy would satisfactorily approximate the output of a gimballed vertical accelerometer. This theoretical result was tested experimentally by comparing displacement spectra from such systems with spectra from a Waverider deployed nearby. Results of the comparison showed no apparent difference between the spectra. A more thorough test was planned for the Experimental Environmental Research Buoy (XERB), which is described in detail by Steele, et al.[8] A buoy-fixed accelerometer and a vertically stabilized accelerometer were installed on the XERB; time series of sensor outputs were recorded on board for analysis at shore.

2. The XERB Buoy

The primary goal of the testing associated with the XERB buoy was the determination of the feasibility of obtaining sea surface directional

spectral estimates in near real time from a large (12-meter diameter, 91,000 kg), remotely operated discus buoy. For these tests, NDBO used an experimental payload, which is based on a 16-bit minicomputer. The payload acquired and processed data into auto- and cross-covariances, which were transmitted to shore for computation of the directional spectral estimate.

A completely separate payload was also installed on board XERB to confirm the proper operation of the experimental system and to report meteorological data from the site. The latter system was a standard NDBO operational payload of the Phase II type, manufactured by the Magnavox Corporation. A Wave Data Analyzer (WDA) subsystem of this payload produced a covariance function estimate at the synoptic hour, which was broadcast to shore for processing into a one-dimensional spectral estimate.

A secondary goal of the XERB project was to provide a test bed on which to mount various sensors. Digitized time series of sensor data would be recorded on the buoy, periodically recovered during service visits, and processed at shore. The time series would form a large data base, thereby allowing sensor performance evaluation, sensor comparison, and analysis of buoy motion.

3. Description of the Experiment

Acceleration Sensors. The buoy-fixed acceleration sensor was a Kistler triaxial servoaccelerometer of the closed-loop, force-balance type. The transducer was oriented with one axis parallel to the buoy mast and one toward the buoy bow. Sensitivity of the mast-parallel axis was 1.02 V/m/sec.

The vertically stabilized accelerometer was a Datawell heave sensor (40 sec), manufactured by Datawell BV, Haarlem, The Netherlands. Vertical stabilization is achieved inertially by mounting the transducing element in a double gimbal with fluid damping. This arrangement is mechanically equivalent to attaching the transducer to a damped spherical pendulum with a 40-second period. Since the longest-period ocean surface wave observed in nature is in the 30-second range, the pendulum is not excited by the wave motion and remains vertically stabilized. In fact, the manufacturer claims that response of the sensor to horizontal acceleration in the wave period range is less than 3 percent of the sensitivity to vertical acceleration, which is 1.00 V/m/sec.

Both sensors were installed below the deck in a center trunk on the buoy symmetry axis. The vertically stabilized sensor was mounted with the manufacturer's prescribed sensing point approximately at the waterline. The buoy-fixed sensor was mounted approximately 0.5 meter below this point and 0.3 meter off the buoy centerline.

Data Recording. In its deployed configuration, 11 analog signals from 5 motion sensors were supplied to a 32-channel multiplexer (mux) input to a 12-bit analog-to-digital converter (A/D) which scaled linearly over the range +10 to -10 volts. The A/D was interfaced to a Data General NOVA 4001 minicomputer, which controlled mux channel selection and A/D conversion. A real-time clock provided the time of year in a buffer available to the minicomputer. The minicomputer was also interfaced to a Kennedy Model 1600 incremental 7-track recorder, which produced a 556 bpi tape in a format compatible with most 7-track computer system tape drives. The experimental payload was operated on a 3-hour cycle based on midnight Greenwich Mean Time (GMT). Immediately following the completion of directional wave data processing at approximately 21 minutes after the synoptic hour, data were acquired and written on tape by the minicomputer. All active channels were sampled essentially simultaneously by the minicomputer in a single scan of the mux, which occurred at 0.5-second intervals. Tape writing took place between scans, with count values for each sensor channel from a scan recorded as a single tape frame. In addition to the sensor data, each frame began with a two-character synchronizing word and ended with a check word, the sum of all data values in the frame. Multiple frames were recorded within a physical record on the tape. A total of 1800 frames of data (15 minutes) were recorded per synoptic report.

Although each six-bit tape data character had a hardware parity bit that was attached by the recorder and checked by the tape reading unit, the checksum proved to be valuable in flagging tape write/read errors. The most common of these was the loss of a character, or "byte dropout". On shore, data from the on-board tape was processed into engineering units prior to storage in the data base. In the event of a tape error as evidenced by the checksum, all data for the offending frame were discarded. Each missing frame was replaced by interpolation between valid data points in the series.

Deployment. The XERB was deployed on March 26, 1977, in the Atlantic Ocean at 30°24'N, 80°08'W, approximately 100 km east of Jacksonville, Florida, on the edge of the continental shelf. A single-point mooring was used to secure the buoy in 200 meters of water.

Upon deployment, the experimental payload began recording data, with operation taking place on a 3-hour cycle based on midnight GMT. Reliable data was obtained for approximately 3 weeks, until hardware problems caused this payload to cease operation. Regular data recording resumed in June 1977 and continued for approximately 4 weeks. At this point, serious payload problems necessitated retrieval of the buoy, ending this phase of the project.

Sea states during the data collection period were light. Significant wave heights ranged from 0.2 to 2.1 meters, and winds ranged from calm to 12 m/sec.

4. Analysis of Data

Once the acceleration time series were stored in engineering unit form in the data base format, a number of standard computer programs could be used to process the data for analysis. Using these programs, the acceleration data were compared through comparison of the time series data by means of plots, and through spectral analysis. The auto-covariance of each time series was computed out to $m \simeq 100$ lags, from which a raw spectral estimate, $S_p(f_k)$, was obtained for frequencies

$$f_k = k/2m\Delta t \qquad (1)$$

where $k = 0, 1, 2, \ldots, m$; $\Delta t = 0.5$ second, and $p = 1, 2$ denotes the particular time series (cf. Bendat and Piersol[9]). The $\tilde{S}_p(f_k)$ were smoothed by Hanning to obtain an acceleration spectral estimate, $\hat{S}_p(f_k)$, having 36 equivalent degrees of freedom.

A cross-covariance function estimate was also computed and used to produce a raw estimate of the cross-spectrum, from which a smoothed estimate

$$\hat{S}_{12}(f_k) = \hat{C}_{12}(f_k) - i\,\hat{Q}_{12}(f_k) \qquad (2)$$

was obtained. A relative phase function

$$\hat{\Theta}_{12}(f_k) = \tan^{-1}\left[\frac{\hat{Q}_{12}(f_k)}{\hat{C}_{12}(f_k)}\right] \qquad (3)$$

was also computed for each frequency. The phase function estimates the phase angle of time series 2 with respect to time series 1 at frequency f_k.

The coherence function between the two time series is defined by

$$\hat{\gamma}^2_{12}(f_k) = \frac{|S_{12}(f_k)|^2}{\hat{S}_1(f_k)\,\hat{S}_2(f_k)} \qquad (4)$$

This function is analogous to the square of a correlation coefficient computed for each frequency, f_k, as described in Jenkins and Watts[10]. The coherence function is a measure of the linear dependence of time series 2 on time series 1 at the frequency f_k, and has the property that if the two time series are related by a constant linear parameter, $\hat{\gamma}^2_{12}(f_k)$ will be unity. Similarly, when the two series are completely unrelated, the coherence function will be zero. If the coherence function is between zero and unity, one or more of the following conditions is satisfied:

- Uncorrelated noise is present in the two time series
- The relationship between the time series is nonlinear
- One or both of the time series is influenced by an extraneous signal.

5. Results

Spectral comparisons of data from the two acceleration sensors were made on 20 different data records taken from the March-April 1977 period. Time series comparisons were also made on selected records from this group. Figure 1 compares the two time series for a period of 1 minute. Note that agreement is quite good, except for an offset in one of the sensors relative to the other.

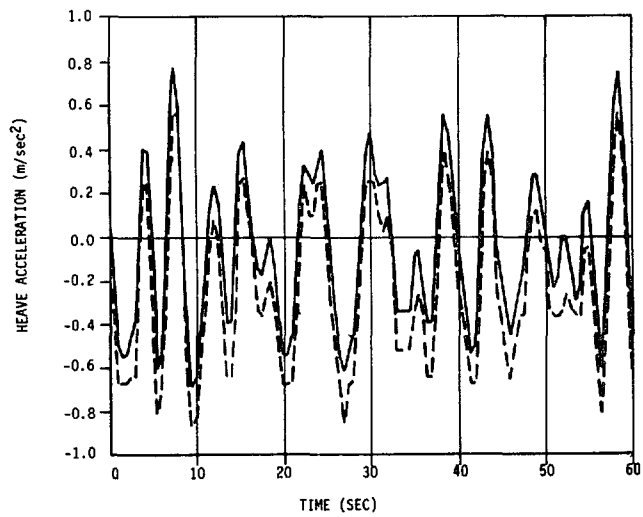

Figure 1. TIME SERIES OF ACCELERATION FROM BUOY-FIXED MAST-PARALLEL ACCELEROMETER AND VERTICALLY STABILIZED ACCELEROMETER. DATA ACQUIRED MARCH 26, 1977, 0700 GMT

Figure 2 compares the power spectrum of acceleration from the gimballed accelerometer with the spectrum from the buoy-fixed acclerometer. Data to compute the spectra shown in Figure 2 were acquired on March 26, 1977, 0700 GMT. The same comparison is made in Figure 3 for waves of higher frequency. Data to produce the latter spectra were acquired on April 2, 1977, 1500 GMT. Agreement in both cases is excellent and is typical of the entire data set.

A displacement spectral estimate

$$\hat{D}_p(f_k) = \hat{S}_p(f_k) \;/\; (2\pi f_k)^4 \qquad (5)$$

was obtained from each acceleration spectrum and used to compute significant wave height via

$$H_{1/3} = 4\sqrt{M_o} \qquad (6)$$

The spectral moment, M_o, was obtained by numerical integration of the displacement spectrum. The displacement spectral density below frequency f_o was set to zero as a noise correction procedure, to prevent the noise level values of acceleration spectral density from contaminating the wave height estimate. The significant wave height values shown in Figures 2 and 3 were computed using $f_o = 0.07$ Hz.

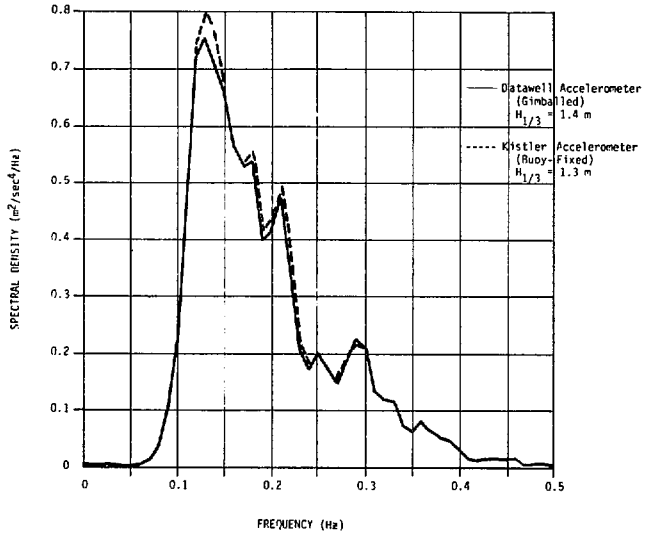

Figure 2. ACCELERATION SPECTRA FROM BUOY-FIXED AND VERTICALLY STABILIZED ACCELEROMETERS COMPUTER FROM DATA ACQUIRED MARCH 26, 1977, 0700 GMT

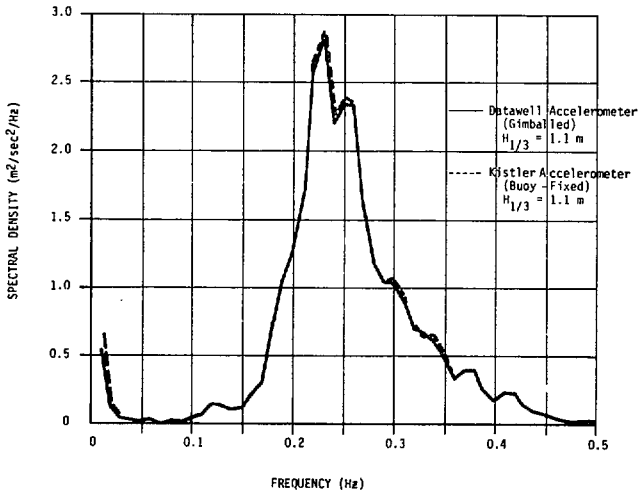

Figure 3. ACCELERATION SPECTRA FROM BUOY-FIXED AND VERTICALLY STABILIZED ACCELEROMETERS COMPUTED FROM DATA ACQUIRED APRIL 2, 1977, 1500 GMT

Figure 4 shows the coherence between the two time series, $\hat{\gamma}^2_{12}(f_k)$, versus frequency, computed for the data of April 2, 1977, 1500 GMT, corresponding to Figure 3. Comparison with the spectrum of Figure 3 indicates that coherence between the gimballed and buoy-fixed accelerometers approaches unity at frequencies for which the power spectrum shows a significant level of acceleration.

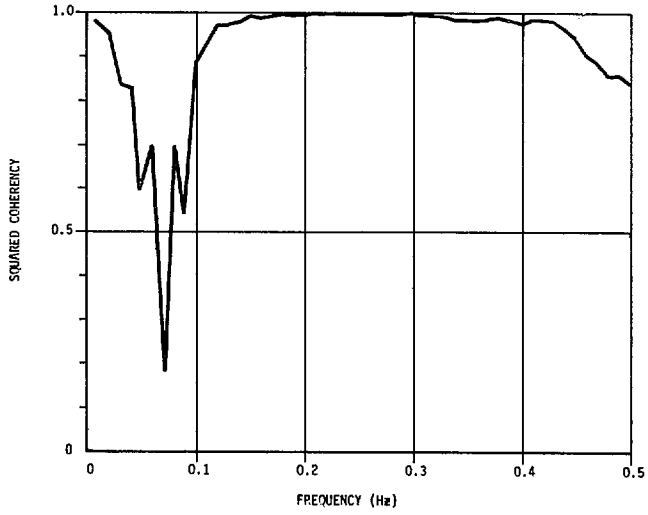

Figure 4. COHERENCE BETWEEN BUOY-FIXED ACCELERATION AND VERTICAL ACCELERATION TIME SERIES AS A FUNCTION OF FREQUENCY. DATA ACQUIRED APRIL 2, 1977, 1500 GMT

Further evidence of this conclusion is presented in Figure 5, which shows $\hat{\gamma}^2_{12}(f_k)$ versus $\hat{S}_1(f_k)$. Note that coherence remains high until the acceleration spectral density diminishes below 0.01 $m^2/sec^4/Hz$, at which level the coherence drops rapidly to zero. The solid curve of Figure 5 represents a "mind's eye fit" of the data. It is interesting to note that the curve does not pass through the origin, but intercepts the abscissa at $\hat{S}_1(f_k) \approx 0.002$ $m^2/sec^4/Hz$. This intercept value is a rough measure of the level of truly random noise in the buoy system.

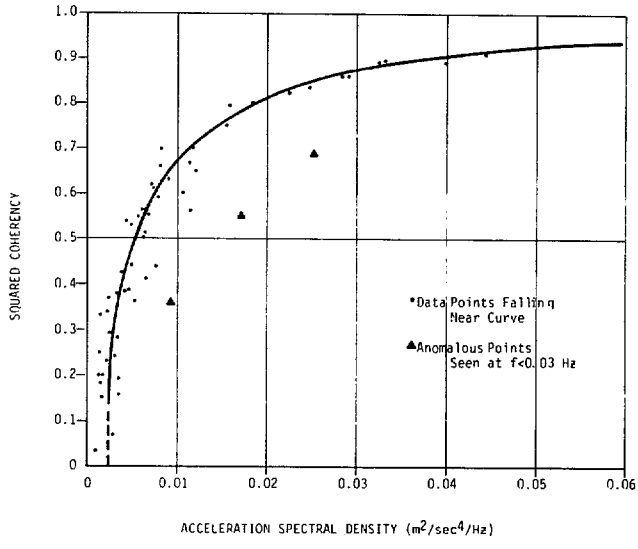

Figure 5. COHERENCE BETWEEN BUOY-FIXED ACCELERATION AND VERTICAL ACCELERATION TIME SERIES PLOTTED AS A FUNCTION OF VERTICAL ACCELERATION SPECTRAL DENSITY. DATA ARE A COMPOSITE OF THREE TIME PERIODS

The phase of buoy-fixed acceleration relative to vertical acceleration is shown in Figure 6, which is a plot of $\Theta_{12}(f_k)$ versus frequency. The data points represent a combination of data from the several records. Points for which the coherence function was less than 0.95 were excluded from the plot in order to minimize the effect of noise. A fit to the linear function

$$\Theta(f) = mf + b \qquad (7)$$

was made by the method of least squares for the plotted data. Estimates of m = -0.138 deg/Hz and b = 0.232 degree were obtained with a correlation coefficient of 0.75. The least squares line is shown in Figure 6 as a solid line. A phase shift that is a linear function of frequency implies a constant time difference between the two time series. In this case, the buoy-fixed accelerometer lags the vertical accelerometer by approximately 38 msec. The phenomenon appears consistently throughout the data; an explanation of a delay of this magnitude has not been found.

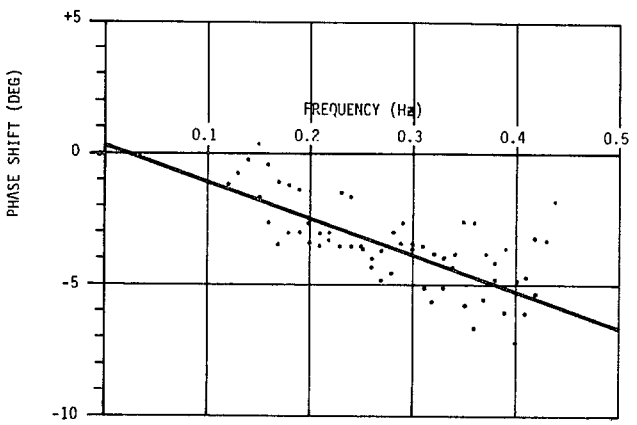

Figure 6. PLOT OF PHASE OF BUOY-FIXED ACCELERATION RELATIVE TO VERTICAL ACCELERATION PLOTTED AS A FUNCTION OF FREQUENCY

6. Conclusions

Results of the data analysis described herein, of which the data in Figures 1 through 6 are typical, confirm the agreement between the buoy-fixed and vertically stabilized accelerometers. However, some care should be exercised in extending the excellent agreement seen at the low to moderate sea states to higher sea states for which no sensor comparison data is available. This is particularly true in view of Tucker's theoretical result, which predicts that the error obtained by the two sensors should increase with the sea state number.

However, the data summarized herein strongly suggest that the buoy-fixed accelerometer is as accurate a sensor as the inertially stabilized vertical accelerometer for the purpose of estimating wave displacement spectra from a large discus buoy. This conclusion has implications beyond the academic, since an inertially stabilized sensor is more expensive than the single-axis, buoy-fixed accelerometer by a factor of from 5 to 10, depending upon the particular single-axis sensor chosen. The buoy-fixed sensor is also smaller by a similar factor. Although this is not a great concern for a large discus buoy, constraints in handling the Datawell sensor are a concern when that accelerometer is employed.

The Datawell sensor remains an obvious choice in some applications; e.g., on board a non-surface-following platform and in situations where an analog displacement signal is required. In NDBO's experience with the heave sensor as an accelerometer and with the Datawell Waverider which uses the same sensor, no failures of the intricate suspension have occurred when handling was conducted per Datawell instructions for these devices.

7. Suggestions for Further Investigation

In view of the excellent agreement between the buoy-fixed and vertically stabilized accelerometers for relatively light sea states, the degree of agreement in heavier sea states should be investigated.

NDBO has introduced several boat-shaped hull NOMAD buoys into its network of operational buoys. These buoys have been equipped with wave systems that use a buoy-fixed accelerometer as the system sensor. Preliminary results of high seas, in situ comparisons between displacement spectra from NOMADs and a GOES-reporting Waverider buoy have shown remarkable agreement.

8. Acknowledgements

The preparation of this paper and the work described herein were supported entirely by the NOAA Data Buoy Office through National Space Technology Laboratories Technical Work Request DB-3T01. The contributions of Mr. K.E. Steele, who conceived and instigated the comparison experiment, and Dr. A. Trampus, under whose auspices the spectral analysis computer programs were developed, are also gratefully acknowledged.

References

1. Tucker, M.J., "A Shipborne Wave Recorder", Transactions of the Institute of Naval Architecture 98, London, p. 236, 1956.

2. Marks, W., and R.G. Tuckerman, "A Telemetering Accelerometer Wave Buoy", Proceedings of the International Conference on Ocean Wave Spectra, p. 281, Prentice-Hall, Inglewood Cliffs, New Jersey, 1963.

3. Tucker, M.J., "The Accuracy of Wave Measurements Made With Vertical Accelerometers", Deep Sea Research 5, p. 185, 1959.

4. Gaul, R.D., and N.L. Brown, "A Comparison of Wave Measurements From a Free-Floating Wave Meter and the Monster Buoy", Transactions of the Second International Buoy Technology Symposium, Marine Technology Society, Washington, D.C., 1967.

5. Verhagen, C.M., P.L. Gerritzen, and J.G.A. von Breugel, "Operation and Service Manual for the Waverider", Datawell, Haarlem, The Netherlands, Doc. No. 5095-67020.

6. Steele, K.E., and A.S. Hananel, "An Analog Wave Spectrum Analyzer System for Operational Buoys", Proceedings of the MTS-IEEE Conference, The Ocean Challenge (OCEANS 78), Washington, D.C., Sept. 6-8, 1978.

7. Steele, K.E., P.A. Wolfgram, A. Trampus, and B.S. Graham, "An Operational High Resolution Wave Data Analyzer System for Buoys", Proceedings of the OCEANS 78 Conference, Washington, D.C., Sept. 13-15, 1976.

8. Steele, K.E. E.L. Burdette, and A. Trampus, "A System for the Routine Measurement of Directional Wave Spectra from Large Discus Buoys", Proceedings of the MTS-IEEE Conference, The Ocean Challenge (OCEANS 78), Washington, D.C., Sept. 6-8, 1978.

9. Bendat, J.S., and A.G. Piersol, Measurement and Analysis of Random Data, John Wiley and Sons, Inc., New York, 1966.

10. Jenkins, G.M., and D.G. Watts, Spectral Analysis and Its Applications, Holden-Day, San Francisco, 1968.

11. Adamo, L.C., K.E. Steele, and E.L. Burdette, "A GOES-Reporting Waverider Buoy", Proceedings of the MTS-IEEE Conference, The Ocean Challenge (OCEANS 78), Washington, D.C., Sept. 6-8, 1978.

A SMALL, WIDE-BAND, LOW-FREQUENCY, HIGH-POWER SOUND SOURCE UTILIZING THE FLEXTENSIONAL TRANSDUCER CONCEPT

J. A. Pagliarini
Ocean Systems Division
Sanders Associates
Nashua, New Hampshire 03060

R. P. White
Ocean Systems Division
Sanders Associates
Nashua, New Hampshire 03060

Abstract

Flextensional transducers have wider bandwidths, lower operating frequencies, and higher power handling capabilities than any other types of transducers of comparable size. They make possible a new class of underwater sound sources having much smaller size while retaining all the other operating characteristics of conventional sound sources. The flextensional concept appeared several years ago. The concept is based on the vibrational modes of an oval cylindrical shell. Mutual coupling between these modes results in potential bandwidths of several octaves. This paper presents the design concept and performance predictions for a small, low-frequency sound source. Test data on an experimental model are presented and compared with predicted values.

1. Introduction

Requirements for transducers of small size, low frequency and wide bandwidth all favor a flexural mode of vibration. The flextensional concept offers improved radiation efficiency and greater depth range compared to other flexural modes such as the flexural bar or flexural disc. It offers a 3:1 bandwidth advantage at frequencies in the 100 Hz to 5 kHz range, and even greater bandwidths if higher order modes are incorporated.

The flextensional transducer consists of a shell which, because of its shape and dimensions, has one or more resonant vibrational modes in the band of interest. A piezoelectric bar is used to excite the desired modes. There are four classes of flextensional transducers, distinguished by their basic shapes, as shown in Figure 1. The subject of this paper is the Class IV flextensional transducer.

The flextensional transducer offers the following advantages:

- Good impedance match to water load.
- Greater bandwidth for a given size (3:1 advantage).
- High efficiency.
- High power density per unit volume.
- High power density per unit weight (30 watts per pound).
- Reduced size and weight.
- System robustness (i.e., bandwidth and power margin).
- Easily implemented ceramic prestress.
- Ruggedness.
- Reliability.

2. Background

Flextensional technology has existed for more than a decade. Elastic wave theory for shell deformation and vibration was developed by Dr. Royster and extended by G. Brigham. W. Toulis performed early work in developing hardware for low frequency high power applications. The coupling between ceramic stack length mode and shell membrane modes represents relatively complex elastic wave theory which resists reduction to practice.

Recently developed engineering design equations formulated through a combined theoretical/empirical approach utilizing the consultant services of G. Brigham of Wheeler Industries now permit greater accuracy in the prediction of transducer performance characteristics. These equations also enable the engineer to extrapolate the design parameters to match other performance requirements.

This effort has resulted in a high degree of confidence in performance predictability of Class IV flextensional designs.

The flextensional transducer has proven itself in a wide variety of applications over the past ten (10) years including the following:

- Project MIMI - ONR/University of Miami
- Deep Star Propagation Program at NUSC
- AFAR - Range - Acoustic Communications Program
- UDL - Mobile Acoustic Communications Program

The AFAR and UDL applications are very important data gathering efforts in the field of acoustic communications. The flextensional transducers utilized in these programs have demonstrated conclusively their reliability, efficiency and broadband response. The salient features of the flextensional design are:

- Minimum size and weight.
- Low transducer Q (3:1 advantage over conventional techniques).
- Greater power handling capability per unit volume (3:1 over conventional techniques).
- System robustness (performance margin against bandwidth and power levels).

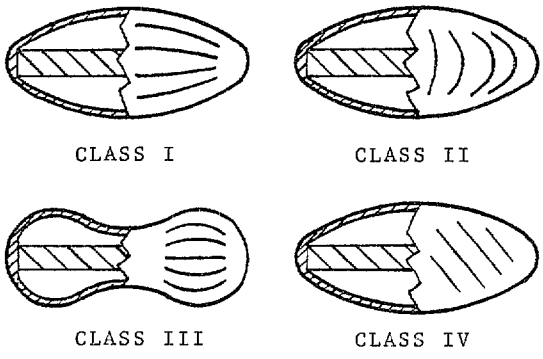

Fig. 1: The four classes of flextensional transducers

3. Design Concept

The Class IV flextensional transducer has a shell which approximates an oval shaped cylinder. A cross-sectional view of a circular cylinder is shown in Figure 2 and the nodal positions for the first flexural mode are shown. As can be seen, the nodes are located at 90-degree intervals, with opposite-phased displacement in adjacent quadrants. A perfectly circular shell in flexure thus has poor radiating characteristics, since equal areas of shell surface are moving outward and inward at the same time. If, however, the cross section is modified to an oval shape, as shown in the same figure, the nodes are displaced toward the ends of the shell. As a result, there are unequal areas moving outward and inward, and the shell is an efficient radiator. The amplitude of vibration of the larger (diaphragm) areas is also greater than that of the end area, further enhancing the radiating efficiency.

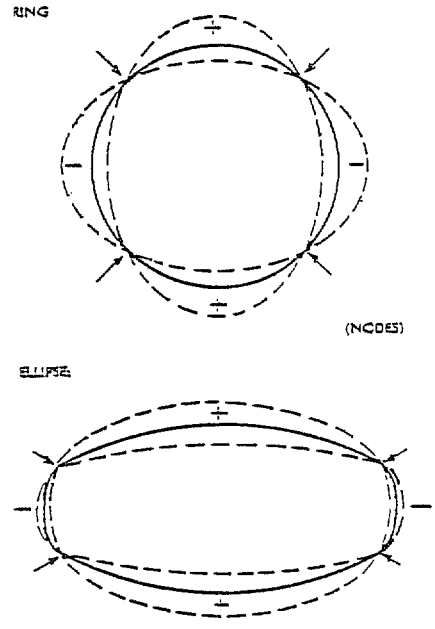

Fig. 2: Fundamental flexural modes of a ring and an ellipse

Some means must be provided to drive the shell into this mode of vibration in response to electrical signals. This is accomplished by inserting a piezoelectric ceramic bar between the ends of the shell, as shown in Figure 3. The bar is made up of ceramic slabs, individually electroded and polarized, and bonded together with epoxy. The electrodes are connected so that all the slabs are driven in parallel in the k_{33} mode. This mode has the highest electroacoustic coupling coefficient, resulting in maximum transfer of energy to the mechanical motion. The use of

many slabs in parallel also results in a low electrical impedance, which facilitates amplifier matching.

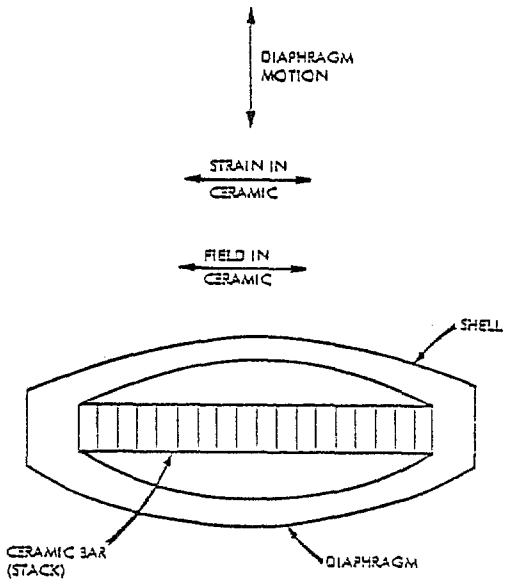

Fig. 3: Basic Flextensional Concept

The electric field applied across each ceramic slab produces a strain in the direction indicated. This forces the ends of the shell to deflect, which in turn produces a deflection in the diaphragms. The amplitude of deflection of the diaphragms is greater than that of the shell ends by the ratio of major to minor axes of the oval. The radiating area of the diaphragms is also much greater than that of the shell ends. As a result, most of the radiation of acoustic energy occurs from the diaphragm surfaces, with very little out-of-phase radiation from the ends. Because of this, the transducer is an efficient radiator. The amplitude step-up, as well as the area step-up between the ceramic stack and the diaphragms, also results in good acoustic impedance match to the water, reflecting significantly increased bandwidth for a given transducer volume. Figure 4 shows construction details for a typical Class IV flextensional unit.

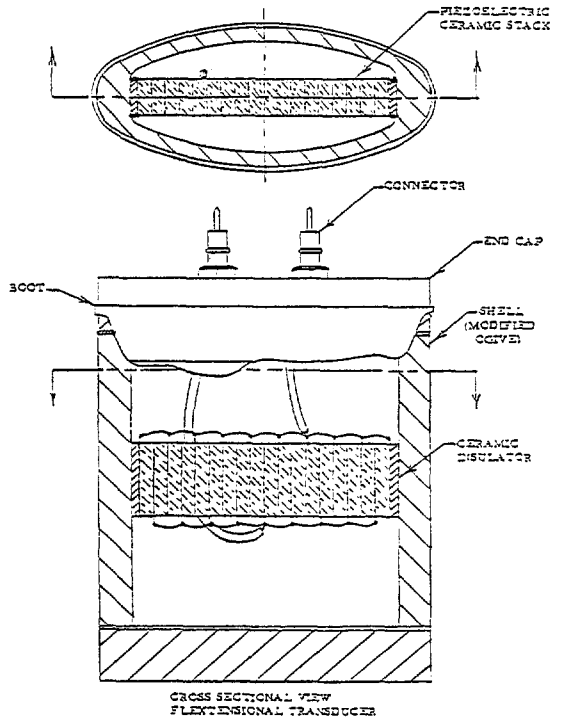

Fig. 4: A Typical Class IV Flextensional Transducer

When designing this type of flextensional transducer the length of the stack is made slightly greater than the length of the opening between the shell ends so that the shell must be expanded to allow stack insertion. Compressive bias is required because hydrostatic pressure on the diaphragms, as well as high drive levels, tend to place the ceramic stack in tension. Bias values must be kept within recommended compressive stress ratings to avoid significant loss of coupling or depoling effects. The lowest compressive bias consistent with maximum operating depth and power is desirable for maximum bandwidth.

To insert the stack, the shell is placed in a hydraulic press and force applied to the two diaphragms. This causes the distance between the shell ends to increase, allowing insertion of the stack. Before insertion, the ends of the stack are coated with epoxy. After stack insertion the force is removed from the shell diaphragms, allowing the shell ends to compress the stack. The transducer is then essentially complete, except for two end covers to prevent flooding of the shell interior.

4. Performance Predictions

The predicted impedance, admittance, and constant-voltage transmitting response curves for a unit of the above design are shown in Figures 5, 6, and 7. In addition, the predicted constant-voltage transmitting response with series tuning is shown in Figure 8.

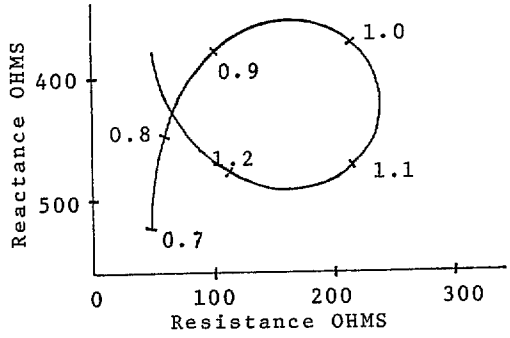

Fig. 5: Predicted Impedance

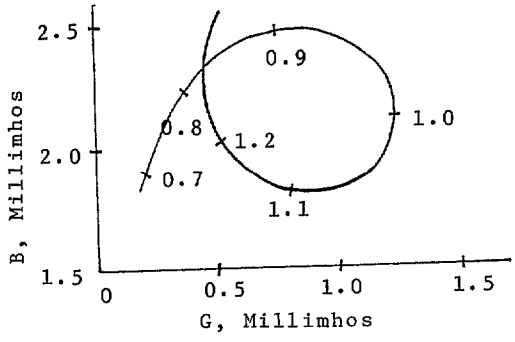

Fig. 6: Predicted Admittance

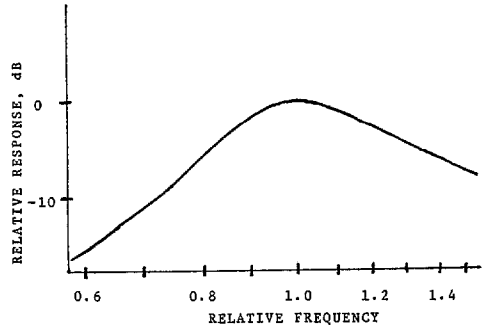

Fig. 7: Predicted Constant-Voltage Transmitting Response (TVR)

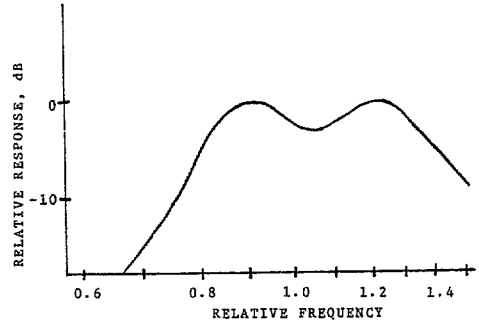

Fig. 8: Predicted TVR with Series Tuning

5. Test Results

Measurements of the above performance parameters were made on several units at Sanders' acoustic calibration facility. In addition, measurements of power linearity and directivity were made. The results of a typical unit are shown in Figures 9-16. The measured values closely match the predicted values. The impedance and admittance curves, as well as the response measurements, show a mechanical Q of approximately 3, which represents a 33 per cent bandwidth. This exceeds by approximately 3 to 1 widths achievable by other transducer types such as the flexural disc. Power linearity is demonstrated up to a level of at least 192 dBμ PA at 1 meter.

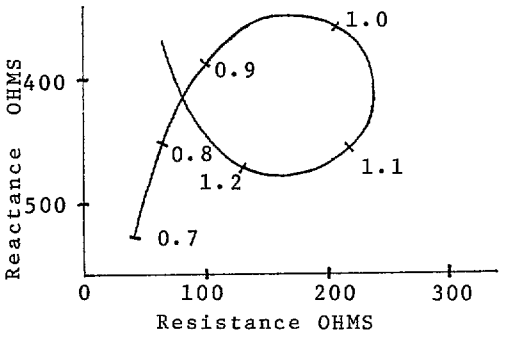

Fig. 9: Measured Impedance

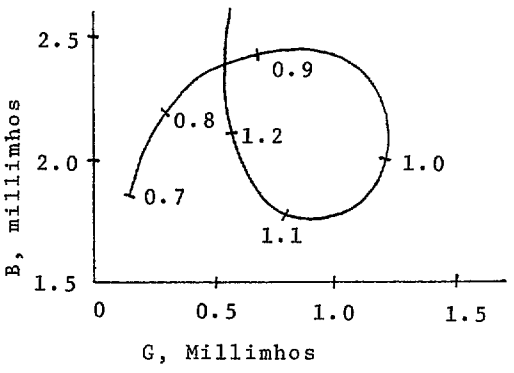

Fig. 10: Measured Admittance

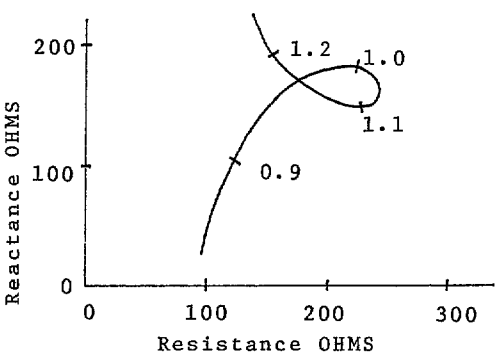

Fig. 11: Measured Impedance with Series Tuning

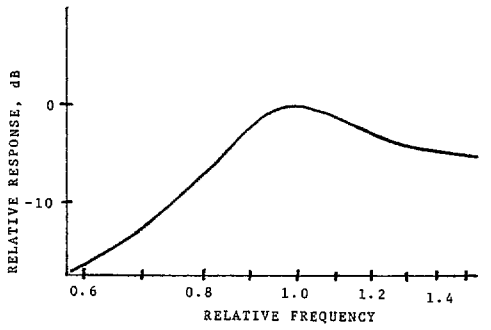

Fig. 12: Measured TVR

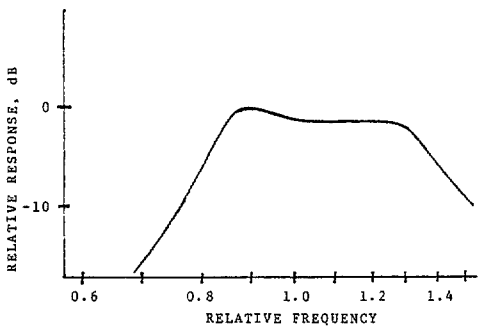

Fig. 13: Measured TVR, with Series Tuning

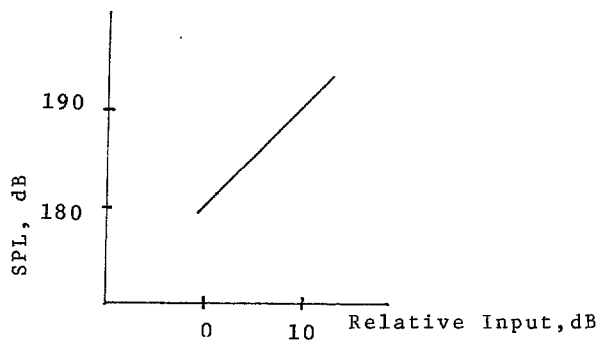

Fig. 14: Measured Power Linearity

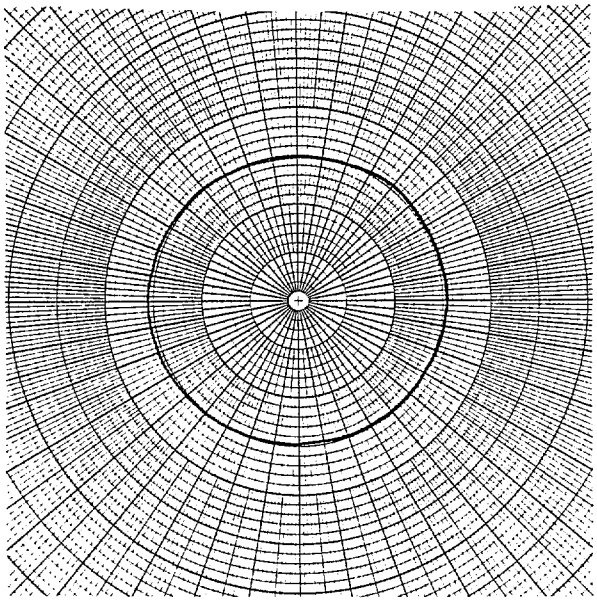

Fig. 15: Measured Pattern, XY Plane (scale - 1dB per division)

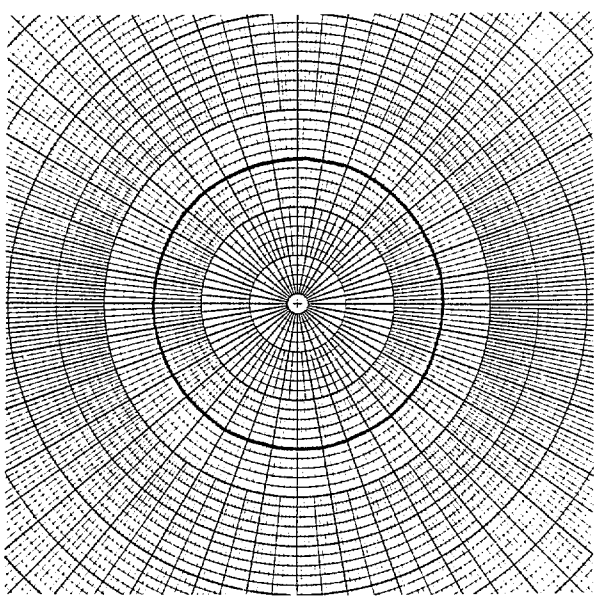

Fig. 16: Measured Pattern, XZ Plane (scale - 1dB per division)

6. Conclusion

In conclusion, a transducer having wider bandwidths, lower operating frequency and higher power handling capability than conventional types of comparable size has been achieved by means of the flextensional concept.

References

1. Brigham, G.A., Design Parameters of the Class IV flextensional transducer, Wheeler Industries Final Report under Sub-contract NFZAC N95 105939M.
2. Royster, L.H. and G.A. Brigham, Present status in the design of flextensional underwater acoustic transducers, J. Acoust. Soc. Am., Vol. 46, p76, 1969.
3. Rutledge and R.A. Royster, Approximate model for predicting operational parameters of the Class IV Flextensional Underwater Transducer J. Acoust. Soc. Am., Vol. 50, p82(A), 1972.
4. Brigham, G.A., An equivalent circuit for oval flextensional transducers, J. Acoust. Soc. Am., 51, 82(A), 1972.
5. Brigham, G.A., Vibrations of oval rings, J. Acoust. Soc. Am., Vol. 42, p. 1203, 1967.
6. Brigham, G.A., Analysis of the Class IV Flextensional Transducer by use of wave mechanics, J. Acoust. Soc. Am., Vol. 56, pp 31-39, 1974.
7. Brigham, G.A., Lumped parameter analysis and equivalent circuit of the Class IV Flextensional Transducer, NUSC Tech. Report, July 1973.

AN ANALYSIS OF THE DISTRIBUTION OF MEASURED BUBBLE PULSE PERIODS OF EXPLOSIVE SOURCES

Richard J. Hecht
Underwater Systems, Inc.
8121 Georgia Avenue
Silver Spring, Maryland 20910

Louis A. Mole
Underwater Systems, Inc.
8121 Georgia Avenue
Silver Spring, Maryland 20910

Abstract

Small explosive charges are often utilized as acoustic sources in the measurement of signal propagation in the ocean. Of particular importance when used as investigative tools is the consistency of the generated power spectrum. A measure of consistency is the degree of variation in the first bubble pulse period, defined as the interval from the onset of the initial shock wave to first bubble pulse maximum. To determine the degree of consistency that can be expected from a series of detonations, an experiment was conducted in which over 1300 charges were detonated at nominal depths of 60 and 300 feet. Using the pressure time histories, the bubble pulse periods were first determined and then analyzed from two viewpoints: first in relation to the charge specifications, and second with regard to the possible physical reasons for the shapes of the distributions. The effects of charge weight, detonation depth, temperature and wave height on the observed bubble pulse period distribution were analyzed.

1. Introduction

The general features of the acoustic waveforms generated by underwater explosives are well known, having been analyzed in detail by a number of individuals[1-5]. The acoustic pressure versus time signature of an underwater explosive source is a sensitive function of the charge weight and the depth of the explosion. The bubble pulse period of an underwater explosion is a function of both the explosive yield and the detonation depth, and, therefore, can be effectively used to monitor the consistency of the resultant acoustic source spectrum and the detonation depth. The bubble pulse period is defined as the time from the beginning of the shock wave to the maximum of the first bubble pulse[6]. The intent of this paper is 1) to present an analysis of an experiment in which 1300 explosives were detonated at depths of 60 and 300 ft, 2) to compare the performance of the explosive sources with the manufacturer's specifications, and 3) to compare the variations in the data with recorded environmental changes.

2. SUS Specifications

The explosive used in this experiment was a Signal, Underwater Sound (SUS), which is a standard U.S. Navy item. Manufacturing specifications for the SUS were obtained from the Naval Weapons Station, and are summaried in Table 1[7-9]. The SUS used in this experiment nominally contain 1.8 lb of TNT and were preset to detonate at pressures equivalent to 60 and 300 ft of depth. The detonation is initiated by mechanical means when the design pressure is attained. The SUS is manufactured under rigorous military specifications so that the performance is consistent from shot to shot.

TABLE 1
SUS MANUFACTURING SPECIFICATIONS[7-9]

	SUS Type	
	Mk 61	Mk 82
Lowest actuating pressure	22 psi	120 psi
Highest actuating pressure	31 psi	147 psi
Detonation depth tolerance	± 10 ft	± 30 ft
Average descent velocity	15 ft/s	15 ft/s
Minimum Explosive (TNT)	1.65 lb	1.65 lb
Booster (Tetryl)	0.07 lb	0.07 lb

3. Experiment

The data was acquired during an exercise in the Northeast Pacific Ocean in September 1973. The SUS shots were launched from the shooting ship over a period of a few days as the ship followed a northerly course from Latitude 29°01' N to 46°45' N. The 60 and 300 ft depth SUS were launched from the ship so as to detonate at two minute intervals. A transducer suspended from the shooting ship was used to receive the SUS signals, which were recorded on analog magnetic tape in the FM mode, along with IRIG B time code and voice communication. Table 2 shows the number of each type of SUS launched and the number that detonated.

TABLE 2
TABULATION OF SUS STATISTICS

	SUS Type	
	Mk 61	Mk 82
Nominal detonation depth	60 ft	300 ft
Number dropped	696	695
Number processed	654	655
Number not recorded	16	14
Duds	26	26

4. Data Processing

The signal processing was performed using a minicomputer that was programmed to analyze the recorded data in real time. A block diagram of the processing system is presented in Figure 1. For each shot, successively, the computer determined: 1) the occurrence of an individual explosive signal, 2) the approximate detonation time, 3) the bubble pulse period, and 4) the error bounds. After these calculations were made, the computer presented the results to the operator for evaluation as to acceptance or rejection. The analog to digital sampling rate of the SUS signal was derived from the 8th harmonic of the time code carrier, which provided a time resolution on the bubble pulse period of 0.125 ms. In addition, this processing procedure removes any speed variation present due to the analog tape recording or playback process. A quality control check on the automatic processing indicated consistent agreement to within 0.15 ms when compared to manually determined bubble pulse periods.

5. Data Statistics

After completion of the processing, the data was analyzed statistically to determine the consistency of the events. Figure 2 presents a histogram of the bubble pulse periods for the Mk 61 SUS. The median bubble pulse period is 127.5 ms which, for a yield of 1.8 lb of TNT, corresponds to a detonation depth of 55 ft. The mean value of the period is 126.9 ms with a standard deviation of 3 ms. The distribution exhibits a strong skewness to the shorter bubble pulse periods, the coefficient of skewness being -1.3.

Figure 3 presents the bubble pulse periods for the Mk 82 SUS. The median bubble pulse is 42.8 ms which, for 1.8 lb of TNT, corresponds to a detonation depth of 291 ft. The mean value of the data is 43.2 ms with a standard deviation of 1.3 ms. The distribution can be considered to be symmetric, since the coefficient of skewness is only -0.40. Note that the data for the two SUS types are similar in that the mean and median values correspond to shallower depths than the expected nominal values.

Since the bubble pulse period is dependent on both the explosive weight and the detonation depth, the relative effects of the construction specifications for each variable were examined with regard to their effect on the bubble pulse period. The explosive specification is at least 1.65 lbs of TNT plus 0.07 lb of booster. The maximum explosive weight is controlled by the "fill line" of the explosive container, which is considered in this analysis to be 1.85 lb[8]. Since both the peak pressure output and the bubble pulse period are proportional to the cube root of the yield, a variation of $\pm$ 2% in the bubble pulse period can be expected for these small variations in yield.

For the Mk 61 sixty foot SUS, a depth specification tolerance of $\pm$ 10 ft is permissible. Therefore, since the bubble pulse period is inversely proportional to depth to the five-sixths power, the corresponding bubble pulse variation is $\pm$10%. Correspondingly, for the Mk 82, three hundred foot SUS, a specification tolerance of $\pm$ 30 ft is permissible, thereby resulting in a $\pm$ 8% variation in bubble pulse period. Because of the insensitivity of the bubble pulse period to yield variations, it must be concluded that the variations are largely controlled by the depth specifications. Examining Figures 2 and 3 it is evident that all but a few of the points for the bubble pulse periods lie within these specifications.

Figure 4 is a plot of the observed bubble pulse period versus time for the Mk 61 SUS. An examination of the figure shows that the majority of the values lie between 125 and 130 ms, which are equivalent to 52.2 and 56.4 feet in depth. This range of values, in which the majority of the points lie, is comparably demonstrated in Figure 2. If we were to set the acceptance criteria for these SUS to be within this range of values, then the depth variation is $\pm$ 2%, which is the same percentage as that for the yield. Because the overwhelming majority of the shots' bubble pulse periods fall within this small window, it is evident that the variation in depth and yield is actually much smaller than the specifications indicate. Using this criterion (bubble pulse period between 125 and 130 ms) for selection of the acceptable SUS for propagation loss measurements, the estimated depth variation of the source is on the order of plus or minus 2 feet. As a matter of interest this is comparable, if not superior, to the depth control that can be maintained for a towed continuous source.

The observed bubble pulse period versus time for the Mk 82 SUS is shown in Figure 5. An examination of the range of values reveals the same spread of data as was observed for the Mk 61 SUS. However, there is an obvious trend, of a decreasing value in the bubble pulse period, during the experiment. As the ship transits northward, the SUS appear to detonate a deeper depths. This trend is discussed in the next section. Although the range of the majority of the points (shown in Figure 3) appears to be 4 ms, if the trend (shown in Figure 5) is taken into account the range is only about 2.5 ms. If this spread of values is used as the criterion for SUS selection, the same narrow range of source depths is achieved as for the Mk 61 shots. It should be noted, however, that the uncertainty of 0.15 ms due to automatic processing increases the range for these deeper shots more than it actually is. To improve the data accuracy at deeper depths, both the sampling rate and, correspondingly, the recording bandwidth would have to be increased.

6. Environmental Factors

In order to obtain a better understanding of the data shown in Figures 4 and 5, hourly averages of the data were determined. These results are shown in Figures 6 and 7 for the Mk 61 and Mk 82 shots, respectively. The straight lines on each of the graphs represent the linear least squares

fit to the data, which emphasizes the increasing depth trend of each curve. Several observations can be made about the data when plotted in this manner. Both data sets demonstrate a trend to lower depths, although the indication is much stronger for the Mk 82s shown in Figure 7. The data of Figure 6 also demonstrates a larger variation in hourly averages during the last thirty hours of the experiment. The data in Figure 4 also show a greater spread of values during this period. These results appear to correlate quite well with sea state, which is plotted in Figure 8 along with the data of Figure 4. The wave height is the sum of swell and wind wave height as recorded from the bridge of the shooting ship. With waves sixteen feet in height, it is possible for the bubble pulse period to be affected by the corresponding dynamic pressure changes of as much as 4 psi.

As noted in the previous section, the sharp downward trend in values shown in Figure 5 is also present in Figure 7. One possible explanation for this may be the temperature decrease in the ocean that occurred as the ship transited northward. Figure 9 shows the time history of the temperature during this period. At the 300 ft depth, the temperature decreases by about 12° C at a linear rate during this period. A possible, but somewhat speculative, cause for the increase in detonation depth may be that more pressure is required to activate the firing mechanism as the "O" ring seals become colder. Although the temperature decreases in a similar fashion at the sixty foot depth, the actions of the waves at the surface appear to make the temperature effect less noticeable.

7. Conclusion

The intent of this paper has been to demonstrate that SUS explosive charges may be used, with a high degree of confidence, as acoustic sources. Specifically, the results demonstrate that 1) the SUS are within manufacturing specifications, 2) if the ranges of the bubble pulse periods that constitute good shots are properly defined, depth uncertainties may be reduced by 25% or more, and 3) the environment can cause perturbations in the observed bubble pulse periods. An appreciation of these factors and their interrelationships is of importance to anyone planning to utilize SUS as acoustic sources.

Acknowledgements

This analysis was made possible by the cooperation of many people, including K. Lackie and V. Sprague from NAVOCEANO, who acquired the data and made it available to us for processing. We would also like to thank Y. McGann and R. Johnson for discussions regarding SUS specifications and performance and P. Bucca for supplying environmental information. The signal processing was performed under the auspices of the LRAPP Office of ONR under Contract N00014-73-C-0484.

References

1. Cole, R. H., Underwater Explosions, Princeton University, Princeton, N.J. (1948).

2. Weston, D. E., "Underwater Explosions as Acoustic Sources," Proc. Phys. Soc. Lond. 76, 233-244 (1960).

3. Slifko, J. P., "Pressure Pulse Characteristics of Deep Explosions as Functions of Depth and Range," Naval Ordnance Laboratory, NOLTR 67-87 (1967).

4. "Manual of Test Procedures for Signal Underwater Sound (SUS)," Vast, Inc., STF-TP-102 (1970).

5. Bedford, N. R., S. K. Mitchell and M. S. Weinstein, "Determination of Source Depth from the Spectra of Small Explosions Observed at Long Ranges," J. Acous. Soc. Amer. 60, No. 4, 825-828 (1976).

6. Gaspin, J. B. and V. K. Shuler, "Source Levels of Shallow Underwater Explosions," Naval Ordnance Laboratory, NOLTR 71-160 (1971).

7. "Experimental and Development Specification, SUS," Bureau of Naval Weapons, Dept. of the Navy, XWS-4660(RU) (1963).

8. "Explosive Section, Underwater Sound Signal," Bureau of Naval Weapons, Dept. of the Navy, MIL-E-23271(WEP) (1962).

9. "Arming and Firing Mechanism," Bureau of Naval Weapons, Dept. of the Navy, XWS-4669(RU) (1963).

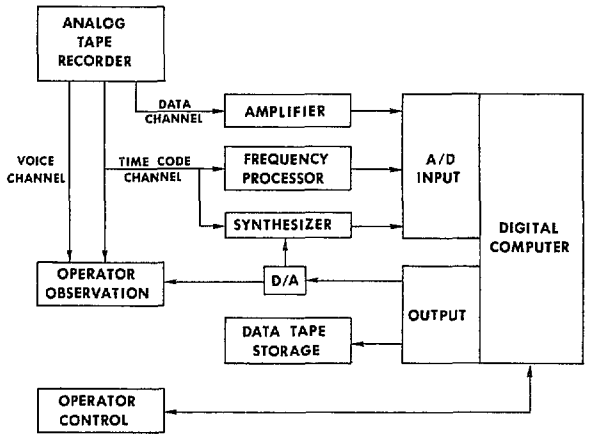

Figure 1. Block Diagram of Bubble Pulse Period Real Time Computer Processing System

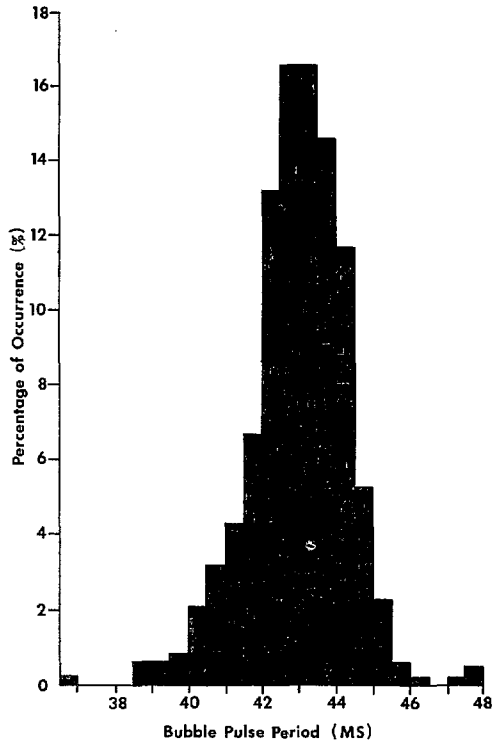

Figure 3. Distribution of Bubble Pulse Periods for the Mk 82 SUS (300 foot)

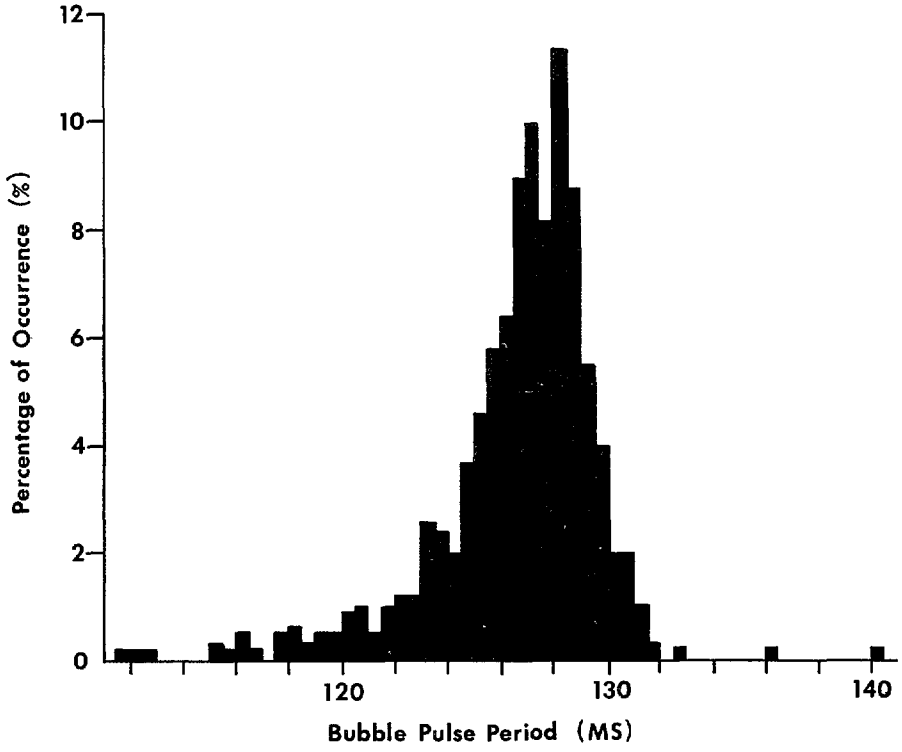

Figure 2. Distribution of Bubble Pulse Periods for the Mk 61 SUS (60 foot)

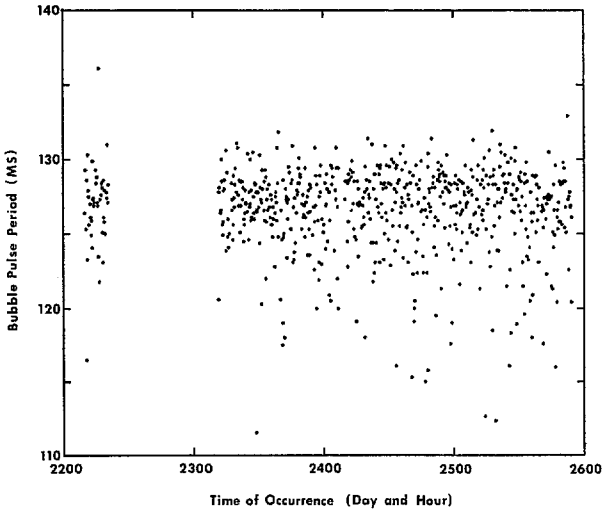

Figure 4. Diagram of Measured Bubble Pulse Period Value Versus Time for the Mk 61 (60 foot)

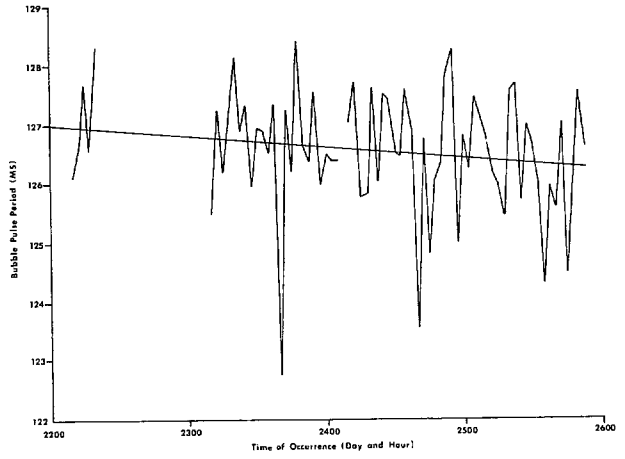

Figure 6. Diagram of Hourly Averages of Bubble Pulse Period Versus Time for the Mk 61 (60 foot)

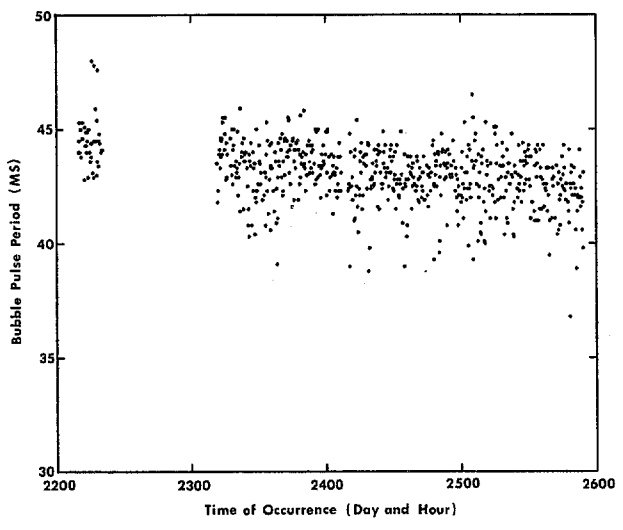

Figure 5. Diagram of Measured Bubble Pulse Period Value Versus Time for the Mk 82 (300 foot)

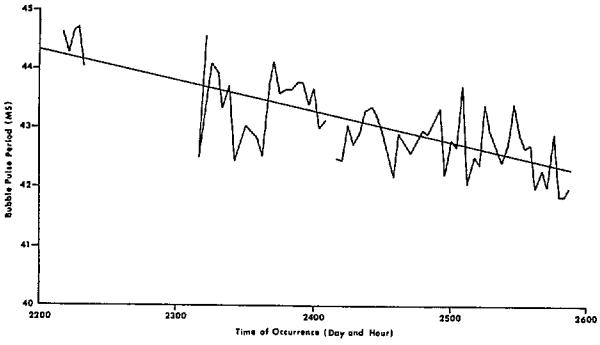

Figure 7. Diagram of Hourly Averages of Bubble Pulse Periods Versus Time for the Mk 82 (300 foot)

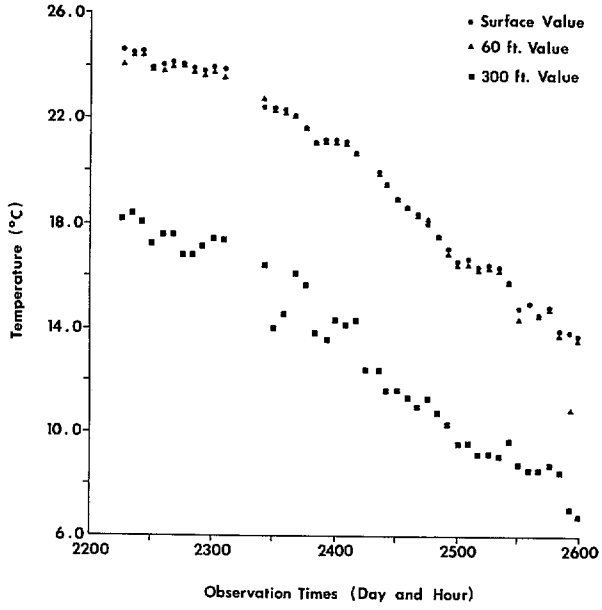

Figure 9. Time History of Temperature Values Measured as Ship Transited Northward

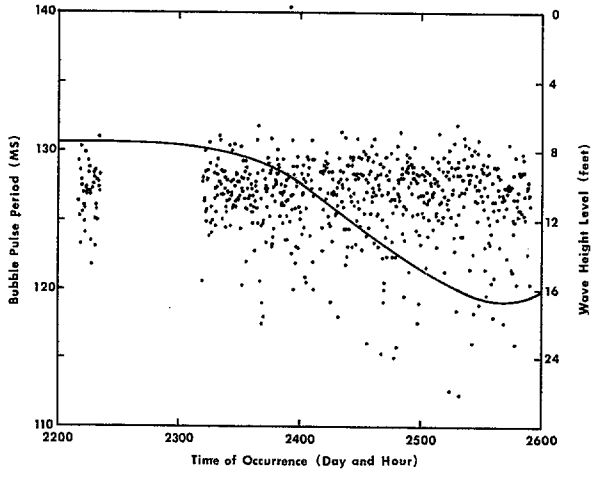

Figure 8. Diagram of Wave Height and Measured Bubble Pulse Period Values Versus Time for the Mk 61 (60 foot)

STATISTICAL MEASURES OF BEAM OUTPUT NOISE DUE TO SHIPPING

M. Moll
Bolt Beranek and Newman Inc.
1701 North Fort Myer Drive
Arlington, Virginia 22209

R. M. Zeskind
Bolt Beranek and Newman Inc.
1701 North Fort Myer Drive
Arlington, Virginia 22209

W. L. Scott
Bolt Beranek and Newman Inc.
1701 North Fort Myer Drive
Arlington, Virginia 22209

Abstract

In a band of rather low frequencies, almost all of the ambient noise in the ocean is generated by ship traffic. If the output of a beamformer in this band of frequencies is squared and averaged, the result would be found to fluctuate in a random manner. This quantity can be regarded as a random variable Y characterized by a probability density function.

This paper presents an algorithm for the calculation of the probability density function of Y, which is organized according to shipping routes in an acoustic basin and the types of ships on those routes.

One of the inputs required by the algorithm is a set of source characteristic functions, one for each type of ship. Additional required inputs include the beam pattern of the array, transmission loss functions, ocean route envelopes, and average numbers of ships on those routes.

1. Introduction

In a band of rather low frequencies, almost all of the ambient noise in the ocean is generated by ship traffic. The performance of sonars operating in this band is limited by this component of background noise; therefore, it is necessary to measure or predict certain statistical measures of beam noise to support system design and deployment decisions.

The probability measures of beam noise depend on many factors: array configuration, orientation, and location (including depth), and season. Thus it would be both expensive and time-consuming to attempt to obtain the required beam noise measures for a large number of sites experimentally. Furthermore, if shipping routes and traffic densities were to change because of strategic or economic causes, the measurements would have to be repeated. There is, therefore, considerable incentive for the development of a capability of predicting statistical measures of array beam noise.

Input data required for the prediction include the following items: array location, orientation, and plane-wave directivity pattern; acoustic source characteristics of various types of ships; ocean route envelopes, and the traffic densities of the various types of ships on those routes; and the transmission loss to the array site as a function of range and direction.

The averaged noise power at the output of a beamformer in a specified passband resulting from ship traffic in an acoustic basin* may be expressed as

$$Y = \sum_{i=1}^{m} \sum_{j=1}^{n} \sum_{k=1}^{A_{ij}} S_{ijk} Z_{ijk} B_{ijk} \qquad (1)$$

where m is the number of routes in the basin,
n is the number of ship types,
A_{ij} is the number of ships of type j on route i; A_{ij} is a random variable,
S_{ijk} is the source intensity of the kth ship of type j on route i; it is a random variable that is statistically independent of the source intensity of any other ship,
Z_{ijk} is the intensity transmission ratio from ship ijk to the receiving point,
B_{ijk} is the gain for a plane-wave arriving at the array from ship ijk.

Various first-order probability measures can be derived from (1); these measures depend on the statistical measures of the random variables in the summand.

2. Characteristic Function for Y

The probability density function for Y can be obtained from its characteristic function

$$\Phi_Y(\omega) = E[\exp j\omega Y] \qquad (2)$$

where E denotes the expectation operator. Substituting (1) in (2) gives

$$\Phi_Y(\omega) = E\left[\exp j\omega \sum_{i=1}^{m} \sum_{j=1}^{n} \sum_{k=1}^{A_{ij}} S_{ijk} Z_{ijk} B_{ijk}\right] \qquad (3)$$

*The acoustic basin in which the array is located is defined by bathymetry (e.g., land masses and high underwater ridges). The intensity of sound from sources outside of the basin is negligible.

$$= E\left[\prod_{i=1}^{m}\prod_{j=1}^{n}\prod_{k=1}^{A_{ij}} \exp j\omega S_{ijk} Z_{ijk} B_{ijk}\right] \tag{4}$$

$$= \prod_{i=1}^{m}\prod_{j=1}^{n} \Phi_{ij}(\omega) \tag{5}$$

where

$$\Phi_{ij}(\omega) = E\left[\prod_{k=1}^{A_{ij}} \exp j\omega S_{ijk} Z_{ijk} B_{ijk}\right] \tag{6}$$

In the sequel it is assumed that

$$Z_{ijk} = z(G_{ijk}, Q_{ijk}) \tag{7}$$

$$B_{ijk} = b(G_{ijk}, Q_{ijk}) \tag{8}$$

where z(,) is a deterministic transmission ratio function; b(,) is a deterministic gain function for a plane-wave; G_{ijk} is the earth-centered angle measuring the longitudinal coordinate (in the direction of the nominal route) of ship ijk; and Q_{ijk} is the earth-centered angle measuring the transverse coordinate (normal to the nominal route) of ship ijk. It is assumed that all ship coordinates are random variables that are mutually independent. Substituting (7) and (8) in (6) and performing the expected-value operation gives

$$\Phi_{ij}(\omega) = \sum_{a=0}^{\infty} p_{ij}(a)\left[\int dg f_{G_i}(g) \int dq f_{Q_i}(q;g) \int ds f_{Sj}(s) \times \exp j\omega s z(g,q) b(g,q)\right]^a \tag{9}$$

where $p_{ij}(a) = P(A_{ij} = a)$; a = 0, 1, 2, 3, ...

$f_{G_i}(\ )$ is the probability density function for G_{ijk}; j = 1, 2, ..., n; k = 1, 2, 3, ...

$f_{Q_i}(\ ,\ )$ is the probability density function for Q_{ijk} depending on the variable g; j = 1, 2, ..., n; k = 1, 2, 3, ...

The inner integral of (9) can be expressed as a characteristic function; thus

$$\Phi_{ij}(\omega) = \sum_{a=0}^{\infty} p_{ij}(a) \{ \int dg F_{Gi}(g) \int dq f_{Qi}(q;g) \times \Phi_{Sj}[\omega z(g,q) b(g,q)]\}^a \tag{10}$$

where $\Phi_{Sj}(\ )$ is the source characteristic function for ships of type j.

In the sequel, it is assumed that A_{ij} is a Poisson random variable; thus, its probabilities are given by

$$p_{ij}(a) = \exp(-a_{ij}) a_{ij}^a \div a!,\ a = 0, 1, 2, 3, \ldots \tag{11}$$

where a_{ij} is the average number of ships of type j in an increment of route i. Substituting (11) into (10) gives

$$\Phi_{ij}(\omega) = \exp(-a_{ij}) \sum_{a=0}^{\infty} \{a_{ij} \int dg f_{Gi}(g) \int dq f_{Qi}(q;g) \times \Phi_{Sj}[\omega z(g,q) b(g,q)]\}^a \div a! \tag{12}$$

The sum is the power series expansion for the exponential of the quantity in braces; thus

$$\Phi_{ij}(\omega) = \exp(-a_{ij}) \exp\{a_{ij} \int dg f_{Gi}(g) \int dq f_{Qi}(q;g) \times \Phi_{Sj}[\omega z(g,q) b(g,q)]\} \tag{13}$$

The cumulant function is the logarithm of the characteristic function:

$$\psi_{ij}(\omega) = a_{ij}\{\int dg f_{Gi}(g) \int dg f_{Qi}(q,g) \times \Phi_{Sj}[\omega z(g,q) b(g,q)] - 1\} \tag{14}$$

If the distributions of the longitudinal coordinates G_{ijk} are uniform over the route, then

$$f_{Gi}(g) = \ell^{-1},\ 0 \le g \le \ell_i$$
$$= 0, \text{ elsewhere} \tag{15}$$

where ℓ_i is the length of route i. Substituting (15) in (14) yields

$$\psi_{ij}(\omega) = \rho k_{ij} \int_0^{\ell_i} dg \int dq f_{Qi}(q,g) \times \Phi_{Sj}[\omega z(g,q) b(g,q)] - \rho \ell_i k_{ij} \tag{16}$$

where ρ is the earth's radius, and k_{ij} is the average number of ships of type j per unit length of route i. In (16) the variables of integration are the route variables g and q; an alternative set of variables is the pair of observation variables related to the range and bearing of point from the sensor.

The characteristic function is the exponential of the cumulant function; thus $\Phi_{ij}(\omega) = \exp \psi_{ij}(\omega)$. Substituting this result in (5) gives the characteristic function of Y:

$$\Phi_Y(\omega) = \sum_{i=1}^{m}\sum_{j=1}^{n} \exp \psi_{ij}(\omega) = \exp \sum_{i=1}^{m}\sum_{j=1}^{n} \psi_{ij}(\omega) \tag{17}$$

The second of these equivalent forms is easier to calculate.

3. Probability Density Function for Y

Once the characteristic function $\Phi_Y(\omega)$ has been found, the corresponding probability density function $f_Y(y)$ can be obtained via the inverse transformation. Because $f_Y(y)$ is real, the inverse transformation is given by

$$f_Y(y) = \frac{1}{\pi}\int_0^\infty R(\omega)\cos\omega y\, d\omega + \frac{1}{\pi}\int_0^\infty I(\omega)\sin\omega y\, d\omega \qquad (18)$$

where $R(\omega)$ is the real part of the characteristic function $\Phi_Y(\omega)$, and $I(\omega)$ is its imaginary part. Simplification of (18) can be achieved by exploiting the fact that Y can only take on positive values; therefore, $f_Y(y) = 0$ for $y < 0$. For $y > 0$, (18) becomes

$$f_Y(-y) = \frac{1}{\pi}\int_0^\infty R(\omega)\cos\omega y\, d\omega - \frac{1}{\pi}\int_0^\infty I(\omega)\sin\omega y\, d\omega = 0 \qquad (19)$$

The use of (19) in (18) yields alternative, simpler expressions for the density function:

$$f_Y(y) = \frac{2}{\pi}\int_0^\infty R(\omega)\cos\omega y\, d\omega \qquad (20)$$

$$= \frac{2}{\pi}\int_0^\infty I(\omega)\sin\omega y\, d\omega \qquad (21)$$

for $y \geq 0$. That is, $f_Y(y)$ can be expressed as a single integral for $y \geq 0$, and either (20) or (21) can be used. This result will reduce the computational load since only the real part of $\Phi_Y(\omega)$ need be calculated and stored, or *vice versa*.

A numerical approximation technique was developed to evaluate the special form of the inverse transform given by (20). It is assumed that $R(\omega)$ is negligible for all ω greater than some ω_N. Assume $R(\omega)$ has been computed at N+1 equally-spaced points in ω, where the first sample point is at $\omega = 0$, and N is an even integer. The range of the integral in (20) is divided into sub-intervals, each containing three sample points. Using a quadratic approximation for $R(\omega)$ in each sub-interval, the integral over each sub-interval can be evaluated analytically. This results in a numerical approximation to (20) of a form that can readily be implemented on a digital computer. This numerical approximation has the desirable property that the selection of the intersample interval is dictated only by $R(\omega)$. Examination of (20) shows that if conventional numerical integration techniques were employed, the selection of intersample intervals would depend on the value of y.

4. Source Characteristic Functions

It is shown in (10) that the calculation of the characteristic function of Y requires a source characteristic function $\Phi_{S_j}(\ )$ for each type of ship. In particular, each of these characteristic functions pertains to the same frequency band as the ambient noise prediction. The required source characteristic functions can be derived from statistical information produced by J. C. Heine and L. M. Gray. [1]

Heine and Gray found it expedient to divide the world's merchant fleet into three types of vessels: fishing, small merchant (ships over 500 long tons and less than 700 feet long), and large merchant (ships over 100 feet long).

For each type of vessel, four noise generating components were characterized: (1) the broadband spectrum that is related to the collapse of propeller cavitation bubbles; (2) the narrowband spectrum (fundamental and harmonics) at the propeller blade rate which are due to the modulation of the cavitation spectrum by the spatially varying inflow to the propeller; (3) the narrowband spectrum (fundamental and harmonics) at the diesel firing rate which are related to the vibratory forces of the main propulsion system; and (4) the narrowband spectrum at the ship's electric plant frequency.

The results of Heine and Gray were in the form of histograms for the source pressure level and source frequency distribution for the fundamental narrowband components. The levels of harmonics relative to the fundamentals were specified by equations.

A procedure was devised to convert the Heine-Gray narrowband data to the distribution of source level in a specified 1-Hz band. If the fundamental is greater than 1 Hz, then no more than one component of the harmonic set can fall in a 1-Hz increment of frequency. Let

C_0 be the event that no component falls in the specified 1-Hz band.

C_1 be the event that the fundamental falls in the specified 1-Hz band.

C_2 be the event that the first harmonic falls in the specified 1-Hz band, and so on.

With the stipulation that the frequency of the fundamental is greater than 1 Hz, these events are mutually exclusive; that is, only one of the events can occur in a single performance of the experiment.

Now let U be the source pressure level in a specified 1-Hz band from a particular narrowband source that radiates harmonics as well as the fundamental. According to the total probability theorem for mutually exclusive events, the probability distribution function for U is

$$F_U(u) = \sum_{i=0}^{\infty} P(U \leq u | C_i) P(C_i) \qquad (22)$$

where P( ) denotes the probability of the argument. The corresponding probability density function is

$$f_U(u) = \frac{d}{du} F_U(u) = \sum_{i=0}^{n} f_U(u|C_i)P(C_i) \qquad (23)$$

The source level density for the fundamental is derived directly from the corresponding histogram; the density is therefore a discontinuous function. For a given harmonic, the same function is employed, displaced by the amount the harmonic level is exceeded by the fundamental level. The probability that the fundamental falls in the specified band is readily determined from the frequency histogram for the fundamental. The same histogram suffices for the first harmonic, except that the frequency scale is doubled, and so on.

As stated previously, the broadband component of the radiated noise is related to the collapse of propeller cavitation bubbles. From a consideration of significant differences in the distributions of peak levels and associated frequencies of the continuous cavitation spectrum, Heine and Gray defined eight broadband classes, each with its characteristic spectrum. The distribution of these broadband classes among types of ships (fishing, small or large merchant) were given by histograms.

These data provide a basis for deriving the probability density function for the broadband source levels for each tpye of ship. First, for a given 1-Hz band, the source level for each broadband class is obtained from the corresponding spectral density functions. Then, the probability of occurrence of each type of ship is determined from the histogram showing the distribution of the broadband class among the types of ships. These data were than employed to construct discrete probability distributions of source levels for each type of ship. Finally, these discrete probabilities were distributed over 10 dB increments of source to obtain density functions for broadband source levels.

For each ship, the total radiated intensity is the sum of those of the four components. For a ship selected at random from a population of a given type, the source intensity is a random variable that is the sum of the source intensities of the four component random variables. Heine and Gray have concluded that the latter are mutually independent.

The procedure for obtaining the source characteristic function for a given type of ship is outlined below.

1. Select a characteristic function with at least two parameters that applies to a non-negative random variable.

2. Calculate the low-order moments of the source intensity of each component. These can be readily obtained from the discontinuous density functions f_{U_k}( ) for the component source levels. For example, the mean value of the source intensity of the kth component is

$$m_i = \int du\, 10^{u \div 10}\, f_{Ui}(u) \qquad (24)$$

3. Determine the low-order moments of the source intensity from the low-order moments of the component source intensities.

4. Determine the values of the parameters of the characteristic function so that its moments match the calculated moments.

The advantage of this procedure is that it avoids the excessive oscillations of the characteristic functions that would be introduced by the direct utilization of the discontinuous density functions.

5. Computer Programs

The algorithms for calculating the probability density of Y have been programmed in FORTRAN for a CDC 6000 digital computer. The algorithms are implemented as three separate programs and associated data files, all represented in Figure 1.

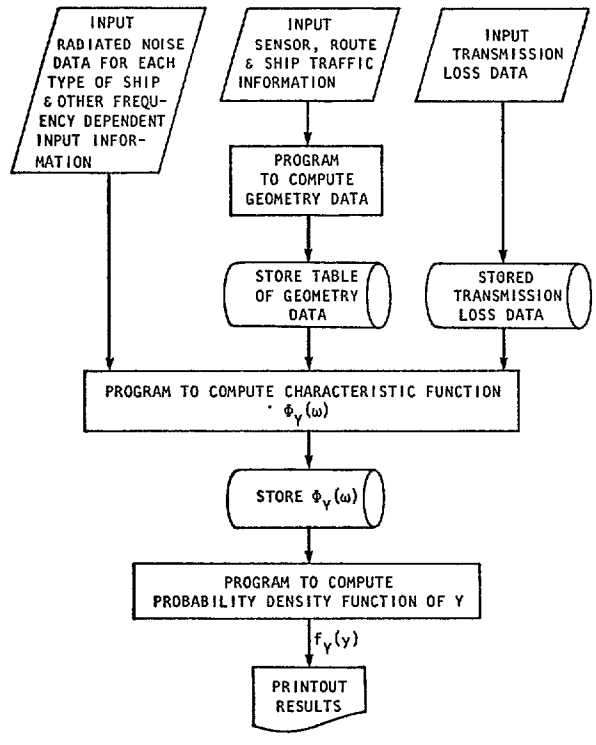

FIGURE 1 Data Flow of Ambient Noise Model.

The input information is divided into three types. Transmission loss data at a given sensor location is read into the computer and stored on a file as a table of transmission loss as a function of range and bearing. One such transmission loss file is created for each frequency of interest. Sensor, route and ship traffic information, which is independent of frequency, is read into the computer. This frequency-independent information is used as the input to a program which computes such quantities as route segment lengths, earth-centered angles between routes and sensor, and other geometric parameters needed in the computation of the characteristic function $\Phi_Y(y)$. The outputs of this geometry program are stored on a file for later use as inputs to the characteristic function program.

The characteristic function of beam noise power is computed via the algorithm derived in Section 2. This program reads in radiated noise data for each type of ship and other frequency-dependent input information such as beam pattern parameters. Beam steering angle and array orientation are also entered at this point. The characteristic function program reads in the data stored in the geometry file and the appropriate transmission loss file. The program calculates the mean and variance of received average noise power as well as its characteristic function and stores the results on a file to be used as input to the final computer program.

The final program computes the probability density function of Y using the numerical algorithm described in Section 3. The mean, variance and probability density function for Y are printed out as the final result.

The structure of the program provides several advantages. The geometric data need be computed only once for a given sensor location and route structure. Since it is independent of frequency and beam steering angle, the same geometry data can be used many times by the characteristic function program. Furthermore, the transmission loss data need be entered only once for a particular sensor location.

6. Discussion

Algorithms and programs have been described for predicting the probability density function for the averaged power Y of the noise output of a beamformer caused by ship traffic. The density is obtained from a calculation of the characteristic function. The programs are capable of utilizing realistic input information regarding ship source characteristics, ocean routes and traffic, and acoustic transmission loss. The assumption that the number of ships of a given type on a given route is a Poisson random variable allows considerable simplification in the calculation of the characteristic function. The relevance of the Poisson variable to this application has been previously examined [2, Appendix B]. The algorithm for the inverse transformation to obtain the probability density function of Y permits the sampling of the characteristic function to be independent of the value of the density variable. Finally, since the distribution of the ships on the sea surface is stated in terms of ocean routes instead of static densities in incremental areas facilitates modification of the programs for calculations of second- [2, Sections 1.3 and 2.0] or higher-order statistical measures; e.g., autocovariance of Y.

References

1. J. C. Heine, L. M. Gray, "A Statistical Model for the Acoustic Source Levels of Merchant Ships," Bolt Beranek and Newman Inc. Report No. 3814, July, 1978.

2. M. Moll, R. M. Zeskind, F. J. M. Sullivan, "Statistical Measures of Ambient Noise: Algorithms, Programs, and Predictions," Bolt Beranek and Newman Inc. Report No. 3390, June, 1977.

Acknowledgements

The development of the ambient noise prediction programs was supported by the Naval Analysis Program, Code 431, Office of Naval Research, The Undersea Surveillance Division, Code 320, Naval Electronic Systems Command, and the Acoustics Division, Code 8160, Naval Research Laboratory.

A WIDEBAND SONAR EQUATION

L. W. Brooks
Binary Systems, Inc.
P.O. Box 1105
Salida, Colo. 81201

Introduction

The controlled impulse generator (CIG) is a technique developed by EDO Corp. for generating nearly arbitrary pressure signatures in the far field of an electro-acoustic projector [1]. As sketched in Figure 1, the technique consists of driving the projector with an equalized voltage which compensates its electro-acoustic transfer function. Using this approach, very short signals (on the order of 150 μsec) can be generated. Such short pulses have the potential to provide extremely good range resolution for advanced mine hunting, swimmer detection and torpedo sonars. A correct evaluation of the CIG sonar performance must include the fact that the sonar environment is frequency dependent; thus the CIG pulse becomes increasingly distorted as a function of range.

Urick [2] gives a very simple technique for evaluating transient signals by replacing the source level in the sonar equation with a more general term which is the transmitted energy flex density divided by the duration of the echo. Unfortunately, Urick does not give a method for computing the echo length. In this paper, a wideband sonar equation is developed which can be used to estimate the pulse distortion over modest ranges. Expressions will be given for the receiver response to the target, ambient noise, self noise, and reverberation.

It is possible to develop a wideband sonar equation in the time domain. In this approach, the receiver output is expressed as the five-fold convolution of the transmit waveform, the environmental impulse response, the target impulse response, the receive transducer impulse response and the receiver filter impulse response. However, most sonar models (propagation loss, target strength, etc., see Urick [2]) are expressed in the frequency domain; thus to make quantitative use of these models it is easier to work in that domain. Of course, if developed correctly, both time and frequency domain representations will be equivalent.

Target Response

Accordingly, let $p_T(t)$ be the time varying, on-axis, far-field, plane-wave pressure corrected to 1 yd and measured in μPa. I.e. for a square pulse of duration T, the source level would be:

$$SL = 10\log\left[\frac{1}{T}\int_0^T p^2(t)\,dt\right] \qquad (1)$$

Next, let $P_T(f)$ denote the complex Fourier transform of $p_T(t)$. Thus;

$$P_T(f) = \int_{-\infty}^{\infty} p_T(t)e^{2\pi ift}\,dt \qquad (2)$$

In direct analogy to the usual sonar equation, the complex Fourier transform of the pressure at the receive transducer is;

$$P_R(f) = P_T(f)\frac{V_T(\theta,\phi,f)}{r^2 10^{.1\alpha r}}\rho(f)e^{2\pi if\tau} \qquad (3)$$

In Equation (3), $V_T(\theta,\phi,f)$ is the one-way complex voltage pattern of the transducer, α is the propagation attenuation, and $\rho(f)$ is the Fourier transform of the target impulse response for a stationary target. We assume $\rho(f)$ is normalized so that the target strength is given by:

$$TS = 10\log|\rho(f)|^2 \qquad (4)$$

Now, let $p_R(t-\tau)$ be the inverse transform of (3); that is the time representation of the pressure pulse

at the transducer for a stationary target. We assume that the effect of a moving target is to produce a time scaling of the received pulse. That is, following Deley [3], the received pressure pulse is written,

$$p_R(t) = a_r p_{R_o}(t-T(t))$$
$$\approx \sqrt{B}\, p_{R_o}((t-\tau)\beta) \qquad (5)$$

where $p_{R_o}(t-\tau)$ is the signal returned by a stationary target, $T(t)$ is the range delay of that part of the signal returning at time t, and β is the time scale factor given by:

$$\beta = 1 - \dot{T}(t) \simeq 1 - \frac{2V}{c} \qquad (6)$$

In (6), V is the radial target velocity. Note that (5) is normalized so that the received pulse energy is independent of the motion. In the frequency domain (5) is written:

$$P_R(f) = \frac{P(f/\beta)}{\beta r^2 10^{.1\alpha r}} V_T(\theta,\phi,f/\beta) \cdot \rho(f/\beta) e^{2\pi i f\tau} \qquad (7)$$

Now, if R(f) represents the complex, on-axis transfer function of the receive transducer and $V_R(\theta,\phi,f)$ is its complex beam pattern, the Fourier transform of the electrical signal at the transducer output is:

$$P_e(f) = \frac{P(f/\beta)}{\beta r^2 10^{.1\alpha r}} V_T(\theta,\phi,f/\beta) V_R(\theta,\phi,f) \cdot \rho(f/\beta) R(f) e^{2\pi i f\tau} \qquad (8)$$

Finally, if the receiver is matched to a spectral shape W(f) with a time scale factor β_o, and a round trip delay τ_o, the output is given by:

$$Z(\tau,\tau_o;\beta,\beta_o) = \frac{1}{\sqrt{\beta\beta_o}} \int_{-\infty}^{\infty} P(f/\beta) \frac{V_T(\theta,\phi,f/\beta) V_R(\theta,\phi,f)}{r^2 10^{.1\alpha r}} \cdot \rho(f/\beta) W^*(f/\beta_o) e^{2\pi i f(\tau-\tau_o)} df \qquad (9)$$

We note that if the target is a point target, the hydrophone response is white, target is on the beam axis and the absorbtion is negligible, (9) becomes proportional to a wideband cross ambiguity function between the p(t) and w(t) (the inverse transform of W(f)) [3].

Equation (9) is general and applies to any waveform. However, here we are interested in baseband CIG pulses whose shape is similar to that sketched in Figure 1. Such short pulses have essentially no capability to resolve time scale differences (i.e. Doppler). Thus (9) can be simplified to:

$$Z(\tau-\tau_o) = \int_{-\infty}^{\infty} P(f) T_E(f) W^*(f) e^{2\pi i f(\tau-\tau_o)} df \qquad (10)$$

where $T_E(f)$ is the "environmental transfer function":

$$T_E(f) = \frac{V_T(\theta,\phi,f) V_R(\theta,\phi,f) \rho(f)}{r^2 10^{.1\alpha r}} \qquad (11)$$

In (10), the peak signal level occurs when $\tau = \tau_o$ and the peak output signal power is $|Z(0)|^2$.

Response to Ambient Noise

The ambient and self noise response may be derived by modeling the noise field as a collection of independent plane waves arriving at all possible angles and frequencies. In this case, one obtains the standard result for the power spectral of the noise at the receiver transducer terminals as, [2],

$$N_n(f) = \frac{N_o(f)}{AG(f)} |R(f)|^2 \qquad (12)$$

where $N_o(f)$ is the noise spectral density at the output of an isotropic hydrophone and AG(f) is the receive transducer noise gain (see [2] pg. 32). Thus the average noise power at the receiver output is given by:

$$N = \int_{-\infty}^{\infty} \frac{N_o(f)}{AG(f)} |R(f)|^2 |W(f)|^2 df \qquad (13)$$

Reverberation

Reverberation is modeled as scattering from a collection of similar "targets" having independent, random amplitudes, phases and positions. This model is a special case of the one used by Middleton [4]. Strictly speaking, since the scatterers are not geometrically identical, the impulse response should be considered a random function; however, it is adequate for our purposes to model the scatterers as having identical impulse response functions except for amplitude and phase. With this assumption we have that the reverberation power at the receiver output can be written [5],

$$P_R(\tau_o) = \sum_{\text{all scatters}} E|a_k Z_R(\tau_k - \tau_o)|^2 \qquad (14)$$

where a_k is the complex amplitude of the kth scattering point, τ_k is its position, and Z_R is given by Equation (10), evaluated for the transform of the reverberation impulse response, i.e. for $\rho_R(f)$. The above equation may be evaluated by counting the average number of scatters at each delay, azimuth, and elevation; thus,

$$P(\tau_o) = \iiint |Z_R(\tau-\tau_o)|^2 |\bar{a}|^2 \eta(\tau,\theta,\phi)\, d\tau d\theta d\phi \qquad (15)$$

where $|\bar{a}|^2$ is the average amplitude squared of the scattering points and η is the average number per unit delay, azimuth, and elevation.

Equation (15) while reasonably general, is not particularly useful since it involves a five-fold iterated integral. It can be simplified by noting that a) for the short CIG pulses $|Z_R(\tau-\tau_o)|^2$ is approximately a Dirac delta function allowing the integration over τ to be evaluated, b) for surface or bottom reverberation $\eta(\tau,\theta,\phi)$ is a Dirac delta function in elevation angle θ, allowing the integration over θ to be evaluated, and c) with the two previous assumptions the only remaining functions which depend on azimuth angle are the transmit and receive beam patterns, thus the integral over ϕ can be replaced by an equivalent beamwidth. The details are too lengthy to be included here and can be found in [5]. The result is:

$$P_s(\tau_o) = \frac{1}{r^4}\int |P(f)R(f)W^*(f)|^2 10^{-.2\alpha r} \cdot S_s(f)\frac{Cr}{2\cos\theta_s}\,\phi(f,\theta_s)df \qquad (16)$$

where $S_s(f)$ is the surface scattering coefficient versus frequency, θ_s is the elevation angle to the surface, and $\phi(f,\theta_s)$ is the equivalent two-way azimuth beam pattern defined by:

$$\phi(f,\theta_s) = \int_{-\pi}^{\pi} |V_T(\theta,\phi,f)V_R(\theta,\phi,f)|^2 d\phi \qquad (17)$$

Evaluation for a Torpedo Application

The key equations which give the target, noise, and reverberation levels at the receiver output (Eqs. (9), (13), (16)) must be evaluated numerically; however, this is not difficult since only a single variable of integration is involved. In our particular application a nine-point Gaussian quadrature formula was found to be adequate.

The example chosen concerned a 1 ft diameter aperture, a 150 μsec pulse, and a peak pressure of 10^{12} μPa (corrected to 1 yd). Figure 2 shows a typical CIG spectrum, and Figure 3 shows the effect of increasing range on the received signal spectrum (at the transducer). For that calculation, the target was assumed to have a constant target strength with frequency of 2 dB, thus the major effect is attenuation which reduces the frequency at which the peak energy occurs as the range increases.

Figures 3 and 4 show the results of numerically evaluating (9), (13) and (16) for a square pass receiver. The ambient noise model versus frequency, $N_o(f)$ was taken from Urick [2]. The torpedo self noise was assumed to be equivalent to sea state 2 at search speed and to increase 15-20 dB at attack speed. The model for surface scattering strength versus frequency required to evaluate (16) was taken from Audreyeva (see [5]).

Note that for such a short pulse, the sonar is ambient or self noise limited at all ranges of interest. Also, the signal-to-noise ratio is better in the higher frequency band (Fig. 4) than in the lower one, even though the lower band corresponds to maximum received signal energy at 3 kyd (see Fig. 2). The reason, of course, is that ambient and self noise are lower in the higher frequency band, and enough so to compensate the loss in signal energy.

References

[1] C. Mazzola "Gen. of Wideband Pulses ..." EDO Rept. 10991, EDO Corp., College Pt. N.Y. 11356, July 7, 1976.

[2] R. J. Urick Principles of Underwater Sound, McGraw Hill, 1975.

[3] G. W. Deley "Waveform Design", in Radar Handbook, M. I. Skolnik ed. McGraw Hill, 1970.

[4] D. Middleton, "A Statistical Theory of Reverberation, Part I and II" IEEE Trans. Vol IT 13, pp 372-414, 1967.

[5] L. Brooks, L. Palmer, and F. Rees, "Wide Band Transient Detection" BSI Rept WB77-12 Binary Systems, Inc. 10750 Columbia Pike, Silver Spring, Md. 20901, Dec. 30, 1977.

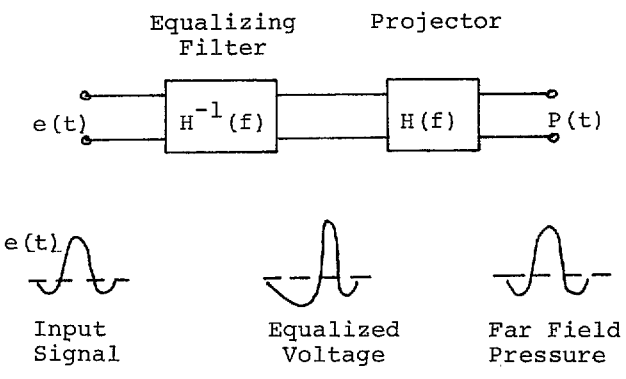

Figure 1. The CIG technique

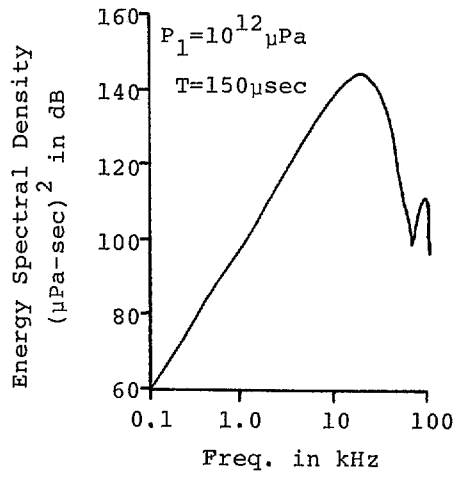

Fig. 2. CIG Pulse Energy Spectrum (Measured at 1 yd)

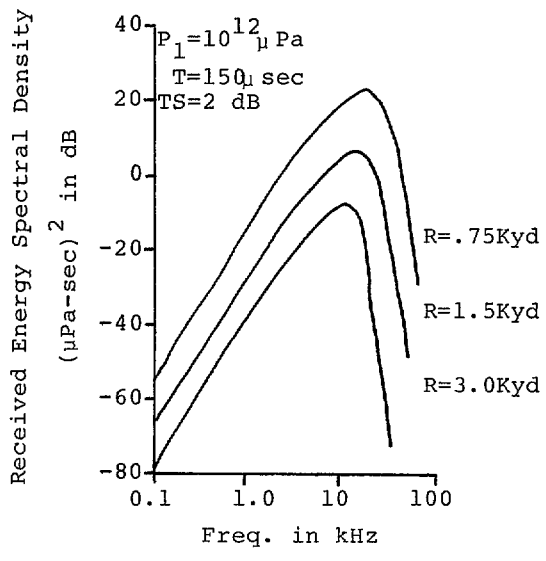

Fig. 3. Received Energy Spectral Density for a Specular Target

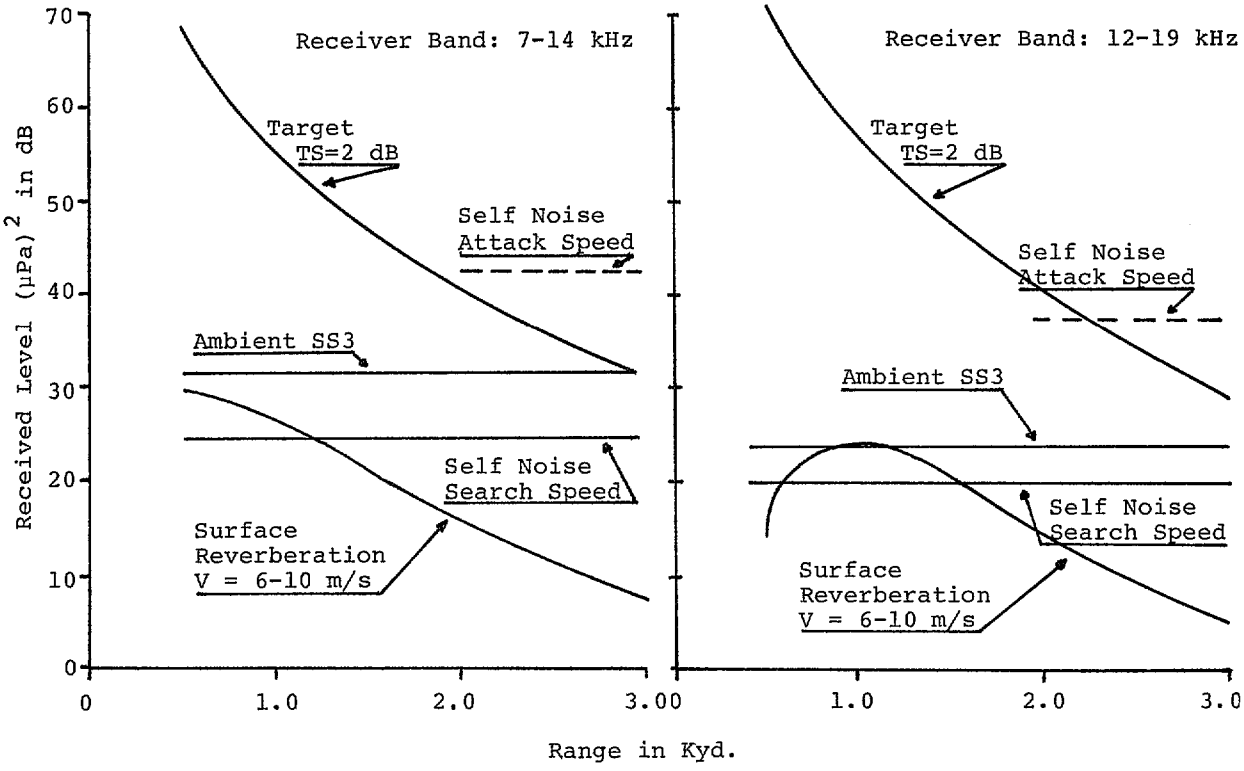

Figure 4. Received Power Levels Versus Range

SYNTHETIC APERTURE IMAGING USING ACOUSTICAL HOLOGRAPHY

W. S. Gan
Acoustical Services Pte Ltd
29, Telok Ayer Street
Singapore 1
Republic of Singapore

Abstract

We develop the mathematical basis for synthetic aperture imaging using acoustical holography in a form suitable for application to underwater viewing. Synthetic aperture technique by itself is a high resolution ultrasonic imaging system. By using acoustical holography we can improve the resolution even further. We preform demodulation and low band-pass filtering on the holographic signal. This is followed by heterodyne detection on the signal. Then we have the superposition of complex images using two frequencies or double exposure acoustical holographic interferometry. We then compare the resolution obtained after applying holographic technique with that before applying. We finally outline a system to test the above principle.

1. Introduction

Synthetic aperture technique is first used in microwave(radar)[1] but has been used in sonar systems as an effective means to get high azimuth resolution.[2] In this paper we apply acoustical holography to a synthetic aperture system. The purpose is to improve the resolution in the range direction and to achieve superresolution. We make use of the method of Sato et al[2] and apply it to the synthetic aperture system of M. L. Dick et al[3]. Sato et al[2] 's method is based on the utilization of superposition of complex images obtained by multiple frequencies of waves. The superposition is performed after the nonlinear heterodyne operation.

2. Demodulation and Low-pass Filtering

We assume that a small transducer moves in a straight line parallel to the x-axis. The y-axis is vertical with the trasnducer located at y = 0 and pointing parallel to the y-axis. The transducer at any time is located at $(x_T,0)$. Assume there is a single point reflector located at (x_r,y_r) and that the transmitted signal is given by

$$s(t) = A_o \sin(\omega_o t).\ w(t)$$

$$w(t) = \begin{cases} 1, & 0 \leq t \leq T_o \\ 0, & \text{otherwise} \end{cases} \qquad (1)$$

where ω_o is the center frequency of the ultrasound pulse

T_o is the pulse duration, which is normally an integral number of half cycles.

The reflected signal is a function of the transducer position and is given by

$$r(x_T,t) = A_1 \sin[\omega_o(t - \tau_r)] .w(t - \tau_r)$$

$$d_r(x_T) = \sqrt{(x_r - x_T)^2 + y_r^2}$$

$$\tau_r = \frac{2.d_r(x_T)}{c} \qquad (2)$$

where c is the velocity of sound

A_1/A_o is the attenuation due to absorption, scattering cross-section, and transducer inefficiency.

The holographic signal is given by

$$h(x_T,t) = s(t) + r(x_T,t) \qquad (3)$$

For demodulation, we make use of both quadrature components. So demodulation yields

$$u_c(x_T,t) = h(x_T,t)\ .\ \cos(\omega_o t)$$

$$= \frac{A_1}{2}\left\{\sin[\omega_o(2t - \tau_r)] - \sin(\omega_o \tau_r)\right\}.\ w(t - \tau_r) + \frac{A_o}{2}$$

$\sin(2\omega_o t) \cdot w(t)$

$$u_s(x_T,t) = r(x_T,t) \cdot \sin(\omega_o t)$$

$$= \frac{A_1}{2}\left\{\cos\left[\omega_o(2t - \tau_r)\right] + \cos(\omega_o \tau_r)\right\} \cdot w(t - \tau_r) + \frac{A_c}{2}(\cos^2\omega_o t - 1) \cdot w(t) \quad (4)$$

This is followed by low-pass filtering to remove the sum frequency from both $u_c(x_T, t)$ and $u_s(x_T,t)$. This filtering yields

$$v_c'(x_T,t) = -\frac{A_1}{2}\sin(\omega_o \tau_r) \cdot w_1'(t - \tau_r) + \frac{A_o}{2}\sin(2\omega_o t) \cdot w_1'(t)$$

$$v_s'(x_T,t) = \frac{A_1}{2}\cos(\omega_o \tau_r) \cdot w_1'(t - \tau_r) + \frac{A_o}{2}(\cos^2\omega_o t - 1) \cdot w_1'(t) \quad (5)$$

where $w_1'(t - \tau_r)$ and $w_1'(t)$ are modifications of the delayed original window, $w(t)$ and the original window, due to the low-pass filter.

3. Utilization of Multiple Frequencies of Waves

When the synthetic aperture technique is used, the azimuth resolution is improved as much as we desire by increasing the aperture to be synthesized. On the other hand, the resolution in range direction is left to the utilization of very short pulsed waves. When the pulse width is reduced extremely to a width as narrow as several wave lengths, the detection of the phase and amplitude of the reflected waves becomes very difficult. This is the result of the decrease of the resistance to noises, besides the difficulty of generation of complete signals of such a short duration. We now make use of multi-frequencies acoustical holographic interferometry to get high range resolution without decreasing the pulse width. The idea of acoustical holographic interferometry is the linear superposition of complex images obtained by multiple frequencies of waves. And it can be shown that by synthesizing the spectrum of multiple frequencies (spectral synthesis) of waves, the images which might be obtained when a very short duration of pulses are used can be obtained by using actual pulses with a relatively long duration.

We first use two frequencies for the interferometrical holography and we let the two frequencies used be ω_1 and ω_2. Then our eqn. (5) becomes

$$u_{c1}(x_T,t) = h(x_T,t) \cdot \cos\omega_1 t \cdot e^{j\omega_1 t - j\theta(t)} + h(x_T,t) \cdot \cos\omega_2 t \cdot e^{j\omega_2 t + j\theta(t)}$$

$$u_{s1}(x_T,t) = h(x_T,t) \cdot \sin\omega_1 t \cdot e^{j\omega_1 t - j\theta(t)} + h(x_T,t) \cdot \sin\omega_2 t \cdot e^{j\omega_2 t + j\theta(t)} \quad (6)$$

The next step is to perform heterodyne processing on (6). Then we have

$$C_{c1}(x_T,t) = \langle u_{c1}(x_T,t)\, s^*(t)\rangle_{T_c} \quad (7)$$

where T_c is the integrating time. Eqn.(7) contains the two-frequencies acoustical holographic interference fringes.

We now use four frequencies for the interferometrical holography and we let the two frequencies used be ω_1, ω_2, ω_3 and ω_4. Then our eqn. (5) becomes

$$u_{c2}(x_T,t) = h(x_T,t) \cdot \cos\omega_1 t \cdot e^{j\omega_1 t - j\theta(t)} + h(x_T,t) \cdot \cos\omega_2 t \cdot e^{j\omega_2 t + j\theta(t)} + h(x_T,t) \cdot \cos\omega_3 t \cdot e^{j\omega_3 t - j\theta(t)} + h(x_T,t) \cdot \cos\omega_4 t \cdot e^{j\omega_4 t + j\theta(t)}$$

$$u_{s2}(x_T,t) = h(x_T,t) \cdot \sin\omega_1 t \cdot e^{j\omega_1 t - j\theta(t)} + h(x_T,t) \cdot \sin\omega_2 t \cdot e^{j\omega_2 t + j\theta(t)} + h(x_T,t) \cdot \sin\omega_3 t \cdot e^{j\omega_3 t - j\theta(t)} + h(x_T,t) \cdot \sin\omega_4 t \cdot e^{j\omega_4 t + j\theta(t)} \quad (8)$$

The next step is to perform heterodyne processing on (8). Then we have

$$C_{c2}(x_T,t) = \langle u_{c2}(x_T,t)\, s^*(t)\rangle_{T_c} \quad (9)$$

Equation (9) contains the four-frequencies

acoustical holographic interference fringes.

For both the two-frequencies and the four-frequencies cases, the reconstructed images are given by the Fourier transformation of eqns. (7) and (9).

4. Comparison of System Resolution before and after the Application of Holography

It is very difficult to show mathematically the amount of improvement in resolution due to the application of multiple frequencies acoustical holographic interferometry. Qualitatively, by applying holography to a synthetic aperture sonar system, we are combining aperture synthesis of synthetic aperture technique with spectral synthesis of multiple frequencies holography to obtain superresolution. The improvement in resolution is in range resolution due to the utilization of very short pulsed waves when the pulse width is reduced to a width as narrow as several wavelengths.

5. System Development

We shall follow the work of Sato et al[2] for the design of our system but with some modifications. This will be to include in electronic instrumentation for demodulation and low-pass filtering works.

References

1. Cutrona, L.J., Vivian, W.E., Leith, E. N., Hall, G.O., "A high-resolution radar combat-surveillance system," IRE Transactions on Military Electronics, MIL-6, 1961, pp. 119.

2. Sato, T., Ikeda, O., Ohshima, H., and Fujikura, H., "A few effective preprocessings in synthetic aperture sonar system," Acoustical Holography, Vol.7, 1977, pp.569.

3. Dick, M.L., Dick, D.E., McLeod, F.D., and Kindig, N.B., "Ultrasonic Synthetic Aperture Imaging," Acoustical Holography, Vol.7, 1977, pp.327.

ENVIRONMENTAL CONSIDERATIONS FOR SITING AN OCEAN THERMAL ENERGY CONVERSION EARLY OCEAN TESTING PLATFORM AT FOUR PROPOSED AREAS

M.D. Sands
Interstate Electronics Corporation
Oceanic Engineering Division
Anaheim, California 92803

Pat Wilde
Lawrence Berkeley Laboratories
University of California
Berkeley, California 94720

Abstract

This presentation summarizes the environmental considerations for siting OTEC-1, the Early Ocean Testing Platform. As you may know, the concept of Ocean Thermal Energy Conversion (OTEC) is not new to the alternative energy source arena. d'Arsonval first proposed the use of the thermal gradient between warm surface and deep cold ocean waters in the late nineteenth century. In the 1950's, the French government considered OTEC, but, after developing some equipment, abandoned the program prior to testing.

With the oil embargo in the early 1970's and the resulting oil price increases, the United States Federal Government, in 1975, established the Energy Research and Development Administration to conduct energy-related research. Presently there are several solar research projects under evaluation, one of which is OTEC, and the Early Ocean Testing Platform for a prototype evaluation has a projected test date in early 1980. The ultimate use of OTEC may be to provide commercial electricity generation in place of the use of fossil or nuclear fuels, or to create floating plant-ship operations for industrial production of aluminum or fertilizers.

As a result of the implementation of the National Environmental Policy Act of 1969, all government-funded activities must consider potential environmental consequences of activities and prepare an Environmental Impact Assessment (EIA). If significant impacts may occur, an Environmental Impact Statement (EIS) must be prepared bringing environmental considerations into the decision-making process. The considerations in assessing impact for OTEC-1 first require a detailed description of the physical system design. Included in the design description are the depth of intake and discharge pipes, volumes discharged, and applicable safety regulations and procedures. The detailed site descriptive information including the biological, chemical, physical oceanographic, and meteorological data must be gathered from all available sources. Particular study areas include the effects of metallic element discharge, ocean water thermal mixing and discharge, effects of impingement and entrainment, biocide effectiveness and toxicity to nontarget biota, working fluid release effects, and worker safety. Also, the international, Federal, state, and local legal implications of siting must be considered. When all relevant data is at hand the predictive process for assessing environmental impact is underway.

1. Introduction

The Oceanic Engineering Division of Interstate Electronics Corporation is under contract to the Department of Energy (DOE) to prepare the Environmental Impact Assessment for the 1-megawatt early ocean test platform. In the EIA, the issues of safety and health, legality of siting and site specific impacts are under evaluation. The potential impacts under study include toxic element effects, biocide release impacts, thermal mixing effects, point and nonpoint source outfall, impingment/entrainment and recommendations for OTEC-1 environmental and system monitoring. Briefly, this presentation will summarize the history of OTEC, OTEC-1 design aspects, the study sites, and report some of the progress to date.

2. OTEC History

The OTEC concept uses the thermal gradient that naturally exists in the oceans to condense and evaporate a working fluid. The minimal temperature difference required is approximately 20°C which limits the geographical region that can be used, to between 35 degrees north and south latitudes.

Ocean Thermal Energy Conversion was first proposed by d'Arsonval in the late 19th century, but the technology available at that time was inadequate to develop the concept further. Georges Claude, between 1929-1930, attempted to use an open cycle pilot plant for electrical power production. Before the cold water pipe was destroyed, Claude did get a small power output and prove the concept. Later, in the 1950's, the French government supported a partially government owned company to construct an OTEC plant on the African Ivory Coast. While several subsystems were designed, built and tested, the work was never

completed. J. Hulbert Anderson and J. H. Anderson, Jr. first proposed the construction of a 100 megawatt plant using the closed cycle approach in 1966.(1)

OTEC was one of the six solar technologies selected by the National Science Foundation's Research Applied to National Needs (RANN) program in the early 70's. In January 1975, the Energy Research and Development Agency (now the Department of Energy) was formed and assumed the lead role for program development. Since the initial budget allocation of $85,000 in fiscal year 1972, the program has grown dramatically to the present funding level for fiscal year 1978 in excess of 35.3 million dollars.(3)

3. OTEC-1 Physical Description

Two types of systems can be used for OTEC power generation--the open or closed cycles. The open cycle utilizes seawater as the working fluid where low-pressure steam is evaporated from the warm-water flow. The closed cycle employs a working fluid with good heat transfer characteristics such as ammonia, freon or propane. The Rankine power cycle includes a pump, condenser, turbine and evaporator. The working fluid is converted to a vapor (power is generated by expansion through the turbine) and condensed by the cold water at the condensers. OTEC-1 is not scheduled to have a turbine, or produce a net energy gain, but to demonstrate and evaluate various technological concepts.(4)

While the platform for the 1-megawatt plant has not been selected, the physical operations specifications have been outlined. Presently, two concepts have been suggested to supply the cold water resource to the platform: a platform-supported sectional pipe string (Figure 1a) or a separately deployed and positioned spar buoy/riser pipe (Figure 1b) which interfaces with the platform through a "quick-disconnect" umbilical. The disconnect mechanism will separate the buoy from the platform in the event of an emergency.

Water Supply: The assumption was made that the cold water pipe will deliver a seawater flow from the 1000 meter depth to the condensers at a flow rate of 257,000 liters per minute (68,000 gal/min). The warm water pumps will deliver 227,000 liters per minute (60,000 gal/min) from the surface waters.

Discharge: The warm and cold water may be mixed and discharged through a common header with extensions over the stern at a depth of 40 meters. The combined flow of 484,000 liters per minute will be discharged at a rate of 308 cm/sec. The method of discharge presently is undefined. In this evaluation, both a horizontal and vertical discharge were considered.

Biofouling Control: The prevention of microfouling on the heat exchanger and condensers surface is a critical aspect for OTEC-1 operation. Buildup on the order of 50 microns will reduce the heat duty 15 to 25 percent.(5) To restrict this buildup, mechanical methods (Amertap and M.A.N. brushes) in conjunction with chemical methods (chlorine) will be used for biofouling control.(4)

4. OTEC-1 Siting Criteria

The site that is selected for OTEC-1 testing must be located within 200 nautical miles off the United States and its properties.(6) The minimum temperature differential must be greater than or equal to 20°C for five continuous months with an overall annual temperature spread of 16°C minimum. The maximum allowable currents shear or velocity gradient must not exceed 1 knot in 50 meters vertically and 1 knot in 200 meters horizontally. Additionally, the water sea state cannot exceed Beaufort No. 4 for 9 months continuous.(6)

In terms of extreme conditions, OTEC-1 will operate in seas with a significant wave height of 4.9 meters, 62 cm/sec surface currents and 15 meters/sec winds. Both the platform and the retracted, detached or modified deployed cold water pipe will survive 12.5 significant wave heights, 1.0 meter/sec surface currents and winds of 51 meters/sec.

The study sites designated for this study by the Department of Energy include Keahole Point, Hawaii; Punta Tuna, Puerto Rico; New Orleans, La; and the West Coast of Florida. Keahole Point is approximately 3.9 kilometers offshore in 960 meters of water. The bottom sediments are basically volcanic sands and silts. The mean flow through the site is between 10-30 cm/sec. The vertical delta T over the year ranges from 19.8 to 22.5°C.(7)

Punta Tuna is approximately 4.6 kilometers offshore in 1,200 meters of water. The bottom sediments are predominately silts and sands high in carbonates. The mean flow through the site is also 10-30 cm/sec; vertical delta T over the year ranges from 20.9 to 23.9°C.(7)

The New Orleans site is approximately 89 kilometers off the southeast pass and 138 kilometers off Mobile Point, Ala. The bottom sediments are primarily terrigenous silts and clays. The annual mean flow through the site is from 35 cm/sec to variable. The vertical delta T over the year ranges from 16.6 to 25.0°C.(7)

The west coast of Florida site is approximately 250 kilometers off Cape San Blas and 272 kilometers off St. Petersburg. The bottom sediments are composed primarily of silts and siltey clays. The flow through the study site is 100 cm/sec and variable. The vertical delta T range for the year is 19.7 to 15.0°C.(8)

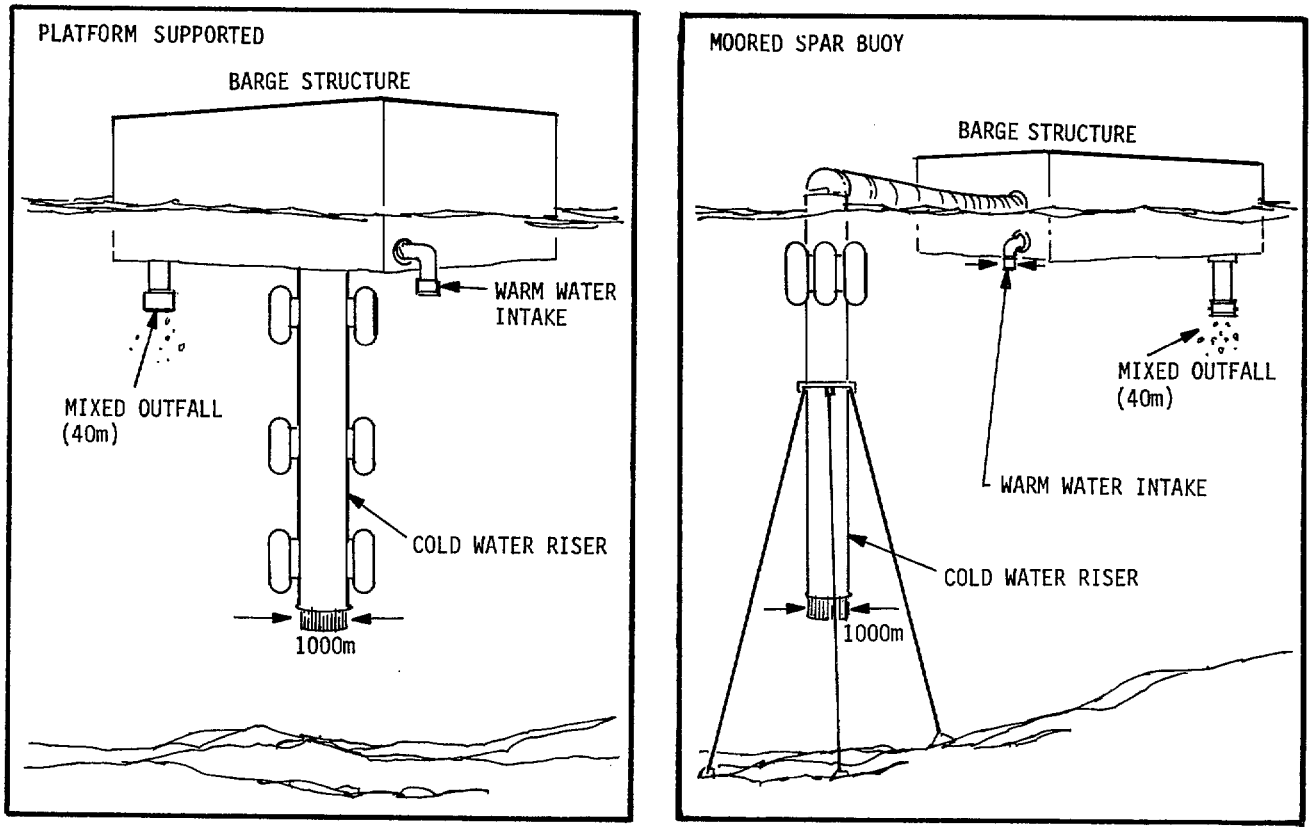

(a) (b)

Figure 1. Alternative Design Concepts for Cold Water Residue

5. Environmental Considerations

The considerations for siting OTEC-1 that must be addressed include health and safety on the platform as well as in the surrounding vicinity, legal or licensing issues of the platform, and the potential environmental consequences that may result from site occupation.

Health and Safety: The safety aspects for OTEC-1 are similar to various operational procedures inherent in most ocean-going vessels. In preparing an evaluation of these issues, at least four department level agencies and fourteen non-governmental organizations will be involved in an advisory or regulatory function.(4,8,9)

Legal Considerations: Several complex national and international legal ramifications surrounding OTEC-1 operations have been discussed by Knight, Nyhart and Stein (1977) who published a comprehensive discussion of the legal, political, and institutional aspects of Ocean Thermal Energy Conversion (under the auspices of the American Society of International Law).(10) Their report covered many of the complex issues of OTEC in general. It is recommended that a similar study, specifically applicable to OTEC-1, be undertaken that will lay the groundwork for the early ocean test platforms.

The Federal agency involvement in licensing is an important siting consideration. Research beyond the territorial sea has been subject to control by the Federal government. Because of the large number of agencies involved in licensing at the Federal and State level, Knight et al. (1977) suggested the designation of a lead agency to coordinate the various approvals required from the administrative bodies involved.

If designation of a lead agency could be made, it would reduce the lead time required to receive permits and would lay the groundwork for future OTEC activities. Congressional approval is required for agency designation. Candidate agencies include (but are not limited to): Army Corps of Engineers, U.S. Coast Guard, or the Department of Commerce (principally NOAA).(11)

Environmental Consequences: The main consideration for the assessment of potential environmental impacts are dependent upon the

near field dispersion of the plume. Once isopleths are prepared for each contaminant introduced to the environment, applicable toxicity data for resident organisms can be compared.

Preliminary evidence obtained from mathematical model predictions and expected density gradients indicate that the 1-megawatt horizontal mixed discharge water would mix in the water column 50 meters below the discharge pipe.(11,12) It is expected that background diurnal fluctuations of up to 1°C would obscure much of the thermal impact at the bottom of the surface mixed layer with the major impact observed within a few hundred meters of the horizontally discharging jet.

If discharged vertically, an entirely different plume behavior will prevail. Essentially the discharged mix will be injected into the top of the main thermocline. Given an initial momentum effect, the discharging jet will reach approximately 60 meters below the discharge pipe before significant entrainment, thus effectively injecting the discharge into the upper portion of the main thermocline. This would, of course, minimize feedback to the warm water intake, but put the discharge at or below the surface mixed-layer depth at each of the four sites during summer conditions.(12)

The environmental impacts that are under evaluation include the impacts that may result from trace element leaching from the heat exchangers, condensers and the platform surface, the effects of biocide release on target and nontarget biota, the effects of nutrient redistribution to the photic zone and the effects of organism impingement on the intake screens and the entrainment of organisms in the system. (13)

Trace Element Release

The heat exchangers, pump impellers, metallic piping and bottom paints are sources of toxic metallic ions. The pump impellers and metallic piping are minor sources; the greatest release will come from the heat exchangers and the bottom paints. The heat exchanger materials likely to be used on OTEC-1 are aluminum and titanium. These materials are relatively nontoxic in the marine environment.

The Hughes Mining Barge, a proposed OTEC-1 platform, is painted with the antifouling paint Kelkote 109AF. The active agent in the paint is cuprous oxide and is applied at a thickness of 6 mils. The amount of release from this surface will vary with the age of the coatings and rate of flow past the hull. The release of 1 kilogram copper would result in a loading to the marine environment of 2 mg/m^2 or 0.2 mg/l, assuming the copper is confined to a 1-cm film over the surface. (14)

Nutrient Redistribution

OTEC-1 site occupation is unlikely to significantly increase primary productivity near the site. After mixing with the surface waters and discharge at the outfall, most of the nutrients will be transported to approximately 90 meters depth where light is expected to be the limiting factor.

Biocide Release

Although chlorine has been specificied for OTEC-1, the method or rate of application is not known at this time. The EPA N.P.D.E.S. Chlorine regulations for cooling water restrict the release of chlorinated waters to no more than 2 hours per day with a 30-day average not to exceed 0.2 mg/l. It is expected that the main influence of release will be on the invertebrates and eggs and larvae stage of fish. The toxicity or bioassay data available for the oceanic species at these sites is very limited. Studies are underway to further evaluate this release.

Impingement/Entrainment

OTEC-1 will circulate millions of liters per day and organisms that reside in the region will be subjected to impingement and entrainment effects. The most serious impingement problem is expected to be with those fish which have the lowest avoidance capabilities, the coelenterates. Organisms entrained in the cold water pipe will suffer 100 percent mortality as a result of the pressure and temperature change and physical abuse, while the warm water intake mortality should be much less. (14) Field programs underway at the OTEC regions will provide the qualitative and quantitative biological data necessary to further evaluate these effects.

Acknowledgement

This OTEC study is funded by the United States Department of Energy under contract number EG-77-C-06-1033.

References

(1) Griffin, Owen M. August 1977. POWER FROM THE OCEANS' THERMAL GRADIENTS. Sea Technology Volume 18, No. 8 p. 11.

(2) W.S. Deptartment of Energy, March 1978. Environmental Development Plan Ocean Thermal Energy Conversion. DOE/EDP/0006 (Available NTIS) p. 48.

(3) Mulcahy, Michael. Aug. 1977. OTEC - FROM 85,000 TO 35 MILLION IN SIX YEARS, Sea Technology Volume 18, No. 8, p. 16.

(4) Sands, M.D. February 1978, "Progress Report for the Environmental Impact Assessment Program for the 1-Megawatt Early Ocean Test Platform", to appear in Proceedings Fifth Anual Conference on Ocean Thermal Energy Conversion, T.N. Veziroglu, Editor; CERI/UM.

(5) Bell, Kenneth J. October 1977. The Effect of Fouling Upon OTEC Heat Exchanger Design, Construction and Operation. Presented at the Biofouling and Corrosion Symposium, coordinated by Battelle Northwest Laboratories and sponsored by the Energy Research and Development Agency.

(6) U.S. Department of Energy, Request for Proposals for System Integration Contractor for OTEC-1, received January. 1978.

(7) OTEC-1 Site Environmental Profile Enclosure A (Revision, January, 1978) DOE Working Document.

(8) United States Coast Guard. 1973. Rules and Regulations for Cargo and Miscellaneous Vessels, subchapter 1. Department of Transportation, Washington, D.C. 179 pp.

(9) Occupational Safety and Health Administration. 1976. General Industry Safety and Health Standards, Department of Labor, Washington, D.C. 649 pp.

(10) Knight, G., Nyhart, J.D., Stein, R.E. 1977. Ocean Thermal Energy Conversion, Lexington Books, Lexington, MA. 230 pp.

(11) Personal communication, K. Bathen, 31 January 1978.

(12) Bathen, K. 1975. An Evaluation of Oceanographic and Socio-Economic Aspects of a Nearshore Ocean Thermal Energy Conversion Pilot Plant in Subtropical Hawaiian Waters. Department of Ocean Engineering, University of Hawaii, Honolulu, Hawaii. 271 pp.

(13) Lewis, L. (ed.) Proceedings, OTEC Environmental and Resource Assessment Workshop, June, 1977.

(14) U.S. Department of Energy. (in press.) ENVIRONMENTAL IMPACT ASSESSMENT FOR OTEC-1. Interstate Electronics Corporation, Anaheim, California.

TECHNOLOGY CONSIDERATIONS IN THE DESIGN OF A COMMERCIAL OFFSHORE ENERGY CONVERSION (OTEC) PLANT

William W. Rogalski, Jr. and Robert J. Scott
Gibbs & Cox, Inc.
2341 Jefferson Davis Highway
Arlington, Virginia 22202

Dr. Julio G. Giannotti
Giannotti & Buck Associates, Inc.
Crestwood Building, Suite 402
5711 Sarvis Avenue
Riverdale, Maryland 20840

Abstract

The design and construction of an OTEC plant slated to produce electricity for commercial consumption in the near future presents a number of unique problems and is forcing the advancement of the state of the art in ocean structures in a number of fields. The successful deployment of a commercially viable OTEC plant is dependent upon identifying these technology areas and developing a program to insure that any potential program obstacles are adequately addressed.

1. Introduction

The concept of OTEC utilizing thermal differentials in the ocean to generate electrical power appears to be one of the more viable methods of transforming solar power into usable forms; however, a number of ocean engineering related problems need to be overcome to reduce the risks inherent with the concept to acceptable levels. This paper will discuss some of the higher risk aspects associated in the development of the platform and cold water pipe (CWP) for an OTEC commercial power plant that utilizes a closed Rankine cycle power system.

The material discussed herein is based on a study done by Gibbs & Cox, Inc. for the U. S. Department of Energy (Reference (1)). This study, one of three parallel efforts, had as its objectives the selection of the optimum plant output and hull configuration for a Commercial OTEC plant and the subsequent conceptual design of the two leading candidates. During this process a number of technology areas requiring further development were identified, the more significant of which are addressed in the subsequent sections of this paper.

2. OTEC Commercial Plant Concepts

To establish a point of reference for the discussion of technology requirements, a brief outline of the baseline designs used in the hull selection process mentioned in the introduction along with the two final conceptual designs will be presented in this section.

The hull forms considered in the optimization process consisted of six generic shapes - ship or barge, vertical cylinder or disc, spar, submersible, semi-submersible, and sphere. In addition, a range of electric power plant outputs was considered, in this case, 50 to 500 megawatts (MW), to bracket what was considered at the time a reasonable variation in size. The upper limit of 500 MW was chosen because it was felt that based on an initial assessment of the state-of-the-art (SOA) in large ocean platform construction, deployment, and operation it represented the upper limit with respect to size, i.e., approximately one million long tons. The evaluation process utilized a figure of merit (FOM) based on an economic benefit to cost relationship and resulted in the final selection of a 400 MW ship and 400 MW semi-submersible for further development. At the same time, Lockheed Missiles and Space Company and M. Rosenblatt and Son, Inc., who were engaged in parallel efforts, each made their recommendations as to size and configuration, and were asked to develop further the ship and spar (Lockheed), and the sphere and spar (Rosenblatt).

The ship and semi-submersible designs by Gibbs & Cox, Inc. underwent a series of iterations until they converged to the point where feasibility was demonstrated and first-cut cost estimates could be made. Table 1 contains the principal characteristics of both the ship and semi-submersible while Figure 1 is an inboard profile of the ship.

Table 1
OTEC Commercial Plant
Principal Characteristics

	Ship	Semi-Submersible
Length (ft.)	620	436
Beam (ft.)	300	436
Depth (ft.)	85	328
Draft (ft.)	45	215
Displacement (full load)*	311,000	451,000
Displacement (light ship)*	126,000	139,000
Nominal Power Output (MW)	400	400

* Displacements are given in long tons; 1 long ton = 2,240 lbs.

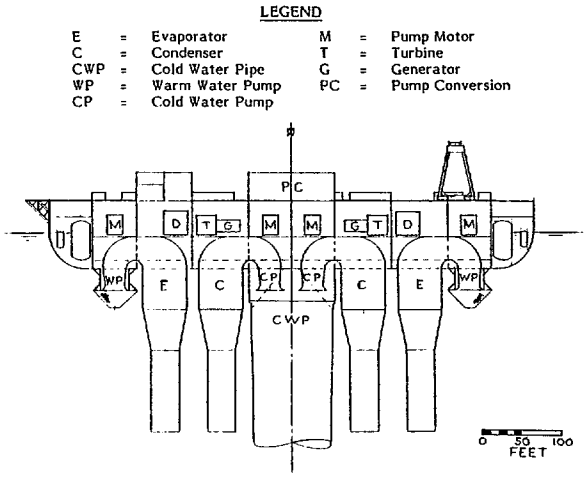

Figure 1 - 400 MW OTEC Plant, Ship Configuration Inboard Profile

The ship is basically a barge-like structure divided into quadrants, with each quadrant containing two 50 MW power plant modules.

Warm water is taken in through screens by the eight warm water pumps, is pumped to eight evaporators (one per module) mounted veritcally below the hull, and is discharged back to the ocean at or near the bottom of the mixed layer through individual discharge pipes (one per heat exchanger). The ammonia vapor is piped to demisters and then to the turbines which are directly coupled to the generators. The turbine exhausts discharge to eight condensers which receive their cooling water via the cold water pipe and cold water pumps, and the condensate is then pumped back to the evaporators. Each of the eight power modules is totally independent and cannot be cross connected. Power conversion equipment, control spaces, and personnel spaces are located on the main deck in deckhouses.

The semi-submersible version is of the vertical column type, and consists of four legs each containing two power system modules with the evaporators, condensers, and warm and cold water pumps mounted externally in a vertical orientation. The columns are joined underwater by a cruciform structure which also serves to support the CWP, and above water by the upper cross structure - a platform that also houses the power conditioning equipment, control spaces, and living quarters for the crew. From a volumetric efficiency standpoint, the semi-submersible was inferior to the ship, but it was hoped that it would have superior seakeeping characteristics as manifested in loads in the CWP.

3. Major Technology Areas

Areas having a significant impact on the success of the OTEC concept will be discussed in the following paragraphs with respect to their position relative to the current SOA.

Size and Configuration. Perhaps one of the most intimidating aspects of the OTEC commercial plants discussed in the previous section is their size. As can be seen from comparing the displacements in Table 1 with those in Table 2 the proposed OTEC plants are structually more massive than any other floating platform, and this fact combined with their unusual configurations (especially when one considers the 3000 foot long 100 foot diameter CWP hanging below the platforms) places them in the forefront of the SOA in ocean structures. To further emphasize this point Figure 2 compares the profiles of the largest existing semi-submersible (ODECO's Ocean Ranger) and the Gibbs & Cox, Inc. semi-submersible.

Table 2
Current SOA in Floating Structures

Type	Dimensions (Length, Beam, Draft)	Displacement (Light Ship)
Tanker (Batillus)	1360 x 261 x 145	78,000
Drill Rigs (Semi-Submersible)	399 x 262 x 152	28,000
Oil Production Platform (Moored Spar)	100 diam. 445 high	20,000

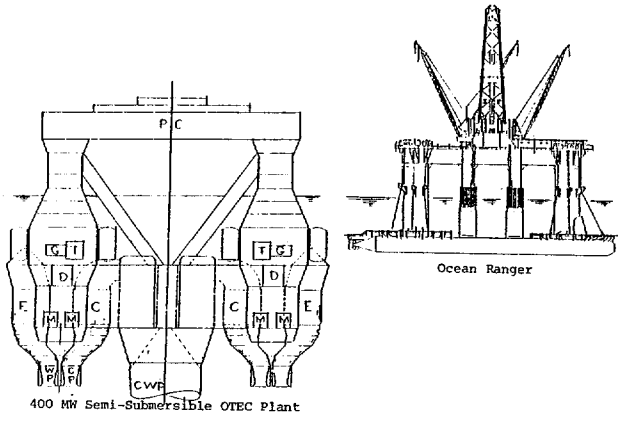

Figure 2 - Semi-Submersible Size Comparison

Aside from the production difficulties (which will be discussed in a subsequent section) associated with such unconventional platforms, the revolutionary nature of the step up to the OTEC Plants as opposed to the normal evolutionary approach taken by the marine industry presents one of the more significant problems with respect to risk and the SOA. The various regulatory agencies (ABS, U.S. Coast Guard) and most insurance companies tend towards the conservative, and although no insurmountable techni-

cal road blocks solely as a result of size and configuration are foreseen, the advancement of the state of art must be pushed forward in a manner analogous to that in the offshore oil industry.

CWP. The CWP is without a doubt the most difficult technical issue facing the OTEC ocean system (non-power plant) designers both from the standpoint of determining the design loads and construction/deployment. A structure with a length of 3000 feet and an inside diameter in the vicinity of 100 feet is unique in the maritime field, and the complications in establishing design criteria and methods are formidable. The pipes developed by Gibbs and Cox, Inc. with the assistance of Giannotti and Buck Associates are stiffened mild steel shells, but other materials such as concrete, glass reinforced plastic, and rubber are being considered to reduce the wave and current induced loads in the CWP's. In the following paragraphs some of the problems involved in establishing those loads will be discussed.

The wave induced motions of the platform in six degrees of freedom give rise to dynamic bending and vertical stresses which could cause structural failure as a result of either single extreme stress excursions or cyclic loadings. Superimposed on these loads is the action of the ocean current velocity which varies with depth and gives rise to steady state bending of the CWP; therefore, a considerable amount of effort during the initial stages of the OTEC platform studies has been devoted to the prediction of these structural loads.

The analysis of steady state current induced drag forces acting on the CWP is fairly straight forward subject to the availability of empirical data on drag coefficients at high Reynolds numbers and vortex shedding at appropriate Strouhal numbers. Studies aimed at developing this information are currently underway and preliminary results have been used in various OTEC platform design studies. Detailed information summarizing this data is given in Reference (1).

The dynamic CWP loads and stresses induced by ocean wave action require rather involved analyses of the complex interaction of waves, platform and CWP. As in any structural dynamics problem the parameters which affect the magnitude and distribution of the loads and the response are geometry, material, structural arrangements, boundary conditions, mass distribution and the characteristics of the dynamic loads (time history, frequency, magnitude, distribution, etc.). In the case of standard ship and ocean platform applications many of the analytical tools for predicting motions and loads induced by the seaway have been validated with experimental data; however, the simulation of the OTEC platform/CWP configuration has not. This will hopefully be accomplished during the next phases of the OTEC program where both scale model testing and full scale experiments on test platforms are expected to be carried out. In the meantime the results obtained from these simulations should be used with caution pending a thorough validation of the theory involved.

In most studies conducted up to now the prediction of the CWP dynamic loads and bending stresses has been carried out using linear frequency domain computer simulations. These tools are fairly economical to use but they are somewhat limited in that the non-linearities of the platform and CWP response are not adequately considered. Such non-linear behavior is best represented in the time domain, Reference (2), but unfortunately this is an expensive technique. The general consensus is that the frequency domain tools should be used to conduct parametric estimates of long term platform behavior in order to allow one to define the worst or critical design conditions. Having accomplished this, the next step would be to conduct a few specific simulations with the time domain tool corresponding to the events associated with the worst case conditions. In this manner the structural response can be determined with due consideration given to the effect of non-linearities without jeopardizing the validity of the design calculations.

For this OTEC study a frequency domain simulation developed by Paulling, Reference (3), was used. The dynamic system under consideration consists of a floating platform with the CWP suspended below it. A linearized frequency domain analysis of the response of the coupled system of platform and pipe to incident waves is performed by the simulation. Responses in random seas are obtained by superimposing the response to a series of regular waves of different frequencies and amplitudes. Results of the analysis include the motions of the platform and a series of points along the pipe, forces at the connection between the pipe and platform, and stresses due to axial force, bending and shear in the pipe.

A typical output of this analysis is shown in Figure 3 where the significant bending stresses in the CWP are plotted against the axial position along the pipe for the ship configuration in random beam seas.

The Paulling simulation is applicable to most conventionally configured platforms such as the ship and semi-submersible developed as part of the current study. Difficulties arise when more unusual forms such as the spar, sphere, and cylinder need to be analysed since in those cases the simulation loses validity because of its inability to accurately calculate the hydrodynamic coefficients for such geometries. Another frequency domain simulation developed by Garrison, Reference (4), presently

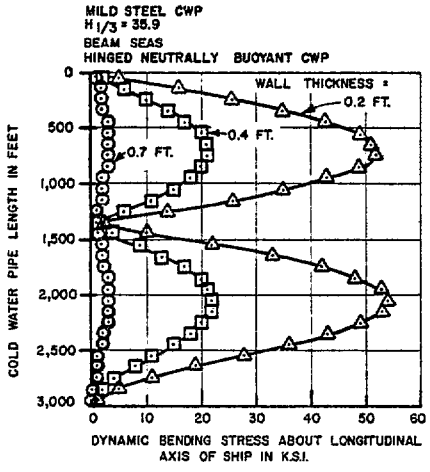

Figure 3 - Typical Results, CWP Loads Simulation

exists which does handle arbitrarily shaped bodies and can be used as an input to the CWP portion of the Paulling simulation; however the previously mentioned limitations still exist, i.e., no full scale or model test verification. In addition the current models do not include all external effects on the CWP such as secondary loads from the current induced pressure distribution (steady state and time dependent) and internal flow.

To adequately reduce the risk in motions and loads predictions for the CWP it will be necessary to develop an all-encompassing simulation in both the frequency and time domain. Their output could be used in one or more of the standard structural analysis programs to develop an optimum structural design. The development of these models is not considered to be beyond present day capabilities, but it is considered an essential advancement of the SOA with respect to the overall development of the CWP. The simulations will then have to be verified with a concerted program of testing instrumented models and partial and full scale pipes on either test platforms or limited scale OTEC plants prior to commitment to the large expenditures required for the commercial plant.

CWP/Hull Interface - The method of attaching the CWP to the platform itself also presents some unique problems in itself. Considering that the CWP developed for the two OTEC commercial plants by Gibbs and Cox, Inc. weighed approximately 20,000 tons in water and that vertical dynamic loads add an additional 2000 tons, it can be seen that the load imposed on the platform structure in the vicinity of the CWP is quite high.

The major problem arises when a compliant joint is considered. In many conditions a device that decouples the CWP and hull in rotation reduces the wave induced bending moments in the upper regions of the pipe, and the device can be configured to facilitate CWP deployment. The critical item in this case is the bearing assembly since it must carry the entire load of the pipe. The ship and semi-submersible designs utilize a universal style joint containing two separate bearing assemblies, each of which carries the entire weight of the pipe. The present SOA in bearing design is very close to that required for such a device. Similar units were developed for the stabilization assembly on the Glomar Explorer, and it is the opinion of several bearing manufacturer that limited development would result in a satisfactory bearing design for the OTEC plant; however, the use of heavier materials such as concrete for the CWP could result in unacceptable loads on a compliant joint. Such a situation would require considerable research and development in bearing design or the addition of expensive buoyancy to the pipe to reduce bearing loads.

Position Keeping System - The environmental conditions at some of the potential OTEC sites - namely peak current velocities up to 6 knots, combined with the large projected underwater areas of the plants result in drag loadings that require position keeping systems beyond the present SOA. Although the watch circle requirements for the plants are not extremely stringent, the drag loading on either the 400 MW ship or semi-submersible plant in a current of only 2 knots is approximately two million pounds requiring the equivalent of 67,000 shaft horsepower to hold the platform stationary. This coupled with the extreme depths at some of the sites under consideration (4650 feet at New Orleans) and the long operating life of the plant (40 years) presents some difficulties with respect to position keeping technology.

Two basic systems are under consideration to meet the position keeping requirements of the OTEC commercial plant; i.e., active (thrusters) and static (mooring lines and anchors). Non directional active units analogous to a conventional ship's propulsion plant with sufficient power to maintain the OTEC plants on station are presently available. In addition 2000 to 3000 horsepower rotatable units that could be mounted in the required quantities are also state-of-the-art, but with both these approaches the parasitic power drain on the plant electrical output would be quite high reducing drastically the power available to the grid or an on-site energy intensive industrial process. This leads to the second choice - the static system..

The combined environmental factors and vessel characteristics mentioned previously make any proposed mooring system beyond the present SOA; however, in most respects the required extrapolation of current technology is not extreme. The 3000 to 5000 foot water depths at the OTEC sites are within the present capabilities of mooring systems, but the problem arises when the loads imposed by the OTEC plants are compared to those of conventional drill rigs. A number of systems, including ones with mooring lines composed of a series of linked pipe sections fabricated from high strength steels, have been proposed by different groups, and the one developed for the Gibbs and Cox, Inc. commercial plant designs by Alan C. McClure Associates of

Houston, Texas is seen to be feasible albiet expensive. It relies on conventional components to make up an unconventional system, and it consists of a 14 point moor using wire rope for the anchor rode and deadweight anchors. The critical problem of long life has been mitigated by the provision for periodic replacement of the wire, and as a logical extension of the present SOA the associated risk is considered to be minimal.

Construction and Deployment - The critical aspects of the large size and unusual configuration of the OTEC plants and the CWP can be distilled down to the difficulties involved in their fabrication, assembly and deployment. Almost all construction facilities in the United States are configured for conventional ships of generally conventional proportions and deal almost exclusively with steel as a building material. On the other hand, the OTEC plants, as should be realized by now, are rather unconventional, and a number of materials have been proposed for their construction - steel and concrete for the hulls, and steel, aluminium, concrete, glass-reinforced plastic (GRP), and reinforced rubber for the CWP's.

The primary issues with most existing fabrication facilities are the building dock dimensions and depth of water. Both the ship and semi-submersible by Gibbs & Cox, Inc., Inc., the spar and ship by Lockheed and the spar and sphere by M. Rosenblatt and Son, Inc. exceed the width and/or draft of all U.S. shipyards unless significant facilities improvement efforts are undertaken or techniques that involve fabrication in sections with final assembly at sea are utilized. The problem is compounded by the scarcity of deep water (50 feet or greater) immediately adjacent to the shoreline which would permit much of the out of dock assembly work to take place in sheltered waters.

The first issue, that of materials technology in shipbuilding, is of course, closely linked with the material chosen for the OTEC plant's hull and CWP. As stated above the U.S. shipbuilding industry is almost exclusively oriented to the production of steel structures. The largest concrete floating structure built in this country to date is an LPG production barge for ARCO which is 461' long, 136' in beam, and 56' in depth and displaces 65,000 tons full load and 29,000 tons light ship, Reference (5). Larger concrete offshore structures have been built, the Ninian Central oil storage platform which displaces approximately 600,000 tons with ballast for example, but most of these have been constructed in dedicated facilities oriented totally towards concrete construction. Additionally these structures sit on the bottom and are not subjected to the full spectrum of loads that a surface platform such as OTEC would be. The point here is that while concrete does not pose any insurmountable technical problems, it would require an extensive investment to convert units of the shipbuilding (or offshore construction) industry over to concrete production. This means that new production procedures must be developed and design criteria established by regulatory agencies which implies a degree of technical risk.

The more exotic materials under consideration for the CWP present similar problems. If GRP or reinforced rubber are chosen for the commerical plant CWP, it will involve a multi order of magnitude increase in the size of any structure made of these materials with a commensurate level of risk.

The second issue, that of the dimensional restrictions of most existing fabrication facilities and the lack of sheltered deep water (with the exception of Puget Sound), will require the advancement of the SOA in offshore construction. Even with such facilities as Offshore Power System's in Jacksonville, Florida, the excessive drafts of the OTEC plants will necessitate a large amount of fabrication, assembly, and deployment work at the operational sites. This is especially true of the CWP. For example the Gibbs and Cox, Inc. ship is projected to be built in halves in a conventional building dock with the halves being joined afloat. The heat exchangers and seawater discharge pipes will be added in deep water (> 300 feet) along with the CWP which will be fabricated on site.

Any heavy construction done offshore is difficult, dangerous and expensive, and the magnitude required to place the proposed OTEC plants in operation exceeds anything yet accomplished in the offshore oil industry. The techniques and equipment required to manipulate and assemble large subassemblies on site must be developed to the point that the risk involved is reduced to acceptable levels.

The magnitude of the problem can be seen when one considers the CWP. If built of steel it will in all probability be fabricated on an assembly barge on site from a series of sub-assemblies, and will grow downwards into the water from this barge as sections are added at the top. When complete, the entire pipe, 3000 feet long and weighing approximately 20,000 tons, will be lowered and moved beneath the OTEC platform where it will be attached. The entire effort is envisioned to take about nine months and during the process severe environmental conditions may be encountered.

Environmental Considerations - The deployment of OTEC plants raises a number of domestic and international environmental problems which must be addressed during the planning and design phases of any future commercial plant.

In order to deal with these possible environmental impact problems, the Department of Energy in cooperation with several academic and industrial organizations has been sponsoring extensive investigations aimed at answering some of the more critical questions. These studies can be grouped into two separate but related areas of study, i.e., near field and far field.

Near field flow computations are of fundamental importance to the OTEC program for two main reasons. First, they determine the inflow temperatures as a function of design and operational parameters and

of the ambient conditions. Second, they are a basic input to far field environmental impact computations since they determine the redistribution of heat, salinity, horizontal momentum, biological species, and nutrients between different ocean layers and the possible addition of biocides and pollutants to certain layers. The near field flow problem has been studied in sufficient depth by several investigators. Their findings are summarized in Reference (1); however, what is needed now is an effort to merge the different analyses and experimental results into a consistent methodology or model which can then be used uniformly in OTEC plant siting and design.

The far field problem has to do with the impact of one or more operating OTEC plants on a specific region of the ocean. Here one must look at the oceanographic processes in a much larger scale than in the case of the near field problem discussed previously. These decisions go beyond the details of the individual plant design as they affect the economic, social, political and environmental structure of the area of concern. Reference (1) summarizes some of the most important far field studies which have been conducted so far under the OTEC program, and as with the near field case, there is a need to synthesize the various analyses into a single prediction model for a number of potential OTEC sites.

In actuality the question of environmental problems associated with OTEC will probably not be fully addressed and identified until the time that environmental impact statements are filed and some operational experience has been gained with some of the proposed test plants.

4. Minor Technology Areas

The previously discussed areas represent the ones most critical to the success of the OTEC concept from an ocean system standpoint, but a number of others with an inherently lesser degree of technological risk also exist. Some of these include the seawater pumps used to pump the warm and cold circulating water through the evaporators and condensers and the maintenance aspects of a ocean structure with a 40 year operational life. In these cases the SOA is very close to that required, and its extension to that point is not anticipated to present any degree of difficulty. As an example the warm water pumps will have to pump about 2.25 million gal/min of water per evaporator. If multi pumps are used then current axial flow designs are sufficient while a single pump of that size does not represent a difficult extension of the present SOA.

5. Summary

None of the technical issues discussed in this paper are seen as a road block to the successful deployment of an OTEC commercial plant in the 400 MW size range provided a well organized, logical, progessive technology advancement program is followed. The revolutionary nature of many of the advancements in the SOA may be reduced to an evolutionary process if such a program is developed and adhered to, using present level offshore technology as a foundation. The approach being taken by the U.S. Department of Energy follows the philosophy and will hopefully culminate in the commercial operation of a number of these large plants in the near future.

References

1. "Ocean Thermal Energy Conversion (OTEC) Platform Configuration and Integration - Final Report," Gibbs & Cox, Inc., Report 18351-10 (W-10,000, 10,010, 10,020), June 1978.

2. Tate, M. B. and Perini, L. L., "Dynamic Loads Induced by Severe Storms in Elastic Cold Water Pipes Attached to OTEC Ships by Fixed and Hinged Connections," Paper presented at the Fifth OTEC Conference, Miami Beach, Florida, February, 1978.

3. Paulling, R. J., Jr., "A Linearized Dynamic Analysis of the Coupled OTEC Cold Water Pipe and the HMB-1 Barge System," Report prepared for Morris Guralnick Associates, Inc., San Francisco, CA, August, 1977.

4. Garrison, C. J. "Hydrodynamics Interaction of Waves With a Large Displacement Floating Body," Naval Postgraduate School Report NPS-69 Gm 77091, September, 1977.

5. Anderson, A. R., "A 65,000-ton Prestressed Concrete Floating Facility for Offshore Storage of LPG," Marine technology, Volume 15, Number 1, January 1978

PHILOSOPHY OF MONITORING, INSPECTION, AND REPAIR FOR FIXED OFFSHORE PLATFORMS

P. W. Marshall
Shell Oil Company
P. O. Box 2099
Houston, Texas 77001

Abstract

The coming energy crisis will require difficult choices--between development vs. stagflation, between various energy sources having different costs and risks, and between allocating our finite resources towards maintaining sufficient energy supply vs. further reductions in pollution in risk.

The philosophy of making rational trade-offs between cost and risk has previously been applied in the selection of design criteria for storm loads, earthquakes, and fatigue. This paper will extend its application to rational decision-making in areas of structural monitoring, inspection, and repair. The role of structural redundancy is discussed, along with current inspection practices and monitoring development.

1. Introduction

There are many risks attendant upon a venture into offshore oil activity--dry holes, political uncertainty, blowouts, collisions, storm damage and earthquakes to name a few. While some of these risks are unavoidable, the risks related to structural design can be minimized by the expenditure of money and technical effort. Here the trade-off between cost and risk can be optimized in terms of rational economic considerations, provided these are formulated to adequately reflect the indirect human and social consequences.

Ideally, the objective of both the engineering effort and the rational value analysis should be directed towards minimizing C in the Veritas equation (ref. 1), regardless of who pays:

$$C = C_I + C_D + \sum_F pr(F) \cdot C_F \quad . \; . \; . \; . \text{(eqn. 1)}$$

where: C is the total cost of a project or structure which is built to produce a given benefit or return

C_I is the initial cost

C_D represents deferred operating costs, capitalized or reduced to present value

F represents an undesirable occurrence or failure

$pr(F)$ is the corresponding probability or risk of failure event F

C_F is the cost (inclusive of <u>all</u> disadvantages) which follows event F, also capitalized at present dollar value.

All risks are internalized; that is, the cost of failure includes expected oil spill clean up expenses, and liability for damages, injury, and possible deaths. The private business risks--loss of income and reserves; platform salvage and replacement costs--also provide substantial incentive for careful evaluation. Total failure cost ranges from 2 to 5 times the initial cost of an API-level platform--e.g. $50 million for a $10 million structure, or $500 million for a $250 million structure.

Zero-risk advocates might argue that unlimited private funds should be expended to achieve public benefits in terms of risk reduction, however out of proportion. In the largest sense, this distinction is artificial, since both public and private resources come from the same finite economic base, and should be allocated wisely. Where both costs and risks are in the public domain--e.g. in the case of flood control--making rational cost-benefit trade-offs is a well-established approach.

2. Strength vs. Load

Occasionally, the offshore civil engineer is asked to evaluate situations involving a finite measure of risk. When this evaluation is made on the basis of a conventionally computed safety factor there is often a tendency to imply that a structure having a safety factor just slightly larger than some arbitrary value is perfectly safe, while one having just slightly less is doomed to failure. Unfortunately, such a black and white answer to the question, "Will this structure fail?" cannot be provided. It becomes necessary to deal with the various shades of grey which are in the realm of probability.

A computed safety factor represents only the ratio of nominal strength to the assumed load. However, structural failure occurs when actual strength is exceeded by the actual load. Both strength and load are random variables, whose distributions include bias and uncertainty, which we shall now examine.

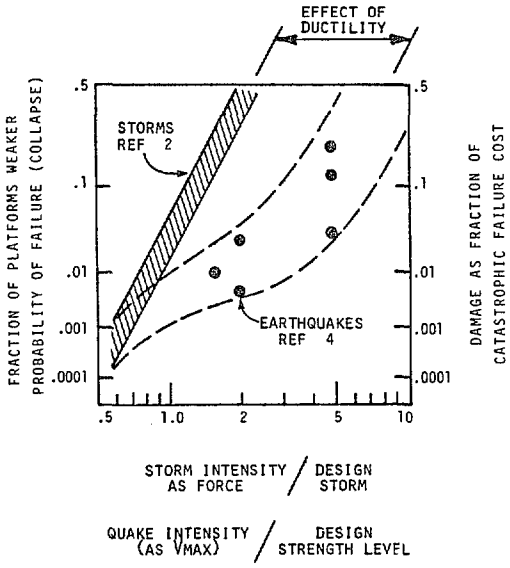

FIGURE 1
RESISTANCE CHARACTERIZATIONS

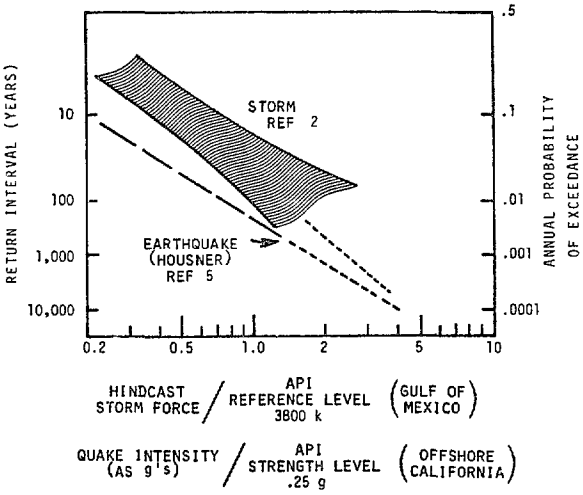

FIGURE 2
APPLIED FORCES

The shaded band in Figure 1 contains various a priori estimates of the relationship between the nominal design strength and the actual failure load of typical Gulf of Mexico drilling platforms subjected to storm forces (ref. 2). The lower tail of the statistical distribution is shown. Among the various models used to evaluate failure modes for offshore structures, the ductile-redundant model, which yields a median failure load of about twice the design load, comes closest to being consistent with survival experience of older platforms subjected to hurricanes. The range of uncertainty shown includes that introduced by wave force calculation procedures.

The upper tail for random variation of extreme storm forces can be found in Figure 2, with the shaded band representing the 95% confidence limits (ref. 2). These forces have been normalized to the current (1977) API reference level design wave, for the Gulf of Mexico.

The annual probability of failure, or risk rate, is obtained by evaluating the overlap of these two distributions (ref. 2, 3). The notional computed risk rate for storm losses comes out to about 1% for deepwater platforms in the Gulf of Mexico, designed to just barely meet API criteria. This result appears to overstate the risk when compared to the historical loss rate of 0.6%, or with the lower risk rates for current designs computed by other investigators (e.g. ref. 4). By way of comparison all-risk marine insurance rates reflect ship casualties of about 2% annually.

Similarly, the lifetime probability of failure is obtained by evaluating the overlap of the strength distribution, with the extreme value distribution for loads experienced during the structure's lifetime.

Now we apply equation 1.

The dollar risks, taken over the platform life, are combined with first cost as shown in Figure 3, with the shaded band covering a range of assumed failure costs, or different degrees of risk aversion versus optimism. Note that increasing the design level relative to API decreases the risk and increases the construction cost. Under optimistic assumptions the API level represents the least total cost (point A). Under more risk-averse assumptions a higher design force can be justified (point B), and some offshore operators elect to exceed the API guidelines. In so doing, they are making a trade-off which puts more steel into platforms and leaves fewer resources available for finding new energy. However, the optimum point is not sharply defined, and there is room for variation between the design criteria of different companies.

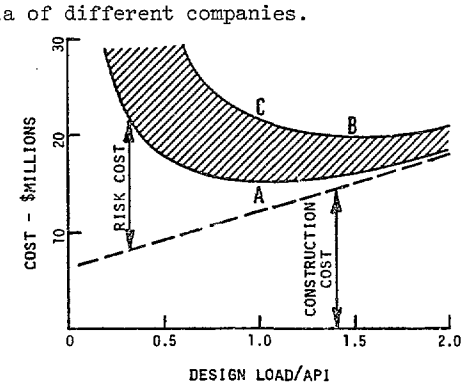

FIGURE 3
ECONOMIC ANALYSIS

Figures 1 and 2 also show resistance and intensity distributions for earthquakes. In the case of storm loading, we are accustomed to dealing with direct forces (e.g. due to waves) which, if not resisted, will cause collapse. Earthquakes, on the other hand, do not produce direct forces on the structure, although most simplified design codes treat them this way. Rather, the earthquake ground motions, transmitted through the stiffness of the foundation elements and super-structure produce distortions of the members, which are in turn related to forces. If the structure is properly detailed to hang together during inelastic excursions, earthquakes beyond its elastic capacity result in permanent distortion, but not collapse. If such distortion can be tolerated, all that fails is the elastic analysis. It is presumed that the wells and production facilities would be designed to avoid catastrophic fire or leakage for the most extreme motions in any case.

The effect of ductility in reducing the consequences of extreme earthquakes can be seen in Figure 1. Plotted points, in terms of damage, come from inelastic dynamic analysis of a typical offshore structure (ref. 4), using several earthquake records at a given nominal intensity. In terms of risk evaluation, we would expect to see a departure from the direct load risk trend at about the design yield level, with the yielding safety-valve effect creating a risk plateau. However, this safety-valve effect has its limits, and when the available ductility is exhausted the risk curve should resume its upward trend, as shown by the dashed lines.

In Figure 2, Housner's intensity distribution for earthquakes at a general site in California is shown. Extrapolation leads to a "maximum credible" event having a site recurrence interval comparable to the next ice age; although on a regional basis, such an event would be more frequent. Specific site studies by geotechnical consultants will generally yield somewhat different results, both in terms of annual probability trends and "maximum credible" events.

Note that both the resistance distribution and intensity distribution for earthquakes fall below the corresponding distributions for storm loading. This implies that more conservative design criteria have been adopted--partly out of concern for the fact that earthquakes occur suddenly, with less time for protective measures than in the case of storms--and partly to compensate for not yet having fully quantified all the uncertainties and risk factors involved in a new technology.

3. Fatigue

The effect of fatigue on failure risk may be illustrated by reference to a case study (ref. 6) of a North Sea steel structure. As originally analyzed, this structure had the following distribution of fatigue lives among 6 parallel members in the critical elevation within the structure:

	CALCULATED D=1 PER AWS	MEDIAN TIME TO FAILURE
1 member @	20 yr	100 yr
2 members @	60 yr	300 yr
3 members @	Over 200 yr	Over 1000 yr

Restricting our attention to braces in the critical elevation being studied, there are several members competing to be the first to fail, and the median time for the first failure is 50 years instead of 100. At year 50, such failure is not certain; there could be no failures or more than one failure. However, in the expected case, we have one failure, which because of multiple parallel load paths still leaves the structure with 80% of its original resistance to lateral loads. With the decreased mean resistance and increased scatter, the risk rate has now increased to about twice its original value. With further passage of time the structure gets progressively weaker, and both the risk rate and the rate of fatigue damage accelerate.

In fail-safe redundant structures, with multiple parallel load paths, the failure of a single brace does not lead immediately to collapse of the structure. Collapse occurs only when an extreme value of the applied load exceeds the remaining strength of the structure, which is reduced by progressive fatigue damage. Over the 20-year life, the added risk of collapse due to fatigue is on the order half the original risk of collapse due to overload. Nevertheless, structures are often designed so that the calculated fatigue life is a multiple of 2 or 3 times the anticipated service life, to further reduce the fatigue risk.

So far, the risk estimate assumes no inspection; that is, any failures would be allowed to progress to ultimate collapse without any kind of intervention. In practice this is not what happens. For the example structure, the expected interval between first failure and subsequent failures is 11 years, with 95% probability that the interval will be at least one year--that is, long enough to permit the damage (complete failure of one brace) to be found in a periodic inspection and repaired. Given inspection opportunity, the lifetime risk of catastrophic total collapse due to fatigue is reduced to less than 0.1%. In most cases of initial failure, detection would permit the structure to be either repaired or abandoned in an orderly fashion.

A large part of this risk reduction is achieved through secondary safety measures such as (1) subsurface safety valves for well control, (2) hurricane shut-in and evacuation procedures, and (3) downrating platforms with known deficiencies. Much of the risk which remains is an economic one on the part of the platform owner, rather than a hazard to human life or the public interest. The strategy of inspection and secondary safety measures is more cost-effective than simply specifying larger safety factors.

4. Inspection Practices

One Gulf of Mexico operator's inspection prac-

tices for fixed offshore platforms during recent years may be summarized as follows:

Extensive underwater inspections are performed each summer on certain platforms selected on basis of age, condition, interval since last inspection, and service history (e.g., unusual loadings, lapses in cathodic protection, etc.). Typically, four to five such inspections are conducted, or about 10% of the major platform population. Platforms which have been subjected to potential overloads in a hurricane are visually inspected under water and above water for major damage immediately after the storm. Above water inspections are performed annually on all platforms, and casual inspections of opportunity are performed in connection with diving for other purposes.

Detailed inspections are basically visual, with documentation in the form of underwater color photographs (sometimes video tape) and of the diver's observations. Techniques do not vary with depth, except that coverage is greatest at shallow depths, with spot checks at deeper levels where diving time becomes much more expensive. Marine growth has been removed by water jet blasting for recent detailed inspections.

Defects found have included the following:

(1) Parted, buckled and missing braces and legs--always the result of overloads from collisions (boats, ice, etc.) and, for older platforms, storms exceeding design criteria.

(2) Cracks in the chord at tubular joints, usually the result of overload in joints with inadequate wall thickness by today's standards.

(3) Breaks, buckles, punctures from objects dropped overboard, and abrasions/chaffing from cables hanging on braces.

(4) General corrosion pitting and selective accelerated loss of weld metal on platforms with incomplete cathodic protection. In severe cases, members may be penetrated (150 mpy pitting rate) or suffer localized 50 percent loss of net section. Knife-edge corrosion of weld heat affected zones has also been noted.

Physical damage, when it occurs, tends to be concentrated near the waterline due to accessibility to boats, localized wave pressures and slamming effects, and to marine growth increasing the effective diameter.

The current state of the art does not permit reliable and cost-effective detection of minor damage and small cracks. Attempts at using ultrasonics for this purpose have usually resulted in copious reports of "cracks" which turn out to be built-in weld discontinuities. However, by providing fail-safe redundancy in the structure, the more certain detection of major damage will suffice.

Costs for detailed underwater inspections range from $10,000-$50,000 for existing Gulf of Mexico structures, to $130,000 in Cook Inlet to $500,000 estimated for the 5-year inspection of a deepwater North Sea platform. Some improvement might be possible through the use of onboard saturation diving systems and an enclosed diver access tube/elevator; and by concentrating the detailed inspection selectivity on a "critical member list." However, a major potential source of savings appears to be the use of continuous structural monitoring (when perfected) as a supplement to underwater inspections to reduce the frequency and extent of the latter.

5. Structural Monitoring

Although measurements of natural periods and damping were obtained on offshore structures in the 1950's, one of the earliest examples of using motion measurements to monitor performance and integrity of manned offshore platforms was on Texas Tower No. 4 shortly before its collapse in 1961. Nicknamed Old Shakey for the noticeable motions which preceeded its collapse, the structure lacked the redundancy of typical template-type fixed platforms.

Shell's MGS Platforms A and C in Cook Inlet, Alaska, have been the subject of myriad monitoring schemes since their completion in 1965 and 1967. The first of these involved accelerometer measurements during 1965-66, with peak accelerations of .05 g reported.

During the period 1968-72, a system was developed which involved velocity transducers instead of accelerometers, with the data recorded on 14-channel FM analog tape, to be later digitized and analyzed using spectral techniques. Relevant objectives of this program (and how they turned out) are as follows:

(a) Verification of calculated natural frequencies from the space frame computer program (accomplished).

(b) Provide baseline measurements for determining feature changes in vibrational characteristics, as might be caused by structural damage. (this was accomplished, and in 1971 after complete loss of a horizontal brace, new readings were taken. These indicated insignificant changes in the natural frequencies, which could be explained by changes in deck mass. This does not necessarily condemn the approach for damage detection since analysis showed this was a redundant member whose loss did not affect either the strength or stiffness of the overall structure. While the "no significant damage" indication was essentially correct, those with unrealistic expectations that the frequency signature method could find lesser damage, e.g., cracks, were disappointed.)

Recently, Schmidt developed an inertial

reference Displacement Meter for this application (ref. 7). Accelerometers are wired to a double-integrating, zero-seeking circuit, which provides displacement output for dynamic and quasi-static motions, while eliminating long-term drift. The entire unit is reliable, highly portable, and can provide both acceleration and displacement output for either direct readout or recording on magnetic tape. The direct readout capability has proved invaluable in correlating structural response with loading events in the field.

In the Gulf of Mexico, measurements of platform response using the displacement meter described above have already yielded valuable feedback for analysis and design procedures, particularly in regard to structural modeling, damping, and overall response level (ref. 8).

These systems have also been operated in an unattended, battery-operated mode to obtain data during hurricane wave loading conditions.

A somewhat parallel technology for using topside motion measurements to monitor platform integrity has been developed in Scotland. Based on analysis and measurements on a laboratory structure, the developers claimed ability to detect damage (removal of jacket braces) by changes in the higher mode natural frequencies of the structure (which are less sensitive to changes in deck mass and foundation stiffness than the first mode). Field testing of their system on structures in the North Sea has led to a more realistic assessment of its capabilities (ref. 9). Baseline measurements are now seen as essential, since the differences between theoretical and actual frequencies are on the same order of magnitude as the shifts caused by damage. Nonlinearities in real structures and noise in field data prevented the identification of more than the first few modes, so that detection of minor damage (e.g., large cracks or the loss of secondary braces) would require mounting a transducer on each individual member. Changes in the frequency signature due to the loss (or restoration) of a major portion of the structure's strength and stiffness could be detected successfully, however, when such change was anticipated.

Based on what is now felt to be a realistic approach on the part of structural monitoring proponents, an opportunity was provided to put them to the acid test. Baseline measurements were made on an about-to-be-salvaged quarters platform in 60 ft. of water. The deck mass was then changed and selected underwater braces removed, giving them a shot at detecting the nature of each change "blind"; i.e., based only on successive motion measurements. Although baseline data was impaired by non-linear behavior of ungrouted piles, the test was a qualified success. Out of four subsequent readings, two correctly identified the condition of the structure, and a third was partially correct. Suffice it to say that a probabilistic statement of predicted changes, similar to Weather Bureau "percent chance of showers" format, now seems more appropriate than having to guess at one of several possible interpretations.

Probabilistic system identification theory should play a key role in structural monitoring efforts. An initial step is to analytically generate a "failure dictionary" of member removal versus changes in the frequency signature; in highly redundant structures, loss of several braces at a given level may be required to produce a significant change. In connection with the problem of detecting fatigue failures, the designer may specify a "critical member" inventory," i.e., a list of the 100 or so members with the shortest calculated fatigue lives. These members would be targeted for detailed inspection and inclusion in the "failure dictionary." A parameter study on the sensitivity of the calculated platform response to foundation stiffness, the various sources of damping, loading parameters (e.g., directional spreading of waves), deck loads, etc.--together with a prior estimate of the range of variability of these various parameters--is also used in a Bayesian sense to update the analytical model of the structure when baseline platform response data becomes available. Hart et al (ref. 10) have now formalized these procedures.

Many attempts have been made to strain gage operating offshore structures in order to obtain a more direct measure of stresses and applied loads. Several operators have instrumented structures in Cook Inlet and the Gulf of Mexico. Most efforts were only partially successful. While the transducers themselves can usually be waterproofed, the cables have proven to be all too vulnerable to environmental damage, presenting an expensive maintenance problem. Retrievable (and therefore maintainable) transducers for down hole measurement of axial loads and bending moments in piles may offer some relief from these problems. However, even where data can be successfully obtained, data interpretation on messy real world structures is clouded by uncertainties in the matter of applied loads and redundant stress paths, and by nonlinearities in the foundation. Only as a specially designed research installation, has Exxon's Ocean Test Structure avoided these problems (ref. 11).

A number of research type measurement programs have been undertaken on concrete gravity platforms in the North Sea. Since these were novel structures, the motivation was to verify their design premises by comparing measured versus calculated response. Up to 70 channels of data were recorded for intermittent 20-minute segments. Data includes wind and wave; accelerations and angular motions at deck, mid-height, and base; strain gages on tower leg rebars; and various foundation response parameters.

Immediate (onboard) data reduction produces zero corrected mean, maximum, minimum, RMS, and zero crossing rate for each data segment, which are plotted on strip charts. A detailed log of platform activities (e.g., tank levels) is also kept.

Subsequent onshore data reduction concentrates on detailed analysis of storm response--using the full design-type mathematical model for the structure and its wave loading, updated on the basis of field measurements. Given the measured wave spec-

trum, this model can be used to compute various response spectra for direct comparison with measured response spectra. Alternatively, the comparison may be made in terms of measured versus computed transfer function. While deterministic wave-by-wave comparisons are also possible, these introduce additional scatter.

The objective of current efforts in this area are to develop a cost effective strategy, and the necessary technology, for monitoring the response of operating offshore platforms as required. Such efforts should provide a basis for project-specific applications to structures scheduled for installation in deep water, earthquake zones, and frontier areas; and focus on design verification, damage detection and realtime data capabilities as outlined below:

(1) Design verification - comparison of predicted versus measured response, given the sea state. Where platforms are sensitive to uncertainties in soil support, damping, or wave load parameters, analysis of response vs. measurements will indicate whether the design assumptions are in the right ball park. Such measurements will provide valuable feedback to subsequent designs. Baseline measurements, system identification, and an updated computer model are also part of most damage detection schemes.

(2) Damage detection - shifts in the frequency signature (or some other aspect of response) may provide an early warning of major deterioration due to corrosion or fatigue failure; or buckling and parting of braces due to hurricanes, earthquakes or collision. Given the use of redundant fail-safe structural configurations which can tolerate the loss of one or several main members, sufficient damage and loss of stiffness can occur prior to imminent collapse to be readily detectable. With an established baseline and continuous monitoring, the absence of major damage indications could be used to justify a less stringent program of in-situ underwater inspection than would otherwise be necessary.

(3) Real time data - such as sea state and gross deck displacement - is monitored as a check on system operation. While such data may also be useful in daily operation on the platform, this function should be approached very cautiously, since false alarms could in themselves create hazards.

6. Repair Philosophy

When one goes looking for structural damage or deterioration, one should have established criteria for what to do when it is found. This is particularly important when regulatory agencies are involved, since ad hoc judgments made in the circumstances of a particular situation may be difficult to justify in the dogmatic atmosphere of subsequent review. Yet trade-offs and judgments are particularly important here, since rigid application to existing structures of criteria adopted for new structures can lead to unconscionable waste.

Ideally, one should be able to evaluate strength and risk for the structure in both the damaged and repaired condition, and then compare the cost of repairs with the risk reduction, making rational trade-offs on a case-by-case basis. However, regulators have a duty to act in the public interest, and may find it difficult to accept private cost-benefit calculations--particularly when there are neither established guidelines on calculation procedures, not explicit agreement on what constitutes an acceptable trade-off.

Figure 4 is an attempt to provide such a guideline. We implicitly take the design criteria and calculation procedures of the reference standard (e.g. API RP 2A) as a consensus representing acceptable trade-off for new construction. Rated strength is the load at which allowable stress (or permissible limit state) is exceeded, using standard calculation procedures--no fancy footwork allowed. Rated strengths less than 100% of the reference standard represent excess risk over that already found to be acceptable; and reduction of this risk can be used to justify the repair cost involved. Curves A, B, and C correspond to various reference strengths and degrees of risk aversion, as shown in Figure 3, for Gulf of Mexico storm loadings. For other types of load (e.g., drilling and production deck load) quite different (steeper) curves would apply.

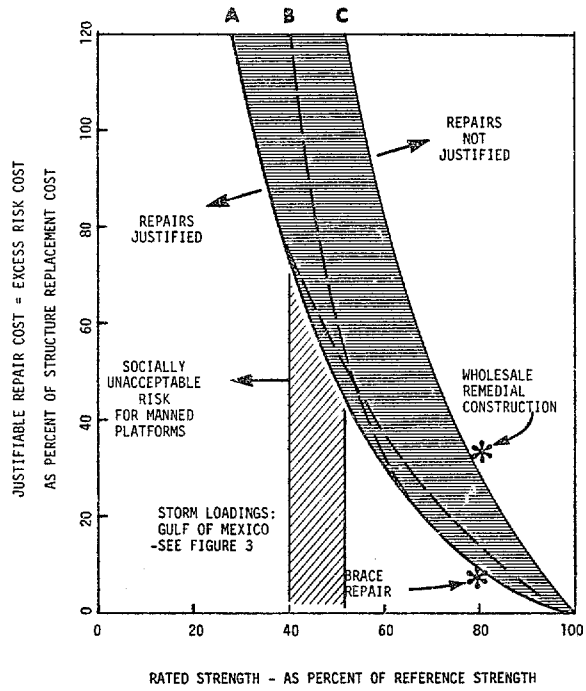

FIGURE 4 - REPAIR GUIDELINE

Two examples are shown, both for structures having replacement cost of $12 million, and found to be rated at only 80% of the reference strength. If the loss in strength is due to damaged braces

costing $1 million to replace, the repair would clearly be justified--except possibly in case B, where the reference strength was very conservative to begin with. If the 80% rating is due to general deterioration, or simply the fact that the platform is an older one designed for 20% lower criteria, the picture changes. The cost of wholesale remedial construction performed offshore and underwater, at $4 million, would not be justified in this example, unless the reference criteria were already below optimum (case C). However, the steeply rising curves provide ample incentive for protective measures which would prevent further degradation.

While the shaded band still leaves room for judgment based on the consequences of failure in each particular case, such a guideline--if adopted in advance--would provide a format in which a degree of flexibility and reasonableness could be incorporated into strict and impartial enforcement of regulations. Although Figure 4 is based on total costs and risks as accounted for by the offshore operator, analysis from a wider viewpoint should still lead to a similar result.

In the Gulf of Mexico, there is sufficient warning for hurricanes that offshore platform personnel can be evacuated and the wells secured against leakage in the event of structural collapse. This is done as a practice of long standing. For periods while the platform is manned and the wells are flowing, the maximum expected winter storm produces only 40% of the API reference lateral load. This is shown on Figure 4 as the limit of socially unacceptable risk; that is, we want the platforms to be fail-safe while manned--defined somewhat arbitrarily in terms of traditional safety factors. The shaded band leaves a margin for undetected damage. Gulf of Mexico platforms can suffer considerable degradation and still meet this criterion.

In other areas like the North Sea, evacuation is not always possible, and offshore platforms may be tested with a design storm while manned; further, the expected annual storm may exceed 70% of the specified design force. There is little if any margin for degradation, and difficult issues involving human risk will inevitably arise. Here it may be possible to define the socially unacceptable limit by reference to risks which have historically been accepted by the public (e.g. other seafaring occupations), or to adverse effects which would ensue if the offshore reserves were to be prematurely abandoned (e.g. more coal miners at risk working to replace the lost energy supply). While this author cannot offer any final answers, these issues deserve to be rationally examined, preferably from the broadest possible viewpoint.

While the socially unacceptable limit might end up being more complex than an arbitrary cutoff value, and the economic trade-off curves would no doubt be steeper, a guideline in the format of Figure 4 should still be feasible for these other offshore areas.

7. Concluding Remarks

In its recent publication, Policies, Practices, and Responsibilities for Safety and Environmental Protection in Oil and Gas Operations on the Outer Continental Shelf, the USGS states as one of its objectives, "to prevent waste of resources by means of an organized and systematic approach to regulations." This suggests that optimizing the allocation of resources in the sense of Figures 3 and 4 is appropriate. Thus, when applying the management principle that "Exploration and development of OCS minerals are carried out in a manner which emphasizes safety of operations and minimizes the risk of environmental damage," one should recognize that regulatory overkill which wastes resources and diminishes the availability of energy is just as harmful to our quality of life as errors in the other direction. Whether we recognize it or not, such trade-offs must inevitably be made.

In the past, offshore operators have traditionally made trade-offs between benefits (reduced risk) and costs. Calculation procedures used by the author for this purpose appear to conservatively overstate the risk. The extent of platform monitoring and inspection was arrived at as a matter of practical judgment, but consistent with the redundancy of our structures and such secondary safety measures as subsurface safety valves and evacuation procedures. When structural deficiencies are found, the decision whether or not to undertake repairs or strengthening has been couched in terms of economic considerations--attempting to rationally balance the cost of repair against the benefit in terms of risk reduction. Because the cost of underwater repairs is often exorbitant in comparison with what a comparable increment in strength would cost during initial construction, such trade-offs often indicate the rational choice is to accept a lower safety factor than is specified for new structures. By recognizing that the platform owner will be held accountable for human casualties, and will bear the full expense of oil spill clean up, as well as such business items as loss of income and loss of investment, making these trade-offs represents responsible behavior, and adequately reflects the national interest.

References

1. Egil Abrahamsen et al, "Safety, Man, and Society", Information from Det Norske Veritas about Safety and Risks, 1977.

2. P. W. Marshall and R. G. Bea, "Failure Modes for Offshore Structures", Proc. BOSS '76 Vol. II, Trondheim, Norway (1976).

3. P. W. Marshall, "Risk Factors for Offshore Structures", Civil Engineering in the Oceans, ASCE Conference, San Francisco (1967).

4. W. E. Gates, P. W. Marshall, and S. A. Mahin, "Analytical Methods for Determining the Ultimate Earthquake Resistance of Fixed Offshore Structures", OTC 2751 (1977).

5. G. W. Housner, "Strong Ground Motion", Earthquake Engineering (1970).

6. P. W. Marshall, "Failure Modes for Offshore Structures - Part II - Fatigue", Methods of Structural Analysis, ASCE Conf., Madison, WI (1976).

7. T. R. Schmidt, "Offshore Platform Displacement Measurement with Inertial Reference System", OTC 2554 (1976).

8. J. A. Ruhl, "Offshore Platforms: Observed Behavior and Comparisons with Theory", OTC 2553 (1976).

9. C. J. Dodds et al, "Experiences in Developing and Operating Integrity Monditoring Systems in the North Sea", OTC 2551 (1976).

10. G. C. Hart and J. T. P. Yao, "System Identification in Structural Dynamics", Dynamic Response of Structures, ASCE-EMD Specialty Conf. (March 1976).

11. R. M. Haring et al, "Improving Platform Design", Ocean Engineering May 1977.

12. S. Fjeld, "Reliability of Offshore Structures", OTC 3027 (1977).

A PROPOSAL CONCERNING TOTAL ENERGY SELF-SUPPLY PLAN FROM OCEAN SURFACES IN JAPAN

Prof. Yoshiro Kasahara
Department of Electronics Engineering
Faculty of Science & Technology
Kinki University
3 - 4 - 1 Kowakae Higashi-Osaka City
Osaka 577 JAPAN

Japan has many isolated islands to the south of her main land in low latitude Pacific Ocean, where the solar radiation is strong enough.

The auther suggests to supply all necessary energy in Japan by utilizing the territorial waters of these islands.

The territorial waters is expanded now till 12 nautical miles off an island. Even a very small island, the area of the territorial waters amounts to 1550 km^2.

The auther recommends to float about 155,000 huge iron rafts upon the territorial waters in Pacific Ocean, each consisting of 100m x 100m square raft unit. The solar radiation power per an island on the surfaces of total rafts reaches to 1.24×10^9 kW.

Suppose the total sun shine hours a year 2,000, then annual solar energy radiated on the territorial waters of a small island is estimates to 2.48×10^{12} kWh.

The auther proposes to transform the solar energy to electrical energy by utilizing silicon solar cells. The conversion efficiency is limited theoritically to 22 ~ 25 %, however, the actual attainable efficiency is now 10 %. Thus if we converge the solar energy into electrical energy, we can obtain 0.248×10^{12}kW per an island.

The total energy demand in Japan never exceeds 5.00×10^{12}kWh per year, this energy generation is realized using 20 small islands lying in the low latitude Pacific Ocean, and to this purpose Japan has enough number of islands.

The output electrical power is applied to decompose water into H_2& O_2gases, and these gases are sent to the mainland of Japan by ships, and used instead of all kinds of presentday fuels, for example, oils, coals etc.

All oil engines & boilers of today shall modify to use H_2 gas as fuels instead of fossil fuels and to used O_2 gas in place of air supply.

The water required to the electrolysis is easily obtained by purifying surrounding sea water of the island through ion exchange resin.

This method of energy supply has following advantages:

1. The realization of large scale electrical energy storage device, which is the most difficult problem to solve, is not necessary.

2. Electrical power transmission line between mainland of Japan and the isolated island is not necessary.

3. As no fossil fuel is used for energy generation, no poisonous gas, for instance, CO, NO_x etc, is produced, and the temperature rise of our Earth is mitigated.

4. Presentday fossil fuels, such as oils and coals shoud be used more significant purposes, for example, manufacturing of various chemical products, artificial fibers etc.

SAR IMAGING OF WAVES IN ICE

Byron R. Dawe and Surendra K. Parashar

Centre for Cold Ocean Resources Engineering
Memorial University of Newfoundland
St. John's, Newfoundland, A1B 3X5, Canada

ABSTRACT

During the months of February and March of 1977 the Environmental Research Institute of Michigan (ERIM) X- and L-band dual polarized synthetic aperture imaging radar (SAR) was used to obtain radar imagery of sea ice off the Labrador coast under Project SAR '77. During the course of imaging specific areas, imagery of ocean swell patterns in consolidated pack ice was obtained. Surface data regarding direction, period and approximate wave height were collected in one particular area. A qualitative analysis of these swell patterns was undertaken using all the frequency-polarization combinations available from the system. Tilt modulation, roughness modulation, orbital velocity and parametric effects models for the SAR imaging of ocean waves were examined for applicability and results are presented. The ability to image these wave patterns is important in enabling ice observers to distinguish between areas of solid ice cover and semi- and unconsolidated pack.

1. INTRODUCTION

During February and March of 1977 simultaneous dual frequency synthetic aperture radar (SAR) imagery was obtained for sea ice and icebergs, including swell patterns in sea ice. The imagery was collected under Project SAR '77, a program funded by C-CORE and the Canadian Government with assistance from the United States Office of Naval Research (Worsfold et al, 1977). The areas imaged were off the coast of Labrador and in the vicinity of Twillingate, Newfoundland (Larson et al, 1977). The purposes of the program were to obtain SAR data over sea ice in both the X- and L-microwave bands using both cross (horizontal transmit - vertical receive, HV) and parallel (horizontal transmit - horizontal receive, HH) polarizations, and to develop expertise in the handling of SAR data at C-CORE.

The Environmental Research Institute of Michigan (ERIM) SAR system, mounted on the Institute's C-46 aircraft, was used to obtain the imagery. The antenna depression angle for all the imagery shown here was 30° and the altitude was 3200 m. The radar data was supplied in photographic form and on computer compatible tapes (CCT's) for certain areas. The imagery had been processed with a spatial resolution of 3 m x 3 m and 6 m x 6 m for the X- and L-band data, respectively. The data was not corrected for the antenna pattern nor has it been slant-to-ground range converted. Because of heavy cloud cover little aerial photographic support data is available, except in isolated cases.

The obtained SAR imagery of ocean swell patterns in sea ice is presented and the possible applicability of various models of SAR imaging of ocean waves is discussed.

2. SURFACE DATA

The area over which the only surface information was available, with regard to swell patterns, was the area where the joint C-CORE and Newfoundland Oceans Research and Development Corporation (NORDCO) Ship-in-the-Ice Project was being carried out (LeDrew and Culshaw, 1977). At the time of the aircraft overpass the sky condition was 10/10 overcast at 300 m, curtailing any aerial photography. Observations made at the time of the SAR data acquisition (LeDrew and Winsor, 1978) show that the ship was surrounded by pancake type ice floes 10 - 15 m in diameter and about 1 m in thickness. The snow cover on the floes was around 20 cm thick, and was new, dense and wet. The floes constituted about 5/10 coverage. The rest of the area was covered with a mixture of slush and shuga of a thickness comparable to that of the ice floes. The general relief was reported to be approximately 1 m (LeDrew and Culshaw, 1977). Figure 1 shows surface photography taken at the time of the overpass.

There was a heavy swell moving through the area in the direction of 230° with a visually estimated period of 12 sec. and an amplitude (crest-to-trough) of 1.8 - 2.4 m. Using photographs taken of the ship's radar (Figure 2) and the geometry (estimated antenna height and shadow zone length), the wave amplitude was measured to be around 1.5 m which is reasonably close to the visual observations considering the possible errors. The wavelength of the swell, also measured from ship's radar, was found to average 227 m. The water depth in the area is about 230 m. Therefore, using deep water wave theory, we find (assuming a 12 sec. period) the theoretical wavelength to be 225 m.

The theoretical phase velocity of the swell pattern is 19 m/s.

3. SAR DATA

The SAR imagery in the vicinity of the ship is shown in Figure 3. This imagery has been obtained by optically processing the signal phase history film for a target moving with a phase velocity of 17 - 18 m/s. By correcting for the angular distortion of the waves due to radar geometry and wave movement (Raney, 1971; Raney and Lowry, 1978) the calculated direction is 228° and the wavelength around 185 m. These values are in reasonable agreement with the surface data. The SAR imagery of a swell pattern in sea ice for another area is shown in Figure 4. It should be noted that floe boundaries are clearly visible in this case.

4. APPLICABLE IMAGING MODELS

Elachi and Brown (1977) examined four theoretical models proposed to explain the method which enables ocean swells to be imaged by SAR. These are: (a) tilt modulation, (b) roughness modulation, (c) orbital velocity, and (d) parametric effects. No single method has been found to be entirely suitable and examples can be found which support or contradict one or more of the above models. In examining these models further Raney and Lowry (1978) have tried to show that for uncrested waves (non-cycloidal gravity waves such as long swells modulated by capillaries) the appropriate imaging model is based on orbital motion of the capillaries with an explicit inclusion of the vertical component of the underlying gravity wave motion. The most suitable model for breaking or crested waves is based on phase velocity of the gravity wave field. A discussion of each model and its possible applicability to the waves imaged in the ice is presented next.

(a) Tilt Modulation

This model is based on the modulation of the radar incidence angle due to the swell pattern. By using the swell information and taking into account the orientation of the waves with respect to the radar at an incidence angle (measured from the vertical or nadir) of 30°, in the image (Figure 3), the maximum variation in incidence angle due to the tilt modulation is about 2°.

To examine the applicability of tilt modulation to the case of waves in ice, the slope of the radar backscatter coefficient, σ^o, vs θ curve without the swell pattern needs to be considered. The only reported measurements of σ^o for sea ice have been for frequencies of 13.3 GHz and 400 MHz (Gray et al, 1977 and Parashar et al, 1974). The X-band imagery presented here is at 9.375 GHz which may make it slightly more sensitive to changes in incidence angle because of the longer wavelength as compared to 13.3 GHz data. At 13.3 GHz (Gray et al, 1977), however, for a modulation of around $\pm 2^o$ about a 30° incidence angle the variation in σ^o is approximately 2-3 db. This would seem to make tilt modulation marginally accountable for HH polarization at 9.375 GHz on this imagery, particularly after processing and compression of the signal range. For HV polarization based on 13.3 GHz data of Gray et al (1977), the effect would be even less. This is not evident from the imagery (Figure 3), however, which seems to indicate that both polarizations are modulated similarly. From the imagery in Figure 3, however, it can be seen that the HV polarization is greatly affected by slight changes in the surface characteristics which could mask the modulation. Thus the data from Gray et al (1977) could come from an area whose surface characteristics differ only slightly, but sufficiently to show a reduced sensitivity to incidence angle. This would help explain the results to some extent.

The L-band (1.28 GHz) data should be even more sensitive to the tilt modulation. The large dark bands are created by antenna pattern anomalies. The slight softening of the image is probably due to the reduction in roughness on the scale of the radar wavelength and the larger resolution cell (6 m as compared to 3 m for X-band) resulting in more averaging. Also the L-band penetration into the surface is greater, making it less susceptible to surface roughness effects.

Thus, in summation, it appears that tilt modulation may be a contributing factor but does not seem sufficient to create the amount of modulation displayed.

(b) Roughness Modulation

In the case of open ocean, the orbital motion of ocean gravity waves causes variable straining of the small capillary type waves. This results in these being shortened and steepened on the forward face and flattened on the backward face (Elachi and Brown, 1977), and leads to modulation of the small scale surface roughness at wavelengths of the same order as that of the radar (Bragg scattering region).

This phenomena may be applicable to waves in ice for some cases depending on the type of ice, its growth history, temperature, and density. The surface ice conditions may result in a flexible mass of ice whose surface roughness and, thereby σ^o value would vary depending on the location on the swell (e.g. crest or trough) due to horizontal stretching and compression of the surface elements.

This phenomena of relative change in surface roughness due to swell was not visually observed during surface truthing, but then, no effort was made to examine whether this occurred. Figure 5 shows the modulation across one area for each of the four frequency - polarization combinations. These are averaged (from Figure 3) over 10 scan lines in the range direction and every 10 pixels (5 resolution cells) in the azimuth direction. No conclusions can be made with regard to the relative

amplitudes because the different system parameters that vary with each combination used are not accounted for (e.g. sensitivity, gain, antenna pattern). The sample was taken in this orientation to minimize the effects of averaging over the incidence angles. It can be seen, however, that the signal modulation is by no means smooth across the swells, as would be expected in a pure tilt modulation model. However, it cannot be stated that roughness modulation may be the cause of this until the statistics of the roughness can be determined.

(c) Orbital Velocity Effects

The orbital velocity of individual particles in different portions of a gravity wave will create a periodic Doppler shift in the returned signal. Small loose particles floating on the surface (as in this situation) maybe subjected to the same velocities. Elachi and Brown (1977) examined this phenomena for ocean waves. From the relationships derived it is shown that the velocities in this situation are insufficient to produce a significant amplitude modulation of the returned signal. However, Raney and Lowry (1978) have stated that the predominant motion, especially in the case of ice, is in the vertical direction (up and down) rather than in the horizontal (lateral) direction. This effect of vertical scatterer motion (wave height modulation) may be the dominant source of Doppler modulation on the radar reflections. The available data is only limited to a few angles of wave directions in ice (relative to radar flight direction) so that this effect cannot be verified.

(d) Parametric Interactions Effects

The frequency shift of the echoes coming from a different part of the wave is different due to change in the local incidence angle. This effect, which would result in a modulated image, has been shown to be negligible in the case of open ocean by Elachi and Brown (1978). In the case of waves in ice, this effect will be equally small.

5. CONCLUSIONS

It appears that tilt modulation, roughness modulation, and effect of vertical scatterer motion are dominant methods of imaging waves in ice through SAR. However, the applicability of these methods needs to be verified by collecting SAR imagery of waves in ice propagating in different directions for different radar frequencies, polarizations and incidence angles. These data need to be available for waves in various ice types and conditions.

ACKNOWLEDGEMENT

The authors would like to acknowledge the assistance of Mr. Randy Raymond in developing the computer programs that were used.

REFERENCES

Elachi, C. and W.E. Brown, Jr. (1977), Models of Radar Imaging of the Ocean Surface Waves, IEEE Transactions on Antennas and Propagation, Vol. AP-25, No. 1, pp. 84-94.

Gray, L., J. Cihlar, S. Parashar, and R. Worsfold (1977), Scatterometer Results from Shorefast and Floating Sea Ice, Proceedings Eleventh International Symposium on Remote Sensing of Environment, Ann Arbor, Michigan, April, pp. 645-657.

Larson, R., C. Liskow, R. Rawson, R. Shuchman, and F. Smith (1977), Areas Imaged during Project SAR '77 using ERIM Four Channel Radar, C-CORE Publication # 77-30, St. John's, Newfoundland, June, 60 pp.

LeDrew, B.R. and S.T. Culshaw (1977), Ship-in-the-Ice - Data Record, C-CORE Report No. 77-28, St. John's, Newfoundland.

LeDrew, B.R. and W.D. Winsor, 1978, Ice Feature Characterization - Labrador Offshore, SAR '77 Field Data Report #14, C-CORE Publication No. 78-4, May, St. John's, Newfoundland, 50 pp.

Parashar, S.K., A.W. Biggs, A.K. Fung, and R.K. Moore (1974), Investigation of Radar Discrimination of Sea Ice, Proceedings Ninth International Symposium on Remote Sensing of Environment, Ann Arbor, Michigan, April, pp. 323-332.

Raney, R.K. and R.T. Lowry (1978), Ocean Wave Imagery and Wave Spectra Distortions by Synthetic Aperture Radar, Proceedings Twelfth International Symposium on Remote Sensing and Environment, Manila, Philippines, April.

Worsfold, R.D., D. Strong, and E. Wedler (1977), Project SAR '77, Proceedings Fourth International Conference on Port and Ocean Engineering under Arctic Conditions, Memorial University of Newfoundland, St. John's, Newfoundland, September.

*now with REMOTEC APPLICATIONS INC.
P.O. Box 5547
St. John's, Newfoundland
A1C 5W5, Canada

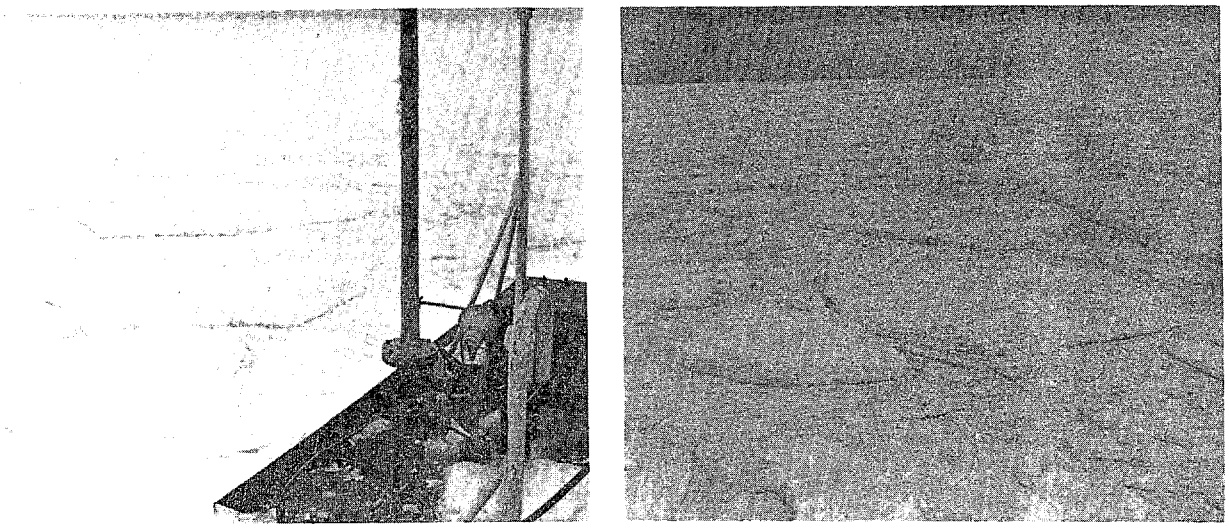

Figure 1 Surface Photography of Sea Ice Cover Around the Ship

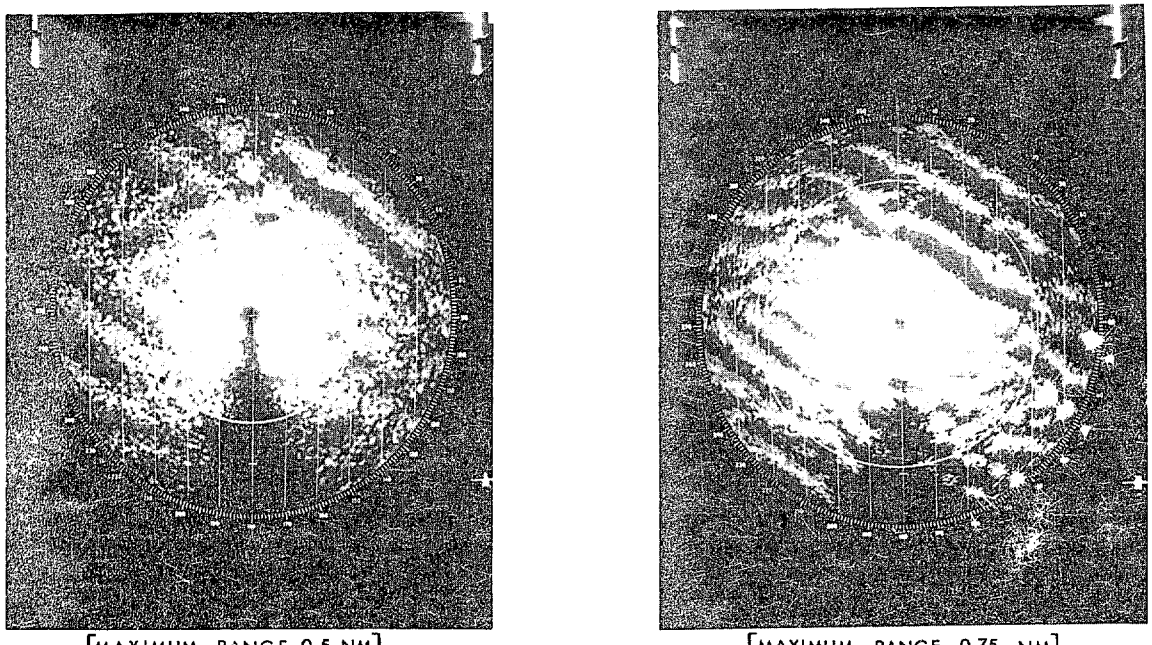

[MAXIMUM RANGE 0.5 NM] [MAXIMUM RANGE 0.75 NM]

Figure 2 Photographs of Ship's PPI Radar Display

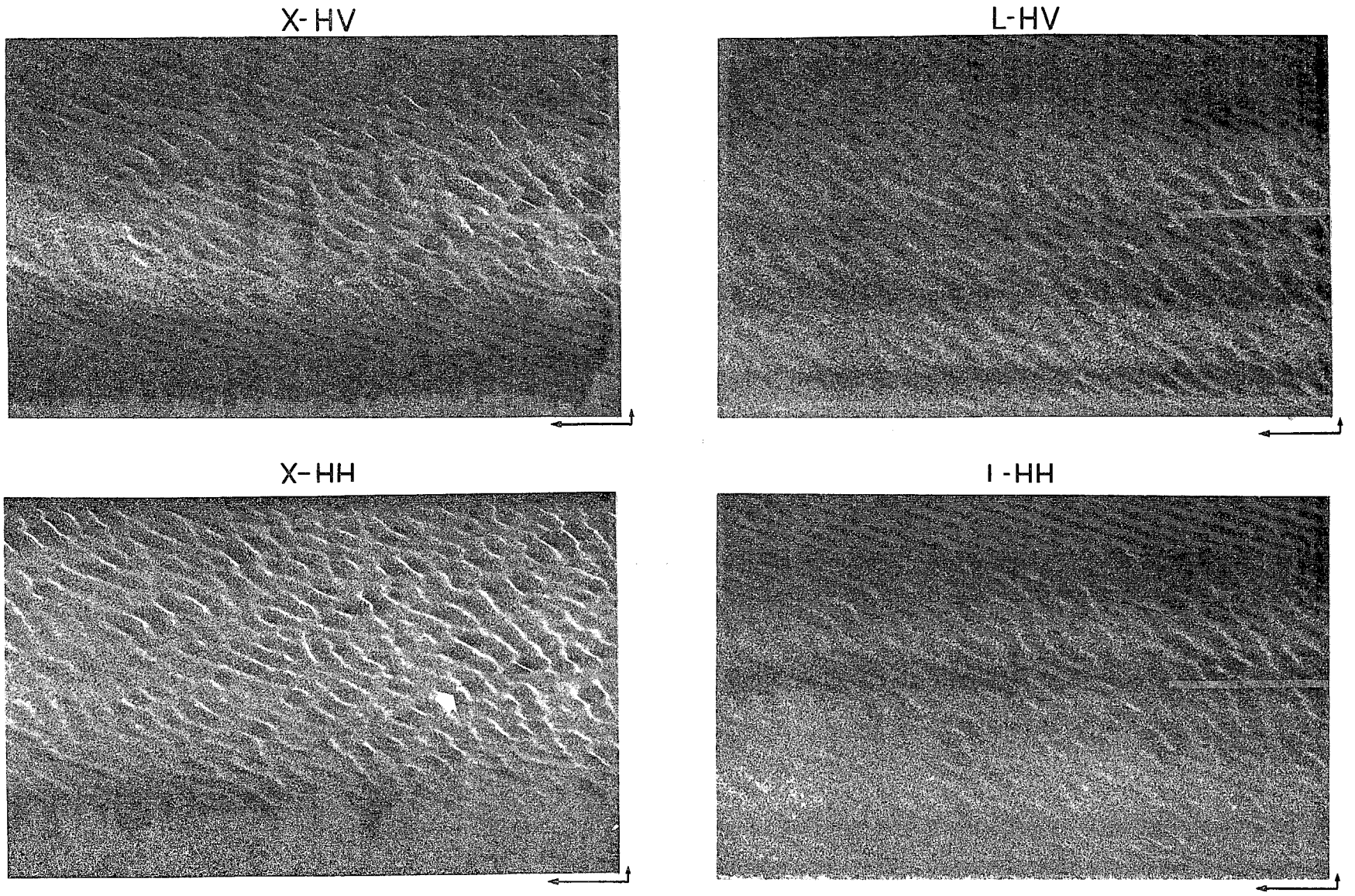

Figure 3 SAR Imagery of Waves in Ice. Location of ship is shown by the arrow. Horizontal lines correspond to the radiance profiles of Figure 5.

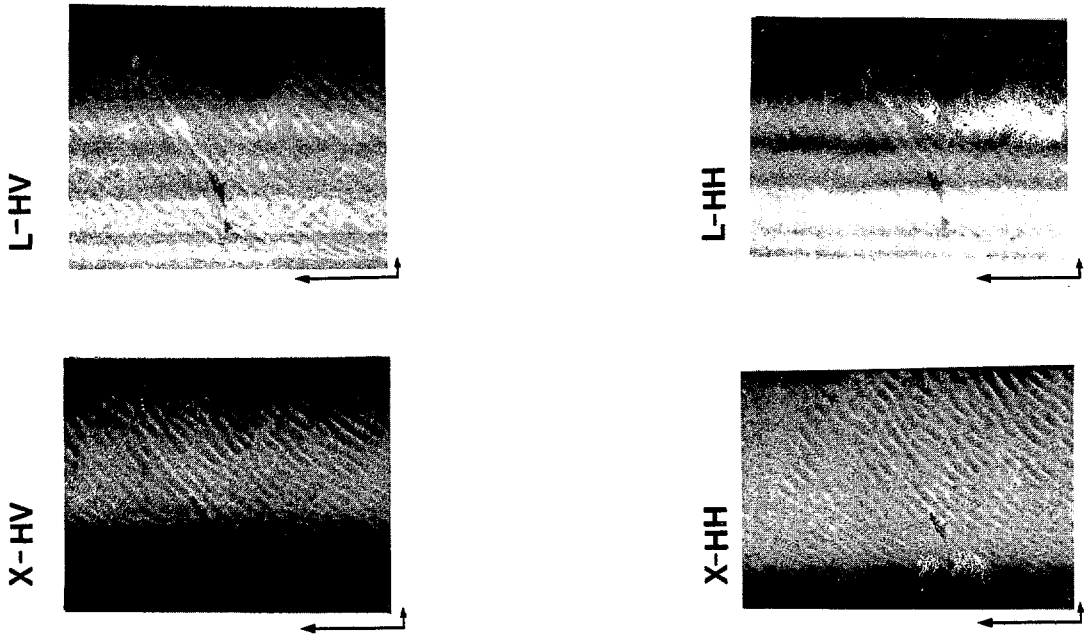

Figure 4 SAR Imagery of Waves in Ice

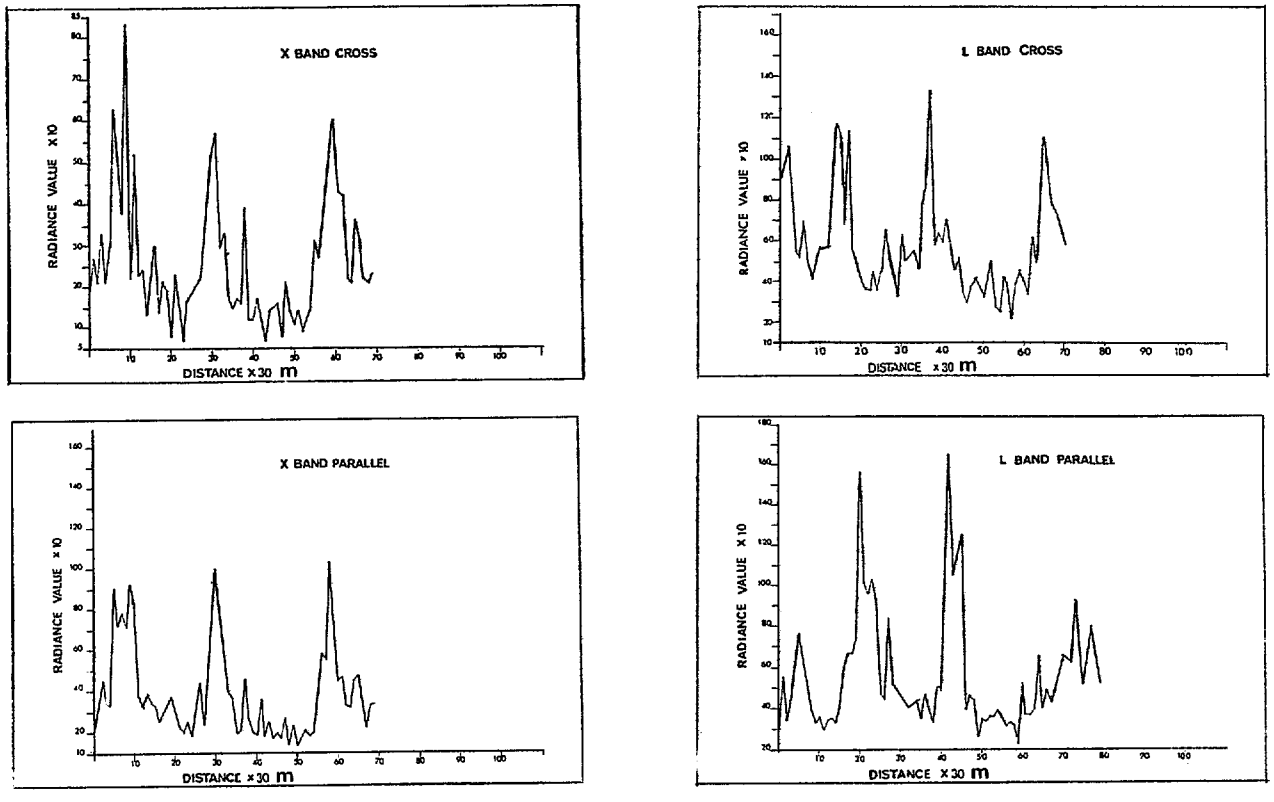

Figure 5 Radiance Profiles Corresponding to Figure 3

THE COMPARISON BETWEEN THE SYNTHETIC APERTURE RADAR IMAGERIES AND THE SURFACE TRUTH OF OCEAN WAVES

S. Vincent Hsiao
Jet Propulsion Laboratory
California Institute of Technology
Pasadena, California 91103

Abstract

Ocean waves measured offshore of Marineland, Florida, by the synthetic aperture radar (SAR) are compared with the surface truth data. The Fourier transform of SAR imageries are taken and the corrections of the wave directions and wave lengths due to the relative velocities between SAR and waves are considered. Favorable comparisons are obtained for the peak frequencies, wave directions, and directional distributions. However, the one-dimensional SAR spectra are quite different from the surface truth wave height spectra.

1. Introduction

The object of this paper is to compare the ocean wave measurements of the synthetic aperture radar (SAR) and the surface truth measurements. From these comparisons we hope to find out what wave informations can be easily obtained from the SAR measurements. The experiment staged offshore of Marineland, Florida, in December 1975 (Shemdin et al., 1975) is an excellent case for the SAR-surface truth comparisons. The SAR data we used in this paper were obtained from the horizontal-transmit horizontal-receive channel of the X-band radar of the Environmental Research Institute of Michigan (ERIM). The surface truth data we used were the wave spectra measured by the pitch-and-roll buoy and the geodolite laser operated by the Sea-Air Interaction Laboratory of the National Oceanic and Atmospheric Administration (NOAA) and the spectra measured by the underwater pressure gauge operated by the Coastal and Oceanographic Engineering Laboratory of the University of Florida. The test site and the sensor locations are shown in Figure 1.

2. SAR spectra

In order to compare the SAR imageries with the surface truth wave spectra, we took the two-dimensional Fourier transforms of the SAR imageries. The two-dimensional SAR spectra $F(k_x, k_y)$ were obtained, where k_x, k_y are the orthogonal components of wave number. Figures 2 and 3 are an example of such Fourier transform pairs. The locations of the maxima of the two-dimensional SAR spectra give us the peak wave numbers and the peak directions. By using dispersion equation, the peak frequency can be found.

From $F(k_x, k_y)$ we can find $F(k,\theta)$ which gives us the directional distributions, where $k^2 = k_x^2 + k_y^2$ and $\theta = \arctan(k_x/k_y)$. Then the one-dimensional spectra $E(f)$ can be calculated by the following equation

$$E(f) = (2\pi k/C_g) \int_0^{2\pi} F(k,\theta)d\theta, \qquad (1)$$

where f is frequency and C_g is group velocity.

3. Wave direction and wave length corrections.

The wave direction and wave length on the SAR imagery need to be corrected due to the relative speed and relative direction between radar and waves. From Figure 4, the directional correction is

$$\delta = \arcsin(C \sin\Theta / V), \qquad (2)$$

where C is the wave phase speed and V is the radar speed. The equation for direction correction had previously been given in a different form by Brown, et al (1976). The true wave direction is

$$\alpha = \Theta + \delta \quad \text{for } \Theta \geqslant 0,$$
$$= \Theta - \delta \quad \text{for } \Theta < 0. \qquad (3)$$

The true wave length is

$$L = \ell \cos\alpha / \cos\Theta, \qquad (4)$$

where l is the observed wave length.

If $\Theta = \pm 90^\circ$, then $\delta = 0$ and

$$L = \ell (V \mp C) / V \qquad (5)$$

4. Peak frequency and direction comparisons.

The comparisons of the peak frequencies and directions between the measurements of SAR, pitch-and-roll buoy, and pressure gauge are listed in Table 1. The spectrum measured by pitch-and-roll buoy is shown in Figure 5. The spectrum measured by pressure gauge and its comparison with pitch-and-roll buoy measurements are shown in Figure 6. The SAR data were taken from the imagery centered

at 15 m depth of water but the pitch-and-roll buoy and the pressure gauge data were taken at 8.5 m depth of water. Thus the corrections of wave directions due to wave refraction are considered here.

The comparisons between the measurements of SAR and the geodolite laser are listed in Table 2. The spectrum measured by laser is shown in Figure 7.

We obtained very good results in the comparisons shown in Tables 1 and 2.

5. Directional distribution comparison.

From the two-dimensional SAR spectra, the directional distribution of each wave number (or frequency) component can be obtained. The SAR directional distribution of wave component f = .122 at Station I is shown as an example in Figure 8.

From the pitch-and-roll buoy measurement, the directional information we can get is only the first five of the Fourier coefficients of the directional distribution, i.e., the coefficients a_0, a_1, a_2, b_1, and b_2 of the series

$$\frac{a_0}{2} + \sum_{n=1}^{\infty} (a_n \cos\theta n + b_n \sin n\theta)$$

Assuming the directional distribution can be represented by the following from

$$A \cos^{2p} [(\theta-\theta_m)/2]$$

p and θ_m were computed from these Fourier components where p represents the narrowness of the directional distribution and θ_m is the peak wave direction. The values of p and θ_m are functions of frequencies (see Longuet-Higgins et al, 1963).

In order to compare the SAR directional distributions and the pitch-and-roll buoy directional measurements the Fourier series of the SAR directional distribution is obtained and the p and θ_m value are calculated. The comparisons of three wave components are shown in Table 3. Favorable results were obtained for both the wave directions and the p values.

6. One-dimensional SAR spectra.

Figure 9 shows the one-dimensional SAR spectrum at Station I. This spectrum is computed from two-dimensional spectrum by using Equation (1). This spectrum, as well as the one-dimensional SAR spectra at Stations II and IIIA, shows that the spectrum increases with wave frequency. Obviously, it is not the one-dimensional wave height spectrum. Two possible reasons are: 1) The SAR measurements are related to some wave properties other than wave height, such as wave slope and wave orbital velocity. 2) The noises are amplified at high frequencies through the use of Equation (1).

7. Summary

The SAR measured peak wave frequency, peak wave direction and the directional distribution match the ground truth very well. It appears that these wave properties can be measured by SAR. The SAR-measured one-dimensional spectrum can not be obtained straightforwardly. More studies are needed to solve this problem.

Acknowledgements

This work was carried out at the Jet Propulsion Laboratory, California Institute of Technology, under contract NAS7-100, sponsored by the National Aeronautics and Space Administration. I thank R.A. Shuchman of ERIM for providing SAR data. I also thank W. McLeish of the Sea-Air Interaction Laboratory of NOAA for providing surface truth data. I acknowledge the helpful discussions of O. H. Shemdin of JPL. The Fourier transforms of SAR imageries were carried out by W. Stromberg of JPL.

References

1. Brown, W. E., T. W. Thompson, and T. Killpack, 1976: Signal-to-noise ratio versus wave detectability. Preliminary Report, Jet Propulsion Lab., Pasadena, California.

2. Longuet-Higgins, M. S., D. E. Cartwright, and N. D. Smith, 1963: Observations of the directional spectrum of sea waves using the motions of a floating buoy. Proc. Conf. Ocean Waves Spectra, Prentice-Hall.

3. Shemdin, O. H., Blue, J. E., and Dunne, J. A., 1975: Seasat-A surface truth program - Marineland test plan. Jet Propulsion Lab. Document No. 622-5, Pasadena, California.

Table 1

	SAR (I)	P-R Buoy	Pressure Gauge
observed peak wave length (m)	80.4		
wave length correction (m)	4.6		
peak wave length (m)	85.0		
peak frequency (Hz)	0.122	0.125	0.117
observed peak direction (degrees toward)	282		
direction correction (SAR)	—6		
direction correction (refraction)	—5		
peak direction	271	270	

Table 2

	SAR (II)	SAR (IIIA)	Laser
observed peak wave length (m)	113.8	124.2	
peak wave length (m)	103.3	112.8	117.4
peak frequency (Hz)	0.113	0.116	0.112
observed peak direction (degrees toward)	299	306	
peak direction	293	299	

Table 3

	SAR	P-R	SAR	P-R	SAR	P-R	
wave length (m)	85.0		62.2		40.2		
frequency (Hz)	0.122	0.125	0.151	0.156	0.195	0.188	0.203
peak direction (degrees toward)	271	270	270	267	266	268	275
P (from 1st harmonic)	21	21	14	10	12	10	7
P (from 2nd harmonic)	19	28	14	11	13	11	8

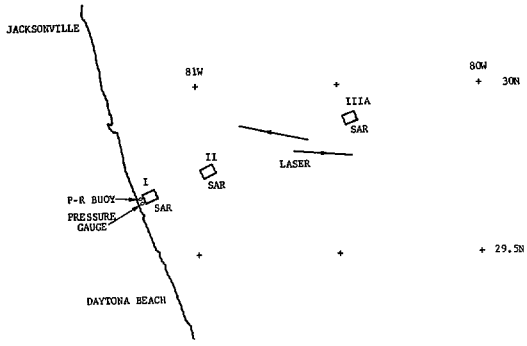

Figure 1. Marineland test site.

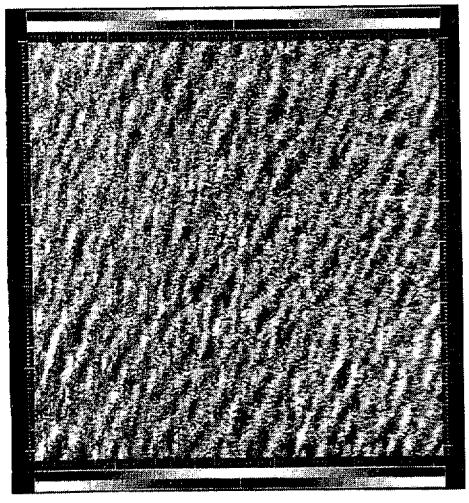

Figure 2. SAR imagery, Marineland Station I, Dec. 14, 1975.

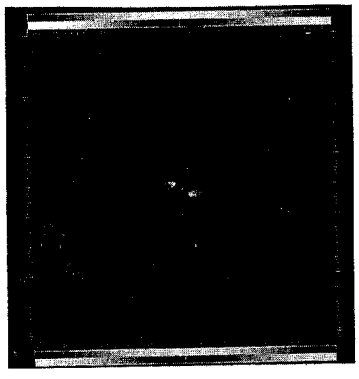

Figure 3. Fourier transform of Figure 2.

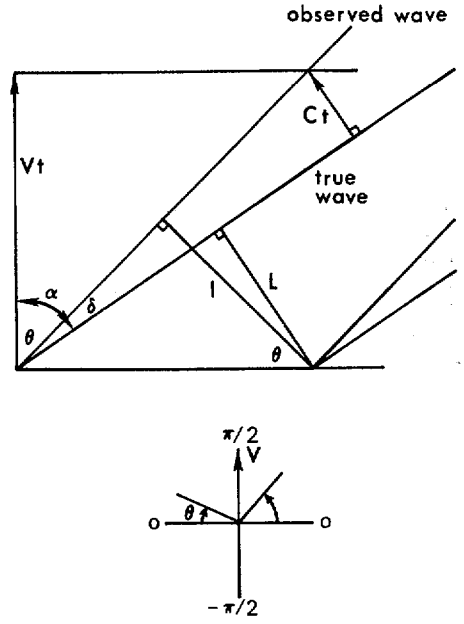

Figure 4. SAR wave direction and wavelength correction.

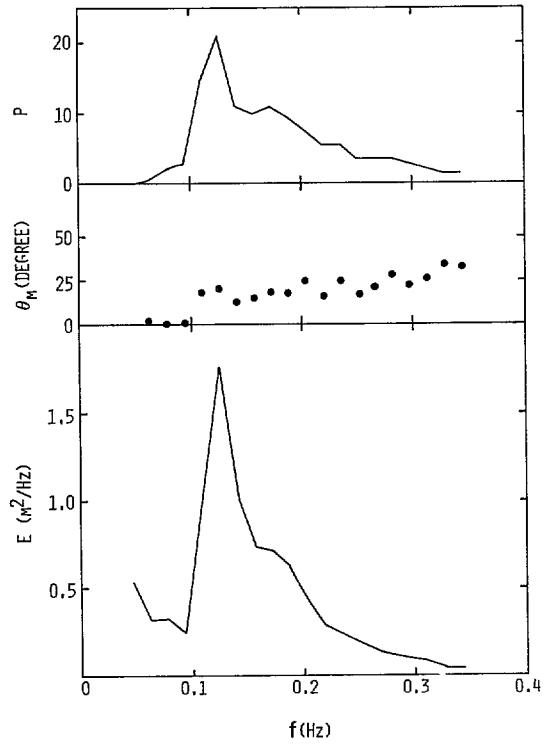

Figure 5. Pitch-and-roll buoy spectrum, Marineland Station I, Dec. 14, 1975.

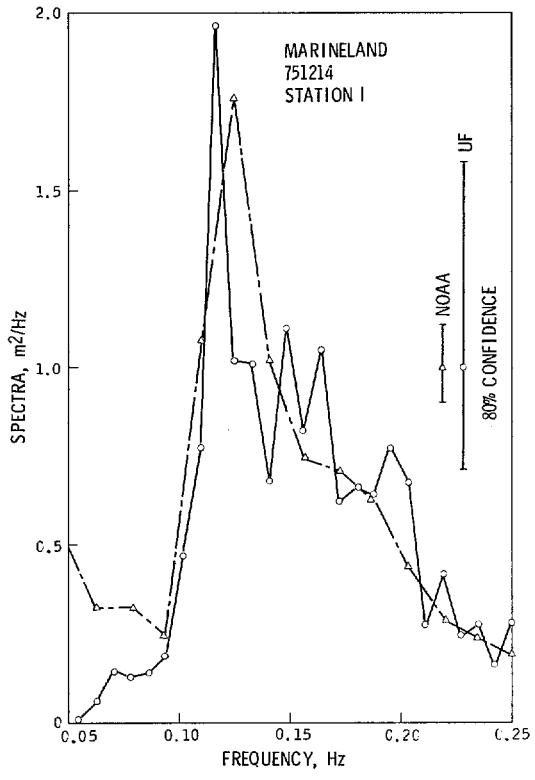

Figure 6. Comparison between pitch-and-roll buoy spectrum (NOAA) and pressure gauge spectrum (UF).

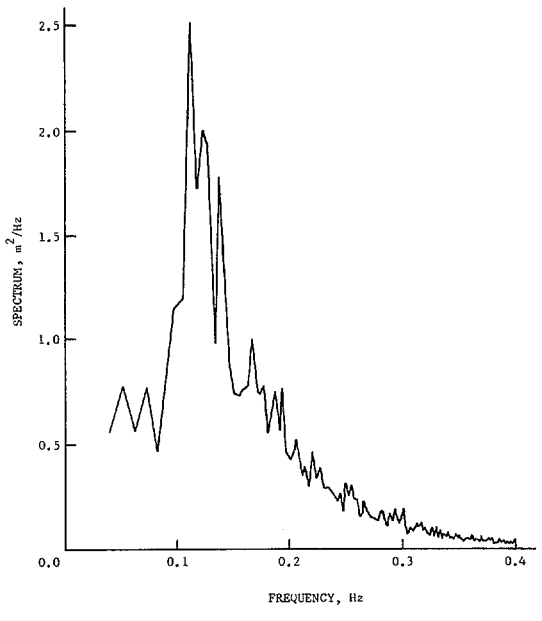

Figure 7. Laser spectrum, Marineland (see Figure 1 for the location of measurements), Dec. 14, 1975.

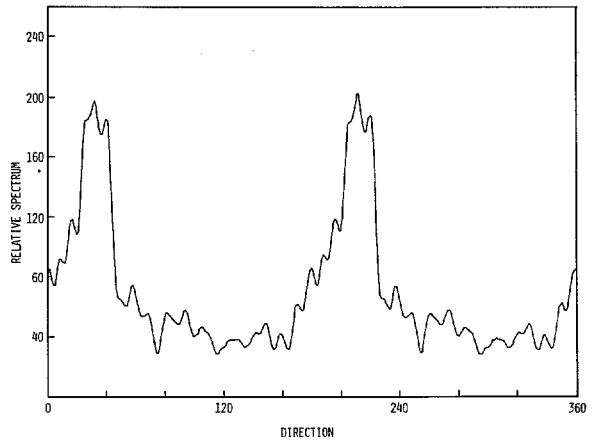

Figure 8. SAR directional distribution of wave component f = .112, Marineland Station I, Dec. 14, 1975.

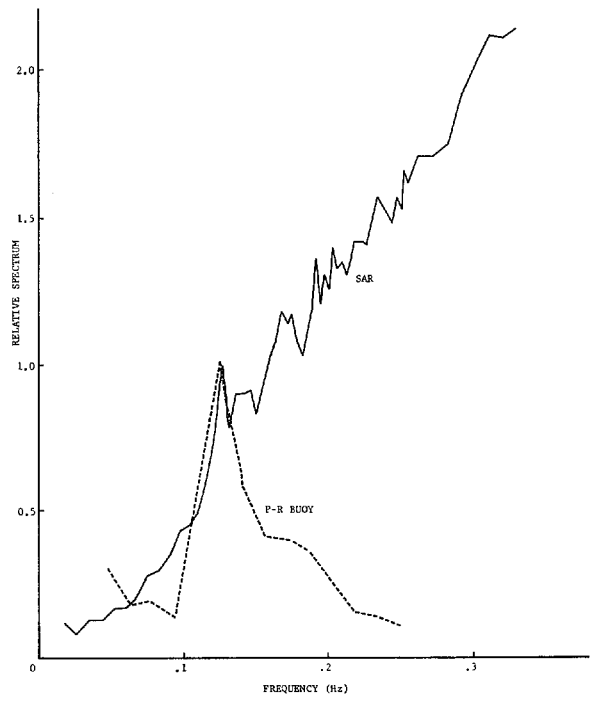

Figure 9. One-dimensional SAR spectrum.

LASER BATHYMETRY FOR NEAR-SHORE CHARTING APPLICATION (PRELIMINARY FIELD TEST RESULTS)

Gary C. Guenther
Lowell R. Goodman
David B. Enabnit
NOAA/National Ocean Survey
EDL, C61
Rockville, Maryland 20852

Robert N. Swift
Robert W.L. Thomas
EG&G/WASC
6801 Kenilworth Avenue
Riverdale, Maryland 20840

Abstract

An airborne lidar* system has been extensively flight tested to study the operational feasibility of using a scanning, rapidly pulsed laser beam, projected into water from a fixed wing aircraft, for near-shore hydrographic applications. Field test results for vertical accuracy, environmental constraints, and effects of system parameters are discussed. Detailed utilization studies indicate that such a system should yield significantly reduced cost as well as increased volume of near-shore bathymetric data for charting purposes.

1. Introduction

During the past ten years, a number of increasingly sophisticated airborne laser ranging (lidar) devices have been tested to determine technical feasibility for hydrographic and other oceanographic applications. (Ref. 1) In 1974, a development program for a versatile airborne laser and data acquisition system, to be sponsored by the NASA Advanced Applications Flight Experiment (AAFE) program, was proposed jointly by NASA/Wallops Flight Center and AVCO Everett Research Laboratory, Inc. The purpose of this collaboration was to produce and demonstrate, for a select community of potential users, a state of the art system utilizing NASA's expertise in space-age technology. Requirements, specifications, evaluation procedures, and applications for this "Airborne Oceanographic Lidar" (AOL) system were solicited and established through a series of meetings with interested parties. (Refs. 2-5) The system evolved with two major and separate modes of operation: bathymetric lidar, and fluorosensing.

Preliminary shakedown and experimentation with the instrument in the bathymetric mode has been sponsored by NOAA/National Ocean Survey (NOS) and the Defense Mapping Agency (DMA), and conducted jointly by NASA and NOS. In this paper we shall discuss the results of the NOS test program. (Ref. 6)

Near-shore bathymetric measurements are presently accomplished by NOS primarily with narrow-beam acoustic (sonar) equipment mounted in small boats which work at relatively low speeds. An airborne laser bathymetric system has the potential to provide a higher quality product with more timely and less costly (Refs. 7 and 8) results in critical coastal and inland waters. It also permits new or improved services and shows great promise as a member of the hydrographic team. The objectives of the Laser Hydrography Development Project within NOS are to determine the capability of an optimized airborne laser system to meet or exceed NOS near-shore vertical accuracy requirements within a bounding set of system variables and environmental parameters; to perform preliminary design work on a realizable, NOS operations oriented system; to assess its cost effectiveness under "typical" operational conditions; and to investigate any potential outstanding problem areas which may develop. Flight testing of the AOL was primarily dedicated to the first of these, while also acting as a valuable input to the second.

2. AOL System Description

The Airborne Oceanographic Lidar (AOL) system, (Ref. 9) designed and built by the AVCO Everett Research Laboratory, Inc. under NASA contract, is installed in the NASA/Wallops Flight Center C-54 aircraft. An open hatch is used to pass transmitted and received energy to and from a large scanning mirror which is mounted between the floor and exterior skin of the aircraft. Water depths are determined for each laser pulse by measuring the time of flight difference between that portion of the pulse reflected back to the receiver from the water's surface and that reflected by the underwater "bottom" topography.

The AOL bathymetric configuration includes the following:

- an AVCO C-5000 gas (neon/nitrogen) laser with an unstable resonator (to improve beam divergence), an adjustable beam expander (for control), and an optional polarizer;

* light detection and ranging: the equivalent of "radar," but at optical frequencies.

- a 56 cm scanner mirror with drive motor and 14-bit angle encoder;
- a 30.5 cm diameter Cassegranian f/4 telescope with adjustable field stop and baffles (0-20 milliradian field of view) and an optional polarizer;
- a narrow band (4Å) interference filter to suppress ambient background;
- a photomultiplier tube (PMT) detector with appropriate electronics;
- 40 charge digitizers (A/D converters);
- CAMAC interface;
- a computer controlled data acquisition, processing, display, and recording subsystem; and
- appropriate power and control provisions.

The laser wavelength of 5401Å (green) is near the minimum of the Jerlov (Ref. 10) curves of diffuse attenuation coefficient for coastal water types. The laser output power is typically 2 kilowatts (peak), while approximately 500 watts (peak) exits the aircraft in the primary beam. Divergence is variable from 0-20 milliradians, and maximum pulse repetition rate is 400 Hz.

The scanner is a nutating design whose mirror normal is offset slightly from the axis of rotation. The resulting pattern on the earth's surface is a tightly interlocked series of pseudo-ellipses (actually slightly "egg"-shaped) which provides relatively uniform areal coverage. The scanner can be operated either at a 5 Hz rotation rate or locked in a fixed position for non-scanning (fixed off-nadir angle) data acquisition. The nominal angle of the output beam with respect to the nadir is adjustable in 5° increments between 0° and 15° maximum deflection (this angle varies slightly during scanner rotation).

An altitude intervalometer, operating in conjunction with a surface return detector, triggers the electronics upon detection of the surface return and permits digitization of just the event data--automatically, independent of aircraft altitude. Delay lines are used to permit digitization of the surface return, as well as the bottom return, in the same output vector. (This feature is extremely important, as it allows use of the surface return shape and location for subsequent analysis.) The altitude data is also utilized to facilitate the removal of wave height variations from the depth calculations; this permits correction of the depths to mean sea level.

The 40 charge digitizers are gated sequentially at 2.5 ns intervals to provide 100 ns (or approximately 10 meters) of usable depth range. The digitized signals are transmitted through the CAMAC interface to a Hewlett-Packard 21 MX minicomputer with disk and tape storage and CRT display capability.

Aircraft attitude and rough positional data are supplied to the computer from a Litton LTN-51 Inertial Navigation System (INS). A Universal Time Code Translator interfaced with the system provides precise "real time of day" for each laser pulse. The entire system (electronics, laser, optics, and computer for both bathymetry and fluorosensing modes) weighs 2100 pounds and fits confortably in a small section of the C-54 cabin.

3. AOL Bathymetric Field Test Program

Goals:

The goals of the NOS flight test program with the AOL system are to: validate the overall feasibility of a bathymetric lidar system to provide high quality data under typical operations-oriented circumstances; determine vertical error under a bounding range of system variables and environmental parameters and correlate error contributions with sources; quantify system and environmental usage constraints to establish the operational "window"; and model major contributions in a return signal strength equation to provide a sound basis for extrapolation of these results to the design specifications of an NOS prototype bathymetric lidar system.

Site Selection:

Site selection for the AOL field tests was based on the following criteria: depths must range between one and ten meters; a combination of both flat and relatively high relief topography is preferred; radar tracking of the aircraft is imperative due to poor performance of the LTN-51; the sites must be logistically easy to reach by both aircraft and ground support vessels; the area must have suitable tide "control"; typical water clarities must be appropriate to permit penetration to the bottom over sufficiently long portions of a flightline; and adequate meteorological support should be available 24 hours in advance for daily mission go/no-go decisions.

Two test sites meeting these requirements were selected (Ref. 11): one in the Atlantic Ocean over Winter Quarter Shoal (several miles offshore from Assateaque Island), and one in Chesapeake Bay -- Tangier Sound between Jane's Island and Smith Island. These dissimilar sites

provided the opportunity to investigate the effects of diversity in water clarity, depth, wind, and surface wave structure. The probability of successful missions in the Wallops Island vicinity based on precipitation, fog, and wind speed data from historical records was calculated and found to be acceptable. (Refs. 11 and 12)

Supporting Data:

A wide variety of ancillary supporting data was required for the flight tests in order to permit quantitative description of the system performance and the environmental restrictions on the operational window. The performance of the AOL is limited primarily by the product of water depth and optical attenuation coefficient. The latter is, for a given location and season, modulated temporally by wind, waveheight, precipitation, and currents; also affecting performance are such things as bottom reflectivity and solar illumination. These parameters interact with system variables such as receiver field-of-view, altitude, scanner angle, and beam divergence to yield a highly complex set of interactions which must be unraveled to permit the quantization of specific effects. Adequate testing of the AOL thus depended on the quality and quantity of ground data specifically tailored to meet needs. Primary support data acquired in support of the flight tests include vertical control, horizontal control, water clarity, sea surface conditions, meteorology, and bottom reflectivity.

Vertical control consists of bathymetry and tide control. A bathymetric survey of the Tangier Sound flightline was conducted by an NOS vessel from the Atlantic Marine Center utilizing standard, automated, acoustic techniques. Horizontal control for this survey was a line-of-sight, high frequency electronic positioning system with ground stations. Tide control was furnished by three continuously recording NOS tide gages at appropriate locations.

Navigation and positioning of the aircraft were accomplished with the tracking radar and plot-board capabilities available at NASA/ Wallops Flight Center. Radar data are smoothed with a Kalman filter program to provide the highest possible accuracy. Radar data are merged with AOL data offline during processing.

Water clarity measurements were made throughout the water column with a narrow beam transmissometer and were backed up with Secchi disk readings. (A well correlated linear regression of beam attenuation coefficient (α) against inverse Secchi depth was noted. This lends credence to both sets of readings.) Measurements were made in the vicinity of the flightline before, during, and after overflights. Attempts to measure diffuse attenuation coefficients (K) were foiled, with few exceptions, by baulky equipment. The observed relationship between α and K, based on a very small data set, is not inconsistent with the Shannon (Ref. 13) equation ($K \cong \alpha/5$).

Winds were measured at the Wallops Island National Weather Service at several levels. Wind, waves, and visibility were measured subjectively from vessels at the flightline.

Bottom reflectivities in green and blue wavelengths were measured with a laboratory reflectometer. Grab samples were transferred in sealed plastic bags. Various handling and sample preparation techniques were investigated and yielded essentially identical results.

The support data was obtained as near to the time of overflights as possible. A total of over one hundred vessel "sorties" or "cruises" were mounted in support of the program. Cruise data was coded directly into an 80-column format and punched onto computer cards for inclusion in a "sea-truth" data base.

Test Description:

"Independent" variables and parameters chosen for investigation during the test phase are: water depth, water clarity, wind speed/ wave height, solar illumination, bottom character, aircraft altitude, scanner off-nadir angle, receiver field of view, transmitter beam divergence, and receiver polarization. "Dependent" variables studied for effects of the above are accuracy (precision and bias), repeatability, hit probabilities, extinction coefficients, system attenuation coefficients, minimum resolvable depth, surface return signal strengths, bottom return signal strengths, noise levels, and detection algorithms. Data for these relationships was obtained within a four phase program. The data base for each mission includes a mission plan, the AOL system output tape(s), a digitized flight log of equipment settings and notes, a digitized ground data log, filtered radar tracking tapes, ground calibration data, a list of tape and data file numbers, a debriefing report, measured tide correctors, and sometimes ancillary materials such as footprint camera films, scope photos, and video tape of the monitor.

In 1977, 18 missions were flown with a total of 161 separate passes for an estimated total distance of 1000 linear nautical miles and 400 minutes of recorded data comprised of five million soundings. Aircraft speed was maintained at approximately 150 knots with altitudes ranging from 150 to 600 meters. Missions were flown in river, bay, and ocean waters, in hot and cold weather, clear and cloudy, night and day, for winds from 0 to 15 knots, with and without capillary waves, in water clarities with narrow beam attenuation coefficients varying from less than $1m^{-1}$ to greater than $4m^{-1}$, and with water depths from 0 to over 10 m.

Data Processing:

The tremendous volume of data acquired on even a single pass causes computer analysis to be mandatory. A wide variety of programs on a number of computers have been developed for data verification, reduction, display, analysis, and troubleshooting. The primary analytic tool for AOL data analysis is a sophisticated multi-function program called the "Processor." (Ref. 14) This program is extremely versatile because it is based on a freeform "keyword" input procedure with liberal defaults. Desired functions or procedures are easily activated and quantified by the inclusion of a single card in the setup deck. Briefly, the Processor unpacks and interpolates the asynchronous system data tape, identifies surface and bottom returns and quantifies their location and amplitude under control of a highly parameterized tracking algorithm, performs wave height correction, prints and plots altitudes, depths, waveforms, statistics, and other requested information, and supplies regressions and correlation values for all combinations of eleven specially selected parameters. An additional program is being developed to compare airborne lidar soundings with corresponding launch acoustic soundings and regress differences against a given parameter set.

4. Results

Preliminary:

Return waveforms from the initial flight tests were badly contaminated with electronic ringing and other spurious but repeatable noise sources whose amplitudes were greater than those of the desired bottom returns. To suppress this noise, a technique was developed which subtracts the system response to a surface return in deep water (with no possible bottom return) from the waveforms with bottom returns to yield a "residual" waveform in which only the bottom return pulse (and any uncorrected noise) appears. This subtraction is parameterized on surface return amplitude which drives the system response. Excellent resolution of bottom returns was achieved for even very weak returns approaching the digitization limit of the system (approximately 50 nanowatts at the scanner). An added benefit of this technique is the resultant subtraction of the surface return (and average solar noise and volume backscatter signal as well) which permits resolution of bottom returns at very shallow depths where they might otherwise be masked. Processor output results indicate bottom resolution to as shallow as approximately 30 cm.

Engineering:

Dominant environmental noise sources for a lidar bathymetric system are solar background reflection in daylight and volume backscattering of the laser pulse in the water column at night. A narrow-band interference filter centered on the laser wavelength reduces solar background level by a large factor. AC-coupling in the electronics further reduces this noise source. Volume backscatter has not been particularly evident in the relatively murky waters used for AOL testing because it occurs very close to the surface return, and because the deep water subtraction technique effectively removes it.

Bottom returns as low as 100 nanowatts can be tracked successfully. Surface returns range from ten to several hundred times larger. Probability of a successful surface return under most circumstances approaches 100% rapidly as the mean surface return signal strength reaches several times the trigger threshold. Typically for the AOL this occurs at about 2.5 microwatts optical power into the scanner. A glassy or mirror-like water surface during totally calm wind conditions causes the surface return probability to decrease while the dynamic range of amplitudes and overall mean amplitude increase. Operation under these conditions would not be recommended.

Penetration capability is probably the most important performance parameter for a laser bathymetric system next to accuracy. The maximum penetration depth, in general, is dependent on a large number of variables and parameters including laser power, altitude, water clarity, bottom reflectivity, off-nadir angle, receiver aperture, receiver field of view, receiver sensitivity, noise sources, and many more (Ref. 9); but for a given (appropriately designed and operated) system, the ultimate concern is water clarity. The reduction in bottom return signal strength with increasing depth can be described by the expression:

$$SSB \sim e^{-2kD}$$

where

SSB = bottom signal strength,

D = depth, and

k ≡ "system" attenuation coefficient as defined by this expression.

The coefficient, k, has no particular theoretical basis, but simply provides a straightforward empirical parameter for describing system performance.

It has been established (Ref. 15) that for a sufficiently large receiver field of view, the value of "k" somewhat coincidentally approaches very close to the value of depth averaged diffuse attenuation coefficient ($\bar{K}$) for the water in question. Because of this fact, the product of $\bar{K}$ and the depth beyond which successful returns cannot be detected (D_{max}) is commonly referred to as the "extinction coefficient" ($\bar{K}\ D_{max}$); and penetration capability is frequently reported in terms of this unitless parameter. In addition, because an apparently linear relationship ($\alpha \cong 5K$) (Ref. 13) exists between diffuse attenuation coefficient (K) and

beam attenuation coefficient (α) for water clarities of interest in coastal waters, extinction coefficients may also be reported in terms of $\bar{\alpha}\ D_{max}$. (AOL results will take this form because most cruise data is for α rather than K).

Calculation of "k" for the AOL (from the slope of ln SSB vs. D curves) resulted in values generally consistent with K. Maximum extinction coefficients observed in processed AOL data are $\bar{\alpha}\ D_{max} = 12$ during the day and $\bar{\alpha}\ D_{max} = 15$ at night! The latter was accomplished in December off Janes' Island with $\bar{\alpha} = 2.75m^{-1}$ and $D_{max} = 5.5m$. These results, cónsidered to be excitingly high for such a low power laser, were defined at the maximum extent of high quality data, where hit probabilities remain in excess of 90% and precision (pulse to pulse agreement) remains no worse than 15-20 cm. Because of the sophisticated processing techniques applied to the raw signals, the loss of soundings at extinction tends to occur quite abruptly at bottom return signal strengths not greatly in excess of the minimum hardware digitization level. Projecting these results to a higher laser power system (100-200 kW peak) leads to expectations of $\bar{\alpha}\ D_{max}$ in the 18-20 range. Such estimates are consistent with independent high power results (Ref. 16).

Wind and wind generated waves (throughout the entire wavelength spectrum from capillaries to off-shore swell) unquestionably influence system performance through a number of intersections, but few are overly significant except at the extremes--considered for our purposes to be 2-20 knots wind speed. Surface return energy from non-nadir scanner angles reaches the receiver only if capillary waves are excited sufficiently to present a large number of tiny facets perpendicular to the beam. These capillaries tend to die out below about 2 knots, and, as noted above, this leads to a reduced hit probability. On the other end of the spectrum, high winds generate waves with sufficient energy and depth to resuspend bottom sediments and decrease water clarity to unacceptable levels. From 2-20 knots, beam spreading through the air/sea interface due to wave slope augmented refraction is not large compared to beam spreading in the water column due to scattering. Surface return amplitudes at higher off-nadir scanner angles actually benefit slightly from higher winds where less variation of amplitude with angle is also noted.

If mean surface return signal strength versus altitude data are estimated with power law curves, the exponents thus obtained range between 1.0 and 2.0 for altitudes from 150-600m. No correlation between the value of the exponent and any variable or parameter (such as off-nadir angle or wind speed) could be established; rather, the value seems to be a complex function of these plus the direction of the beam relative to the wind direction. The median exponent value observed is approximately 1.3, which indicates that the surface returns generally contain a high specular component, rather than being diffuse in nature (for typical illuminated areas from 0.5-6m in diameter at the water's surface).

The effect of altitude on bottom return signal strength is indirect. The amount of bottom return energy reaching the receiver depends on the fraction of the bottom return energy refracted through the air/sea interface (in the direction of the receiver) within the field of view of the receiver. The factors determining that fraction are water clarity, depth, altitude, wind speed, and receiver field of view. An analytic model has been developed which calculates the field of view necessary to intercept 90% of the potential bottom return energy for specific values of the other parameters. This model is in good agreement with experimental data and can be used for future system design applications.

The off-nadir "scanner" angle affects both surface and bottom return signal strengths. Surface returns at nadir are quite strong and can easily exceed the input capabilities of the system. With increasing off-nadir angle, the returns decrease rapidly in the first five degrees and then much more slowly thereafter. Bottom return signal strength is also highest at nadir but falls off more gradually with increasing angles. A scanner pattern which does not intersect the nadir is highly desirable because it avoids the dynamic range problem caused by the strong nadir surface returns. Although the AOL was configured for a maximum off-nadir angle of 15°, extrapolations of test data indicate that angles of up to 30° or more may not be unreasonable. At such large angles, calculations of a depth bias due to pulse stretching from long slant ranges would become increasingly more important.

The transmitter beam divergence, varied from two to ten milliradians, had virtually no effect on results. The only potential restriction is that the beam must be large enough to provide high surface return probability; resolution is not degraded with a larger divergence because the beam spreading in the water is several orders of magnitude greater.

Dark, muddy bottoms, typical in Chesapeake Bay, caused no bottom detection difficulties. Reflectivities for sediments consisting of various grades of mud, sand, and shell fragments ranged between 4% and 12% with a median of approximately 9%. Significant bottom vegetation was present in neither test site. Future testing of the system will be planned for bottoms populated by various forms of broad and narrow leaf plants. It is expected that various types of vegetation will attenuate the bottom signal or cause a shallow bias in soundings.

Sunglint proved to be no problem in AOL testing, because scanner off-nadir angles were not large enough to permit viewing of the glint

pattern at the 38° latitude of the test sites. For low latitudes, noon-time summer operations might be difficult, and a system with larger scan angle could experience a glint problem.

Vertical Accuracy:

Investigation of the basic sounding accuracy of the system to date has been based on data acquired in the "fixed" or non-scanning mode at various off-nadir angles. This technique permits simple comparisons with acoustic data and precludes additional errors due to possible uncertainties in wave correction procedures. (Scanning data contains large variations in air to sea slant range caused by scanner eccentricity and aircraft roll and pitch.) Wave correction procedures for scanning data based on careful modeling of the aircraft and scanner parameters are presently being investigated. Wave correction for non-scanning data is accomplished with a simple averaging technique based on altitude intervalometer data.

Accuracy is divided into two basic measures: precision and bias. Precision is a measure of self-consistency and is related to random noise, while bias errors are determined by comparison with an external "standard" and are fixed offset or "systematic" errors.

An upper bound on the actual system precision under given conditions can be estimated as the lower bound of the RMS deviation of given data about a linear fit to the data over a representative interval (typically chosen to be a single page of computer output: 40 points, or about 15 meters of track length). This is true, because this measure also unavoidably includes actual small bottom variations and residual uncorrected wave noise in addition to actual system random noise components. This worst case measure will henceforth be called "precision" for purposes of discussion.

A mean "precision" of 4-5 cm for data with reasonable signal strengths was observed during a low wind/wave test (without wave correction) with a 15° off-nadir scan angle. This value compares favorably with simulation results (Ref. 17) undertaken to derive a model of expected system performance based on laser pulse width and shape, charge digitizer gate width, photon arrival rates, pulse detection algorithms, and similar matters. At low bottom return signal strengths (several times the mimimum detectable limit) the "precision" may typically increase into the 10-20 cm range (trending as predicted by the simulation). Because of limitations in the AOL altitude intervalometer (minimum discrete jumps of 15 cm, as operated), the mean precision for wave corrected data generally has a minimum of about 10 cm. Wave correction thus adds about 5 cm error to the optimum performance level, but on the other hand performs admirably for the more usual case where wave heights above 10 cm predominate.

Fully automated comparisons of AOL soundings with NOS acoustic soundings are not yet available (though pending), and the comparison has consequently involved comparisons of several data sets by hand--a tedious task. Results in general are encouraging. Datum free comparisons of laser and acoustic bottom profiles yield mean RMS deviations in the range of 5-15 cm. With appropriate datums applied, however, distinct biases of about 30 cm have been observed in several cases. Careful analysis of the data indicates no apparent fault with the basic techniques, and hardware anomalies are suspected. Ground test data (from simulated bottom and surface targets), presently being analyzed to test this hypothesis, appear to contain somewhat similar inconsistencies. Biases as a class are generally causal and hence correctable; the high "precision" noted in the data is considered to be a better measure of system performance at this point in time. Ultimately, biases of less than approximately $\pm$ 15 cm are desired. Detailed error budgets, calculated for the AOL and for an optimized design, indicate that this is a quite reasonable goal in the reasonably shallow coastal waters of interest.

5. Conclusions

1) The feasibility of obtaining high precision bathymetric soundings in a typical operational environment with a scanning airborne lidar system has been confirmed.

2) Excellent penetration ($\bar{\alpha}$ D $\cong$ 15) of typical coastal waters has been achieved with a relatively low power laser.

3) Performance in the scanning mode at off-nadir angles up to 15° is satisfactory for performing bathymetry.

4) The operational window for various system variables and environmental parameters is not unduly restrictive and should not lead to unreasonable mission constraints.

5) The mean precision of AOL soundings is excellent (typically less than 20 cm) and predictable with an existing model.

6) Biases of up to 30 cm presently noted in a limited number of soundings are slightly greater than NOS accuracy standards but are expected to be explainable (in terms of hardware instabilities) if not correctable. Such biases are not expected to appear in a well designed system.

7) Wave correction using altitude intervalometer data has been successfully demonstrated for non-scanning data. Further work is required to extend this result to scanning data.

8) Sophisticated peak detection and location software has been developed and is performing well in low signal-to-noise ratio conditions.

9) Separate studies indicate that a relatively high powered (200 kW peak), eye safe, lidar bathymetry system can be configured to operate from a small (Beech "King Air") aircraft (Ref. 18) and should provide a significant gain in cost-effectiveness over present acoustic techniques (Refs. 7 and 8).

6. Acknowledgements

AOL bathymetry mode testing could not have been accomplished without the dedication of over forty individuals. We wish to specifically thank Frank Arbusto, Wayne Barbley, Chris Blue, Kurt Borman, Marion Butler, Bob Chase, Earl Frederick, Tom Harmon, Frank Hoge, Doug Mason, Roger Navarro, and Bill Townsend for their assistance, and the aircrew who flew long, tedious missions at low altitude. Finally, we owe a special debt of gratitude to Bill Krabill whose unending faith, support, and ideas made it all possible.

References

1. Kim, H., P. Cervenka, and C. Lankford, "Development of an Airborne Laser Bathymeter," NASA Technical Note TND-8079, October 1975.

2. "Laser Hydrography User Requirements Workshop Minutes," edited by L.R. Goodman, NOAA; January 1975.

3. "Minutes of the Laser Fluorosensor Workshop," NERC/Las Vegas, S.R. Melfi, Chairman, February 1975.

4. "Laser Hydrography Technical Review Workshop Minutes," edited by L.R. Goodman, NOAA; August 1976.

5. "Presentation for Airborne Oceanographic Lidar System Applications Workshop Seminar," AVCO-Everett Research Laboratories, Inc., December 1976.

6. "Laser Hydrography Development Project Plan, A Working Document," L.R. Goodman, February 1977.

7. "Laser Hydrography Analysis (A Cost Comparison Study)," prepared under contract for NOAA/NOS by GKY & Associates, Inc., January 1977.

8. "Cost Benefit Analysis Study of Airborne Laser Hydrography," prepared under contract #7-35364 for NOAA/NOS by GKY & Associates, Inc., February 1978.

9. "Airborne Oceanographic Lidar System," NASA Contractor Report CR-141407, prepared under contract # NAS6-2653 by AVCO-Everett Research Laboratory, Inc., October 1975.

10. Jerlov, N.G., Optical Oceanography, (Elsevier, Amsterdam), 1968.

11. Swift, R.N., "Preliminary Report on Pre-Flight Seatruthing for the Airborne Oceanographic Lidar Project," prepared for NASA/Wallops Flight Center, February 1977.

12. Scott, R., "Probability of Success of AOL Bathymetry," NOS Internal Report, December 1976.

13. Shannon, J.G., "Correlation of Beam and Diffuse Attenuation Coefficients Measured in Selected Ocean Waters," SPIE Ocean Optics, Vol. 64, p. 3, 1975.

14. "Airborne Oceanographic Lidar Post-flight Bathymetry Processor Program Documentation, Version 4.0, K. Borman, EG&G/WASC Planetary Sciences Department Report #004-78, March 1978.

15. Witt, A.K., et. al., "Air/Underwater Laser Radar Test Results, Analysis, and Performance Predictions," Naval Air Development Center Report #NADC-76005-20, January 1976, (Report is classified "CONFIDENTIAL").

16. Petri, K., Naval Air Development Center, personal communication.

17. "A Quantitative Analysis of Errors in the Interpretation of AOL Charge Digitizer Output," R.W.L. Thomas, EG&G/WASC Report # 4820-10, January 1977.

18. "Airborne Hydrography System Limited Design Report," prepared under contract #7-35373 for NOAA/NOS by AVCO-Everett Research Laboratory, Inc., January 1978.

REGIONAL INTEGRATION, VALIDATION, AND APPLICATION OF SEASAT-A SATELLITE SCATTEROMETER (SASS) DATA

V. E. Delnore
Department of Meteorology and Physical Oceanography
Cook College, Rutgers University
Box 231
New Brunswick, New Jersey 08903

Abstract

Seasat-A is scheduled for launch during the summer of 1978. Several experiments are planned for verification of the expected data. An accurate account of these experiments is premature as this conference digest goes to press; therefore only a very brief overview will be given here. It is expected that some preliminary results will be available at the conference.

1. Concept

The Seasat-A satellite for oceanography is scheduled for launch by NASA during the summer of 1978. The satellite will be placed in a nearly polar orbit, providing extensive coverage of most areas of the world's oceans on a dense time scale. Several active and passive instruments will be aboard--among them the Seasat-A Satellite Scatterometer (SASS), a 14.6-GHz radar designed to measure the scattering coefficient of the sea surface. This frequency was chosen in order that the radar backscatter be proportional to the vector wavenumber spectrum of capillary waves generated by the near-surface wind.

With its fourteen orbits per day, the SASS is expected to provide wind velocity measurements at 50-km resolution over a 1000-km wide sub-track swath. Wind speed measurements will be accurate to the greater of $\pm$ 2 m/sec or $\pm$ 10%, over the range 4-24 m/sec. Wind direction will be determined to $\pm$ 20° in any direction.[1] The algorithm for inferring near-surface winds from normalized radar cross section (and thus from the backscatter) has been described by Jones, Wentz, and Schroeder.[2]

2. Data verification

An initial validation phase of the SASS experiment involves an aircraft carrying a scatterometer similar to that aboard the spacecraft. The airborne instrument will be operated at times and places coincident with the satellite's swath, and at the same look-angles. Other validation exercises will rely on selected ships, buoys, and fixed sea-based platforms for surface truth.[3]

To determine the usefulness and accuracy of high-resolution radar scattering measurements from space is the main purpose of the SASS experiment. The data will lend themselves to many geophysical applications involving land, ice, and sea, but the emphasis will be on oceanographic studies.

3. Regional applications

Several experiments have been planned by various investigators. Many of the experiments make use of the second-order dependence of scatterometer data on large-scale wave characteristics, various meteorological variables, and on the ability of the scatterometer to differentiate type and age of land and sea ice. Movements of the Inter-Tropical Convergence Zone and of sea level anomalies accompanying tropical storms are among the regional oceanographic phenomena to be studied.

References

1. Seasat-A Scatterometer Validation and Experiment Plan (draft). Langley Res. Center, NASA, 1978.
2. Jones, W.L., F. J. Wentz, and L.C. Schroeder. Algorithm for inferring wind stress from Seasat-A. Pres. at AIAA Conf on Satellite Applications to Marine Operations, New Orleans, Nov. 1977.
3. NOAA Seasat-A Catalog of Potential Platforms for *in situ* Data Collection. NOAA Seasat-A Project Office, Washington, Mar. 1978.

REGIONAL ASPECTS OF OCEAN MANAGEMENT

Lewis M. Alexander
Chairman
Department of Geography and Marine Affairs
University of Rhode Island
Kingston, RI 02881

Abstract

Regional approaches to ocean management are but one component of global management systems. The world ocean is, in a sense, a single geographical unit, with various interacting forms and processes. At one end of the management spectrum are global rules and regulations, such as those developed by IMCO for issues of vessel source pollution. At the other end are national, state, and local standards which are applicable for internal and territorial waters. With the coming of the exclusive economic zone, some of these national standards will also come to apply out to 200 miles from shore. In between these extremes is the management of "regional" areas - that is, of some geographic entities which lie between national and global. In this article it is suggested that there are at least three geographical sub-categories within this group: subregional, regional and extra-regional.

The term "region" refers to an area of the earth's surface within which there exists some distinguishing feature or group of features, and, with respect to these features, is somehow distinguishable from surrounding areas. The most easily recognizable regions of the world ocean are the semi-enclosed seas, as well as the Arctic and the Antarctic. The Atlantic and Pacific Oceans are also susceptible of division into regions, such as the North Atlantic, the North Pacific, and the West Central Pacific. Within each marine region, there are subregions, for example, the Eastern Caribbean Islands, the Adriatic and Aegean Seas, and the Gulf of Thailand. In terms of management functions, these subregions often lend themselves to more stringent regulatory actions than may be possible for the region as a whole.

Subregional units may be bilateral or multilateral. Sometimes the offshore jurisdictional zones of two opposite or adjacent states may cover all of a subregion, such as the blanketing of the former ICNAF area by the exclusive fisheries zones of the United States and Canada. But a subregion such as the Gulf of Thailand is bordered by four littoral states.

Extra-territorial units are taken to be those involving two or more marine regions. The United Nations Environment Programme, for example, is planning a "regional seas" action off Western Africa involving the coastal areas from Mauritania south to Namibia, or Southwest Africa. Although termed the "Gulf of Guinea Action Plan" the area involved covers parts of at least three "physical" marine regions - Northwest Africa, the Gulf of Guinea, and Southwest Africa.

1. Recent Developments in Marine Regional Arrangements

Interest in marine regional issues is a fairly recent phenomenon. At the turn of the century the International Council for the Exploration of the Sea (ICES) was formed to carry out scientific activities with respect to fisheries in Northwest Europe, and in 1911 the North Pacific Fur Seal Convention was signed with Canada, Japan, Russia and the United States as members. But the real impetus for regional fisheries organizations did not begin until after World War II. At present there are 27 regional fisheries organizations, six of them directly related to FAO, the Food and Agriculture Organization of the UN. The other fisheries units, although independent of FAO, cooperate closely with it. Most of the regional fisheries organizations are concerned with data collection on fisheries stocks within this area, as well as with data assessment. A few recommend regulatory measures in the interests of conservation although these regulations may not be binding on all member states. More centralized management functions such as enforcement of regulations or allocation of the catch among member states is almost non existent. And it should be noted that with the advent of the 200-mile exclusive fisheries or economic zone, even some of the existing management functions regional organizations such as ICNAF had in the waters beyond territorial limits will probably disappear. Thus the short-term future for regional fisheries bodies is not particularly bright, except insofar as they may be successful in carrying out other functions generally assigned to them such as that of helping member states develop and strengthen their own domestic fishing industries.

A second category of regional marine arrangement involves scientific research. Here the Intergovernmental Oceanographic Commission of UNESCO is the lead agency. It has developed a regional program for the Caribbean, IOCARIB, which supports a series of regional scientific programs, dealing with such topics as fisheries and submarine geology. IOC is also associated with a somewhat similar scientific organization in the Mediter-

ranean, CIM. But perhaps the best-known activities of IOC are the ad hoc, cooperating investigations of certain regional phenomena, such as upwelling off South America, the Kuroshio current off Japan, and the Tsunamis of the Pacific.

In addition to IOC's activities there are two independent regional science organizations. The best-known is the International Council for the Exploration of the Sea, located in Denmark, which for over 75 years has carried out high level research, particularly with respect to fisheries, in Northwestern Europe. The other unit is ICSEM, a private marine science organization for the Mediterranean, which is based in Monaco.

A third category concerns pollution control and abatement. Hence there are two groups. First are the separate treaties set up largely to control oil pollution in Northwestern Europe, including the Baltic. Littoral states came together and decided to impose for the areas higher pollution control standards than are generally recognized internationally.

A second group is under UNEP, the United Nations Environment Programme. Formed after the 1972 Stockholm Conference on the Human Environment, UNEP has established a "Regional Seas" Programme which will develop and implement action plans for certain regional areas. These plans must embrace both environmental and development objectives, and strongly involve the respective Governments of each region. In 1975, the first of the regional action plans - that for the Mediterranean Sea - was adopted by the governments of the Mediterranean states (except Albania) and is now being implemented. Other regional seas for which action plans are anticipated include the Caribbean, the Persian (Arabian) Gulf, the Red Sea, the West African Coast, and the East Asian Waters.

Beyond these three categories relatively little has been done in regional marine activities except with respect to development. The United Nations Development Programme, for example, has six on-going regional fisheries projects, and the World Bank has contributed also to regional marine-related projects such as fisheries and port complexes. The regional commissions of ECOSOC, the UN Economic and Social Council, has also funded projects associated with the marine environment. Two regional units exist in the Southeast Asia/ Western Pacific area to coordinate and develop exploratory work for offshore oil and gas.

Clearly in the field of development, regional and subregional marine efforts are expanding They are also growing with respect to environmental control. What the future is in terms of scientific research depends largely on the future of the theory political problem of access for foreign research to the exclusive economic zones of other countries. There has been little regional activity with respect to shipping, to dispute settlement, or to education and training, despite the several regional conferences held on this topic by IOC's Working Group on Training and Mutual Assistance (TEMA). It has already been noted that regional fisheries management organizations face a dim future so far as management is concerned, at least for the next two years. Another possibility is regional approaches to seabed mining - the conclusion of "mini-treaties" in the event that UNCLOS III cannot come up with a global region for the seabed.

2. Future Directions for Marine Regionalism

With respect to the use of outside development funds and other forms of assistance, I would anticipate that regional and subregional arrangements among developing countries should continue to grow. Cooperative action often is more efficient than aid dispersed on a county-by-country basis. In fact, donor nations are in a position to considerably strengthen certain forms of regional cooperation through the terms of their assistance much as the United States did in Western Europe with the advent of the Marshall Plan. But most donor states will not rely exclusively on regional aid. Often there are one or two countries which are considered to be especially significant to the donor, and thus warrant special treatment over and above that given to other members of the region.

UNEP's regional action plans may be slow in developing (after the initial waves of enthusiasm) because the costs of regional efforts at pollution control are high, because the dangers from pollution and the necessary steps to control it may be seen differently by different states of the region and because there appears to be no large-scale economic assistance coming from outside sources for the regional action plans. IOC's regional program for the Caribbean will grow slowly but steadily (its initial time frame is only six years but it can be renewed), and the Commission is anxious to set up similar organizations for other marine areas. But IOC faces a number of political problems. Among them the tie-in between participation by a developing coastal state in a regional science project under IOC, and the implication that, through participation, the same state agrees to grant access in its economic zone to oceanographic vessels of other member countries of the project.

The number of well-defined enclosed or semi-enclosed seas of the world are limited in number, and there is even a finite number of partially-enclosed (or otherwise easily recognizable) water bodies, such as the Gulf of Guinea, or the Coral Sea. People tend to think in terms of their geographic entities, and it follows that quite a number of future regional arrangements will be made with respect to traditional seas, gulfs, and bays. For the time at least, most of these arrangements will deal with one - or possibly two - marine-related activities to the exclusion of others. But fisheries issues in the Caribbean or the Red Sea have at least some associations with issues of scientific research and of environmental control in the same water body. Which raises the question of future "linkages" within the same geographic area between two or more regional marine arrangements, each dealing with a different activity. Can the managers of the arrangements be induced to work closely together, even though the regional institutions

they represent may be funded from different sources? Will there be competition as to which of the organizations is the "lead" agency? Might some form of coordinated super-agency eventually be formed to manage one or more of the regional seas?

It should be noted that there is very little in the Informal Composite Negotiations Text (ICNT) with respect to regional activities, other than extolling states to join together in regional and subregional programs. One of the most troublesome regional issues in the Text refers to the rights of land-locked and geographically disadvantaged to utilize the surplus catch within the economic zone of coastal states of the same "region". There may in time be some differences in the definition of "regions" for West Africa, Southern Africa, or Southeast Asia.

The policies governments adopt toward participation in marine regional activities depend in part on how they perceive the costs and benefits of regional - as opposed to unilateral or global-activities. These perceptions are based upon their relationships with the sea, in terms of such factors as accessibility to the ocean and its resources, investment in marine-related activities, and dependence of the country on the sea and its well-being. But perceptions are also based upon the objectives countries seek from their marine activities, procurement of wealth, protection of national security, exclusion of certain foreign vessels from their offshore waters, etc. What is needed by planners and policy makers is a well-conceived paradigm of national ocean interests which can provide the basis for analysis of national decisions and decision-makers with respect to regional action.

A final note on directions for marine regionalism concerns the dichotomy between developmental and restrictive regional arrangements. Developmental are these which benefit the member of a marine-regional organization economically and/or in times of environmental protection. Restrictive arrangements are those which tend to shut out the vessels of non-littoral states, even though such exclusion does not materially benefit the economic or environmental interests of the littoral countries. Banning the oceanographic research vessels of one or more "outsider" countries within the waters of a semi-enclosed sea, such as the Black Sea or the Mediterranean, would be a restriction on it, since the littoral states themselves would have no demonstrable benefits from such exclusion. Since virtually all of the waters of the world's semi-enclosed seas are completely shut off by the overlapping exclusive economic zones of the littoral states, and since within these economic zones coastal states presumably have exclusive rights with respect to oceanographic research by foreign countries, as well as to environmental protection, it follows that all or most of the littoral states of such seas could, in theory at least, ban together to exclude from the seas the oceanographic vessels or "potential polluters" of one or more non-littoral power.

In conclusion, this paper suggests that what is needed now is considerably more research and analyses on the whole topic of marine regionalism. Can we define "regions" and "subregions" more carefully? Can we develop general guidelines for management institutions with input to various categories of marine-related activities? Perhaps through case studies of specific regions, their marine processes and problems, certain types of models might be developed which would have relevance in other parts of the world.

Marine regional arrangements are still in their early stages. With the advent of the 200-mile economic zone a period of intense nationalism will be upon us which will serve to frustrate binding regional arguments. But seen in the midst of this nationalist period plans must be developed for promoting and supporting regional and subregional activities, because they are so necessary to the efficient functioning of our management activities. Study and debate will therefore continue as we accustom ourselves to this new form of ocean management.

THE PROPOSED INTERNATIONAL SEABED AUTHORITY: A UNIQUE INSTITUTION?

Lee Kimball
United Methodist LOS Project
100 Maryland Avenue, N.E.
Washington, D.C. 20002

Sam Levering
U.S. Committee For the Oceans
245 2nd Street, N.E.
Washington, D.C. 20002

Abstract

The attempt of the United Nations Law of the Sea Conference to devise "international machinery" to administer the new regime for deep seabed mining may well spawn models and precedents for other problems of international scope such as resource management or arms control. Not only will the composition and voting procedures point the way toward equitable representation in other international forums, but the scope of the institution itself will be unique. It will at the same time manage the development of an international resource, taking into account both conservation and price stabilization, take part in mining as an international business enterprise, and serve as a self-supporting, profit-making aid institution. It will also take part as an independent actor on the world scene, contracting with private companies, appearing before international courts, and assuming liability for damages caused by it.

There is general agreement at the United Nations Law of the Sea Conference, now in its resumed sixth substantive session in New York, that there should be an International Seabed Authority to administer the part of the prospective comprehensive ocean treaty dealing with the development of mineral resources in manganese nodules on the deep seabed.

Although final agreement has not yet been reached on the structure and operation of the proposed Authority, many of its features have been generally accepted. This is a far cry from the situation in 1967 and 1970 when the United Nations blithely endorsed the creation of "international machinery" for this purpose. To some this meant merely the establishment of a licensing agency to record claims in the deep seabed area. To others it took on the hue of a comprehensive ocean authority governing all ocean use and development. Many saw the promise of seabed riches as breathing new life into the whole system of international institutions. Others expected bonanzas for national development.

Obviously none of these conceptions was quite accurate. But what has evolved in the Law of the Sea Conference discussions does in fact represent a unique departure from existing international institutions, both in scope and in structure.

First, the International Authority will actually manage and supervise the development of a resource of material value through contracts with private mining companies or state enterprises as well as through its own mining arm, the Enterprise. In the past, unclaimed resources have always been divided up among nations which themselves managed exploitation. What functions were performed by international agencies were to coordinate and harmonize national policies and regulations.

Second, through the Enterprise, which will be comparable to a state mining company, the Authority will undertake its own mining operations. The Enterprise is meant to become self-sufficient and generate its own capital and income. It represents the first truly international business enterprise, as we proceed from the national to the multinational to the transnational enterprise and now beyond.

As the administrator of resource development, the International Authority will participate in international commodity conferences and arrangements as an independent developer. (One question yet to be resolved in the Conference is whether the Authority in these arrangements will be able to vote production resulting from contracts with private companies or state enterprises, or merely that for which the Enterprise is responsible.) But in so doing it will come to the conference table representing both producers and consumers, as well as the bulk of the world's nations not substantially involved in either, but which still have a stake in the development, conservation and fair and stable pricing of natural resources.

Through its dealings with private companies mining the deep seabed, it will have the opportunity to forge new directions for harnessing their strength and efficiency for the common weal in a manner acceptable to all parties. This will apply to the transfer of technology as well as to financial terms which promote development yet fairly divide the costs and the risks. On the one hand there is a great deal of fear among the multinational mining consortia that they will be denied a fair deal. On the other hand, the majority of the world's nations fear that once again they may be 'had' by these same consortia. What may be arrived at is a balance which for the first time

permits the companies equitable mining terms and conditions without circumscribing their initiative, while at the same time fosters the evolution of a system of resource development which prevents "exploitation".

Third, once mining is well underway, the operating income of the Authority will come primarily from mining activities under its supervision and not from member states' grants. It is hoped that the Authority will soon become self-sufficient.

Needless to say, both the initial administrative expenses of the Authority and the initial administrative expenses of the Enterprise as well as its first complete mining operation will be financed by funds from member states. In the case of the Authority, these will be contributions, and in the case of the Enterprise, guaranteed loans. Both will be assessed according to the United Nations budget scale of assessments. Thus these unique institutions spring from traditional patterns of funding international institutions.

Fourth, the impetus behind the International Authority differs explicitly from most other international institutions. It has been agreed that the benefits from deep seabed mining are to go primarily to the developing nations. Thus the nations of the world have agreed to set up what will be a self-sufficient international aid institution, one not dependent on voluntary contributions from national coffers and one whose funds derive from an international source of wealth. Not only will this one be allowed to make a profit, it will be urged to make as high a profit as possible. Although it is unlikely that net revenues will amount to much certainly before the end of this century, the profit-making authorization is a significantly different mandate from that of existing international aid institutions.

Fifth, the International Authority will deal directly with mining entities, rather than through their governments (except in the case of state-sponsored enterprises). Compliance will be expected from the companies and enforcement sanctions exercised against the companies rather than on nations, although states parties have the ultimate responsibility to ensure that activities undertaken by persons under their jurisdiction are carried out in conformity with the Convention. For the first time, individuals and corporations will be able to take part in the international dispute settlement procedures established to deal with seabed-related disputes. Both the mining entities and the International Authority or its mining arm, the Enterprise, will be liable for damages caused by them.

Finally, we come to the key point: can, in fact, a decision-making structure be devised for the International Authority which all nations feel adequately protects their interests? The Law of the Sea Conference is closer than any other effort in United Nations voting reform to achieving some mechanism which both protects the interests of the industrialized nation minority and skirts the politically-sensitive issue of veto power by the minority. In what began as an adamant Third World endorsement of one-nation/one-vote decision-making majorities, we now have a plenary Assembly with overall decision-making powers and a 36-member Council which will be responsible for the key day-to-day operational decisions. The composition and voting of the Council is the all-important factor.

It is already agreed in the Conference that half of the Council's membership will represent special interests and half will be selected according to the principle of equitable geographic distribution. Special interests include those nations which have made the greatest contributions to the exploration for and exploitation of the resources as demonstrated by substantial investments or advanced technology, major importers, major exporters from areas under their jurisdiction whose exports have substantial bearing upon their economies, large populations, land-locked and geographically disadvantaged nations, and least developed nations. The precise formula, however, has not yet been identified. To quote Ambassador Richardson, "the parallelism of the system will in large measure be influenced by the manner in which the Council is composed and voting provisions". (June 16, 1978, Testimony before the Senate Foreign Relations Committee) The application of third-party dispute settlement procedures to these decisions must also be blended in the crucible.

As more and more of the decisions facing national governments take on international dimensions, the ability to make them outstrips existing structures of international decision-making. For this reason, the efforts of the United Nations Conference on the Law of the Sea to devise new structures and voting procedures may well evolve into a model for use in other areas. The International Authority might well establish precedents and gain experience applicable to other international bodies such as an International Arms Control and Disarmament Authority, which would be essential to administer and assure compliance with an Arms Control and Disarmament Treaty, if this could be achieved. It could also be a model for the use and development of other "common heritage" resources such as outer space or the Antarctic.

THE IMPACT OF UNCLOS III ON MARINE SCIENTIFIC RESEARCH

William L. Sullivan, Jr.
Director, Office of Marine
Science and Technology Affairs
Department of State
Washington, D.C. 20520

Abstract

UNCLOS III is attempting to reach international agreement on a broad range of ocean issues, one of which is marine scientific research. If an LOS treaty is produced, it will provide the basic governance for marine scientific research. The existence of UNCLOS III itself has had and will continue to have an impact on the conduct of marine scientific research, whether or not there is an LOS treaty. The negotiations have brought marine scientific research squarely to the limelight. This has made national officials conscious of the political, economic, and security implications of marine scientific research. Coupling the suspicions of the developing countries over the real motives of the developed world with such things as the new international economic order has produced a climate which is at best suspicious of and in many respects hostile to marine science. Nations are already turning this into claims to national jurisdiction, and the number will continue to grow. Accordingly, even if there is no LOS treaty, our scientists will be confronted by national claims over marine science in a very significant area, making research much more difficult. Costs will be increased. In the long run science may still benefit. But it may be a long time before we see this.

* * *

The Third United Nations Conference on the Law of the Sea (UNCLOS III) is attempting to reach international agreement on a broad range of issues. These include deep seabed mining, the breadth of the territorial sea, fisheries and other economic uses of 200 mile offshore zones, passage through straits, boundary delimitations, and marine pollution. Many of these topics have been substantially agreed, while others are still under discussion at the resumed Seventh Session of UNCLOS III which is taking place in New York at the time of delivery of this paper.

One of the topics still under discussion, that of concern here, is marine scientific research. If agreement is reached on an LOS treaty, one section of it will provide the basic governance under which a large portion of marine scientific research will be conducted for many years to come. That section will deal primarily with the band of ocean lying within 200 miles of the coast, an area which encompasses 37% of the ocean, or one-quarter of the earth's entire surface. Scientifically the 200 mile zone with its boundary currents and relatively shallow waters is perhaps more important than the rest of the ocean.

It is not the intent of this paper to discuss the potential science articles in an LOS treaty or the impact of alternative formulations of those articles on the future conduct of marine scientific research. Rather, it is to discuss the impact that the existence of UNCLOS III itself has had and will continue to have on the conduct of marine scientific research as one of the institutional aspects of ocean development. It is clear that this impact exists now, and will continue, whether or not there is an LOS treaty.

The long and difficult negotiations toward an LOS treaty involve a host of highly charged legal, political, economic, social, and security issues. Many of these issues have had a direct impact on the concept of and the positions which have been taken on marine scientific research. The oceanographers who have been participating in the conference have had to become experts on many matters little dreamed of when they were students, or when they later pursued their scientific calling leading to the expertise which resulted in their being drafted to provide the necessary scientific input to the Conference. Likewise, the lawyers and other participants have come to know more about marine scientific research than many of them probably ever wanted to know.

Even though science was one of the formerly lesser-known aspects of the LOS negotiations from the perspective of the world at large, the protracted discussions and the necessity

U.S. Government work not protected by U.S. copyright.

to try to reconcile often widely differing viewpoints have brought marine scientific research squarely into the limelight in the eyes of most national governments. This is true in particular with respect to their foreign, finance, justice, resource, and defense ministries, each of which has a special interest in or responsibility for some aspect of the prospective 200 mile zone agreement which UNCLOS III may reach. Of these, the only ones which in the past were most likely to have been directly involved with marine science in what might become the 200 mile zone were the navies. This is because the principal entities responsible for marine science in most developing countries, which constitute the vast majority of UNCLOS III participants, were the navies, but then primarily from a technical sense. During the Conference, however, most navies' attention turned toward national security concerns about the nature of foreign marine scientific research which might be conducted within their zones, because of a perception that such marine scientific research might be a cover for espionage, or because of the feeling that the knowledge gained by the foreign scientists might be put to use in some way which imperiled national security. However, as the Conference went on, the focus on marine scientific research has shifted more to the resource people as the Conference focused more and more on control over and access to resources.

In addition to the security implications -- real or imagined -- of marine scientific research, this limelight has made national officials of numerous ministries conscious of the political and economic implications of marine scientific research, again -- real or imagined. They have become acutely aware of the power they might exert by controlling scientific research within 200 miles of their coast. Perhaps more importantly, though, many of them have become convinced that knowledge itself is power, and that this power has direct implications for economic interests. They have become convinced that any scientific research, no matter how abstract the science or how "ivory tower" the scientist, might be used by developed countries to their own advantage in negotiating resource arrangements, whether they be for oil drilling or fishing by foreign vessels in the zone.

These feelings have been intensified by the international scene in which we have lived in recent decades. We have seen a vast increase in the number of nation-states, and of the emergence of their determination to exert their weight in international fora, including UNCLOS. One of the heritages of the colonial past has been a suspicion of the real motives of the developed world, and in particular such leading nations as the United States. Thus, when we took the lead in advocating the freedom of scientific research beyond the projected twelve mile territorial sea, many of the developing country participants wondered what we really had in mind. It was too simplistic to believe that we really think it is important to expand knowledge about the more than 70% of this planet which is ocean, that such expanded knowledge would ultimately benefit everyone.

Even those who perceive this, however, believe in many instances that the developed countries would be the only ones to benefit initially, because only we have the technology and the resources to put whatever knowledge which might be gained from marine scientific research to practical application in "their" waters.

In a world of epidemic nationalism and new credos such as the "New International Economic Order", the suspicions about the developed world have heightened and thus have those about our real intent with regard to marine scientific research. While they are really extraneous to the question of marine scientific research, such episodes as the cases of the USS Pueblo and the Glomar Explorer also served to heighten suspicions of our real motives with regard to marine scientific research and other ocean activities. Thus, we have a climate which is at best suspicious of and in many respects hostile to marine scientific research.

In UNCLOS, this climate in turn produced a perception of the need to exercise complete control over marine scientific research in broad areas off national coasts, if not to prevent it outright. Thus, we have seen UNCLOS moving steadily toward a discretionary 200 mile consent regime over marine scientific research, in spite of our protestations of the harm this could do to mankind in both the short and long term. Moreover, the suspicions of the developing countries are so great that they have turned our reasonable proposals on guidelines and conditions under which marine scientific research might be conducted into long and complicated details in the LOS drafts. Many of these are so complex and unclear that they are perceived by many scientists as being more inimical to marine scientific research than the concept of a discretionary consent regime within 200 miles itself.

However, the notion of 200 mile exclusive economic zones, including a consent regime for marine scientific research, has become so pervasive that it is already becoming a reality. Approximately 50 nations have already asserted 200 mile jurisdiction which includes marine scientific research. Three others, at least, have asserted 200 mile jurisdiction over fisheries research, and four have asserted archipelagic jurisdiction which is similar in its broad extent to 200 mile jurisdiction. Some

dozen or so others have asserted jurisdiction which includes science to varying distances beyond 12 miles, some as much as 150 miles. Some 16 others have asserted fisheries jurisdiction only to 200 miles. It is clear that many of them have conversion to a full economic zone jurisdiction in mind at some time. Other nations have such legislation pending, while others have indicated that they intend to exercise such jurisdiction but prefer to await the outcome of UNCLOS III. (All figures as of June 1, 1978.)

Accordingly, even in the absence of an LOS treaty governing marine science, scientists are confronted by national claims over marine science in a very significant portion of the world ocean. This portion will continue to grow, regardless of the outcome of UNCLOS III, until the 200 mile offshore area of most nations will fall under their perceived science jurisdiction.

Thus, with or without an LOS treaty, the conduct of a significant portion of marine scientific research will be much more difficult for some time to come. If done at all in these areas, costs, particularly, for marine science will increase. There will be a pressing need to produce tangible results -- real or perceived -- of benefits to the coastal nation involved. The more theoretical science, which might hold the potential for the greatest long-term benefit, will suffer at the expense of more applied research with more immediate pay-off. There will be a need to produce technical assistance and technology transfer as part of the research program, either as part of individual projects or as part of overall relations between developed and developing countries concerning marine scientific research. All of this will cost. And the cost and effort will be on top of what must be done to achieve the research objectives themselves. Thus, marine scientific research has come to a new era, from one of almost complete -- or at least one of relative -- freedom to one of operating under national controls. In effect, oceanographers are now in the same boat with terrestrial scientists in having to cope with land-based controls. To make this more complicated, a single research project may be subject to several, possibly conflicting, sets of national rules and regulations because of the extent of the area that many of them are required to cover. Oceanic processes in one 200 mile zone may well produce effects in another hundreds of miles away or on the land mass of a far distant country.

Some of these contraints would have come to pass anyway. But it is safe to say that it was UNCLOS III itself which made most national lawmakers and rulemakers conscious of marine scientific research.

Although marine scientific research is facing a most difficult period of adjustment, this is not meant to imply that marine science will wither or die. Marine scientists will find some way to accommodate themselves to the new problems and at least many of the new rules. Changes are already taking place. In the long run this may even lead to a new flowering of marine science. As the developing countries receive benefits from these activities, and their marine science infrastructures build up, their perceptions of the advantages of marine science and the necessity of international cooperation in its conduct should produce demands for more science and more benefits for all concerned. The suspicions they now hold may be eliminated gradually as their development of ocean resources progresses and their scientific capabilities increase. With the decline in suspicions should come a more conscious desire to promote rather than impede marine scientific research. However, it may well be quite some time before we see a conscious movement in this direction.

NOTE: The views expressed herein are those of the author, based on over seventeen years of experience in dealing with international marine science activities, and do not necessarily reflect those of the Department of State.

CAESAR, SOSUS, AND SUBMARINES: ECONOMIC AND INSTITUTIONAL IMPLICATIONS OF ASW TECHNOLOGIES

by Harvey B. Silverstein*

Department of Government and International Studies
University of South Carolina, Columbia, South Carolina 29208

Technological developments and deployments in antisubmarine warfare have advanced so dramatically in the last few years that many full-time observers of ocean affairs are not aware of current and projected capabilities. This paper sets forth the nature of American capabilities to monitor foreign submarines.

American efforts to monitor Soviet submarines, particularly those carrying strategic missiles, are likely to lead to responses on the part of the U.S.S.R. which can have undesirable and destabilizing implications.

Existing systems of ocean surveillance could be utilized in alternative institutional frameworks for economic and other benefits for the larger international community while preventing a further acceleration of the U.S.-U.S.S.R. arms race.

A naval ensign is sitting in front of a CRT console somewhere near San Diego, California. On the television-like screen in front of him is an electronically drawn map of part of the Sea of Japan. Appearing on the screen are hundreds of little blips, each representing a source of sound in that particular area of the world's oceans. The ensign picks up what looks like a tiny pistol. It is not a gun but a light pen which he focuses on one of the blips on his screen. He presses a button on the pistol-like light pen and within less than a minute on another screen appears the information that the blip he identified is a ship, the ship is a submarine, the submarine is a Soviet submarine of the Delta II class, and the name of the Captain of that particular sub is Captain Balaschnikov.

A scene from an updated Dr. Strangelove--not quite, for the nature of activities described above represent fairly closely the capabilities which the United States has developed in anti-submarine warfare. Although in practice we may not yet be able to identify the specific captain of a particular Soviet vessel, the United States is rapidly reaching the point where we can monitor the location of Soviet strategic missile sumarines almost anywhere in the world's oceans. Unfortunately, in almost none of the available sources dealing with the nature of our technological capabilities in anti-submarine warfare has there appeared any serious discussion of the full implications that deployment of these particular technologies would bring.[1] The intent of this paper is three-fold: to set forth the nature and extent of developments of anti-submarine warfare, assess some of the strategic implications of those developments, and finally to put forth an alternative institutional scheme for utilizing these technologies which could have important and beneficial economic and political spillovers.

1. ASW Technologies

Anti-submarine warfare actually involves several distinct operations, detection of the submarine, classification of what has been detected, localization to specific geographic coordinates, and finally destruction when desired of the offending submarine. Of all of these operations, detection has historically proven to be the most difficult phase to carry out successfully. Highly sophisticated technology has not only been developed but has also been deployed to carry out all of these phases through the localization operation. Most of these technologies are dependent upon the use of various types of acoustics or sonar as it is often called. Sonar can be active in which one sends out a sound impulse which is reflected off a target submarine indicating its position, or it can be passive in which one listens with very sensitive hydrophones to the sound impulses given off by various machinery within an operating submarine. In principle, these technologies operate in much the same way as the ASDIC used during World War II. In practice, however, the devices which the United States has deployed today bear as much relation to World War II type sonar as a color television set bears to a Marconi wireless.

In addition, we use some new technologies for tracking submarines. MAD or magnetic anomaly detectors prove very useful when a submarine is very close to the surface or in pinpointing an exact location. There are experiments now going on using optical systems with low light level television, although again this seems useful primarily for ultimate localization. There is also some scuttlebutt that the Navy may be looking into the use of neutrinos and neutrino detection systems (neutrinos are given off by any nuclear reactor) as a means of detecting submarines.[2] It has also been suggested that a special type of blue-green laser could also be used in an ASW capability. Despite the sex appeal of these rather exotic sounding technologies, it is acoustic systems which are the backbone of submarine detection, classification, and localization activities around the world.

The intention here is not to present an exhaustive list of every device we have developed but to present a survey of the range of systems and, more importantly, describe how they interrelate.

Before proceeding with an elaboration of these technologies, it is important to recognize that there is a sense of unreality about acoustical operations within both the oceanographic scientific community and those military officers not intimately involved with anti-submarine warfare. Conversations with many of these individuals suggest that while there is wide recognition of the terrible difficulties in picking up and identifying miniscule sounds across thousands of miles of ocean, there is also little awareness of the tremendous strides acoustical technology has taken in the isolation and identification of noise profiles.

Perhaps the most impressive and certainly among the most secret of our ASW surveillance systems are the fixed arrays and sonobuoys that we have implanted in the ocean. These include such projects as AFAR (Azores Fixed Acoustic Range) with sonar installed on three towers at deptsh of 300-600 meters off the island of Santa Maria for surveillance of traffic through the straits of Gibraltar and project SOSUS (Sonar Surveillance System) which is our major underwater passive acoustic submarine detection and classification system. It consists of a series of hydrophones and special sonars linked by cable to shore base installations that process the received signals. Possible range may extend to 9,600 miles. It is based on the periphery of the oceans and has the capability of locating a submarine within a ten mile square area from a 2,000 mile distance. This includes such projects as "Barrier" and "Bronco" believed to be located on the territory of American allies such as the Azores, New Zealand, Australia, Norway, Shetland Islands, Iceland, and Greenland. This system has undergone several generations and was actually first installed back in 1954. The first SOSUS system, the grandaddy of them all, is project CAESAR. This includes highly sophisticated sonars (AN/FQQ-6 and AN/FQQ-9V) and spectrum analyzers (AN/UQA-5). CAESAR is now in its fifth generation of development and recently got a glimmer of public attention during the Panama Canal debate when it was revealed that Galeta Island, which is in the Canal zone, is also the site of part of our SOSUS network.[3] Colossus is an advanced version of CAESAR and was installed beginning in 1964 off the west coast of the United States using a more advanced form of sonar (AN/FQQ-10 [V]).

"Sea Spider" was to be anchored in the deep ocean rather than the coastal peripheries of the ocean and incorporate hydrophones three meters in diameter which were to be anchored at 5,500 meter depths by three 8,000 meter cables and was to be powered by a nuclear battery. Whether or not this system was ultimately deployed as it was supposed to be off the north coast of Hawaii is somewhat questionable, although one account of the recovery of the Russian submarine by Hughes Glomar Explorer describes the web of Sea Spider as the largest undersea acoustic detection system ever placed in operation with a capability of continuous surveillance of all vessels in its 1,300 mile network, and also being the key technology utilized in the breakup and subsequent localization of the Soviet submarine which went down north of Hawaii in March, 1968.[4] A final system which has been moved back to low priority because of some recent technological advances in towed arrays is the Suspended Array System (SAS) which was truly a monster system with a tripod tower anchored at a 4,900 meter depth with each leg roughly 10 kilometers from each other. This system was to be so sensitive that only one such tower would be necessary to completely monitor an entire ocean basin.

In terms of cost effectiveness, portability, ease of deployment, accuracy, and adaptability, the towed arrays and the sonobuoy systems have become the rage in submarine surveillance. These include such systems as TASS (towed surveillance system), TACTLASS (tactical towed linear array sonar system), SURTASS (surface towed array sensor system), and ITASS (interim towed array sonar system) which are all sonar systems towed by either surface ships or submarines to be used in both tactical and strategic localization of submarines with a maximum range in the case of the TASS system of almost 6,000 miles. These towed array systems can be coupled with sonobuoy systems which are, in essence, hydrophones dropped by ships, planes, helicopters, or other submarines at a fixed point to help provide localization of a submarine. These include both active and passive sonars. Sonobuoy systems include DICTASS (directional command activated sonobuoy system) which can be remotely commanded via a data link and also will send its signals to a helicopter or airplane, VLAD (vertical line array DIFAR [Directional Low Frequency Analyzer and Ranging] which extends a sonobuoy system from the surface layer into the deep sound channels below and covers a very long vertical area of the ocean, SLVA (steered vertical line array) which is also a localization system, and FDS (fixed distributed system) which can be used for protection of restricted bays and sounds and is an essentially upward looking sonar network to detect objects passing through it. Finally, we have a unique sonar system developed for our own strategic nuclear subs consisting of a towed array sonar (AN/BQR-15) and a passive sonar receiver (AN/BQR-19) as well as an improved DIMUS consisting of a digital multibeam steering improved version of currently installed integrated sonar (AN/BQR-2/BQ-4).

In addition to these particular sonar systems, it is important to note that there are several specific airborne systems which are used essentially as ASW platforms and incorporate many different kinds of sonar technology, data reporting, and systems links as well as anti-submarine bombs, mines, torpedos, and rockets. The most important of these include the Lockheed Orion P-3C which has the capability to not only locate and track submarines, but to do it in real time and link that real time tracking data with ships, other aircraft, and even with land-based stations through direct satellite links. It can deploy 87 sonobuoys over a wide area, and in coordination with surface ships and helicopters this airplane can accurately pinpoint the location of a submarine. The Lockheed Viking S-3A, another aircraft which can be computer controlled during flight, provides a little different mixture of endurance and speed. Helicopters designed specifically for anti-submarine warfare are the Sikorsky S-61, the Sea King SH3 or SH3H, and the LAMPS (Light Airborne Multi-Purpose System). They can be used for localization of submarines after detection by a ship's sonar, sanitation of areas around a naval operation, an effective extension of the range of ship weapons systems, and an additional data link in the entire system for tracking submarines. The LAMP

helicopter also carries two torpedos and could be used to deliver a final coup de grace.

Financially these systems have also come to absorb an increasingly larger percentage of the Navy's budget. "The Navy now spends 6.5 billion dollars or 15 percent of its total budget on anti-submarine warfare."[5]

The single outstanding factor which has converted this cornucopia of sonar systems into an effective, accurate, fast, tracking mechanism of Soviet submarines has been the deployment of ever more advanced computers and data link systems. It is only through the use of sophisticated programs and extremely powerful computers that submarine generated noise can be separated from that of any other ship, from the clicking of shrimp and the whistling of whales, as well as pinpoint its direction when confronted by the terrible anomalies of temperature, current, sea state, and interference. Naval scientists using these computers have succeeded in developing compensating equations to deal with all of these anomalies faced by soundwaves traveling through a water medium. This is perhaps the most miraculous part of the entire anti-submarine warfare technology development effort. Once an acoustic profile of a ship or a submarine is obtained, it is a fairly simple matter to store it and later match it against an unknown signal. The principle underlying this is identical to that used in the development and application of voice prints. In this way scientific developments have combined with technological advance to provide the capability to locate and identify foreign submarines.

The collection of all of the signals picked up by the variety of sensors previously described, analysis of the information, and programming to enable command and control decisions regarding any submarines that are localized is coming about through a new system, Project Seaguard, developed by the Defense Advanced Research Project Agency (DARPA). At the heart of Project Seaguard is ILLIAC IV, described by the Director of DARPA as the world's largest computer. Located at the Acoustic Research Center in Moffett Field, California, ILLIAC IV is linked to a variety of acoustic arrays by secure satellite link.[6] This incredible computer's ability to coordinate sensor data from 64 separate inputs and parallel process them gives the Navy the ability to not only localize, identify, and track submarines, but to do them in real time. "Real time," of course, means the ability to carry out these operations just as they are happening. Therefore, the image of a Naval ensign following a blip across an electronic screen exactly as a Soviet submarine is crossing that area of the Sea of Japan no longer represents an unattainable ideal.

A final stage in the completion of an ASW mission is the communication of the intelligence derived by Seaguard back to the operational units on land, afloat, and in the air. To enhance this capability the Navy is now developing Project OSIS (Ocean Surveillance Information System) which will correlate and distribute information and commands from sources to operating forces all over the world.

2. Strategic Implications

I have gone into some detail here in presenting technological information which is all generally known among the anti-submarine warfare community. However, conversations with officials from the Arms Control and Disarmament Agency, State Department, U.S. Navy, U.S. Army, C.I.A., and academics specializing in defense and strategic issues have convinced me that there is a woeful ignorance of not only the nature and extent of these technological developments, but particularly their strategic implications. Although there are a number of additional innovations in anti-submarine warfare, the technologies herein described should make it apparent that even if we may not yet be able to track Soviet strategic missile submarines everywhere, all the time as of this writing, we are moving toward that goal.

Initially, expenditures by the Navy on anti-submarine warfare were justified on the ground of their necessity for protection of naval ships at sea and to enable the Navy to carry out its mission of keeping the sea lanes open. As a result of the rapid advance of ASW technology those rather limited goals initially set forth by Naval leaders have evolved to the point where research administrators and admirals have explicitly professed the heightened objectives of tracking submarines from the moment they leave their home port until they return in real time.[7]

The strategic implication of these developments which is most serious is at the same time both simple and disconcerting. If the United States indeed is attaining the ability to monitor Soviet submarines wherever they wander in the world's oceans, this means that we could conceivably deploy forces to interdict and destroy those submarines. If, indeed, this can be accomplished in a very short period of time regarding Soviet ballistic missile submarines (SSBN's), the Soviet Union can no longer depend upon the guaranteed existence of a second strike capability, or in other words, the maintenance of a deterrent force. Therefore, the continuing development of ASW technology can and may already have dramatically upset the balance of strategic nuclear forces between the Soviet Union and the United States.

Although the Soviet Union has also been developing anti-submarine warfare technology, it has not deployed the great variety of fixed array and deep ocean devices that the United States has and is considerably behind the American Navy in its technological capability. As Admiral Long of the United States Navy described: "The Soviets will undoubtedly continue to expand both the quantity and quality of the forces committed to open ocean ASW over the next several years. In general, these forces will represent current state of the art and incremental improvements based on experience with existing forces. <u>I want to emphasize that the U.S. SSBN force is secure today and we know of no breakthrough that jeopardizes the security of the SSBN forces in the near future.</u>"[8]

The basis of any further negotiations on SALT II rest upon the concept of mutual deterrence and maintenance of MAD--Mutual Assured Destruction. The uncertainty to the members of the Politburo and the Soviet high command of the viability of their sea launched ballistic missiles brought on by the evolution of American ASW technology could have many possible outcomes. The Soviets may lessen reliance on their missile submarines and turn to the construction of more land-based and land-based mobile missile systems as a suitable deterrent force.

There is some suggestion that this may indeed be happening already. One result of this policy option would most likely be an increase in the deployment of missiles by the United States in response, thus raising the overall nuclear ante.

Another response by the Soviets would be to undertake a crash program in the development of their own ASW capabilities. This would, of course, be followed by the United States' development of counter-ASW technologies, and, in fact, this has already happened. The U.S. has developed such systems as SAWS (submarine acoustic warfare systems) and NIXIE[9] as well as sonobuoy countermeasures to provide evasion capabilities against a variety of acoustically targeted weapons. In other words, there would be an escalation of ASW measures followed by counter-measures and the investment of billions and billions of more dollars by both the United States and the Soviet Union without the purchase of any additional security. That cycle has already begun.

There is another dimension of the anti-submarine warfare capability deployed and in development by the U.S. which puts the Soviet Union at an additional disadvantage. Not only can we keep track of their missile carrying submarines, but we can also follow whatever hunter killer submarines they put on the tail of our missile carrying submarines. While very good from the standpoint of the protection of American Naval forces, this can only reinforce perceptions of strategic insecurity by the Soviets.

It is also becoming increasingly difficult for the United States to maintain a monopoly in the most advanced fields of anti-submarine warfare. In the May 1978 issue of Sea Technology there was not only a story of how the General Services Administration had mistakenly sold ten classified Navy sonars to a local entrepreneur for $12.00 apiece, but there was also an ad by a Silver Spring, Maryland corporation advertising custom underwater detection systems built to order to solve security problems. Incidents such as these are suggestive of the difficulty the U.S. Navy will have maintaining a lock on this type of technology which does have some commercial applications.

3. Institutional Applications--GLOMO

This brings me to my proposal regarding institutional implications of ASW technologies. Rather than continuing the acoustic race of technology and counter-technology, array and wider array, sonobuoy and counter-sonobuoy, at every increasing cost, and greater instabilities regarding national security, I propose that we make the oceans transparent to all. Instead of playing hide and seek and cat and mouse, between the Russians and the United States and any other powers that may enter the fray, let there be created a new international institution which monitors everything going on in the oceans, on the oceans, and above the oceans. The information collected would be available to anyone willing to purchase it The provision of such information could not only serve to guarantee the integrity of American and Soviet missile submarines, but would also be able to provide many commercial and economic benefits to both nation states and private interests.

What I envision is a Global Ocean Monitoring Organization (GLOMO) operated much like INTELSAT or MARISAT in which there is a peculiar mixture of government and private interests represented. In this way the United States could contract out the services provided by its existing ASW collection and evaluation nets. Other states or private interests could then buy into the technology or the services provided by the technology. In this way any nation that wanted to buy into GLOMO could obtain information about all submarines, American and Soviet, running around the world. It would then become apparent who was tracking whose submarines, how frequently, and under what conditions. Therefore, it would also be readily apparent when there was a concerted threat posed to the strategic submarine forces of either side. In this way, a deterrent force for both super powers could be preserved without a continuing escalation of non-productive investments in ocean warfare technology.

An additional benefit from GLOMO would come from the system's capability to identify any type of sound in the ocean. Not only submarine but merchant ships of every size, type, and description could be individually programmed on the massive computers employed. This would create the potential ability to identify and track any ship, anywhere, at any time. Although this can be done to some extent by satellite now, it is the acoustical signature of a particular ship's engines that enable definite identification. This tracking technology would enable shipowners and shippers to know at any time exactly where their ships are located to better program cargo routing, and to monitor fishing grounds. It could be utilized in the enforcement of pollution laws and would be invaluable in many types of rescue operations both to rescue ships in trouble and to warn other ships faced with hurricanes, tidal waves, etc. Nations could apply this capability for better enforcement of customs laws and drug laws. In fact, on a number of occasions the CAESAR system has been used, sub rosa, to assist U.S. Customs officers in the tracking and location of suspected drug smuggling vessels in the Caribbean. Scientists would also find GLOMO invaluable because it could be designed to monitor and follow movements of everything from shrimp to whales and, consequently, observe some of the secrets of marine creature migration. If and when a treaty on the law of the sea is finally signed and put into effect, the technologies employed in anti-submarine warfare could also be used to follow the operations of deep sea drilling and mining enterprises. Again, many interests--national, commercial, scientific, and even humanitarian--may be interested in purchasing the type of services that could be provided by GLOMO.

The creation of the kind of institution suggested here would not be totally unique and has been accomplished in communications and soon will be in maritime navigation. The operation of acoustical monitoring systems by such an international or shall I say transnational institution could not only better contribute to the maintenance of national security but provide a host of beneficial services. Simultaneously, the incentives for the deployment of more and more elaborate military systems in the oceans would be decreased. In this way the sea frontier may remain one of exploration rather than of conflict.

* I'd like to indicate a special thanks to William R. Cope whose help, diligence, and persistence made this article possible.

NOTES

[1] Exceptions are Tactical and Strategic Anti-Submarine Warfare by Kosta Tsipis, a SIPRI monograph, the MIT Press, Cambridge, Mass., 1974 and Richard L. Garwin, "Anti-Submarine Warfare and National Security," Scientific American, July 1972, Volume 227, No. 1, pp. 14-25.

[2] Sea Technology, May 1978, p. 7.

[3] The State, Sunday, February 26, 1978, Columbia, South Carolina.

[4] See Clyde W. Burleson, the Jennifer Project, Prentice-Hall, Inc., Englewood Cliffs, New Jersey, see especially pp. 16-17, 24-25.

[5] George C. Wilson, "U.S. Leads in Sub Hunting," the Washington Post, Sunday, May 28, 1978, p. C-2. More detailed information on the technical ASW systemsdescribed above can be found in TSIPIS, Op. Cit., the last five years of Sea Technology, in Hearings before the House Appropriations Committee, Sub-Committee on Defense Appropriations, and the Senate Armed Services Committee.

[6] See the statement of Dr. George H. Heilmeier, Director of DARPA, Hearings before the Defense Appropriations Sub-Committee of the Committee on Appropriations, United States Senate, 95th Congress, First session on H.R. 7933, Department of Defense Appropriations for Fiscal Year 1978, U.S. GPO, 1977, pp. 54-91.

[7] See statements by Dr. Curry in Sea Technology, March 1977, pp. 31-33 and statement by Dr. George H. Heilmeier, Op. Cit., and previously cited Hearings before the Senate Committee on Appropriations regarding Defense Department Appropriations for 1978.

[8] Hearings before a Sub-committee on Appropriations, House of Representatives, 95th Congress, First session, GPO 1977, Department of Defense Appropriations for 1978, pp. 213 and 214. [Emphasis mine.]

[9] See TSIPIS, p. 96.

THE ECONOMIC POTENTIAL OF THE OCEANS AND AFRICAN STATES

Penelope Simoes Ferreira
Institute of African Affairs and School of Law,
Duquesne University,
Pittsburgh, Pennsylvania 15219.

Abstract

The positions of African states are related both to substantive national economic interests and wider political goals in their approach to the development of ocean resources. The major interests of African states in coastal hydrocarbon and fishery resources and in the benefits and effects of sea-bed mining are outlined. Areas of conflict between coastal and non-coastal states, and between national and group interests, are shown, and some trends toward their resolution are indicated.

1. Introduction

The forty-nine independent countries of Africa are all developing countries, with the exception of South Africa, and with an overall per capita GNP of $370 U.S.[1] the continent is the second poorest in the world. An ECOSOC study named sixteen as among the least-developed[2] (the number has since increased), and per capita income of several, including Ethiopia, Zaire, Upper Volta, Mali, Guinea, Malawi, Niger, Rwanda, Chad, Burundi, Somalia and Lesotho, is under $100 U.S.[3] Further, the external debt of Africa, over $21 billion in December 1973[4] continues to grow. The effects of inflation have been particularly severe since all but a few countries have to import all their requirements in oil and manufactured goods. At the same time, African economies are still heavily reliant on the export of primary products and raw materials subject to, at best, price fluctuations which make systematic economic planning extremely difficult. In some cases there have been drastic declines in raw materials prices: the price of copper, on which Zambia relies for over 90% of its earnings, dropped from $1.50 a pound in 1974 to $0.60. The quadrupling of crude oil prices in 1973/4 dealt a devastating blow to already weak economies, and had a perceptible effect on national policy and on UNCLOS III, just beginning in New York - most noticeably in the shift of emphasis from the common heritage toward coastal state interests.

Within this broad framework of poverty there are wide devergencies in national wealth. The land-locked countries of Africa, of which there are thirteen[5] number among them nine of the least-developed in the world but there are also several coastal states in the disadvantaged category who are extremely poor in resources. Thus there is some conflict of interest between these states and the wealthier coastal states particularly with regard to the exploitation of coastal resources.

National economic interests also conflict with continental (Organization of African Unity) and global (Group of 77) policy goals in some areas. As members of the OAU, independent African states share a common commitment to the preservation of African unity in political affairs, and the maintenance of a common position in global negotiations. The considerable success of the African Group in the UNCLOS III negotiations in maintaining group unity attests to the strength of this commitment, but it has been severely strained by the clash between the African coastal and disadvantaged states.

As developing nations, African countries are members of the Group of 77 as well, and committed to the long-term policy goals of the Group, such as the establishment of a new economic order and world commodities policy. Membership of this group has also been a source of strength in the preservation of national interests, particularly with regard to the prevention of adverse economic effects on land-based producers of sea-bed minerals, as well as the establishment of a strong international authority.

2. Substantive economic interests in marine resources.

The three marine resources of major concern to African countries are sea-bed minerals, viewed both as a promise of benefit to developing countries generally, and a threat to African land-based producers, hydrocarbons and fisheries.

1) Sea-bed Minerals

Ever since the idea of the common heritage came into being the developing countries,

including the Africans, have stressed the importance of establishing a regime that would benefit developing states, and take into account their special needs and interests. Statements in the General Assembly, the Sea-bed Committee and regional meetings emphasized the need for a strong international machinery, empowered to exploit sea-bed resources and distribute the benefits among the needy, as well as facilitate technical training and technology transfer. However, with the growing movement towards extended national jurisdiction it became apparent that the exploitable resources would not include oil and gas but would be confined to manganese nodules for the foreseeable future. As the United Nations report of the "Economic Significance, in terms of Sea-bed mineral resources, of the Various Limits proposed for National Jurisdiction" points out[6], with national limits at 200 miles and 3000 meters (the margin limit), the petroleum production potential of the international area is about 12.50% and 7.36% respectively. Because of the great costs of operations at below 300 meters only very large fields will be viable and it is unlikely that oil or gas can be exploited economically for some decades[7]. Even as to the nodules, it was demonstrated early on that after paying for administrative and production costs the authority would have little left to distribute, at least initially.

Given these realities, the strong opposition of African land-locked and disadvantaged countries to wide national zones was inevitable. They protested these claims in OAU and Sea-bed Committee meetings, and opposed the economic zone concept unless land-locked states were given equal access to both fisheries and mineral resources in the zone. Thirteen African disadvantaged states co-sponsored the resolution which resulted in the "Economic Significance" report mentioned above, drawing attention to the erosive effect on the common heritage of extended national zones. The Kampala Declaration[8] of developing land-locked and disadvantaged states emphasized the right to exploit all resources; these concerns were repeated in the Sea-bed Committee and at the Caracas and subsequent sessions of the Conference by Uganda, Zambia and others and Draft articles providing for regional economic zones were submitted. However, African coastal states have remained firm in their opposition to the granting of rights in mineral resources. These conflicts caused a serious split in the African Group, with threats of withdrawal of all rights of access being directed against the recalcitrant land-locked. A further concession was made at the recent Geneva session regarding the surplus but it is clear that no further rights will be conceded in the economic zone.

As regards manganese nodules, not only were the prospects of economic benefits diminishing but some African land-based producers feared that sea-bed production would disrupt their export markets and cause serious price declines. The minerals concerned are copper, cobalt and manganese (nickel production is dominated by Canada, New Caledonia and the Soviet Union), and the countries most affected are Zambia, Zaire and Gabon.

Copper exports accounted for 93% of Zambian and 73% (80% in 1975) of Zairean total exports in 1974[9]. Both countries have suffered severe economic disruption by the drop in copper prices since 1974 and have attempted unsuccessfully to reverse the trend. Together with Peru, a 15% reduction in output has been put into effect, and Zaire has gone so far as to purchase copper on the London Metal Exchange to make up for shortages to its customers[10]. As a result there have been some increases of copper prices but they still stand at about 60 cents a pound, up from 55 cents in February. Clearly, such effort by CIPEC (Inter-Governmental Council of Copper Exporting Countries) to shore up copper prices has been ineffective, partly because Chile, the fourth member of the Council, has lower production costs than the others. Any substantial increase in production from sea-bed sources is likely to pose a considerable problem to the Zambian and Zairean economies. However, estimated sea-bed copper production in the first decade is in the region of 1.3% of total world demand,[11] and such a low production increase is unlikely to cause a substantial drop in prices.

Manganese is produced in Africa by South Africa, the largest world producer (over 3½ million metric tons in 1974), Gabon (over 2 mill. metric tons), Ghana (over 300,000), Zaire (over 300,000) and Morocco (about 150,000)[12]. It is a major export earner for Gabon - 27.5% of total exports in 1972, 11.7% in 1973. However, as these figures indicate, Gabon has been able to diversify, largely due to increased earnings from petroleum production: export earnings from petroleum, at $804 U.S.millions in 1974, far exceeded manganese earnings of $42 million in the same period[13]. Nevertheless, United Nations estimates that nodule manganese production may amount to 13% of world demand in the first decade indicate that manganese prices will drop considerably. Further, the uncertainties surrounding sea-bed manganese production affects long-term planning decisions and contributes to economic disruption.

Sea-bed cobalt production is likely to have

a significantly greater impact - United Nations reports indicate that cobalt from nodules will account for over one half of world demand in the first decade and reduce prices to two-thirds of present levels[11]. As cobalt export earnings amounted to 10.4% and 8.7% of Zaire's total exports in 1973 and 1974 (the figures for Zambia and Morocco are between 0.8% and 0.6% respectively), the effect could be serious for the Zairean economy. One estimate puts the decline in export earnings at about $88 million a year[15].

Hydrocarbons

The growth of offshore oil and gas production in Africa has been very rapid. With virtually no production in 1961, by 1972 oil from Africa, particularly Nigeria, Gabon, and Angola, was 13% of total world output, at 309.4 million barrels[16]. Over one hundred new offshore wells were drilled in 1972 and 1973, and the quadrupling of crude oil prices coupled with technical advances making feasible drilling at great depths further stimulated exploration efforts. In 1974 Nigerian daily oil output averaged 2 to 3 million barrels. For each barrel of oil produced about 1000 to 2000 cubic feet of natural gas was "flared" or burned and wasted, largely because of the huge capital outlays required for gas storage and transportation to the markets in Europe and the United States. However, Nigeria is now making a considerable investment in gas production: $2.2 billion in being spent on two gas liquefaction plants, and ten or twelve ships with insulated containers, each costing $50 million, will be used to transport the gas to the U.S.[17].

Since offshore hydrocarbon potential relates to the width of the continental margin and the thickness of sediments, it is not surprising that production potential in Africa, with relatively narrow continental margins[18], is in the medium potential (17 countries), low potential (10) or no potential (16) categories. Only one country, Libya, is in the high potential category[19]. Further, the countries with low or no potential are among the poorest in Africa. In view of the high production costs at greater depths, these countries have little or no chance of benefitting from their own areas. This explains their emphasis on the common heritage and the international area, their opposition to extended national zones, and demands for a share in the resources and revenue sharing. These objectives conflict with those of African coastal states with viable hydrocarbon potential, and in fact have been virtually overridden by the numerical strength of coastal states at UNCLOS III. A 200 nautical mile economic zone is a fait accompli in the ICNT, and the continental shelf limit is defined in Article 76 as "the outer edge of the continental margin or to a distance of 200 nautical miles...where the outer edge... does not extend up to that distance"[20]. As regards revenue sharing, the only obligation of the coastal state relates to revenues from beyond 200 miles, payments to begin after the fifth year of production at a rate of 1% a year increasing to a maximum of 5%. As production starts to decline after about five years the revenues generated under this provision are a far cry from the idea of the common heritage. Although this issue is still the subject of negotiation, the discussion on the subject at the 1978 Geneva session were concerned with defining the margin, not restricting the limits.

Fisheries

Except for tuna, the important fishery resources (pelagic, demersal and crustaceans) of Africa are concentrated on the continental shelf. The richest fishing grounds are found in areas of seasonal upwellings, particularly in the CECAF (East Central Atlantic) area from Mauritania down to Guinea and in the Gulf of Guinea in part, the ICSEAF (South East Atlantic Region) area around the South West coast, and northern Kenya and Somalia[21]. Thus the richest fishing grounds are found off desert coasts with low populations and little traditional fishery industry, while the most highly populated states such as Ghana, Nigeria and Ivory Coast have relatively poor resources. The latter countries apart from their local artesenal fisheries, have traditionally fished off the coasts of their neighbours; several, including Algeria, Cameroon Ghana, Nigeria, Ivory Coast, Senegal and Mauritania, are expanding their medium and large fleets[22]. The most severe constraints on the development of fisheries are the high costs, the lack of the basic infrastructure of shore-based facilities and trained personnel, and the lack of information-gathering mechanisms.

The rapid growth in catch in the Atlantic, and to a lesser extent in the Indian Ocean as well, has brought the additional problem of over-fishing. In the CECAF area the catch increased over 150% from 1964 to 1972, but the main beneficiaries are non-coastal states. The Soviet Union, Spain, Japan, South Africa and Norway increased their catch by 240%, compared with a coastal-state increase of 70%. Senegal, with the most important fishery in West Africa, took only 8% of the catch in 1971, compared with the Soviet Union catch which almost equalled the combined catch of all West African countries north of the Congo[23]. In the ICSEAF area,

traditionally dominated by the three coastal states, Angola, Namibia and South Africa, the Soviet catch increased from 167 thousand metric tons (tmt) to 423 tmt between 1964 and 1970. The same pattern is evident in the Indian Ocean where the Soviet catch showed an explosive growth from 4.6 tmt to 242.4 tmt in 1971. By comparison, the coastal state with the greatest catch in the area, Tanzania, took only 28.6 tmt in the same period.

Viewing these foreign fishing activities as an unjust plundering of their resources, African coastal states took steps to gain control over their marine areas by claiming extensions of national jurisdiction. Between 1970 and the Caracas session of the Conference in June 1974 fourteen African states extended their territorial sea limits[24]. Three claims were beyond or up to 100 miles: Gabon (100 miles), Sierra Leone (200 miles) and Somalia (200 miles). Morocco and Senegal claimed exclusive fishing zones of 70 and 132 miles respectively.

The pace of unilateralism slowed down somewhat after the Caracas session, although the countries that gained independence in that period were quick to assert wider limits than those prevailing under colonial rule. Guinea-Bissau and Cape Verde claimed territorial seas of 150 miles and 100 miles respectively, Angola established a 200 mile exclusive fishing zone and Comoros and Benin 200 mile economic zones. In 1976 Senegal again extended its national jurisdiction, this time in claiming a territorial sea of 150 miles, while establishing the continental shelf limit at 200 miles[25] While it can be argued that these claims merely reflect the consensus on coastal state rights at UNCLOS III they also establish a pattern for the future, even in the event that no treaty results.

The efforts of the land-locked and disadvantaged states to obtain rights to exploit living resources in coastal zones of neighboring states have been marked by some success at UNCLOS III. Articles 69 and 70 of the ICNT[20] provide for the participation of developing land-locked and geographically disadvantaged states in the exploitation of living resources, conditional on agreement with the coastal states concerned. However, the coastal state is empowered to determine the allowable catch and is obliged to give other states access to the <u>surplus</u> only. Even this is only after taking into account its own economic and other national interests (Article 62). In view of this provision the coastal state may well grant licenses to the highest bidder, thus obtaining maximum benefits for its own economy. As the highest bidder is likely to be a developed distant-water state[26], the result will be the effective exclusion of neighboring states. Seeing their rights under these provisions as being largely illusory, the land-locked and disadvantaged pressed for preferential or priority participation, and called for amendments to Articles 69 and 70 to include express reference to that effect. Coastal states on the other hand, contended that such preferential rights were implicit in these two articles. In the recent Geneva session Negotiating Group 4 was established to deal with these problems and a compromise formula was reached.[27] Article 62 was amended to read "...(Where the coastal State does not have the capacity to harvest the entire allowable catch)...it shall... give other States access to the surplus of the allowable catch <u>having particular regard to the provisions of articles 69 and 70, especially in relation to the developing States mentioned therein</u>." Articles 69 and 70 are amended to provide for access of the land-locked and disadvantaged to "<u>an appropriate part of the surplus</u>" of the living resources of economic zones of coastal states "in the <u>same subregion or region</u>", and the interests and needs of both coastal and disadvantaged states that are to be taken into account are specified. Further, where the coastal state is approaching the point of being able to harvest the <u>entire</u> allowable catch it is now obliged to establish equitable arrangements for the participation of developing land-locked States (and developing States with special geographical characteristics) of the same region or sub-region, as appropriate. As explained by the Chairman of the Negotiating Group in his explanatory memorandum, this provision will enable developing land-locked and geographically disadvantaged states to have adequate participation in any joint ventures established. This provision thus goes a long way to alleviate the fears of the land-locked that they will be excluded when the coastal state is able to harvest the entire catch in joint ventures with distant water states.

3. Continental and Global Policy Goals.

As mentioned above, African states policies in relation to the development of marine resources have also been influenced by their membership of the OAU and the Group of 77.

For some time prior to UNCLOS III efforts were made to develop a unified continental position on law of the sea issues. The OAU first stated its position in three resolutions issued by the Council of Ministers in June 1971[28]. These resolutions stressed the need to harmonize African positions so as to maximize the impact of African states as a group in negotiations. The right of states to exercise permanent sovereigny over their natural resources, including the resources of the superjacent waters of the

continental shelf, so as to "further the economic development of African coastal states" was proclaimed. These resolutions mark a clear shift of emphasis from the common heritage toward coastal state rights.

The resulting protests of African land-locked countries in the OAU led to a search for a compromise, which was found in the economic zone concept. This concept was initiated by Kenya at the January 1972 meeting of the Afro-Asian Legal Consultative Committee and in the Kenyan Draft Articles on the Economic Zone concept submitted to the Sea-bed Committee in August the same year[29]. It was further developed in the African States Regional Seminar on the Law of the Sea held in Yaounde, Cameroon, in June, 1972,[30] and adopted by the OAU Declaration on the Issues of the Law of the Sea in May 1973[31].

The economic zone was conceived as not merely a resource-management zone; although it provided for coastal state sovereignty over both living and non-living resources, jurisdiction over scientific research and pollution control were also prescribed. Similar to the patrimonial sea concept outlined in the Declaration of Santo Domingo in June 1972[32], it contains two essential differences: neighboring land-locked and disadvantaged countries are given specific rights of access to the sea and to living resources in the zone, and continental shelf limits are fixed at the limit for the economic zone, 200 miles. These provisions both represent a concession to the interests of non-coastal and disadvantaged states members of the OAU.

On the international area the position of African states is a unified one. The OAU Declaration firmly supported the common heritage principle and the Declaration of Principles, and stressed the need for international machinery with strong and comprehensive powers of direct exploitation and regulation. Further, the Authority was to be empowered to control sea-bed mineral production so as to minimize adverse economic effects on land-based producers, and to distribute the benefits from sea-bed production to developing countries, particularly the most needy. Control over scientific research and environmental protection in the area was also provided for.

The position of the OAU on sea-bed resources corresponds to that of the Group of 77: in all areas where the interests of developing states are concerned the positions of the African Group and the Group of 77 converge. This fact has contributed to the considerable strength of the developing countries in protecting their interests in the common heritage at UNCLOS III, despite the fact that the industrialized countries are in exclusive possession of the technology and finance.

Further, African states, particularly Algeria, Tanzania and Mauritania, have actively promoted the efforts of the Group of 77 to establish a new economic order. The link between the sea-bed and world commodities policies was first established in the Committee I negotiations but by Geneva in 1975 it was being extended to areas in the other committees as well, where possible trade-offs in relation to such issues as straits were discussed. It is clear that the new international economic order is regarded as a substantive issue that is an integral part of the negotiations by many African states, not only the radicals among them. As a result, there was a noticeable hardening of attitudes in the Group[33].

4. Conclusion.

As shown above, African interests in the development of marine resources conflict in some areas and converge in others. In the areas of conflict considerable effort has been made by the African Group to reconcile divergent interests and the present status of the ICNT as amended in the recent Geneva session represents the considerable success achieved. In the areas where national and group interests converge, group membership of the African Group and the Group of 77 has played an important part in enabling African states to get a treaty that protects their interests.

References

1. World Bank, 1977.
2. Burundi, Central African Empire, Chad, Benin, Ethiopia, Gambia, Guinea, Lesotho, Malawi, Mali, Niger, Rwanda, Somalia, Sudan, Tanzania Upper Volta. E/AC.54/L.72, cited in L. Alexander and R. Hodgson, "The Role of the Geographically Disadvantaged States in the Law of the Sea", 13 San Diego Law Review, 1976, pp.558-582.
3. Colin Legum, ed. African Contemporary Record 1975/6.(New York: Africana Pub.Co.1976) 129.
4. Examples of external public debt figures as of December 1973, in $US millions: Algeria 4,788; Egypt 1,746; Zaire 1,016; Morocco 978.5; Tunisia 818.9; Nigeria 707; Ghana 615.4; Ivory Coast 566; Zambia 535. Source: World Bank, External Public Debt Outstanding in 86 Developing Countries, December, 1973.

5. Land-locked: Botswana, Burundi, Central African Empire, Chad, Lesotho, Malawi, Mali, Rwanda, Swaziland, Upper Volta, Uganda, Zambia Niger.
24 have limited coastlines: Congo, Benin, Gambia, Mauritius, Sao Tome & Principe, Togo, Zaire, Seycheiles, Comores (-100 miles) Cameroon, Equatorial Guinea, Guinea (100 - 200 miles); Cape Verde, Gabon, Ghana, Guinea Bissau, Ivory Coast, Kenya, Liberia, Mauritania, Nigeria, Senegal, Sierra Leone, Sudan (200-500 miles).
Small continental margins/Economic Zones: Togo, Zaire, (under 1000 sq. meters); Cameroon (100-5000), Congo, Benin, Gambia (5000-10,000). Comores, Seychelles.
Shelf-locked: Ethipia, Sudan.
Zone-locked: Zaire.
Many African states are small island states.
Source: Alexander and Hodgson, supra n.2.

6. A/AC.138/87, June 1973. GAOR 28th Session, Supplement No. 21 (A/9021).

7. UN Sec. Gen. "Economic Implications of Sea-bed Mineral Development in the International Area", Doc. A/CONF.62/37, 18 Feb. 1975, reprinted in 4 UNCLOS III, p.122.

8. A/CONF.62/23, 2 May 1974, in 3 UNCLOSIII, p.3

9. IMF, International Financial Statistics, cited in D. Leipziger and J.Mudge, Sea-bed Mineral Resources and the Economic Interests of Developing Countries. (Cambridge, Mass.: Ballinger, 1976) Table 5-3, p. 134.

10. Wall Street Journal, April 11, 1978, p.38.

11. UN, Reports of the Secretary General, Doc. A/CONF.62/25, May 1974, 3 UNCLOS III Doc. A/CONF.62/37, Feb. 1975, 4 UNCLOS III, 122

12. Bureau of Mines, Minerals Yearbook (1973/4) and Commodity Data Summaries (1974, 1976) cited in Leipziger and Mudge, supra n.9, p 125

13. ibid, p. 136.
14. Ibid. p.20

15. Ibid. p. 163

16. Ibid, p.6.

17. Ibid, p.21, note 18.

18. the average is about 30 miles, with variations from 5.8 miles off Benin, Togo, Ivory Coast, to more than 100 miles off Guinea and Guinea-Bissau, for example.

19. Leipziger and Mudge, op cit, Table 1-5, p.23
Medium Potential: Angola, Cameroon, Egypt, Ethiopia, Gabon, Ghana, Guinea, Ivory Coast, Malagasy Republic, Mauritania, Morocco, Mozambique, Nigeria, Senegal, South Africa, Tanzania, Tunisia.
Low Potential: Benin, Congo, Gambia, Guinea-Bissau, Kenya, Liberia, Sierra Leone, Sudan, Togo, Zaire.
No Potential: the thirteen land-locked countries plus Algeria, Mauritius, Somalia.

20. Informal Composite Negotiating Text, Doc.A/CONF. 62/W.P.10, 15 July, 1977.

21. F. Christy, Transitions in the Management and Distribution of International Fisheries (Washington, D.C., Resources for the Future, 1977); J. Crutchfield and R.Lawson West African Marine Fisheries (RFF, 1974) A. Tussing and R.Hiebert, Fisheries of the Indian Ocean, (RFF, 1974); E. Bayagbone, "Alternative Legal and Economic Arrangements for the Fishery of West Africa", Proc. of the 7th Annual Conference of the Law of the Sea Institute, Kingston, R.I.1972

22. Christy, op.cit., p. 245

23. Crutchfield, op.cit, p.9

24. Territorial, Sea, 12 miles: Equatorial Guinea, Tunisia, Zaire; 30 miles: Congo, Ghana, Mauritania, Mauritius, Nigeria.
50 miles: Gambia, Madagascar, Tanzania.
100 miles: Gabon (1972);
200 miles: Sierra Leone, Somalia.

Exclusive Fishery Zones: Morocco (70 miles) Senegal (132 miles).

Source: U.S. Office of the Geographer, Limits in the Seas, no.36 (Washington, D.C. 1973, December 23); see also R.Smith and R. Hodgson, "Unilateralism: the Wave of the Future?", in E. Miles and J.K. Gamble(eds.) Proc. of the 10th Annual Conference of the Law of the Sea Institute, University of Rhode Island, (New York:Ballinger, 1977), 146.

25. Ibid (Limits in the Seas)

26. Christy, op.cit., p. 251.

27. NG4/9/Rev.2, and Explanatory Memorandum by the Chairman of NG4, NG4/10, in UNCLOS III 7th Session, Geneva, Report of the Committees and Negotiating Groups, 19 May, 1978

28. B. Buzan, Sea-bed Politics (N.Y.:Praeger, 1976), pp.184-5.
29. A/AC.138/S.C.II/L.10, August 7, 1972, reprinted in I.L.M. Vol.XII, 1973, p.33.

30. Reprinted in Int.Leg.Mat.(XII), p. 210.
31. Reprinted in 3 UNCLOS III (1975), p.63.
32. Reprinted in ST/LEG/SER.B/16 (1974), p.599.
33. E. Miles, "The Structure and Effects of the Decision Process in the Seabed Committee and the 3d. UN Conference on the Law of the Sea" 31, Int'l Organization (Spring, 1977) 159.

SATELLITE IMAGERY AND THE GEOMORPHOLOGY OF BERMUDA

S. A. Ashmore
Geography Department
University of Maryland
College Park, Maryland 20742

Abstract

LANDSAT multispectral scanner (MSS) imagery provides a unique tool for investigations of coastal and shallow-water geomorphology. Small scale patterns (1 to 10^2 kilometers) are much easier to detect from a vantage point in space than they are from the ocean surface or from conventional aircraft photos.

The extensive Bermuda platform has been a puzzle in geomorphology for many years. Recent LANDSAT scenes have allowed the development of a new hypothesis which can be checked by conventional geological and geophysical field investigations. The hypothesis states that the gross morphology of subaerial and submarine Bermuda resulted from lateral transportation of sediments and that modern analogs of Bermuda's relict spits and bars can be found along many other coastal areas.

1. Introduction

Central to the progress of science is the generation of ideas which can be converted to hypotheses and tested. Often what is needed to generate such ideas is to look at an old problem in a new way or from a different "viewpoint". Remote sensing in general, and LANDSAT in particular, has been remarkably successful in providing a different perspective in both the subaerial province and to an increasing extent in submarine areas. The unique advantage of high orbital LANDSAT imagery over low altitude or surface investigations is that with decreased scale, oceanographic and geomorphological patterns, which were previously undetectable, become apparent.

Such was the case in Bermuda where inspection of a LANDSAT band 4 image led to the formulation of the "spit hypothesis" which is now being tested by seismic surveys, coring, and submarine drilling. The spit hypothesis was from its inception controversial and is by no means proven and is only one of several viable hypotheses in the explanation of Bermuda's submarine morphology. The intent of this paper is not to prove or disprove any of the conflicting ideas but rather to show how an idea derived from orbital spacecraft imagery can be investigated employing the latest techniques available to submarine scientific investigators.

2. The Spit Hypothesis

Figure 1 is an annotated band 4 image obtained on 23 March 1976 by LANDSAT 2. The particular advantage of band 4, of course, is that the sensor in the blue-green portion of the spectrum penetrates up to 20 meters of clear water. The cloud patterns present are a deterrent to interpretation of submarine morphology but very useful as an example of the effect of rising air over an isolated island. It is the pattern of recurves (here labeled relict spits), however, that is of primary interest. Particularly engaging is the similarity between the submarine "hook" at the lower left and the subaerial, hotel encrusted, one on the right. The smaller hook in the center follows a log spiral pattern which is characteristic of spits formed by wave refraction.

What were obviously spits to one geomorphologist, however, proved to be less convincing to others, particularly those who have long considered Bermuda a classic example of calcareous dune formation. To these geologists the recurves were merely concentric sand dunes piled up by the wind and not recurved spits formed by the action of waves and currents.

3. Testing The Hypothesis

Fortunately Peter Garrett, an investigator from the University of California, Santa Barbara, found the spit argument compatible with a barrier island hypothesis he had developed to test against other ideas which included the sand dune, the volcanic cone, and the karst solution hypotheses. Very briefly, the sand dune theory argues that Bermuda's islands and submarine ridges owe their basic shape to dunes piled up during prior glacial sea-level changes. The volcanic cone school holds that the proven existence of an extinct volcano about 80 meters below sea-level exerts a primary influence on the present geomorphology. The karst solution idea is supported by similarities between Bermuda and other sink-hole topographies.

In May 1978 a sub-bottom survey, using a EG&G Uniboom high resolution seismic profiling system, was run on the Bermuda platform as part of the

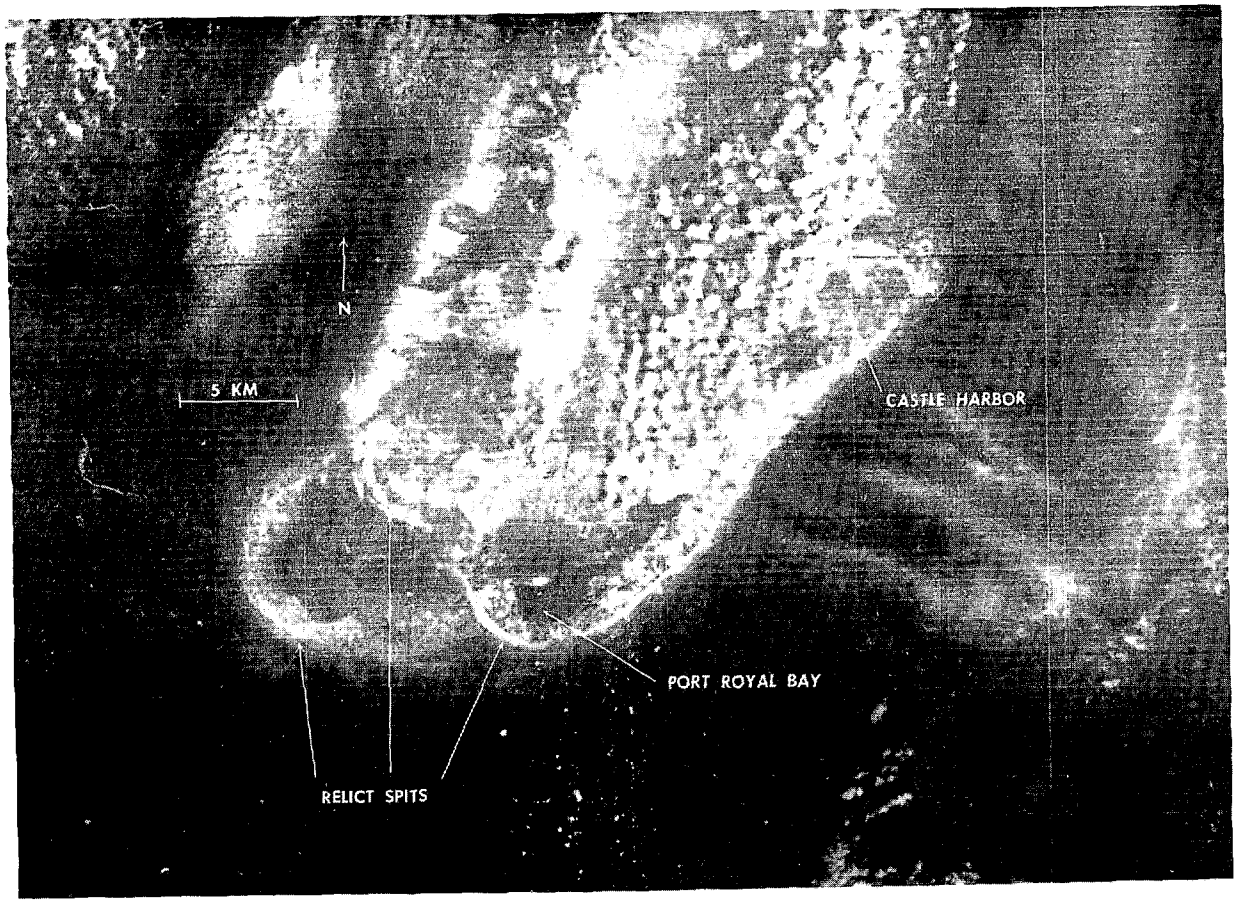

Figure 1. LANDSAT (MSS 4, 3/23/76) imagery of Bermuda

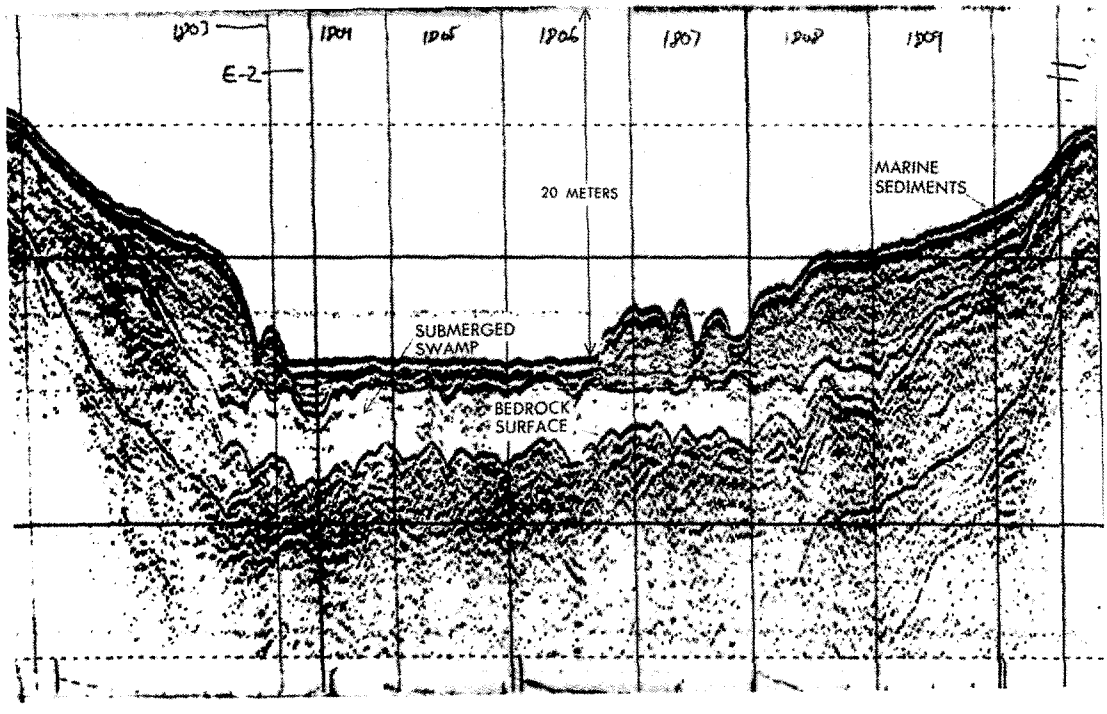

Figure 2. South to North sub-bottom profile across Port Royal Bay, Bermuda. Feature labels are based on insufficient data and are therefore tentative.

Peter Garrett study. The Uniboom was operated by Albert Hine of the University of North Carolina. The excellent data obtained from this survey disclosed a myriad of previously unknown buried "landforms" which required further investigations. One such area, Port Royal Bay (figure 2), is presently under intensive investigation by the author. Here the seismic instrument recorded a very unusual acoustically "transparent" layer which is tentatively called the Port Royal Swamp.

To further explore the unusual Port Royal Bay profile, an ingenious instrument, devised by the paleoclimate group at the University of Wisconsin, to study lake bottom sediments was used. This corer (figure 3) is simply a pointed pipe which is filled with dry ice (solid CO_2) and alcohol. A cap with an escape hole for excess CO_2 is fitted to the open end and lines are attached for retrieval. Allowed to free-fall into soft sediments it gives up to 2 meters penetration. After about five minutes in the bottom the pipe is recovered with several centimeters of sediment frozen to the outside. Once the dry ice/alcohol mixture is emptied, sea water poured into the pipe allows the "core" to be slipped off the pipe and retired to the ice box for later study. Since the sediment layers are up to 10 meters thick, however, additional work with a conventional vibracorer is also planned.

The reef areas and rock layers of the Bermuda platform necessitated the use of a submarine core drill. The devise used was developed by Eugene Shinn of the U. S. Geological Survey and is operated on the ocean floor by SCUBA divers. The machine is powered hydraulically from a surface launch. Drilling, which is not yet complete, disclosed a surprising depth of recent coral growth on the outer reefs. This is somewhat in conflict with the spit hypothesis which assumed lateral transport of sediment rather than reef growth as the dominant morphological agent.

Whether or not the spit hypothesis is substantiated, the use of LANDSAT imagery has proven its value in idea generation which is the prime ingredient of any submarine scientific research project. While the space program and submarine research are usually pictured as being competitors, it seems apparent that remote sensing from high earth orbit will be a significant factor in many future underwater investigations.

Figure 3. Sediment probe

UTILITY OF POLARIZED VISIBLE RADIATION IN OCEANOGRAPHY

Harold V. Soule
OAO Corporation
50/50 Powder Mill Road
Beltsville, Maryland 20705

Abstract

In a brief manner what is presently known about the polarization of visible radiation over oceanographic environments is presented. This data indicates that present sensors are not recording all of the radiation information available so considerable radiometric information is being ignored.

Over oceans, surface reflected and underwater scattered radiation is quite highly polarized. A review of the overall ocean radiance gives an idea of the characteristics of the Stokes parameters which completely describe remotely sensed radiation characteristics. Conclusions and an evaluation of the potential utility of imaged Stokes parameters is made.

Proposed research on the feasibility and proof of concept of a relatively simple sensing and imaging technique is outlined.

1. Introduction

Most remote imaging sensors are not measuring all of the radiation information coming from the ocean environment. The purpose of this paper is to review the reasons why additional measurements should be made and propose a simple experiment which would indicate a way in which many of the objectives of remote oceanographic sensing could be more easily and reliably attained.

Over a century ago Stokes developed a set of four parameters completely describing the overall characteristics of radiation.[1] Imaging of these parameters can and has been done.[2] They represent the present commonly measured spectral radiance, the degree of linear polarization and its orientation, and if circular, the degree and its rotational direction. Thus, the complete characteristics of incoherent radiation are described.

Although sunlight is essentially not polarized, when it interacts with matter it becomes partly polarized. All matter selectively absorbs and reflects radiation dependent upon the e-vector orientation with respect to the material surface. The amount that radiation is polarized is also dependent upon the angular direction in which it is reflected. In remote sensing these angles can be determined. In oceanographic environments selective e-vector reflection and scattering is quite large and if imaged in the same manner as, for instance, Landsat, it should greatly aid in radiometric/physical phenomena correlations.

One basic remote sensing goal of most oceanographic earth research scientists is determining whether there is a high correlation between imaged radiometric data and physical phenomena. Using the radiation information currently being recorded, a number of spatial and temporal varying parameters plus sensor-produced errors makes the probability of a high correlation of similar phenomena over wide areas, quite small. In general, ground truth/remote sensor data has shown a high correlation only on a very limited spatial and temporal basis (i.e., a few dozen acres and a few successive clear cloudless days).[3] Over land areas this has resulted in the need for a very large number of ground truth sites.[4] Weather, atmospheric, and aerosol effects which are variable and difficult to estimate or measure are all responsible to some extent for this type problem.[5] However, the situation can be improved by measuring all of the reflected radiation information.

A method of recording and imaging all of the Stokes parameters which will permit immediate and rapid evaluation of their utility is proposed. The principal objective will be to determine whether there is a high correlation between widely separated, similar target areas and the imaged Stokes parameters. In addition, any advantages resulting from using differences and ratios in the polarization equations, thus reducing the many unknowns present in the first Stokes parameter to second order effects, should be investigated.

Display and manipulation of the first Stokes parameter is common practice. A number of techniques which will effectively display vector lengths and orientations in black and white or color have been developed. In the initial studies, high radiometric accuracy would not be feasible or necessary to establish whether really useful oceanographic information was being rerecorded.

In oceanographic remote sensing the characteristics of the water surface, underwater phenomena and in shallow water, the ocean floor are of interest. Correlation of reflected, scattered, and transmitted solar radiation with the characteristics of these oceanographic phenomena is a very difficult and expensive problem. There are so many factors involved, that in a short paper all that can be done is to put available oceanographic polarization literature into perspective.

2. Overall Oceanographic Radiances

Less than half the horizon-to-horizon ocean area will permit underwater phenomena viewing. As indicated by Plass and his associates in the typical horizon-to-horizon diagram (figure 1), solar glare and skylight reflection exceed the underwater radiances and polarization in the rest of the area. As indicated in figure 2, even in the area which permits underwater viewing, skylight and sunlight surface reflections are still present, producing image noise. Polarization filtering, eliminating some of the polarized ocean surface reflections, should greatly enhance the useful underwater signal to noise ratio.

3. Wind/Wave Phenomena

Polarized reflected solar radiation dominates a portion of the central area in figure 1; its position is dependent upon the sun's elevation. Several studies have been made of the possibility of determining wind speed and direction based upon the extent and characteristics of the solar glare pattern. It is quite probable that because of their nature, the imaged Stokes parameters will greatly improve the chances of success in this type investigation.

4. Underwater Phenomena

An overall indication of the characteristics of underwater polarization (see figure 4) was given by Waterman quite some time ago. The downward transmittance of polarized radiation by the water surface is also indicated in this figure, suggesting that underwater polarized radiation will be transmitted to the atmosphere with little attenuation or change.

The amount of underwater polarization and its orientation are highly dependent upon the physical characteristics of water suspended materials. The sun and observation angles are also quite important but these angles are known and their influence on the physical/optical correlation can be predicted.

Although no remote oceanographic imaged Stokes algorithms are available in the literature, a number of underwater polarization measurements have been made during the past few decades. Those made by Waterman and Westell in figures 3 and 5 indicate the change in e-vector orientation as a function of solar bearing. Figure 6 indicates the typical correlation between sea water scattering coefficient and the degree of polarization at right angles to incident solar radiation. It will be noted that up to 80% polarization was measured by Ivanoff in the Western Mediterranean.

A number of conclusions can be drawn from these and other underwater measurements:

- Daylight reaching any observable submarine point from all possible directions has been found to be partially polarized.[8]
- Most underwater polarization phenomena is produced by irregular particles having a size distribution from that of the wavelength of light to over a factor of two larger.[9,10]
- The percent polarization is in the 10 to 75% range and is variable depending to some extent upon water clarity.[9]
- The e-vector orientation is dependent upon sun orientation and is predictable.[7]
- At near-shore locations elliptical polarization is present underwater.
- Polarized skylight is as prominent underwater as it is above the water surface.[5]
- It has been possible to differentiate between Mediterranean and Atlantic Ocean waters flowing back and forth between these two bodies of water using their polarization characteristics. No similar information was available in their radiances.[10]

A surprising aspect of underwater polarization is the fact that surface effects do not appear to influence it. On the basis of surface polarization physics, one would expect a large increase in the vertical e-vector component and vertical polarization underwater. It has never been observed. Because of this and refraction effects, a considerable difference between surface and underwater phenomena should be noted when all of the Stokes parameters are imaged and analyzed.

5. Surface Reflected Skylight

Very little published data exists on the characteristics of polarized skylight reflected from the water surface. The percent polarization reflected is almost independent of e-vector orientation. The only exception is at the critical angle for radiation having its e-vector oriented parallel to the principal plane. It is quite probable that elliptical polarization is present but has never been recorded in the literature.

It is very difficult to predict the potential utility of Stokes images of ocean surface reflected skylight when no data exists and correlation with physical phenomena is thus impossible.

6. Potential Utility Summary

The additional radiation information produced by imaged Stokes parameters should aid in the determination of:

- o Surface wind speeds and possibly direction.
- o Subsurface suspended particulates.
- o The relative concentration and nature of pollution.
- o Ocean current characteristics, location, boundaries, etc.
- o Near-shore bottom characteristics.
- o Deeper water characteristics than currently feasible should be recorded because of the reduction of surface reflection interference effects.

The second, third, and fourth Stokes parameters are essentially the difference between two measurements of the same target points. This radiation travels both to the target and then to the sensor along the same atmospheric paths. As a result, the effects of angular reflection changes (bidirectional reflection) should be greatly reduced compared to standard radiance measurements, (the first Stokes parameter). The effects of changes in atmospheric transmittance and path radiance for each target area should also be small. These effects are one of the principal factors causing diffulty in correlating physical phenomena with radiation for widely separated similar targets at present.

Sky polarization effects due to Rayleigh and Mie scattering can be predicted. This type polarization is added to the sensor-received signal directly and via ocean surface reflection. A number of presently unknown factors will make it necessary to undertake theoretical and experimental studies of this problem.

7. Stokes Algorithm Imaging

Stokes vector imagery using data taken through polarized filters is relatively easy to implement. Using standard computer techniques the results can be made to appear the same as any synthetic photographic image product.

A beam of incoherent radiation can be completely described at any given wavelength by the Stokes parameters:[11]

$$\begin{vmatrix} L_o \\ L_1 \\ L_2 \\ L_3 \end{vmatrix}$$

Where L_o is the commonly measured radiation intensity. L_1, L_2, and L_3 are observables describing independent features of the e-vector. L_1 gives the vector length and L_2 the angular displacement of the vector. L_3 represents the degree and rotational direction of circular polarization.

Perhaps the simplest method of determining the additional radiometric information is to take calibrated photographs of the scene at several different wavelengths using a plane polarized filter at four (Θ) orientations.

The film density (ρ) recorded in each of the four photographs can be related to the polarized radiation intensity and used to determine the Stokes parameters in a given wavelength region. The Stokes vectors are determined as follows:

$$L_o = \Sigma L_{(\Theta)} \text{ or } \simeq \Sigma\rho\Theta$$

$$L_1 = L_{(0^o)} - L_{(90^o)} \text{ or } \simeq \rho_{(0^o)} - \rho_{(90^o)}$$

$$L_2 = L_{(45^o)} - L_{(135^o)} \text{ or } \simeq \rho_{(45^o)} - \rho_{(135^o)}$$

L_3 = circular polarization rotational direction and amount.

Each photograph in a set of four, taken at e-vector polarization angles related to the plane of the sun/target area/sensor (the principal plane), is scanned and digitized. Correction should be made for the film radiance measuring nonlinearities*. Then the equations are used to compute the intensity and polarization of each pixel of the image.

When discussing polarization, it is much easier to think in terms of the magnitude, P, and the phase angle Θ_o, of the polarization. These values can be determined in the following manner:

$$P = (L_1^2 + L_2^2)^{\frac{1}{2}}/L_o \simeq \text{the normalized polarization.}$$

$$\text{and } \Theta_o = \tan^{-1}(L_2/L_1) \simeq \text{the phase angle of the Stokes vector.}$$

The two (P and Θ) values should be computed on a corresponding pixel-by-pixel basis using data from each of the four pictures. There are a number of ways of displaying and recording vectors, both in black and white intensities and in color.

---

*The radiation response of film is not linear so corrections should be made, particularly at high and low radiances. Film has no known selective sensitivity to radiation polarization.

8. Comments and Summary

As indicated in figure 7, almost the entire oceanographic physical environment produces partly polarized radiation. In that the degree and e-vector orientation of the sensed radiation will vary as a function of its origin, wavelength, and other parameters, its physical phenomena correlation utility should offer a considerable improvement over present remote sensing techniques.

It should be noted that past unsuccessful attempts to apply polarimetry information to various types of earth resource work have had about the same difficulties as those which have prevented the widespread application of high accuracy radiometric information to this type work. There are pointing, calibration, and temporal error problems which do not greatly effect the utility of Landsat-type image data. In earth resource imaging, the lack of a high correlation between exact radiometric measurements and image target measurements has not impeded the wide range of utility of this type earth resource data.

The prime utility of Landsat data is based on relative contrast changes in various narrowband spectral regions. Atmospheric effects, in addition to its polarization sensitivity* at the longer wavelengths, make high recorded radiometric accuracy impossible. It is therefore proposed that the same philosophy be used in the generation of the Stokes parameters using film in the initial studies. Without this type data it is impossible to determine the real utility of using these type algorithms in determining any possible correlation between all of the radiometric information and the physical phenomena producing it.

In initial studies considerable low altitude flight data which can be correlated with in situ physical measurements will be required. A number of opportunities will be available if the underflight/ship measurement programs such as those planned for the Nimbus G Coastal Zone Scanner are implemented.

* To enhance its near-infrared imaging capabilities, multiple reflection in the photomultiplier faceplate was used. Since there was nothing in the specification limiting polarization sensitivity, this parameter was never measured in Landsats 1 and 2.

References

1. Stokes, G.G., Trans, Camb, Phil. Soc., 9, 399 (1852).

2. Walraven, R. "Polarization Imagery", Proc. of Soc. of Photo-Opt. Instr. Engrs, V. 12, Optical Polarimetry, p. 164 (Aug 1977).

3. Nalepka, R.F. and J.P. Morgenstern, Signature Extension: An Approach to Operational Multispectral Surveys, ERIM 31650-152-T NASA JSC Earth Observations Div. NAS9-9784.

4. Grandfield, A.L. Large Area Crop Production Inventory Acreage Estimation (LACIE) NASA 77W70488 LBJ Space Center Houston, Tex. (re: Problems related to agricultural machine inventory methods).

5. Horvath, R., M. Spencer, and R. Turner, Atmospheric Correction and Simulation of Space-Acquired Remote Sensor Data: 0.4 to 1.0 μm Spectral Range. WRL 10657 - 5-F NAS 9-12269.

6. Plass, G.N. et al, Radiance Distribution Over a Ruffled Sea: Contributions from Glitter, Sky and Ocean, App. Opt. p. 3161, December 1976.

7. Waterman, T.H., and Westell W.E., Quantative Effect of the Sun's Position on Submarine Light Polarization, J. of Marine Res. #15 p. 149 (1965).

8. Waterman, T.H., Polarization Patterns in Submarine Illumination, Science p. 927 December 1954.

9. Ivanoff, A., Quelques resultats concernant les properiétés diffusantes des eaux de mer, in 1960 Helsinki Symposium, Int. Union Géod. Géophys Intern Monographie 10 - p. 45 (1961)

10. Ivanoff, A., Polarization Measurements in the Sea in the book Optical Aspects of Oceanography, Academic Press (1974).

11. The National Bureau of Standards in an attempt to make the symbols self-consistant and standardize them has changed some of the current literature nomenclature. However, in introducing them, the symbols currently being used should be identified in an attempt to keep misunderstanding to a minimum. In particular L replaces I for intensity and:

$$L = \begin{vmatrix} L_0 \\ L_1 \\ L_2 \\ L_3 \end{vmatrix} \quad \text{replaces} \quad \begin{vmatrix} I \\ Q \\ U \\ V \end{vmatrix} \quad \text{in the Stokes parameters}$$

Nicodemus, F.E., editor, "Self-Study Manual on Optical Radiation Measurements, "NBS Tech. Note 910-1, 2, 3 and 6.

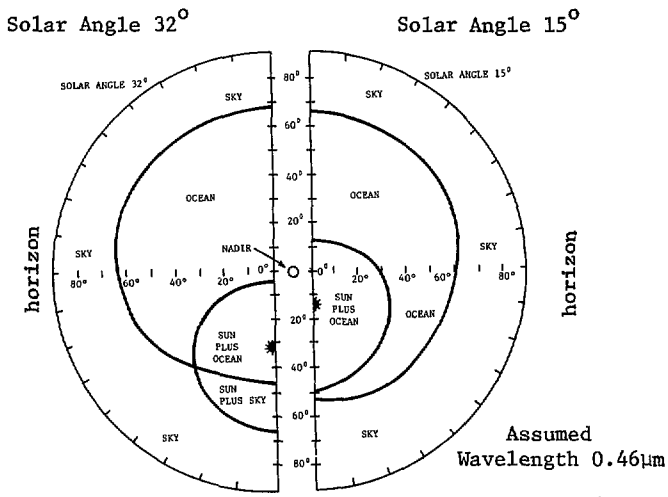

Figure 1. Dominant parameters in upwelling from the ocean surface. Only half the ocean is shown for each solar angle because it is symmetric about the center line. Solar glitter dominates the sun plus ocean area, reflected skylight, the sky area and underwater upwelling photons, the ocean area; waves appropriate for a 20 knot wind assumed (ref. Plass et al)[6].

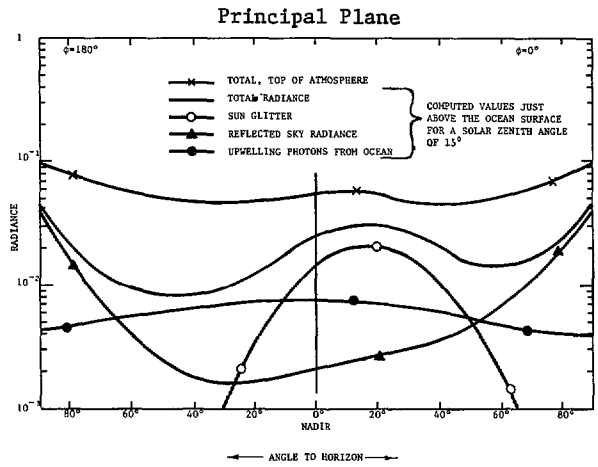

Figure 2. Typical radiances above the ocean surface for a 15° solar zenith angle. The solar horizon is at the left edge, nadir, at the center and antisolar horizon at the right edge. Waves appropriate for a 20 knot wind and a spectral wavelength of 0.46μm assumed. (ref. Plass et al).[6]

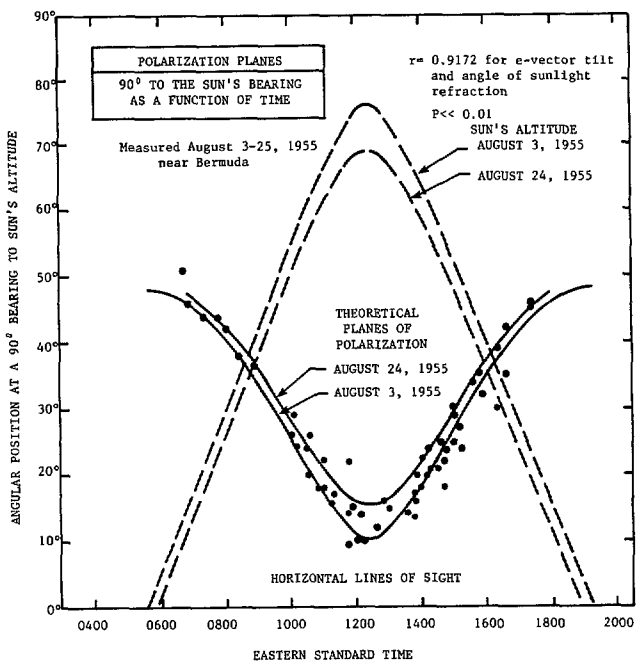

Figure 3. Effect of the sun's altitude on the submarine polarization plane (e-vector) observed 90° to the solar bearing. This was plotted with time as the abscissa; 72 individual observations are shown as black circles. For reference, the sun's altitude has been indicated by the broken curves for two particular days, one at the beginning and one at the end of the observation period. The calculated angles of sunlight refraction (r) which theoretically would be the same as the e-vector tilt from horizontal have been drawn for the same days (continuous curves). Observed planes of polarization and the calculated angles of refraction are strongly correlated in a statistically significant way. (ref. Waterman and Westell)[7]

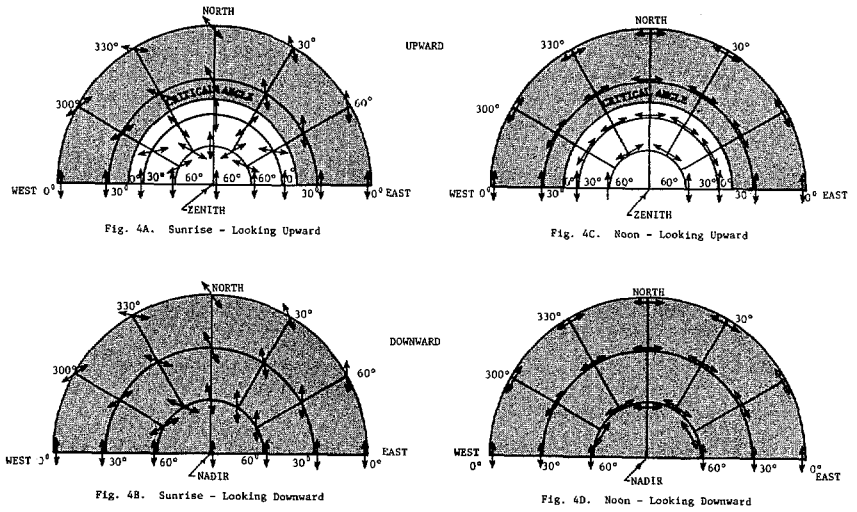

Fig. 4A. Sunrise - Looking Upward

Fig. 4C. Noon - Looking Upward

Fig. 4B. Sunrise - Looking Downward

Fig. 4D. Noon - Looking Downward

Figure 4. Polarization planes of submarine illumination as seen from a point a few meters under water at two different times of a clear cloudless day (diagrammatic). In A and B the pattern shown is that observed at sunrise with the sun on the horizon directly east. In C and D the pattern is that observed at noon with the sun directly overhead in the zenith. The diagrams are plotted on polar coordinates with azimuths represented by radii, and elevation or depression of the observer's line of sight as concentric circles. The outermost circle (0°) in each case is the underwater horizontal--that is, the edge of a plane passing through the observer and normal to the vertical.

Diagrams A and C show polarization appearing when the line of sight is raised upward toward the zenith; B and D show polarization planes seen when it is depressed downward to the nadir. In looking upward, when the critical angle (about 42°) elevation) is reached, the sky and its polarization are seen, as they are at all greater elevations. The areas showing sky polarization as seen underwater are unshaded; those where the polarization is produced by sunlight in the water itself are gray. The numbers labeling angles between the critical angle and the zenith are altitudes in the sky measured from the water-level horizon (0° inside the semicircles). These are distorted by refraction as the plot shows.

In all cases the polarization planes are represented by vectors whose angular relationship to the azimuthal radius that they intersect is the same as that between the e-vector of the polarized light and the vertical at the point plotted. The pattern of light polarization in the observer's other visual hemisphere would be a mirror image of that in the hemisphere diagramed. Intensities of polarization are not represented in this figure but varied markedly. (ref. Waterman)[8] Copyright 1954 by Amer. Assoc. for the Advancement of Science.

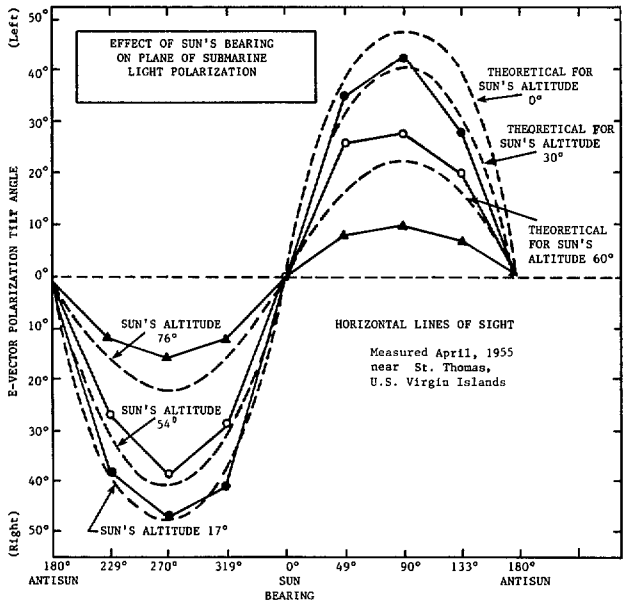

Figure 5. Effect of the sun's bearing on the submarine (e-vector) polarization plane observed at different solar altitudes. Observations are indicated by circles and crosses. For comparison, theoretical curves (broken lines) computed for the angle of sunlight refraction are shown. The curves were computed using tan P=tan r sin Θ, where P is the e-vector and the horizontal angle, r is the sunlight refraction angle computed from the solar altitude, and Θ is the angle between solar bearing and line of sight. Agreement between simple theory and observations appears good. (ref. Waterman and Westell)[7].

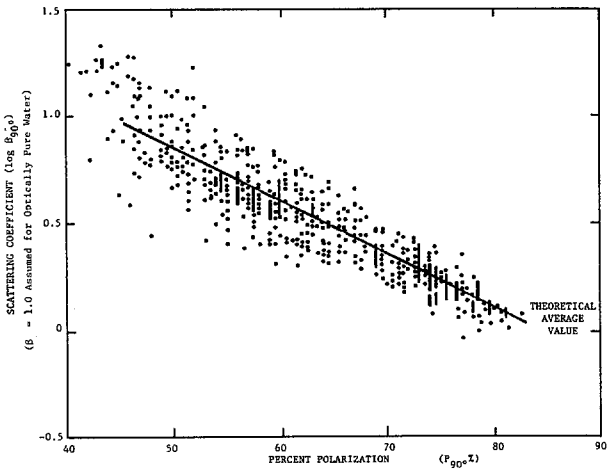

Figure 6. Scattering coefficient at right angles to the source and corresponding degree of polarization for all the sea water samples studied by Ivanoff (1961) during a cruise in the Western Mediterranean.[9,10]

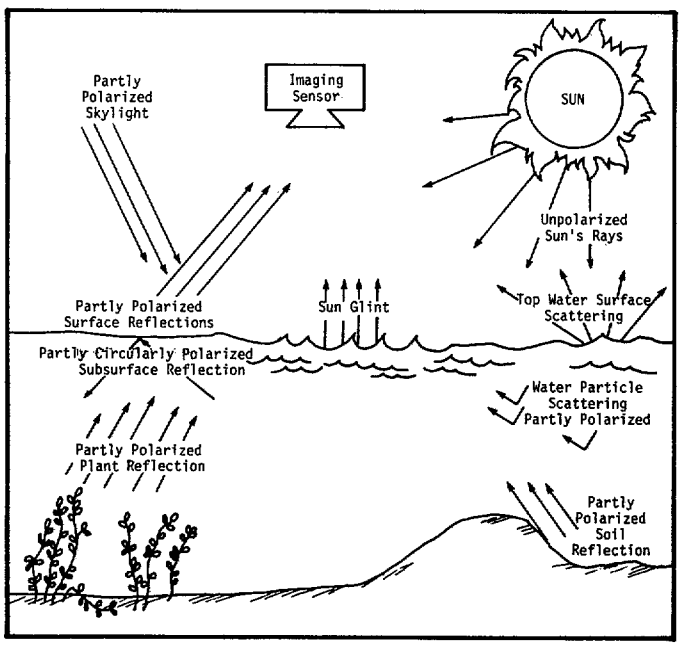

Figure 7. Physical factors producing polarization in reflecting and scattering the unpolarized sun's radiation.

SATELLITE OCEAN-RELATED IMAGERY APPLICATIONS PROGRAM

Edward Wedler
Centre for Cold Ocean Resources Engineering (C-CORE)
Memorial University of Newfoundland
St. John's, Newfoundland, Canada
A1B 3X5

Richard D. Worsfold
REMOTEC Applications Inc.
P.O. Box 5547
St. John's, Newfoundland, Canada
A1C 5W4

Abstract

Sea ice distribution, sea surface temperature contouring, and Iceberg/Ocean Vessel Detection and Identification have been identified as areas of immediate concern to marine activities off the Canadian East Coast. These are areas, also, in which LANDSAT and NOAA data from the Shoe Cove Satellite Receiving Station have been investigated and found both useful and operational with respect to providing data to users. The Satellite Ocean-Related Imagery Applications Program allowed the demonstration of this transfer of satellite technology to ocean interests.

1. Introduction

The objective of the Satellite Ocean-Related Imagery Applications Program (SORIAP) is to evaluate the usefulness of both LANDSAT and NOAA Imagery and computer compatible tapes (CCT's) obtained at the newly operating Shoe Cove Satellite Receiving Station (SCSRS), with respect to providing worthwhile data products to the ocean user community. The program is being carried out by the Centre for Cold Ocean Resources Engineering (C-CORE) for the Canada Centre for Remote Sensing (CCRS) under a subcontract from the Newfoundland Ocean Research and Development Company (NORDCO).

Application areas of study have been chosen which, it is felt, would produce immediate benefits to user groups and represent an extension into geographic areas not concentrated on previously. The application areas include:

(1) Sea Surface Temperature Contouring

(2) Sea Ice Distribution

(3) Iceberg/Ocean Vessel Detection and Identification

The geographic areas of interest are (Figure 1):

(1) Grand Banks - Flemish Cap

(2) Labrador Sea - Davis Strait

Fishing and hydrocarbon exploration activities are at present a major concern in these areas, particulary within Canada's 200 mile economic zone.

The four-phase program involves the acquisition and handling of Shoe Cove satellite data (Table 1), the use of all ground truth support data (Table 2) for the interpretation of the satellite images; the conducting of various test experiments in the application areas; and the conducting of one or two selected, potentially most valuable near real-time experiments. Interaction with user groups constitutes the most important part of the SORIAP program. It is through these groups that the 'true' evaluation of the satellite data product will be made.

Sea Ice Distribution

The coastal areas of the Labrador Sea and Davis Strait are ice covered for a large part of the year (Figure 2). Ice cover is an important consideration in the strategic and tactical movement of ocean vessels in the fishery, in exploration and development, and in shipping activities.

Near real-time data analysis and data dissemination is an important step in providing up-to-date ice information, especially during times of limited flight coverage by the Canadian ice reconnaissance aircraft. LANDSAT and NOAA data from Shoe Cove provides a locally available source of ice information. Though limited by cloud cover, the data frequency is suitable for sea ice distribution studies.

Experiments involving sea ice distribution in the program include:

(1) Locating ice leads for seal hunters.

(2) Indicating ice boundaries and distribution for a Canadian Coast Guard Vessel Traffic Management Centre.

(3) Providing repetitive coverage for several days over one area for pack ice movement studies.

(4) Comparing Shoe Cove data with GOES imagery in locating ice boundaries.

Sea Surface Temperature Contouring

The Grand Banks - Flemish Cap and surrounding areas are themally complex (Figure 3). It is an

area important to the fishing industry, yet it is an area frequented annually by sea ice and icebergs. A knowledge of the sea surface temperature is important in locating thermal fronts and upwelling zones, predicting deterioration rates of sea ice and icebergs and locating the area of potential freezing spray conditions.

Since sea surface temperature is dynamic, a near real-time availability of sea surface temperature is most useful. Although NOAA satellite information is presently received at Shoe Cove, necessary calibration data is yet to be incorporated with the CCT's for quantitative data analysis. Once this problem is resolved, the developed software can then be implemented. LANDSAT 3 thermal channel data is not expected to be available within the time frame of this program.

Experiments involving sea surface temperature include:

(1) Large scale data collecting in conjunction with the Canadian Federal Fishery Observer Program.

(2) Temperature contouring for current studies in the Grand Banks.

(3) Temperature contouring for iceberg deterioration rates.

Iceberg/Ocean Vessel Detection and Identification

Icebergs have been monitored annually by the International Ice Patrol (IIP) for over 60 years in the Grand Banks. Icebergs pose a potential hazard to offshore activities in the area. A continual surveillance of these icebergs is necessary for the safe movement and operation of vessels. As part of the Canadian Federal Fishery Surveillance Program, a knowledge of all fishing vessels operating within the 200 mile economic zone is important to the proper management of the fishery resources off the Grand Banks.

The cloud cover and data frequency limitations of LANDSAT, in assisting the continual surveillance of icebergs and ocean vessels, are well understood. LANDSAT may be used, however, as support data on an opportunity basis and as a data source for areas not normally surveyed (Figure 4).

Experiments involving iceberg/ocean vessel detection and identification include:

(1) Detecting and reporting 'suspected vessels' located by LANDSAT using CCT's within the surveillance and reporting zones of the Canadian Federal Fisheries and the Canadian Coast Guard.

(2) Detecting icebergs using ship, shore and IIP aircraft verification data.

SORIAP Program Follow-up

The results of the SORIAP program, using data at the Shoe Cove Satellite Receiving Station, are to be documented. Included in the documentation will be: the procedures used and results obtained in each of the various application areas; an evaluation of the interaction with users of the data with respect to quality and value to their operations; and, recommendations to the Shoe Cove Satellite Receiving Stations for improvement of the existing data collection, processing and dissemination.

LANDSAT 2 and 3; NOAA 4 and 5

Image Size	Format
185 mm	Paper, B & W
185 mm	Film Negative, B & W
185 mm	Film Positive, B & W
70 mm	Film Negative, B & W
70 mm	Film Positive, B & W
	Microfiche (LANDSAT only)
	CCT (9 track 1600 bpi)
	Photo-facsimile

Table 1 Data Available from the Shoe Cove Satellite Receiving Station

Sea Surface Temperatures

Canadian Federal Fisheries - observer program experiment
METOC, Halifax - weekly chart
AES, Halifas - daily, coded ship reports
IIP - occasional PRT 5 line trace, during spring

Ice Reports

Canadian Coast Guard - occasional ECAREG Reports
- ice reporting light-stations
AES, OTTAWA - ice charts (1 - 3 days)
- 30 day ice forecast notice
U.S. Navy - weekly Eastern Arctic Ice Analysis Chart
- monthly, 30 day ice edge forecast chart
AES, Halifax - daily, coded ship reports
NOAA-NESS - weekly GOES Labrador ice analysis chart

Iceberg Reports

IIP - weekly bulletin and chart during spring
CCG - occasional ECAREG Reports

Table 2 Ground Truth Support Data Available for the Study Areas

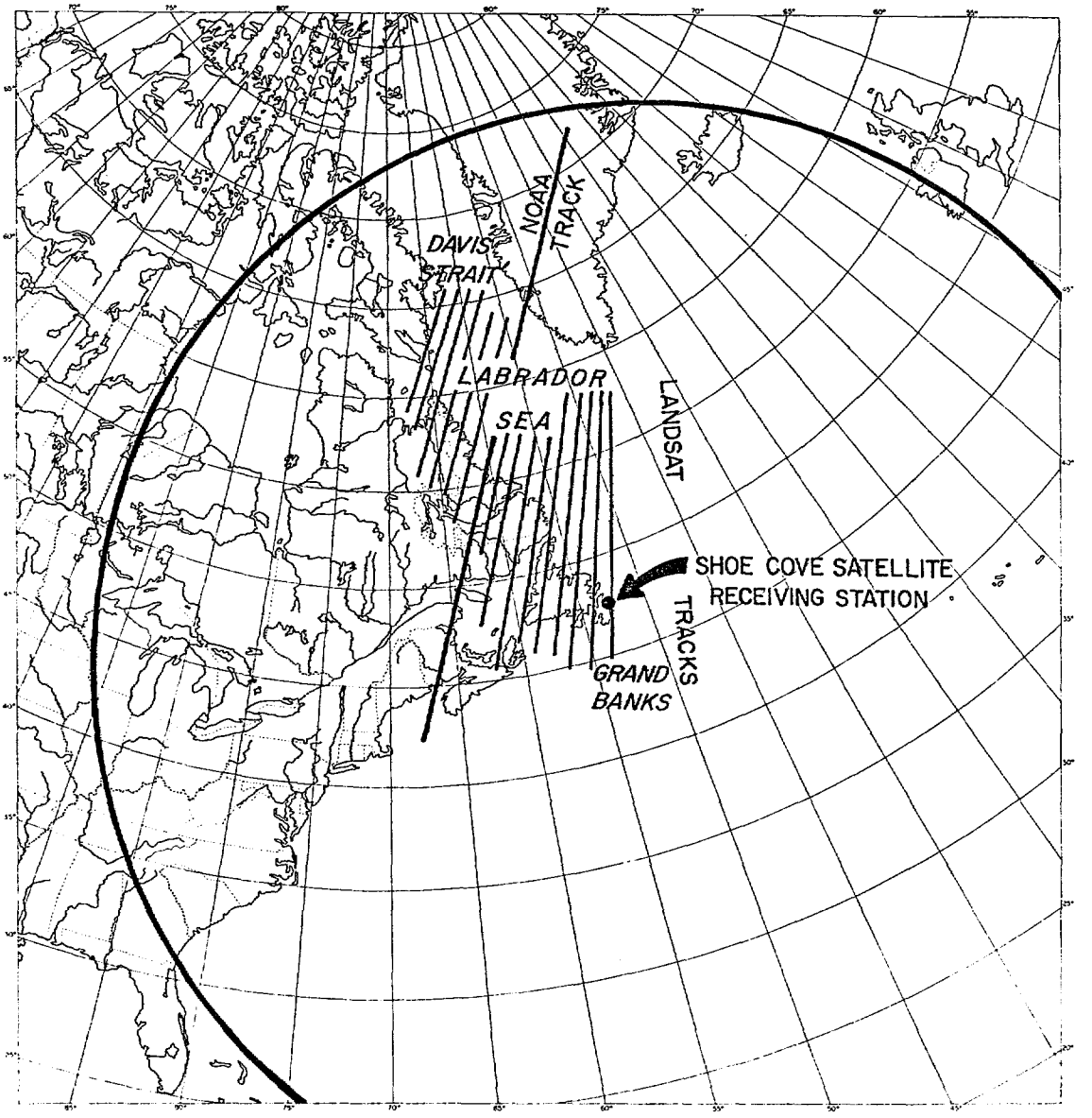

Figure 1 Shoe Cove Satellite Receiving Station and LANDSAT and NOAA orbits tracked in the study areas.

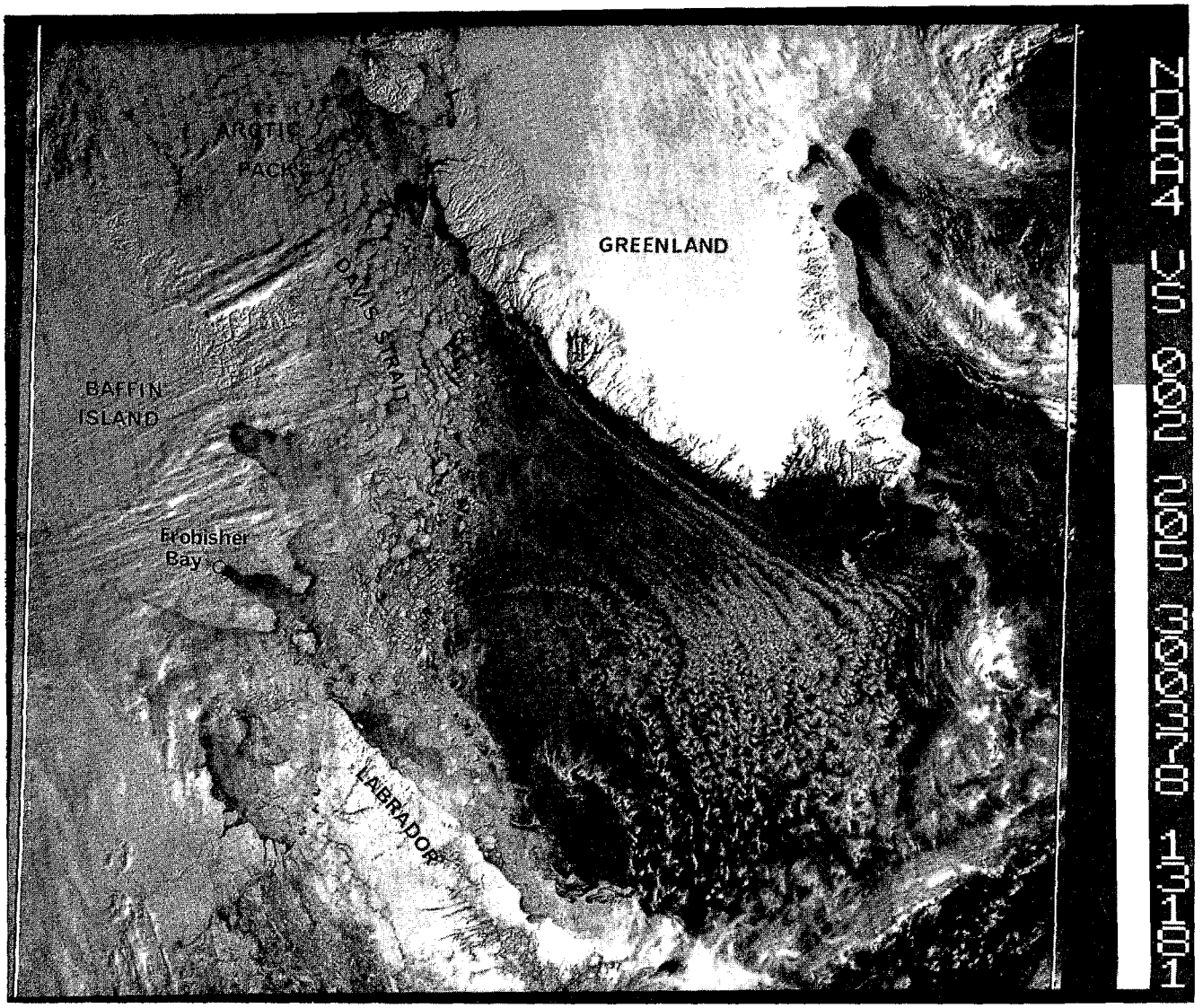

This direct readout NOAA 4 image illustrates the Arctic pack with large floes breaking off into Davis Strait. These floes drift southerly with the currents along the Labrador coast. Easterly moving air masses move over cold land and ice and pick up moisture over the warmer Labrador Sea, creating steaming cloud patterns.

Figure 2 Sea Ice Distribution in the Labrador Sea and Davis Strait, 30 March 1978.

NOAA 4 SATELLITE IMAGERY

19 APR 78 1234 GMT

visible

thermal

Major thermal fronts are seen with significant intermixing of Gulf Stream and Labrador waters. Fog is seen off the South and North-East coasts of Nova Scotia. Ice temperatures are not significantly different from the surrounding cold waters.

Figure 3 Thermal detail as seen by NOAA 4 in the area near the Grand Banks, 19 April 1978.

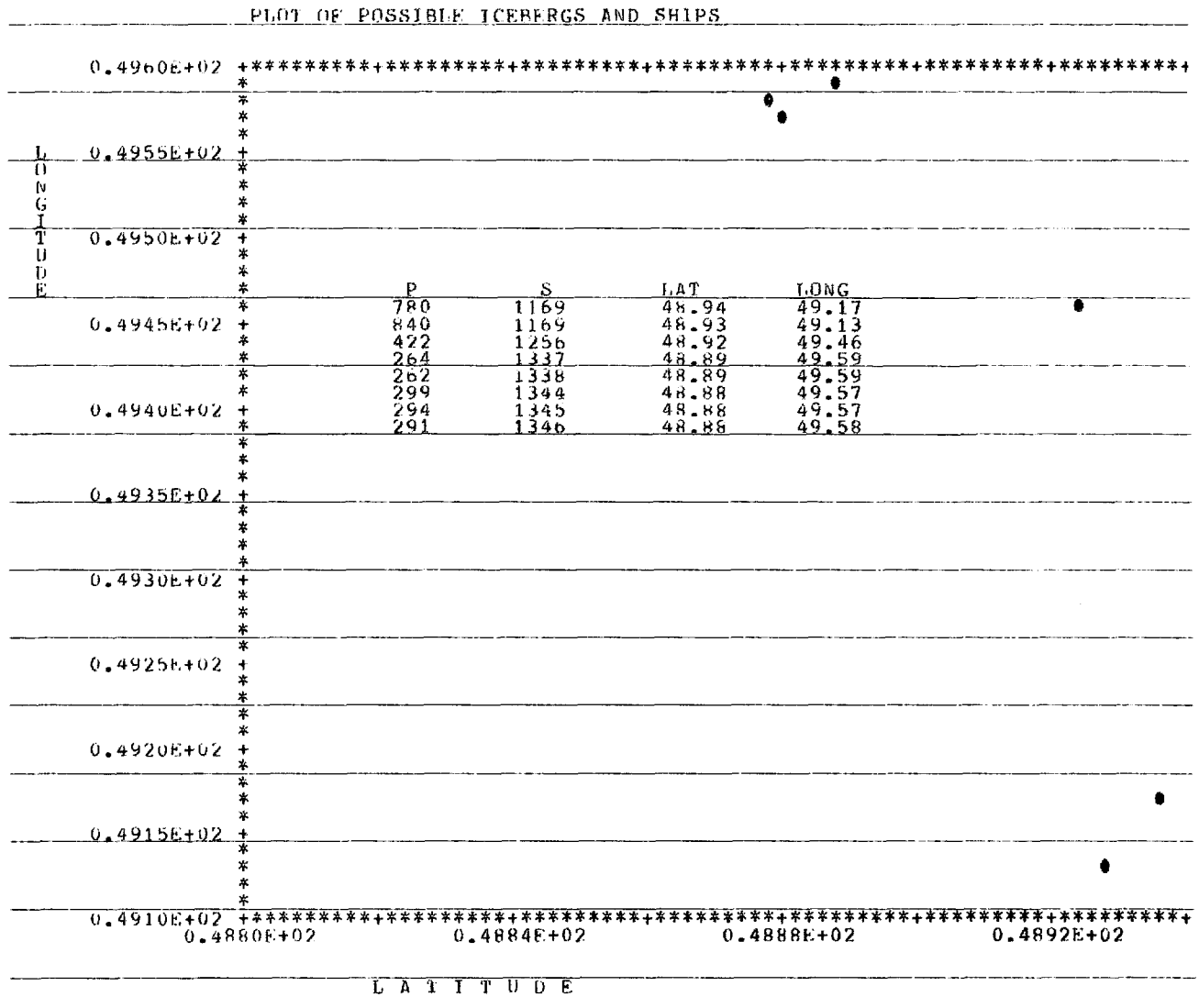

Figure 4 Results of LANDSAT 'HUNT' for objects seen in the ocean.

SOME AUTOMATIC DIGITAL TECHNIQUES FOR ENHANCING AND EXTRACTING OCEANIC FEATURES FROM SATELLITE INFRA-RED PICTURES

D. G. Nichol
Code 315
Naval Underwater Systems Center
New London Laboratory
New London, Connecticut 06320

Abstract

Infra-red images have proved extremely useful in obtaining synoptic views of sea-surface temperatures. This paper describes several techniques for displaying and processing such pictures. These include a method to automatically assign the grey-levels in the displayed pictures to minimize information loss. Also discussed are techniques to reduce random uncorrelated noise and enhance oceanic features such as fronts.

1. Introduction

Some algorithms to process digital satellite images are discussed. The aims of the processing are twofold, firstly to improve the quality of the image for visual inspection and secondly to reduce the noise content to facilitate easier machine processing in future computer analysis. To achieve the first of these a technique for optimally and automatically setting the thresholds for grey-level assignment is described. This is 'optimal' from a minimum entropy loss viewpoint. For the second aim a simple technique of cascaded filters is used to reduce the uncorrelated (white) noise and then to sharpen the edges in the resultant low-pass filtered picture. This latter aspect is particularly useful in the oceanographic applications discussed because the location of ocean fronts, such as the edge of the Gulf Stream, is of primary importance. The examples given are obtained from NOAA-5 very high resolution (VHRR) infra-red (IR) data but the techniques can be applied to any satellite image, visible as well as IR.

2. Grey scale assignment

2.1 Basic considerations

Figure 1 shows a typical VHRR IR image as obtained from the Satellite Data Service of NOAA.

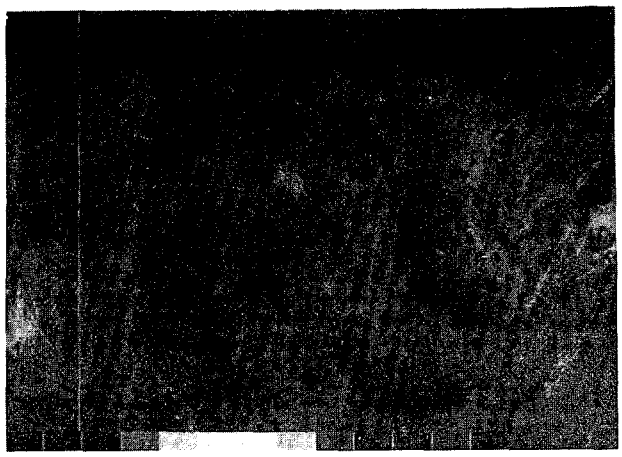

Fig. 1. NOAA-5 IR Image of Gulf of Mexico, 1421, 10 April 1977.

This shows the loop current in the Gulf of Mexico. The photographic process used to display the image has effectively only 8 to 12 grey shades but the data itself is digitized to 256 levels. Thus the original 8 bits of information is reduced to 3-3.5 bits for display. That is, for each picture element ('pixel') some 4 to 4.5 bits of potential information is being lost.

2.2 Minimum entropy loss algorithm

Suppose the data can assume the N values $f_1, f_2, f_3 \cdots f_N$ and the effective K grey levels are $g_1, g_2, g_3 \cdots g_K$. We assume N>K (usually N>>K). The assignment of grey levels can then be thought of as a many-one mapping from the set $\{f_1, f_2, f_3, \cdots f_N\}$ to the set $\{g_1, g_2, g_3, \cdots g_K\}$. Denoting the probability density function of the f's by ψ_n and of the g's by ϕ_k then a measure of the information content of the stored and displayed pictures is given by the entropy functions:

$$I_S = - \sum_{n=1}^{N} \psi_n \log_e \psi_n \qquad (1)$$

and $$I_D = \sum_{k=1}^{K} \phi_k \log_e \phi_k \qquad (2).$$

U.S. Government work not protected by U.S. copyright.

Now because the mapping is many-one, it is clear that at least one of the ϕ's must consist of the sum of two or more ψ's. It can then be shown that because of this I_D is always less than I_S. Thus entropy, or potential information, is being lost. The assignment method suggested is to minimize this loss. As I_S is constant for a given picture, this means that I_D must be maximized.

From basic Information Theory it is well known that an expression such as (2) is maximized when:

$$\phi_i = \phi_j \quad \text{for all } i,j \in \{1,2,\cdots K\} \qquad (3)$$

Thus the mapping required is one which most closely produces a uniform distribution of grey-scale values.

A further constraint is that the assigned grey levels should increase monotonically with data values. Thus in IR pictures the higher the surface temperature, and thus the pixel value (a 'count'), the darker the point plotted.

Thus the following algorithm to select grey levels has been developed:

(1) Measure the probability density function for the given picture.

(2) Select integer boundaries $z_0, z_1 \cdots z_K$ where $z_K > z_{K-1} > z_{K-2} \cdots > z$ and such that, as closely as possible,

$$\phi_i = \phi_j \quad \text{for all } i,j \in \{1,2,\cdots K\}$$

where

$$\phi_k = \sum_{n=z_{k-1}}^{z_{k-1}} \psi_n \qquad (4)$$

Thus the resulting ϕ_k is the best approximation to a uniform distribution.

Fig. 2. Same image as above in the grey-scale assigned by minimum entropy loss algorithm

Figure 2 shows the region shown in fig. 1 processed with this algorithm. It is clear that more water structure is visible in the processed than in the original picture. Figure 3 shows the Tasman Sea area processed in the same manner.

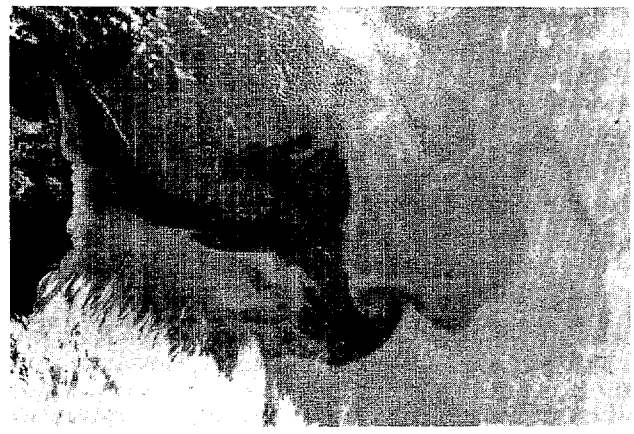

Fig. 3. Tasman Sea showing East Australia current, 2257, 13 October 1977. Processed by minimum entropy loss algorithm.

In this case, however, the presence of clouds would distort the measured density function ψ_n so only those values of f_n greater than a threshold θ have been included in ψ_n. This is possible because in general clouds are colder than the ocean and as the IR counts increase with temperature it is quite realistic to assume that, at these latitudes, all values less than say the equivalent of 15° C are cloud. Accordingly in this picture the available grey scale range is matched to the sea surface water temperature as desired. Many interesting features are brought out by this matching.

3. Random noise reduction and ocean front enhancement

3.1 Random noise

The VHRR data is comparatively low noise compared to say the low resolution scanning radiometer (SR) images from the same satellite. However, there is still a considerable component of both correlated and uncorrelated ('white') noise present. This is not as apparent in fig. 2 because each pixel plotted is the sum of 4 data points and thus the uncorrelated noise has its standard deviation reduced by a factor of $1/\sqrt{4}$, that is 0.5. (The original data covered in fig. 2 covers 1024 x 1024 pixels but these are plotted as a 512 x 512 picture.) However, by not summing the data in this region the sub-picture shown in fig. 4 is obtained.

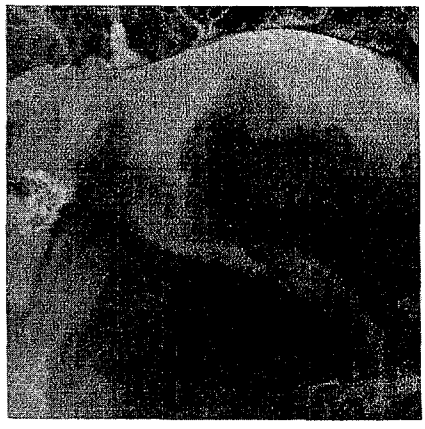

Fig. 4. Part of same region shown in fig. 2. No pre-integrations lead to noisier image.

This covers 1/4 of the image of fig. 2 and the grey scale has been assigned by the algorithm developed in section 2.2. The background noise is very apparent. One way to reduce this is to smooth the picture by convolving it with a smoothing window. Thus for a given image P(x,y) the smoothed image is given by:

$$P_s(x,y) = \sum_{x'} \sum_{y'} w(x-x', y-y') P(x',y') \qquad (5)$$

where the integration is carried out over the picture region where the weighting function w(x,y) is non-zero. Figure 5 shows the effect of a uniformly weighted rectangular window of size 5 x 5 applied to fig. 4.

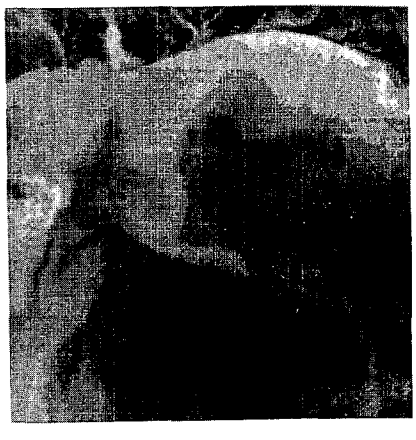

Fig. 5. Smoothing by 5 x 5 window leads to significant reduction in noise.

The noise is clearly considerably reduced by this smoothing. In fact assuming a stationary noise process over the convolution region implies that the non-correlated noise has its standard deviation reduced by a factor of $1/\sqrt{n_c}$ where n_c is the number of pixels in this region. In this case the noise has a new standard deviation of 0.2 times the original.

This convolution is of course a form of low-pass filtering and by changing the weighting function different filters may be designed. For a given size window, however, the noise reduction will be less than for a uniform weighting.

3.2 Front enhancement

One of the problems with the smoothed image is that edges tend to become blurred. One of the major aims of this processing is to locate and extract ocean fronts which are characterized by sharp temperature gradients. This smearing tends to make this localization more difficult. To improve the image an edge sharpening technique previously described[1] is used. This is to use a smaller multiplicative window on the smoothed image. This non-linear transformation has the effect of suppressing pixels on the 'low' side of an edge because low valued pixels are included in the window.

Thus the image $P_s(x,y)$ is transformed to:

$$P_{sm}(x,y) = \prod_{(x',y') \in R_{xy}} P_s(x',y') \qquad (6)$$

where R_{xy} is the window centered on (x,y). Figure 6 shows the result of applying such a transformation to fig. 5.

Fig. 6. Previous figure processed with multiplicative transform to enhance the edges of front.

The window used was a 3 x 3 rectangular window. The front location is now easier to determine.

4. Concluding remarks

The simple local techniques described are capable of producing a significantly improved image without operator involvement. The final image obtained is particularly suitable for automatic edge detection as the non-linear transformation is severe on noise and the track chosen will be easier to find.

References

1. Nichol, D. G., "The Analysis of Bathythermograph Data: A Picture Analysis Approach," Pattern Recognition, May, 1976.

SATELLITE INTERFEROMETRY FOR OCEAN SURVEILLANCE

R. S. Orr
Stanford Telecommunications Inc.
1307 Dolley Madison Blvd.
McLean, VA 22101

Abstract

A system employing satellite-borne interferometry to provide cooperative monitoring and surveillance of ocean vessels at low cost to the user is proposed in this paper. L-band signals transmitted by a vessel are received at a geostationary satellite equipped with a crossed-boom, long baseline interferometer pair. The signals received at each interferometer element are translated to an appropriate downlink frequency (e.g. C-band) and are FDMA downlinked to a shore station for processing. The shore station extracts position, vessel ID, and mission-related data from the received signals. Signals from four calibration stations of known position are continually monitored for attitude correction and compensation of thermal deflections of the booms. A high accuracy (0.5 km 1σ) position update can be obtained with 90% probability for each of 3000 vessels every 6 min.

1. Introduction

A satellite-based interferometer system for monitoring and surveillance of ocean vessels is proposed in this paper. Typical users might be oil tankers or fishing vessels. The system operates as follows (Figure 1): a vessel periodically transmits a CW burst of a few seconds duration which is modulated by low rate information such as vessel ID, cargo data, etc. The transmission is of low power and at L-band (1.6 GHz). The transmissions are received at a space-borne crossed-boom interferometer which is mounted aboard a geostationary satellite at the 100° W.L. orbital slot. The satellite is a repeater which translates the signal at each interferometer antenna to C-band, and all the antenna signals are downlinked to a shore station or satellite control center. Using the downlinked data, this center performs the functions of acquisition, direction finding, position fixing, and data detection. No forward link to the vessel is required.

There are many potential users of such a system (up to 3000 vessels) and each must access the satellite in some manner. In the absence of a forward link from shore to ship, no control channel is available to give timing information or to implement polled TDMA. Instead, each user transmits a number of replicas of his message at randomly selected times within a designated update interval. The combination of time diversity so achieved and frequency diversity which results from the combination of long term instability of the transmit oscillator and very narrow-band signalling is sufficient to allow the entire user population to be serviced with a high accuracy (0.5 km 1σ) position update once per 6 min with 90% probability.

2. Interferometer System

Specification of an interferometer system is largely an exercise in resolution of conflicting demands. The Appendix summarizes a disciplined approach to handling the trade-offs among (i) coverage, (ii) accuracy, (iii) signal-to-noise ratio, and (iv) ambiguity resolution. In brief, high accuracy demands long baselines. Conversely, wide

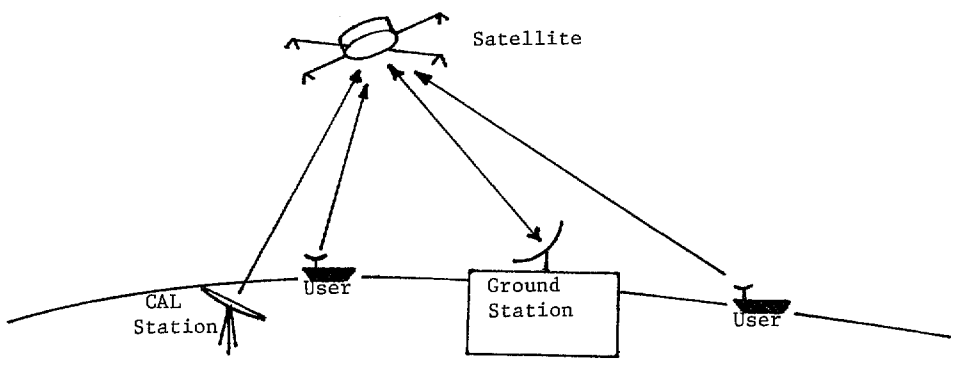

Figure 1. Elements of Satellite Interferometer System

coverage requires narrow baselines to eliminate ambiguous estimates. An attempt to meet these objectives simultaneously with a single interferometer pair necessitates an inordinately high signal-to-noise ratio. One solution is well known: use a sequence of disparate baselines such that the highly accurate but ambiguous estimate made by the long baseline pair can be resolved by a succession of shorter baseline estimates which are less accurate but also less ambiguous. The design technique presented in the Appendix provides a fixed probability of correct ambiguity resolution at each stage and a systematic approach to the baseline and SNR calculations as a function of coverage and accuracy.

Figure 2 illustrates the coverage and accuracy goals, which are 0.5 km (1σ) position accuracy within $\pm 45°$ of the Equator (subsatellite point). These goals imply an angle estimation requirement of $\sigma_{\sin\alpha} = 5.4 \times 10^{-3}$ mrad.

For this problem, a two-stage interferometer (in each coordinate) appears to be preferable. The baselines are 300λ (57.15 m) and 4λ (76 cm), which requires a 40 dB SNR in order to achieve the desired angular accuracy. The system is configured to have 46 dB, arising from an uplink C/N_o = 40 dB-Hz and a 4 s integration time per transmission. Correct ambiguity resolution occurs with 0.65 probability, which would be sufficient to maintain track with a simple outlier test in the tracker.

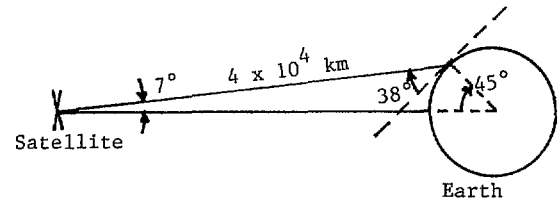

Goal: σ_{Total} 0.5 km (1σ) accuracy within $\pm 45°$ of the subsatellite point

$$\sigma_{Lat} = \sigma_{Long} = \sigma_{Total}/\sqrt{2}$$

$$\sigma_{Total} = \underbrace{\sqrt{2}\ \sigma_{\sin\alpha}}_{\text{sine angle error}} \times \underbrace{\sec 7°}_{\text{converts to angle error}} \times \underbrace{\csc 38°}_{\text{minimum sat. el.}} \times \underbrace{4 \times 10^4 \text{ km}}_{\text{range to sat.}}$$

$$\Rightarrow \sigma_{\sin\alpha} = 5.4 \times 10^{-3} \text{ mrad}$$

Figure 2. Coverage and Accuracy Goals

The link budget (Figure 3) shows that 10W CW into an upper-hemispherical antenna provides the desired uplink C/N_o, assuming earth coverage antennas on the interferometer. The preamp noise figure (5 dB) is within state of the art.

Figure 3

L-BAND UPLINK BUDGET

TRANSMITTER POWER	10.0 dBW
TRANSMITTER ANTENNA GAIN	3.0 dB
EDGE OF BEAM LOSS	-3.0 dB
PATH LOSS (1.6 GHz)	-188.0 dB
INTERFEROMETER ANTENNA GAIN	17.0 dB
NOISE (5 dB NF)	-201.0 dBW/Hz
C/N_o	40.0 dB-Hz

3. Satellite Downlink

Aboard the spacecraft, there are seven interferometer antennas (two pairs in each direction, with one shared central antenna) as shown in Figure 4. The signals from these seven are mixed to seven parallel frequency channels at C-band and downlinked FDM to the satellite control center. The shipboard oscillator is assumed to have long term stability 1 pp 10^5, resulting in about +15 kHz frequency uncertainty at 1.6 GHz. In addition to this 30-kHz band, each interferometer channel must also pass the signals from each of four calibration stations on the ground. These are located two at either side of the user band; calibration oscillator stability is 1 pp 10^6 (3-kHz uncertainty). Including guard bands, a channel bandwidth of 52 kHz is required. The seven channels can be downlinked in less than 400 kHz, as shown in Figure 5.

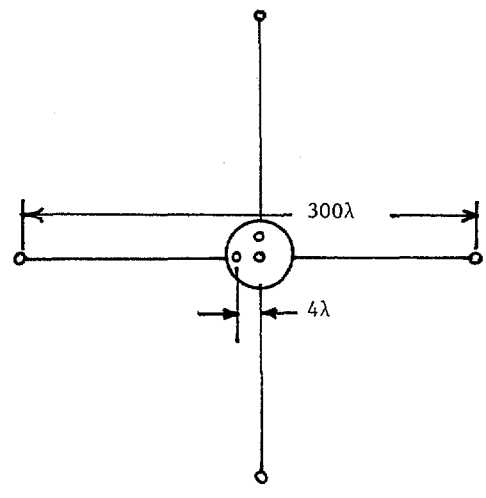

Figure 4. Interferometer Antenna Dimensions

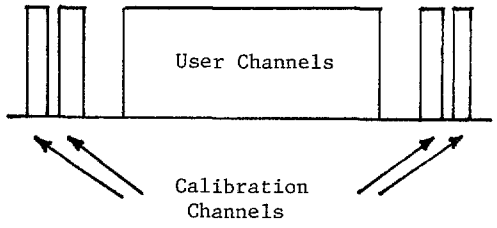

User Channels: 30 kHz
CAL Channels : 3 kHz
4kHz guard band next to user channels
1kHz guard band between CAL channels

Total : 52 kHz x 7 + guard bands
< 400 kHz

Figure 5. Downlink Spectrum

4. Signal Format

The signal format contain 1 s of unmodulated carrier for acquisition and 3 s of 30 bps-modulated DPSK data. Thus 90 bits can be transmitted per update, only 12 of which are needed for ID (16 may be used to provide a set of ID codewords having a guaranteed minimum distance exceeding 1). Thus at least 74 bits are available for other data. Because of the very high SNR within a bit time (25.2 dB), the probability of erroneous ID decode is negligible.

A bandwidth of 60 Hz will pass all the required information from one user at the ground station. There are 500 60-Hz bands within the 30-kHz downlink user band, providing a factor of 500 in frequency diversity. If the 3000 (maximum) users were spread uniformly across the band, there would be six per narrowband channel. The processor performance has been optimized for 10 users/channel.

5. Multiple Access Processing

If a position update is wanted every 6 min, there are (360 s ÷ 4 s/user) = 90 slots available to the (assumed) 10 users. From the point of view of optimum random access, this 11% channel loading is too light; a 33% loading is more nearly optimum. Thus each user transmits with random timing <u>three</u> times per update interval (6 min). The probability of a successful update becomes 0.9.

The reason for the long transmission and integration times is, of course, the need for accurate differential phase measurements for angle estimation. In order to make the phase measurement, the receiver must first acquire, then phase-lock to the signal and finally provide the two interferometer signals to a phase meter. Each of these functions is discussed below.

The pulse traffic arrival rate at the shore station is (3000 users/update x 3 pulses/user ÷ 360 s/update) = 25 pulses/s or 100 pulses/pulse length (4 s). Since there are 500 frequency channels of width 60 Hz, the average arrival rate per channel is 0.2 pulses/pulse length. For acquisition, then, one of the seven satellite downlink channels is filtered by a bank of 500 60-Hz filters; the outputs of these channels are energy detected and when signal is detected in a channel, its output is connected to one of a bank of time-shared phase-lock loops (PLL). One hundred PLL's would suffice to acquire <u>all</u> the downlinked pulses if arrivals occurred in nonoverlapping TDM. Since detection of one in three is all that is required, a lesser number would actually suffice.

When phase lock is accomplished (this is estimated to require a fraction of a second), the loop bandwidth can be narrowed and the modulation stripped off, enabling accurate phase measurement. Since the signal is coherently demodulated, differentially coherent PSK reception of the data is possible. Data detection need be done on only one channel, but after acquisition lock has been detected, all seven channels must be phase-locked to secure the differential phase estimates.

6. Calibration Stations

Four calibration stations are employed. Each station transmits uninterrupted CW towards the satellite; the transmitter power can be quite low because a directive antenna pointed at the satellite can be used to achieve high EIRP. The frequency of each station is known to within 3 kHz (1 pp 10^6 long term stability) and each frequency lies in a distinct band. The transmission is modulated with a station ID code once every 5 s.

The functions of the calibration stations are to provide to the satellite control center data which is used to remove fixed or slowly varying biases from the user data upon which the position fixes are based. If the satellite/interferometer complex were electrically ideal and perfectly rigid, attitude control information could be ascertained from the transmission of one centrally located calibration (CAL) station. The LAT-LONG errors in the interferometer estimate of the CAL station position determine instantaneous attitude error. Other electro-mechanical errors which are present necessitate additional stations.

The mechanical errors are primarily bending and twisting of the interferometer booms due to thermal deflections arising from uneven solar heating. Twisting results in pointing error of the interferometer antenna, with resulting decrease in gain. This is compensated by beam broadening of the antenna pattern, which uses up only a small amount of margin in the link budget. The current

technology of space-qualified deployable long booms is such that twisting can be held within a few degrees ($\pm 5^\circ$ conservatively) and as such is not a source of major system error.

Bending is the primary distortion which must be calibrated out. Even a 1° boom tip deflection out of the ideal crossed-baseline plane (a state-of-the-art number) results in a 2.6λ displacement of a 150λ boom. In a system which is trying to resolve differential phase to within a fraction of a wavelength, this is intolerable. The displacement is doubled in an anti-symetric vibration mode.

Boom bending can result in an apparent attitude drift which differs from that of the spacecraft body itself, and it is this apparent drift which must be calibrated electrically. Were it not for the baseline variations introduced by symmetric mode vibrations, apparent attitude could be calibrated out by one station; two additional stations provide enough data to track the lat-long baseline variations.*

Typical angular rates of variation in the baseline are on the order of 10^{-5} rad/s. The "multiplier" for a 300λ baseline ($2\pi \times 300$) converts this to an electrical angle rate of about 1°/s maximum which must be calibrated. The CAL channels have higher SNR than the user channels and can be integrated for longer periods of time and with time constants chosen to balance the lag vs smoothing trade-off in order to achieve this.

A fourth station permits elimination of electrically induced phase bias errors due to unequal cable cuts, varying transponder channel characteristics, etc.

7. Discussion

A concept for a system to provide a marine monitoring and surveillance service suited to anticipated Coast Guard requirements has been outlined in this paper. In order to evaluate the utility of the satellite interferometer solution to this problem, alternative solutions (both space and non-space systems) must be offered and comparisons made. Relative to the system concept in this paper, it is concluded that although the thermo-mechanical engineering of the space segment is important to the success of a spaceborne interferometer system, it is the design challenge in the electrical portion of the system which would be the pacing item in a totally successful execution of the interferometer monitoring system.

---

*Apparent baseline changes due to frequency uncertainty in the uplink signals can be taken into account after the narrow band processing at the ground.

APPENDIX

The design procedure developed for the interferometer problem is summarized below.

Assumptions:

1. Emitters to be located lie within an angular range $|\theta| \leq \theta_m$.
2. The rms accuracy desired in the estimate of $\sin\theta$ is σ^* (assumed to be $\ll \sin\theta_m$).
3. Ambiguity resolution at a given stage will be successful if the resolving estimate lies within $\pm k$ standard deviations of its mean.

Results:

1. A set of N baselines are defined for an N-pair interferometer. The spacing of the n-th pair is:

$$\frac{D_n}{\lambda} = \frac{1}{2\sin\theta_m}\left[\frac{\sin\theta_m}{k\sigma^*}\right]^{(n-1)/N} \quad ; 1 \leq n \leq N$$

2. The required signal-to-noise ratio is:

$$S/N = \left(\frac{k}{\pi}\right)^2 \left[\frac{\sin\theta_m}{k\sigma^*}\right]^{2/N}$$

3. The rms error in the n-th estimate is:

$$\sigma_n = \sigma_{\sin\hat{\theta}_n} = \sigma^* \left[\frac{\sin\theta_m}{k\sigma^*}\right]^{1-n/N} \quad ; 1 \leq n \leq N$$

4. The overall probability of correct ambiguity resolution is:

$$P_c^{(N)} = \left[1-2Q(k)\right]^{N-1}$$

where

$$Q(x) = \int_x^\infty du \frac{1}{\sqrt{2\pi}} e^{-u^2/2}$$

Reference

1. Program Plan for Satellite-Aided Coastal Zone Monitoring, NASA Goddard Space Fight Center, Greenbelt, Md., 14 September 1977.

ADVANCEMENTS IN OIL SPILL TRAJECTORY MODELLING

D.R. Garver
Process and Computer Engineering
Dow Chemical Company
Freeport, Texas 77566

G.N. Williams
Computing Science
Texas A&M University
College Station, Texas 77843

Abstract

The continuing increase in offshore crude oil production and transportation is presently coupled with widespread concern over protection of the environment. This has led to interest by members of the petrochemical community, in the development of suitable methods for quickly predicting the probable transport path and coastal impact time of a possible oil spill in the offshore environment. An oil slick simulator of the stochastic trajectory type has been enhanced in an effort to provide such methods.

In particular, four areas will be addressed. First, both the Fay radial spreading equations and a long-term dispersive algorithm are now provided. Additionally, the slick may now assume an elliptical shape. Secondly, wind and current forcing functions may now be generated with the use of Markov state transition matrices as well as through the use of input time histories. Thirdly, the model will adaptively calculate coefficients for the transport equations in an attempt to correct for deficiencies in the particular equations used. Finally, the model will now execute in a real-time mode with an on-line computer terminal to allow tracking to occur during an actual spill.

1. Introduction

An oil slick simulator of the stochastic trajectory type has been previously described by Williams, Hann, and James (8). This model, the result of two research projects carried out under the auspices of the National Sea Grant Program and SEADOCK, Inc., is a predictive oil slick tracker designed to aid in the assessment of environmental impacts from catastrophic oil spills. The model simulates the movement of an oil patch in an offshore environment with boundary lengths on the order of 10^6 meters, and slick travel times ranging from several hours to several months. It also models the physical processes acting to dissipate a slick, of which the most notable are evaporation and dissolution.

The physical processes affecting oil spilled on the surface of a body of water are of two types: those causing the transport of the centroid of the slick, and those causing changes in the properties of the slick, such as its size, shape, orientation, and chemical composition. These properties have been modelled analytically and numerically by various entities (2,7). For this particular model, the slick transport is simulated by a vector sum of the wind and current at the slick centroid, of the form

$$\Delta\vec{P}_i = 0.03\,\vec{W}_{Fi} + S\vec{C}_{Fi}$$

where $\Delta\vec{P}_i$ is the positional change vector during the ith time step, $\vec{W}_{Fi}$ is the offshore wind vector during the ith time step, and $S\vec{C}_{Fi}$ is the surface current vector during the ith time step. For a slick within five miles of the coast line, this equation is modified to represent the appearance of other forcing factors.

The modelling of physical changes to the slick is accomplished in two parts. Physical spreading is modelled using the Fay equations (1), while the degradation of the slick follows the first order rate process described by Moore, Dwyer, and Katz (3).

Subsequent to the completion of the model of Williams, et al., it became apparent that the utility of the model would be increased by extending its scope to include deterministic as well as stochastic modes. Additionally, it was desired to add certain technical improvements in an attempt to include in one model all such analytical techniques as are presently considered to be the state-of-the-art for simulating the physical processes affecting an oil slick. The remainder of this paper will address these extentions and modifications.

2. Trajectory Forcing Functions

The transport equations in the base model assume wind and current fields which are time-variant but spatially invariant. It is doubtful that the assumption of spatially invariant winds is justifiable given the physical scale of interest; however, it is a workable approach in terms of the limited quantities of wind and current information which is available for offshore regions. In some few cases, such data has been collected over a fairly long time base, but such histories are generally limited to single stations.

The initial model utilized an offshore wind and current data base consisting of observations at three hour intervals for a time span of approximately 23 months. While this type of data structure is ideal for generating coastal impact probabilities, it presents several disadvantages for the general user. Among these are the inability of the model to accept real-time data from an existing spill, and the limitation of slick simulations to the time frame of the data. The enhanced model, therefore, while retaining this time history format, additionally provides two alternate sources of forcing function data in order to circumvent these difficulties.

By means of a set of manipulations on the time history data of the form discussed above, a set of monthly Markov state transition matrices may be constructed. With the aid of a suitable random number generator, such matrices provide a means for generating a statistically probable set of wind and current values based on a previous observation. Although the quantity of time history data required to generate statistically valid matrices of this type is not trivial, once generated, such matrices eliminate the restriction of simulations to the period of data collection, since it is assumed that the probabilities implied by the method remain time-invariant over a period of years. Furthermore, the statistical nature of such an approach seems to lend itself to the base assumption of spatial invariance, since probability should be much less sensitive to position than is actual time history data.

As incorporated in the enhanced model, similar matrices exist for offshore and onshore winds and for offshore currents. Each driving force is defined in terms of a three matrix set for each month, where one first order Markov state transition matrix is used to generate a direction based on the last previous observation. These directional matrices are built based on a 16 point compass. The additional two matrices include a two dimensional probability distribution for velocity as a function of direction, and a one dimensional vector for directional probability which is used to select the initial direction of the particular driving force. In operation, at each time step the proper monthly set of matrices is determined, and a random number between 0 and 1 is obtained from a uniformly distributed random number generator. Associating the previous time step's direction with the appropriate directional transition matrix, the random number identifies the direction for the new time step. This direction can then be used with a new random number to select a corresponding velocity for the desired driving force.

The probabilistic method described here is well suited for generating a large number of simulated slick tracks for use in environmental assessment studies. It was felt, however, that for maximal usefulness the model should have the capability of using time history data; therefore provision was included for generating simulations from such data, either from a time history data base of the type described previously, or through the input of actual values entered from an interactive terminal during real-time. When such data is available it replaces the Markov-generated values. One additional facility is included for use in deterministic tracking applications. Should the model be used to predict the coastal impact point of an actual oil slick in real-time, data on the direction and velocity of the various driving forces will obviously not be known for the entire period of the simulation. In this case, the last known observation will be used as the initial value for probabilistic data generation using the Markov matrices as described above. Then, 100 simultaneous directions and velocities will be generated and averaged at each time step, in order to generate a "most probable" slick path. It is expected that this averaging will improve the ability of the model to predict the path of a spill as it occurs.

3. Adaptive Tracking

Initially, the slick simulator discussed here was designed for use in environmental impact assessment studies. Subsequently, it was desired to enhance the model by adding the capacity to predict a shoreline impact point for a hypothetical oil slick during the first critical hours following a spill. A deterministic solution to such a problem is impossible to achieve since no data on the wind and current driving forces is available. It may be assumed, however, that the wind and current components are known at the spill location. This initial measurement will provide a reasonable basis for the use of the Markov matrices discussed previously, resulting in a "most probable" impact point. Such a solution is correct only if the actual driving forces happen to equal the most probable ones, which is unlikely. The driving forces for the first time interval are known, however, and thus the first movement increment can be calculated in a deterministic manner. At some later time, a second slick location will be known, with the error between the actual and predicted slick locations calculatable. Such error is attributable in part to variations in the winds and currents during one modelling interval, and in part to inaccuracies in the transport equations. Variations in the driving forces cannot be accounted for, but may be assumed to be distributed around the known values, and may be neglected when averaged over several intervals. Error due to inaccuracies in the modelling equations may, however, be accounted for to some degree.

As discussed previously, the basic transport equation for the model is a first order vector sum of winds and currents at the slick location, of the form

$$\Delta\vec{P}_i = C_1\vec{W}_{Fi} + C_2\vec{SC}_{Fi}$$

where C_1 and C_2 are scalar constants. By placing an arbitrary orthogonal grid on the modelling plane and describing the wind and current vectors as vector components in the directions of the coordinate axes, the transport equation may be expressed as a set of two linear equations

$$\Delta P_{i,x} = C_1 W_{Fi,x} + C_2 SC_{Fi,x}$$

$$\Delta P_{i,y} = C_1 W_{Fi,y} + C_2 SC_{Fi,y}$$

where C_1 is usually set to the commonly used wind

drift factor 0.03 and C_2 is set to 1.0 to account for current effects not due to wind shear. It should be noted that such a vector combination approach to slick advection is poorly supported theoretically (7). It was felt, however, that the limited data on the behavior of actual oil slicks does not justify the use of a more rigorous modelling method for a general use model of the type described here.

Much of the debate over the suitability of the vector combination approach centers on disagreement over the values for the proportionality constants C_1 and C_2. Various values have been quoted in the literature, and 0.03 and 1.0 are supportable choices. As such, they may be modified in order to more accurately reflect actual conditions. In the model described here, an attempt is made to adjust the coefficients as additional data for a slick become available. Given any two observations of slick location, and $\vec{W}_{Fi}$, $\vec{SC}_{Fi}$ at the initial position, it is possible to solve the transport equations analytically for C_1 and C_2:

$$C_1 = \frac{SC_x \Delta P_y - SC_y \Delta P_x}{W_y - SC_y W_x}$$

$$C_2 = \frac{\Delta P_x - C_1 W_x}{SC_x}$$

Thus, given n+1 distinct observations, we may calculate n sets of $C_{1,i}$ and $C_{2,i}$ which are averaged in a weighted manner with the latest observation having the greatest weight:

$$C_1' = \frac{\sum_{i=1}^{n} i * C_{1,i}}{\sum_{i=1}^{n} i}$$

$$C_2' = \frac{\sum_{i=1}^{n} i * C_{2,i}}{\sum_{i=1}^{n} i}$$

These averaged C_1', C_2' are now usable in the transport equations to predict further slick movement.

4. Dispersion

The Fay equations, used in the model to describe the physical spread of oil on the ocean surface, predict a terminal radius for a slick of a given mass, at which time those forces tending to cause slick spreading are balanced by those forces tending to retard such spreading. If oil slicks remained connected regions for their entire life span, this concept would be valid. Observation has shown, however, that after a given time slicks tend to fragment into smaller patches, which advect and spread independently (4). Such breakup is beyond the ability of a non-hydrodynamic numerical model to simulate. If, however, an aggregate of patches is treated as a simply connected region with a centroid of mass and equivalent radius enclosing some arbitrary percentage of the total slick mass, then the spread of the slick may be treated statistically as a dispersive model (5). The simulation of an oil slick by such a model imposes no theoretical upper bound on the size of a slick. The model is, therefore, well suited for simulating oil slicks which remain at sea for significant periods, as dispersive forces tend increasingly to dominate over physical spreading forces for times exceeding 10^5 seconds (7).

The analysis for a dispersive model presumes a circular slick with some equivalent radius, R_e, within which lies 95% of the slick mass. This idealized slick is treated as having a normal concentration distribution; therefore, we may define an equivalent variance, $\sigma^2_{r_e}$. R_e is thus equal to $3\sigma_{r_e}$. The available data for dye patch dispersion in the ocean show a relationship between $\sigma^2_{r_e}$ and time which may be characterized as

$$\sigma^2_{r_e} = 0.0108t^{2.34}$$

where $\sigma^2_{r_e}$ is in cm^2 and t is in seconds (6). This equation applies to a circular spill, whereas it is well documented that oil slicks do not remain circular, but tend to assume an elliptical form.

The quantity of work which has been done in attempting the simulation of two-dimensional dispersion processes is minimal; however, it was deemed desirable to attempt such a modification to the slick model described here. It must be emphasized that the dispersion model discussed below is at best a first approximation to actual behavior, but the lack of dispersion data makes a more sophisticated analysis infeasible.

Rather than a single size parameter $\sigma^2_{r_e}$, an elliptical spill may be characterized by two such parameters, σ_x and σ_y, where x and y are respectively the major and minor axes of the slick. In order to describe the growth of an elliptical spill, it is necessary to describe the growth of σ_x and σ_y with time. Unfortunately, there is at present insufficient data in the literature to accomplish this. As an alternate approach, we may describe the elongation of an oil slick, ρ, in terms of the ratio of the major and minor axes

$$\rho = \frac{\sigma_y}{\sigma_x}$$

Data for ρ is available with respect to time for many of the dye patch studies used to derive the time dependence of $\sigma^2_{r_e}$. As a first approximation, ρ may be described by

$$\rho = -0.175 \log_{10}(t) + 1.168 \quad (t{:}sec).$$

Combining the relationships

$$\rho = \frac{\sigma_y}{\sigma_x}$$

and

$$\sigma^2_{r_e} = 2\sigma_x \sigma_y$$

and given $\sigma^2_{r_e}(t)$ and $\rho(t)$, an implicit relationship for σ_x and σ_y may be derived

$$\sigma_x = (\sigma^2_{r_e}/2\rho)^{1/2}$$

$$\sigma_y = \rho\sigma_x$$

Thus, an equivalent ellipse containing 95% of the slick volume will have a major axis length of $2\sigma_x$ and a minor axis length of $2\sigma_y$, where the major axis may be assumed to lie along the direction of the mean current vector.

Elongation data do not extend beyond $4*10^5$ seconds. Slicks with travel times greater than this are presumed to reach a constant elongation of approximately $\rho=0.15$.

5. Implementation

No simulation methodology, regardless of its level of sophistication, is useful if its implementation is difficult to use or its results hard to understand. A primary objective of the modelling implementation discussed here was to provide to the user a complete package with which either probabilistic environmental impact studies or deterministic real-time slick track prediction could be accomplished. The package was designed to require a minimum of specialized knowledge, either of slick modelling fundamentals or of programming. With this objective in mind, the primary user interface is an interactive dialogue designed to be used with a time-sharing terminal. This dialogue carries the user through a logical sequence of questions which define what input data is available to the model and what forms of analysis and output are desired. The model capabilities include the generation of multiple simulations for environmental assessment as well as the prediction of the impact point for a single slick for which location and driving forces are known. The model generates printed output as well as a time history file which may be used as input to additional analyses such as impact counters, plot generators, and a simulator of oil fractions in the water column below the slick. The model may be applied to any offshore region by providing the proper data to describe the areal geometry. Additionally, the input data requirements are heirarchical in nature, so that the model will generate a prediction based on whatever data a given user can provide, from slick location alone to a full time history of winds and currents.

6. Conclusions

Oil slick simulation has been shown to be a useful tool for environmental impact studies by the petrochemical and transportation industries. The model discussed with associated modifications described represent an attempt to provide to the petroleum community the best simulation techniques which may be reasonably applied, within the constraints of present knowledge.

7. Acknowledgements

. This work was partially sponsored by SEADOCK, Inc. and the NOAA Sea Grant Program.

References

1. Fay, J.A., "Physical Processes in the Spread of Oil on a Water Surface," Proceedings of the Joint Conference on Prevention and Control of Oil Spills, pp. 463-67, New York, American Petroleum Institute, 1971.

2. James, W.P., et al., Environmental Aspects of a Supertanker Port on the Texas Gulf Coast, Texas A&M University, Sea Grant Report TAMU-SG-73-201.

3. Moore, S., R.L. Dwyer, and A.M. Katz, A Preliminary Assessment of the Environmental Vulnerability of Machias Bay, Maine to Oil Supertankers, No. MITSG 73-6, Massachusetts Institute of Technology, 1973.

4. Murley, T.S., and M.L. Khandekar, "Simulation of Movement of Oil Slicks in the Strait of Georgia Using Simple Atmosphere and Ocean Dynamics," Proceedings of the Joint Conference on Prevention and Control of Oil Spills, Washington, D.C., 13-15 March 1973, pp. 541-546.

5. Okubo, A., "A Review of Theoretical Models of Turbulent Diffusion in the Sea," Technical Report 30, Chesapeake Bay Institute, Johns Hopkins University, 1962.

6. Okubo, A., "A New Set of Oceanic Diffusion Diagrams," Technical Report 30, Chesapeake Bay Institute, Johns Hopkins University, 1968.

7. Stolzenback, K.D., O.S. Madsen, E.E. Adams, A.M. Pollack, and C.K. Cooper, A Review and Evaluation of Basic Techniques for Predicting the Behavior of Surface Oil Slicks, Massachusetts Institute of Technology, Ralph M. Parsons Laboratory, Report No. 222, February 1977.

8. Williams, G.N., R.P. Hann, and W.P. James, "Predicting the Fate of Oil in the Marine Environment," Proceedings of the Conference on Prevention and Control of Oil Pollution, San Fransisco, California, March 1975.

MARINE POLLUTION IN KUWAIT

B. L. Oostdam
Millersville State College
Millersville, PA 17551

Abstract

Rapid development of a single natural resource and resulting industrialization and urbanization have put a severe stress on the fragile nearshore environment off Kuwait. Major pollution hazards are oil spills, industrial wastes, thermal pollution, fecal coliform, and solid waste.

Good progress is reported in abatement of ammonia and hydrogen sulphide, chief pollutants in the Shuaiba Industrial Area. In Shuaikh, mercury pollution from chlorine plants associated with large desalination plants appear localized. Thermal pollution constitutes recirculation problems and fecal coliform and solid waste are serious along the Kuwait City Waterfront. Although very active in international programs, improvements are required in local cooperation so as to establish an effective environmental protection program to counteract the strong industrial development interests.

1. Introduction

The study of marine pollution in Kuwait is of particular interest because it constitutes a case history of the impact on a tropical nearshore marine environment of extremely rapid single resource development, industrialization and urbanization. The semi-enclosed Gulf between Arabia and Iran is characterized by high temperatures and salinities, and by low wave energy, so that mixing and dilution as well as oxygenation are relatively ineffective agents in counteracting most forms of pollution. A major oil spill would not only have a disastrous effect on such fragile yet important marine resources as shrimp, but also seriously impair the water supply from seawater destillation plants on which Kuwait is vitally dependent. On the other hand, high solar radiation would aid rapid decomposition of spilled oil, and direct effects of spill-landings on the predominant desert shores would be less serious than along densely populated coasts or at well-developed beach resorts.

Since the first export of oil from Kuwait in 1946,and at an accelerating pace since 1973, most industrial developments in the small (17,303 km^2) State of Kuwait (Figure 1) have been concentrated along its shores, where investments to-date exceed US $40,000,000 per kilometer. The population growth, mainly by immigration, has been spectacular, so that the City of Kuwait has to cope with all usual problems of rapid urbanization. The resulting most serious actual or potential sources of pollution are: oil spills, industrial wastes from petrochemical industries and brines from desalination, excess heat from vast cooling plants, fecal coliform, and solid waste.

2. Oil Spills

Exports of crude oil and refined products averaged 120 million m^3 per year from 1955 to 1976. The average annual number of spill accidents reported during this period amounted to 109 , and is decreasing, possibly because of increasingly heavy fines. The estimated amount of oil spilled in Kuwaiti waters averaged 183 m^3 per year, with a maximum of 472 m^3 during 1971. Actual figures are higher, since the numbers and sizes of spills from sources outside Kuwaiti waters are difficult to calculate.

Adequate oil spill cleanup facilities for spills below 1,000 m^3 are available in the form of stockpiled detergents. To deal with major spills, the oil companies in the Gulf have executed a cooperative agreement for mutual aid. Present monitoring and enforcement measures are inadequate, as are facilities for deballasting and slop disposal. As to research on the effects of pollution on indigenous marine species, a program was initiated in 1977, using varying concentrations of oil and refined products, detergents, and combinations of oils and detergents in 96 hour LC-50 continuous flow-through systems; preliminary results are in press.

Tarball surveys were made during the latter half of 1977 along the beaches south of Kuwait City (Oostdam and Anderlini, 1978). During two sampling periods, it was found that tar was concentrated along the high tide swash lines, and rarely occurred on tidal flats or exposed bars. Concentrations decreased from South to North and from fall to winter, 1977, and are summarized in Table I.

TABLE I - TARBALLS ALONG COAST OF SOUTH KUWAIT, 1977

Period	Beaches Sampled*	Grams of tar per m^2	Grams of tar per m	Total Tar**
Sept/Oct	12	7.7 ± 2.8	208 ± 252	29
Nov/Dec	19	3.3 ± 3.6	148 ± 122	20

*three(3) profiles each
**(m^3) along South Coast

From the few published figures available for comparison, and from surveys of beaches along the Indian Ocean made by the author in 1978, the tar pollution of Kuwaiti beaches can be characterized as slight to moderate.

Assuming a 1:3 ratio of tar stranded to oil spilled, the maximum average residence times of tar in a tropical environment is 180 days.

3. Industrial Wastes

Kuwait's main industrial complex,the Shuaiba Area, is located 50 kms South of Kuwait City, and contains harbor-facilities, oil-pipelines, power and seawater desalination plants, refineries and fertilizer plants. The 1977 production capacities of liquid ammonia, sulphuric acid, ammonium sulphate and urea were between 400 and 550 m^3 per day each.

An Air and Water Pollution Control Center was established in 1970 to monitor the various effluents and to set desirable limits and maximum threshold hazard values. Improvements have been impressive, because it is generally recognized that problems of recirculation of the waste water makes effective control mandatory. For example, the immediate deleterious effects of ammonia, one of the main pollutants, are that it attacks the cupro-nickel tubes of cooling water exchangers,increases the system's chlorine demand, and affects the pH of the product water. Its concentrations, as measured at the seawater intakes, have decreased from 3.17 to 0.25 ppm between 1973 and 1977. Similarly, hydrogen sulphide values in waste water outfalls decreased from 7.8 to 5.8 ppm (average) and from 28 to 8 ppm (max) during this period (Sharman & Dourgham, 1977).

Because of the location of the refinery and fertilizer plants, and the configuration of outfalls and intakes, it is virtually impossible to avoid recirculation of waste water into the cooling water inlets before sufficient dilution has taken place. Therefore, projects are underway to recover sulphur and ammonia, and to use suitable land-disposal of waste waters, instead of marine outfalls.

A secondary industrial complex, located in Shuaikh, immediately West of Kuwait City, houses the main power and desalination plants. In 1976, a daily average of 56 million liters of water was distilled from seawater, yielding as by-products over 15,000 tons of salt, and 5,000 tons of chlorine. Because the mercury cell process is used in the chlorine production, the author and his co-workers were requested to study the effects of losses of mercury to the nearshore marine environment (Szucs & Oostdam, 1978). Reported overall mercury losses total 0.2 kgs per ton of chlorine produced. The average effluent discharge was over 2,100 m^3 per hour, and contained 2.17 ± 0.46 micrograms of mercury per liter. Calculations show that only as little as 10% of the total losses of mercury may be directly to the sea.

Seawater samples collected near the outfall of the Salt and Chlorine Division averaged 1.67 ± 0.81 (unfiltered) and 1.06 ± 1.87 (filtered) micrograms per liter, compared to (unfiltered) values of 0.17 ± 0.19 in Kuwait Bay and 0.10 ± 0.11 off the Kuwait coast. Mercury in 31 sediment cores analyzed at 2 cm depth intervals decreased with distance from the outfall (Figure 2) and depth in the sediment column (Figure 3). Mercury averages for the top 10 cms in the outfall area amounted to 3.54 ± 4.33 ppm, as opposed to 0.05 ± 0.04 ppm for 4 cores collected on tidal flats along the Kuwait coast,and 1.74 ± 2.87 ppm for 11 worldwide nearshore areas from the literature. Similar, but less pronounced trends were shown in the outfall area for trace elements with chemical affinities to mercury: 1.83 ± 0.39 for silver in the top 10 cms, 2.18 ± 0.98 for cadmium, 27.36 ± 6.11 for lead,and 14.96 ± 9.36 for zinc (all in ppm's).

Consequently, there is little doubt about the anthropogenic origin of the bulk of the mercury, but the effects of the outfall are restricted to a limited area. A contributory cause of high mercury values in the sediments may be the agitation caused by the adjacent spent seawater cooling water outfall, which stirs up the sediments. This suspended sediment scavenges dissolved trace elements from the ambient water, and subsequently settles in more quiescent waters, thus conveying more mercury to the sediments.

4. Thermal Pollution

Field studies were performed to evaluate the dispersal of waste water, including spent seawater cooling water, in the Shuaiba Nearshore Area. In 1970, The Rhein Ruhr A.G. used drogues followed by boats, and in 1975, Cremer & Warner, (1976) used rhodamine dye and helicopter surveys. The generally warmer discharge waters establish an artificial thermocline, whereas the seawater intake ports are placed as close to the seafloor as possible. Yet under certain conditions, e.g., low tide, onshore winds, and high summer temperatures, the artificial thermocline descends, because the effluents are piled "down" against the shoreline. Under such circumstances, intakes may take in warmer and polluted waters. While industrial effluents measured 39°C, intake water temperatures have been found as high as 31°C, disturbingly close to the critical maximum design temperature for sea cooling water exchanges 32.2°C. Additional field and mathematical, as well as physical modeling studies, have been proposed to recommend improved configurations and procedures.

Problems may also be anticipated with the

power and desalination plants at Doha (Figure 1), located within Kuwait Bay. Too little attention appears to have been given to the Bay's natural circulation and generally elevated temperatures and salinities. Yet the amount of seawater to be circulated by the plant presently completed and the approved additions, are equivalent to the flow of a medium size river (170 m^3 per second), while the anticipated ΔT is of the order of 8°C. This suggests the need for developing countries to accept the practice of preparing environmental impact statements, and of heeding them.

5. Sewage and Solid Waste

In Kuwait City itself, the greater portion of a storm water system had been constructed by 1967 so as to achieve a complete separation of drainage systems. The Main Treatment Plant processes approximately 25,000 m^3 per day, mainly household wastes, of which 60% enters the Bay as secondarily treated water (Al-Shamaly, 1977). In addition, however, much raw sewage still enters the sea from small coastal communities, emergency outfall lines from each of ten pumping stations and from the Main Plant,as well as from numerous illegal hookups to the storm sewage drains. Two additional sewage treatment plants are planned for Fahaheel and Jahra (Figure 1), which should be operational by 1979.

The Occupational Health and Pollution Control Section of the Ministry of Public Health (Al-Zaher, 1976),measured the level of bacterial pollution along the Kuwaiti coast in 1974, at 21 locations, totalling 374 samples. Using a limit of 800 coliform per liter as criterion of pollution, 52 samples exceeded this value, mainly along the coast of the City itself. Highest values (81-8% of 11, and 45% of 20 samples) occurred near Shuaikh Port, and near the Amiri Hospital (35% of 20 samples).

The Kuwait Institute for Scientific Research performed a preliminary assessment of sewage pollution in 1977, monitoring 21 sites adjacent to major storm drains and public beaches. Samples were collected from a launch at high tide, and were processed for fecal coliform, using a count of over 100 per 100 ml as criterion for pollution. Forty-eight percent of all samples were unpolluted, 24% slightly polluted, 19% polluted, and 9% highly polluted. The latter occurred near to recently constructed very large storm drains, in the vicinity of two major hotels. The maximum count was 3,702 fecal coliform per 100 ml.

Immediately after 1977's major rainstorms a survey of all storm sewers in Kuwait City showed suspended sediment values up to 589 ppm with 21% organic matter, against a background average of 36 ppm and 30%. The lowest suspended sediment concentrations 26 ppm,were associated with the highest percentages organics, 62%, and occurred near the hospital complex West of Shuaikh (Figure 1).

A potential hazard is the indiscriminate dumping along the shoreline of vast amounts of "landfill." Although it mainly consists of demolition debris, it also contains such varied substances as old carbodies, watertanks, refrigerators, steel rods and wire, boxes, cans, glass bottles, tires and plain household garbage. Besides the obvious bad quality of these materials for foundations or shoreline protection,and their lack of aesthetic appeal, leaching will contribute to the degradation of the water quality of the nearshore environment, which, at the same time, is the subject of a major coastal recreational development project.

6. Conclusion

Present pollution problems in Kuwait are mainly localized, manageable and not yet as serious as in many other countries. Emphasis should be on: 1) abatement, 2) improved monitoring and fieldwork,preferably by data-buoys, 3) establishment or strengthening of rapid response capability to major disasters, 4) legislative action, setting realistic standards, 5) enforcement.

7. Acknowledgements

The author thanks the Kuwait Institute for Scientific Research for their cooperation during 1976/8,when he served as consultant and Director of the Marine Pollution Program. The cooperation of the Shuaiba Area Authority, Ministries of Public Health,Public Works & Planning,and Kuwait University,is gratefully acknowledged. Finally,thanks are due to Millersville State College for extending a sabbatical leave and a leave of absence,thus allowing the author to expand his professional experiences.

References

1. Al-Shamaly, Ministry of Public Works, 1977: personal communication.

2. Al-Zahner, A.A., 1976: Report on Beaches Regarding Water Quality and Meteorology; Occupational Health & Pollution Control Section, Min. of Public Health, internal report, 12 p.

3. Anderlini, V. & M. Salama, 1977: Preliminary Assessment of Sewage Pollution in Kuwait Bay; internal report, Kuwait Instit. for Scientific Research, 5 p.

4. Cremer & Warner, 1976: Transport of Pollutants through the Environment at Shuaiba. Section 9.0 of Report to Shuaiba Area Authority, p. III, - 187/203.

5. Oostdam, B.L. & V. Anderlini, 1978: Oil spills and Tar Pollution Along the Coast of Kuwait, internal report, Kuwait Instit. for Scientific Research, 54 p.

6. Sharma, Y. & F. Dourgham, 1977: Improvements and Achievements Attained by Pollution Control Within Shuaiba Industrial Area-A Case History (1971-78); stencilled report, Shuaiba Area Authority, 21 p.

7. Szucs, F. K. & B.L. Oostdam, 1978: The Effects of Mercury from the Effluent of the Salt & Chlorine Division Plants on the Nearshore Environment of Kuwait; A report submitted to The Salt & Chlorine Div. of the Petrochemical Industries, 192 p.

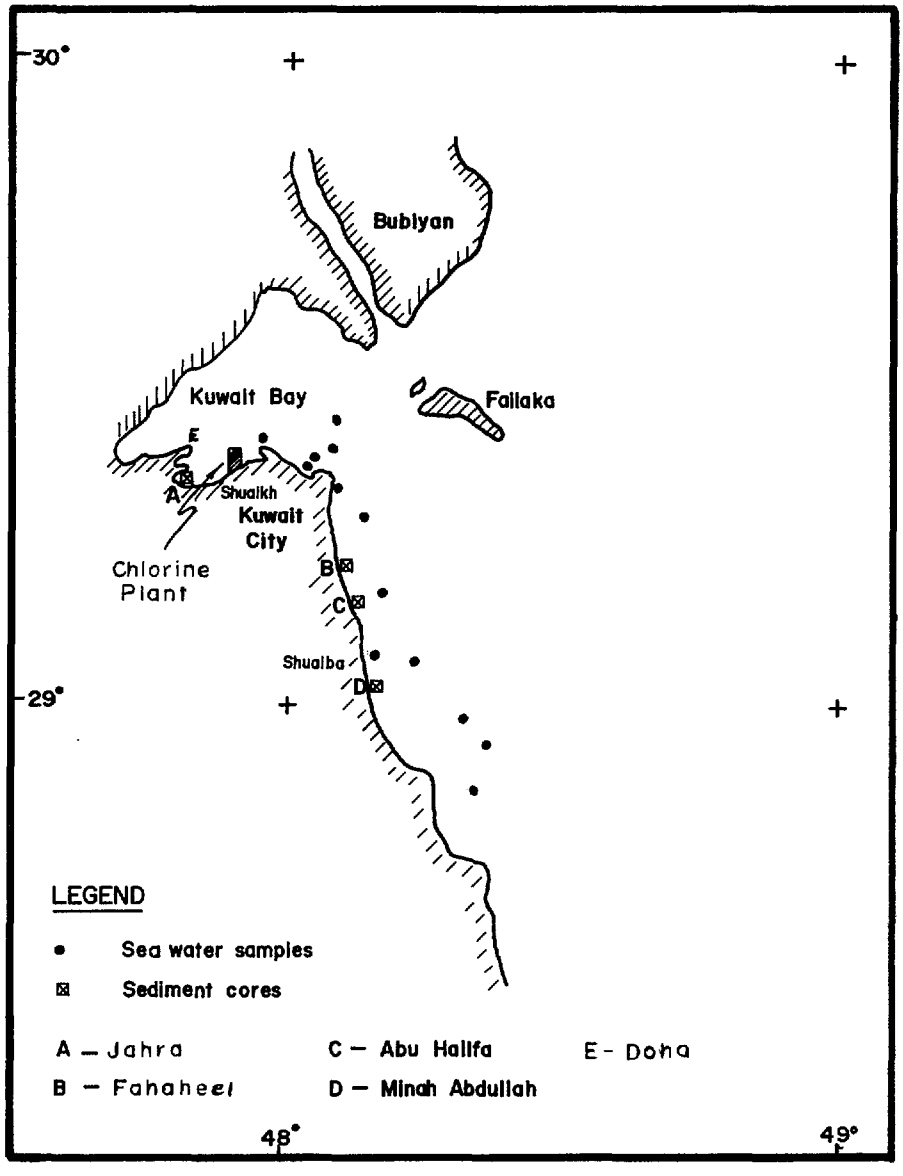

FIGURE 1: Locations of seawater samples and sediment cores collected along the coast of Kuwait, 1977.

FIGURE 2

AREAL DISTRIBUTION OF MERCURY CONTENT (PPM)
IN TOP 10 CMS OF SEDIMENT, S.C.D. NEARSHORE AREA

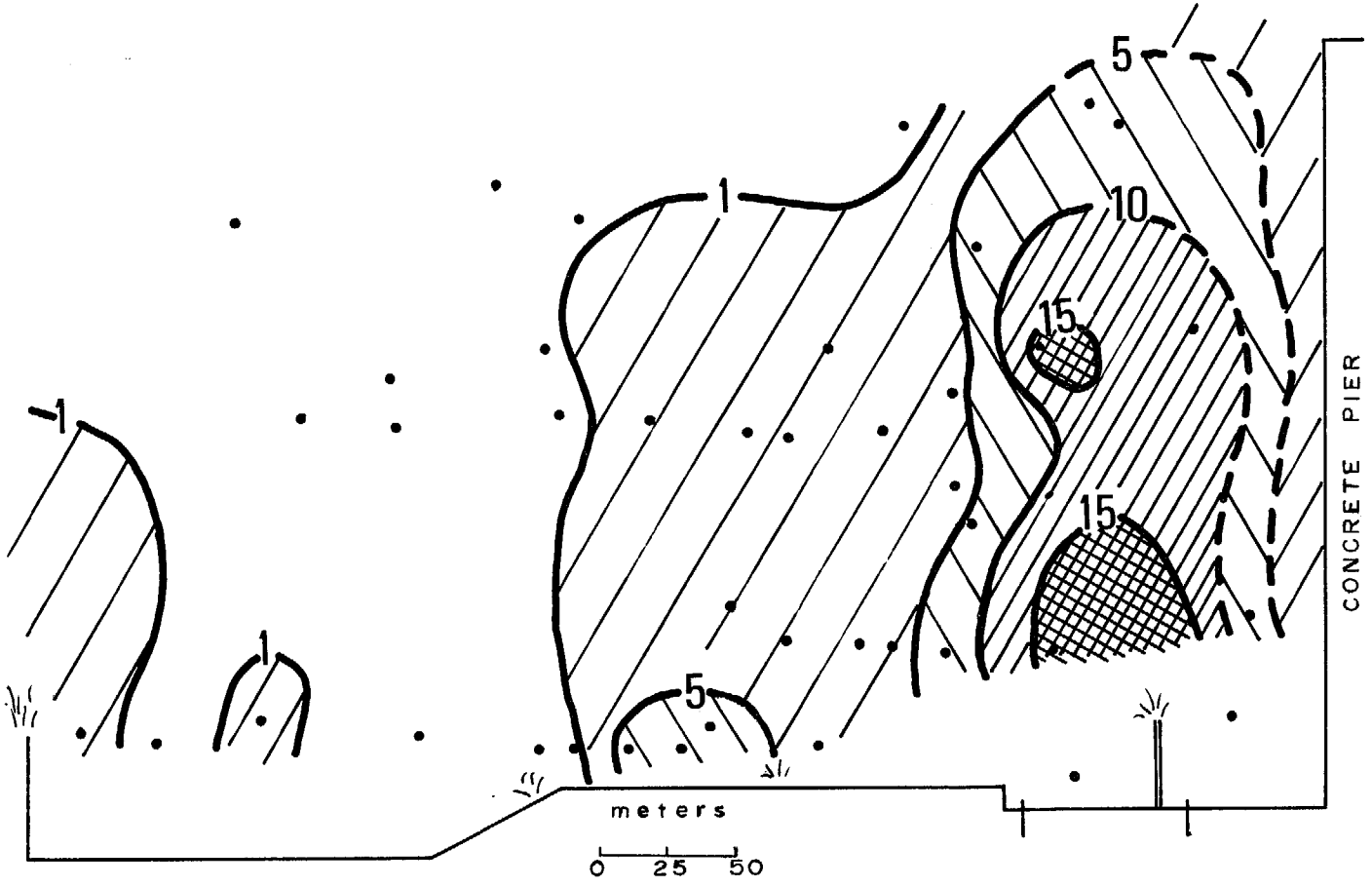

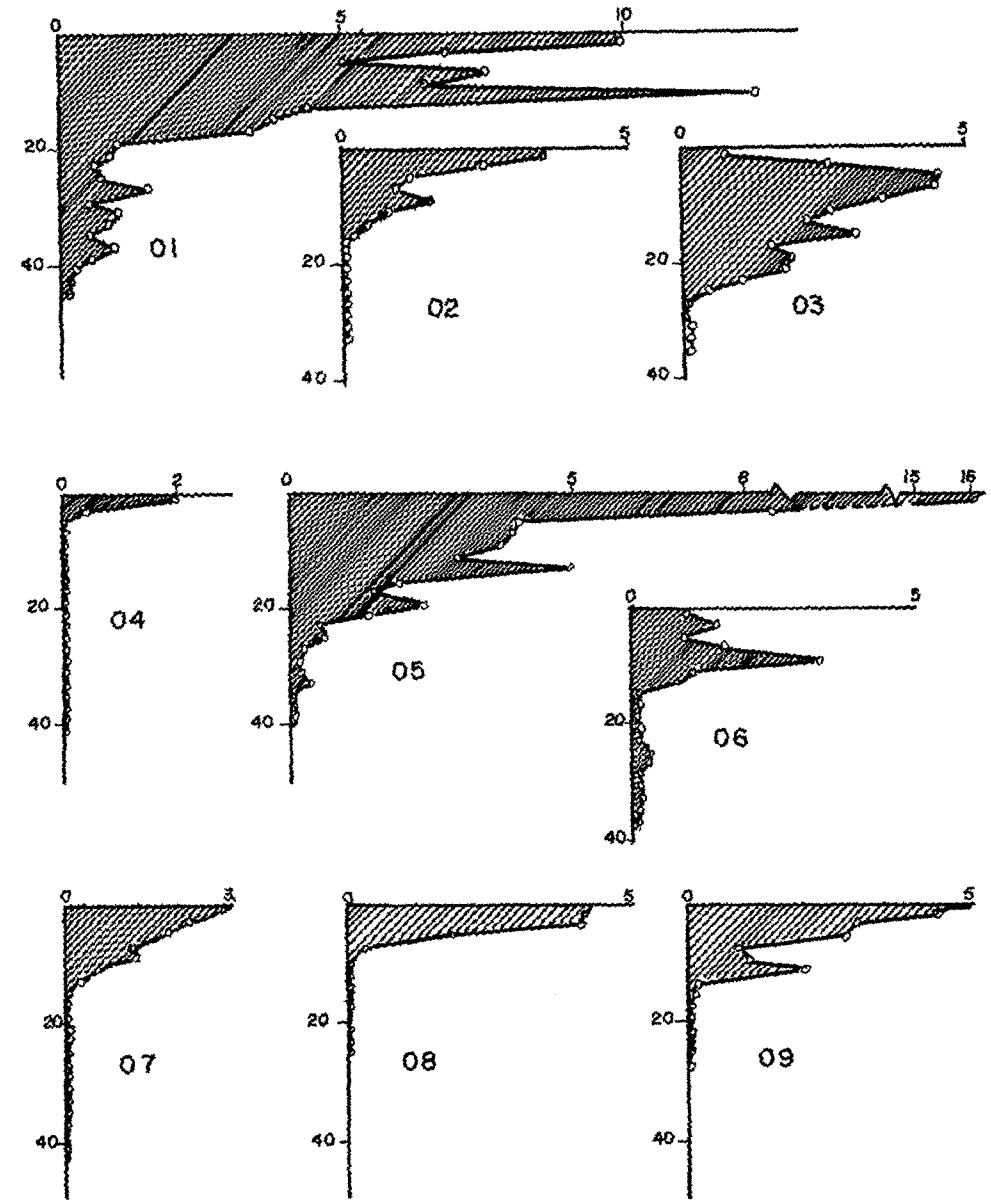

LEGEND :

CORE SERIES

EMP-70613-..

hor. scale = Mercury concentration (in ppm)

vert. scale = Depth below seafloor (in cms)

FIGURE 3 - Variations in mercury concentrations with depth below the seafloor, SCO Nearshore Area, June 1977.

STRATIFIED WATER CIRCULATION FORECASTING FOR WATER QUALITY MANAGEMENT PLANNING IN THE COASTAL ZONE

S.G. Chamberlain, P.V. Tawari, and W.J. Comery

Raytheon Company, Environmental & Oceanographic Services
Portsmouth, Rhode Island

Abstract

Hydrodynamic and water quality models provide a capability to forecast the effects of coastal zone management decisions on waste-receiving coastal and estuarine waterways. This paper discusses the hydrodynamic component of the RAMSES Model, a management planning model designed to simulate stratified estuaries. The need for such a model to bridge the gap in complexity between the simple, but often limited, single layer models and the complex, but often expensive to apply, multi-strata models, is discussed. The model is described in terms of its basic hydrodynamic equations and its numerical solution approach. Processes incorporated in the model, including vertical entrainment and interfacial friction, are identified. The ability of the model to simulate stratified waterways is demonstrated by application to Penobscot Bay.

1. Introduction

Hydrodynamic and water quality models provide a capability to forecast the effects of coastal zone management decisions on waste-receiving coastal and estuarine waterways. The accuracy of the forecasts is a function of the degree to which the models represent fully and correctly all important processes active in the waterway. Two characteristics which are important in adequately simulating stratified waterways are interstrata mass transfer and strata thickness. Stratification has the effect of limiting, but not eliminating the exchange of mass between the strata (or layers) of the waterway, thereby reducing the effective mixing volume for materials discharged to a given layer. Stratification also effects the water circulation patterns in the waterway, thereby affecting the longitudinal and transverse transport of water quality constituents and the resulting spatial distributions. Hence, models used in management planning for stratified coastal or estuarine waterways should be capable of appropriately representing these phenomena.

This paper discusses the hydrodynamic component of the RAMSES Model, a management planning model designed to simulate stratified estuaries. The RAMSES Model (RAytheon Model for Stratified Estuary Systems) is being developed for the U.S. Environmental Protection Agency, under Research Grant No. R805170010 [1]. The need for a model such as RAMSES is established by discussing limitations of existing estuary hydrodynamic models. The RAMSES Model is described in terms of the basic hydrodynamic equations in the model and the numerical approach used to solve the equations. Processes included in the model are described, including external driving forces (tide, runoff, wind), internal horizontal factors (bottom friction, surface gradients, density gradients) and internal vertical processes (interfacial friction, vertical entrainment). The applicability of the model to stratified estuaries is demonstrated by application to a real estuary.

2. Limitations of Existing Models

A number of estuary models currently exist. These include single-layer (vertically-averaged) dynamic models [2-6], used to represent stratified estuaries with a vertically-averaged approximation, steady-state models [7-9], used to represent only the mean distributions of estuary properties, and stratified hydrodynamic models [10-12], used to represent the vertical and horizontal variations in the circulation patterns of stratified estuaries. Each of the existing models, however, has characteristics which may limit its usefulness in water quality management applications. The single-layer dynamic models are inadequate for representing the vertical variations in water quality properties in stratified estuaries. The lack of dynamic representation in the steady-state models eliminates them from consideration for many estuary applications. Existing stratified hydrodynamic models are often limited in their applicability to estuaries either by failure to represent one of the important physical phenomena or by excessive cost and computer requirements. These limitations have focused attention on the need for the development of a less complex, layered hydrodynamic model that can be applied within the fiscal and facility constraints of water quality management planning programs for stratified estuaries.

3. The RAMSES Model

The RAMSES Model includes the essential dynamics and stratification features of estuaries in a form that bridges the gap in complexity between the simple, but often limited, single-layer models, and

the existing complex, but often expensive, multi-strata models. The model is dynamic, in that time variations in water flows are produced. Stratification is included by incorporating mass and momentum transfers between layers and by forecasting layer thicknesses and densities. Complexity of the model and costs to apply the model are kept to a minimum by limiting vertical resolution to two layers, and by utilizing a network of interconnected one-dimensional channels (links) and water masses (nodes) to represent horizontal flows in each layer.

The RAMSES Model includes hydrodynamic and water quality models connected in tandem. The hydrodynamic model forecasts water flows and layer thicknesses, and feeds these as inputs to the water quality model. The water quality model then forecasts distributions of water quality constituents throughout the estuary. Water circulation forecasting is the subject of this paper, so only the hydrodynamic model is discussed here. When the designation RAMSES Model is used in this paper, the hydrodynamic component of the RAMSES Model is intended unless otherwise stated.

The model solves the basic equations of mass and momentum conservation. Being non-linear, the equations cannot in general be solved analytically. The use of the link-node approach simplifies the equations to provide a set of equations which can be solved numerically on the computer. The equations consist of two types, those relating to nodes (or water masses) and those relating to links (or channels) which connect the nodes. Derivation of these equations is to appear in a forthcoming paper [13]. The node equations for the thickness (H) of each node, and for salinity (c) in each node, are:

$$\frac{\partial H}{\partial t} = \frac{\Sigma \rho(c_i) Q_i - \frac{\partial \rho}{\partial c} \Sigma c_i Q_i}{A\left[\rho - c \frac{\partial \rho}{\partial c}\right]} \tag{1}$$

$$\frac{\partial c}{\partial t} = \frac{\rho \Sigma c_i Q_i - c \Sigma \rho(c_i) Q_i}{AH\left[\rho - c \frac{\partial \rho}{\partial c}\right]} \tag{2}$$

where:

ρ = mass density of the node

c_i = salinity of i th channel connected to the node

Q_i = volumetric flow rate of i th channel connected to the node

A = surface area of the node

The channel equations, for flow velocities (U_1,U_2) and channel thicknesses (H_1,H_2) in the surface and bottom layers (subscripts 1 and 2 respectively, are:

$$\frac{\partial U_1}{\partial t} - \frac{U_1}{H_1}\frac{\partial H_1}{\partial t} = \frac{C^* \rho_a w_a^2}{H_1 \rho_1}\cos(\psi) - \frac{\nu_o}{H_1}(U_1 - U_2)\,|U_1 - U_2| - \frac{gH_1}{2\rho_1}\frac{\partial \rho_1}{\partial x} + \frac{U_1^2}{H_1}\frac{\partial H_1}{\partial x} - g\frac{\partial \eta_1}{\partial x} \tag{3}$$

$$\frac{\partial U_2}{\partial t} - \frac{U_2}{H_2}\frac{\partial H_2}{\partial t} = -\frac{g\,U_2\,|U_2|}{H C_z^2} + \frac{\nu_o}{H_2}(U_1 - U_2)\,|U_1 - U_2| - \frac{gH_2}{2\rho_2}\frac{\partial \rho_2}{\partial x} + \frac{U_2^2}{H_2}\frac{\partial H_2}{\partial x} - g\frac{\partial \eta_2}{\partial x} - g\frac{\rho_1}{\rho_2}\frac{\partial H_1}{\partial x} \tag{4}$$

where:

C^* = Eckman coefficient

ρ_a = density of air

w_a = wind velocity

ψ = angle between wind direction and channel axis

ρ_i = density of surface layer channel (i = 1), bottom layer channel (i = 2)

ν_o = interfacial friction coefficient

g = gravitational acceleration constant

η_1 = surface elevation (= $H_1 + H_2 + E_B$)

E_B = bottom elevation

η_2 = interface elevation (= $H_2 + E_B$)

C_z = Chezy coefficient

In the surface layer equation (3), the terms on the right side of the equality sign represent respectively: wind stress, interfacial friction, horizontal density gradient, layer thickness gradient and surface gradient. The terms on the right hand side of the bottom layer equation (4) are, respectively: bottom friction, interfacial friction, horizontal density gradient, bottom layer thickness gradient, interfacial elevation gradient and a gravitational force due to surface layer thickness gradient.

Vertical transport of mass is included in the node equations where the vertical flow rate (Q_v) is taken as a function of the difference in flow velocities in the surface and bottom layers:

$$Q_v = \frac{KA(U_1 - U_2)^3}{g\bar{H}\frac{\Delta\rho}{\rho}} \quad (5)$$

where:

K = vertical entrainment coefficient

A = channel surface area

U_i = surface (i = 1) and bottom (i = 2) layer velocities

ρ = average of surface and bottom layer densities (ρ_1, ρ_2)

$\Delta\rho = \rho_2 - \rho_1$

$\bar{H}$ = average of surface and bottom layer thicknesses

4. Solution Approach

The node and link equations given above are solved by discretizing space in such a manner that the partial differential equations above become a set of ordinary differential equations. Spatial discretizations are accomplished by laying out a network of nodes, representing masses of water, and links, representing channels which connect the nodes, throughout the waterway of interest, as illustrated in Figure 1. The two-layered representation of an estuary is illustrated in Figure 2. Partial derivatives are approximated as finite differences between upstream and downstream values.

The coupled set of ordinary differential equations are solved by discretizing time and using a fourth order Runge Kutta algorithm to solve the resulting difference equations.

The model can be driven by appropriate selection of upstream and downstream boundary conditions. Upstream flows and downstream tidal elevations, both as functions of time, are specified as inputs.

The model produces forecasts (outputs) of the flows in each channel and in each layer throughout the link-node network as a function of time throughout the simulation period. It also produces forecasts of the thicknesses and salinities of each layer at each node throughout the link-node network, also as a function of time throughout the simulation period.

5. Application to Penobscot Bay

To demonstrate the applicability of the model, the simulation of simplified tidal flows and river runoff in Penobscot Bay is presented. Circulation in Penobscot Bay, located on the coastline of Maine, consists of a two-layer flow regime produced by the flow of lower salinity, less dense runoff water over higher salinity, more dense ocean water. Saline tidal waters enter and leave the Bay at two ocean boundaries, shown in Figure 3, and fresh water flows out from the Penobscot River. Stratified flow is characterized by the entrainment of lower waters into the surface layer.

To carry out the simulation, data on the Bay were reviewed, a simulation period was selected, data for that period were selected and prepared for use with the model, and the simulation was carried out. Model inputs, derived from field data made available by the Central Maine Power Company [14,15] include boundary conditions (river runoff at the upstream boundary and tidal elevation and ocean salinity at the downstream boundaries), and initial conditions (layer depths (i.e., stratification) and salinities in the layers). Layer salinities were taken as 27 ppt and 31 ppt in the surface and bottom layers, respectively. River runoff from the Penobscot River was taken as $164 m^3/s$. At the downstream boundaries, tidal elevations were taken as a sinusoidal function of time, with tidal period of 12.4 hours, an amplitude of 1.47m and a mean value of 1.40m above MLW.

Flows across three key cross-sections of the Bay are important for comparison with model forecasts. The three cross-sections, as shown in Figure 3, are East Passage (EP), West Passage (WP) and Sears Island (SI). Measurement data on these flows indicate the following characteristics of Penobscot Bay waters:

(i) A strong tidal influence exists in the Bay.

(ii) Flow is predominantly two-layered.

(iii) A net current exists in the Bay due to runoff from the Penobscot River.

(iv) There is a net outward flow in the surface layer and a net inward flow in the bottom layer.

To simulate the flows in Penobscot Bay, a simplified network of nodes and links was selected, as shown in Figure 3. Uniform depths, salinities, and channel lengths and widths were used to simplify the analyses. The channel cross-sectional areas were equal to the average cross-sectional areas of the EP, WP, and SI transects. This allows flows across these cross-sections to be properly simulated in the model.

Flows produced by the model across the three cross-sections are shown in Table 1. Flood and ebb flows given in the table are the total flows integrated over the flood and ebb portions, respectively, of the tidal cycle. Negative (positive) values are into (out of) the Bay. The flows forecasted by the model, as given in Table 1, show the following characteristics:

(i) Flows are oscillating (positive and negative) due to the ebb and flood tidal waters.

(ii) Flows in the top and bottom layers are different, due to the differing velocities in the two layers.

(iii) Flows from the Penobscot River influence flows across the three cross-sections.

(iv) Net flow is out of the Bay (positive) in the surface layer and into the Bay (negative) in the bottom layer.

These characteristics of the forecast flows agree with the characteristics of Penobscot Bay waters derived from field measurements. This agreement is for the major flow characteristics of the Bay, which is all that was simulated. Additional simulations utilizing a finer grid and a more complete set of data can be carried out. However, agreement betwen the model forecasts and characteristics derived from field data, as discussed above, demonstrates the applicability of the model to stratified estuaries, such as Penobscot Bay.

6. Conclusions

The RAMSES Hydrodynamic Model has been developed for use as a planning tool for forecasting the effects of potential coastal zone management decisions on stratified waste-receiving coastal and estuarine waterways. This model fills the gap in complexity between simple, but often limited, single-layer models, and existing complex, but often expensive, multi-strata models. The RAMSES Model incorporates inter-strata mass transfers and strata (i.e., layer) thicknesses which are important in adequately simulating stratified waterways. The applicability of the model to stratified waterways has been demonstrated by a simplified simulation of stratified flows in Penobscot Bay.

7. References

1. Tawari, P.V., S.G. Chamberlain, and W.J. Comery, Development of a Dynamic, Two-Layer Hydrodynamic Model for Stratified Estuaries, Raytheon Interim Report to U.S. Environmental Protection Agency, Research Grant No. R805170010, June 1978

2. Raytheon Company, Environmental & Oceanographic Services. New England River Basins Modeling Project, Vol. 1, RECEIV-II Water Quantity & Quality Model Documentation Report. U.S. Environmental Protection Agency, Contract 68-01-1890, 1974. 289 pp.

3. Feigner, K.D., and H.S. Harris. Documentation Report, FWQA Dynamic Estuary Model. U.S. Department of the Interior. FWQA, July 1970. 248 pp.

4. Leendertse, J.J. Aspects of a Computational Model for Long-Period Water-Wave Propagation. Rand Corp., Santa Monica, Memo. No. RM-5294-PR, May 1967. 165 pp.

5. Laevastu, T. A Vertically Integrated Hydrodynamical-Numerical Model, Part 1, ENVPREPRSCHFAC Technical Note No. 1-74, Environmental Prediction Research Facility, Naval Post Graduate School, Monterey, California, January 1974. 63 pp.

6. TRACOR, Inc. Estuarine Modeling: An Assessment. Water Quality Office, Environmental Protection Agency, Washington, DC. Report No. 16070 DZV 02/71. February 1971. 497 pp.

7. Ippen, A.T. and D.R.F. Harleman. One-dimensional Analysis of Salinity Intrusion in Estuaries Tech. Bull. No. 5. Committee of Tidal Hydraulics, Corps of Engineers, U.S. Army, Vicksburg, Mississippi, June 1961. 51 pp.

8. Fisher, J.S., J.D. Ditmars and A.T. Ippen. Mathematical Simulation of Tidal Time-Averages of Salinity and Velocity Profiles in Estuaries Massachusetts Institute of Technology, Report No. MITSG 72-11, November 1972. 193 pp.

9. Thomann, R.V. Systems Analysis and Water Quality Management. Environmental Science Services Division, Environmental Research and Applications, Inc., New York, 1972.

10. Laevastu, T. and G.D. Hamilton. Computation of Real-Time Currents off Southern California with Multi-Layer Hydrodynamical-Numerical Models. Environmental Prediction Research Facility, Naval Post Graduate School. Monterey, California. 1974.

11. Leendertse, J.J. and S.K. Liu. A Three Dimensional Model for Estuaries and Coastal Seas: Volume II, Aspects of Computation. Rand Corp., Santa Monica, California. 1975. 123 pp.

12. Wang, J.D. Mathematical Modeling of Near Coastal Circulation. Ph.D. Dissertation, Mass. Inst. Tech., Cambridge, Mass., 1975.

13. Chamberlain, S.G., P.V. Tawari, and W.J. Comery. "The RAMSES Hydrodynamic Model: A Numerical Model for Stratified Estuary Systems", to be submitted.

14. Normandeau Associates. Environmental Survey of Upper Penobscot Bay, Maine. Second Quarterly Report for Central Maine Power Company, April 1975. 385 pp.

15. Normandeau Associates. Preliminary Data Package for Anchor-Station Transect Survey of Upper Penobscot Bay Conducted on March 19, 1975, Phase I (Update) and Phase II for Central Maine Power Company, July 3, 1975.

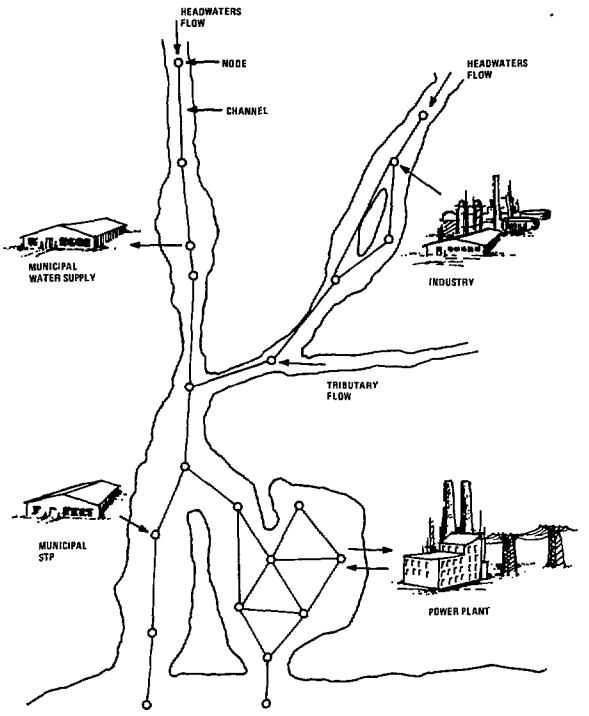

Figure 1. Illustration of RAMSES spatial framework. (adapted from reference [1])

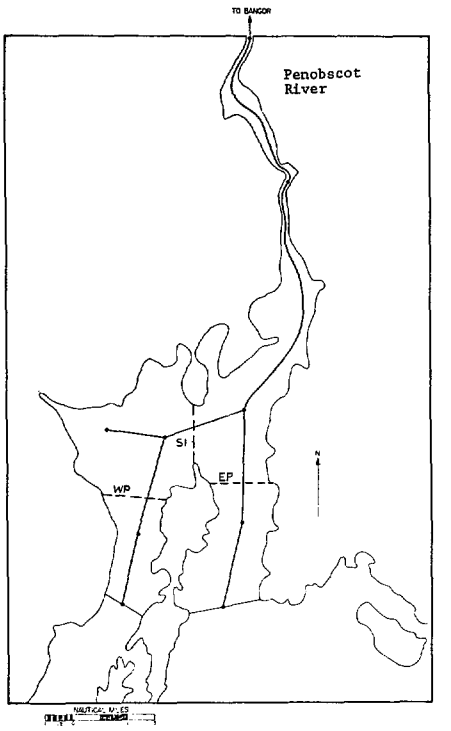

Figure 3. Model simulation network of Penobscot Bay

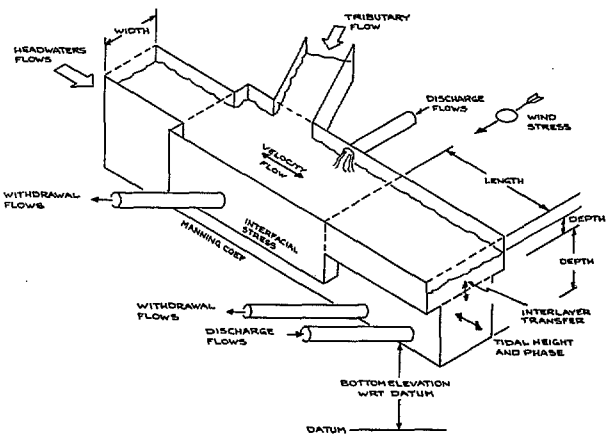

Figure 2. Illustration of estuary layeredness for hydrodynamic computations in the RAMSES model.

Figure 2. Illustration of estuary layeredness for hydrodynamic computations in the RAMSES model

	Average Flow Over Tidal Cycle	Flood Flow	Ebb Flow
EAST PASSAGE			
Top Layer	0.90	-1.72	2.62
Bottom Layer	-0.34	-9.51	9.17
SEARS ISLAND			
Top Layer	0.77	0.01	0.76
Bottom Layer	-0.25	-1.52	1.27
WEST PASSAGE			
Top Layer	0.90	-1.53	2.43
Bottom Layer	-0.36	-8.80	8.44

Table 1. Model forecasts of flows across three cross-sections ($x10^7$ cubic meters)

OCEAN DISPOSAL IN THE MID-ATLANTIC BIGHT

W. C. Muir
U.S. Environmental Protection Agency
Philadelphia, Pa. 19106

G. M. Horwitz
U.S. EPA
Philadelphia, Pa. 19106

G. D. Pence
U.S. EPA
Philadelphia, Pa. 19106

Abstract

With the passage of the Marine Protection, Research, and Sanctuaries Act of 1972, the U.S. Environmental Protection Agency has been given the lead role in the protection of the nation's oceans from the disposal of toxic pollutants. Through the establishment of a permit program, the U.S. EPA's Middle Atlantic Region III has brought the indiscriminate disposal of municipal and industrial wastes under control. The goal is to eliminate ocean disposal of harmful waste by January, 1981 through the development of sound, reasonable and environmentally acceptable land based alternatives. Until that goal is attained, an intensive monitoring program has been established to assess the fate and effects of all pollutants dumped into the Region's waters.

INTRODUCTION

About ten percent of the pollutants entering the world's oceans are introduced as a result of someone's collecting wastes, putting them on a barge or ship, and taking them out for disposal at sea.[1] Prior to 1972, there was little governmental control over ocean dumping. Disposal of waste materials at sea began with an application to the District Office of the U.S. Army Corps of Engineers. The application was circulated to other federal agencies and the Corps issued a "letter of no objection." The sole criteria for issuance or denial was whether navigation would be impeded or obstructed.

The revelations of the late 1960's and 1970's concerning dumping of nerve gas and petroleum off the Florida Coast, dumping of enormous quantities of sewage sludge, each day from New York and Philadelphia, and a number of other similar instances, spawned legislation to regulate ocean dumping. Relying heavily on the Council of Environmental Quality's April, 1970 report, Ocean Dumping - - A National Policy, and the Environmental Protection Agency's 1971 report, Ocean Disposal of Barge - Delivered Liquid and Solid Wastes from U.S. Coastal Cities, Congress passed the Marine Protection, Research, and Sanctuaries Act of 1972 which became effective April 23, 1973. The Congress has made the findings that:

> ...it is the policy of the United States to regulate the dumping of all types of materials into ocean waters and to prevent or strictly limit the dumping into ocean waters of any material which would adversely affect human health, welfare, or amenitities, or the marine environment, ecological systems, or economic potentialities.

The Act is divided into three major parts. Of prime importance to ocean dumping is Title I which establishes criteria and regulations to control all future dumping. The Environmental Protection Agency has the prime responsibility for regulation of all dumping except dredged material. The Act, while banning certain materials, allows dumping under EPA permits. In establishing criteria for evaluation of permit applications, the Administrator must consider the need for the proposed dumping, the ecological ramifications of the dumping and the alternatives to ocean disposal available.

The Act was amended twice, once on March 22, 1974, to clarify the interpretation of oil as it relates to the requirements of the Federal Water Pollution Control Act, and again on November 4, 1977, to place a date final for all ocean dumping which does not meet the criteria. That date being December 31, 1981.

Pursuant to the Act, the Administrator of EPA promulgated regulations and criteria for ocean disposal on October 15, 1973 and Final Revised Regulations and Criteria on January 11, 1977. The Administrator further promulgated procedural regulations on November 28, 1977. These regulations and criteria constitute the entire body of rules governing ocean dumping.

The EPA and the Corps of Engineers (for dredged spoils) regulates ocean dumping through the issuance of ocean dumping permits. There are six categories: General, Special, Interim, Research, Emergency, and Ocean Incineration. The Regional Office is responsible for Special and Interim permits which are defined as:

U.S. Government work not protected by U.S. copyright.

Special Permits - issued for certain materials which satisfy all relevant ocean dumping criteria.

Interim Permits - issued for materials exceeding criteria. No interim permits will be in effect after December 31, 1981 and no interim permits will be issued after April 23, 1978 unless the dumper is on an implementation plan to meet the criteria or phase out dumping by December 31, 1981.

The criteria for determination of acceptability are divided into three parts; prohibited materials; constituents prohibited as other than trace contaminants; and materials which will not endanger or degrade the marine environment.

Prohibited - include biological, chemical, or radiological warfare agents; high-level radioactive wastes; and persistent inert synthetic or natural floating materials.

Constituents prohibited as other than trace contaminants - organohalogen compounds; mercury; cadmium; oil; and carcinogens, mutagens or teratogens.

Materials permitted for ocean disposal - any materials not containing prohibited constituents or contaminants in no greater than trace concentrations.

REGIONAL ACTIVITIES

At the onset of the ocean disposal program, the EPA Region III administered four disposal sites as shown in Figure I. Site (1) is the old sewage sludge site. This site was authorized by

FIGURE I OCEAN DISPOSAL SITES

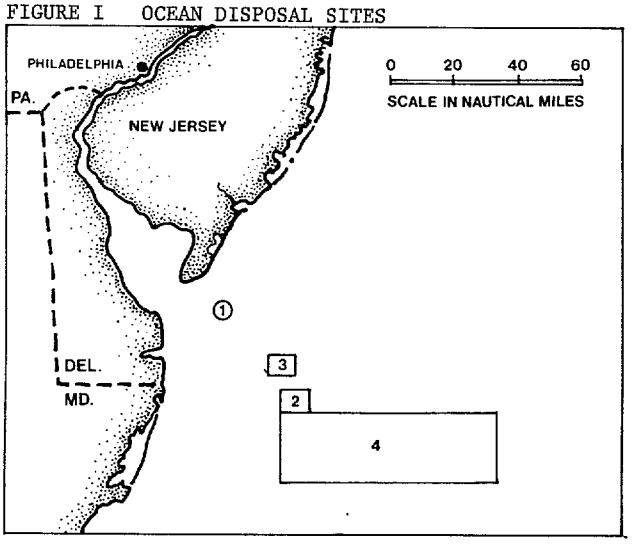

TABLE I OCEAN DISPOSAL

Site	Gallons x 10^6	Kilograms x 10^6
1. Old sewage sludge site (1961-1973)	960.4	3,746.4
2. New sewage sludge site (1973-1977)	718.4	2,802.4
3. Acid Waste Site (1973-1977)	964.5	3,696.8
4. Arsenic Site (1966-1974)	28.6	109.6

the United States Corps of Engineers in 1961 for the disposal of the City of Philadelphia's sewage sludge. In 1966, the City of Camden began using the same site. The site was closed on May 8, 1973 and both dumpers were moved to Site (2), the new sewage sludge site. Dupont disposed of acid wastes at Site (3) from 1968 to 1977 at which time its dumping was moved off the Continental Shelf. Site (4) was designated as the arsenic site and had been used intermittently for a number of years by various industries but no records were kept until 1966. From 1966 to 1974 this site was used to dispose of caustic and white water oil emulsion from the Sun Oil Company. A summary of the total site usage is shown in Table I.

The Region has attempted to rigorously enforce the mandate set forth by Congress. Table II shows the status of permit activities within the Region. Each application received a critical review to determine if there was a real need to dump, what the potential environmental effects of dumping would be, and, how the effects could be minimized if dumping was necessary. All permits that were issued contained requirements that the dumper develop alternatives as soon as possible.

Presently, there is only one active dumping site in the Region. This site (Number 2) is used by the City of Philadelphia. Except for Dupont and Crompton & Knowles, Inc., which have been moved to the '106' site controlled by Region II, all other dumping which originated within the Region has been phased out. The remaining dumpers are on strict schedules to phase out all dumping by 1981.

MONITORING

To comply with the intent of the Act, that permits be conditioned upon knowledge of effects on the marine environment, Region III initiated an intensive field monitoring program in May, 1973. The objectives of the program were to provide a system for the evaluation, control and regulation of ocean disposal.

The design of the monitoring program was based upon the assumption that the ocean is a

TABLE II OCEAN DUMPING PERMIT APPLICATIONS

State	Applicant	Issued/Denied	Phase Out
Delaware			
	Dupont-Edgemoor	issued	1980
	Rollins Env. Serv.	issued	1975
	Barcroft Lo.	denied	
District of Columbia			
	U.S. Army Corps of Engineers	denied	
New Jersey			
	City of Camden	issued	1978
	New Jersey Zinc	denied	
Ohio			
	U.S. Air Force	denied	
Pennsylvania			
	City of Philadelphia	issued	1980
	Sun Oil Company	issued	1975
	Modern Transport - Sewage	issued	1975
	Modern Transport - Industrial	issued	1975
	ABM Disposal Ser.	denied	
	Integrity Shipping Company	denied	
	Whitmoyer Laboratories	denied	
	McAdoo & Allen, Inc.	denied	
	Crompton & Knowles, Inc.	issued	1979
Virginia			
	Hampton Roads Sanitation District	denied	
West Virginia			
	Dupont-Belle	issued	1976
Wisconsin			
	Ansul Co.	denied	

dynamic medium and that any material injected into it will be acted upon by physical, chemical and biological processes. The interaction of the processes has been described by Ketchum quite well.[2] Our program is split into two distinct tasks. The first is to assess the immediate effects of the pollutants upon impact into the ocean. The second is to determine the ultimate fate and effects on the marine environment.

Prime objectives of the short-term study were to determine safe discharge rates (F.R. 198 pt. II, 1977) and to determine how the pollutants behaved. These objectives were accomplished by determining the initial dilution factors, the dispersion with time, and the toxicity on the organisms as the pollutants were diluted.

The prime objectives of the long-term study were: first, to determine an environmental baseline from which the effects of the dumping can be compared; second, to determine the ultimate fate of pollutants and the pathways by which pollutants are distributed; third, to assess the impact of these pollutants on the marine biota; and last, to predict the potential for impact before irreversible effects occur.[3]

FIG.11. MID-PLUME DATA; WAKEFALL, SEPTEMBER 1975[6]

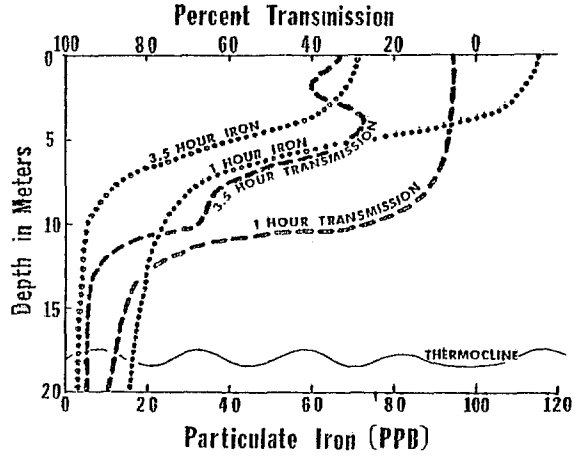

Short-Term Studies

To determine the dilution and dispersion of the wastes, plume tracking experiments have been conducted on the acid wastes and the sewage sludge being dumped. For sewage sludge a good correlation exists between total suspended matter and extinction coefficient.[4] Transmissiometer profiles with separate CSTD's and hydrocasts for heavy metals and bacterial content were made in the barge wake during special surveys in 1975 and 1976.[5,6] Figure II indicates how the material dispersed with time.

Conclusions from the sludge plume studies were that the plume does not penetrate deeply into the water column; the plume remains as a narrow ribbon for several hours with maximum concentrations near the surface and the centerline of the long axis; and, initial dilution was approximately 1:4200, and after four hours 1:10,000, for metals and 1:100,000 for coliform bacteria.

Through the permit system, EG & G, environmental consultants, conducted plume studies of Dupont's acid waste. Instead of transmissivity, EG & G used pH and iron to identify the plume. Interestingly, they found initial mixing to be about 1:5,000 and after four hours 1:100,000. This compared roughly with the sludge dispersion.

In conjunction with the studies of initial dilution and dispersion, EPA has the various wastes tested for toxicity. Bioassays have been shown to be a valuable analytical technique where chemical examination alone of complex industrial and municipal wastes does not provide sufficient information on their effects on the aquatic biota for the protection of the aquatic environment. Short-term bioassays are used as a range-finding technique to indicate relative toxicity of a complex waste. Long-term bioassays are used to determine effects on life cycles such as growth, reproduction, development of sex products, maturation, spawning, success of spawning, hatching success, survival of larvae or fry growth and survival of different life stages, behavior, and bioaccumulation.

The results of these assays were used to define release conditions under which the wastes would present no harm to the marine environment. As an example, Dupont was required to conduct both acute and chronic toxicity bioassays. Assays were done on Acartia tonsa (a marine copepod), Cyprinodon variegatus (a fin fish), and Mysidopsis bahia (a marine shrimp). Figure III shows how the data from these bioassays are used to determine the release time for a barge.

Long-Term Studies

The Region has spent the bulk of its efforts in establishing the long-term trends associated with specific dumping practices. Trend surveys have been conducted on a semiannual basis since the program's conception in 1973. More than twenty surveys have been conducted. Emphasis has been placed upon the bottom environment because long-term changes or trends associated with disposal of wastes are more detectable in this less transient system. The sands and shellfish do not move about as much as do fin fish, plankton, and water.

Persistent contaminants, those which do not readily degrade, contained in industrial and municipal wastes are a primary environmental concern. As an example, heavy metals and chlorinated hydrocarbons are persistent contaminants and represent a hazard to marine life.

One portion of our surveys centered on studying the distribution of selected metals in the bottom environment, specifically in two common species of shellfish. Both Dupont and the City of Philadelphia dumped many metric tons of metals annually. Dupont's waste accounted for most of the iron, manganese, titanium and vandium dumped in this area of the continental shelf. Philadelphia sludge accounted for most of the copper, silver, lead, nickel, and cadmium. Two species of shellfish, Artica islandica (mahogany clams), and Placopecten megellanicus (sea scallops) were

FIGURE III Bioassay and Release Time (Falk 1976) Relationship for Dupont Barge

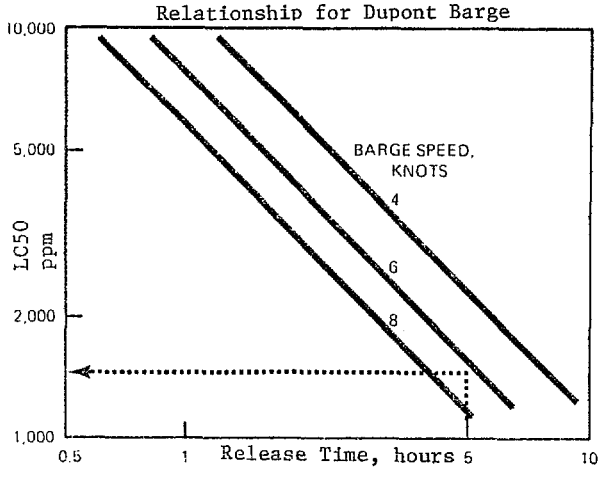

collected over a wide area of the Mid-Atlantic shelf and analyzed for 13 heavy metals. The data were then subjected to several statistical analyses. Among these were the One Way Analysis of Variance and Duncan's Multiple Range Test. Dr. Gerald G. Pesch, an EPA research biologist at the EPA's Environmental Research Laboratory in Narragansett, Rhode Island, gave a detailed explanation of how the statistical tests were used to show causal relationships between metals in the organisms and the wastes dumped.[5] Based in part on Dr. Pesch's work, an EPA hearing officer concluded that Dupont should move its dumping activity to an area off-the-continental shelf which has a lower level of productivity, has no potential marketable quantities of shellfish, and due to the greater depths and distance to shore, should provide for much greater dispersion and dilution of the wastes.

Community structure of micro-organisms also provide a tool for trend analysis. In 1975, study of the infauna community indicated an aberrancy south of the municipal sludge release site. A grid of stations at relatively close intervals was established and indicated several areas of apparent sludge accumulation immediately to the south of the release site. Investigations of these areas indicated accumulations of organic carbon, metals characteristic of the sludge waste, PCB's (a synthetic organohalogen) and coprostanol (a steroid biochemical excreted from the intestines of warm-blooded animals and indicative of sewage pollution).[7]

In April 1978 EPA and the Food and Drug Administration conducted a joint expedition to assess the extent of distribution of sewage indicator bacteria (coliform, fecal coliform) associated with municipal sludge dumping. Previous investigations indicated the general absence of these indicators of public health significant in the water column, except immediately behind the barge while dumping. The preliminary results did indicate, however, the presence in sediments. The results of the April 1978 survey conclusively showed contamination in the bottom sediments in an area of at least 165 nautical miles square.[8]

Independent of EPA's field surveys, the City of Philadelphia was required to do prediction studies on its sludge. A mathematical model simulating the hydrographic characteristics of this Region and the nature of the wastes, done by Raytheon Corporation under contract to the City of Philadelphia, indicated the probable repositories of barged waste materials. The model's prediction of this area of probable impact correlates very well with the actual field data collected by the EPA.

Region III's concern in the sludge dumping has led to the requirement that the City phase out

all of its dumping by 1981. The Region had proposed to move the City of Philadelphia off-the-continental shelf in the interim, based on the impact shown, and the presence of commercially harvestable shellfish within and around the site. A Public Hearing was held at Tom's River, New Jersey in May of 1977 to review the move. The final decision was made by Thomas C. Jorling, Assistant Administrator for Water and Hazardous Materials in EPA Headquarters. He concluded that while there was conclusive evidence of impact, "...the economic impact of the closure of the present site (Philadelphia sludge site) to shellfishing for an additional three years is not significant."

Special Studies

The Region has worked in cooperation with many different agencies to develop new research techniques useful for ocean application. Some of the more successful programs are described below.

Remote Tracking of Wastes

The University of Delaware and the National Atmospheric and Space Administration has developed a technique for synoptically observing currents and monitoring pollutants. A Lagrangian current tracking system using radio-signal-emitting current drogues has provided EPA with a new picture of how the currents transport materials dumped at sea. These results have proved especially useful in our attempts to determine the ultimate fate of pollutants and to better understand the data we had collected relating to heavy metals in sediments. Remote multispectral imagery from the Earth Resources Technology Satellite (ERTS-1), and medium and high altitude aircraft have been used to provide a visual trace of the actual pollutant plume.[9,10]

In-Site Bioassays

As described earlier in this paper, bioassays provide us with insight as to how the pollutants effect the biota. Laboratory static and flow-through bioassays attempt to approximate the real world but in-site bioassays provide the ultimate in combining all of the synergistic and antagonistic effects into a single assay. EPA's National Marine Water Quality Laboratory in Rhode Island frontiered this work in our area using specially designed benthic cages in which scallops (Placopecten megellanicus) were placed for three months. While the immediate results were inconclusive, the technique shows great promise.

Parasitology and Histopathology

The National Marine Fisheries Services Laboratory, Oxford, Maryland is doing research on the parasitology and histopathology of the rock and Jonah crabs (Cancer irroratus and Cancer borealis) at the sludge disposal site. Initial conclusions are that the incidence of discoloration and gill fouling is a function of proximity to the sludge dumpsite. Further work is also being done to correlate this work with black necrotic lesions in the Cancer crabs, usually found near the sewage sludge disposits.

ALTERNATIVES TO OCEAN DUMPING

Region III has taken a restrictive approach toward applying the criteria embodied in the Act. The Region has required all dumpers to actively seek alternatives to ocean dumping. The marine environment is only a part of the total environment which must be used for the ultimate disposal of wastes, and problems which affect the marine environment and solutions to these problems must be viewed in terms of their interrelation with the total environment. Some acceptable form of disposal must be developed for each waste that is phased out of ocean dumping. Considerable research is going into the development of alternative methods of disposal which will reduce the environmental effects of the ultimate disposal of the unavoidable residue - be it solid, liquid, or gas - either on the land, in the water, or in the air. EPA is concerned particularly about the problem of the ultimate disposal of sewage sludge, which will be produced in ever increasing quantities as municipalities install more advanced forms of sewage treatment.

EPA plans to continue its comprehensive program for municipal wastewater sludge management, including the development of a strategy to coordinate the various Agency activities regarding sludge management. This program will concentrate on demonstration of new technologies which will recycle or reuse sludges, or recover residuals contained in the sludges. For example, new technologies are being examined to determine if there are cost-effective methods for processing of sludge into products including metals recovery, organic acids, fertilizer bases, soil conditioners, methane, and the recovery of process heat. The program will also provide guidance for controlling land disposal practices under the Resource Conservation and Recovery Act of 1976.

One alternative which has been successfully demonstrated is the composting of sludge with various bulking agents such as wood chips, bark or solid waste. EPA has a joint project with the Department of Agriculture in Beltsville, Maryland and has conducted a composting demonstration program in Bangor, Maine. Composting stabilizes the sludge and if designed properly can kill pathogens in the process. The land area required for composting as a means of stabilizing sludges is small, and in some cases an energy saving can be realized by using this method. The product resulting from composting has been shown to be an excellent soil conditioner.

In November 1976, the City of Camden was ordered by EPA to discontinue the dumping of its sewage sludge. The City was, however, allowed 18 months to dispose of this residue at a more remote

site and implement an alternative. EPA recommended the composting of its wastewater sludge by the forced aeration system developed in Beltsville, Maryland, by the Agricultural Research Service and Maryland Environmental Service. As a result of the joint efforts of the Camden County Municipal Utilities Authority, the City of Camden, the New Jersey Department of Environmental Protection, EPA, and Cook College, a program of plant rehabilitation, site improvement, composting facility design and construction, and research was initiated. By June 1978, ocean dumping ceased.

Another alternative being used by many cities is the direct application of liquid or dried sludge to farm land. EPA estimates that about 25% of the municipal sludges are currently being disposed of in this manner. This method has been frequently used to provide all or part of the fertilizer requirements for growing forage crops and grain. Such direct applications of sludge have also been used to reclaim strip mined or otherwise disturbed lands (shifting sand dunes, mine spoils, etc). EPA has initiated studies to survey the results of such programs to document more adequately current nationwide practices in land application of sludges.

The City of Philadelphia is required to end ocean dumping of sewage sludge. To meet the 1980 deadline, Philadelphia has a program underway to select and implement alternatives. Land application of sludge to strip mines is being instituted on a pilot basis and large scale composting is presently being implemented. The City is exploring other technologies such as the EPA funded Eco-Rock research process which produces highway aggregate material by means of co-fusion of incinerator ash and sludge.

In addition, Philadelphia has begun a sludge giveaway program (Philorganic) using aged lagooned sludge as a source. Following installation of dewatering equipment they hope to use stabilized daily-generated sludge as the source. Philadelphia has promulgated pretreatment regulations effective July 1977 in order to improve the quality of the sludge by reducing concentrations of heavy metals entering the treatment plants.

The Dupont Company has been ocean dumping its metal laden, acid wastes since 1968. EPA gave Dupont a choice of implementing a costly waste treatment system or an equivalent recycle process. The Company was able to devise a plan of resource recovery of ferric chloride from its two major waste streams. Dupont forecasts marketing of all ferric chloride by 1980.

References

1. Report of the United States Delegation to the Intergovernmental Conference on the Convention of Ocean Dumping of Wastes at Sea, held at London, October 30, November 13, 1972.

2. Ketchum, B. H. (1967). Man's Resources in the Marine Environment, in Pollution and Marine Ecology, T. A. Olson and F. J. Burgess, Eds., Interscience, New York.

3. National Academy of Sciences. (1971). Marine Environmental Quality: Suggested Research Programs for understanding Man's Effect on the Oceans, National Research Council, Ocean Affairs Board, Washington, D.C.

4. Callaway, R. J., and A. M. Teeter, Dispersion of Sewage Sludge Discharged from Vessels to New York Bight waters. In special symposium on the Middle Atlantic Continental Shelf and New York Bight held in New York, in November, 1975.

5. Pesch, G. G. (1976). Statement of Public Hearing in Georgetown, Del. on Ocean Dumping Permit for City of Philadelphia. EPA ERL, Narragansett, R.I. April 28, 1976.

6. Phelps, D. K., and B. H. Renyolds (1977). Progress Report: Monitoring of the Ocean Dumpsites Used by the City of Philadelphia and the Dupont Corporation, July 1, 1977, U.S. EPA ERL, Narragansett, R.I.

7. Lear, D. W., S. K. Smith and M. L. O'Malley (Eds.) 1976. Effects of Ocean Dumping Activities, Mid-Atlantic Bight-1976, Interim Report. U.S. Environmental Protection Agency, Region III. EPA 903/9-77-029.

8. Verber, James L. (1978). "Bacteriological Data and Sample Locations for Operation Ridge Runner, April 11-16, 1978," presented at Ocean Dumping Hearing for City of Philadelphia on May 11, 1978. Georgetown, Delaware.

9. Klemas, V., G. R. Davis and D. J. Lew, Current Drogue and Waste Observations at the Dupont Waste Disposal Site. University of Delaware pub. CRS. 3-76, Newark, Delaware.

10. Lewis, B. W., and Vernon G. Collins, Remotely Sensed and Laboratory Spectral Signatures of an Ocean-Dumped Acid Waste. NASA Technical Note, NASA TN D-8467, July 1977, Hampton, Virginia.

11. Falk, L.L. (1976). Statement on behalf of E. I. Dupont at Public Hearing on Ocean Disposal Permit, presented at Ocean Dumping Permit Hearing for Dupont on October 13, 1976. Georgetown, Delaware.

SUBMERSIBLE ACOUSTIC NAVIGATION FOR PRECISE UNDERWATER SURVEYS

Robert C. Abbott
AMF Sea-Link Systems
3001 Centreville Road
Herndon, Virginia 22070

Abstract

With submersibles playing an increasingly important role in the offshore oil industry for performing surveys and inspections, rapid, accurate positioning becomes imperative. The ability to accurately navigate and record track and survey data is vital to a successful survey.

Until recently, size and cost constraints made navigation equipment in the submersible impractical, so tracking of submersibles was done on the surface, and the pilot guided via underwater telephone. Now based upon microprocessor technology and past acoustic navigation experience, Sea-Link Systems has developed a miniaturized navigation system which fits inside a manned submersible and provides navigation data directly to the pilot. Using data from the acoustic ranging system, a doppler velocity sensor and compass, the system provides the pilot with course-line navigation guidance to precisely cover a pre-determined grid survey pattern allowing the pilot to complete his survey with greater accuracy and speed.

1. Introduction

In order to conduct an accurate, complete survey of the seabed, a manned submersible requires a navigation system which fulfills two basic requirements. The first is to provide guidance to the pilot to assure complete coverage with minimum overlap of survey lines. The better this function is performed, the faster and hence, cheaper the survey can be completed. If the navigation presentation is clear and updates are rapid, the submersible can also operate at a higher rate of speed further reducing survey time. The second, and perhaps more important requirement, is to maintain an accurate record of submersible position during the entire dive to be used in interpreting the survey results during post-mission data processing.

The system described here integrates acoustic transponder ranging, acoustic doppler sonar, compass and depth sensors to compute a continuous sub's track. The submersible position is compared with a pre-programmed survey grid pattern and the distance to the end of the current track line, along with the distance off the current track presented to the pilot. The convenience and clarity of this navigation display allows higher speed operation with the pilot concentrating on his other duties to speed and simplify the survey. A cassette recorder and data acquisition sub-system allow all navigation data and survey sensor data to be recorded on a single tape for ease of post-processing.

2. Surface-Based Submersible Navigation

Many submersible operators are currently using a surface acoustic system to precisely measure the track of a submersible during an underwater survey. This type of system is attractive because it merely requires the attachment of an acoustic transponder or precise beacon to the manned submersible. This simple installation, however, is paid for in a more awkward and less accurate system. In this method, the shipboard equipment interrogates the bottom transponder array on a frequency, F1, to measure the ranges from the ship to the bottom transponders, R1, R2, etc., in Figure 1. This range is used to determine the ship's position, and a series of interrogations allows the ship's track to be determined. The system then sends a pulse on a different frequency, F2, to interrogate the transponder on the submersible which replies on frequency F1 measuring range RS in the figure. Since this reply is on frequency F1, it also interrogates the bottom transponder array determining the total range RS plus RS1 plus R1, etc. With these measurements, it is then possible to determine the position of the submersible. This result can contain significant errors caused by difficulty in estimating the ship's exact position at the time of the interrogation. This technique, known as a "sing-around" measurement, is in wide use today, and gives errors of two to three times the errors of a direct range-range-measurement system as is used for the ship's position. Once this submersible position is known on the surface, it is then necessary to contact the submersible using a means such as an underwater telephone to provide direction to the pilot. This is a slow, and often unreliable means of communication which results in significant wandering of the submersible's track when ideally the submersible would follow a straight-line grid pattern.

An additional problem is introduced as well, in that the submersible position data is being recorded on the surface while the sensor data is recorded in the submersible. It is then necessary to have accurate, synchronized time bases so that

the data can be later correlated to provide the bottom map desired during post-processing.

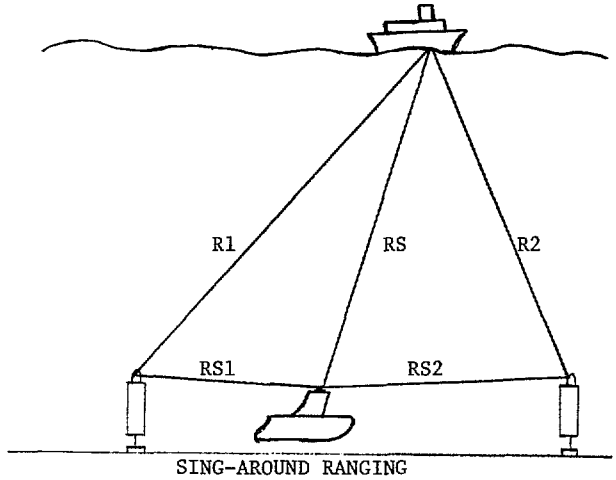

SING-AROUND RANGING

FIGURE 1

3. Submersible System

By installing a multi-channel ranging receiver and microprocessor in the submersible, it is possible to receive the replies from the bottom transponder array resulting in a direct measurement of RS1, RS2, etc. This data is sufficient to determine the position of the submersible directly with only an ambiguity as to whether the submersible is above or below the transponder array plane. By resolving this ambiguity, either directly through measured pressure depth or through a manual input, it is possible to provide highly accurate East/North position information to the submersible pilot to aid in his navigation. Since the ranges measured are not sing-around ranges, but are direct two-way acoustic ranges, the position of the submersible is determined to the same accuracy possible for the ship's position using a surface acoustic system. Since a submersible is usually operating near the bottom, and near the plane of the transponder array, the measurement of the depth acoustically is very difficult due to the awkward geometry involved, and it is necessary to either manually insert the depth information or preferably to have an auxiliary input of the pressure depth from the system in the submersible.

4. Complementary Navigational Sensors

Because of the low data rate of an acoustic transponder system with interrogations available at best, once every ten to fifteen seconds, and possibly no more often than once in thirty seconds, it is desirable to include acoustic doppler sonar and compass data to allow the submersible track to be continuously output based upon a combination of the doppler and the acoustic transponder information. The two systems, having complementary characteristics, operate together to provide a superior tracking system. The use of the doppler data to measure the submersible position between acoustic fixes also results in significantly better operation of the range gates in the transponder portion of the system.

Each measuring subsystem has its own error characteristics which can be compared to the other subsystems to much better estimate the submersible's continuous track position and estimate these errors. The acoustic transponder system has a scale-factor error caused by sound velocity estimates, and has a position error caused by random measurement errors. The acoustic doppler system is essentially a velocity sensor measuring the velocities along and perpendicular to the heading of the submersible. This system has a rotational error that is a function of installation, usually very small, and it has a scale factor error in the velocity which translates to a time-increasing position error. The compass has an additional offset in the heading. The depth sensor can have a variety of errors which convert to an offset and a scale factor error which can usually be ignored. In operation far removed from the ocean bottom, there is also an error introduced when the doppler sonar is not in bottom-lock, but is giving water reference velocity. This error is the speed of the ocean current at this location, and while this is not an error in the strict sense of the word, it also contributes to the position error. For near-bottom operation discussed here, this is not a factor.

5. Integration and Filtering

The doppler system is used to provide a continuous track between transponder fixes and an improved estimate of vehicle position at the instant of the succeeding transponder interrogation allowing improved operation of range gates.

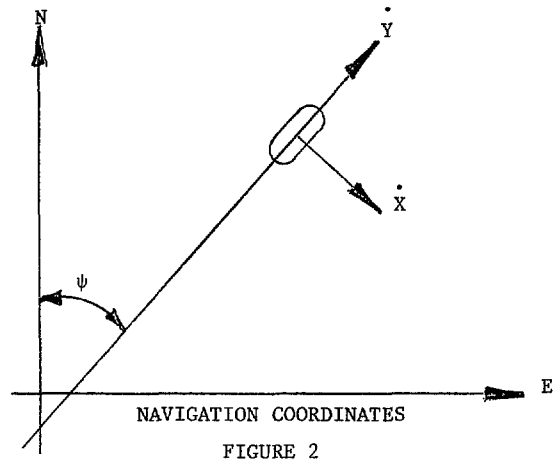

NAVIGATION COORDINATES

FIGURE 2

Transponder System Output E_M, N_M

Doppler System Output $\dot{X}_D, \dot{Y}_D$

Compass Output ψ_M

Heading $\psi = \psi_M + \psi_c$

$$\dot{X} = K_D \dot{X}_D$$

$$\dot{Y} = K_D \dot{Y}_D$$

$$\dot{E} = \dot{X} \cos \psi + \dot{Y} \sin \psi$$

$$\dot{N} = \dot{Y} \cos \psi + \dot{X} \sin \psi$$

At the time of a transponder interrogation, a position fix is computed and used to update the position of the sub. The doppler system is then used to provide a continuous track, in this case one update per second. The X, Y velocity from the doppler is scaled and rotated through the compass angle ψ to yield $\dot{E}$ and $\dot{N}$, east and north velocities, to update position.

$$E = E + \dot{E}\,\Delta t$$

$$N = N + \dot{N}\,\Delta t$$

$$\Delta t = 1 \text{ Sec normally}$$

At the instant of the next transponder interrogation, the doppler position is saved as E_e, N_e to be used as estimates in the fix computation and filter. The measured acoustic ranges are passed through a range gate and a least squares fix (E_M, N_M) computed using transponder ranges only.

A filtered position fix is then computed for the sub at the interrogate time.

$$\hat{E} = E_E + \alpha\,(E_M - E_E)$$

$$\hat{N} = N_E + \alpha\,(N_M - N_E)$$

α = position smoothing coefficient with the doppler position updated by the difference between the doppler track and the transponder fix weighted by a smoothing coefficient. The present doppler track is also updated by this same quantity:

$$E = E + \alpha\,(E_M - E_E)$$

$$N = N + \alpha\,(N_M - N_E)$$

The coefficient K of the doppler system and the compass error ψ_c must now be updated based upon the error of the last fix. The measured travel is compared with the doppler travel to obtain error in magnitude (error of K) and a directional error (compass error) to correct these coefficients.

Doppler Travel $S_D = \sqrt{(E_E - \hat{E}_{i-1})^2 + (N_E - \hat{N}_{i-1})^2}$

Measured Travel $S_M = \sqrt{(\hat{E}_i - \hat{E}_{i-1})^2 + (\hat{N}_i - \hat{N}_{i-1})^2}$

Doppler Direction $\phi_D = \tan^{-1} \dfrac{(E_E - \hat{E}_{i-1})}{S_D}$

Measured Direction $\phi_M = \tan^{-1} \dfrac{(\hat{E}_i - \hat{E}_{i-1})}{S_D}$

and we update

$$K = K + \beta_1 \cdot \delta K = K + \beta_1 K \cdot \frac{(S_M - S_D)}{S_D}$$

$$\psi_c = \psi_c + \beta_2 \cdot (\phi_M - \phi_D)$$

so as to approach correct doppler operation between acoustic fixes.

The coefficient alpha (α) is a weighting function between zero and one which determines the weight placed upon transponder vs doppler position values. In the limit of zero, we have a pure doppler system and for a value of one, a pure transponder system. Alpha is chosen based upon the ratio of the expected errors between the two sensors, and is usually chosen to favor the transponder measurements. i.e., 0.7-0.9

The adjustments to the doppler scale factor K are smoothed by coefficient beta one which reduces the update from the total error. Since K is near unity and very slow varying, it is preferable to limit updates to a very small value by a value of beta one of .1 or smaller. Likewise, compass error correction ψ_c will vary quite slowly and beta two, its coefficient, is also on this order. In some cases it is preferable to ignore compass error altogether by reducing beta two to zero.

In a system without a doppler sonar, it is possible to perform a similar operation in which a sub's velocity estimate is derived from previous fixes and used to dead reckon between fixes. In this case, no details of track between fixes are known and, of course, the coefficients favor the current measured transponder fix very strongly.

$$\hat{E} = E_E + \alpha\,(E_M - E_E) \qquad \alpha \simeq .95$$

$$\hat{N} = N_E + \alpha\,(N_M - N_E)$$

$$\hat{\dot{E}}_i = \hat{\dot{E}}_{i-1} + \beta\,\frac{(E_M - E_E)}{\Delta t} \qquad \beta \simeq .8$$

$$\hat{\dot{N}}_i = \hat{\dot{N}}_{i-1} + \beta\,\frac{(N_M - N_E)}{\Delta t}$$

6. Course-Line Navigation

Rather than provide the submersible pilot with a track-plot of the submersible path through the transponder array, the course-line navigation feature provides the pilot with a very simple display which tells him the distance from his submersible to the next way-point or end of grid line, and provides him with the distance, left or right, that he is deviating from the selected course-line.

By entering into the computer the end point of each of the grid-lines in the survey, it is possible for the pilot to get course-line guidance throughout the entire dive. In Figure 3, we can see the selected way-point, and the previous way-point which make up the current course-line, and see the distance to way-point and off-course distance. By reading this information from the pilot's display, we can see how it is possible for the pilot to interpret his position and stay on the selected survey line with minimal effort. By having a continuous display of his position relative to the selected course-line, the submersible pilot can follow the selected path, and obtain optimum survey coverage in a minimum time.

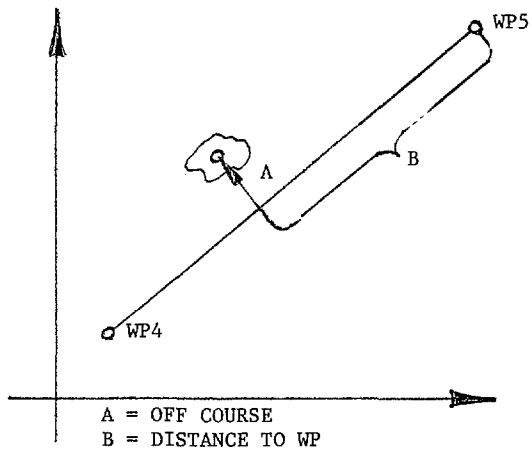

WAY-POINT NAVIGATION

FIGURE 3

7. Data Recording

A further advantage of having self-contained navigation capability within the submersible, is the ability to record on one tape cassette the raw navigation data, the submersible position information, the output from auxiliary navigation sensors, and the outputs of the survey sensors. This one tape can be processed after the dive to create the contour maps that are the desired output of the survey. An essentially unlimited number of analog and digital sensors can be accommodated, restricted only by tape capacity and processor data rates.

It is also possible to process the navigation data after the dive with improved array calibration or other navigational improvements to provide a more accurate bottom map. The post-processing also allows the user to reverse-filter the navigation data to further reduce the effect of doppler drift between acoustic transponder fixes. By starting at a fix, and computing backward in time, the doppler system error can then be reduced to zero at each end of the interval to cut the maximum drift error in half compared to what is possible in real time.

8. Summary and Conclusions

In conclusion, we have shown a self contained submersible navigation system which provides higher accuracy primarily as a result of eliminating the sing-around technique, and more convenience with the ability to record all data on one tape. The self-contained system precludes the requirement for submersible directions through the underwater telephone. This system offers much greater economy due to the higher precision and speed with which the survey can be run with the elimination of the overlap and wasted lines that are required to assure full coverage in a conventional system.

References

1. Campbell, Dudley E., "Precise Acoustic Navigation and Position Keeping," Journal of the Institute of Navigation, Vol. 17, No. 2, Summer 1970.

2. Cestone, J. A., Cyr, R. J., Roesler, G. and St. George, E., Jr., "Latest Highlights in Acoustic Underwater Navigation," Journal of the Institute of Navigation, Vol. 24, No. 1, Spring 1977.

3. Heckman, D. B. and Abbott, R. C., "An Acoustic Navigation Technique," 1973 IEEE Conference on the Ocean Environment.

4. Van Calcar, H., "Precision Subsea Navigation System," Journal of the Institute of Navigation, Vol. 17, No. 2, Summer 1970.

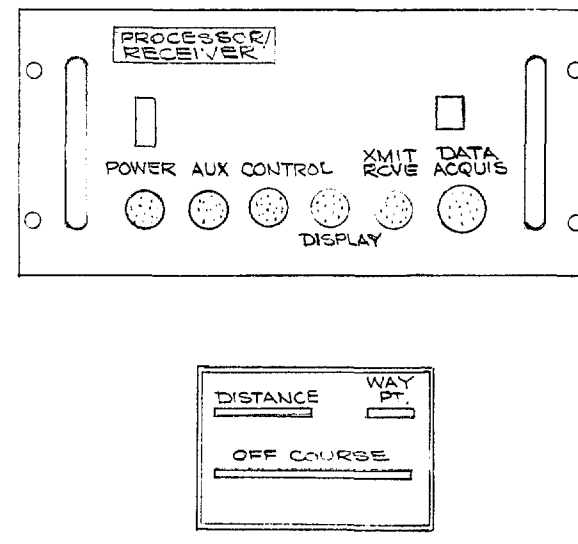

SUBATNAV SYSTEM

FIGURE 4

OPTIMAL ESTIMATION OF UNDERSEA ACOUSTIC TRANSPONDER LOCATIONS*

David G. Carta
Jet Propulsion Laboratory
California Institute of Technology
Pasadena, California 91103

Abstract

Using principles from multilateration and optimal estimation theories an approach is derived for estimating the relative positions of three or more submerged and anchored acoustic transponders. The procedure is not constrained to processing range data collected at special points or on special trajectories. While the data normally collected over transponders and between transponder pairs can be processed, simultaneous ranges from anywhere on the surface to three or more transponders can also be processed. Simulated examples involving four stations in different geometries with different range collection schemes demonstrate the effectiveness of the procedure.

1. Introduction

In order for an underwater vehicle to navigate relative to acoustic transponders anchored to the ocean floor, it is necessary to survey the transponder positions. Currently, the survey is accomplished by taking simultaneous range measurements from a surface vessel. For the three transponder case, six data collection runs are usually made: three approximately over each transponder and three approximately halfway between pairs of transponder. These ranges (corrected for known errors) are used in an iterative residual-reducing routine to estimate relative transponder coordinates [1]. The rationale is that the first three runs determine transponder depths while the latter three determine lateral spacing. No claim is made concerning the efficiency, optimality or accuracy of the procedure other than that it reduces residuals between observed and calculated ranges to reasonably small values.

In this paper a procedure is presented by which simultaneous ranging data from a vessel located anywhere on the ocean surface may be directly processed in an optimal fashion. By optimal is meant that all known error sources are appropriately considered and weighted. The tool used for optimal estimation will be one of the stable variants of the Kalman filter.

The output of the procedure will be an estimate of the transponder relative coordinates and a covariance matrix for errors in those coordinates.

*This paper presents the results of one phase of research carried out at the Jet Propulsion Laboratory, California Institute of Technology, under Contract No. NAS 7-100, sponsored by the National Aeronautics and Space Administration.

2. Range Error Model for Multiple Transponders

Although the term range data is commonly used, what are actually measured are times between the emitting of a pulse and the return to the surface of the acoustic transponder repeated pulses. This is the process which will be modeled in detail so that the effects of various error sources may be properly considered. The geometry of a single "range" measurement is depicted in Figure 1. It is assumed that the survey vessel is bobbing on the surface and is subject to known and unknown drift currents. The independently-calculated average sound velocity is assumed to contain a random error, and the instrument measuring elapsed time is also subject to random errors. Non-flatness of the earth is also accounted for.

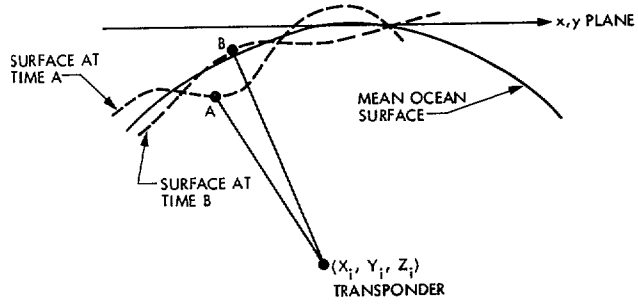

Figure 1. Geometry for a Single "Range" Measurement

At the time the pulse is emitted, the surface vessel is at Position A. The coordinates of this point are taken as $(x, y, z_{xy}+w_D)$ where z_{xy} is the displacement of the mean surface below the flat-earth reference plane at the point (x,y) (Appendix A) and w_D is the random wave displacement from the mean ocean surface. The travel time Δt_D to transponder i with coordinates (X_i, Y_i, Z_i) is

$$\Delta t_D = \frac{1}{\bar{c}_i+\delta_i}\sqrt{[(X_i-x)^2+(Y_i-y)^2+(Z_i-z_{xy}-w_D)^2]} \quad (1)$$

where $\bar{c}_i$ is the calculated mean sound velocity over the path and δ_i is the error in that calculated value. After a (calibrated) time delay of Δt_{T_i} seconds, a return pulse is emitted. This return

pulse is received at position B. The surface vessel arrives at position B: $[x + \Delta t_i(v_x + u),\ y + t_i(v_y + v),\ z_{xy} + w_i]$ by drifting both known and random distances and by the changing wave height. The return pulse travel time is then

$$t_U = \frac{1}{\bar{c}_i + \delta_i}\sqrt{[X_i - x - \Delta t_i(v_x+u)]^2 + [Y_i - y - \Delta t_i(v_y+v)]^2 + (Z_i - z_{xy} - w_i)^2} \qquad (2)$$

where v_x and v_y are the known drifts while u and v are the random drifts. The total measured elapsed time is then

$$\Delta t_i = \Delta t_U + \Delta t_D + \Delta t_{T_i} + e_i \qquad (3)$$

where e_i is the random error introduced by the time measuring device.

Substituting from Eqs. (1) and (2) into (3) and expanding to first order in $(X_i, Y_i, Z_i, x, y, \bar{c})$ yields

$$\Delta t_i = \frac{2R_i}{\bar{c}} + \Delta t_{T_i} - \frac{1}{\bar{c}R_i}\Big[(2R_i^2/\bar{c}\,\delta_i + (Z_i - z_{xy})w_D + \Delta t_i(X_i - x)u + \Delta t_i(y_i - y)v + (Z_i - z_{xy})w_i + \Delta t_i(X_i - x)v_x + \Delta t_i(Y_i - y)v_y\Big] + e_i \qquad (4)$$

where

$$R_i = \left[(X_i - x)^2 + (Y_i - y)^2 + (Z_i - z_{xy})^2\right]^{1/2}$$

Letting $\rho_i = \bar{c}(\Delta t_i - \Delta t_{T_i})/2$, Eq. (4) becomes

$$\rho_i = R_i - \frac{1}{2R_i}\Big[(2R_i^2/\bar{c})\delta_i + (Z_i - z_{xy})w_D + \Delta t_i(X_i - x)u + \Delta t_i(Y_i - y)v + (Z_i - z_{xy})w_i + \Delta t_i(X_i - x)v_x + \Delta t_i(Y_i - y)v_y - R_i\bar{c}e_i\Big] \qquad (5)$$

The above equation relates the measurement derived ranges ρ_i to the unperturbed true ranges R_i. The effects of error sources are exhibited as linear perturbations to the true ranges. To prepare for the estimation technique to be used, one further operation will be performed here. Squaring both sides of Eq. (5) and retaining perturbations to first order gives

$$\rho_i^2 = R_i^2 - \Big[(2\rho_1^2/\bar{c})\delta_i + (Z_i - z_{xy})w_D + \Delta t_i(X_i - x)u + \Delta t_i(Y_i - y)v + (Z_i - z_{xy})w_i + \Delta t_i(X_i - x)v_x + \Delta t_i(Y_i - y)v_y - \rho_i\bar{c}\,e_i\Big] \qquad (6)$$

where additionally to with first order accuracy ρ_i has been substituted for R_i in the coefficients for δ_i and e_i. For later reference Eq. (6) is written as

$$\rho_i^2 = (X_i - x)^2 + (Y_i - y)^2 + (Z_i - z_{xy})^2 - \Delta t_i(X_i - x)v_x + \Delta t_i(Y_i - y)v_y + D_i\underline{v} \qquad (7)$$

$$i = 1, \ldots, r, s$$

where

$$\underline{v} = [w_D, u, v, \delta_1, \ldots, \delta_s, w_1, \ldots, w_s, e_1, \ldots, e_s]^T \qquad (8)$$

and

$$\underline{D}_i = [(z_{xy} - Z_i),\ \Delta t_i(x - X_i),\ \Delta t_i(y - Y_i), \ldots, -2\rho_i^2/\bar{c}, \ldots, \ldots, \ldots, (z_{xy} - Z_i), \ldots, \ldots, \rho_i\bar{c}, \ldots] \qquad (9)$$

All terms not explicitly exhibited in D_i are zero.

3. Reduction to Standard Form

To estimate transponder coordinates, a combination of two approaches is used: multilateration and optimal estimation. The essence of multilateration is to mathematically eliminate the surface vessel coordinates [2]. The step that led to Eq. (6) was to prepare for this elimination. The essence of optimal estimation is to correctly consider the effects of perturbing errors on the estimation process. It is for this reason that error terms have been treated with such great care.

The multilateration step is accomplished as follows: Eq. (7) represents s equations. Information from the last two (i=r and s) will be used to eliminate the unknown surface position, (x,y). Subtracting each of the last two equations from the first gives

$$\rho_1^2 - \rho_r^2 = (X_1^2 - X_r^2) + (Y_1^2 - Y_r^2) + (Z_1 - z_{xy})^2 - (Z_r - z_{xy})^2 - [2(X_1 - X_r) - (\Delta t_1 - \Delta t_r)v_x]x - [2(Y_1 - Y_r) - (\Delta t_1 - \Delta t_r)v_y]y - (\Delta t_1 X_1 - \Delta t_r X_r)v_x - (\Delta t_1 Y_1 - \Delta t_r Y_r)v_y + (D_1 - D_r)\underline{v} \qquad (10)$$

and an identical equation with s replacing r. These two equations are linear in x and y and can be written in vector-matrix form as

$$A\underline{x} = \underline{b} \qquad (11)$$

where

$$A = \begin{bmatrix} 2(X_1 - X_r) - (\Delta t_1 - \Delta t_r)v_x & 2(Y_1 - Y_r) - (\Delta t_1 - \Delta t_r)v_y \\ 2(X_1 - X_s) - (\Delta t_1 - \Delta t_s)v_x & 2(Y_1 - Y_s) - (\Delta t_1 - \Delta t_s)v_y \end{bmatrix} \qquad (12)$$

$$b = \begin{bmatrix} (X_1^2 - X_r^2) + (Y_1^2 - Y_r^2) + (Z_1 - z_{xy})^2 - (Z_r - z_{xy})^2 - (\rho_1^2 - \rho_r^2) - (\Delta t_1 X_1 - \Delta t_r X_r)v_x - (\Delta t_1 Y_1 - \Delta t_r Y_r)v_y + (D_1 - D_r)\underline{v} \\ (X_1^2 - X_s^2) + (Y_1^2 - Y_s^2) + (Z_1 - z_{xy})^2 - (Z_s - z_{xy})^2 - (\rho_1^2 - \rho_s^2) - (\Delta t_1 X_1 - \Delta t_s X_s)v_x - (\Delta t_1 Y_1 - \Delta t_s Y_s)v_y + (D_1 - D_s)\underline{v} \end{bmatrix} \qquad (13)$$

and $\underline{x} = (x,y)^T$. From Eq. (12) it can be seen that if the images of transponders 1, r, and s (corrected for small drift components) projected on the z = 0 plane are not colinear, then $\underline{x}$ may be solved for. This is assumed to be the case so that $\underline{x} = A^{-1}\underline{b}$. Functionally, then $\underline{x} = \underline{x}(\underline{X}_1, \underline{X}_r, \underline{X}_s, \underline{v})$ where $\underline{X}_i = (X_i, Y_i, Z_i)^T$. This relationship can now

be substituted for $\underline{x}$ in the first s-2 of Eqs. (7). The last two of Eqs. (7) can be discarded. The information they contained is carried in $\underline{x}$. Functionally, Eqs. (7) can now be written as

$$\begin{aligned} \rho_1^2 &= h_1(X_1,\ \underline{x}(X_1,X_r,X_s,v),v) \\ &\cdots \\ \rho_{s-2}^2 &= h_{s-2}(\underline{X}_{s-2},\underline{x}(\underline{X}_1,\ \underline{X}_r,\ \underline{X}_s,\underline{v}),\underline{v}) \end{aligned} \tag{14}$$

or as

$$\underline{z}_k = \underline{h}(\underline{X}_1,\ldots,\underline{X}_{s-2},\underline{x}(\underline{X}_1,\underline{X}_r,\underline{X}_s,\underline{v}),\underline{v}) \tag{15}$$

where

$$\underline{z}_k = \left[\rho_1^2,\ldots,\rho_{s-2}^2\right]^T \quad \text{and} \quad \underline{h} = \left[h_1,\ldots,h_{s-2}\right]^T$$

The subscript k indicates the k-th time ranges are collected to all s transponders. Eq. (15) is in the classical form to be processed by a sequential estimator.

4. Nonlinear Sequential Estimation

Consider the estimation of constant parameters $[\underline{X}^T,\underline{X}^T,\ldots,\underline{X}^T]_T = \underline{X}^T$ given multiple observations $[z_1,\ldots,z_m] = \underline{z}^T$ related to $\underline{X}$ at observation time k by the nonlinear equation

$$\underline{z}_k = \underline{h}_k(\underline{X},\ \underline{v}_k)\ . \tag{16}$$

It is assumed that each observation is corrupted by errors $\underline{v}_k$ described only by the statistics $E[\underline{v}_k] = \underline{0}$, $E[\underline{v}_k\ \underline{v}_j^T] = \delta_{jk}R_k$. It is assumed that an initial (a priori) estimate $\underline{X}_o$ is known as well as an initial guess P_o of its error covariance, i.e.

$$P_o = E[(\underline{X}-\hat{\underline{X}}_o)\ (\underline{X}-\hat{\underline{X}}_o)]^T. \tag{17}$$

where $\underline{X}$ is the true value. The classical extend Kalman filter (estimator) update [3] is then

$$G_k = P_{k-1}H_k^T\left(H_kP_{k-1}H_k^T + L_kR_kL_k^T\right)^{-1} \tag{18}$$

$$P_k = P_{k-1} - G_k\left(P_{k-1}\ H_k^T\right)^T \tag{19}$$

$$\hat{\underline{X}}_k = \hat{\underline{X}}_{k-1} + G_k\left[\underline{z}_k - \underline{h}_k(\underline{X},0) - H_k(\hat{\underline{X}}_{k-1} - \bar{\underline{X}})\right] \tag{20}$$

where $\hat{\underline{X}}_k$ is the estimate of $\underline{X}$ after measurement $\underline{z}_k$ has been processed. $\bar{\underline{X}}$ is a nominal value about which nonlinearities are expanded, and P_k is the covariance of the error in $\underline{X}_k$. Additionally,

$$H_k = \left.\frac{\partial \underline{h}_k}{\partial \underline{X}^T}\right|_{\substack{\underline{X}=\bar{\underline{X}} \\ \underline{v}=\underline{0}}} \tag{21}$$

and

$$L_k = \left.\frac{\underline{h}_k}{\underline{v}_k^T}\right|_{\substack{\underline{X}=\bar{\underline{X}} \\ \underline{v}_k=\underline{0}}} \tag{22}$$

At least two passes will be made through the filter. On the first, at each iteration step we let the nominal $\bar{\underline{X}} = \hat{\underline{X}}_{k-1}$, the most recently obtained best estimate; on subsequent passes, for all iteration steps we let $\bar{\underline{X}} = \hat{\underline{X}}_N$, the best estimate after the most recent pass through all the data.

At this point, an interesting and well-known observation is that with nominal values for the transponder locations and a knowledge of the form and magnitude of the measurement errors, Eqs. (18) and (19) above can be used to generate the covariances of the estimates which would be produced by Eq. (20) without actually generating the estimates. Thus, without collecting data it is possible to determine the positional accuracies (covariances) achievable with any hypothetical transponder array and surface vessel collection process.

Because the Kalman form of the covariance update, Eqs. (18) and (19), is known to be numerically ill-conditioned, actual computations were performed using an algebraically equivalent but computationally stable covariance square-root variant of the update. [4]

5. Transponder Location Estimation

In order to proceed with the estimation procedure the derivatives

$$L_k = \frac{\partial \underline{h}}{\partial \underline{v}^T} \tag{23}$$

and

$$H_k = \frac{\partial \underline{h}}{\partial \underline{X}^T} = \left[\frac{\partial \underline{h}}{\partial \underline{X}_1^T},\ldots,\ \frac{\partial h}{\partial \underline{X}_s^T}\right] \tag{24}$$

are required. (Note that the subscript k on $\underline{h}_k$ has been suppressed.) To obtain these derivatives from Eq. (15) the chain rule is employed which in vector-matrix notation takes the compact form:

$$\frac{\partial \underline{h}}{\partial \underline{X}_i^T} = \left(\frac{\partial \underline{h}}{\partial \underline{X}_i^T}\right)_{x\ \text{constant}} + \left(\frac{\partial \underline{h}}{\partial \underline{x}^T}\right)\left(\frac{\partial \underline{x}}{\partial \underline{X}_i^T}\right) \tag{25}$$

and

$$\frac{\partial \underline{h}}{\partial \underline{v}^T} = \left(\frac{\partial \underline{h}}{\partial \underline{v}^T}\right)_{x\ \text{constant}} + \left(\frac{\partial \underline{h}}{\partial \underline{x}^T}\right)\left(\frac{\partial \underline{x}}{\partial \underline{v}^T}\right) \tag{26}$$

The above partial derivatives are then evaluated at the nominal values $\underline{X} = \bar{\underline{X}}$, $\underline{v} = \underline{0}$, and $\underline{x} = \bar{\underline{x}} = \underline{x}(\underline{X}_1,\underline{X}_r,\underline{X}_s,\underline{0}) = (A)^{-1}\bar{\underline{b}}$. Referring to Eq. (7), the partial derivatives are found as

$$\left(\frac{\partial \underline{h}}{\partial \underline{X}_i^T}\right)_{\bar{\underline{x}}} = \begin{bmatrix} 0 & 0 & 0 \\ \vdots & \vdots & \vdots \\ 0 & 0 & 0 \\ 2(\bar{X}_i-\bar{x})-t_iv_x & 2(\bar{Y}_i-\bar{y})-t_iv_y & 2(\bar{Z}-z_{xy}) \\ 0 & 0 & 0 \\ \vdots & \vdots & \vdots \\ 0 & 0 & 0 \end{bmatrix} \begin{array}{l} \\ \\ \\ \leftarrow \text{row } i \\ \leftarrow = C_i \\ \\ \\ \leftarrow \text{row } s-2 \end{array} \tag{27}$$

for $i = 1,\ldots,s-2$. For $i > s-2$, $C_i = 0$.

$$\left(\frac{\partial \underline{h}}{\partial \underline{v}^T}\right)_{\bar{\underline{x}}} = \begin{bmatrix} \bar{D}_1 \\ \vdots \\ \bar{D}_{s-2} \end{bmatrix} = D \tag{28}$$

$$\frac{\partial \underline{h}}{\partial \underline{x}^T} = \begin{bmatrix} 2(x-X_1)+\Delta t_1v_x & 2(y-Y_1)+\Delta t_1v_y \\ \vdots & \vdots \\ 2(x-X_{s-2})+\Delta t_{s-2}v_x & 2(y-Y_{s-2})+\Delta t_{s-2}v_y \end{bmatrix} = H_x \tag{29}$$

The remaining partial derivatives are found by using Eqs. (11), (12) and (13). Taking the partial of Eq. (11) w.r.t X_1 (the first component of $\underline{X}_1$) gives:

$$\frac{\partial A}{\partial X_1}\,\underline{x} + A\,\frac{\partial \underline{x}}{\partial X_1} = \frac{\partial \underline{b}}{\partial X_1}. \tag{30}$$

Evaluating the partials using Eqs. (12) and (13) gives

$$\begin{bmatrix} 2 & 0 \\ 2 & 0 \end{bmatrix}\begin{bmatrix} x \\ y \end{bmatrix} + A\,\frac{\partial \underline{x}}{\partial X_1} = \begin{bmatrix} 2X_1 - \Delta t_1 v_x \\ 2X_1 - \Delta t_1 v_x \end{bmatrix} \tag{31}$$

or

$$\bar{A}\,\frac{\partial \underline{x}}{\partial X_1} = \begin{bmatrix} 2(\bar{X}_1 - \bar{x}) - \Delta t_1 v_x \\ 2(\bar{X}_1 - \bar{x}) - \Delta t_1 v_x \end{bmatrix} \tag{32}$$

where we have evaluated quantities at their nominal values. Similarly,

$$A\,\frac{\partial \underline{x}}{\partial Y_1} = \begin{bmatrix} 2(\bar{Y}_i - y) - \Delta t_1 v_y \\ 2(\bar{Y}_i - y) - \Delta t_k v_y \end{bmatrix} \tag{33}$$

and

$$A\,\frac{\partial \underline{x}}{\partial Z_1} = \begin{bmatrix} 2(\bar{Z}_1 - z_{xy}) \\ 2(\bar{Z}_1 - z_{xy}) \end{bmatrix}. \tag{34}$$

Assembling (32), (33) and (34) into a single vector equation gives

$$\bar{A}\,\frac{\partial \underline{x}}{\partial \underline{X}_1^T} = B_1 \tag{35}$$

where

$$B_1 = \begin{bmatrix} 2(\bar{X}_1 - \bar{x}) - \Delta t_1 v_x & 2(\bar{Y}_1 - \bar{y}) - \Delta t_1 v_y & 2(\bar{Z}_1 - z_{xy}) \\ 2(\bar{X}_1 - \bar{x}) - \Delta t_1 v_x & 2(\bar{Y}_1 - \bar{y}) - \Delta t_1 v_y & 2(\bar{Z}_1 - z_{xy}) \end{bmatrix} \tag{36}$$

Since A has already been assumed invertible, we have

$$\frac{\partial \underline{x}}{\partial \underline{X}_1^T} = \bar{A}^{-1} B_1 . \tag{37}$$

Similarly,

$$\bar{A}\frac{\partial \underline{x}}{\partial \underline{X}_r^T} = B_r = \begin{bmatrix} 2(\bar{x} - \bar{X}_r) + \Delta t_r v_x & 2(\bar{y} - \bar{Y}_r) + \Delta t_r v_y & -2(\bar{Z}_r - z_{xy}) \\ 0 & 0 & 0 \end{bmatrix} \tag{38}$$

$$\bar{A}\frac{\partial \underline{x}}{\partial \underline{X}_s^T} = B_s = \begin{bmatrix} 0 & 0 & 0 \\ 2(\bar{x} - \bar{X}_s) + \Delta t_s v_x & 2(\bar{y} - \bar{Y}_s) + \Delta t_s v_y & -2(\bar{Z}_s - z_{xy}) \end{bmatrix} \tag{39}$$

and

$$\bar{A}\,\frac{\partial \underline{x}}{\partial \underline{v}^T} = B_v = \begin{bmatrix} \bar{D}_1 - \bar{D}_r \\ \bar{D}_1 - \bar{D}_s \end{bmatrix} \tag{40}$$

The above information is now assembled into the vectors H_k and L_k. Let

$$H_k = [H_1, \ldots, H_s] \tag{41}$$

Then

$$H_1 = C_1 + H_x\,\bar{A}^{-1} B_1$$

$$\begin{aligned} H_2 &= C_2 \\ &\ldots \\ H_{s-2} &= C_{s-2} \\ H_r &= H_x\,\bar{A}^{-1} B_r \\ H_s &= H_x\,\bar{A}^{-1} B_s \end{aligned} \tag{42}$$

$$\text{and} \quad L_k = D + H_x \bar{A}^{-1} B_v \tag{43}$$

All the necessary elements for estimating transponder coordinates and their error covariance are now derived.

6. Inclusion of Depth Measurements

Suppose data is collected by maneuvering nearly above each transponder and measuring its minimum range. Letting $x = X_i + \varepsilon_x$, $y = Y_i + \varepsilon_y$ and maintaining small quantities only to first order, the range ρ_i in Eq. (5) becomes

$$\rho_i = |Z_i - Z_{xy}| - \frac{\rho_i}{\bar{c}}\,\delta_i - \frac{1}{2}(w_D + w_i) + \frac{\bar{c}}{2}\,e_i \tag{44}$$

or

$$\rho_1 - z_{xy} = -Z_i + v_i \tag{45}$$

where

$$E[v_i] = 0 \tag{46}$$

$$E[v_i^2] = \frac{\rho_i\,\sigma_\delta^2}{\bar{c}} + \frac{1}{2}\sigma_w^2 + \frac{\bar{c}\,\sigma_e^2}{2} \tag{47}$$

These measurements do not require processing by the filter. The coordinate of $\hat{\underline{X}}_o$ which corresponds to Z_i is simply initialized to $z_{xy} - \rho_i$ and its corresponding variance element in P_o initialized to $E[v_i^2]$.

7. Multilateration Treatment of Line Crossing Measurements

Traditionally, line crossing data is collected by crossing the approximate centerpoint between transponders i and j and finding the minimum sum of ranges. The development below, which uses a multilateration approach, has no requirement for the line crossing to be near the centerpoint.

Let (x,y) be on the line from (X_i, Y_i) to (X_j, Y_j) at a distance λ. Then

$$x = X_i + \lambda(X_j - X_i) = X_j + (1-\lambda)(X_i - X_j) \tag{48}$$

$$y = Y_i + \lambda(Y_j - Y_i) = Y_j + (1-\lambda)(Y_i - Y_j) \tag{49}$$

and from Eq. (7), written for subscripts i and j, the minimum ranges ρ_i and ρ_j can be expressed as:

$$\rho_i^2 = \lambda^2[(X_i - X_j)^2 + (Y_i - Y_j)^2] + (Z_i - z_{xy})^2 - [v_x(X_i - X_j) + v_j(Y_i - Y_j)]\Delta t_i \lambda + D_i \underline{v} \tag{50}$$

and

$$\rho_j^2 = (1-\lambda)^2[(X_i-X_j)^2+(Y_i-Y_j)^2]+(Z_j-z_{xy})^2$$
$$+ [v_x(X_i-X_j)+v_y(Y_i-Y_j)]\Delta t_j(1-\lambda)+ D_j\underline{v} \qquad (51)$$

Subtracting Eq. (50) from (51) gives

$$\rho_j^2-\rho_i^2 = (1-2\lambda)[(X_i-X_j)^2+(Y_i-Y_j)^2]+(Z_j-z_{xy})^2$$
$$- (Z_i-z_{xy})^2+[v_x(X_i-X_j)+v_y(Y_i-Y_j)]$$
$$[\Delta t_j-\lambda(\Delta t_j-\Delta t_i)] + (D_j-D_i)\underline{v} \qquad (52)$$

Eq. (52) yields $\lambda = \lambda(\underline{X}_i, \underline{X}_j, \underline{v})$:

$$\lambda = \frac{(X_i-X_j)^2+(Y_i-Y_j)^2+(Z_j-z_{xy})^2-(Z_i-z_{xy})^2+\rho_i^2-\rho_j^2 + [v_x(X_i-X_j)+v_y(Y_i-Y_j)]\Delta t_j+(D_j-D_i)\underline{v}}{2[(X_i-X_j)^2+(Y_i-Y_j)^2]+(\Delta t_j-\Delta t_i)[v_x(X_i-X_j)+v_y(Y_i-Y_j)]} = b/a \qquad (53)$$

Substitution of this λ into Eq. (50) will yield a scalar measurement equation suitable for processing by the sequential estimator described in Section 4. Making the substitution yields

$$\rho_i^2 = h(\underline{X}_i, \underline{X}_j, \lambda(\underline{X}_i, \underline{X}_j, \underline{v}), \underline{v}) \qquad (54)$$

As before we will need $\partial h/\partial \underline{X}^T = H$ and $\partial h/\partial \underline{v}^T = L$ which will be developed by the chain rule Eqs. (25) and (26). From Eq. (50):

$$\left(\frac{\partial h}{\partial \underline{x}_i^T}\right)_{\lambda\text{const}} = [2(\bar{X}_i-\bar{X}_j)\bar{\lambda}^2-v_x\Delta t_i\bar{\lambda},\ 2(\bar{Y}_i-\bar{Y}_j)\bar{\lambda}^2-v_y\Delta t_i\bar{\lambda},\ 2(\bar{Z}_i-z_{xy})] = E_i \qquad (55)$$

$$\left(\frac{\partial h}{\partial \underline{x}_j^T}\right)_{\lambda\text{const}} = [-2(\bar{X}_i-\bar{X}_j)\bar{\lambda}^2+v_x\Delta t_i\bar{\lambda},\ -2(\bar{Y}_i-\bar{Y}_j)\bar{\lambda}^2+v_y\Delta t_i\bar{\lambda},\ 0\ ] = E_j \qquad (56)$$

$$\left(\frac{\partial h}{\partial \underline{v}^T}\right)_{\lambda\text{const}} = \bar{D}_i \qquad (57)$$

Also,

$$\frac{\partial h}{\partial \lambda} = 2\bar{\lambda}[(\bar{X}_i-\bar{X}_j)^2+(\bar{Y}_i-\bar{Y}_j)^2]-\Delta t_i[v_x(\bar{X}_i-\bar{X}_j)+v_y(\bar{Y}_i-\bar{Y}_j)=H_\lambda \qquad (58)$$

Writing Eq. (53) as $a\lambda = b$ and differentiating w.r.t $\underline{X}_i^T$ yields

$$\frac{\partial a}{\partial \underline{X}_i^T}\lambda + a\frac{\partial \lambda}{\partial \underline{X}_i^T} = \frac{\partial b}{\partial \underline{X}_i^T} \qquad (59)$$

Evaluating the derivatives and using nominal values

$$\frac{\partial \lambda}{\partial \underline{X}_i^T} = \frac{1}{\bar{a}}\begin{bmatrix} 2(\bar{X}_i-\bar{X}_j)+v_x\Delta t_j-\bar{\lambda}[4(\bar{X}_i-\bar{X}_j)+v_x(\Delta t_j-\Delta t_i)] \\ 2(\bar{Y}_i-\bar{Y}_j)+v_y\Delta t_j-\bar{\lambda}[4(\bar{Y}_i-\bar{Y}_j)+v_y(\Delta t_j-\Delta t_i)] \\ -2(\bar{Z}_i-z_{xy}) \end{bmatrix}^T = F_i \qquad (60)$$

Similarly,

$$\frac{\partial \lambda}{\partial \underline{X}_j^T} = \frac{1}{\bar{a}}\begin{bmatrix} -2(\bar{X}_i-\bar{X}_j)-v_x\Delta t_j-\bar{\lambda}[-4(\bar{X}_i-\bar{X}_j)-v_x(\Delta t_j-\Delta t_i) \\ -2(\bar{Y}_i-\bar{Y}_j)-v_y\Delta t_j-\bar{\lambda}[-4(\bar{Y}_i-\bar{Y}_j)-v_y(\Delta t_j-\Delta t_i) \\ 2(\bar{Z}_j-z_{xy}) \end{bmatrix}^T = F_j \qquad (61)$$

and
$$\frac{\partial \lambda}{\partial \underline{v}^T} = \frac{1}{\bar{a}}(\bar{D}_j-\bar{D}_i)\ . \qquad (62)$$

For this problem H takes the form

$$H = [0,\ldots,0,\ H_i,\ 0,\ldots,0,\ H_j,0,\ldots,0] \qquad (63)$$

Then
$$H_i = E_i + H_\lambda F_i \qquad (64)$$
$$H_j = E_j + H_\lambda F_j \qquad (65)$$

and
$$L = \bar{D}_i + H_\lambda[\frac{1}{\bar{a}}(D_j-D_i)] \qquad (66)$$

With H and L now in hand formulas Eqs. (18), (19), and (20) can be used to update the estimate of the two interrogated transponders.

8. Initializing the Estimator

In order to begin the estimation process, values are needed for the initial transponder coordinates and their error covariances. As noted in [1] six coordinates may be chosen arbitrarily. Fixing the appropriate three removes translational ambiguity and fixing three others removes rotational ambiguity. By referencing all ranges to a surface vessel nominally located on a plane, one translational and two rotational degrees of freedom are used up. As in [1] the three remaining ambiguities are removed by choosing $X_1 = Y_1 = Y_2 = 0$. I.e., the origin is arbitrarily located at transponder number 1 and the x-axis made to pass through transponder number 2. This information is conveyed to the estimator by taking $\hat{\underline{X}}_o = [0,0,\hat{Z}_1(0),\ \hat{X}_2(0),0,\hat{Z}_2(0),\ \hat{X}_3(0),\hat{Y}_3(0),\hat{Z}_3(0),\ldots]^T$. The estimated values of X_1, Y_1 and Y_2 are prevented from drifting from their initial zero values by choosing their corresponding error sigmas to be small relative to the expected final accuracy of the other coordinates. Sigmas of one centimeter were chosen.

Assume that the initial z-coordinates $\hat{Z}_1(0), \ldots, \hat{Z}_s(0)$ are estimated as in Section 6 by depth measurements over the transponders, and the corresponding standard deviations are 50 cm. Assume also that the initial relative lateral positions $\hat{X}_1(0), \hat{X}_3(0), \ldots,$ and $\hat{Y}_3(0), \hat{Y}_4(0), \ldots,$ are taken to be those of where the transponders were dropped and are known to only a one sigma of 100 meters. The initial covariance matrix then becomes:

$$P_o = \text{diag}[(1\text{cm})^2,(1\text{cm})^2,(100\text{m})^2,(1\text{cm})^2,(50\text{cm})^2,$$
$$(100\text{m})^2,(100\text{m})^2,(50\text{cm})^2,(100\text{m})^2,(100\text{m})^2,$$
$$(50\text{cm})^2,\ldots,(100\text{m})^2,(100\text{m})^2,(50\text{cm})^2] \qquad (67)$$

9. Simulations

Two four-transponder geometries were chosen for study. For each geometry two data collection patterns were examined: the first consists of four legs passing roughly between transponders; the second, of four legs passing over transponders. The scenarios are described pictorially below. Triangles are transponders, dotted lines the surface vessel paths.

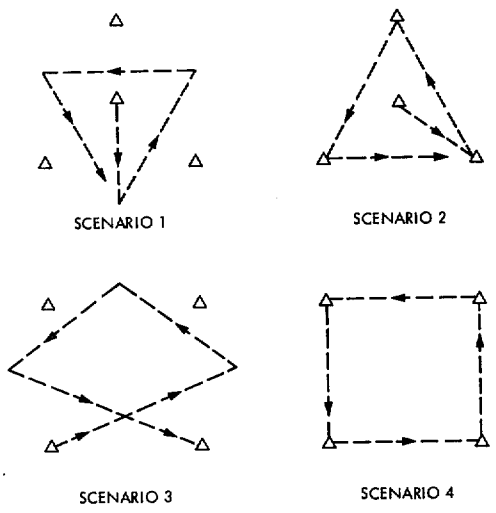

Transponders were assumed anchored at a depth of 5000m and, except for the center of the triangles, separated by 5000m. Using Eqs. (1),(2) and (3) simultaneous "range" data was simulated to all four stations at twelve evenly spaced points on each leg. All error sources were assumed normally distributed and chosen as realistically as possible:

$$\delta_i = N(b,\sigma_\delta) \qquad b = 0.1 \text{ m/sec}$$
$$\sigma_\delta = 0.1 \text{ m/sec}$$
$$w_i, w_D = N(0,\sigma_w) \qquad \sigma_w = 0.25 \text{ m}$$
$$u,v = N(0,\sigma_u) \qquad \sigma_u = 0.25 \text{ m/sec}$$
$$e_i = N(0,\sigma_e) \qquad \sigma_e = 0.0003 \text{ sec}$$

Note that the sound speed error is simulated with a bias as well as a random component. The nominal average speed of sound and the deterministic drift rates were chosen as

$$\bar{c} = 1500 \text{ m/sec}$$
$$v_x = v_y = 1.0 \text{ m/sec} \quad .$$

A pessimistic set of noise levels was also simulated for each of the scenarios. For these runs the values of $\sigma_\delta, \sigma_w, \sigma_u, \sigma_e, v_x$, and v_y were double the realistic values. The average and maximum errors in estimated transponder positions for all scenarios under both sets of noise conditions are presented in Table 1.

Table 1. Summary of Simulation Results

A. Realistic Level of Measurement Noise

Scenario	Average Error	Maximum Error
1	0.69 m	0.89 m
2	0.74 m	0.79 m
3	1.01 m	1.66 m
4	1.56 m	2.03 m

B. Pessimistic Level of Measurement Noise

Scenario	Average Error	Maximum Error
1	0.99 m	1.46 m
2	1.15 m	1.25 m
3	1.47 m	2.90 m
4	2.56 m	3.35 m

For the square configuration, if a limited data collection run must be made, it appears preferable to pass between transponders rather than directly over them. For the triangle, either collection pattern does about as well. Simulation of other transponder numbers and geometries and other data collection patterns will be reported on later.

10. Conclusions

A new approach has been presented for locating the relative positions of acoustic transponders. This approach combines the modern methods of multilateration and estimation theory to allow processing of simultaneous range measurements from anywhere on the ocean surface. A number of simulated examples demonstrate the effectiveness of the approach.

In closing it will be mentioned that with simultaneous ranges to four or more transponder the three dimensional position of the ranging vessel can be mathematically eliminated. Thus, data collected from a randomly located submersible can be processed to obtain transponder coordinates. An analysis of this case is available from the author.

References

1. Cestone, J. A., et. al, "Latest Highlights in Acoustic Underwater Navigation," Navigation: J. Inst. of Nav., V. 24, No. 1, Spring, 1977.

2. Escobal, P. R., et. al, 3-D Multilateration: A Precision Geodetic Measuring System, TM 33-605, Jet Propulsion Laboratory, Pasadena, Ca., 91103, March 15, 1973.

3. Sage, A. P., and Melsa, J. L., Estimation Theory with Applications to Optimal Control, pp. 268, 460, 462, McGraw-Hill Book Co., New York, 1971.

4. Kaminski, P. G., et. al, "Discrete Square Root Filtering: A Survey of Current Techniques," IEEE Trans. Automatic Control, Vol. AC-16, No.6, December, 1971, pp. 727-735.

Appendix A derivation was deleted for lack of space. $z_{xy} \approx (x^2 + y^2)/2R$ where R = Mean earth radius.

"ACCURATE AND CONTINUOUS GEOPHYSICAL NAVIGATION CONTROL WITH NEWLY DEVELOPED RADIO SYSTEM"

DR. LEO E. OTT

NAV-CON, INC.

ABSTRACT

The current medium range radio positioning equipment relies completely on its ability to maintain a constant frequency source for measuring phase angles or time of travel. Achievable accuracy depends on the stabilization of this frequency standard.

The NANO-NAV System is a range-range system utilizing the Cesium Beam atomic clock (the most accurate frequency reference available), and ground wave radio transmission to provide positioning accuracy to distances of 400 miles under normal conditions. Ability to recover lane identification at sea without return to a known base is also of prime importance. The versatility of the NANO-NAV central processing unit provides a complete stand-alone system for real time navigation and positioning control.

1. Introduction

To achieve positioning accuracies of 20 meters or less in a continuous real time situation, the use of radio positioning equipment is required. Radar systems can easily provide this accuracy or better, and it is not uncommon for these systems to be in the 3-5 meter accuracy range. However, radar has one basic deficiency which limits usage to coastal waters; signals cannot be transmitted further than 50 miles because radar's radio waves travel in straight lines. Therefore, to obtain longer ranges, the transmitted frequency is reduced to achieve a ground wave mode of transmission.

As offshore exploration efforts move to deeper ocean regions further from shore, radio navigation systems reach maximum limitations in maintaining the ability to position marine vessels. Two familiar systems that were developed to obviate these limitations are the Loran-C and Omega Systems. The operation range of Loran-C is approximately 3000 km, and the range of Omega is worldwide. However, the achievable accuracies are 100 meters and 1500 meters, respectively, if appropriate data handling of the radio system is accomplished. Each of these systems possesses the range but lacks the accuracy that is required for detailed ocean surveys.

This paper describes the new NANO-NAV System^{tm} which was developed to provide an accurate short-medium range navigation system to cover the gap between the long-range Loran-C and the short-range radar systems. NANO-NAV was developed to approach the accuracy of radar systems and the range of Loran-C. The NANO-NAV System and design concepts will be presented with some preliminary results obtained while at sea.

2. Design Objectives

To date, there is not an ideal radio navigation system that will provide continuous worldwide coverage to an accuracy sufficient for detailed marine surveying. The next best approach is to design a sub-optimal system that will provide the accuracy needed for a large area; however, there are obvious trade-offs. In general, longer ranges can be achieved with lower transmitted frequencies; but higher accuracies are the reverse of this. The NANO-NAV System was designed to operate in the 1.6 to 1.8 MHZ frequency band which was the closest available frequency band that would provide the best trade-off between ranges and accuracy.

Realizing the high cost of operating a marine crew, the NANO-NAV System was designed to provide reliable navigation information, as well as increase daily productivity at longer ranges. This was accomplished by two means: 1. A system less susceptible to sky wave interference, thus allowing longer and more continuous work periods. This is accomplished by eliminating much of the energy that produces the sky wave signal at the transmitter station. 2. A system with the ability to re-establish one's position without returning to a calibration point in the event signals are lost.

The NANO-NAV System is a completely passive system, which allows an unlimited number of users of the same shore based stations. This also provides location security for users such as secret military applications. Another advantage for the NANO-NAV System was the inclusion of a central processing unit, which provides real time navigation with versatile control functions, such as the coordination and digital tape recording of other peripheral survey data.

3. Time Reference Development

The NANO-NAV System is a unique high accuracy range-range (rho-rho) positioning system using Cesium Beam Frequency Standards. These highly accurate clocks possess sufficient stability to permit transit time and phase measurements of radio waves transmitted from one atomic clock to another. The NANO-NAV System uses Hewlett Packard Cesium Beam Frequency Standards with the high performance tube and goes one step further to assure the best positioning accuracy and re-positioning by including a Delta Frequency Compensator, which allows the user a calibrated means of matching frequency standards. Selecting one clock as a master, usually shore based, a long-term phase drift run is performed to determine the phase drift. Typical drift rates are 1°/9000 sec; therefore, the Delta Frequency Compensator is adjusted to provide a 1° phase shift to the clock every 9000 sec. With this procedure, all clocks are calibrated in the laboratory before placing them in the field for installation. This pre-calibration procedure is allowed because of the long-term stability of the Cesium Beam Frequency Standards. The clock drift calibrations are monitored periodically, thus assuring minimal errors caused by erronous clock drifts. In the NANO-NAV System, a 1° phase shift represents approximately one foot in position change.

To ensure the constant availability of the system for navigation without re-calibration, the clocks are maintained in a running condition at all times. This is accomplished by providing three-hour 24vdc battery backup to the clocks in the event AC power is lost. Of course, if the probability of AC power outage of longer duration exists, extra batteries are included to extend the time. Sufficient accuracy to eliminate timing errors between remote frequency standards with an extremely high probability of success can be maintained with this arrangement.

4. Base Stations

The NANO-NAV System uses double side band suppressed carrier modulation in the frequency band of 1.6 MHZ to 1.8 MHZ with a transmit frequency selectable in 100 HZ steps. Figure 1. shows a block diagram of the NANO-BASE System. The 5 MHZ signal from the Cesium Beam Standard is fed to the Delta Frequency Compensator. In turn, the phase corrected frequency is fed into the frequency synthesizer, which generates the desired carrier frequency Fc and a 500 HZ tone. These two coherent signals are then fed to a balanced modulator which generates two frequencies separated by 1000 HZ. The signals are then amplified and fed to a loading box which matches the output impedence of the amplifier to the tower.

This transmitting tower is a critical element of the entire chain. The transmit site consists of a 100 foot insulated tower with a top hat assembly which has the effect of lengthening the tower and a sufficient ground plane to operate as a counter poise. Appropriate tuning and impedence matching accomplished by the loading box will in effect make the tower appear to be 5/8 of a wavelength in length. This effective tower length will direct the majority of the radiated power horizontally with the ground, which will then minimize the vertical radiated power as illustrated in the ITT Engineer's Handbook (1). The purpose of directing as much of the radiated power horizontally and minimizing the vertical is to reduce skywave interference. Figure 2. illustrates the path that the radiated waves can travel from the transmitter to the receiver. The desired ground wave travels along the surface of the earth and is received at the ship. Simultaneously, a radio wave also leaves the transmitter and is reflected from the ionosphere to the ship. However, this wave does not arrive at the same time as the ground wave, thereby producing a positioning error due to an inaccurate phase measurement. This usually becomes a problem during sunset and sunrise hours when the atmosphere is moving up and down due to the sun setting and rising. In the NANO-NAV System the skywave interference is minimal due to the method described in the preceeding section to minimize the vertical radiation pattern.

5. RECEIVER SYSTEM

The NANO-NAV mobile receivers use a technique of synchronous reception and detection (also known as coherent detection). Figure 3. shows a basic block diagram flow of signals in the receiver units. The Cesium Beam clock, which is known to be in phase with the transmitter clock by means of the Delta Frequency Compensator, is used to synthesize the necessary frequencies to detect and measure the received ground wave signals. The R. F. block receives the desired frequencies and amplifies them in order to drive a mixer which heterodynes the signal to the I.F. frequency. A series of filters and amplifiers in the I.F. section drives another coherent mixer thereby producing a 1000 HZ signal and a 25 KHZ signal. Each of these signals is phase compared with 1000 HZ and 25 KHZ signals derived from the synthesizer. These synthesized signals are again coherent in phase with the transmitted signal due to the Delta Frequency Compensator. Thus, any phase difference is a result of the mobile receiver not being at the transmitter sites. This is the basis for all phase measuring radio navigation systems. The phase reading of the receivers is proportional to the distance from the transmitting station. A 0° to 360° phase measurement of the 25 KHZ signal represents a distance of approximately 200 meters, and the resolution of the phase measurement is 1/100 of this or 2 meters. This 0° to 360° phase measurement represents a fine lane, and in order to keep track of the lanes, an up/down counter is employed. That is, if the phase measurement changes from 359.9^{o} to 0.1^{o}, the lane counter is incremented; in the reverse situation the lane counter would decrement.

The phase comparison of 1000 HZ signal provides a course measurement whose $0\text{-}360^{o}$ phase rotation represents approximately 200 km. This phase measurement has a resolution of 100 meters, and accuracy sufficient to determine the correct lane

count if signals should be lost at sea. There is a phase ambiguity every 200 km however, which is easily reconciled by the operator of the system who will be able to estimate his position within 200 km.

When the NANO-NAV System is first put into the field, the system must be at a known position at one time in order to determine the initial lane counts. This initial lane count is determined by calculating the distance between the ship's position and the base station location and dividing by the wavelength for the frequency of this transmitter site.

The major advantage of this receiver is the fact that the System can accomplish lane identifications, which means that if signals are lost at sea, the correct fine lane can be recovered without returning the ship to a known location.

6. INTEGRATION OF RECEIVERS AND CPU

The NANO-NAV System is a complete stand-alone navigation system capable of producing real time control and positioning information which is accomplished by implementing a central processing unit with the receiver units. Figure 4. is a block schematic of a typical NANO-NAV stand-alone system. This configuration shows three NANO-NAV receivers, thus providing three range measurements to the CPU, which are then processed to provide a latitude and longitude. The System, with its three receivers, has the distinct advantage of producing a redundant range reading since only two range measurements are needed for a position fix.

The computer has direct control of the video terminal, cassette tape drive, keyboard and line printer. The video terminal displays velocity north and east, latitude and longitude, steerage parameters consisting of track angle, distance on and off course, velocity on and off course, and bearing and range to a desired point. Additional parameters are displayed in response to manual entry commands as entered through the keyboard. The printer supplies hard copy of the video display at predetermined time intervals. Computer derived positional information, as well as the raw data, are recorded on cassette tapes for off line analysis.

The interface is an output device that controls external devices. It provides an external closure based on time or distances traveled as well as a means to log the navigation data to an external recording system. The interface also drives a two pen strip chart recorder for monitoring the outputs of two radio receivers.

7. PRESENT AND FUTURE STATUS

The NANO-NAV System is presently undergoing tests in the Gulf of Mexico. Five permanent base stations are in operation. Initial tests look promising, with lane identification successfully demonstrated at ranges between 70 to 350 nautical miles. Twenty-four hour operation of the System has been demonstrated at ranges of 300 nautical miles. However, sufficient data has not yet been obtained from the field to establish the ultimate ranges and accuracies for a year-round operational role.

A central processing unit incorporated in the NANO-NAV System allows further expansion of the system to interface and include other navigational aids. We are currently undergoing implementation of a Loran-C receiver and a satellite receiver into the System for backup and remote transmit station positioning. Loran-C also provides a means of checking the fine lane count as redundancy. The satellite receiver will provide absolute position fixes on the average of every 1 1/2 to 2 hours depending on the user latitudes described in OTT (2). The accuracy of each position fix will provide a further lane identification check and verify the Loran-C system. A major use of the satellite receiver will be to provide surveys of base station sites in remote areas of the world where readily available land surveys do not exist. This will be accomplished with normal satellite 3D solution and translation techniques as described in Spradley (3) and Hatch (4).

8. CONCLUSIONS

The NANO-NAV System is a viable system that can fill the gap between the high accuracy short-range radar systems and the medium to long-range systems. It will approach the accuracies quoted by the radar systems while consistently extending the range. Ultimate range of the NANO-NAV System should be from 400 to 600 nautical miles.

The NANO-NAV System is similar to other methods but has the distinct advantage of being able to redetermine the proper lane count when signals are lost at sea, thus eliminating the costly procedure of returning the vessel to a known calibration point. Another advantage is that the System is completely passive, thereby permitting an infinite number of users of the same shore based stations. It also incorporates a central processing unit which is expandable to include Loran-C and satellite navigation to provide the safety and redundancy of accurate positioning desired by the offshore industry.

The NANO-NAV System provides accurate real time navigation for the offshore marine and the airborne industries including geophysical exploration, pipeline positioning, submersible tracking systems, air search and rescue missions, oceanographic surveys, hydrographic surveys, and airborne mine sweeping operations, as well as numberous other commercial and military applications.

9. References

1. ITT Radio Engineer's Handbook, Published by Howard W. Sams, Inc. Indianapolis, March 1970 Third Printing, Fifth Edition.

2. Ott, L. E. "A Totally Integrated Navigation System", Eighth Annual Offshore Technology Conference, Houston, May 2-6, 1976.

3. Spradley, L. H. "Translocation Fix Update for Geophysical Navigation", Society of Exploration Geophysicists, October, 1976.

4. Hatch, R. R. "Point Positioning and Translocation Via The Transit Satellite System", Society of Exploration Geophysicists, October 1976.

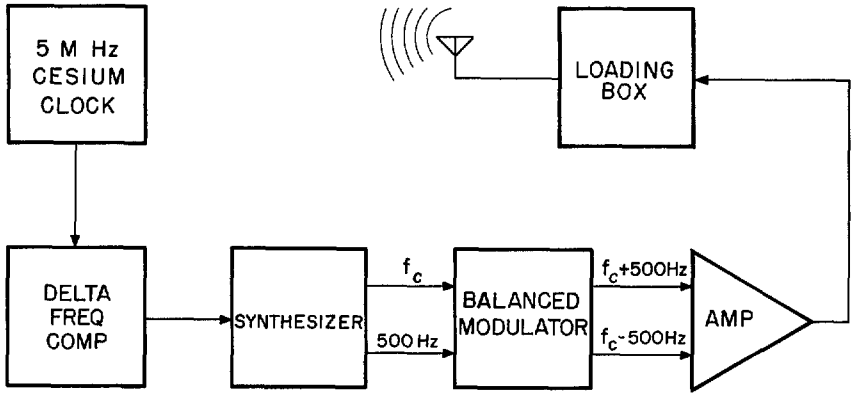

Figure 1. Block diagram of Nano-Base transmitting station showing how transmitted signal is developed.

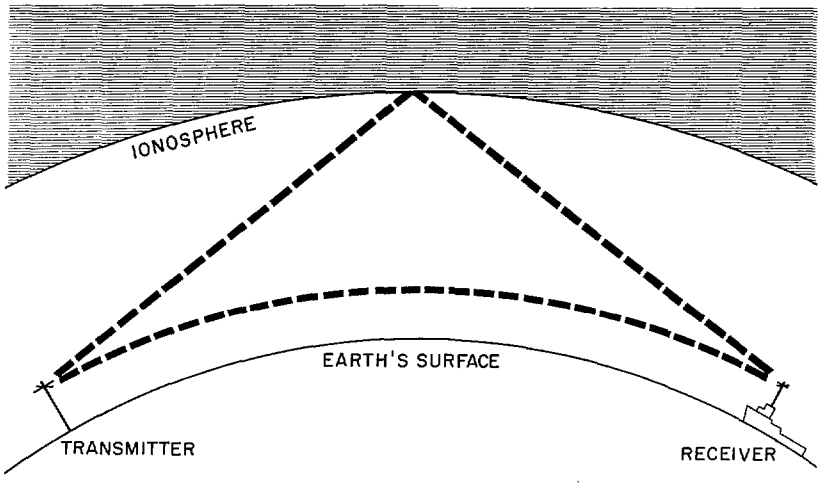

Figure 2. Pictorial view of paths radio waves travel from transmitter to receiver and the effect of sky wave.

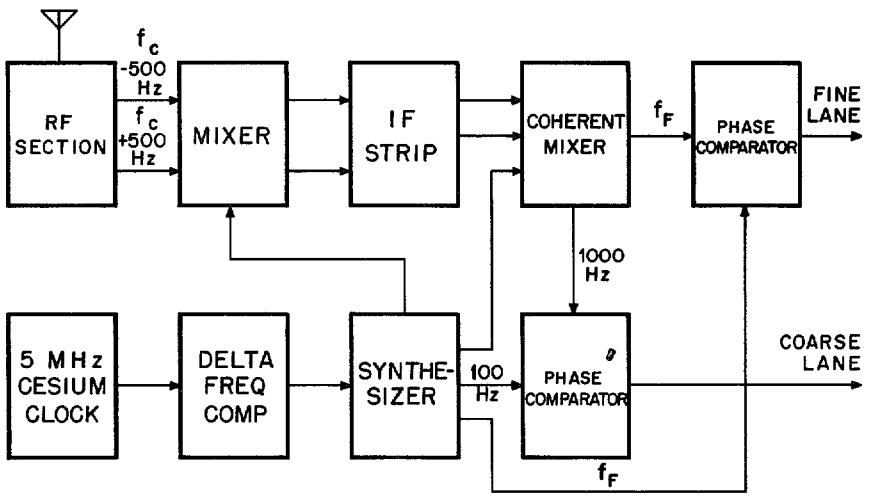

Figure 3. Block schematic of signal paths of Nano-Nav receivers

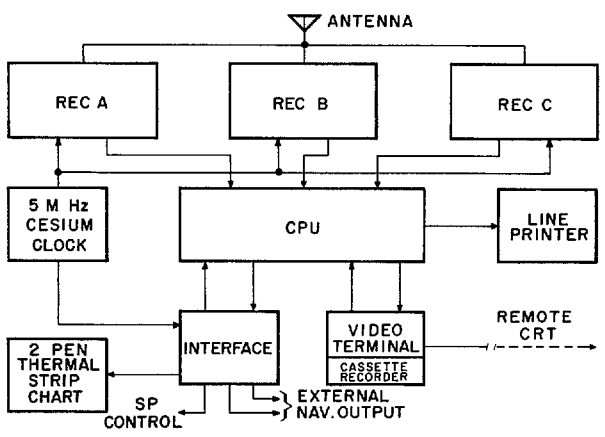

Figure 4. Block schematic of Nano-Nav stand alone navigation system.

HOW TO ADD SATELLITE NAVIGATIONAL ACCURACY AND STABILITY TO EXISTING OFFSHORE NAV SYSTEMS

Phineas J. Icenbice, Jr., Senior Member IEEE
Director, Advanced Technology

JMR Instruments, Inc.
20621 Plummer Street
Chatsworth, CA 91311 USA

ABSTRACT

This paper describes how to employ the accuracy and reliability of the NNSS (TRANSIT) satellite receiver data, as an input to improve the accuracy of a "NAV" SYSTEM which has multiple input data ports. The multiple sensor data from ten or more inputs are accepted by the covariance matrix computational microprocessor, along with the position fix signals from the JMR-2 Doppler Survey Receiving Sub-system. These data are processed to provide multiple outputs for navigation, survey, control and data logging. The helmsperson is provided with a display and the data are recorded on tape. Since different applications require different sensors, this universal design is capable of accepting signals from many sensors with different characteristics.

1. INTRODUCTION

The need for Offshore position fixing ACCURACY and RELIABILITY is recognized by most exploration, geodetic, and hydrographic survey teams as two of the most sought-after performance characteristics. Since most data is collected, collated, and referenced to a position fix, the ability to return accurately and reliably to a geographical location in terms of latitude and longitude, is of great significance in terms of time and dollars spent. Satellites provide the basis for the required position fix accuracy and stability, so it is then only necessary to combine in an optimum combiner the other selected sensor signals as needed to develop the desired system performance. The optimum combining technique is accomplished in the microprocessor. The software is written to basically accept the asynchronous sensor signals and accumulate them in the form of a covariance matrix. The output signals which result from the basic matrix computation in the microprocessor is then placed in the appropriate data format to drive the output ports for interfacing the displays, controls, and other data logging features.

2. SYSTEM DESCRIPTION

Figure 1.0 is the system diagram showing the input sensors on the upper half of the page, and the output devices on the lower half of the page with the processor sub-system in the center. Six input ports are shown for simplicity, but the actual number of inputs is expandable to several dozen if needed. Nine output ports are shown, but again the design is flexible and expandable to several dozen if needed. Three types of tape interfacing schemes are shown, one for cassettes, one for multi-track, and one with RS 232C specifications. Display devices are shown on the lower left and comprise - digital 20ma TTY, RS 232C Track Plotter, ship's speed log and heading, time nav. and sounding, and CRT with expandable capabilities. Special contact closure, time-event-marker outputs are also available. The processor sub-system is a microprocessor capable of interfacing a multiple of devices both input and output with command, control, logic, arithmetic, and other programmable functions. The key inputs are located at the top of the page. The manual keyboard and time inputs are for directing and/or controlling the system directly or indirectly through the microprocessor. The four main signal sensor inputs are:

1) JMR-2 Satellite NAV
2) Radio Position NAV
3) Echo Sounding
4) Ship's Speed Log & Heading

3. NEED FOR INTEGRATED SYSTEMS

Practical experience with LORAN C in the Gulf of Mexico by my good friend and colleague, Jim Moyer, is proof of the need and value of employing an integrated systems approach to improve surveying accuracy. Jim was one of the first to fully realize and analyze that a stand-alone LORAN C system was subject to variations

SYSTEM DIAGRAM

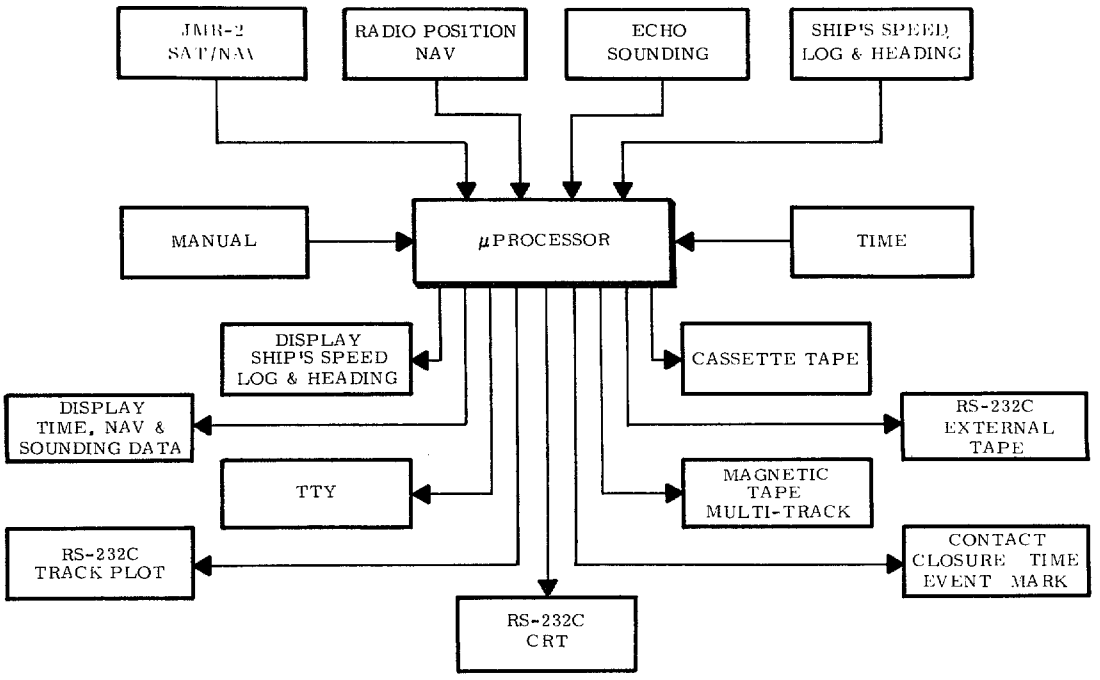

Figure 1

P.J.I. 78

SATELLITE FIXES REQUIRED TO VERIFY LANE OF CW RADIO NAVIGATION AID

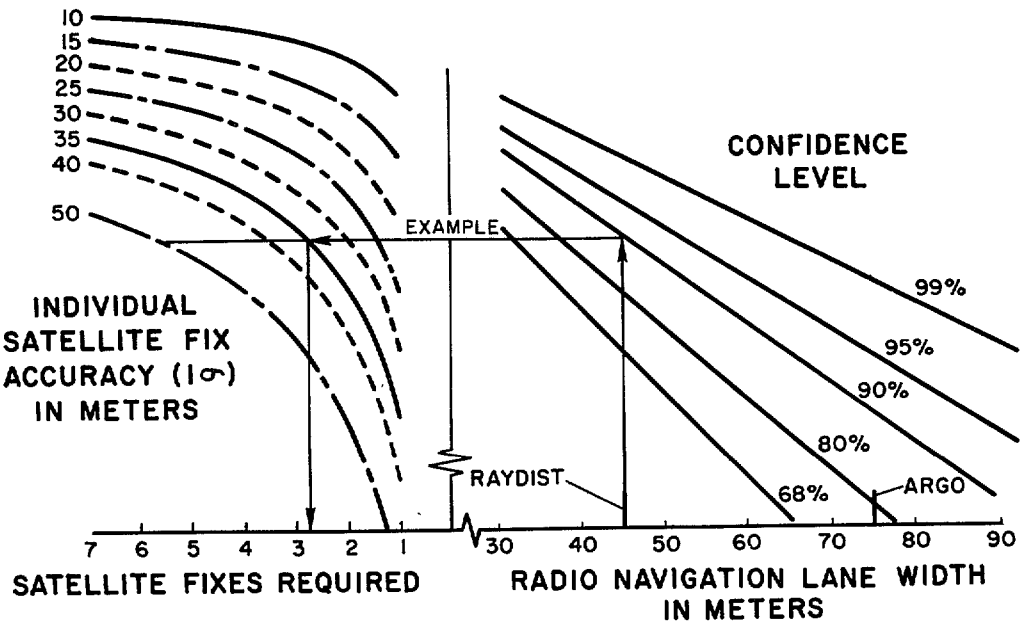

Figure 2

P.J.I. 78

as large as 2400 meters. LORAN C ground wave signals are very stable under most conditions, except during local thunderstorms or squall lines along the range sector between the ship and the stations. Also, radical changes often occur at sunrise and sunset. Repeatability has been demonstrated in the range of 50 to 150 feet for range-range (rho-rho) systems in good signal strength areas with adequate LOP crossing angles. Reliability and stability are needed and satellite systems supply this needed stability, but a moving satellite system required good velocity inputs to compute good fixes. So the Integrated System is needed. CW radio systems can provide excellent velocity by measuring rate of change lines of position. CW radio "NAV" systems suffer from serious ambiguity problems since most cannot differentiate one lane from another. Satellite fixes can differentiate lanes.

The attached Figure 2.0 demonstrates how effectively satellite fixes can be used to verify proper lane counts for CW radio systems. The figure is in the form of a nomogram, which is entered with the known radio system lane width (DRS Raydist and ARGO shown for examples). The procedure is then to rise vertically to the desired confidence level, travel horizontally to the expected one sigma satellite fix accuracy, and finally descend vertically to obtain the number of sequential satellite fixes required to verify the actual CW lane count to the specified confidence level (round up to the nearest integer). Previous theoretical analyses have predicted satellite one sigma accuracies of 30 to 40 meters for an integrated satellite/ARGO system. This figure shows that the proper ARGO lane can be identified to 95% confidence by fixes of 32 meters or less on a single pass and within two passes for fix accuracies to about 43 meters.

The data in Figure 2.0 correlates exceptionally well with actual practice. On a survey off the West Coast of Greenland using an integrated satellite/ARGO system, it was demonstrated that the satellite fix gave the proper ARGO lane 93% of the time. This figure would indicate that the integrated system was producing satellite fix accuracies of approximately 33 to 34 meters one sigma - well within the anticipated performance range.

4. COMMON OFFSHORE NAV SYSTEMS

Common offshore navigational systems are usually composed of one or more of the following basic systems or sensors:

1) SAT-NAV (two channel)
2) Inertial (Gyro-or IMU-Inertial Measurement Unit)
3) RADIO (LORAN C/Raydist/ARGO/OMEGA)
4) SONAR

The JMR Integrated Systems group is concerned with combining and weighting selected input data from multiple sensor inputs in an optimum way in order to predict and project for display the most probable position fix, course and heading information. The following is a simplified functional description of the basic integrated NAV system emphasizing the software organization for positional tracking.

The basic elements of the microprocessor are shown in Figure 2A. The individual data transfer loops are cycled at rates appropriate for the type or sensor signals and sensor measurement accuracies. For clarity, a single radio navigation sensor is shown integrated with a satellite receiver, but additional sensors may be simply incorporated by expanding the measurement prediction and adaptive navigational filter modules and by adding a separate tracking filter for each new sensor. The heart of the software lies in the adaptive navigational filter. This module combines all sensor measurements into statistically optimal estimates of a vessel's position, velocity, and sensor bias errors whenever an adequate level of redundancy exists.

A more graphic display of the performance of an integrated satellite/LORAN C system is presented in Figure 3. This takes a typical, and actual fix distribution and applies it to the "nominal" LORAN C error growth rate. The dashed line indicates the error potential in a vessel equipped only with a stand-alone LORAN C system perfectly calibrated about 50 minutes before the day begins. The lower saw-toothed line demonstrates the constraints on error build up which the satellite fixes can provide. It is interesting to note that on this particular day the realtime error exceeded 100 meters only twice for a total duration of only 2 1/2 hours. The worst excursion during this day amounted to just 150 meters.

5. RADIO-NAV SENSORS & INTEGRATION

Many basic radio types of navigational systems are available today such as DECCA, LORAN C, OMEGA, RAYDIST, ARGO, and others. Each system is considered a good candidate, navigational sensor, in an integrated NAV system, and it is recognized that each offers special advantages and disadvantages. The purpose here is

FUNCTIONAL DIAGRAM
INTEGRATED NAV TRACKING LOOP

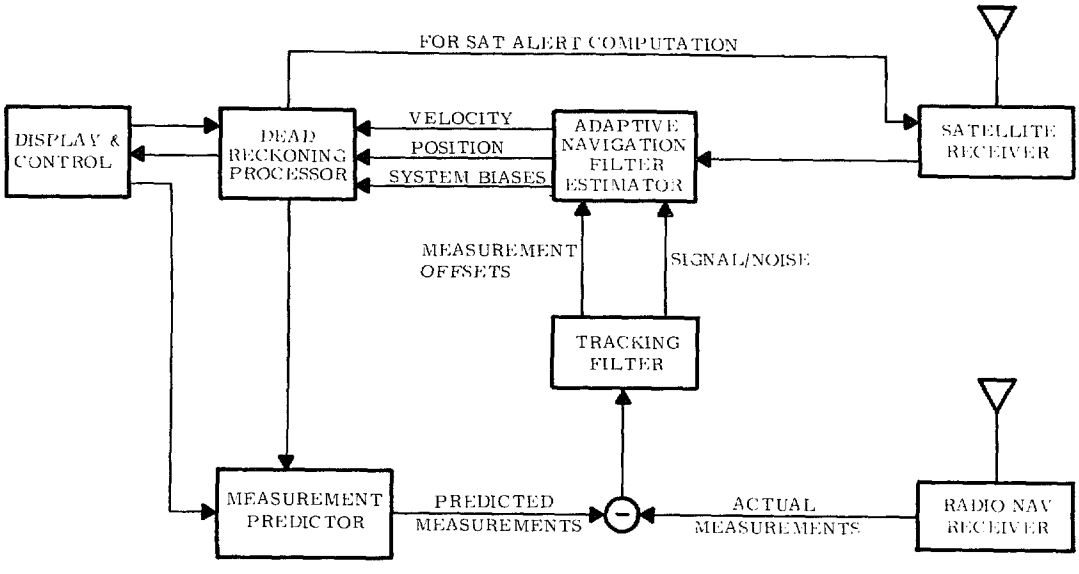

Figure 2A

P.J.I. 78

GROUND CONDUCTIVITY PHASE ERRORS
(TYPICAL DAY OF LORAN C)

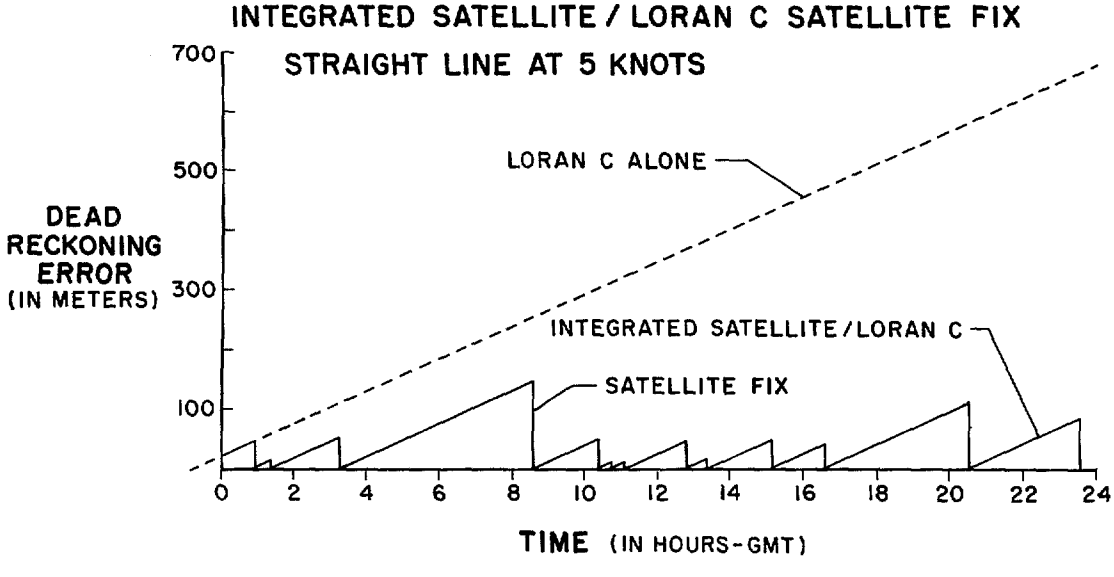

Figure 3

P.J.I. 78

to use LORAN C as an example of a good candidate sensor and show some of the advantages of the integrated systems approach. Other systems often operate on frequencies other than 100 KHz, some higher, and some lower in frequency. Most employ different types of modulation and occupy different bandwidths. Each set of system performance specifications results in some outstanding features. However, one common performance feature that is often missing is the ability to identify the correct lane.

Our discussions are not designed to aid in the selection of one system sensor over another, but rather to show some detail for a typical sensor-LORAN C as an example. The 100 KHz transmissions of LORAN C penetrate over 100 feet into the Earth, and the difference between the propagation velocity in the Earth and in the free air tends to distort the wave front at the surface. Vehicles traveling at the surface, ships, and land vehicles, are often significantly effected by the distorted wave front while aircraft are not subjected to the phenomenon.

All current LORAN C charts show lines of position computed by using a propagation velocity based on a "standard sea water path." All automated LORAN C navigators which produce readouts of latitude and longitude employ the same technique. The assumption of a standard sea water path can lead to enormous position errors - approaching several miles under certain conditions.

Jim Moyer was one of the first to fully analyze this situation in the early 1970's after conducting a survey in the Gulf of Mexico using a stand-alone, hyperbolic LORAN C system which he misplaced a significant portion of the survey lines by over 8000 feet. Fortunately, he also had a backup satellite system which he believed had failed, due to the large differences in realtime with the LORAN C positions. After some considerable analysis of the problem, he was able to develop a contouring algorithm which converted the difference between predicted LORAN C LOPs based on over 500 satellite fixes in the area and the measured LORAN C LOPs into coefficients of a ground conductivity model which was applicable over a broad area. The effectiveness of the model was verified by placing a survey vessel on anchor at seven test points throughout the Eastern Gulf of Mexico and averaging 24 hours of satellite and LORAN C data at each site. While the original survey lines remained 8000 feet from their desired location, he was most fortunate to be able to prove that they were now correctly positioned to an accuracy of 150 feet.

The success in averting the initial disaster resulted in numerous contracts to reprocess data collected by other surveying contractors using stand-alone LORAN C systems, and gave him an almost exclusive on LORAN C surveying for several years. This bit of history is intended to emphasize the reality of the problems associated with LORAN C phase errors due to ground conductivity.

The attached Figures 4A & 4B shows the actual contours of the phase errors in LORAN C signals measured in two areas of significant interest to navigation - the Gulf of Alaska near the approaches to Cook Inlet, and off the East Coast of the U. S. These contours were developed with Jim Moyer's original algorithm by Digicon, Inc., and are based on continuous DRS Raydist positions in Alaska and on thousands of satellite fixes off the East Coast.

The contours, difference between theoretical LOPs and actual LORAN C measurements are shown in 0.10 microsecond intervals. While they are in reality hyperbolic LOPs, they can be qualitatively evaluated easier by assuming they are range errors. Since one microsecond represents about 983 feet, the transit from one contour line to the next would result in a change in position error of 98.3 feet.

To illustrate the potential magnitude of the dead-reckoning errors which can be generated by the spacial variability of ground conductivity phase delays, consider a survey vessel sailing a straight line at 5 knots in the "worst" case regions, as indicated on Figures 4A and 4B. Assume that there are no instrumentation errors, perfect station geometry, and that at the initial point the receiver is perfectly calibrated so measured LOPs equal exactly the theoretical values.

The relative changes in phase delay as derived for each of the two area "worst" case paths are shown on the 4th figure. The third error growth curve labled "nominal" corresponds to a report from a major oil company as their experienced nominal LORAN C dead reckoning in the general U. S. East Coast area (some sectors were worse, some better). As can be seen, a vessel with only a stand-alone LORAN C system in Alaskan waters could be in error by half a mile within 12 hours. Similarly, the worst case East Coast error would approach 2000 feet. Even the nominal situation errors would exceed 1000 feet over the half-day interval. While dead-reckoning errors grow dramatically due to changes in ground conductivity, velocities derived from the rate of change

of LOPs are not significantly altered. The worst case Alaska path introduces a velocity error of only 0.05 knots which would cause only a 17-meter satellite fix error even if it were to all occur along a North-South axis. The nominal case generated a 0.015 knot velocity for a maximum satellite fix velocity induced error of 5.6 meters. Therefore, even in the presence of variable ground conductivity, velocities derived from LORAN C LOP changes are sufficiently accurate to provide excellent satellite fixes.

6. SAT-NAV INTEGRATION EFFECTIVENESS

To demonstrate the effectiveness of satellite integration in constraining the LORAN C dead-reckoning error (see Figure 4) growth eight days of satellite alerts were run for the two latitudes used in the example (59°N and 39°N). These alerts were culled of high (above 70° elevation angle) and low (below 15°) passes and conflicts where two or more satellites would simultaneously produce very similar doppler offsets were eliminated. It was also assumed the satellite receiver was of the automatic acquisition type, but was not aided in the selection of passes either by a computer or manually. Therefore, good passes which had rise times within the tracking period of an unacceptable pass were also eliminated since the standard receiver would have acquired the poor pass without the knowledge that the acceptable pass was to arise shortly thereafter. While the number of passes which would provide fixes varied significantly between the individual days, the total number of fixes over the eight-day period amounted to 125 for 59°N, and 95 for 39°N. The average number of passes per day came to 15.6 for 59°N, and 11.9 for 39°N.

The statistical distribution of the satellite fixes are indicated on the dead-reckoning curves "not to exceed" percentages. This is to say that, in the Alaskan case, 100 per cent of the satellite fixes were spaced six hours or less apart so that at no time during the eight-day period examined would the dead-reckoning error have exceeded 1730 feet (527 meters). Similarly, 80% of the fixes would have constrained the error to about 200 meters and 50% to just over 100 meters.

The longest time between passes for the East Coast ran to eleven hours, so the maximum error extended to 1800 feet for the "worst" case, but 50% of the fixes constrained the error to approximately 200 feet (61 meters). On the nominal East Coast case, about 85% of the satellite fixes would restrict the realtime dead-reckoning error growth to under 100 meters. This level of realtime navigation precision is highly acceptable for all survey operations except for the small amount of work involving "3D" geophysical data collection, or the small area site surveys. Since Since the ground conductivity phase errors are very stable in time, they can be assumed linear functions between satellite fixes and, therefore, are easily removed by post-mission processing.

7. HOW TO ADD ACCURACY

One common radio NAV sensor was used as an example, up to this point, to show how accuracy is improved by processing two data sources of different characteristics from real world data. Different applications may, and usually do, require more and different NAV sensors. The universal JMR design is capable of accepting signals from echo sounders, log gyros, RS232C compatible sensors, LORAN C, inertial, and most currently available marine sensors capable of RS232C interfacing. Accuracy is achieved in the system's unique ability to estimate, track, collate, weight, and synergistically combine the best data at the best time for an accurate output. When a set of measurements contain systematic errors, then the precision of the measurement is better than the accuracy. However, in the limit of no systematic errors, a measure of the precision is identical to that of accuracy (as described by the standard of measure in use). The objective is to adjust the processing and filtering to limit the systematic errors to as low a value as possible. The random errors are reducible by the square root of the number of possible measurements per unit of time, available.

8. SUMMARY AND CONCLUSIONS

The charter to accurately locate a position without ambiguity, on or near the surface of the Earth, is now delegated universally to satellite surveying systems. The shape and size of the Earth is also precisely defined as a result of ten years of satellite and other geodetic measurements for WGS-72. Atomic instrumentation of time interval measurements and epoch synchronization between distant points is adding confidence and accuracy to satellite measurements which are already capable of establishing position fixes (of stationary points) to fractional meter accuracy. Artificial satellites rise and set with the regularity of the sun and their VHF/UHF signals are processed automatically into the latitude and longitude by the receiver. Since 1964, many thousands of usable satellite passes, predictably on schedule, have provided the statistical proof of this high reliability and confidence. It is this continuous and world-wide proof of performance by JMR satellite systems

in the field that is now available to improve offshore navigational technology. Good heading and velocity measurements are available from many different "navigational sensors" covered in this paper. These short-term sensors are very accurate and provide the conjugate match when the data are properly integrated and weighted with accurate two-channel JMR quality satellite navigational data.

Several classes of navigational dead-reckoning sensors have been briefly examined. The efficiency of satellite integration into two widely popular radio navigation systems has been graphically demonstrated.

The conclusion is that position fixing accuracy and reliability are maximized with a well-implemented integrated offshore navigational system. The well-planned mission scenario that includes multiple SAT-NAV calibration points at zero velocity is desirable to produce the best accuracy. The geometry formed by the calibration points should be selected for its strength and accuracy. Just as the ideal selection of the sensors should be based upon the stability and overall system accuracy desired; the JMR system integration is dedicated to provide the optimal signal combining processor for best accuracy and stability.

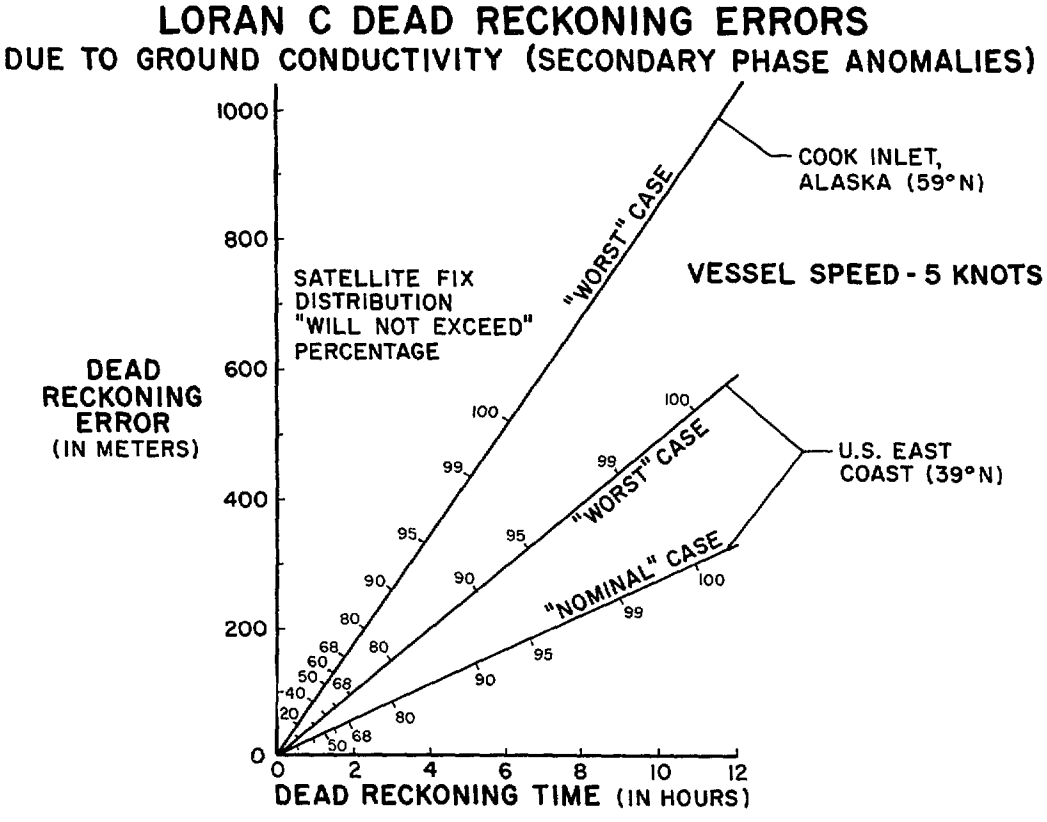

Figure 4

P.J.I. 78

Note: Contour charts deleted due to page limitations. Charts are available from JMR upon request. (Figures 4A & 4B)

PERFORMANCE OF A REAL WORLD MINIMUM VARIANCE INTEGRATED NAVIGATION SYSTEM

R. F. McPherson
Sperry Marine Systems
Charlottesville, Virginia 22906

Abstract

Performance of an integrated navigation system presently used on large oil tankers is investigated through simulation techniques. A description of the system operation is followed by a discussion of simulation methods and results. Results include performance characteristics as a function of sensor errors and ship turning parameters.

1. Introduction

Integrated navigation systems have been developed for various uses ranging from accurate positioning to ocean bottom surveys. The system analyzed in this paper was developed for general navigation aboard large commercial ships. Six systems are in use today on oil tankers operating between Valdez, Alaska, and the West Coast of the United States.

Performance of the system was evaluated during sea trials and through computer simulation. Sea trials were held in September 1977, the results of which are presented in Reference 1. Sensitivity of the system to its various sensors was analyzed with a dynamic computer simulation. A UNIVAC 1108 computer was used.

Following a brief functional description of the navigation system, simulation development and results are discussed. Results include system error as a function of sensor errors and system performance during turns.

2. Functional System Description

Two algorithms compose the integrated navigation system: a dead reckoning function and a minimum variance filter. The filter is used to periodically update dead reckoning calculations that are then used as a position input for the next filter estimate. System output is the position determined by the dead reckoning algorithm. Figure 1 presents a block diagram of the system.

Ocean current and position estimates are calculated by the minimum variance filter using position fixes from sensors and dead reckoned position. Position sensors are a Loran C receiver, satellite receiver, and radar data processed by the channel navigation function. Every 60 seconds, positions from sensors reporting during the interval are mixed with the dead reckoned position to obtain an estimate of own ship's position and ocean current.

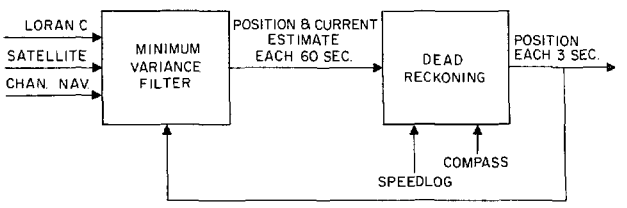

Figure 1. System Block Diagram

Weights of each input used to calculate final estimates are inversely proportional to the inputs' variance. For sensors that have not been reported during a filter interval, their weight is set to zero effectively ignoring that sensor's input. These updated position and current estimates are used to reinitialize the dead reckoning algorithm.

Dead reckoning is used to obtain own ship's position between the 60-second filter intervals. The algorithm integrates own ship's northerly and easterly velocity components over time to calculate the change in location from the last filter position estimate. Integration interval was 3 seconds. Inputs from the ship's speed log, compass, and the estimate of ocean current from the filter are used to compute northerly and easterly velocity components. At the end of the 60-second filter interval, the present dead reckoned position is fed back as an input to the filter. After calculating the new estimate of own ship's position, the filter updates the dead reckoning algorithm. The dead reckoning module output is used for the integrated navigation display.

3. Simulation

Simulation of the integrated navigation system consisted of three parts: a model of the navigation system was developed, the system environment was modeled, and signals representing outputs of various sensors were simulated. A flow chart of the simulation is presented in Figure 2. The integrated navigation system was simulated by the interconnection of these models.

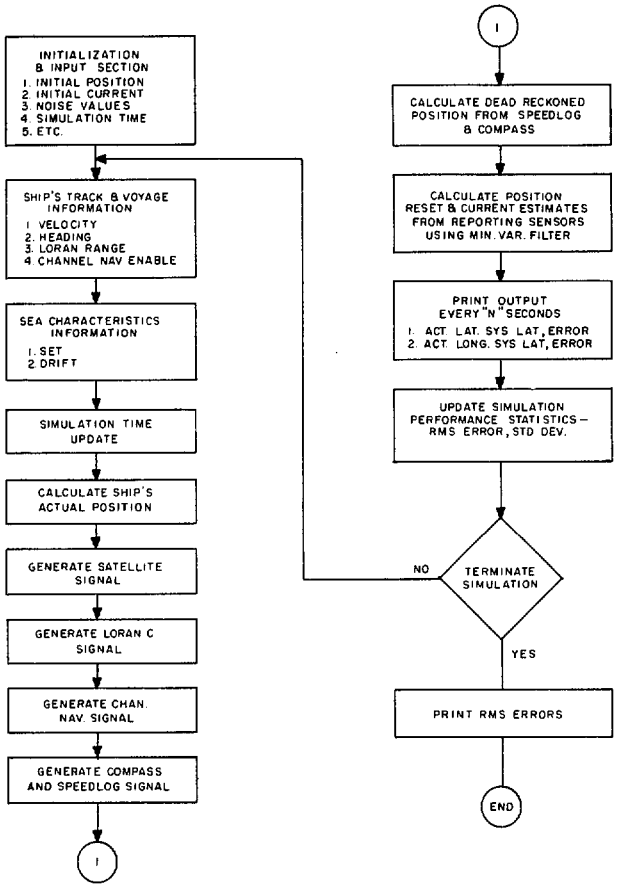

Figure 2. Navigation Simulation Flow Chart

The actual algorithms for the filter and dead reckoning formed the basis of the navigation system model. Because these algorithms were digital no approximations were necessary. These algorithms were converted into FORTRAN for inclusion in the simulation. Inputs to the algorithms were from simulated sensor signals. Filter estimates of ocean current and position, generated every 60 seconds, were used to update the dead reckoning calculation. The latest dead reckoned position was fed back to the filter for each 60-second filter update.

The navigation system model was operated in a simulated environment. By using the stored values of the ship's actual dynamic motion parameters (velocity, heading, turn rate, and the like) and ocean current parameters, the ship's true position, heading, and velocity were tracked. This model supplied the reference information needed to check performance of the navigation system.

The navigation model used simulated sensor signals. These signals were modeled by adding noise, characteristic of the particular sensor, to the values of the sensed parameters obtained from the environmental model. No attempt was made to model the sensor because only the output signal was of interest for this study. Sensor signals were generated at intervals that corresponded to actual occurrence rates. These simulated signals were applied to the appropriate navigation algorithms.

Verification of the simulation was accomplished through selected test runs. Simple tests with known results were used to exercise various models comprising the simulation. With the aid of diagnostic outputs these test runs provided checks for proper functioning of the models.

4. Simulation Results

Simulation was used to obtain system sensitivities to various sensor errors. A baseline level for errors was chosen as a reference. This baseline came from a study entitled, "The Effects of Sensor Errors in Certain Marine Collision Avoidance and Threat Assessment Systems," (2). Their magnitudes are typical of values of errors present in commercial marine navigations sensors. By perturbating errors around the baseline, system performance sensitivity was measured. Tests, using turns of various radii, turn rates, and drift angles, along with the sensor errors, set to baseline levels, provided data on the system performance during maneuvers. Baseline sensor error levels were:

Error Type	Magnitude
Compass bias	1 degree
Compass deck plane	1 degree rms
Compass Schuler pendulum	0.1 degree rms
Compass jitter	0.1 degree rms
Speed log bias	0.1 knot
Speed log fluctuation	0.1 knot rms
Speed log jitter	0.1 knot rms
Loran C	500 feet +10 feet rms

To find the worst case conditions, the sensor errors and ship motions were chosen such that error contributed by each sensor

was additive. No error cancellation from one sensor by another sensor was allowed. Except for the maneuver test runs, a straight track for own ship was used. Current was held constant in magnitude with direction changing by 90 degrees in about four simulation days. This is comparable to the current in open ocean between San Francisco and Valdez.

Loran C error was varied under three system configurations: operating on Loran C only, operating with satellite signals, and operating with channel navigation radar signals. Figure 3 shows the results of the three cases. With the system using only Loran C signals, position error ranged from 500 feet to 1,340 feet rms as the Loran C error varied from 500 feet to 1,500 feet. This was improved to 460 feet to 1,215 feet rms with the addition of satellite fixes. When operating with channel navigation radar signals, the system error was improved to 220 feet rms in the 500-foot Loran C error range to 310 feet rms in the 1,500-foot range. In terms of ship length, this represents an error about the quarter of the length of a medium size oil tanker for operation in a ship channel.

Compass errors affect system performance as exhibited in Figures 4 to 6. The system shows higher sensitivity to Schuler pendulum error than either bias or deck plane, but this is the smallest source of error in the compass. Compass bias appears to have the most deteramental effect on performance in terms of error magnitudes that might occur during operation. With the bias error at 4 degrees (typical 1 degree) the system error was 680 feet rms. This compares to about 500 feet rms with all sensor errors at the baseline condition.

Speed log bias and fluctuation errors were varied up to ten times their normal values. These results are shown in Figures 7 and 8. System error with a 1.0-knot speed log bias is 720 feet rms. A 1.0-knot rms fluctuation gives rise to a 615-knot rms error. The speed log bias error curve can be used to estimate the system error for manually inputted values of the ship velocity. This situation could occur if the speed log fails and another source is used to estimate speeds such as engine rpm.

Both compass and speed log jitter errors were perturbed from their baseline level. No significant change in system performance was noted. This was expected as both the speed log and compass signals are passed through low pass filters before entering the navigation algorithms.

Performance of the system during turns was evaluated, using the specified baseline error levels. In addition, the effect of channel navigation and satellite fixes on performance while turning was investigated. The ship's track was altered to a circular path for this analysis. Various turn rates and turn radii were tried with no change in system performance. This characteristic was attributed to the speed of response of the navigation system. The system can respond to velocity and heading changes that are much faster than the ship can realize during a turn. Drift angle, however, had a very definite effect on system performance. Figure 9 shows the results of various drift angles during turns. The drift angle was varied from 0 to 15 degrees. Results show improvement in system response with the addition of channel navigation and satellite fixes. With a 15-degree drift angle, a 200-foot improvement in system error can be achieved. Because large drift angle turns are usually encountered in tight harbor situations, this improvement is significant.

5. Conclusions

Integrated navigation systems do perform with greater accuracy than single sensor systems. The data presented in this paper supports the claim. Not only is accuracy increased with multiple sensors, but degradation of performance is minimized as sensors begin to fail. If one sensor becomes increasingly less accurate, the others help to compensate. This adds a greater measure of reliability to integrated navigation systems.

6. References

1. "Performance Analysis of an Integrated Navigation System for Tankers Transporting Alaskan Oil," R. F. McPherson and H. S. Gentry, Sperry Marine Systems, Copyright 1978, Offshore Technology Conference.

2. "The Effects of Sensor Errors in Certain Marine Collision Avoidance and Threat Assessment Systems," R. F. Riggs, Sperry Marine Systems, Navigation: Journal of The Institute of Navigation. (Spring, 1974) Vol. 21, No. 1.

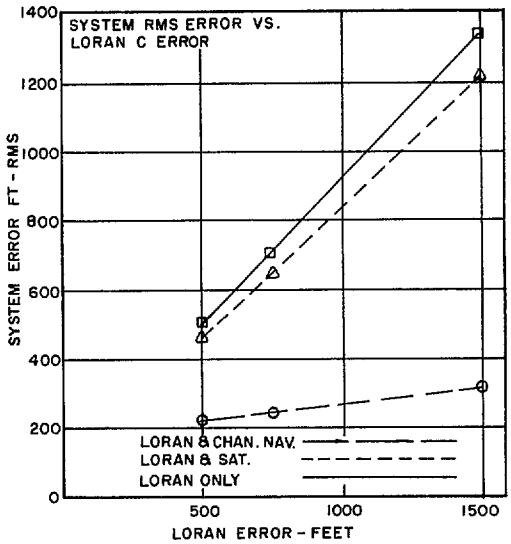

Figure 3. System RMS Error Versus Loran C Error

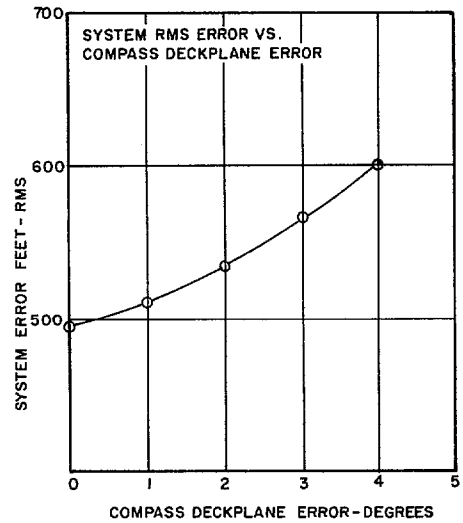

Figure 5. System RMS Error Versus Compass Deck Plane Error

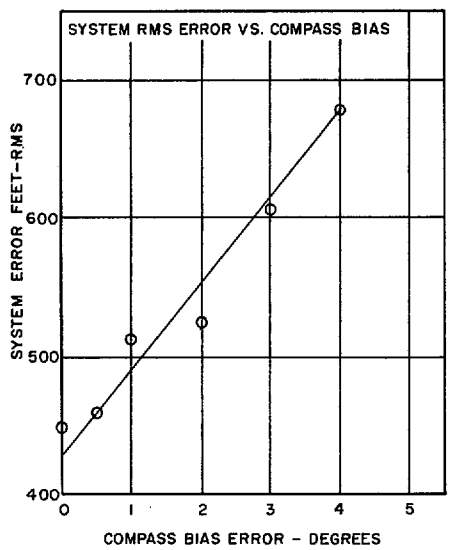

Figure 4. System RMS Error Versus Compass Bias

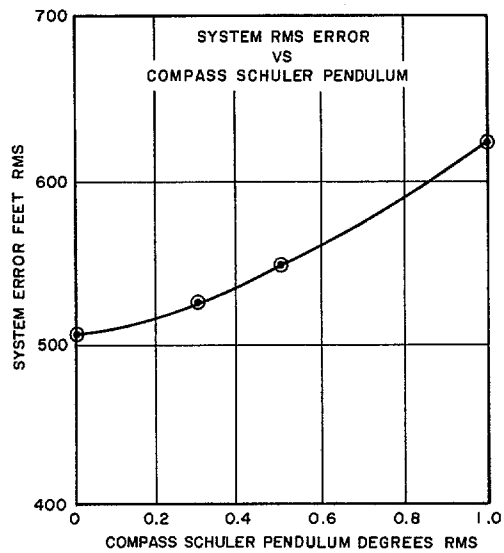

Figure 6. System Error Versus Compass Schuler Pendulum

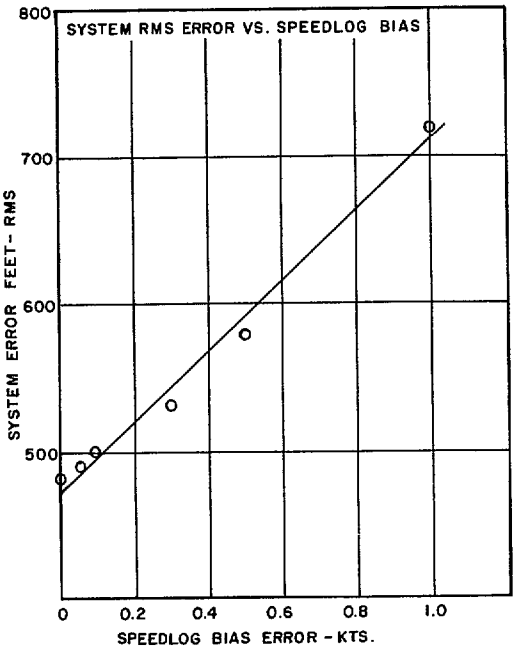

Figure 7. System RMS Error Versus Speed Log Bias

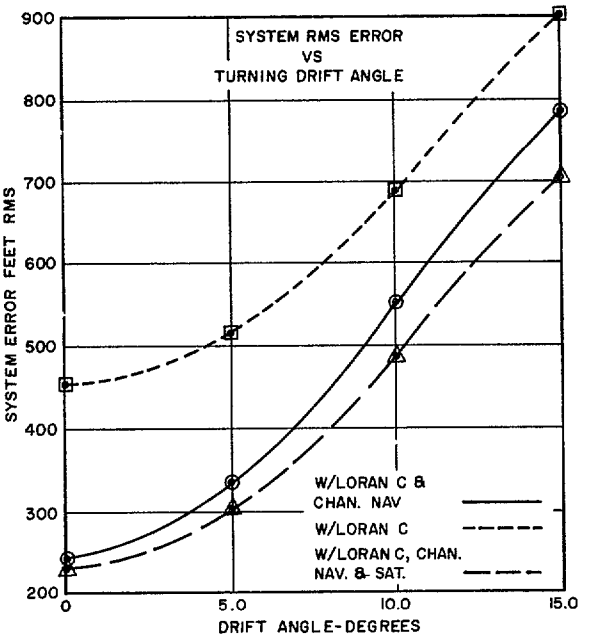

Figure 9. System RMS Error Versus Turning Drift Angle

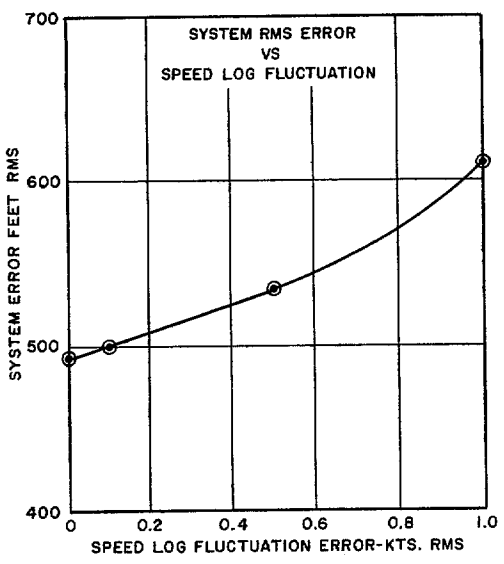

Figure 8. System RMS Error Versus Speed Log Fluctuation

A SATELLITE-BASED SYSTEM FOR REDUNDANT MARITIME DISTRESS SIGNALING

Walter C. Scales
The MITRE Corporation
Metrek Division
Mail Stop W535
7925 Westpark Drive
McLean, VA 22102

1. Introduction

In March 1971, the Texaco Oklahoma suffered a structural failure and broke in two off Cape Hatteras. The stern section, with 31 survivors aboard, remained afloat for 27 hours. The survivors used lifeboat radio, lights, and flares to signal for help. Although there were at least 18 other vessels within 120 miles of the floating stern section, the signaling equipment available to the survivors proved to be useless.

On February 1, 1972, the SS V.A. Fogg was damaged by an explosion and sank quickly off the Texas coast. If there was an opportunity to transmit a radio distress signal, it was never received. A search was initiated only when the ship was reported overdue. It took 11 days to find the sunken hull. The entire crew was lost.

These and other recent maritime disasters underscore the need for quick, reliable, long range emergency alerting. Life expectancy at sea decreases hour by hour after a sudden disaster. Death from exposure, untreated injuries, drowning, and other hazards can be reliably thwarted only by quick rescue. Although some disasters afford an opportunity for signaling by conventional means, there remains a significant number of accidents in which no such opportunity exists. In the case of deep sea trawlers, for example, vessels that suddenly vanish without a trace represent only about five percent of all vessel casualties, but these accidents cause about twenty-five percent of the deaths.(1) Similar statistics can be assumed to apply for other vessel categories.

It is clear, then, that there is a need for an alerting system that would provide for rapid rescue under circumstances which prevent contact by conventional radio. As a minimum, such a system should have the following characteristics:

1. Global Coverage - Figure 1 shows the projected 1980 worldwide average distribution of merchant ships. Only the polar regions are substantially free of activity. Implementation of a local alerting system would leave much of the problem unsolved.

2. Immediate Alerting - The need for quick rescue after a serious accident is paramount. There is no time to be lost in trying to establish contact on an unpredictable channel or in waiting for the next passage of a low orbiting satellite. Automatic monitoring for distress signals is highly desirable.

3. Automatic Activation - The emergency signaling device should be packaged as a buoy that would float free and activate in case of a rapid sinking. A manual means of activation should also be provided.

4. Identification and Location - Transmissions from the ship/buoy should carry the identification of the stricken vessel (in coded form). From the ship's schedule and last reported location, the approximate area of the accident can be determined. More accurate location data is obviously needed to complete the rescue, and this should be obtainable within a short time after the initial alert.

5. Low Cost - In order to be effective, the cost of the emergency signaling device must be acceptable to the owners of small vessels. The cost to the country or countries providing the land portion of the system must also be reasonable.

We present here a redundant satellite-based system that is expected to meet all of the above requirements. It has been conservatively estimated that such a satellite-based system would save more than sixteen lives and more than $5 million worth of property annually in the U.S. maritime region alone.(2) If these figures are indicative of the potential benefits in other maritime regions, then the total benefit for an emergency alerting system with worldwide coverage would appear to justify the implementation of such a system.

The system described has grown out of studies by NASA, the U.S. Coast Guard, the Canadian Government, and the U.S. Maritime Administration. It is, in fact, a marriage of the two concepts that evolved from the NASA/Canadian Study and the efforts of the Maritime Administration.

2. Present Emergency Signaling Techniques

With the possible exception of a few small pleasure craft, virtually every vessel capable of operating on the high seas is provided some form of emergency radio signaling capability. Unfortunately, many

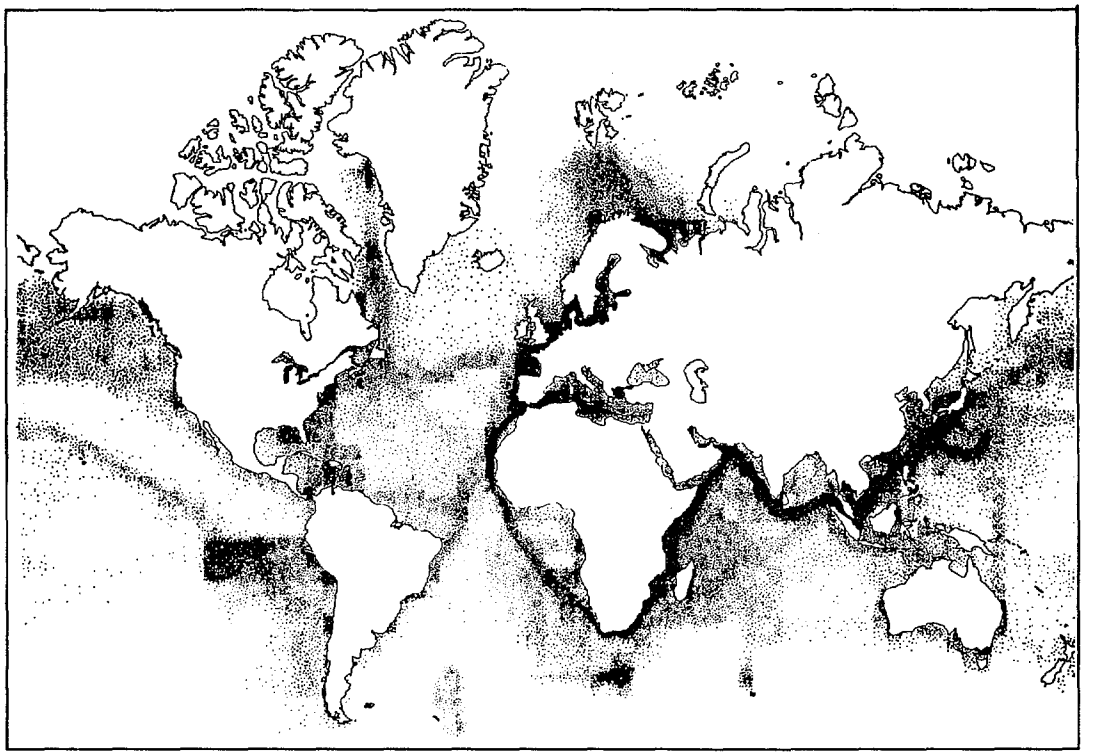

FIGURE 1

1980 PROJECTED WORLDWIDE MERCHANT SHIP DISTRIBUTION

of the present capabilities are of limited value because of their short operational range, high cost or unreliable propagation mode. Table 1 provides a summary of present emergency signaling methods and their limitations; detailed descriptions can be found in references 2 and 3.

TABLE 1

CONVENTIONAL EMERGENCY SIGNALING

METHOD	COMMENTS
500 kHz Radiotelegraph	200-700 nmi typical range
Survival Radio (500 kHz/8364 kHz)	Low power
2182 kHz Radiotelephone	60-140 nmi typical range
2182 kHz Survival Transmitter	Low power, 40 nmi range
2182 kHz EPIRB	Low power, 9-16 nmi typical range
HF Radiotelephone and Radiotelegraph	Variable propagation, Lack of shipboard watch-keeping
VHF Radiotelephone	22-54 nmi typical range
121.5/243 MHz EPIRBs	Line-of-sight
Marisat Terminals	High cost ($60,000 purchase or $1500/mo. lease)

3. Present and Planned Maritime Communication Satellites

Two distinct types of satellite systems have been offered for distress applications.

a. The geostationary satellite based system utilizes the enormous "earth footprint" view from the geostationary communication satellite to obtain very nearly global, continuous reporting of distress situations. Typically, such a system would be included as part of a commercial maritime communication satellite. This system has the inherent disadvantages of long-path space attenuation of the signal, which requires a higher EPIRB power output, and the need for auxiliary means (which could prove to be quite expensive) to provide position data.

b. The low altitude polar orbit satellite system, on the other hand, has a nearly complementary set of advantages and disadvantages. Satellite visibility periods in this case can be several hours apart and last only a few minutes. However, independent position fixing of the emergency transmitter (EPIRB) is easily achieved from the doppler shift of the signals recieved by the satellite. This type of system could be a "piggyback" package on a meteorological satellite. Signal processing for position determination could be accomplished on board the satellite, or on the

ground via "bent pipe" relay from the satellite. Because of the reduced path length, the low altitude polar orbit satellite system requires considerably less EPIRB power than does the geostationary satellite-based system.

Both systems have the merits common to satellite based communication systems: a high grade communications channel and automated telecommunication to a fixed number of designated Earth stations. A properly constituted system could provide the means for rapid detection of an emergency situation, and on-the-scene command level, or regional coordination of rescue efforts consistent with those in the present establishment. Such a system also offers the potential for global coordination.

4. Emergency Signaling Via Low-Orbiting Satellite--The Joint NASA/Canada Study (4)

For the past several years, both the United States and Canada have been studying the application of satellite technology to Search and Rescue (SAR) requirements. This work has included examination of user requirements and investigation of various concepts culminating in limited proof-of-concept experiments using the AMSAT OSCAR satellites during 1975 and 1976. Up to this point, these studies and experiments were conducted separately and independently by both countries. Since late 1976, joint meetings have been held to explore the possibility of a joint program and to develop a tentative cooperative work plan.

The baseline system consists of near polar orbiting, nominal 850 km altitude satellites (TIROS-N series spacecraft) incorporating spacecraft SAR mission instruments, and multiple Local User Terminals (LUTs) which can process and receive information to detect and locate both ELTs* and EPIRBs that are currently in the field operating at 121.5/243.0 MHz and a new class of ELT/EPIRBs would operate on a frequency of 406 MHz.** The new ELT/EPIRBs would access the satellite via a coded address and would provide an identification (I.D.) of the user as well as the capability for situation coding.

The ELTs and EPIRBs in all three bands will transmit their signals to the orbiting spacecraft. Within each band, there can be one or more simultaneous ELT/EPIRB emissions as well as other non-ELT/EPIRB emissions. The spacecraft instrument will multiplex each band into a composite signal and relay the composite signal, in real time, to the LUTs. At an LUT the composite signal will be demultiplexed into the three individual bands. Each ELT/EPIRB signal will be individually detected and processed to determine position location information, which will be displayed at the LUT control console for subsequent forwarding to the nearest Rescue Coordination Center (RCC) where the SAR forces will be alerted and deployed.

The LUTs will use a three meter diameter parabolic antenna with program tracking of the satellite. The relayed ELT/EPIRB signals will be available for processing to determine the position location of the distress incident only when the satellite is mutually in view of both the ELT/EPIRB and the LUT.

Partial signal processing of the "new" ELT/EPIRB emissions at 406 MHz will also be performed on-board the satellite, in addition to the real time relaying of the 406 MHz signals to the LUT for complete processing. The spacecraft SAR mission instrument will look for and accept only valid ELT/EPIRB 406 MHz emissions and subsequently determine the I.D. and measure the frequency of the doppler-shifted signal. The doppler frequency measurement, appropriately time tagged and including the I.D., will simultaneously be transmitted in real time and also stored on-board the satellite for later transmission to a NOAA earth station. This approach will allow the ELT/EPIRB emissions to be received and partially processed when the satellite is not in view of an LUT. The partially processed data will be stored for subsequent readout and transmission to a NOAA earth station for relaying to a processing center. In either the real-time or stored data mode, the data will then be further processed to compute the position location of the distress, to identify the person or vehicle in distress, and to display the message* concerning the distress situation (e.g., ship on fire, sinking, or medical emergency).

5. Emergency Signaling Via Geosynchronous Satellite

Overview

The use of geosynchronous satellites for maritime distress alerting would offer near-global coverage** and immediate alerting. These attractive features have given rise to a number of proposals, the most significant of which are summarized in Table 2.

SCULPT

The SCULPT (Satellite Communication Using Low Power Techniques) system is designed to provide emergency signaling via existing or planned maritime communication satellites (9,10). No modifications or additions to the satellites would be required. SCULPT signals will be below the ambient noise level of the satellite receiver and will not produce interference with conventional communications satellite users. The use of "direct sequence" spread spectrum techniques, together with

*Emergency Locator Transmitters used for distress signaling by aircraft.

**The new ELT/EPIRB would also radiate at 121.5 and/or 243 MHz at a low level for use by the SAR forces in the final location phase.

*Situation coding will be an optional feature of the new ELT/EPIRB primarily designed for maritime use.

**Polar regions are not easily covered.

considerable signal integration, provides the high processing gain required to detect data reliably.

TABLE 2

SUMMARY OF PROPOSALS FOR EMERGENCY SIGNALING VIA GEOSYNCHRONOUS SATELLITE

CONCEPT	SPONSOR	COMMENTS
DRCS	ESRO/ESA	L-band, FSK signaling (5,6)
	TSC	PN coding, PSK signaling (7)
	Japan	406 MHz, Similar to DRCS (8)
SCULPT	MARAD	L-band, Spread Spectrum (9,10)

The SCULPT concept employs a phase shift keyed (PSK) pseudo random (PN) coded sequence to spread the transmitted signal over the bandwidth of a conventional communication satellite. The transmitted data is modulated onto the PN sequence so that data bits consist of an integral number of PN sequences. The signal received by the satellite is so far below the noise level (as seen by conventional users) that many SCULPT signals can be transmitted without interference to the conventional voice and Telex service. This is the important "transparency" feature of low power spread spectrum communications, i.e., conventional users cannot "see" the SCULPT signals and the SCULPT system is not significantly affected by the conventional users.

This sharing of the satellite bandwidth is possible because the conventional users cannot occupy the entire satellite bandwidth with conventional frequency division multiple access (FDMA) techniques. The low-level SCULPT signals utilize so little satellite power that their presence is negligible.

A simplified functional block diagram of the SCULPT system is illustrated in Figure 2. Data containing ship identification (stored within the SCULPT transmitter), together with externally entered data such as distress code and location, are formatted and repeatedly modulated onto the repetitive, spectrum-spreading PN code in the transmitter. This baseband spread spectrum signal is shifted up to L-band, amplified to a level of about 10 watts, and transmitted to the satellite repeater. The satellite translates the SCULPT signals (along with signals from conventional users) to C-band, amplifying them before and after the translation process. At an earth station, the C-band signals are shifted to an intermediate frequency, where they enter the SCULPT receiver.

The SCULPT receiver is based on the use of matched filters (implemented with charge transfer devices) to provide for rapid PN code acquisition relative to correlation-type receivers. The first function of the receiver is to establish code timing. This is accomplished by the extensive noncoherent integration of successive code cycles (after the matched filters) to bring the input signal to noise ratio from about -10 dB (at the matched filter output) to 9 or 10 dB. After the code has been acquired, the carrier is acquired to provide for coherent detection. The result of the coherent detection is a highly corrupted, sampled-data version of the baseband data signal. This signal is integrated over several dozen message cycles to improve its signal-to-noise ratio before bit decisions are made in the data detector. The final detected message exhibits a worst-case bit error rate on the order of 10^{-5}.

6. Proposed Dual EPIRB System

In reviewing the various proposals for emergency signaling via satellite, it becomes clear that no single approach will satisfy all of the perceived requirements. The use of low-orbiting satellites will provide for accurate position determination via Doppler techniques, but cannot provide for immediate alerting. The use of geostationary satellites provides for immediate reporting, but does not allow for accurate position determination (except perhaps in a system with a relatively large number of satellites).

The alternatives are (1) to develop and implement a single system that does not meet all of the requirements or (2) to develop and implement a redundant system that employs geostationary satellites as well as low-orbiting satellites. We suggest that a redundant emergency signaling system will prove to be the better choice, both from the viewpoint of fulfilling operational requirements and in terms of cost effectiveness. Such systems would combine the low-orbiting satellite system advocated by NASA with a system under study by the Maritime Administration which signals via existing or planned commercial geosynchronous communication satellites.

Functional Characteristics

The proposed system could provide the following capabilities:

1. Immediate alerting via geosynchronous satellite.

2. Automatic monitoring for rescue alert.

3. Incorporation of location and distress code data in the first alert whenever conditions on the stricken vessel permit.

4. Location via Doppler fixes from low-orbiting satellites within a short time after the first alert. This data will provide for reducing the search area to about 100 km^2 even if it is not possible for a survivor to manually enter location data on the stricken vessel.

5. Worldwide coverage. In this respect, the coverage areas of the two satellite subsystems are complementary. The low-orbiting meterological satellites (in polar orbit) provide excellent coverage of polar and subpolar regions, while the geosynchronous communica-

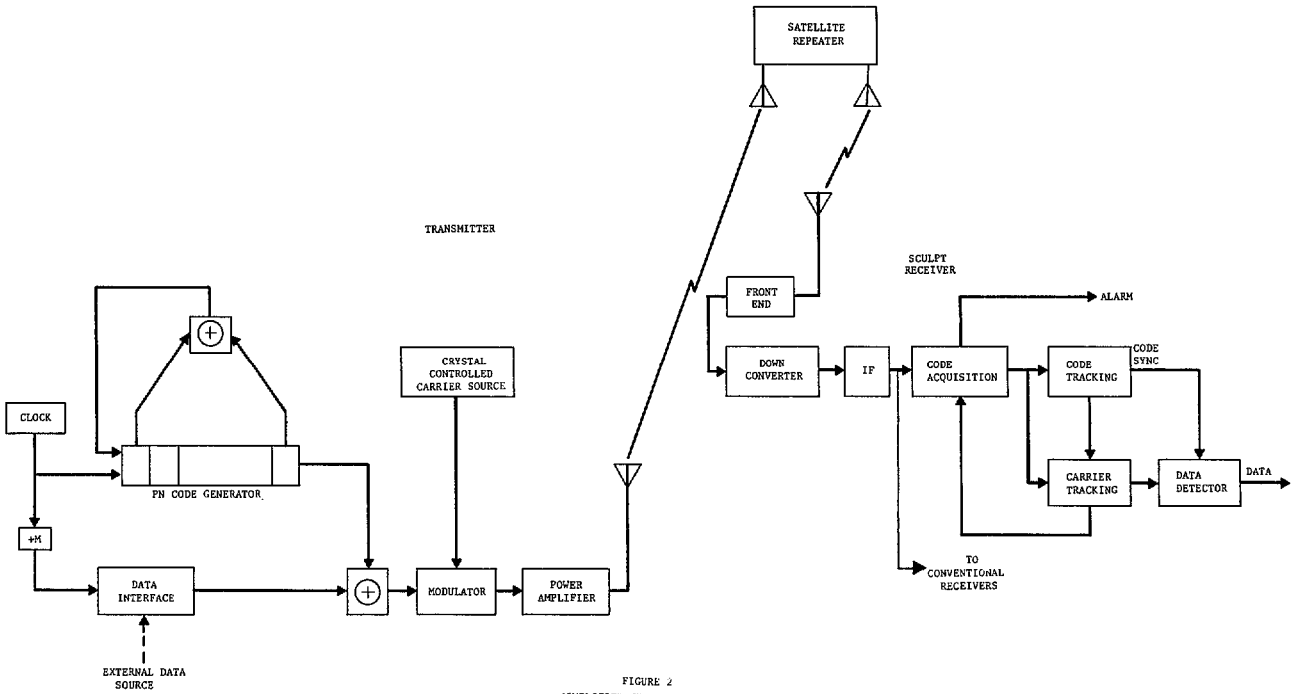

FIGURE 2
SIMPLIFIED FUNCTIONAL DIAGRAM OF SCULPT SYSTEM

tions satellites provide better coverage of equatorial and temperate zones.

6. Automatic or manual activation. The dual EPIRB would float free and activate automatically in case of a sudden sinking. Means for manual activation would also be provided.

7. Maximum use of existing and planned satellite systems. The system would not require any dedicated satellites or earth stations.

8. Redundancy in most segments of the system. Normally single failures of satellites or earth stations would not prevent distress messages from getting through.

Activation of the EPIRB, either by manual or automatic means, would result in the immediate reception of an alert through one of these geosynchronous maritime communication satellites and its associated earth station. The alert, containing the identity of the stricken vessel, and a manually entered distress code, would be immediately relayed to the SAR mission control and the rescue coordination center(s) associated with the earth station at which the alert was received. The alert would also be available for transmission to SAR mission control centers with jurisdiction over the estimated location of the ship. The alert from the EPIRB to the earth station would be repeated periodically.

Simultaneously, the EPIRB would begin to transmit periodic messages at 406 MHz for relay by meteorological satellites in polar orbit. The first meteorological satellite to pass within range of the activated EPIRB will retransmit the EPIRB signals in real time on 1543 MHz. If the real time signals are received by a local user terminal (LUT), they are processed at the LUT to extract a Doppler fix on the EPIRB. This mode of contact is limited to cases in which both the EPIRB and an LUT are in mutual view of a particular meteorological satellite. Worldwide, there will obviously be many locations that will be out of satellite range to any LUT. For this reason, Doppler information will also be extracted on the satellite and stored for later transmission to an earth station equipped to receive meteorological and distress alerting data from the satellites. In either case, the location data will eventually reach the appropriate SAR mission control center.

The maximum waiting time to receive a Doppler fix on the EPIRB is a function of (1) the number of meterological satellites equipped for the relay of distress messages, (2) the system configuration and (3) the EPIRB latitude. In polar regions (85° latitude) the worst-case waiting time varies from 48 minutes to 1176 minutes depending on the system configuration and the number of satellites. (The lower waiting times corresponds to a four-satellite system.) At the equator, the worst-case waiting time varies from 250 minutes to 1270 minutes (4).

The accuracy of the location data (2 to 5 km) will be sufficient for rescue teams to make quick visual contact in many circumstances. When radio homing is required in the final search phase, this can be

accomplished either by use of a future homing capability on 406 MHz, or by a separate lifeboat EPIRB on 2182 kHz, 243 MHz, or by lifeboat survival radio (500 kHz and 8364 kHz), all of which are currently available and are small enough for lifeboat use.

Technical Characteristics

EPIRB

The proposed EPIRB would transmit on 406 MHz and 1.6 GHz. The technical parameters of the 406 MHz transmitter are summarized in Table 3. The use of narrowband signals in an available bandwidth of 100 kHz (406.0-406.1 MHz), together with a low duty cycle (2%) provide for access of a single meteorological satellite by several active EPIRBs within its field of view.

TABLE 3

406 MHz TRANSMITTER CHARACTERISTICS

Frequency	406.05 MHz ±0.003%
EIRP	5 W
Spurious Output	50 dB below 5 W
VSWR	infinite-without damage
Modulation	continuous phase FSK
Transmitter Lifetime	100 h
Temperature	-40°C* to +50°C
Bit Rate	128 b/s
Data Coding	Manchester
Message Length	115 bits
CW Preamble	102 ms
Transmission Time	1 s
Repetition Rate	50 s
Oscillator Drift	< 4 Hz/10 min
Incidental FM	< 5 Hz peak-to-peak

*May not be low enough for sub-polar areas.

The technical characteristics of the 1.6 GHz transmitter are summarized in Table 4. In this case, a multiple access capability is inherent in the spread spectrum signaling format. This inherent capability is expanded by the use of a low transmitter duty cycle (2 to 50%).

TABLE 4

1.6 GHz TRANSMITTER CHARACTERISTICS (TYPICAL)

Frequency	1640 MHz
EIRP	6.2 W
Spurious Output	50 dB below 6.2 W
VSWR	infinite-without damage
Modulation	PN code/biphase PSK
Transmitter Lifetime	100 h
Temperature	-40°C to +50°C
Chip Rate	128 kHz
Data Rate	≈ 2 b/s
Data Coding	differential
Message Length	15-50 data bits
Sync Word	20 bit Neuman-Hofman sequence
Transmission Time	2 min
Repetition Rate	4 min to 100 min
Carrier Stability	10 ppm
Code/Data Clock Stability	1 ppm

7. Conclusions

Present means for maritime distress alerting are not always adequate. The consequent loss of property and lives in disasters at sea represents a problem that is global in scope and which demands a global solution.

A number of approaches to satellite-aided maritime distress alerting have been proposed. Each would make use of either low-orbiting satellites or geosynchronous satellites. Used as a radio relay, each type of satellite system has a nearly complementary set of advantages and disadvantages, to the extent that it is not possible to meet all of the perceived system requirements using one type of satellite exclusively. Since the use of dedicated satellites is not required, the increment of cost to the satellite segment is minimal so long as modifications to the satellites are kept small. For this reason, the use of geosynchronous satellites and low-orbiting satellites within the same system is suggested. The advantages of both types of systems are combined, and the marginal cost of adding the use of geosynchronous satellites should be small compared with the cost of the low-orbit system alone.

References

1. "Sudden Disasters at Sea," United Kingdom Department of Trade, Published in "Report of Atlantic International Air and Surface Search and Rescue Seminar," April 22-25, 1975, pp. 142-145; NTIS No. AD-A019776.

2. "Interagency Committee for Search and Rescue Ad Hoc Working Group Report on Satellites for Distress Alerting and Locating," Final Report, October 1976, p. 6-27.

3. "Study of Alerting and Locating Techniques and Their Impact," Prepared for the U.S. Coast Guard by Computer Sciences Corporation, December 1976.

4. "Preliminary System Definition, Joint NASA/Canada Satellite-Aided Search and Rescue (SAR) Mission," First Draft, Goddard Space Flight Center, May 19, 1977.

5. "European Communications Experiments in L-band with ATS-6," ESRO, Rep. No. NOX/0206/YG/16, Volume 6: Distress Buoy System Design, Instrumentation and Experiment, October 1975.

6. "Proposal for a Maritime Distress Alerting System at INMARSAT--Description of a Field-Approved System," Submitted by the Federal Republic of Germany to the INMARSAT Preparatory Committee Technical Panel, October 10, 1977.

7. "Distress Buoy System Analysis," Proteon Associates, Inc., Tech. Memo A113.

8. K. Kimura, M. Kimura, T. Hata, and Y. Yoshimura, "Emergency Position Indicating Radio Beacon Systems Using 406 MHz Band Mobile-Satellite Service," International Conference on Maritime and Aeronautical Satellite Communication and Navigation, London, March 7-9, 1978.

9. Aaron Weinberg, Yaroslav Kaminsky, and Feisal Keblawi, "A Novel Concept for a Satellite-Based Maritime Search and Rescue System," IEEE Journal of Oceanic Engineering, Volume OE-2, No. 3, July 1977, pp. 274-285.

10. A. Weinberg, "Characteristics and Performance Aspects of a Concept for Satellite-Based Maritime Search and Rescue," AIAA/IEEE Conference on Satellite Applications to Marine Operations, New Orleans, LA, November 15-17, 1977.

ADHESIVE RESISTANCE OF UNDERCONSOLIDATED SEDIMENTS

T.R. Chari, S.N. Guha and K. Muthukrishnaiah
Faculty of Engineering & Applied Science
Memorial University of Newfoundland
St. John's, (Newfoundland)Canada A1B 3X5

Abstract

The top few meters of the ocean floor is generally underconsolidated. Properties of such sediments have not yet been well researched. Adhesive resistance of these sediments has great application in all activities involving the sea floor. This paper describes laboratory pull-out tests on objects of different material embedded in artificially sedimented clay.

1. Introduction

Surficial ocean sediments are generally characterised by high liquidity index and underconsolidation in contrast to terrestrial soils as well as to soils at larger depths below ocean floor. The thickness of these sediments could vary from a few centimeters to several meters depending on the location. Properties of these weak sediments have not yet been well researched. Offshore operations such as ship salvage, submarine rescue, recovery of sunken fishing trawlers, relocation of submarine pipe lines, submersible offshore structure designs, and retrieval of core samplers necessitate a thorough understanding of the adhesive resistance of these sediments, in addition to other properties such as strength and compressibility. One other application of the adhesive property in the cold environment is in the ice-soil interaction and sea bed scouring.

Considerable research has been reported on skin friction between terrestrial soils and various construction materials. Very little work seems to have been carried out to evaluate the adhesive resistance of very weak soils resembling the surficial ocean sediments.

Meyerhof (1961) reported the ratio of adhesion to cohesion for smooth steel flats in the order of 0.1 to 0.3 from direct shear tests. Witney (1968) conducted experiments using clay with a shear strength of about 2.6 kPa (54psf) and reported an adhesion of 11% of the shear strength for clay-glass interface.

Erchul and Smith (1969) investigated the resistance to penetration of objects into sediment. Coated and uncoated steel plates were dropped into a sediment having a cohesion of 7.2 kPa (150 psf). The maximum sediment adhesion for uncoated plates was reported to be in the order of 1.2 to 1.7 kPa (25 to 35 psf) which is about 17 to 24% of the cohesion of the sediment. The maximum adhesion on coated plates was in the order of 16 to 20% of cohesion.

Vesic (1971) opined that adhesion could equal cohesion within a few days to about 6 months after an object comes in contact with sediment. He suggested the need for further work to study the development of adhesion at early stages of sedimentation when the shear strength of the sediment will be low.

Wang, Demars and Nacci (1977), in their investigation on the breakout capacity of suction anchors in soil, found an adhesion to cohesion ratio of 0.75 when the cohesion was 0.55 kPa (11.5 psf) and 0.67 when the cohesion was 1.03 kPa (21.6 psf), for acrylic.

A continuous program of research is going on at the Naval Civil Engineering Laboratory, Port Hueneme, California (Lee 1972, Liu 1969, Muga 1966, Muga 1968) with analytical and model studies as well as field trials to determine the breakout resistance of objects partially and fully embedded in ocean muds.

Finn and Byrne (1972) proposed that an upper limit for the breakout force for an object buried to a shallow depth in a cohesive soil could be obtained by assuming that the failure mechanism is similar to that for a bearing capacity failure with the direction of movement reversed.

Byrne and Liam Finn (1978), based on small scale laboratory tests, concluded that the maximum uplift pressure required to dislodge an object buried to a shallow depth in the ocean floor can be predicted from bearing capacity theory.

This paper describes laboratory tests conducted with artificially sedimented clay to study the adhesive resistance of soils having strength comparable to surficial ocean sediments. Pull-out tests were conducted using a plate of plexiglas, an ice sheet and objects of different shapes and materials partially embedded in artificially sedimented clay. The soil-object adhesive resistance was measured in each case. A list of experiments conducted is given in Table I.

2. Experimental Facility

The experimental facility (Fig. 1) consists of a glass container of 27 cm (10.5 inches) diameter, 29 cm (11.5 inches) deep, in which a soil slurry was prepared. The average bulk unit weight and moisture content of the slurry immediately after a thorough mixing of the soil were 14.8 kN/m^3 (94.3 pcf) and 89% respectively.

Two series of tests were conducted. In the first series, pull-out tests were conducted using plate models of plexiglas, stainless steel, brass, mild steel (rough as well as painted) and on ice sheet. In the second series, partially embedded prismatic object of plexiglas of square cross-section was used.

In all the tests, the object was suspended through a load cell into the soil to a desired depth immediately after the slurry was thoroughly mixed. The weight of the object as well as the weight of the connecting rods and of the load cell was counterbalanced by weights placed on a pan, shown in Fig.1.

At the end of a desired period of sedimentation the shear strength of the soil at different depths was determined by a modified vane shear apparatus. Additional weights were then placed on the pan in steps in quick succession till the onset of pull-out as indicated by the load cell reading.

The soil used in the experiments was commercially available potter's clay. The properties of the soil are presented in Table II. The surface roughness of the plate models was determined by Taylor-Hobson stylus method and expressed in terms of center line average (C.L.A). The C.L.A. values are presented in Table III.

3. Results and Discussion

The average unit adhesion computed from the measured maximum pull-out resistance is plotted as a function of the average shear strength of the sediment in Fig. 2. Adhesion increases with cohesion, as well as with the surface roughness of the object, as seen in Fig. 2, except in the case of plexiglas. Even though the microscopic roughness of plexiglas is the least among the different objects tested, the adhesion is maximum. This anomaly is attributed to the surface undulations on plexiglas sheets which is common with this material.

An average adhesion of 5.3 Pa (0.11 psf) was measured during tests on ice sheet models in a soil of 153 Pa (3.2 psf) strength. The adhesion-cohesion ratio is very small (3%) as can be expected for ice.

The adhesion-cohesion ratio, α, is plotted as a function of cohesion in Fig. 3 which shows that adhesion is not a constant proportion of cohesion for different values of cohesion. This observation is true for all objects having different surface roughnesses. The results indicate that α increases with increasing shear strength.

Fig. 4 shows the relationship between α and the liquidity index of the sediment. The value of α increases with decreasing liquidity index and approaches a constant value at lower liquidity index values.

4. Partially Embedded Prismatic Object

The pull-out load due to resistance at the base of a plexiglas prism of square cross-section was computed as the difference between the total measured pull-out resistance and the resistance due to adhesion on the sides of the prism. The unit adhesion on the sides of the prism is obtained from tests on plate models. The resistance at the base of the prism can be called base suction since a differential pressure develops at the base due to quick pull-out of the object. The relationship between the base suction, expressed as a ratio of the cohesion at the same level, and the depth-width ratio of the object is shown in Fig. 5. The base suction obtained from the empirical bearing capacity formulae of Hansen (1961) as well as of Lee (1972) are also shown in Fig. 5. It may be noted that the above empirical formulae ignore the side adhesion. Fig. 5 shows that the base suction values obtained from the laboratory tests are lower than those predicted from Hansen (1961) and Lee (1972) models. They increase with increasing depth-width ratio.

The variation of base suction as a function of cohesion at the base is shown in Fig. 6 which indicates that base suction increases with increasing values of cohesion.

5. Summary and Conclusions

Pull-out tests were conducted in the laboratory to study the adhesive resistance of underconsolidated sediments. Plate models of plexiglas, brass, stainless steel and mild steel (rusted as well as painted) and prismatical object made of plexiglas were embedded in artificially sedimented clay and pulled out when the sediment attains desired strengths.

The results based on plate models show that the adhesive resistance is a function of both surface roughness and sediment strength. It was found that the unit adhesion is not a constant proportion of the sediment strength. Adhesion-cohesion ratio is larger at larger sediment strengths. Even ice-sediment interface exhibits adhesive resistance, though small.

Results of pull-out tests on partially embedded prismatic plexiglas object suggest that the suction at the base of the object is far in excess of the cohesion of the soil at the same level. However, a comparison of the base suction with values predicted from empirical reverse bearing capacity formulae of Hansen (1961) and Lee (1972) indicate that the observed values are less than those predicted from the above formulae.

This work is part of ongoing marine geotechnical studies at Memorial Unversity.

Acknowledgements

The sustained interest shown in the research by Dr. R.T. Dempster, Dean of Engineering and Dr. G.R. Peters, Group leader of Ocean Engineering is gratefully acknowledged. The work was partly funded through grant A-3710 from the National Research Council of Canada.

References

1. Byrne, P.M. and Liam Finn, W.D., "Breakout of submerged structures buried to a shallow depth", Canadian Geotechnical Journal, Vol.15, No. 2, May 1978, pp 146-154.

2. Erchul, R.A. and Smith, R.J., "Lubricant and polymer reduction of sediment adhesion", Proceedings, ASCE Conference: Civil Engineering in the Oceans II, December 1969, pp 621-640.

3. Finn, W.D.L. and Byrne, P.M., "The evaluation of the break-out force for a submerged ocean platform", 4th Offshore Technology Conference, Houston, Texas, Paper No. OTC 1604, Vol. I, 1972, pp 863 - 868.

4. Hansen, J.B., "A general formula for bearing capacity", Ingeniøren-International Edition, Vol. 5, No. 2, 1961, pp 38-46.

5. Lee, H.J., "Unaided breakout of partially embedded objects from cohesive seafloor soils", Technical Report R-755, Naval Civil Engineering Laboratory, Port Hueneme, California, February 1972.

6. Liu, C.L., "Ocean sediment holding strength against breakout of embedded objects", Technical Report R-635, Naval Civil Engineering Laboratory, Port Hueneme, California, August 1969.

7. Meyerhof, G.G., "Some problems in the design of rigid retaining walls", Proceedings, 15th Canadian Soil Mechanics Conference, Ottawa, 1961, pp 59-79.

8. Muga, B.J., "Breakout forces", Technical Note N-863, Naval Civil Engineering Laboratory, Port Hueneme, California, September 1966.

9. Muga, B.J., "Ocean bottom breakout forces, including field test data and the development of an analytical method", Technical Report R-591, Naval Civil Engineering Laboratory, Port Hueneme, California, June 1968.

10. Vesic, A.S., "Breakout resistance of objects embedded in ocean bottom", Journal of Soil Mechanics and Foundations Division, Proceedings ASCE, Vol. 97, No. SM9, September 1971, pp 1183-1205.

11. Wang, M.C., Demars, K.R. and Nacci, V.A., "Breakout capacity of model suction anchors in soil", Canadian Geotechnical Journal, Vol. 14, No. 2, May 1977, pp 246-257.

12. Witney, B.D., "The determination of soil particle movement in two-dimensional failure", Journal of Terramechanics, Vol. 5, No.1, 1968, pp 39-52.

Table I List of Experiments Conducted

Series	Type of Object	Material	Soil Sedimentation Period (hours)	Experiment Number
I	Plate Models 25.4 cm x 15.2 cm	Plexiglas	2,4,6,8,10,12 16,20,24,48,72	PP2, PP4 PP6, PP8 PP10,PP12,PP16,PP20 PP24,PP48,PP72
	(10" x 6")	Brass	2,10,16,24,48,72	BP2,BP10,BP16 BP24,BP48,BP72
		Stainless Steel	2,10,16,24,48,72	SP2, SP10,SP16,SP24 SP48,SP72
		Mild Steel, Painted	2,10,16,24,48,72	MP2, MP10,MP16 MP24,MP48,MP72
		Mild Steel, Rough	2,10,16,24,48,72	MRP2, MRP10, MRP16 MRP24,MRP48, MRP72
II	Prismatic Model of Square Cross-Section 7.9 cm (3.1 inch) Side	Plexiglas	2,10,16,24,48,72	PS2, PS10,PS16 PS24,PS48,PS72

Table II Properties of Soil Used in the Experiments

Color	Brown
Liquid Limit(%)	30
Plastic Limit(%)	16
Plasticity Index	14
Clay Size Fraction	15%
Silt Size Fraction	15%
Sand Size Fraction	70%
Specific Gravity of Solids	2.73
Mineral Composition:	Predominantly Illite, with traces of Chlorite and Kaolinite

Table III Surface Roughness of Objects Tested

Plexiglas	1.2	μ - inch	per	0.01 inch
Brass	1.75		do	
Mildsteel, (Painted)	7.0		do	
Stainless Steel	7.5		do	
Mild Steel, (Rusted)	155		do	

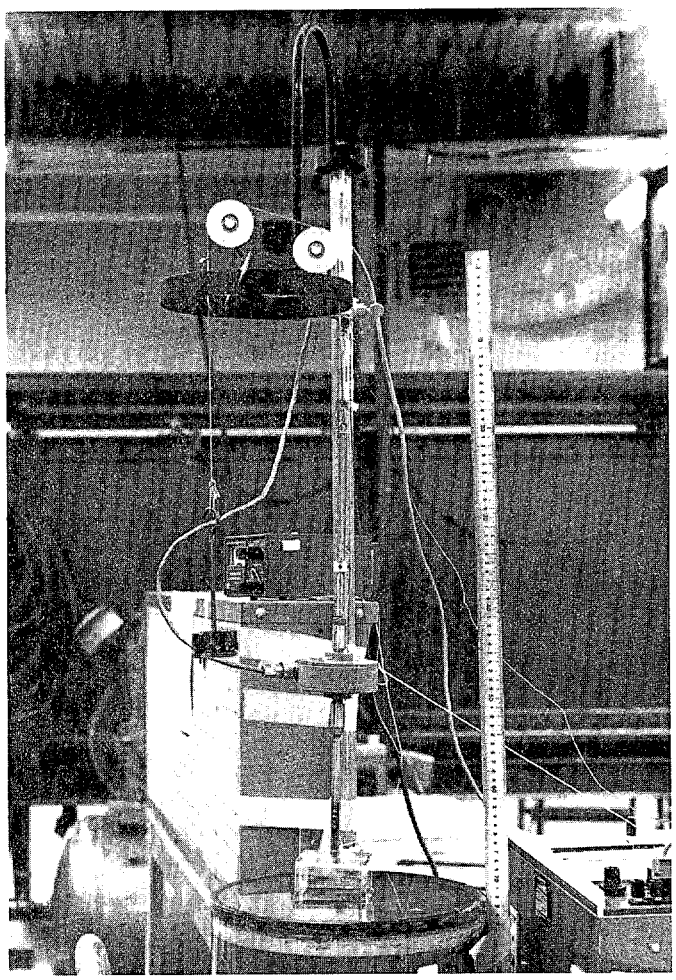

FIGURE 1 LABORATORY TEST ASSEMBLY

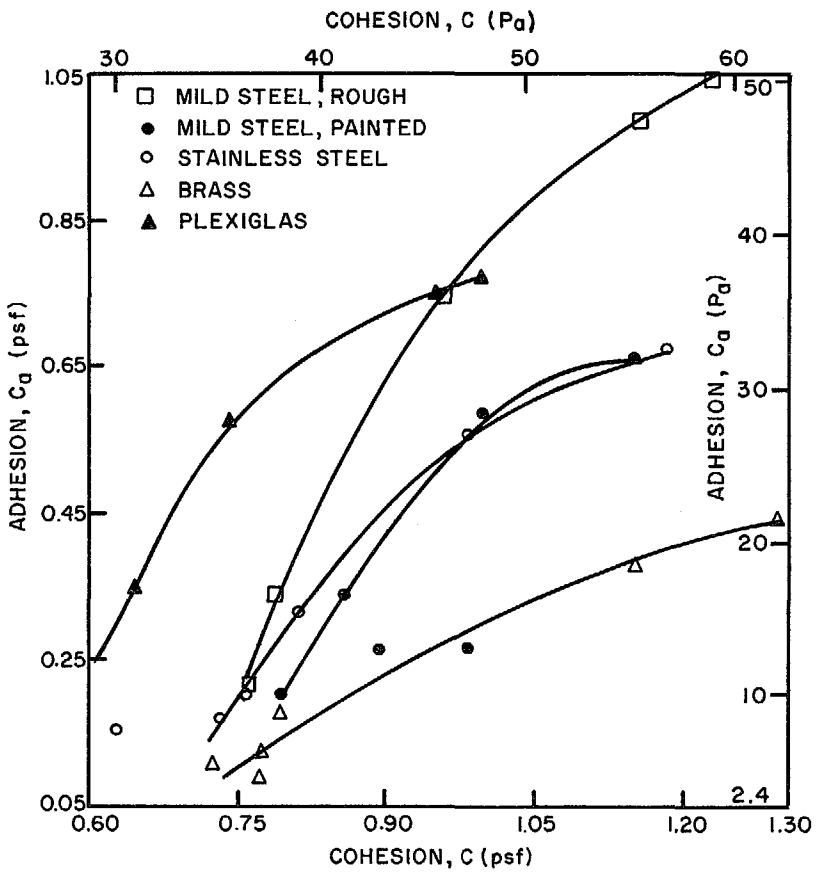

FIGURE 2 UNIT AVERAGE SEDIMENT ADHESION FOR PLATE MODELS

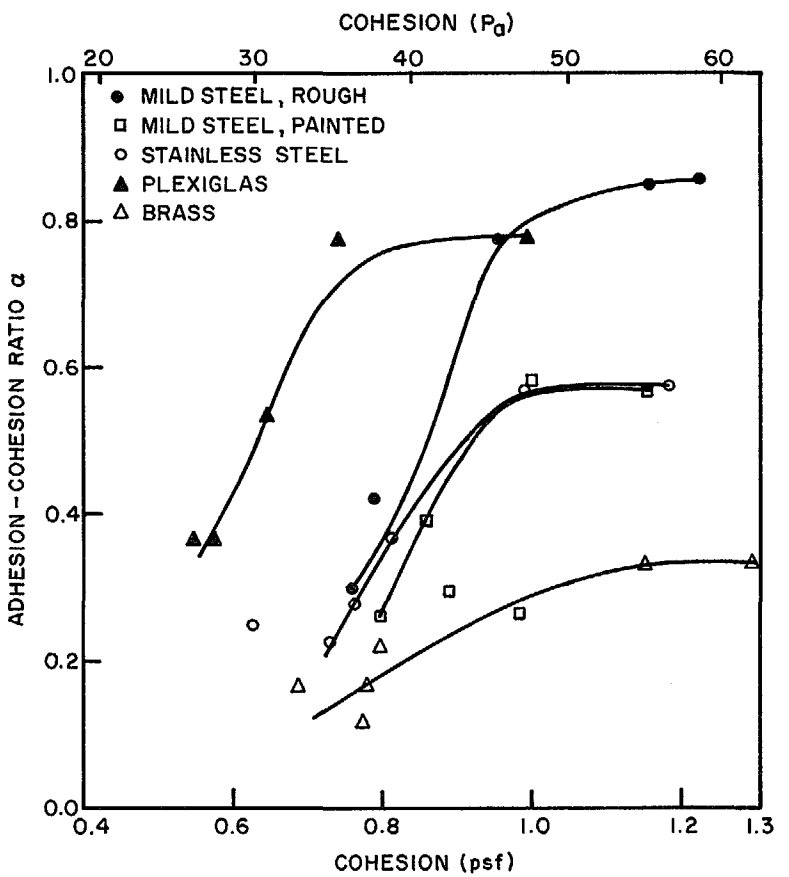

FIGURE 3 RELATIONSHIP BETWEEN

α AND SHEAR STRENGTH OF THE SEDIMENT FOR PLATE MODELS

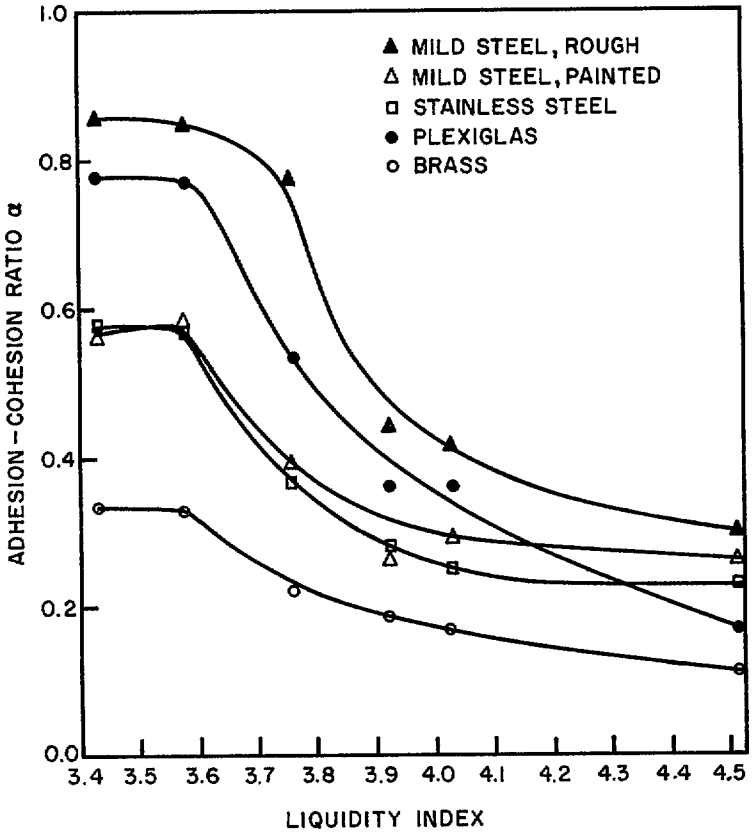

FIGURE 4 VARIATION OF α WITH LIQUIDITY INDEX

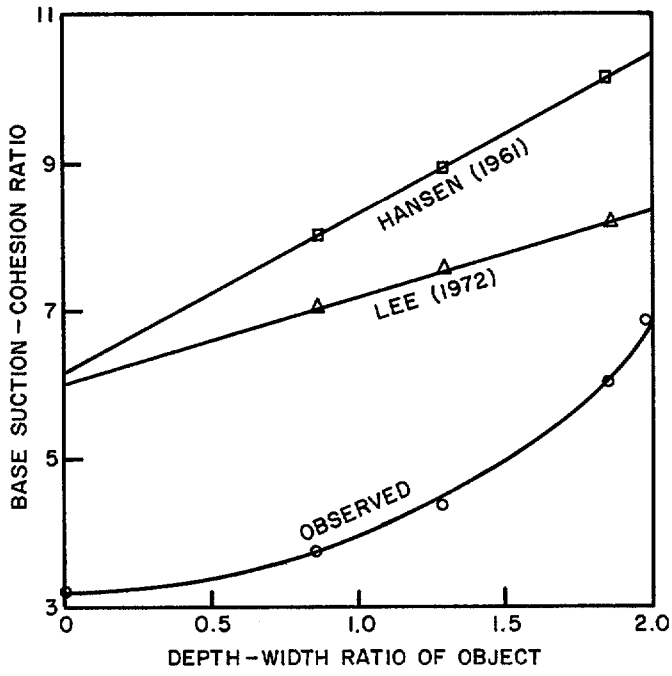

FIGURE 5 BASE SUCTION Vs DEPTH OF EMBEDMENT

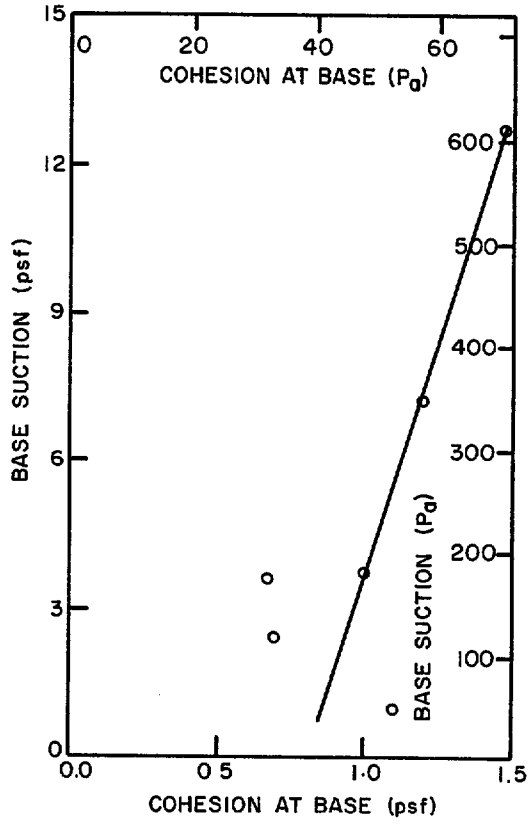

FIGURE 6 BASE SUCTION Vs SEDIMENT STRENGTH

SUBMARINE LANDSLIDES - EAST COAST CONTINENTAL SLOPE AND UPPER RISE

Alexander Malahoff
National Ocean Survey
Rockville, Maryland 20852

Robert W. Embley
Lamont-Doherty Geological Observatory
Palisades, New York 10964

Richard B. Perry
National Ocean Survey
Rockville, Maryland 20852

Abstract

Potential hydrocarbon reservoirs are located beneath the continental slope of the East Coast of North America. The slope marks the site of major sediment slides. The size, configuration, origin and history of such a submarine landslide located off Baltimore Canyon was examined through studies using detailed, precision navigated hydrographic and subbottom high-resolution seismic reflection profiling. The shipboard data were visually confirmed through a series of submersible traverses aboard the DSV ALVIN. The survey delineated a complex pattern of incised valleys and ridges some of which encroach onto the continental shelf. A 50 m thick stratified sediment sheet has moved through faulting and sliding from the valley slopes and deposited in the valley axes as unlayered acoustically incoherent deposits merging into an extensive sediment fan beyond the 2900 m isobath.

1. Introduction

When a submarine earthquake occurred under the Grand Banks off Newfoundland in 1929 (Heezen and Ewing 1952), the transatlantic cable companies were puzzled by the great number of cable breaks that took place on the ocean floor at that time. Cables were not only broken during the time of the earthquake itself but hours later, and at distances of 400 miles downslope from the focus of the earthquake, which was located in a water depth of 2400 meters. As disruptive as the cable-breaks were to transatlantic communications, the data from these breaks provided an invaluable insight into catastrophic submarine processes operating over great distances and unmatched in scale by similar events occurring on land. The invaluable insight was gained by Ewing and Heezen (1952) who plotted the times of the breaks of the cables. Within a circle of 150 kilometers in diameter all cables broke at the time of the earthquake, but further down the continental slope and out onto the upper rise the cables broke sequentially, the last break taking place thirteen hours later at a distance of 600 kilometers from the focus and at a water depth of 5600 meters. Using the time and distance between the cable breaks, Ewing and Heezen concluded that the earthquake had mobilized the sediments on the continental slope and created a dense, heavy sediment laden turbidity current which under the force of gravity gained momentum and moved down the slope at speeds of up to 100 kilometers per hour, eroding the ocean floor and cutting the submarine cables.

More recent regional studies of the continental margins of northwest Africa (Embley, 1975, 1976; Jacobi, 1976) have demonstrated the ubiquitous existence of large scale sediment slides that had transported sediments into deep waters away from the continental margin. These slides appear to be similar in nature to the one that occurred as a result of the 1929 Grand Banks earthquake. Embley and Jacobi (1977) further showed the widespread occurrences of sediment slides and debris flow fans along both the east and west Atlantic margins. One area where they reported the existence of such a large debris flow fan is on the eastern U.S. continental slope and rise southeast of Baltimore Canyon. The flow located south of Baltimore Canyon offers an excellent opportunity to study in detail the origin, source and history of an Atlantic margin sediment slump and flow that had taken place in the locale of proposed U.S. offshore petroleum development. In order to study the sediment source as well as the history of this particular flow a detailed hydrographic survey of the shelf, slope and upper rise was carried out in this region by the NOAA vessel MT. MITCHELL in 1976 (Figure 1). A portion of this region was resurveyed in May, 1977 by the MT. MITCHELL using a towed, high-resolution subbottom penetrating 3.5 kHz echo sounder. To provide ground truth, three DSV ALVIN dives were carried out in the survey area during June, 1977. This paper presents the results of the study in light of continuing interests in the hydrocarbon resources of the deeper parts of the continental shelf, slope and upper rise of North America.

2. Offshore Petroleum Development and Submarine Landslides

Until extensive offshore oil exploration and development took place, the presence of ocean floor turbidity currents and debris flows could be regarded as of deep scientific interest but

of relatively mild economic impact. If however, the move to ever deeper waters takes place in the search for petroleum resources leading to the emplacement on the ocean floor of ever-more expensive installations such as well heads, pumps, petroleum pipelines, etc., a careful reexamination is needed of the set of events that took place on the Grand Banks in 1929.

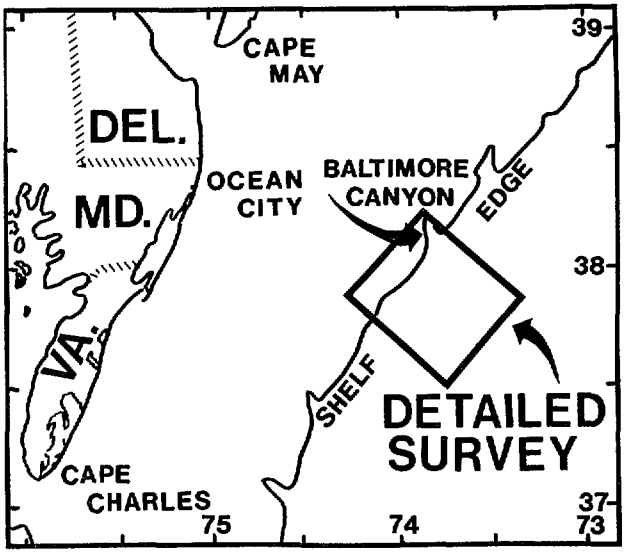

Figure 1.
Site of detailed surveys of submarine landslides located on the continental slope south of Baltimore Canyon

The turbidity current that broke the transatlantic cables in 1929 had to have had a sediment source. The cable-breaks that were coincident in time with the earthquake occurred over an area, represented by a circle 150 kilometers in diameter, or equivalent to an area of 17,000 square kilometers. The cable-breaks in this area probably occurred as a result of submarine landslides triggered by the earthquake. The ocean floor sediments, displaced by the landslides and slumps then became mobilized into a turbidity flow which cut the cables sequentially down the slope and down the continental rise.

The submarine landslides of the 1929 Grand Banks earthquake occurred over a depth range extending from the edge of the continental shelf located at about 160 meters out to the bottom of the continental slope at 4000 meters.

The continental shelf and slope regions of the east coast of North American mark sites of favorable hydrocarbon deposits. Geological studies of this area by commercial exploration companies and the U.S. Geological Survey (Grow and Markl, 1977) show that some of the thickest sediments and hence those with the best prospect underlie the continental slope and portions of the upper rise, the surfaces of which are apparently excavated extensively by submarine erosion processes, the most striking of which is mass erosion resulting from submarine slumps, slides and debris flows.

3. Bathymetry

In order to examine the relationship between the physiography of the continental slope and erosion processes present, especially those attributable to extensive submarine landsliding, a detailed bathymetric map (Figure 1) was produced over the Baltimore Canyon area. The area of survey selected extends between Norfolk and Baltimore Canyons and is adjacent to some hydrocarbon lease areas. Contouring of the intricate bathymetric features seen in Figure 1 was made possible by a 1.3 to 2.2 km track line spacing utilizing a shore based navigation system (HYDROTRAK) with an estimated horizontal accuracy of $\pm$ 50 meters.

The most striking features within the area are the Baltimore and Washington Canyons. The important morphologic characteristics of these canyons have been discussed previously by Veatch and Smith (1939), Pratt (1967), and Kelling and Stanley (1970). In addition to these major canyons, which have cut back more than 10 km shoreward of the shelf break, the entire upper rise and slope is dissected by numerous valleys and canyons, creating a surface that resembles an environment of desert erosion. Numerous "mesa" and "butte" like remnants of eroded ridges are present on the slope, as well as extensive sediment fans at the base of the slope. There is a large, previously unmapped shelf canyon about halfway between Baltimore and Washington Canyons which has cut back about 4 km beyond the shelf break. The head of this canyon (henceforth named the Delaware Canyon) also has the "northward hook" similar to that seen in the Wilmington, Baltimore, and Washington Canyons. Kelling and Stanley (1970) have suggested that the northward trending sections of these canyons were cut by the north-south drainage systems developed across the continental shelves during glacial low sea-level stands. Numerous similar "embryonic" canyons are present, for instance the feature located directly southwest of the Delaware Canyon. These "embryonic" canyons which indent the 200 meter contour of the shelf-slope break by one or two kilometers apparently have not captured the sediment source required for further headward erosion and development onto the continental shelf.

The upper portion of the slope between water depths of 300 and 1500 meters which is marked by the numerous flat-topped "mesa" and "butte" like structures also contains irregular block like features. Visual submersible observations and subbottom profiles confirmed the presence of erosional remnants as well as of individual slumped sediment blocks on the slope.

Steep valley slopes, 500 meters high and with gradients of as much as 40°, narrow V shaped valleys, sharp ridges are all encountered at depths ranging between 300 and 1250 meters. The individual ridges extend out to 50 kilometers

beyond the edge of the shelf-slope break into water depths of 1500 meters where a much smoother upper rise is evident.

4. Subbottom High Resolution Acoustic Profiling

In order to determine the sediment source, the extent, the history and possible mechanisms of recent sediment slide events in the study area, a high resolution, towed, 3.5 kHz subbottom penetrating acoustic survey was conducted with an EDO system aboard the MT. MITCHELL (Figure 3 dashed lines). The survey was focused upon obtaining data that would provide the geological setting for the slide events and delineate the extent of encroachment of the sediment flows onto the upper slope. The data were gathered in the form of closely spaced

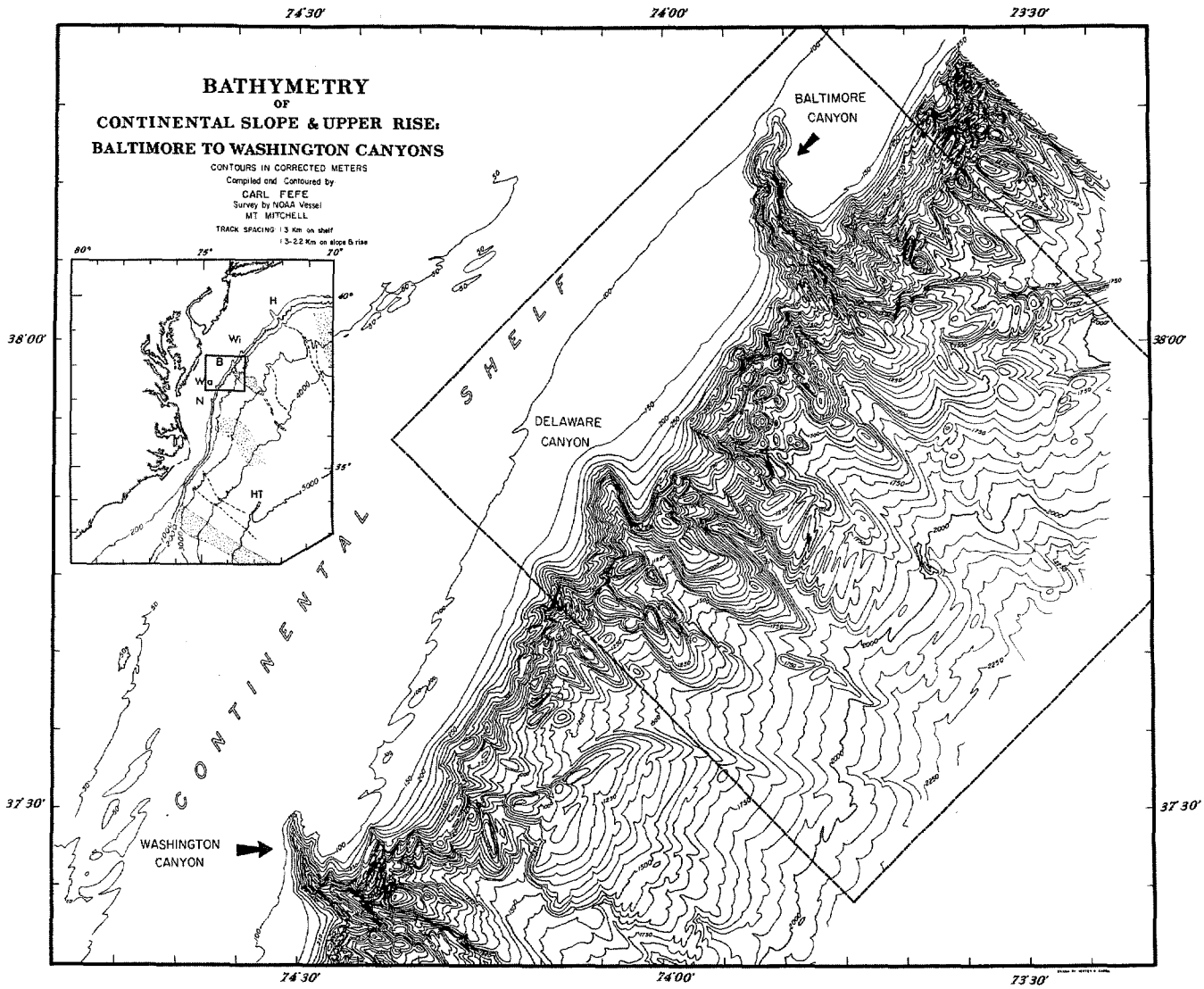

Figure 2.
Bathymetry of the Continental Slope and Upper Rise between the Baltimore and Washington Canyons. Contour interval 50 meters. Dashed rectangle shows area of study described in paper and located in Figure 1. Inset shows location of major sediment flows (stippled) described and mapped previously and located near the following canyons: H - Hudson Canyon; Wi - Wilmington Canyon; B - Baltimore Canyon; Wa - Washington Canyon; N - Norfolk Canyon; H - Hatteras Canyon

high resolution acoustic reflection profiles. Analysis of the profiles delineated four major acoustic provinces present in the study area:

(A) Sharp ocean acoustic return with poor penetration, a single subbottom acoustic horizon present. This is a characteristic of the continental shelf sediments.

(B) Many acoustic horizons present (Figure 3). Moderate subbottom penetration down to 100 meters. Typical of the sediments perched on the crests of the erosional ridges.

(C) Acoustic penetration but with no distinct acoustic horizons discernable in the record (Figure 3). Typical of the flow sediments deposited along the valley floors.

(B/C) Good acoustic penetration acoustically unstratified over stratified sediments. Typical of the deeper parts of the slope and the upper rise.

Interpretation of the acoustic reflection data suggests that the acoustic type A is associated with quartzose-foraminiferal sands of the Late Pleistocene sand lens (Milliman et al 1972) located on the continental shelf. The acoustic type B is seen to reflect layered hemipelagic sediments overlying the crests of the erosional ridges, while the acoustic type C reflects the sediments of the slumped hemipelagic sheet deposited in the valley axes below. At greater depths a sequence of acoustically unlayered sediments is seen to overlie a layered sequence (B/C). This phenomenon probably resulted from younger mobilized flow sediments overriding and covering older layered sediments at depth.

A 3.5 kHz acoustic reflection record taken over the ridge and valley complex of the continental slope is shown in profile E-W in Figure 3. Profile E-W illustrates the relationships and possible mechanisms of separation between the acoustically stratified sediments (B) overlying the ridge and the acoustically transparent mass of the flow sediments (C) located below along the valley floor. The central ridge in the

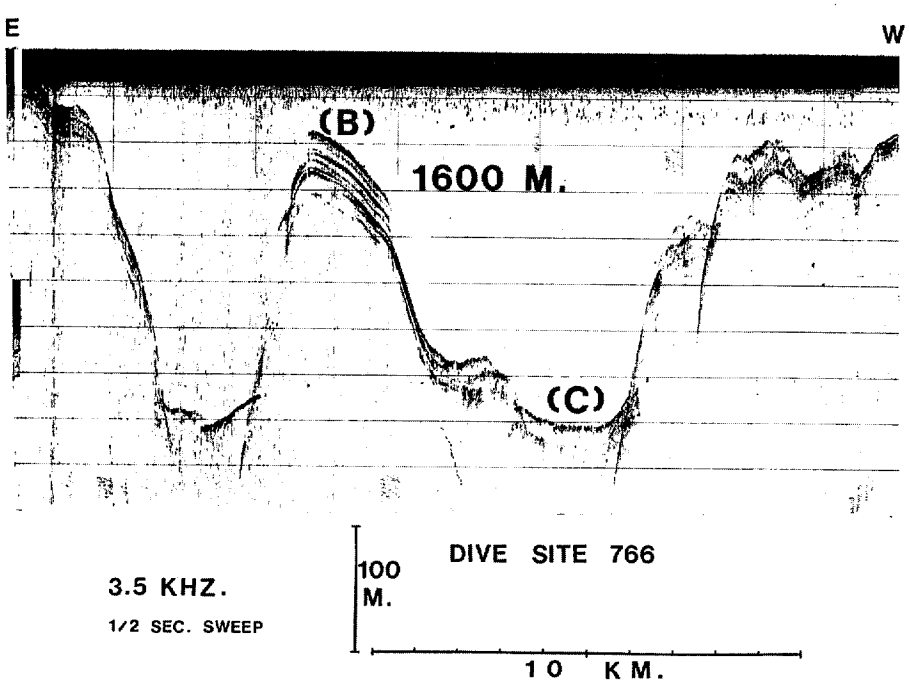

Figure 3.
High resolution 3.5 kHz acoustic reflection profile E-W (see Figure 4 for location) extending across the ridge and valley complex of the continental slope. Note perched acoustically stratified sediments (B) along the ridge crest and acoustically transparent (slumped) sediments (C) along the valley floor. ALVIN dive 766 traverse extends from the valley floor across the slump scarp and along the stratified sediments on the ridge crest.

figure is seen to be capped by about 50 meters of the acoustically stratified sediments (B) which are terminated abruptly along the western flank of the ridge. An acoustically incoherent, transparent sediment mass (C) is located at the base of the ridge. It may be interpreted from the examination of the profile that a portion of the sheet of the layered sediments parted at the scarp located along the western edge of the ridge, slid down the glide plane and ended up as a jumbled mass of sediments resting in the valley floor at the base of the ridge.

Figure 4 represents an acoustic facies map constructed from the detailed examination of thirty reflection profiles taken in the study area (dashed lines in Figure 3). The acoustic facies were drawn according to the scheme described above. Examination of the acoustic profiles in Figure 4 shows the ubiquitous presence of the 50-meter thick stratified sediment sheet (B) along the crests of the ridges, the presence of a 50-meter scarp where the sediments have parted and the presence of finger-line extensions of sediment flow (C) filled valleys onto the edge of the

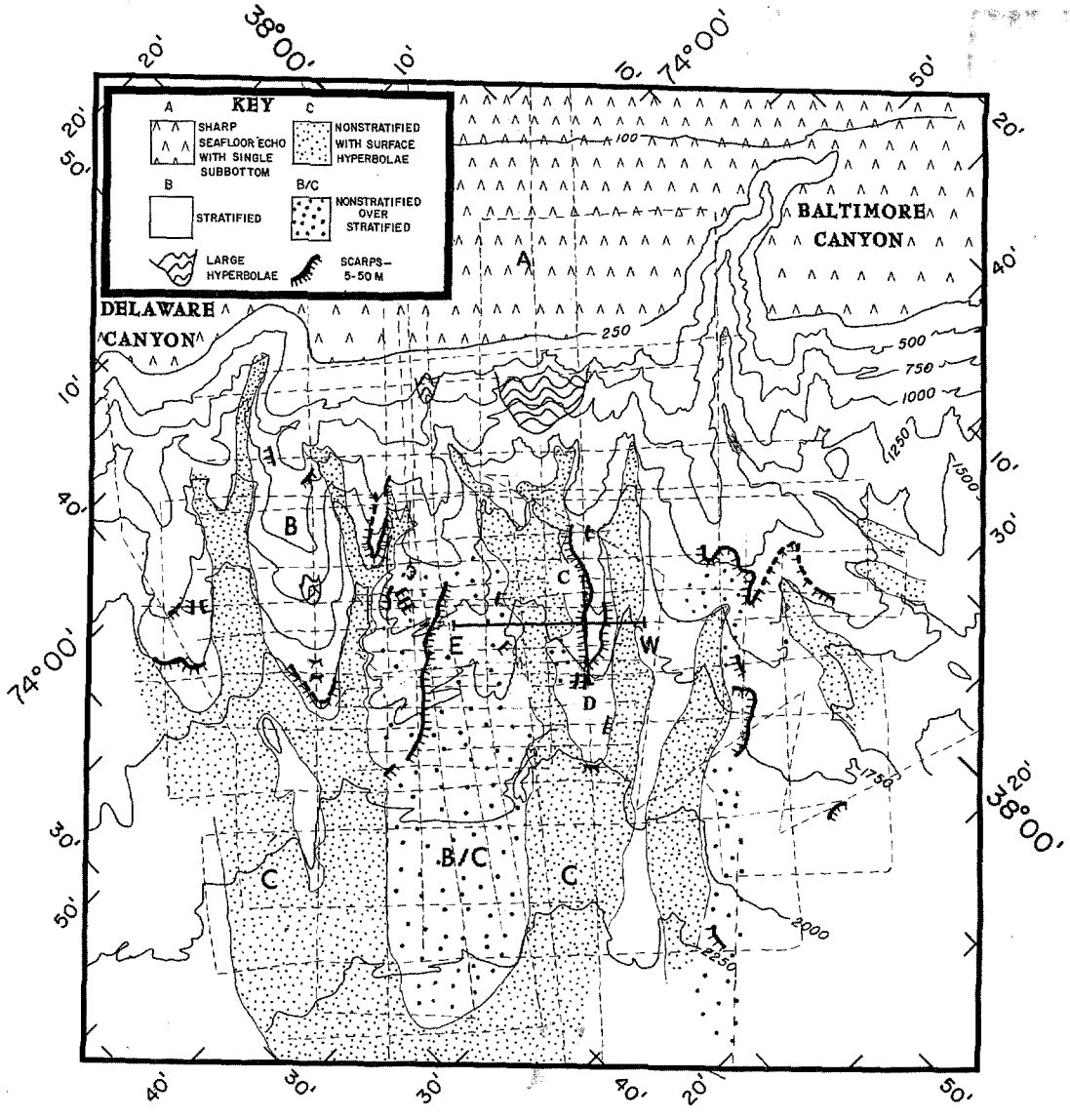

Figure 4.
Acoustic Facies Map of the sediments of the continental shelf and slope south of Baltimore Canyon. Facies based on echo character and presence of acoustic layering in high resolution 3.5 kHz acoustic reflection profiles (dashed lines show locations). Key to facies as follows: A - poor penetration, single sub-bottom return; B - good penetration, presence of acoustic stratification; C - good penetration, absence of stratification; B/C - acoustically transparent, overlying acoustically stratified sediments.

shelf-slope break. The data suggest that one episode of sedimentation was responsible for the deposition of the 50-meter thick acoustically stratified but poorly consolidated sediment sheet. Later episodes of earthquake activity or additional sediment loading gave rise to sediment instability and subsequent downslope sliding of portions of the sediment sheet. An alternative interpretation would point to a single episode of strong earthquake activity during the Holocene that could have led to wholesale sediment failure and sliding in the study area.

In order to determine the periodicity of the sediment slumping events in the study area, coring was conducted at a few selected sites. A box core recovered at 72°34'N; 73°99'W in a water depth of 2800 meters showed the presence of large 2-3 cm inclusions of material in a clay matrix. A radio-carbon date of 5265 ± 210 years BP for the boundary between hemipelagic capping sediments and the debris flow in the box core suggest that sediment slides have occurred on the continental slope in the Baltimore Canyon area during the Holocene and are not solely a phenomenon of Pleistocene glaciation.

5. Submersible Observations

Three ocean floor traverses using the DSV ALVIN were carried out during May 1977 across the following features:

(a) the sediment slump, glide-plane, and fault scarp of the valley-ridge section shown in Figure 3, (See Figure 4 for location of profile) depth range 1830 to 1000 meters;

(b) valley and ridge terrain of the upper slope, depth range 1300 to 850 meters;

(c) shelf-slope break, depth range 450 to 250 meters.

The three traverses were planned to visually examine the microphysiography of the surface of the continental rise and to determine the presence of recent fault scarps and glide planes, sediment waves, and other evidence of intense bottom current activity and rapid sediment transport along the ocean floor.

Common to the three traverses was the ubiquitous presence of a fine grained, light grey hemipelagic sediment blanket. This sediment blanket was determined through coring to be 40 centimeters in thickness and was found to cover the face of the sediment slump scarp and the flow sediments shown in Figure 3.

The visual examination and sampling of the slump scarp suggests that the 40 centimeters of hemipelagic sediments have accumulated since the last faulting and sliding episode took place, the episode that mobilized the 50 meter thick stratified sediment sheet shown in Figure 3. Lateral examination of the scarp showed the scarp to be indented throughout by secondary erosional scarring.

No ripple marks, scours or erosion scarps were observed within the hemipelagic sediments deposited on the valley floor. The valley flanks were also seen to be covered by the unconsolidated hemipelagic sediments which were thrown into suspension when disturbed by the hull of the ALVIN.

The 40 centimeter thick hemipelagic blanket appears to have covered all rock outcrops. The substratum was only seen to be exposed along the crests of ridges where intense excavation by benthic organisms, especially red crabs has produced deep burrows (30-70 centimeters deep, 50-80 centimeters wide).

6. Discussion

Detailed hydrographic surveys of the continental slope south of Baltimore Canyon have shown the surface of the slope to be heavily eroded. Visual examination of the high resolution 3.5 kHz acoustic reflection profiles suggests that much of the erosion has been accomplished through the mechanical failure of unconsolidated sediments leading to slumping and sliding of the sediments down from the ridges into the valleys below.

The valleys were observed to be filled with the acoustically transparent flow sediments which extend down along the valleys into deeper water. At a distance of 100 kilometers from the shelf-slope break, in water depths greater than 2250 meters, the individual sediment flows, filling the sediment floors, coalesce into large flow sheets, that cover much of the upper rise. The inset in Figure 2 shows the location of the sediment flow sheets off the east coast of North America.

Whether failure of the sediments is triggered by earthquakes or other phenomenon is not as yet fully understood. Studies of the effects of the 1929 Grand Banks earthquake upon the sediments of the shelf, slope and upper rise of that area would however suggest that earthquakes appear to be the prime triggering mechanism for mass slumping of sediments deposited on the continental slope. The frequency of such events is not as yet known for the Baltimore Canyon area. The radio-carbon date of the 5265 ± 210 years BP date for the period of the last major sediment slump event, together with the presence of the hemipelagic blanket, that covers the slump scar surfaces, suggest that the continental slope immediately south of Baltimore Canyon has not experienced any major submarine landslides, therefore possibly earthquakes during, historical time.

7. Conclusions

1. Detailed bathymetry of a section of the slope and upper rise located between the Baltimore and Washington Canyons, and above a major sediment flow of the continental rise

has shown this section of the ocean floor to be extensively excavated by erosional processes creating a landscape of ridges, valleys and "mesa" and "butte" like features on the ocean floor. The study section is representative of the configuration of the continental slope and upper rise of the northeastern Atlantic margin of North America.

2. The most recent erosional event in the study area appears to have taken place 5265 ± 210 years ago in the form of area wide slumping and sliding of the uppermost 50 meters of stratified sediments, from the ridge flanks down into the neighboring valleys. Only the ridge crests maintain undisturbed sections of the stratified layer.

3. Slumping and sliding of the sediments has occurred along glide planes located along the submarine ridge and valley flanks. The slumped sediments appear to form sediment flows along the valley floors which at depth coalesce into large sediment flow fans covering sections of the upper rise.

4. Submersible observations show the presence of a 40 centimeter thick hemipelagic sediment blanket that appears to cover all of the slump scarps as well as the flow sediments located in the study area.

5. No evidence for present day active, area wide erosional processes was collected during the investigations.

6. The present day ocean floor environment of the slope and upper rise in the study area appears to be that of quiescent hemipelagic sedimentation, disturbed in places only by the activities of benthic marine organisms.

7. Earthquake activity is assumed to be the principal triggering mechanism for area wide mechanical failures of surficial marine sediments deposited on the continental slope, such as those mapped in the study area and inferred from submarine cable breaks on the continental slope of the Grand Banks.

8. References

Embley, R.W., "Studies of deep-sea sedimentation processes using high frequency seismic data," Ph.D. Thesis, Columbia Univ., 1975, 344 pp.

Embley, R.W., "New evidence for the occurrence of debris flow deposits in the deep sea," Geology, Vol. 4, 1976, pp. 317-374.

Embley, R.W. and R. Jacobi, "Distribution and morphology of large submarine sediment slides and slumps on Atlantic continental margins," Marine Geotechnology, Vol. 2, 1977, pp. 205-228.

Grow, J.C. and R.G. Markl, "IPOD-USGS multichannel seismic reflection profile from Cape Hatteras to the Mid-Atlantic Ridge," Geology, Vol. 5, 1977, pp. 625-630.

Heezen, B.C. and M. Ewing, "Turbidity currents and submarine slumps and the 1929 Grand Banks earthquake," Amer. Jour. Sci., Vol. 250, 1952, pp. 849-873.

Jacobi, R. "Sediment slide on the northwestern continental margin of Africa," Mar. Geol., Vol. 27, 1976, pp. 157-173.

Kelling, G. and D.J. Stanley, "Morphology and structure of Wilmington and Baltimore submarine canyons, eastern United States," Geol. Soc. Amer. Bull., Vol. 78, 1970, pp. 637-680.

Milliman, J.D., O.H. Pilkey, and D.A. Ross, "Sediments of the continental margin off the eastern United States," Geol. Soc. Amer. Bull., Vol. 83, 1972, pp. 1315-1344.

Pratt, R.M. "The seaward extension of submarine canyons off the northeast coast of the United States," Deep-Sea Research, Vol. 14, 1967, pp. 409-420.

Veatch, A.C. and P.A. Smith, "Atlantic submarine valleys of the United States and the Congo Submarine Valley," Geol. Soc. Amer., Spec. Paper 7, 1939, 101 pp.

DESIGN OF AN OCEAN BOTTOM SEISMOMETER WITH RESPONSE FROM 25 Hz TO 100 SECONDS[1]

R. G. Bookbinder, A. C. Hubbard, W. G. McDonald and P. W. Pomeroy
Lamont-Doherty Geological Observatory
of Columbia University
Palisades, New York 10964

Abstract

A new ocean bottom seismometer for seismicity study, evaluation of seismic hazard, and for collection of refraction data has been designed. The basic system contains a feedback controlled long-period vertical seismometer, a short-period vertical seismometer and a pressure-compensated crystal hydrophone. The long-period seismometer response models a standard 15 second long-period suspension - 100 second galvanometer combination allowing study of long-period phenomena never before recorded on a free-fall/pop-up ocean bottom seismometer. The entire system is under the control of a cosmos microprocessor. The microprocessor produces modified IRIG time code and such housekeeping functions as delayed turn on; cage, uncage and centering for the long-period suspension; in situ calibration and timed ballast release. The ocean bottom seismometer also includes an acoustic transponder for location, navigation and release.

This paper describes the design of a new generation of seismographs for operation on the bottom of the ocean. These new units are of the free-fall "pop-up" type. That is, they return to the sea surface from the ocean floor after a fixed time interval, up to 30 days, or upon receiving a coded acoustic signal from a surface vessel. After surfacing, the units can be serviced and redeployed for another recording period. The principal new features of the system are:

1) A long-period vertical seismometer capable of recording data in the 10 to 100 second period band.

2) Recording duration to 30 days using analog tape recording at a recording speed of 1/120 inch per second. The short-period data are recorded in the direct mode and the long-period data in the digital mode.

3) Acoustic recall capability allowing greater flexibility in ship schedules during recovery of the instruments.

4) Microprocessor control to perform "housekeeping" functions and to provide IRIG time code.

In addition, features found on the earlier Lamont-Doherty Geological Observatory instruments are also present in the new configuration. These include:

1) a short-period (2 Hz) seismometer;

2) a hydrophone; and

3) radio and visual recovery beacons.

The entire instrument package of the new system is housed in a cylindrical pressure case with a low profile to minimize the vibration effects of ocean currents acting on the package. The instrument package is also designed to penetrate loosely consolidated sedimentary material to insure good coupling between the package and the ocean bottom. The new system is shown in Figure 1.

1. Introduction

The Lamont-Doherty Geological Observatory has long been engaged in seismological studies of the ocean bottom. The VELA-UNIFORM program motivated by the need to improve discrimination between explosions and earthquakes, heightened the Observatory's activity in the design and deployment of ocean bottom seismographs. That program culminated with the installation of an ocean bottom observatory 90 miles off Point Arena, California in 1966. That seismic observatory (Sutton et al)[1] was "hard wired" to a land recording site and produced a wealth of seismic data during its 6 1/3 years of operation. The Point Arena installation contained 3 component short- and long-period seismometers and represented the only previous effort to record long-period seismic data on the sea floor. The long-period instrument described in this paper is the direct outgrowth of the highly successful Point Arena instrument.

---

[1] Lamont-Doherty Geological Observatory Contribution Number 2694.

In 1972, a renwed interest in portable short-period seismographs for use on the ocean bottom resulted in the development of a first generation pop-up OBS (McDonald et al.)[2]. A number of those instruments were built and have been successfully deployed around the world. A total of 91 deployments were made between December 1972 and December 1977. During the early part of this time period, the emphasis of shipboard programs was on seismic refraction profiles and, in general, only a few instruments were involved in recording the signals generated by a large number of explosive charges. In the past few years, however, many experiments have been carried out in active seismic areas such as the Gulf of Alaska, the Caribbean, and the mid-Atlantic ridge to monitor earthquake or micro-earthquake activity. These experiments were highly successful although only a few instruments were utilized. The results, however, clearly indicated that future experiments would require larger numbers of instruments operating for intervals up to 1 month. A need for a long-period seismograph on the ocean bottom was also clearly indicated. The new instruments described here are specifically designed to meet the requirements of these future, more sophisticated, experiments.

2. Problems With Previous Systems

Profile

Previous designs of ocean bottom seismographs have ranged in height above the sediment from approximately eight feet to two feet; in frequency response from 2-12 Hz to 1-100 Hz; in recording duration from six hours to ten days and in coupling configuration from a cement flower pot to a tripod with footpads. Now, with the experience gained from several years of experiments, optimum height, frequency response, recording time and mechanical coupling configuration have been incorporated in the design of the new LDGO instruments.

Since bottom currents of 1-2 knots have been measured in the first few meters in what was thought to be still bottom water, the optimum instrument should have the least cross sectional area, lowest profile and most streamlined shape possible. Moreover, the instrument would not have a protruding antenna or flag.

Coupling

The experience gained with coupling is difficult to quantify but straightforward to describe. An instrument that settles gently on the extremely loose sediment typical of the ocean floor, is very poorly coupled to the actual motions of the consolidated bedrock underlying the sediment cover. High-frequency seismic energy is rapidly attenuated in sediment and, moreover, the recording of waves generated in the sediment may not be desired for many ground motion studies. There is controversy within the scientific community on the best method of alleviating this problem. One idea is to make the density of the seismometer package equivalent to that of the surrounding sediment. The other approach is to insure that the instrument package penetrates the sediment until a reasonably consolidated sediment is reached. The latter approach is usually used by land based seismologists and is the criteria adopted for the instrument described here. Penetration of one to two feet into the sediment should result in adequate coupling of the instrument package to the more consolidated underlying sediments.

Frequency Response

The frequency response and dynamic range are tailored to the seismic energy of interest. The 2 to 30 Hz range is excellent for recording short-period body wave signals, but the long-period range from 1 to 100 sec has, up to now, remained unrecorded in portable ocean bottom instruments and yet has provided a wealth of information to land based seismology. If, on the other hand, the bottom unit is to be used for refraction studies, then information in the high frequency direct water wave (50-150 Hz) must be recorded.

Last, but certainly not least, is the ease with which a large number of instruments can be checked out, deployed and recovered from a surface vessel. In future experiments, array deployment using 8 to 10 instruments will be necessary, and limited shiptime and personnel require more reliable, easily handled systems.

3. New System

With the problems mentioned above in mind, the design of a new ocean bottom seismometer was undertaken in late 1977. The starting point of the design of the new system was that it would be a free-fall, pop-up configuration rather than a tethered or cabled system. Operational problems with tethered or cabled systems, when more than a few systems are deployed on a temporary basis, become prohibitively complex. The configuration of the new instrument, shown in Figure 1, insures a minimal protrusion above the sediment/water interface, approximately twenty-five inches. Note in Figure 1, that the welded steel frame has four spikes extending from the bottom instead of the footpads used in older instruments. These spikes are lead filled and will provide significantly improved coupling through the water/sediment interface. The frame also acts as ballast and is left on the bottom upon release.

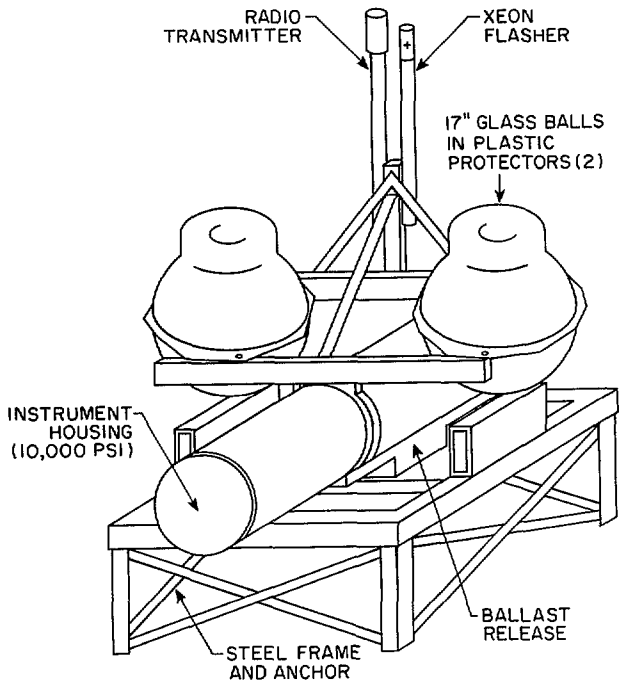

Figure 1: An outline drawing of the LDGO ocean bottom seismometer showing low profile and spikes. To enhance coupling to the sediment.

The frequency response (Figure 2) is broken down into three bands. The first band is between 1 and 30 Hz. Transducers recording this band include a short-period vertical and horizontal seismometer and the short-period hydrophone. Signals from these transducers, after preamplification and filtering, are recorded on analog magnetic tape in the direct record mode. Each short-period channel has dynamic range in excess of 50 db through the use of two recording tracks separated by 26 db. The second band is 1-100 seconds. Instruments recording in this band include a long-period vertical seismometer and long-period hydrophone each of which is sampled three times per second and recorded digitally with a dynamic range of 72 db. The third band is between 50 and 150 Hz and is used to record water waves (50-150 Hz) which are detected, band limited and recorded direct on a timing channel.

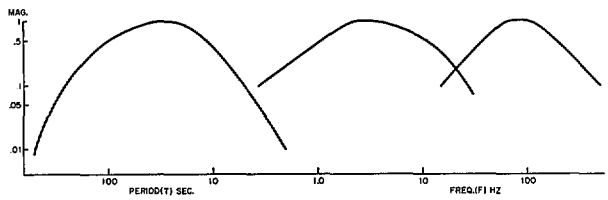

Figure 2: Frequency response showing recorded spectrum. Covers nearly six decades.

We have taken advantage of advances in state-of-the-art electronics since our earlier ocean bottom seismometer was designed, by replacing the random logic time code generator and system programmer with a low-power microprocessor.

From earlier experience we have found that the optimum transducer complement varied from one experiment to the next. Three component short-period seismometers were more useful for certain experiments; while at other times, a short-period hydrophone and two seismometers were required. In the new instrument the long- and short-period channels can be easily reconfigured to provide a maximum of three short-period signals or two short-period and two long-period signals in addition to time code. Thus, in any experiment the instrument can record those signals that are of prime interest to the experimenter.

In addition to the interchangeability of the transducer compliment, the recording mode may be changed. Normally, the system records continuously for thirty days. In the future, however, with the addition of a buffer memory, a software event detector, and a higher speed tape recorder, the system can be used in an event-detect mode. Space is provided for the additional memory, and the event-detector algorithm can be implemented in the microprocessor. Thus, in the new design, changes have been made to overcome many of the problems present in earlier designs and to meet the future requirements placed on ocean bottom systems.

4. System Components

Long-Period Transducer

Over the past two decades, major advances in knowledge of seismic source functions for earthquakes and explosions, and in understanding of propagation path characteristics have been made using body and surface wave observations made on land based long-period seismograph systems (Kovach)(3). In the past, it has not been possible to observe "oceanic" earthquakes along purely oceanic paths. The addition of a long-period transducer (T_0 = 15 seconds) in an ocean bottom instrument package will allow observations of that type. Moreover, phase and group velocity measurements of fundamental and higher mode surface waves of the Rayleigh type on segments of the oceanic lithosphere of differing ages can be obtained. The long-period first motions of the compressional waves emitted from seismic sources beneath the ocean floors can now be measured close to those sources with the new instruments. Source parameters previously measured poorly, if at all, can be accurately determined and inversion techniques can be applied to the entire long-period seismogram to obtain source and propagation path parameters. In short, the addition of long-period seismographs to bottom instrument systems opens an entire spectrum of measurements on the ocean floor comparable to the enhancement of knowledge that resulted from the development

of an operational vertical long-period seismograph by Press and Ewing in the early 1950's.

The requirements on a long-period seismic transducer on the ocean floor are severe yet the Point Arena installation clearly demonstrated that such operation is possible. The long-period instrument constructed at LDGO is a LaCoste suspension design and is a physically scaled down version of the Point Arena vertical instrument. The free period of the unit is 15 seconds and the unit is designed to operate at critical damping. A differential capacitance transducer is used to provide a displacement response and a coil is attached for damping, calibration, and fine centering of the seismic mass. The characteristics and system design are similar to the instruments described in Sutton and Latham(4). The output of the displacement transducer (see block diagram, Figure 3) is amplified and passed through a second order low pass filter with a corner period of 100 seconds. The response is then approximately that of a seismometer-displacement transducer-galvanometer combination with a galvanometer free period of 100 seconds. Negative feedback with a time constant of 6300 sec is used to stabilize the long-period system. This feedback signal can be used to provide an output showing the vertical component of solid earth tides.

The long-period data is converted to 12 bit digital data and is then recorded.

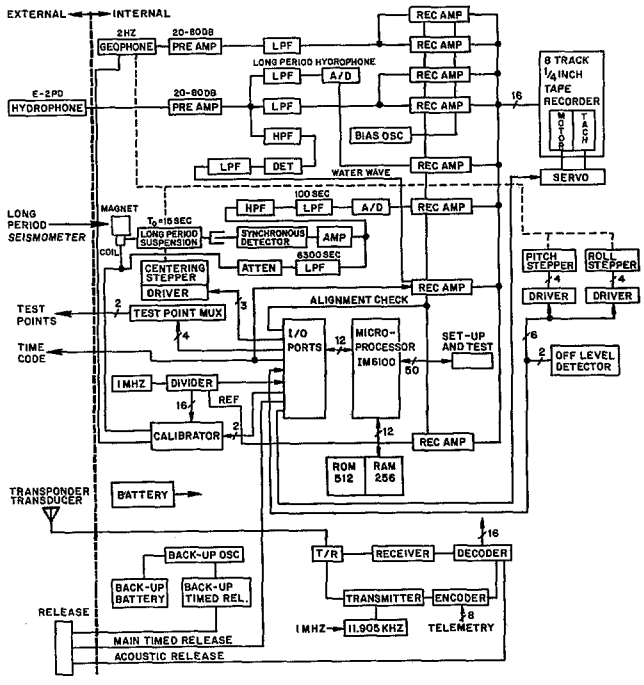

Figure 3: Block diagram of the OBS showing signal conditioning, microprocessor, and transponder.

Short-Period Transducers

Short-period components consist of Geospace Inc. HS10-2 (2 Hz natural frequency, 300 v/m/s output, 4100 ohm coil) vertical seismometers, and HS10-2 horizontal seismometers, and/or an Ocean and Atmospheric Sciences Inc. E-2PD pressure compensated crystal hydrophone. In the standard configuration, the short-period vertical seismometer is mounted beside the long period suspension on the gimbal system to insure a true vertical measurement and the horizontal, when used, is mounted in place of the long-period assembly. Hydrophone sensitivity is -92 dbv dyne^{-1} cm^{2}. High ambient pressure is equalized between exterior and interior through a threshold valve. Hydrophone capacitance is .05 MFD which allows the use of a conventional high quality, high input impedence preamplifier.

Short-period signals enter a micropower instrument operational amplifier (National LH0036) with input impedence adjusted to provide 70% critical damping for the seismometers and a -3 db point of 2 Hz for the hydrophone. This section of the preamp can provide a voltage gain of 0 to 60 db with the adjustment of one resistor. The following stage provides a fixed voltage gain of 20 db and a DC signal to correct for offset in the first amplifier. The equivalent input noise represents approximately a one millimicron ground displacement at 2 Hz. The seismometer signals are then low-pass filtered (12 db/oct at 40 Hz) and sent to the high and low gain record amplifiers. The hydrophone signal is also low-pass filtered (12 db/oct at 40 Hz) and sent to high and low gain record amplifiers. The preamp signal is also sent to a high-pass filter (12 db/oct at 50 Hz). This high frequency signal is detected, band limited to a rise time of 13 msec and recorded with the time code. By limiting the rise time of the water wave channel the detected signal can be frequency demultiplexed from the time code during playback. The hydrophone signal is also low-pass filtered and digitized to provide long-period data.

Microprocessor

Accurate time keeping on the ocean floor is a problem ocean bottom instrument designers have had to contend with from the start. At LDGO, we have now designed the third generation of low-power time code generators. The first was a cosmos random logic IRIG-C generator design implemented on a printed circuit card approximately one foot square. The second generation was also cosmos, but was built on a 6" x 6" wire wrap card. A second 6" x 6" wire wrap card was devoted to system programming functions. The third generation now uses a cosmos microprocessor (Intersil IM6100) for implementation of a modified IRIG-C (20 Hz carrier) time code and direction of all system functions. It is wire wrapped on a 9.5 inch diameter round printed circuit card with space for significant expansion of control capability.

The microprocessor was chosen over a random logic design because of its reliability and flexibility. The microprocessor system will be more reliable simply because it has fewer IC's to fail. The random logic time code generator and programmer used approximately 200 IC's while the microprocessor uses approximately 30 IC's. The software operating system will allow major additions and modifications without major hardware changes. The system's program is contained in a low-power EPROM (erasable programmable read only memory) (512 bytes), and can be expanded by simply adding more bytes of memory.

Clock

The time base is provided by a Vectron Inc. 1 mHz temperature compensated crystal oscillator that is quoted as stable to within $\pm$ 3 part in 10^8 over the temperature range 0-5° C. Since the ocean bottom environment is stable to within a few hundredths of a degree, timing errors on the order of $\pm$ 3 parts in 10^9 can be expected. This 1 mHz oscillator is divided down to provide a 50 MS interrupt for the microprocessor and is further divided to provide calibration frequencies for the long- and short-period seismometers. When the time code that the microprocessor generates from the 50 MS interrupt is compared to a standard (WWV or sat. nav.) before and after each 30 day deployment, the crystal aging term (1 part in 10^8 per day) and the initial setting error term can be eliminated and an overall timing resolution of $\pm$ 10 MS for a 30 day mission is achieved. For ease of operation, time code is always available on an external feedthru connector in the pressure case.

Operational Sequence

In addition to time code generation, the microprocessor supervises the following operations in sequence:

1) Delayed turn on. From the time the OBS is armed on ship, a 0-7 hour delayed turn on is available to allow the instrument time to get to the ocean floor. During the delay an acoustic transponder can transmit and, after the delay, the recorder is turned on and the transponder is shut down.

2) Pitch and roll leveling. The main gimbal which supports both the long- and short-period seismometers is leveled on two axes after the initial delay and is releveled whenever roll exceeds .25° or pitch exceeds 2° thereafter. The gimbal drive consists of two DC stepping motors with worm gear reductions.

3) Uncage LPZ. The long-period vertical seismometer is mechanically caged during deployment to prevent damage and is uncaged after leveling.

4) Centering LPZ. The long-period seismometer is centered after thermal stabilization and is recentered when necessary. This is accomplished with a DC stepping motor and a series of gears for reduction.

5) Calibration. Once every 24 hours, the seismometers receive a time domain calibration and once every 5 days they are calibrated in the frequency domain.

6) Release. Upon receiving a release command from either the acoustic transponder, main timed release, backup timed release or leak detector, the long-period seismometer is caged, the telemetry is turned on and the release is activated.

Calibration and Test

In situ calibration in both the time and frequency domain is provided for all seismometers. Every twenty-four hours (at 0000) the long- and short-period calibration coils are sent a series of four current steps separated by 10 db with each lasting 5 minutes. Then once every five days (at 1200) the seismometer calibration coils receive a series of four cycles of a digitally synthesized sinusoidal current. The short-period instrument receives four cycles each of 1, 2, 4, 8, 16, 32 and 64 Hz and the long-period receives four cycles each of 2, 4, 8, 16, 32, 64 and 128 seconds. This series is repeated at four amplitudes separated by 10 db. The sequence takes approximately one hour.

After the package is sealed and ready for deployment, a test point multiplexer allows a shipboard technician to monitor twenty analog signals on just two external feedthrough pins. The sensors are checked at various points along the signal path along with the different battery voltages and telemetry inputs. Thus, a very thorough system checkout can be accomplished in the ten minutes it takes to step through the test points.

Tape Recording

A specially modified tape recorder is required for 30 days of continuous recording. An Uher 4000C was chosen for modification because of its small outside dimensions and rugged all metal construction. The heads and electronics are removed and two Nortronics four track interlaced record-heads (model PBQL4F) are substituted. A servo motor with DC tachometer and reduction gearhead (Escap type 16GIC204/104) drives a worm gear for capstan and take up reel drive. The motor is controlled by a simple servo. Tape speed is 0.212 mm/sec (1/120 ips) which produces 30 days of recording on 1800 feet of Scotch 295 low speed tape. In tests, this recorder keeps unfiltered peak-to-peak wow and flutter to within 6% (P-P).

Each short-period signal is recorded by two constant current record amps driving two tracks separated by 26 db in amplitude. Thus, these

signals are recorded with a midband dynamic range in excess of 50 db. The long-period signals are recorded digitally using a Non-Return-To-Zero format (clocking is provided by time code track). The two outer tracks (one on each head) are used for timing and water wave detection. The modified IRIG time code is recorded on one head along with the water wave signal. The other outer track records a 20 Hz reference signal which is used in playback to generate a sampling clock. The reference signal will allow digitization of the analog signals with removal of the wow and flutter terms.

Once every hour, a 0.5 second, 20 Hz tone is recorded on all eight tracks. This signal serves two purposes. First, it allows removal of any residual skew in the two record or playback heads. Second, it provides backup timing information if time code is not recorded.

Transponder

Originally an acoustic pinger was incorporated into a test configuration to identify failure modes of lost instruments. This telemetry proved so useful that pingers were subsequently used on all bottom instrumentation. The acoustic system provides engineering status data, tracking, and unit identification by pinging once per second at 12 kHz and sending an eight bit code block every two minutes. The new ocean bottom seismometer includes an acoustic transponder telemeter system. By adding a receiver/decoder to our existing pinger-telemeter, we now have full acoustic command capabilities.

The acoustic transponder telemeter (ATT) can receive up to 16 possible commands including but not limited to all units transpond, unit X transpond, unit X release, etc. In addition with each response, the bottom unit replies with an eight bit code, one of twelve identification codes and a clock to ease visual decoding of data and identification codes. As with the previous acoustic pinger, the ATT transmits and receives on the same frequency (12 kHz) which allows transmission and reception on PDR's, PGR's, PESR's, etc., which are universally used on marine geophysical research vessels.

The ATT is all low power and may be switched on and off under microprocessor control. In the receive mode the ATT uses approximately 30 milliwatts and when transmitting once per second, average power consumption is 2.9 watts.

The addition of a transponder will not only allow accurate location of bottom units with respect to a ship, and capabilities of maneuvering the ship toward ascending OBS's, but will also allow acoustic release instead of predetermined timed release. This feature allows much more flexibility in ship movement and prevents the necessity for recovery in very heavy seas or fog. With multiple array deployments forecast for the future, acoustic release is a necessity to minimize precious ship time and allow for the quick location of all units in an array. The acoustic transponder also provides a bottom beacon for precise navigation while shooting refraction lines. Precise navigation is necessary in refraction experiments studying the uppermost portion of the oceanic crust.

5. Conclusions

The new generation of ocean bottom instruments described in this paper opens up a new spectrum of long-period recording using temporarily placed pop-up instruments. The long-period system will allow determinations of earthquake source mechanisms and parameters as well as detailed oceanic crust and upper mantle investigations. The frequency response of the system covers nearly six decades, from several hundred seconds to nearly 200 Hz. The new system will record this spectrum for a time period up to 30 days. This extended recording time is essential for monitoring natural seismicity and allows a variety of experimental programs hitherto impossible with shorter term recorders. The addition of acoustic transpond recall functions and the use of a microprocessor greatly enhance the flexibility of ocean bottom experiments; allowing a wide range of performance modifications without hardware changes. The entire system has been specifically designed to meet the requirements of more sophisticated experiments contemplated during the next decade.

6. Acknowledgements

The design effort described above was supported by the National Science Foundation under Grant Number EAR 77-17115 and by Institutional Funds. We thank Dr. Manik Talwani for his continuing encouragement and support. Ivars Bitte and George Gunther have been responsible for building the electronic systems and Kerry Oxner for construction of the mechanical system. The paper was critically reviewed by C. H. Scholz and A. J. Murphy.

References

1. Sutton, G.H., W.G. McDonald, D.D. Prentiss and S.N. Thanos, "Ocean-bottom seismic observatories," Proceedings of the IEEE, Vol. 53, 1965, pp. 1909-1921.

2. McDonald, W.G., A.C. Hubbard, R.G. Bookbinder and K. McCamy, "Design and shipboard operation of a multipurpose ocean bottom seismograph," Marine Geophysical Researches, Vol. 3, 1977, pp. 179-196.

3. Kovach, R.L., "Seismic surface waves and crustal and upper mantle structure," Reviews of Geophysics and Space Physics, Vol. 16, 1978, pp. 1-13.

4. Sutton, G.H. and G.V. Latham, "Analysis of a feedback-controlled seismometer," Journal of Geophysical Research, Vol. 69, 1964, pp. 3865-3882.

A UNIQUE OCEAN TEST RANGE

J. Blaine Davidson
Florida Atlantic University
Boca Raton, Florida 33431

Abstract

Construction of an offshore acoustic range near Boca Raton, Florida is described. The range consists of a track which can be used to hold a side scan sonar or other instrumentation when careful measurements, with no instrument motion, are required.

The Department of Ocean Engineering at Florida Atlantic University in Boca Raton, Florida has constructed a unique underwater range in the Atlantic waters off Boca Raton.

For some years the Department has had a research grant from a German company, Metellgesellschaft, A.G. to study the possibilities of utilizing side scan sonar in the search for manganese nodules in the deep oceans of the world. In pursuing the research recorded magnetic tapes of side scan sonar returns from manganese nodule fields and various types of bottoms not containing nodules have been studied seeking unique features of the returns from nodule fields. This study has led to a general interest in the echo formation process in side scan sonar, and a need for data which does not contain some of the variables found in normal towed side scan returns thus developed. In particular, data with no variables caused by uncontrolled tow-fish motion was desired. It was determined that this type of data could best be obtained by mounting the side scan sonar on a track and moving the fish along the track by incremental amounts or by pulling it at some constant speed. This idea gave rise to plans for constructing an offshore range.

It was determined that an offshore area near Boca Raton was suitable for the project. The area, in forty feet of water contained a wide flat sand bottom and offered an unobstructed horizontal range area some 100 meters by 50 meters. Since the area is regularly used by sport fishermen trolling for game fish it was determined that a permanent structure would not be in order, and plans were made to construct the range as a portable unit which could be installed in the morning prior to a data taking session and removed in the evening after the session was completed.

The support structure for the track consists of two inch steel pipes twenty feet in length. To hold each of these vertical supports a ten foot piece of two inch pipe is jetted into the sand with only about six inches remaining above the bottom. These permanent foundation pieces are capped when not in use to protect the threads. When the range is to be assembled the caps are removed and the twenty feet support sections are screwed into the foundations using two inch couplings. In addition to this basic structure each vertical support is supplied with three guy wires, attached to the support near its top and fitted with snap hooks at the other end. Three additional ten foot sections of pipe are jetted into the sand around each vertical support. Each of these sections is fitted with a cap and eye bolt so that the guy wires can be snapped into them when the vertical pieces are screwed into place. Thus, each of the four vertical supports provides a rigid foundation for the track.

The track itself consists of three twenty-five feet sections of aluminum angle, fitted so that it can be set on top of the vertical supports and each section secured with a single nut at each end. An experienced team of divers can assemble the track in about one and one-half hours and can disassemble the structure in about one hour. A sketch of the track in place is included as Figure 1.

The side scan sonar, or other instrumentation rides on a wheeled carriage which can be pulled along the track by a line and pulley system attached to a boat moored overhead, or it can be moved from one fixed position to another by a diver. A further refinement will provide a remotely controlled motor to position the fish. When the range was initially planned only a single position for the track was suggested. However, the progress of studies between the time the range was planned and when it was actually installed revealed the need to look at targets from front, rear and side positions as well as from the variable angle which could be produced by moving the sensor along the track. It was concluded that this improvement could be provided with no substantial increase in cost by simply providing three sets of foundations for the track, on three sides of the area in which targets can be installed. Figure 2, illustrating the entire range area, shows how this is accomplished. This permits installing the track in one location, collecting data from this location, moving the track to a second location, depending on the variable being studied, to collect a second set of data, and the possibility of a third move if needed.

The project was planned in December, 1977 and shortly thereafter a letter was sent to five fed-

eral and state agencies requesting permission to make the installation. The incidents involved in obtaining a permit are probably more interesting than the technical features of the range and a paper entitled "Bureaucracy at its Best" had been considered to replace this one. However, a few of the highlights of the encounters with bureaucracy will suffice to illustrate the point.

The first to reply of those solicited for a permit, was the Coast Guard. They determined that a lighted buoy would be required and an application form for a lighted buoy was enclosed in the reply. A quick response to the Coast Guard explained that the range was portable, that it would never be used at night, and that at all times when the range is installed a boat, flying an appropriate obstruction signal would be anchored directly over the range. They agreed to blow out the light but still insisted on an unlighted buoy and sent along an application form for an unlighted buoy.

Next came the Corps of Engineers. The letter application was sent to the Jacksonville Office but a reply was received from a branch office in Miami. The letter, signed by a lieutenant, listed a number of things that would have to be done to obtain a permit, and another application form and a pamphlet containing procedures for obtaining permits for construction on submerged lands was included. Several days later, while the letter from the Miami office was still being considered, a letter from the Jacksonville office arrived including a permit for the range, complete with permit number and reference to Corps of Engineers instructions which authorized such installations. This letter was signed by the colonel himself and even school teachers know that colonels outrank lieutenants. This led to a break of diplomatic relations with the Miami Office and no further submission to the Corps of Engineers.

State offices proved to be the most troublesome. One required a detailed survey of the area so that the University could be given an easement of title to the land. This was finally accomplished by jetting pipes into the bottom at the position of the range boundaries, tying empty plastic bottles to the pipes using just enough line to permit the bottles to float and tying the bottles into permanent survey marks provided in city plats with transits from surveyed locations on the beach. There was some concern about disturbing the reefs in the area so plastic bottles were also tied to outcroppings on the nearest reefs in the area and these were also cut in during the survey. The result is illustrated in Figure 3.

Final authority to build the range, from all concerned had not been received at the date provided for submission of this paper but it is anticipated that this will be received and that pictures of the actual installation will be available in time for OCEANS 78.

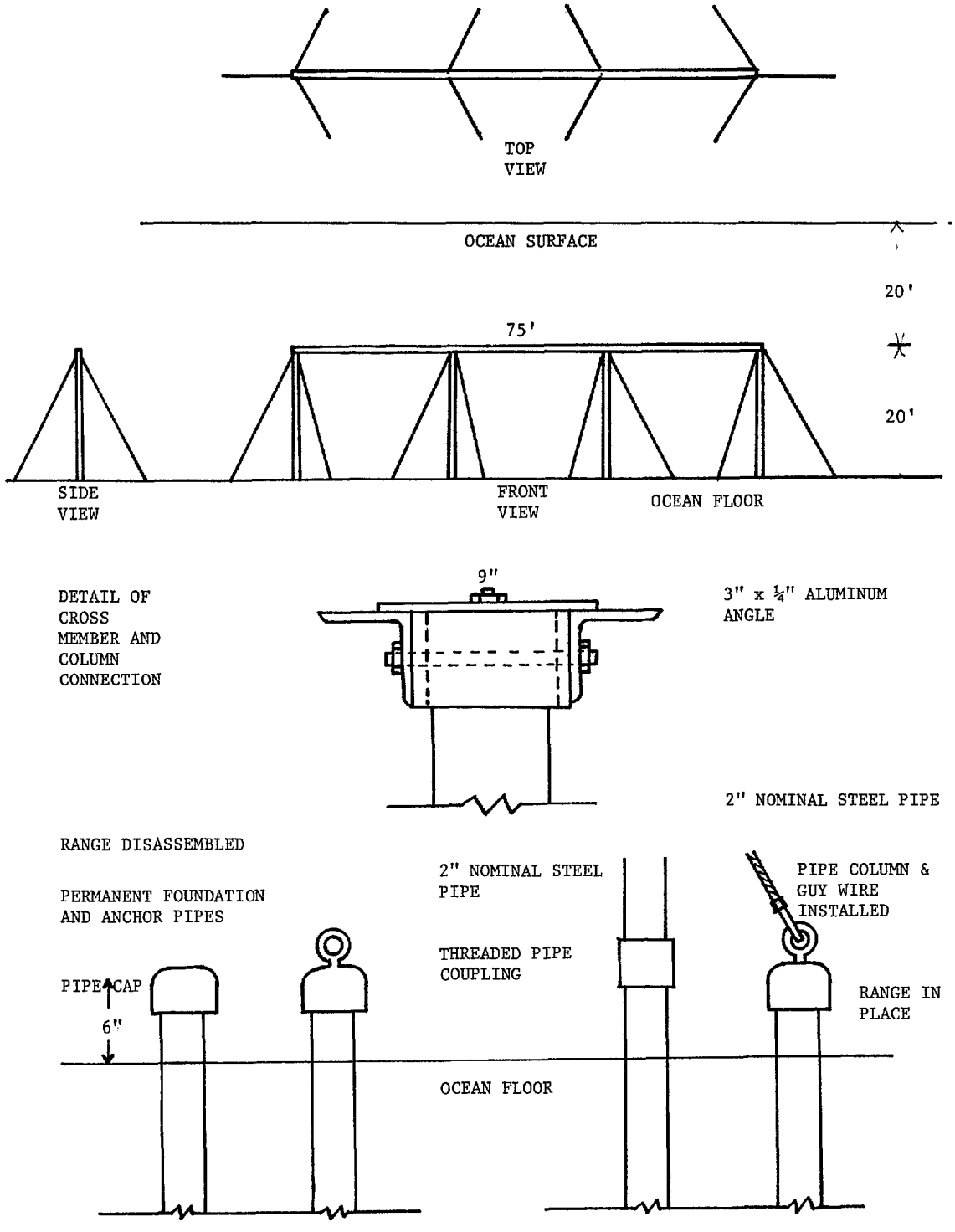
TOP
VIEW
OCEAN SURFACE
20'
75'
20'
SIDE
VIEW
FRONT
VIEW
OCEAN FLOOR
DETAIL OF
CROSS
MEMBER AND
COLUMN
CONNECTION
9"
3" x ¼" ALUMINUM
ANGLE
2" NOMINAL STEEL PIPE
RANGE DISASSEMBLED
PERMANENT FOUNDATION
AND ANCHOR PIPES
PIPE CAP
6"
2" NOMINAL STEEL
PIPE
THREADED PIPE
COUPLING
PIPE COLUMN &
GUY WIRE
INSTALLED
RANGE IN
PLACE
OCEAN FLOOR

FIGURE 1

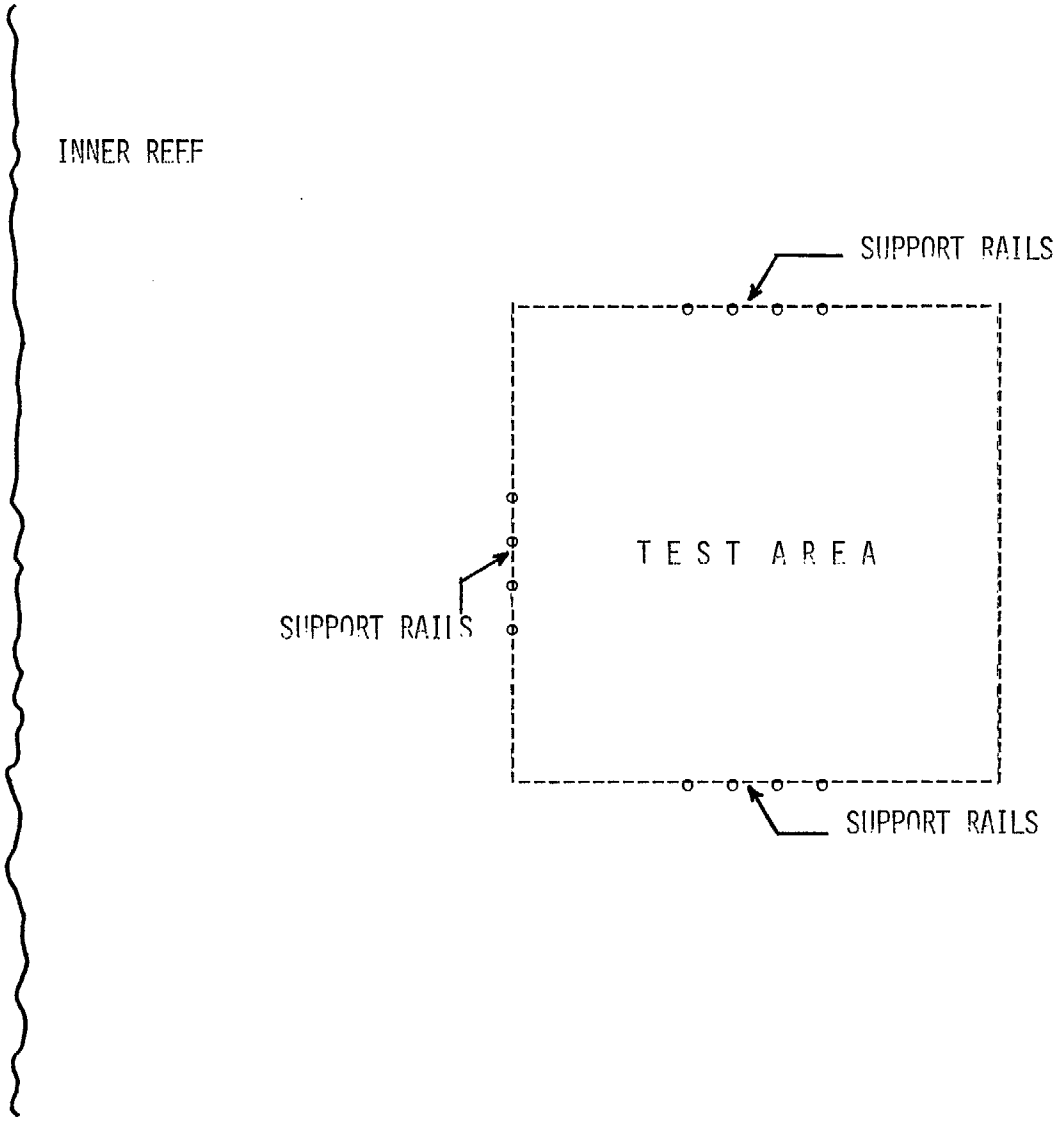
INNER REEF
SUPPORT RAILS
TEST AREA
SUPPORT RAILS
SUPPORT RAILS

FIGURE 2

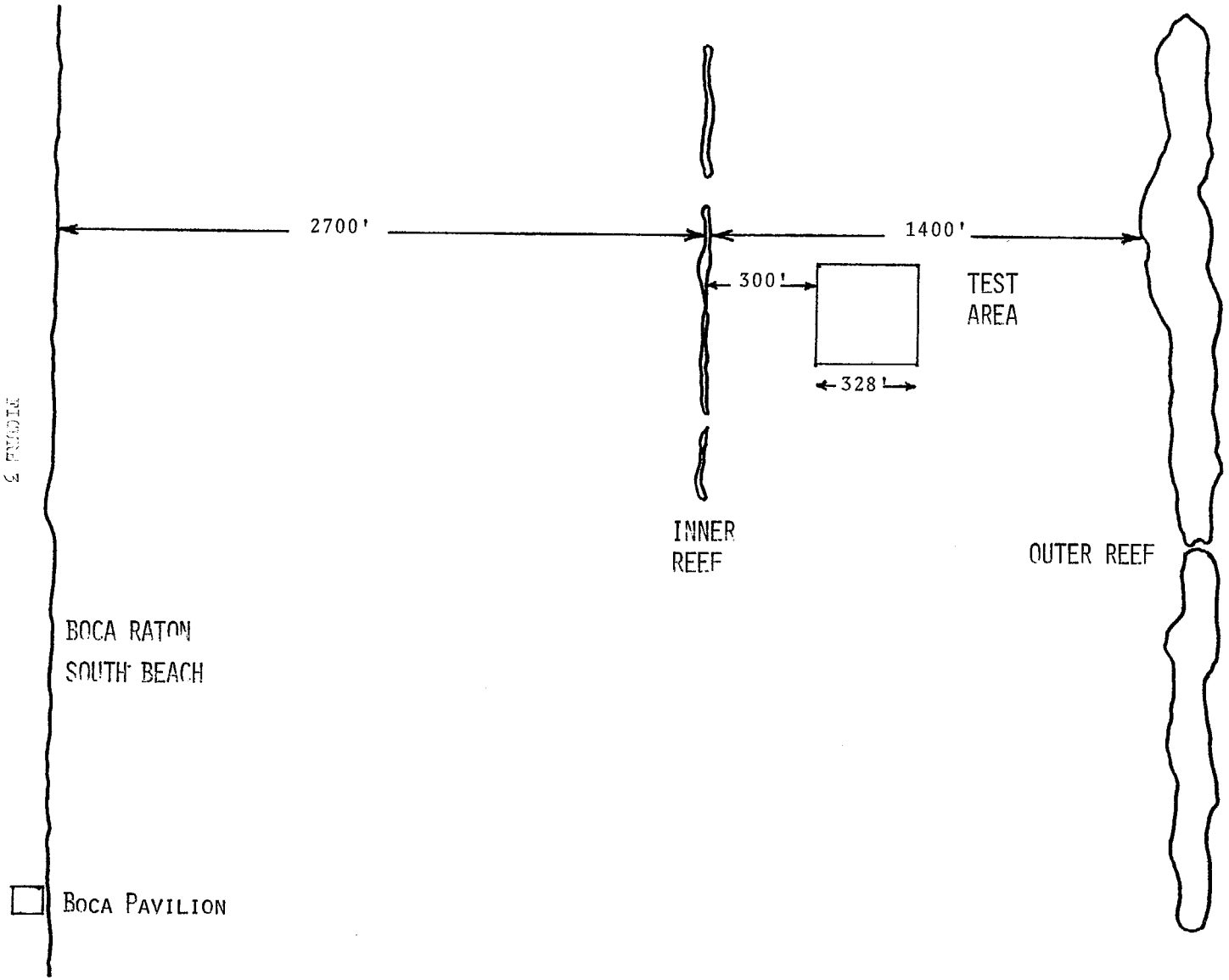
2700'
1400'
300'
TEST
AREA
328'
INNER
REEF
OUTER REEF
BOCA RATON
SOUTH BEACH
BOCA PAVILION

FIGURE 3

BROADBAND SEISMIC DATA USED FOR SEAFLOOR SEDIMENT CLASSIFICATION

A.D. Dunsiger
Faculty of Engineering & Applied Science
Memorial University of Newfoundland
St. John's, Newfoundland
Canada, A1B 3X5

R.R. MacIsaac*
Acres Consulting Services, Ltd.
5259 Dorchester Road
Niagara Falls, Ontario
Canada, L2E 6W1

Abstract

The echo returns from a broadband deep towed seismic system are examined. It is shown to be possible to separate four different sediment types based on two metrics. These are i) the maximum value of the normalized cross-correlation function and ii) the normalized water-sediment interface energy. For the small data base used these two metrics give complete separation of the four sediment types.

1. Introduction

With the current interest in the exploitation of off-shore resources a need exists for a rapid, reliable and automatic method of determining the composition and properties of the ocean floor. Such information aids in the design and siting of off-shore structures and pipe line routing, provides an inventory of the mineral resources for economic development and planning and improves our understanding of the geophysical structure of the seabed.

Acoustic sources provide a rapid, non-intrusive method of remotely sensing the ocean floor. The use of a high resolution system permits the examination of small areas of the seafloor at frequent spatial intervals. Generally the echo returns require ground truthing by conventional methods such as core and grab samples, but with proper interpretation acoustic techniques can supply averaged information over large bottom swaths.

The coherent reflected energy from a smooth bottom yields an initial echo pulse from the sediment which is closely related in shape to the transmitted pulse. The echo returns from a completely rough bottom result in a time elongation of the transmission duration with no clearly discernable initial replica pulse. Intermediate values of roughness result in echoes which contain both a reduced coherent portion and an elongated tail. A measurement of the amount of coherent return from the ocean floor gives a measure of sediment roughness. This roughness may then be associated with a particular sediment type.

For normal incidence the acoustic energy returned from the ocean sediment is the sum of i) the energy specularly reflected from the water-sediment interface, ii) the energy scattered from the interface within the illuminated area, and iii) the energy returned from scatterers within a particular layer. It is these latter two components which contribute to the elongation of the echo. For multilayered sediments this process repeats at each interface.

Two complementary methods of evaluating the proportion of coherent and incoherent energy are used. The first is based on the stability of the coherent echoes with small spatial translation. The second method is used to estimate the coherent energy component within a single echo. In both cases ping to ping averaging, effectively spatial averaging for a transiting towed body, is used to decrease the fluctuation of the measurement.

Using data from a high resolution broadband acoustic source the resulting complementary metrics enable an algorithmic categorization of four sediment types found along the Eastern Continental Shelf (Fig. 1). These metrics are not to be taken as unique means for sediment classification but are to be used in addition to such other techniques as reflection coefficient measurement and graphic profile interpretation.

2. HUNTEC Deep Tow Seismic (DTS) System.

The DTS System (Hutchins et al. 1976) is a broadband boomer-type sound source. It has a maximum energy output of 600 Joules and a nominal sub-bottom penetration capability of the order of 50 m. dependent on sediment type. The source is mounted in a towed body. This results in a sub-bottom window equal to the fish depth which is free of surface reflections. The echoes are recorded at sea on analog magnetic tape. They are digitized ashore using a sampling frequency of 50 kHz with an 82 msec window corresponding to a water equivalent path of 60 m. Bandpass filtering from 1 kHz to 10 kHz is accomplished after digitization using frequency domain filters.

Due to the fixed aperture of the transmitting plate (60 cm diameter) the broadband pulse shape and hence the frequency spectrum varies with beam

---

** This work was done while the author was at Memorial University of Newfoundland.*

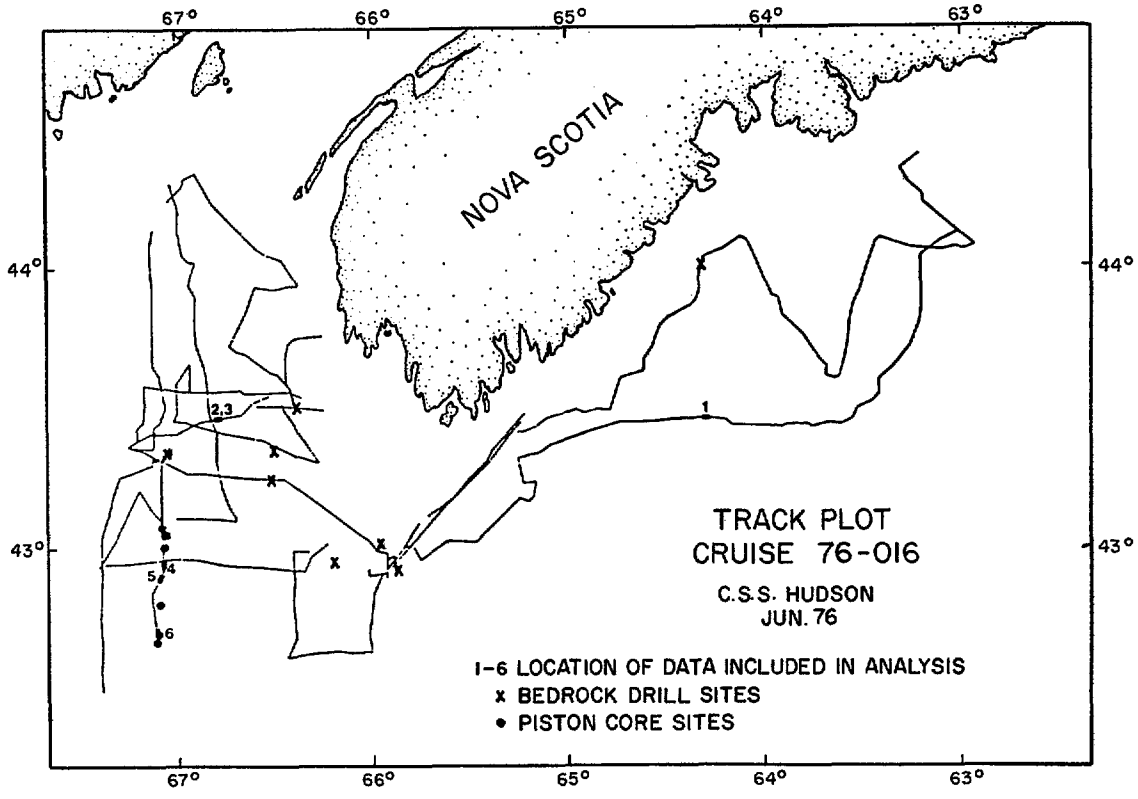

Figure 1. Locations of Acoustic Data Analysis Sites. Emerald Silt - 4, 6; Sambro Sand - 2, 3; La Have Clay - 1; Scotia Shelf Drift - 5.

angle. In the interpretation of the data the characteristics of the DTS System have not been removed from the measurements. With the dependency of frequency content on beam angle, some care should be taken in the interpretation of the results in application to other systems.

3. The Sediment Model

Clay and Leong (1974) show that completely rough bottoms return acoustic energy by means of a scattering mechanism, while totally smooth bottoms reflect acoustic energy in a coherent manner. Between these two extremes, intermediate degrees of roughness return proportions of reflected and scattered (coherent and incoherent) energy. Coherent energy reflected from a smooth bottom yields an echo that is closely correlated to the transmitted pulse. Echoes returned from a completely rough bottom (where the dimensions of the scattering elements are of the same order of magnitude as the wavelength of the incident acoustic energy) result in a time elongated signal containing no discernable correlation to the transmitted pulse. Intermediate degrees of roughness result in echoes that contain both a reduced coherent portion and an elongated reverberation tail. Drapeau and King (1972) associate bottom roughness characteristics with sediment type. Using this association, a measure of the amount of coherent energy in a bottom return yields a measure of sediment roughness which may be associated with a particular sediment type.

Two complementary methods of evaluating the proportion of coherent versus incoherent energy in the bottom echo are used. Their use in sediment classification was suggested in MacIsaac and Dunsiger (1978).

4. Echo to Echo Correlation

The first method is based on the assumption that for spatial translation of the sound source, the reflected component of an echo changes slowly while the scattered component fluctuates rapidly from ping to ping. It is expected, that echoes from smooth sediments would be highly coherent while those from rough sediments would fluctuate widely over a short time span. The measure of coherence used is the maximum value of the normalized cross-correlation function between successive echoes.

Representing the echo returns by

$$\{x(t)\} = x_1(t),\ x_2(t),\ \ldots,\ x_n(t)$$

the normalized cross-correlation function is defined as

$$\rho_{i,i+1}(\tau) = \frac{R_{i,i+1}(\tau)}{[R_i(0)R_{i+1}(0)]^{\frac{1}{2}}} \qquad (1)$$

where the cross-correlation between the ith and the (i+1)th echo is defined by

$$R_{i,i+1}(\tau) = \langle x_i(t)\ x_{i+1}(t-\tau)\rangle \qquad (2)$$

where < • > denotes a time average

and $$R_i(0) = \langle x_i^2(t)\rangle \qquad (3)$$

is the energy in the echo $x_i(t)$. The maximum value of the normalized cross-correlation, i.e., the correlation coefficient, is used as the parameter related to bottom roughness and is defined by

$$\rho_{i,i+1} = \text{Max}\ [\rho_{i,i+1}(\tau)] \qquad (4)$$

where $|\rho_{i,i+1}| \leq 1$. It is expected that smooth flat bottoms will exhibit high values of correlation coefficient while rough bottoms, due to the random nature of the roughness, will produce low coefficient values.

Using a 40 msec window this method of analysis is applied to acoustic data from four different sedimentary regions. The sediment classification of these regions is based on the surficial geology maps of Drapeau and King (1972) and Fader et al (1977). The individual correlation coefficients were determined for the four sediment types over a total track of 7.1 km. The running average of $\rho_{i,i+1}$ over 50 successive events (corresponding to approximately a 100 m. track) was evaluated. A bar over the parameter is used to denote spatial averages. Figure 2 shows a selection of these values over a 500 meter track for each sediment type. Using thresholds which optimize the separation of sediment types, the scatter matrix for all the data analyzed is shown in table 1. The weighted average of correct classification using the correlation coefficient is 69%.

Table 1. Classification of sediment type based on the maximum of the normalized cross-correlation compared with the reference classification of Drapeau and King (1972) and Fader et al. (1977). Classification thresholds, ρ_T, are at the following levels. i) Emerald Silt, $0.725 < \rho_T < 1.0$, ii) Sambro Sand, Gravel, $0.625 < \rho_T < 0.725$, iii) La Have Clay, $0.575 < \rho_T < 0.625$, iv) Scotia Shelf Drift, $0.3 < \rho_T < 0.575$. Values shown are percentages.

Correlation Coefficient Classification	Reference: Emerald Silt	Reference: Sambro Sand	Base: La Have Clay	Scotia Shelf Drift
Emerald Silt	70	28	-	-
Sambro Sand	27	53	-	-
La Have Clay	3	18	84	-
Scotia Shelf Drift	-	1	16	100
N° of Events	1725	1076	432	270
Track Length (km)	3.5	2.2	0.9	0.5

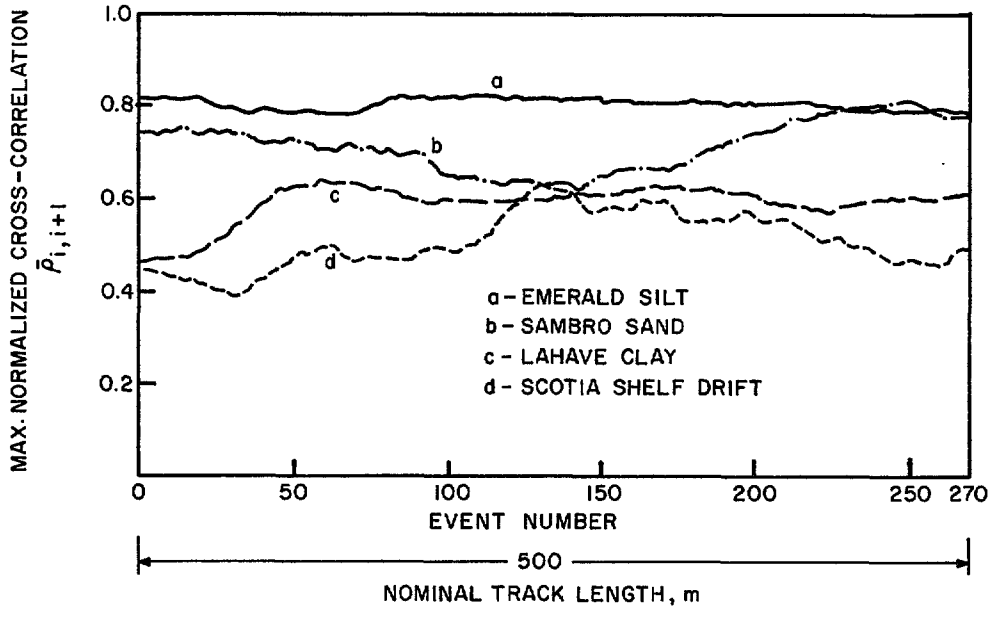

Figure 2. Typical Values of Correlation Coefficient (running mean averaged over 50 echos pairs) vs. Track Length.

5. Coherent Interface Energy

The second indicator of the degree of coherent energy in a return follows the methods of Knott et al (1977). The normalized cumulative energy function, NCE(t), is formed. This function is the cumulative integral of the magnitude squared of the echo normalized by the total energy contained in the return, i.e.,

$$\begin{aligned} NCE(t) &= \frac{1}{E_T} \int_0^t x_i^2(t)dt \qquad t < T \\ &= 1 \qquad\qquad\qquad\qquad t \geq T \end{aligned} \tag{5}$$

where E_T is the total energy in the window T. Typical plots of NCE(t) for the four sediments are shown in Figure 3.

By determining NCE(t) over a time window Δt equal to the transmitted pulse length and beginning at the water sediment interface, an estimate of the proportion of coherent energy in a return is obtained. This value of the NCE(t) function is designated the normalized interface energy, E_Δ. E_Δ only approximates the coherent energy in the return, since the portion of the return within Δt also contains incoherent (noise) energy.

For rough bottoms, low values of normalized interface energy are expected. For smooth bottoms, E_Δ can be large or small dependant on whether the sediment is homogeneous or stratified.

Figure 4 shows a selection of E_Δ values for the four sediment types. A value of T = 40 msec was used for all the data except clay where T = 10 msec was selected. The track is over the same 500 m as shown in Figure 2. These values have also been averaged over 50 successive events where again the bar over the parameter denotes a spatial average. In total, the normalized interface energy was evaluated over a track length of 5.2 km. By using thresholds which optimize the separation of sediment types the resulting scatter matrix for all the data is shown in Table 2. The weighted average of correct classification based solely on the normalized interface energy, E_Δ, is 55%.

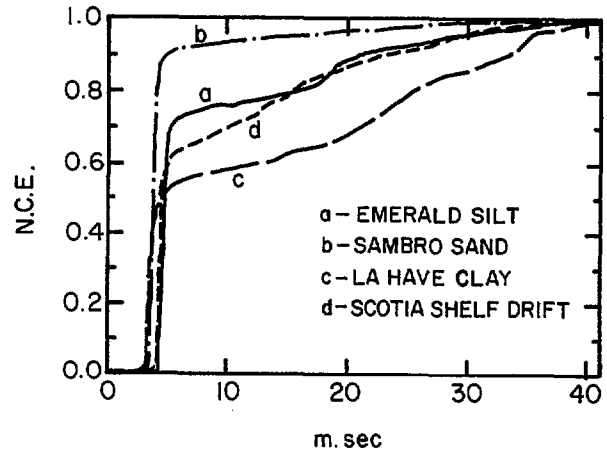

Figure 3. Normalized Cumulative Energy Functions for the Four Sediment types.

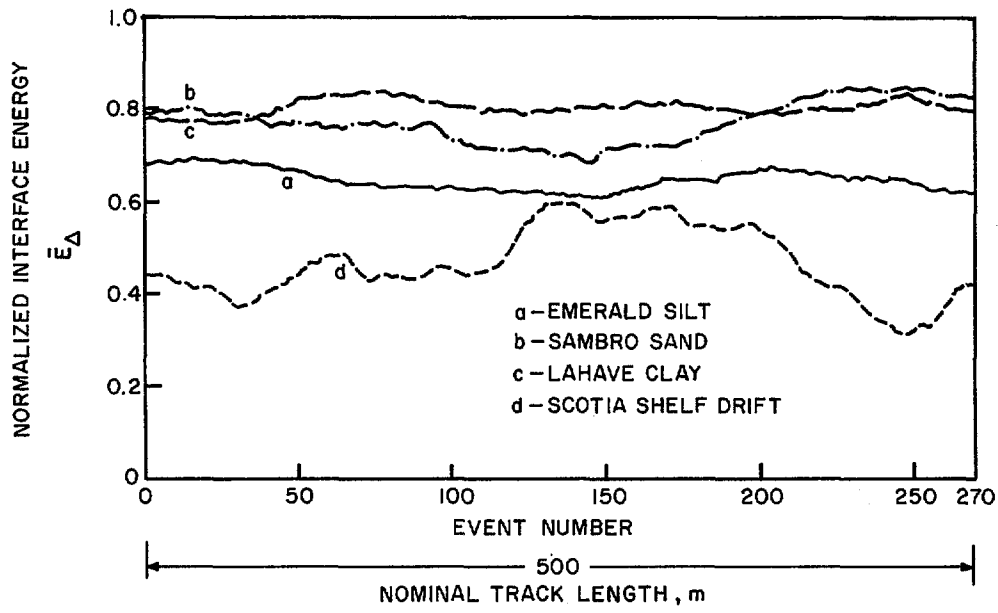

Figure 4. Typical Values of Normalized Interface Energy (running mean averaged over 50 echoes) vs. Track Length.

Table 2. Classification of sediment type based on the normalized interface energy compared with the reference classification of Drapeau and King (1972) and Fader et al (1977). Classification thresholds, E_T, are at the following levels; i) La Have Clay, $0.8 < E_T < 1.0$, ii) Sambro Sand, Gravel, $0.7 < E_T < 0.8$, iii) Emerald Silt, $0.5 < E_T < 0.7$, iv) Scotia Shelf Drift, $0.3 < E_T < 0.5$. Values shown are percentages.

Interface Energy Classification	Emerald Silt	Reference Sambro Sand	Base La Have Clay	Scotia Shelf Drift
Emerald Silt	64	30	1	33
Sambro Sand	-	49	53	-
La Have Clay	-	21	46	-
Scotia Shelf Drift	36	-	-	67
N° of Events	800	1140	380	270
Track Length (km)	1.6	2.3	0.8	0.5

6. Complementary Metrics

Classification errors arise when the values of the correlation coefficient or the normalized interface energy approach the thresholds separating sediment types. By combining both measures the complementary nature of the two metrics can be used to resolve the decision ambiguity.

A plot of the correlation coefficient, $\bar{\rho}_{i,i+1}$, versus the normalized interface energy, $\bar{E}_\Delta$ is shown in Figure 5. For the limited data base complete separation of the sediments is possible.

Silt is a smooth stratified sediment. This results in consistant echoes from the various layers and thus a high value of correlation coefficient. Proportionally less energy is reflected from the water sediment interface resulting in low values of normalized interface energy. Sand is a smooth homogeneous sediment resulting in high values of correlation coefficient and normalized interface energy. Fine grained clay is again a smooth homogeneous sediment but on the Scotian Shelf it is generally found in depressions in other

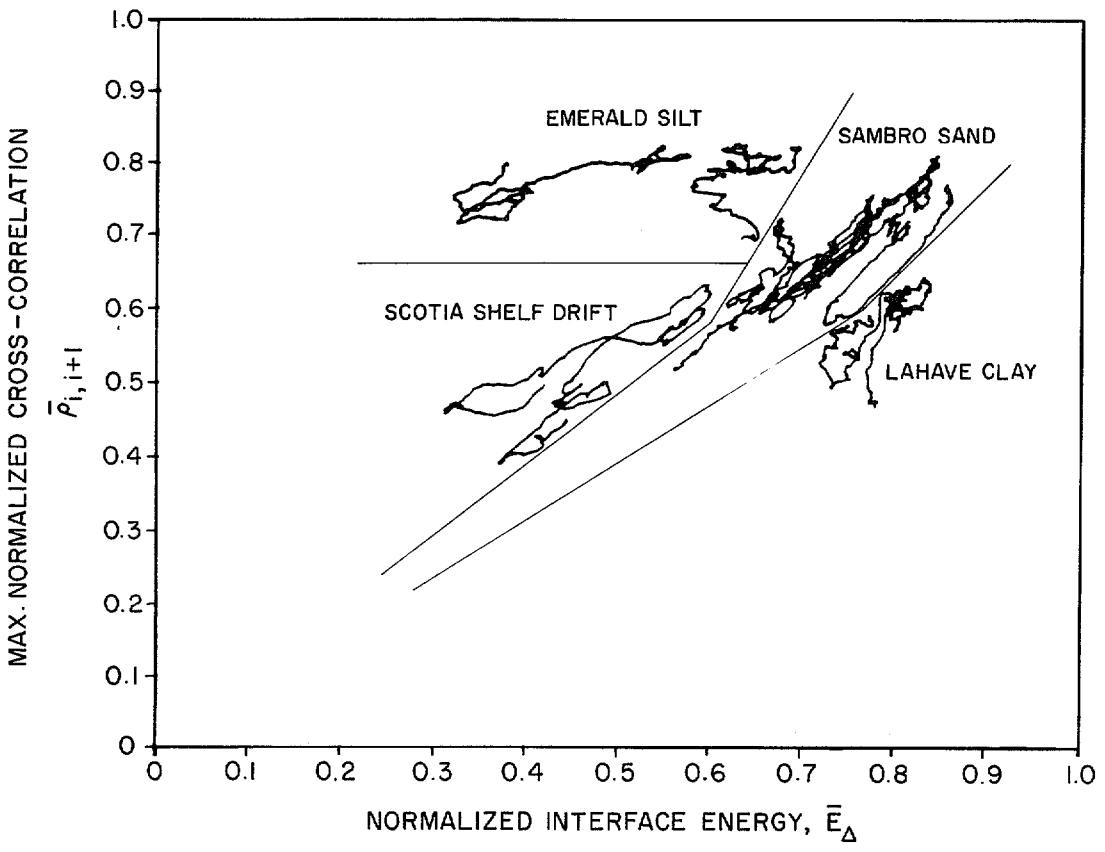

Figure 5. Classification Diagram Showing Separation of the Plane into Four Distinct Areas.

sediment types. It is highly transparent acoustically and this results in a large contribution to the total echo from the underlying layers. Thus the values of correlation coefficient shown for clay also depend on the underlying sediment. The high values of E_Δ are obtained by shortening the analysis window to eliminate the effects of the underlying sediments. Due to the high proportion of internal and surface scatterers the results for the Scotia Shelf drift exhibit the lowest values of correlation coefficient and of normalized interface energy.

7. Summary and Conclusions

Using a limited data base complete and automatic separation of four different sediment types is accomplished. The separation is based on two measures of echo coherency and their relationship to sediment roughness. The correlation coefficient gives a measure of overall likeness of two successive echoes where the magnitude of the coefficient decreases as the sediment roughness increases. The normalized interface energy measures the proportion of coherent energy returned from the water-sediment interface. In a complementary fashion the two measures aid in resolving classification ambiguities.

For a larger data base it is expected that overlap would occur in the classification zones. As a result additional metrics, e.g. the reflection coefficient, are needed to maintain separation among the various sediment types.

ACKNOWLEDGEMENTS

We would like to thank L.H. King and D.I. Ross (now of NORDCO Ltd.) of the Bedford Institute of Oceanography (Atlantic Geoscience Centre) particularly for making space available to us aboard C.S.S. Hudson during cruise 76-016. We would also like to thank P.G. Simpkin, R. Hutchins, and D.R. Parrot of HUNTEC ('70) Ltd. for access to the DTS equipment and for data support. Both groups have allowed us liberal access to the Seabed Research Programme.

The work is partially supported by a National Research Council of Canada operating grant.

REFERENCES

Clay, C.S. and Leong, W.K. (1974); "Acoustic Estimates of the Topography and Roughness Spectrum of the Seafloor Southwest of Iberian Pennisula." In Physics of Sound in Marine Sediments, Edited by Loyd Hampton, Plenum Press, pp. 373-446.

Drapeau, G. and L.H. King (1972); "Surficial Geology of the Yarmouth-Browns Bank Map Area." Ottawa, Information Canada, Marine Science Paper 2, pp. 6.

Fader, G., L.H. King and B. MacLean (1977); "Surficial Geology of the Eastern Gulf of Maine and Bay of Fundy." Marine Science Paper 19, Geological Survey of Canada, Paper 76-17.

Hutchins, R.W., D.L. McKeown and L.H. King (1976); "A Deep Tow High Resolution Seismic System for Continental Shelf Mapping." Geoscience Canada, Vol. 3, No. 2, pp. 95-100.

Knott, S.T., Hoskins, H. and LaCasce, E.O. (1977); "The Energetics of Normal Incidence Marine Seismic Profiles and Estimation of the Acoustic Impedance Structure of the Seabed." Proc. of International Symposium on Computer-Aided Seismic Analysis and Discrimination. Falmouth, Mass., U.S.A., IEEE Computer Soc.

MacIsaac, R.R., and A.D. Dunsiger (1978); "Ocean Sediment Properties using Acoustic Sensing." Proc. of 4th Int. Conf. on Port and Ocean Engineering under Arctic Conditions (POAC '77), pp. 1074-1086.

A MICROPROCESSOR ACOUSTIC DATA BUOY

R. C. Spindel K. R. Peal D. E. Koelsch

Woods Hole Oceanographic Institution
Woods Hole, Massachusetts 02543

Abstract

A unique microprocessor controlled digital instrument has been developed for the remote acquisition of underwater acoustic data. The buoy is designed to receive and process long range, low frequency transmissions. Currently it processes complement phase maximal-length shift-register sequences with a carrier frequency of 220 Hz, receives and processes transmissions from nearby moored beacons for phase tracking of buoy motion, and continuously records ambient temperature and time. Matched or inverse filtering of the pseudorandom sequences allows separation of acoustic multipaths for individual study of amplitude and travel time fluctuations. Software control results in a flexible system that is readily reprogrammed to accomodate different transmission parameters and types. The primary advantage of the microprocessor controller is that it enables sophisticated in situ processing and significant power and space economy.

1. Introduction

Several types of self-contained recording capsules have been used to receive underwater acoustic transmissions for the purpose of studying propagation effects. One class of instruments is characterized by analog recording techniques and the other by digital recording. Analog recorders usually offer greater data capacity, but have limited dynamic range and poor phase tracking between recorded channels.[1] Digital recorders are capable of wide dynamic ranges and excellent phase tracking, however, extensive signal processing is required to compress the data in order to achieve recording times comparable to analog systems. Data compression has been achieved through combinations of analog and hardwired digital processing leading to rather inflexible data acquisition systems whose specifications were suited only for a particular type of signal transmission.[2] The advent of the microprocessor allows the design of data gathering buoys with digital signal processing algorithms that can be readily changed simply by altering software routines. The result is a compact system that is adaptable to a wide variety of signal types.

The recording buoy described in this paper was designed to be fixed to deep ocean moorings at depths up to 5000 m. Included in this paper is a brief description of its first deployments where it was used to process and record phase encoded transmissions for the purpose of measuring acoustic travel time variations between a moored source and moored receiver over distances up to 1000 km.

2. The Receiving Buoy

A block diagram of the data gathering functions of the buoy is shown in Figure 1.

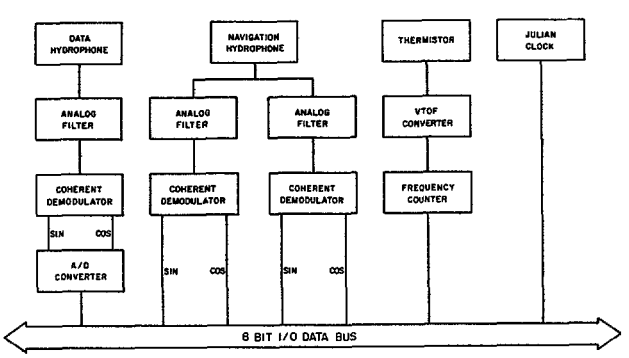

Fig. 1 Block diagram of acoustic buoy data inputs.

The system is oriented around an 8-bit data bus which interconnects all input-output functions. Acoustic propagation data is received by the data hydrophone, is bandpass filtered, coherently demodulated and converted to digital form (12 bits) before routing to the bus. The acoustic buoy is equipped with a Doppler navigation system to measure mooring motion, i.e. to measure horizontal displacements of the buoy and its data hydrophone. This system has been described in detail elsewhere.[3,4] Briefly, it consists of acoustic beacons rigidly moored near the ocean bottom. A continuous tone from each beacon is received by

a hydrophone on the data buoy. The transmit frequencies of these beacons (near 13 kHz) are known so that departures from the nominal beacon frequencies can be measured in the buoy. Such departures are Doppler shifts induced by buoy motion. Point-to-point displacements of as little as a few centimeters can be measured with this system. Ambient ocean temperature and time information is also applied to the bus. Additional I/O ports are available for other sensors, such as pressure or sound velocity.

In Figure 2 the digital portion of the system is shown with the analog inputs compressed into a single box. An RCA 1802 microprocessor was selected for this application simply because it is constructed using CMOS technology and therefore requires little operating power.

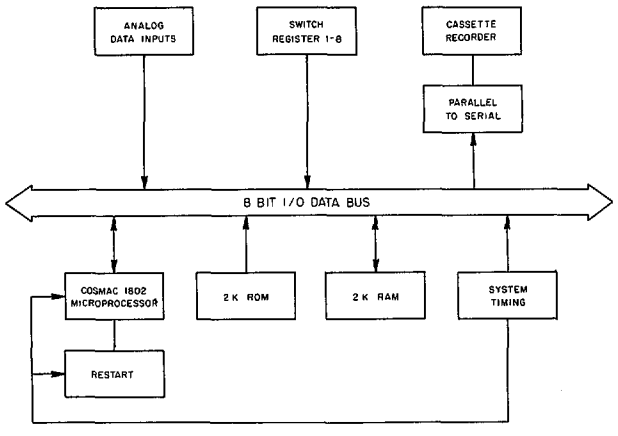

Fig.2 Block diagram of digital portion of the acoustic data buoy.

This is a vital consideration in remote, in situ, battery powered devices such as the present buoy. Similarly, system ROM (Harris 6611) and RAM (AMI 5101) are also CMOS devices. A total of 4096 8-bit bytes is shared equally between ROM and RAM. Under normal conditions the system program, including all control and processing algorithms, is stored in ROM while all data manipulation takes place in RAM. Eight 8-bit switch registers are provided to enable operator adjustment of software parameters without reprogramming. All data are recorded on a digital cassette which stores 10^7 bits on 300 ft. of 1/8" tape.[5]

Since the buoy is a remote device, designed to be deployed for periods up to one year, precautions must be taken to insure reliable operation. Each time data is recorded a hardware restart timer is set and after a predetermined period of time has elapsed a restart procedure is executed unless the timer has been reset. Several software restart procedures are included as well. The first memory location after the program in ROM contains the sum of all program instructions times minus one. A check is made after each program cycle by summing all the program instructions and the quantity stored in this location. A sum other than zero forces a program restart. Only a single 1K RAM is used for data manipulation. Alternate 1K RAMs are used during successive iterations of the ROM program while the inactive RAM is exercised with a test program. In the event that an error is detected during the test, the program prevents further use of this RAM until the failure clears. To further reliability, software timers are used whenever the 1802 must wait for an external event. If the timer overflows the event is bypassed and the program continues. These timers are used for tape writes, clock reads, A/D conversions and for any data transfers requested by external devices. Thus a failure of any of these functions does not permanently halt data acquisition.

The entire system is packaged in a cylindrical pressure housing 15 cm in diameter, 1.3 m long and rated for 10,000 psi (Figure 3). Navigation and data hydrophones can be attached directly to the pressure case or they can be mounted remotely. Power is supplied by a lithium battery stack which is packaged separately in a smaller cylindrical container. Total power consumption is about 0.75 watts for the entire

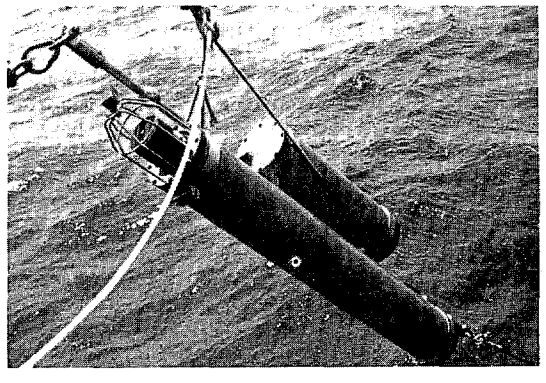

Fig. 3 Photograph of the data buoy during deployment. The smaller cylindrical case contains the lithium battery stack.

system plus an additional 0.25 watts for a precision crystal oscillator and oven.

3. An Application

During its first deployments the buoy was used to receive and process complement phase, maximal-length, shift register sequences that were transmitted with a carrier frequency of 220 Hz. The experiment consisted of transmitting the signal between a moored acoustic source and several acoustic data buoys moored at various ranges. The acoustic travel time between source and receiver is a measure of the average sound velocity structure of the intervening ocean path. Dynamic variations in the ocean cause corresponding changes in average temperature (as well as salinity, density, etc.). Sound velocity is a strong function of temperature so that variations in acoustic travel time as a function of time yield a time series that can be related to ocean dynamics. The transmitted signal was a broadband code, recompressed upon reception in order to measure travel time.

A travel time resolution of approximately 0.1 s and a sampling rate of 15 samples/hour was required. These parameters are consistent with the time between groups of early arrivals in SOFAR transmissions (about 0.5 s), the expected variation in travel time due to large scale (100 km) ocean features (about 0.1 to 0.5 s), expected spreading of a 0.1 s pulse due to relatively rapid time variations in the medium (about 15 msec at 500 km), and the correlation time of the ocean for the particular frequency and ranges employed (about 5 min at 200 Hz and 500 km). A coded signal was transmitted to limit transmitter peak power requirements. The specific pseudorandom code employed has minimal side lobes upon recompression.

Figure 4 illustrates these ideas. Shown is a schematic representation of the multipath reception of a single infinitely narrow pulse transmitted between source and receiver on the axis of the deep sound channel.[6] The multipaths arrive in groups; each group is usually composed of three constituent arrivals if the source and receiver are exactly on the axis. If one is slightly off axis four arrivals are usual. The transmitted signal will not resolve group constituents, but rather resolves the entire group itself. At the bottom of the figure an expected shift in group arrival time due to ocean dynamic changes is shown. Travel time changes of this order are associated with dynamic processes having distance scales of about 100 km (called the mesoscale) and time scales of about 30 days.

The specific transmitted signal consisted of a 63 digit pseudorandom sequence with alternate digits encoded by ±45° phase changes of the 220 Hz carrier. Each digit was d = 0.1 s long and contained 22 cycles of the carrier. The total sequence lasted 63 digits x 0.1 s/digit =

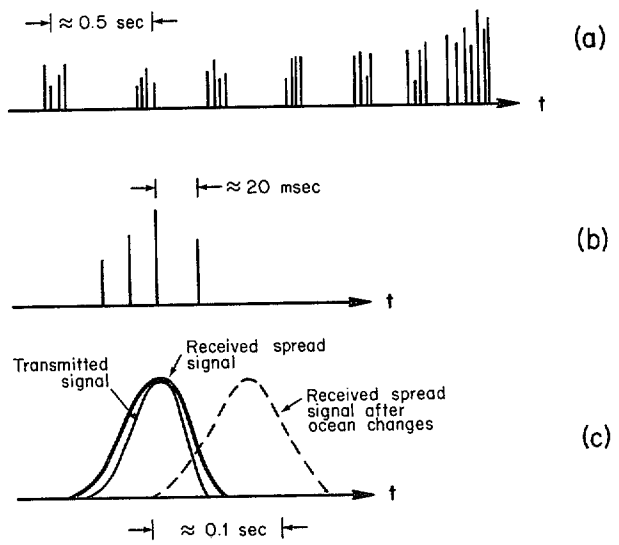

Fig. 4 Typical pulse arrival sequence for an impulsive source and receiver near the axis of the deep sound channel (a), a group of arrivals (b), and expected shift of actual received pulse whose resolution cannot resolve constituent arrivals within a group (c).

6.3 s and was repeated 10 times during a 63 s interval. Repetitive transmissions of the 63 second signal occurred every four minutes.

The frequency spectrum of the transmitted signal is shown in Figure 5a, its correlation function in Figure 5b. Half the transmitted power is contained in the carrier line at 220 Hz and half of the remaining power is spread over an 8.8 Hz -3 db bandwidth. The received signal can be match filtered for optimum signal-to-noise or it can be inverse filtered for optimum time resolution. The time resolution of the signal is determined by the transmitted bandwidth and is decreased by any filtering of the received signal. Unfortunately, inverse filtering requires that there be no zeros in the spectrum of the transmitted signal so it was sharply filtered in a B = 15 Hz band centered on the carrier. Resolution is therefore limited to about 0.13 s.

The digital buoy receives, processes and records a signal with the following waveform

$$r(t) = \sum_{k=-K}^{K} c_k e^{j\frac{2\pi k}{L}(t-\tau)} e^{j2\pi f_0 (t-\tau)}$$

where the c_k are the Fourier coefficients for the sequence, τ is the gross delay encountered in traveling from source to receiver, L is the length of the sequence (6.3 s) and f_o is the

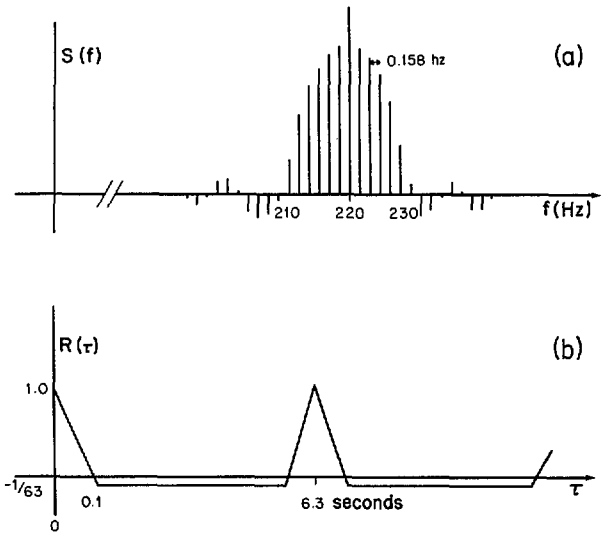

Fig. 5 Power spectrum of transmitted pseudo-random sequence (a), and autocorrelation function of an infinite number of sound sequences repeated every 6.3 seconds.

220 Hz carrier frequency. K is the largest integer less than BL/2 thereby assuring the absence of zeros in the spectrum of the transmitted signal. The program in the data capsule removes τ (which is preset via sense switches). Analog conditioning heterodynes the signal to baseband (0 Hz) and produces the demodulates

$$r_o(t) = \sum_{k=-K}^{K} c_k \left[\cos \frac{2\pi k t}{L} + j \sin \frac{2\pi k t}{L}\right].$$

They are converted to digital form and sampled at s = 10 Hz yielding one sample per transmitted digit. The samples from each of the 10 consecutive repetitions of the basic 6.3 s sequence are averaged in memory before writing on tape. Tape writes are through Direct Memory Access (DMA). The program also causes an appropriate calibration signal to be written as well as navigation information, temperature and time data. With this type of processing a single 300 ft cassette can store 12 continuous days of data.

4. Results

Examples of data recorded with the microprocessor buoy are shown in Figures 6 and 7. Figure 6a shows 40 minutes of recompressed pulse data taken with the instrument in the laboratory. The signal was fed directly to the data buoy with no noise present; it had an arbitrary fixed delay of about 4.2 seconds. Figure 6b shows about three hours of data taken with the buoy at sea and with the receiving hydrophone attached to a radio-telemetering free drifting buoy. The source was moored in 5000 m of water at a depth of 1050 m. During the time period shown the hydrophone drifted first towards the source and then away from the source evidenced by a decreasing followed by an increasing arrival time. Source to receiver range was about 4 km. Figure 6c shows one hour of data taken at a range of 100 km with the source and receiver both moored at a depth of 1050 m. The received signal is somewhat noisier than in Figure 6b. No data is available presently for a long enough period of time to observe travel time variations due to mesoscale (100 km) ocean changes, however, at the present time three receiving buoys are deployed for a two month period in order to make such measurements.

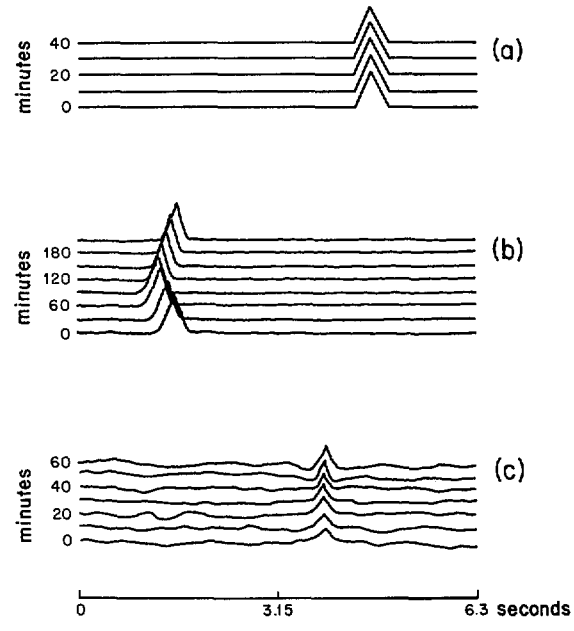

Fig. 6 Example of data received by the buoy. In (a) a noise free input signal was simulated in the laboratory; in (b) the input was from a drifting hydrophone; in (c) the buoy was moored 100 km from the source.

Figure 7 shows data buoy motion for a 5½ day period measured via the navigation hydrophone and bottom moored beacons. Motion is primarily tidal with two complete cycles/day. This is consistent with previous observations taken with a digital hardwired instrument.[4]

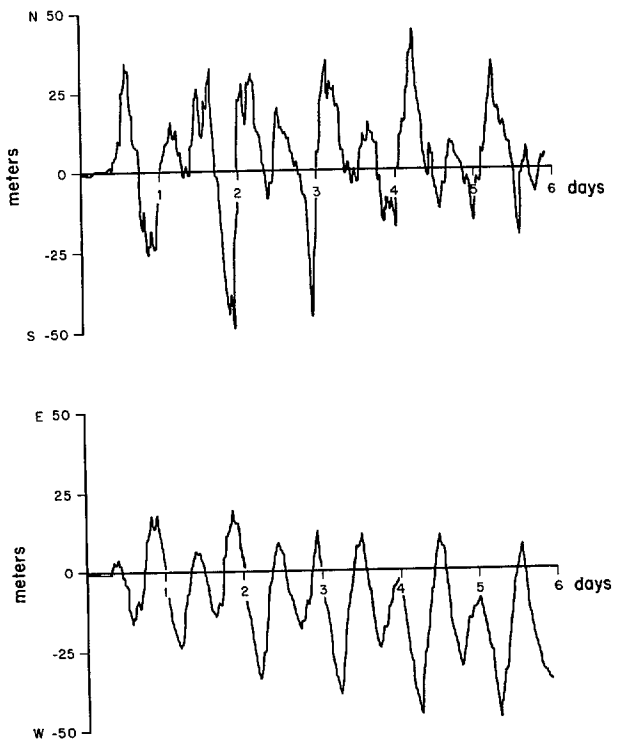

Fig. 7 Data buoy motion in the north-south and east-west directions. The buoy was attached to a single point mooring about 3000 m above the ocean bottom. Peak excursions are about 100 m and peak energy is at the tidal frequency of 2 cycles/day.

5. Summary

We have described the basic configuration of a microprocessor based acoustic data buoy and have shown some examples of its operation when used to record complex underwater signal transmissions. The microprocessor is an ideal choice for signal processing and data formatting in a remote instrument of this type. It is easily reprogrammed to accomodate different data inputs, it is compact, and if a CMOS type is chosen it is power conservative.

This development was supported by ONR contract N00014-77-C-0196 and ONR contract N00014-74-C-0262;NR 083-004. This is contribution number 4168 of the Woods Hole Oceanographic Institution.

References

1. A typical example of an analog system is the Acoustic Data Capsule (ACODAC). See Daubin et al, "The ACODAC System", Woods Hole Oceanographic Institution, Woods Hole, Massachusetts, Technical Report WHOI 72-87, November 1972.

2. A typical example of such a digital system is the Digital Buoy System (DIBOS). See Spindel et al, "A Mobile Coherent Low-Frequency Acoustic Range". IEEE J.Oceanic Eng., OE-2, 331-337, 1977.

3. Spindel, R. C., Porter, R. P., Marquet, W. M. and Durham, J. L., "A High-Resolution Pulse-Doppler Underwater Acoustic Navigation System", IEEE J.Oceanic Eng., OE-1, 6-13, 1976.

4. Spindel, R. C., Porter,R. P., and Schwoerer, J. A., "Acoustic Phase Tracking of Ocean Moorings", IEEE J.Oceanic Eng., OE-3, 27-30, 1978.

5. Sea Data Corporation, Newton, Massachusetts.

6. The deep sound is the locus of all points at the depth of the sound velocity minimum in the water column. At mid-latitudes in the Atlantic (say at 30°N) it is about 1200 m deep. In the Pacific it is about 100 m deep at the same latitude.

A LOW-POWER MICROPROCESSOR SYSTEM FOR DEEP-SEA FREE VEHICLE APPLICATIONS

R. E. Ackermann, C. M. Butler and R. F. Weiss
Scripps Institution of Oceanography
University of California, San Diego
La Jolla, California 92093

Abstract

A microprocessor system is being developed for control of a deep-ocean free vehicle. The RCA COSMAC microprocessor was selected for its architecture and CMOS support circuits. A CPU card, using CMOS UV PROM, can operate alone or in conjunction with support cards such as I/O and mass storage. I/O is accomplished either by interrupt and status techniques or with CPU strobing. The development system consists of an HP 9845 desk top computer connected to a development card-cage by an RS232 link. The development cage contains a PROM programmer, circuits under test, and other testing aids. This system, using a BASIC editor and assembler, facilitates rapid programming and hardware checkout. Flexibility in troubleshooting is provided by combined use of signature analysis and monitor diagnostic firmware.

Introduction

The microprocessor system described here is being developed for control of a deep-ocean free vehicle, the MANOP Bottom Lander, which will carry out measurements at the sediment-water interface related to the formation of ferromanganese nodules. The Lander is designed for deployments lasting as long as one year during which water and sediment samples will be collected from each of three chambers in which chemical and biological processes are being monitored. In addition to the sampling program, the Lander will be capable of monitoring pH and dissolved oxygen and of injecting tracers into each of the chambers. The preliminary design of the Lander is described by Weiss et al. (1977).

The process control functions of the Lander are summarized in Figure 1. Each chamber is controlled by its own dedicated processor and centralized Lander functions such as acoustic communications, ballast release and data storage will be controlled by the data microprocessor. Although this microprocessor system is still in fabrication, we hope that by presenting our work at this stage we will inspire worthwhile dialogue within the oceanographic community.

COSMAC 1802

In a free vehicle operating on stored energy, power consumption is a major concern. Choices of microprocessors are thus reduced to three. The SBP-9900 (I^2L) processor (Texas

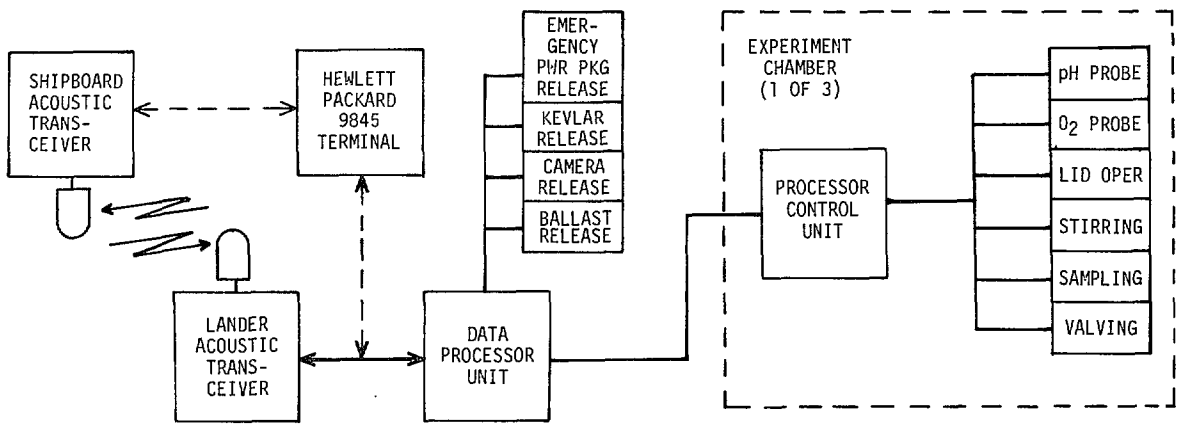

Figure 1. Microprocessor control functions for the MANOP Bottom Lander. The acoustic link is used during the deployment for control and operational verification. The Hewlett-Packard 9845 terminal is used for pre-deployment programming and system checkout, as well as for acoustic communication and data reduction.

Instruments) is currently supported by TTL circuits which consume unreasonably large amounts of current for this application. The 6100 processor (Harris and Intersil) is supported by a family of CMOS circuits, but its cumbersome data transfer structure and non-standard 12-bit word length are less than ideal. However, because the 6100 is compatible with DEC's PDP-8 software, those laboratories which have access to a PDP-8 computer may find this approach more advantageous. The COSMAC 1802 processor (RCA) is supported by CMOS circuits, and has 16-bit addressing in conjunction with a separate 8-bit data bus. This 8-bit capability is valuable, since most data is handled in 8-bit bytes and since most terminals use ASCII characters which are formatted in 8 bits.

System Architecture

The main factor determining system architechture, aside from the selected CPU device, is the geometry of the available space. Constrained by cylindrical pressure housings of 15 cm maximum inside diameter and considering the need for flexibility of the hardware configuration, circular-type plug-in boards were chosen. For ease of troubleshooting it is necessary that the CPU card be able to stand alone. This requires that it contain the CPU device, some RAM, some ROM, an I/O port, and a clock generator. The presence of an I/O port requires I/O select circuits and an interrupt structure (both described below). RAM and ROM on the CPU card are limited by the physical space needed for other required circuits to only 640 bytes (512 bytes of Intersil IM-6604 UV PROM and 128 bytes of static RCA CDP-1823 RAM). Because of the need to supply additional modular memory and still preserve the simplicity of the memory chip select circuitry, a 2k-byte "piggyback" memory was designed for use with the CPU card. The same "piggyback" memory added to a 2k memory card gives a 4k-byte module. This approach results in a memory hierarchy of sixteen 4k-byte pages. Each page contains four 1k=byte sectors, and each sector can be either RAM or UV PROM.

The system bus architecture is shown schematically in Figure 2. All signals necessary for interconnecting memory cards, I/O cards, and the CPU card are provided by a 50-conductor ribbon cable back-plane running the length of the pressure housing with 50-pin connectors spaced at 1.8 cm intervals. Memory cards are distinguished from I/O cards by the selection system: memory is selected by the address bus using two 8-bit bytes and I/O cards are selected by the I/O select bus. Any other connections, such as those which lead outside the microprocessor system, are accomplished by connectors peculiar to the specific I/O card.

Interface

I/O devices provide, in some configuration, the means of data collection, control, and communication with other systems. The I/O cards are addressed by the CPU using the 7 program=controlled lines of the I/O select bus. Further selection within each I/O card is accomplished by the device bus. I/O devices transferring information to the CPU initiate the process via a priority encoder which generates an interrupt on the interrupt bus and sets an identification code on the status bus. Any individual input port can generate interrupts through the priority encoder. The CPU can poll the I/O devices via the I/O select bus and identify the interrupter via the status bus. Any interrupt or status signal can be disabled by the CPU.

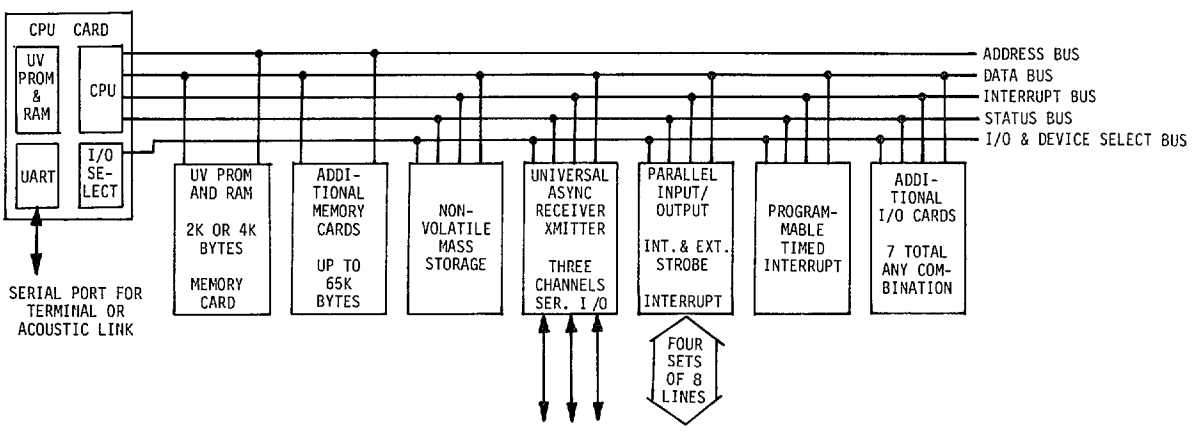

Figure 2. Bus architecture for an individual microprocessor system. I/O and memory cards are shown as they are connected to the 50-conductor ribbon cable back-plane. Signals entering or leaving the microprocessor system are shown vertically.

The parallel input/output (PIO) card has four 8-bit ports with associated strobes: one of fixed input, one of fixed output, and two which are defined by how the chips are inserted into the board. Through software control, the input ports can strobe incoming data, either by external signals causing an interrupt or by CPU strobing.

The UART card has 3 universal asynchronous receiver transmitters which provide for serial information transfers. This card, like the PIO, uses the interrupt, I/O select, and I/O device busses.

The non-volatile mass storage card is an I/O device which allows large amounts of data to be stored without direct memory addressing and without meeting the constraints of CPU memory timing. Several storage techniques, including magnetic bubbles, have been explored but no design has yet been selected.

The programmable timed interrupt card provides the CPU with a hardware interrupt used for timekeeping and for initiating repetitive operations. Time-interval programming and interrupt suppression are under control of the device bus in conjunction with an I/O select line.

Hardware and Software Development System

In order to write and debug a microprocessor program, some sort of computer and software are required. A minimal system consists of the processor for which the program is intended, a firmware monitor, and a terminal. However, programming with such a system is generally slow, tedious, and prone to error. Several alternatives exist, including an emulator, run on a time-shared system. In this approach programs are loaded, edited, and run on hardware other than that for which they are intended, so that the use of custom interfaces can create problems. Another alternative is to load, edit, and assemble programs on a general purpose computer which is interfaced to the processor for which the program is intended. Assembled programs can then be loaded into the microprocessor using a firmware monitor and run under real conditions. Still another alternative is the in-circuit emulator (ICE) which is a dedicated system specifically designed to write and debug microprocessor software. These systems run the programs on the microprocessor under real conditions. An ICE is probably the most time-efficient method of producing microprocessor software, however such a system is expensive and is sometimes rendered obsolete by rapidly advancing technology.

In the case of the Lander project, a small general-purpose computer is required for data reduction and to handle shipboard acoustic communication with the Lander. Since the need for microprocessor software development is expected to diminish once the Lander deployments are underway, and since only small-to-moderate amounts of software are required, the use of such a computer to write and debug microprocessor programs represents an ideal solution. To meet these needs, the Lander project has acquired a Hewlett-Packard 9845S desk-top computer. This machine is interfaced to the RCA 1802 microprocessor system via an RS232 link using a version of the RCA CDPR512D monitor. Currently, an editor and assembler, written in BASIC, are running on the HP9845 and a linking loader is now being written. With these programs, and with the use of structured programming on the microprocessor software, we feel that programmer efficiency can come close to an ICE and still remain sufficiently flexible to keep pace with the development of new components.

To further facilitate the debugging process we have built a development card-cage in

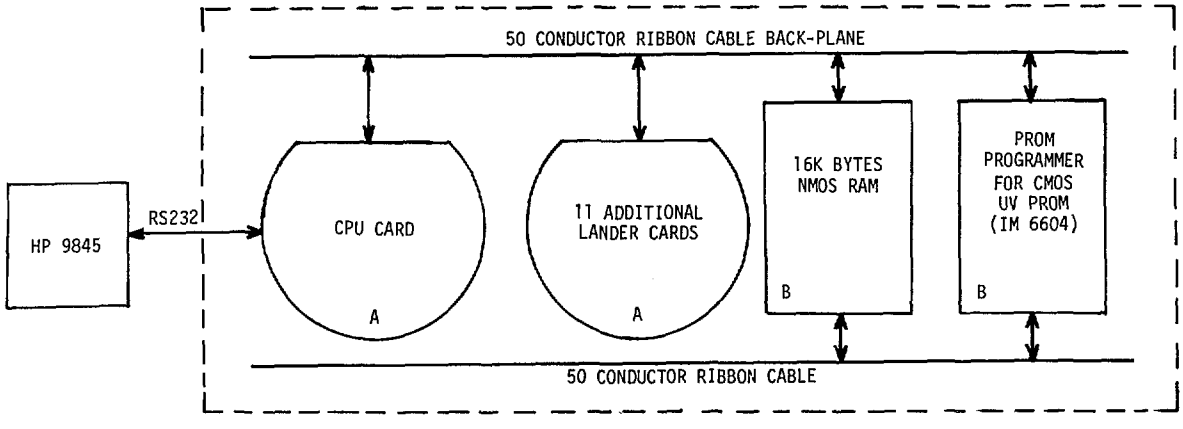

Figure 3. Block diagram for the development card-cage. Cards designated "A" and shown as circular segments are Lander cards. The CPU card is needed for the card-cage operation and the additional slots are used to test other Lander cards. Cards designated "B" and shown as rectangles are required to program UV PROMs, developing software, etc. (see text).

which cards can be conveniently operated on the bench. This card-cage also accomodates a PROM programmer, one or more 16k RAM boards, and other testing aids. As indicated by the card-cage block diagram shown in Figure 3, this card-cage duplicates the 50-conductor ribbon cable back-plane in the Lander hardware and provides an additional 50-conductor ribbon cable for interconnecting testing aids, a PROM programmer, and any additional cards which cannot be supported by the Lander back-plane. This card-cage accomodates up to 12 Lander cards and 5 support cards.

Troubleshooting

The microprocessor system hardware can be tested and faults can be located precisely by means of two different approaches. The most direct approach is an internal diagnostic program called from the terminal by the monitor diagnostic firmware. Troubleshooting of memory and I/O cards can be accomplished via the terminal and the monitor firmware. This mode of troubleshooting expedites location of faulty circuit cards but, depending upon the availability of spare boards, may require use of the signature analyzer to locate faulty IC's (see Hewlett-Packard Application Note 222, 1977).

In the event that the problem is such that the diagnostic program does not function, then signature analysis is a useful troubleshooting aid. A switch on the CPU card modifies the address decoding such that program operation begins in the signature analysis firmware (starting address 2048) at power-up. For this program to execute properly, only the CPU clock, self-test UV PROM, CPU device, and the first byte address latch must be operating. The program runs in a tight loop enabling a signature analyzer to examine the bus nodes for their characteristic signatures. If the signature pattern of a node does not match that generated during proper operation, then the source or loads of that node are defective. By isolating the loads the defective IC can be located. The first test-loop is tight and exercises the minimum number of ICs. Additional loops can be entered by loading selective sense lines with a test lead. As the number of ICs involved in the loop is increased, the testing becomes more nearly complete. Each node and every IC can be tested in this way.

Summary

Although the microprocessor system we describe has been designed for application to a specific free vehicle, the MANOP Bottom Lander, we believe that this system may easily be adapted to other oceanographic instruments which depend upon limited in situ power sources. The system is easily packaged in conventional pressure housings and is modular to the extent that the complexity and function of the system can be varied by the selection of appropriate memory and I/O cards. For a medium-sized system, the total power consumption is on the order of 10 milliwatts. Location and repair of faults are greatly facilitated by the use of diagnostic programs and signature analysis.

Acknowledgements

We thank F. K. Mansir, whose craftsmanship and ideas are helping to make the hardware a reality. This work is supported by the U. S. National Science Foundation as part of the International Decade of Ocean Exploration, Manganese Nodule Program.

References

Hewlett-Packard Company, "A designer's guide to signature analysis", Application Note 222, 50 pp (1977).

Weiss, R. F., O. H. Kirsten and R. Ackermann, Free vehicle instrumentation for the in situ measurement of processes controlling the formation of deep-sea ferromanganese nodules, in Oceans '77 Conference Record, paper 44D, Marine Technology Society and Institute of Electrical and Electronics Engineers (1977).

REAL TIME OCEANOGRAPHIC DATA FROM GEORGES BANK

Robert N. Lobecker Gary Milano Ron Franklin Earl Lind

Raytheon Environmental and Oceanographic Services
P.O. Box 360, Portsmouth, R.I. 02871
Telephone 401-847-8000

Abstract

A complete data system has been developed to gather, process and telemeter oceanographic data from Georges Bank on the outer continental shelf. It consists of a microprocessor based central processing unit collecting data, performing calculations and controlling interfacing devices; sensors for measuring current speed, magnetic heading, conductivity, temperature and bottom pressure; an on-board tape recorder; and a satellite telemetry link.

The microprocessor allows extensive in-situ calculations to be accomplished including sensor nonlinearity corrections, salinity from conductivity and temperature, resolution of current and heading into NS/EW vectors, digital filtering, mean product calculation and data averaging. Hourly transmissions of processed data are immediately available for viewing and analysis. Operational units were deployed beginning in the fall of 1977.

I. Introduction

In 1976 the U.S. Bureau of Land Management initiated a physical oceanographic study as part of the environmental studies program for the New England outer continental shelf. The Georges Bank region of the outer shelf is soon to undergo test drillings for gas and oil. A three-fold data collection program was launched to acquire information on surface currents, subsurface currents and associated parameters, and hydrography. This paper deals with the data acquisition system developed to measure subsurface currents.

The oceanography of Georges Bank is extremely complex being bound on one side by the North Atlantic and a cyclical seasonal frontal zone and on the other by the Gulf of Maine and the Bay of Fundy with its extreme tides. Additionally, meandering Gulf Stream eddies, wind driven currents, and deep reaching waves are expected to color the data. A known elliptical tidal circulation predominates on Georges Bank.[2,5] What is desired is to further define the seasonal variations of this flow and to model the residence times and eventual trajectories of parcels of water. The Argo Merchant spill of December 1976 occurred immediately adjacent to the study area providing a before-the-fact calibration of models and underlining the necessity for undertaking the study.

Design of the system was initiated in September of 1976. A prototype mooring was deployed on Nantucket Shoals in March of 1977. A fully-instrumented engineering model successfully operated in September 1977. Two systems were deployed in the Georges Bank study area during the winter 1977-78 and three during June of 1978 to monitor spring and summer conditions.

The mechanical and mooring designs of the buoy platform are discussed in reference 1.

II. System Design

Parameters required to be measured include current speed and direction, conductivity, temperature, and bottom pressure. Current, conductivity, and temperature are required at three depths: near-surface, mid-depth, and near-bottom; temperature is additionally sensed at 10-meter intervals between the primary measuring depths. Calculations of salinity (from conductivity and temperature)[4], NS-EW current velocities and mean products of current with salinity and temperature are required at the three primary depths. The measured and calculated data are averaged over 30-minute periods.

The calculation of salinity, resolved currents and mean products is undertaken in-situ rather than later during data reduction in order to obtain a valid mean product. The mean of the products $(\overline{C \times S, T})$ calculated prior to averaging will differ from the product of the means $(\bar{C} \times \bar{S}, \bar{T})$ as a function of the phase relationships of the input variables. The mean product is important in characterizing mass transport.

Input information, derived from wave particle motion or from mooring motion, having periods 3 seconds and larger is filtered from processed data. Smaller period waves only exist near the surface and their effects are not felt at the 10-meter depth of the upper sensor package.[6,8] Analysis of mooring dynamics indicates that no

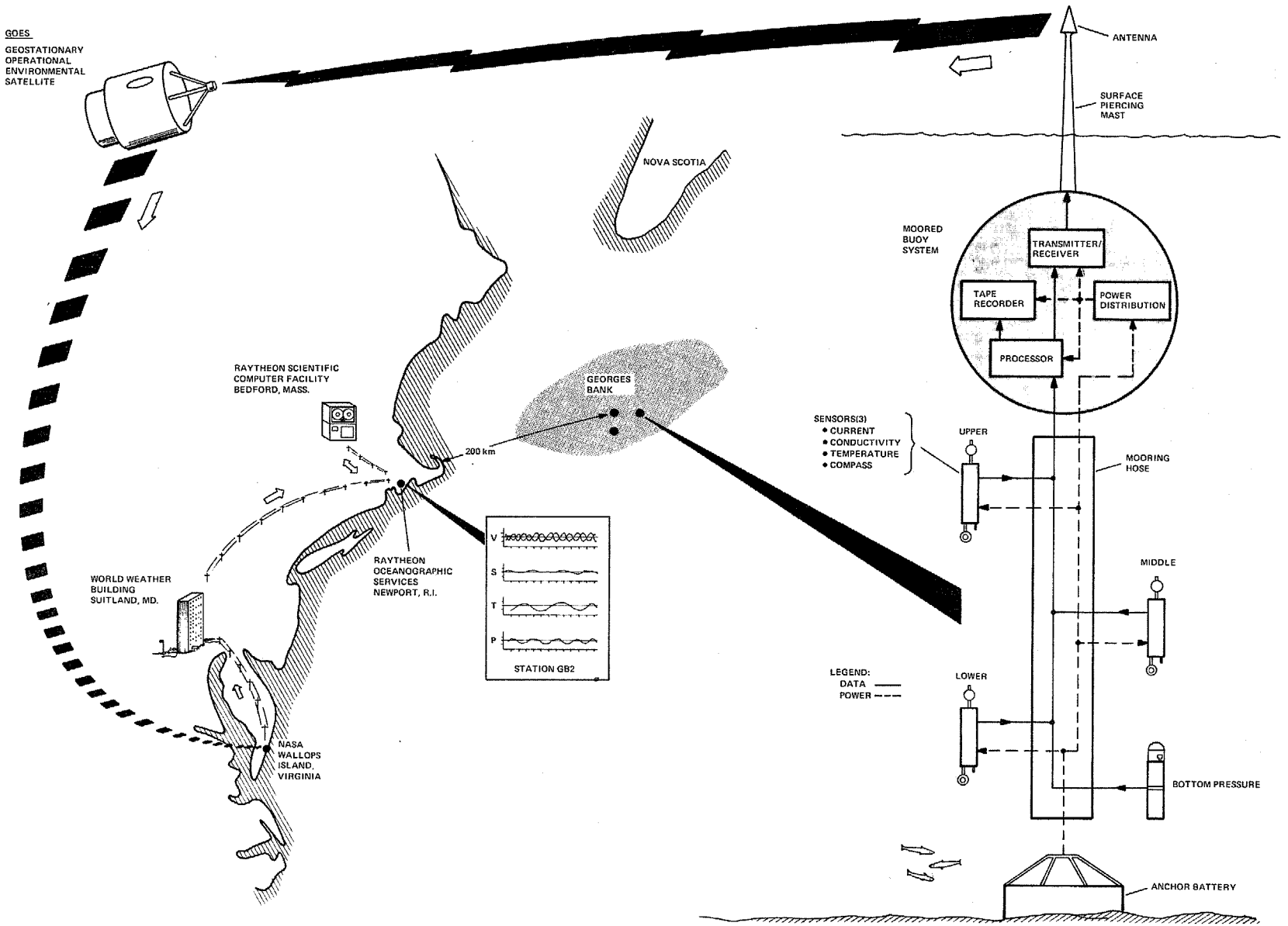

Figure 1. Oceanographic Data Acquisition System

mooring motions having periods shorter than 3 seconds will occur.[3] Accordingly, the sample rate for current and compass data is set at one second. The current and compass sensors have matching short time constants of one to two seconds in order to accurately resolve small period inputs while maintaining their phase relationships before the in-situ resolution calculation is made. After this calculation a digital filter having a time constant of 30 seconds is applied. A wave period of two seconds is theoretically resolvable according to the Nyquist criteria.

Conductivity and temperature are not affected by wave action to the extent of current and compass data, so their sampling rates are set at 4 seconds. Additionally, a single pole filter (τ = 30 seconds) is applied to their outputs prior to sampling.

Preserved data, that which is included in the 30-minute average, have periods greater than 30 sec and include internal waves and other phenomena having periods between 30 sec and one hour. Note that these are not resolved, since a 30-minute average is being taken. Aliasing of data caused by discrete sampling has been reduced to negligible levels with the above described sampling plan.[9]

Bottom pressure samples taken once each half hour are integrated for a period of 3.6 minutes, thus eliminating surface wave-induced pressures which would otherwise contaminate data.[10]

At the front end of the data acquisition system are the sensors. In order to resolve anticipated vertical variations in salinity and temperature, and particularly to compute the small cross-isobath transport, extremely accurate sensors are required. Accordingly, meticulous care has gone into their specification and calibration. Primary, traceable standards have been utilized in current, conductivity and temperature calibrations.

A telemetry link providing real time viewing of data has been incorporated into the data acquisition system. The GOES (Geostationary Operational Environmental Satellite) system is utilized with printouts of data available for review and analysis immediately as it is taken.

A final requirement of the system is to record on command several days of raw unaveraged data. A bank of sequentially activated tape recorders is included to record current and compass values once each second and conductivity and temperature once each four seconds. Short period (2 hour to 30 second) spectral analyses can be performed on this information using appropriate Fourier techniques and weighting functions to account for attenuated information.

III. Processor

At the heart of the buoy system is the Intel 8080 based microprocessor subsystem. The processor controls the operation of other buoy subsystems, collects data from the remote sensor units, preprocesses this data, and effects data storage and transmission.

Hardware Description

The microprocessor subsystem is composed of four main components; the processor card cage and function modules, the power distribution unit, the magnetic tape storage unit, and the secondary battery power units. The microprocessor subsystem requires an average of 25 watts power, about half of which is due to conversion inefficiency.

A block diagram of the processor subsystem is given in Figure 2. The entire subsystem is contained within the subsurface mooring buoy.

The card cage contains thirteen modules which perform thirteen distinct functions:

- Central Processing (CPU)
- Random Access Memory (RAM)—2K
- Programmable Read Only Memory (PROM)—8K
- Real Time Clock
- Watch Dog Timer
- Interrupting Timer
- Tape Storage Unit Interface
- Telemetry Subsystem Buffer/Interface
- Switching Control for the Tape Unit
- Sensor Package Addressing
- Data Multiplexing of Sensor Information
- A/D Conversion of Analog Data
- Bottom Pressure Sensor Interface

Each module is a low power version of Raytheon's family of modular, plug-in printed circuit modules (Watchstander™ modules). To ensure failure-free (or nearly so) performance during field deployments, high reliability (military grade "B-2") components have been used throughout. The modules are currently being used in other industrial and maritime applications where reliability, maintainability and ruggedness are essential.

The power distribution unit provides for the power conversion to the appropriate voltage levels required for operation of the processor modules, magnetic tape unit, and telemetry subsystem. It also contains the switching relays to power strobe the magnetic tape unit.

During telemetry transmission, a large current drain (~8A) is experienced on the 14 volt supply line to that subsystem. For this reason, a separate battery is provided within the subsurface mooring buoy to eliminate large surges on the power lines from the main battery in the anchor. Circuitry is provided to recharge this battery pack between transmissions.

The power distribution unit is powered from either of two sources: the primary anchor battery or a set of deployment batteries located in the subsurface buoy. During deployment the processor subsystem is fully powered from these secondary deployment batteries,

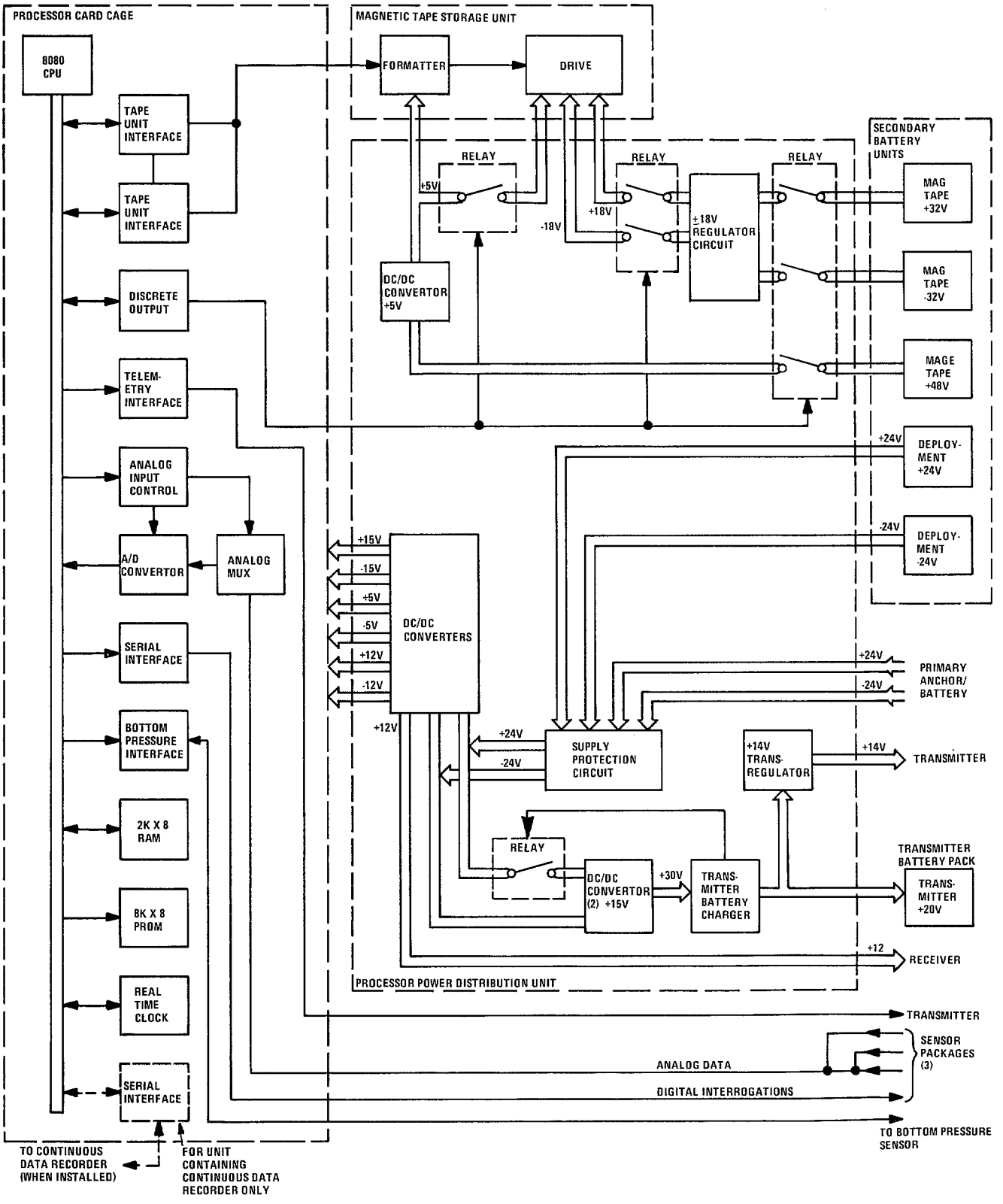

Figure 2. Processor Block Diagram

while system initialization and checkout are completed. The final step of deployment is to connect the primary anchor power supply to the buoy system.

The processor subsystem also contains the magnetic tape storage unit providing a backup data collection device in the event of telemetry link failure. The tape unit is strobed on only during the data recording cycle (2 sec out of every hour), greatly reducing average power consumption. This enables the entire unit to be powered directly from separate battery packs contained within the subsurface buoy. Utilizing a separate power source for this electro-mechanical system additionally enhances the overall system reliability.

Functional Description

The processor is driven by a continuous sequence of one second interrupts to perform its preprogrammed functions. At deployment time, the precise time of day and day of year are entered into the processor via a temporary hookup to a data entry terminal. At that point, the processor starts operating to a preprogrammed schedule of events timed by the one-second interrupts. A flowchart of these events is given in Figure 3. The overall cycle of operation is one hour. During that hour data is collected, preprocessed and averaged over two half hour periods and passed to the telemetry data buffer for transmission.

This data is also logged onto magnetic tape. Each half hour's worth of data consists of a maximum of twenty-one temperature samples measured along the mooring hose, six current speed measurements (current speed N-S and E-W from each of three sensor packages), three calculated salinities (one from each sensor package), and twelve mean product values composed of the product of the currents with salinity and temperature for each sensor package. Each of these data values is an average over one half hour. Along with this data is one sample from the bottom pressure sensor. Information on data validity is also kept with each half hour's group of data. This information is indicated by a flag bit for each data point. The flag is raised if, in a half hour period, a predetermined number of samples are found to be unstable.

An hour's data collection cycle consists of two half hour groups of data as just described plus a group of housekeeping voltages selected as indicators of overall system performance.

Data from each sensor package are sampled according to a carefully determined sample plan as previously described. Current speeds and compass heading data are sampled once per second, and corrected by a generalized current meter correction curve. A compass magnitude calculation is made to account for local variability of earth's field. These data are then used to formulate north-south and east-west components of current speed. The resultant vectors are then passed through a digital filter having a thirty-second time constant. The output of the digital filter is sampled once every four seconds along with the temperature and conductivity data from the sensor packages. Temperature and conductivity values are ratiometrically compensated to account for any voltage reference drift. The temperature data are also corrected based on a generalized thermistor correction curve to account for thermistor non-linearities.

Within the microprocessor, processing is divided into four pieces to avoid overloading any single interrupt servicing cycle. On the first of a group of four second interrupts, samples are taken and required data correction or data formatting is carried out. On the subsequent interrupt, salinity for the first sensor package is calculated and cross products are determined for that sensor package. During the third and fourth interrupt, these calculations are done for the second and third sensor packages, respectively. At the end of a four second cycle, all data points are added to the accumulated thirty-minute sums. After 448 such cycles (1792 seconds) the software executive routine computes the averages and readies the data for transmission and logging. The executive also formulates data validity flags and samples housekeeping data. Two such half hour cycles worth of data (except for housekeeping—only one group) are buffered to be transmitted via telemetry and logged on the tape unit.

The processor subsystem contains a watch dog timer function which monitors the operation of the processor by detecting the execution of a special computer instruction. In the event the instruction is not executed within a predetermined period of time (8 second), a system reset is automatically operated to re-start the processor. This function provides a "second chance" in the event of an abnormal pause in program flow in a deployed buoy system.

During pre-deployment check-out, special diagnostic software is installed in the processor subsystem to re-configure it as a test and diagnostic computer. This Diagnostic Test Unit (DTU) is accessed through a TTY terminal. In this configuration all subparts of the data acquisition system can be tested. Complete checkout of all units of the moored instrumentation system can be accomplished in about 30 minutes.

IV. Telemetry Link

Since the contemplated locations of the buoys on Georges Bank are up to 400 km from the nearest land, there were only two choices for the radio transmission; ground wave low frequency transmission, or line-of-sight relay through a satellite. Tidal and wave detuning effects on the surface piercing mast and antenna eliminated low frequency transmission from consideration.

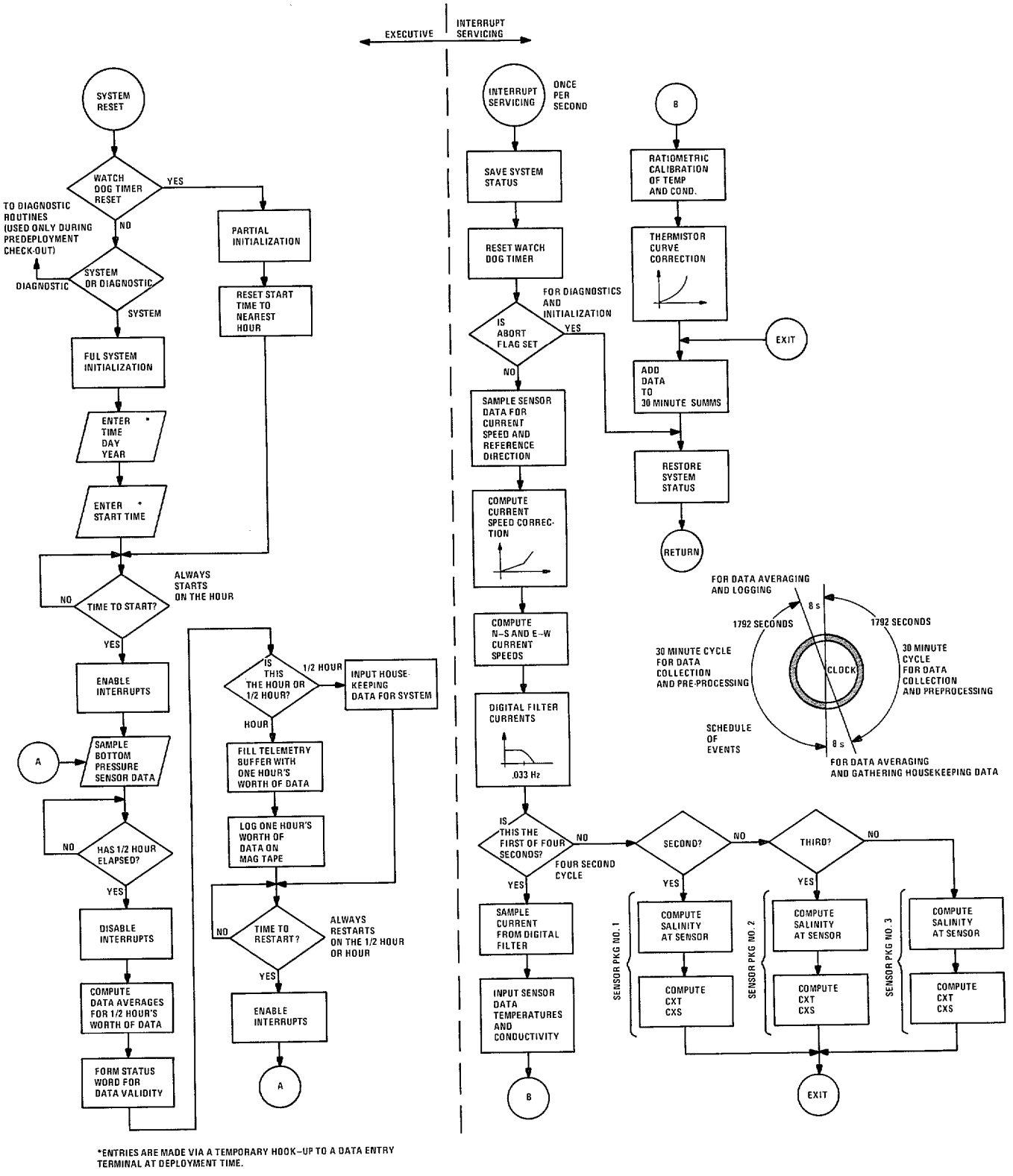

*ENTRIES ARE MADE VIA A TEMPORARY HOOK-UP TO A DATA ENTRY TERMINAL AT DEPLOYMENT TIME.

Figure 3. Software Flow Diagram

The GOES (Geostationary Operational Environmental Satellite) System operated by NESS (National Environmental Satellite Service) granted Raytheon an assignment on interrogatable channel 106, with transmitting frequency of 401.858569 MHz and receiving frequency of 468.8375 MHz. The interrogatable channel was selected because:

- This system has the additional capability to use a secondary command to activate the continuous data recorder on board the buoy.
- On an interrogatable channel, the buoys will be interrogated each hour, with up to 3 tries to get error free data. On a self timed channel, the transmission cycle would be once every three hours. A missed 3 hour transmission would put a severe gap in the data.

The equipment selected to implement the buoy transmission subsystem consists of:

- AEL Model DCP-IIR radio set consisting of two cylinders 11.3 cm in diameter, with the transmitter 57.2 cm long and the receiver 30.5 cm long. The power output is 40 watts. All critical specifications are controlled through NESS certification requirements.
- CHU Associates antenna is a cone 100 cm high with a base diameter of 44.5 cm. The pattern has a gain of 4 dB at an elevation of 40 degrees above the horizon with a ±20 degree beamwidth to accommodate the expected worst tilt angle of the antenna. The pattern in the horizontal plane is circular to ± 1 dB at the 40 degree elevation to accommodate the random orientation of the buoy in this plane.

The data is ingested by the transmitter from the microprocessor/telemetry interface in 6 bit bytes. Then 2 bits are added by the transmitter to make basic 8 bit ASCII characters. With the preambles and identification coding, the two sets of 42 channels of oceanographic data, and the 37 channels of housekeeping data results in a transmission time of approximately 32 seconds at 100 bits per second.

The basic total data communications procedure consists of the following steps:

- Interrogation is transmitted from Wallops, Virginia, to the satellite at 75°W Longitude.
- Satellite repeats interrogation on Channel 106 to the buoy.
- Buoy replies on assigned channel to satellite.
- Satellite relays data to Wallops.
- Wallops wirelines data to NESS in Suitland, Maryland, where it is stored on disk.
- Raytheon obtains data by accessing the disk by dial-up wireline.

The telemetering feature of the system allows real time viewing of the data, and more importantly, indicates the operational status of the system. Previous investigators on Georges Bank have experienced poor data returns due to instrument failures and/or equipment losses due to weather or conflict with fishing activity. It was felt that data returns could be maximized over the relatively short period of the study, if it were known whether the data gathering systems were in fact operating. Prudently planned servicings could then be undertaken to repair those indicating malfunctions or eliminated for satisfactorily operating systems.

V. Current, Direction, Temperature, Conductivity, and Bottom Pressure Sensors

Ocean Data Equipment Company (ODEC)[7] has supplied the sensor package measuring current, conductivity, magnetic heading and temperature. All sensors and electronics are housed in a PVC package 19 cm in diameter, 155 cm long, and weighing 29 kg out of the water and 8 kg in the water. The unit is tested to operate to depths of 300 meters. The sensor packages are mounted in cages at approximately top, middle, and bottom levels in the mooring. Data samples are controlled via interrogations from the central processing unit in the subsurface buoy. Power is provided from the anchor/battery. Each sensor package requires 120 ma of power at ± 12 volts. Electrical conductors providing power and carrying data are contained inside the mooring strength member, a 7.6 cm diameter polyester reinforced rubber hose. Sensor accuracies are shown in Table 1.

Table 1. Sensor Specifications

	Compass	Current Speed
Sensor:	Fluxgate Magnetometer	Electromagnetic
Range:	0-360°	± 150 cm/sec
Accuracy:	3°	The larger of 2% of reading or 2.1 cm/sec

	Temperature	Conductivity
Sensor:	Thermistor	Toroidal Cell
Range:	0-25°C	0-60 mmho
Accuracy:	0.01°C local 0.1°C remote	0.02 mmho

	Bottom Pressure/Depth
Sensor:	Pressure sensitive crystal
Range:	0-270 meters
Accuracy:	2.7 cm

Current speed is measured with the Marsh-McBirney model 555 electromagnetic current sensor. "Golden" sensors were calibrated at the David Taylor Model Basin and later used as transfer standards in the Marsh-McBirney closed flow calibration unit. Outputs of the sensors are x and y components of current. The current sensor exhibits a repeatable non-linearity. Corrective equations are stored in the processor and applied to the incoming data:

$$|\text{Input}| < 25 \text{ cm/sec } V_A = 1.19\ V_I \quad (1)$$

$$|\text{Input}| > 25 \text{ cm/sec } V_A = 0.95\ (V_I + 5) \quad (2)$$

where: V_A is actual velocity and V_I is indicated velocity.

A Neil Brown model C10073 fluxgate magnetic compass senses package heading and outputs sine θ and cosine θ, where θ is local magnetic North. Allowance is made in the in-situ program for storage of individual compass deviation corrections. It has been unnecessary to make use of the capability, however, since all compasses have been well within the 3° specification. Since the output of a fluxgate compass is sensitive to the magnitude of the earth's magnetic field, a correction is computed in the processor according to the following equation.

$$\sin\theta_A = \frac{H_E \sin\theta_I}{\left(H_E^2 \sin^2\theta_I + H_E^2 \cos^2\theta_I\right)^{1/2}} \quad (3)$$

where: θ_A is actual magnetic heading and $H_E \sin\theta_I$ and $H_E \cos\theta_I$ are the indicated sensor outputs and include both earth's field and heading components.

Ocean Data provides the sensors and electronics for measuring conductivity and temperature. A 5 cm diameter toroidal conductivity sensor and linearized Yellow Springs thermistors are utilized. The extreme accuracy specifications on temperature and conductivity necessitated calibration at the NOAA Northwest Regional Calibration Center (NRCC) in Bellevue, Washington. Controlled temperature/salinity tanks large enough to totally immerse the sensor package are available there. Along with the sensors incorporated in the package, each unit is capable of servicing six remote temperature sensors.

The YSI linearized thermistors used are accurate to 0.1°C and a second order curve correction is necessary to achieve the 0.01°C specification. A look-up table is stored in the processor memory and corrections are applied to temperature data as it is taken. The correction curve is common to all thermistors.

Small drifts of reference voltages and zero point offsets in the sensor packages are accounted for by measuring them and accounting for deviations according to the following calculation:

$$T_A = \left\{T_I - Z_I\right\} \frac{V_R}{V_{RI} - Z_I} \quad (4)$$

where: T_A is the actual value, T_I is the indicated value, Z_I is the indicated zero voltage point, V_R is the expected voltage reference and V_{RI} is the indicated voltage reference.

The bottom pressure sensor is an Aanderaa model TG4-A modified for long-line external interrogation and data transmittals to the processor in the buoy.

VI. Anchor/Battery

Power for all systems is provided from the anchor/battery, consisting of 38 two volt cells, supplying ±26 volts to the buoy system and ±12 volts to the sensor packages. The cells are C&D Batteries KCPSA-787 stationary cells designed for long-term slow discharge at cold temperatures. This lead acid cell uses a lead calcium alloy to limit battery gassing and to provide a low self discharge. Cell capacity limitation is acid starvation in this application so a 1.300 specific gravity electrolyte is used. A glass fiber is wrapped on the plates to improve cell life at this high specific gravity. Each cell provides 1100 A-hr. at a 2000 hour discharge rate. This is sufficient to operate the system for 4 months. These cells are mounted in circular steel case, oil-filled and pressure equalized to the sea.

VII. Data Retrieval and Processing

Data from the buoy system is handled in two phases. The first or retrieval stage includes actual receipt of the telemetered message from NESS onto cassette storage at Raytheon's Newport, R.I. facility. The second or processing phase begins with a first level operational evaluation of the system and ends with permanent storage of quality annotated data ready for further dissemination.

Retrieval

After making parity checks and completing necessary reinterrogations NESS stores all messages on disc. Messages are available on demand using a 1200 baud dial up port. A Texas Instrument Model 742 intelligent data terminal with cassette storage is used for retrieval. It performs a CRC check and through an "Acknowledge/Not Acknowledge" blocked protocol scheme ensures data integrity over telephone lines. A typical message containing platform address, time of receipt and data is seen in Figure 4(a).

Processing

Each hour's transmission contains two 30 minute averages of the 42 channels of oceanographic data and single samples of the 37 channels of housekeeping data. Housekeeping includes battery, regulated and precision reference voltages along with computer generated status

```
B2604349 165131602 eErEReu♦yaoalakakaoaTgbZYb{cD]SgcZFBcNkNfNlavacNZNz`|X}rn`XZM
`Y^9BYNtapazaoapakaOez\zrJdb]KaS_eAtCox99999999eEuEReu♦yaoalakajaoaQgY]_bzcf^PgZ
]9BeNBO4NlauadN\NgaS\}rRaD]W`J_DAZNtapazaoapakaqeH^zreda^Sae_9CtCCy99999999XuytM
sIs[}pL[}JshuCuEs{rV}pLM}Fs♦umuSsHsW}tLT}Ss[♦Z♦x}w}{~PB9999AE
```

Figure 4(a). Typical GOES Message

```
DAY/TIME     +12   -12 7.5-7.5 TEMP   CRNT   COND   LOGIC
                                                ♦♦♦ +24   -24   ±14   +36   Q+5   90   5 PS
165131602   12.5 12.5 7.5 7.5 4.799 1.000 4.801 3.999
            12.5 12.6 7.5 7.5 4.795  .998 4.781 3.994
            12.6 12.6 7.5 7.5 4.794 1.000 4.789 4.011
                                                ♦♦♦ 27.4 27.4 14.1 36.2 5.12 PB 99 99
```

Figure 4(b). Typical Housekeeping Report

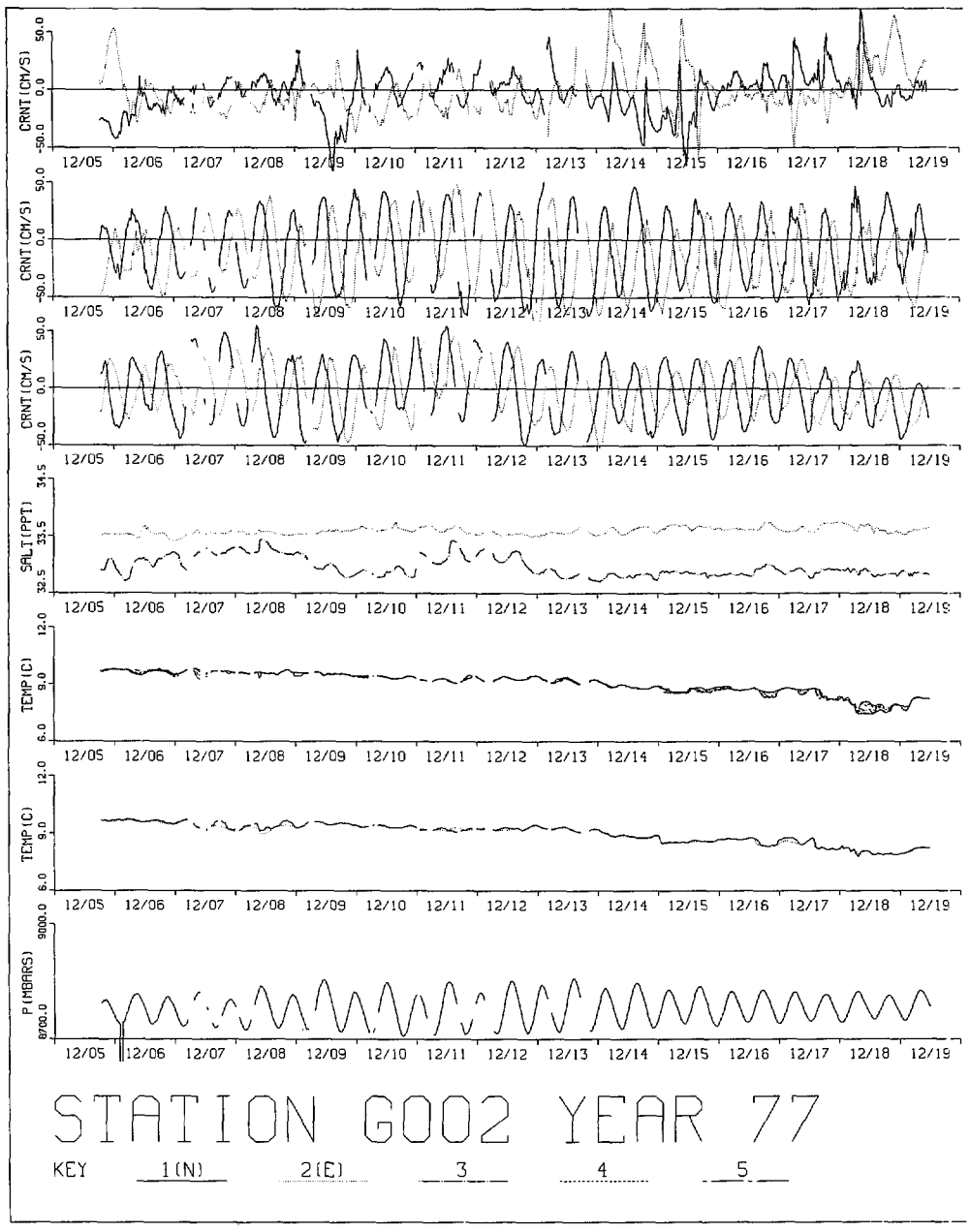

Figure 4(c). Typical Data Plot

flags which indicate sensor input variabilities, out-of-range calculations, and subsystem (bottom pressure, tape recorder, processor sub-module) abnormalities.

The first step in processing is to immediately extract the housekeeping data using programs executed on the T1742. A housekeeping report is distributed daily to system support personnel. Evaluation of servicing requirements, data quality and percent data return are thus addressed on a day-to-day basis. A typical housekeeping report is seen in Figure 4(b).

Data is then prepared for transfer to a CDC Cyber 174 computer at Raytheon's Scientific Computer Center in Bedford, Mass. for further processing and archiving in the Raytheon Oceanographic Data System (RODS). Again, a scheme of parity and LRC (Longitudinal Redundancy Check) ensures data integrity during transmission over land telephone lines.

As each day's data enters the data system, a tabulated data report is produced. During this process, the data is routed through a series of preliminary quality control routines. These routines detect and highlight missing or duplicate data messages, step changes in a data channel, data out of expected ranges, or other anomalies which may be of interest. Values such as step size or ranges are selectable by buoy and parameter in order to allow close monitoring of each system. Each anomaly is annotated on the tabulated output and is carried with the data point within the data system.

At desired intervals, stacked plots are produced showing each parameter as a function of time to allow analysis of trending and an intercomparison of data from different sensors at different levels. A typical plot of data is seen in Figure 4(c). Other types of analysis and graphics are produced on an "as requested" basis for analysis and evaluation by scientific personnel.

Following retrieval of on-board tapes during servicing cruises, a series of software routines are used to compare these tapes with the telemetered data for verification. Data lost during telemetry outages is then merged into the data base.

VIII. System Performance

At this writing (June 1978) six buoy deployments have taken place. An engineering model deployed in Block Island Sound in September of 1977 performed satisfactorily for a month before being retrieved for evaluation. One system deployed on Georges Bank in November of 1977 failed after 19 days due to a power supply failure. A second deployed on the Bank in December 1977 telemetered data for 62 days and collected data (on magnetic tape) for 90 days. Upon servicing at 120 days, water was found to have entered a connector, causing the loss of telemetry. The system remained operational for its 90-day planned deployment. Data quality deteriorated near the end of the deployment, however, due to intermittents in two sensor input cables as a result of conductor fatigue. These and other problems encountered during the first phase of the program have been corrected.

Three systems are currently deployed and performing satisfactorily. They are scheduled for servicing in September of 1978.

Overall percent data return through the telemetry link has been a phenomenal 96%. The collection of data through telemetry has been found to be more efficient than the traditional in-situ recording methods. The ability to collect and evaluate system performance and data on a real-time basis eliminates loss of data due to faults not normally detected until instruments are retrieved.

IX. Summary

The Data Acquisition System described has advanced the gathering of offshore oceanographic data into the realm of microprocessor, satellite telemetry and in-situ data processing. It provides researchers with the ability to manipulate and correct data unconstrained by fixed sampling schemes and non-linear sensors. It allows engineers to monitor system operation and plan servicings to optimize data return. And above all, it has proven itself in the hostile North Atlantic winter.

Acknowledgements

The buoy systems were developed by the Raytheon Company, Oceanographic & Environmental Services, under contract AA550-CT6-53, with the U.S. Bureau of Land Management. Many individuals not listed as authors contributed to the development effort, among them: Paul Higley, Les Stroup, David Cook, Arthur Joyal, Richard Neidich, Robert Day, and Captain Robert Hanson. The current-temperature-conductivity sensors were developed by Ocean Data Equipment Corporation (ODEC). Technical monitoring of the contract for the Bureau was accomplished by Kenneth Berger and Eiji Imamura.

References

1. Higley, P.D. and Joyal, A.J., New Mooring Design for a Telemetering Offshore Oceanographic Buoy, Proceedings OCEAN '78.
2. Beardsley, R.C. and B. Butman, Circulation on the New England Continental Shelf; Response to Strong Winter Storm Department of Meteorology, M.I.T. and Woods Hole Oceanographic Institute, 1974.
3. Berteaux, H., Buoy Engineering, Wiley Interscience, 1976.

4. Bennett, A.S., Conversion of In-Situ Measurements of Conductivity to Salinity, Deep Sea Research, 1976, Vol. 23, pp. 157 to 165.

5. Bumpus, Dean F., Review of the Physical Oceanography of Georges Bank, Woods Hole Oceanographic Institute, 1975.

6. McCormick, M.E., Ocean Engineering Wave Mechanics, John Wiley and Sons, 1973.

7. Ocean Data Equipment, East Providence, Rhode Island.

8. Von Arx, An Introduction to Physical Oceanography, Addison-Wesley Publishing Company, 1962.

9. Laurence W. Gardenhire, The Use of Digital Data Systems, Presented at the National Telemetering Conference, Albuquerque, New Mexico, May 1963.

10. Aanderaa Instruments Ltd., Instruction Manual Model TG4-A Water Level Gauge.

USE OF INDUSTRY STANDARDS FOR SHIPBOARD DATA SYSTEMS

K. R. Peal A. M. Bradley

Woods Hole Oceanographic Institution
Woods Hole, Massachusetts 02543

Abstract

The problem of shipboard data acquisition is examined from a general point of view. A bus-oriented system is recommended where all elements of the system interface to a common bus. When the IEEE 488 bus is used, a wide variety of system controllers, tape units and printers can be used. System implementation is easy and the design remains basically unchanged as the system develops from an experimental one to a self-contained production unit. Bit serial current loop transmission is used for remote sensors providing noise immunity and easy system check-out.

1. Introduction

The problem of acquiring data from sensors aboard ships appears to be a simple one. Data rates are usually low (of the order of Hertz), the number of sensors is not large (less than 100), adequate AC power is often available, and the physical environment (vibration, ambient temperature) may be unpleasant but is usually not severe. Yet over the years a vast array of acquisition and logging devices has been created, many of which have enjoyed only a very short useful lifetime. Why has so much money and effort been expended on an apparently simple job? We believe that the job is not quite as simple as it first appears and further that technology has limited the breadth of applicability of many schemes.

The typical shipboard data acquisition requirements cannot be met by the standard industrial-style logger consisting of a multi-channel analog scanner, analog to digital converter, clock and digital recorder. Some such systems are capable of scanning hundreds of channels with special signal conditioning available. These are clearly more powerful and more expensive than we need or can justify. Our sensors are often spaced throughout the ship necessitating transmission of analog data in an electrically noisy environment. Sometimes the "sensors" do not take the form of analog voltages but are in fact digital outputs from some other system. Furthermore, we often require the clock and timing to be accessible to other devices or to be generated externally. It soon becomes apparent that ours is not a "standard" application.

Independent analysis of the problem often leads to a computer-based system built around a network of minicomputers, operating with sophisticated multiprogramming software systems. In the past few years reliable versions of such systems have become available with very attractive purchase prices; in many cases they provide a good solution to the shipboard data acquisition problem. However, there is another class of problems for which even these solutions are ill-suited. The high turn-on and operating costs of these systems makes them unsuitable where the scale of requirements varies greatly from cruise to cruise. In addition, many applications require simply real time display of engineering units to verify correct operation but do not require the capability for massive sophisticated processing and display provided by the minicomputer systems. In many cases, portable self-contained systems are required for use on ships of opportunity.

Experience has taught us that no device can be a truly general purpose acquisition and logging system. There are always cases where at least parts of a general purpose system are not suitable. We are presenting rather a design philosophy leading to specific recommendations which will ease the problems of system specification, integration, and implementation.

2. Design Philosophy

The traditional acquisition and logging system looks in block-diagram form as shown in Figure 1. It is diagrams such as this that lead to the creation of another new logger because one portion of the system is always different from previous applications. Let us concentrate on the interfaces between the modules - labelled A, B, C, D, E. If these were well defined, it might be possible to change only the block which is different when creating a new system.

Consider the sensor portion of the system. We are using the term sensor in a broad sense - it includes true sensors such as resistive temperature devices but also includes any subsystem which senses something of interest; for example, XBT or

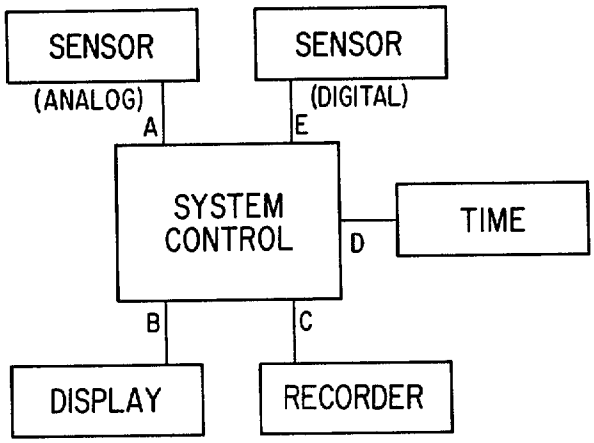

Figure 1. Conventional system block diagram.

navigation receivers. If the sensor interface can be thoroughly defined with a simple specification (say no more than one page) it becomes really practical for different scientists to integrate the sensors they need into their system on a short term basis. Also, some of the problems of mounting expeditions on unfamiliar ships would be considerably reduced if sensor interfaces were standard and well defined.

In the case of the system controller the problem is more severe since it must access all the interfaces identified in Figure 1. In many cases, interfaces B and C to recording and display devices are not very different from each other. Also, digital sensor interfaces are not conceptually different from B and C. One quickly realizes that the concept of a bidirectional electronic bus greatly simplifies the problem - Figure 2. One implication of such a concept is that digitization must take place at the sensor so that the sensor's system outputs are bus-compatible digital signals. With today's technology the economic burden represented by this implication is relatively minor and, in an increasing number of examples, is an advantage as digital sensing systems are exploited to give increased resolution.

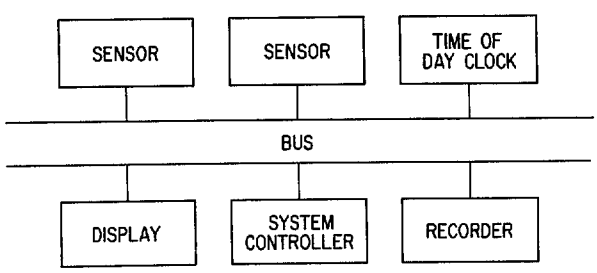

Figure 2. Bus oriented system block diagram.

Since the shipboard data acquisition problem is unique, a good case can be made for designing a bus system optimized for our needs. We feel that the oceanographic community is too small and diverse to define and utilize an in-house standard effectively. Instead, we examine the several candidate busses from the larger field of digital instrumentation and discuss their applicability to our environment. Well defined buses which might be considered are as follows:

- EIA RS-232C - a bit serial voltage interface (reference 1).
- Teletype current loop - similar to 232 but current driven.

These two are actually not buses but certainly have applicability to this discussion.

- IEEE488 - 1975 - the GPIB or HPIB, a byte serial ASCII interface bus with simple hand-shaking (reference 2).
- IEEE583 - 1975 - CAMAC - an extensive electronic and mechanical specification with will-defined operations and related software (reference 3).
- S100 - the "hobby computer standard" based on ALTAIR computer's I/O bus (reference 4).
- Unibus - DEC's PDP-11 backplane which has much industry support (A/D converters, printers, etc.).

We believe that the first 3 in the above list can be used to great advantage in solving this problem. The CAMAC standard has the advantage of expandability and flexibility but the initial cost is very high in both hardware and software. Also, the standard CAMAC packaging is often unsuitable for use on ships of opportunity where small size is required with a simple operator's panel.

The Unibus seems unattractive since its use limits the choice of system controllers to the PDP-11 product line. Use of the S100 bus inherently limits one to very short runs, mostly in the realm of "pure" electronic design with microprocessors.

By using the GPIB as the heart of the system, a variety of controllers can be used. In cases where the system is created quickly, perhaps for one or two expeditions, the controller could be a desk-top calculator programmed in BASIC. In cases where more extensive data processing and display are required, a minicomputer could access the bus simply as a listener in conjunction with a calculator controller, or it could serve as the sole controller on the bus. In cases where a portable self-contained system is required for use on ships of opportunity, the controller could be reduced to a microprocessor-based special. Note that use of the GPIB allows these and other changes to the controller to be made without necessitating changes to other parts of the system.

The recording device in most cases would be a digital magnetic tape recorder. The DC300A cartridge is suitable for this type of system and sometimes is available as a subsystem in the controller (Tektronix 4051). However, at least one company produces a ½" digital tape system which connects to the GPIB. In most cases then, the data can easily be recorded in ASCII form (reference 5) which greatly simplifies system checkout and data processing. Another important feature of this class of recorder is read-after-write check. This is performed with a second tape head to read the data on tape immediately after it is written. Generally the tape controller ensures valid data by rewriting blocks which give a bad read-after-write check. Display devices such as printer and plotter are available to connect to the bus. Their importance in a given application depends on the amount of real time data validation required.

As stated earlier, sensor outputs to the system bus must be digital. Where appropriate, several sensors may be clustered to make use of a common A to D converter. However, the interface seen by the system must be the standard digital bus.

Since the sensors are often located in remote parts of the ship consideration must be given to some sort of bus extender. By definition, the GPIB is limited in length to 15 m. Although electronic tricks can be used to extend this limit, it appears wiser to adhere strictly to the standard, thus avoiding a system which doesn't quite meet the required specifications. If only one or a few long runs are required, converters between the bus and a two-wire twisted pair are available (Figure 3). However, oceanographic applications often require a large number of long runs to remote sensors, making this approach cumbersome and expensive.

In this case the bus extension is better performed by conversion to bit-serial digital links to which the sensors are directly interfaced. The links should be either current loop or RS-232. The 20 mA current loop is a widely accepted standard and is ideal in the electrically noisy shipboard environment. The RS-232 standard is suitable for longer runs using modems. Conversion between the two is easy. Whether the current loop or the RS-232 standard is used, it is important that the data be coded in ASCII. This simplifies the system checkout and the bus conversion.

In summary we suggest that sensors to be used for shipboard data logging utilize either the GPIB or a 20 mA current loop with serial ASCII data for their data output (Figure 4). Although some software specification is still needed to program the system, the nightmare of a multitude of one-of-a-kind interfaces or data loggers is prevented.

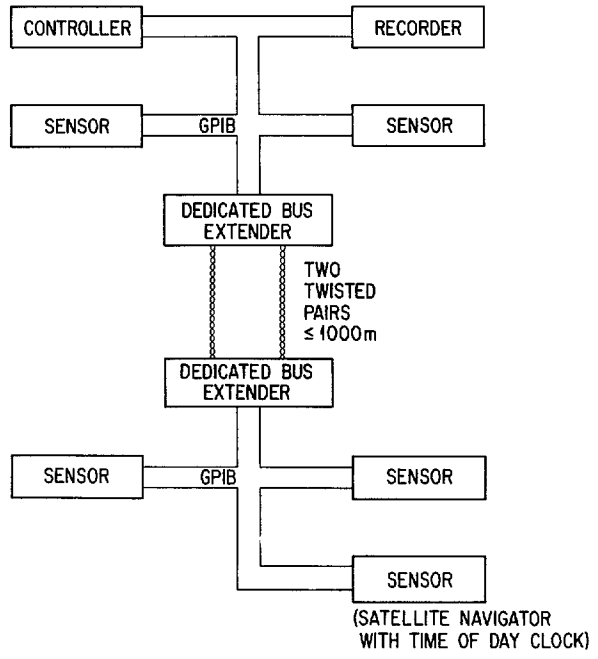

Figure 3. A dedicated pair of bus extenders can be used to connect a remote site to a central controller and recorder.

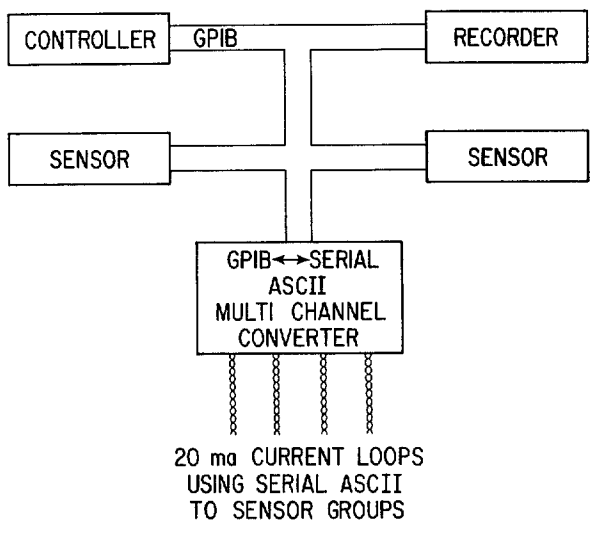

Figure 4. Conversion to 20 mA current loop is advisable when sensors at several remote sites must be accessed.

3. Implementing a System

Based on the above philosophy we have built a system on one of our research ships to record and display meteorological data.

The system is shown in block diagram form in Figure 5. The GPIB is at the heart of the system with a Commodore PET serving as the controller. The PET CRT provides a live display in engineering units of the data being acquired. The printer provides occasional hard copy output. The cartridge tape recorder provides the permanent logged output of the system.

The central multiplexer allows for the addition of more remote acquisition units at other locations on the ship. The remote acquisition unit is based on an RCA COSMAC microprocessor which we were familiar with from use in underwater instruments. The presence of a microprocessor allows us to access the ship's gyro and speed log, neither of which provide a conventional analog voltage output. The use of RS-232 and current loop for the transmission allows us to use the ship's patch panel wiring, greatly simplifying the installation. Also we are able to use a standard computer terminal to check out the various modules of the system.

Data acquisition is performed by these remote units continuously. Messages are sent from the PET to control this acquisition: sample rates, filter constants and average periods can be set in this way. To write a program for the PET to control this system, then, a specification is provided to describe the format and meaning of the various messages.

4. System Changes

It is important to note that changes can be made to this system without affecting its basic operation. For example, a likely requirement would be to log the fixes from a satellite navigation receiver. A new remote acquisition unit would be built to interface to this unit, then its output connected to the central multiplexer. A change to the BASIC program running in the PET would be necessary to acquire and log the data.

Similarly new sensors to measure such parameters as insolation and conductivity could be added to the present remote acquisition unit.

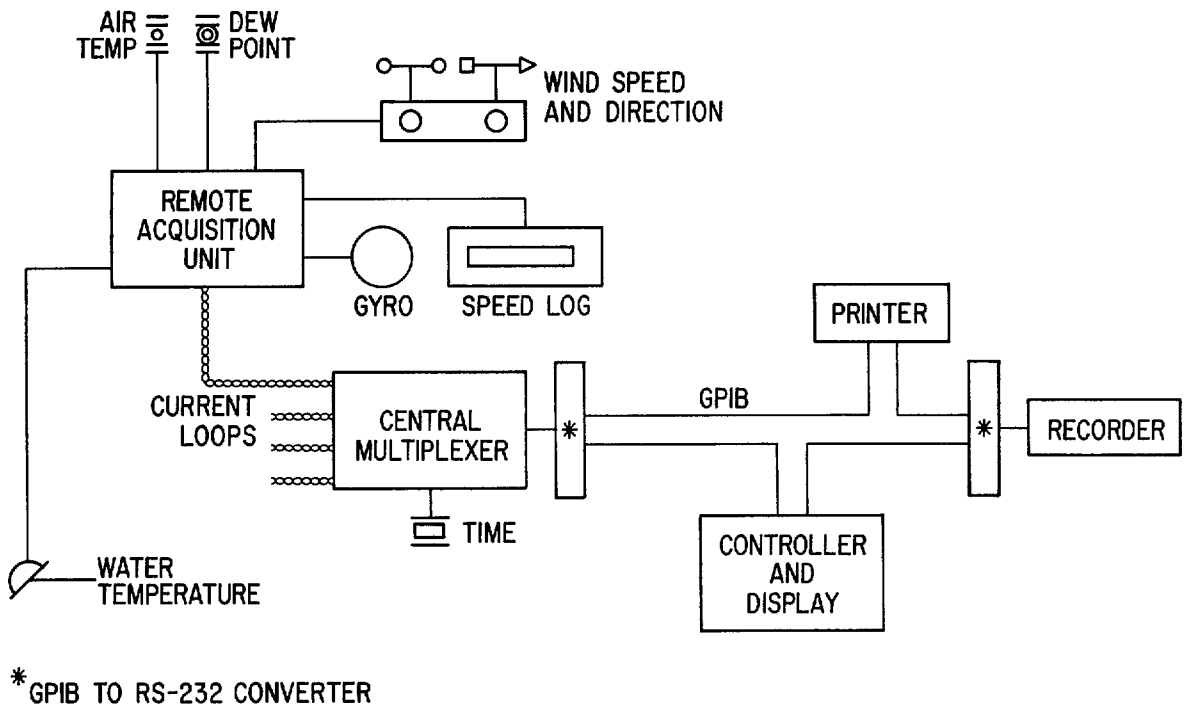

Figure 5. Implementation of a simple system which can be easily expanded or changed to meet future needs.

A change to the PET program would tell the remote acquisition unit to start logging data from these sensors. No hardware change to the system would be necessary.

If it were desirable to do much mathematics in the remote acquisition unit (for filtering or units conversion, for example) it may be appropriate to use a different microprocessor. This change could be implemented without necessitating other changes to the system since the new module still uses current loops to transmit data to the central multiplexer.

5. Acknowledgements

This work is funded by NSF contract OCE76-80174. The authors appreciate the encouragement and assistance offered by S. Wilson of ONR, and D. Webb and R. Spindel of W.H.O.I. This is contribution number 4177 of the Woods Hole Oceanographic Institution.

References

1. Interface Between Data Terminal Equipment and Data Communication Equipment Employing Serial Binary Data Interchange, EIA RS-232-C, Engineering Department, Electronic Industries Association, August, 1969.

2. IEEE Standard Digital Interface for Programmable Instrumentation, IEEE Standard 488-1975, Institute of Electrical and Electronics Engineers Inc., April, 1975.

3. IEEE Standard Modular Instrumentation and Digital Interface System (CAMAC), IEEE Standard 583-1975, Institute of Electrical and Electronics Engineers, Inc., November, 1975.

4. Morrow, George and Howard Fullmer, Proposed Standard for the S-100 Bus, IEEE Computer, vol. 11, no. 5, May, 1978.

5. USA Standard Code for Information Interchange, USAS X3.4-1968, American National Standards Institute, N.Y.

A MICROCOMPUTER BASED OCEAN OBSERVATION SYSTEM

D. A. Munoz
Department of Meteorology
San Jose State University
San Jose, California 95192

Abstract

A low cost, reliable, and flexible instrument package carried by a drifting buoy has been designed. Reliability and low cost, important factors if we are to obtain the spatial resolution required, have been achieved through the use of recently developed semiconductor technology, such as semiconductor transducers and LSI devices. The use of Intel's 8080 microprocessor permits a system of high performance at only a small increase in cost. The basic design is flexible, i.e., it can not only take care of the initial set of measurements (air temperature, sea surface temperature, and atmospheric pressure), but can readily be adapted to measure other parameters of interest.

1. Introduction

The system presented in this paper was designed to become the basic cell of a data acquisition network that would provide detailed information, on a routine basis, on the physical characteristics and on the phenomenons that occur over the Peruvian coastal waters, which have dramatic impact on the economy of the country. To develop such network the basic data acquisition cell should meet certain general characteristics to operate in an economic way, applicable even if it would be deployed over other regions of the world. These basic characteristics are:

Low cost
Expendable
Reliable and dependable
Limited life span

in this way the system obtained is a low cost drifting buoy, that has a life span limited by the time its batteries take to discharge, or when the buoy can not communicate with shore. The reliability and dependability are further enhanced by an on-board microcomputer that provides a large processing-controlling capability without a significant increase in cost.

The basic set of parameters that the prototype measures have been selected mainly because of their importance to describe the environmental characteristics, and also by their feasibility. They are:

Air temperature
Sea surface temperature
Atmospheric pressure

Since this set will be necessarilly altered, the data acquisition module has been designed flexible enough to add new parameters as needed.

2. Instrumentation

Figure 1 is a block diagram of the system's instrumentation. It consists of three basic modules:

- Data Acquisition. Consists of the transducers and their signal conditioning circuitry that condition the sensors' signals to adequate analog levels before they are digitized by the microprocessor for calibration and filtration purposes. The prototype will measure an initial set of parameters as described in the previous section.

The sensors selected for the temperature measurements, both air and sea surface, are National Semiconductors' LX5700 that take advantage of the linear dependance of a PN junction voltage with temperature. The LX5700 is a self contained transducer-on-a-chip that has -20 mV per degree Kelvin voltage-temperature ratio. Their encapsulation has been modified by mounting each inside a single ended, epoxy coated, metal tube, which can be made of monel, admiralty brass, or stainless steel 316. The tube is sealed with Silicon rubber to prevent water leakage. The purpose of this modification is to protect the transducer from the environmental stress and to increase its time response to about 15 seconds in water. The performance of the transducer has been successful. Since their design permits feedback, it is possible to increase their accuracy and linearity; obtaining in that way better results than with thermistors, which are several times more expensive. The accuracy obtained is .2 ^{o}K, but there is evidence that it can be further improved if required.

For the pressure measurement, the transducer used is the LX1701AF from National Semiconductors. The sensor is based on the pressure

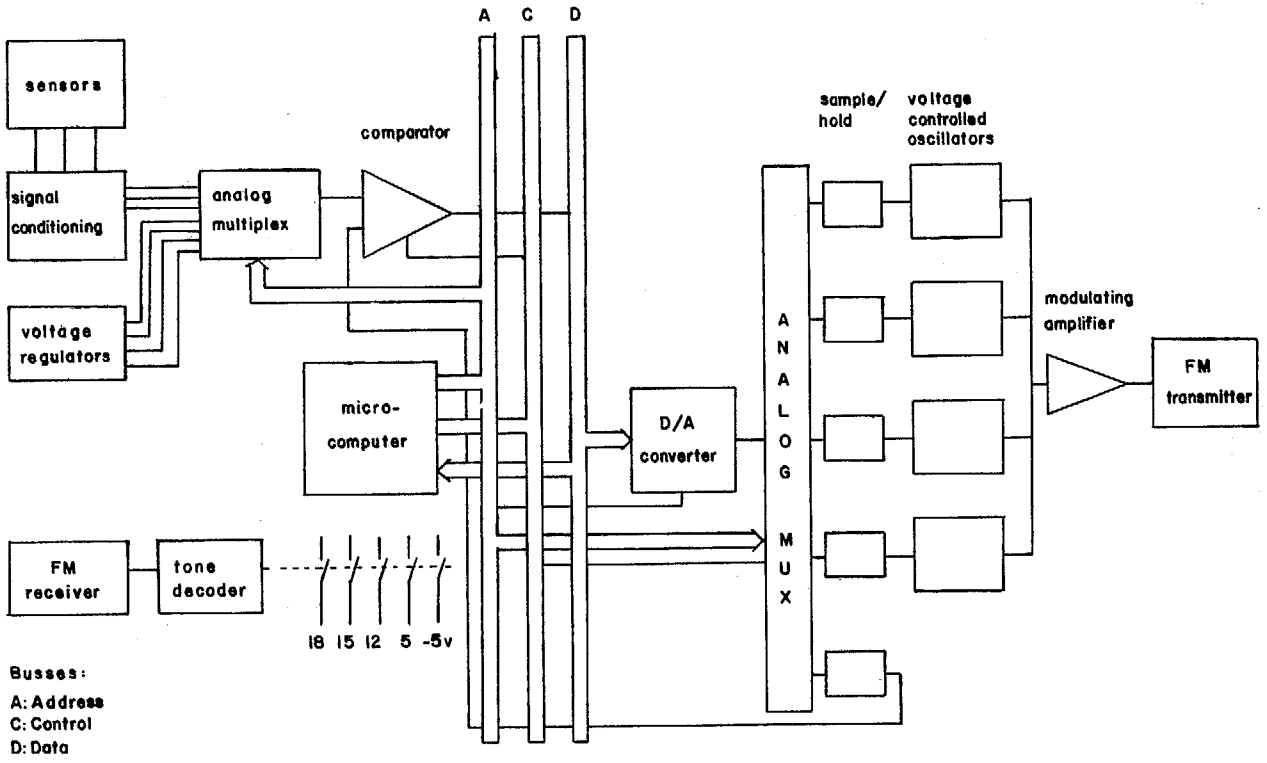

Fig. 1. BLOCK DIAGRAM

dependance of a thin crystal layer's frequency of vibration. The transducer outputs a voltage linear dependent with pressure. Since only thirty percent of its full range is used, its accuracy can be improved to 1.5 mb by a careful mounting, by using high quality components in its conditioning circuitry, and by the processing done by the microcomputer, as described ahead. It has the advantage of being relatively inexpensive as compared to other pressure transducers, and most of all, the effects of the environment are minimized because it is mounted inside a Zinc cover filled with Silicon oil. Since its short response time can be aesily modified, its signal has to averaged over 15 seconds to filter the effects of the platform movement.

For a system of this nature, these semiconductor transducers to be a good alternative, for their low cost and for the ease to manipulate their signals.

These three parameters are only a basic minimum set that can be altered according to the needs. To add flexibility to the system, provisions have been made to readily mount wind, humidity, and radiation sensors; and the instrumentation has been designed in such way that the addition of a new parameter is transparent to the measurements of the others, the only module that is affected is the processing module, which can be readily adapted by changing the microcomputer's software. Wind has not been included in the basic set because there is a need of a more economic way to measure it; at a cost compatible with an expendable system.

- Communications. The data will be transmitted to shore via an FM transmitter working at 174 MHz; and an FM receiver working at 132 MHz, will receive the transmit command from shore.

To simplify the operations, the system is intended to to have only two states: stand-by and transmit. In the first state it will remain idle to conserve batteries; the second state, transmit, which occurs after detecting the right addressing tone, the whole system is turned on and transmits data and status information to shore.

The sensor signature is first converted to voltage to be digitized and processed by the microcomputer; once the processing is completed, it applies binary combinations to drive voltage controlled oscillators, one for each item. In that way, the aim is to encode the data in frequency. These signals, status and data, are added in the modulating amplifier to form a telemetry band. In the prototype the following frequency assignments have been done:

100- 2000 Hz	address tone
2100- 3200 "	air temperature
4600- 6600 "	atmospheric pressure
9300-13600 "	sea surface temperature
14000-18000 "	system status

This is the base band that will modulate the 174 MHz carrier; the transmitter outputs 5 w to a ground-plane vertical antenna.

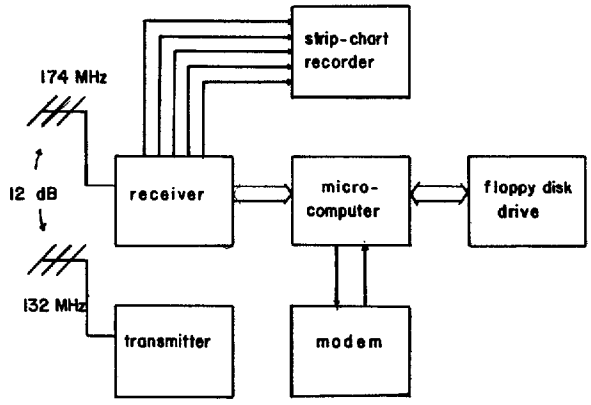

Fig.2.- Shore station

Figure 2 shows the scheme of a proposed shore station operating in the VHF band. By selecting appropriate locations for 21 of these stations along the western branch of the Andes, most of the fishing zone can be covered. In this way, an oceanic strip 2100 Km long and 70 Km average width would be covered. The stations of this proposed array would operate in pairs of a master and a slave station to locate the buoys The position of the buoys can be obtained by calculating the point of convergence of the two antennas of the stations. The worst case uncertainty would be a square of 8 Km a side. Obviously a wider area could be covered if systems like OMEGA or Loran C would be available in the region. For this the communications scheme needs to be altered accordingly.

The third module, control and processing, is described in the next section.

3. Control and processing module

As mentioned before, the system has two modes of operation: stand-by and transmit. During the first mode the whole system is turned off with the exception of the receiver, FM demodulator, and the tone decoder; refer to figure 1. When it is time to retrieve data, a shore station sends an 'addressing' tone that serves as identification for the particular buoy that is fetched. If the tone decoder (a phase locked loop) receives from the FM demodulator (also a PLL) the tone corresponding to the system, it will apply a voltage to a relay that will close its contacts to feed the rest of the circuitry with their appropriate supply voltages. This starts the transmit mode. The addressing tone can be resolved within several Hz.

Once the system is turned on, the microcomputer, basicly an 8080A with its support chips, 2 Kbytes of PROM and 256 bytes of RAM, is the main processor. The transmission is analog to avoid a complicated transmission scheme that may require some kind of protocol. The microcomputer

digitizes the signals as required, once they are ready to be transmitted, it converts them to analog levels again.

The microcomputer performs the following tasks:

a) Filtration. To filter the DC noise and the wave effects, it samples the analog output of each channel every second during fifteen seconds; at the end of this period calculates an average value and converts it to an analog level to be transmitted.

b) Linearization. In the prototype this function is performed only on the pressure channel. Previous to deployment, the pressure transducer is calibrated at 256 points of its full range (900 to 1100 mb); these laboratory readings are stored in a PROM so once the system is operational, and a 15 seconds average has been obtained, the processor uses the PROM as a look-up table to obtain a more accurate measurement and transmit it to shore.

c) Error check. Once the data averages have been completed, the processor applies a known voltage at the inputs of the signal conditioning circuits and goes through a similar 15 second averaging. Compares each reading to an expected one, and sets a data line if the reading is within an acceptable error range, otherwise clears the data line.

d) Self test. Monitors the supply voltages at the output of each voltage regulator (18, 12,+5, and -5 V) and sets or resets a data line as in error checking.

The error check and self test result in a status byte that is also converted to analog to be transmitted to shore.

The software required for these functions is limited to the following:

Main program
I/O routine
A/D conversion routine
Arithmetic and logic routines.

4. Conclusions

The system described has been tested succesfully and will be deployed off-shore California to be monitored from the oceanographic vessel "Cayuse" in August 1978. For this, the platform that will be used is a vertical cylinder surface buoy with a ballast 10 m below the surface to stabilize and minimize its drift. The overall cost of the system is around fifteen hundred dollars; an alternate design without the on-board microcomputer costs around one thousand dollars. It is obvious that the increased cost of the computerized system is justifiable since it has a much better performance. The cost of the microcomputer will be further reduced if ordered in large quantities, as required by a network. Similarly, the software cost will be distributed over many units. The power level required to operate is expected to be reduced with the introduction of CMOS versions of the 8080, as several manufacturers have already announced.

The microprocessor technology has not been fully exploited in this application; there are improvements and additions that can be done, such are a navigational aid, e.g. LoranC, more adequate sampling techniques, hardware control and correction, and others that will provide a high processing and controlling capability at only a reduced increase in cost.

References

1. Intel Corp. 8080 Microcomputer Systems User's Manual. September 1975.

2. Kerr, K. P. "Stability characteristics of various buoy configurations," Trans. of the 1964 Buoy Tech. Symp. pp 1-16.

3. Nat. Acad. of Engineering. Directions for Data Buoy Technology 1978-1983. Washington D.C. 1974.

4. National Semiconductor. Pressure Transducer Handbook. 1977.

5. National Semiconductor. Linear Applications, Vol. 2. 1976.

6. NOAA Data Buoy Office. Practical experience with buoys developed by the NOAA Data Buoy Office. COM-74-10084, NOAA 73121303. Nov. 1973.

SHIPS THRUSTER ALLOCATION LOGIC WITH RUDDER INTERACTION

D. O. Molnar
Principal Development Engineer
Advanced Development Group
Marine Systems Center
Honeywell
5303 Shilshole Avenue Northwest
Seattle, Washington 98107

M. R. Cramer
Development Engineer
Commercial Marine Operations
Marine Systems Center
Honeywell
5303 Shilshole Avenue Northwest
Seattle, Washington 98107

Abstract

The minimum energy control of a ship's motion with available thrusters is of interest. Precision control is needed for various ocean transfer and/or oil drilling support operations. Specialized ships are outfitted with fixed/steerable thrusters in addition to the usual main screw(s) and rudder(s). The control of the available thrusters (thrust force and direction) to meet some desired surge, sway (forward, sideways) and moment command is sought. Often the number of thrusters to be controlled is greater than the number of commands (3). In this case, a unique minimum energy solution is selected from the infinite set of possible solutions. The present solution is a dynamic programming approach made efficient by special tactics for this class of problems. The methodology reported here is considered more general and provides a better solution in the sense of minimum energy and avoids the jump discontinuities encountered previously.

1. Introduction

The problem considered here is the allocation of thruster force in order to meet a commanded surge, sway, and moment. The problem is complicated by (a) more thrusters available than commands, (b) the nonlinear effect of the rudder, and (c) limits on maximum thruster output and rudder angle. A general solution to this class of problems is sought.

It was deemed desirable to avoid jumps in the thruster/rudder solutions if the commands are slightly varied. Furthermore, the rudder variations were to be kept to a minimum. The rudder-main screw effect is treated as a constrained steerable thruster, see Figures 1 and 2. A steerable thruster is initially treated as two independent orthogonal thrusters, then the appropriate constraint is imposed--as indicated in Figure 2.

The thruster allocation problem is one of optimization. The cost function to be minimized is the weighted measure between the commanded and achievable force. The weighted measure is used to prioritize the commands; the achievable force is that which can be delivered by the constrained thrusters.

The solution method developed here can be considered to be analogous to dynamic programming, but more efficient in that larger steps are taken in the attempted solution search iterations. The larger solution steps are possible because of the segmented linearity of the problem and large signal separability). The problem is linear in each of the four quadrants of the space spanned by the main screws.

The "pseudo inverse matrix" [1] solution method was selected because it results in minimum energy expenditure. Another reason for this choice was the rudder effect uncertainty. Assuming that the rudder effect is a separable function in a small neighborhood, the solution tactic must yield interim solutions that converge in small steps to the final solution. The sequential processing matrix inverse [3] method used can provide these interim solutions.

Linear Programming [2] was initially rejected because of the nonlinearity of the problem and the difficulty of prioritizing the commands. Budget and time constraints prevented a thorough investigation. The algorithms used for spacecraft attitude control might be adapted to this application. Furthermore, the algorithm has been considered for the control of a submersible vehicle; that is, the algorithm is still applicable with increased number of degrees of freedom.

2. Problem Formulation

An analytic solution to the unconstrained problem is presented. This serves as an introduction to the more practical computer formulation given in Section 3.

Consider the ship thruster configuration indicated in Figure 1, and described by the

force balance Equation (2.1). Note that for simplicity we restrict the thrust direction of the forward thruster (x_3) so that it is parallel to the fixed thrust directions (x_4).

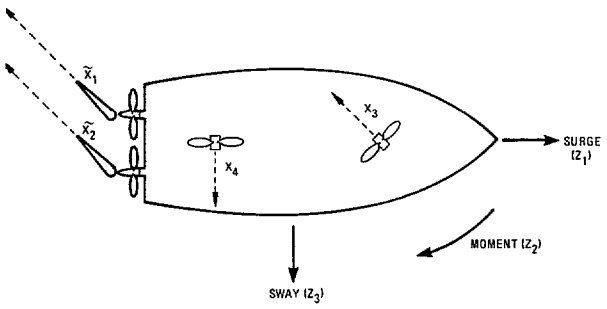

Figure 1. Desired Command: (Zi) = Surge, Moment, Sway; Available "Thrusters" (Xi)

$$\begin{bmatrix} z_1 \\ z_2 \\ z_3 \end{bmatrix} = \begin{bmatrix} c_1 & c_2 & 0 & 0 \\ r_1 & -r_2 & a_3 & a_4 \\ s_1 & s_2 & 1 & 1 \end{bmatrix} \begin{bmatrix} \tilde{x}_1 \\ \tilde{x}_2 \\ x_3 \\ x_4 \end{bmatrix} \quad (2.1)$$

The matrix parameters in Equation (2.1) are defined in Figure 3.

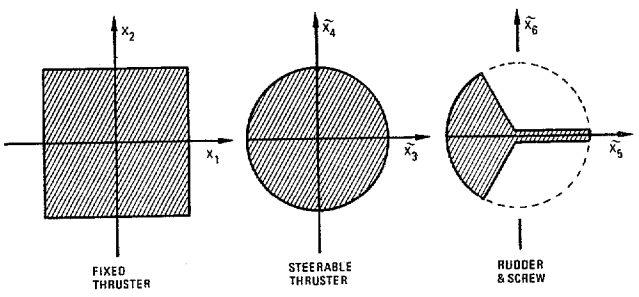

Figure 2. Limited Thruster Resources, Force Constraint Sets. *Note that rudder and screw is a special case of the steerable thruster constrain set.*

In order to illustrate the problem, let us assume the rudder effect, in mathematical terms, is a separable, ideal, lossless function redirecting the main screw's forward thrust; see Figure 3.

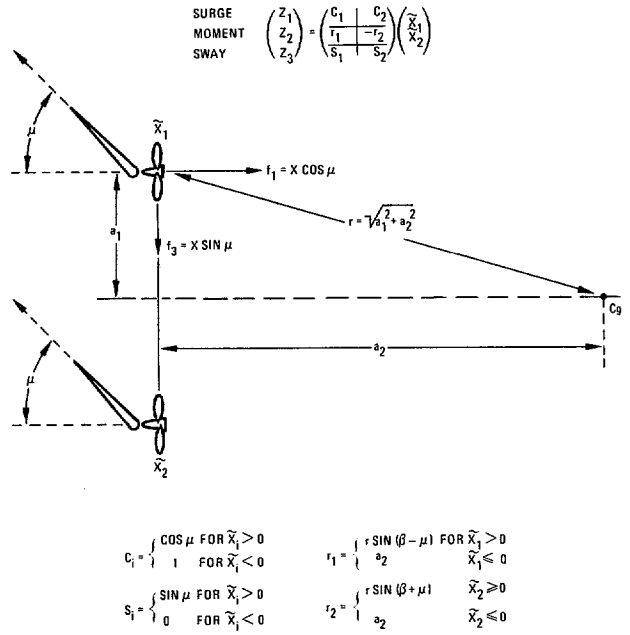

Figure 3. Nonlinear Rudder Effect – No Directivity When Backing Down.

Where

z = (3 x 1) vector of commands, in order of priority, z(1) = surge; z(2) = moment; z(3) = sway

x = (4 x 1) vector of thrusters
x(1) and x(2) = main screws
x(3) and (x(4) = two lateral thrusters

r, a = moment arms

H = H(μ) the projection matrix mapping x into z as a function of the rudder angle μ. The separability of main screw force and rudder effect is a key assumption which is guiding the solution approach.

$$S \triangleq \left\{ x(i) : |x(i)| \leq X_{mi} \text{ and } \mu \in (-\mu_m, \mu_m) \right\}$$

where X_{mi} is the maximum force limit of the i'th thruster.

Since rudder variations are to be kept to a minimum. We attempt first to find a solution at the current rudder angle. An inability to satisfy the desired command at this angle may dictate changes in rudder angle. In Section 5 we present an alternate approach which is more efficient computationally but does not permit fixing of the rudder angle or of the orientation of the steerable thruster.

3. Unconstrained Thruster Solution

Given: command vector z and command/thruster relationship, Eq. 2.1

Find: thruster solution x* such that

$$z = Hx^* \tag{3.1}$$

and $\|x^*\|$ is minimum with respect to all possible x satisfying 3.1

Discussion: since x is of degree 4 and z is of degree 3, no unique solution exists, that is, matrix H is not invertible. The H matrix is a projection operator mapping 4-space into three space.

If we want the solution nearest some arbitrary point, x(o) then we can always find a unique solution, i.e., the "pseudo inverse" matrix gives the solution nearest to the origin as derived next:

3.1 The Unconstrained Pseudo Inverse Solution

It is convenient to reform Eq. 3.1 and define a cost function L as given by Eq. (3.1) and (3.2).

Given: $f = H(u)x - z = 0$ (3.1)

$$L = 1/2x^T Ix + 1/2\ b\mu^2 \tag{3.2}$$

Find: $\min_{u,x} L$

Adjoin the system equation (3.1) to the cost function (3.2) by the undetermined multipliers λ as follows:

$$A = L + \lambda^T f = L + \lambda^T (Hx - z) \tag{3.3}$$

A necessary condition for the existence of the minimum of L is that the partial derivatives of A with respect to x and u be equal to zero.

$$A_x = x^T + \lambda^T H = 0 \tag{3.4}$$

$$A_u = b_\mu + \lambda^T H_\mu X = 0 \tag{3.5}$$

Multiplying Eq. 3.4 by H and substituting into Eq. 3.1 gives:

$$\lambda = -(HH^T)^{-1} z \tag{3.6}$$

inserting (3.6) into (3.4) gives:

$$X = H^T (HH^T)^{-1} z \tag{3.7}$$

which is the pseudo inverse matrix solution sought. Substituting Eq. (3.7) and (3.6) into (3.5) gives:

$$b\mu = z^T (HH^T)^{-1} H_\mu H^T (HH^T)^{-1} z \tag{3.8}$$

Equation 3.8 defines the unconstrained rudder angle that minimizes the cost function of 3.2. Note that the scalar b can be made arbitrarily small; hence, the rudder angle solution gives the "minimum energy." In other words, the factor bu^2 in the cost function is not an energy term, which can be removed by letting $b \to 0$.

The sufficient condition for a local minimum of L is that the second partial derivative (Eq. 3.9) be positive definite

$$\left(\frac{\partial^2 L}{\partial z^2}\right)\Bigg|_{f=0} > 0 \tag{3.9}$$

The solution for the best rudder angle u indicated by Eq. 3.8 has not been implemented because of the complexity of the matrix solution. The rudder angle solution method that is considered more practical is described in Section 5.

There exists a convenient algorithm for carrying out the solution indicated by Eq. (3.7). This algorithm is a sequential processing matrix inversion routine that is much used in Kalman filtering. [3] The computer algorithm has the desirable flexibility for including prioritization of the commands z.

The prioritization of commands is a natural step, in the allocation of the limited thruster resources. In the next section the problem of constrained thrusters is considered.

4. The Constrained Thruster Allocation Problem

If the solution given by Eq. 3.7 is in the feasible set S, then the problem is solved with the possible exception of some rudder adjustment to reduce the thruster energy. In this section the problem of unattainable commands is considered; hence, we have the problem of allocating the limited thruster resources in a manner consistent with the priority of the commands.

Consider the problem where the commanded force z cannot be attained due to the thruster constraints. This conflict of requirements represents a singularity. In order to deal with this singularity, we relax the command constraints in an order consistent with our priorities. The command equations can now be considered "soft" constraints, and the nearest boundaries of the feasibility sets S are "hard" constraints.

Let us assume that we have an unconstrained solution from Section 3 that is not feasible, i.e., x&S. Consider the augmented problem where the original commands are no longer a "hard" requirement, and the adjacent constraints of S are augmented to the original command equations. (See Eq. 4.1).

$$\left\{\begin{array}{l}\text{COMMANDS}\\ \\ \text{CONSTRAINT}\\ \text{BOUNDARY}\\ \text{SELECT SIGN}\\ \text{BASED ON}\\ \text{UNCONSTRAINED}\\ \text{SOLUTION}\end{array}\right\} \begin{bmatrix} z_1 \\ z_2 \\ z_3 \\ X_{mi} \\ \vdots \\ X'_{mj} \end{bmatrix} = \begin{bmatrix} h_1 & & & & \\ & h_2 & & & \\ & & h_3 & & \\ & & & 1 & \\ & & & & \ddots \\ & & & & & 1 \end{bmatrix} \begin{bmatrix} X_1 \\ \vdots \\ X_n \end{bmatrix} + \begin{bmatrix} V_1 \\ V_2 \\ V_3 \\ 0 \\ \vdots \\ 0 \end{bmatrix} \quad (4.1)$$

(ALLOCATION OF LIMITED RESOURCES IN ACCORDANCE TO PRIORITY)

REDUCE LOWEST PRIORITY COMMAND TO MAKE SOLUTION "FEASABLE"

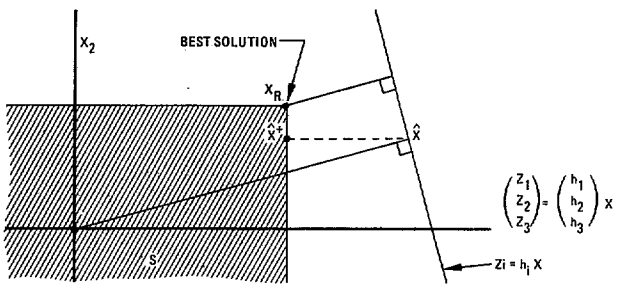

S = {X: ATTAINABLE}

$\tilde{X}$ = {X: X∉S, EXCEEDED CONSTRAINTS}

Zi IN ORDER OF PRIORITY

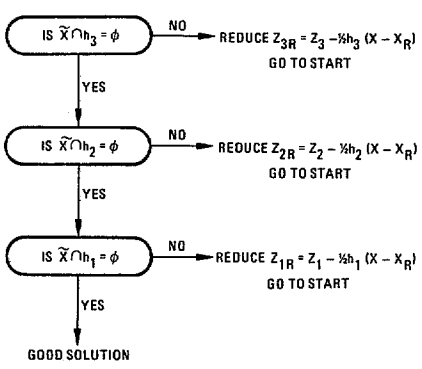

Figure 4. Constrained Thruster Solution Tactic

Figure 4 indicates a constrained thruster solution tactic, given that we cannot satisfy a command with our constrained thrusters. Briefly, the solution tactic is to attempt solutions of three command groups (z_1), (z_1, z_2), and (z_1, z_2, z_3). After each solution attempt, the last command is reduced to that attainable. The command reduction to attainable value is accomplished as follows: Nonfeasible solutions are projected on to the feasibility boundary at the same time as these boundaries are selected for augmentation to the current prioritized command grouping for a second solution attempt.

This second augmented solution attempt is necessary to find the prioritized command intersection with the feasibility boundary. The results of the second solution attempt are adjusted as necessary by projection to the feasibility boundary before proceeding to the next command grouping.

In summary, for each of the command groups (z_1), , (z_1, z_2), , and (z_1, z_2, z_3) , a solution attempt has four steps:

(a) Unconstrained solution

R = 0, P = I, equation 4.8

(b) Projection to nearest constraint boundary (if necessary).

(c) Augment "hard" (R = 0) constraint boundaries onto the "soft" i(th) command and solve by Equation 4.8.

(d) Project results of step (c) to appropriate feasibility boundary before proceeding onto next command grouping and step (a).

Steps (a) through (d) are carried out for each quadrant of the $x_1 - x_2$ space (main screws) since it is not known a-priory which quadrant contains the best solution.

The solution tactics above have been implemented to demonstrate the basic methodology. Improvement in both computer burden and algorithm performance is considered possible. For example, the solution tactic above might be abbreviated considerably by proper choice of P and R at the intermediate solution points.

A nice feature is the generality of the solution methodology suggested by equation 4.8. Once the solution tactic is perfected, a new ship configuration need only be inserted in the H- matrix and the thrust/rudder allocation problem is solved.

The generality of Equation 4.8 is demonstrated by its use in the "best" rudder angle solution search presented next. This formulation negates the 4-quadrant solution search in the $x_1 - x_2$ space. The two "steerable thrusters" x_1, x_2 are treated initially as four independent orthogonal forces. With the imposition of constraints (Figure 2), the independance of the forces is removed and the rudder angle becomes available from the components; see next section.

5. Solution for New Rudder Angle

Once the best thruster solution at the current rudder angle is obtained, it may be desirable to change the rudder in order to (a) reduce thruster energy output or (b) more nearly achieve a command that is not obtainable due to saturation.

One solution method is the extension of Equation 3.8 to contain the appropriate boundaries of S and then find the roots. If there are more roots than one, the best rudder angle can be chosen by substitution into 3.1.

The solution method outlined here involves treating a steerable thruster initially as two independent orthogonal thrusters. Subsequently, the constraints indicated in Figure 2 are imposed. Because of the nonlinearity of the constraints, various solution methods were attempted. Consider Equation 4.1, the constraints, assume X_1 and X_2 are orthogonal components of screw force $\tilde{X}_1$. Assume X_1 is the force in the highest priority command, then the constraint on X_2 is computed as $X_{m2} = \pm(\tilde{X}_{m1}^2 - X_1^2)^{1/2}$ where $\tilde{X}_{m1}$ is the maximum thruster output and $|X_1| < \tilde{X}_{m1}$ otherwise $X_1 = \tilde{X}_{m1}$ and $X_2 = 0$. The above is summarized in Figure 5a,b. Note that Figure 5c represents an improvement over Figure 5b, in that the best solution is returned in one step, whereas the method of Figure 5b requires iterative steps.

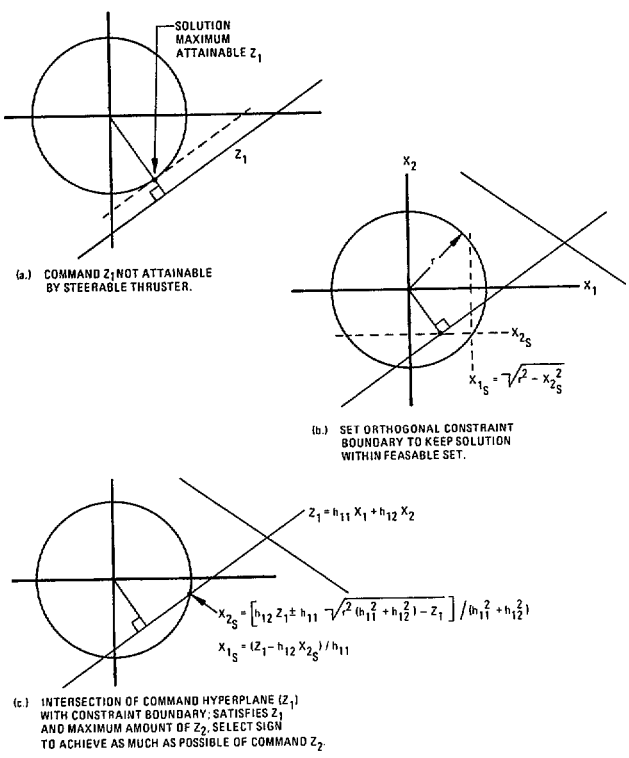

Figure 5. Steerable Thruster Solution Options: (a.) Steer to Maximize Highest Priority Command, (b.) Orthogonal Constraints for Linear Solution, (c.) Nonlinear Solution

The "orthogonal constraint" method indicated in Figure 5b is currently being utilized. We rewrite Equation (2.1) by breaking up the rudder (steerable thruster) into orthogonal components. We define the $\{y_i\}$ variables in terms of the S_i, C_i, X_i variables of Equation (2.1) as follows:

$$(y_i) = (c_1 x_1, s_1 x_1, c_2 x_2, s_2 x_2 x_3, x_4) \qquad (5.1)$$

The moment command constraint (z Equation 2.1) expressed in terms of orthogonal moment arms (Figure 3) results in the desired component form of Equation 2.1, given by Equation 5.2.

$$\begin{bmatrix} Z_1 \\ Z_2 \\ Z_3 \end{bmatrix} = \begin{bmatrix} 1 & 0 & 1 & 0 & 0 & 0 \\ a_1 & -a_2 & -a_1 & a_2 & a_3 & -a_4 \\ 0 & 1 & 0 & 1 & 0 & 0 \end{bmatrix} \begin{bmatrix} y_1 \\ y_2 \\ y_3 \\ y_4 \\ y_5 \\ y_6 \end{bmatrix} \qquad (5.2)$$

In this form the rudder angle variable is no longer explicitly present. By imposing the appropraite constraints (Figure 2,5) the rudder angle solution is obtainable from the components:

$$\mu_1 = \tan^{-1}\left(\frac{y_2}{y_1}\right)$$

The above approach does not readily permit the modulation of a command without changing the direction of the steerable thruster. In contrast, the method presented in Section 4 was developed so that command variations would result in only thruster magnitude changes, and the steering of thruster/rudder would be attempted only if necessary.

The solution tactic for allocation of the thruster resources are the same for the above formulation as for the previous formulation in Section 3.

Conclusion

The general problem of controlling a ship's three degrees of freedom with constrained thrusters has been formulated. The allocation of limited thruster resources to achieve prioritized commands has been solved. The solution tactics above may be varied as new constraints develop, i.e., penalty on rudder motion, thruster wash interaction, etc.

REFERENCES

1. Gelb, A. (ed) "Applied Optimal Estimation," MIT Press, 1974, pp

2. Gass, S. I., "Linear Programming," 3rd Edition, McGraw-Hill, 1969

3. Leondes, C. T. (Ed), "Advances in Control Systems, Theory and Applications," 1966, H. W. Sorenson Contributing Author on "Kalman Filtering Techniques," pp 256-260

THE MARINE TECHNOLOGIST

Roger M. Lloyd, Jr.
Director of Marine Technology
Florida Junior College-South Campus
P.O. Box 114
Jacksonville, Florida 32216

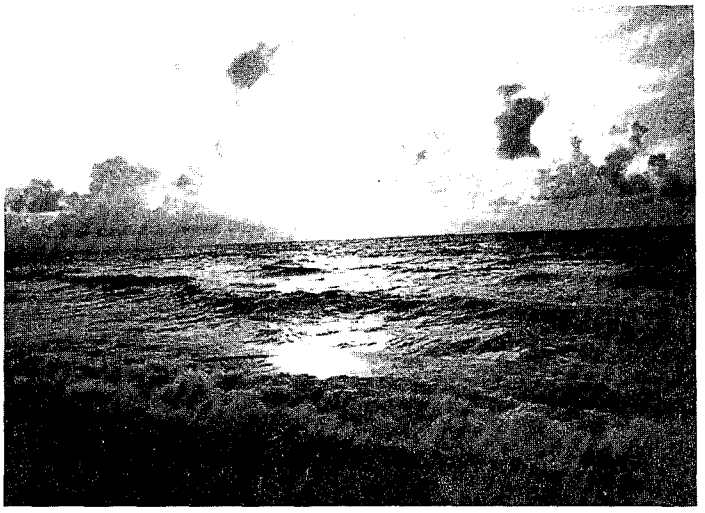

Yonder is the sea, great and of wide extent;
Therein are living things innumerable,
Living creatures both small and great.
There the ships make their course;
There is the great leviathan whom thou has
formed to sport therein.
These all wait upon thee,
That thou mayest give them food in due season...

Psalm 104
Book of Psalms

Since the time that man's cranial capacity exceeded 1200 cc's in volume, he has diligently searched for explanations which would help clarify the awesome phenomena presented by the world's oceans. The sea with all her mysteries stands before us. The prospect of her bearing foods, minerals, and raw materials is unyielding. In the near future, the oceans may become the environmental site for large motile cities.

At present, the nation as a whole has only dealt in piecemeal fashion with its interest in and action toward the total air-warer-land-sea bottom environment. There is a serious need to produce educated people with the acquired ability to think out the relationship of the various parts to the whole. The attendant need for broadening education to allow for the capacity of this type of thinking can only come through extensive, specific curriculum modifications at every academic level; from kindergarten through college.

With the help of the National Oceanic and Atmospheric Administration (Sea Grant), the U.S. Navy and Jacksonville Shipyards, Florida Junior College at Jacksonville initiated a Marine Technology Program in September of 1974. The designers of this program spent many hours and traveled many miles collecting ideas and information from other marine-oriented programs at different universities. After a year of critical research, the Marine Technology Program was constructed, and became a specialty program of study at Florida Junior College at Jacksonville, Fla.

The program itself is unique for the students graduate with an Associate in Arts Degree (with special emphasis in Marine Technology). This allows the graduates to pursue higher educational goals without loss of credits during the upper division transfer process. To help in this aspect also, Florida Junior College has formulated articulation agreements with several universities in the southeast. Each articulating school offers a different type of upper division degree. Agreements include Florida Atlantic University with a Bachelors in Ocean Engineering, Florida Institute of Technology with a Bachelors of Technology, University of West Florida with a Bachelors in Marine Biology, and University of North Florida with a Bachelors in Biology. Students are counseled to explore their far-reaching interests. When the students decide which aspect of marine science they wish to pursue, their curriculum is altered slightly to include the peculiarities of that particular school's requirements. The exact requirements for each school are listed in Table 1. Although several differences in curriculum occur, as a whole the program remains the same.

The program is a rigorous one. Within the two-year period the Marine Technology students are introduced to the ocean and her inhabitants through core courses including Introductory Oceanography, Marine Biology, Ichthyology, and Marine Instrumentation. There is practical experience in marine specimen collection and statistical research in Marine Field Sampling. The practical experience can be executed when the students learn the skills offered in the courses of Scuba Diving, and Navigation and Small Boat Handling. With the use of the sixty-eight foot U.S. Navy Special Services Survey boat the "WACCAMAW", the students learn navigational abilities and how to collect important data used for Introductory Oceanography laboratories. A local shrimper has assisted us in teaching students how an otter trawl operates.

In addition to core courses, as a minimum the

Table 1

COMPARISON OF ARTICULATION

INSTITUTION	CREDIT HOURS	DEGREE REQUIRED	MATH THROUGH CAL III REQ.	MATH THROUGH CAL II REQ.	MATH THROUGH CAL I REQ.	PHYSICS WITH CALCULUS REQ.	SCUBA REQUIRED	SMALL BOAT HANDLING REQ.	DRAFTING & ENG. DRAWING REQ.	NO. OF CREDIT HOURS AFTER A.A.	TYPE OF DEGREE OFFERED	BIOLOGY BACKGROUND	MARINE INSTRUMENTATION REQUIRED
Florida Institute of Technology	78	AA		X			X	X		117	Bachelor of Technology	16	X
Florida Atlantic University	62	AA	X			X		X	X	90	Bachelor of Ocean Engineering		X
University of West Florida	78	AA		X			X	X		71	Bachelor of Marine Biology	16	X
Mississippi State University	62	AA		X				X	X	68	Bachelor of Marine Engineering Technology		X
University of North Florida	78	AA		X			X	X		92-96	Bachelor of Biology	16	X
Jacksonville University	79	AA		X			X	X		65	Bachelor of Marine Science	12	

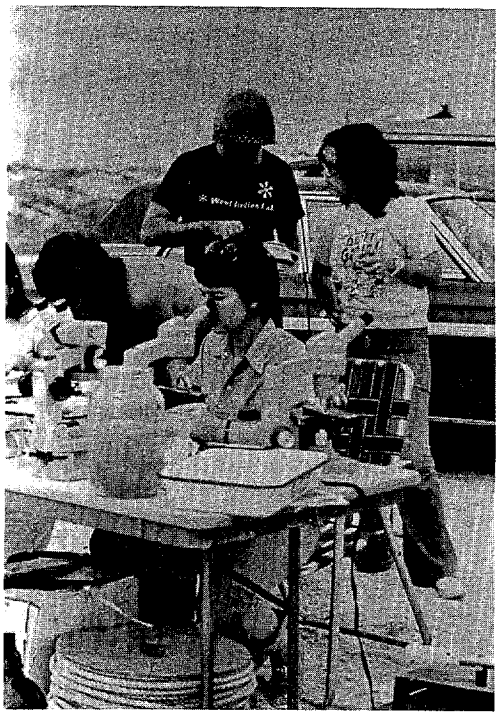

Marine specimen identification in the field.

students must complete Calculus I and II, College Chemistry, and College Physics along with the required English, History, and Humanities courses.

There are no dead ends for motivated students; after graduation from Florida Junior College there are many alternatives for the graduate. As mentioned previously the Marine Technology Program has articulating agreements with several universities in the southeast. For those students ready to work; agreements have been formulated with many agencies. Sources of employment include area power companies, consulting firms, shipyards, drafting firms, diving companies, and local, state, and federal governments. Salaries range from $9,000 to $18,000.

The Marine Technology Program has not limited itself to the present only; the curriculum is designed to grow with the changing needs of the community and country.

With state tuitions soaring higher, it is a relief to many oceanography-oriented students to learn of a Junior College offering a challenging first-rate curriculum in Marine Technology. It is no wonder that from 1974 to 1977 the number of students has tripled.

Skills for marine field technologists vary widely from operating, calibrating, and adjusting instruments used in the field, to specimen collection and identification. The work load for the technologist may include laboratory analysis, pulling dredges and nets, sieving sediments, plotting data, maintaining aquacultures, photographing data, and many other jobs.

Employment for technologists who have had sufficient course work and field experience is

Seining for specimens at the West Palm mangroves.

quite good currently. In addition, there are cooperative education programs and private scholarships available for ambitious student graduates interested in a career in ship construction and repair.

Ocean Science education is as boundless, complex, and dynamic as the ocean itself. In order to cope with today's demands, the young Marine Technologist must be one part mathematician, one part engineer, one part chemist, one part biologist, one part physicist, and one part mechanic.

Students learn to use the Salinity-Conductivity-Temperature meter on the U.S.Navy's "WACCAMAW".

EDUCATION--THE BRIDGE TO OCEAN EXPLORATION

Matilene S. Berryman
Professor of Marine Science
University of the District of Columbia
(Van Ness Campus)
2226 Randolph Street, N.E.
Washington, D.C. 20018

Abstract

Institutions make an impact on society basically through the product they produce. One of the most important and least expensive of these products is EDUCATION, its benefits as a commodity is priceless to people whose concern is with the Economics and Energy of our Environment. The University of the District of Columbia, Van Ness Campus (formerly Washington Technical Institute) received Sea Grant funds of $208,000 from the National Oceanic and Atmospheric Administration, Department of Commerce, between 1972 and 1974 to develop a Marine Science Technology Program. This paper details that program.

1. Introduction

Nationally and internationally, the chief articulated concerns of society are:

ENVIRONMENT
ENERGY
ECONOMICS

All command the attention of today's society in view of the dwindling natural resources within the bowels of the earth, the rising cost of fuel, and the lack of land for the production of food resources.

In consideration of these issues, the last three decades have witnessed an inordinate technological venture into the realms of the oceans (2/3 of Planet Earth) in search of the energy resources to insure continuing economic benefits for an affluent society, and to lessen the burden on the environment that the rape of land resources has produced. However, just as space exploration--and the spectacular walk on the moon--was carried out by only a small fraction of this society of 220 million Americans, so is the technology of the sea a tool and market place for but a handful of the American public.

2. The Role of Education

In our concern for the benefits of a benevolent universe and the three E's of Environment, Energy, and Economics, we have minimized the importance of the biggest issue - the E of Education. Lack of programs of education in the ocean sciences at major educational institutions accounts for the fact that the greater mass of people have little appreciation for problems and possibilities of the 330 million cubic miles of water called the oceans. It stands to reason that if the oceans are to provide the world with the important energy and food resources for tomorrow; if the oceans are to be explored, exploited and preserved; if the oceans are to be the career arena for the future, then it is imperative that the greater public receive the benefit of education in the Ocean Sciences.

Oceanography, the science that explores the oceans and seas, has been an expanding science since early World War II when the Navy was faced with the defense of American shores from possible invasion of enemy submarines and underwater missiles. This branch of science has been offered mainly by graduate and undergraduate institutions since 1950, despite the awakening awareness that the oceans may be man's last bastion for survival.

3. Role of Institutions in Ocean Exploration

The largest single employer of Oceanographers for the last three decades has been the Naval Oceanographic Office (formerly of Suitland, Maryland, now at Bay St. Louis, Mississippi). This institution has been in the forefront of ocean exploration since the early 1950's.

Basically, however, educational institutions engaged in ocean exploration have been Big Ten and Ivy League universities where operating budgets are already large and faculty and staff are necessarily adequate to engage in research on a large scale. Few smaller universities receive major grant funds from the chief government source of funding--The National Sea Grant Office of the National Oceanic and Atmospheric Administration, Department of Commerce. The annual budget of from 872.5 million in 1976 to 956.6 million in 1977 is spread over twelve (12) agencies including the Department of Commerce, the Department of the Interior, Health, Education and Welfare, the National Science Foundation, The Environmental Protection Agency, the National Aeronautics and

Space Agency, the State Department, the Department of Defense, to name a few. Additionally, $800 million has been set aside over the next 10 years as a Coastal Energy Impact Statement Fund, and another $400 million over the next 8 years in Formula Grants for Coastal Zone Management. Fundamentally, these agencies control the research and development activities of our oceans and coastal areas; whether for the extraction of oil, gas, minerals, for fish, for navigation, for recreation, for enforcement of Law of the Sea concepts, or otherwise. The goals are:

(1) To expand the technological capability of man to utilize the natural environment of our world with its huge energy resources, and

(2) To assure that our economic potential may be increased without endangering the natural bounds from which these resources are produced.

Education, then would seem to be the root from which the other goals could be achieved.

If smaller institutions have been engaged in ocean exploration it has been primarily Technical Institutions and Community colleges implementing programs in Marine Science Technology.

4. Marine Science Technology at the University of the District of Columbia Van Ness Campus (formerly Washington Technical Institute)

Marine Science, the applied aspect of oceanography, began to appear in the program offerings of Community Colleges and Technical Schools in 1966, with the establishment of the National Sea Grant Office, the principal national instrument for cooperative programs in ocean development and coastal zone management. It was established by Congress for the purpose of fostering marine resource development, ocean technology, environmental research, education, training, and advisory services. The principal recipients of Sea Grant have been state and local governments, academic institutions and industry.

In 1970, a planning grant of $13,200 was provided by the Sea Grant Office and Link Foundation to the Washington Technical Institute to establish a Marine Science Technology Program. These funds were used to do a feasibility study and to bring together ocean scientists and engineers from government and private industry to plan a curricula of marine science for implementation at a two-year technical institution to award an Associate of Applied Science Degree (AAS).

The program began in 1970 with approximately 15 students, but it was not until September 1971 that the curriculum was revised to strengthen the program and to assure a stronger base in the physical sciences. A proposal was then submitted to the National Sea Grant Office, and $208,000 was subsequently awarded to continue development and implementation of the program at the Washington Technical Institute. Approximately twenty-five (25) students were recipients of an AAS Degree and 25 additional students received direct benefit of Sea Grant to this technical institution.

5. Implementation Problems

The University of the District of Columbia has an open door policy, consequently many students seeking careers in the technological fields do not have ample preparation in the mathematics and science fields and most pursue studies in remedial courses before admittance to a single technology program. This problem was deemed to be the central reason for the high dropout rate in the Marine Science Program in early 1971. To stem the tide of low student enrollment and a high dropout rate, a foundation course entitled "Science of Man's Environment" was introduced as a motivational tool to challenge the thinking and conceptual ability of the students, and to aid them in their acquisition of scientific and technological know-how. This course is a meshing of research materials of an interdisciplinary nature and treats the Universe of Atmosphere, (air - gas) the Hydrosphere (water - liquid) and the Lithosphere (land - solid) each as a piece of the puzzle that contributes to an understanding of the whole. The student receives indoctrination into the concept of the earth as existing as three states of matter, i.e., gas, liquid, solid, and as responding to the forces of heat and pressure to reshape and reform the universe into the products which we utilize materially. The student fully understands the necessity of chemistry, physics, mathematics, biology and geology as cornerstones in this technological base, and have readily adapted their thinking to a full consideration of the sciences as understandable and exciting in their quest for knowledge of the real world. This course was subsequently adopted as a science requirement for the programs in Police Science, Technical Teaching Training, Business Administration and off-campus programs under contract with government agencies. More than 1200 students have enrolled in this course since 1972.

6. Career Placement of Graduates

Since 1973, more than 30 students have graduated from the Marine Science Technology Program, or are employed in major ocean related disciplines across the nation. The majority of those employed are with the National Oceanic and Atmospheric Administration (NOAA), others are continuing in undergraduate programs of oceanography or environmental science programs at George Washington University, Howard University, American University and Maryland University. Two of the students are enrolled in masters programs. For the past two summers, a black female in the Marine Science Program has been employed as a co-op student aboard the NOAA research vessel cruising the Atlantic Ocean from its bases in

Miami, Florida and Galveston, Texas. This program has been the major vehicle for the black student entry into the world of oceanography/ marine science, in terms of long range capability and contribution to this field of technology.

7. Future Expansion

The program at UDC has not expanded to reflect the continuing national effort. There are several reasons for this, the chief of which are:

(1) Lack of adequate funding

(2) Lack of adequate trained faculty

(3) Change of calendar

The grant funding to this program was not renewed on the basis that UDC did not exhibit the research capability of Sea Grant Institutions, and that the desired mission of the Sea Grant Office was not necessarily the promotion of education in the ocean sciences. Thus, the Marine Science Program has lacked funds to expand and hire capable faculty to engage in wholesale ocean exploration.

The second major drawback has been a lack of faculty with both academic and technical preparation in the ocean sciences. The objective of the Marine Science Program is to provide the student with applied techniques so that he can work as an ocean technician in:

Tides and Currents
Waves
Underwater Acoustics
Physical Properties
Biological Properties
Geological properties
Instrumentation
Scuba Diving

Consequently, if a student is to learn to read Tide Tables; if he is to have a knowledge of wave theory and the principles and techniques of the engineer; if he is to utilize the principles of underwater acoustics to determine the path of acoustic wave travel (draw ray diagrams) if he is to use the Salinometer, or the STD recorder and understand the principles; if he is to statistically analyze data of temperature, salinity, and sound velocity - if he is to have practice in the above principles; then there must be at least 6 trained faculty to provide the students with this base. At UDC this program implementation has been carried on by a minimal of faculty.

In June 1978, the University of the District of Columbia consolidated into one-all of its program offerings of the three colleges that comprise this University; i.e. the Washington Technical Institute (Van Ness Campus); the Federal City College (Mt. Vernon Square Campus); and the District of Columbia Teachers College (Georgia-Harvard Campus). In this process, programs that were formerly offered under the quarterly calendar had to be converted to the semester calendar. This calendar change was very detrimental to the Marine Science Technology program in terms of content of the program. A major revision of the program is necessary if the students are to continue to receive a strong base in the physical sciences and directly apply these concepts to a practical solution of problems in the oceans.

It is envisioned that a four year program of oceanography may be a future possibility. The University of the District of Columbia is primarily a four-year institution, the Marine Science Technology program is but one of the few two-year programs presently ongoing.

Whatever is the future for this program, it has had a fundamental impact on the lives of those students of the District of Columbia who have been beneficiaries of its implementation, and who, without the funding provided by the National Sea Grant Office, would not be widening the horizons of their employment possibilities by a view of the world of the oceans.

8. Summary and Conclusion

The environment, with its natural storehouse of ENERGY, and the ECONOMICS to be derived therefrom; these are the articulated issues of our society today; EDUCATION, the key issue is missing from the hierarchy of a concerned society. Specifically, the world has moved from the wilderness of land to be developed, to the 2/3 of our world which the oceans represent, the 330 million cubic miles of water and the vastness of resources to be explored, exploited, and expanded for the wealth of mankind. Education of the masses has not kept pace with this expansion.

The planned budget of the United States for ocean and environmental studies is close to 4 billion dollars a year for the next several years. These funds are to be utilized for research and development of ocean and marine resources; for providing energy sources; for laws of policy that regulate and deregulate the environment and the oceans; for coastal zone management.

Few of the smaller educational institutions receive funding to assure capability in marine science and other educational programs that build a knowledge of the sea for the greater mass of people with no "literacy" on the problems and possibilities of the ocean world. Education must be at the forefront of ocean exploration if the maximum benefit is to inure to the 220 million people of America.

Two-Year Program in
Marine Science Technology Curriculum

Description	Class-room Hrs.	Lab Hours	Credit
General Chemistry I	2	4	4
Data Processing	3	0	3
Communications I	3	0	3
Science of Man's Environment	3	3	4
Technical Math I	3	0	3
			17
Second Quarter			
General Chemistry II	2	4	4
Communications II	3	0	3
Marine Instrumentation	3	6	5
Technical Math II	3	0	3
Humanities Elective	3	0	3
			18
Third Quarter			
Technical Writing	3	0	3
Biological Oceanography	4	6	6
Technical Math III	3	0	3
Physics I	2	4	4
			16
Fourth Quarter			
Basic Electronics I	3	3	4
Physical Oceanography I	3	3	4
Environmental Statistics I	3	0	3
Physics II	3	3	4
Social Science I	3	0	3
			18
Fifth Quarter			
Physical Oceanography II	3	3	4
Environmental Statistics II	3	0	3
Physics III	3	3	4
Social Science II	3	0	3
Technology Elective	3	3	4
			18
Sixth Quarter			
Environmental Microbiology I	2	4	4
Data Handling & Analysis	3	3	4
Geological Oceanography	3	9	6
Scuba Diving	2	3	3
			17
Environmental Law (Elective)	3	0	3

Students co-op for one or two quarters depending on the availability of such experiences.

References

1. G. Tyler Miller, Jr., "Living in the Environment," Wadsworth Pub. Co., Inc., 1975.

2. Matilene S. Berryman, "Careers in Environmental Sciences," 1974 Proceedings, Shoreham Americana Hotel, Washington, D.C. & Sea Grant Marine Science Technology Program at Washington Technical Institute, October, 1974.

3. Environmental Protection Agency, Research Highlights, 1977; EPA 600-9-77044, Dec. 1977, Washington, D.C.

4. EPA, Who's Who in the Interagency Energy/Environment R & D Program.

UNDERGRADUATE PREPARATION FOR A CAREER IN PHYSICAL OCEANOGRAPHY

V. E. Delnore
Department of Meteorology and Physical Oceanography
Cook College, Rutgers University
New Brunswick, New Jersey 08903

Abstract

A survey of academic institutions, employers, and placement officers was undertaken to examine the desirability of undergraduate education in physical oceanography. This subject is approached from the viewpoints of graduate school admission and employability of degree recipients. The results of the study indicate that students anticipating careers in physical oceanography would do well to earn a bachelor's degree in a basic physical science or engineering (rather than in physical oceanography). However, the results also indicate a need for elective introductory courses in physical oceanography.

1. Introduction

Enrollments in U. S. undergraduate degree programs in marine physical science are increasing. 237 bachelor's degrees were awarded in that field during 1973-74, and 253 were awarded the following year, all by less than a dozen schools.[1,2] Students are eager to study oceanography (one school had 312 students enrolled in in its bachelor's degree program last year), in spite of decreasing optimism in job forecasts.[3,4,5] It becomes important, then, to examine undergraduate education in oceanography, and to seek suggestions for students and educators. These suggestions should enable universities to continue to be responsive to the nation's need for qualified marine scientists.

The premise is made here that jobs are available in oceanography, and that they will be filled by qualified persons. The question is raised as to the sort of undergraduate academic preparation most useful in qualifying a person to enter the field of oceanography. To answer this question, at least for physical oceanography, opinions and experiences were solicited from educators and employers. It was found that the most desirable strategy for a university student planning a career in physical oceanography includes earning a bachelor's degree in a basic physical science or in mathematics or engineering, followed by graduate study or initial work experience in physical oceanography.

2. Definitions

This study is concerned only with academic preparation for careers in physical oceanography; no effort was made to include vocational training such as would be pursued by a person interested in a career as a marine technician. Likewise, the study does not include ocean engineering, marine biology, or other fields of marine science and oceanography outside of physical oceanography.

For brevity, the term "oceanography" will mean only physical oceanography. The term "marine science" is used here to mean general oceanography, or geological, biological, chemical, and physical oceanography taken together.

The terms "basic science" or "physical science" are taken here to include the usual physical sciences, including mathematics. "Engineering" includes all fields of engineering study, although the emphasis in oceanography would be on electrical, chemical, and mechanical engineering.

3. Methodology

Faculty members of twelve undergraduate departments and several graduate departments offering degrees, degree options, or substantial course work in oceanography were contacted by telephone or through personal interview. The undergraduate departments contacted include virtually all those in the United States with such programs, except for the service and maritime academies. (These were excluded because their graduates do not normally enter the open job market.) Placement offices, government agencies, industrial firms, and environmental consulting companies were also contacted. Each contact consisted of a discussion during which several questions were asked.

In the case of the undergraduate departments, the questions were concerned with:

- reason a degree was, or was not, offered
- the curriculum
- student response to the courses and/or program
- success of students in obtaining jobs or admission to graduate study.

Graduate school admission officers were asked what undergraduate preparation was the most desirable for graduate study in oceanography.

For industrial and consulting firms and government agencies, inquiry was made about past and projected needs for persons trained in oceanography at the baccalaureate level. Also, information was sought concerning the hiring of persons with degrees in other fields to do oceanographic work.

Placement officers were asked about their own perceptions of oceanography and about experience in placing graduates in that field.

It should be noted that all persons contacted were most enthusiastic about the study, and were eager to provide input.

Because of the small number of departments involved in undergraduate education in oceanography, no statistical analyses were attempted. No attempt was made to evaluate the quality of any particular program. In addition to the telephone and personal surveys, several monographs and compilations, as referenced, were consulted.

4. Results

Undergraduate programs

A directory of academic programs in oceanography[5] lists a large number of institutions offering undergraduate courses in that field. The telephone survey showed that only six (nine, if the service and merchant marine academies are included) of these institutions offer a baccalaureate degree in oceanography, in name or in fact. One of these six and three additional schools offer oceanography options within a basic science degree program. Another one of the six, plus a tenth institution, offer oceanography as a double (or second) major. The other major must be in one of the basic sciences.

The six different oceanography degree curricula surveyed may be characterized as follows:

- Three are structured around mathematics and physics, and require only two or three courses in oceanography, to be taken over the four years. One of these curricula was designed specifically to prepare students for admission to graduate school in oceanography.
- Two are effectively physics programs for the first three years, followed by a year of courses admittedly borrowed from the first year of the graduate program in oceanography.
- One is built around the subject material of oceanography. Students are required to take eight oceanography courses, such as air-sea interaction, dynamical oceanography, etc.

In the cases in which an oceanography option is available, it is usually offered within the requirements for a traditional basic science degree, usually physics. One faculty member of the institution offering both a degree in oceanography and an oceanography option within the physics degree said that a student seriously interested in oceanography would be better off majoring in physics. He advises students accordingly.

Of the two schools offering the double major, one grants the bachelor's degree in oceanography only when course work in that field is completed in addition to all the requirements for a degree in a basic science. The same institution also offers a single-major program in marine science, intended for students not planning careers in oceanography. The other double major is actually a five-year degree granted jointly with either mathematics or physics.

In all cases, it was found that student enthusiasm for undergraduate education in oceanography was high. Strong and active oceanography clubs exist at most of the institutions. This enthusiasm has led, in part, to the establishment and maintenance of many of the oceanography degree and option programs now in existence.

Several of the academic departments contacted offer graduate degree programs and/or undergraduate course work in oceanography, but no bachelor's degree in that field. The reason most often given for the lack of an undergraduate program (expressed, in some cases, adamantly!) was that the learning of a basic science should be the object of an undergraduate education, while the study of a specialized field such as oceanography should be delayed until graduate school or initial employment.

Graduate school admissions

All of the schools offering undergraduate oceanography degrees reported reasonable success in having students admitted to graduate study in various fields. However, some expressed the feeling that many graduate schools of oceanography discriminate against applicants with baccalaureate degrees in that field. Further telephone conversations, with faculty members of these graduate schools, confirmed this notion. Admissions officers said, for the most part, that oceanography should be taught only at the graduate level, and then on a foundation of skills in any one of the basic sciences or engineering. Many of them felt that a student with only a bachelor's degree in oceanography would necessarily be deficient in the fundamental tools to do graduate work. Further, most felt that an undergraduate has little to gain by taking watered-down versions of courses (in oceanography) which will still have to be taken in graduate school. One admissions officer stated that a student who studies oceanography as an undergraduate at the expense of courses in a basic science and then tries to study oceanography as a graduate student will never be able to adequately function in his/her chosen field; probably that student would spend an entire working lifetime trying to learn the basics which should have been learned during the undergraduate years.

Employment prospects

Most employers contacted reported that, for B. S. level positions in oceanography, a competent graduate in any one of the physical sciences or engineering would be acceptable. The only exception to this was one of the U. S. Navy laboratories, which actively seeks, through the civil service system, two or three persons a year who actually hold bachelor's degrees in oceanography. During 1977 one agency responsible for much of the nation's non-defence effort in oceanography hired only six bachelor's degree recipients to perform work in oceanography, and not all six had degrees in that field. That agency and others reported having received applications from far more oceanographers (at all degree levels) than could be placed.

Several professional organizations and industrial firms, mostly oil and consulting companies, expressed a preference for graduates in fields other than oceanography to perform work in oceanography. This is reflected both in the telephone contacts made for this study and in recruiting literature available in placement offices. One brochure[6] specifies undergraduate study in a basic science or engineering as preparation for a career in oceanography.

It was pointed out by federal employment officers that the civil service requirements for entry-level oceanography positions specify a bachelor's degree in any one of several basic sciences or in oceanography or in engineering, but these officers felt for the most part that any specific training in oceanography should be in addition to, not instead of, training in a basic science. One recruiter stated that a physics or math major could reasonably be hired into an oceanography position, but that for the converse to occur would be most unlikely.

5. Recommendations

The following recommendations are offered, based on the results of this study:

1) A student interested in a career in oceanography should avoid enrolling for an undergraduate degree in a field outside of the basic sciences or engineering.

2) An undergraduate interested in a nontechnical (writing, public policy, etc.) career in oceanography could reasonably enroll in a degree program in marine science.

3) For academic departments with an established degree program in oceanography, any curriculum built around oceanography itself should be changed in order to emphasize mathematics and/or physics. The requirements should be patterned after one or the other of those two fields, with a small number of courses (perhaps three at the most) in oceanography.

4) A better alternative for such a department, however, would be the gradual de-emphasis of the degree program in oceanography in favor of cooperation with a mathematics, physics, or engineering department to provide an option or second major in oceanography within or in addition to one of those basic disciplines. The direct benefit of this strategy would be that an existing oceanography department could then tap into a larger pool of technically oriented students than would ordinarily enroll in oceanography, and offer these students something (the option or second major) that their primary departments cannot.

5) Introductory undergraduate courses in oceanography should be offered as science electives or as option requirements. The former would satisfy the interests of science and nonscience majors alike, and the latter could be used as specified above. There is probably a need to increase the number of introductory oceanography courses available as electives.

6) Members of oceanographic and academic institutions should welcome opportunities to explain to guidance counselors and to prospective students and their parents the nature of work in oceanography and the academic preparation required. That oceanography is not itself a basic science, rather a field of application of many basic sciences, should be emphasized. Also to be emphasized is the relationship between undergraduate and graduate education, stated under Results.

It is hoped that the above recommendations will be of use to educators wishing to satisfy the interests of students while providing them with thorough training.

Acknowledgement. Funding for this study was provided by the Department of Meteorology and Physical Oceanography, Rutgers University.

References

1. "Digest of Education Statistics, 1976." Department of Health, Education, and Welfare, NCES 77-401. U.S.G.P.O., Washington, 1977.

2. "Curricula in the Atmospheric and Oceanographic Sciences, 1978." American Meteorological Society, Boston, MA, 1978.

3. "The Oceans and You." Marine Technology Society, Washington, 1973.

4. "Occupational Outlook Handbook, 1977." Department of Labor, Bull. 1955. U.S.G.P.O., Washington, 1977.

5. As for 4, above, but for 1978.

6. "Careers in Exploration Geophysics." Society of Exploration Geophysicists, undated.

SUBMARINE RADIOMETRY AND PHYSICAL ENVIRONMENT MONITORING

Joël A. VANDENBERGHE
Institut Supérieur d'Electronique
du Nord
59046 LILLE CEDEX - FRANCE

Robert KLING
Laboratoire d'Algologie
Université des Sciences et Techniques Lille I
59650 VILLENEUVE D'ASCQ - FRANCE

Abstract

A multidisciplinary project is described which involved research people, engineering faculty and student work.

The aim was to design a station able to monitor physical parameters in a marine environment, especially under-water light radiation measurement in tidal zone.

Description of the work and of the final project leads to some conclusions pertinent to engineering education.

Introduction

Project DITERASOL (DIspositif de TElemesure du RAyonnement SOLaire) was set up three years ago, as a multidisciplinary work involving research people from the Laboratoire d'Algologie, Faculté des Sciences, Université de Lille I (France) and the Institut Supérieur d'Electronique du Nord (Lille-France), a College of Engineering, specializing in electronic engineering.

The basic requirements as stated by the research people are presented below. The engineering solutions are then detailed and a conclusion is drawn about the educational aspects of this work.

I - SPECIFICATIONS

A thesis work in vegetable biology deals with the growth condition of a red alga, *Gracilaria Verrucosa* ; this plant grows on a silted rock facies of Eastern Channel, (50°N-1°35'W). The annual temperature conditions allow only a poorer algological flora than on the coast of Britanny, yet an interesting development is due to the outcrop of conglomerate kimmeridgian and portlandian : one can find good quantities of green, brown and red algae, especially *Gracilaria verrucosa*, *Gigartina stellata* and *Chondrus crispus*, of well-know economical interest (production of agar and carageen) In order to determine the best conditions of growth with respect to physico-chemical parameters (light being the most important), the best solution appeared to be to determine by measurement the conditions under which those species are developing.

The specifications of the device have been set up according to the known photosynthetic activity of the algae. The pigments used in this process have their peak absorption in blue, green, red and yellow range portions of the visible spectrum.

As the photosynthetic efficiency is coupled to the energy of the received radiation and to the spectral distribution of it, it was important to define an equipment able to identify and measure this energy at different times and different depths (between 0 and 50m).

The specifications are as follows :

- Measurement of oncoming radiation in a 2π steradian angle (half-space) in W/m^2.
- Analysis of the spectral distribution in 100 nm bands centered at 450 nm, 550 nm, 700 nm.
- Measurement of the water level above the equipment
- Turbidity of environmental medium
- Temperature

The interest of this work is two-fold :

- Theoretical : the availability of physical data in the actual environment will enable an *in vitro* simulation of those physical parameters and help in the study of growth for those algae.
- Practical : the equipment could be used to monitor the pollution on coastal zone, and help in determining the best suitable location for implement sea-farms for production or agar and carrageen producing algae.

II - RUNNING OF THE PROJECT

This project, as outlined before, has been submitted to successive groups of final year students in I.S.E.N. (Institut Supérieur d'Electronique du Nord, FRANCE), for three years now. As part of their curriculum, these students undertake in groups of two to three an externally sponsored project, the subject of which is generally provided by a company or a research laboratory. Engineering scope is frequently in a rather narrow field, but in this case, students trained in electronics technology had to deal with many problems which were completely new to them : physical measurements, environment, mechanical design, etc...

During the first year, the study led to the definition of transducers, signal conditionning and timing of the measurement sequences. In a first attempt, the equipment was designed to be connected by means of a transmission cable to an earth station providing power and recording facilities. After consulting marine technology specialist, this solution had to be abandoned, because of the foreseeable difficulties in maintaining a physical link of a sufficient strength to stand tidal movements. The year after, an other group of students used the work of their predecessors to design a new equip-

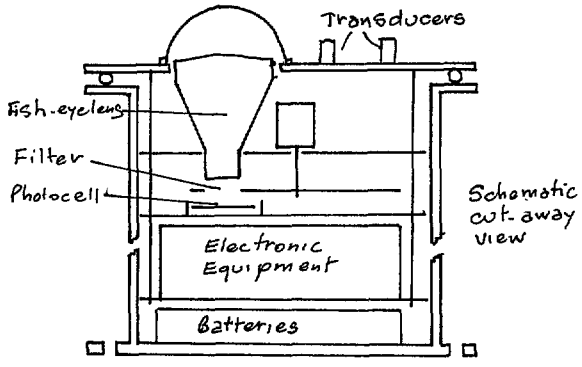

ment which could stand alone and record the physical parameters, the data being processed off-line, by removal of the recording equipment and use of computer equipment on earth.

They had to specify and choose the recording equipment, designed the container and started the realization of the control functions associated with equipment ; the specification of the digital recordind equipment helped them to build, in the same time, the software for processing data on a mini-computer.

At the end of the year, all of the equipment was available, but no test had already been undertaken at normal scale.

This year, a third group of students was assigned the responsibility of assembling the equipment and conducting the first series of measurements.

At the time when this paper is written, the assembling is coming to an end and the final adjustment of electronic equipment are performed. Experimentation should be undertaken during this coming summer.

The long term project has suffered many delays due to :

a) necessity of having each group of students deeply involved with the subject and with the work of the previous group.

b) delays in design and realization of the container, with the help of C.N.E.X.O. (Centre National pour l'Exploitation des Océans).

One can wonder, at this point, whether the opportunity given to the students of undertaking a major engineering project involving investigation in many fields was consistent with their eagerness to lead design of an equipment to a practical end, which did not happen in this case. It is possible that some of them felt slightly frustated by their apparent lack of results, because they had no means to evaluate from an objective stand point their achievement in this work ; nevertheless, the experience they gained in (a) investigating a new field of engineering and (b) dealing with the work of other people, was highly valuable and could make them appreciate the difficulties related to communication of knowledge and know-how.

III - DESCRIPTION OF THE EQUIPMENT

The equipments consist in a number of transducers, the signals of which are conditionned to be recorded in a digital way. The data acquisition system is built around a DATEL LPS 16 digital recorder, containing a 16 analog multiplexer, A/D conversion and related logic circuit. The record is made on digital cassete, which is subsquently read on a cassette reader connected to a mini-computer for data processing.

All of the measuring equipment is contained in a leak proof container made of a section of pipe tube (27 cm in diameter and 80 cm length). The equipment is attached to a removable cover for easy servicing and replacement of the cassette containing recorded data.

The bloc diagram is as follows :

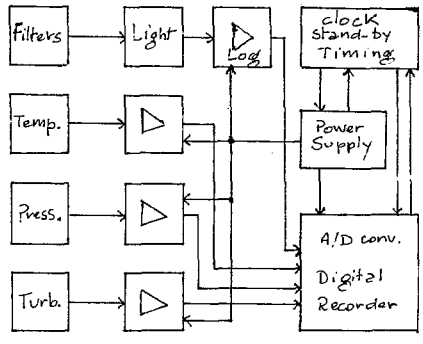

The ADC can accomodate 16 analog channels, out of which 9 are actually in use. Future applications could make use of the remaining ones.

3.1. Transducers

3.1.1. Light

Light has to be collected in a 2 steradians angle (half a space), above the tank container and has to be filtered before falling on the transducer.

We have imagined, instead of using a diffusor and transducer placed away so as to follow the correct law, to use a fish-eye lens (orthographic projection) and to place the filters between the rear lens and the transducer.

The lens in a NIKKOR, 10 mm, f/5,6, designed for light measurement and which transmits illumination without alteration. The low relative aperture of the optical system reduces the overall efficiency of the system (equivalent to a 2.5 mm2 useful area, whereas the photocell in use is a 5.6 cm disc on to which the image is located inside a 2 cm circle), but the advantage is the possibility of inserting filters very easily in front of the transducer.

The transducer is a silicon photocell and its short-circuit current is measured as an indication of the oncoming light.

The short-circuit current is directly proportional to the quantity of light falling on the device, and the combination of the transmission curves of each item and of the response curve of the photocell make possible an absolute evaluation of the irradiating energy.

The cell has been calibrated for relative and absolute response : Icc=1,23mAper mm2at830nm

The filters are positioned on a rotating disc, the movement of which is controlled by the timing and control system.

3.1.2. Temperature

Temperature of water and inside the tank are measured by means of resistances inserted into bridges.

3.1.3. Pressure

A pressure transducer, ranging from 0 to 7 bars, is used as an indicator of water height above the tank.

The transducer is Schaevitz made, type P 701 0002 0 to 100 PSI.

3.1.4. Turbidity

Turbidity of water is determined arbitarily by measuring the transmission of infrared light between a LED and phototransistor set 10 cm apart on the cover of the tank.

3.2. Signal conditioning and recording

- The imput of the A/D converter is rated at ± 5 V full-scale. The short circuit current of the photocell is amplified through a current-voltage converter designed around an operational amplifier and a logarithmic amplifier which allows suitable compression before A/D conversion ;

6 decades are recorded without having to change any range control.

- The resistance bridges are designed so as to give a useful signal according to the accuracy of the A/D converter, the same for the amplifier following the pressure gauge.

The data acquisition system (DATEL LPS 16) is controlled by a timing device and generates status signals which help in scheduling the stream of measurements.

The system is held unoperative (power-supply off) and activated at selected time intervals by a master stand-by clock.

When activated, a series of measurements is made (temp, press, light through three filters, test, file gap) and the system comes to a stop. It can be immediately reactivated for up to three measurements streams, thus giving the user the possibility of averaging measurements to avoid some errors.

- Time intervals between measurements is adjustable from 30 s to 1 h, the time taken for a set of measurements is 15 s (this is due to the time necessary for placing the filters between lens and photocell.

- The master stand-by clock is permanently powered and uses low-power logic. It activates the providing reset signals to a control card : this card then generates the control signals for the recording equipment.

- Power is supplied by a set of alcaline batteries and the autonomy is sufficient to insure a complete record of the available magnetic tape. (120 000 x 16 bit words). (e.g. : one measurement every 15 mm gives an autonomy of 140 days).

3.3 Container

The container is made of a pipe section, 80 cm high and 27 cm in diameter. One extremity is closed and on the other one a flange is welded which is used to fix the cover.

On the cover are attached all of the equipments : transducers are through leak-proof passages, electronic gear is attached to discs supported by four threaded rods and help in position with the help of spacers strung on the rods.

The cover is fixed to the container flange by a set of screws, water-tightness is made with a toroidal joint.

3.4. On site installation

The container is installed on the sea-shore, in such a position that it will be uncovered at low-tide. Provision must be made that the cover is always under water, to prevent the deposition on the hemispheric lens.

In order to enable the on-site removal of the cover ant the replacement of the magnetic tape, we have designed a concrete structure which is to be built if the equipment must stay for a long time.

For short term tests, which need not more than the recording of one cassette, the tank is attached to the sea floor by means of a simple concrete sole, it is removed at the end of the session and the cover is detached off-site (in the lab).

3.5. Data processing

The processing of recorded data is made with the help of a mini-computer (Intertechnique Multi 20).

The cassette is read with an ordinary cassette reader and all of the information is transfered on a disc storage for subsequent processing.

The correct filing of the recorded data is made during this transfer and a first correction is made according to the calibration of the transducers, so that the stored values can be taken as the physical parameter values.

When the information is available on the disc, any kind of subsequent processing (averaging, comparison, statistics, etc...) can be made by software means.

The programs developed for the specific project deal with the data storage on disc and with the edition of the raw parameter values on the printer.

IV - CONCLUSION

The equipment has been built and the computer programs are written. The first experiments are on the way while this paper is written and adjustments will certainly be necessary. From the experience we gathered out to this project-work, some viewpoints stand rather clearly, which we can quote without logical order :

- It takes a considerable amount of time to have a group of students to be involved in a multidisciplinary project and to make them widen their views in engineering field. For those students who have been trained for four years in fundamentals and in electronic engineering, the simple fact of designing a leak-proof metallic tank requires a lot of documentation and contacts with people of different training : communication ability is a must and they proved to be able to overcome these difficulties.

- Conducting a project from a year to another one without overlapping requires much time to have

the group accepting the objectives as stated before and preventing them from redesigning totally the work done preciously.

- Final year engineering students are not prepared to undertake a project which has to stand industrial requirements, neither are they to report on the work done so that an other team be able to carry on the work from where it was stopped. In spite of many endeavours to have them leave usable documents, the instructors or project supervisors had to take much time to make this work acceptable for the following team.

- The particular aspects of technology linked to the ocean environment have only been studied on paper : the available documents helped the conception of the system, and interviews with people from CNEXO or from French Navy Labs helped in designing the tank and its stand, but no platform test in a real marine environment has been undertaken by the student group.

The tests will now be conducted by the research people for whom the equipment was designed and it is possible that a group of students will be involved in the running of those tests and in the final work of transducer adjustments and evaluation, as well as in the design of specific software programs for scientific purposes, using the disc stored data.

In conclusion, we can state that this work was proved to be very interesting for the students involved, that they have schown, great abilities to adapt themselves to a kind of project which in non traditional in this College, yet it takes a lot of efforts for correctly managing those activities.

From the faculty viewpoint, this project has led to a widening of the normal field of interest or of contacts and has increased the comprehension between faculty people from different universities, in the same time it confronted us with real engineering problems not so likely evident in an academic environment.

SIMPLIFIED GUIDANCE FOR ENGINEERS ASSOCIATED WITH DESIGN, CONSTRUCTION, AND CERTIFICATION OF HYPERBARIC RESEARCH FACILITIES

Terry H. Hayes
Electrical Engineer
Naval Facilities Engineering Command
Alexandria, Virginia

ABSTRACT

Because of potential hazards associated with diving in deep ocean simulation facilities, a procedure has been developed by which these facilities can be certified for safe operation. One of the major steps involved in this procedure is the review of documentation associated with the design, fabrication and construction of these facilities. The review process affords the certifying authority the opportunity to evaluate the adequacy of design rationale, the adequacy of fabrication techniques and the conformance of these items with existing codes and standards. This paper concerns itself with the philosophy of the certification process and the rationale employed during the documentation review and evaluation.

1. INTRODUCTION

Diving, whether in the open ocean or in research facilities, is dangerous. The U. S. Navy, being a fore-runner in ocean research, have sought means to minimize endangerment to life in developing a program by which its hyperbaric research facilities can be certified for safe operations. The program is intended to assure (1) that the operators of the facility are qualified, (2) that the procedures for operation are adequate, and (3) that the rationale, methods and processes employed during the design and construction of these facilities are the most effective. This paper will address the latter, and will concern itself with the review and evaluation of documentation associated with design, fabrication and construction.

2. BACKGROUND INFORMATION

To combat the restraints of time, cost, limited knowledge, endangerment to life, and also to provide a controlled means by which both man and machine can be tested in simulated ocean environment, hyperbaric research facilities have been developed. These facilities provide a technological complex which simulates ocean environments by precisely controlling the magnitude and rate of change of pressure, temperature, salinity, turbidity and other ocean characteristics. These research chambers also provide a means by which the composition and condition of the confined atmosphere can be varied. From tests and experiments conducted in these facilities, the physiological effects of the ocean environment on man, his behavior, his ability to perform useful work, and the durability of machines can be evaluated.

Diver's safety, when the facility is operational, is the primary objective of certification. While confined within the facility (see figure 1), divers are subjected to such hazards as uncontrolled depressurization, fire, hypoxia, high noise levels, CO and CO_2 poisoning, narcosis, electrocution, embolism and toxicity. Of these, the two most feared are uncontrolled depressurization and fire. To date, 90 percent of all reported hyperbaric chamber casualities have resulted from fire.

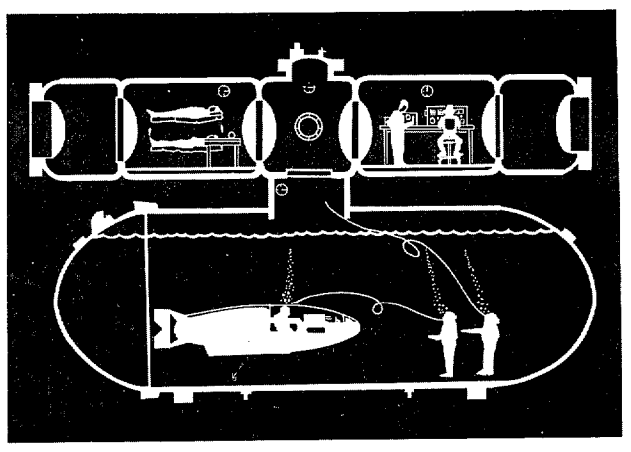

Figure 1 - Elevation of a Hyperbaric Research Facility

U.S. Government work not protected by U.S. copyright.

To ensure the safety of divers and operators of these complex facilities, the U. S. Navy has developed a safety certification program. Certification is defined as "The procedures, including application independent review, survey and approval, to insure the adequacy of the facility to perform safely over its operational/emergency spectrum" (1).

The Naval Facilities Engineering Command is the System Certification Authority (SCA) for all shore based, Navy owned or leased hyperbaric facilities. The Naval Sea Systems Command is the SCA for all sea going facilities. The U. S. Coast Guard has established a program for certifying commercial facilities.

3. MAJOR CERTIFICATION EVENTS

The evolution of events occuring during the certification process are illustrated in figure 2 and summarized below:

a. The applicant, owner or his agent, makes an application for certification of his facility. In his application, he defines objectives, summarizes descriptions, lists overall parameters and states the desired tenure period.

b. The applicant and the System Certification Authority (SCA) negotiate the certification scope, milestone event schedule, documentation rerequirements and cost.

c. The applicant collects and submits to the SCA documentation related to design, fabrication, construction and testing.

d. The SCA reviews and evaluates the documentation.

e. The SCA performs an on-site survey of the facilities and identifies any deficiencies which may exist.

f. The applicant performs an operational test for the SCA, during which any irregularties are identified.

g. The applicant or his agent corrects all deficiencies or irregularties.

h. The SCA issues a certificate of certification.

i. The applicant sustains certification throughout the effective tenure.

The entire process can not be discussed in this paper. However, one of the most important events is the documentation review, for it is here that useful design and fabrication information can be obtained.

4. DOCUMENTATION REVIEW

As previously stated, the applicant collects and submits to the SCA documentation related to design, fabrication, construction and testing. With regards to design, these documents usually consist of design drawings and specifications, design calculations, stress analyses, base material selection evaluation, failure modes and effects analyses, flexibility analyses, manufacturer's catalog sheets, manufacturer's certification statements and other documents or information necessary to substantiate the adequacy of the facility to perform safely within the design parameters.

With regards to fabrication, and testing during fabrication, these documents usually consists of welding or brazing procedures and procedure qualifications; welding or brazing operator qualification and qualification acceptance tests; welding or brazing equipment qualification; non destructive examination (NDE) equipment qualification; NDE procedures and results; qualification of NDE operators, interpreters and inspectors; methods of forming base metal; ductile

MAJOR CERTIFICATION EVENTS

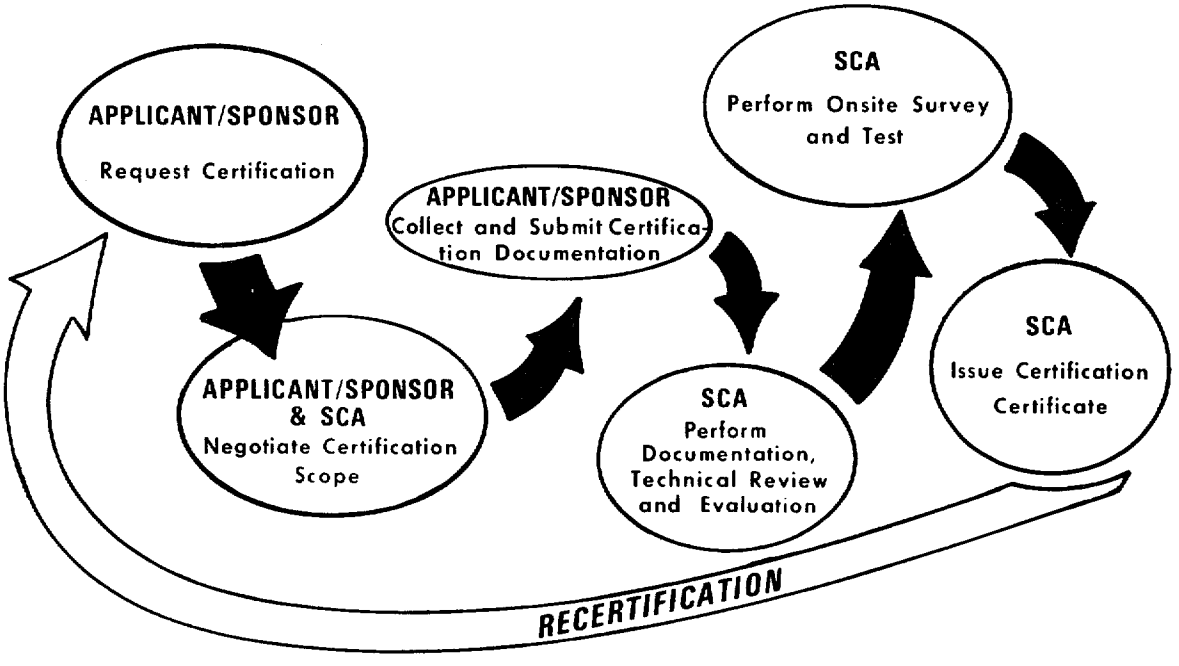

brittle transition test; post fabrication treatment; material traceability records; and records of material and component evaluation.

Additional documents are submitted and are related to systems cleaning; operational, emergency and maintenance procedures; quality of breathing gases; flammability and toxicity of materials; electrical insulation and continuity test; and other documents attesting to the safety of the facility.

The SCA then reviews these documents for evidence of such things as adequacy of design practices, built in redundancies, validity of design assumption and design rationale, adequacy of fabrication techniques, adequacy of construction practices and conformance with the applicable codes and standards to ensure that the facility as designed and constructed will not imperil the safety of the divers and operators.

A major problem often encountered by design engineers and fabricators is unfamiliarity with existing codes and standards applicable to the design and construction of hyperbaric research facilities. For some applications, codes and standards do not exist. However, there are many existing codes and standards which are applicable to the design and construction of these facilities.

The ones which most designers and fabricators are familiar are Section VIII, Divisions 1 and 2 of the American Society of Mechanical Engineers' (ASME) Boiler and Pressure Vessel Code (2,3). However, if one is referring to a man rated pressure vessel, these are not the governing codes. The American National Standard Institute (ANSI) and ASME standard ANSI/ASME PVHO-1(4) is the governing standard. As a supplement to Section VIII Divisions 1 and 2 this standard, establishes the rules governing the design, fabrication, and inspection during construction for man rated pressure vessels, their appurtenances and viewports. It should be emphasized however, that Section VIII Divisions (1) and (2) are the criteria and basis of PVHO-1.

It also must be understood and realized that a hyperbaric research facility is more than a pressure vessel. It is an intricate connection of the pressure vessel with its supporting systems. Systems typical of a hyperbaric research facility include the following:

1. The Pressure Vessel, its Appurtenances and Supports
2. The Atmospheric Conditioning System
3. The Potable Water System
4. The Waste Disposal and Sanitary System
5. The Gas Storage System
6. The Wet Chamber Water Conditioning System
7. The Oxygen Make-up System
8. The Gas Pressurization and Vent System
9. The Fire Extinguishing System
10. The Built-in Breathing (BIB) System
11. The Electrical System
12. The Communication System
13. The Gas Analysis System
14. The Panel System

Codes and standards applicable to the design and construction of these systems are summarized in Table (1). Abbreviations have been used to conserve space. Full titles are given in the references.

	Pressure Vessel	Cat I & II Piping Systems	Cat III Piping Systems	O_2 Piping	Electrical/ Communication	Life Support	Fire Extinguish Systems
Design	Div 1&2(2,3) DM-39(6) PVHO-1(4)	B31.1(7) Div 1&2(2,3) M.S. 438(8) M.S. 777(9)	B31.1 (7) MS 777(9) DM-39(6)	B31.1(7) DM-24(23) NFPA50-1(24)	NFPA 56D(10) NFPA 70 (15) DM-39(6)	MS 777(9) DM-39(6) SEA 9010(11)	NFPA 56D(10) DM-39(6)
Fabrication/ Installation	Sh 9010(12) M.S. 271(20)	B31.1(7)	B31.7(7)	Sh 7000(13) M.S. 777(9)	NFPA 70(15)	B31.1	M.S 777(9) B31.1(7)
Cleaning	N/A	Sh 9230.12 (16) Sh 9230.15 (17) P-9290(1)	Sh 9230.12 (16) Sh 9230.15 (17) P-9290 (1)	Sh 9230.12 (16) Sh 9230.15 (17) P-9290(1) MS - 1330 (18) MS 1359 (19)		Sh 9230.12 (16) Sh 9230.15 (17) P-9290 (1) MS - 1330	Sh 9230.15 (16) P-9290(1)
Hydro and Pneumatic Test	Div 1&2(2,3) DM 39(6)	B31.1(7)	B31.1(7)	B31.1(7)		B31.1(7)	B31.1(7)
Non Destructive Examination	ASME V (22) DIV 1&2(2,3) MS 453(21)	B31.1(7)	B31.1(7)	B31.1(7)		B31.1(7)	B31.1(7)

TABLE I
CODES & STANDARDS APPLICABLE TO
HYPERBARIC RESEARCH FACILITIES

The standards manuals and codes listed in Table (1) can not be considered to be all inclusive. There are many standards and codes governing the design and fabrication of the many components of these systems. Nevertheless, when these systems are designed with sound engineering judgement, fabricated and constructed with high quality workmanship, and when the design and fabrication techniques conform with the requirements of the codes and standards listed in Table (1), it can be assured that the facility will be safe for operation. A by-product of this effort would surely be an easier task for the System Certification Authority.

5. PHILSOPHY OF HAZARD LEVELS

In determining the codes and standards appliable to the design and fabrication of the aforementioned systems, consideration has to be given to the different modes of failure of the components and the effect such failures would have on the safety of the divers. A method was needed which would allow an evaluation of the failure on the basis of its severity. MIL-STD-882 (5) was helpful in providing guidance. It offers a procedure for categorizing failures into hazard severity levels. Using this procedure, components of the system can be evaluated during the failure mode and effect analysis, and dependent upon the effect such failures would have on the safety of the divers, assigned a hazard severity number The more severe the effect of the failure, the lower the severity number. The hazard severity evaluation criteria adopted for certification purposes are as follows:

a. Category I Catastrophic - Diver fatality or injury is highly probable. Failure management or means to circumvent the failure or malfunction is not possible.

b. Category II - Critical - Diver injury is imminent. Failure management is possible and necessary to sustain life.

c. Category III - Marginal - No diver injury. Failure management required to prevent injury.

d. Category IV - Negligible - No diver injury. Failure management performed at the discretion and convenience of the owners.

In adopting this approach it can readily be seen that the lower the hazard severity category number, the more stringent the code governing the design, the fabrication methods and techniques and the construction practices.

6. CONCLUSIONS AND SUMMARY

The process of certification is viewed by some as being an unnecessary process. The question often asked is "Why should a double check be made of design practices and fabrication techniques?" To date, for every hyperbaric research facility that has been constructed and certified, the certification process has uncovered areas of potential hazards. This in no way implies incompetance on the part of designers and fabricators, for they are very much concerned with the safety of these facilities. It must be realized that these facilities are among the first generation of ocean facilities. Where there is room for error, mistakes will be made. Even with the process of certification, there is no guarantee that diving casualties will not result. Yet it is comforting to know that in the minds of the designers, fabricators, builders and certifiers, the facility will perform safely.

Man in the oceans will eventually be required for any meaningful exploitive purposes. His being there will require the use of some type of liveable facility. The realiability and safety of these facilities will in many ways be dependent upon the research being conducted today in hyperbaric

facilities. Designers and fabricators will have obtained valuable knowledge in the design and construction of these needed facilities, requirements will be better defined and new criteria will evolved. From these requirements and new criteria, safety standards and codes will be developed. With a continued conscious effort toward safety, realiability and operability, certification will have paved the way and proven its effectiveness.

7. REFERENCES

1. Naval Material Command (NAVMAT) P-9290, "System Certification Procedures and Criteria Manual for Deep Submergence Systems," June 1976.

2. ASME Section VIII, Division 1, "Pressure Vessel Code".

3. ASME Section VIII, Division 2, "Presure Vessel Code, Alternative Rules".

4. ANSI/ASME PVHO-1, "Safety Standard for Pressure Vessels for Human Occupancy".

5. Military Standard (MIL-STD) 882A, System Safety Program Requirements".

6. NAVFAC Design Manual DM-39, "Hyperbaric Facilities".

7. ANSI B31.1, "Code for Pressure Piping, Power Piping".

8. MIL-STD-438E, "Schedule for Piping, Valves, Fittings and Associated Piping Components for Submarine Service".

9. MIL-STD-777C, "Schedule of Piping, Valves, Fittings and Associated Piping Components for Surface Ships".

10. National Fire Protection Association (NFPA) 56-D, "Hyperbaric Facilities".

11. NAVSEA 0994-LP-001-9010

12. NAVSHIPS-0900-006-9010, "Fabrication Welding and Inspection of HY-80 Submarine Hulls".

13. NAVSHIPS 0900-01-7000, "Fabrication and Inspection of Brazed Piping Systems".

14. MIL-STD 1693(YD), "Fabrication, Welding and Inspection of Hyperbaric Chambers and Other Critical Land-Based Structures."

15. NFPA-70, "National Electrical Code".

16. NAVSHIPS 9230.12A

17. NAVSHIPS 9230.15

18. MIL-STD-1330B, "Cleaning and Testing of Oxygen and Nitrogen Piping System".

19. MIL-STD-1359, "Cleaning Methods and Procedures for Breathing Oxygen Equipment".

20. MIL-STD-271E, "Non Destructive Testing Requirements for Metals".

21. MIL-STD-453A, "Radiographic Inspection".

22. ASME Section V, "Non Destructive Examination".

23. NAVFAC DM-24, "Land Operational Facilities".

24. NFPA 50-1, "Bulk Oxygen Systems".

DYNAMIC DAM FOR HARNESSING OCEAN AND RIVER CURRENTS AND TIDAL POWER*

James T. Yen
Research Department
Grumman Aerospace Corporation
Bethpage, N.Y. 11714

John Isaacs
Scripps Institute of Oceanography
University of California
LaJolla, California

Abstract

A new type of power system is proposed for creating economically viable systems for harnessing ocean and tidal energies. Based on the "dynamic dam" concept, immense amounts of ocean or river energy can be collected with low cost structures and concentrated into compact tur ines. Since the collecting surfaces do not encounter large hydrostatic pressures, as different from a static dam, they can be anchored in open oceans or wide rivers. Through an extended concept, this system can provide economical powerplants for harnessing even low level tides.

Vast amounts of clean and renewable energy may be derived from ocean and river currents and tides. However, their energy density is very low such that large collectors are needed for producing desirable amounts of energy and for bringing out the full potential of these sources. In addition, the ocean environment is corrosive and hostile. Hence, it is a formidable task and a tremendous challenge for scientists and engineers to come up with economically viable systems for harnessing ocean and tidal energies.

Wind energy has similar difficulties and its unpredictable fluctuations give additional trouble. To overcome these difficulties, the Tornado-type wind energy system and its extension have been proposed and first reported in References 1 and 2. Experimental and analytical investigations of the wind energy system itself are being sponsored by the U.S. Department of Energy.

The Dynamic Dam system is another extension of the above wind energy system. Figure 1 shows that a stationary collector "A" is used to collect ocean or river currents and maintain a water vortex within the collector. Due to the interaction between the vortex and the ambient atmosphere, a cavity is formed at the core of the vortex, and the atmospheric pressure is extended downward into the depth of the cavity. A water turbine is situated below both an inlet pipe and the bottom of the cavity, or between a high water head H_1 and a low head H_2, the latter is lowered by the vortex and the cavity. A large water head difference $\Delta H = H_1 - H_2$ is then maintained across the turbine, resulting in a high power density from the turbine. Immense amounts of ocean or river currents are collected by collctor "A" and concentrated through the action of the vortex and the cavity into a small and compact turbine. Of course, to maintain the cavity and the flow through the turbine, water has to be continuously exhausted through the pumping action of collectors "B" and "C". These are submerged collectors. Their vortices produce water-filled vortex cores which serve as low-pressure exhaust reservoirs for the collector "A" and the turbine. Two additional turbines, one each at the base of collector "B" and "C", can

---

* The Dynamic Dam concept for harnesseing ocean and river currents was invented by the second author in June 1976. Its extension to tidal power was made by the first author in July 1976. Professor Isaacs is very modest in insisting that he be the second author.

be installed. Also, collector "B" or " "C" can operate independently as a powerplant for harnessing ocean or river currents, without collector "A".

If the top of the collector "A" is sealed by a solid plate fitted with a vent pipe (Figure 2) then the entire assembly may be submerged and anchored to the bottom of the ocean. The vent pipe connects the vortex in collector "A" with the atmosphere and hence maintains the function of the cavity. However, when the ocean surface is raised by tides, the water head difference driving the turbine is increased from ΔH to $\Delta H' = \Delta H + \Delta H_T$. In this way, even a low-level tidal energy can be economically harnessed.

The system depicted in Figure 1 is called a Dynamic Dam by the second author. It maintains a head difference by the dynamic action of its vortex; in contrast, the conventional static dam uses a stationary surface to dam a river and maintain a head difference. The static dam has to sustain immense forces due to the head difference and it has to be anchored into solid rocks of mountains bordering the river. In general, it is expensive to build such dams and they cannot exist in open oceans or across rivers which are not bordered by rocky mountains.

The dynamic dam, on the other hand, does not encounter severe static or dynamic loads because due to the vortex action, there is little pressure difference across its peripheral walls. Thus its walls can be made of light weight, cheap and corrosion resistant materials and it can be placed in open oceans or wide rivers. The development of these systems would give us economical and practical power plants for harnessing the vast amounts of energy in ocean and river currents and in tides.

References

1. J.T. Yen, "Tornado-type Wind Energy System", Proceedings 10th InterSociety Energy Conversion Engineering Conf., Oct. 1975, pp. 987-994.

2. J.T. Yen, "A Combined System for Wind Power, Solar and Fossil Energy", Proceedings, Simposio Intern. sobre Fuentes de Energia y Desarrollo, Barcelona, Spain, Oct. 1977.

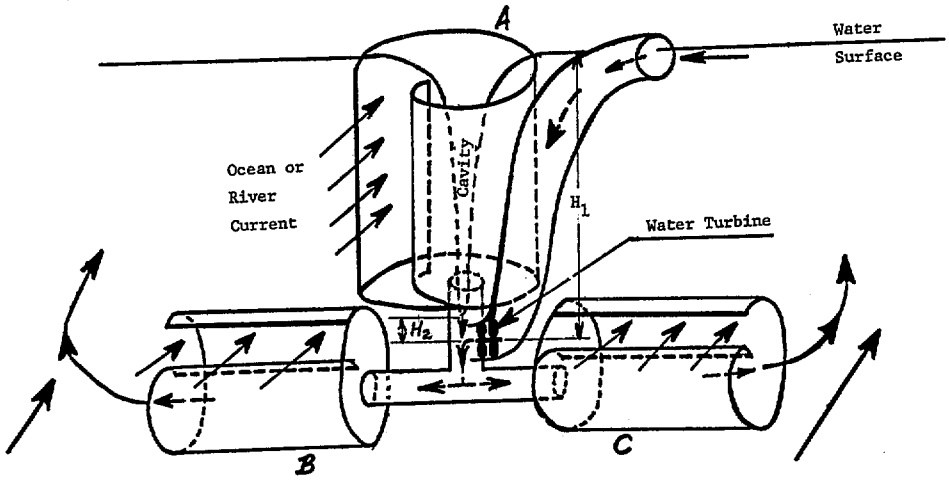

DYNAMIC DAM

Figure 1 A Sketch of the Dynamic Dam System for Harnessing Ocean and River Currents

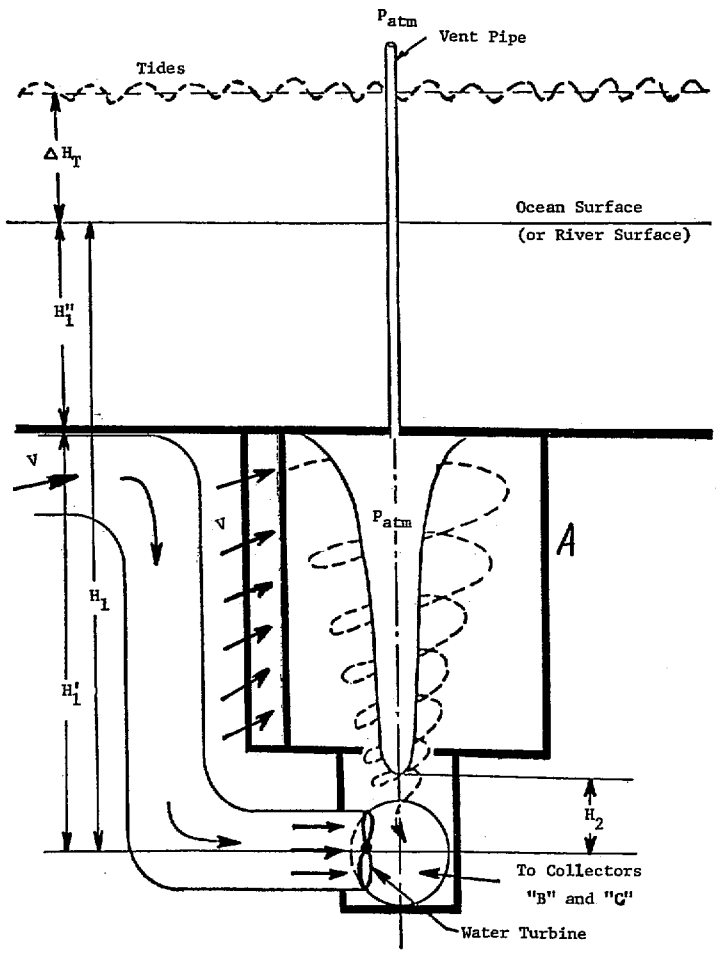

Figure 2 Dynamic Dam for Harnessing Tidal Energy

A WAVE ACTIVATED ELECTRIC GENERATOR

T. Omholt
Engineering Department
State University of New York
Maritime College
Fort Schuyler, Bronx, N.Y. 10465

Abstract

A large number of devices have been proposed for extracting energy from ocean surface waves. This paper proposes yet another which operates on the same principles as alternating current generators. The device froms a two-degree of freedom mechanical system producing power by electro-magnetic induction. The equations governing the system's motion, as well as, the rate of power generation is presented. These are solved in a special case, which for a typical set of operating conditions, lead to energy extraction from the waves of 35 percent.

1. Introduction

The power in ocean surface waves is considerable and many interesting ideas have been proposed for converting this energy into practical use. Recently, because of the energy crisis, interest has intensified. Slotta[1] has presented an extensive review and list of many of the concepts proposed over the last one hundred years. The number of possible devices seem to be inexhaustible.

More recently, serious effort has concentrated on the development of five power systems: (1) the Salter cam[2,3] being developed in England; (2) a hinged float type, also, developed in England[4]; (3) a pressure activated submerged generator developed by Kayser in Germany[5,6] (4) the wave powered pump developed at Scripp's Institution of Oceanography[6,9] and (5) a pneumatic wave converter originally developed by Masuda in Japan[7,8]. The first four systems are being considered for large scale energy generation, whereas, the last type is being used as low level power supplies for navigation buoys. It is in this latter category of uses that the proposed design is thought to have some utility.

Basically, the design consists of an electric power generator enclosed in a buoy. The generator (see Fig. 1) consists of a rectangular wire loop of N turns, directly supported by the buoy frame, and a system containing two permanent magnets which are supported by helical springs to the buoy. The wire loop which moves between the magnets, and the magnets form a two degree of freedom system excited by the wave induced motion of the buoy. Since the system has no exposed moving parts, fouling should not be a problem.

2. Generator System

If an electric conductor is moved relative to a magnetic field, an induced electric potential sets up a current in the conductor and, thereby, generates electric power. A simple system capable of generating power by this principle is shown below (Fig. 1)

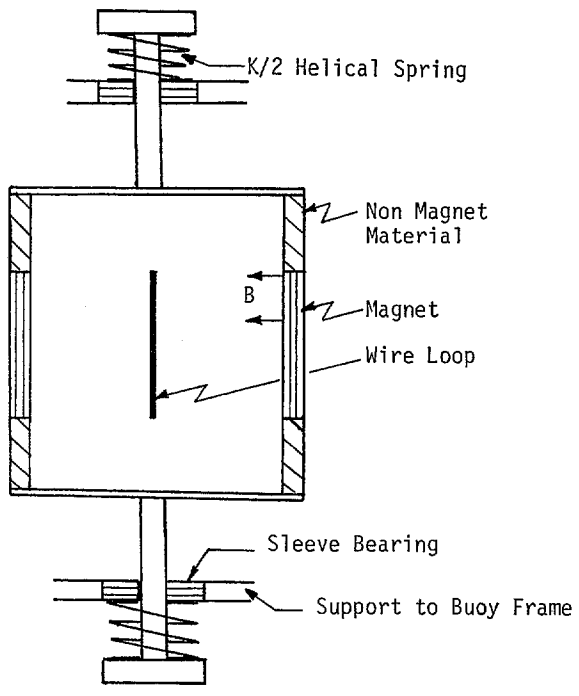

FIG. 1. GENERATOR SYSTEM

If V_r is the relative motion of wire loop with respect to magnet, the electrical power generated is

$$P = \frac{N^2 B^2 L^2 V_r^2}{R} \qquad (1)$$

where B is the magnetic induction, R is the load resistance in the wire loop, and L is the wire length (within magnetic field) in the plane perpendicular to the page. As a result of the current flow, a force will also act on the loop opposing its motion. This force is given by

$$F = \frac{N^2 B^2 L^2 V_r}{R} \qquad (2)$$

An equal but opposite force also acts on the magnets.

3. Motion of Buoy and Generator

The general equation of motion for a buoy can be stated as

Inertia Forces + Damping Forces + Restoring Forces = Excitation Forces (3)

Referring to the simplified diagrams (Fig. 2) for the buoy-generator motion, and assuming infitesimal waves, cylindrical buoy and only vertical motion, equation 3 can also be written as

$$(m+m_a)\ddot{Z} + b\dot{Z} + \rho g A Z = \rho g K_p A_a \cos(wt) - \frac{B^2 N^2 L^2}{R}(\dot{Z} - \dot{X}) - K(Z-X) \qquad (4)$$

where m is the buoy mass (excluding the mass of the spring supported magnetic system), m_a is the added mass, b is the damping coefficient, ρ is the water density, K_p is the pressure response factor (e^{-kd}), a is the wave amplitude, K is the total spring constant, κ and ω are the wave number and frequency. It has also been assumed that the buoy diameter is small compared to the wave length.

The system containing the permanent magnets has a mass m_m which is excited by the induced force (F) and the transmitted force through the two helical springs. The motion of m_m can therefore be expressed as

$$m_m\ddot{X} = -\frac{B^2 N^2 L^2}{R}(\dot{X} - \dot{Z}) - K(X - Z) \qquad (5)$$

It is clear from equations (4) and (5) that the two simple cases of $X = Z$ and $\dot{X} = \dot{Z}$ are not possible or energy generating motions. So that the phase angle between the two motions (X and Z) must be greater than 0 but less than 180.

If we let, $\tau = wt$, $w_B = (\rho g A/m+ma)^{1/2}/w$,

$$w_m = \left(\frac{k}{m_m}\right)^{1/2}/w,$$

$$\delta = \frac{B^2 L^2 N^2}{2R\sqrt{km_m}}, \quad \varepsilon = \frac{m_m}{(m + m_a)}, \quad X_1 = Z/a, \quad X_2 = X/a$$

and $\delta_0 = \frac{b}{2\sqrt{km_m}}$, so as to reduce the number of variables, equations (4) and (5) become

$$\ddot{X}_1 + 2w_m\varepsilon(\delta + \delta_0)\dot{X}_1 + (\varepsilon w_m^2 + w_B^2)X_1 = 2\delta w_m\varepsilon\dot{X}_2 + \varepsilon w_m^2 X_2 + w_B^2 K_p \cos\tau \qquad (6)$$

and

$$\ddot{X}_2 + 2\delta w_m\varepsilon\dot{X}_2 + w_m^2 X_2 = 2\delta w_m X_1 + w_m^2 X_1 \qquad (7)$$

These equations have the general solutions

$$X_1 = w_B^2 K_p R_e(\bar{X}_1 e^{i\tau}) = w_B^2 K_p \bar{X}_1 \cos(\tau+\psi_1) \qquad (8)$$

and

$$X_2 = w_B^2 K_p R_e(\bar{X}_2 e^{i\tau}) = w_B^2 K_p \bar{X}_2 \cos(\tau+\psi_2) \qquad (9)$$

To simplify the analysis, we will only look at the special case of $\psi_1 - \psi_2 = \frac{\pi}{2}$. Under this condition the buoy motion leads the motion of the magnets by 90 degrees.

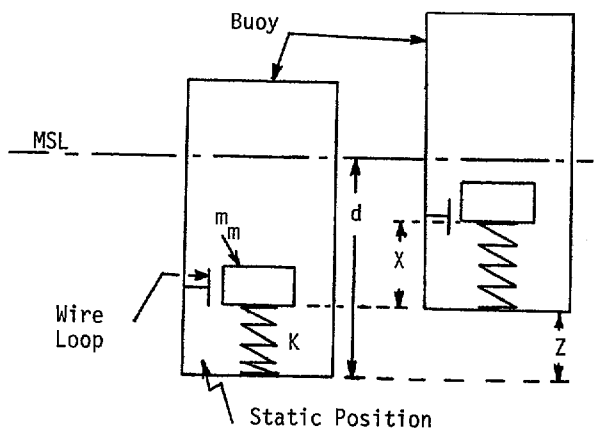

FIG. 2. SCHEMATIC DIAGRAM OF BUOY GENERATOR SYSTEM

4. Rate of Energy Generation

From equation (1), the rate of electric power generation is

$$P = \frac{B^2 N^2 L^2}{R} (\dot{Y} - \dot{X})^2 \tag{10}$$

and the average power over one wave period (T) is

$$\overline{P} = \frac{1}{T}\int_0^T P dt = \frac{B^2 N^2 L^2 a^2 W_B^4 K_p^2}{2R\left(\frac{T}{2\pi}\right)^2}\left[\overline{X}_1^2 + \overline{X}_2^2 - 2\overline{X}_1 \overline{X}_2 \cos(\psi_1 - \psi_2)\right] \tag{11}$$

If the buoy has a diameter equal to (D), then the average wave energy flux contained in a wave crest of length (D) is

$$P_w = \frac{\rho g^2 a^2 TD}{8\pi} \tag{12}$$

Taking the ratio of $\overline{P}/P_w$ we have the fractional part of the wave energy convered to electric energy. This is given by

$$\frac{\overline{P}}{P_w} = (2\pi)^2 \left(\frac{D}{\lambda}\right) W_B^2 \quad Kp^2 \, \delta w_m \varepsilon \, (H) \tag{13}$$

where λ is the wave length and (H) is given by

$$(H) = \frac{1}{2}\left[\overline{X}_1^2 + \overline{X}_2^2 - 2\overline{X}_1 \overline{X}_2 \cos(\psi_1 - \psi_2)\right] \tag{14}$$

The solutions of Eqs. (4) and (5) are straightforward but cumbersome to deal with. Therefore, the special case when $\psi_1 - \psi_2$ equals 90°degrees is considered. This allows for considerable simplification of $\overline{X}_1$ and $\overline{X}_2$. With the above restriction we have

$$\overline{X}_2 = \frac{\sqrt{1-4\delta^2}}{2\delta} \overline{X}_1 \tag{15}$$

and

$$\overline{X}_1 = \frac{2\delta}{\left[4\delta^2 (w_B^2 - 1)^2 + \varepsilon^2 (1-4\delta^2)(4\delta_0\delta+1)^2\right]^{1/2}} \tag{16}$$

with the requirement also that

$$w_m = \sqrt{1 - 4\delta^2} \tag{17}$$

Note that $w_m<1$ and that $\delta<.5$. The first of these conditions means that the natural period of the magnet-spring system is larger than the wave period. Also, for $\delta< \sqrt{1/8}$, $\overline{X}_2>\overline{X}_1$ and $\delta>\sqrt{1/8}$, $\overline{X}_2<\overline{X}_1$. With the above specification, Equation (13) for the power ratio becomes

$$\frac{\overline{P}}{P_w} = \frac{2\pi^2 \left(\frac{D}{\lambda}\right) K_p^2 \, \varepsilon w_B^2 \, \delta \, (1 - 4\delta^2)^{1/2}}{\left[4\delta^2 (w_B^2 - 1)^2 + \varepsilon^2 (1 - 4\delta^2)(4\delta_0\delta+1)^2\right]} \tag{18}$$

It can be shown that $\frac{\overline{P}}{P_w}$ is a maximum when

$$w_B^2 = \left[1 + \frac{\varepsilon^2 (1 - 4\delta^2)(4\delta_0\delta + 1)^2}{4\delta^2}\right]^{1/2} \tag{19}$$

So that, substituting Eq. (19) back into (18) gives

$$\frac{\overline{P}}{P_w} = \frac{\pi^2 \frac{D}{\lambda} K_p^2 \, \varepsilon (1 - 4\delta^2)^{1/2}}{2\{4\delta^2 + \varepsilon^2 (1-4\delta^2)(4\delta_0\delta + 1)^2\}^{1/2} - 2\delta\}} \tag{20}$$

and equation (16) becomes

$$\overline{X}_1 = \frac{\delta\sqrt{2}}{[4\delta^2 + \varepsilon^2(1-4\delta^2)(4\delta_0\delta+1)^{1/4}\{[4\delta^2 + \varepsilon^2 \cdot (1-4\delta^2)(4\delta_0\delta+1)]^{1/2} - 2\delta\}^{1/2}} \tag{21}$$

Equations (20) and (21) can not be further reduced by maximizing with respect to δ and ε Since for these variables, the maximums in general exist outside their allowable range of values.

5. Discussion

To obtain an idea of the power conversion effectiveness of this device under the conditions stated in section (4), the special case of $\varepsilon = .1$ and $4\delta_0 = 1$ is examined. Results for this condition is shown below (Fig. 3.). If we take $\delta = .3$, then we have that

$$\frac{\overline{P}}{P_w} = 4.5\pi^2 \left(\frac{D}{\lambda}\right) K_p^2 \tag{22}$$

and

$$\overline{X}_1 = 5.8$$

$$\overline{X}_2 = 7.7 \tag{23}$$

Since X_1 and X_2 are normalized with respect to the wave amplitude, the buoy height must be large. This, unfortunately, means that K_p^2 can become quite small for large values of $\overline{X}_1$ or $\overline{X}_2$.

If we choose, as being representative of a real system, the following values:

(1) D = 10 ft; (2) λ = 100 ft; (3) a = 3 ft; and (4) d = 20 ft, the value of $\overline{P}/P_w$ IS .35 (i.e. 35 per cent conversion of the wave energy into electrical energy). Both the buoy and magnets, under these conditions oscillate near resonance (W_B = 1 and W_m = .8). The above efficiency compares favorably with the maximum possible efficiency of 50 per cent reported by Mei[10] and a 25 per cent efficiency that can be determined from McCormick's[11] theoretical analysis of the pneumatic wave converter (his data from section D and the peak average power from Fig. 3 at 15 feet.

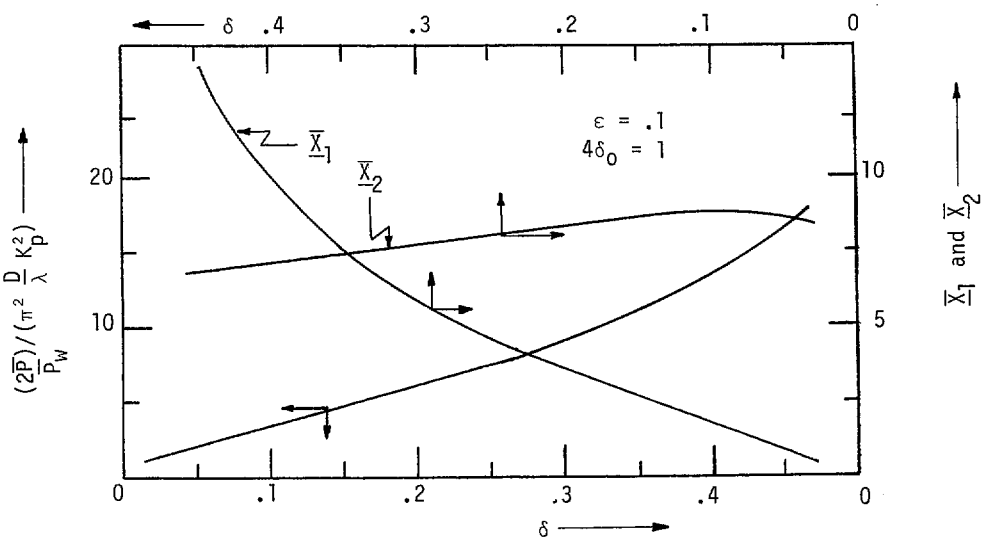

FIG. 3. EFFICIENCY AND MOTION OF SYSTEM

One feature of the system that has not been explored is the possibility of easily tuning it for maximum efficiency with changing wave conditions. This could be accomplished by changing the variable δ which involves the load resistance (R). This resistance could easily be changed, if the system also includes the recharging of batteries. Thus, by changing the rate of charging R could be increased or decreased. However, this is a matter that needs further investigation

REFERENCES

[1] Slotta, L. S., "Recoverable wave power concepts," (Proceedings) wave and salinity gradient energy conversion workshop, Univ. of Delaware, May 1976, pp. H 1 - H 186.

[2] Salter, S. H., "Wave Power," Nature, Vol. 249, June 1974, pp. 720-724.

[3] Salter, S. H., "Characteristics of a Rocking Wave Power Device," Nature, Vol. 254, April 1975, pp. 504-506.

[4] Wolley, M. and J. Platts, "Energy on the Crest of a Wave," New Scientist, May 1975, pp. 241 - 243.

[5] Kayser, H., "Energy Generation from Sea Waves," Proceedings, Ocean '74, IEEE Conference, Halifax, N. S., Canada, Vol. 1, 1974 pp. 240-243

[6] Isaacs, J. D., G. L. Wick and W. R. Schmitt, "Utilization of Energy from Ocean Waves," (Proceedings) Wave and salinity gradient energy conversion workshop, Univ. of Delaware, May 1976, pp. F 1 - F 36.

[7] Masuda, Y., "Wave Activated Generator," Intern Colloquim on the Expositions of the Ocean (Trans.) Bordeau, France, March 1971, pp. 1-18.

[8] McCormick, M. E., "A Modified Linear Analysis of a Wave Energy Conversion Buoy," Ocean Engng., Vol. 3, 1976, pp. 133-144.

[9] Isaacs, J. D., Castel and G. L. Wick, "Utilization of the Energy in Ocean Waves," Ocean Engng., Vol. 3, 1976, pp. 175-187.

[10] Mei, C. C., "Power Extraction from Water Waves," J. of Ship Research, Vol. 2, 1976, pp. 63-66.

[11] McCormick, M. E., "Analysis of a Wave Energy Conversion Buoy," J. of Hydronautics, Vol. 8, 1974, pp. 77-82.

ENERGY FROM SEA WAVES: SYSTEM OPTIMIZATION BY DIFFRACTION THEORY

G. Sebastiani, M. Berta, A. Blandino

Tecnomare S.p.A., S. Marco 2091, 30124 Venezia

Abstract

The paper deals with a computerized method for the determination of the optimal conditions for an efficient extraction of energy from sea waves. The analyzed system is a floating cylinder connected to an energy extracting device.
The system has been studied parametrically, by calculating its maximum efficiency in function of the geometric dimensions and layout configuration. The diffraction theory has been used in order to calculate the hydrodynamic terms (forces, added masses, damping coefficients) taking into account the real interaction between the body and the sea. Moreover a true statistic of waves is used in order to compare the efficiency of various systems in real sea conditions.
The results obtained have confirmed the possibility of optimizing the system efficiency with respect to the parameters examined.

1. INTRODUCTION

Many systems for the conversion of sea wave energy have been proposed in recent years. But the most important problem in this field is an optimization analysis for the energy transfer process from the sea to the equipment, taking into account the interaction effects between the system and the waves and between the system components (diffraction effects).
Moreover the performances of the system, like extracted energy and efficiency, must be evaluated with reference to an effective annual statistical distribution of sea states.
Infact, the theoric incident energy is distributed in a variable way into classes of waves of characteristics H and T (fig. 3) and it is strongly disuniform in time. Therefore only the average annual values of absorbed power and efficiency are significant in order to compare the different systems.
For this reason the entire analysis has been performed on the basis of the annual statistical distribution of the waves in a real sea: the Sicily Channel.
The system here analyzed - vertical floating cylinder with absorption device - is very simple; but it is schematically representative of the whole family of the wave energy extracting machines based on the large floating bodies motions.
The present study is based on a parametric dynamic analysis of the system in function of the geometric dimensions (radius, draft and distance between two components) and of the linearized damping (D_M), representative of the machine absorption. In order to obtain a correct calculation of the dynamic response, especially for waves of great height H, the linearized drag effects are included in the motion equations.
The solution of the dynamic equations for each couple of values H and T gives the motions of the body as well as the extracted energy.
By applying the procedure to all waves we obtain the total and average annual values of the extracted energy and then the average efficiency.
In this way it has been possible to compare the effective behaviour of the various systems by means of their real efficiency.

2. DYNAMIC ANALYSIS BY DIFFRACTION THEORY

The most important aspect of the present analysis has been performed by using our computer program DINDIF, which calculates the dynamic frequency response of a large body of arbitrary form, on the basis of the tridimensional diffraction theory. The sink-source numerical technique is used to arrive at the solution.
The capabilities of the program include the following calculations:
- global forces and moment
- added mass and damping matrix
- linear motions in six degrees of freedom
- dynamic pressure on the wet surface of the body, including or not the body motions
- velocity, accelerations and pressures for points in the surrounding fluid including or not the body motions.

The results of this computer program have been checked by experimental tests.

Synthetical review of diffraction theory

The mathematical approach is based on the potential fluid theory. The solution of the problem is obtained by determining a total velocity potential ϕ_t by the superimposition of the incident wave potential and of the perturbative effects induced by presence and motions of the body /1/, /2/:

$$\phi_t = \phi_o + \phi_7 + \sum_{j=1}^{6} \dot{s}_j \phi_j \qquad (1)$$

where:

ϕ_o = incident wave velocity potential (Airy)

ϕ_7 = diffracted potential due to the fixed body

ϕ_j j=1,6 = velocity potential due to the six degrees of freedom of the body.

The different contributions of the potential must satisfay the Laplace equation;

$$\nabla^2 \phi_j = 0 \text{ in the fluid field} \qquad (2)$$

and the boundary conditions on the free surface, on the sea bottom and at the infinite.
Finally the following boundary conditions on the wet surface of the body are applied:

$$\frac{\partial \phi_j}{\partial n} = n_j \quad j = 1,6 \qquad (3)$$

$$\frac{\partial \phi_7}{\partial n} = -\frac{\partial \phi_o}{\partial n} \qquad (4)$$

where $\frac{\partial}{\partial n}$ is the normal derivative in the direction of the outward generalized normal vector.
For each term ϕ_j (j=1,7) the solution of the problem is given by the following integral expression

$$\phi_j (x,y,z) = \iint_S Q_j(\xi,\eta,\zeta).G(x,y,z;\xi,\eta,\zeta)dS \qquad (5)$$

where:

- G is the Green function which, for different cases, assumes the formulations of Wehause, Laitone /3/ or Garrison /4/, /5/
- Q_j (j=1,7) is the unknown source density.

For each point of the mesh the values of Q_j are carried out by the solution of an integral equation obtained by applying to the expression (5) the boundary conditions (3) and (4).
The solution obtained for j=7 gives the forces (F_j) as well as the solution for j=1,6 gives the added mass matrix (A_{jk}) and the damping coefficients matrix (D_{jk}).
Then it is possible to solve the linear equation of the body motions:

$$\sum_{k=1}^{6} (M_{jk}+A_{jk})\ddot{s}_k + D_{jk}\dot{s}_k + C_{jk} s_k = F_j e^{-i\omega t} \qquad (6)$$

Finally this procedure has been extended to the case of two indipendent bodies.

Introduction of the linearized drag effects

Mainly near to the resonance condition and for great values of H it is necessary to consider the viscous drag resistance on the body.
In order to linearize the drag effect in the heave equation, we assume:

$$\frac{1}{2}\rho A C_D \dot{s}_3 |\dot{s}_3| = \frac{1}{2}\rho A C_D \frac{8}{3\pi} \dot{s}_{03} \dot{s}_3 \qquad (7)$$

where $\dot{s}_{03}$ is the heave velocity amplitude.
So, in the equation (6) the heave damping coefficient becomes:

$$D'_{33} = D_{33} + \frac{1}{2}\rho A C_D \frac{8}{3\pi} \dot{s}_{03} \qquad (8)$$

In this case the algebraic equation associated to the differential equation (6) is non-linear and the value of $\dot{s}_{03}$ is found by a convergence method; moreover, now the solution must be performed for each wave height.

Schematization of the energy extracting device

In the present analysis we assume that the energy extracting device behaves as an energy linear absorber D_M, which acts only for the heave motion.
Thus the total damping is changed again and becomes

$$D''_{33} = D_{33} + \frac{1}{2}\rho A C_D \frac{8}{3\pi} \dot{s}_{03} + D_M \qquad (9)$$

In order, the three terms of the total damping, from an energy point of view, represent:
- the energy irradiated from the body
- the energy dissipated for viscous effects
- the useful energy absorbed by the device.

As the dynamic equation (6), with the total damping coefficient D''_{33}, is solved, we obtain the dynamic response of the system including the absorbed energy.

3. INCIDENT ENERGY AND EXTRACTED ENERGY

Theoric content of wave energy

The mean power transferred by a sinusoidal wave of height H and period T through a vertical strip of unit width is /7/

$$P = \frac{\rho g^2}{16\pi} H^2 T f \qquad (10)$$

where:
f = 1 in shallow water
f = 0.5 in deep water.

The total energy (kinetic plus potential) transferred in a period T is:

$$E = P\,T \qquad (11)$$

The total theoric annual energy in a geographical area for which is assigned the statistical distribution of Hs and Tz (significant height and mean zero up-crossing period) is easily evaluated when the distribution of the number of waves (N_{jk}) into classes of H_j and T_k is obtained.
So the total annual incident energy is:

$$E_i = \frac{\rho g^2}{16\pi} \sum_j \sum_k H_j^2\, T_j^2\, N_{jk}\, f_k \qquad (12)$$

By applying the method to some significant cases, starting from basic wave statistics, the following values of mean annual power incident for meter of crest elevation have been found:

- Hebrydes Islands 55 kw/m
- North Sea (Ekofisk) 36 kw/m
- Sicily Channel 26 kw/m
- North Adriatic 22 kw/m

These values are lightly lower than those obtained by U.K. National Engineering Laboratory /6/.

For each wave of characteristics H and T the energy absorbed by a machine characterized by a linear absorber D_M is:

$$E_a = \frac{2\pi^2}{T} D_M\, s_{03}^2 \text{ (in one period)} \qquad (13)$$

When the system response is calculated for all couples H_j, T_k we can calculate the total energy extracted annually by:

$$E_a = 2\pi^2 D_M \sum_j \sum_k \frac{N_{jk}\, s_{03}^2 (H_j, T_k)}{T_k} \qquad (14)$$

where:

$s_{03}(H_j, T_k)$ is the heave amplitude of the floating cylinder, obtained by the solution of the equation (6) with the condition (9).

Efficiency of the system

We assume as average efficiency of the system the ratio:

$$\eta^* = \frac{Ea}{Ei} = \frac{\text{Total annual extracted energy}}{\text{Total annual incident energy}} \qquad (15)$$

where Ei refers to a wave front equal to the dimension of the body along the crest elevation.
This efficiency is the principal parameter to perform a comparison between different systems.

4. ANALYSIS AND RESULTS

Analysis performed

A parametric series of dynamic calculations has been performed with reference to a vertical floating cylinder connected to a device with absorption D_M relevant to the heave motion.
The parameters studied in the analysis are:
- radius of the cylinder (from 5 m to 40 m)
- draft of the body (from 2 m to 16 m)
  equivalent damping (D_M) of the device
- distance between the two equal components of a double system.

For all calculations a water depth of 100 m has been assumed.
The general procedure for the calculation of the system efficiency is shown in the block diagram of figure 2.
For each geometric configuration, having been assumed a suitable mesh (fig. 1), a preliminary analysis is carried out by computer program DINDIF, to calculate forces, added mass matrix and damping coefficient matrix for each period T.
Then, for each body a parametric analysis of the efficiency in function of D_M has been performed to calculate the value of D_M corresponding to the maximum average annual efficiency.

Results

The diffraction theory calculations have allowed us to take into account in the analysis the effective forces and hydrodynamic coefficients for each body. In fact, forces, added masses and damping coefficients are variable with the body geometry and with the period (fig. 4).

The importance of the choice of the equivalent damping of the machine D_M is confirmed by the results plotted in fig. 5. The maximum global efficiency for the system examined is 22.2% and is obtained for $D_M/D_o = 0.625$
In the curve efficiency versus T (fig. 5) it can be seen that for $D_M/D_o = 0.2$ the efficiency can reach a peak value of 39% for T=9 s, which is approximately the resonance period. But, as shown in fig. 8, for this value of D_M/D_o we have a low global efficiency (16%).
The curve of the global efficiency versus draft (fig. 5), shows the existence of a maximum for draft = 3-4 m.
Fig. 5 also shows the curve of the global efficiency versus radius.

Figs 7 and 8 show the effects of the interaction between two equal bodies in function of their mutual distance.
Fig. 7 shows the curves of the hydrodynamic coefficients of one body of the double system in ratio

to the same values of the single body.
The mutual influence is important especially on damping coefficient.
Fig. 8 shows how the mutual interaction can increase the average global efficiency of each single component of the double system; in fact it increases from 22.2 to 26.6 for bodies of radius 15 m and draft 12 m.

6. CONCLUSIONS

The results obtained by the present analysis confirm that today the most important problem concerning the extraction of energy from sea waves, for each proposed device, is an accurate parametric analysis to obtain the conditions of maximum efficiency. It is very important in this type of analysis to use diffraction theory methods, in order to take into account the effective interaction between the system and the sea and between the system components.
Furthermore the performances of different systems can be compared only on the basis of the average annual efficiency, obtained by starting from the seasonal and directional wave statistics.
With regard to the system analyzed it has been demonstrated that without this kind of optimization a very poor efficiency may be obtained. In fact the calculated values of the efficiency come within the range 10% - 30%.
Moreover the results have shown that taking advantage of the interaction between the two components of a double system, the efficiency can be considerably increased again.

REFERENCES

/1/ Loken, A.E., and Olsen, O.A.: "Diffraction Theory and Statistical Methods to Predict Wave Induced Motions and Loads for Large Structures", OTC 2502, 1976

/2/ Faltinsen, O.M., and Michelsen, F.: "Motions of Large Structures in Waves at Zero Froude Number", Proceedings of International Symposium on the Dynamics of Marine Vehicles and Structures in Waves, University College London, 1974

/3/ Wehausen, J.V., and Laitone, E.E.: "Surface Waves", Handbuch der Physik, 9.1969, Springer-Verlag Berlin, 1969

/4/ Garrison, C.J., and Berklite, R.B.: "Hydrodynamic Loads Induced by Earthquakes" OTC 1554, 1972

/5/ Garrison, C.J., and Chow, P.Y.: "Waves Forces on Submerged Bodies", Journal of the Waterways, Harbors and Coastal Engineering Division - ASCE, Aug. 1972

/6/ Leishman, J.M., and Scobie, G., UK N.E.L.: "The Development of Wave Power - A techno Economic Study", 1975

/7/ Kinsman, B.: "Wind Waves", Prentice-Hall, 1965

ACKNOWLEDGEMENT

The authors wish to thank their colleagues Mr. R. Pesaresi for his important contribution to the theoretical approach and Mrs E. Bognolo and I. Piussi for the preparation of this paper.

NOMENCLATURE

A	πR^2
A^*_{33}	Heave added mass for each single body of a two body system
C_D	Drag coefficient
C_{jk}	Hydrostatic restoring matrix (j,k=1,6)
d	Draft
D_M	Device damping coefficient
D^*_{33}	Heave damping coefficient for each single body of a two body system
D_o	$\rho V\sqrt{g/R}$
Ea	Absorbed energy
Ei	Incident energy
f, f_k	Incident energy factor
F^*_3	Heave force on each single body of a two body system
g	Gravity constant
H	Wave height
M_{jk}	Mass matrix of the body (j,k=1,6)
n_j	Surface generalized normal
N_{jk}	Number of waves into classes of height H_j and period T_k
R	Radius of the body
s_j	Body motions (j=1,6)
s_{oj}	Motions amplitude (j=1,6)
S	Wet surface of the body
T	Wave period
V	Displaced volume
ρ	Mass density of water
ω	Circular frequency of wave

FLOATING BODY GEOMETRY

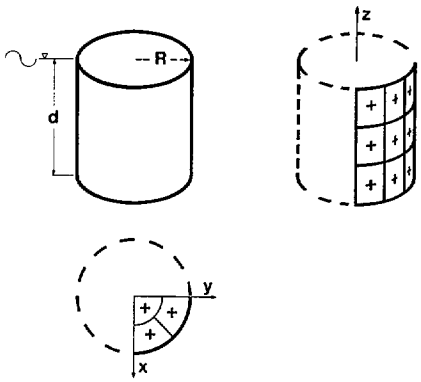

Fig. 1 - Mesh used in DINDIF calculations

PROCEDURE FOR SYSTEM EFFICIENCY EVALUATION

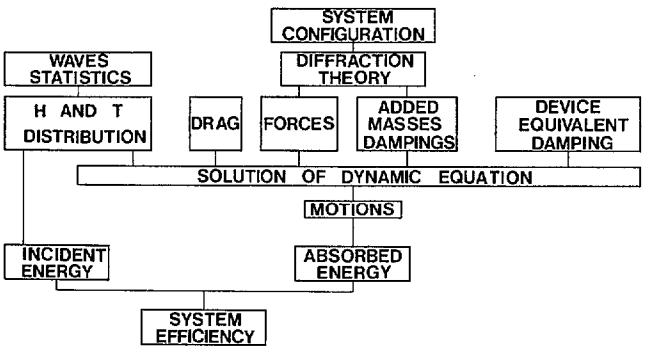

Fig. 2

INCIDENT WAVE ENERGY

AVERAGE ANNUAL DISTRIBUTION

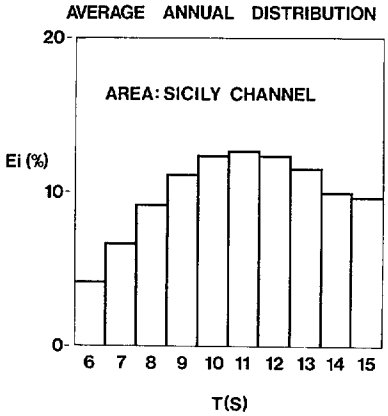

Fig. 3

VERTICAL FORCE

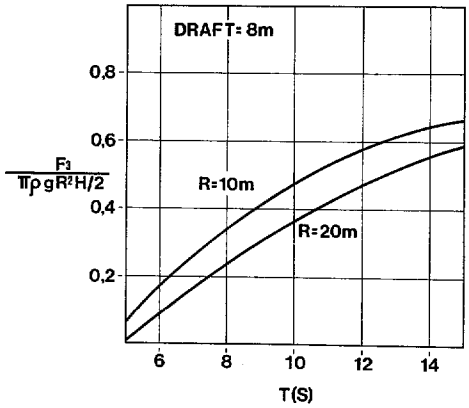

ADDED MASS

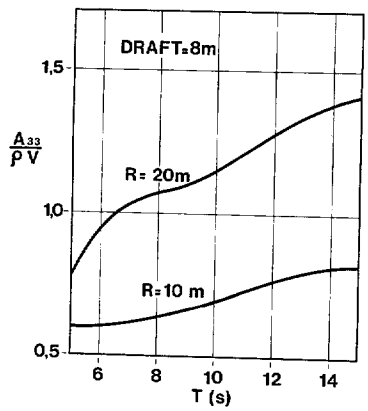

DAMPING COEFFICIENT

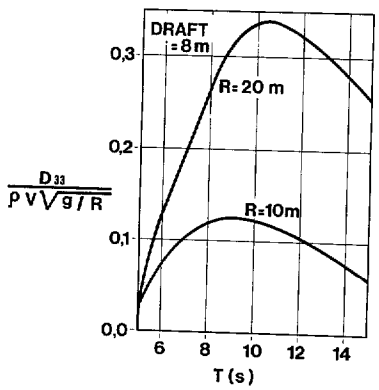

Fig. 4 - Heave hydrodynamic terms by diffraction theory

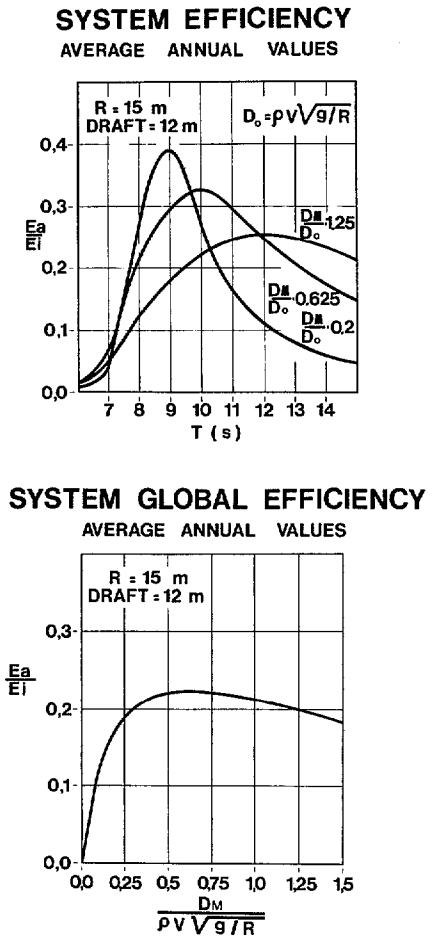

Fig. 5 - Efficiency Vs period and device absorption

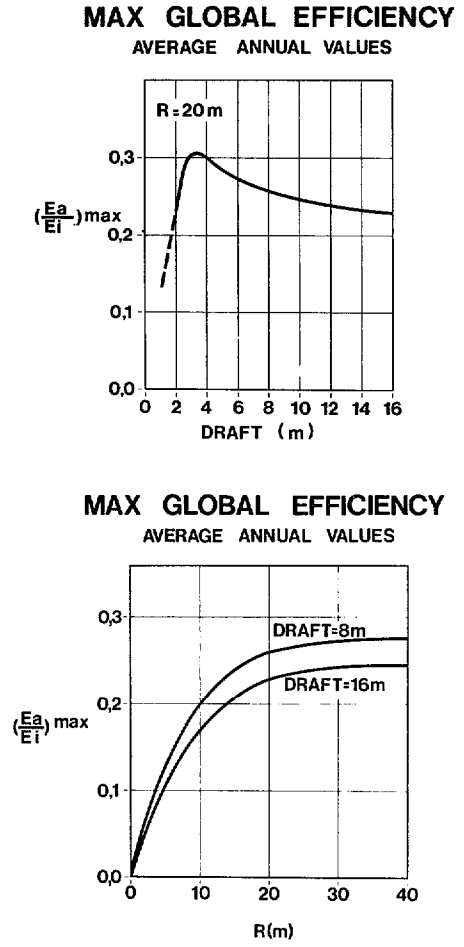

Fig. 6 - Max efficiency Vs radius and draft

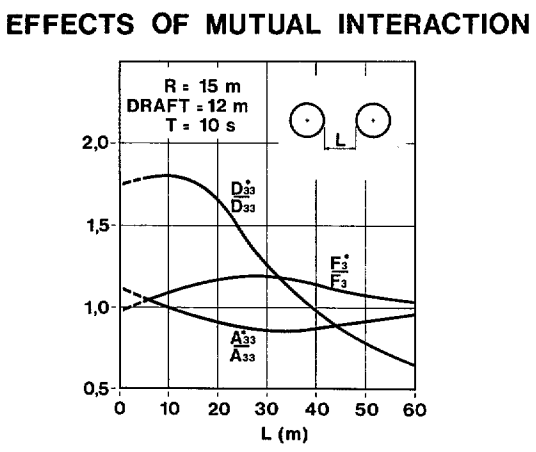

Fig. 7 - Heave hydrodynamic terms ratio between two body system and single body system

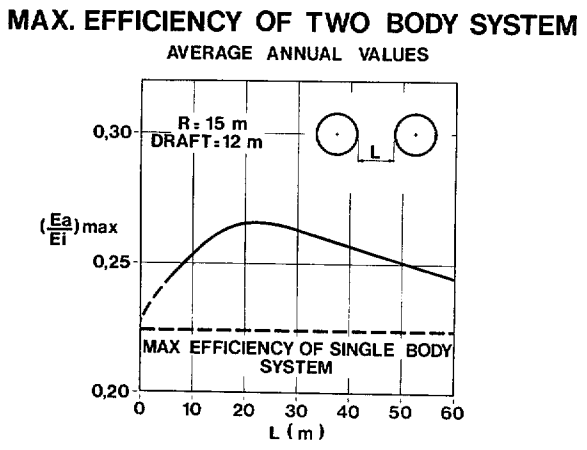

Fig. 8 - Efficiency comparison between two body system and single body system

A HYDROSTATICALLY ACTUATED PISTON AND HYDRAULIC SYSTEM FOR DEEP-SEA FREE VEHICLE APPLICATIONS

O. H. Kirsten and R. F. Weiss
Scripps Institution of Oceanography
University of California, San Diego
La Jolla, California 92093

Abstract

A piston actuated by hydrostatic pressure at ocean depths up to 6 km is used to provide a controlled source of hydraulic fluid at above-ambient pressure. This fluid energy is used to collect box cores of deep-sea sediment and ferromanganese nodules from a free-vehicle instrument platform. At the completion of the coring operation, the same hydrostatically actuated piston is used to release ballast and to extract the vehicle and its cores from the sediment.

Introduction

Several investigators have used hydrostatic energy as a means of performing work in the deep sea (Lisitzin et al., 1954; Rosfelder, 1966). However, widespread application of this technique has been limited by problems in the design of seals and housing, and in methods of controlling large differential pressures in the actuating fluid. Nevertheless, this approach has remained extremely attractive because the amount of available work is extremely large. Consider a mechanism in which a piston is driven against an evacuated internal displaced volume V by a fluid at hydrostatic pressure P. Neglecting frictional losses, the available work is simply the product PV. In the sea, the work available per kilometer of depth per liter of internal displaced volume is thus $\sim 10^4$ joules, or $\sim 10^3$ kilogram-meters.

This paper describes a hydrostatically actuated piston designed to perform a series of specific tasks on a deep-ocean free vehicle, the MANOP Bottom Lander, which will carry out measurements at the sediment-water interface related to the formation of ferromanganese nodules. The Lander will operate at depths up to 6 km and will carry out in situ chemical flux experiments by collecting a time-series of water samples from three chambers emplanted in the sea floor. The Lander will also inject the chambers with chemical and biological tracers and monitor pH and dissolved oxygen. The preliminary design of the Lander is summarized by Weiss et al. (1977).

At the close of the experiment, which may last as long as one year, the Lander will collect box cores of the sediment and nodules underlying each of the three chambers, release ballast, extract itself out of the sediment, and then rise to the surface. These operations will require exceptional amounts of energy which must be stored for the full deployment period. We have decided to use ambient hydrostatic pressure to actuate a single piston which will supply the force needed to perform all these operations. Although the device is still undergoing development, we hope that by presenting our work at this stage we will inspire worthwhile dialogue with other members of the oceanographic community.

The Mechanism

The Lander's hydrostatically actuated system is shown schematically in Figure 1. Its principal components are a compressible reservoir filled with silicone fluid at hydrostatic pressure, a control valve fired by an explosive cartridge, a flow restrictor, a primary actuating cylinder, a secondary cylinder to supply pressurized hydraulic fluid, and a ball-lock ballast release mechanism.

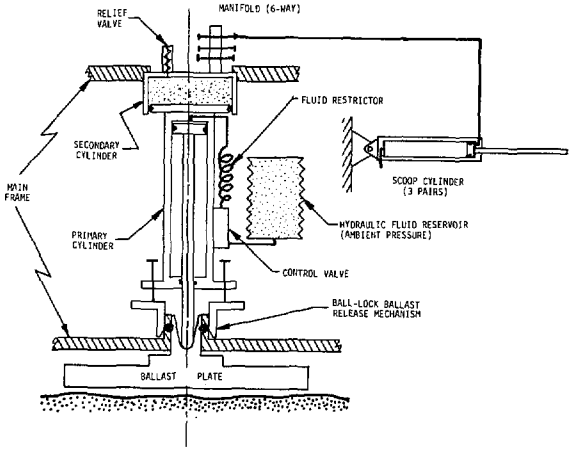

Figure 1. Schematic representation of the hydrostatically actuated system for the MANOP Bottom Lander. The positions of all the components are shown prior to actuation. For simplicity, only one of the six scoop-closing hydraulic cylinders is shown.

A sectional view of the control valve is shown in Figure 2. The design is an adaptation of a deep-sea time release mechanism developed by Sessions and Marshall (1971). Instead of a conventional valve design, an aluminum disc is used to seal the primary cylinder against the hydrostatically pressurized silicone fluid. In this way, the sealing of the valve depends entirely on the integrity of reliable static seals which are not exposed to seawater. On a signal from the Lander's microprocessor control system (Ackermann et al., 1978) or from a backup control mechanism (Weiss et al., 1977) the explosive cartridge is fired and a piston is propelled toward the aluminum disc. The piston is designed to pierce the disc, allowing the silicone fluid to flow into the valve, through a sintered metal filter to trap particulate impurities, and out toward the flow restrictor. Experience with the Sessions and Marshall release device has shown that these explosive cartridges, which are manufactured for critical aerospace applications, are of exceptionally high reliability, so that we consider this approach to be superior to the use of conventional high-pressure valves.

The flow restrictor has the geometry of a long spiral tube of sufficiently small internal diameter to control the rate at which the inrushing silicone fluid actuates the primary piston. The exact length and internal diameter of the flow restrictor depend upon the volume of the primary cylinder, the desired actuation time, the hydrostatic pressure, and the viscosity of the silicone fluid as a function of temperature and pressure. We propose to adjust the dimensions of the restrictor so that the actuation will occur over a period of approximately 10 minutes. This should allow sufficient time for the suction which is created under the box cores during the push-out process to be relieved.

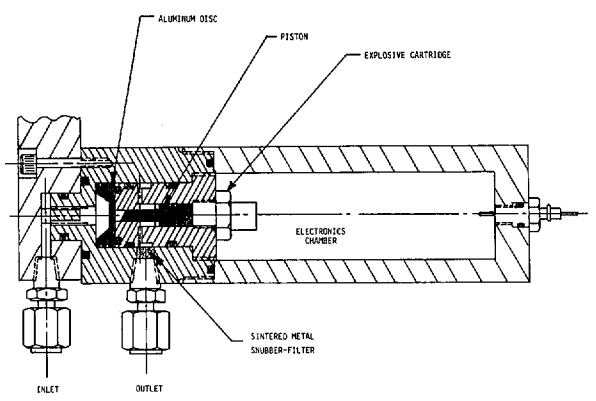

Figure 2. Sectional view of the control valve showing the explosive cartridge, the piston, and the aluminum disc which is punctured during actuation.

The primary cylinder and piston provide the mechanical driving force for the entire hydrostatically actuated system. As the silicone fluid flows from the restrictor into the upper portion of the primary cylinder, the primary piston is driven toward the displaced internal volume below the piston. This volume is either evacuated or filled with air at 1 atmosphere. The available force is thus given by the pressure differential across the piston multiplied by the difference between the cross-sectional area of the piston and the cross-sectional area of the cylinder rod. This cross-sectional area difference is ~ 4.5 cm^2. For deployments in shallower waters, a primary cylinder with a larger cross-section can be substituted to compensate for reduced hydrostatic pressure.

Because the cylinder rod is constrained by the main frame through the ball-lock mechanism, the full force of the primary cylinder is first applied upward against the piston of the secondary cylinder. Silicone fluid in the secondary cylinder is thus pressurized above ambient pressure, providing a convenient source of hydraulic fluid to drive the scoop-closing mechanisms on the three independent box cores. This system is designed to operate at a maximum pressure of ~ 14 atm above ambient pressure. A relief valve set at this differential pressure is used to vent excess fluid at the completion of the scoop-closing operation. The secondary cylinder has an internal diameter of ~ 14 cm and a full stroke of ~ 7 cm, so that ~ 1.1 liters of pressurized hydraulic fluid are available. The fully actuated secondary cylinder is shown schematically in Figure 3.

During the last centimeter of the secondary cylinder actuation, the skirt at the base of the primary cylinder raises the liftrods attached to the retainer ring on the ball-lock release mechanism (Figure 3). This allows the locking balls to fall free and the ballast plate to separate from the Lander's main frame. As the stroke of the primary cylinder continues, its full force is applied against the released ballast by the primary cylinder rod. The ballast plate thus acts as a foot against which the now-buoyant Lander can push itself and its closed box corers out of the sediment. Primary cylinder actuation continues until its full 46 cm stroke is completed.

Because the pushout and coring operations are dependent on the actuation of a single primary piston, failure of this piston to actuate cannot leave the Lander anchored to the bottom with its coring scoops closed. As a backup release mechanism, a separate set of liftrods can be used to raise the retainer ring and release the ballast plate. As long as the coring scoops are not closed, the Lander will then become sufficiently buoyant to free itself from the bottom without the aid of the primary piston.

Seals and Materials

The reliability of the hydrostatically actuated system depends heavily on the design of seals and on the choice of materials. For static seals used in the primary cylinder chamber, integrity is improved by the use of multiple seals: a face seal O-ring followed by a sleeve seal T-ring with dual backup rings. This redundant design provides long-term sealing where corrosive undercutting and pitting of seal surfaces can be a problem. The dynamic seals on the piston and cylinder rod are also of the T-ring type. The surface on which they ride are honed to a 8-10 RMS finish and are coated with molybdenum disulfide and silicone grease. The single T-ring piston seal is not exposed to differential pressure until the control valve is fired. The cylinder rod seal is composed of dual T-rings to provide the desired redundancy and also to protect the inner seal against acquiring a long-term pressure "set".

The primary and secondary cylinders are made of high-strength 7075-T6 aluminum and the cylinder bulkheads are made of 6061-T6 aluminum. All face seal surfaces are hard-anodized and coated with a urethane layer applied electrostatically and baked. The sleeve seal surfaces are only anodized. The corrosion resistance of these aluminum components depends upon the use of high-quality coating and on avoiding damage to these coatings during assembly. As an additional precaution, sacrificial zinc anodes are attached at strategic locations.

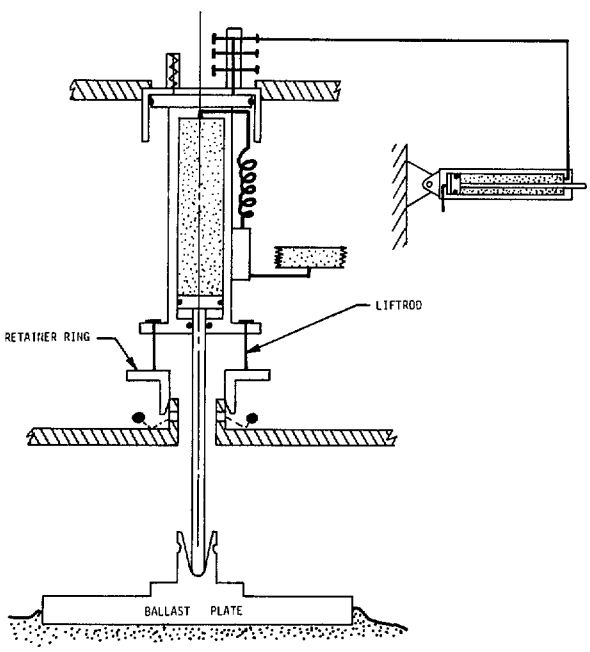

Figure 3. Schematic representation of the system after actuation is complete. The individual components are as labeled in Figure 1. Note that the ballast plate has been released by raising the retainer ring, thus allowing the locking balls to fall free (see text).

The remaining materials used in the actuator system are titanium used for the cylinder rod and tie rods, and electropolished and passivated stainless steel used for high-pressure tube fittings. The titanium is carefully isolated from electrical contact with the aluminum using non-conducting plastics. Titanium is preferable to stainless steel because of its higher strength-to-weight ratio and because it is not susceptible to undercutting and pitting in occluded areas filled with oxygen-depleted seawater.

Summary

Compared to other mechanical, chemical or electrical methods of storing large amounts of energy for mechanical applications in deep-sea instrumentation, we believe that a hydrostatically actuated system offers several distinct advantages. The mechanism is simple, light, and compact, and is essentially immune to degradation over long storage periods. Although the system we describe has been designed for use with a specific free vehicle, the MANOP Bottom Lander, the method is easily adapted to a number of deep-sea applications.

Acknowledgements

We thank A. Krause for his invaluable advice and assistance in the fabrication of this device, and M. H. Sessions for giving us the benefits of his experience in explosive release technology. This work is supported by the U. S. National Science Foundation as part of the International Decade for Ocean Exploration, Manganese Nodule Program.

References

Ackermann, R. E,, C. M. Butler and R. F. Weiss, A low-power microprocessor system for deep-sea free vehicle applications, in Oceans '78 Conference Record, Marine Technology Society and Institute of Electrical and Electronics Engineers (1978).

Lisitzin, A. P., V. P. Petelin and G. B. Udintzev A new achievement of the Soviet marine geology, the Svsoev-Kudinov hydrostatic core sampler, Priroda, 6, 63-66 (1954), [transl. by E. R. Hope, Def. Res. Board Canada, 1965].

Rosfelder, A. M., Hydrostatic actuation of deep-sea instruments, J. Ocean Technology, 1, 53-63 (1966).

Sessions, M. H. and P. M. Marshall, A precision deep-sea time release, Scripps Institution of Oceanography Reference Series, 71-5, University of California, San Diego, 18 pp (1971).

Weiss, R. F., O. H. Kirsten and R. Ackermann, Free vehicle instrumentation for the in situ measurement of processes controlling the formation of deep-sea ferromanganese nodules, in Oceans '77 Conference Record, paper 44D, Marine Technology Society and Institute of Electrical and Electronics Engineers (1977).

THE USE OF OCEAN ENERGY - A HYDROSTATIC MOTOR

S. Selwyn
Lamont-Doherty Geological Observatory
of Columbia University
Palisades, New York 10964

F.W. McCoy
Lamont-Doherty Geological Observatory
of Columbia University
Palisades, New York 10964

Abstract

A device which utilizes the hydrostatic gradient at sea is described. The apparatus is currently configured to drive a deep-sea sediment sampler but could be used for virtually any power requirement. A simplified schematic diagram is presented to illustrate the working principle, and sample calculations of the power available are provided.

1. Introduction

The concept described herein is a remote energy source usable in the deep-sea without umbilical hoses, electrical wires, or additional control cables. These features are appealing and desirable for operating equipment such as corers, rock drills, anchoring devices, or, for functioning as a low frequency sound source. Specialized conduits transmitting electricity, pneumatic pressure, or hydraulic fluids are the most commonly used methods for conveying energy or providing control to equipment at depth from surface vessels. With these methods, power losses due to friction or electrical resistance can be significant, especially at deeper depths; as are handling difficulties on deck with multiple cables and tubes and winches, not to mention entanglement problems with the main lowering cable during lowerings. All of these factors compound the problem of controllable energy sources in the deep ocean. Impact or remotely triggered explosive devices provide only brief sources of energy.

In bottom sampler designs, for example, portable power units utilizing energy derived from either surface vessels or from self-contained storage systems have been used in the vibro-corer, an air-driven, vibrating sampler, or in the "SEACORE 50", an electrically driven rotary drill usable only to 1,000 ft. water depths. The severe restrictions in using this equipment at deeper water depths due to line losses through electrical cables or hydraulic lines, in addition to high costs of purchasing and using cables and lines, severely limit their effectiveness. At extreme water depths, an additional problem arises for surface-supplied, pneumatically- or hydraulically-driven devices -- pressure differentials are reduced leading to a significant reduction in their inherent efficiency. To overcome line losses, self-contained power sources on sediment samplers have utilized energy stored in the form of compressed air, springs, electrical batteries, hydraulic accumulators, stretched rubber bands (Greene, 1971), or explosives (Andresen, et al., 1965). None of these has proven completely successful; as one example, the Norwegian Geotechnical Institute Gas-Operated, Sea-Floor Sampler (Andresen, et al., 1965) was driven into the sea-floor by igniting rocket propellent but after a few tests has not seen extensive use.

Hydrostatic pressure differentials have been used, but so far are capable of providing only brief pulses of usable power. A rotary rock drill, which has successfully drilled short cores in igneous rocks from the Mid-Atlantic Ridge (Brooke and Pelletier, 1970; Gilbert and Brook 1969) utilized hydrostatic pressure to drive a rotary hydraulic motor developing 3 h.p. for ten minutes from an air chamber initially pressurized at 15 p.s.i.. Yet the hydrostatic pressure differential represents an enormous source of potential energy - a source that is inherent to the oceans, non-polluting and inexhaustable, although constrained by water depth.

In order to apply our concepts relating to the use of hydrostatic pressure we have designed and are building an improved bottom sampler, a Hydrostatic Motor at the Lamont-Doherty Geological Observatory. It utilizes hydrostatic pressure differentials as a source for extended and controllable power. While our immediate application of the Hydrostatic Motor will be for driving corers into bottom sediments to sample longer stratigraphic sections than those now obtainable by conventional piston corers, the concept obviously could have wide applicability. We present here our fundamental design for the Hydrostatic Motor; discussion of the Hydrostatic Corer will be presented later in other publications.

2. Description of the Equipment

The utilization of hydrostatic pressure requires only that a pressure differential between atmospheric (or near atmospheric) conditions in

the upper water column and those encountered at depth be established between two chambers, both connected in such a way that controlled pressure equalization will force a movable piston to provide harnessable mechanical energy. Oceanic pressure gradients are approximately 0.5 p.s.i. for every one foot increase in water depth. It is not a linear increase due to small changes in sea-water density, but, as an approximation, every foot of submersion in sea water would produce an increase of about 0.5 p.s.i..

Transfer of this high pressure to a chamber maintaining lower (near surface) pressures results in a tremendous work availability - in the example cited, the initial work potential stored in a 12,000 cubic inch volume represents (neglecting friction) 15,000,000 pound-feet. In this design (Fig. 1) five principle components would control pressure equalization and convert this potential energy to mechanical work: chambers [1] and [2] are hollow, rigid, and connected chambers capable of withstanding ambient external pressure. Chamber [2] senses higher hydrostatic pressures by either being open to sea-water, as pictured in Fig. 1, or through a sealed membrane if hydraulic oils are used. Chamber [1] retains near-surface, lower, pressures. In our example, the piston [3] is free to slide within chamber [2], unless mechanically restrained. Valves [4] and [5] are flow control valves. When mechanically released under the influence of high hydrostatic pressure, piston [3] tends to move to the right (velocity is controlled through the use of a flow restricting orifice - not shown) into the region of lower pressure providing the power stroke. The piston is returned to its initial position by closing valve [5] and opening valve [4], thus allowing high ambient pressure water to enter behind the piston which is now exposed to equal water pressure on both faces and the unbalanced force of the compressed spring on the right, it therefore moves to the left where it is again mechanically restrained. Closing valve [4] it is isolated from external pressure and opening valve [5] allows water to drain from chamber [1] into the low pressure chamber [2], thus reestablishing a low pressure area behind the piston and completing the cycle.

The unit will continue to operate provided the valves are properly sequenced and piston restraint continues until the low pressure chamber is nearly filled with water. The number of cycles is approximately equal to the ratio of the volumes of the cylinder to the low pressure chamber. Cycling of valves would be controlled by piston movement by means of cams affixed to the piston rod.

Because the total work which can be done by the device is equal to the force applied to the piston times the total distance, piston travel is not a function of piston area or the length of the cylinder, and the energy stored is only a function of the volume of chamber [2] and the ambient pressure.

Accordingly, as a function of water depth (external pressure) the hydrostatic head can be harnessed to provide an enormous source of energy. Use of the device at greater depths corresponding to higher hydrostatic pressures and increased hydrostatic heads, results in increased energy availability. Simply increasing the low pressure storage volume allows utilization of hydrostatic pressure differentials in even shallower water depths and increases the work potential at any depth.

The Hydrostatic Motor represents an effective method for converting hydrostatic pressure gradients into usable energy. By simply raising the device to shallower depths the system will be recharged. Energy losses in transferring the equipment, by winches, for example, vertically through pressure gradients, prohibit any large-scale use for manufacturing significant power, such as in the generation of electrical power for use on land, although naturally occurring hydrostatic pressure changes while the Hydrostatic Motor remains in place such as perhaps produced by internal waves might even make this feasible. As the moment, we do see immediate application to power requirements necessary for deep-ocean instrumentation.

3. Acknowledgements

Preliminary design was financed through Office of Naval Research (Grant N00014-75-C-0210) and the National Science Foundation (Grant OCE 76-18049) as part of their support to the Lamont-Doherty Geological Observatory Core Laboratory and Repository. Prototype development is now supported by the Office of Naval Research through Grant N00014-75-C-0210 (Hydrostatic Corer). We appreciate comments by R. Stoll and N. Opdyke. Original concept is covered under preliminary patent protection to S. Selwyn with appropriate releases and usage for scientific research given according to National Science Foundation and Office of Naval Research stipulations.

References

1. Andresen, A., S. Sollie and A.F. Richards, "N.G.I. Gas-operated sea-floor sampler," Proc. 6th Int. Conf. of Soil Mechanics and Foundation Eng., 1965, pp. 8-11.

2. Brooke, J. and B. Pelletier, "Sea drilling techniques of the Bedford Institute," Underwater Science and Technology Journal, Vol. 2, No. 3, 1970, pp. 165-167.

3. Gilbert, R.L.G. and J. Brooke, "A hydrostatic power system," Atlantic Oceanographic Institute of Canada, Proc. Oceanology International, 69, Paper #54, 1969.

4. Greene, M.L., "A line cutter and a coring device powered by elastic bands," MTS Journal, Vol. 5, No. 3, pp. 48-50.

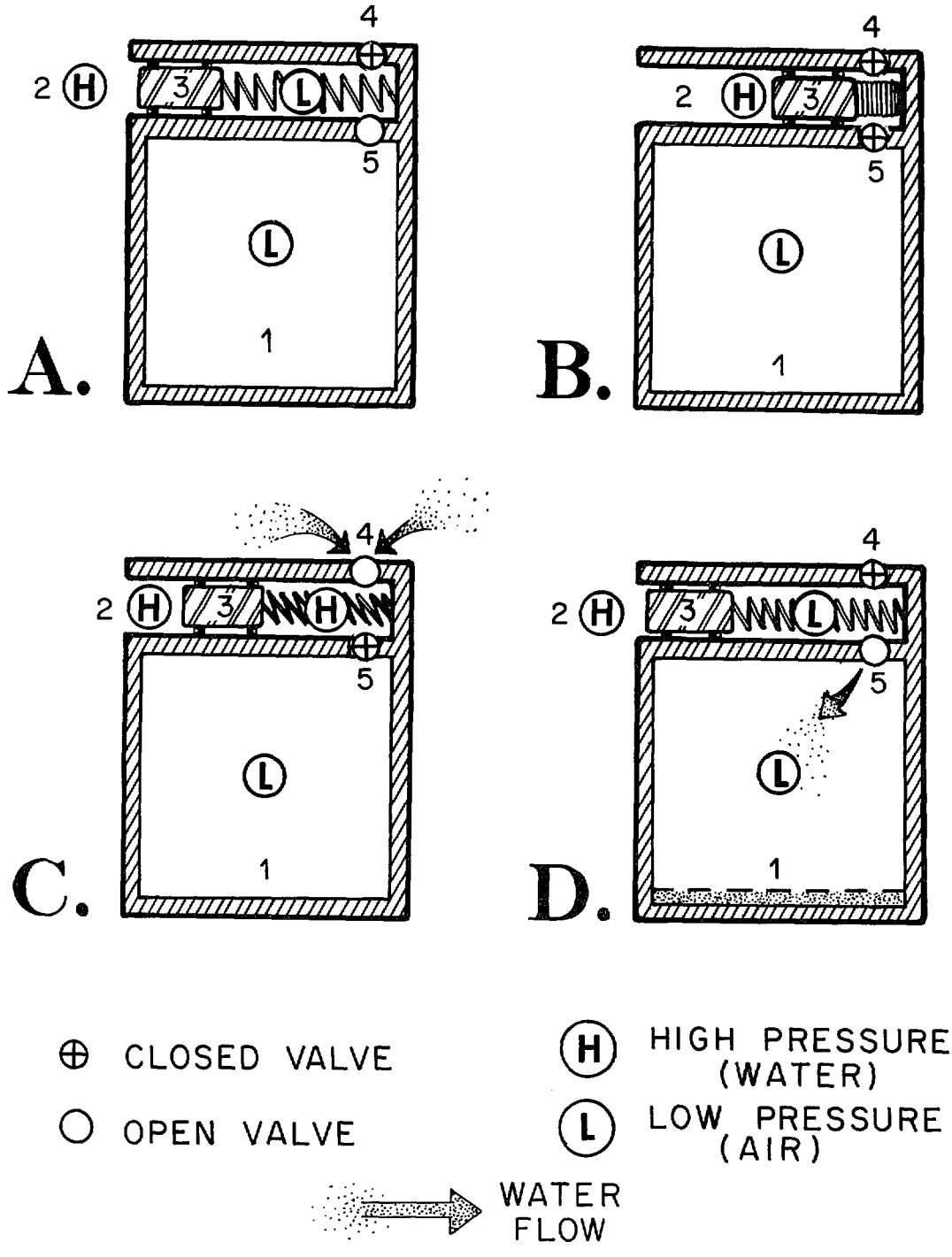

Figure 1: Schematic of Hydrostatic Motor operation. See text for explanation of numbered components. Letters A, B, C and D refer to operating sequence.

ACTIVITIES AND ECONOMICS OF EXISTING MANGANESE NODULE MINING CONSORTIA

C. Richard Tinsley
Second Vice President
Continental Bank
231 South LaSalle Street
Chicago, Illinois 60693

ABSTRACT

Previous capital cost estimates for manganese nodule mining consortia have not discussed the specific assumptions underlying the estimates. This paper, based on a rigorous analysis of the published literature and various project fundamentals, details the capital cost estimates for the five major groups currently involved in research and development in manganese nodule mining, namely: The Kennecott consortium, Deepsea Ventures, The Inco consortium, The Lockheed consortium, and Afernod. The capital cost estimates are listed in a schedule of annual expenditures based on the best case development assumptions.

INTRODUCTION

Capital costs and the expenditure schedules are presented for each consortium based on a study of the international literature, fundamental analysis of the mining and processing economics, and discussions for the record with members of the consortia. A great deal of material must necessarily remain unpublished but hopefully this properly tempers the conclusions.

The evaluation of nodule capital costs and the underlying economics is a dynamic process subject to continuous study and revisions to feasibility studies. It can be expected that the effort continues to trim capital and operating costs per unit. One must consider the capital costs as merely an expected value within a range of numbers. The range is difficult to determine but is probably within the ± 30% common for detailed scoping analysis.

KENNECOTT CONSORTIUM

The Kennecott consortium was formalized in January 1974. The members of the unincorporated joint venture are Kennecott Copper Corp. (50%), Rio Tinto Zinc (10%), Consolidated Gold Fields (10%), British Petroleum Co. - sub BP Minerals (10%), Mitsubishi Corp. (10%), and Noranda Mines Ltd. (10%). The Kennecott consortium's game plan calls for a phased program with the intention to be able to enter production at the end of the five-year, $50 million, development program (1979), if warranted. Phase 1, which involved testing large-scale mining equipment, was completed at the end of 1975. The next phase will require "massive equipment and large ships."[1] It is thought a large-scale mining test at sea will be undertaken in 1979 with a towed dredge at the end of a near-vertical pipe string.[2]

In the past, Kennecott talked of operations typically being 5,000-15,000 tons per day and Welling estimates that this would involve up to a 20-inch-diameter pipe and such a full-scale test would cost $75-$100 million.[2] Considering the announced budget, the large-scale test might be at one-third or one-half of the full production capacity. Kennecott is reported to be working on robot seabottom nodule collectors.[3]

Kennecott is usually regarded as favoring hydraulic hoisting and the 1978-1979 tests may use a series of in-line submerged pumps.[4] Presumably some ship conversion or modified drillship will be used, but no announcement has yet been made on vessel selection.

The Kennecott group is thought to be focusing on a single-ship, 2.7 million-mtpy mining vessel and ocean transportation of the nodules to a US-based processing plant using the Cuprion process to recover nickel, copper, cobalt, and molybdenum. Capital cost ranges of $500-$750 million are recognized by Kennecott and it is assumed that the estimate is toward the middle of the range with the size of the mining operation more than adequately offset by the lower comparative capital costs of the Cuprion process plant. The best insight is provided by Moncrieff and Smale-Adams who refer to a Kennecott-type operation. Burgess' five-year development period is assumed broken down into one year for financing and four years for plant construction and commissioning.[5]

A top-down estimate of Kennecott's capital costs, excluding R&D, working capital, and exploration, might look like the following guesstimate:

The analysis and opinions are the author's own and must not be attributed in any way to Continental Bank.

	$ million
Mid-point	625
Less $50 million program	(50)
Less further R&D	(75)
Less Working Capital	(50)
Net Investment	$450

This draws from Kennecott's own statements and uses Moncrieff & Smale-Adams' estimate for working capital.

The capital cost estimate from the bottom up is somewhat easier. Kennecott says its process plant will have a low capital cost which equates to about $320 million in 1977$. A separate communication outlined the following (in 1977$ million):

Ore Preparation	$25-35
Reduction	50-70
Leach, Metal Rec.	150-200
Auxiliaries	40-60
	$250-350

Summary of Assumed Capital Costs ($ million)

Cuprion Process Plant	$310
Mining Ship	100
Pipe, bottom equipment	20
Port facilities	10
Other	10
Total	$450

This assumes a scale-up from prior estimates of the ocean mining vessel and port which is confirmed by unpublished research. The plant and bottom equipment are adjusted from numbers published by Kennecott or its associates.

Optimistic Capital Investment Schedule*
($ million)

	1981	1982	1983	1984	Total
1977$	50	150	150	100	450
Escalated$	72	233	252	181	738

*Excludes Exploration, R&D, Working Capital

	Production Rate	Recovery
Mine	2.7 million tpy	NA
Ni	31,600 mtpy	90%
Cu	27,300 mtpy	92
Co	5,700 mtpy	85
Mo	?	?

Process
Hydrometallurgy, Cuprion Process

OCEAN MINING ASSOCIATES

Ocean Mining Associates (OMA) in its present form was formalized in March 1977, OMA is a management company comprised of US Steel Corp, sub Essex Minerals Co.; Sun Co. Inc. sub. Sun Ocean Ventures Inc.; and Union Miniere SA sub. Union Seas Inc. OMA has an operating agreement with Deepsea Ventures, formerly a Tenneco subsidiary.

Deepsea Ventures conducted air-lift testing in a 750-foot-high test loop in an abandoned mine shaft in 1968. The first successful multi-stage air-lift dredging test was conducted on the Blake Plateau in August 1970 at a water depth of 2400 feet. Phase 1 of Deepsea's expanded development program included pilot-scale mining. Under tight scheduling, the 560-foot iron ore carrier, the Weser Ore, was converted into the R/V Deepsea Miner II in Galveston in 1976.

It was reported that the vessel commenced a one-fifth scale test early in 1977 on the OMA claim site in 15,000 ft of water. It was planned to recover 15,000 tons of nodules for pilot plant testing. No word has emerged from the test program except that some pipe problems were encountered. A full-scale OMA mining operation would be 1.35 million wet mtpy (0.95 million dry mtpy) with additional or replacement units eventually boosting capacity to 4 million wet mtpy (2.9 million dry mtpy).

A number of capital cost figures have been mentioned for the OMA consortium which is generally regarded as starting with a small, 1 million mtpy operation. After a 3-4 year feasibility period, Deepsea personnel have stated that it would take at least three years to get metal to market. The total development costs are commonly referred to by Deepsea as $340 million (in 1977$). This should be adjusted as follows to eliminate exploration, R&D, and working capital.

	1977$
Total	$340 million
Original Program	20
Phase 1	30
Further R&D	15
Working Capital	40
Other	10
	$225 million

This number is low for a chloride process, but is purposefully chosen on the presumption OMA will not use a chloride approach and will tend toward a lower capital intensive hydrometallurgical approach which will nevertheless yield manganese.

Optimistic Capital Investment Schedule*
($ million)

	1980	1981	1982	1983	Total
1977$	40	60	60	65	225
Escalated$	53	86	92	109	340

*Excluding Exploration, R&D, Working Capital

	Production Rate	Recovery
Mine	0.95 million mtpy	
Ni	11,900 mtpy	96%
Cu	9,800 mtpy	94
Co	2,300 mtpy	96
Mn	256,200 mtpy	93

Process
Hydrometallurgy, Chloride leach

OCEAN MANAGEMENT INC.

This group was formalized in April 1975 and the partners at that time included Inco. Inc. sub. Inco Ltd.; Deep Ocean Mining Co. (DOMCO); and Arbeitsgemeinschaft Meerestechnich Gewinnbare

Rohstoffe (AMR). Sedco Inc. joined the consortium in November 1975. Each group has an equal interest in the venture. Ocean Management Inc. (OMI) of Bellevue, Washington, has a management contract. AMR consists of the West German companies Metallgesellschaft AG, Preussag AG, and Salzgitter AG. The Japanese Domco has six members of the Sumitomo group, Marubeni, Dowa Mining, Nippon Mining, Nissho-Iwai, Mitsui OSK Alliance, Toyo Menka Kaisha, Idemitsu Kosan, Komatsu, Kyokuyo, Shinko Electric, Tokyo Rope, and Ataka. OMI has embarked on a four-year $33-million program incorporating a phased technology development program followed by a one year feasibility study. Inco recently announced a halt to this program.

Some sophisticated mining methods have been suggested and constructed by the West Germans e.g. a crawler-mounted sweep arm miner. Various dredges have also been examined. Inco reckons it should provide for losing two dredges per year per mining vessel.[6] Inco is apparently planning to use a hydrolift and/or an airlift hoisting system. A two-ship operation should yield 3 million dmtpy from 16,500 feet through two 14-in. diameter pipes. The ship will be expected to travel at 1-2 knots and be capable of computer-controlled navigation.[6]

The drillship Sedco 445 was a natural candidate for OMI's one-fifth scale mining test, which successfully mined nodules in 15,000 feet in the North Pacific in April 1978. Conversion was undertaken in October 1977 and it was planned to mine 5000 tons of nodules.[7] Air-lift injections were to be tested at depths ranging from 5,000-8,000 ft. but submersible pumps at about 3,000 ft. were used for the successful test. The nodules in the converted mud pits were to be off-loaded every 30 days or so since the vessel is not designed for storage.

The most reliable source of capital cost information on OMI appears to be from a paper presented in Japan.[6] This gave capital costs as follows (in 1976$):

Mining System	$137 million
Port, Process Plant	327
Total	464
Working Capital	(55)
Total	$409 million

This translates to $435 million in 1977$ and I have added $15 million for other capital costs. A three-year construction period would lead to production at the beginning of year four. The "optimistic" schedule below is now highly unlikely to be met due to the deferral of the OMI development program.

Optimistic Capital Investment Schedule*
($ million)

	1982	1983	1984	1985	Total
1977$	60	160	220	10	450
Escalated$	93	269	398	20	780

*Excluding Exploration, R&D, Working Capital

	Production Rate	Product	Recovery %
Mine	3 million dmtpy	Ore	NA
Ni	35,000 dmtpy	Granules	90
Cu	29,700 dmtpy	Cathode	90
Co	5,300 dmtpy	Electro	70
Mn	695,000 dmtpy	Fe Mn	80

Process
Pyrometallurgy, Smelt to matte, leach.

OCEAN MINING COMPANY

The Amoco consortium was formalized in November 1977. The members of Ocean Mining Co. (Ominco) are Amoco Minerals Co., sub. of Standard Oil Co. (Indiana); Billiton BV, a member of the Royal Dutch/Shell group; BKW Ocean Minerals BV, sub. of Bos Kalis Westminster Group NV; and Lockheed Missiles & Space Co., sub. of Lockheed Corp. Lockheed has been engaged as the prime contractor for Ominco.

The Ominco group will use the Glomar Explorer for their prototype test mining. The test miner, which Lockheed has tested in a simulated sea-floor mud pit as well as submerged in a wet tank, has a productive capacity of approximately 20-25% of the planned operational unit. "Successful tests of the miner will provide engineering data required for the production miner."[2] Lockheed was keeping its options open between an air-lift and hydrolift in 1976.

Lockheed has thoroughly examined the systems aspects of nodule mining through a series of planned and phased risk management milestones[2] which can be characterized as an Economic Evaluation Methodology. Once funded, the next phase calls for "proof testing at sea of a test miner and initiation of process scale-up." It would be expected to have a three to four year development period.

The only capital cost recognized by Lockheed to date is $300-$500 million for the total development of a complete ocean mining system including both the mining and land processing plant. Mineral economic studies done to date show economic feasibility and favorable cost comparisons for similar sized land mining "per annual pound of capacity"[8] e.g. nickel laterites.

It is assumed that Ominco would require $400 million, the mid-point of the range mentioned by Messrs. Wenzel and Welling. Assuming a $75 million R&D effort, $25 million for exploration, and $50 million working capital, the net investment is guesstimated at $250 million. According to Welling: "The economics of ocean mining should be based upon the extraction and marketing of nickel, copper and cobalt, and limited consideration be placed upon manganese and other metals."[9] Welling adds later that the nodule porosity "makes them rather easily processed by acid leaching." This is the only processing approach cited by any Lockheed references examined. It is assumed that Lockheed was not working on a hydrochloric acid leach since that seems to be the domain of Deepsea Ventures. Therefore, a sulfuric acid leach would

be the only alternative and is so assumed. The 3-4 year development period mentioned by Mr. Wenzel is assumed to get underway in 1981 given the most optimistic assumptions.

Optimistic Capital Investment Schedule*
($ million)

	1980	1981	1982	1983	1984	1985	Total
1977$	30	40	50	50		30	250
Escalated$	40	58	77	84	91	58	408

*Excludes Exploration, R&D, Working Capital

	Production Rate	
Mine	1.5 million mtpy	Recovery
Ni	18,300 mtpy	95%
Cu	15,100 mtpy	90
Co	2,300 mtpy	60

Process
Hydrometallurgy, Sulfuric Acid Leach

AFERNOD*

This group has been conducting exploration since 1970 and five companies formalized a nodule mining program in mid-1977. The group members each have a 20% interest and are Gov't National Ocean Exploration Center (CNEXO); Gov't Atomic Energy Commission (CEA); Imetal sub. Soc. Le Nickel (SLN); Empain Schneider sub. Dunkirk Shipyards (CFD); and Gov't Mining & Geology Research Bureau (BRGM).

CNEXO participated in the 1972 continuous line bucket (CLB) test and has since played a leading role in CLB development especially for a two-ship CLB design. This system has undergone model tests in the Brest testing basin and work continues with Afernod and six other French companies. The advanced-design dredge buckets would be attached to a 16,000-m polypropylene or dacron cable loop with a 2000-mt breaking strength. The continuous loop would travel at 1 m/sec for a mining rate of 10,000 mtpd. The CLB principle entails driving the loop through shipboard traction motors with the buckets dragging a path over the ocean bottom and the full buckets attached to the loop pulled up to be dumped on board the rear ship.

The latest capital costs estimate for a two-ship CLB system were given by Mero as follows ($ million):

Expenditures to date	$1.5
Production tests	10
Two 100,000-ton ore carriers	$70
Two sets CLB machinery	20
Processing Plant	160
Total Costs*	$250

*Excluding R&D, Exploration, Working Capital

(This would be escalated to $265 million in 1977$).

Process
Hydrometallurgical

*Afernod: Acronym for Association Francaise pour l' Exploration Nodules

JAPANESE DOMA

DOMA is comprised of C. Itoh, Dowa Mining, Furukawa Mining, Hitachi Shipbuilding & Engineering, Ishikawajima-Harima Heavy Industries, Japan Metals & Chemicals, Kanematsu-Gosho, Kawasaki Heavy Industries, Kawasaki Steel, Marubeni Corp., Mitsubishi Corp., Mitsubishi Electric, Mitsubishi Heavy Industries, Mitsubishi Metal Corp., Mitsui & Co., Mitsui Mining & Smelting, Mitsui Shipbuilding & Engineering, Nichimen, Nippon Kokan, Nippon Mining, Nippon Steel Corp., Nippon Yakin Kogyo, Nissho-Iwai, Nittetsu Mining, Pacific Metals, Sasebo Heavy Industries, Sumitomo Metal Industries, Sumitomo Metal Mining, Sumitomo Shoji, Sumitomo Shipbuilding & Machinery, and Tokyo Shibaura Electric.

A Japanese engineer invented the CLB system but the Japanese have not done much development sine the 1972 CLB test. Plans also call for development of a hydraulic suction mining device. Mining testwork was scheduled for completion in 1979. Capital costs are not estimable.

REFERENCES

1) Tinsley, C. R., "A New Picture Emerges in Deep Ocean Mining," Mining Engineering, April 1976.

2) Welling, C. G., "Next Step in Ocean Mining-Large Scale Test," Mining Congress Journal, December 1976, p 46-51.

3) Barrons, November 25, 1976.

4) Tinsley, C. R., "Nodule Miners Ready for Prototype Testing," E/MJ, January 1977, p 80-81, 101.

5) Burgess, C. H., Testimony to US House subcommittee, May 16, 1972.

6) Shaw, J. L., "The Economics of an Ocean Mining Project," 4th International Ocean Development Conference, Tokyo, 1976.

7) Ocean Industry, "Converted Drillship will Begin Deepsea Mining Test in October," June 1977, p 79-84.

8) Wenzel, J. G., Testimony before US Senate Subcommittee, November 7, 1975.

9) Welling, C. G., "Strategic Importance of Deep Ocean Mining to the United States," Mining Congress Journal, September 1976.

CAPITAL COST ESTIMATE ASSUMPTIONS

Nodule Grade: 1.3% Nickel, 1.1% Copper, 0.25% Cobalt, and 29.0% Manganese; North Pacific mine; and internal rate of return greater than 12% sufficient to attract entry. Expenditure schedules are very optimistic since they assume some means of investment protection on either a national or international scale in place by 1980.

TECHNOLOGICAL GAPS IN DEEP OCEAN MINING

John B. Herbich
Professor and Head
Ocean Engineering Program
Texas A&M University
College Station, Texas 77843

John E. Flipse
Visiting Professor
Ocean Engineering Program
Texas A&M University
College Station, Texas 77843

Abstract

The need for several minerals found on the deep ocean floor has increased the world's interest in deep ocean mining. Several large international consortia have been formed and some are currently testing mining systems. The authors examine the incentives for these test programs and report on their status. Limitations, with associated penalties, of current exploration, surveying and resource mapping systems are discussed. Problems associated with the collector-sea floor interface and the ship-dredge system interface are defined. Instrumentation, data collections and transmittal, system control and system evaluation techniques are developed with attention focused on areas where present technology is deficient or difficult/uneconomic to apply. The authors consider the impact and recommendations of several recent investigations in deep ocean mining.

1. Introduction

In early 1977, a resource manager of the United States Steel Company calmly informed the U.S. House of Representatives' Merchant Marine and Fisheries Committee, during a hearing on Deep Ocean Mining legislation, that the free world reserve of manganese is sufficient for 29 years of normal steel production. This estimate was based on the continuing uninterrupted mining of high quality ore from Gabon and the Republic of South Africa. The forecast recognized the ore grade problems and nationalization of some South American mines and the disappearance of the "basket mines" of North Africa and India. The rapid five-fold rise in the price of ferromanganese has, unfortunately, been offset by worldwide inflation with its impact on infrastructure costs providing little hope for reopening uneconomic mines.

Recent events on the African Continent suggest that the free world's principle source of cobalt is now at great risk. Zaire (formerly the Belgian Congo) in addition to its role in cobalt has long been a major source of copper from ores assaying over 5% as contrasted to the assay of less than 1% for the last-opened U.S. copper mine. And, in spite of the current oversupply of nickel, the long-range prospects of laterite ores as a major nickel source have appreciably diminished. Certainly world events continue to provide major incentives for the development of deep-ocean hard-mineral resources.

As this paper goes to press, two major test programs are being successfully concluded. Although schedules and technical approaches differed, the tests demonstrated that ocean mining systems can be deployed in great depths at sea and sea bed resources pumped to the surface. Nonproprietary technical difficulties will be considered below. We look forward to timely additions to the technical literature from the sponsoring organizations.

2. Exploration, Surveying and Mapping System Limitations

Finding a deposit of manganese nodules on the floor of the deep ocean is appreciably easier today than it was twenty years ago, thanks to the many fine technical papers, maps and books that have become available over the past two decades. Broadly defining the deposit (sometimes called exploration) or thoroughly defining the deposit (surveying) is still accomplished by the same techniques albeit with considerably improved equipment. Television, free-fall samplers, dredges, corers, P.D.R.s and the still camera continue as the practitioners' dependable tools.

Determination of precise bathymetric relief and preparation of an accurate bathymetric and slope charts (maps) using narrow beam echo sounding and integrated navigation system inputs is now routinely accomplished by the ocean mining operators using the computer and its plotter to record and present the data. The ore assay, determined on board or ashore by atomic absorption analysis, is added to the map with less location precision than the bathymetric data but with enough accuracy to satisfy all but the most terrestrial-bound economic geologist.

What is missing? The second generation surveying machine yielding, ideally, from in situ observation and analysis, the nodule concentration and assay (by principle metal constituents), the nodule sample seabed location, and the seabed characteristics (slope, bearing and shear strengths) all automatically recorded and displayed by the computer and its peripheral equipment. Although the foregoing capability may sound fanciful, several first attempts have been undertaken with funding as the primary constraint.

Even with adequate funding, the development of an accurate and dependable in situ surveying system will be very challenging!

3. Major Interface Problems

Inasmuch as this is a technical paper, we may consider the Industry/Government, Government/Public and U.S./UN ocean mining interfaces as minor. This leaves the mining platform (ship)/mining system (pipeline) and the collector (dredge head)/sea floor as the major interfaces where technical problems abound. Let us consider each in some detail.

Of the six degrees of freedom of ship motion (roll, pitch, yaw,heave, surge and sway) only three are amenable to direct mechanical treatment. A structurally adequate gimbal will accommodate the rotational motions of roll and pitch while judicious placement of the pipe handling systems near the longitudinal center of gravity of the ship will minimize the effects of the third rotational motion, yaw, while reducing pitch amplitudes. The major linear motion, heave, can be adequately handled by mounting the gimballed derrick on cushioned hydraulic cylinders which can be tuned to compensate for rather large vertical motions thereby minimizing vertical accelerations and associated forces acting on the pipe system. Since the ship dredges at low speed (½ to 3 knots) surge should present few problems unless wave lengths approach or exceed ship length. The effect of the last linear motion, sway or athwartship translation, is likely to be unimportant while dredging with the ship headed into or away from the dominant wave pattern, but could be a severe problem if the ship must be turned in a high-sea state while the pipe is deployed.

In fact, the storm or survival situation is what causes this interface to be so difficult. The trade-offs of the derrick location and geometry (toppling or pendulating, etc.), the pipe system characteristics (length of sections, joint configuration, etc.) and the ship and moon-pool geometry become increasingly complicated as the motion amplitude assumptions are made more severe. Expedient compromises and due dilligence during the recent testing permitted successful operations. In-depth analysis with exhaustive trade-off studies are required before an all-weather commercial system can be built and put into service.

The second major interface is between the collector, dredge-head or seabed vehicle (as proposed by some) and the ocean floor itself. The geotechnical properties of the seabed have been extensively studied by the several consortia, NOAA through DOMES and by Lehigh University, among others. Although this information provides design data that has sufficed for the system tests, it is not sufficiently comprehensive or extensive to permit confident design of a commercial system. Much more data, analysis and understanding are required.

Another relatively unknown influence of this interface is the transmittal of ship and/or pipeline motions to the dredge head and their influence on the orderly transit of this key system component across the seabed while performing its essential task of picking up the nodules. Unfortunately, a highly empirical or "brute-force" solution to this poorly understood problem has potentially serious environmental implications. Again, in-depth analysis of expanded relative data and, perhaps, modeling is indicated.

Although not an interface, or an interface problem, a major problem does exist in the use of electric power and signals in the ocean depths. Let us briefly identify the nasty working difficulties that interrupt and delay the current tests and therefore threaten the dependability and "on line" time of any commercial deep-ocean mining system.

Thirty years ago, the U.S. Navy seriously studied the flow of cable insulation and "fillers" at bulkhead penetrations so that submarine compartments could "pass" air pressure tests. The problem is intentionally understated. Today, power-cable jacket flooding has caused serious power failures in spite of meticulous attention to terminations and cable armor. In some cases the workmanship of/at the connectors can be identified as the problem but in other cases subsequent cable failure at or near the connector appears to be the cause of the flooding. Ghosts of the past, perhaps?

No discussion of electricity at sea can be concluded without noting the delays and frustrations caused by cursed connectors. There is no lack of effort, nor accompanying increase in cost, on the part of the manufacturers, installers and users but any component that depends upon the absence of a hair or particle of lint under the o-ring and the artistic application of a "smidge" of grease (of the proper type, naturally) in field use must represent a technological gap. A fellow traveler, but of different technical origin, is the oil-immersed pressure compensated submersible motor. Why do they regularly get in serious trouble, with massive sequential costs and delays?

4. Instrumentation, Data Collection and Transmittal Deficiencies

Mining in deep water presents some unique problems, in many aspects the problems encountered are more difficult than those experienced by the oil and gas offshore industry. Most of the systems now being considered, or tested employ a drag head which is remotely controlled. The drag head is either towed or self-propelled. The continuous-line bucket dredge is an exception.

The nodules must be brought to the surface through a pipe employing mixed flow hydraulic pumps or an air-lift.

Measurement, transmission and recording of various parameters is obviously necessary for two reasons:

(a) to evaluate performance of the operating system engineered to recover nodules. This will provide sufficient data to improve the efficiency of the system,
(b) to evaluate the environmental impacts of the deep ocean mining operation.

To provide data for item (a), the following instrumentation is necessary:

(1) To measure the rate of the three-phase flow (water, air and nodules). Measurements of three-phase flow are difficult and instrumentation must be improved. At present a magnetic flow meter may be used to measure the mass flow, a nuclear density meter may be used to measure the density of the mixture and a production meter has been developed to combine the inputs from the magnetic and density meters to give the rate of solids flow in say, tons per hour. The magnetic flow meters are quite rugged and sufficiently accurate for measurement of total flow. Density meters should be developed for underwater operation, as the density of material may have to be monitored from the initial pick-up location (at the drag head) to the discharge point on the vessel. Since continuous pumping is not only desired, but necessary, it is important to know the density of mixture being pumped. Instrumentation to detect the air flow and the ratio of liquid/air and fluid/solid flow is also needed.

(2) Instrumentation to measure the total velocity and velocities of liquid, solids and air would also be desirable so that intelligent decisions can be made by the operator to assure continuous and efficient operation of the system. Velocities inside the pipe would be most difficult, if not impossible, but the velocities may be obtained from the meters described above.

(3) Pressure in the pipe must also be monitored along the pipe to obtain information on friction head losses. Rugged pressure sensors operating under large hydrostatic pressures must be used.

(4) Inertial coefficients for vessels, pipelines, suction drag heads; drag coefficients - Reynolds Number relationship; added mass for bodies; vortex shedding; vibration all must be known for successful, efficient design for the ocean mining system. Instrumentation must be adopted or developed for measurement of various parameters mentioned above.

5. System Control and Performance Evaluation

As the preceding section suggests, measuring, transmitting and recording performance data for later reduction, analysis and application in the system design process is not without its problems. Displaying at least some of this data so that it can be understood and applied in the real-time control of a complex system with the "person"-in-the-loop identifies additional technological gaps in this developing industry. The proposition that the system is too complex to admit to human control is rejected on the basis that the cost of automation and optimization by computer could/would negatively impact the development of deep-ocean mining while the prototype systems did, indeed, function successfully.

A ship, moving at slow speed in a real random sea, subject to wind and current influences presents some control difficulties even when assisted by bow and stern thrusters. Attach to the ship through a "soft" connection three miles of steel pipe and cable with a ten-ton vehicle at its end to be towed over uncertain terrain of variable load-bearing characteristics and we further complicate the total vehicle control problem. The dynamics and vibratory behavior of the system is also influenced by the product being pumped up the pipe -- liquid, liquid and solid, or liquid, solid and air. In spite of the prototype tests performed, much analysis, modeling and optimization remain to be done before an efficient commercial system can be designed, built and placed in service.

6. The National Research Council, Assembly of Engineering Marine Mining Technology Panel Report Implications

Since some of you might have missed reading the NOAA's Marine Minerals Workshop Proceedings[2] and the National Academy of Engineering's Report[3], the more important recommendations and conclusions are quoted directly from the reports.

1. NOAA's Workshop[2]

(i) The environmental assessment of manganese nodule mining has been underway as part of NOAA's Deep Ocean Mining Environmental Study (DOMES). Further government/industry cooperative e-fort to acquire and evaluate data on the changes and disturbances of the deep ocean marine environment caused by pilot nodule-mining operations is recommended.

(ii) The environmental impact of the on-shore processed nodule residue dumped at sea should be evaluated. The beneficial uses of solid wastes resulting from processing plants should be considered.

(iii) Factual information on the worldwide distribution of potential nodule deposits is needed to provide more accurate estimates of reserves.

(iv) Environmental physical oceanographic parameters for the potential mining sites should be obtained and made available.

(v) Research on behavior of materials in sea water should continue and should be encouraged.

(vi) Micro-topographical maps are needed for detailed resource assessment.

(vii) A better understanding of the sediments in the equatorial Pacific is needed for the design of future mining systems.

(viii) A study of repopulation rates of the benthos during the post-mining period is recommended.

(ix) Technology transfer of non-classified material from the defense agencies to industry is recommended.

(x) In the event of a possible failure of the Law of the Sea Conference, the bilateral and multilateral treaties should be considered.

(xi) Economic impact of the various methods proposed to regulate the exploitation of deep-ocean manganese nodules should be evaluated.

2. NRC Panel (quoted directly from Reference 3)

(i) "Environmental impact studies (EIS) of marine mining should be modified to focus on the elucidation of significant ecological processes which are affected by mining activities as distinguished from generally descriptive studies. The approach should be one in which hypotheses are proposed and tested. A set of procedures to be followed to incorporate studies into the EIS process were identified.

(ii) Government weather data service as presently available in the eastern tropical Pacific should be expanded to include the principal areas of nodule mining interest.

(iii) Research should be undertaken on the genesis of shell and placer deposits.

(iv) There should be an extension of high resolution bathymetric charts, with contour intervals of 5 or 10 meters throughout the 200-mile economic zone with emphasis on the most promising zones of exploitation.

(v) The federal government should encourage the rapid development of the NAVSTAR global positioning system or equivalent, and foster the development of improved subsurface acoustical location fixing systems required for ocean mining operations and related environmental investigations.

(vi) Development should proceed to provide improved capabilities for determining the thickness and physical properties of unconsolidated shelf sediments.

(vii) The federal government should increase the voluntary exchange of technical information between the ocean mining industry and relevant sectors of government and academic institutions. It should also explore with other nations the feasibility of voluntary exchange of research information and of jointly planned and carried out research programs on assessment of environmental change relevant to ocean mining.

(viii) The federal government should assist in providing a better knowledge base for the development of new or improved ocean mining and extraction technology."

The writers generally agree with the NRC panel recommendations.

It appears that the present weather and sea forecasting services provided by the government are adequate for most deep ocean mining purposes. The exception may occur if a mining site is in a remote location. It can be argued that it is not the role of the government to provide localized wave forecasts for shipping and other marine-related activities such as ocean mining. This type of service should be performed by a commercial forecasting firm, unless the government wishes to promote the ocean mining in the name of national interest. The government should, however, provide the tropical cyclone advisories, tsunami warnings and sea ice forecasts, if appropriate.

The exchange of information in the ocean engineering area would undoubtedly reduce the development time for ocean mining companies. The Navy has an extensive ocean engineering program, not only as a result of its in-house capabilities but also because it includes facilities and operations that directly utilize private industrial research organizations and the academia. The body of technical data is related to the following technologies: materials and structural design; sensors, navigation and control; acoustic oceanography, communications; man-in-the-sea and diver support; energy conversion and machinery; sea floor engineering; and environmental prediction and oceanographic survey. Unfortunately, there is no organized system for the archiving, or disseminating the data to the ocean engineering community.

Also there are many government ocean engineering test facilities which could be identified and made available to industry at minimum cost.

There is a definite need to establish a focal point in government for monitoring and evaluating technological developments in terms of their applicability to improving reliability and performance of commercial ocean mining. This agency could provide an active mechanism for transferring this information and identify the technological gaps that may interfere with future mining efficiency and capacity to meet regulatory and environmental requirements.

7. Conclusions

The recent testing of deep ocean mining systems has demonstrated the technical feasibility of deploying the needed equipment at sea and dredging manganese nodules from the deep ocean floor. As anticipated, the exercise may have raised more questions than it has answered. The need for in-depth analysis and systems optimization is demonstrated.

The technical and system similarities, in both problems and solutions, re-enforced by the very high cost of the experimentation, suggests that the emerging industry may be ready, even at this early stage, to pool their technical findings in the interest of the rapid and cost-effective development of deep ocean mining.

The contest has passed from the technical innovators and entrepreneurs to the lawyers, accountants, management committees and the politicians. Is it not time for the marine technical community to close ranks and fight the real enemy, the sea?

8. References

1. Herbich, J.B., Coastal and Deep Ocean Dredging, Gulf Publishing Co., Houston, Texas, 1975.

2. U.S. Department of Commerce, National Oceanic and Atmospheric Administration, Proceedings of the Marine Minerals Workshop, March 23-25, 1976, Silver Spring, Maryland, Government Printing Office, Washington, D.C., 1976.

3. National Academy of Sciences, "Marine Mining Technology: Research Needs and the Government

Role," a report prepared by the Panel on Marine Mining Technology of the Marine Board, Assembly of Engineering, National Research Council, Washington, D.C., 1977.

4. Kaufman, R. and A. J. Rothstein, "Recent Developments on Deep Ocean Mining," Marine Technology Society, 6th Annual Preprints, Vol. 2, Washington, D.C., 1970.

5. Brown, R., D. Fuerstenau, J. B. Herbich, R. Kaufman, R. Moore and W. Normark, "Marine Mining Technology: Current Capability and Future Demands," Marine Minerals Technology Workshop, 1977. Available from the Marine Board, Assembly of Engineering, National Research Council, Washington, D.C.

6. Duane, D. B., D. Fuerstenau, R. Gerard, and J. Herbich, "Geological Processes: Dynamics of the System." Prepared for the Marine Minerals Technology Workshop, 1977. Available from the Marine Board, Assembly of Engineering, National Research Council, Washington, D.C.

7. Kaufman, R. "National Needs, Current Capabilities, and Engineering Research Requirements (Offshore Mining Industry)," 1976. Available from the Marine Board, Assembly of Engineering, National Research Council, Washington, D.C.

8. MacCutcheon, E.M., "Technical Deficiencies and Improvement Opportunities in Marine Mining," 1976. Available from the Marine Board, Assembly of Engineering, National Research Council, Washington, D.C.

UTILIZATION OF AVAILABLE TECHNOLOGY TO SUPPORT OCEAN MINING

Sam Rothman
Department of Engineering Administration
School of Engineering and Applied Science
George Washington University
Washington, D.C. 20052

Robert J. Lynch
Department of Engineering Administration
School of Engineering and Applied Science
George Washington University
Washington, D.C. 20052

Abstract

With the large capital investment and high operating costs associated with ocean mining, it is vitally important that maximum use be made of existing technologies. To accomplish this, the ocean mining community should have a central focal point to which its members can address their technology needs and expect to get an authoritative response. It is further necessary that the industry be kept apprised of available technologies which have potential application to ocean mining. These functions can best be accomplished through the use of an ocean mining oriented technology broker to bring the users with the needs together with the technology producers on a person-to-person basis.

1. Introduction

Because of the generally depressed state of the metals market and the uncertain political situation, it appears that there may be a temporary hiatus in further deep ocean mining prototype testing such as recently completed in the Pacific. This will inhibit identification of the full range of technological needs to support future deep ocean mining operations. It is at such times as these that it becomes particularly important for the Federal government to provide initiatives and mechanisms to determine the technological needs of the ocean mining industry in order to:

- identify U.S. Government developed technologies which can be transferred to meet these needs, and
- identify those technological requirements for which no technology is available; and, in cooperation with industry, determine whether the development of a specific technology should be an industry, government, or joint effort.

Effective utilization of available technologies by the ocean mining community depends upon a mechanism which can provide quick responses to a user's stated technological need by:

- identifying a pertinent transferable technology to meet the need, or
- indicating the non-availability of such a technology.

This is the "Technology Pull" mode of the Generalized Technology Transfer Process illustrated by Figure 1. There is a further requirement to ensure that the ocean mining community is kept apprised of relevant technologies developed for another purpose which might be adapted to meet needs of the industry. This constitutes the "Technology Push" mode of the generalized model.

2. Technology Pull

The technology users exert "technology pull" when they encounter a problem beyond their capabilities and look elsewhere for the technology to solve the problem. Such users, through their previously established contacts, may know an authoritative source who can point them toward the technology producer(s) with the technology to fulfill their need. If the user does not know such a source, he may refer to various product and service directories such as The Sea Technology Buyers Guide/Directory, the Worldwide Directory of Offshore Contractors and Equipment, the Geophysical Directory, and others to identify specific contacts in the area of the technology need (Step 1 of the Process shown on Figure 1).

If no contacts can be made or if contacts prove to be nonproductive, the user may elect to access information/data systems; that is search the Abstracting and Indexing Publications or query the computerized information/data services for references relating to the needed technology. (Step 4).

All of the significant unclassified Abstracting and Indexing Services are commercially available in computerized form. The Lockheed DIALOG, the Systems Development Corporation ORBIT, and the National Technical Information Service Bibliographic Data Files provide computerized services which cumulatively include abstracts of much of the published technology information relevant to ocean mining. These services are also utilized by other government agencies, industry, and academia.

While these time honored sources and others are readily available, the user is frequently overwhelmed with the number of citations provided in response to a specific technology question. Information contained in the systems is generally over six months old because of the time lags between a development and publication. Further, not all relevant technology information is published. These shortcomings illustrate that effective technology transfer can only be accomplished through person-to-person contact between the ocean mining community and the expertise in the pertinent technology areas. The key step in the technology transfer process is to match the user having a stated need with the producer having the technology which may be adapted to fulfill that need.

3. Technology Push

Since ocean mining is in its development stage, there is serious question as to whether the industry is fully aware of its technological requirements, which probably span the total spectrum of ocean engineering. As a consequence, a Technology Transfer Process relying only on "technology pull" will not meet the requirement to ensure utilization of available technologies by the ocean mining community. Therefore, there is a need to provide users with a "catalog" type service showing available technologies from which they may choose those of potential use to meet their, as yet unspecified, needs. This is the "Technology Push" mode of the Generalized Technology Transfer Process.

Industrial technology producers utilize the "technology push" approach in their marketing efforts. The classical government example of "technology push" is the Department of Agriculture Extension Service which disseminates USDA supported research results, on a person-to-person basis, to every state and county of the nation using approximately 17,500 extension service employees nationwide. The NASA Technology Utilization Program is another example of technology push whereby the program attempts to ensure that new aerospace technology is brought to the attention of American industry and others (including Federal, state and local government agencies) so that it may be adapted and applied for the user's benefit. The Navy conducts a modest technology push program through the publication of a monthly Navy Technology Transfer Fact Sheet. The NOAA Marine Advisory Service, employing about 275 extension agents, assists those who are interested in and responsible for development, utilization, and management of the ocean and its resources. The results of research, availability of services, experience of industry and other sources of information are made available to users on a person-to-person basis.

The "technology push" approach assumes, as experience has indicated, that the users either cannot or will not bother to articulate their technology needs. They are more responsive to direct personal assistance to help identify their technology requirements and need to be shown how a given technology can be applied to solve their problem.

"Technology push" is initiated by a commercial producer motivated by the profit incentive. Federal agencies are motivated by the national policy to ensure that results of research and development sponsored by their agencies are made available to State and local governments, and the private sector. Communication channels for promotional efforts to transfer technology include:

- Formalized marketing efforts
- Extension agents
- Symposia,conferences, and exhibits
- Selective dissemination of information
- Primary Publications
- Newsletters and Information Exchange Groups
- Research in progress reporting

4. Technology Broker

An effective technology transfer process will incorporate a combination of "technology pull" and "technology push" capabilities. Ocean mining is a relatively new industry with extensive and varied technological needs. Consequently, the industry is handicapped in its ability to identify the sources of expertise in the various technology areas. The transfer process described in this paper lacks an ocean mining specific structure. The process needs an ocean mining technology broker between the users and producers of relevant technologies. The broker would function in the role of matching the technology needs with the available technologies.

5. Location of the Ocean Mining Technology Broker

NOAA, with its responsibility to assure that the ocean environment and its resources are wisely used in a balanced way --- for the national well being, would appear to be the logical location for an ocean mining technology brokerage effort, perhaps as a part of an overall ocean engineering effort. However, there is somewhat of an organizational problem with respect to such an operation in NOAA. While NOAA is the lead civil agency in ocean related matters, it is clear that the bulk of the developing technology for potential transfer exists outside the lead agency. Most current Federal transfer operations have the more limited objective of moving their own organizations' technology into a wider market.

The principal Federal government source of technology related to ocean mining resides with the Navy. The development of such technologies is diffused throughout the various naval commands and research activities in both classisfied and unclassified programs. It is difficult for a civil organization without a contractual affinity with the DOD to easily identify available relevant technologies. Since the Navy's role is primarily defense related, it appears necessary to have the broker for ocean mining technology within a civil agency which has a close working relationship with the Navy. NOAA is the organization with such a relationship and is consequently the preferred location.

References

Federal Council for Science and Technology. 1975. Directory of Federal Technology Transfer. Washington, Government Printing Office.

Marine Board, Assembly of Engineering, NRC, NAS/NAE. 1977. Priorities for Research in Marine Mining Technology. Washington, National Academy of Sciences.

Marine Board, Assembly of Engineering, NRC, NAS/NAE. 1975. Mining in the Outer Continental Shelf and in the Deep Ocean. Washington, National Academy of Sciences.

National Science Foundation. 1975 Federal Technology Transfer; an Analysis of Current Program Characteristics and Practices. Washington, NTIS PB 253-104.

Rothman, S. and others. 1977. NOAA Office of Marine Minerals Technology Transfer Study, Final Report. Washington D.C., The George Washington University.

Rothman, S. and others. 1978. NOAA Ocean Engineering Technology Transfer Operation, Final Report, Washington, D.C., The George Washington University.

FIGURE -1

GENERALIZED
TECHNOLOGY TRANSFER PROCESS

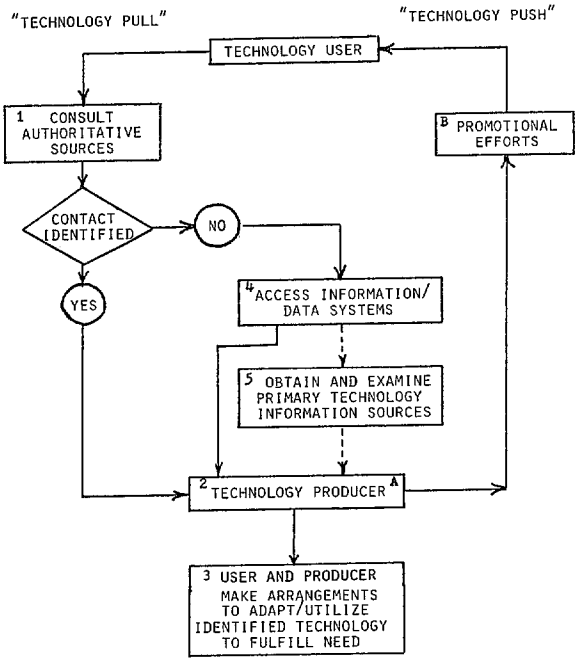

A SYSTEM FOR THE ROUTINE MEASUREMENT OF DIRECTIONAL WAVE SPECTRA FROM LARGE DISCUS BUOYS

K.E. Steele
NOAA Data Buoy Office
National Space Technology Laboratories
NSTL Station, Mississippi 39529

E.L. Burdette
Computer Sciences Corporation
National Space Technology Laboratories
NSTL Station, Mississippi 39529

A. Trampus
Federal Energy Regulatory Commission
825 North Capitol Street
Washington, D.C. 20426

Abstract

The NOAA Data Buoy Office (NDBO) devised a concept for a directional wave spectra measurement system suitable for routine use on board its large discus buoys. The concept was translated into an experimental system and mounted on a buoy deployed in the Atlantic Ocean. This system was operated briefly and evaluated. The system concept was based on the measurement of body-fixed pitch and roll of a surface-following discus hull, the heading of the buoy, and the buoy heave. The time series records of these parameters were processed on board the buoy to reduce the quantity of data sent to shore. This paper reviews the technical considerations that led to the selection of the measurement technique. The hardware configuration is described, and the problems encountered are identified. The data handling methods are outlined, but an analysis of the data is not included. An analysis of the data is provided in a companion paper. The methods used to evaluate the data are described herein.

1. Introduction

In late 1974, NDBO demonstrated that one-dimensional wave displacement spectra could be routinely measured from buoys and reported to users in near real time.[1] Consideration was then given to the practicality of reporting directional wave spectra on a routine synoptic basis from NDBO's operational continental shelf and deep ocean buoys. These buoys include 12-, 10-, and 5-meter diameter discuses, and boat-shaped NOMADS. NDBO predominantly uses the 10- and 12-meter diameter discuses with approximately 10-meter high masts.

Panicker[2] reviewed the techniques for the measurement of directional wave spectra from buoys. The experience of Pierson[3] and Nierenberg[4] along with various reports[5,6] of activity in the United Kingdom also provided useful information for NDBO's planning. These sources and the references cited by Panicker indicated that it would be practical to measure low-resolution directional spectra through the measurements of heave, heading, pitch, and roll of a moored discus hull. Systems designed to determine high-resolution directional spectra through the measurement of sea surface curvature were rejected because of their complexity.

Numerous constraints had to be met in the adaptation of the chosen measurement technique to operational buoys. The system had to be reliable, provide limited data to relay to shore in near real time at synoptic hours, consume no more power than is readily available on board an operational buoy, interface both mechanically and electrically to existing or planned on-board data reporting systems, be small enough to be mounted in the hull, and be cost effective. During 1974 and 1975, NDBO devised a system to satisfy these constraints.

During 1976 and early 1977, NDBO integrated a special buoy to evaluate the practicality of the concept. The buoy has commonly been called XERB (Experimental Environmental Research Buoy). The XERB buoy included a 12-meter discus hull with center-mounted aluminum mast salvaged from an experimental boat-shaped hull buoy (Figure 1). Two independent marine data acquisition and reporting systems, or payloads, were mounted on the buoy. These were identified at that time as "EB-05" and "EB-06". The EB-06 payload was to provide directional wave and other experimental data, while EB-05 was to provide comparison data to establish that EB-06 was functioning properly. XERB was deployed in the Atlantic Ocean in 1977. Both the EB-05 and EB-06 payloads functioned successfully for several weeks, until a major failure aboard XERB forced its return to shore.

During its operational life, XERB produced much useful data and largely fulfilled its mission. The data demonstrated that NDBO's concept for the routine measurement of directional wave spectra needed only some slight modifications. Section 2 explains how the characteristics of the XERB hull affected the design for the directional measurement system. Sections 3 and 4 describe the EB-06 and EB-05 payloads. Section 5 discusses the relationship between the data taken by the two payloads. Section 6 describes the evaluation of the data. The adequacy of the EB-06 directional measurement system is discussed in Section 7. On-board hardware and software are both discussed, but only an overview of algorithms is included since a review of the data processing techniques is given in a companion paper[7], which also shows some of the data produced by the XERB systems.

The authors of this paper contributed significantly to the work described, but that contribution was only a fraction of the total

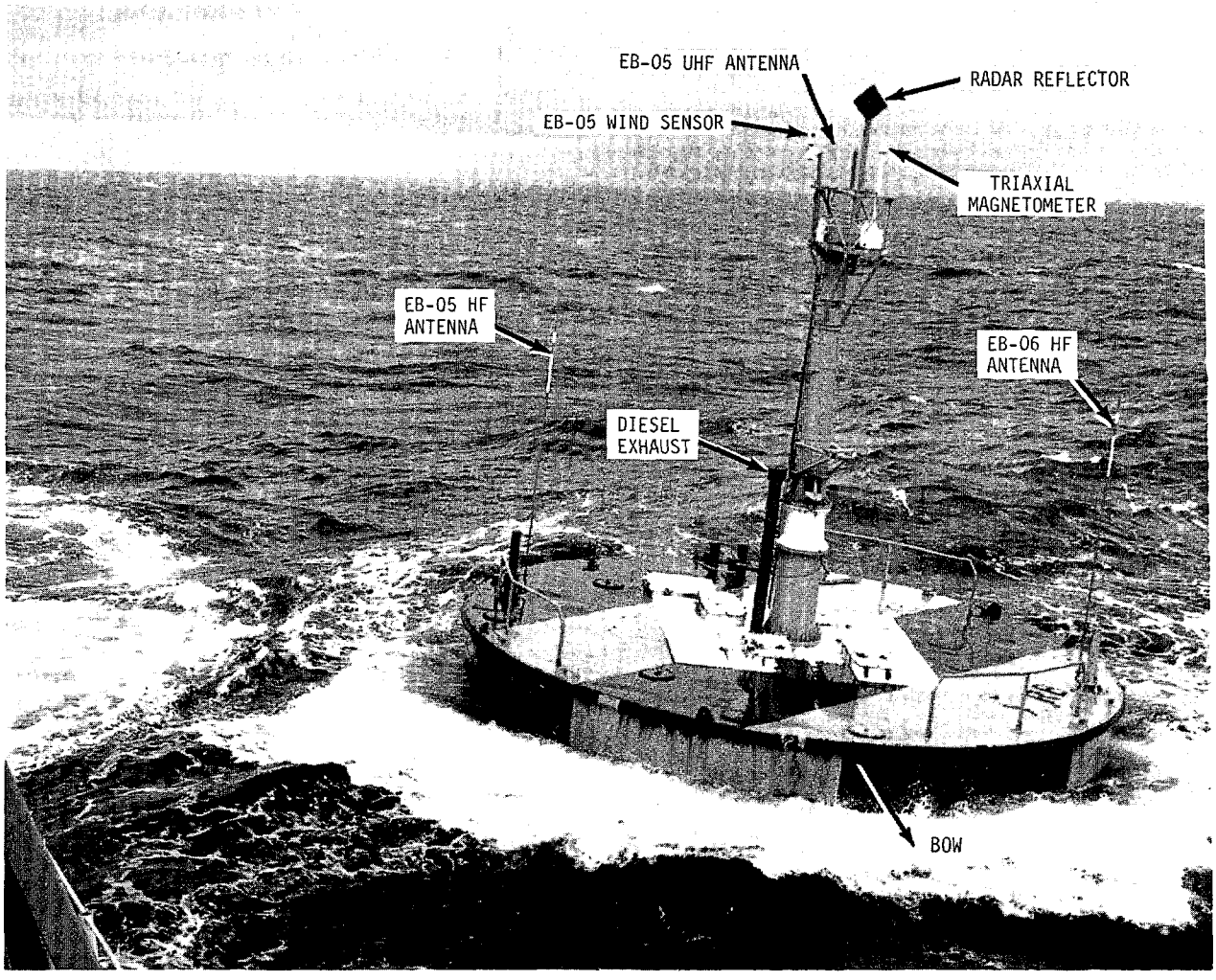

Figure 1. XERB

effort. We have tried to credit everyone fairly in Section 8.

2. Hull Considerations

An estimate of directional wave spectra consisting of the first five terms of the Fourier series expansion in the azimuthal angle requires the measurement of three time series. If $\eta(x,y,t)$ represents the elevation of sea surface above the mean sea level at location (x,y) in an earth-fixed frame of reference, it is necessary to measure records, perhaps 20 minutes in duration, of

$$\left(\frac{\partial^2\eta}{\partial t^2}\right)_{x,y} \equiv \ddot{\eta}\ , \quad \left(\frac{\partial\eta}{\partial x}\right)_{y,t} \equiv \eta_x, \text{ and } \left(\frac{\partial\eta}{\partial y}\right)_{t,x} \equiv \eta_y,$$

in which x points east and y points north. Figure 2 shows the buoy fixed frame of reference.

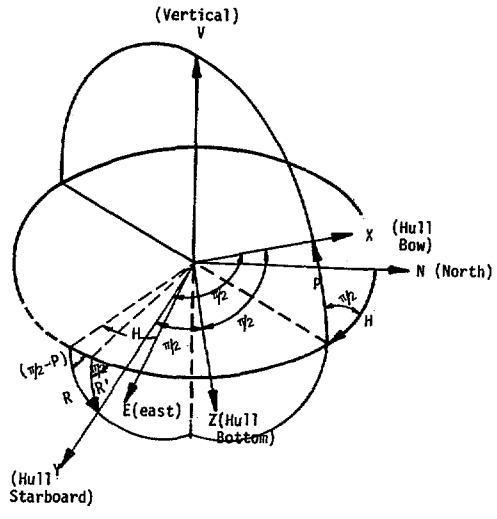

Figure 2. BUOY FIXED FRAME OF REFERENCE

There are several reasons why it may not be possible to approximate these records by measuring the corresponding heave acceleration, and corresponding east and north slopes of the discus hull. For example, because the discus buoys are moored, the ocean currents could cause horizontal motion, or a stationary or non-stationary nearly constant tilt of the hull large enough to affect the measurement adversely. Also, the wave motion tends to move the hull with a periodic circular motion in a plane parallel to the direction of wave propagation. The heave, pitch, and roll responses of the hull are frequency dependent, and measurements made at frequencies sufficiently high that the response deviates significantly from perfect coupling of hull to sea could cause difficulty. Measuring or analyzing these effects in the real world under all conditions is essentially impossible. Simplifying assumptions based on engineering judgment were necessary in the design of the EB-06 directional system. Accordingly, we assumed that records of $\ddot{\eta}$, η_x and η_y at the location of the hull at the time data acquisition began could be approximated by records of vertical acceleration ($\ddot{z}$), east slope (z_x) and north slope (z_y) of the discus hull.

NDBO knew that Fleet Numerical Weather Central's (FNWC's) directional spectral ocean wave model[8] made predictions only up through 0.164 Hz. Thus, for FNWC purposes at that time, there appeared to be no compelling reason to attempt measurements above 0.17 Hz. We also recognized that one of our most serious problems in the routine reporting of directional spectra to shore would be the large quantity of data transmitted. If very many buoys were to report over a frequency band that was too wide, the telemetry link could become overloaded.

Computer calculations made by the NDBO Hull/Mooring Dynamics Program [9] indicated that, for frequencies up to 0.17 Hz, the hull phase shift angles for heave and pitch should be small and perhaps negligible. (See Figure 3.) With little phase shifting, fewer words per frequency could be sent to shore to reproduce directional spectra. This minimization of words sent to shore made it desirable to limit the frequency range to 0.17 Hz or less.

The basic sampling rate chosen for directional sensors was 0.68 Hz, or a Nyquist frequency of 0.34 Hz. Thus, the lowest-frequency aliased energy contaminating the spectrum at 0.17 Hz was to come from [0.34 + (0.34 - 0.17)] = 0.51 Hz. The heave displacement power transfer function for 0.51 Hz is about 0.008. Thus, at this frequency, the 12-meter discus hull was expected to filter out virtually all sea energy for all sensors. Reversing this logic, i.e., limiting the upper frequency of interest to 0.17 Hz, was expected to allow sampling on a 12-meter discus hull at 0.68 Hz with no noticeable aliasing due to sea energy. Assuming that no electrical noise energy would be present above 0.51 Hz, it seemed unlikely that it would be necessary to filter the sensor outputs electronically to avoid aliasing, thus simplifying the system and reducing its cost.

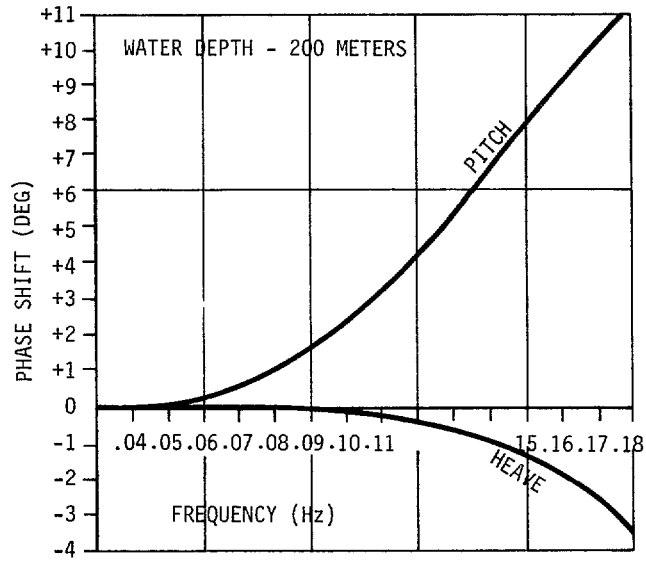

Figure 3. PHASE SHIFTS OF 12-METER UNMOORED DISCUS BUOY

These considerations and others, relating to the on-board data processing technique, led to the selection of an upper frequency limit of 0.17 Hz for the routine measurement of directional spectra.

3. The EB-06 Payload

The major elements of the EB-06 payload are shown in Figure 4 and described herein.

Power Source. Power for the EB-06 payload was provided by an on-board diesel generator similar to that used on earlier NDBO buoys.

Computer. The on-board data processing system was a modified Data General 4001 NOVA minicomputer that had been in service for several years. Although it consumed a great deal of power and was not designed for use in a non-laboratory environment, this model was chosen because it was readily available, because our algorithms could be inserted into an existing software system already functioning with the computer, and because it was only needed for a short time to test the system concept.

Data was input to this computer through 11 analog channels to which hull attitude and motion sensors were connected. A multiplexer and analog-to-digital converter controlled by the computer software produced 12-bit words for the computer.

Tape Recorder. A Kennedy Model 1600 digital tape recorder was connected to the minicomputer. It had been interfaced to the Data General computer, but it was not part of the concept for a system to routinely report directional spectra.

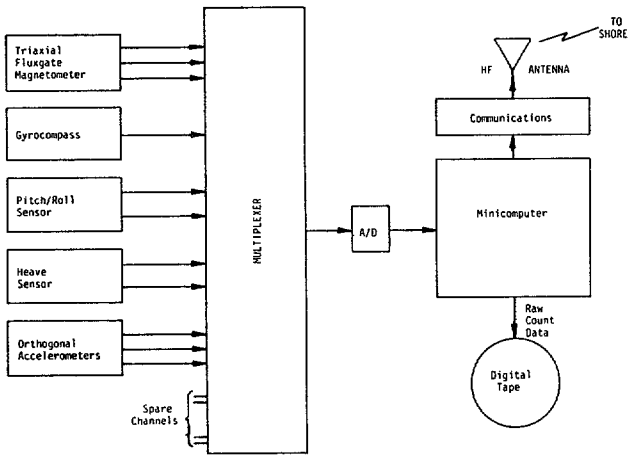

Figure 4. EB-06 PAYLOAD BLOCK DIAGRAM

It was included in EB-06 so that raw records would be available at shore to verify the near-real-time data.

Orthogonal Accelerometers. A container housing three orthogonal linear Kistler accelerometers was mounted as shown in Figure 5. The axes of two of these accelerometers were parallel to the deck. The axis of the third was parallel to the mast. The inclusion of these accelerometers in EB-06 was indirectly related to the development of directional spectra. NDBO had found that one-dimensional wave spectra derived from an accelerometer fixed parallel to a discus buoy mast did not differ noticeably from simultaneously acquired Waverider spectra derived from a vertically stabilized accelerometer. As a result, fixed accelerometers had commonly been used on NDBO's operational buoys. We were confident that the less expensive fixed accelerometers were producing quality one-dimensional spectra; but, to eliminate any uncertainty, simultaneous times series records were needed from both fixed and vertically stabilized accelerometers collocated on board the same discus hull. Raw count records from the three accelerometers were written on the on-board tape, and a comparison of the two mounting techniques has since been made.[10]

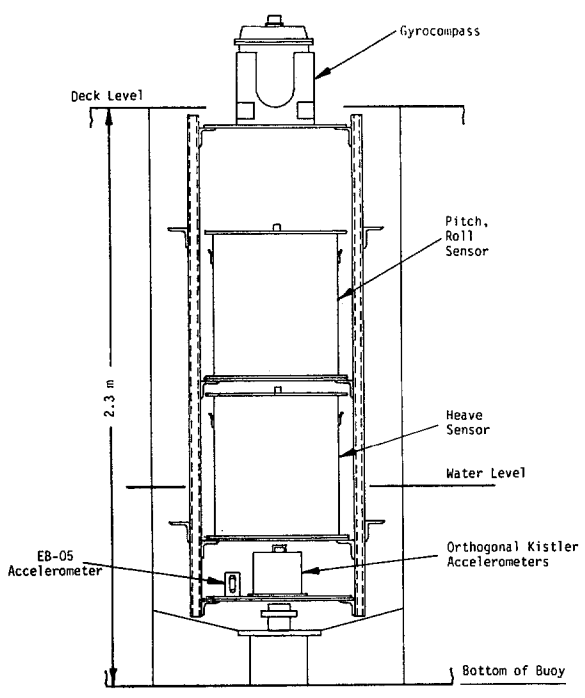

Figure 5. SENSOR MOUNTING ARRANGEMENT

If directional spectra could be measured with a vertically stabilized accelerometer, we believed it could be done as well using a fixed accelerometer with no serious loss of accuracy. Data from the fixed accelerometers was to verify this belief.

Heave Sensor. The Datawell heave sensor (40 sec) provided analogs of acceleration and displacement, either of which can, in principle, be used to compute directional spectra. The mechanical elements of this sensor are similar to those of the Datawell Waverider[11], which has a proven reliability record. The heave sensor was mounted on XERB as shown in Figure 5, on the centerline near the water level. The first configuration of EB-06 payload made use of samples of acceleration, $\ddot{z}(n)$, in which n enumerates the number of samples. The $\ddot{z}(n)$ was initially chosen for two reasons. First, NDBO thought that the total system would be more reliable if the output of the accelerometer were digitized rather than the output of the electronically more complex accelerometer plus double integrator. Also, it was hoped that at a later date the needed vertical acceleration could be obtained from a small, inexpensive fixed accelerometer rather than from the Datawell sensor. The uncertainty about whether $\ddot{z}(n)$ and $z(n)$ would be best for the calculation of directional spectra led NDBO to connect the analog of each into the EB-06 computer.

Pitch/Roll Sensor. The Datawell pitch/roll sensor (PIRO 40 sec) was mounted as shown in Figure 5. It provided angle analogs that, although not truly body-fixed pitch and roll, allowed their computation. The variables reproduced in engineering units in the EB-06 computer for the nth pair of samples taken from the sensor were $\sin P(n)$ and $\sin R'(n) = \cos P(n) \sin R(n)$. The $P(n)$ and $R(n)$ were true hull pitch and roll angles, respectively, and $R'(n)$ was the angle shown in Figure 2.

The Datawell heave and pitch/roll sensors were chosen because of low power consumption and proven reliability, despite such limitations as bulky housings, fairly high costs, and the overseas source.

Gyrocompass. Mounted inside of XERB's aluminum mast just above deck level was a modified

Sperry Mark 37 ship gyrocompass, as shown in Figure 5. It provided heading angle H(n), relative to true north.

Triaxial Magnetometer. A triaxial buoy-fixed fluxgate magnetometer, Superconducting Technology, Inc., Model F203, was mounted on top of the aluminum mast. It was not aligned with the buoy fixed frame of reference shown in Figure 2. Alignment was not necessary, and other hardware at the top of the mast made it inconvenient.

The counts produced in the EB-06 computer by the magnetometer outputs were proportional to the vector components of the local magnetic field parallel to the axes of the three magnetometers, $B_1(n)$, $B_2(n)$, and $B_3(n)$. The local magnetic field comprises $\vec{B}_e(n)$, the earth's field in the absence of the buoy, and $\vec{B}_b(n)$, a magnetic vector due to the buoy. The gyrocompass was to determine whether or not the magnetic interference of the hull would prevent an accurate determination of heading angle by the magnetometer. This was not expected to occur, and NDBO planned to use the magnetometer to determine H(n) for the directional measurement. A triaxial fluxgate magnetometer was chosen for compactness, low power consumption, and reliability.

Data Processing. The software for the EB-06 minicomputer routinely initiated a cycle beginning with the acquisition of one-dimensional wave displacement spectra. Except for the use of the Datawell heave sensor acceleration analog in place of a fixed accelerometer analog, data processing was identical to that of an earlier NDBO system.[1] The sampling rate was one per second. Autocovariances were computed, scaled, and stored for transmission to shore during the 15 minutes preceding the synoptic hour. Displacement spectra between 0.03 and 0.5 Hz with a resolution of 0.01 Hz, both corrected and not corrected for filtering of the hull, were calculated at shore.

At the beginning of the synoptic hour, sampling of sensors was begun to determine the near-real-time directional spectra. The time between samples was 1.47 seconds. At the initial deployment of XERB, the PIRO and gyrocompass were sampled virtually simultaneously, and the east $[z_x(n)]$ and north $[z_y(n)]$ slopes of the discus hull were calculated. Later, after EB-06 tape records had been analyzed at shore and had shown that these slopes could be calculated from the triaxial magnetometer and PIRO outputs, the EB-06 software was reprogrammed to derive H(n) from P(n), R(n), $B_1(n)$, $B_2(n)$, and $B_3(n)$. A schematic diagram of the reprogrammed version of the EB-06 directional data processing is shown in Figure 6.

The time series records $\ddot{z}(n)$, $z_x(n)$ and $z_y(n)$ were numerically filtered between samples. Total records were not stored. The filtered records were subsampled at a rate of 0.34 Hz. The subsampled records were used to compute the auto-

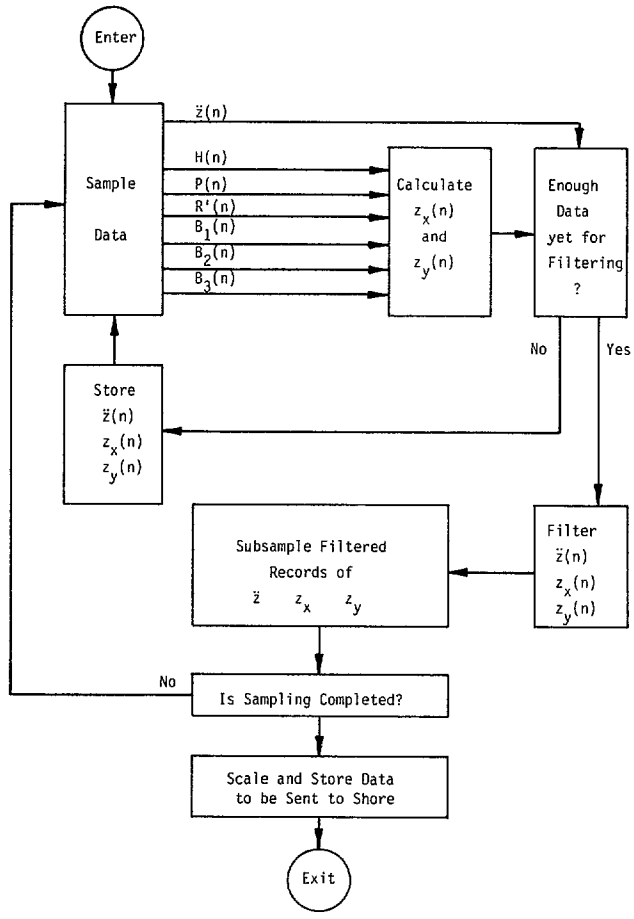

Figure 6. SCHEMATIC OF EB-06 DATA PROCESSING FOR DIRECTIONAL SPECTRA

and cross-covariances between the $\ddot{z}(n)$, $z_x(n)$, and $z_y(n)$ time series. It had been assumed that, in the frequency range up to 0.17 Hz, coupling between the hull and sea would be very good. On that assumption, the cross-covariances that should have been negligibly small were not transmitted to shore. The other auto- and cross-covariances were scaled and, by about 20 minutes after the synoptic hour, stored for transmission to shore. A more detailed description of the data processing techniques is provided in the companion paper.

Beginning at about 20 minutes after the synoptic hour, 12-bit raw samples were taken each half second for about 15 minutes from each of the 11 transducer outputs and recorded on the digital tape. Upon request from shore, EB-06 transmitted the one-dimensional and directional wave data to shore.

The directional data in the telemetry message sent to shore consisted of 132 sixteen-bit words. The approximate 28 seconds required to transmit a message of this length was not excessive for a routinely reporting system.

4. The EB-05 Payload

The EB-05 payload consisted of a battery-powered Magnavox Phase II data acquisition and reporting system.[12] This payload measured and reported barometric pressure, air temperature, surface water temperature, north and east components of wind speed, and one-dimensional wave spectra up to a frequency of 0.25 Hz. The Wave Data Analyzer (WDA) system of EB-05 was a modification of the system described in a 1975 paper.[13] Data was relayed to shore by EB-05 every 3 hours through both HF and UHF telemetry links. Wave data was acquired for a 15-minute period ending at the hour.

The accelerometer driving the EB-05 WDA was mounted next to the three orthogonal accelerometers of EB-06, with its axis fixed parallel to the mast, as shown in Figure 5. Thus, two accelerometers with axes fixed parallel to the mast, and one in the Datawell heave sensor vertically stabilized, were all mounted within about 0.3 meter of each other.

5. Relationship Between EB-05 and EB-06 Data

Figure 7 shows the time relationship between data acquired every 3 hours by EB-05 and EB-06. In the 15 minutes preceding the synoptic hour, the spectral data acquired by EB-06 and EB-05 were expected to be similar. Slight differences were expected for several reasons, including (1) the accelerometers driving the two systems were separated by about 0.3 meter, (2) the EB-06

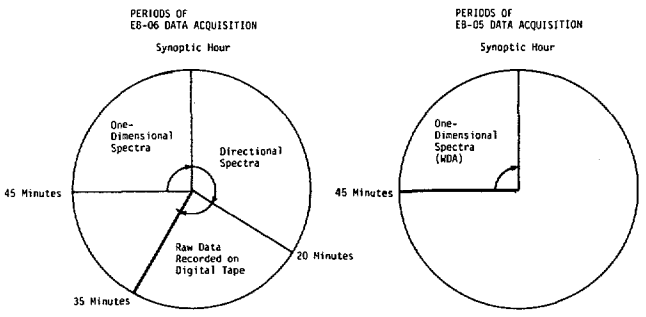

Figure 7. RELATIONSHIP BETWEEN EB-05 AND EB-06 WAVE DATA ACQUISITION TIMES

accelerometer was vertically stabilized, whereas the EB-05 accelerometer had its axis fixed parallel to the mast, and (3) the hardware, sampling rates, filtering characteristics, and other details of the EB-05 and EB-06 systems differed. Comparisons of these one-dimensional spectra were to determine whether or not there were noticeable differences between spectra produced by fixed and stabilized accelerometers.

The battery-powered EB-05 system had an analog six-pole Butterworth filter with a half-power frequency of 0.25 Hz to protect against aliasing. It was expected to have less electrical noise than the diesel-powered EB-06. EB-05 was therefore expected to produce the better one-dimensional spectra. We planned to compare it, as well as the one-dimensional spectra directly produced by EB-06, to the one-dimensional spectra derived by summing the directional spectra of EB-06 over all directions. The small differences between times of acquisition were not expected to be a serious factor. This three-way comparison was intended to verify the performance of each of the three systems.

NDBO had various computer programs at shore to produce wave data, including directional spectra, from the EB-06 tape records. These raw records were to be the ultimate source of data in the event of disagreements among the real-time data sources.

6. Data Evaluation

XERB was moored in the Atlantic Ocean at $30^{\circ}24'$N latitude and $80^{\circ}08'$W longitude in March 1977. At this location on the continental shelf, about 100 km from Jacksonville, Florida, the water depth is about 200 meters. The Gulf Stream current varies up to 2 meters/second and perhaps to near 3 meters/second at times. The sea states were light during the spring of 1977. The EB-05 and EB-06 payloads functioned well during the first 3 weeks of deployment, after which the EB-06 computer failed. It was repaired, and EB-06 began functioning again in June. Data from both payloads was successfully acquired for another 4 weeks. Telemetered data acquired daily from the two payloads was analyzed through hindcasting by an NDBO contractor. The contractor's first evaluation[14] of the correctness of the telemetered directional wave spectra was inconclusive, because the very light sea states prevalent at the time of data acquisition made evaluation difficult. NDBO had the raw digital data, which had been sampled during the same period at a higher rate than that of near-real-time data, processed to produce directional spectra. The contractor then evaluated these data. The report[15] of this second evaluation, along with our own evaluations, clarified several questions. The spectra were found to be fundamentally in agreement with known sea state conditions. Some of this data is presented in the companion paper.

The directional data from EB-06 was to be evaluated against independent directional measurements made by other systems, but a failure of the diesel exhaust system of XERB, which could only be corrected by return of the buoy to shore, prevented this effort.

7. Conclusions

A problem arose with the use of $\ddot{z}(n)$, which required the conversion of acceleration spectra to displacement spectra through a multiplication by ω^{-4}. Either high noise or higher than expected aliasing levels in the samples led to a degradation of the calculation when the sea state was

very light. Of course, this difficulty was not a fault of the $\ddot{z}(n)$ output of the Datawell sensor, but rather of the use made of it in the original configuration of EB-06. The Datawell heave sensor itself is a satisfactory choice for the measurement of vertical displacement, and it should be mounted approximately as it was on XERB. Its displacement output should be used, because the double integrator acts as a filter and provides a cleaner analog. NDBO believes that directional spectra can be measured accurately enough with the output of only an analog-filtered linear accelerometer with its axis fixed parallel to the mast; but, since this simplification has not yet been proven, we do not recommend it at present.

The Datawell PIRO 40 second sensor is a satisfactory source for body-fixed pitch and roll data. It should be placed approximately as it was on XERB. However, its location is not believed to be critical to its proper functioning.

The triaxial fluxgate magnetometer proved to be a satisfactory means of measuring H(n). Also, equations relating A(n) to P(n), R(n), $B_1(n)$, $B_2(n)$, and $B_3(n)$ worked well. Offsets were included in these equations to compensate for the effect of hull magnetization. Since the mast was aluminum, these offsets were small. If the magnetometer were mounted on the mast of one of NDBO's discus hulls with larger permanent magnetization, greater offsets would be required to compensate, but we believe accuracy would be maintained.

Although additional costs are incurred, active filters should be used on all six outputs of the recommended sensors, to eliminate uncertainty about aliasing. With aliasing and noise at a sufficiently low level, acceleration can probably be used in place of displacement.

A modern, low-power microcomputer with a multiplexer providing at least six input channels to the analog-to-digital converter should effect the on-board data processing. The analog-to-digital converter should have a 12-bit sampling capability, and sufficient storage capacity should be available to hold records of either the raw data from the six transducers or z(n), $z_x(n)$, and $z_y(n)$. It could be that 10 bits/sample is sufficient, but finding out exactly appears to us to be more trouble than simply measuring with 12-bit accuracy. This microcomputer should be ruggedized to withstand the unavoidably rough treatment it will receive at sea as a routinely operating measurement system.

The assumption that, at or below 0.17 Hz phase and amplitude shifting by the hull of sea pitch, roll and heave would be negligible, was found to be false. This finding translates into a requirement for more data words to be sent to shore, to allow corrections for the phase and amplitude shifting of the hull. These are not major complications of the concept, and should not be difficult to implement. Nevertheless, the non-trivial phase and amplitude shifting will require the experimental measurement of these transfer characteristics.

Once the correction for phase and amplitude shifts has been introduced, the upper frequency bound for measurements is limited mainly by the on-board method of calculation and by the need to limit the quantity of data produced. The need to limit the quantity of data results mainly from the greater energy consumed in telemetering a larger quantity of data that would, as a further disadvantage, have a lower probability of being error free. It also arises from the greater cost and other disadvantages related to the shoreside data processing.

We believe that more data words than the EB-06 directional system sent to shore can, and should, be tolerated. Telemetry errors in the HF messages were tolerable, and results with UHF telemetry should be better. On a large discus hull, the additional energy required to telemeter a somewhat longer message does not seriously impact the power budget. The companion paper explains in some detail the rationale for increasing the number of transmitted words from 132 to 186.

Our choice of an on-board data processing technique for directional spectra was not ideal for routine operations. It unnecessarily limited the frequency range in which data could be acquired. It did, however, function correctly and allowed us to gain experience with all aspects of the routine acquisition and reporting of directional wave spectra. Based on this experience, we believe that an on-board fast Fourier transform algorithm should be used, in place of the method used on XERB, to transform the two slopes and heave into the frequency domain.

The companion paper provides a more detailed explanation of the on-board and shorebased data processing techniques for directional spectra. Included are examples of both the near-real-time data produced, and data from the tape records. These demonstrate the utility of a system capable of reporting directional spectra.

The WDA system for the measurement of one-dimensional spectra includes a microcomputer fed by an accelerometer fixed parallel to the mast. Estimating the directional spectra in the manner described requires a microcomputer of similar cost. In addition, sensors to measure heading, pitch, and roll are needed, and heave displacement may be needed in place of acceleration. We estimate that these added sensors would cost approximately $10,000. Thus, after development has been completed, the incremental cost of hardware to measure directional spectra rather than one-dimensional spectra should be approximately $11,000.

8. Acknowledgements

Numerous individuals associated with NDBO

contributed to the success of the work described. Some of these are listed here.

Mr. Frank Remond of Sperry Support Services participated in the system design, sensor testing, and integrated system tests. In addition to writing the procedures, he supervised the tests, analyzed the data, and designed special test equipment to simulate sensor outputs under hypothetical sea states.

Mr. James Stewart of Sperry programmed the algorithms for the EB-06 on-board data processing system. He also programmed the shorebased system that completed the calculations to produce directional spectra.

Mr. Bobby Redmon of Sperry interrogated the EB-06 system daily to retrieve the near-real-time data.

Mr. R. Crowder, formerly of Sperry, served as project engineer for the integration of the XERB buoy hardware.

Mr. Ralph Dagnall of Sperry coordinated integration of the XERB hardware with the preparation and installation of revised software, and offered much useful advice to the total project.

Mr. James Tapley and Mr. Norm Negrete of Sperry were major contributors in the actual assembly of the XERB. They also advised on the configuration of the buoy, and accompanied it to sea.

Mr. Billy Graham of Sperry planned the shorebased portion of the EB-06 data processing system. He also prepared and tested the software test routines to assure proper functioning of the system.

Mrs. Deborah Hojem edited the paper, and Mrs. Linda Bridges suffered through the typing of numerous drafts, as well as the final copy.

References

1. Steele, K.E., J.M. Hall, and F.X. Remond, "Routine Measurement of Heave Displacement Spectra from Large Discus Buoys in the Deep Ocean," Proceedings of the First Combined IEEE Conference on Engineering in the Ocean Environment and the Annual Meeting of the Marine Technology Society (OCEANS 75), Sept. 1975.

2. Panicker, N.N., "Review of Techniques for Wave Spectra," International Symposium on Ocean Wave Measurement and Analysis (WAVES 74), Vol. I, p. 669, Sept. 9-11, 1974.

3. Pierson, W., "Recording, Measuring, and Reporting Ocean Wave Properties with National Data Buoys on a Synoptic Basis," New York University, Dept. of Oceanography, May 1972.

4. Nierenberg, Dr. W.A., "An Ocean Wave Measuring Buoy," Scripps Institution of Oceanography, University of California, San Diego, Advanced Ocean Engineering Laboratory, AOEL Report #56, Jan. 1974.

5. "UK Develops Buoy Prototype for Monitoring in North Sea," IMS Newsletter, International Marine Science, No. 7, Dec. 1974.

6. Rusby, Dr. S., "The Data Buoy Scene," New Science, Nov. 13, 1975.

7. Burdette, E.L., K. Steele, and A. Trampus, "Directional Wave Spectral Data from a Large Discus Buoy," Proceedings of the MTS-IEEE Conference, The Ocean Challenge (OCEANS 78), Washington, D.C., Sept. 6-8, 1978.

8. Lazanoff, S.M. and N.M. Stevenson, "An Evaluation of a Hemispheric Operational Wave Spectral Model," Fleet Numerical Weather Central, Monterey, CA, Technical Note No. 75-3, June 1975.

9. Niederman, CDR.C.S., Lt. C.B. Doherty, D.M. Brooks, and Lt. (jg) H.E. Beasley, "Mooring Handbook," NOAA Data Buoy Office, 1976.

10. Burdette, E.L., "The Comparison of Discus Buoy Wave Spectra Produced by Body-fixed and Vertically Stabilized Accelerometers," Proceedings of the MTS-IEEE Conference, The Ocean Challenge (OCEANS 78), Washington, D.C., Sept. 6-8, 1978.

11. Verhagen, C.M., P.L. Gerritzen, and J.G.A. von Breugel, "Operation and Service Manual for the Waverider," Datawell, Haarlem, The Netherlands, Doc. No. 5095-67020.

12. "Equipment Operations Manual for Phase II Payload System," prepared under Contract NAS 13-16 for the NOAA Data Buoy Office by Magnavox Government & Electronics Company, July 1976.

13. Steele, K.E., P.A. Wolfgram, A. Trampus, and B.S. Graham, "An Operational High Resolution Wave Data Analyzer System for Buoys," Proceedings of the OCEANS 76 Conference, Washington, D.C., Sept. 13-15, 1976.

14. Hubert, W.E., "Evaluation of Environmental Data from XERB," Ocean Data Systems, Inc., Final Technical Report (Task Order No. 9), May 1977.

15. Hubert, W.E., "Evaluation of Broadband (Recorded) Directional Spectra from XERB," Ocean Data Systems, Inc., Preliminary Final Technical Report (Task Order No. 10), October 1977.

DIRECTIONAL WAVE SPECTRAL DATA FROM A LARGE DISCUS BUOY

E.L. Burdette
Computer Sciences Corporation
National Space Technology Laboratories
NSTL Station, Mississippi 39529

K.E. Steele
NOAA Data Buoy Office
National Space Technology Laboratories
NSTL Station, Mississippi 39529

A. Trampus
Federal Energy Regulatory Commission
825 North Capitol Street
Washington, D.C. 20426

Abstract

A 12-meter diameter discus buoy was instrumented by the NOAA Data Buoy Office (NDBO) for the measurement and near-real-time reporting of wave directional spectra. Time series of buoy heave displacement, pitch, roll, and heading angles were processed into covariance functions on board the buoy. The covariances were then telemetered to shore for further processing into a Fourier series azimuthal approximation of the wave energy frequency/direction spectrum. The data processing procedures are described and examples of the data are presented herein. Plans for continued development of the technique are also outlined.

1. Introduction

An automated data acquisition and processing system based on a 16-bit minicomputer was installed and operated on board a 12-meter discus buoy (XERB) by NDBO, to obtain near-real-time estimates of the sea surface directional spectrum via the technique of Longuet-Higgins, Cartwright, and Smith[1]. Buoy motion was measured by a heave sensor, a pitch/roll sensor, and a gyrocompass (later replaced by a triaxial magnetometer). Digitized time series of sensor outputs were processed into covariances on the buoy for transmission to shore via an HF radio link. Further processing was performed on shore to produce the directional spectral estimate. Digitized sensor data was also stored on board the buoy on magnetic tape. (A more detailed description of the system hardware is contained in a companion paper.[2]) This paper describes the techniques used for handling and processing the data, the methods used to evaluate the processed data, and some preliminary results. Modifications made to and proposed for the data processing procedure, and NDBO plans for further development of a directional spectral measurement capability, are also presented.

2. Description of the Technique

The buoy motion sensors were rigidly mounted in a coordinate system, X, fixed in the buoy, which may be taken to be as shown in Figure 2 of Steele, et al.[2] However, the spectral estimate $S(f,\phi)$ is computed from time series of three quantities which are expressed in an earth-fixed system, x, having the +x-axis in the east direction and the +z-axis toward the zenith. The quantities required for the spectral estimate, expressed in continuous notation, are

$$\eta_o(t) = \frac{d^2}{dt^2}\eta\ (x_o,y_o,t) \qquad (1)$$

where $\eta(x,y,t)$ = sea surface elevation at (x,y) at time t,

$$\eta_x(t) = \frac{\partial}{\partial x}\eta\ (x,y,t)\ \Big|_{x = x_o,\ y = y_o} \qquad (2)$$

and

$$\eta_y(t) = \frac{\partial}{\partial y}\eta\ (x,y,t)\ \Big|_{x = x_o,\ y = y_o}\ . \qquad (3)$$

It was assumed that the buoy remained sufficiently near to (x_o, y_o) during the data acquisition cycle and that the buoy followed the sea surface adequately to allow $\ddot{\eta}_o$, η_x, and η_y to be approximated by the corresponding motion of the buoy, $\ddot{z}$, z_x, and z_y.

Four analog sensor voltage levels—heave acceleration, pitch, pseudo-roll, and heading angle—were sampled and digitized essentially simultaneously for a period T. N' samples of each voltage level were acquired, yielding four time series consisting of discrete values separated in time by $\Delta t = T/(N'-1)$.

The vertical acceleration, $\ddot{z}$, was read directly from the heave sensor, while z_x and z_y were computed from the outputs of the pitch-roll sensor and gyrocompass as described by Saenger[3].

The three resulting time series may be represented by

$$\begin{aligned} y_1(j) &= \ddot{z}\ (t_o + (j-1)\cdot\Delta t), \\ y_2(j) &= z_x(t_o + (j-1)\cdot\Delta t), \text{ and} \\ y_3(j) &= z_y(t_o + (j-1)\cdot\Delta t), \end{aligned} \qquad (4)$$

where t_o represents the beginning of the time series and $j = 1, 2, 3, \ldots, N'$. Each time

series was filtered numerically by a moving-average type of low-pass filter as in Powell[4], where each filtered sample was a weighted average of m_f consecutive unfiltered samples.

Each of the filtered time series was subsampled, or decimated, to produce three new time series, $x_i(n) = F\langle y_i(2n-1)\rangle$, i = 1, 2, 3, where F represents the operation of the filter and n = 1, 2, 3, . . ., N. The number of samples in the filtered and unfiltered time series are related as $N = [(1/2)\ (N'-m_f)] + 1$.

Filtering was used to prevent aliasing from the y_i time series into the subsampled x_i. Table I shows the actual values of the various parameters used in the on-board computation of the directional spectrum.

TABLE I

PARAMETERS EMPLOYED IN ON-BOARD COMPUTATION OF DIRECTIONAL SPECTRA

PARAMETER	SYMBOL	NUMERICAL VALUE
T	Length of sampling period	20.48 min
N'	Number of data samples in each time series	837
Δt	Time between samples in original time series	1.47 sec
N	Number of data samples in subsampled time series	408
m_f	Number of data samples used to compute a filtered sample	23
M	Number of lags in covariance computation	17

Six elements of the covariance matrix, $Cov_{pq}(\ell)$, for lag ℓ= 0, 1, 2, ..., M, were computed for the three time series (cf. Bendat and Piersol[5]) for transmission to shore. In the original software configuration, $Cov_{11}(\ell)$, $Cov_{12}(\ell)$, $Cov_{13}(\ell)$, $Cov_{22}(\ell)$, $Cov_{33}(\ell)$, and $Cov_{23}(\ell)$ for each of 18 lags were telemetered from the buoy in the form of 12-bit integer words. Additional data on mean, minimum, and maximum values of the time series was also reported, so that the directional wave message consisted of 132 twelve-bit data words.

The directional wave message was received at shore as a part of the overall buoy data message, and then converted from integer to engineering unit form. The time series values were printed out for a quick-look check of system performance, while the covariance matrix elements were used to compute elements of the raw spectral matrix, $\tilde{S}_{pq}(f_k)$, by means of the discrete Fourier transform. The spectral matrix was computed for frequencies $f_k = k\cdot(f_N/M)$, where k = 0, 1, 2, ..., M, and f_N is the Nyquist frequency. The raw spectral elements were smoothed by Hanning to obtain the elements of the acceleration matrix, $\hat{S}'_{pq}(f_k)$, which were then converted to an estimate of the displacement spectral matrix via

$$\hat{S}_{pq}(f_k) = \alpha_p \alpha_q \hat{S}'_{pq}(f_k) \qquad (5)$$

where

$$\alpha_p = -\left(\frac{1}{2\pi f_k}\right)^2 \quad \text{for } p = 1$$

$$\alpha_p = 1 \qquad \text{for } p = 2, 3.$$

The elements of the spectral matrix are complex, of the form

$$S_{pq}(f) = C_{pq}(f) - iQ_{pq}(f) \quad . \qquad (6)$$

However, it may be shown that, for a hull that is a perfect surface follower,

$$S_{pq}(f) = \begin{bmatrix} C_{11}(f) & -iQ_{12}(f) & -iQ_{13}(f) \\ iQ_{12}(f) & C_{22}(f) & C_{23}(f) \\ iQ_{13}(f) & C_{23}(f) & C_{33}(f) \end{bmatrix} \qquad (7)$$

The elements of the $S_{pq}(f)$ matrix were estimated by $\hat{S}_{pq}(f_k)$ and were used to obtain the first five Fourier coefficients of the angular distribution of the displacement spectral density function from which the weighted Fourier expansion

$$S\ (f_k,\phi) = 1/2a_o + c_1(a_1 \cos\phi + b_1 \sin\phi) + c_2(a_2 \cos 2\phi + b_2 \sin 2\phi) \qquad (8)$$

of Longuet-Higgins, et al., was computed. The weighting coefficients, $c_1 = 2/3$ and $c_2 = 1/6$, were chosen to reduce negative values of the azimuthal expansion. A minor change in convention was adopted to facilitate interpretation of the directional wave data through comparison with conventional wind field data, where the wind direction is that direction from which the wind comes. The vector wave number was defined as

$$\vec{\kappa} = (\kappa \sin\phi,\ \kappa \cos\phi) \qquad (9)$$

so that ϕ indicated the direction with respect to the north of $-\vec{\kappa}$, or that direction from which the wave energy at frequency f_k was arriving at (x_o,y_o). Also, to facilitate data evaluation further, $S(f_k,\phi)$ was expressed in units of m^2/Hz-degree, requiring the expansion coefficients to take the form

$$a_o(f_k) = \frac{\delta}{\kappa} C_{11}(f_k)$$
$$a_1(f_k) = \frac{\delta}{\kappa} Q_{13}(f_k)$$
$$b_1(f_k) = \frac{\delta}{\kappa} Q_{12}(f_k) \qquad (10)$$
$$a_2(f_k) = \frac{\delta}{\kappa^2} [C_{33}(f_k) - C_{22}(f_k)]$$
$$b_2(f_k) = \frac{2\delta}{\kappa^2} C_{23}(f_k)$$

with $\delta = 1/180^o$. A mean wave direction for each frequency band was also computed; i.e.,

$$\bar{\phi}(f_k) = \tan^{-1} [b_1(f_k)/a_1(f_k)] \quad . \qquad (11)$$

The number of degrees of freedom of the spectral estimate obtained by this technique is $n = 2N/M$; for the parameters of Table I, $n = 24$.

3. Data Evaluation

In addition to the directional wave system, termed the EB-06 buoy payload, XERB carried a completely independent sensor, data processing, and telemetry system, termed the EB-05 payload, which reported meteorological and one-dimensional wave spectral data. EB-05 was an NDBO operational payload, which produced proven high-quality wave data. The one-dimensional wave spectra from this payload provided the primary source of comparison data for the on-board directional wave system. Integration of $S(f_k,\phi)$ of eq. (8) over the azimuthal angle yielded a one-dimensional spectral estimate. Comparison of data from EB-06 with the EB-05 data gave a good indication of proper operation of the experimental system.

The sensor data recorded on magnetic tape by the EB-06 payload provided a second source of comparison data and a means for verifying the wave direction. The recorded time series were digitized at a higher sampling rate ($\Delta t = 0.5$ sec) than the data used in the on-board directional system, thereby allowing spectral analysis over a frequency range from 0 to 1.0 Hz. These data were processed at shore in two ways: (1) The on-board data processing was duplicated in a 16-bit minicomputer similar to that on board the buoy, and (2) the other spectral analysis, including a 0 to 1.0 Hz directional spectral estimate, was performed on a large-scale 36-bit computer.

The on-board directional spectral estimate was obtained from $\dot{z}$, z_x, and z_y, with $\ddot{z}$ obtained from the Datawell heave accelerometer, but the tape data processing was not so limited. In fact, excellent results were obtained by estimating the directional spectrum from z, z_x, and z_y, with z obtained from the displacement output of the Datawell sensor. The availability of tape recorded sensor data for subsequent shoreside examination and processing by various techniques proved to be one of the most valuable aspects of the initial stage of the XERB project.

The 0 to 1.0 Hz directional spectral estimate, termed the boardband spectrum, was not compensated for the buoy hull transfer function, which deviated significantly from unity for frequencies greater than about 0.27 Hz. Spectral data for higher frequencies was therefore suspect. While waves in the 0.25 Hz range should not necessarily be in equilibrium with the local wind, the wave direction should approach the wind after several hours of steady wind direction. Also, the XERB deployment site (30°24'N, 80°08'W) had a directional window on open water from an azimuth of about 35° through 140°. Waves incident from other directions were limited in fetch from approximately 100 to 500 km. Valid wave directions at lower frequencies must lie within the open-water window. These two constraints were used to test the validity of the broadband directional spectrum, which was then compared with the on-board directional spectrum. Minor statistical differences between the EB-05, EB-06 on-board, and broadband spectra were expected because the data for the estimates were acquired during three approximately contiguous time intervals.

Hindcasting was also used with some success, although the lack of clearly identifiable localized wave sources in the North Atlantic during early summer relegated this technique to a secondary role. The unpredictable effect of the Gulf Stream on wave directions also made hindcasting difficult.

A thorough examination of the XERB directional wave data was performed by an independent NDBO contractor[6] using techniques similar to those described herein. Partial results of this evaluation are included in this paper.

4. Preliminary Results

The experimental results presented herein are for an interesting period of data that began on March 31, 1977. Figure 1 compares one-dimensional wave height spectra for March 31, 0000 GMT, obtained from the EB-05 payload, the EB-06 on-board directional payload, and the broadband spectral estimate. Comparisons of mean wave direction, $\bar{\phi}(f_k)$, are also shown for the on-board and broadband directional spectral estimates.

The excellent agreement between the EB-05 data and the broadband spectrum computed from displacement is typical of the XERB data. Note the separate spectral peaks at 0.09 Hz and 0.15-0.16 Hz, which indicate the presence of two low-frequency swell trains. The poor agreement between the on-board directional data and the other two data sets is also typical of the initial XERB data.

Mean wave direction for the EB-06 on-board estimate does not agree closely with that of the broadband estimate, but the extent of the agreement is surprising in view of the poor agreement between the one-dimensional spectra. Wind direction was obtained from the EB-05 sensor and from National Weather Service (NWS) facsimile charts. The latter is more likely to be a measure of wind

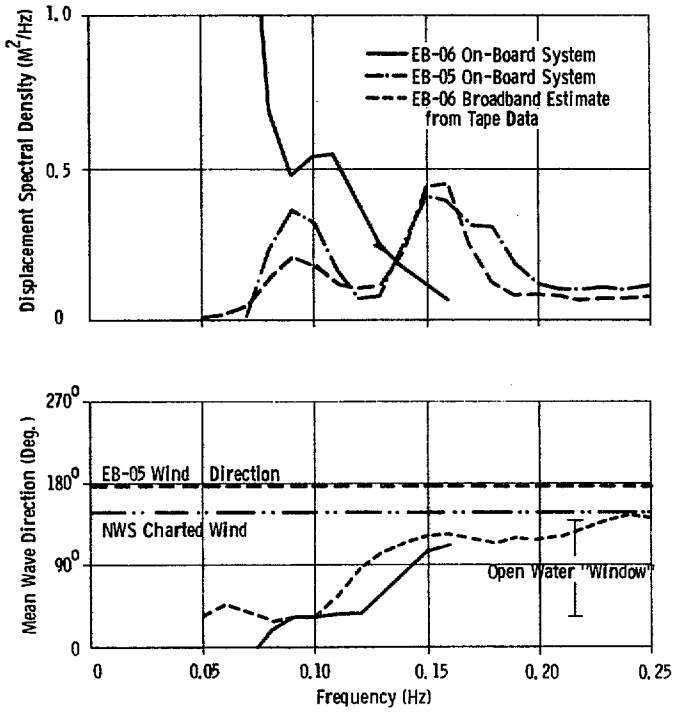

Figure 1. COMPARISON OF XERB DATA FOR MARCH 31, 1977, 0000 GMT

direction over an area large enough to generate waves at 0.25 Hz, while the former indicates actual local wind. Note that the wave direction at higher frequencies approaches that of the local wind.

Figure 2 is a time series of local wind direction together with a time series of 0.27 Hz mean wave direction from the broadband spectral estimate for the period March 24 through April 6, taken from Hubert[6]. Of interest here are the abrupt wind shifts of April 1 and 2, which were caused by a frontal passage to which the high-frequency wave direction responded. The apparent

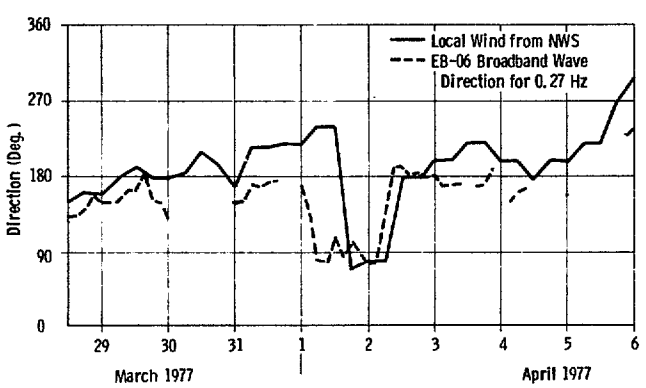

Figure 2. COMPARISON OF XERB 0.27 Hz MEAN WAVE DIRECTION WITH LOCAL WIND DIRECTION (WAVE DIRECTION IS FROM BROADBAND SPECTRAL ESTIMATE COMPUTED AT SHORE FROM BUOY DATA RECORD)

anticipation of the direction shift is thought to be due to the fact that waves of 0.27 Hz frequency are generated at some distance from the buoy, resulting in an apparent hysteresis. Discrepancies between the two directions may be due to wave refraction caused by the Gulf Stream, which has a current greater than 2 m/sec at this location. Gaps in the wave direction time series were caused by on-board recorder problems.

The high-frequency agreement with wind direction indicated by Figure 2, together with the fact that low-frequency data typically fell within the open-water window, confirmed the accuracy of the broadband spectral estimate, thereby confirming that the sensor and data acquisition systems of EB-06 were functioning properly. Hence, the tape recorded data could be assumed to be reliable.

The tape recorded sensor data was processed at shore through a bench system which estimated the on-board data processing and telemetry of EB-06. Extensive tests were performed to determine the cause of the poor agreement between data produced by the on-board directional system and data from other sources. It was determined that the bias seen in the spectral estimate at lower frequencies (<0.10 Hz) was due to a combination of system noise and aliased sensor data from frequencies above 0.57 Hz amplified tremendously by the acceleration to displacement transformation which produced $\hat{S}_{pq}(f_L)$. At higher frequencies (0.13 to 0.17 Hz), the on-board directional spectral estimate was attenuated by the rolloff of the digital anti-aliasing filter. This was expected and plans were already underway to compensate the spectral estimate. Based on the simulation results, modifications to the on-board data processing technique to overcome these problems were made and tested in the bench system.

5. Modifications to the Technique

An in-house study performed by NDBO had shown that a triaxial magnetometer could be used to determine the magnetic heading of a buoy, if compensation for the effects of the ferromagnetic hull could be provided. One goal of the XERB project was to test this concept. Data from the EB-06 on-board tape, which was recorded during the first week of deployed operation, allowed the computed magnetic heading to be compared with the reading of the buoy gyrocompass. Based on these results, the on-board computational software was modified to compute the sine and cosine of heading by means of the magnetometer. This software modification was actually implemented on board XERB in early June 1977.

A more extensive modification to the on-board and shorebased software was planned and tested using tape data, but was not implemented due to on-board hardware problems. These modifications included (1) conversion to computation of the directional spectral estimate from time series of z, z_x, and z_y, rather than $\ddot{z}$, z_x, and z_y; (2) addition of a routine to compensate for

the transfer effects of buoy hull, heave sensor double integration circuitry, and the numerical anti-aliasing filter; (3) addition of a correction for finite water depth in computation of the Fourier coefficients; and (4) correction for system noise.

Conversion to Displacement. The initial technique of transformation from acceleration to displacement in the frequency domain caused amplification of noise, as previously described. This difficulty was overcome by using the displacement signal from the heave sensor rather than acceleration. The sensor performs the acceleration to displacement transformation in the time domain at the expense of introduction of a significant phase/amplitude shift in the signal. This problem was corrected by a second software change to compensate the transfer function.

Correction for Transfer Effects. The time series, y_i, used to compute the spectral estimate are not the true sea surface motions, w_i, but are related to them as follows:

$$y_i(j) = h_i(j)\ w_i(j) \tag{12}$$

where

$$\begin{aligned} w_1(j) &= n(t_o + (j-1)\cdot\Delta t) \\ w_2(j) &= n_x(t_o + (j-1).\Delta t) \\ w_3(j) &= n_y(t_o + (j-1)\cdot\Delta t). \end{aligned} \tag{13}$$

The h_i values are time domain representations of the transfer effects of the sensors, hull, and filtering process. The spectral matrix corresponding to the sea surface time series is

$$T_{pq}\ (f_k) = \frac{S_{pq}\ (f_k)}{H_p^*(f_k)\ H_q(f_k)} \tag{14}$$

where $H_i(f_k)$ is the complex frequency domain counterpart of $h_i(j)$. The $\hat{T}_{pq}(f_k)$ elements were used to compute the Fourier coefficients for the directional spectral estimate. A transfer function for each time series was generated by combining the effects of the numerical filter, sensors, and buoy hull (obtained by numerical modeling).

In order to perform the correction indicated by eq. (14), it was necessary to transmit additional data from the buoy in the form of three additional covariances, $Cov_{21}(\ell)$, $Cov_{31}(\ell)$ and $Cov_{32}(\ell)$, for each of 18 values of ℓ. This increased the transmitted data message to 186 words.

Correction for Water Depth. The water depth, h, at the XERB site required inclusion of the shallow-water correction, $\omega^2 = \kappa g \tanh \kappa h$, in the computation of κ for the Fourier coefficients. No attempt was made to correct for the more complex effect of refraction due to shoaling.

Noise Correction. System noise produced occasional bimodal spikes in the directional spectrum at low frequencies. However, a corresponding error in the one-dimensional spectrum obtained by an azimuthal integration was not seen. This result was attributed to aliasing of pitch/roll motion from 0.6 to 0.7 Hz. The aliased signal was greatly attenuated, so the effect was troublesome only when high-frequency wave motion was significant and low-frequency wave motion was slight. Since no aliasing was seen in the heave displacement spectrum, a simple threshold technique was employed as a correction. When $T_{11}(f_k)$ was less than the threshold value, $\Theta(f_k)$, all elements of $T_{pq}(f_k)$ were set to zero for that particular frequency band.

Figure 3 shows the results of the corrections obtained by simulating the modified on-board system using EB-06 tape data for 3/31/77, 0000 GMT. The broadband spectral data of Figure 1 is included for comparison. Figure 4 shows the same comparison for data of 3/31/77, 0600 GMT. Figure 5 is a contour plot of the modified on-board directional spectral estimate for 3/31/77, 0000 GMT; corresponding data from the broadband directional estimate is shown in Figure 6.

The agreement between the modified on-board and the broadband directional spectral estimates over the range of 0 to 0.15 Hz indicated by Figures 3 through 6 is typical of the test data. Unfortunately, hardware problems with EB-06 forced the retrieval of XERB from its deployment site. The modifications to the EB-06 software-system were therefore never implemented.

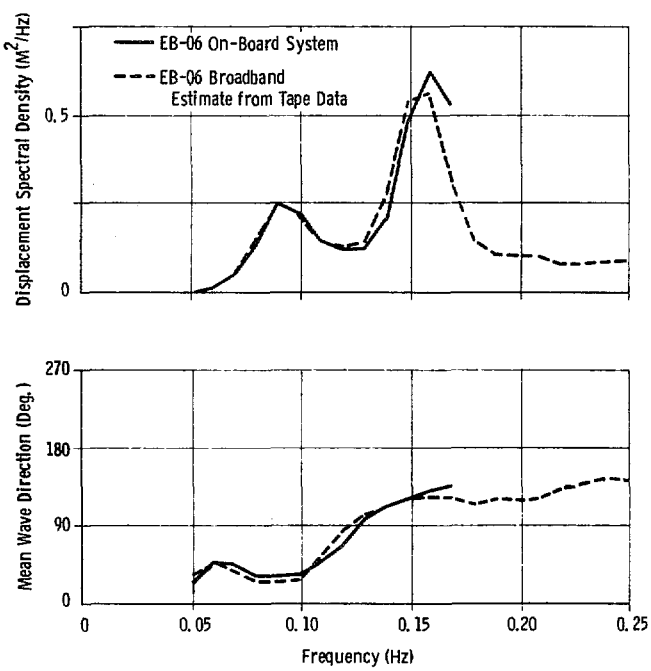

Figure 3. COMPARISON OF MODIFIED ON-BOARD DIRECTIONAL SYSTEM DATA WITH BROADBAND DIRECTIONAL DATA FOR MARCH 31, 1977, 0000 GMT

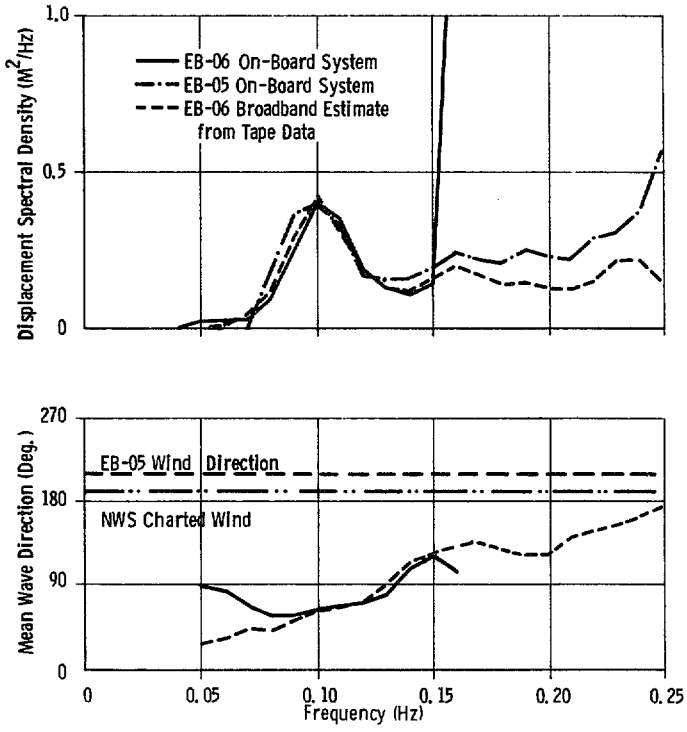

Figure 4. COMPARISON OF MODIFIED ON-BOARD DIRECTIONAL SYSTEM DATA WITH BROADBAND DIRECTIONAL DATA AND EB-05 DATA FOR MARCH 31, 1977, 0600 GMT

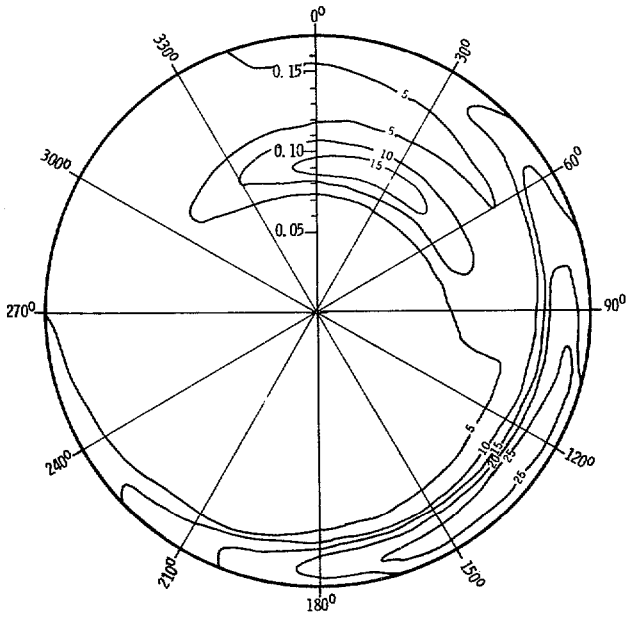

Figure 5. CONTOURS OF EQUAL SPECTRAL DENSITY IN MODIFIED ON-BOARD DIRECTIONAL SPECTRAL ESTIMATE, MARCH 31, 1977, 0000 GMT (SPECTRAL DENSITY IS IN UNITS OF M^2/Hz-DEG: RADIAL COORDINATE IS FREQUENCY IN Hz; AZIMUTHAL COORDINATE IS DIRECTION (TRUE) FROM WHICH ENERGY IS INCIDENT)

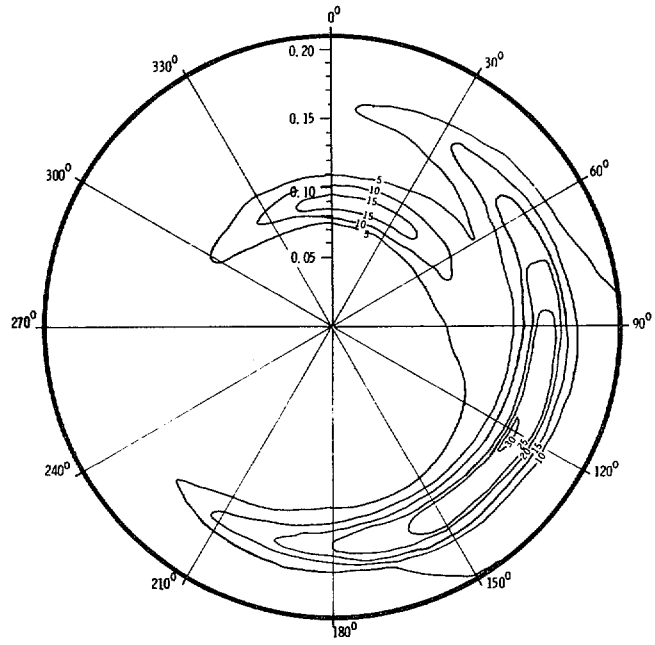

Figure 6. CONTOURS OF EQUAL SPECTRAL DENSITY IN BROADBAND DIRECTIONAL SPECTRAL ESTIMATE, MARCH 31, 1977, 0000 GMT (SPECTRAL DENSITY IS IN UNITS OF M^2/Hz-DEG; RADIAL COORDINATE IS FREQUENCY IN Hz: AZIMUTHAL COORDINATE IS DIRECTION (TRUE) FROM WHICH ENERGY IS INCIDENT)

6. Conclusions

Extensive comparisons of the type indicated herein made over the full period of operation of the EB-06 directional system indicate that adaptation of the Longuet-Higgins, Cartwright, and Smith technique is a practical means for obtaining directional spectra from a pitch/roll buoy in a real-time mode. Based on experience with XERB, a number of improvements are planned in addition to the modification described in Section 5.

7. Plans for Future Work

The XERB experiment is being continued by NDBO, with changes being planned for both system hardware and software. Initially, the directional wave system hardware will be upgraded to a ruggedized, 16-bit minicomputer which utilizes a set of machine instructions and a system architecture identical to that of the old EB-06 NOVA computer. The modified software described in Section 5 will thus be utilized both on board and at shore. The telemetry mode will also be changed from HF radio to the more reliable UHF/GOES link of the NOAA National Environmental Satellite Service.

The next phase of the experiment will util-

ize this newer hardware with extensive changes to both on-board and shorebased software. In place of the covariance procedure of Longuet-Higgins, et al., the new on-board procedure will employ a technique based on the segmented record fast Fourier transform. This technique has been employed in a similar application on the National Institute of Oceanography DB-1.[7] The amount of shorebased processing will be reduced, as will the amount of telemetered data per spectral estimate. The upgraded software will use a high-level computer language to facilitate its adaptation to future systems.

A calibration experiment is also planned for XERB. The buoy will be moored near an offshore tower equipped with a wave staff array from which a ground-truth directional spectral estimate will be obtained. Following thorough testing of the XERB system, NDBO plans to adapt the pitch/roll buoy on-board computational technique to a cost-effective, low-power microprocessor-based system for operational use in the data buoy network. Methods for the dissemination of directional wave data to users over the NWS teletype network will also be investigated. Initial implementation will likely consist of augmentation of NDBO's present one-dimensional spectral reports to include a mean wave direction for each frequency band.

References

1. Longuet-Higgins, M.S., D.E. Cartwright, and N.D. Smith, "Observations of the Directional Spectrum of Sea Waves Using the Motions of a Floating Buoy," Proceedings of the International Symposium on Ocean Wave Spectra, Prentice Hall, 1963.

2. Steele, K.E., E.L. Burdette, and A. Trampus, "A System for the Routine Measurement of Directional Wave Spectra from Large Discus Buoys," Proceedings of the MTS-IEEE Conference, The Ocean Challenge (OCEANS 78), Washington, D.C., Sept. 6-8, 1978.

3. Saenger, R.A., "Measurement of the Statistical Properties of the Ocean Surface with Instrumented Surfact Floats — Part II: Engineering and Data Processing," Geophysical Sciences Laboratory TR-69-10, New York University School of Engineering and Science, University Heights, New York, 1969.

4. Powell, S.W., "Methods of Digital Filtering," Aeroballistics Internal Note No. 37-63, George C. Marshall Space Flight Center, Aeroballistics Division, Huntsville, Alabama, 1963.

5. Bendat, J.S., and A.G. Piersol, "Measurement and Analysis of Random Data," John Wiley and Sons, Inc., New York, 1966.

6. Hubert, W.E., "Evaluation of Broadband (Recorded) Directional Spectra from XERB," Ocean Data Systems, Inc., Technical Report, 1977.

7. Clayson, C.H., and J.A. Ewing, "The Buoy as a Directional Wave Sensor," U.K. Data Buoy (DB1) Symposium, Wormley, Godalming, Surrey, U.K., 1976.

DIRECTIONAL WAVE-SPECTRA MONITORING HORIZONTAL-SPAR BUOY

Andrew Van Baird
Department of Ocean Engineering
Massachusetts Institute of Technology
Cambridge, Massachusetts 02139

Abstract

A center-tethered lightly ballasted spar will be driven parallel to the crests of a uni-directional wavetrain.

The application of this phenomenon has been proposed in the design of a wave direction monitoring buoy. Such a system would provide a reliable and inexpensive means for measurement of the direction of the maximum wave energy in an ocean environment. The performance of this system is discussed from both a theoretical and an operational point of view.

Model and field test results are presented which reaffirm the viability of the design, with potential developments postulated.

1. Introduction

Of many natural phenomena observed and studied for centuries, waves remain yet as one of the most complex and least understood processes of the ocean. With a growing scientific and engineering concern over the mechanisms involved in wave formation and propagation, motivated by an increasing outreach to the seas as a source of minerals and food, the need has developed for an instrument capable of measuring wave amplitude, period and direction.

In the recent past, few oceanographic systems have been available to monitor and record all the properties of a wave spectrum. Those which are employed (e.g. multiple bottom mounted pressure sensors, multiple wave staffs, etc.) tend to be excessively costly, unreliable or limited in use for baseline environmental surveys. Consequently, the art of wave measurement has remained out of the hands of the main industrial echelon.

The discussion presented in this paper evaluates an instrument aimed at meeting these requirements. The system described employs a center-tethered lightly ballasted horizontal spar for measuring wave direction. Wave amplitude and period can also be monitored by the addition of an accelerometer/magnetometer unit to the buoy.

2. Background

The concept of employing a horizontal spar for measuring wave direction originated from work begun at ENDECO (Environmental Devices Corporation)[1]. From contacts with industry, they realized the value of an inexpensive and reliable system which could monitor waves and provide a "good first-order measurement" of their structure. Observing that a spar with a high length to draft ratio would align parallel to the crests of waves, ENDECO proposed an initial design of a lightly ballasted cylindrical buoy as the vehicle for their wave monitoring unit.

In the summer of 1977, a prototype buoy was constructed which measured 5.80 m in length and 0.23 m in diameter (Figure 1). The buoy was outfitted with a recording compass. In addition, after at-sea tests, a roll axis inclinometer was installed for removing a 180° ambiguity which was found to exist. This instrumentation package, along with the batteries and pipe, produced a draft of 0.06 m.

Field tests were conducted with the prototype (now designated Type 864 Insitu Wave Direction Recorder) from August 30, 1977 to September 15, 1977 in Buzzards Bay, Massachusetts. The buoy was moored 91.4 m bearing 135 from the Cleveland Ledge Light Tower. Observed wave direction was obtained from wind data supplied by the Wings Neck Light (7.4 km north of the test site) since the waves in the bay are wind driven in origin. The Type 864 Buoy recorded wave direction every 15 minutes; wind direction was obtained every 4 hours. During data reduction, wave direction from the buoy was derived from an average of data $\pm$ 1 hour referenced to the wind direction observations. Figure 2 is a time series presentation of this data.

Armed now with the reassurance of a reasonable correlation between the observed and recorded wave directions, ENDECO approached the Massachusetts Institute of Technology, through the Sea Grant Program, with a proposal to investigate the buoy's motions and optimize the design. This offer was accepted and a Sea Grant internship was formally created, under the guidance of Professor Robert Van Houten, in October, 1977.

3. Model Tests

The first step taken in the theoretical investigation of the buoy's motion was a series of scale model tests of the spar being acted upon by plane sinusoidal waves. These experiments were conducted in the MIT Ocean Engineering Laboratory employing models of various drafts, lengths and diameters with a scale ratio of 1:10.

The performance of the models was evaluated by measuring the radial velocity of the spars in aligning with impacting waves. This response was determined with the use of a camera and a strobe employing multi-flash, single exposure techniques (Figure 3).

The results of these first tests highlighted several features peculiar to the buoy:

1. Increasing the draft will rapidly deteriorate the buoy's performance. When the draft equals the spar's radius, the buoy will not align at all.
2. An imposed mooring force is essential for the desired response and this force must act at the center of the buoy for no bias to exist.
3. Increasing the buoy's length will nominally improve performance; however, when its length equals or exceeds the incoming waves' length, imposed hydrodynamic forces counteract and decrease the radial velocity.
4. Increasing the diameter will nominally enhance the response, assuming that the draft remains constant for increasing radii of pipe.
5. The radial velocity of the spar is linearly proportional to the slope (k_oA) of the incoming wave.
6. Centering the ballast (instrumentation package) will significantly improve performance.

4. Theory of Operation

The mechanism by which the spars align with incoming waves can best be visualized in a uni-directional wave field. If a buoy lies at an angle to the wave train, the leading portion of the spar will be elevated as a crest nears, creating an inherently unstable position for the system. To revert to a stable configuration with no static imbalances, the buoy will tend to "slide down" the crest and, because of imposed mooring forces, rotate about its center until it is parallel to the waves. A similar mechanism exists when the leading section dips into the trough and the "tail" rides the crest.

Resisting this restoring force, the generated drag can significantly delay or inhibit the response. Consequently, the underwater profile determines to a large extent the efficiency of the buoy.

Other forces present are insignificant when compared to the acting inertial forces. Typical of these are the particle orbit velocities which cancel out over the cycle of a wave; current and particle drift velocities which, by reason of their magnitudes[2], can be expected to be of inconsequence; and wind velocities which have little effect due to the slight density of air with respect to seawater.

In empirically describing the above process, attempts have been made to non-dimensionalize the parameters involved and graphically illustrate the buoys' performances (Figure 4). Difficulties arise in execution, however, for as the buoy's length approaches the incoming wavelength, its response deteriorates due to rather complicated interactions. Nonetheless, this problem is essentially inconsequential, in as much as one can expect typical ocean waves to exceed six meters in length[3].

5. Type 864 Buoy Design

The configuration of the Type 864 Buoy is given in Figure 1. The spar utilizes a fiberglass filament wound pipe with a PVC liner. This pipe is marketed under the name "Permastran" and is manufactured by the John Manville Company. This construction was chosen to provide light weight with strength.

The tether is attached at the midpoint of the spar and, similarly, a high intensity xenon strobe light is mounted at the center. Electronics and batteries are accessible from the ends of the buoy and are likewise positioned to provide symmetrical ballasting. This weight balance is necessary to insure a decipherable response, free of bias.

The wave direction monitoring system employs a Rustrak type recorder and solenoid operated potentiometric compass programmed by a quartz crystal clock. The output is recorded every 15 minutes for a duration of 3.75 seconds. The strip chart is advanced between readings with a significant gap produced every 24 hours to allow for daily time correlations.

An averaging circuit monitors the output of a single-axis roll potentiometric inclinometer. A voltage comparator senses if the roll is greater than 5° away from the ambiguous face of the buoy. Such a signal would denote the forward face of the spar, since the buoy tends to roll away from an advancing wave train. When this condition occurs during the compass sampling interval, a solenoid event marker is energized to signal for the 180° correlation during data processing.

6. Field Tests

In January, 1978, three full-scale models of the wave monitoring buoy were constructed. These were identical in draft and diameter to the Type 864 Buoy. The three spars had

lengths of 5.80 m, 4.88 m and 3.66 m and utilized iron ballast in place of the normal electronics unit.

In February, 1978, these buoys were moored 100 m off the southeast face of the Buzzards Bay Light Tower. They were spaced approximately 100 m apart.

Visual observations were made of their movements by means of a pelorus-like sighting instrument, from February 21 to February 28. Current data was determined with an ENDECO Type 110 Remote Reading Current Meter, situated 1.8 m below the water's surface, under the tower. Wind data was provided by meteorological instrumentation installed on the tower. Three critical features of the system were apparent at the conclusion of the tests:

1. The buoys were not influenced by currents up to 0.44 m/sec in strength, even in very calm seas.
2. While length was shown to increase response velocity in towing tank tests, no significant discrepancies in performance were measured for the three buoys in this coastal ocean environment.
3. The buoys would respond to a complex wave spectrum such that a single attitude of alignment would exist, with complimentary oscillations of $\pm$ 18° (or less). As can be expected from actual sea conditions (as opposed to a sinusoidal wave field), a bias was induced by the shorter breaking waves of greater than normal steepness[4]

7. Future Plans

Environmental Devices Corporation is completing the design of a digital recording buoy which includes wave height and period measurements. The deployed system will utilize a vertical axis accelerometer with roll correction obtained from a two-axis horizontal magnetometer which will be rigidly mounted without gimbals. This magnetometer will also provide heading information.

Research at the Massachusetts Institute of Technology will continue to investigate the theoretical aspects of the spar's motion in a regular wave field. Also, attempts will be made to analyze the directional components of the wave spectra which the buoy tracks.

8. Conclusion

A uni-directional wavetrain will force a lightly ballasted spar perpendicular to its direction of motion. Utilization of this phenomenon can provide for a cost effective and reliable buoy capable of providing a first order measurement of the wavetrain's direction of propagation.

The observations discussed in this paper may also find use in the study of small craft dynamics in the open ocean environment.

9. References

1. Brainard II, Edward C., "Horizontal Spar Wave Direction Monitoring Buoy," Offshore Technology Conference, May, 1978.
2. Lozow, Jeffrey B., Second Order Dynamics of Small Bodies in Waves, Doctor of Philosophy Thesis, MIT, January, 1977.
3. Craven, John P., Ocean Engineering Systems, MIT Press, Cambridge, Massachusetts, 1971.
4. Longuet-Higgins, M.S., "On the Statistical Distribution of the Heights of Sea Waves," Journal of Marine Research, Volume XI-3, 1952.

Figure 1 - ENDECO Type 864 In-situ Wave Direction Monitoring Buoy

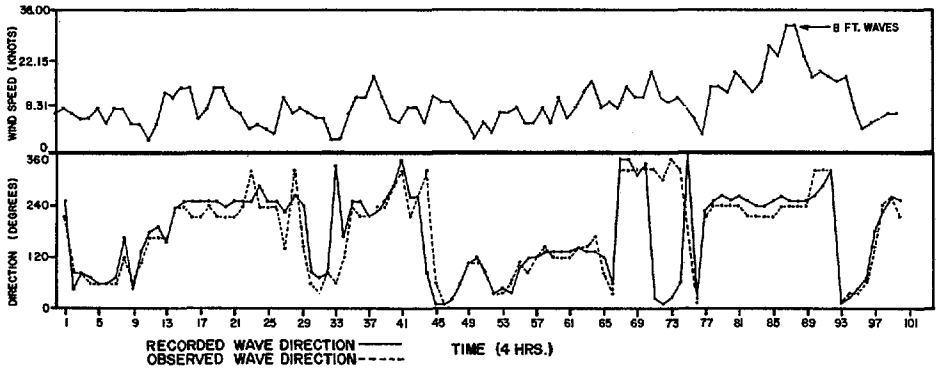

Figure 2 - Observed and Recorded Wave Directions and Wind Speed
Cleveland Ledge Data; 8/30/77 - 9/15/77

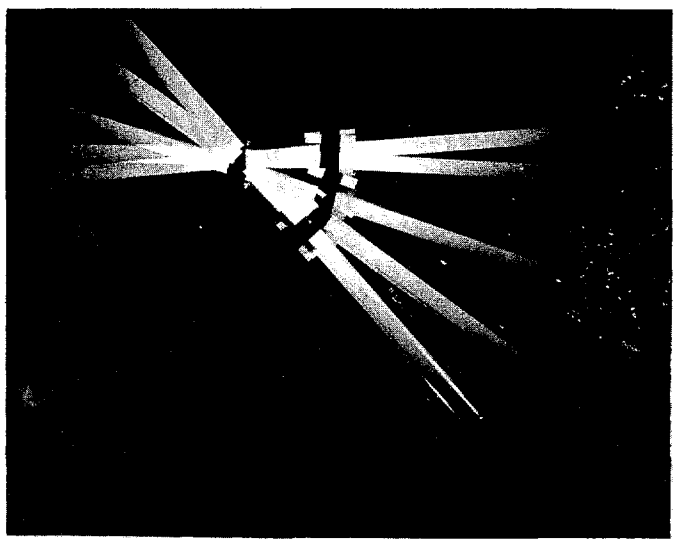

Figure 3 - Multi-flash Exposure of a Model Spar
MIT Towing Tank; 11/13/77

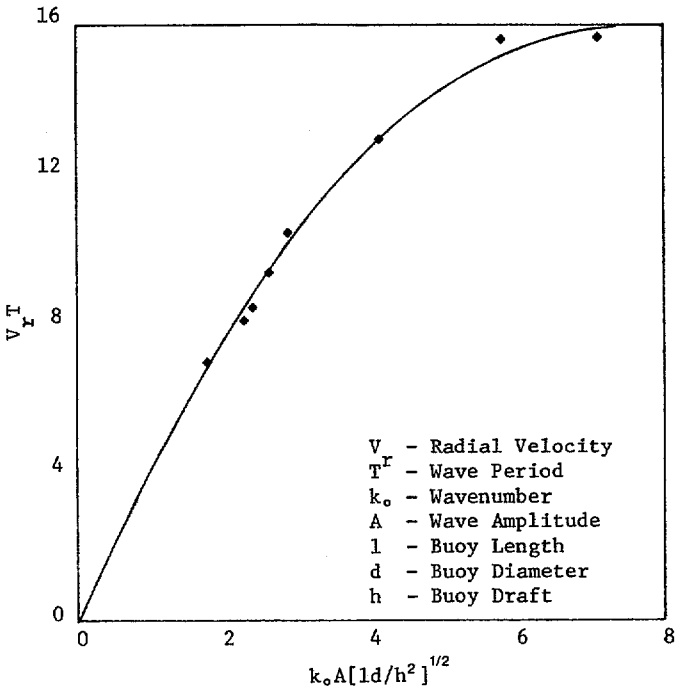

Figure 4 - Non-dimensional Analysis of a Horizontal Spar in a Uni-directional Sinusoidal Wave Field

MEASUREMENT OF DIRECTIONAL OCEAN WAVE SPECTRA FROM FIXED PLATFORMS

Leon E. Borgman

Evangelos Yfantis

Department of Statistics
University of Wyoming
Laramie, WY 82071

ABSTRACT

Various instrument systems providing measurements which can be analyzed to estimate the directional ocean wave spectral density are reviewed. These include (a) electromagnetic current meters with wave staff, and (b) a wave staff with satellite bottom pressure sensors. In addition, general mathematical procedures are presented for arbitrary space arrays of measuring devices. Eigenvector procedures are introduced to remove equation redundancy. Choices of directional spreading functions, including a new four-parameter formula, for modelling the output of the analysis of wave sensor data are outlined.

Data was constructed to have about the same scatter as real measurements and used to illustrate the analysis, presentation, and problems in interpretation of directional spectra estimates. Such topics as directional resolution and estimate stability, as they relate to length of record, digitization increment, and other similar details of data collection are discussed.

INTRODUCTION

It is difficult to continuously maintain recording instruments in the ocean environment. Arrays of in situ measuring devices for determining the directional wave spectrum ordinarily consist of only a few strategically placed sensors--generally fewer than 10. A problem which would be simple with 100 sensors becomes substantially more difficult with just a few measuring instruments.

Fixed platforms provide convenient structural support for measuring instruments. The recording devices can be out of the water and shielded from weather. Regular servicing is simplified. Generally the instruments have a good chance of surviving severe storm conditions. Several disadvantages are the high initial cost of constructing the platform and possible shielding and interference effects from the structural supports which may distort measurements. The relatively small lateral extent of most platforms has statistical advantages and disadvantages. Large scale statistical nonstationarities in space, which devil space arrays, are relatively unimportant if the sensors are not too far from each other in the horizontal plane. On the other hand, the lateral closeness of the instruments make them highly correlated, particularly for waves with long wave length. Thus, a number of sensors may not give much more information than a single sensor. In this situation the emphasis has to be placed on an array of different types of sensors, rather than a space array of instruments measuring the same thing.

In the following discussion, procedures will be given for an array consisting of (a) wave staffs, (b) velocity meters measuring horizontal components of the water particle velocity, and (c) bottom pressure transducers.

CROSS-SPECTRAL DENSITIES

Let $\eta(x,y,t)$, $v_x(x,y,z,t)$, $v_y(x,y,z,t)$, and $p(x,y,z,t)$ denote the sea surface elevation above mean water level, the horizontal x- and y-components of the water particle velocities, and the pressure fluctuations about static pressure, respectively at the coordinate positions indicated. The reference coordinate axis will be taken to be right-handed with origin at the sea floor, z positive upward, and x and y horizontal. Further, let K_v and K_p represent

$$\begin{aligned} K_v(z) &= 2\pi f \cosh kz/\sinh kd \\ K_p(z) &= \rho g \cosh kz/\cosh kd \end{aligned} \qquad (1)$$

where f is the frequency in Hertz, ρ is the water density, g is the acceleration due to gravity, d is the water depth, and $k = 2\pi/L$ is the wave number (L = wave length).

In the follwoing wave property pairs, the first property is measured at (x,y,z_1) while the second property listed is measured at $(x+X,y+Y,z_2)$, both as functions of time. The co-spectrum (c.s.) and quad-spectrum (q.s.) formulas will be written in matrix form for compactness.

$$\begin{Bmatrix} \text{c.s.} \\ \text{q.s.} \end{Bmatrix} \text{between} \begin{pmatrix} \eta, \eta \\ \eta, v_x \\ \eta, v_y \\ \eta, p \\ v_x, v_x \\ v_x, v_y \\ v_x, p \\ v_y, v_y \\ v_y, p \\ p, p \end{pmatrix} = \begin{pmatrix} 1.0 \\ K_v(Z_2) \\ K_v(Z_2) \\ K_p(Z_2) \\ K_v(A_1)K_v(Z_2) \\ K_v(Z_1)K_v(Z_2) \\ K_v(Z_1)K_p(Z_2) \\ K_v(Z_1)K_v(Z_2) \\ K_v(Z_1)K_p(Z_2) \\ K_p(Z_1)K_p(Z_2) \end{pmatrix} \text{times}$$

$$\cdot S(f)\int_0^{2\pi} D_f(\theta)\begin{Bmatrix}1.0\\ \cos\theta\\ \sin\theta\\ 1.0\\ \cos^2\theta\\ \cos\theta\sin\theta\\ \cos\theta\\ \sin^2\theta\\ \sin\theta\\ 1.0\end{Bmatrix}\binom{\cos}{\sin}(kX\cos\theta+kY\sin\theta)d\theta \qquad (2)$$

Here $S(f)$ is the usual wave amplitude frequency spectral density and $D_f(\theta)$ is spreading function at frequency, f. The spreading function is a non-negative, unit area function relative to integration over $(0 < \theta < 2\pi)$.

THE BASIC PROBLEM

Since the frequency spectrum, $S(f)$, can be estimated easily by standard procedures, the basic problem in the determination of the directional spectrum is the estimation of $D_f(\theta)$ at selected frequencies. This, in turn, may be regarded as the problem of inverting the above set of integral equations in which there are two equations (co-spectral and quad-spectral relations) for each sensor pair and single equation for the spectral density for each sensor. Thus, in theory, an array of n-sensors would produce n^2 integral equations $(n(n-1)/2$ pairs plus n spectral densities). In practice, some of the equations provide no information. For example, if $X = 0$ and $Y = 0$, the quad-spectral densities are all zero for the above wave properties.

The solution of the set of integral equations may be attempted by a variety of methods. Two useful procedures follow from (a) the use of a general shape formula for $D_f(\theta)$ with a finite unknown parameter set, and (b) a truncated Fourier series representation for $D_f(\theta)$. The former procedure requires in its most general sense, a search in parameter space for the "best" values which with numerical integration satisfy the equations in an optimal manner (e.g., least-square error). The second procedure reduces the integral equations to a set of linear equations with the Fourier coefficients as unknowns. If there are sufficient gage pairs so that there are enough linear equations to solve for all non-negligible Fourier coefficients, the second procedure gives a complete answer. Unfortunately, this is usually not the case. The Fourier series must, ordinarily, be truncated to fewer terms than are needed to adequately represent $D_f(\theta)$.

Thus the two procedures may be characterized as a mathematically satisfactory but computationally difficult method (a search for the parameters in a system of nonlinear integral equations) versus a relatively easy linear matrix solution (the Fourier series) which may give an estimate with known defects. Obviously a variety of subjective choices must be made for the particular array under study. It is often possible to proceed sequentially, first using the Fourier series method, and then introducing a parameterized model to further refine the estimate.

A SUB-CIRCLE EXPANSION

Let the spreading function be approximated by

$$D_f(\theta) = \frac{1}{T}+\sum_{m=1}^{M}\left[a_m(f)\cos\frac{2\pi m(\theta-\theta_0)}{T}+b_m(f)\sin\frac{2\pi m(\theta-\theta_0)}{T}\right] \qquad (3)$$

where it has been assumed that $D_f(\theta)$ assumes non-negligible values only on the interval (θ_0,θ_0+T). For full circle coverage, $\theta_0 = 0$ and $T = 2\pi$. However, often it is known a priori from meteorological or other information that no appreciable energy is traveling in certain sectors of the circle. Then, the Fourier expansion over a part of the circle may be mathematically preferable.

If the sub-circle Fourier expansion is substituted into the theoretical formulas and equated to the data spectra, an equation of the following form is obtained.

$$\frac{T}{\hat{S}(f)K_1K_2}\begin{Bmatrix}\hat{c}_{12}(f)\\ \hat{q}_{12}(f)\end{Bmatrix} = \int_{\theta_0}^{\theta_0+T} R_1(\theta)R_2(\theta)\binom{\cos}{\sin}$$

$$\cdot\ (kX\cos\theta+kY\sin\theta)d\theta + \sum_{m=1}^{N}\hat{a}_m(f)\int_{\theta_0}^{\theta_0+T} R_1(\theta)R_2(\theta)$$

$$\cdot\ \binom{\cos}{\sin}(kX\cos\theta+kY\sin\theta)\cos\frac{2\pi m(\theta-\theta_0)}{T}\,d\theta$$

$$+\sum_{m=1}^{N}\hat{b}_m(f)\int_{\theta_0}^{\theta_0+T} R_1(\theta)R_2(\theta)\binom{\cos}{\sin}(kX\cos\theta+kY\sin\theta)$$

$$\cdot\ \sin\frac{2\pi m(\theta-\theta_0)}{T}\,d\theta \qquad (4)$$

where K_i is the appropriate frequency function just right of the equal sign in eq. (2) and $R_i(\theta)$ is the corresponding function of frequency listed in first vector after the integral sign in eq. (2).

This system of equations can be manipulated into the form $S = M\beta+\varepsilon$ where S is vector of modified spectral estimates, M is the matrix whose elements are in integrals in eq. (4), β is the vector of Fourier coefficients, $\hat{a}_m$ and $\hat{b}_m$, and ε is the error vector. Let W be a matrix with its non-diagonal elements equal to zero and its diagonal elements being a subjectively selected number which represents the reliability of the particular gage pair contributing the corresponding equation. Then the weighted least-square normal equations are $M'WM\beta = M'WS$.

In most data arrays from fixed platforms, $M'WM$ will be almost singular if N in eq. (4) is too large. A reasonable approach then is to determine the number of non-negligible eigenvalues of $M'WM$ and to require 2N to be less than that number. This may require more truncation than is physically desirable, but the data just does not contain enough information for more.

HYBRID METHODS

A graph of the truncated Fourier series may suggest a reasonable model for $D_f(\theta)$. Thus, if the graph appears to be a unimodal, approximately symmetrical, bell-shaped function, a reasonable model might be one of the following:

wrapped Normal

$$\pi D_f(\theta) = \pi \sum_{k=-\infty}^{\infty} \frac{e^{-\frac{1}{2}(\theta-\mu-2\pi k)^2/\sigma^2}}{\sqrt{2\pi}\,\sigma} = 0.5+\sum_{m=1}^{\infty} e^{-m^2\sigma^2/2} \cdot \cos[m(\theta-\mu)] \quad (5)$$

von Mises

$$\pi D_f(\theta) = \frac{e^{a\cos(\theta-\alpha)}}{2I_0(a)} = 0.5+\sum_{m=1}^{\infty} \frac{I_m(a)}{I_0(a)}\cos[m(\theta-\alpha)] \quad (6)$$

exponential Fourier

$$\pi D_f(\theta) = C\ \exp\{a\cos(\theta-\alpha)+b\cos[2(\theta-\beta)]\} \quad (7)$$

(In the above, $I_m(a)$ is the modified Bessel function of order m). If a unidirectional sea appears to be present the model might be $\sigma^2\delta(\theta-\theta^*)$ where $\delta(x)$ is the Dirac delta and θ^* is the direction of travel.

In any case, a model is selected for subjective reasons and its theoretical Fourier coefficients are compared to the first few harmonics developed from the least-squares. Usually the parameters of the model can be estimated from this comparison. This, in turn, allows a prediction of the Fourier series tail, consistent with the model, which was truncated off in eq. (4). The tail approximation which is usually relatively small is subtracted from the left side of eq. (4) and the lower harmonics are re-estimated. Alternation of these two procedures continues until there is no change.

EXACT COEFFICIENT DETERMINATION

If the gages are located at the same (x,y) position, substantial simplifications occur. For example, consider a wave staff and three velocity meters, each determining (x,y) components of velocity, located on the same piling as the staff. A full circle expansion will be used. Then eq. (2) reduces to

$$\text{c.s. between} \begin{pmatrix} \eta, \eta \\ \eta, v_x \\ \eta, v_y \\ v_x, v_x \\ v_x, v_y \\ v_y, v_y \end{pmatrix} = \begin{pmatrix} 1.0 \\ K_v(Z_2) \\ K_v(Z_2) \\ K_v(Z_1)K_v(Z_2) \\ K_v(Z_1)K_v(Z_2) \\ K_v(Z_1)K_v(Z_2) \end{pmatrix}$$

$$\cdot\ S(f)\int_0^{2\pi} D_f(\theta) \begin{pmatrix} 1.0 \\ \cos\theta \\ \sin\theta \\ \cos^2\theta \\ \cos\theta\sin\theta \\ \sin^2\theta \end{pmatrix} d\theta \quad (8)$$

By trigonometric identities, all of the equations become simple algebraic expressions involving the first two harmonics of $D_f(\theta)$.

Such an array can produce a number of estimates of a_1, b_1, a_2, b_2, at each frequency. However, there is no possibility of estimating higher harmonics. Paradoxically, the estimates are exact and have no error due to truncation of the Fourier series. The mathematics truncates the Fourier series rather than the analyst.

AN EXAMPLE

Values of s(f), a_1, b_1, a_2, b_2, μ, and σ for an artificial data set are shown in Table I. Although the values are not taken from actual data because the immediately available examples are still proprietary, the general range and scatter are consistent with cross-spectral estimates with 20 degrees of freedom and a resolution of .01 H_z. It is anticipated that clearance will be received before Oceans '78 so that actual data will be presented later in the verbal presentation.

The pre-supposed instrument array for the example consists of a wave staff and three velocity gages at various depths directly below the wave staff measuring horizontal components.

The appropriate formulas follow from eq. (8). For the velocity meter at a given position

$\{[\text{c.s. between } (v_x,v_x)]^2+[\text{c.s. between } (v_y,v_y)]^2\}$

divided by $S(f) = K_v^2(z)$. From the definition of the full circle Fourier coefficients

$$\begin{pmatrix} a_m \\ b_m \end{pmatrix} = \frac{1}{\pi}\int_0^{2\pi} D_p(\theta)\begin{pmatrix}\cos \\ \sin\end{pmatrix} m\theta\ d\theta$$

it follows from eq. (8) that for all gage pairs of the type indicated

$$a_1 = [\text{c.s. } \eta, v_x] \ / \ [\pi S(f)K_v(Z)]$$

$$b_1 = [\text{c.s. } \eta, v_y] \ / \ [\pi S(f)K_v(Z)]$$

$$a_2 = (2/\pi)\{([\text{c.s. } v_x,v_x] \ / \ [S(f)K_v(Z)]) - 0.5\}$$

$$= (2/\pi)\{0.5-([\text{c.s. } v_y,v_y] \ / \ [S(f)K_v(Z_1)K_v(Z_2)]\}$$

$$b_2 = (2/\pi)\{[\text{c.s. } v_x v_y] \ / \ [S(f)K_v(Z_1)K(Z_2)]\}$$

As an example of the use of these formulas, a typical set of possible values for cross-spectral density estimates at f = 0.1 H_z is shown in Table III. The scatter shown is typical of real data with spectral estimates having the resolution and degrees of freedom previously mentioned.

Various methods could be used to distill a single set of coefficients from all those displayed in Table III. Least-square methods or some type of weighted average could be used. However, for the artificial example given, a simple average is listed for the coefficients at f = 0.1 H_z in Table I.

The formulas for the fit of the wrapped-normal follow from eq. (5)

$$a_1 = (1/\pi)e^{-\sigma^2/2}\cos\mu; \qquad b_1 = (1/\pi)e^{-\sigma^2/2}\sin\mu$$

Thus

$$\mu = \arctan(b_1/a_1); \qquad \sigma^2 = -2\ln[\pi\sqrt{a_1^2 + b_1^2}]$$

Values of μ and σ stated in degrees are listed in the last column of Table I. A similar set of equations for μ and σ^2 can be obtained from a_2 and b_2, or alternately, various more sophisticated methods using all four coefficients could be introduced. The simplest approach using only a_1 and b_1 was followed in the listed example.

Studies in which the above general procedures were applied to ocean measurements are described by Forristall, et. al. (1978a,b).

The Fourier series, least-square approach with subsequent model-fitting as outlined in the preceeding, depend critically on the stability and accuracy of the cross-spectral estimates. As many degrees of freedom as possible should be obtained in the spectral estimation. This, in turn, depends on the length of data and the resolution imposed. Let T be the length of record which is digitized at increment, Δt. Then $N = T/\Delta t$ = number of measurements in the data sequence and the basic frequency increment will be $\Delta f = 1/T$. The number of FFT lines in a resolution interval (or interval of spectral averaging) R will be $R/\Delta f = RT$. There are two degrees of freedom per line, so the degrees of freedom perspectral estimate will be 2RT. Thus, statistical stability increases with record length and coarseness of resolution.

Many researchers have worked on directional spectral estimation in one way oranother during the last 15 years. A complete bibliography would be too long for inclusion in this paper. Rather than providing an incomplete list, two references will be given which, in turn, provide a fairly complete bibliography as well as more details on the general approach which has been followed in the foregoing presentation, (Panicker, et.al (1974), Borgman (1978))

TABLE I

AN ILLUSTRATIVE EXAMPLE (ARTIFICIAL DATA) OF SPECTRAL DENSITY, FOURIER COEFFICIENTS, AND WRAPPED-NORMAL PARAMETER ESTIMATES

f	$\hat{S}(f)$	$\hat{a}_1$	$\hat{b}_1$	$\hat{a}_2$	$\hat{b}_2$	μ^*	σ^*
.07	5.1	-.294	-.064	.239	.082	192°	19°
.08	40.3	-.301	-.075	.248	.166	194°	13°
.09	128.6	-.302	-.081	.232	.175	195°	11°
.10	162.8	-.290	-.110	.225	.189	201°	13°
.11	100.0	-.279	-.129	.217	.196	205°	15°
.12	50.2	-.250	-.158	.128	.173	212°	22°
.13	44.7	-.211	-.195	.048	.193	223°	26°
.14	35.2	-.202	-.216	.026	.192	227°	22°
.15	31.9	-.223	-.207	.044	.211	223°	17°
.16	23.5	-.221	-.192	.050	.175	221°	23°
.17	20.8	-.218	-.154	.076	.130	215°	34°
.18	19.8	-.220	-.174	.063	.143	218°	29°
.19	15.6	-.188	-.189	.041	.151	225°	34°
.20	12.2	-.164	-.178	.051	.107	227°	42°

TABLE II

AN ILLUSTRATIVE EXAMPLE (ARTIFICIAL DATA) OF CROSS-SPECTRAL DENSITIES AT f = 0.1 Hz.
(Spectrum on main diagonal, co-spectrum above diagonal, quad-spectrum below diagonal)

	η	v_{x1}	v_{y1}	v_{x2}	v_{y2}	v_{x3}	v_{y3}
η	162.8	-72.2	-26.7	-64.6	-22.9	-62.3	-25.6
v_{x1}	- .40	32.8	10.7	28.9	9.9	28.0	10.7
v_{y1}	.60	- .52	5.4	10.1	4.5	9.6	3.1
v_{x2}	- .06	- .11	.36	26.2	8.8	24.9	8.7
v_{y2}	- .90	.31	.40	.60	4.2	8.4	4.5
v_{x3}	- .80	.95	.81	.93	- .22	24.4	9.3
v_{y3}	-1.12	.42	.23	.71	.23	.67	5.1

REFERENCES

Panicker, N.N. and Borgman, L.E. (1974). "Enhancement of Directional Wave Spectrum Estimates," Proc. 14th Coastal Eng. Conf., Copenhagen, Denmark, ASCE, New York.

Borgman, L. E. (1978). "Directional Wave Spectra from Wave Sensors," Ocean Wave Climate (M. Earle, ed.), Plenum Press, (Scheduled 1978 or 1979).

Forristall, G. Z.; Ward, E. G.; Borgman, L. E.; and Cardone, V. J. (1978a). "Storm Wave Kinematics," OTC 3227, pp. 1503-1514, Offshore Technology Conference, Houston.

_____, (1978b). "The Directional Spectra and Kinematics of Surface Waves in Tropical Storm Delia." (Submitted to Jour.Physical Oceanography)

TABLE III
AN ILLUSTRATIVE EXAMPLE (ARTIFICIAL DATA) OF COEFFICIENT ESTIMATES CONSISTENT WITH TABLE II NUMBERS

(a) Separate estimates of a_1 at f = 0.1 Hz.

	v_{x1}	v_{x2}	v_{x3}
η	-.292	-.292	-.286

(b) Separate estimates of b_1 at f = 0.1 Hz

	v_{y1}	v_{y2}	v_{y3}
η	-.108	-.104	-.117

(c) Separate estimates of a_2 at f = 0.1 Hz.

	v_{x1}	v_{y1}	v_{x2}	v_{y2}	v_{x3}	v_{y3}
v_{x1}	.229					
v_{y1}		.228				
v_{x2}	.222		.231			
v_{y2}		.234		.230		
v_{x3}	.213		.211		.207	
v_{y3}		.260		.223		.208

(d) Separate estimates of b_2 at f = 0.1 Hz.

	v_{x1}	v_{y1}	v_{x2}	v_{y2}	v_{x3}
v_{x1}					
v_{y1}	.200				
v_{x2}		.189			
v_{y2}	.185		.184		
v_{x3}		.182		.174	
v_{y3}	.202		.185		.200

OCEAN WAVE DETECTION AND DIRECTION MEASUREMENTS WITH MICROWAVE RADARS

Paul G. Teleki
U. S. Geological Survey
915 National Center
Reston, Virginia 22092

Robert A. Shuchman
Environmental Research Institute
P. O. Box 618
Ann Arbor, Michigan 48107

Walter E. Brown, Jr.
Jet Propulsion Laboratory
California Institute of Technology
Pasadena, California 91103

William McLeish
Sea Air Interaction Laboratory
National Oceanic and Atmospheric Administration
Miami, Florida 33149

Duncan Ross
Sea Air Interaction Laboratory
National Oceanic and Atmospheric Adminstration
Miami, Florida 33149

Michael Mattie
U.S. Army
Coastal Engineering Research Center
Fort Belvoir, Virginia 22060

Abstract

Electromagnetic energy at microwave frequencies is backscattered by the short-wave component of the ocean wave spectrum. Complex scattering models, which include both Bragg resonance and Rayleigh scattering, have been postulated to describe the amplitude of radar return. The actual return is complicated by the intensity and distribution of the facets of infra-gravity waves. Furthermore, long gravity waves modulate short waves, their tilt and displacement depending on their instantaneous position relative to the long wave profile and extraneous vector quantities such as surface current gradients.

As the maximum modulation is in the direction of wave motion, the discernibility of ocean waves is dependent on the radar look direction. Waves traveling or containing components in the azimuth direction (along track direction of the flight) are sensitive to defocusing due to Doppler shifts in the case of the synthetic aperture radar (SAR), introduced primarily by velocity components such as perturbations due to long wave orbital velocities, Bragg wave velocities, and surface current velocities. For a given velocity component, defocusing is greater at L-band frequencies than at X-band, resulting from the longer residence time of a moving target in the L-band aperture, given equivalent resolution.

The principal uses of radar imagery for wave studies are to derive direction and length information. While length and direction are determinable from the radar signal, the accuracy with which this information can be established had to be tested against more conventional ocean instrumentation. Data obtained with a pitch-and-roll buoy and current meters were compared to X-band SAR wave imagery obtained simultaneously over a test site offshore of Florida. Analysis shows that the wave direction at the peak frequency of the wave spectrum from buoy and current meter measurements agrees with the frequency-averaged radar directions within 2 degrees. Agreement in the data is considered exceptional, given that the measurements were made in 8-12 m water depth, where wave refraction is strong.

Shore-based radars have also been used to derive wave direction and length information. Comparison between the measured wave directions for the principal wave trains, as seen on aerial photographs and shore-based radar images, simultaneously obtained show agreements within 3 degrees.

In the case of airborne real-aperture radars, wave length information derived from the radar is in good agreement with that determined from simultaneous laser profilometer spectra, and the direction observed is essentially the same as the local wind.

With case-by-case determination of the modulation depth and focusing parameters, the SEASAT-A L-band SAR will produce much needed information for wave refraction studies on continental shelves.

1. Introduction

Imaging radars are active devices that sense the environment with short wavelength electromagnetic waves. With the advent of the SEASAT-A data on dynamic ocean properties, interest in understanding the uses and limitations of radars has been increasing. As active sensors, radars provide their own illumination in the microwave region of the electromagnetic spectrum and thus are not affected by diurnal changes in emitted or reflected from the earth's surface. Most radars operate in the frequency region of 300 MHz (1 m) to 30 GHz (1 cm), and bandwidths within this region are commonly designated by letters. Radars discussed in this paper are designated as L-band (23.5 cm), X-band (3.2 cm) and Ka-band (0.86 cm), all having been operated as airborne side-looking radars, and one X-band (3 cm) PPI (plan position indicator) radar operated in a fixed position.

Side-looking radars use pulse ranging, whereby the radar antenna attached to a moving aircraft

illuminates a section of the ground and the amplitude, phase and polarization of the returned echoes are processed to determine the distance to the scene and to obtain the measure of relative strength of the return (σ_o). In real-aperture systems, the resolution in azimuth is limited by the beamwidth (i.e. the physical length) of the antenna. Synthetic aperture radars utilize the Doppler history (change of phase) associated with the motion of the aircraft, recording both the phase and the amplitude of the backscattered energy, thus improving the azimuthal resolution. The longer the radar length, the greater improvement in the along-track resolution of the system.

Conventional radars of the PPI presentation commonly use a fixed pulse repetition frequency and CRT (cathode ray tube) displays of the brightness pattern (energy scattered by surfaces and objects) that represents topographic features in view of the azimuth scanning radar antenna. The CRT displays the returned echoes by representing azimuth as an angle and range as radial distance. The X-band shore-based radar described is of the PPI type used in measuring the sea-echo in nearshore waters.

Among the recognized advantages of radars are their ability to image the earth's surface independently of weather conditions or solar illumination and to provide synoptic views at high resolution. These attributes make space-borne radars attractive to studies of surface dynamics of the oceans. The synthetic aperture radar (SAR) on SEASAT-A, operating a L-band (1.275 MHz) in horizonal polarization was designed to image principally ocean wave patterns. Potentially, the SAR can also provide information on the dominant wavelength and direction of surface waves, on wave height, surface currents, and internal waves. Insofar that the principal aim of the SAR Experiment, relative to oceans, is the derivation of two-dimensional wave spectra, it should be noted that until now few meaningful SAR ocean spectra have been generated (Brown, et al. 1976). Wave height information is theoretically obtainable from SAR, but an algorithm has yet to be developed. Elachi and Apel (1976) and Moskowitz (1973) published radar imagery with features that resemble, respectively, internal waves and surface currents, but these observations were not supported with in-situ measurements.

In the course of designing the SEASAT-A SAR, it was realized that in the absence of experience with spaceborne SARs and in view of the limited amount of ocean data existing at L-band, aircraft based experiments had to be conducted prior to launch of the satellite. The aim of these experiments was to study the physical coupling between electromagnetic waves and water waves (Shemdin, et al. 1975). Thus, in December 1975, an experiment took place near Marineland, Florida, wherein X- and L-band synthetic aperture radars were flown on aircraft to image waves in varying meteorological conditions and sea states on the adjacent continental shelf. Wave height and direction and the amplitude and direction and the amplitude and direction of currents (due to orbital motion in waves and due to wind) were measured by an array of in-situ instruments, of which data obtained by a pitch-and-roll buoy and paired orthogonal current meters are relevant to this study. With regard to wave direction measurements, this report quantifies results, reported by Shemdin et al. (1977), for tests conducted on December 14.

2. Radar concepts

Imaging mechanisms: The principle in imaging any surface with a radar is that in the backscatter of microwave energy (echo) received by the radar antenna contains information on the roughness characteristics (shapes, dimensions and orientation) of the reflecting area. These parameters that influence the echo received from ocean waves include the motion of the scattering surfaces, the so-called speckle effect, system resolution, digital sampling, non-coherent integration and thermal noise level and contributions attributable to wind, surface currents and surface tension. Factors described herein are those pertaining to wave orbital velocity, Bragg scatterer velocity, and long (or resolvable) wave phase velocity. To illustrate the various effects, relatively simple models have been chosen.

Several models exist that attempt to explain wave image formation with synthetic aperture radars. In general, static models show dependence on instantaneous surface features and dynamic models draw on surface velocities. Considerable debate exists on the acceptability of either model. We attempt to draw together both analytical and experimental results and use arguments from both types of models.

The three principal static models for the backscatter (σ_o) from the ocean are the facet, Bragg-Rice, and the Rayleigh scattering models. The tangent plane or facet model is based on reflections from areas whose slopes are oriented normal to the line of sight. It is assumed that the surface radius of curvature exceeds the radar's wavelength and that one can neglect random scattering and shadowing effects (Brown, et al. 1976). The radar cross section of the facet model, according to Beckman and Spizzichino (1963) is

$$\sigma_o\ (\theta) = \cot^2\beta_o \exp\ (-\tan\theta/\tan\beta_o)^2 \qquad (1)$$

where θ in the radar incidence angle, and $\tan\beta_o = 2\ \sigma/T$, T being the autocorrelation distance for a rough surface whose heights are distributed with standard deviations σ.

The Bragg-Rice model uses the concept that the ocean surface can be represented by a combination of periodic surfaces, so that the dominant backscatter will match some portion of the ocean wave spectrum. The model assumes that the number of favorable additions satisfy the criterion of adequate sample size, the height and slopes of the backscattering elements are small relative to the incident wavelength and that their distribution is isotropic. The maximum return, as measured by Wright (1966), is obtained when

$$k_w = 2\ k \sin\theta \qquad (2)$$

where $k_w = 2\ \pi/L$ and $K = 2\ \pi/\lambda$ are the wave numbers and L and λ the wavelengths, respectively, of the capillary waves and the radar. For this model, the

cross section

$$\sigma_o(\theta) = 4\pi k^4 \cos^4\theta \, R(\theta,\psi) \, W(k) \qquad (3)$$

where $R(\theta,\psi)$ is the reflectivity as function of the surface electromagnetic properties and the incidence and polarization angles and where $W(k)$ is the energy density spectrum of surface height variation evaluated at the Bragg resonant condition in Eq. 2. According to Trunk (1976), Phillips (1966) gives a bound for $W(k)$ as Bk^{-4}, where B is approximately 6×10^{-3} for gravity waves and 1.5×10^{-2} for capillary waves. Trunk shows, that this model, which can be related to breaking or steep-crested waves, is dependent on short-pulse radars.

Backscatter from the sea is composed of contributions from many fluctuating individual scatterers, which in the Rayleigh scattering model are represented by segments of spheres or complex shapes that are small relative to the radar wavelength. The resultant echo varies in time, reflecting relative phase differences among the echoes received from each scattering element (Skolnik, 1970). The resultant cross section, which is relatively insensitive to look-direction because the scattering elements are moving randomly and are distributed nearly isotropically, is described by a probability density function. According to Trunk (1976), the Rayleigh scattering is more sensitive to vertical polarization and more applicable to wide pulse widths, wherein the received echo contains returns from several breaking waves, added non-coherently.

Two of the static models, the facet and Bragg-Rice scattering models were evaluated with data from the Marineland experiment. Analysis indicates the facet model agrees only marginally with the data obtained with the synthetic aperture radars operated by the Environmental Research Institute of Michigan (ERIM). Results shown in Fig. 1 include the range of data reported by Bechman and Spizzichino (1963), and X-band (λ=3.2 cm) and L-band (λ=23.5 cm) measurements normalized to the 12 knot wind speed measured at Marineland (equivalent to β_o = 10°).

In comparison, the Bragg-Rice model offers more promise, at least for the L-band data. Data summarized by Guinard and Daley (1970), together with data obtained by ERIM on December 15, 1975, are shown on Fig. 2 for X-band and in Fig. 3 for L-band. The Bragg-Rice-Phillips upper bound is shown as a solid line. For the limited range of incidence angles agreement between theory and data is good.

Static models are particularly applicable to imaging with real-aperture radars. Synthetic aperture radars, however, are very sensitive to Doppler velocity components present in the imaged scene. Effects of aircraft motion on wave elements present in SAR imagery, include in order of importance, displacement, image smearing and loss of focus in the azimuth direction, reduction of wave contrast and loss of focus in the range direction. Because the origin of these effects is in the velocity components present on the ocean surface, dynamic models applied to SAR imaging concentrate on either the phase velocity or on the orbital velocity of ocean waves. Early attempts to explain these effects

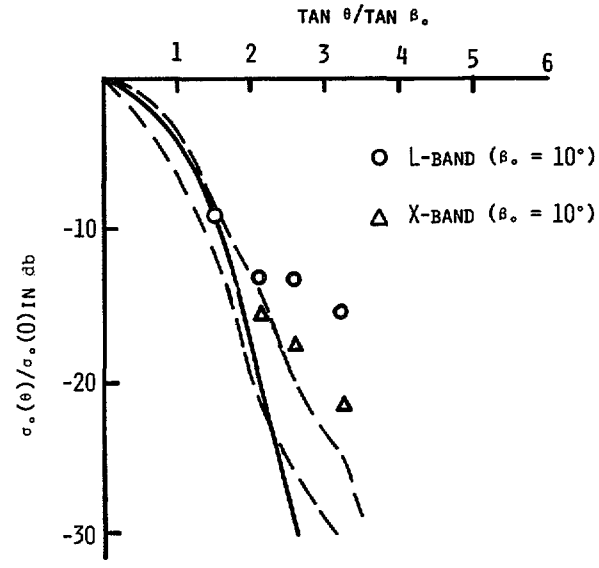

Fig. 1 Comparison of X-band and L-band data obtained at Marineland on December 15, 1975, with the facet model (solid line) and with the range of data reported by Beckman and Spizzichino (dashed lines).

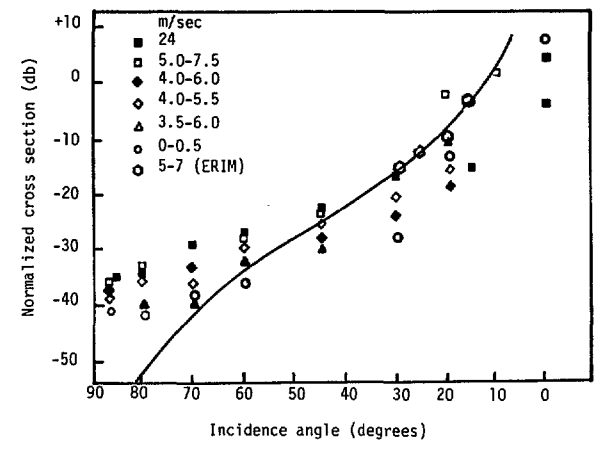

Fig. 2 Variation of the normalized σ_o (HH) at X-band with incidence angle and wind speed. The line represents the Bragg scattering relationship. Data from Guinard and Daley (1970) and the ERIM radar.

observed in SAR wave imagery based arguments on phase velocity; more recent work tends to develop models dependent on orbital motion. The topic is an exciting and controversial one in that experimental evidence exists to support aspects of both approaches. However, the degrees of freedom associated with coherent SAR processing are not sufficient to uniquely explore cause/effect relationships for the image perturbations cited. In addition, influence of spatially distributed currents, including those generated by wind stress are just beginning to be investigated (Weissman and Thompson, 1977).

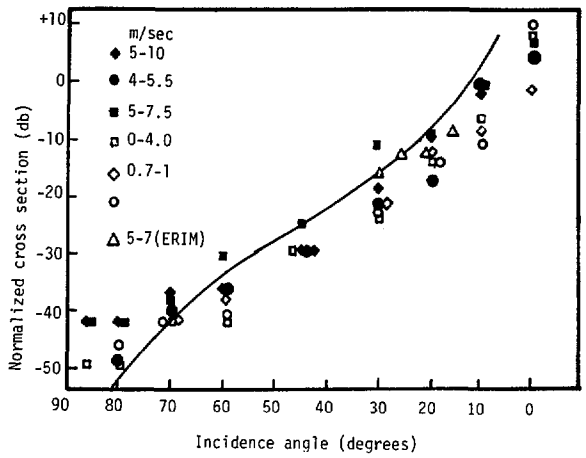

Fig. 3. Variation of the normalized σ_0 (HH) at L-band with incidence angle and wind speed. The line represents the Bragg scattering relationship. Data from Guinard and Daley (1970) and the ERIM radar.

Geometry and motion effects. There are two inherent problems in the collection of ocean wave data with synthetic aperture radars that must be accounted for before dominant wavelength and directional information can be obtained. The two problems are geometry and wave motion effects.

Figure 4 shows the typical configuration of the SAR and the resulting distortion near nadir. Two aspects of the slant range geometry must be considered. First, wave imagery will be compressed, introducing a high range-frequency component with increasing slant range, so that a Fourier transform of a large area containing waves will include a wide range of frequency-modulated wave components. This smears the spectrum and reduces the signal-to-noise ration. Optical or digital slant-to-ground range conversions alleviate this problem.

Another aspect of geometry is the distortion of imagery near nadir resulting from the time delay in range shown in Fig. 5. This, however, is routinely correctable by digital techniques.

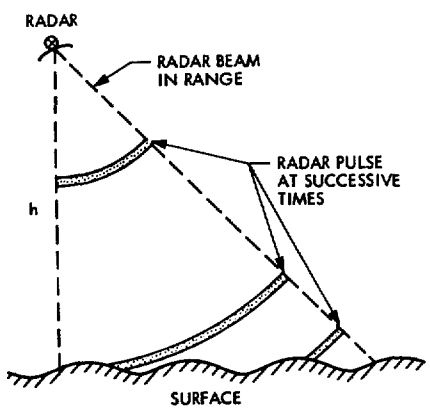

Fig. 4 Range geometry of side-looking radars.

Ocean waves imaged by a SAR system may be blurred if the wave move a substantial distance during the time they are in the radar antenna beamwidth. These blurring effects may, in some cases, be removed by compensatory adjustments of the optical correlator. Azimuthal velocity compensation is achieved by adjusting the correlator azimuth focus according to an algorithm utilizing radar, processor and moving target parameters. Similarly, the blurring effects of range traveling waves may be removed by suitable

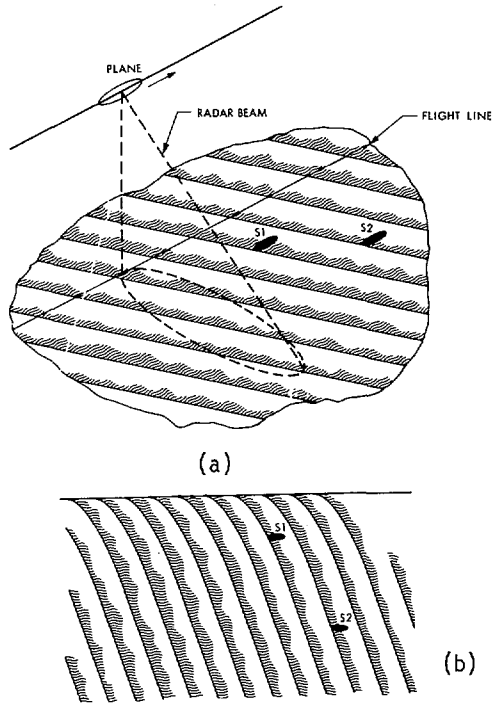

Fig. 5 Relationship between the radar look direction (a) and the corresponding image (b).

rotation of cylindrical optical elements in the correlator. For azimuth traveling waves, the focus correction needed to produce the best azimuth focus can be explained assuming the radar scatterer moves at the phase velocity of the ocean wave. This is not the case, however, for range traveling waves where a point scatterer moving at the phase velocity of the wave would displace, but not defocus the wave image. The observed defocusing can be accounted for by assuming the radar signals are reflected from a stationary scattering surface with variable reflectivity modulated by the passage of a moving ocean wave.

The appropriate model assumes that the energy returned to the radar receiver is reflected or scattered from an ocean surface that is stationary relative to its geographic location. The reflecting surface may, in fact, be moving slowly relative to the phase velocity of the wave, such as the orbital velocity of the wave that usually is an order of magnitude lower than its phase velocity. In this case, the stationary surface model would still apply, since the scattering surface is more nearly stationary compared to the phase velocity of the wave. This is consistent with the fact that the predominant echo

in Bragg scattering is from waves either traveling toward or away from the radar.

This model is based on the following observations made on the ERIM-SAR optical correlator: 1. Measurement of the azimuth Doppler spectrum shift for a series of range traveling waves indicate a scattering surface velocity, at most an order of magnitude lower in value than the phase velocity of the waves; 2. Radar image contrast for range traveling waves is maximized when the cylindrical optics used to focus the azimuth signal histories are rotated an amount proportional to the waves phase velocity; 3. Wave images made from separated Doppler spectral bonds show range displacements equal to the wave phase velocity times the equivalent time between the two Doppler spectra for a stationary traget at the same radar range; 4. Azimuth traveling waves are defocused an amount equal in magnitude to that produced by radar reflectors moving at the phase velocity of the wave and defocusing is more pronounced at L-band than at X-band.

Figure 6 demonstrates dependence of azimuth traveling ocean waves on focus setting in the SAR processor. Modulation depth, defined as the variation in image intensity associated with individual wave returns (wave crest to trough contrast), is plotted against focus shift for an area of waves simultaneously imaged by X- and L-band SAR. Results show the relative insensitivity of X-band to focusing while an optimum detectability (high modulation depth) occurs at L-band at a setting shifted 1.0 mm from a stationary (land) object. Similar results were reported by Jain (1978). Analysis of Marineland

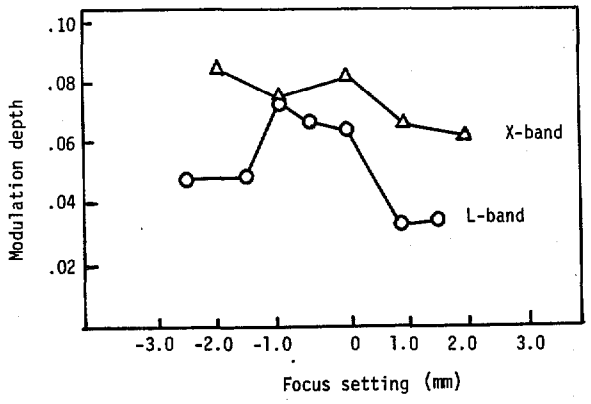

Fig. 6 Modulation depth as function of focus shift for X- and L-band data from Pass 9, Location E, Marineland, Florida, December 14, 1975. Zero represents the stationary focus.

data indicates that optimum wave images result when the radar is looking essentially up-wave or down-wave, that is when waves propagate towards or away from the aircraft in the range direction as is shown in Fig. 7. This principally indicates Bragg-type scattering. Because in the range direction the SAR uses a train of very short pulses, waves traveling in range appear quasi-stationary relative to the sampling time. Differences in modulation depth of range traveling waves (Fig. 8) also indicate that better quality wave images can be generated with

Radar look direction up-wave. Waves are essentially traveling in the range direction

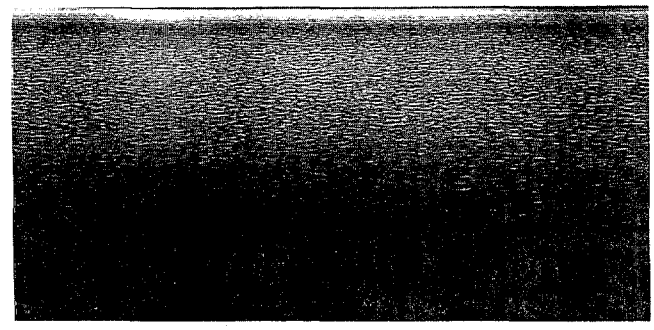

Radar look direction cross-wave. Waves are essentially traveling in the azimuth direction

Fig. 7 Identical ocean area imaged on December 14, 1975, with X-band radar and processed to 3 x 5 meter resolution. Radar flight line from left to right. Radar look direction toward bottom of page with a scale of 5 km in range.

X-band at parallel polarization than with L-band radar. Simultaneously obtained, identical resolution and signal-to-noise ratio X-band (HH) ocean wave images are compared to L-band (HH) images of the same area in Fig. 9. Scans of image density in the direction perpendicular to the dominant crest direction show higher crest-to-trough modulation for X-band. Consequently, wave spectral peaks derived from X-band images can be more accurately defined than those from L-band.

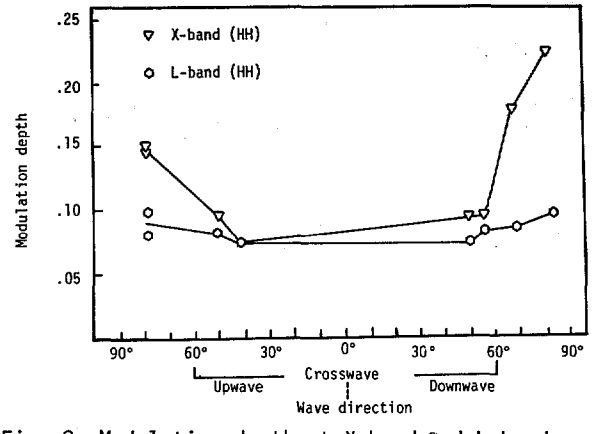

Fig. 8 Modulation depth at X-band and L-band as function of the direction of wave propagation.

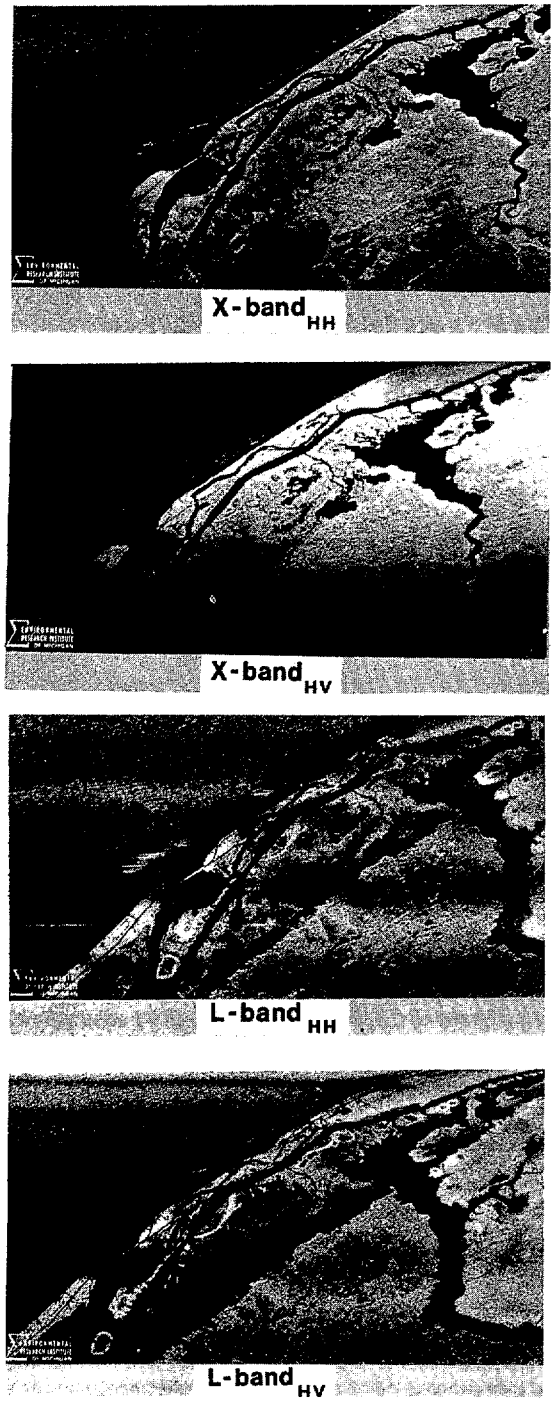

Fig. 9 Radar imagery of the nearshore area at Marineland, Florida, on December 15, 1975, at X- and L-band frequencies and parallel and cross-polarizations.

A possible explanation for the higher quality of X-band imagery was given by Shuchman and Zelenka (1977), who suggested that X-band data have a larger depth of focus than L-band, and therefore the waves moving in the azimuth direction are not appreciably defocused as commonly occurs on L-band images of comparable resolution. The X-band also incorporates a shorter synthetic-aperture length or integration time than L-band, hence reducing motion errors. Also, Trunk (1976) noted that data at horizontal polarization have larger echo spreads than at vertical polarization, and that L-band data have larger clutter spreads than X-band data.

Aspect angle. Besides such factors as sea state and radar frequency and polarization, the intensity of the backscatter return (σ_o) from a SAR also depends on the radar look direction (aspect angle) relative to wind speed and direction. Variation of σ_o at X-band with incidence angle and wind speed was given in Fig. 2. The data indicate that the reduction in the incidence angle toward nadir corresponds to an increase in σ_o. In a comparison of four frequencies, K-band (0.89 cm), X-band (3.2 cm), S-band (15 cm), and L-band (23.5 cm), Long (1956) has shown that the general trend also indicates σ_o increases toward nadir, but correlation of these data to wind speed or direction is not demonstrable. It is known, however, that the backscatter is usually higher in the upwind direction, and in a recent report Fontanel (1978) mentions a 6 db difference at X-band.

3. Data acquisition

The Marineland experiment, whose objectives have been described by Shemdin et al. (1975), took place in December 1975. Data we have analyzed were collected on December 14, with airborne X- and L-band dual-polarized synthetic aperture radars flown on ERIM's C-47 aircraft. In-situ data on wave properties were collected by a pitch-and-roll buoy (wave height and direction) operated by NOAA's Atlantic Oceanographic and Meteorological Laboratory (AOML) and an instrumentation package consisting of a pressure gauge and orthogonally mounted current meters on a sea-sled (wave height, orbital velocities and mean current velocities) operated by the U.S. Army's Coastal Engineering Research Center (CERC). Additional data presented herein were obtained with two real-aperture systems, one an X-band (3 cm) stationary scanning (Raytheon 1020/9XR) radar operated by CERC and a Ka-band (APD-7) radar operated on NP3C aircraft by AOML. Data obtained by these radars were in geographic areas and at times different from those of the Marineland experiment. We included this information to exemplify techniques by which wave spectra and direction can be obtained.

Characteristics of the ERIM SAR system have been described by Shuchman and Zelenka (1977). The CERC radar uses a nine foot slotted array antenna with a beamwidth of 0.9° at 3 db rotating at the rate of 33 rpm. Pulse width is 0.05 μsec which results in a range resolution of 10-20 m. This will generally permit imaging waves of 30 m length. The PPI has a 10-inch CRT with a fast decay phosphor photographed with a Bolex 16 mm reflex camera. The radius of the region displayed may be varied by discrete steps from 3/8 of a nautical mile (0.695 km) to 24 nautical miles (44.4 km). Signal-to-noise limitations restrict wave imaging to a range of 3 nmi or less. The optimum range for obtaining information on wave direction depends on the length and height of the incident waves.

The real-aperture Ka-band radar, operated by NOAA is a military version of the APQ-97 system developed by Westinghouse, that uses a narrow transmitted pulse width to achieve a range resolution of 8 m.

Physical charteristics and operational modes of the sea-sled instrumentation have been reported by Teleki, et al. (1975). The pitch-and-roll buoy operated by NOAA is the type described by Ewing (1969).

4. Wave spectra

In converting raw SAR data to wave spectra, two basic steps are used: 1) to generate an image by correlating the SAR signal amplitude and phase histories and 2) to derive the wave frequency and wave number spectra. In this procedure SAR signal data were digitized and corrected for geometry. The slant-to-ground range conversion, $R_g=(R_s^2 - h^2)^{1/2}$, where R_g and R_s are the ground and slant range distances and h is the altitude of the aircraft, also requires knowledge of the sampling interval and geoidal surface elevation. Using the antenna gain as a function of angle, each image element in range was weighted to account for the two-way propagation loss that is proportional to range (Lowry, et al., 1977). A form of radiometric correction, it involves calculating the average intensity in each range cell.

Figure 10 is a geometrically corrected image of wave conditions at Marineland on December 14, 1975, obtained with the ERIM X-band (HH) radar and processed at the Jet Propulsion Laboratory. Location of the pitch-and-roll buoy (PRB) is marked. The local water depth, adjusted for the tide was 12 m. The sea-sled gauges were operating in 7.7 m water depth directly shoreward of the buoy. For the square subarea in which the buoy was operating, an FFT transform of the radar image was generated in digital form. After averaging, the two-dimensional energy density spectrum E (k, θ), was mapped (Fig. 11) that shows presence of two wave trains. The dominant energy is at k=0.076 rad/m (L=82m) with wave direction α=270°. The contour interval is 2.718.

Pitch-and-roll buoy data were digitized at two samples/second and cross correlated to obtain the directional distribution of wave energy, E (f,θ). After applying the shallow water correction to the radar data using the dispersion relationship $\omega^2 = gk \tanh kd$, where $\omega = 2\pi f$ and d is the local water depth, the frequency-dependent energy density spectra of the buoy and radar measurements were calculated. This is shown in the lower half of Fig. 12 wherein the peak of the spectra match at the frequency of 0.124 Hz. In order to compare the spectral shapes, especially in the high frequency region of the spectrum, ln(f) was plotted again ln (E(f)) in Fig. 13. Comparison of the slopes of the radar and buoy spectra indicate both sensors having measured the same wave components.

5. Wave direction

Wave direction was computed from the radar, pitch-and-roll buoy and the current meter data (Table 1) for the total frequency range observed.

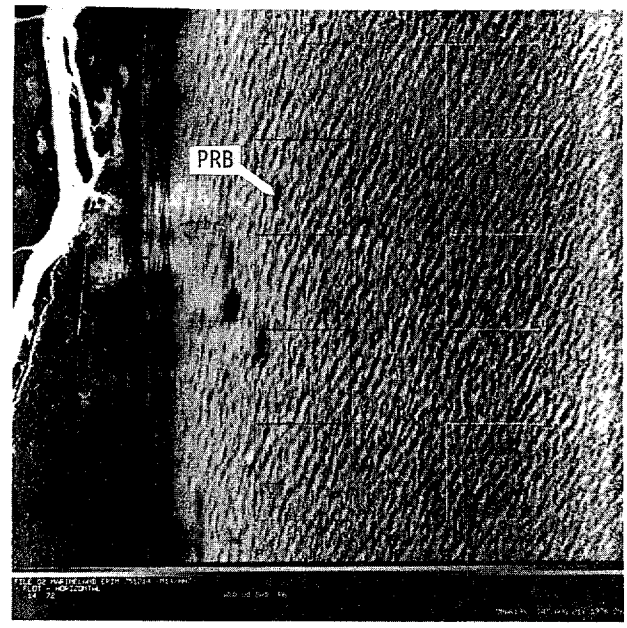

Fig. 10 Geometrically corrected radar imagery of ocean wave conditions on December 14, 1975, at Marineland.

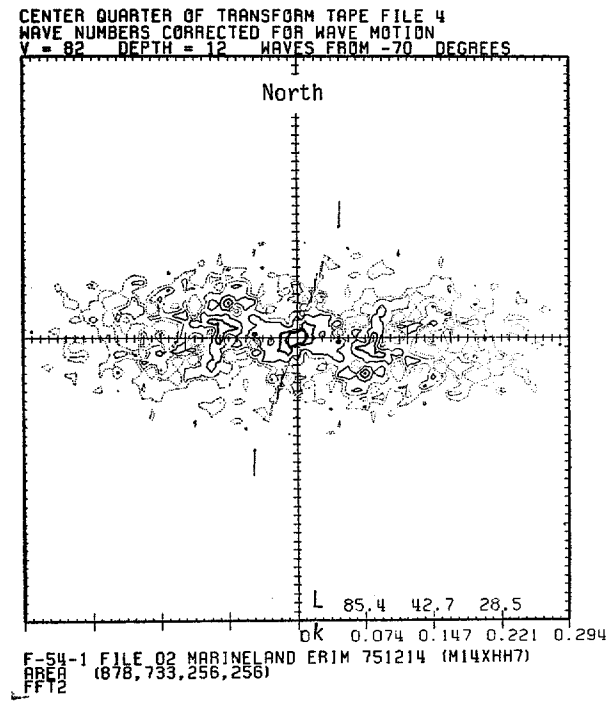

Fig. 11 Contour plot of E(k,θ) derived from X-band radar data at the location of the buoy in Fig. 10. Scales of L and k are in m and rad/m.

Because different algorithms were used to compute directions from the current meter data, the frequency bands do not match those of the other sensors. Results shown in the upper half of Fig. 12 indicate very good agreement for wave directions for all three measurements in the region 0.12<f<0.22 Hz. At the peak of the spectra the difference between radar and

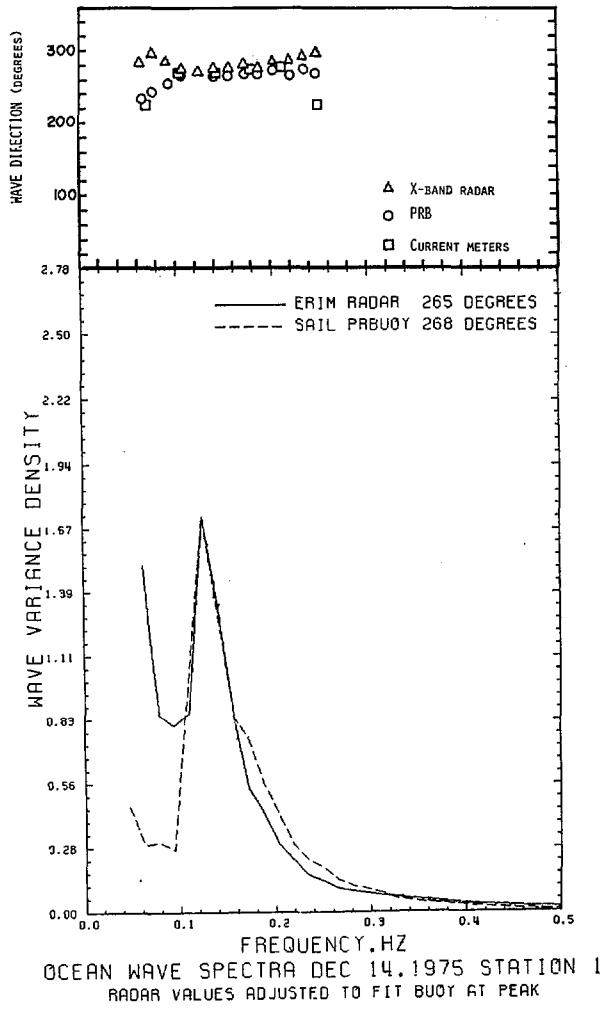

Fig. 12 Ocean wave spectra and wave direction computed for the area identified in Fig. 10 and 11. Energy density is in units of m^2/Hz.

buoy measurements is 2°. In the current meter data, the peak frequency lies between .107<f<.143 with 270°<α<271°. This agrees to within 2° of the buoy data and within 1° of the wave directions measured with the SAR. Calculation of the weighted averages of wave directions over 3 frequency bands centered on the peak frequency (0.124 Hz) gave results of 273° for the radar. The equivalent averaged direction for the buoy was 266°.

Data are also shown from real aperture radars. For the CERC radar experiments, U2 aerial photographic missions were flown off the California coast in the area of San Diego, during the West Coast Experiment in March of 1977. Simultaneously, radar images of the waves were obtained with the CERC radar system (Fig. 14), located at Mission Beach. From data obtained on March 14 and 29, 1977, directions of long crested wave trains detectable on the radar image and the U2 photographs were measured manually (Table 2) referenced to the bearing of 275° from the NUC tower to the radar site. On both dates, two wave trains were detected with the radar, whose

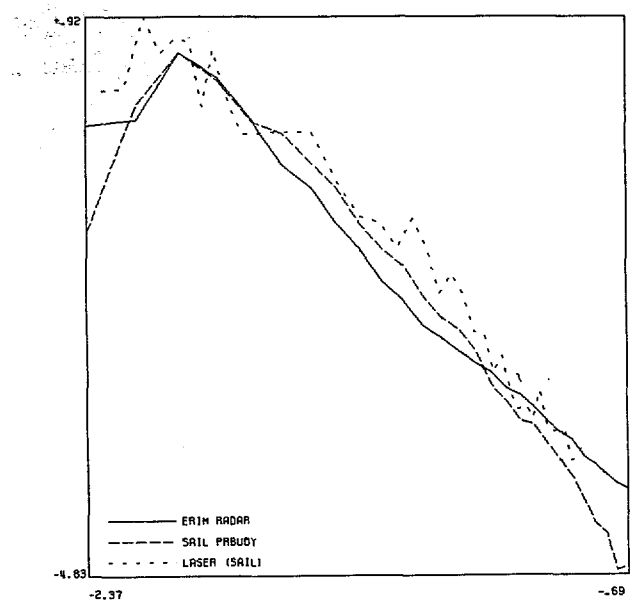

Fig. 13 Logarithmic distribution of wave spectra shown in Fig. 12.

directions agree well with those obtained from U2 images. A third wave train, with short wavelength was seen in the aerial but not in the radar images. Its absence in the radar may have resulted from a misadjustment of the pulse width, so that the radar's resolution became too degraded to image the short waves. With proper adjustment, it is expected that the radar could image waves with lengths on the order of 30 m, as lengths of 35 m have already been measured with radar similar in resolution to the CERC system.

Table 1 Summary of wave direction computations (in degrees) at Marineland, Florida, December 14, 1975.

f	(1)	(2)	(3)	(4)
.063	235	288	283	-
.071	-	-	-	225
.078	242	296	296	-
.094	254	287	287	-
.107	-	-	-	270
.109	266	277	275	-
.125	268	270	270	-
.141	263	275	275	-
.143	-	-	-	271
.156	265	282	277	-
.172	267	285	280	-
.179	-	-	-	275
.188	267	281	275	-
.203	272	290	285	-
.219	266	289	287	-
.234	275	288	292	-
.250	269	295	296	224

(1) NOAA pitch-and-roll buoy
(2) ERIM X-band data shown in Fig. 10
(3) ERIM X-band data, with image elements of the ship having been removed
(4) CERC sea-sled based current measurements

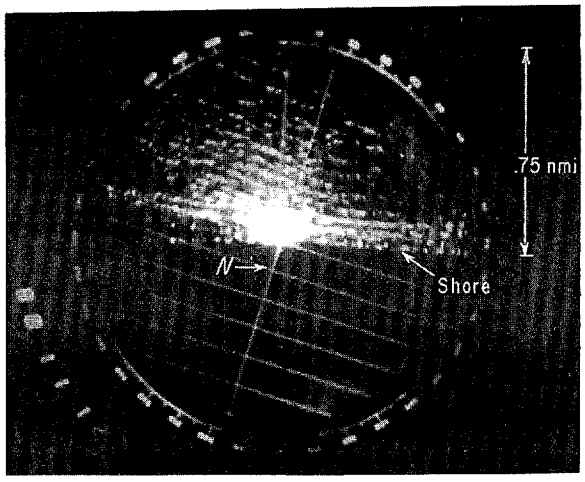

Fig. 14 Radar image of waves in the Mission Beach area, San Diego, California, obtained on March 29, 1977, with the CERC X-band radar. Radar range is 0.75 nautical mile.

Table 2 Comparison of wave directions measured with the shore radar to those observed on photos.

Date (1977)	Time	CERC RADAR (α)	CERC RADAR (L)	U2 AERIAL PHOTO (α)	U2 AERIAL PHOTO (L)
3/14	11:30	281°±4°	84±11m	284°±2°	long
		263°±4°	168±22m	264°±3°	longest
				316°±2°	short
3/29	11:00	284°±4°	132±21m	288°±2°	long
		257°±4°	168±22m	257°±2°	longest
				320°±2°	short

The NOAA Ka-band radar was flown in May 1978, near the coast of Puerto Rico. Fig. 15a and Fig. 15b are examples, respectively of deep ocean and coastal waves imaged with this system. The waves apparent in Fig. 15a have a wavelength of 110-130 m compared to the value of 130 m derived from a wave spectrum (Fig. 16), for which data were obtained with a laser profilometer operated simultaneously onboard the aircraft. The waves are propagating in the downwind direction.

6. Conclusions

As demonstrated in comparison of radar and in-situ data, radar imagery of the ocean surface can be used to measure wave direction. Hence, SEASAT-A SAR data should prove useful to studies of wave refraction, provided shortcomings in present knowledge about radar backscatter of ocean waves are recognized. This study shows that, the Bragg-Rice model appears to give good results for the incidence angles investigated. Dynamic models are still in the development stage, therefore, one can only conclude that investigations on the causes of Doppler effects will have to continue on a case-by-case basis and with assistance from adequate and properly calibrated in-situ sensors. The principal task in the geophysical evaluation of SEASAT-A SAR data, therefore, will have to include testing of both the scattering principles and the limits of imagibility in a wide range of wave and wind conditions.

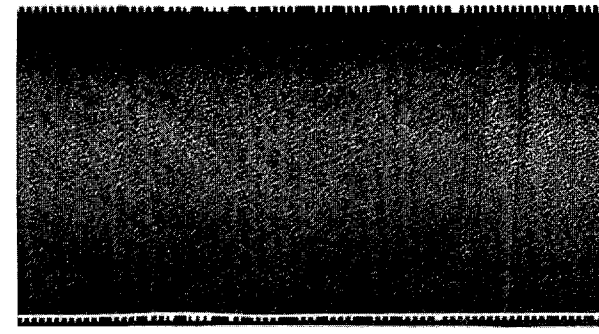

(a)

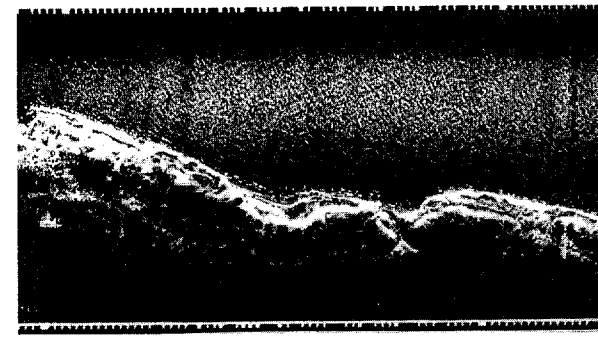

(b)

Fig. 15 Waves imaged (a) in deep water, (b) in coastal area near Puerto Rico with the NOAA Ka-band radar in May 1978.

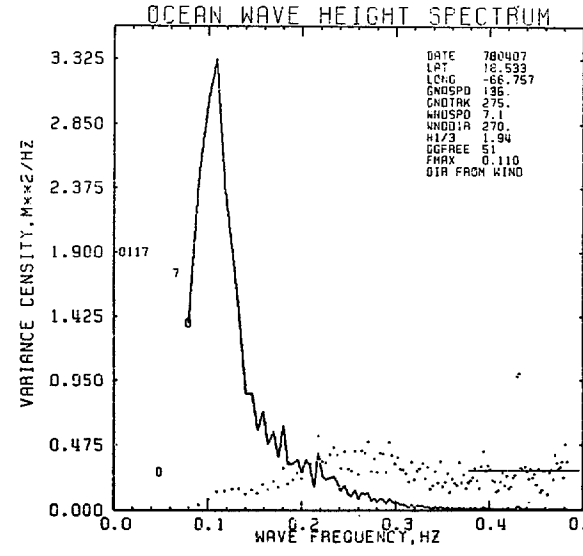

Fig. 16 One-dimensional wave spectra associated with the image of Fig. 15a. Dots represent the equilibrium range constant α, assuming an f^{-5} form of the spectrum

Acknowledgements

The ERIM contribution was the result of work performed under ONR contract N00014-76-C-1048 and NOAA/NESS grant No. 04-6-158-44078. The authors benefited from discussions with members of the SEASAT-A SAR Experiment Team.

References

Beckman, P. and A. Spizzichino, "The scattering of electromagnetic waves from rough surfaces," McMillan Co., New York, 1963.

Brown, W. E., Jr., C. Elachi, and T. W. Thompson, "Radar imaging of ocean surface patterns," Jour. of Geophys. Res., v. 81, 1976, pp 2657-2667.

Elachi, C., and J. R. Apel, "Internal wave observations made with an airborne synthetic aperture imaging radar," Geophys. Res. Letters, v. 3, 1976, pp. 647-650.

Ewing, J. A., "Some measurements of the directional wave spectrum," Jour. Mar. Res., v. 27, 1969, pp. 163-171.

Fontanel, A., "Experiences d'étude de l'état de la mer par radar latéral," Actes. Colloq., no. 5, CNEXO, 1978, (in press).

Guinard, N. W. and J. C. Daley, "An experimental study of a sea clutter model," Proc. IEEE, v. 58, 1978, pp. 543-550.

Jain, A., "Focusing effects in the synthetic aperture radar imaging of ocean waves," Jour. Appl. Phys., v. 15, 1978, pp. 323-333.

Long, M. W., "On the polarization and wavelength dependence of sea echo," IEEE Trans. on Ant. & Propag., v. AP-13, 1965, pp. 749-754.

Lowry, R. T., D. G. Goodenough, J. S. Zelenka, and R. A. Shuchman, "On the analysis of airborne synthetic aperture radar imagery of the ocean," Proc. 4th Canadian Symp. on Rem. Sensing, Quebec City, 1977, pp. 480-505.

Moskowitz, L. I., "The feasibility of ocean current mapping via synthetic aperture radar methods," Proc. Fall Conv., Amer. Soc. Photogrammetry, 1973, pp. 760-771.

Phillips, O. M., "The dynamics of the upper ocean," Cambridge Univ. Press, London, 1966.

Shemdin, O. H., J. E. Blue, and J. A. Dunne, "SEASAT-A surface truth program: Marineland test plan," Jet Propulsion Laboratory Rept. 622-6, 1975.

Shemdin, O. H., W. E. Brown, Jr., F. G. Staudhammer, R. Shuchman, R. Rawson, J. Zelenka, D. B. Ross, W. McLeish, and R. A. Berles, "Comparison of in-situ and remotely sensed ocean waves off Marineland, Florida," Boundary Layer Meteorology, v. 13, 1977, pp. 225-234.

Shuchman, R. A., and J. S. Zelenka, "Processing of ocean wave data from a synthetic aperture radar," Boundary Layer Meteorology, v. 13, 1977, pp. 181-192.

Skolnik, M. I., "Sea echo," Ch. 26 in M. I. Skolnik (ed.): Radar handbook, McGraw-Hill, New York, 1970.

Teleki, P. G., F. R. Musialowski and D. A. Prins, "Data acquisition methods for coastal currents," Proc. ASCE Conf. on Civil Eng. in the Oceans/III, 1975, pp. 1190-1210.

Trunk, G. V., "Non-Rayleigh sea clutter: properties and detection of targets," NRL Rept. 7986, 1976.

Weissman, D. E. and T. W. Thompson, "Detection and interpretation of ocean roughness variations across the Gulf Stream inferred from radar cross section observations," Proc. Oceans '77, 1977, pp. 14B/1-10.

Wright, J. W., "Backscattering from capillary waves with application to sea clutter," IEEE Trans. Ant. and Propag., v. AP-14, 1966, pp. 749-754.

OFFSHORE PETROLEUM DEVELOPMENT FINANCING

Arthur C. Eschenlauer

Morgan Guaranty Trust Company of New York
23 Wall Street
New York, New York 10015

Abstract

Offshore hydrocarbon development financing often is "non recourse", because project sponsors wish to mitigate the risks of such large scale, costly, and complex undertakings with their long term exposures to technical, economic, and political uncertainties. Lenders first forecast the economics of the project in light of all risks, and then work with project sponsors to build a suitable financial plan. This plan usually will be negotiated with the host government and other lenders before it is implemented. The entire effort is demanding and costly, and it requires many decisions and tradeoffs to optimize the technical, economic, political, safety and environmental criteria. The enterprise system and market orientation play an important role in motivating and disciplining the financing effort and guiding the decisions and tradeoffs that must be made.

1. Introduction

Financing for offshore hydrocarbon development projects is shaped primarily by the nature of the projects themselves. Let's begin by looking at the characteristics of such projects as they affect the financing. In the first place they typically are huge in cost. It is not uncommon for them to run into the multi-billions of dollars. Also they are vast in physical scale and complexity, and each is unique. This requires a problem solving approach that draws tremendously on the financial and human resources of the sponsors and the suppliers of the hardware. It also means that the projects often have several years of lead time.

2. Characteristics of Offshore Developments

Offshore developments are fraught with many risks. There are those of a technical nature: Are the hydrocarbons really in place? Can they be produced? Is the technical development plan adequate to produce them? Is the plan itself feasible? Is it consistent with environmental and safety standards? Will the political environment remain stable and dependable after the facility is in place and producing hydrocarbons? What will happen in case of a casualty caused by weather, accident, sabotage or war? Efforts to cope with these risks are affected considerably by the fact that the projects usually have multiple sponsors. This arises from the fact that the cost and uncertainty of the hydrocarbon exploration effort is so great that most such wildcatting is done not by single companies but rather by groups of companies who have banded together to obtain the required exploration license and carry out the project.

Therefore, it is unusual for one company to make a discovery and be able and willing to undertake the development of an offshore project by itself. Often the membership of a group arranging to finance the development is quite heterogenous in that it includes both large oil companies as well as some more modest-sized ones and even some entities who may be primarily in such other businesses as chemicals, minerals or gas transmission. Also, sponsor groups occasionally include some very small independent oil and gas producing companies. The heterogeneity is increased by the fact that the participants may be of different nationalities, have different tax situations to cope with, and have different needs and uses for the hydrocarbons produced. As an example of the last point, one partner may have a refining and marketing operation in the country where the offshore project is located, while another may not. The latter company, therefore, would be looking to sell the hydrocarbons in the world market, or possibly transport them to another jurisdiction where it has refining and marketing operations.

Finally, offshore development financing is conditioned by the political situation in the host country. Not only does this mean the attitude of the host government toward free market development of hydrocarbon resources, but also the degree to which it wants its own national oil company involved, and the general outlook for the stability of political framework under which the sponsor group has obtained its license, rights, and obligations relating to the project.

All the foregoing characteristics of offshore development contribute to a desire in many cases for the owners to do what is called "project financing" to develop the hydrocarbon resource. Project financing differs from the corporate financing which banks ordinarily engage in. In the

usual corporate term loan the bank looks to repayment out of the cash produced by a strong and well-known corporation engaging in a business in which it has had a successful history. Often there is a diversity of sources of cash within the corporate structure. In any event, the future can to some degree be projected from past history. By contrast, in developmental project financings there is no past history, because the project has not existed. The project lender therefore looks primarily to cash flow from a single project to pay the principal and interest on his loan. The loan typically is made upon completion of the project, but sometimes in advance of completion if the corporations sponsoring the project have given adequate undertakings to see it through to completion. Because there is no past record which can be extrapolated into the future, the analysis of a project requires a rigorous and intensive prospective effort on the part of lenders.

From the viewpoint of the sponsor companies project financing has considerable appeal. This is not to say that sponsors always opt for project financing; they don't. However, there are situations in which even the largest companies with no need to borrow to finance the project do choose project financing. Perhaps a discussion of how project financing can help cope with a few of the problems of offshore development will suggest why. First, the problem of size: Even a major company could well be unwilling to subject itself to such a concentration of capital exposure as is required for an offshore development program. These projects involve an awesome "bet" on a very few platforms, wells, and reservoirs. The risk is compounded by the fact that the development may be in a foreign political environment, leaving the sponsor company feeling it would further increase its already large exposure to that host country if it were to add hundreds of millions or even billions of dollars of development funds to the great value of the hydrocarbons in place. One way to avoid such concentration of risk is to do project financing on the development. If the project fails, the sponsor company will lose only the equity invested in the project, because there is no recourse by the lender to anything but the project. If for economic, technical, or political reasons the project proves disappointing, or even worthless, the loss would fall first upon the sponsor to the extent of its equity, and secondly, upon the project lender.

3. Bankers Viewpoint and Analysis

Now let's assume that a project sponsor has decided that it wants to do this so called project or non-recourse financing of the development program. How does the banker proceed? Let's walk through both the analytical and implementation phases of such a project.

To begin, the banker identifies the stream of cash expected to flow from the project, which would be available to pay principal and interest on the loan. This stream of cash is partially determined by the economics of the project itself. But in part it is determined also by negotiation with the project sponsor, because the sponsor can undertake to provide assurances as to various elements of the project economics, thereby reducing the risk assumed by the lender. This in turn can result in financing in a larger amount, or at a lower rate of interest. It should be recognized that when the sponsor gives such assurances, the financing departs from an absolute project orientation. In practice, there are very, very few pure project financings done. Nearly all that are given this label have some degree of corporate undertaking behind them. In other words, instead of being truly "non-recourse", these financings involve limited recourse to the sponsor companies.

Our banker looking at a project's economics begins with an engineering estimate of the hydrocarbons in place, the amount that will be produced in each year of the project's life and the split among oil, gas, and natural gas liquids, the estimated price at which these hydrocarbons will be sold, the royalty share of the host government, operating expenses that will be incurred, any further capital expenditures that will have to be undertaken to attain the programmed production, the corporate taxes that will be borne by the project as well as any special petroleum taxes might apply. As mentioned above, the project sponsor may wish to remove or eliminate the uncertainties relating to any of these elements, but at least the sponsor will commit to operate the project up to some kind of economic limit. In other words, the sponsor would be relieved of the obligation to operate when operating costs would exceed revenue. Several ways in which economic uncertainties could be eliminated or reduced may be of interest. The project sponsor could undertake, as a corporate matter, to operate the project and pay all operating expenses. Or, alternatively, he could agree to pay all operating expenses over and above an agreed upon level. The project sponsor could agree to purchase at an agreed price the hydrocarbons produced. Occasionally, the project sponsor may prefer to bear the technical risks, because he feels he knows and understands them and does not want to pay any price in terms of interest rate to the bank lending group for bearing such risks. In such a case the project sponsor may, in effect, guarantee the volumes and timing of hydrocarbon production by agreeing to pay to the lenders the amount of revenue that would be obtained if the project did in fact produce planned volumes at the scheduled times.

In any event, by analysis and negotiation the lender will have determined the base case cash flow stream over the life of the project. His next task is to determine how big a loan this cash flow will support and to tailor the debt service burden - i.e. principal and interest payments - of that loan to the projected stream of cash. Because the cash flow stream contains uncertainties, the banker will need to build in a margin of safety. He does this by limiting the debt service in each year to an amount smaller

than the base case stream of cash available in that year to pay principal and interest. This technique allows the banker what is called "coverage" of his debt service requirements by the cash flow stream available. The amount of such coverage is determined in light of the risks of the project. These risks include those mentioned before like the goodness and feasibility of the operating plan, hydrocarbon prices, reserves in place, producibility of those reserves, taxation, economic limit, operating costs, and the like, and in addition such considerations as foreign exchange risks, the convertibility of currencies and ability to apply the cash from the project to service the foreign obligations of the project, the cost of providing for the safety of workmen on the project and for environmental protection, and the risk of interruption of the cash flow stream through force majeure of some kind. The lenders will consider these risks in light of the remedies available to them if cash flow available for debt service does fall short. Realistically, speaking, however, where a project is being operated by a knowledgeable and well capitalized major oil company, there is little effective remedy available to the lender who has taken project risk. It would be a rare case in which the lender could step into the shoes of such an oil company and operate the property in a way that would increase the cash available for debt service.

In trying to understand and appraise these risks as they might affect the coverage of debt service, the banker will build a model of the project and then test the sensitivity of the cash flow stream to various assumptions with respect to each of the elements of uncertainty. As a result of this exercise he will become familiar with the nature of the cash flows, and through repeated cutting and fitting, gradually reach the point where he feels he has sufficient base case coverage of his debt service. He will look at and eventually express this coverage in at least two ways. First, the coverage over the life of the loan, which is the excess of the cumulative cash flow available for debt service over the term of the loan over the debt service requirement of the loan for that same original term. Secondly, the coverage over the life of the hydrocarbon reserves, which is the excess of the cumulative projected cash flow available for debt service for the entire life of the project over the debt service requirement of the loan for its original term. This life of reserve cash flow would be determined from an analysis of the hydrocarbons in place and the plan for their recovery.

The reason for looking at the life of loan coverage is to determine the probability that the loan can be serviced within its intended term. The reasoning behind the analysis of coverage over the entire life of the reserves is that the lender wants to know what the situation would be if the loan had to be extended. For example, the lender might well be satisfied with a loan which provides very thin coverage of debt service over the targeted life of the loan, so long as there is ample coverage over the entire life of the project. The lender might, in these circumstances, decide that while he is undertaking a risk that his loan will be extended in time, he is taking little risk that it will not ultimately be paid. By contrast, a lender might feel uncomfortable with a reasonably full coverage over the life of the loan but with a coverage over the life of the project that is thin, as would occur in a case where the term of the loan approached the life of the reserves, leaving relatively little projected cash flow beyond the original term of the loan.

There are other considerations in the design of a non-recourse loan: such things as the bank's willingness to put out funds for a long term in light of its need to manage its own assets and its willingness to be exposed to the political risks in the country where the project is located.

Eventually, then, in light of the constraints of the cash flow stream available for debt service and the term for which the bank is willing to lend, the banker will reach a judgment regarding the amount of his loan, the schedule for the repayments of principal, and all the other elements involved in any ordinary term bank loan. When this has been done, the banker negotiates with the project sponsor until both parties agree on the financial and all other aspects of the financing. At that time the banker begins to work with counsel and the client to guide the preparation of all the legal documentation required to bring the transaction ultimately to closing.

4. Syndication and Structuring

There are other tasks to be performed, also. The banker and project sponsor will work together to determine the group of lending banks. Just as the risk of the project would be very great for one sponsor company, it would be extremely great for one lending bank. Banks do not expose hundreds of millions of dollars to a single project. Therefore, a participation effort is needed in nearly all cases. The banks to participate will be chosen on the basis of their relationship with the sponsor company, their knowledge and capability in offshore oil and gas project financing, their standing in the host country, their size and ability to provide a significant share of the financing required, their probable willingness to work well with the bank group in the event the project develops difficulties. The bank and the project sponsor will try to put together a strong team that can be expected to be cooperative and effective at all stages of the transaction, from negotiation right through to ultimate repayment.

As discussions with the lead bank proceed, the project sponsor will be keeping the host country as well as its national oil company, oil industry regulatory group or groups, and its central bank apprised of the financing program. It is often felt that this widening of the conversation from a bipartite one between oil company

and host government to a tripartite one in which the lead bank joins increases the degree of confidence among all parties. If the environment is right, all three can come away from these discussions feeling that the financing is sound. The purposes of discussions with host country representatives is to inform them candidly and completely of the plan for financing a project which oftentimes is of tremendous importance to their country, to be sure that they will give the consents which may be necessary to enable the financing to take place on the terms intended, and to satisfy the oil company and the lender that there is no opposition within the host government to the idea of the oil company doing non-recourse financing of the development program.

The lead banker will, by now, have begun to work on another of his responsibilities as agent: to plan the communications between the project sponsor and the bank lending group. In order to be sure that all prospective bank participant banks fully understand the project, the agent bank will work with the sponsor to prepare a detailed offering memorandum. This will describe the project and the financing program, including the report of independent consulting petroleum engineers, who will confirm that they find the reservoir, production program, development plan and hardware satisfactory and sufficient for the project as planned.

After prospective participating banks have received this offering memorandum the agent bank will continue to supply them information and answers to questions and suggestions they might have. Initially this is by telephone, but eventually an information meeting will take place. At such a meeting the project sponsor, the agent bank, the independent consulting engineers, and the bank lending group meet face to face for most of a day to discuss the project in depth. Following that, the participating bankers are expected to commit their institutions to the financing. This is followed by the closing of the transaction and the drawdown of funds.

5. Complicating Factors

The above discussion has been vastly oversimplified. In the real world it is never so easy. For example, it was assumed that the project would be complete at the time the funds were committed and disbursed. This is seldom the case. More often, a completion undertaking must be negotiated with the project sponsor or sponsors. This requires a definition of completion and the terms and conditions under which the sponsor's obligations will fall away upon completion. Secondly, we spoke as if there were only a single project sponsor and that he were both the operator of the property and had sole control of operating decisions. This is by no means always the case. Sometime a project financing is sought by a sponsor who is not the operator or, even if he is operator, does not have unilateral control of the operating decisions. This requires the lenders to satisfy themselves that in some fashion they can be comfortable with the mechanics by which operating decisions will be made and by which those decisions will be implemented. In lending to a company that does not have control over operating decisions, the banker must realize that in event of default, he cannot expect to determine the operations of the project. He must be satisfied with whatever operating decisions the group makes. This is an uncomfortable position for a banker, who normally likes to delegate all operating decisions to the borrower, but have the right, if the loan goes into default, to have a significant say in how the business is operated.

A further simplifying assumption has been that there is no national oil company of the host country participating in the transaction. Where there is, there are always special considerations arising from the fact that the national oil company will have certain privileges and rights preferential to those of other participants.

Another greatly simplifying assumption is that we have not dealt with the issues of the transportation of hydrocarbons by ship or pipeline, the refining or other processing of hydrocarbons such as the liquification of natural gas, the stripping out of the natural gas liquids, the use of the hydrocarbons in electric power generation or gas distribution, and the like. Frequently these transportation, refining and hydrocarbon usage programs are intimately involved with a project financing. Where this is the case, the transporters and offtakers of the hydrocarbons can also be projects rather than large well-established corporate credits. In such cases a separate analysis must be done on each of the projects involved so as to be sure that all elements of the overall program will be accomplished satisfactorily. This will be essential to the cash flow stream. For example, if an offtaker were to fail to pay for the hydrocarbons produced there could be a shortfall in revenue; if a pipeline project to carry the hydrocarbons were to fail for any reason, there could be a slowdown or cessation of hydrocarbons production. We are all familiar with the reduced production of Alaskan crude oil which inevitably followed when a portion of the Trans Alaska Pipeline capacity was lost because of an outage of one of its pump stations.

6. Conclusion

In real projects all of these complications, and more, can occur, and all must be foreseen and dealt with in the planning process. Therefore, project financings take years and years. In fact, the financial planning of them takes place more or less in tandem with the design of the project itself and is an integral part thereof. The whole exercise requires tremendous dedication on the part of all parties involved: lenders as well as project sponsors. It amounts to a vast commitment of corporate opportunity both in terms of funds and man hours. There are a myriad of problems to be solved and decisions to be made, and the underlying force that guides the effort is primarily the financial

incentive provided by the expected opportunity to sell the hydrocarbons at a profit.

FINANCIAL REQUIREMENTS FOR OCEAN THERMAL ENERGY CONVERSION (OTEC)

Frederick E. Naef and Rosendo J. Pont

Lockheed Missiles and Space Company

Ocean Thermal Energy Conversion (OTEC) is a solar energy technology that utilizes the surface layers of the ocean as a solar collector and thermal energy storage medium, and converts that thermal energy into electricity by using a closed cycle Rankine heat engine. The technology is currently being developed into a practical commercial venture by private enterprise working in collaboration with the Department of Energy. After the government demonstration is completed, commercial development of OTEC systems will create a significant financial requirement.

A baseline 400 Mwe OTEC plant is described, and the financial requirements to build such an installation are established. Since each OTEC plant consists of several identical modules, it is suggested that lease-finance techniques may facilitate the accumulation of the necessary capital. An economic analysis is presented that relates the cost of delivered electricity (mils/kwh) to the return on investment of the plant owner/operator and power module lessor.

Presentation Outline

I. Introduction

II. What is OTEC?

- A. Basic principles
- B. DOE program
- C. An energy industry

III. An OTEC Plant Concept

- A. Systems characteristics
- B. Assumptions
- C. The Technology Delivery System

IV. Ownership and Financial Arrangements

- A. Outright ownership
- B. Maritime lease finance
- C. Application of maritime financial aids
- D. Assumptions

V. Marketing Arrangements

- A. Bareboat Charter
- B. Period Charter
- C. "Take & Pay" Charter
- D. Assumptions

VI. Economics

- A. Unit costs
- B. C&M costs
- C. Transmission cost
- D. Return on Investment (ROI)
- E. ROI/Risk relationships

VII. Market Projections & Sensitivity Analysis

- A. Potential sites and applicants
- B. Projected time/cost relationships
- C. Projected market

VIII. Assessment of Risks and Benefits

- A. Pro ownership considerations
- B. Pro charter considerations

IX. Conclusions

COST STANDARDS FOR OCEAN RESEARCH VESSELS

William L. Martino
Assistant Director - CED
6001 Executive Boulevard
Washington Science Building #1
Room 214
Rockville, Maryland 20852

Abstract

A standarized and uniform vessel accounting system is proposed for the Federal oceanographic fleet. Currently, a number of Federal organizations fund and manage the Nation's research and survey vessels. No single agency is responsible for overall coordination or management of the fleet or its operations. As a result, each agency has its own accounting standards for determining vessel operating costs. Thus, comparative cost analysis are difficult to undertake because of the different criteria used. By establishing standardized accounting procedures, Federal managers could be assured they are using the most efficient and economical vessels to achieve their objective if uniform accounting standards were implemented.

Commentary

This past June the Comptroller General recommended that a standardized and uniform vessel accounting system be established for the Federal oceanographic fleet. The basis of this recommendation was a year long study made by the GAO of the management of the Nation's ocean research and survey vessels.

GAO believes that complete and adequate accounting standards would provide federal managers with the necessary data to determine and compare vessel costs for similar services from government and commercial sources. With a uniform accounting system managers would be assured that they are using the most efficient and economical vessel(s) to achieve their objective.

Federal oceanic activities are conducted by 21 organizations in 6 departments and 5 agencies. Five of the 21 organizations fund and manage the Nation's oceanographic fleet to support these activities. No single agency is responsible for the overall coordination or management of the fleet or its operations.

Last year the Federal Government spent over $126 million to maintain and operate a fleet of 79 research and survey vessels -- An average cost of $7,658 per vessel for each operating day -- Because each activity operating federally owned or funded oceanographic vessels is independent of the other, different criteria for defining and accounting for days at sea and for determining the associated cost per day is used.

Cost is a major consideration in evaluating most Government operations, and oceanographic vessel operations are no exception. The price of working in or on the oceans is high and becoming more expensive each year. Consequently, it is imperative that federal agencies can identify what costs are associated with providing research vessel services in order to determine if the derived benefits are worth the associated costs. Any accounting system should provide sufficient costs data to allow for comparison with other means of obtaining the service including the cost of similar services to other agencies. There should be enough similarity among the various agencies accounting systems to allow for reasonable cost comparisons.

Cost per operating day is the primary measurement for comparison purposes between the costs of research and survey vessels. However, the items which are included (or excluded) in the cost per operating day varies by organization. Let me give you some examples:

1. Research and survey vessels are basically mobile platforms designed to accomodate scientists and technicians conducting research programs or surveys. One organization provides program expertise (i.e. scientific and technical personnel) as part of the ship's crew; other organizations do not. Since crew costs are part of ship operating costs, the treatment of this expense is not consistent.

2. One organization uses an estimated cost per day which is charged to the various users on a daily basis. If a profit or loss is realized as a result of the estimated daily rate an adjustment is made in subsequent years to return or recover the cost. Other organizations

charge actual rather than estimated costs. Needless to say, the practice of using estimated costs and subsequent adjustments tends to distort true cost figures.

3. One organization considers special supplies, some vessel alterations, and crew overtime during a unique voyage as reimbursable costs not to be included in the cost per operating day. Other organizations consider these costs as part of the cost per operating day.

4. One organization excluded some maintenance costs while other organizations included these costs in determining the cost per operating day.

5. The commonly used method for measuring vessel productivity is "Days at Sea." Different federal organizations have different criteria. For example, one organization defines a day at sea as any 24 hour period for a vessel to qualify for a "Day at Sea."

This discussion on costs is not intended to be all encompasing. Instead it points to a problem which, we believe, can be solved by coordination among the various agencies and the adoption of a uniform vessel accounting standards for the Federal oceanographic fleet. This accounting system could provide for cost comparability on an item-by-item basis and also for total vessel operating costs. For example, crew salaries and fringe benefits could be accounted for under one cost category while costs such as equipment and maintenance could be accounted for under other cost categories. Uniform accounting systems would provide federal managers a basis for determining the efficiency and economy of various vessels.

In summary, the mission - oriented approach of the various agencies involved in funding and managing the Nation's oceanographic fleet has resulted in a fragmented, incomplete and inadequate vessel accounting standards and made it difficult, if not impossible to determine and compare vessel costs for similar services. GAO believes this problem is symbolic of the lack of a coordinated and definitive U.S. Government ocean policy.

Until a comprehensive national ocean policy is established, GAO has recommended a single manager - (or a Government-wide Fleet Allocation Council which would have the same authority as a single manager) - for coordination and efficient use of Government civilian agency oceanographic vessel operations. This single manager would have the authority and responsibility to effectively manage the Nation's oceanographic fleet. Included in the manager's responsibilities would be the establishment of a standardized and uniform vessel accounting system. GAO believes this approach will resolve most of the problems we have discussed today.

A DYNAMIC HYDROTHERMAL EXPERIMENTAL SYSTEM

K. Andrew Gustajtis
Centre for Cold Ocean Resources Engineering
Memorial University of Newfoundland
St. John's, Newfoundland
A1B 3X5, Canada

Abstract

A unique dynamic hydrothermal system has been built to study the alteration reactions between seawater and basalt in the temperature range of 0 to 180°C. The purpose of the system was to approximate in the laboratory the type of geochemical reactions which would occur in a submarine hydrothermal circulation of seawater at active mid-ocean spreading centres. A total hydrostatic pressure of at least 1000 bars (± 10 bars) and a temperature difference of 0°C to 180°C could be established between interconnected reaction chambers containing seawater and basalt. Basalt/seawater ratios as great (or greater) than 1:50 where used. The use of a large volume reservoir of seawater allowed a continuous flow of fresh seawater through the basalt with the ability to sample the seawater continuously without disturbing the temperature or pressure of the experimental system.

Introduction

Associated with the concepts of seafloor spreading and plate tectonics, there has recently been a growing consensus that seawater may take part in submarine hydrothermal circulation in the crestal provinces of mid-ocean ridges (Elder, 1965; Palmason, 1967; Talwani, et al, 1971; Bodvarsson, et al 1972; Lister, 1972; Williams, et al, 1974). Field observations suggest that such hydrothermal circulation system(s) beneath mid-ocean ridges may lead to significant alteration of not only the basaltic crust but also the geochemical mass balance of the marine environment (Spooner and Fyfe, 1973; Hart, R., 1973a and 1973b).

A hydrothermal system was designed and built which allowed the close approximation in the laboratory of the envisaged and recently proposed convective flow of seawater through oceanic basalts in regions of high heat flow. Unlike all presently available experimental hydrothermal systems known to the author, which are limited to a basalt/seawater ratio of between 1:1 to 1:5, the system developed here permitted ratios as great (or greater) than 1:50. The purpose of this equipment was to test experimentally the ability of circulating seawater to leach specific elements (particularly iron and manganese) from basalt, as well as to provide a means of studying the behaviour of such elements while being transported in the seawater at various temperatures.

The unique design of this hydrothermal system permitted the variation of four parameters, duplicating the conditions envisaged beneath the seafloor. Pressure could be maintained constant to at least 1000 bars (±10 bars) which is equivalent to a water depth of 10 km. Temperature differences of 0 to 180°C could be established between the basalt samples. The use of a large volume reservoir of seawater allowed a continuous flow of fresh seawater which in turn permitted the system to operate for weeks without requiring a shut-down. Finally, a provision was made for sampling the seawater continuously without disturbing the temperature or pressure of the experimental system.

Hydrothermal Circulation

Since the early heat flow measurements by Bullard (1954; et al 1956) near the axis of the Mid-Atlantic Ridge, it has been recognized that high heat flow values were frequently associated with the crest of active ocean ridge systems. The subsequent accumulation of data has substantiated that the average heat flow at the Mid-Atlantic Ridge, the East Pacific Rise and the Indian Ocean Ridge are considerably above the oceanic mean, with a surface flux of between four (Deffeyes, 1970) and eight (Langseth and von Herzen, 1970) times the earth's average. However, although these anomalies have proven to be larger and more consistent than any other in the heat flow field (McKenzie, 1967), a number of major discrepancies exist between predicted and measured heat flow patterns close to the mid-ocean ridge crests (Talwani et al, 1971; Hyndman and Rankin, 1972; LePichon and Langseth, 1969; Sclater and Klitgord, 1973; Williams et al, 1974).

Detailed heat flow studies from various active spreading centers such as the Juan de Fuca Ridge (Lister, 1970), Reykjanes Ridge (Talwani et al, 1971), the Mid-Altantic Ridge at 45°N (Hyndman and Rankin, 1972), and the Galapagos Spreading Center (Sclater and Klitgord, 1973) all show similar scatter in measured heat flow values, and their mean distribution indicate a significant discrepancy between observed and theoretically calculated heat flow. This scatter can be attributed only in part

to instrumental error, topographic relief or uneven sediment distribution (Langseth and von Herzen, 1970). Active hydrothermal circulation directly or indirectly has been proposed to explain this conspicuously large variance, as well as the anomalously low values commonly observed in heat flow measurements near the ridge crests and flanks (Lister, 1972; Williams and von Herzen, 1974).

The motion arises from the buoyancy forces produced by density variations in a field of non-uniform temperatures. This results from the fact that a given volume of seawater would expand with increasing temperature, the expansion would contribute to a decrease in density and an upward flow would occur. For example, the change in density over a temperature range can be approximated by the following expression,

$$\rho = \rho_0 \left[(1 - a)\,(T - T_0)\right] \qquad (1)$$

where ρ is the calculated density at temperature T, and ρ_0 is the original density at temperature T_0, and a is the coefficient of thermal expansion. Extrapolating Wilson and Bradley's (1966) data on the thermal expansion of seawater to 300°C, at a total hydrostatic pressure of 700 bars, equation (1), was plotted for the temperature range 0 - 300°C (Fig. 1), and illustrates a 40 percent decrease in total density.

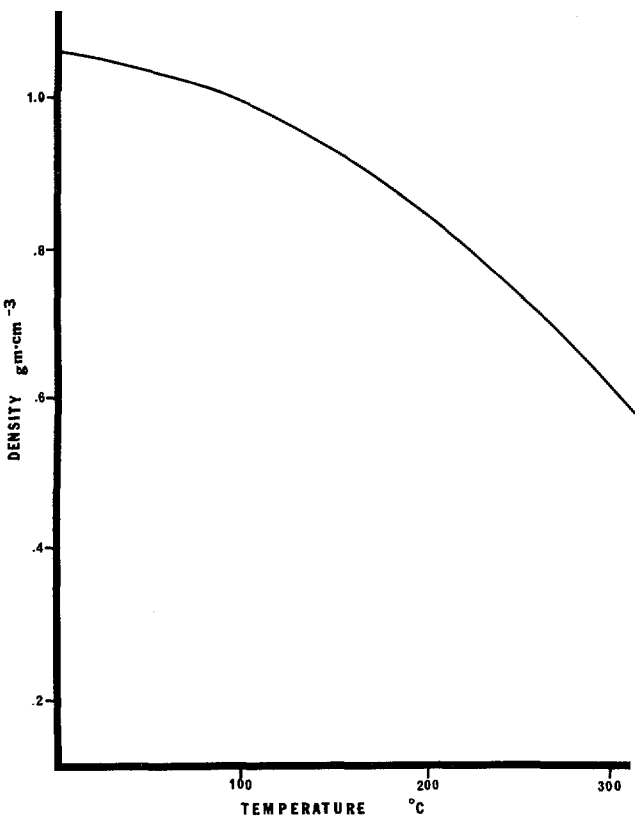

Fig. 1 Change in seawater (35°/oo density (gm/cm^3) from 0-300°C at 700 bars total pressure.

The Experimental System

The system which was designed and built is illustrated in Fig. 2 and Fig. 3. The essential components are two large pressure vessels (O.D. 4 3/8", depth 21", capacity 1,040 ml.), connected in series, each of which is referred to as a pressure vessel, within which specially designed reaction chambers, were held. The first pressure vessel was usually maintained at an elevated temperature, whereas the second was either at room temperature or cooled to 0°C.

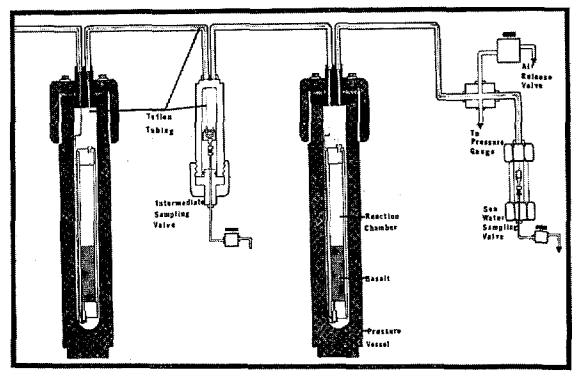

Fig. 2 The flow through hydrothermal system illustrating the two reaction chambers connected in series with an intermediate valve between the two, and an exit valve at the far right.

The seawater-basalt system was entirely surrounded by transformer oil which acted as the pressurizing fluid. The pressure was created and maintained, by a compressed air operated hydraulic pump. Since a continuous flow through the hydrothermal system was required, the hydraulic pump was maintained in a dynamic mode, this insured a pressure within ±50 psi of any desired setting, providing the temperature and flow rate remained constant.

The seawater was held in a large pressure vessel referred to as the reservoir chamber, which is not shown in Fig. 2, but can be seen in Fig. 3. The seawater was contained in a series of (a maximum of three) large (15 litre) collapsible polyethylene bags. To minimize the risk of a tearing while lowering the bags into the reservoir chamber, they were only partially filled, containing no more than 7 litres of seawater each, resulting in total maximum capacity of 21 litres of seawater. An exit tube of Teflon through which the seawater could flow, ran inside a high pressure tube from the reservoir chamber into pressure vessel one, entering the base of reaction chamber one.

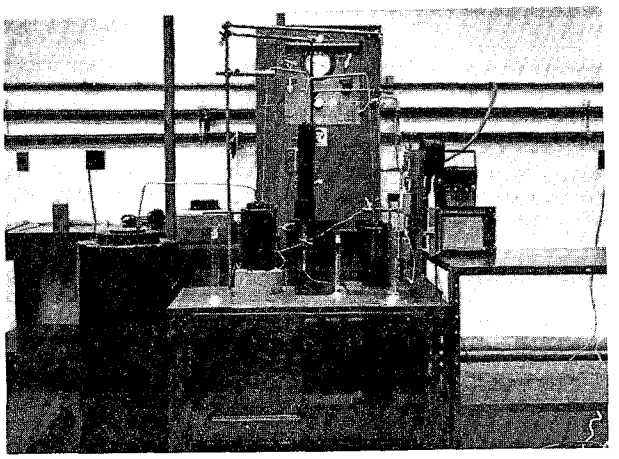

Fig. 3 The hydrothermal system illustrated in Fig. 2. The hydrostatic pump is located in the background, and is connected to the large reservoir chamber at the left, which is in turn connected to the first pressure chamber that is enclosed in a sand bath containing an electric heating element. The intermediate valve and the second pressure chamber are also seen in the photograph.

Pressure vessel one, was enclosed in a sand bath heated by electric element which was connected to a variable transformer. An alumel-chromel thermocouple was lowered into a specially designed well at the top of the pressure vessel. This thermocouple was connected to a strip chart recorder and provided a continuous direct temperature trace.

The seawater would flow through the reaction chamber number one, where it would react with the powdered basalt, and proceed through more Teflon tubing to pressure vessel number two. The valve arrangement as shown in Fig. 2 was installed between these two pressure vessels. This valve made of chromatronix fittings would allow passage of the seawater unobstructively as long as it remained closed. When opened, a sample of seawater in transit between pressure chambers one and two could be extracted.

The final exit sampling valve illustrated in Fig. 4 when opened allowed the seawater to flow through the entire system from the reservoir, through reaction chamber one and reaction chamber two. This valve was maintained open for the duration of an experimental run.

Extreme care was necessary in adjusting the flow, particularly when temperature over 100°C were involved and since both the seawater and oil were essentially incompressible, the removal of even a small amount resulted in a significant pressure drop. Removal of seawater automatically resulted in a slight pressure decrease in the system. As long as this pressure decrease was small, it would be accommodated by deformation of the reservoir polyethylene bags. However, if the pressure differential was substantial enough or if seawater could not flow freely enough through the system, rupture of the internal reaction system would occur, resulting in contamination of the seawater with oil and termination of the run. As long as the rupture was past the last reaction chamber, contamination of basalt was minimal and useful chemical results were obtained.

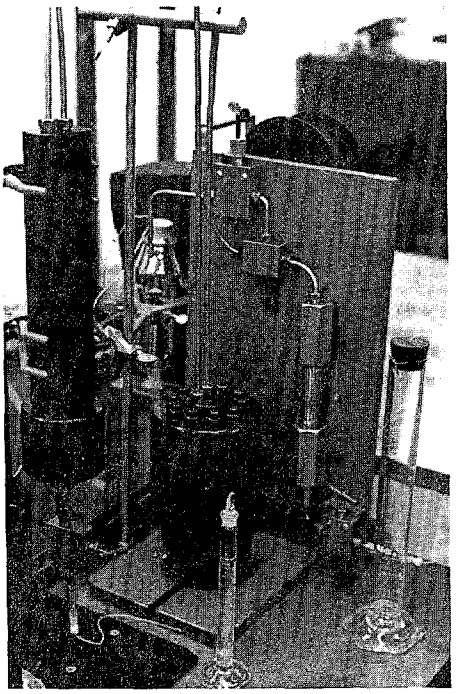

Fig. 4 The final exit sampling valve which allowed a continuous flow of seawater.

A critical component in this exit value assembly was the actual valve itself, which required very delicate adjusting to ensure the slow flow rate required. The flow was monitored by means of a flow meter and the seawater volume collected over time indicated the average flow rate.

The design and manufacture of the reaction chambers, had to meet a number of criteria. The first and most obvious was for material which would be chemically inert to insure that chemical changes in either the basalt or the seawater were not due to contamination from the chamber.

To meet these requirements, the first choice was a thick walled Teflon tube of suitable diameter with tightly machined Teflon plugs. The reaction chambers performed flawlessly at the lower temperature range (less than 85°C) but various minor problems were continually encountered if the temperature was increased above 100°C. Minor leaks in which oil would enter the reaction chambers were encountered, since the Teflon plugs themselves would slowly deform and prevent adequate sealing. Another common problem was the fine basalt powder, would plug the Teflon tube at the base of the reaction chamber.

As a result of these repeated problems, it was finally decided to design a pair of stainless steel reaction chambers. To prevent contamination from the stainless steel, the final solution adopted was to use heat shrink Teflon tubing. The tube was preshrunk to approximately the inside diameter of the reaction chamber, the ends were flared, and the inside surfaces of the top and bottom plugs were coated with the epoxy resin. The Teflon tube was then packed with basalt powder. The additional advantage of this procedure, which worked well, was that the Teflon tube could be removed at the end of the run with minimal disruption of the actual basalt sample.

Discussion and Conclusions

Among the major imperatives in any laboratory attempt to duplicate natural processes, there needs to be concerted effort to insure that the physical and chemical parameters involved in nature are realistically accounted for. It is of course impossible to duplicate all the parameters exactly, nor would it be advantageous to do so, because of the associated incomprehensible complexity and especially the time limitations. Therefore, almost by definition, the laboratory scientist is at an unavoidable disadvantage - faced with investigating the real world with an unrealistic model.

Geology, among the various sciences, is perhaps the most vulnerable to this laboratory paradox because of the essentially infinite time available for the natural processes in the real world. Alteration reactions, whether diagenetic or metamorphic, have been generally assumed to be infinitely slow, and that mineral phases found in chemical or physical disequilibrium require infinite time to readjust. This assumption of very slow reaction rates need not be the case. There are rate determined reactions which are too slow for practical laboratory investigations, but in many cases, particularly for reactions involving aqueous solutions and elevated temperatures, the reaction kinetics are such that providing the other parameters are duplicated the system can prove to be suitable for laboratory experimentation.

In the hydrothermal alteration reactions, the most important physical parameters are not only temperature and pressure but flowing seawater as well. Without flowing seawater, one deals with a stagnant system, which is an unrealistic compromise. In the alteration reaction in nature, the seawater would be continually renewed, and the elements leached from the rock due to the flowing seawater would be relocalized or removed.

Seawater flowing through a basalt column in the seafloor would not only undergo changes in temperature, but also in composition (see Fig. 5). The importance of these changes are clearly indicated in the behaviour of iron in the basaltic material examined in the two reaction chambers that were connected in series (see Table 1). The ramification of these results are obvious; elevated temperatures are not particularly important

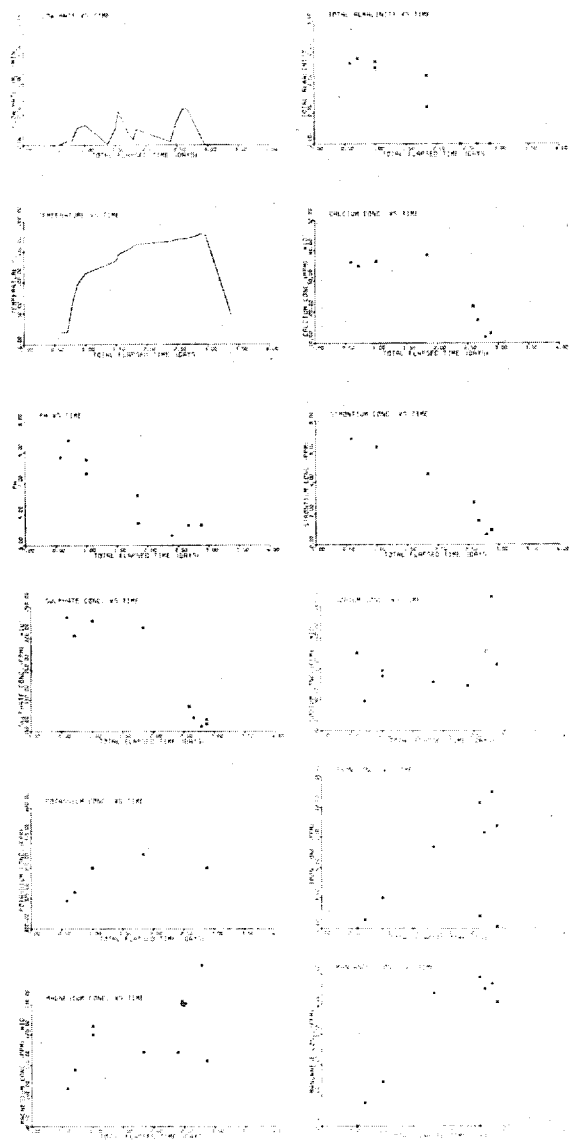

Fig. 5 Illustrated in these graphs are chemical changes that were observed in seawater, as a result of flow through two interconnected reaction chambers as discussed in the text. The temperature trace is for the first reaction chamber in series and it attained a maximum temperature of 180°C. The second reaction chamber was maintained at 0°C. The chemical analysis of the basalt are included in Table 1.

TABLE 1. Basalt Analysis (Major Elements in %)

	Samples					
	Original Basalt	High Temperature NO. 1	No. 2	No. 3	Low Temperature No. 1	Standard Deviation
SiO_2	50.52	48.13	48.13	46.69	48.05	0.30
Al_2O_3	14.58	14.48	14.36	14.96	14.66	0.06
Fe_2O_3T*	10.50	10.07	10.18	10.10	10.02	0.11
MnO	0.182	0.173	0.177	0.175	0.176	0.002
MgO	9.08	9.08	8.95	9.10	8.86	0.11
CaO	11.49	11.06	11.25	11.32	11.05	0.17
Na_2O	2.13	2.42	2.58	2.56	2.32	0.04
K_2O	0.256	0.214	0.206	0.224	0.250	0.004
TiO_2	1.07	1.04	1.03	1.01	1.06	0.11
P_2O_5	0.38	0.32	0.32	0.30	0.33	-
CO_2	--	--	--	--	--	-
H_2O+	0.55	1.04	1.18	--	1.11	-
TOTAL	100.74	98.03	98.35	96.52	97.89	
Fe_2O_3	2.35	2.21	2.56	2.02	1.85	
FeO	8.15	7.86	7.62	8.08	8.17	0.07

*Total Iron as Fe_2O_3

in the removal of iron and manganese by the circulating seawater. The elevated temperatures are, however, important in modifying the seawater from essentially an oxidative neutral solution to one that is reducing and acidic, which in turn makes it a much more effective solvent.

The overall purpose of this equipment has been met, it has provided a means of studying both the ability of seawater to reach specific elements, as well as a way of monitoring the behaviour of such elements while being transported in the seawater at various temperatures.

Acknowledgements

The experimental system discussed here, was built at Dalhousie University, Halifax, Nova Scotia when the author was a graduate student there. Dr. R. Cooke (Dalhousie University) was instrumented in providing the design suggestions for the original system. Funding was provided through a research grant obtained by Dr. F. Aumento (Dalhousie University) from the Canadian Department of Energy, Mines and Resource. The author would also like to thank C-CORE for aiding in the production of this paper.

References

Bodvarsson, G. and Lowell, R.P., (1972). Ocean Floor Heat Flow and the Circulation of Intersitial Waters. J. Geophys. Res. 77. pp. 4472-4475.

Bullard, E.C., (1954). The Flow of Heat through the Floor of the Atlantic Ocean. Proc. Roy. Soc. Lond. A, 222, pp. 408-429.

Bullard, E.C., Maxwell, A.E. and Revelle, R., (1956). Heat Flow through the Deep Sea Floor. Advan. Geophys. 3. pp. 153-181.

Deffeynes, K.S., (1970). The Axial Valley; A Steady State Feature of the Terrain. The Megatechonics of Continents and Oceans, Ch. 9, pp. 194-222. (edited by) Johnson, H., and Smith, B.L. Rutgers University Press , New Brunswick, New Jersey, 282 p.

Elder, J.W., (1965). Physical Processes in Geothermal Areas. Am. Geophys. Un. Mono., Ch. 8. pp. 211-239.

Hart, R.A., (1973a). A Model for Chemical Exchange in the Basalt Sea Water System of Oceanic Layer II. Can. J. Earth Sci., 10(6). pp. 779-816.

Hart, R.A., (1973b). Geochemical and Geophysical Implications of the Reaction between Sea Water and Ocean Crust. Nature, 243. pp. 76-78.

Hyndman, R.D. and Rankin, D.S. (1972). The Mid-Atlantic Ridge near 45°N SVIII Heat Flow Measurements. Can. J. of Earth Sci. pp. 664-670.

Langseth, M.G. and Von Herzen, R.P. (1970. Heat Flow through the Floor of the World Oceans, in The Sea, 4.

LePichon, X. and Langseth, M.G. (Jr.), (1969). Heat Flow from the Mid-Ocean Ridges and Sea Floor Spreading. Techonophysics, 8. pp. 319-344.

Lister, C.R.B. (1970). Heat Flow West of the Juan de Fuca Ridge, Geophys. J., 75. pp. 2648-2654.

Lister, C.R.B. (1972). On the Thermal Balance of a Mid-Ocean Ridge. Geophys. J. R. Astr. Soc., 26. pp. 515-537.

McKenzie, D.P. (1967). Some Remarks on Heat Flow and Gravity Anomalies, J. Geophys. Res., 72. pp. 6261-6273.

Palmason, G. (1967). On Heat Flow in Iceland in Relation to the Mid- Atlantic Ridge. Iceland and Mid-Ocean Ridges, Publ. 38, edited by Bjornsson, S., Soc. Sci. Islandica, Reykjavik. pp. 111-127.

Sclater, J.G. and Klitgord, K.D. (1973). A Detail Heat Flow Topographic, and Magnetic Survey across the Galapagos Spreading Center at 80°W. J. Geophys. Res., 78. pp. 6951-6975.

Spooner, E.T.C. and Fyfe, W.S. (1973). Sub-Sea Floor Metamorphism, Heat and Mass Transfer. Cont. Mineral. and Petrol., 42. pp. 287-304.

Talwani, M., Windisch, C.C. and Langseth, M.G., Jr. (1971). Rekjanes Ridge Crust: A Detail Geophysical Study. J. Geophys. Res., 76(2). pp. 473-517.

Williams, D.L., Von Herzen, R.P., Sclater, J.G. and Anderson, R.N. (1974). The Galapagos Spreading Centre: Lithospheric Cooling and Hydrothermal Circulation. Geophys. J. R. Astr. Soc., 38. pp. 589-608.

Wilson, W.D. and Bradley, D.L. (1966). Specific Volume, Thermal Expansion and Isothermal Compressibility of Sea Water, U.S. Naval Ordance Laboratory NOLTR 66-103.

DEPLOYMENT OF LONG-TERM SEAFLOOR MINERAL EXPOSURE EXPERIMENTS TO MEASURE CHANGES OF MINERALOGY AND COMPOSITION OF MANGANESE NODULES

Roger G. Burns, Virginia Mee Burns, Harlon W. Stockman and Christine T. Stockman
Department of Earth and Planetary Sciences, Massachusetts Institute of Technology,
Cambridge, Massachusetts 02139
and
Martin D. Benson,
Marine Physical Laboratory, Scripps Institution of Oceanography,
San Diego, California 92132

Abstract

Long-term mineral exposure experiments near the seafloors at two stations in the north equatorial Pacific have been designed around long-life transponders left behind after the completion of Deep Tow surveys during the October 1977 INDOMED expedition of R/V Melville for the NSF-IDOE Manganese Nodule Project Attached to each transponder remaining at Site M (metalliferous rise-crest sediments; 8°46'N, 103°58'W; 3040m.) and at Site H (hemipelagic sediments; 6°33', 92°46'W; 3470m.) are a dozen flow-through plastic capsules containing a variety of natural and synthetic hydrated oxides of manganese and iron, including minerals found in deep-sea manganese nodules. When the two stations are re-occupied in 1980-81, the transponders will be recalled and measurements made on materials in the capsules to determine phase changes, metal-uptake capacity, and oxidation products of the various Mn and Fe oxides.

1. Introduction

Manganese nodules cover large areas of the seafloor beneath most oceans. In some areas, these concretions of manganese-iron oxides contain significant concentrations of nickel, copper, cobalt and, to lesser extents, zinc, molybdenum, barium and lead. Nodules from the north equatorial Pacific in a region bounded by the Clarion and Clipperton Fracture Zones consistently show Ni and Cu concentrations each in excess of 1·0 - 1·5 weight percent, whereas nodules dredged from seamounts in the South Pacific frequently are cobalt-rich. The abundance of deep-sea manganese nodules and their high Ni, Cu and Co contents make them objects of great interest to the ocean mining industry, mineral economists, environmentalists, and delegates to the United Nations Law of the Sea Conference.[1] The nodules also pose intriguing scientific problems and are currently the focus of active geochemical research.[2]

In the United States, an inter-university investigation of processes controlling the distribution and composition of manganese nodules is being conducted by the Manganese Nodule Project (MANOP) of the International Decade of Oceanography (IDOE), funded by the National Science Foundation. One of the main objectives of the integrated research efforts of MANOP is to determine the factors responsible for variations of transition-metal concentrations in deep-sea manganese nodules. To this end, detailed *in situ* geochemical measurements are being planned around the MANOP Bottom Lander,[3] a free vehicle instrumentation device designed to house time-series chemical flux experiments at the sediment-seawater boundaries of five major deep-sea sediment-types in the Pacific Ocean -- siliceous ooze, calcareous ooze, hemipelagic clay, metalliferous (rise crest) sediments, and pelagic brown ("red") clay. Before selecting locations to deploy the Bottom Lander, five sites representative of the five different sediment facies have been, or will be, surveyed by the Deep Tow system of the Scripps Institution of Oceanography, Marine Physical Laboratory.[4] The long-life bottom transponder array that Deep Tow uses for navigation during its surveys will be used to accurately emplace the Bottom Lander for subsequent *in situ* measurements. The transponders left behind at the proposed MANOP sites provide unique opportunities to carryout long-term mineral exposure experiments near the seafloor. These experiments are designed to measure changes of mineralogy and chemical composition of Mn and Fe oxide phases, either precursors to or occurring in manganese nodules. In this paper we describe the design of the mineral exposure experiments, and outline the problems being addressed by the various synthetic and natural Mn and Fe oxide phases encapsulated in plastic flow-through capsules attached to transponders left at two of the MANOP sites.

2. Mineralogy of Manganese Nodules

The manganese oxide minerals most frequently reported in manganese nodules are todorokite, birnessite and delta-MnO_2.[5] Birnessite, the so-called "7Å manganite" phase in early literature on manganese nodules, appears to be more common in nodules from shallower seafloors and seamounts. Todorokite in terrestrial ore deposits is recognized as a constituent of manganese nodules by two diagnostic lines around 9·6Å and 4·8Å in x-ray diffraction (XRD) patterns. These lines also appear in XRD patterns of a synthetic sodium manganese (IV) oxide hydrate, the so-called "10Å

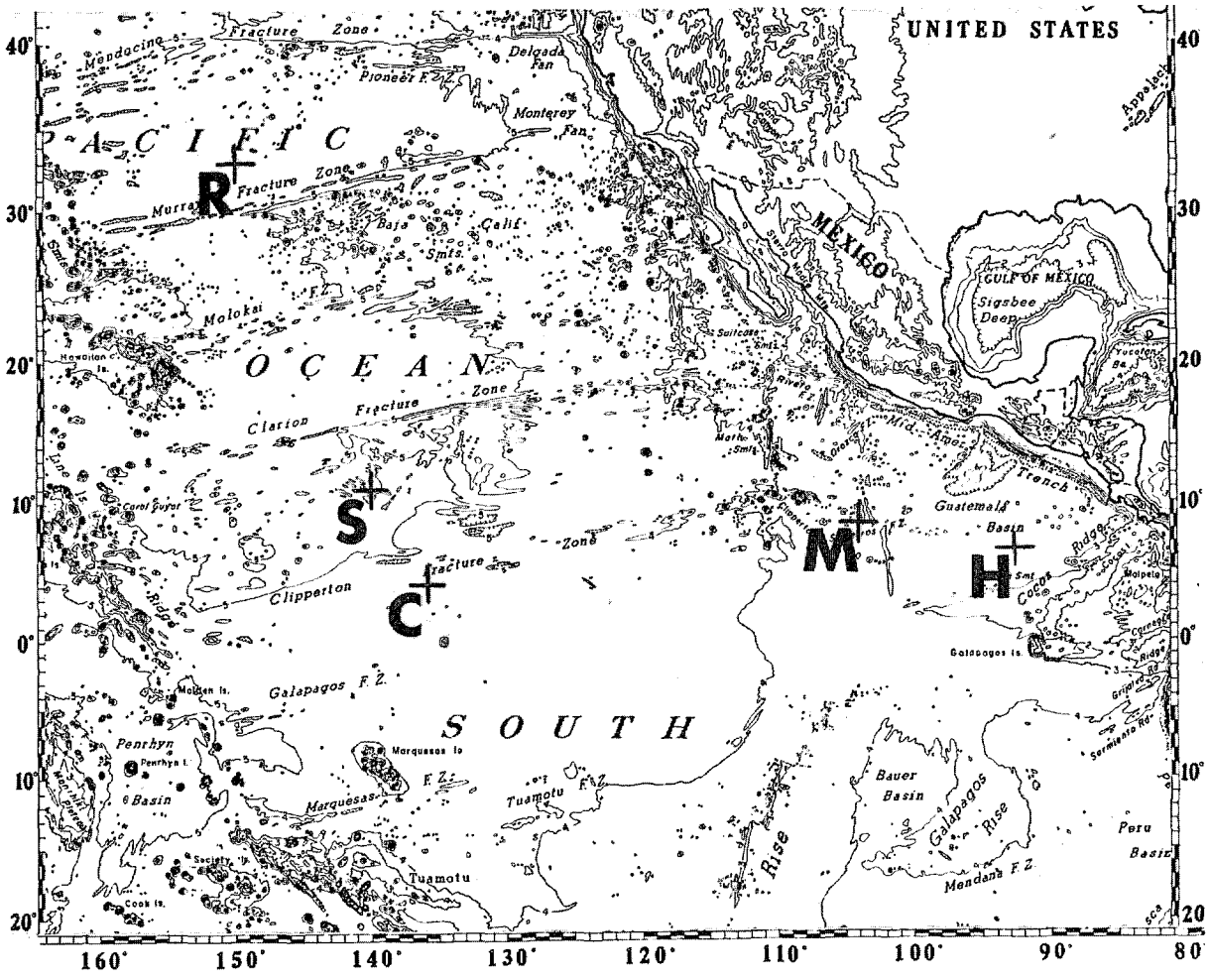

Figure 1. Proposed MANOP Sites.

manganite" phase in early literature on manganese nodules. This synthetic Na derivative was recently named buserite and is sometimes used in European literature on manganese nodules. Sodium buserite is unstable and dehydrates to birnessite. It can only be synthesized at temperatures below about 10°C. Various calcium and transition metal derivatives of buserite may be synthesized by exchanging Na for Ca, Cu, Co, Ni, Zn, Mg, etc., and these compounds appear to be more resistant to decomposition.

The XRD powder photographs of outermost surfaces of nodules are often featureless with considerable darkening of the films, suggesting that the microsamples consist of phases amorphous to X-rays. Occasionally, broad diffuse lines centered around 2·40-2·45Å and 1·40-1·42Å are observed, which are attributed to δ-MnO_2, a cryptocrystalline, structurally disordered form of birnessite. Although most nodules contain significant concentrations of Fe, the iron-bearing phases in most pelagic nodules appear to be amorphous to X-rays. Recently, an iron oxide phase in nodules was named and formulated as feroxyhyte, δ'-FeOOH, and suggested to be a disordered precursor to goethite (α-FeOOH).

3. Proposed MANOP Sites

Features of the five sediment-facies MANOP sites shown in Figure 1 are summarized below.

Site S. (siliceous clay, 11°N, 140°W). This is in the equatorial zone of biogenic-rich siliceous sediments containing radiolarian and diatom tests. Manganese nodules from this area are generally enriched in Ni and Cu, and todorokite is the most frequently identified mineral. Site S was surveyed during leg 4 of the PLEIADES expedition of R/V Melville in Summer 1976 (station 20).[6] It is planned to deploy Bottom Landers within the northeastern quadrant of this area during Spring 1979, Fall 1979 and Fall 1981.

The depth of the seafloor at Site S is relatively large (around 5000m) and below the carbonate compensation depth.

Site M. (metalliferous sediment, East Pacific Rise, 8°46'N, 103°58'W). This is a site where the sediments are dominantly of hydrothermal origin. The seafloor at Site M is about 3000m and is significantly shallower than that at Site S. Site M was surveyed during leg 1 of the

INDOMED expedition of R/V Melville in Fall 1977,[7] and long-life Sonatec transponders were left at this site. The transponders are to be recalled to the surface when Site M is occupied by Bottom Landers during mid-1980. The 2-3 year period during which the transponders remain on the seafloor is currently being used in the mineral exposure experiments.

Site H. (hemipelagic sediments, 6°33'N, 92°46'W). This site has a thin layer of oxidized material overlying reduced hemipelagic clay. The seafloor at Site H, about 3500m, is again significantly shallower than that at Site S. Site H was surveyed during leg 1 of the INDOMED expedition of R/V Melville in Fall 1977, and again long-life transponders were left behind at this site. It is planned to return to Site H and to deploy Bottom Landers there during Spring 1981. Again, the 3-4 year period during which the transponders stay near the seafloor at Site H is being utilized in our mineral exposure experiments.

Site C. (calcareous ooze, approximately 4°N, 136°W). This site lies beneath the most biologically productive surface waters of the equatorial Pacific, where relatively rapid deposition of calcareous sediments occurs. A preliminary Deep Tow survey was undertaken during leg 4 of the PLEIADES expedition of R/V Melville in Summer 1976 (Station 21),[6] and a few marble-sized nodules were observed and sampled. Site C is to be surveyed in greater detail by Deep Tow in Fall 1980, and is to be occupied by Bottom Landers in Fall 1981 and Spring 1982. Long-life transponders will remain on the seafloor at Site C during that 1-2 year period.

Site R. (brown clays, approximately 33°N, 150°W). This site lies to the north of siliceous clay sediments, and is characterized by a lack of calcareous and siliceous microfossils and by more tranquil sedimentation. This site will be the last one surveyed under the long-range plans of MANOP. Deep Tow surveying is planned for Fall 1980, and Bottom Lander deployments are planned for mid-1982 and 1983.

4. Design of the Mineral Exposure Experiments.

The 2-3 year duration between Deep Tow surveys and Bottom Lander deployments at Site M and Site H obviates against battery-powered pumping of seawater over mineral samples attached to long-life transponders. Instead, natural diffusion gradients or current action near the seafloor must be relied upon for equilibration of seawater with mineral samples used in our mineral exposure experiments. Therefore, it is essential that sample holders be sufficiently permeable to seawater and yet be efficient at retaining very fine-grained particles (>5 micron) of synthetic phases during the life-time of the experiment. In our mineral exposure experiments, we have modified the design of plastic flow-through capsules used by Dr. S. Honjo (Woods Hole) in his titanium-bellows pump.[8] The plastic capsule assembly is illustrated in Figures 2 and 3. The capsules were fabricated from 4cm diameter plastic rods, and consist of cylindrical vials (length 4cm, internal diameter 2.5cm, capacity 20ml) with screw-on tops and bottoms. The latter each contain three types of filter held in place by a plastic grid: 1.2cm diameter millipore pre-filters, 2.5cm diameter polypropylene membrane filters, and 2.5cm diameter gauze. This system retains particles of synthetic minerals exceeding about 5 microns, and equilibrates with submerged aqueous solutions in 10-15 minutes.

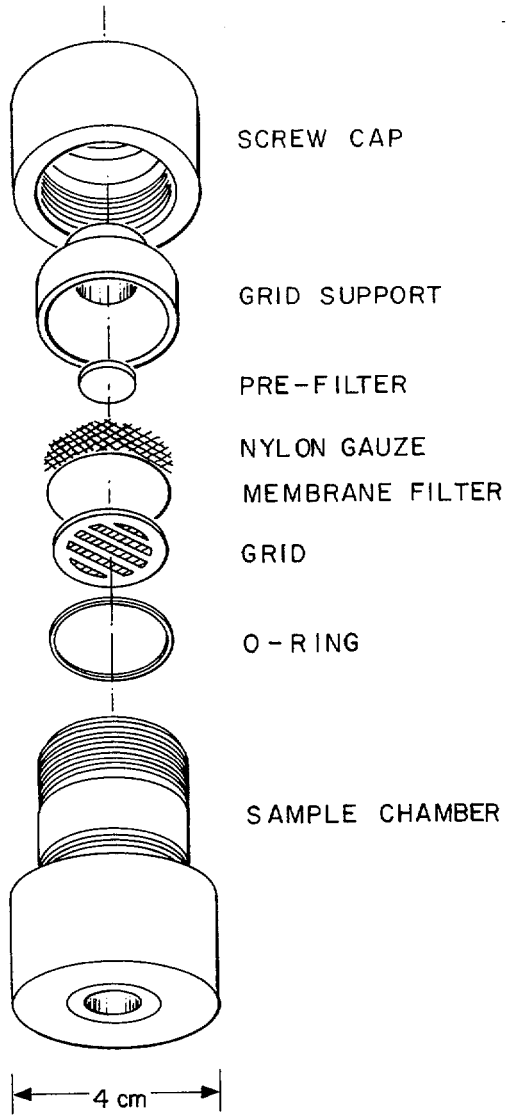

Figure 2. Design of the Plastic Flow-Through Capsules Used in the Mineral Exposure Experiments

To date, two long-term mineral exposure experiments, each consisting of a dozen plastic capsules containing a variety of mineral substrates, have been launched, one at Site M and the

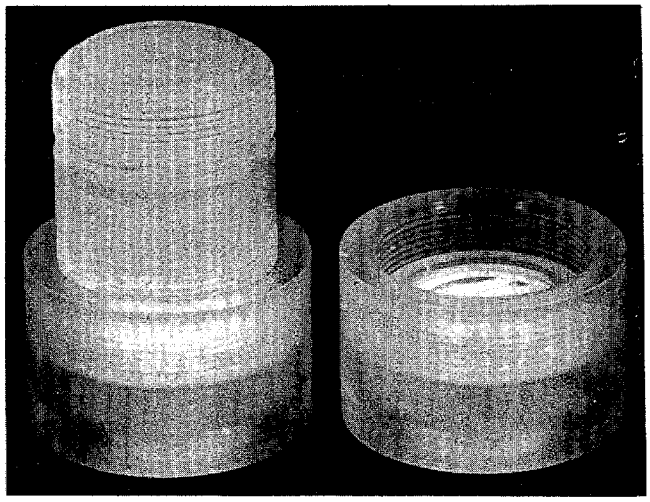

Figure 3. View of a Partly Assembled Sample Holder

other at Site H. The lay-out of the experiment near the seafloor is depicted in Figure 4. The capsules are bound to flag-poles of the flotation system attached to transponders anchored at Site M and Site H, and are situated about 100m above the seafloor.

When the mineral exposure experiments were launched during the Fall 1977 leg 1 INDOMED expedition of R/V Melville, great care was taken to avoid thermal decomposition of some of the minerals before they reached the cold seafloor. The capsules had been kept refrigerated and were attached to the flotation system only a few minutes before the transponders were deployed. It is assumed that the poor thermal conductivity of the plastic capsules and the slow permeability of the filter system ensured the mineral samples remained cold during the passage of the transponders to the seafloor.

In order to test whether the plastic capsules were functioning satisfactorily, one vial was attached to a short-term transponder deployed while R/V Melville was on station at Site M. The capsule was retrieved ten days later when the transponder was recovered at the completion of the Deep Tow survey. Chemical analysis of the solution in the capsule indicated the presence of Mg^{2+} and SO_4^{2-}, demonstrating that the original encapsulated 0.7m NaCl solution had equilibrated with seawater. The capsule had also retained the synthetic Na buserite loaded into it.

5. Description of the Mineral Exposure Experiments

Materials loaded into the capsules deployed at Site M and Site H were selected to elucidate several problems of manganese nodule geochemistry. They include:

(i) Todorokite and buserite. Todorokite, or its possible synthetic analogue buserite, is the predominant mineral in manganese nodules from siliceous clay sediments in the north equatorial Pacific (e.g. Site S), and is responsible for the high Ni-Cu enrichments in these nodules. The

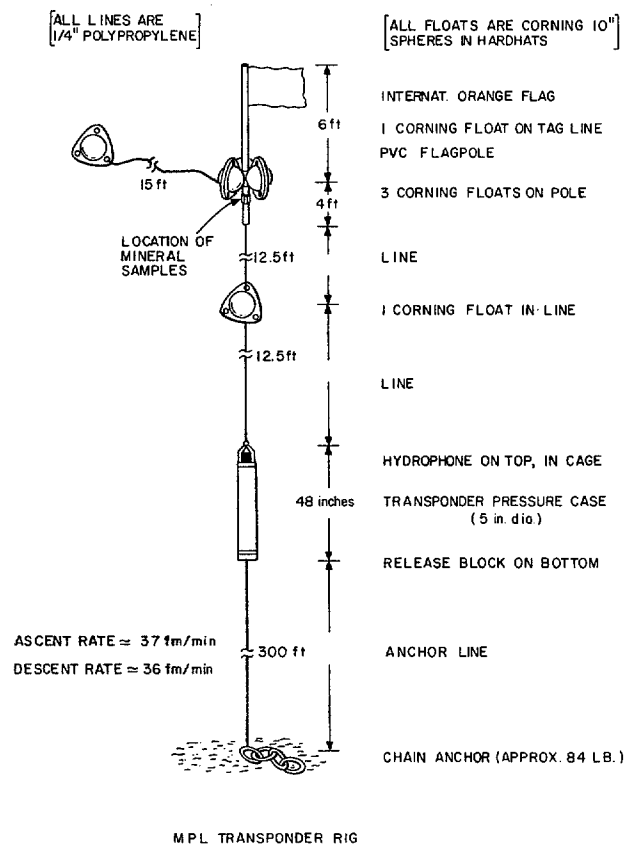

Figure 4. Location of the Mineral Exposure Experiment Attached to the Long-life Transponder Rig.

todorokite-bearing nodules at Site S occur at depths greater than the seafloors at Site M and Site H. Do todorokite and buserite decompose at these shallow depths?

To test this possibility, natural todorokite, and synthetic Na, Ca, Cu and Co buserites are being used. A sample of Na buserite contained in the capsule returned after 10 days when the Deep Tow survey of Site M was completed had not yet decomposed to birnessite.

(ii) Birnessite and Delta-MnO_2. These two minerals are most commonly reported in nodules from seamounts and shallow seafloors. Delta MnO_2 is also believed to be responsible for enriching Co in these nodules. Can the uptake of Ni, Cu, and particularly Co be induced in the two minerals over 2-3 years? To examine this possibility, synthetic Na birnessite and δ-MnO_2 devoid of Co, Ni and Cu are being used at Site M and Site H.

(iii) Iron Oxide Hydroxide Phases. Amorphous or crytocrystalline Fe(III) oxyhydroxides are intimately associated with hydrated Mn(IV) oxides (todorokite, birnessite, δ-MnO_2) in manganese nodules. Do these FeOOH phases have specific uptake and fixation properties for heavy metals in seawater?

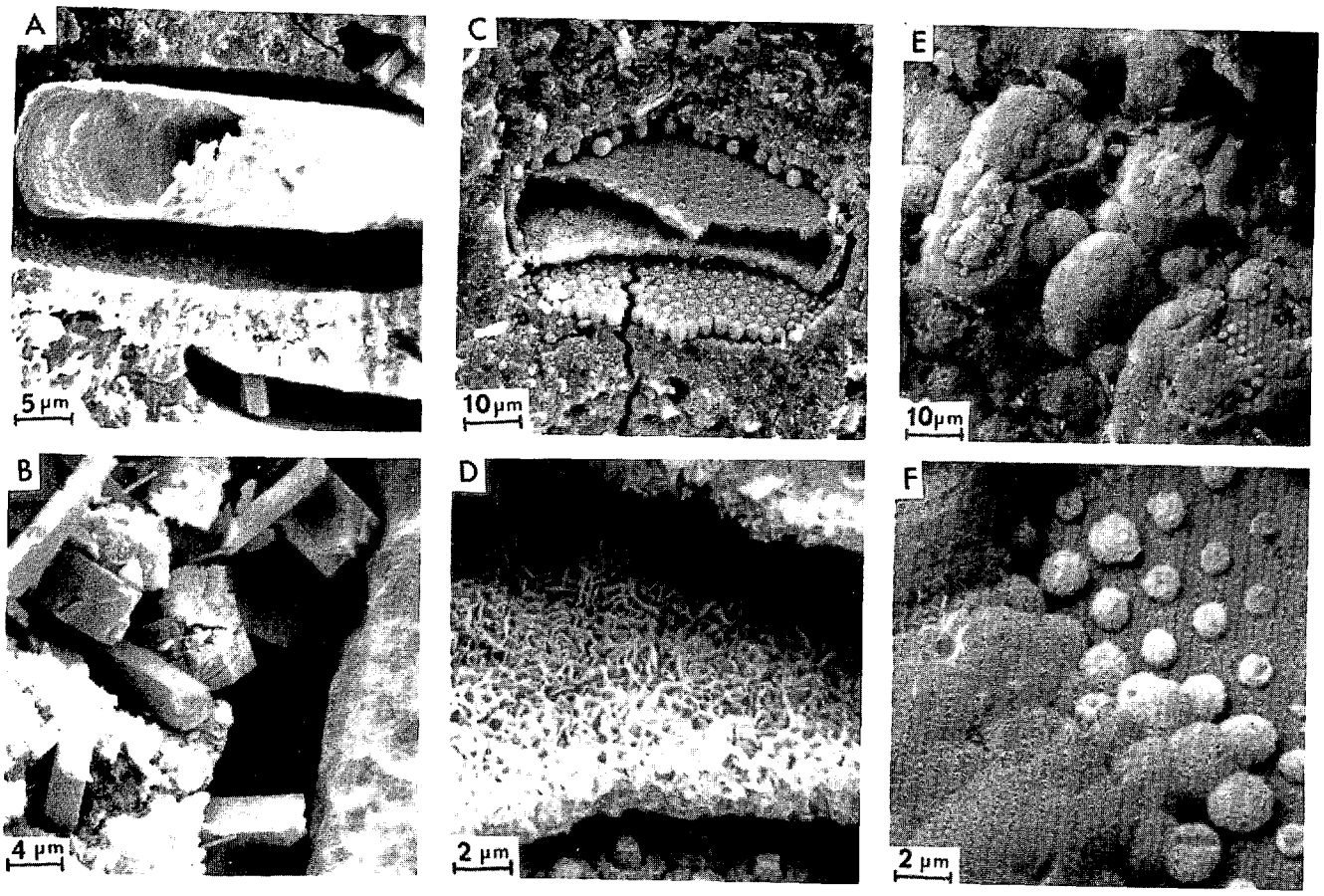

Figure 5. Scanning Electron Microscope Photographs Showing Post-Depositional Recrystallization Features Inside a Manganese Nodule from Site S.

A. Biogenic siliceous debris showing dissolution textures. Phillipsite crystals are forming in the leached regions;

B. Phillipsite crystals and clusters of todorokite crystallites growing adjacent to remnant siliceous debris;

C,D. Meshwork of todorokite crystallites containing Ni and Cu coating biogenic debris;

E,F. Clusters of todorokite enriched in Ni, Cu and Zn infilling voids where biogenic debris once occurred.

Dr. J. W. Murray (University of Washington) has supplied samples of synthetic α-FeOOH (goethite) and β-FeOOH (akaganeite) to test the relative affinities of these two polymorphs to absorb trace metals from seawater at Site M and Site H.

(iv) Nodules Atypical of Relatively Shallow Marine Environments. What happens to foreign nodules, such as a fresh water nodule (Lake Oneida, New York) and a Ni-Cu-rich nodule (Site S), when they are exposed to different aquatic regimes? We have encapsulated small slabs of each of these two nodules, which were characterized by x-ray diffraction, scanning electron microscopy, and electron microprobe analyses. We plan to investigate whether degradation of existing minerals occurs, chemical compositions change, and new phases nucleate on these manganese nodule samples alien to the environments at Site M and Site H.

(v) Mixtures of δ-MnO_2, FeOOH, Siliceous Ooze and Palagonite. The authigenic zeolite mineral phillipsite has been observed [9] by scanning electron microscopy in interiors of nodules from Site S, and appears to have formed adjacent to areas where extensive leaching of biogenic siliceous debris has occurred. Clusters of todorokite crystallites enriched in Ni and Cu fill fissures adjacent to the phillipsite, coat biogenic debris, and infill voids where biogenic debris once occurred in interiors of nodules. Examples of these features are shown in Figure 5. We have suggested that the post-depositional growth of phillipsite and the recrystallization of δ-MnO_2 to todorokite inside manganese nodules is promoted by the dissolution of biogenic siliceous debris and palagonite, and that FeOOH coating phillipsite and detritus forms a substrate for the nucleation and epitaxial growth of todorokite. To test whether any of these diage-

netic reactions can be induced, a mixture of δ-MnO_2, FeOOH, siliceous ooze and palagonite has been encapsulated at Site M and Site H. A similar long-term experiment is planned at Site S where the reaction is most appropriate during 1979-1982. The experiments at Site M and Site H are intended to be monitors for the later experiment at Site S.

(vi)Mixtures of Synthetic Mn(IV) Oxides and Transition Metal Salts. One of the objectives of the experiments listed under (i) and (ii) above is to measure the uptake of Ni, Cu, and Co from seawater into synthetic Mn(IV) oxides. However, the concentrations of these metals in seawater is extremely small. Can the uptake and fixation of transition metals be induced into synthetic Mn(IV) oxides under hydrostatic pressures and low temperatures prevailing at Site M and Site H? To examine this possibility, mixtures of $NiSO_4$, $NiCl_2$, $CoCl_2$ and $CuSO_4$ crystals have been encapsulated with synthetic Na buserite, Na birnessite or δ-MnO_2.

(vii) Other Minerals of Mn and Fe. One capsule left at Site H contains crystals of the following minerals: Rhodocrocite ($MnCO_3$), siderite ($FeCO_3$), manganite (γ-MnOOH), nsutite (Mn^{2+}, Mn^{4+}) $(O,OH)_2$. Oxidation of Mn^{2+}, Mn^{3+} and Fe^{3+} ions might be induced and measured at high pressures and low temperatures near the seafloor at Site H.

6. Future Experiments

Future mineral exposure experiments planned in collaboration with Dr. P. Brewer (Woods Hole) and Dr. J. Murray (Univ. of Washington) will employ a Honjo-designed titanium-bellows pump to increase and control the flow rate of seawater over the various Mn and Fe oxide phases. Such experiments will again take place deep in the water column, but last for shorter time periods (1-6 months).

More relevant to the environment of manganese nodule growth, however, are the additional natural flow-rate experiments being planned at the sediment-seawater interface at each MANOP site. Here, the plastic flow-through capsules will lie on the seafloor and be attached to the Bottom Lander or to anchors of transponders or sediment trap moorings. Such long-term in situ mineral exposure experiments, particularly at Site S, should provide a better understanding of the mechanism of uptake of transition metals into deep-sea manganese nodules.

Acknowledgments

We are grateful to Drs. P. Brewer, S. Honjo, J. Murray, F. N. Spiess, R. Collier, and R. Weiss for advice and helpful discussions, to Tom Harris and Sharon Witherow for assistance in deploying the mineral exposure experiments, and to Paul Gabriel for fabricating the plastic capsules. This research is supported by the NSF-IDOE (grant no. OCE-28480).

References

1. G. P. Glasby (ed.), Marine Manganese Deposits, Elsevier Publ. Co., 523 p. (1977).
2. S. V. Margolis and R.G. Burns, "Pacific deep-sea Manganese nodules: their distribution, composition, and origin." Ann. Rev. Earth Planet. Sci., 4, 229 (1976).
3. R. F. Weiss, O. H. Kirsten, and R. Ackermann, "Free vehicle instrumentation for the in situ measurement of processes controlling the formation of deep-sea ferromanganese nodules." MTS-IEEE Oceans 77, Conf. Rec., 2 44D (1977)
4. F. N. Spiess and J. D. Mudie, in: The Sea , (A. E. Maxwell, ed.), 4, 205 (1970).
5. R. G. Burns and V. M. Burns, "Mineralogy of Manganese Nodules". Chapt. 7 in Ref. 1, p. 185 (1977)
6. F. N. Spiess and J. Greenslate, "PLEIADES expedition leg 04,Mn-01, RV Melville preliminary cruise report." Scripps Inst. Oceanogr. MANOP Tech. Rept. 15, 87p. (1976)
7. F. N. Spiess and P. Lonsdale, "INDOMED expedition leg 01, Mn-OZ, RV Melville preliminary cruise report" in preparation.
8. S. Honjo and J. Erez, "Dissolution rates of calcium carbonate in deep oceans: an in situ experiment in the North Atlantic Ocean" Earth Planet. Sci. Lett., in press (1978)
9. V. M. Burns and R. G. Burns, "Post-depositional metal enrichment processes inside manganese nodules from the north equatorial Pacific." Earth Planet. Sci. Lett., in press (1978).

"MOBILE INITIAL CONDITION INDICATOR", A DYNAMIC APPROACH TO MARINE EXPLORATION

Lawrence H. Befferman
President
Em-Log Enterprises
3316 Colden Avenue
New York, N.Y. 10469

Abstract

Changes in procedure have been initiated to increase the effectiveness of search vehicle operations. Many of the routine functions that were previously done at the surface are now being performed during active exploration. A "Mobile Initial Condition Indicator" MICI continously tests for mineral concentration in four uniquely constructed sampling tubes. The concentration in each is determined by precise chemical measurements. Any differences in content between the four tubes are monitored by computer which then provides data to the control system. The computer is capable of deciding whether the level of concentration is increasing at a rate that indicates deposits of commercial value to be within the submersibles range. This results in an ability to make decisions concerning mission parameters based on actual condition at the time of sampling.

1. Introduction

A "Mobile Initial Condition Indicator" MICI is a vehicle designed with search features that can save costs of exploration. It's description will follow a detailed survey of how valuable concentrations of minerals give off tracers that an MICI was designed to follow. Although much heralded, the production of valuable heavy minerals from the sea floor such as ilmenite, rutile, zircon, tin, monozite, iron, gold and diamonds, is relatively small, probably under one hundred million dollars per year. In many of these examples, the economic placer deposits of the minerals lie within a few km of the original igneous sources. Unfortunately, exploration to date has not been very successful in locating such igneous sources. Sediments have been able to mask the underlying volcanic relief in a few centuries. An MICI is designed to locate placer deposits of valuable minerals on the sea floor.

Just as non-conventional sources of energy are becoming economically attractive in the late 1970s because of rising prices at conventional sources, the ocean's mineral reserves will become more attractive as land-based materials shortages developed, thus driving prices up, i.e. the costs of material recovery must compete with high grade deposits found on land. Hydrocarbons (natural gas and oil) from the continental shelves are one ocean resource involving retrieval and exploitation that is in response to the relative economic forces. In addition to minerals located beneath the sea floor, seawater contains compounds of economically valuable elements such as magnesium, bromine, molybdenum, uranium, gold, silver, lead, copper and many others. Many of these elements are presently being extracted on a commercial scale while others are present in such low concentration, or if not, present such process difficulties, that no economical method of extracting them has yet been developed. Because of uncertainties in choosing specific elements for production, an MICI is designed to provide an accurate description of mineral or element concentrations at the chosen site.

As a consequence of the mixing processes of the oceans, trace elements are dispersed or fractionated in the course of these geochemical actions. They become distributed among phases of which they are not the essential constituent and which they did not create. These trace elements serve in their turn as tracers for the geochemical phenomena. It is similar to the process of erosion of rocks throughout geologic time, which has brought innumerable mineral deposits into the oceans by streams and rivers. The function of an MICI is to detect these trace elements and follow them to their source.

The oceans of the world are being extensively explored, and many years of recording and sampling reveal vast potential mineral reserves. Because of this, exploration efforts of governments and private interests are receiving high priority. Improving search vehicle performance is an essential part of these priorities. The detection equipment on these vehicles must be such that venture capital has assurances of sufficient mineral quantity to be economically removed, i.e. as the ability to discover areas of high concentration improve, the greater these assurances will be. An MICI supports the requirements of such commercial ventures. It assures accurate parameter information concerning mineral concentrations so that cost effectiveness studies aimed at determining the trade off between the value of a specific mineral find, and the costs to mine at that depth, are realistic.

2. Locating mineral concentrations with an MICI

About sixty of the first ninety elements in the periodic table have been detected in sea water. The major constituents are compounds of sodium, potassium, magnesium, calcium and strontium. Other compounds are sulfates, chlorides, bromides, fluorides, carbonic and boric acids. They are found everywhere in the ocean in virtually the same proportions. This makes up almost all the total dissolved salts. The minor constituents are all the rest of the elements. They in turn can be separated into conservative and nonconservative elements. The conservative elements, like the major constituents, are found everywhere in constant proportion to the total salts. The non-conservative elements show a variation in their relative concentration. All elements are recorded in terms of average concentration when describing their abundance in sea water. (the elements range from an average of twenty thousand PPM for chlorine to one part per billion billion of radium). The function of an MICI is to decern a variation or anomaly in these average concentrations, especially in the non-conservative elements. There are differences between the specific non-conservative elements found in coastal waters and deep sea.

At present, statistics show that exploration activity has been intense at the continental shelf and rise within less than 100M depth of water. This coastal area is only a small percentage of the ocean floor. There are many reasons why this activity has been justified. Cost of recovery is an important factor, and mineral concentrations are greater in this area of ocean floor due to the influx of eroded land materials. In addition, waters close to the continental shelf contain more suspended matter because of greater current action. The total quantity of suspended materials in various areas of the ocean is well documented. This data is used in certain calculations, however, the concentration of the mineral and particle size significantly effect the vehicles search coordinates. Lying near shore areas along the coast line are economic concentrations of minerals commonly found in land placers. They offer the advantages common to land placer deposits in that nature has provided the necessary liberation action of crushing and grinding with a degree of sizing and concentration. Concentration results when the waves reach out and carry the low specific gravity minerals out to sea. Precious metals survive attritional chemical weathering, and will concentrate in shallow coastal waters. Similarly, all minerals have areas of high concentration throughout the world because of many factors such as rivers, volcanic activity, friction of currents passing over the bottom causing turbulence, etc. These various processes lead to the transport and mixing of minerals in waters of the sea. With each change in the mineral of the sediment, changes in element ratio of the surrounding water takes place. Traveling over distances in a search vehicle confirms the great variability of the sediment on the sea floor. Although this research is extensive, very little is known about the formation of minerals on the sea floor by the diffusion and absorption of elements in and on sediments. In a study of waste disposal on continental shelves it was assumed that canyons are natural conduits to the deep ocean basins and hence ideal depositories for refuse to be carried away from the coasts. However, current and sediment transport studies made by submersibles suggest the existance of significant transport at times up the canyons, as well as down. An MICI adjusts for increased off-shore currents or concentrations of suspended materials, i.e. titanium in combination with magnetite and most iron silicates are found in depths characteristic of coastal waters.

At one time the deep sea was thought of as a flat expanse. It is now understood that the historical topography is at least as complex as the continents. There are innumerable sea mounds from volcanoes, faults or trenches dissect the sea floor, magnetic anomalies indicate complications in the rocks, denuded oceanic crust is bared by continental shift, and many more geologic formations are found in the ocean basins. Turbidity currents transport sediments considerable distances from the continental shelf. Also volcanoes introduce many trace elements into sea water. The suspended gold content is 3.4 PPB but if this increases, it suggests a volcanic source. In the area of volcanic ridges, there may be considerable variations in the nickel, copper and cobalt content of nodules over a distance of a few miles. What causes these rapid variations in composition is not fully understood, i.e. there may be ten layers of rock in one area and one layer in another close by. Earthquakes fault rock, allowing escaping minerals, MgO, FeO, Fe_2O_3, Al_2O_3, CaO and Na_2O are some of the mineral released by deep faults. There are networks of currents interlacing the worlds' oceans. The continual motion of the sea, horizontal, and to some extent vertical, blend and stir the minerals. Where the currents are most active such as the gulf stream, enormous amount of minerals are carried and deposited over great distances. Upwelling is a process of mixing in the marine environment by which subsurface water is displaced toward the surface. It is believed to be caused by a junction of deep and diverging currents. An important factor in this motion is that it sometimes creates a concentration of salt in the surface area above a mature sub-sea dome which often contains Petroleum, gypsum and sulfur. The last major method of deep sea mineral dispersion is marine life. Analysis of trace constituents of sea water such as nitrogen, phosphorous, iron, copper and manganese indicate these to be essential micronutrients. Because of enrichment by marine life, concentrations of 1.0 - 6.0 PPM of silver in certain areas is thousands of times greater than the expected average sea water levels.

In exploring the continental shelf and deep ocean, very little work has been undertaken to establish the extent of local variations in the grade of materials. Ingeous and metamorphic rock have been found to contain veins of massive

deposits of nonferrous and precious metals. Also, valuable minerals have been washing into the sea for millions of years collecting in oozes, clays, and sediments, sometimes concentrating in rich deposits. When considering the basis for most studies on deep sea sediments, wherein relatively few sample are randomly collected, and the extrapolation of data over great distances is commonplace, information from many of these investigations are incomplete. An MICI is a vehicle designed for the complex processes and variations which are the rule rather than the exception. When selective samples are taken continuously, an appreciation is gained for such things as (1) sporadic concentrations of material and (2) transport as influenced by local features. In interpreting analysis of surfaces and suspended materials, careful considerations have to be given to the entent to which their original composition may have been altered by deposition and assimilation of current borne material. The MICI provides a continuous plot of data in which decisions are made from small differences in the nature and magnitude of agents or processes at work on the sea floor, i.e. concentrations of manganese deposits have to do with water motion in areas of vulcanism and proximity to dissolved manganese. The MICI can make decisions on location as to changes in scope and plan of observations especially in the dynamic process of the mineral search. The economical use occurs when a contact is made and the vehicle provides unparalleled control in the direction of the mineral buildup toward the source.

The ability to collect samples from precise sites relative to one another is important. This insures that anomalous features are considered in perspective and can be judged as significant. It is possible that attempts will not yield economic concentrations from areas selected. At times, an increase in measurable materials does not result in locating an area of abundant particles which are a desired size. These occurrences are minimized, however, because (1) computer comparisons of instrument response in calibrated samples and actual samples and actual samples of various sizes, (2) rapid recognition of potentially valuable materials, (3) use of mathematical methods which will predict distance of an economic concentration, and (4) computer interpretation of compounds which have previously resulted in locating elements of commercial value. In these areas an MICI conforms with the latest design features of submersibles because it is a fully integrated system which insures a high effective utilization rate.

3. Design and method of operation

An MICI can operate as a tethered deep submersible vehicle with a line supplying information to a surface computer, or a vehicle with a crew for increased capability. It is a self-contained laboratory whose function is to reduce the search area by specifically directing the location of test samples using constant instant analysis. The unexplored ocean is vast, and present day techniques of exploration involves a method of random sampling procedures which are costly and time consuming. As mentioned in the introduction, platinum, oil, gold, etc., deposits are localized in the ocean and a sample could miss an important find. A "hit" may be a matter of luck. In addition to detecting desired elements in solution and sediments, an MICI can navigate in the direction of increasing concentration. The series of measurements is based on analyzing a constant flow of data, much as a geiger counter provides increased pulse frequency for identifying the mineral, and its best approach. The vehicle computes direction based on strongest element concentration or their compounds. Calculations of the variation in material distribution is then precisely made. Use of precise chemical analyzers, precipitation devices, computer statistical computations and other tests in detecting material presence, directs the MICI toward mineral deposits when contact of a slight quantity has been made.

The basic configuration is composed of four main hollow feeder tubes containing some of the detection equipment, and which eminate from corners of a square plate. Each tube continually processes the samples and analyzes them. The chair-like assembly is attached to the deep submersible through seals in the hull. An MICI vehicle is best described as having the appearance of a large four-legged stool which has fallen on its side and attached in this position to the forward section of the submersible. A continuous sample analysis is supplied to a computer which provides coordinate data to thrusters capable of propulsion in all directions. Any gradient in mineral concentration between the four tubes at time of contact results in direction change. Vehicle motion is directed toward the side containing higher concentrations of desired mineral. This "pointing" effect is unique in present deep submersibles. Each of the four feeder tubes have smaller perpendicular sampling tubes along its length which are arranged to receive samples of less quantity. Holes in the grid like smaller sampling tubes allow water near the sea bed surface to be drawn in, or expelled simultaneously, or individually, when analysis is completed, by a pump located in the vehicle. A laboratory test was recently performed to locate a small amount of copper in a vat of salt solution. Using probes as feeder tubes, laboratory equipment detected the distortion by the sample of an electric field introduced in the vat. This was translated into coordinates and the samples location was determined. Laboratory equipment is now sufficiently sensitive to detect differences in mineral concentration within several meters, or as little as a teaspoon of a substance in twenty cubic miles. In an area of highly localized mineral deposits, the surrounding water contains trace quantities in solution, although oozes and other surface debri are present. Rods on the bottom and sides of an MICI are used to agitate the sediment or canyon walls at a promising location. If a mineral concentration level exists in sediment, samples brought up by agitating the surface will show increased materials in the lower tubes as

sea water is swept past, i.e. slightly more material in one tube, whether it is in a side, upper or lower tube, will cause the vehicle to proceed in that direction.

A partial list of equipment that can be used for sea water analysis, and whose accuracy is within detection requirements of an MICI are: atomic absorption spectrophotometer which is used in research of trace or ultra trace metals and water pollution investigations of trace hydrocarbons and petrochemical substances, gamma ray spectrometer for discriminating uranium potassium and thorium minerals from non-economic gamma ray sources, x-ray fluorescence spectrometer which is second to the wet chemical methods in determination of trace elements especially above sodium in the periodic table, and the gas chromatographs which are presently used in chemical analysis research. These instruments can detect um size particles, weighing a mg, in concentrations of 0.002 ug/ml for silver and 0.005 ug/ml for potassium with 95% certainty. Some have the capability of detecting pg weights of many elements. Vehicle velocity relative to water current must be integrated into the computer for a navigation position fix at regular intervals. Doppler-sonar beam patterns can be used to determine speed directly and frees dead reckoning calculations of accurate current measurements. The computer continuously generates ship position in this working coordinate system. Gyroscopes measure roll, pitch, or heading angles, and with supplementary sensors depth, altitude, and water current speed can be calculated. This is an important factor in navigation since six degrees of freedom must be present for response to the complex search pattern. Simultaneous operation of all thrusters, (these are fixed or tillable design arrangements) is very difficult without automatic propulsion control when heave, yaw, and surge is included. The computer acts through analogue and digital I/O buffers to a control display unit with data storage and finally to activators of solenoid servo-valves for speed or direction control. The building of a mineral in one feeder tube gives digital information to its thrusters speed control by increased signal strenght. Obstacles in the path must be detected and avoided. Constant and close surveilance of the forward and side looking sonar transducers are used to anticipate terrain variations and to avoid obstacles. In addition, depth and altitude sonar transducers also supply information to the computer when search patterns are required in the cruise mode. This occurs when samples are showing constant concentration in each tube. The search pattern requires traveling in a spiral and alternately ascending and descending in altitude to insure an acceptable probability of detection. Weight, dimensions (large feeder tubes are 8m) and vehicle power depends on the equipment included, i.e. specific chemical analysis equipment use high power for burning, and ventilation would then be required. It can be seen that the search features of an MICI is automatically controlled and entail a highly integrated system. For this reason, display and manual control equipment is essential if this configuration requires over-ride in any mode.

4. Central computer and mathematics

All search functions are led entirely by computer. Automatic control includes sampling, analysis of data, direction of vehicle and storage of results. An auto-sampler directs valves in the large and small feeder tubes to inject surrounding water into the analysis equipment. The sample is then expelled or portions stored in accordance with a sequence of timed events in the computers memory. Hundreds of method files control complex analysis at regular intervals, including calibration of equipment and comparing samples against standards. The computer performs all curve fitting calibrations by determining mean value, standard distribution, sensitivity, detection limit parameters, and choosing maximum precision method for the specific elements in order of increasing concentraion. The on line data acquisition and processing is "hardwired" in ROM, assuring that accidental erasure is not possible during real time computation or changes in mineral information. Hundreds of samples are processed unattended, however, it is possible to override preset handling and analysis control functions. Following analysis, output is recorded on an electrostatic printer/plotter and visual display terminal. These recorders have a multiple input range and can log many measurements in concentration unit format per second. It also includes automatic error diagnosis in post-processing and a warning signal or cycle shutdown if comparisons between the program in memory and actual data differ due to a blocked feeder tube. A library of stored and blank magnetic cards with reader is required for particle size, count, and weight of the various elements. The central computer directs the results of these multi-element analysis to the propulsion system. It performs the necessary integrations to overcome non-linearities due to buildup of minerals in one feeder tube over another by the action of currents and speed. A further function is the manner in which sample parameter selection takes place, i.e. an element is instantly expelled after analysis; it is allowed to remain in a storage tank of the large feeder tube if samples contain very small quantities of desired element; test time is varied if detection threshold to noise ratio is excessive. Only peaks that pass a test for slope, width and shape as compared to an internal standard are stored. Finally, a quick look capability is provided, which offers a check on instrument analytic accuracy, presence of redundant data, and whether go-no go commands are initiated for anomalies.

The complexity in reduction of data from these scanning modes, requires statistical formulation. The mathematical model of the computer program is a matrix designed to establish priorities in seconds. Decisions to redirect the search as anomalies are observed, must be made continually. When a feeder tube indicates a mineral increase, the programmed search pattern may be halted. This decision is based on a formula that predicts the probable distance of an economic

concentration taken from the first five or six data points. A modified Weibull distribution is used for the cumulative function. Inherent in this formula are the properties of a growth curve, that is, a function which is always increasing, but approaches some maturation level asymtotically. Construction of the preliminary curve consists of plotting the ordinate P (particle of average size at each sample interval), P0 through P6. The abscissa is represented by d, 6 samples equally spaced between d0-d6 corresponding to P. The least square method of optimum fit is applied to the formula $P=PC-Ne^{-Kd}$, where PC= largest predicted particle size (P can also represent weight or count) and where constants N, K are within specific confidence levels obtained by computer minimization techniques. This brief description indicates that the computer is programmed not to proceed in the direction of a material which is predicted to lie outside the vehicles range, since currents may have carried the mineral hundreds of km. In addition to this computation, the computer must consider whether the mineral or element is worth investigating on economic terms, even when the deposit appears to be within a realistic distance. A third major factor is whether the compound is a species common to the waters or not valuable as a tracer. Boron's main dissolved species which is common to all oceans is H_3BO_3 and $B(OH)_4$, aluminum $Al(OH)_3$ etc.. There are, however, hydrogenous components that create compounds not common to all waters and which empirical evidence has shown are valuable indicators of nearby deposits. The three factors (distance, worth, tracer) are interrelated and must be balanced to assure an effective search pattern. The computer considers these in terms of ratios, and as such, the probabilities are multiplied, not summed, when an optimum is desired, i.e. the cost effective probability of the search. An MICI central computer is required to furnish solutions for many facets of the vehicles operation. Other functions that will assure mission success involves display of vehicle performance, and a potential hazard warning system. The computers function is designed to analyze data at the time of occurrence without surface support for optimal vehicle utilization.

5. Summary and conclusion

Sedimentary red clay, globigerina, distom and radiolarian ooze which are sometimes of value themselves, cover deposits of oil, gas, sulfur, coal, iron, etc.. Iron and coal are being mined while drilling rigs remove oil, gas and sulfur at off-shore sites. Deep ocean basaltic rocks contain chromite, platinum, etc., and loosely consolidated chemical precipitates of manganese, nickel, copper, cobalt, cover the surfact. These valuable mineral deposits, and many more, present a persistent case for supporting a fully integrated exploration vehicle that can cut search time significantly, by tracing elements to their highest concentration. An MICI makes use of a unique design concept which also utilizes the computers computation speed to control state of the art scientific equipment. The complex environment of the oceans requires technological precision on this level. A prototype of the vehicle design is undergoing testing, and extensive appraisal of results in both laboratory and sea water locations indicates excellent conformity to performance requirements. In the laboratory, precipitation equipment which can perform electrolytic filtration, solvent extraction, ultracentrification, and magnetic separation are being used to prepare samples for element analysis. Several of these equipments will be chosen for use in the large feeder tubes. Also being tested in this location are three units common to most submersibles, an interferometer index of refraction, salinometer, and a unit for conductivity measurements. Each of these will have their own water storage tank where sample accumulation is desired. In an unmanned submersible design, many analytic functions are possible, i.e. detection of indicators such as iron, gas seepage, or the radio-active decay tracers, uranium and radium. However, several sophisticated chemical analysis units require human interpretation. The spectrophotometer involves statistical computation in measuring some trace elements, and wet chemical methods are often visually oriented. The last phase of actual sea water testing presently being undertaking, involves procedures for dividing, storing and defining the level of concentration or dispersion of trace minerals. These definitions involve automated analysis routines for determining variability; the standard deviation and variance of the sample distribution.

The rate at which man is using many minerals is placing a heavy demand on present land sources. Eventually the production of ocean reserves will be required to augment supply. Commercial ventures specializing in recovery of deep sea minerals must be assured a high concentration level. An MICI will direct the search operation toward such a deposit, and map the size so that realistic estimates can be formed as to its value.

References

1. Deep Sea Sediments, edited by Anton L. Inderbitzen, Plenum Press, New York 1974

2. The Persian Gulf, edited by B. H. Purser, Springer Verlag 1973

3. Introduction to Marine Chemistry, J.P. Riley Academic Press 1971

4. Submersibles and Their Use in Oceanography and Ocean Engineering, Richard A. Geyer, Elsevier Scientific Publishing Company 1977

5. Heavy Minerals in Alaska Beach Sand Deposits, Donald J. Cook, Mineral Industry Research Laboratory - University of Alaska College, Alaska 99701

6. A.I. Tugarinov, Recent Contributions to Geochemistry and Analytical Chemistry, Keter Publishing House, Jerusalem Ltd. 1975

7. Modern Method of Geochemical Analysis Wainerdi, Plenum Press 1971

8. Introduction to Geochemistry, C.J. Allegre D. Reidel Publishing Company 1974

9. Handbook of Geochemistry, Springer-Verlag Berlin - Heidelberg, New York 1972

COMPREHENSIVE OCEANOGRAPHIC MONITORING PROGRAM IN THE ARABIAN GULF

C.S. Ahn, Ph.D.

KSEC, Executive Consultant
2700 Kennedy Blvd., Jersey City,N.J.07306

Abstract

In contrast to the significance of industrial expansion in the Arabian Gulf region, this part of the water body is least understood scientifically. Obtaining a complete spectrum of oceanographic and water quality data is very important for planning and development in the fast growing industries in this region.

Several instrumented offshore monitoring stations are established to measure current, temperature,conductivity,wind,DO,PH,and chloride. Each monitoring platform contains sensor instrumentation,data processor and telemetry unit. The Central Station serves to interrogate and control timing,sampling and data quality via the shore stations. The received data is logged on an IBM compatible 9-track tape recorder,which is played back,displayed or analyzed through computer.

The integrated technology of the real-time data acquisition system ,the state-of-art knowledge of the oceanographic process,and their industrial applications in the Arabian Gulf are discussed.

1. Introduction

The Arabian Gulf is one of the fastest growing industrial regions and plays a vital role in world economics. Despite its industrial significance,the water body of Arabian Gulf is little understood scientifically. The effective utilization of coastal areas for industrial development,coupled with the need for environmental protection, has necessiated a systemetic integrated approach of oceanographic study in this region.

Coastal processes in the Arabian Gulf are very complex due to dynamic interactions of many different factors(1) over wide temporal and spatial ranges. This complexity requires the identification of important parameters and interactions between data gathering and predictive techniques. Mathematical models are a cost-and time-saving tool where only a limited amount of field data is available. Such a model (1) will lead to prediction of industrial waste dispersion, drifting oil spills, coastal erosion and harbor protection.

2. System Approach

Although there are fragmented studies as needed, a complete understanding of oceanographic processes in this water body is a far -reaching goal. Due to constraints of trained manpower, difficult operational environment,and budgetary consideration an integrated system approach is needed to reach this enormous scientific goal. Relatively little oceanographic data are available in the Arabian Gulf region. Only wind data have been adequately summarized. Most data are spotty samples over short periods which reveals a lack of coordination and regularity.

Therefore, the first important task is to obtain reliable,meaningful oceanographic data. Oceanographic processes in this region results from the complex interactions of many different factors(1) such as macro-scale circulation, tidal oscillations,wind stress,surface and internal waves ,density gradients, precipitation,evaporation, and various radiation processes. Economic factors impose limitations on oceanographic measurement system so that complex phenomena should be understood based on a limited number of measurements of a few physical parameters. The detailed planning for implementation of adequate data acquistion systems is a very important phase of the total program. Furthermore, the mathematical modeling efforts should be tightly coupled with this field measurement program.

An overall system perspective should be adopted to ensure that essential subsystems are consonant with each other. A reconnaissance survey of the regional area will be accomplished in search of general phenomena and establishment of topographic features. Updating aerial photographs and utilization of observational satellites will provide adequate information for changes of urban development,recent construction, coastal erosion and sedimentation. Intensive surveys will be applied subsequently to define areas of particular interest such as industrial development sites. This data will help in a general understanding of oceanographic processes and will verify the numerical prediction model. Ocean boundary conditions such as mass flux and tide are relatively easy to establish in the Strait of Hormuz. Utilizing the current and tide at the ocean boundary and the wind data in the inner region, the general circulation pattern will be predicted in the Arabian Gulf. Such a model will facilitate an understanding of the pollutant dynamics in the Gulf region and will eventually be applied to planning for industrial expansion and environmental protection.

In order to achieve scientifically valid data and a better understanding of oceanographic process, the following system concept is emphasized.

Extensive sensing of important parameters,

- Acquisition of synoptic real-time data,
- Cost-effective utilization of data sensing, processing,and storage,
- Efficient computerized technique for realistic numerical simulation.

Program Tasks	Scientific Objective
A. Oceanographic Field Experiment:	
1) Intensive platform monitoring in the inner part:	Establishment of temporal pattern of important parameters in key area.
2) Vertical profile of current,temperature, salinity and tide in the Strait of Hormuz:	Establishment of boundary conditions at ocean boundary for math model.
3) Aerial photograph and Remote Sensing:	Synoptic coverage of general phenomena and topographic features.
B. Data Processing and Analysis:	
1) Data acquisition and management:	Storage in computer compatible format.
2) Data manipulation:	Compute statistics and provide graphical display.
3) Data analysis:	Scientific interpretation provision of input data for math model.
C. Numerical Predictive Model:	
1) Development of hydrodynamic model:	Prediction of circulation pattern by one or two layer model.
2) Development of Dispersion model:	Prediction of specific pollutants (thermal, chemicals,oil slicks).

3. Oceanographic Monitoring Concept

1) Overall System

A real-time oceanographic data acquisition system is initiated by KISR(2) which involves an integration of modern marine technology and proven concepts. These concepts are refined and applied in such a way as to achieve realistic data collection in the Arabian Gulf and in particular in the near-shore Kuwait area, providing a logical, expandable capability in anticipation of a broader range of requirements. The data acquisition system with the latest developed oceanographic instruments is installed on the monitoring platforms to provide real time oceanographic and environmental data.

Each oceanographic monitoring platform contains sensor instrumentation, and an in situ processor and telemetry unit. The RF telemetering link is provided between the monitoring platforms and the local shore station which collects,checks,and stores data on a magnetic tape. The central station,via the shore station, serves to interrogate and control the timing ,sampling and data quality.

2) Measuring Parameters

Each monitoring station consists of the following parameters:

Current Speed:	2 levels every 30 min.
Current Direction:	2 levels every 30 min.
Water Temperature:	2 levels every 30 min.
Conductivity:	2 levels every 30 min.
Disolved Oxygen:	1 level every 1 hour.
PH:	1 level every 1 hour.
Chloride:	1 level every 1 hour.
Wave Height:	@ 20 min. continuously every 6 hr.
Wind Speed:	1 level every 30 min.
Wind Direction:	1 level every 30 min.

3) Functional Requirements

The conceptual aspects of the functional requirements of the overall data acquisition system are:

- Proven oceanographic and water quality sensors are installed at the various monitoring stations in accordance with the scientifically recognized standards.
- Parameter accuracy is ensured by analogue to digital conversion directly at the monitoring station using a binary format of sufficient bit size. The accuracy of output data is limited only by the sensor itself and no data degradation will occur in transmission and recording.
- A common data format will be used at all monitoring stations ensuring efficient data merging and processing plus equipment interchange-ability in the field.
- Current speed and direction are sampled once per second for a 2 minute duration and vector averaged by means of the micro-processor. Burst average data are available in the "real-time" operating mode and for the specified 30 minute current reading.
- Because of slower fluctuations of temperature and salinity(conductivity) they are sampled every 7.5 minutes with four readings averaged to obtain 30 minute averages. They are formatted along with current data and these readings are available on demand for the real-time mode.
- Wind speed and direction are sampled at 7.5 second intervals to properly average fluctuations caused by buoy motion and are vector averaged over 30 minutes as with current readings.
- The water quality data (DO,PH,chloride) are converted analog to digital every 7.5 minutes in the normal mode and the average of these four data points for each sensor are transmitted to shore station along with other oceanographic data.
- The wave height sensor is scanned at two samples per second for 20 minutes continuously every 6 hours which is transmitted to shore station via telemetry link and stored on magnetic tape.
- Proven telemetry concepts are used at all monitoring stations,the shore station and the central base station.
- Reliability of data acquisition plus assurance of a common time frame are maintained by independent time keeping.

4) Telemetry System

The telemetry system handles all communications among the monitoring stations, the shore stations and the central base station. It is a crucial link in the performance of the data-acquisition system. There are two basic paths from the monitoring platforms to the local shore stations and from the shore station to the central base station. The central base station transmits control signal to the shore station. The shore repeater station retransmits control signals and receives data from the remote ocean monitoring stations. Use of the repeater station at shore allows low power transceivers to be employed at the ocean sensor sites which provides large cost savings both in capital equipment outlay and in operational costs. Frequency modulated transceivers provide greater noise immunity than amplitude modulated transceivers. RF power output of the

remote transmitters can be adjusted for optimum communication and power conservation.

4. Ocean Monitoring Platforms

The major concerns for selecting platforms are;

- Platform ruggedness and long term survivability,
- Minimum distortion of sensing instruments due to dynamic environmental effects,
- Flexibility and adaptability to changing program requirements,
- Transmission reliability, and
- Cost.

Two types of oceanographic monitoring platforms are chosen;

1) Surface Buoy Station

Surface buoy provides oceanographic and meteorological sensing stations where real time data can be acquired continuously and transmitted to the shore station. The surface buoys are stationed with a taut line mooring with housing for a sensor interface device, power supply and telemetry tube. An integral tower provides for the required positioning of meteorological sensors, telemetry system and navgational light,as well as the solar panels. Data retrieval and operational service are easily done from the surface buoy. The surface buoy is subject to continuous stressing of the buoy system due to wave action,although it meets sensing requirements, telemetering and easy service.

2) Subsurface Buoys

Subsurface buoys are inexpensive and minimizes dynamic effects,such as winds and waves, to mooring cables and instruments. Majority are subsurface buoy systems except those requiring meteorological sensing instruments. The spherical subsurface buoy,taut moored to the bottom, is quite stable,reliable and a proven underwater platform for the oceanographic data acquisition system. The mooring lines can be easily extended to any depth of water if measurement locations are changed in future. The response of this subsurface system to wave action and high current flow has been investigated and found to be minimal.

5. Control Stations

1) Central Base Station

The central base station is the major facility of monitoring control,data acquisition,processing and analysis. It initiates the action of the Remote Control Units, synchronizes the sampling networks, gathers the data from RCU's on a preset schedule, stores the data on a disc, prosesses and subsequently analyzes the data. It controls also quality of data, prints the received data on demand, and produces a permanent data archive onto IBM compatible magnetic tape. In summary, the central base station serves the following;

- Control the ocean monitoring stations and local shore station,
- On-line and off-line data processing, and
- Quality control of data.

The data control consol consists of the following modules;

- Digital clock including day counter,
- Ocean monitoring station generator,
- Telemetry data recovery module,
- Tape recorder (9-track IBM compatible),
- Data display panel, and
- Transmitter-receiver control panel.

2) Local Shore Stations

Data from each ocean monitoring station are transmitted sequentially to the local stations established at the shores. It could be established at the existing industrial facilities or mobil stations at the remote areas. The local shore station receives data and transmits to the central base station. At the same time, the data received from the ocean monitoring stations are recovered and used for local display for diagnosis. The data are logged also on a 9-track IBM compatible tape recorder as a backup for the shore-central station radio link.

Normally all control of the ocean monitoring station is achieved under the direction of the central station. However, for trouble shooting or in case of shore-central RF breakdown, all ocean station control can be handled by the shore station. The remote readout contains its own receiver which feeds the computer summaries to a printer and optimally to a CRT display.

3) Data Processing and Analysis

Many types of data are gathered in myriad formats and with a wide variation in regularity and periodicity. The unassessed data should be processed into the format most useful for subsequent. analysis. Frequently there is an overemphasis on producing (collecting) data and underemphasis on putting data into usable format.

Collecting and processing voluminous data of many types requires a specialized discipline (data tech or system analysis). Rapid recognition of common patterns, general trends and statistical analyses are to be conducted systematically in conjuction with computer generated graphical display (3) which makes scientific interpretation significantly easier. Such expensively collected valuable data ought to be utilized for multi-purpose (3&4) in the most efficient manner.

6. Physical Environment

The Arabian Gulf (5) is a shallow semi-enclosed sea in a highly arid climatic zone. The strong evaporation exceeds the precipitation which accounts for high salinities in the inner part of the Gulf. A deep-reaching thermo-haline convection of high saline water outflows in the bottom layers through the Strait of Hormuz. In the middle part of the Gulf the isohalines tilt as do the isotherms. The system of surface and bottom currents is further complexed by the transversal direction of the monsoon in the region which yields eddies with large fluctuations for different seasons and years. From the estimation of annual evaporation and salinities of the inflowing and outflowing waters, the average current velocity of the outflowing bottom water is in the order of 10 cm/sec and is therefore significantly below that of the tidal current which are in the order of 50 to 100 cm/sec. The stratification in the Strait of Hormuz may not be limited to a double layer. The water from the Gulf of Oman flows mainly off the Iranian coast whereas the deeper outflowing water moves over the Arabian shallow shelf according to the Corilis force.

Excess of evaporation over precipitation also causes a lowering of the sea level of the Arabian Gulf and,as a result, a strong surface current of

about three knots flows into the Gulf through the Strait of Hormuz. This current generates a weak counter-clockwise gyre in the surface waters of the Gulf and a compensating outflow of high salinity water at deeper levels.

The tides are basically a combination of diurnal and semi-diurnal features ranging from 1½ to 4 meters. The tidal range is least in the center of the Gulf, about 1½ meters. At the eastern and western ends of the Gulf the tidal range is greater. The corresponding tide range at the northwest end is about 2½ meters, and the section between Dubai (UAE) and Lengeh(Iran) ranges from 3 to 4 meters.

The summer months are uniformly hot with only weak northerly winds and almost no precipitation. Sea temperatures rise to 31-33°C in shallow coastal areas. Despite the shallowness, a temperature stratification develops in the central Gulf, the bottom water being 10°C cooler than the surface. During winter, winds are generally northerly. Average water temperatures drop to 20°C and considerably lower in shallow areas.

7. Mathematical Modeling Effort

Although the main pattern of circulation of the Gulf is known, it is not solidly based on quantitative measurements and not detailed enough to be practically useful. The main objective of the mathematical modeling effort is to develop a realistic predictive method of determining the current circulation pattern and a conservative pollutant dispersion in the Arabian Gulf. There are different kinds (1&3) of mathematical modeling approaches depending upon its objective and emphasis (i.e. formulation type,solution method,system of governing equations,and flow regions). In the course of developing general circulation models in the Arabian Gulf the following particular features are to be considered;

- Significant tidal influence,
- Surface wind stress,
- Coriolis Force,
- Stratification (temperature and salinity gradient),
- Transient phenomena, and
- Unique topographic configuration and bathymetry.

We therefore limit our attention to the application of the Finite Element Method to the general circulation problem. The finite element method, initially developed for structual applications, is a powerful and efficient computational tool to analyze complex flow problems. The mathematical formulation of two layer stratified flow and the solution strategy is discussed (6),except Coriolis and tidal effects which can be modified without difficulty. The flow field is divided into two layers which are coupled by kinematic and dynamic conditions through the interface. Vertically integrated continuity and momentum equations are derived for upper and lower layers. The method of weighted residual is applied to generate an integral statement which is the basis for the finite element discretization.

Satisfying the governing equation with the appropriate boundary condition is equivalent to requiring the weighted residual to vanish for arbitrary functions. The weighting function has the same shape function as the variables to be solved for (Galerkin's scheme). This two layer finite element model calculates transient behavior of the surface and the interface elevations, and the velocity distribution in both layers.

8. Concluding Remarks

Many of the marine ecosystems in the Arabian Gulf are seriously threatened by industrial development, such as oil pollution, thermal pollution, and chemical effluents. The oceanographic study in the Arabian Gulf is considered of fundamental importance in the water resources planning and environmental quality management. A complete spectrum of temporal and spatial variability of oceanographic and water quality data at the essential locations is to be obtained systematically.

At present, KISR is conducting a multi-dimensional systematic study in the near-shore area of Kuwait utilizing modern marine technology and proven concepts. In order to establish a sound base of important oceanographic study program in the Arabian Gulf, a similar concept should be broadly applied with more regional support.

References

1. Ahn,C.S., "Coastal oceanography for industrial application" presented at the Third Seminar on Environment and Pollution at Kuwait University, May 16-17,1977.
2. Ahn,C.S.,"A preliminary proposal to Shuaiba Area Authority, Phase II: Hydrographic Monitoring Program" Kuwait Institute for Scientific Research,Sept. 1977.
3. Ahn,C.S. and Smith,P.F., "The First Report of a study to forecast Nuclear Power Plant Effects on coastal zone", U.S. Atomic Energy Commission ,Dec. 1972.
4. Ahn,C.S.,"Pollutant Dispersion in shallow coastal water", Ocean 74 Conference, Nova Scotia, Canada.
5. UNESCO,"Marine Sciences in the Gulf Area", Unesco Technical Papers in Marine Sciences 26, 1976.
6. Watanabe,H., Harleman,D.R.F. and Connor,J., "Finite element model for transient two-layer cooling pond behavior", M.I.T.Water Resources and Hydrodynamic Laboratory, Report No.202, July,1975.

Acknowledgement

Much of this work was performed while the auther was a visiting Research Scientist at Kuwait Institute for Scientific Research in 1977.

A SYSTEMS APPROACH TO UNDERWATER CAMERA DATA CORRELATION AND INTERPRETATION

Gary G. Hayward and William D. McElroy, Jr.
Benthos, Inc.
Edgerton Drive
No. Falmouth, MA 02556

David S. Hosom and William M. Marquet
Woods Hole Oceanographic Institution
Woods Hole, MA 02543

Abstract

By recording pertinent information relating to deep ocean photographs digitally on the film, it is possible to reduce significantly the labor involved in correlating ancillary operational and oceanographic data with the photographs. This paper discusses the details of such a system with specific reference to the one employed by the DSRV ALVIN. In the ALVIN system, time, depth, height off the bottom, compass bearing, and dive number are recorded on each picture. The data recording is accomplished by a 16-digit LED display photographed simultaneously with each picture. Circuit details of the system, as well as photographic examples are presented.

1. Introduction

Because of the expense and effort involved in carrying out underwater photographic programs for either research or survey purposes, the camera systems employed are usually designed to take a very large number of photographs on one loading of film. This can be more than 6,000, but is usually of the order of a thousand exposures. It is also not uncommon, given the circumstances of such underwater studies, that the resulting photographs in a sequence are overall indistinguishably similar in appearance one to another. This similarity does not diminish their value or information content, but, because of this and the quantity of photographs, it does impose on the interpretation process significant data handling complications. This problem was recognized early in the development of underwater cameras and at the time provision was made to photograph the dials of a clock and pressure gauge, as well as a handwritten data card within the camera (Ref. 1). This "analog" data usually was not adjacent to the related photograph, but its usefulness nevertheless is obvious.

2. General Description

The present complete data recording system has provisions to accept most, if not all, the correlary data which will be needed with each photograph and is designed to facilitate handling this data subsequently. Thus the new system can process a wide range of data inputs and record this information on each of the corresponding photographs in an immediately-readable digital form. This recorded data includes time as well as an event number plus a variety of sensor output signals as discussed below. Furthermore, the system is configured to be used aboard either submersibles or towed unmanned autonomous vehicles or from fixed platforms.

The heart of this underwater camera data recording system is a digital data chamber and decoder as shown in Figure 1. This unit is positioned behind the film plate in the camera and, as can be seen, has its own optical system for imaging the data display onto the emulsion. This is accomplished through the back of the film which makes possible recording the data directly on to the corresponding exposure frame. Light emitting diodes are used to generate the digital display and since a mirror is employed in the optical path, the information is directly readable on the light emitting diodes, as well as being correct on the film and the print. In addition to the standard sensors, other user-choice external sensors can be handled.

3. System Details

The camera data system consists of a programmer, an encoder, a decoder, the 16-digit LED optical display, along with the sensors and their associated formatters, if required. The block diagram of Figure 2 illustrates a typical system configuration. The encoder (built on two printed circuit boards) accepts the sensor inputs as positive true binary coded decimal data (64 BCD bits total), formats the data, and transmits it to the camera on a single line during each picture taking sequence. The data is pulse-width coded and transmitted by means of optical isolators enabling complete isolation between the camera system and data

system when required. The encoder also accepts interrput signals from the sensor formatters to insure that the data inputs are valid and not being updated when transmission starts. All data inputs are buffered to allow any input level from 5V to 15VDC to be used. The transmitted data is received by the decoder (another printed circuit board), mounted on the camera chassis, decoded, and presented to the drivers and displays within the data chamber. The displayed data is reflected by a mirror and focused by the data lens on the edge of the film frame (through the back of the film). (See Figures 3 and 4).

Certain inputs are usually standard with a camera system: time (in hours, minutes, and seconds), date (numerically), altitude, and compass heading. Most sensors that have parallel BCD outputs available can be tied directly to the encoder. In addition, interface printed circuit boards have been designed to accept sensors which do not have a BCD output. Thus the camera is extremely flexible and provides for recording the data required by the user.

Data transmission to the data chamber is initiated by a negative transition on the camera program line as shown in the Block Diagram. This transition also triggers the picture taking sequence (shutter and strobe), thereby ensuring proper correlation of the recorded data with the photograph. Data transmission takes approximately 224 ms so the program line must be held for at least this length of time to enable all the data to be recorded. The positive transition on the program line initiates film advance for next exposure. Typically 250 ms is used. A photograph taken in the Benthos test pool is shown in Figure 3. This shows the digital information in the lower left of the frame and is a photograph of an underwater test grid.

4. The DSRV ALVIN Camera System

Under the sponsorship of O.N.R., A.R.P.A., and more recently N.S.F.*, an advanced photographic mapping system has been developed for ALVIN. This system centers around a bottom acoustic transponder navigation system and an eight-channel analog data logger which act as a mobile frame of reference to which observations, samples, and pictures can be related. It is possible with this system to map features to an accuracy of 10-15 meters and with bearing accuracies of 5 degrees. Although this system operated with surprising reliability in the Mid-Atlantic Ridge as a part of Project FAMOUS, a large amount of scientific information was lost due to an inability to relate photographic information to the track of the submersible. It was possible to know, for example, the orientation and position of the vehicle within a relative time frame of 2-3 seconds, while it was impossible on the average to resolve photographic information to less than 5 minutes. This was due primarily to a poor original camera system aboard ALVIN. As a result, a camera system built upon the above design was installed. Not only is the optical quality superior to the previous system, but also it has greatly reduced the manpower needed in data reduction and insured a major increase in the amount of useful photographic information.

The ALVIN camera system consists of two Model 372 Benthos 35 mm cameras with 35 mm lenses, mounted above the forward viewport and aimed at a point about 12 feet in front of the submarine, as shown in the diagrams of Figure 3 and the photograph, Figure 4. (See Ref. 4). Each camera may be triggered separately or they may be triggered together for stereo pairs. The cameras may be loaded with black and white (Plus-X) or color (High Speed Ektachrome) and each has a capacity of 750 frames. In addition to manual triggering, a timer is incorporated in the internal controls allowing the cameras to be triggered at 4 to 14 second intervals.

Each camera has one of the present data recording systems which puts information on each frame of every picture. Figure 6 shows the format of this data which includes time to the nearest second; the last two digits of the ALVIN dive number which effectively gives the date; the last three digits of depth in meters; the submersible's heading (direction) in degrees from true north, and the submersible altitude in feet. An example of one frame taken of the bottom during a 4000 meter test dive in New Providence Channel on 22 May 1978 at 1143 hours is given in Figure 7. These photographs are now refered to as "TAGED" for: Time, Altitude, Gyro, Event, Depth.

*Office of Naval Research, Advanced Research Project Agency of the Department of Defense, and National Science Foundation.

5. Conclusion

When the ocean scientist or ocean engineer was interested only in obtaining qualitative information from underwater photographs, the photographs themselves or these together with an accompanying photograph of dials to show time and the like was sufficient. Recently, however, new technical and scientific demands related to expensive offshore operations for resource assessment, engineering surveys or research purposes have put new levels of demands upon the users of these photographs. They must be measured and the information quantified. The new system described here is designed to meet these demands. Now, in addition to the time of the photograph, each photo may also be permanently marked with the depth and altitude of the camera, the geographic heading of the assembly (towed "fish" or submersible), and an event number which identifies the run, lowering or dive number. Now more photographs can be assimilated systematically and their information content quantified in what has become to be known as a

"cost effective" manner.

References

1. Hersey, J. B., ed., Deep Sea Photography, 1967, Chapter 3, pp. 52.
2. Bland, E. L., Donnelly, J. D., Shumaker, L. A., ALVIN Users Manual, Woods Hole Oceanographic Institution Technical Memorandum No. 3-46, November 1976.

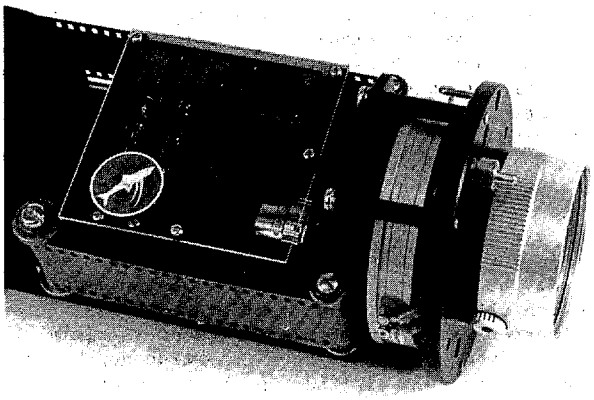

FIGURE 1. Photograph of Benthos Camera Digital Data Chamber.

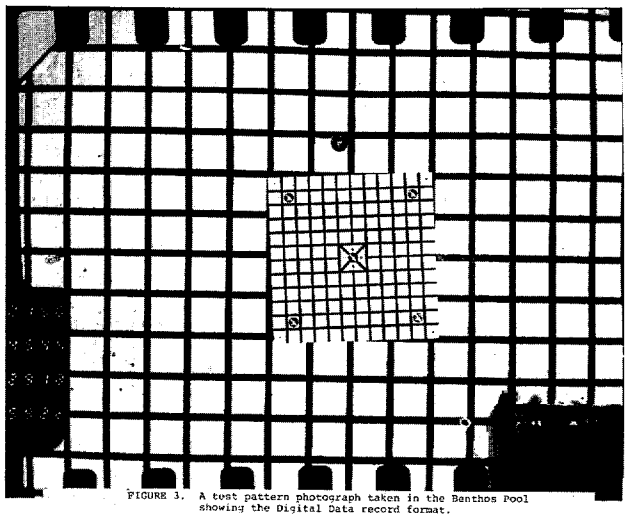

FIGURE 3. A test pattern photograph taken in the Benthos Pool showing the Digital Data record format.

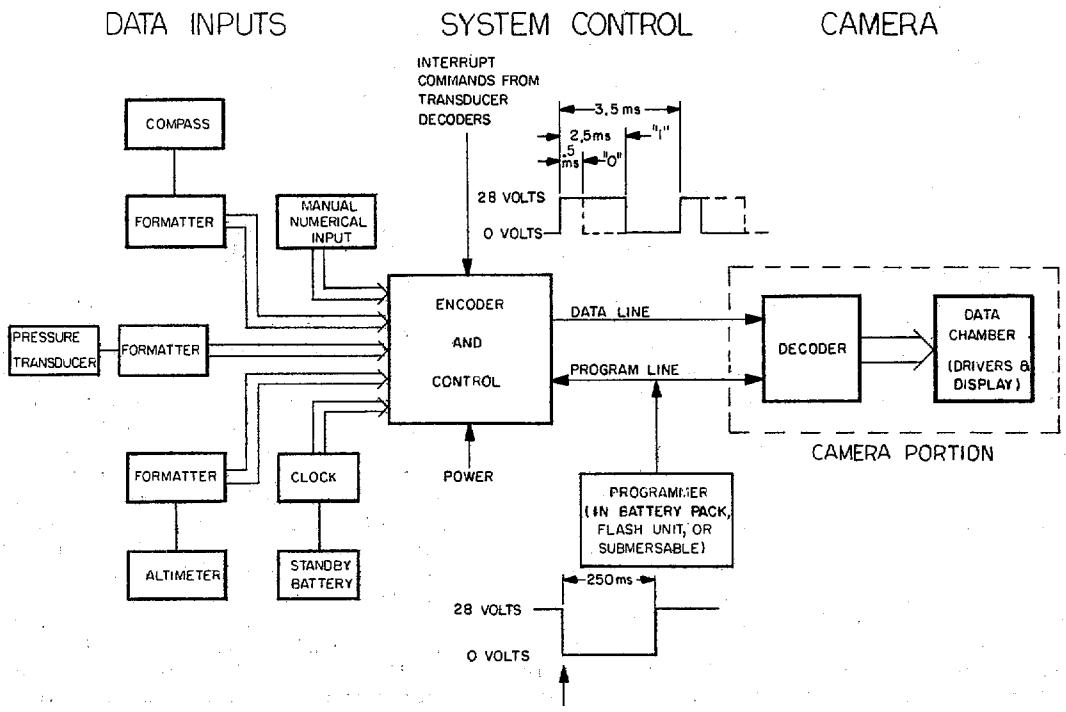

FIGURE 2. BLOCK DIAGRAM OF A TYPICAL DATA RECORDING UNDERWATER PHOTOGRPHIC SYSTEM

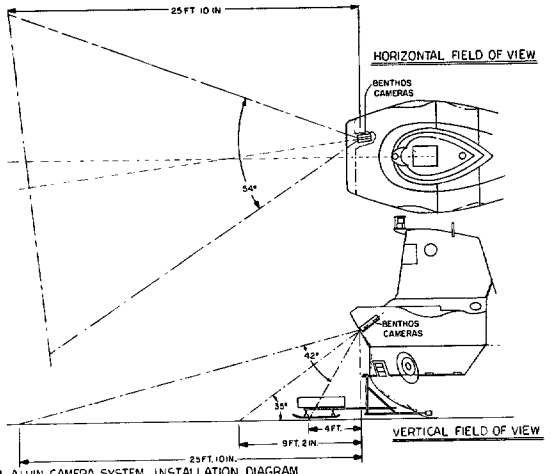

FIGURE 4. ALVIN CAMERA SYSTEM INSTALLATION DIAGRAM
(FROM FIGURES 7 AND 8 WHOI TECHNICAL MEMORANDUM 3-76)

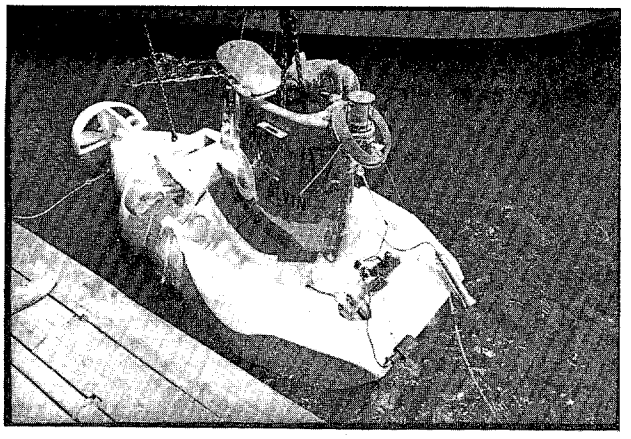

FIGURE 5. Photograph of DSRV showing Benthos Camera and Strobe installation.

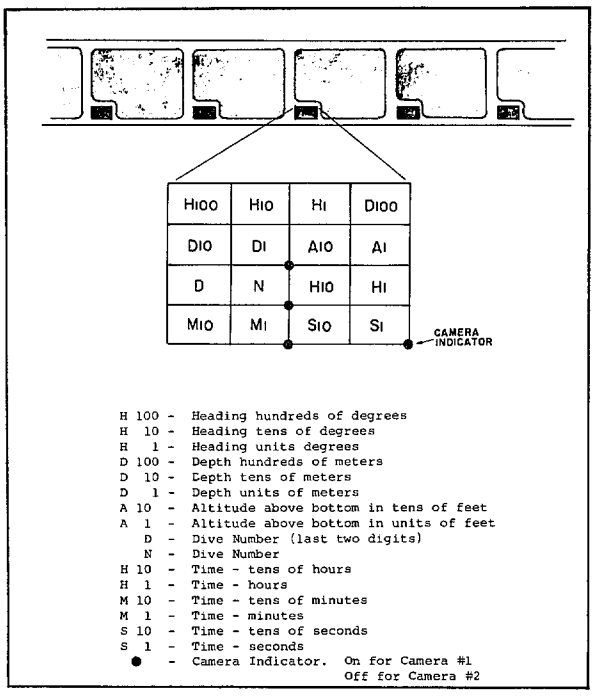

Figure 6. The DSRV ALVIN Benthos Camera System data recording format. (From Figure 9, Ref. 2).

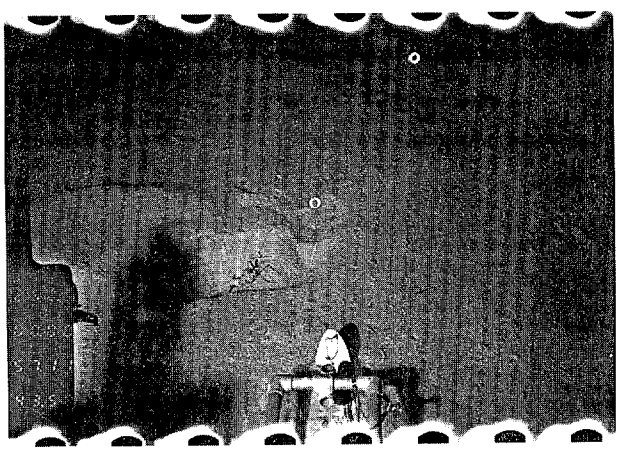

FIGURE 7. "TAGED" Bottom photograph taken during an ALVIN Test Dive at 4000m in New Providence Channel, Bahamas, on 22 May 1978 at 1143 hours 58 seconds on a heading of 268 degrees.

ICEBERG ALARM SYSTEM

R. Boetes B.P. Sukhov R.W. Crocker W.E. Russell

NORDCO Limited
P.O. Box 8833
St. John's, Newfoundland, Canada

Abstract

This paper proposes a hydro-acoustical alarm system that will warn personnel on drillships, production platforms or support vessels about approaching icebergs with sufficient draft to endanger bottom installations. The system would basically consist of two underwater units anchored such that the horizontal line between them defines the alarm limit. The principle of operation is described and block diagrams are presented.

1. Introduction

The threat posed by icebergs to offshore oil activities is one that has been the topic of much discussion and many papers have been written on the subject (1,2,3,). During the exploration stage, the greatest danger is the possibility of collision with drilling platforms. If an iceberg threatens to approach a platform too closely, a certain time must be allowed to disconnect the drill string and move off the well. One has to be constantly alert with respect to the movements of icebergs around the platforms in order to make the disconnect-decision at the correct time.

When a well reaches a production stage another aspect of the dangerous nature of the iceberg becomes clear, namely its draft. Icebergs are a potential hazard to the bottom installations. If an iceberg has sufficient draft, it can destroy well heads and flow lines on the bottom with disastrous results to the environment and enormous financial losses. In essence, this aspect of iceberg threat is much more serious since visual inspection of the berg does not give any information concerning its draft. Consequently, no conclusions can be drawn on whether the berg poses a threat. Fortunately, the course of an iceberg can be changed by towing to prevent it from entering an area with bottom installations. However, this effort is not necessary if the berg in question does not have a dangerous draft. It follows, therefore, that cost savings can be realized if iceberg draft can be easily classified.

This paper describes an iceberg alarm system which will provide the required information.

2. Description of the System

The basic principle of the system is presented in Figure 1. A and B are underwater units, placed a certain height h, above the seabed. This height h, equals the water depth H, minus the maximum tolerable draft, D, of an iceberg. The maximum tolerable draft depends, of course, on the height of the bottom installations above the seabed. Unit A is the master unit, which contains a clock. Unit A is connected to a surface buoy which contains a radio transceiver. Unit B is a repeater, which transmits an acoustic pulse when it receives a pulse from unit A. Unit A transmits a pulse every time the surface buoy receives a coded signal from a base station located on a ship or on shore. The operation is as follows:

- Unit A transmits omnidirectional acoustic pulses periodically. Simultaneously a clock is started in unit A.
- The first signal to arrive at unit B will trigger the transmitter in this unit which then transmits a pulse of a different frequency. The first signal to arrive at unit B will be the signal which followed the direct path, i.e. the shortest distance between units A and B. After this first signal, a number of bottom and surface reflections will be received by unit B, but these will be ignored by the circuitry in this unit.
- The pulse emitted by unit B will propagate to unit A and, when it is received, the clock in this unit is stopped. The elapsed time is proportional to the shortest distance between the units. This time is stored in a memory and the process is repeated.
- Each time unit A receives a signal from unit B, the elapsed time is compared to the stored time. If the measured time equals the stored time, within certain limits, the stored time is replaced by the last measured time.
- If, however, an iceberg interrupts the direct signal path between the two units,

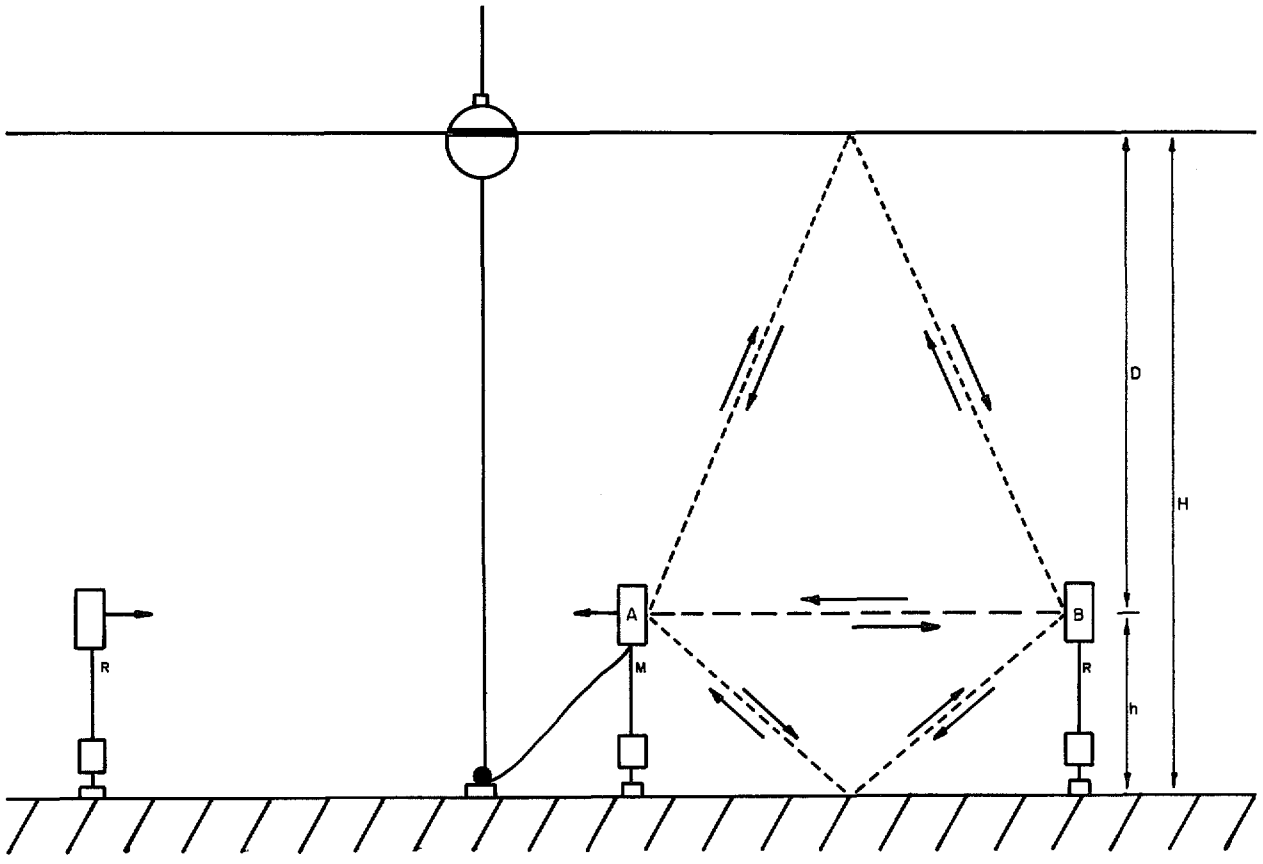

Figure 1. Concept

a direct signal will no longer be possible. In this case the first signal to be received at unit B will be a bottom reflection. This will result in a measured time, proportionally longer than the stored time. When this occurs, the stored time remains the same and the alarm transmitter in the surface buoy will be activated. The alarm will be received at the base station, thus giving operational personnel the information that a berg with hazardous draft has entered the danger zone.

The underwater units will be a large distance apart (i.e., in the order of kilometers) and the pulse repetition rate will be in the order of seconds. Considering these facts, it is felt that any changes in the temperature or salinity of the water between the units will remain essentially constant between transmissions.

The system may be expanded as required, for example, an array of master- and repeater-units can be placed around a wellhead, a drillship or any object that has to be protected from icebergs. It is also possible to place the units in a linear array.

3. Block-Diagram

Figure 2 presents the block diagram of the master unit. The circuitry enclosed by the interrupted line is contained in the surface buoy. Only the receiver and the decoder are continuously activated. When a certain code is received from the base-station, the decoder activates a relay which supplies power to the rest of the system. When the system is thus activated, the controller causes the high voltage generator to send a high voltage pulse to the transducer which emits an acoustic pulse. Simultaneously, input #2 of and-gates A and B goes high so that the counters start counting pulses from the oscillators. The acoustic receiver is also activated.

The acoustic pulse, then travels to the repeater units which results in the transmission of two pulses with two different frequencies. These two pulses are then received by the receiver of the master-unit. The filter separates the two pulses. After passing through the two pulse-shapers, they are fed into the controller, which drives the #2 inputs of gates A and B low, causing the counters to stop. The output of the counters is converted to BCD code and stored in the shift registers, because the #2 inputs of gates C and D are driven high by

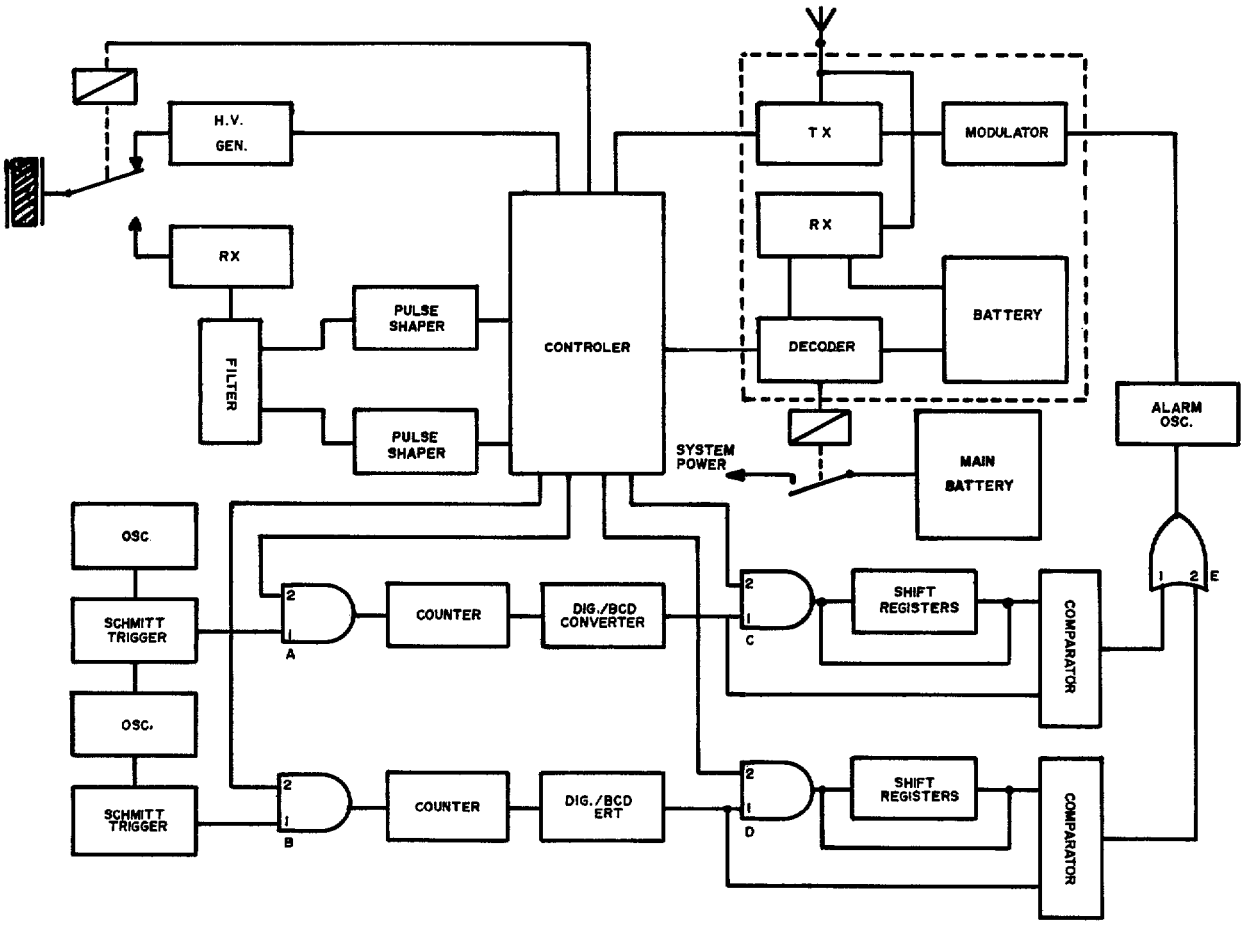

Figure 2. Blockdiagram Master Unit

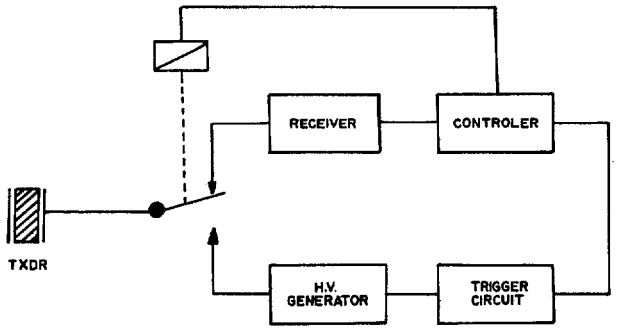

Figure 3.
Blockdiagram Repeater Unit

the controller.

After a specific time, the master transducer transmits its next pulse and the process repeats itself. This time, however, the #2 inputs of gates C and D are kept low by the controller so that the output of the digital to BCD converters is not stored in the shift-registers, but is compared with the contents of the shift registers in the comparators. If both values are equal, within certain limits, the output of the digital to BCD converter overwrites the contents of the shift-register and the cycle is repeated. If the output of a converter is not equal to the contents of the corresponding shift-register, the output of the comparator goes high and activates the alarm oscillator and, at the same time, the radio transmitter in the surface buoy is switched on, which results in the transmission of an alarm signal. The alarm signal is transmitted as long as the measured time does not correspond with the stored time in either of the two channels. This time depends on the size and speed of the berg.

After the berg has passed, the alarm signal will cease and the system will continue to function as before since the last propagation time that was measured before the berg interrupted the direct signal path is still stored in the shift-registers.

Figure 3 shows a block diagram for a repeater unit. When the unit receives a pulse from the master unit, it switches from receive to transmit and the high voltage generator is triggered. This causes the transducer to transmit an acoustic pulse of a different frequency. The frequency separation will be sufficient to avoid interference between signals.

4. Conclusions

A system has been described which initiates a radio frequency alarm if an iceberg with a dangerous draft approaches a production site.

The system has the following properties:
- It is self-contained and automatic;
- It is capable of long term deployment;
- It is not affected by long term temperature changes in the water;
- It is recoverable by acoustic release.

References

1. Duval, J., "Icebergs. A New Problem for Oil Exploration and Production," Earth Science Symposium on Offshore Eastern Canada, Geol. Surv. Can., Paper 71-23, 1973, pp 639-652.

2. Bruneau, A., "Science Seeks a Way to Predict Path of Icebergs Ahead of Time," Offshore, 1972, Vol. 32 (1), pp. 32-33.

3. Duval, J., "Arctic Offshore Problems Examined" Petroleum Engineer International, 1970, Vol. 42, pp. 14-18.

USE OF FREE FALL PENETROMETER IN SEA FLOOR ENGINEERING

T.R. Chari, W.G. Smith and A. Zielinski

Faculty of Engineering and Applied Science
Memorial University of Newfoundland
St. John's, Newfoundland, Canada A1B 3X5

Abstract

In-situ evaluation of shear strength is an important aspect of geotechnical testing of the ocean floor. The free fall penetrometer is one such test device, capable of quickly examining the top few meters of the surficial sediments. A description of the penetrometer and preliminary results from its sea trials south of Newfoundland during May 1978 are presented in this paper.

1. Introduction

Most of the techniques used in sea floor engineering are extensions or modifications of the methods for terrestrial soils. Conventionally, building foundations are designed after testing "undisturbed" bore hole samples. Similar procedure in the oceans is generally expensive. Samples obtained by other methods are generally much disturbed. Samples from the ocean floor undergo additional disturbance when brought to the surface by expansion of the pore water and the release of dissolved gases. Such disturbance could cause as much as 20% or more increase (Ferguson et al. 1977) in the volume. Laboratory tests on such samples will be gross underestimates of the shear strength.

The practice of collecting soil samples will continue in sea floor investigations in terms of the need to visually see, identify and conduct laboratory tests. However, in-situ tests will always be needed in ocean floor studies to supplement sampling and increase the confidence level.

In-situ devices generally measure a characteristic property of the soil in its natural state. This can then be related to the shear strength and soil bearing capacity through appropriate semi-empirical formulation. Among various in-situ test devices, vane shear apparatus and the penetrometer have found common acceptance among offshore engineers. Vane shear measurement is a quick way of finding the undrained shear strength of the soil. But the test itself has to be performed in conjunction with either a bottom supported rig (Richards et al. 1972) or inside a bore hole (Doyle et al. 1971).

2. Penetrometers

Penetrometers used in the ocean environment fall under three broad categories; (a) static cone penetrometers, (b) dynamic or quasi-dynamic penetrometers and (c) free fall penetrometers. Static cone penetrometer tests (CPT) have been used for more than thirty years, mostly in Europe, in terrestrial geotechnical engineering. Use of this instrument in North Sea offshore investigations has been reported to be successful. Static penetrometers require seabed rigs (De Ruiter 1975, Zuidberg 1975) to test surficial sediments and drill string attachment (Ferguson et al. 1977) for tests inside bore holes. For site-specific foundation studies, static penetration tests appear to be extremely relevant and useful.

Several types of dynamic penetration tests for sea floor have been reported. Scott (1967) and Preslan (1970) measured the deceleration of a gravity corer and attempted to correlate the soil characteristics. Colp et al. (1975) reported measurements with a 3 inch (75 mm) diameter 5 foot (150 cm) long disposable penetrometer with a tapered nose section. True (1975) reported studies with dynamic penetrometers of different shapes. Beard (1977) developed a disposable penetrometer with Doppler telemetry for velocity measurement. A 2 inch (50 mm) diameter dynamic penetrometer driven by repeated blows of a freely falling weight was reported by Kolbe (1975). A bullet system is reported to be (Anon 1977) under development at the University of Newcastle upon Tyne. Research on dynamic penetration theory has been in progress at the Scandia Laboratories (Thompson and Colp 1970) for nearly 15 years. Standardization and interpretation of dynamic penetration tests is still an area for further work.

3. Free Fall Penetrometer

A free fall penetrometer has been developed at Memorial University (Dayal 1974) as an instrument for a quick and economical evaluation of the surficial sediments. A penetration of 10 meters of the ocean floor is envisaged with such an instrument. This has a good potential in geotechnical surveys and investigation of large tracts

such as those for pipeline routing. The penetrometer used in the initial trials (Allen et al. 1975) was similar to the standard 1.4 inch (35.6 mm) diameter static penetrometer (Figure 1) with a 60° cone tip and 23.25 sq. inch (150 sq.cm) friction sleeve. In addition to the cone tip resistance and sleeve friction, the deceleration was measured during penetration. Weights up to 180 lb (800 N) were attached at the top of the field penetrometer. Laboratory tests with this tool were quite successful, but there were problems during sea trials. The slender 1.4 inch (35.6 cm) shaft failed frequently (Jones 1976) by buckling.

A completely redesigned version of the penetrometer which is now 3 inch (75 mm) diameter is shown in Figure 2. The accelerometer, cone and sleeve load cells are all located in the instrumented tip assembly which was pressure tested to 350 psi (2.4 MPa). The ballast is uniformly distributed in the penetrometer stem, thus improving the structural and kinematic stability of the instrument. A twelve conductor umbilical cable transmitted the signals to a tape recorder on board. The penetrometer which weighed 350 lb (1.56 kN) was lowered from a winch (Figure 3) and tripped by a counter weight giving a free fall of 50 feet (15 meters). A Doppler telemetry system was also housed inside the stabilizer and was used in conjunction with a hydrophone hung over-board. Velocity thus measured was compared with that computed from the accelerometer record.

4. Preliminary Results

Out of a total twenty drops in water depths of 180 to 250 meters (100 to 135 fathoms), successful records were obtained in sixteen cases. Four tests failed due to flooding of the cable connector. Penetrometer results as well as the core samples from this sea trial are being analyzed.

Figure 4 is a typical trace of the deceleration, cone thrust and sleeve friction resistance. A penetration of the entire 12.25 ft. (3.7 m) length of the penetrometer was obtained in medium to stiff clay. At stations where the clay was overlain by sand, the velocity profile clearly identified the layering as shown in Figure 5. A preliminary comparison of the velocity directly measured and that integrated from the deceleration record is shown in Figure 6. The agreement is excellent with a maximum difference of only 3%.

After the recent successful sea trials, it is felt that this type of instrument has high potential in geotechnical surveys. Further development is in progress. Laboratory tests are also in progress to correlate the instrument with static penetration and triaxial shear tests.

5. Summary

Sea trials of the free fall penetrometer described above prove it to be a useful in-situ equipment. Penetration up to 30 ft. (9 m) is easily possible in its present stage of development.

The entire operation of deploying the penetrometer and retrieving takes only about 20 minutes. The instrument is a very useful ground truth equipment for deep tow acoustic surveys.

6. Acknowledgements

The constant encouragement and assistance provided by R.T. Dempster, Dean of Engineering and G.R. Peters, leader of the Ocean Group is gratefully acknowledged. The authors wish to express their appreciation to G.A. Fowler of Bedford Institute of Oceanography and A. Bursey for their invaluable assistance during sea trials. Meticulous assembly of the penetrometer by the University Technical Services in time for the cruise is gratefully appreciated. Thanks are due to A.D. Dunsiger, J.S. Rao, S.N. Chaudhuri, M.N. Abdel Salam, S.M. Abdel Gawad, D. Tilley and K. Manuel for their assistance at various stages of the project.

References

1. Allen, J.H., Dayal, U. and Jones, J.M., "Development of marine sediment impact penetrometer", Proceedings, Oceanology International Conference, 1975, pp. 244-248.

2. Anon., "Bullet system profiles sediments", Offshore, December 1977, pp. 154-156.

3. Beard, R.M., "Expendable Doppler penetrometer: A performance evaluation", Civil Engineering Laboratory, U.S. Naval Facilities Engineering Command, Technical Report 855, July 1977.

4. Colp, J.L., Caudle, W.N. and Schuster, C.L., "Penetrometer system for measuring in-situ properties of marine sediments", Ocean '75, Proceedings, IEEE Conference, 1975, pp. 405-411.

5. Dayal, U., "Instrumented impact cone penetrometer", Ph.D. Thesis, Memorial University of Newfoundland, Canada, 1974, 222 p.

6. DeRuiter, J., "The use of in-situ testing for North Sea soil studies", Proceedings, Offshore Europe '75, Aberdeen, 1975, pp. 219.1-219.10.

7. Doyle, E.H., McClelland, B. and Ferguson, G.H., "Wire line vane probe for deep penetration measurement of ocean sediment strength", 3rd Offshore Technology Conference, Houston, OTC 1327, Vol. I, 1971, pp. 121-127.

8. Ferguson, G.H., McClelland, B. and Bell, W.D., "Seafloor cone penetrometer for deep penetration measurements of ocean sediment strength", 9th Offshore Technology Conference, OTC 2787, Vol. I, 1977, pp. 471-478.

9. Jones, J.M., "The use of an impact penetrometer in remote sensing study of the sea bed properties", 2nd CSCE Hydrotechnical Conference, Atlantic Region, Amherst, N.S.

10. Kolbe, R., "The design and development of an ocean sediment probe", Ph.D. Thesis, University of New Hampshire, Durham, 1975, 206 p.

11. Preslan, W.L., "Accelerometer-monitored coring", Proceedings, Civil Engineering in the Oceans II, American Society of Civil Engineers, 1970, pp. 637-641.

12. Richards, A.F., McDonald, V.J., Olson, R.E. and Keller, G.H., "In-place measurement of deep sea soil shear strength", Underwater Soil Sampling, Testing and Construction Control, ASTM STP 501, American Society for Testing

13. Scott, R.F., "In-place soil mechanics measurements", Marine Geotechnique, Editor: A.F. Richards, University of Illinois Press, 1967, pp. 264-271.

14. Thompson, L.J. and Colp, J.L., "Application of earth penetration technology to ocean bottom penetration", 2nd Offshore Technology Conference, OTC 1203, Vol. I, 1970, pp. 571-576.

15. True, D.G., "Penetration of projectiles into seafloor soils", U.S. Naval Civil Engineering Laboratory, Technical Report R-822, May 1975.

16. Zuidberg, H.M., "The Sea Calf, a submersible cone penetrometer rig", Marine Geotechnology, Vol. I, No. 1, 1975, pp. 15-32.

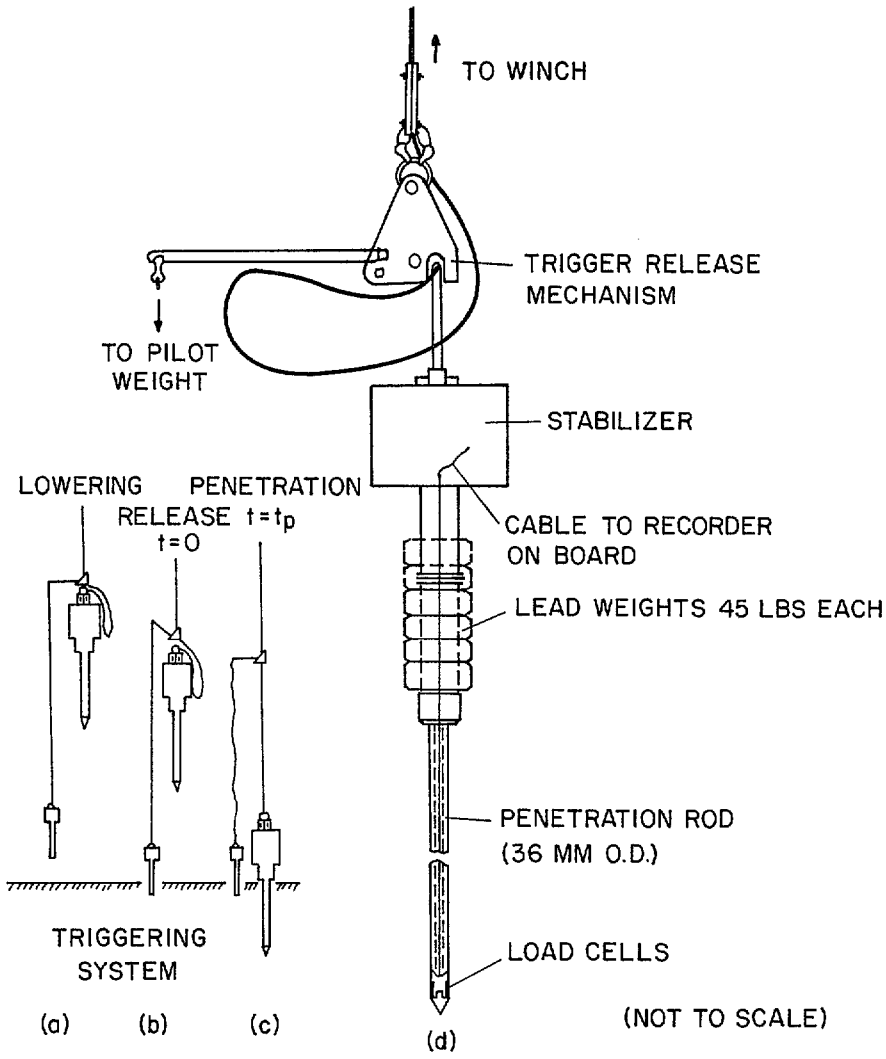

FIG. 1: FREE FALL PENETROMETER (35.6 mm DIAMETER)

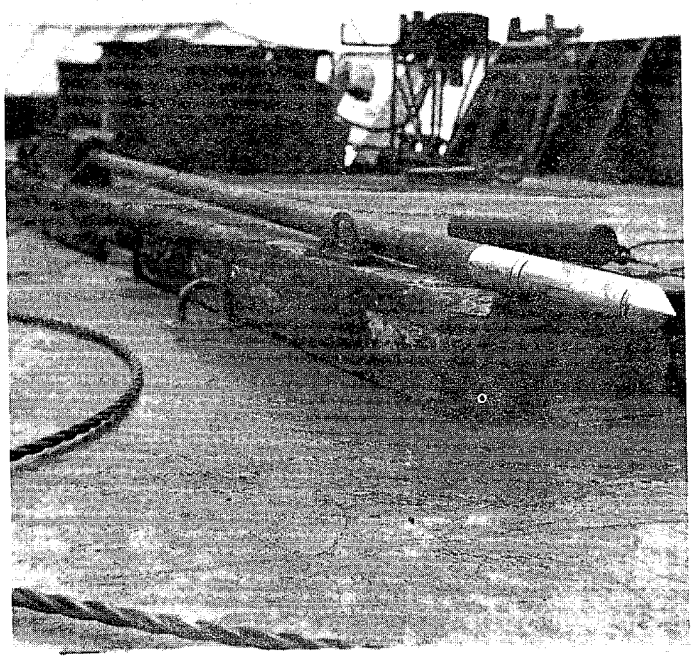

FIG. 2: REDESIGNED 75 mm DIAMETER PENETROMETER

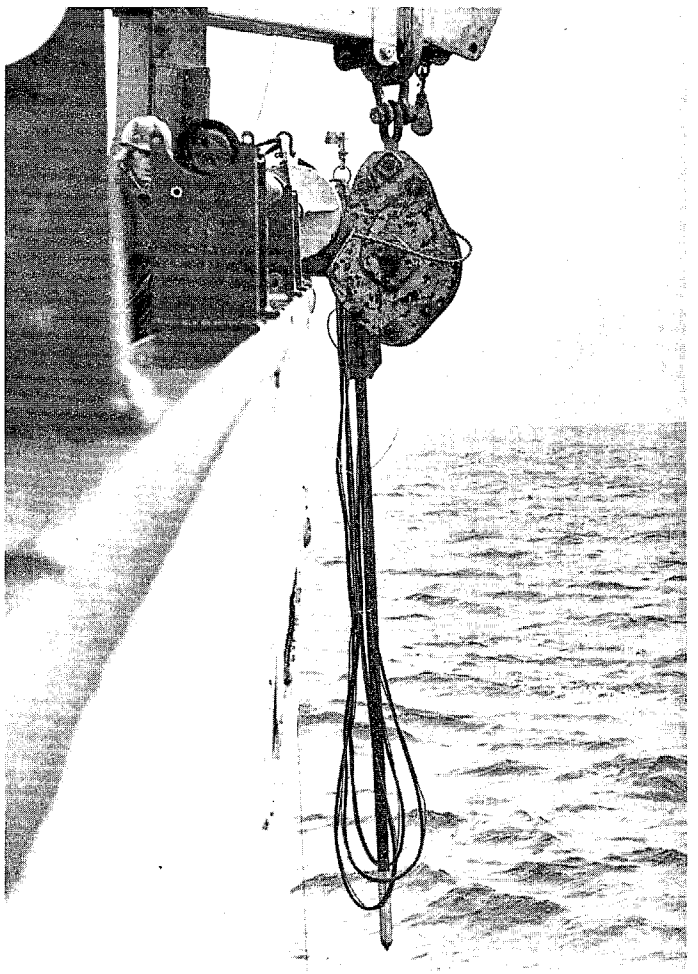

FIG. 3: PENETROMETER BEING DEPLOYED

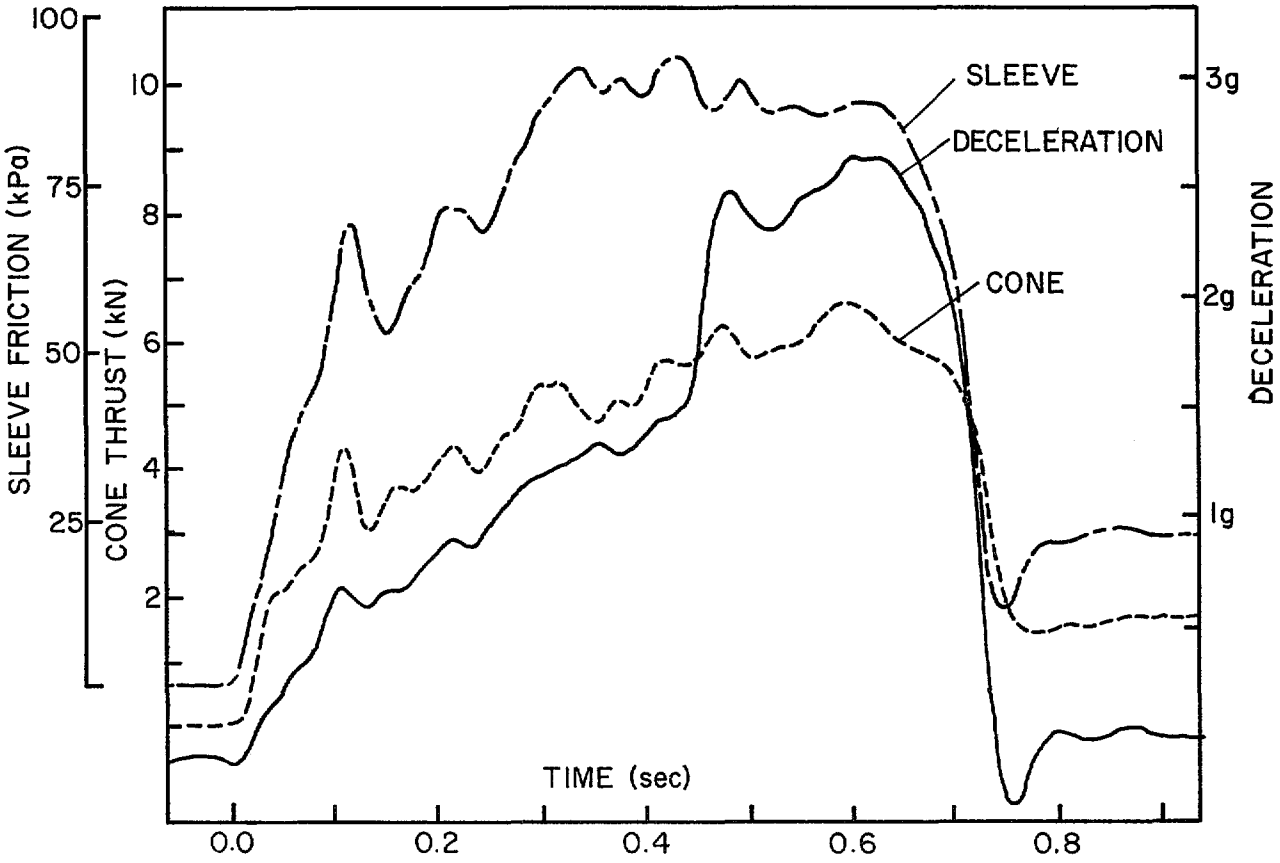

FIG. 4: TYPICAL OUTPUT OF DECELERATION, CONE THRUST AND SLEEVE FRICTION

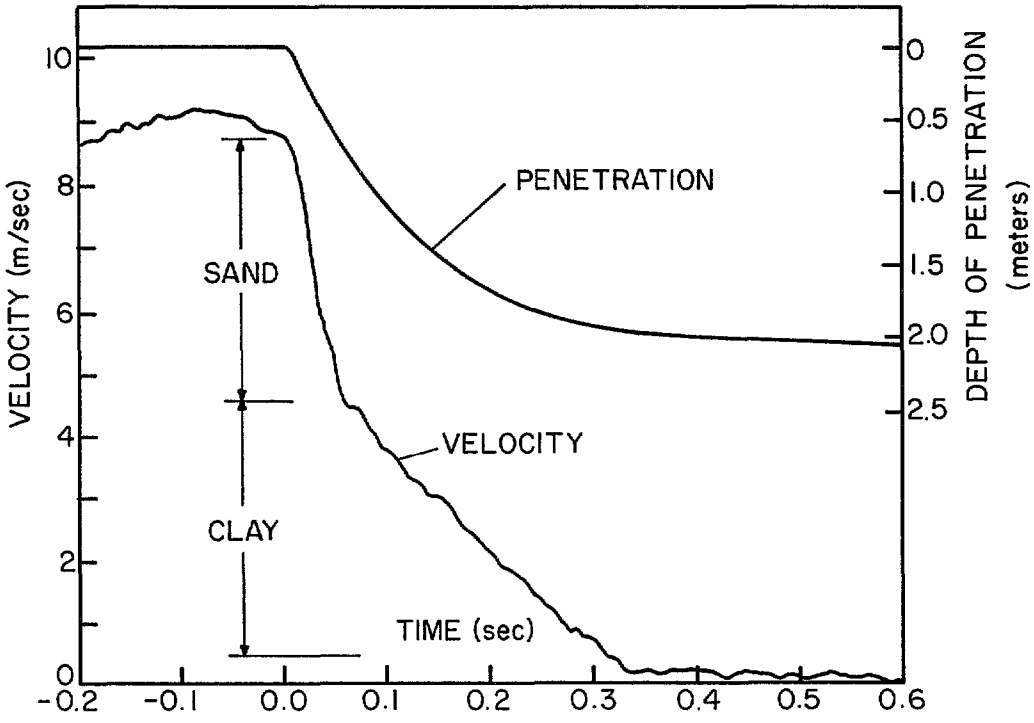

FIG. 5: VELOCITY PROFILE IN LAYERED MEDIUM

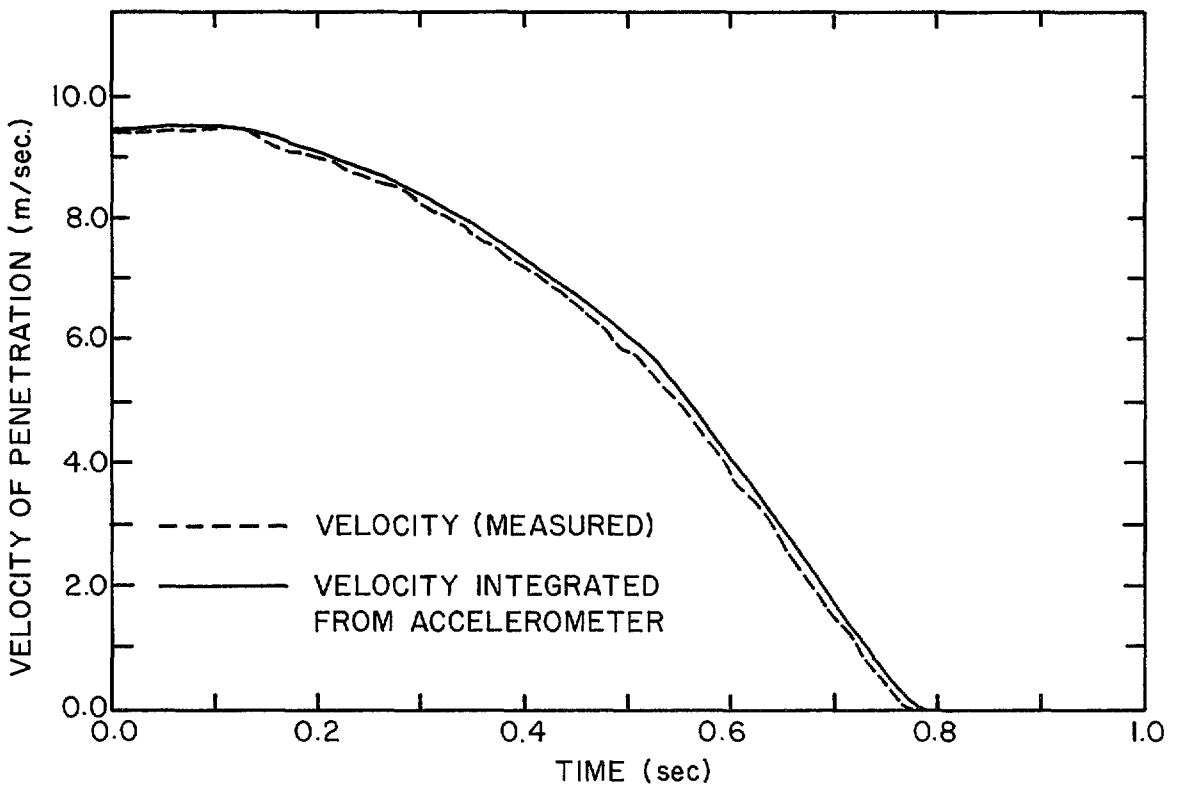

FIG. 6: COMPARISON OF DOPPLER TELEMETRY AND HARDWIRED OUTPUT

THE DEVELOPMENT OF A SEAFLOOR EARTHQUAKE MEASUREMENT SYSTEM*

David E. Ryerson
Instrumentation Systems Division
Sandia Laboratories
Albuquerque, New Mexico 87185

Eric W. Reece
Instrumentation Development Division
Sandia Laboratories
Albuquerque, New Mexico 87185

Abstract

A Seafloor Earthquake Measurement System is being developed at Sandia to measure marine sediment response to seismic activity. The system will use an acoustic telemetry system to transmit commands to and collect data from the seafloor package. The seafloor package contains a microprocessor which controls the data collection, data processing, and acoustic telemetry. A one million bit magnetic bubble memory is used for storage of seismic data obtained from a three-axis accelerometer package. The microprocessor continuously compares the incoming data in mass memory and saves the "best" data for later readout by the acoustic telemetry system. The seafloor package consists of a ballast emplaced pressure vessel and probe containing the accelerometer. After the probe is inserted into the sediment, the ballast weight is removed and a section of the probe is retracted to mechanically isolate the accelerometers.

1. Introduction

Sandia Laboratories, under the sponsorship of the Department of Energy (DOE) and the U.S. Geological Survey (USGS), is developing a Seafloor Earthquake Measurement System (SEMS) to measure the response of ocean floor sediments to seismic activity. The data available for the design and regulation of offshore structures in seismically active areas are very limited. Since future exploration and production of oil and gas will be extended in seismically active areas such as the Alaskan offshore and the California offshore, the data on environmental hazards and engineering forces needs to be greatly expanded. This system is designed to demonstrate a means of gathering the seismic data which will aid the design and regulation of safe, cost-effective offshore production facilities.

* This work supported by the U.S. Department of Energy and the U.S. Geological Survey.

The SEMS uses an acoustic telemetry system developed by Sandia in 1977 to transfer data from the seafloor to the ocean surface. The acoustic telemetry system was tested in Lake Mead, Nevada, the Gulf of Mexico, and the Gulf of Alaska. It reliably transmitted data at 2400 bits per second in water depths of 300 and 600 feet.

The seafloor data gathering package and the surface command and recording package both use similar microcomputers for data acquisition, processing, and storage. The seafloor data are transmitted to the surface on command from the surface package. In addition, the seafloor package can be commanded to change its operating parameters. With this capability, the status of the seafloor package and the data are available at any time and the operating parameters can be changed as necessary to gather the best data.

The first system will be installed in the Santa Barbara area off the California coast in the fall of 1978. This system is designed to operate for one year. Two or three additional systems are to be installed in the summer of 1979.

2. System Description

The Seafloor Earthquake Measurement System (SEMS) consists of three main subsystems as follows:

1. The DAta Gathering Subsystem (DAGS), a pressure vessel and probe containing accelerometers, microprocessor, solid state memory, batteries, and acoustic telemetry link;
2. The Command And Recording Subsystem (CARS), a portable receiving/recording station that provides surface command and data recording capabilities; and
3. The Buoy RElay Subsystem (BRES), an optional buoy relay station between the DAGS and the CARS with communication between the BRES and the CARS being over a radio frequency link.

All three subsystems are controlled by similar microcomputers consisting of an RCA 1802 microprocessor, programmable read-only

memory (PROM), read/write random access memory (RAM), a real time clock, a universal asynchronous receiver/transmitter (UART) and additional input/output devices as required. Low power analog circuitry and CMOS digital circuitry are used throughout the system to minimize power consumption.

Figure 1 is a block diagram of the DAGS. Its main sensor is a three-axis force-balance quartz-suspension accelerometer package capable of measuring acceleration levels from 0.1 millig to 1 g and from DC to 20 Hz. In addition, it has a two-axis magnetometer mounted with the accelerometers for determination of the horizontal orientation of the accelerometers and a temperature sensor mounted in the electronics section of the pressure vessel. The mass memory consists of 1.08 million bits of magnetic bubble memory (MBM). MBM was chosen since it is nonvolatile and can be powered off except when it is being written or read. The package is powered by 32 large silver-zinc cells. The design life of the DAGS is one year.

Figure 2 is a drawing of the DAGS after installation. The accelerometers and magnetometers are located in the probe tip. A 20-inch section of the probe has been retracted and only an umbilical cable connects the probe tip to the pressure vessel. This gives good mechanical isolation between the probe tip and pressure vessel. The probe tip is 11.5 feet below the seafloor mudline. The pressure vessel, which is 26 inches in diameter and 30 inches high, contains the batteries and electronics and has the acoustic transducer for the telemetry system mounted on its top.

The block diagram of the CARS is shown in Figure 3. In addition to the microcomputer, the CARS has a 10-million bit cassette display for operator control, a radio frequency receiver/transmitter for communication with the BRES when used, an optional line printer for received data printout, and an optional magnetic tape reader for checking of recorded tapes. The CARS is contained in a metal suitcase

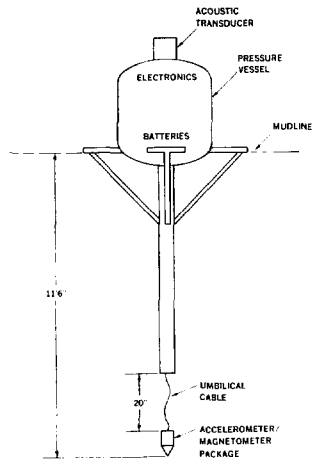

SEAFLOOR EARTHQUAKE MEASUREMENT SYSTEM (SEMS)
DATA GATHERING SUBSYSTEM (DAGS)

Fig. 2 - Data Gathering Subsystem (DAGS)

of approximately 16 inches on a side. It is powered by an external 12 volt lead-acid battery. The optional printer and tape reader are also external devices which require 110 volt AC power.

The acoustic telemetry system uses 110-degree beam transducers for communication. This requires that the surface acoustic transducer be within a circle above the seafloor package of radius 1.4 times the water depth. If it is difficult to keep the receiving station ship within this circle, the BRES can be used. It is a buoy containing a radio frequency to acoustic repeater. With the BRES moored over the DAGS, the ship is only required to keep the BRES within line of sight. The BRES uses the above described microcomputer to receive and retransmit commands or data. It also checks for errors in the received information. If a command is in error, it is not retransmitted. Data are always retransmitted but the number of

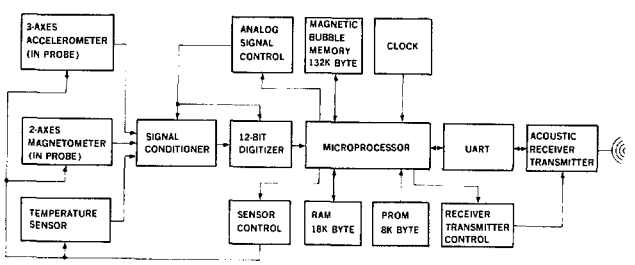

SEAFLOOR EARTHQUAKE MEASUREMENT SYSTEM (SEMS)
DATA GATHERING SUBSYSTEM (DAGS)

Fig. 1 - Data Gathering Subsystem (DAGS) Block Diagram

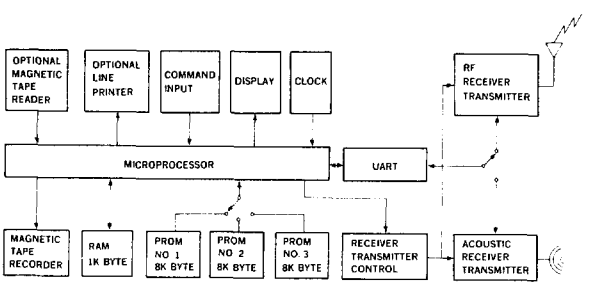

SEAFLOOR EARTHQUAKE MEASUREMENT SYSTEM (SEMS)
COMMAND AND RECORDING SUBSYSTEM (CARS)

Fig. 3 - Command and Recording Subsystem (CARS) Block Diagram

data errors are added to the data block as information to the CARS so that the operator can determine if errors are occurring in the acoustic or radio frequency link.

3. Acoustic Telemetry System

The acoustic telemetry system uses 110 degree beam conical transducers on both the seafloor and surface packages to transmit commands and data vertically through the water. Conical transducers are used to reduce the transmission and reception of bottom and surface reflected signals.

Asynchronous digital data are transmitted using frequency-shift keying. A data bit zero is transmitted at 68.3 kHz and a data bit one is transmitted at 76.8 kHz. Commands are transmitted at a serial bit rate of 75 bits per second from the CARS to the DAGS and data at 2400 bits per second from the DAGS to the CARS. The non-return to zero serial bit stream consists of eleven bit words with one word being a start bit, eight data bits, a parity bit, and a stop bit. Commands consist of blocks of three to eight words per block and data consists of 4 to 250 words per block. For every command sent, the seafloor package responds with a block of data requested by the command or a verification that the command has been performed. This is a half-duplex system; that is, it can only transmit in one direction at a time.

The acoustic transmitter consists of a voltage controlled oscillator modulated with the serial bit stream followed by a five watt transistor amplifier. The receiver starts with a field-effect transistor pre-amplifier, followed by several stages of a bandpass-filter limiting amplifier, a phase-locked loop discriminator, and a lowpass data filter. The universal asynchronous receiver/transmitter (UART) connected to the microprocessor is used to generate and decode the serial bit streams.

When the BRES is used, the 70 kHz frequency-shift keyed signal is frequency modulated on a 218 MHz radio frequency carrier using standard telemetry receivers and transmitters. A one watt transmitter is used which will give a range longer than the line of sight distance from the ship to the buoy.

4. Seismic Recording Procedure

The seafloor package, the DAGS, has enough magnetic bubble mass memory to store 204.8 seconds of seismic data in eight 25.6-second blocks. A single seismic event can take from one to eight blocks depending upon the length and size of the event. Therefore, the system can store eight short events, one long event, or any combination in between. The microcomputer examines the incoming data and runs comparisons with data in mass memory so that it can keep the "best" data. This section describes the procedure for finding the best data.

All three accelerometer axes are monitored every ten milliseconds and the data are stored in a 1.7-second precursor ring buffer. The vertical axis input is used for all decisions in determining the "best" data. A 1.28-second short term average and a 20.48-second long term average of the absolute value of the vertical axis input are calculated every sample interval. When the ratio of the short term average to the long term average exceeds a trigger threshold, previously set by command, an event is declared (Ref. 1 and 2).

When an event is declared, the long term average and the precursor ring buffer are fixed. Next, 25.6 seconds of data are gathered in a temporary buffer as the first block of data in this event. In addition, the average of the short term average for this first block is calculated and defined as the event size for the entire event. Even though an event may consist of more than one 25.6-second data block, the event size is always calculated using data from the first block in the event. This block of data is stored in a vacant mass memory block if one exists; but if none exists, and if the event size of this new event exceeds the event size of any event in mass memory, all the memory blocks for the smallest event are declared vacant and the new data are recorded in one of these vacant blocks. Finally, if the new block cannot be recorded because of too small an event size, the event is declared over and the system restarts, looking for another event. If the new event data are recorded, the precursor buffer and time are also stored in the same mass memory block.

If the first data block of the new event is recorded, the system gathers another 25.6 seconds of data. It also calculates the average of the short term average of this new block, which is defined to be the block size. For the first data block in an event, this average is called the event size, but for all subsequent blocks, it is called block size. If the ratio of the block size to the long term average is less than a shutdown threshold, previously set by command, the event is declared over; this data block is discarded, and the DAGS begins looking for another event. If the ratio is greater than the shutdown threshold, this block is recorded in a vacant mass memory block. If no vacant blocks exist and the event size of this event exceeds the event size of the smallest event presently in mass memory, the blocks for that smallest event are declared vacant and the new block is recorded. Otherwise, the event is declared over and search for another event begins.

The above procedure continues until the event is declared over or eight data blocks are recorded. If eight data blocks are

recorded for a single event, the event is assumed to be so important that the system stops looking for new events until commanded from the surface to restart. After the data are collected by the surface package, the CARS, a command is sent to declare all mass memory blocks vacant so that new smaller events can be recorded.

5. Testing and Installation

The acoustic telemetry system was tested in the summer of 1977 (Ref. 3). By using known test patterns, the system demonstrated that it could reliably transmit data at 2400 bits per second in water depths up to 600 feet. In addition, a microcomputer similar to the one being used in the SEMS was tested and proven in the acoustic telemetry tests.

The seafloor seismic recording software and hardware are being tested with the system shown in Figure 4. Strong motion earthquake data were obtained from the National Information Service for Earthquake Engineering at the California Institute of Technology on magnetic tape (Ref. 4). These data are fed into a minicomputer which scales and outputs them at correct time intervals to a three-channel digital-to-analog converter. The three analog signals are input to the accelerometer input ports of the DAGS. After the DAGS processes the data, the CARS is used to readout the data to a cassette tape. Finally the cassette tape data are fed back into the minicomputer for comparison with the original data. This test system allows one to check if a large event will indeed record over a small event and if the data are distorted in recording.

The first prototype package is to be installed off the coast of California in the Santa Barbara area in the fall of 1978. General Motors 137-foot research vessel SWAN will be used to install the system. A large weight ranging from 3500 to 7500 pounds will be used to insert the DAGS probe into seafloor clay. After insertion, the weight will be removed and a 20-inch section of the probe will be retracted for mechanical isolation of the accelerometers from the pressure vessel. The system will be installed near an onshore station so that comparison with land data can be made.

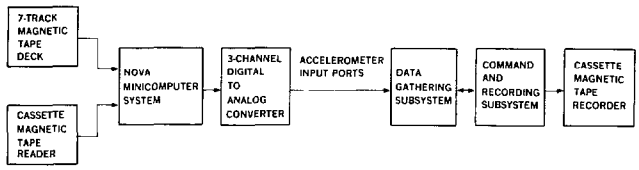

SEMS EARTHQUAKE RECORDING TEST SYSTEM

Fig. 4 - Seismic Recording Test System Block Diagram

6. Conclusion

A Seafloor Earthquake Measurement System is being developed which will provide a unique, and heretofore unavailable, capability in measuring the response of marine sediments to seismic activity. The broad dynamic range of the system (10^{-4} to 1 g) provides the ability to sense both weak and strong ground motion. The solid state, microcomputer-controlled data gathering system can operate for up to one year in remote offshore locations. The acoustic telemetry provides flexible, cost-effective data retrieval. In summary, the SEMS will afford both government and private industry a means of gathering much needed seafloor earthquake data for usein the design and regulation of offshore structures.

References

1. Eterno, John S. et al: "Special Event Detection for an Unattended Seismic Observatory," Charles Starr Draper Laboratory, Cambridge, Mass., Report No. R-765, March 1974.

2. Stearns, S. D. and Durham, H. B.: "Unmanned Seismological Observatory--Seismometers and Signal Processing," Sandia Laboratories, Albuquerque, NM, Report No. SAND-74-0205, Sept. 1974.

3. Reece, Eric W. and Ryerson, David E.: "Development of an Experimental Marine Sediment Instrumentation System," Tenth Offshore Technology Conference, Houston, TX, May 1978.

4. California Institute of Technology: "Strong Motion Earthquake Accelerograms," Earthquake Engineering Research Laboratory, Pasadena, CA, Report No. 71-50, Sept. 1971.

MICROWAVE DETECTION OF ADSORPTION AND SPREADING FILMS AT THE AIR-WATER INTERFACE.

R. Cini
Professor, Istituto di Chimica-Fisica
University of Florence, Italy
Via Gino Capponi 9, Firenze, Italy

P.P. Lombardini
Professor, Istituto di Fisica Generale
University of Turin, Italy
Corso Massimo D'Azeglio 46, Torino, Italy

Abstract

Preliminary microwave experiments are described giving ratio of surface waves damping in water in the presence and in the absence of adsorption filmes and spreading monolayers. The dependence of damping ratio by surface concentration is evidenced. Sea water samples are also tested. The possibility of making use of microwave doppler techniques for the remote sensing of surface pollutants in natural water systems is envisaged.

1. Introduction

The quantitative study of the physico-chemical properties of the air-sea interface is becoming increasingly important (1) (2). Hitherto the most convenient way of acquiring significant parameters in this field of the optical or mechanical measurements of the damping coefficient of capillary waves (3). However, these methods can not be easily extended to include the band of short gravity waves. Yet, this band appears to be particularly important in the wind-sea energy transfer problem.

In the laboratory experiment reported here we have found that a microwave sensor, smilar to the one devised by J.W. Wright (4), can be very† rippled water, and lends itself to qualitative measurements of damping phenomena throughout the band of transition between capillary and gravity waves. Using this method we have discovered a resonance effect in the function relating frequency to the ratio of damping coefficients of waves on a water surface covered by a monolayer, and waves with pure liquid surface. This resonance is theoretically justified (5), and may open the door to possible remote identification of water pollutants from measurement of the water waves spectrum obtained with radar techniques.

2. Laboratory experiments

The experimental set-ip used was as shown in Fig. 1. In essence the method makes use of a microwave sensor, a water tank, and a mechanical wave maker.

In our tests we used water tanks of varied areas: 30.7 x 21.5 cm^2, 54 x 44 cm^2, 700 x 400 cm^2, and depths: 1.5 cm, 5 cm, 70 cm, respectively.

† sensitive to small amounts of surfactant in

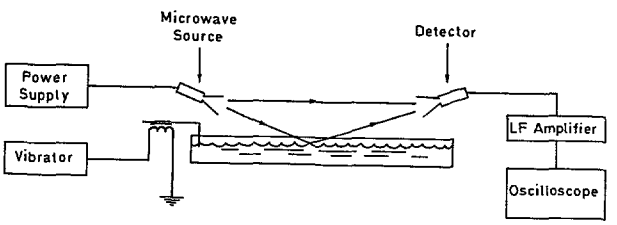

Fig. 1 Experimental set-up

The liquid surface was kept in oscillation with the help of a teflon shaker periodically swung by an electronically controlled vibrator, the frequency of which could be varied from one Hertz to several hundred Hertz. Frequency and position of vibrator were chosen in such a way as to create monochromatic progressive waves on the surface of the tank.

The sensor included a microwave c.w. source and a crystal detector, followed by a low-frequency amplifier and an oscilloscope. Source and detector exchange radiation through horns oriented so that the received field results from both a direct path from the source and forward reflection at grazing angle from the stirred surface. Liquid and radio waves have similar wavelengths and parallel wavefronts. The output of the amplifier displayed on the oscilloscope, being the effect of the time-varying phase comparison of the two links, monitors the water wave.

The frequency of the mechanical vibrator was varied until the oscilloscope showed a pure sinusoidal signal. This condition indicated an output which proved to be proportional to the ampli-

tude of the liquid wave.

Measurements of damping effects were obtained by setting the system into resonance when the tanks was filled with surface pure water, and subsequently observing the decrease of signal caused by the introduction of known quantities of substance in the water. After each test it was verified that the addition of powdered active charcoal in the liquid brought the output signal to an intensity very close to that observed in the initial conditions.

Both adsorption films and insoluble spreading fils have been tested. In the first case the surfactant was Triton X100, having surface activity of $2 \cdot 10^4$ mN·m^2/mole, in concentration $10^{-2} \div 10^{-1}$ ppm, as well as soap in the neighborhood of cmc. In the second case, the surface active material was stearic acid dissolved in exane, which was added to pure water using standard techniques until reaching a condensed monolayered film on the surface of the tank.

Three types of surface pure water were alternatively used: distilled water, tap water and sea water. Distilled water was surface purified with a technique described elsewhere (6). Tap water and sea water were initially micro - strained in order to eliminate colloidal parti - cles, subsequently passed through a column of granulated active charcoal, and finally micro - strained again. The surface activity of all samples was tested "in situ" with the surface dynamic tension method (7).

Fig. 2 shows the behaviour of the ratio of the oscilloscope outputs for undamped vs. damped water as a function of concentration for: (a) - Triton X100, and (b) - Stearic acid, both observed at the microwave frequency of 9.8 GHz.

Fig. 3 shows the oscilloscope output ratios for undamped vs. damped water waves observed at various water wave frequencies. Triton X100, making a saturated film, was tested at the microwave frequencies of 0.9, 1.4, 1.9, 9.8, 17 and 37 GHz. (solid squares). Stearic acid (solid circles) was tested at 1.9 and 9.8 GHz. The continuous lines and the empty squares appearing in the figure will be discussed in section 3.

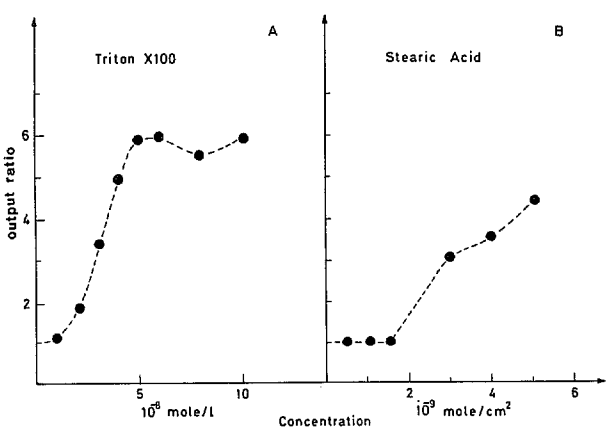

Fig. 2 Signal ratio for surface pure and film covered water vs. molecular concentration for: (a) Triton X100, (b) Stearic acid.

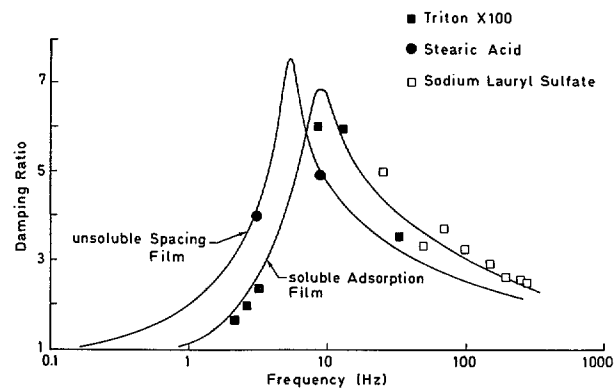

Fig. 3 Damping ratio vs. liquid wave frequency.

3. Discussion and conclusive remarks.

The plot of Fig. 2-a indicates an increasing damping up-to-saturation surface excess vs. massive concentration of an aqueous solution of Triton X100. This is in good agreement with what we have found for the same substance and span of concentrations in measurements of surface dynamic pressure (6). This behaviour may be explained in terms of the relationship binding the damping coefficient with the visco-elastic parameter (8). A similar trend may be noticed in the plots of damping coefficient vs. (log c) for sodium lauryl sulphate in water given by Davies and Rideal (9).
Taking into account the different nature of the two films and notwithstanding that we used a non-ionic solvent, the similarity of the two results is so good to induce infering that our oscilloscope output ratio represents the damping ratio.
Analogous conclusions may be drawn from Fig. 2-b.

On the basis, in the ordinate of Fig. 3 we have identified oscilloscope output ratios and damping ratios.

Turning now to Fig. 3, we observe that the output ratios obtained with Triton X100 are ordered around a maximum, at circa 10 Hz. Elsewhere (5) we have shown that an elaboration of existing theories leads to the deduction that the relationship between the frequency and the damping ratio of surface waves in the presence and in the absence of a monolayer passes through a maximum.

The solid curve of Fig. 3 is a plot of the theoretical function adapted to fit the observed data. For the sake of comparison, we have reported in the figure the damping ratios for sodium sulphate (empty squares) obtained by dividing computed viscous attenuation coefficients by the damping coefficients given by Davies and Rideal (9). The fair agreement of all the squares on the same theoretical curve seems to imply a common trend for different adsorption films in condition of saturation.

In Fig. 3 only two data of a spreading film are reported. In spite of the paucity of data these points are sufficiently displaced from the others to allow the suggestion that in this case the resonance occurs at a different frequency, as shown by the curve.
The different behaviour of the two films may be associated to the fact that in a spreading film the diffusional phenomena are missing.

In conclusion, we believe that further investigation along these lines may lead to a possible identification of the nature of water pollutants based on the proper interpretation of the capillary range of a remotely measured sea wave spectrum.

References

1. R.A. Horne, "Marine chemistry", Wiley-Interscience, New York, N.Y., 1969.
2. W.D. Garrett, "Impact of natural and man-made surface films on the properties of the air-sea interface, in The changing chemistry of the oceans, Nobel Symposium 20, Almqvist & Wiksell, Stockholm, Sweden, 972.
3. E.H. Lucassen-Reynders, J. Lucassen, "Properties of capillary waves", in Advances in Colloid and Interface Science, Elzevier Publishing Company, Amsterdam, Holland, 1969
4. J.W. Wright, "Backscattering from capillary waves with application to sea clutter" IEEE Transactions on Antenna and Propagation, AP-14, 1966, p. 749-754.
5. P.P. Lombardini, R. Cini, "Damping effect of monolayers on surface wave motion in a liquid" J. Colloid & Interface Sci., 1978 (in print)
6. R. Cini, G. Loglio, A. Ficalbi, "Temperature dependence of the surface tension of water by the equilibrium ring method", J. Colloid & Interface Sci., 41, 1972, p. 287-298.
7. R. Cini, A. Ficalbi, G. Loglio, "A simple physico-chemical method of detecting traces of surfactants in water". Microchimica Acta, Wien 1974, p. 203-212.
8. V.G. Levich, "Physico-chemical hydrodynamics", Prentice-Hall, Englewood, N.J. 1962.
9. J.T. Davies, E.K. Rideal, "Interfacial phenomena", Academic Press, New York, N.Y. 1963 (page 270).

ELECTRODEPOSITION OF MINERALS IN SEAWATER

Wolf H. Hilbertz

Marine Science Institute
The University of Texas
Austin, Texas 78712

Abstract

By establishing a direct electrical current between electrodes in an electrolyte like seawater, calcium carbonates, magnesium hydroxides, and hydrogen are precipitated at the cathode, while the anode produces oxygen and chlorine. Recent experiments have demonstrated in part the feasibility of using the electrodeposited minerals as building materials for a wide variety of purposes, including the construction of artificial reefs. Several of these experiments are described and some implications for marine building technology are discussed.

1. Introduction

Sea water contains nine major elements: sodium, magnesium, calcium, potassium, strontium, chlorine, sulfur, bromine, and carbon. These elements comprise more than 99.9% of the total dissolved salts in the ocean(Milliman, Müller, Förstner, 1974; Sverdrup et al., 1942; Culkin, 1965; Goldberg, 1965). The constancy of the ratios of the major elements throughout the oceans has long been well-known (Ditmar, 1884).

In 1837, following Davy's work on the protection of iron by zinc anodes, Mallet showed that zinc so used became covered with a thick layer of zinc oxide and calciferous crystals which blocked the zinc surface (Morgan, 1960; Lynes, 1954).

In 1940 and 1947, G.C. Cox was issued U.S. Patents No. 2,200,469 and No. 2,417,064, outlining methods of cathodic cleaning and protection of metallic surfaces submerged in sea water by means of a direct electrical current. During the cleaning process, a coating is also formed cathodically, consisting of magnesium and calcium salts (Eickhoff and Shaw, 1948). If these coatings are hard and continuous, they afford a considerable degree of corrosion protection to the enclosed metal (Humble, 1948, 1949).

Lower marine organisms utilize the minerals in solution surrounding them to build structural formations. Mollusk shells, for instance, are generally composed of calcium carbonate crystals enclosed in an organic matrix. A significant proportion of the soluble protein of the matrix is composed of a repeating sequence of aspartic acid separated by either glycine or serine (Gregoire et al., 1955; Piez, 1961; Hare, 1963; Hedley, 1958; Simkiss, 1963; Jope, 1971). This sequence, comprising regular repeating negative charges, could bind Ca^{2+} ions and thus perform an important function in mineralization of the template (Weiner and Hood, 1975).

Although impressed current produced $CaCo_3$ / $Mg(OH)_2$ formations were precipitated since the 1940's, these were never thought of as possible building materials until recently. Consequently, only few publications outline structural testing of these materials, describe experiments and techniques using the electrodeposited material for a wide variety of structural purposes, and report on the possible suitability of the material as a substrate for biological growth in mariculture facilities and as a primary construction material for same (Hilbertz, 1970, 1974, 1975, 1976, 1977; Hilbertz et al., 1977).

2. General Experiments

Large-scale studies with galvanized iron mesh cathodes and iron/lead anodes immersed in sea water have provided evidence for the role of electrochemical processes in the accretion of minerals (Hilbertz, 1976). A preliminary qualitative model for these processes has been proposed (Fig. 1).

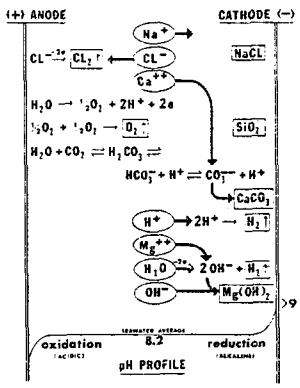

Fig. 1

Potentially, minerals can be accreted by three methods: 1. concentration gradients, 2. ionic

attraction, and 3. electric migration. Concentration gradients are most likely the cause, but combinations of the three methods cannot be precluded (Hilbertz et al., 1977).

In order to devise methods which would allow the solid accretion of a three-dimensional cathode, the "onion" experiment was devised. This cathodic cube consisted of 7 insulated layers of 1/8" galvanized hardware cloth. Immersed in seawater containing a lead anode, layer 1 was connected to the power supply. After sufficient accretion thickness was achieved, layer 2 was connected, and so forth. A solidly accreted cube was obtained. (Figure 2), (Hilbertz, 1976).

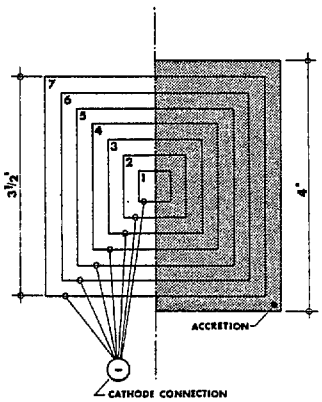

Fig. 2

Parts of beach sand volumes, between electrodes contained in 10 gallon tanks and saturated with sea water, can be solidified. Figure 3 shows a cemented sheet of sand after flushing of loose sand particles.

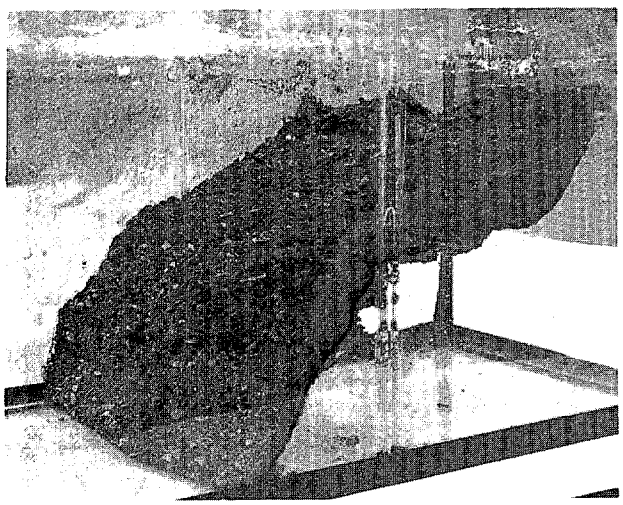

Fig. 3

All previous mineral accretion experiments were performed in water depths ranging from 0-15 ft. An experiment was devised to accrete on a 15 cm by 15 cm ½" galvanized hardware cloth cathode with a 1mm x 15mm x 30mm lead anode at a depth of 450 ft. at Cane Bay, St. Croix for 42 h. A control experiment using the same equipment, power input, and time span was performed at a depth of 1 ft. in Tague Bay, St. Croix. Identical accretion thickness was achieved in both experiments (Fig. 4), (Hilbertz, 1977).

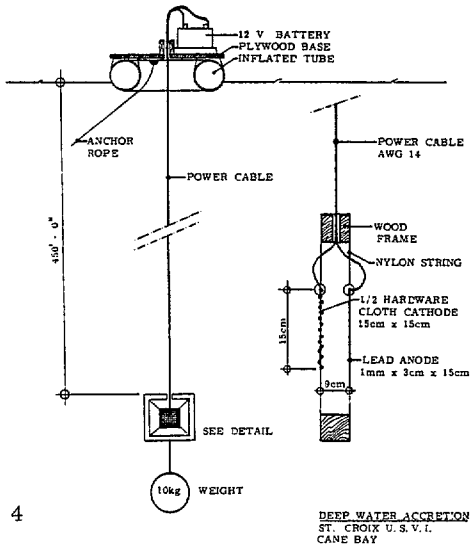

Fig. 4

Samples of electrodeposited materials obtained at St. Croix and at Port Aransas sites were analyzed on a Philips X-ray Diffractometer. Involving an error factor of approximately ±10%, some results are given in Figure 5.

	Compounds and Percentages					
Sample #	Brucite $Mg(OH)_2$	Calcite $CaCO_3$	Aragonite $CaCO_3$	Halite NaCl	Quartz SiO_2	Other
1	80	T	12	T	--	8
2	60	7	17	5	7	4
3	58	2	7	3	4	26
4	40	1	8	2	2	47
5	69	1	24	5	1	--
7	44	T	18	15	--	23
10	77	6	5	12	--	--
11	57	3	25	10	5	--
17	79	2	15	5	--	1
19	83	1	12	4	--	--
20	50	T	15	T	T	35
21	60	3	6	15	--	16
22	50	T	6	T	--	44
23	60	T	5	T	--	35
24	70	9	7	14	--	--
25	45	T	16	--	--	38
26	90	T	10	T	T	--
27	70	T	15	15	--	--
28	73	T	7	20	--	--
30	65	4	18	11	2	--
31	61	1	5	20	T	13
32	40	1	3	2	T	54
33	50	4	10	--	1	35
34	80	2	10	2	1	5
35	33	1	15	4	2	43
36	79	3	5	2	--	11
37	70	1	15	10	1	3
38	50	3	26	8	--	13
42	50	1	25	--	T	24
44	40	4	17	5	1	33
46	68	3	5	8	1	15
47	80	T	4	T	T	16
49	65	T	5	--	--	30
54	80	5	6	2	1	6
60	61	2	10	12	1	14
66	60	3	4	10	--	23
67	68	5	12	4	4	7
73	70	4	25	--	--	1
79	79	3	18	--	--	--
82	88	4	3	5	T	--
86	69	--	20	10	--	1
87	50	4	32	2	3	9
88	89	T	8	3	--	--
92	80	1	18	T	T	--
93	50	3	10	5	T	32
94	58	2	9	8	1	22
95	98	T	2	T	T	--
96	51	1	13	3	T	32
97	70	1	3	1	--	25
98	80	1	8	8	3	--
99	70	2	22	T	T	6
100	25	T	5	15	T	55
101	90	T	7	T	T	3

Fig. 5

A typical section of electrodeposited materials on ½" galvanized hardware cloth is given in Fig. 6. The clearly discernable "rings" reflect periods of time under electric power and without power. It cannot be precluded, however, that seasonal changes also might be reflected.

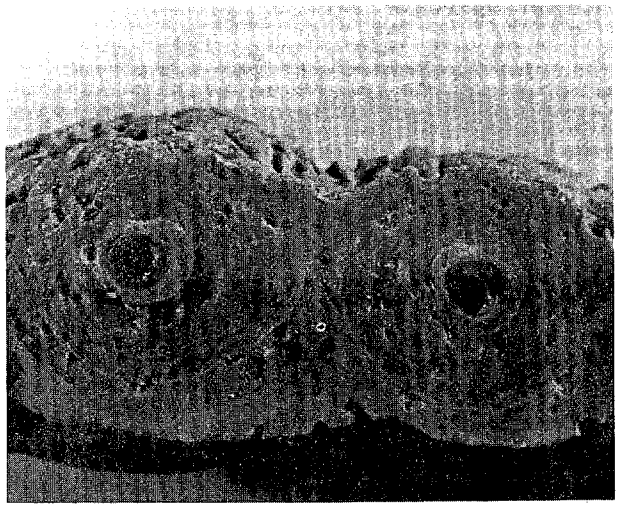

Fig. 6

In order to determine accretion thickness as a function of proximity of electrodes and location of negative pole cable connection, several 72" by 2" $\frac{1}{4}$" galvanized hardware cloth test strips were accreted for 52 hours and mineral deposits were measured every 6 in. (Fig. 7).

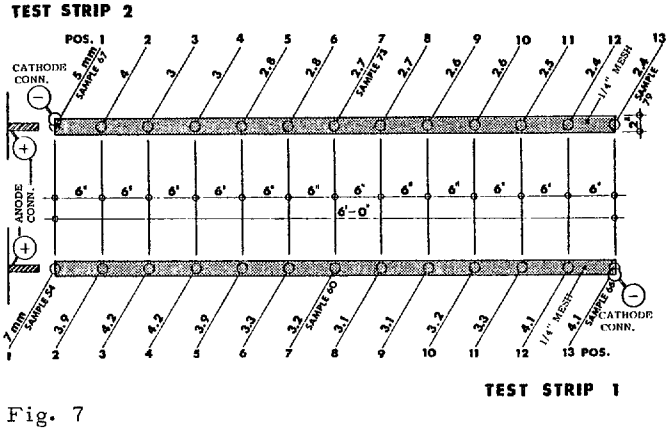

Fig. 7

Direct current was supplied at 10V, ranging between 4 and 10A. As evidenced, multiple cathode cable connections should be spaced evenly to achieve uniform current densities and thereby uniform accretion sections (Hilbertz, 1976).

During 1977 the construction of a cathodic hull for a boat was completed (Hilbertz, 1977). The frame consists of $1\frac{1}{2}$" by $1\frac{1}{2}$" yellow pine to which the double-layered $\frac{1}{2}$" galvanized hardware cloth form is stapled. Spacing between layers is 3/8". This hull is being accreted at the present, consuming DC at typically 12V and 1.5A (Fig. 8).

Fig. 8

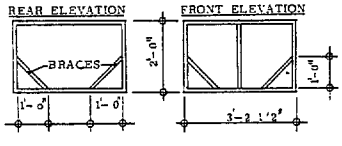

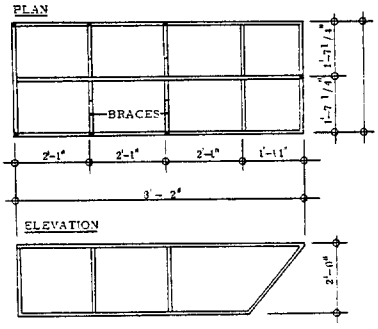

Fig. 8

3. Building Components

To investigate the use of mineral electrodeposition for the construction of building components, several experiments involving large cathodic surfaces were devised. The catenary structure measures 5ft. by 4ft. by 2ft. and is of double-shelled ($\frac{1}{4}$" spacing) $\frac{1}{4}$" galvanized hardware cloth construction (Hilbertz, 1977). Fig. 9 shows the catenary formation before accretion, Fig. 10 after approximately 1000 h of accretion, consuming DC typically at 6V, 5A. The lead sheet anode is in the center of Fig. 9.

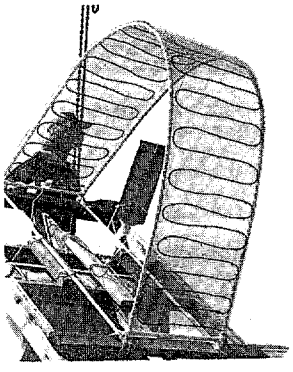

Fig. 9

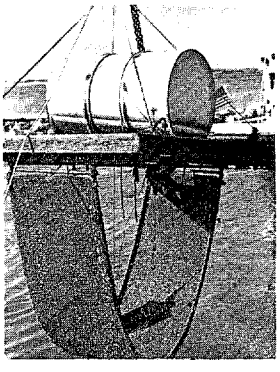

Fig. 10

The 1/2 circle formation is of similar construction (Fig. 11).

Fig. 11

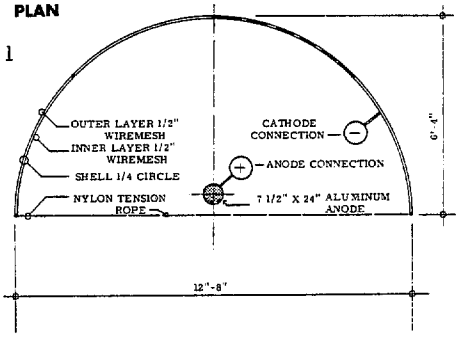

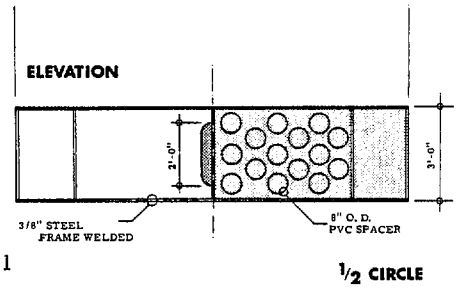

Fig. 11

Hung from a flotation device, it assumed a catenary configuration. The formation was supplied with DC by a winddriven generator located on the site, producing a peak output of 200 W (Fig.12, 13).

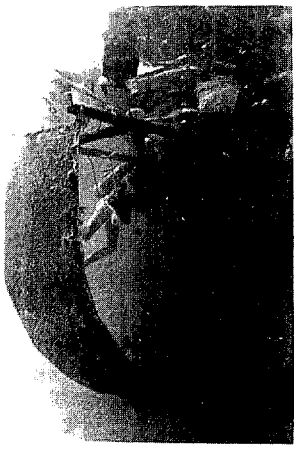

Fig. 12

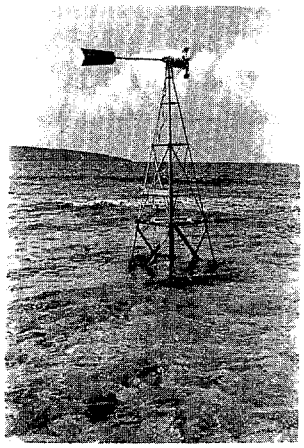

Fig. 13

Likewise, the $7\frac{1}{2}$ ft. by 15 ft. circular column was supplied with DC from two wind-driven generators with a peak output of 200 W each, (Hilbertz, 1977), (Fig. 14).

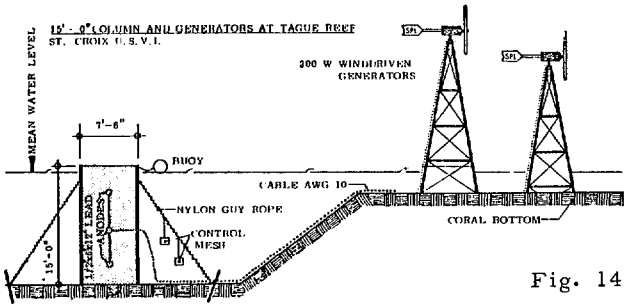

Fig. 14

The structure was of $\frac{1}{2}$" galvanized hardware cloth double-shelled construction with approximately 1" spacing. Three $\frac{1}{2}$" x 6" x 12" lead anodes were positioned along the longitudinal axis of the column.

4. Testing of Mechanical Properties

Twenty samples of electrodeposited minerals obtained on $\frac{1}{2}$" galvanized hardware cloth were prepared and tested at the UT Austin Structural Testing Laboratory. Following standard procedure for concrete testing, compression forces were recorded at the point of breakage (Hilbertz, 1977). Individual and averaged test results reflecting p. s. i. strength are shown in Fig. 15.

TEST P.S.I. IN COMPRESSION OF ACCRETED MINERALS

1/2" HARDWARE CLOTH EMBEDDED IN TEST SAMPLES

SAMPLE #	
1	4350 P.S.I.
2	4470 "
3	4230 "
4	5350 "
5	4410 "
6	4020 "
7	4350 "
8	4380 "
9	4500 "
10	4750 "
11	4530 "
12	5100 "
13	4260 "
14	3990 "
15	3960 "
16	3930 "
17	3960 "
18	3870 "
19	3720 "
20	3930 "

85350 : 20 = 4267.5 P.S.I. AVERAGE

TEST MATERIALS INCLUDED ACCRETIONS
FROM PORT ARANSAS/TEXAS AND ST. CROIX/U.S.V.I.

Fig. 15

For comparison, concrete with 3500 p. s. i. (probable 28th day strength, normal Portland cement Type 1, 15% less than recommended by ACI Joint Commitee) is typically used for stairs and steps, sidewalks, driveways, slabs on grade, and basement wall construction (Olin, 1975).

5. Artificial Reefs

It has long been evident that prominent substrate to which marine organisms can attach and in which organisms can find shelter attracts fish populations. The oldest recorded establishment of artificial reefs dates back to the early 1800's in Japanese waters (Edmond, 1960; Stone, 1975). Since the early 1950's american marine fishery interests have been investigating the possibility of using artificial reefs as management tools for manipulation of fish populations (Stone et al., 1973; Stroud and Massman, 1966). Calculations of fish populations on artificial reefs as compared with control areas or before reef placement showed increases of between 3 to 16 times (Kami, 1959; Arve, 1960; Turner, 1964).
Since the choice of material determines to a large extent transportation, construction, and maintenance costs of artificial reefs and their design, this factor becomes very important.

Preliminary investigations indicate that the mineral accretion process produces a very suitable substrate for marine growth and, at the same time, a strong primary building material (Hilbertz, 1976, 1977). Accreted wire mesh components also present a reduced profile, compared to solid components, which reduces resistance to water currents, thus increasing stability while offering open volumes and entrances for shelter to marine organisms. Placement of steel mats or wire mesh as an artificial substrate in areas predominated by soft, fine-grained sediments has been suggested (De Sylva, 1962). Accordingly, the use of accreted wire mesh may be particularily well suited for these areas.

Two artificial reefs were constructed and placed in Tague Bay, St. Croix in August, 1976. These constructions were built to determine the parameters of the electrodeposition process onto large surfaces as substrate for marine growth, and to support the hypothesis that wire mesh formations covered by electrodeposited minerals can support marine communities usually found inhabiting natural reef formations (Hilbertz, 1976).

Both of these reef components were placed in shallow waters, approximately 8 ft. m.l.t., on relatively barren and sandy substrate with small amounts of seagrass (Thalassia) present. Direct electric current is supplied intermittantly to the components by an unregulated power supply in the range of 12-16V/15-30A. Reef One and Reef Two have been in the water 22 months, and approximately 11 months under power.

Reef One consists of an assembly of regular and irregular shapes constructed with wire mesh having a total surface area of 253 sq.ft. Overall dimensions of the reef are 4ft. x 12.67ft. x 3ft. Average accretion thickness on the wire mesh is 3/8", with thickness in some areas up to 3 in. (Fig. 16). Fish censuses performed $4\frac{1}{2}$ months and 15 months after placement indicated 127 individuals (5 species), and 483 individuals (19 species), respectively. The most dominant fishes were were medium-sized grunts, parrotfish and damselfish.

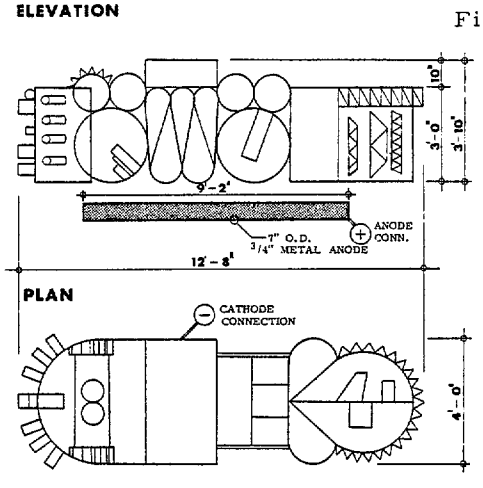

Fig. 16

Reef Two consists of identically folded wire mesh formations of 2 different gauges with a total surface area of 144 sq.ft. Overall dimensions are 7.5ft. x 7.5ft. x 6ft. (Fig, 17).

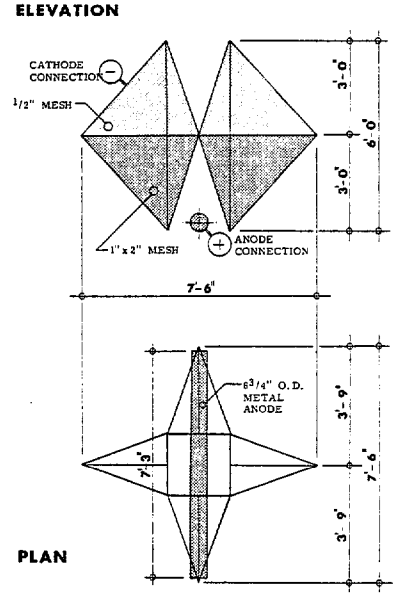

Fig. 17

Fish censuses performed $4\frac{1}{2}$ months and $16\frac{1}{2}$ months after placement indicated 92 individuals (6 species) and 142 individuals (14 species), respectively. Again, the fish population was dominated by grunts, parrotfish, and damselfish. Fig. 18 and Fig. 19 show portions of Reef One after 4 months and 16 months of placement, respectively.

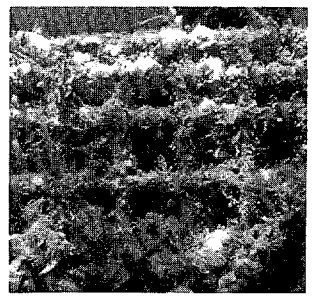

Fig. 18

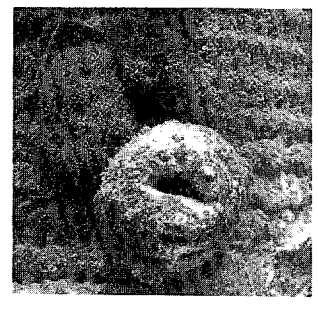

Fig. 19

In order to determine to what degree the electrodeposited minerals on wire mesh formations enhance the development of marine communities, and to what degree the wire mesh formation simply acts as an attractant, two reef components were constructed and submerged in August, 1977

in Tague Bay. Both components are identical in size and construction, each consisting of folded plate $\frac{1}{2}$" galvanized wire mesh formations having a total surface area of 192 sq. ft. and overall dimensions of approximately 19.5ft. by 5ft. by 4.5 ft. in height (Fig, 20).

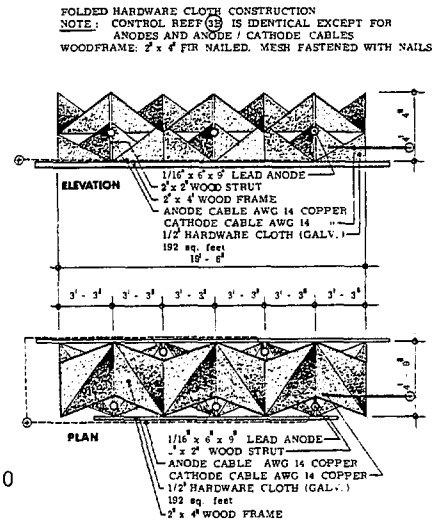

Fig. 20

Both components are situated in 15 ft. m.l.t. on a relatively barren, sandy bottom with a small amount of seagrass (Thalassia) present. One component (Reef 3a) is supplied with DC from an unregulated power supply in the range of 12V/20A; the other component, Reef 3b, is not under power, thus acting as a control since no electrodeposition occurs, and is situated approximately 265 ft. from Reef 3a. Floral and faunal censuses are taken every 6 weeks at both the accreting reef and the control reef. Fish counts taken $6\frac{1}{2}$ months and 8 months after placement of Reef 3a (under power) indicated 17 individuals (8 species) and 33 individuals (35 species), respectively. Fish counts taken at the same time on Reef 3b indicated 33 individuals (10 species) and 16 ind. (7 species). More than 39 spiny lobsters (Panulirus argus) were seen in Reef 3a, while none were seen in Reef 3b, 8 months after placement.

Two artificial reef assemblies are proposed along the Texas coast, utilizing the mineral accretion process on wire mesh components. The two reef assemblies will be supplied with DC each by a 600 W wind-driven alternator, allowing the utilization of locally available energy (coastal winds) to power the components. Accreted wire mesh formations as reef material may also represent a considerable reduction in transportation and material costs when compared to concrete block or tire reefs, as the bulk material (substrate for marine growth) is assimilated directly on the site. In addition, the initial layer of electrodeposited material prevents corrosion of the wire mesh template.

Each reef assembly will consist of 10 folded plate wire mesh components having overall dimensions of 3ft. x 4ft. x 10ft. (Fig. 21).

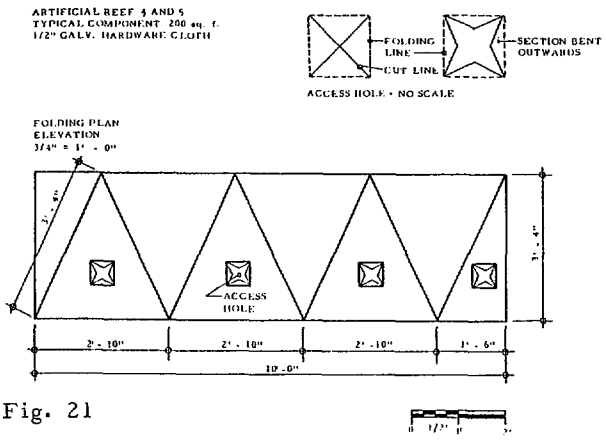

Fig. 21

Total surface area of the wire mesh used in each assembly is 2000 sq, ft. The components will be arranged uniformly over a 46ft. x 18ft. area (828 sq. ft.) (Fig. 22).

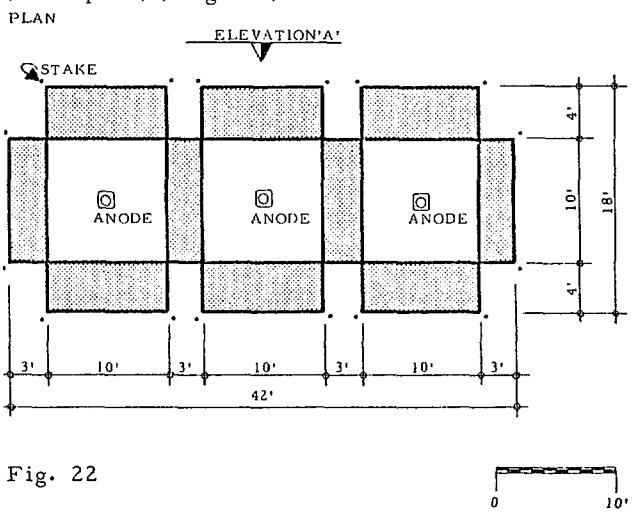

Fig. 22

6. OTEC Facility Proposal

The mineral accretion process potentially can contribute significantly to the solution of formidable engineering tasks which will be undertaken in the oceans, like the construction of Ocean Thermal Energy Conversion plants. It is evident, for example, that the use of traditional engineering materials like steel or fiber reinforced concrete and tubular steel for the construction of OTEC systems cold water supply pipe will produce enormous costs because the system will have to be overdesigned in respect to unknown or only vaguely defined parameters.

Quite to the contrary, a relatively light aquadynamic cathodic tube configuration (Fig. 23) which

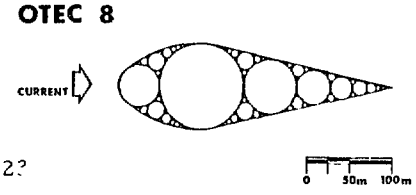

Fig. 23

permits assembly on the plant on-site, can be accreted selectively in order to effectively withstand changing and unpredictably occurring forces (e.g. changing currents).

In case of slowly or suddenly occurring damage to the wall section, the tube can be repaired by placing an anode in the vicinity of the damaged portion, thus facilitating, for instance, cementation of cracks, replacement of lost materials, and reinforcement of previously deposited mineral layers. The OTEC plant is moored and moves with prevailing currents (Fig. 24).

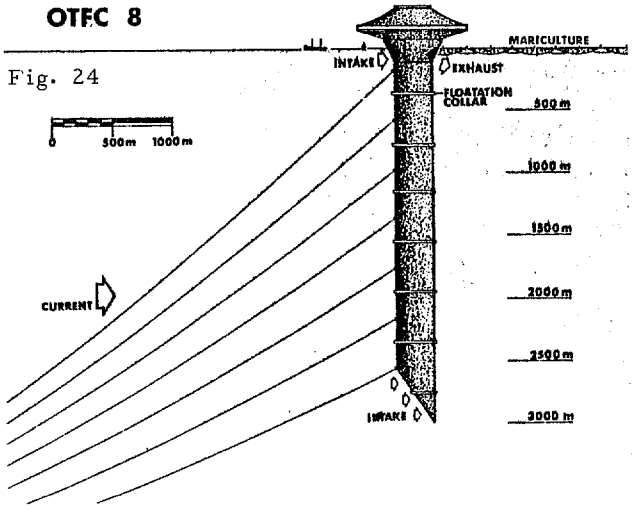

Fig. 24

Aside from converting ocean thermal energy into electricity, the plant can also produce cryogenized hydrogen, ammonia, and $Mg(OH)_2$ (brucite) as a byproduct of the electrolysis process used to provide uplift of cold water in the deep water pipes (Fig. 25).

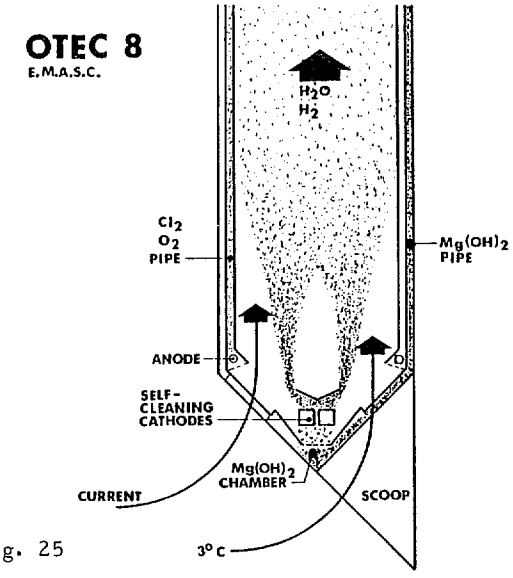

Fig. 25

Through the application of heat, brucite can be directly reduced to the mineral periclase (MgO). Thus, the plant may produce refractory magnesia at potentially competitive cost and additionally provide raw material for magnesium production. The Cl_2 gas, resulting from electrolysis, can also be utilized. While building a considerable, but not yet calculated head, the upwelled water/gas mixture can drive turbines. The nutrient rich deep water should be utilized at the surface as a mariculture medium.

7. Summary and Conclusions

Electrochemical accretion of minerals in sea water and other media (e.g. blood serum=internalized ocean) appears to be as old as life itself and seems to have proven its worth in evolutionary time.

Artifactual building methods, as used at the present, are mainly brainchildren of the first industrial revolution with built-in limits (Hilbertz, 1970). Example: A concrete or steel element in sea water, once broken or decayed, is useless because it cannot meet its design specifications unless it is repaired. In most cases repair necessitates removal from the site and repositioning, thus incurring unreasonably high cost.

An element produced by electrodeposition, however, can be repaired or reconditioned in situ after failure. With renewed electrical power input the same conditions and resources which formed the element initially can be utilized again. This characteristic is not found in any commonly used construction method or material.

When, for instance, a reinforced concrete volume is cured and has left the form, its structural and formal characteristics can be altered only by major operations. Thus, strict limits concerning the element's adaptability to changing conditions are enforced.

Applications for the electrochemical accretion process can be seen readily: floating habitats and industrial islands (Spilhaus), (Fig. 26), using clay refuse (bauxite) as a construction material, stabilized by mineral accretion.

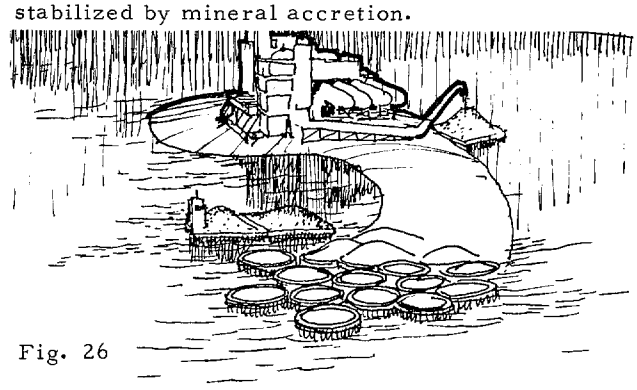

Fig. 26

Settlements on banks, seamounts, and the continental shelf (Fig. 27), mariculture facilities, underwater storage tanks, dams and jetties, pipelines, bridges, tunnels, airports, beach accretions, current diverters, building components for use on land, etc.

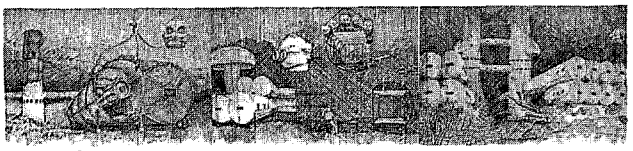

Fig. 27

Moveable articulated form generators can be designed for a wide variety of purposes (Fig. 28).

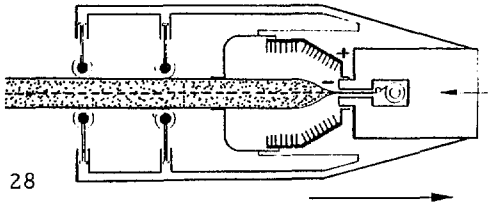

Fig. 28

The medium for construction, maintenance, modification, repair, and reclamation of structures produced by this process covers 70.8% of this planet.

Energy requirements for electrochemical mineral accretion are modest and can be met everywhere locally by utilizing solar energy in its various forms.

References

Arve, J., Ches. Sci., 1 (1): 58-65, 1960.

Culkin, F., in Chemical Oceanography, J.P. Riley and G. Skirrow, eds., (Academic Press, London 1965), Vol. 1, p. 121-161.

De Sylva, D. P., in Base for Reefs, SFI Bull. (125): 4-5, 1962.

Dittmar, W., Challenger Repts., Phys. and Chem., (1), 1-251, 1884.

Edmond, L., Foreign Service Dispatch No. 180 (4pp), Am. Emb., Tokyo, Dept. of State, Washington, D.C., 1960.

Eickhoff, A.J. and W.E. Shaw, Corrosion, 4: 463-474, 1948.

Goldberg, E.C., in: Chemical Oceanography, J.P. Riley and G. Skirrow, eds., (Academic Press, London, 1965), p. 163-196.

Gregoire, C., G. Duchateau, M. Florkin, Am. Inst. Oceanogr., 31 (1), 1955.

Hare, P.E., Science, 139 (216): 1, 1963.

Hedley, R.H., Proc. Zool. Soc., (130): 569, 1958.

Hilbertz, W.H., Progressive Architecture, pp. 98-103, May, 1970.

_____, in: The Responsive House, E. Allen, ed. (MIT Press, Cambridge, 1974), p. 272.

_____, Submarin, 6: pp. 40-41, 1975.

_____, Ind. Forum, 6 (2): pp. 53-56, 1975.

_____, Arch. Sci. Review, 19 (4): pp. 84-86, 1976.

_____, Man- Env. Syst., 6: pp. 60-62, 1976.

_____, Seagrant Rept. No. 04-6-158-44111, 1976.

_____, SPL Rept. No. 2, The U. of Tex., 1977.

_____, Deutsche Bauzeit., (5): 14, 1977.

_____, in Minimal-Konstruktionen, Bubner, Baier, Koenen, Oelbermann, eds., (Verlagsgesellschaft Rudolf Müller, Köln- Braunsfeld, 1977), pp. 191-203.

_____, D. Fletcher, C.R. Krausse, Ind. Forum, 8 (4-5): pp. 75-84, 1977.

Humble, H.A., Corrosion, 4: pp. 358-370, 1948.

_____, Corrosion, 4(9): pp. 292-302, 1949.

Jope, M., in: Comprehensive Biochemistry, M. Florkin and E.H. Stotz, eds., (Elsevier, Amsterdam, 1971), Vol. 26, Part C, p. 749.

Kami, H.T., USFWSFA Hawaii F-5-R-8 (Job 10) Job Completion Rept. (Unpub. Ms.), 1959.

Lynes, R.M., Corrosion, 10 (2): 59, 1954.

Milliman, JD., G. Müller, U. Förstner, Marine Carbonates, (Springer-Verlag, N.Y., 1974).

Morgan, J.H., Cathodic Protection, (MacMillan, N.Y., 1960).

Olin, H.B., Construction, (The Institute of Fin. Educ., Chicago, 1975), Sec. 203-3.

Piez, K.A., Science, 134: 841, 1961.

Simkiss, K., Comp. Biochem. Physiol., 16: 427, 1963.

Spilhaus, A., personal comm.

Stone, R.B., C.C. Buchanan, R.O. Parker, Jr., Final Report, Murrels Inlet, S.C., 1973.

_____, Exxon, U.S.A., 1975.

Stroud, R.H., W.H. Massman, SFI Bull. (1970): 1-8, 1966.

Sverdrup, H.V., M.W. Johnson, R.H. Fleming, The Oceans: Their Physics, Chemistry, and General Biology, (Prentiss-Hall, Inc., N.J., 1942.

Turner, C.H., Underwater Soc. Amer., Fifth Ann. Conv., Mexico, D.F., (Unpub. Ms.), 1964.

Weiner, S., L. Hood, Science, 190 (4218): pp. 987-989, 1975.

Acknowledgement:

This work was in part supported by NOAA/Seagrant, the University of Texas Marine Science Institute, the University of Texas Research Institute, and the Texas Coastal and Marine Council. Much help has been given by the West Indies Laboratory, St. Croix, Fairleigh Dickinson University.

JANUS IV CONSTRUCTION DIVING AT 460 M (1509 FT)
NEW WORLD RECORD AT 501 M (1644 FT)

H. G. DeLauze
Comex Industries
287 Chemin de la Madraque Ville
B. P. 49
13314 Marseille Cedex 3
France

J. L. Chasserot
Comex Industries
287 Chemin de la Madraque Ville
B. P. 49
13314 Marseille Cedex 3
France

Abstract

New compression tables developed by Comex for the experimental diving project, JANUS IV, extend diving capabilities. Divers were at bottom pressure for about 60 hrs. Three men made excursion dives to 501 m (1644 ft).

Three factors contributed to the success of the project:

+ new compression tables that minimize the effects of high pressure nervous syndrome (HPNS) through control of nitrogen during compression.
+ diver confidence in the proven reliability and quality of the equipment used.
+ high capability of the divers.

A diving team, with Comex as operator, set the new diving depth record and at the same time effectively doubled the depth at which men can work at ambient pressure by conducting pipeline connection operations at 460 m (1509 ft).

1. Introduction

The dives were made from the dynamically positioned drillship Petrel, off the south coast of France between the Ile de Levant and Cap Benat in the Mediterranean Sea. Involved with Comex were the Centre National Pour l'Exploitation des Oceans (CNEXO) and the French Navy. The Elf-Aquitaine Group loaned the $71,000/day drillship Petrel as a surface base:

Operation JANUS IV had two main aims:

+ to prove that it is possible for divers to descend in the open sea to 460 m (1509 ft).
+ to prove that, once there, divers could successfully undertake the type of tasks currently performed at lesser depths of 215 m (705 ft) and occasionally at 300 m (about 1000 ft).

The schedule called for diver compression to begin during the morning of Oct. 15, 1977. This would be followed by 3 days of diving and work with the end of saturation taking place in Marseille on Oct. 28. Six divers - 4 from Comex and 2 from the French Navy - undertook the operation.

Divers setting the record for the excursion dives to 501 m (1644 ft) were Jacques Verpeaux of Comex, and Chief Petty Officer Gerard Vial of the French Navy, with Patrick Raude of Comex operating the bell. The record was set between 3:20 and 4:20 P.M. Oct. 20, 1977. The second diving team, which continued the pipe connecting operation at 460 m (1509 ft), consisted of Phillipe Jeantot and Louis Schneider, both of Comex, and Senior Chief Petty Officer Emile Sevellec, French Navy.

2. JANUS I, II, III: 3 Earlier Operations

JANUS IV stemmed from 3 earlier stages which built up to the 460 m dive. Nine years

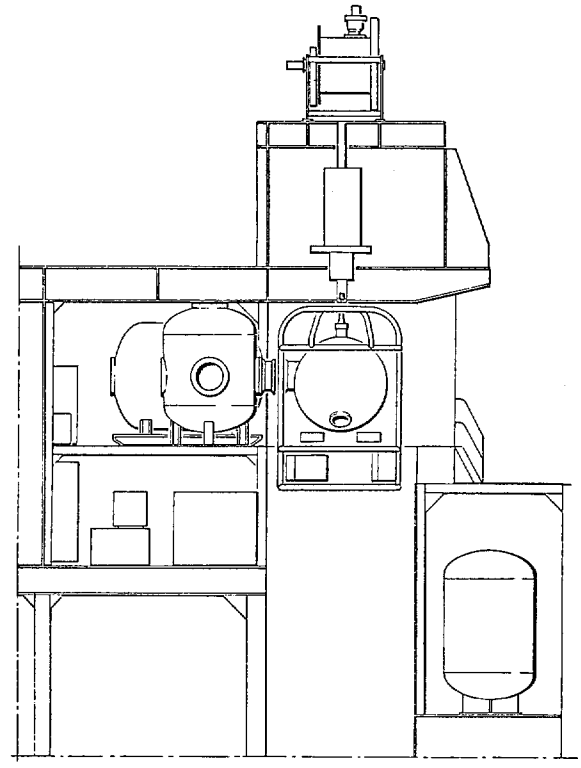

Plane view of diving system aboard Petrel

prior to Janus IV, Elf, Comex and the French Navy had jointly financed and organized JANUS I. At 150 m (500 ft) on the side of the Fosse de Cassidaigne, off Cassis, also in the Mediterranean Sea, two 2-man diving teams worked successively on an offshore wellhead, each team being saturated six days. This was the first time such an operation was performed by divers living in saturation chambers aboard a surface vessel.

Almost two years later, CNEXO, Elf and Comex jointly sponsored JANUS II, which further advanced deep diving capability. The location was Bay of Ajaccio, off Corsica, and the depth tackled was 253 m (830 ft). Three Comex divers descended twice daily to an actual work site, successfully cutting a pipeline and welding the connection.

The fact that 13 dives, 26 hours of bell bottom time, and 35 man-operating hours were logged proved that specially trained and equipped divers could work at such great depths.

The depths at which men can work are, of course, linked to the solution of physiological and biotechnological factors. JANUS III took place at the hyperbaric facilities of Comex in Marseille in April, 1975. Simulated working dives could be conducted there in water pressurized to the equivalent of 390 to 450 m (1280 to 1475 ft).

The success of this work was reinforced when, in June 1975, a team of Comex divers performed a subsea operation at the unprecedented depth of 326 m (1070 ft) off the Labrador coast. Recovery of a wellhead was done from the dynamically positioned drillship Havdrill in water at a bone-chilling temperature of -2° C!

3. JANUS IV: Dive Preparations

Following JANUS III, JANUS IV got underway in Oct. 1976. The 4th stage consisted of three phases: two preparatory and the actual open ocean dive a year later in Oct. 1977.

The first phase of JANUS IV was designed to select the divers most suited to the very deep diving and the work likely to be done. Twenty pre-screened volunteers were subjected to 7 tests in the 180 to 210 m range (590 to 690 ft). These tests, in addition to the usual obligatory medical control, evaluated:

+ Sensitivity to decompression. A watch was kept for trembling, dizziness, nausea, dysmetria, and high pressure articular syndrome.
+ Sensitivity to high pressure. An electroencephalogram (EEG) checked for the slow waves characteristic of high pressure nervous syndrome (HPNS).
+ Alertness. Psychosensory tests were made of such items as visual choice reaction time. Intellectual tests measured such items as number sequence and perception of sign barriers. The tests were accompanied by EEG and pulse-rate measurements.
+ Manual dexterity. A test was used on the arrangement and insertion of pegs in holes.
+ Function study. Measurement was made of cardio-respiratory adjustment to physical work, of ventilatory mechanics, vital capacities, electrical impedance and air bubble detection.
+ Physiological reactions analyzed by urinalysis.
+ Self-evaluation capacity measured by questionnaires completed by the divers.

As a result of Phase I, eight French Navy and Comex divers were selected. Phase II in Dec. 1976 reduced the number to six and checked out the performance of all equipment for the final open sea phase. Phase II was effectively a dress rehearsal for Phase III, simulating as closely as possible in the carefully controlled conditions of the Comex hyperbaric modular complex, the 460 m (1509 ft) pressure depth to be encountered in the open sea.

4. Phase II of JANUS IV: A Preparatory Hyperbaric Dive to 480 m (1575 ft)

Eight divers lived for 8 consecutive days at a pressure corresponding to 400 m (1310 ft). From this depth, excursion dives were made in a special pressurized pool to 430 m, 445 m, 460 m and 480 m.

During the first two days, 6 dives, which totaled 9 hours 15 minutes work time - indicated an ability to work in 430 m (1410 ft) of water at 4° C. Four additional work dives were made to 445 m (1460 ft) for 5 hours altogether. Then, to simulate the sea goal, 12 work dives over 3 days achieved 12 hours 15 minutes at 460 m (1509 ft). Finally, a dive to an unprecedented 480 m (1575 ft) was made for 10 minutes in 6° C water. The task tackled was the assembling and tightening up of a puzzle-assembly of twenty elements of 2-inch pipe.

The 6-man team selected was now ready for Phase III. Over the 3-day period of the work dives, they would make an 8-inch pipeline tie-in with the Comector mechanical connector, which achieves a tight seal entirely by mechanical compression. There are no hydraulically operated devices or epoxy injections with the Comector. Once set, it remains rigid even if pipeline pressure is released. It can be reset easily or uncoupled, and ample adjustment is provided to facilitate connection of misaligned pipes. Applications range from riser repair and installation to tanker loading hose connections.

5. The Working Dives: October 18-21, 1977

Prior to the Janus IV operation, certain special equipment was added to the surface support vessel Petrel. One piece of equipment was a work table patterned after an exact replica of a typical subsea pipe laying situation, built on a 10 x 10 m (1076 sq. ft.) metal base.

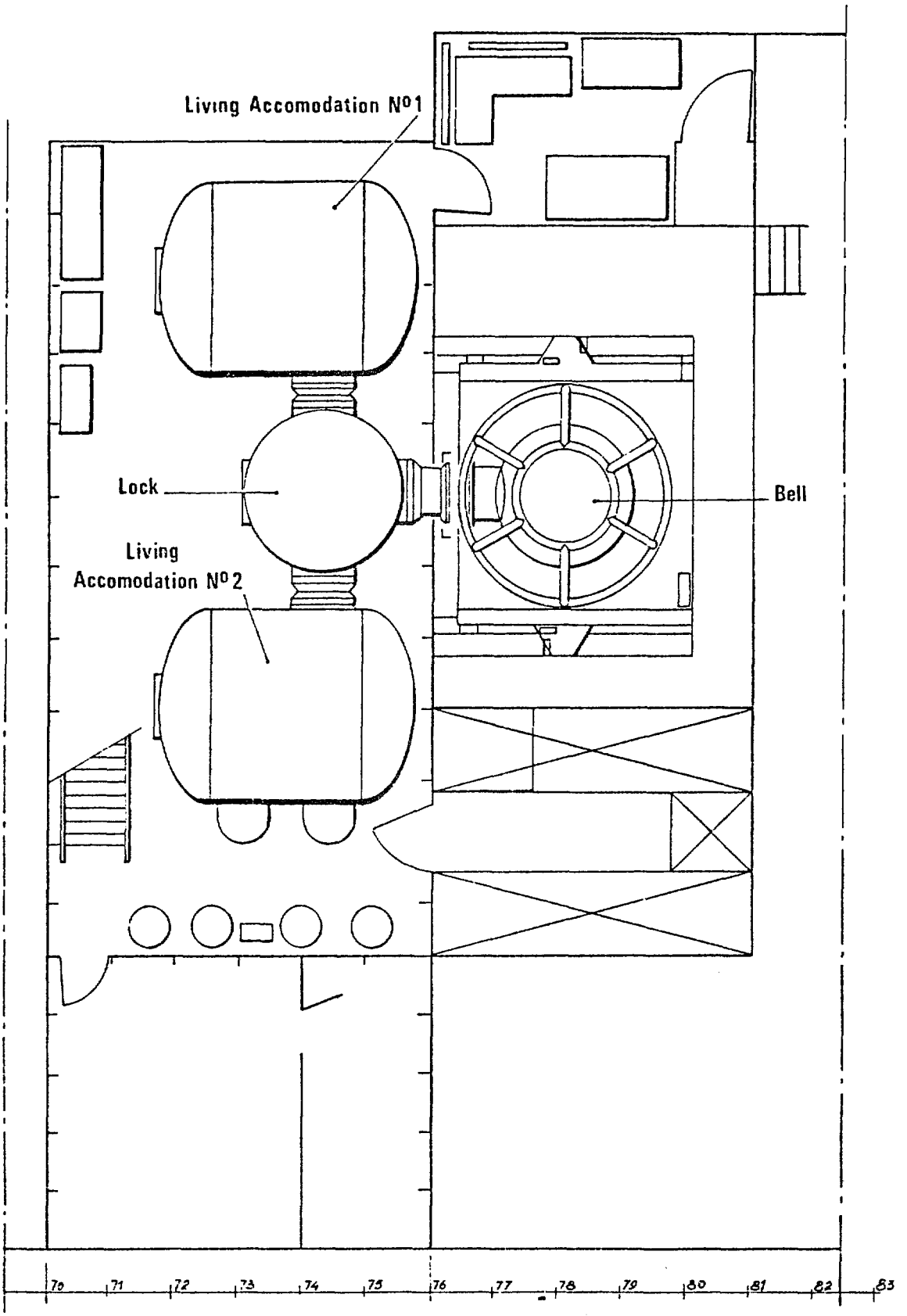

Elevation of Diving System aboard Petrel

The work table contained two pipeline sections with all the material required to connect them:

+ crosscut circular saw
+ welding station
+ Comector

The work table was submerged to a depth of 460 m (1509 ft) through the moon pool, through which, ordinarily, goes the BOP stack and riser.

Onboard Petrel, the six divers were saturated to a living depth of 430 m (1410 ft) in two teams of three. They descended from the life chamber in which they were confined onboard Petrel to a depth near the work table via the diving bell. The two teams of divers alternated traveling in the bell to 450 m (1475 ft) and diving to the 460 m (1509 ft) working depth. Each diver was outside the bell twice. The working dives, conducted between 10:42 A.M. on October 18 and 12:15 A.M. on October 21, totaled ten hours.

6. The Record Breaking Dive: October 20, 1977

On October 20 between 3:20 and 4:20 P.M., divers undertook two 10-minute dives to 501 m (1644 ft) and thereby broke the previous world depth record, 350 m (1148 ft) established in 1975 by the U.S. Navy.

The success of JANUS IV was the joint accomplishment of a closeknit, homogenous team comprised of personnel from Comex, CNEXO, DRET, the French Navy (Gismer) and the Petrel.

Approximately 100 doctors, scientists, engineers and technicians took turns in a round-the-clock surveillance of the six divers confined to hyperbaric chambers on Petrel. Their monitoring activities ensured that operations progressed satisfactorily and reminded one of the ground crew's role during a manned spaceflight.

Using data from television monitors, remote control networks, pressure gauges and gas manifolds, support team members prepared breathing mixtures, distributed the gas to the onboard chambers or the submerged bell, and supervised the regeneration of gases and control of the aquanauts' environment. Other support team members made sure that the underwater missions assigned each diver were correctly carried out. The medical team monitored the divers' behavior during compression and decompression. Engineers controlled the functioning of equipment they had put into use.

The combined efforts of all team members is how, over a 6-day period, divers were able to work effectively at a depth of 460 m (1509 ft) for ten hours. During this time, the divers performed all required tasks (pipe cutting out, welding, alignment, fitting of a Comector) with a physical, as well as psychological, ease which surprised all observers.

7. Undersea Work Results

Results of undersea work assignments performed by JANUS IV divers indicated that divers are able to perform pipeline connections identical to those commonly made in the 100-200 m (330-655 ft) range, but now at substantially greater depths. The work assignments were:

A) Welding and oxyarc-cutting feasibility trials. The main purposes of the trials were:
   + to determine the reliability of the underwater welding equipment pressure-equalized at 45 bars,
   + to try out the electrodes which had been modified by Comex for in-the-wet welding,
   + to determine the operational validity of cutting and welding at a water depth of 460 m.

B) 8" pipeline connection with a mechanical connector. The connection was made with the 8" Comector under the worst possible conditions:
   + using inflatable air bags,
   + without any rigid base or structure on which a crossbar could be mounted,
   + sustaining a heave of approximately 1 m (3.3 ft).

8. Decompression

An ultrasonic "Doppler-effect" device, developed by Comex, the I.N.S.A., and the C.E.R.T.S.E.M., was used to detect moving nitrogen bubbles. This portable apparatus, which can be used in a pressurized chamber, detects nitrogen bubbles in the heart and the pulmonary artery before they reach the lungs by means of a subcutaneous sensing element placed over the precordium. Only a trained operator can differentiate between the bubble stages.

9. The Future

Successful completion of JANUS IV would have been simplified had compression to 500 m (1640 ft) been feasible from the start. Since equipment on Petrel limited initial compression to 430 m (1410 ft), the additional 30 m had to be added during descent. The breathing mixture was mostly helium with 1% oxygen and a few parts nitrogen. Compression to 430 m took 30 hours and an additional half-hour was added for compression to 460 m. Decompression time from 460 m to 430 m took about an hour. Decompression time from 430 m to end of saturation was just over 7 days and 17 hours.

When will JANUS V take place and at what depth? No one yet feels the need to say. In perfecting the technology which now enables men to work at a depth of 460 m (1509 ft), Comex has given the oil industry access to areas where possible commercial exploitation has been seen but for which the diving technology was not available for production operations, even

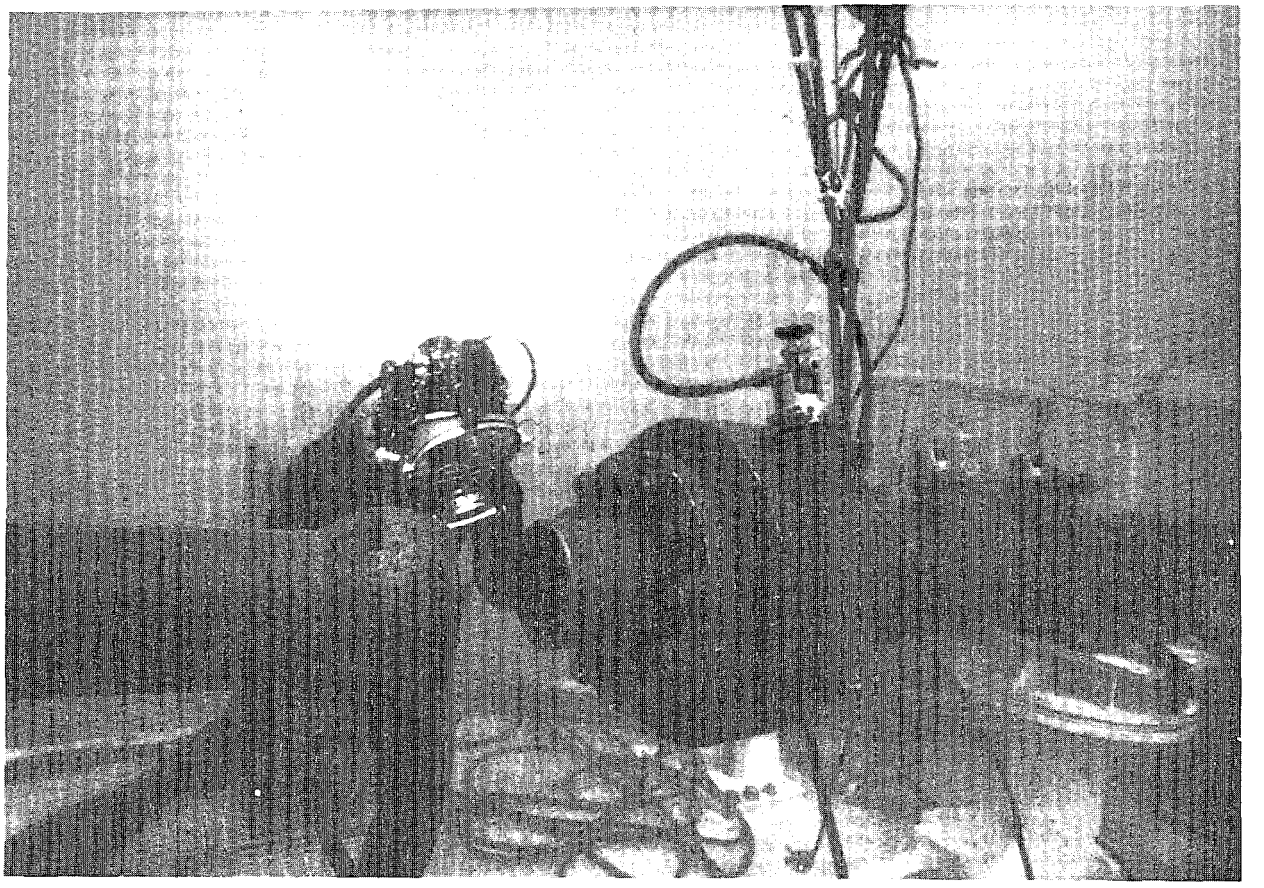

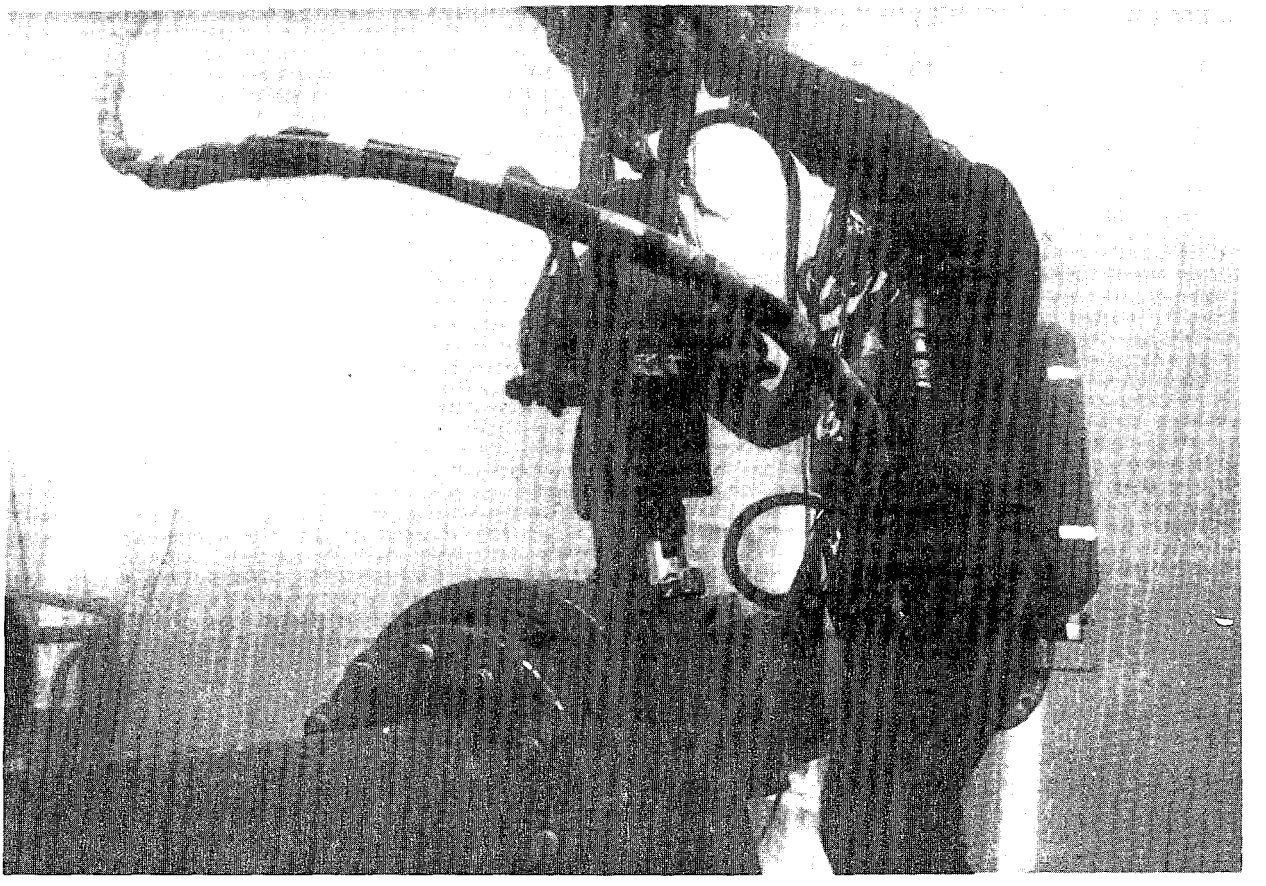

Installation of Comector during Phase III of JANUS IV

though drilling has been satisfactorily performed at these depths. The commercial significance of JANUS IV is enormous, now that the experience, technology, and equipment is available for work in these depths.

10. Conclusion

On Saturday, October 29, 1977 at 5:30 P.M., the six divers came out of the hyperbaric chambers in which they had been confined for a total of 14 days. Waiting to greet them was an enthusiastic crowd of friends and personalities including Mr. Henri DeLauze and Mr. Antoine Rufenacht.

To Mr. DeLauze this moment marked the latest achievement of his continuing efforts during fifteen years as founder and head of Comex to establish his company and his country as a world leader in the conquest of the ocean depths. Mr. Rufenacht, Secretary of State, came to announce to the six aquanauts that the President of the French Republic had accorded them the honor of "Chevalier de l'Ordre du Merite National". This distinction is shared among all those who contributed in making the JANUS IV operation a successful "first" in diving technology.

About the Authors

Mr. H.G. DeLauze is founder, chief executive officer, and a major stockholder in the Comex Group of international diving and underwater products and services companies, headquartered in Marseille, France. Mr. DeLauze has received international recognition for his pioneering achievements over the years in diving and underwater technology.

Mr. J.L. Chasserot is Assistant Commercial Director of Comex Industries, which is the equipment manufacturing company in the Comex Group, supplying submersibles, hyperbaric centers, and diving systems to governmental and commercial organizations worldwide. An industrial engineer by training, Mr. Chasserot has worked in major shipyards in the United States and Europe prior to joining Comex Industries.

SUBSURFACE LAYERED MEDIA PARAMETER ESTIMATION USING A LINEARIZED MULTIPLE REFLECTION MODEL

Ferial M. El-Hawary
Faculty of Engineering & Applied Science
Memorial University of Newfoundland
St. John's, Canada, A1B 3X5

William J. Vetter
Faculty of Engineering & Applied Science
Memorial University of Newfoundland
St. John's, Canada, A1B 3X5

ABSTRACT

The purpose of this paper is to address the problem of determining the geometry of subsurface sediment layers and rock strata. This has considerable importance in diverse activities in the ocean environment. We use a multiple - reflection model that gives the mathematical description of the effects of layered media on the response to implusive type acoustic excitations in the water. The parameters of the model are propagation delays and reflection/transmission coefficients at the boundaries between layers. Least squares criteria are employed in estimating parameters such that the response of the model shows good correspondence with field data. In the present paper we apply a linearization procedure to the composite pulses to accommodate the inherent time delay phenomena. Efficient estimators developed and computational experience related to field data studies performed are discussed.

1. Introduction

Acoustic wave propagation and reflections in water and in the underlying sediments and rock formations for a broadband pulse-type source signal are considered in this paper. Use is made of a model closely related to those introduced and used by Robinson [1-2], Mendel [3], Nahi and Mendel [4], Mendel and Kormylo [5]. The model characterizes the subsurface in terms of multi-layered media. The parameters are time delays in the various layers associated with the wave propagation and amplitude parameters which are functions of the reflection coefficients at the interfaces. The thickness can be estimated (given the velocity of propagation in the medium) with the estimated travel time in the sediment or rock layer.

Much of the work reported in the literature was largely motivated by seismic exploration for hydrocarbons in the land-based environment. The approach and techniques are, however, equally applicable to deep-seismic exploration and for shallow-seismic studies of sediments and rock strata under the ocean. In the latter case, the potential uses include identification of layer topology and media properties towards siting of off-shore structures and pipelines and as possible sources of building material. The modeling activity and analysis of experimental data contributes towards an increased understanding of propagation effects and signal deterioration in the various media, and to the general knowledge of subsurface properties.

A recent paper [6] reports on efforts by the authors towards estimation of parameters characterizing the dominant acoustical characteristics and geometry of layered subsurface media. A cross-correlation type estimation scheme has been developed which generates estimates for return pulse delay parameters and near minimum variance estimates for return pulse amplitude parameters. The present effort is directed towards improving discrimination for composite pulses, relating the return factor estimates $\hat{a}_i$ and return delay factor estimates $\hat{\tau}_i$ to the individual layers in a medium. For this purpose a novel linearization scheme is employed which results in an efficient implementation procedure.

2. A Model For Layered Media

The phenomena of Sound propagation (in water and Solids) for a single medium can be described by partial differential equations in pressure, scaler velocity potential and velocity of propagation in medium. At an interface between two media the physics of the situation impose boundary conditions of compatibility of pressure at the boundary and of continuity of particle velocity across the boundary. The propagation phenomena are not readily described in a tractable solution form in general. Exceptions to this include the cases of simple geometries, parallel interfaces, normal incidence and lossless media. In the latter case and for a medium of infinite extent, the local pressure waveform will be a direct replica of the signal source pressure waveform (at a far field distance of a real source) delayed by a time $D(x) = x/c$. If pressure pulses impinge on boundaries between media at normal incidence, then energy is partly transmitted and partly reflected. Each reflection and multiple reflections contribute to amplitude scaling of the respectively incident pressure signal. No further reflections occur from a pulse which has entered the "basement" medium.

The multiple-reflections result in a received pressure signal in the water above subsurface which consists of a sum of replicas of the source pulse. Each replica has an amplitude scaled by the respective reflections-transmissions encountered, and is delayed in accordance with the respective propagation time in the media traversed. The input-output relationship, obtainable either by ray tracing or from the layer geometries following for example Mendel's formulation [3] can be written as

$$y(t) = \sum_{i=1}^{\infty} a_i \, m(t-\tau_i) + v(t) \qquad (1)$$

where each term $a_i \, m(t-\tau_i)$ is a replica component. These components may arise from primary, secondary, and higher order reflections, i.e. a_i are functionally related to reflection coefficients r_i at the interfaces between layers, and τ_i are related to the layer delay coefficients D_i. The "measurement noise" $v(t)$ is the aggregate of effects not accomodated by the model such as acoustical disturbances, primarily scattering and reverbration, together with instrumentation inaccuracies.

The infinite series in (1) is assumed to be truncated at n terms, the remainder is incorporated into $v(t)$. Thus our model takes on the form

$$y(t) = \sum_{i=1}^{n} a_i m(t-\tau_i) + v(t) \qquad (2)$$

of interest to us is the determination of sufficiently accurate estimates of the a_i's and τ_i's.

3. Linearized Model

Reference [6] describes a procedure for evaluating estimates of the delays τ_i and the amplitudes a_i based on cross correlation type estimation schemes developed by the authors. Presently we assume that rough estimates of the delays namely $\hat{\tau}_i$ are available and that we are required to find

$$\Delta\tau_i \triangleq \hat{\tau}_i - \tau_i \qquad (3)$$

We employ the following truncated Taylor series

$$m(t-\tau_i) = m(t-\hat{\tau}_i) - (\Delta\tau_i)m'(t-\hat{\tau}_i) \qquad (4)$$

The truncation is appropriate since the $\Delta\tau_i$'s are assumed of small magnitudes. The prime denotes time derivative in the above equation. As a result an approximate form of (2) is given by

$$y(t) = \sum_{i=1}^{n} a_i m(t-\hat{\tau}_i) + \sum_{i=1}^{n} b_i m'(t-\hat{\tau}_i) + v(t) \qquad (5)$$

Here we introduced the new variable b_i

$$b_i = (a_i)(\Delta\tau_i) \qquad (6)$$

Our problem is simply to estimate a_i and b_i, given $\hat{\tau}_i$, $m(t)$ and consequently $m'(t)$. We remark here that the introduction of the new variables b_i renders linear-estimation equations instead of a nonlinear version that would result if direct solution for a_i and $\Delta\tau_i$ is sought.

From (5) we may write for $t=t_o, t_1, \ldots t_k, \ldots t_{N-1}$

$$y = [M \quad \tilde{M}] \begin{bmatrix} a \\ b \end{bmatrix} + v \qquad (7)$$

Where we have defined the following vectors and matrices

$$y = \begin{bmatrix} y(t_o) \\ y(t_1) \\ \cdot \\ \cdot \\ \cdot \\ y(t_{N-1}) \end{bmatrix}$$

$$M = \begin{bmatrix} m(t_o-\hat{\tau}_1) & m(t_o-\hat{\tau}_2)\ldots. \\ m(t_1-\hat{\tau}_1) & m(t_1-\hat{\tau}_2)\ldots. \\ \cdot & \\ \cdot & \\ \cdot & \\ m(t_{N-1}-\hat{\tau}_1) & m(t_{N-1}-\hat{\tau}_2)\ldots \end{bmatrix}$$

$$\tilde{M} = \begin{bmatrix} m'(t_o-\hat{\tau}_1) & m'(t_o-\hat{\tau}_2)\ldots. \\ m'(t_1-\hat{\tau}_1) & m'(t_1-\hat{\tau}_2)\ldots. \\ \cdot & \\ \cdot & \\ \cdot & \\ m'(t_{N-1}-\hat{\tau}_1) & m'(t_{N-1}-\hat{\tau}_2)\ldots. \end{bmatrix}$$

$$a^T = [a_1 \; a_2 \; \ldots \; a_n]$$

$$b^T = [b_1 \; b_2 \; \ldots \; b_n]$$

$$v^T = [v(t_o) \; v(t_1) \; \ldots \; v(t_{N-1})]$$

Our problem is thus to obtain estimates of a and b given y, M, and $\tilde{M}$.

4. Some Results from Estimation Theory

Consider the vector-matrix equation (7) written in the form

$$y = Hp + v \qquad (8)$$

where y is a vector of measured quantities, H is a matrix of known entries, v is a "noise" vector, and p is a vector of the unknown parameters. This general structure is introduced here to put some general results for estimation criteria and algorithms into perspective. In eq. (8), the matrix H is given for our present case by:

$$H = [M \quad \tilde{M}]$$

As detailed elsewhere (e.g. Deutsch [7], Sage [8], Vetter [9]) for a-priori information with

$$E\{v\} = 0,\ E\{vv^T\} \triangleq V,$$

$$E\{p\} = \bar{p},\ E\{(p-\bar{p})(p-\bar{p})^T\} \triangleq P \quad \text{and}$$

$$E\{pv^T\} = 0.$$

, all unbiased linear estimates of the parameter vector p are of the form

$$\overset{*}{p} = \bar{p} + K(y - H\bar{p}) \tag{9}$$

with associated error covariance

$$\overset{*}{P} \triangleq E\{(p-\overset{*}{p})(p-\overset{*}{p})^T\}$$

This turns out to be

$$\overset{*}{P} = (I-KH)P\ (I-KH)^T + KVK^T \tag{10}$$

For a least squares criterion with weighting both of deviations from the a-priori estimate $\bar{p}$ and of a quadratic form in the observation residuals, i.e.

$$J_{WLS} = (p-\bar{p})^T A(p-\bar{p}) + (y-Hp)^T B(y-Hp), \tag{11}$$

where A and B are positve definite and $A + H^TBH$ must be non-singular, K takes the form

$$K_{WLS} = (A+H^TBH)^{-1}H^TB \tag{12}$$

For the minimum variance criterion

$$J_{MV} = \text{trace } E\{(p-\bar{p})(p-\bar{p})^T\}, \tag{13}$$

K takes the form

$$K_{MV} \triangleq \hat{K} = PH^T(HPH^T+V)^{-1} \tag{14}$$

From (12) and (14) it also follows that the particular least square weightings $A = kP^{-1}$ and $B=kV^{-1}$ lead to the minimum variance condition (Vetter, [9]) and that

$$\hat{K} = PH^T(HPH^T+V)^{-1} = (P^{-1}+H^TV^{-1}H)^{-1}H^TV^{-1} \tag{15}$$

For the minimum variance situation, the covariance matrix takes the particular form

$$\begin{aligned}\overset{*}{P}_{MV} \triangleq \hat{P} &= PH^T(HPH^T+V)^{-1}HP \\ &= (P^{-1}+H^TV^{-1}H)^{-1},\end{aligned} \tag{16}$$

the second form of (16) being obtained by use of the matrix inversion lemma (e.g. Sage [8]).

5. Implementation Aspects

An estimation algorithm based on the theory detailed above has been developed. With an estimate $\hat{\tau}_i$ for τ_i previously determined we use (8) and the minimum variance estimator, equation (9) with (15), to obtain the estimate

$$\hat{p} = \bar{p} + (P^{-1}+H^TV^{-1}H)^{-1}H^TV^{-1}\ (y - H\bar{p}) \tag{17}$$

In the absence of a-priori information one sets $\bar{p} \to 0$ and $P^{-1} \to 0$ (or $P \to \infty$), which reflects the complete prior ignorance for estimates of the parameters. In this case equation (17) reduces to

$$\hat{P} = \hat{K}y \tag{18}$$

with

$$\hat{K} = [H^TV^{-1}H]^{-1}H^TV^{-1} \tag{19}$$

Entries for the covariance matrix of the disturbance must be chosen to reflect the disturbance activity. A special case is one with

$$V = \sigma_v^2\ I$$

For which we have

$$\hat{K} = [H^TH]^{-1}\ H^T \tag{20}$$

6. Test Results

A program based on the proposed estimation algorithm has been developed for operation on the HP 5451 Fourier Analyzer System. The program was tested using both simulated data records and field data. In situations where overlapp of replicas occurs, the program improved the discrimination of the composite wavelets.

Figure 1, shows the calibrated signal "Huntec" which is a broad-band type source signal.

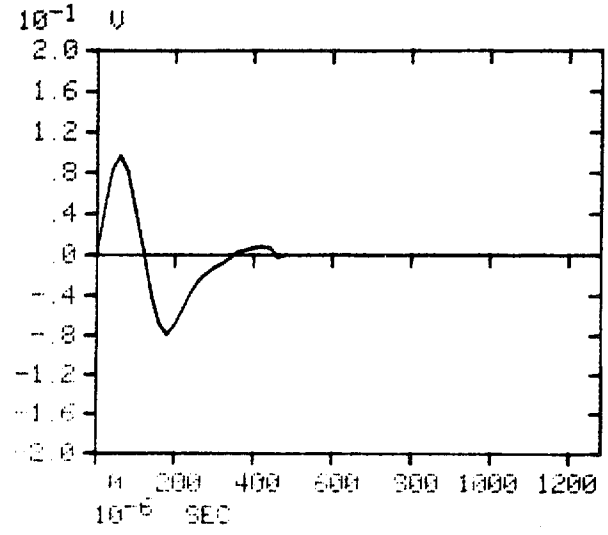

Figure 1. Calibrated Source Signal

Figure 2 shows the second half of a single record from the Huntec DTS system [10] from a sea trial over the western part of the Scotian Shelf and in the eastern part of the Gulf of Maine aboard CSS Hudson in June 1976. Figure 3, shows the preliminary results of estimating the location $\hat{\tau}_i$ and magnitude of wavelets using the procedure detailed in ref. [6].

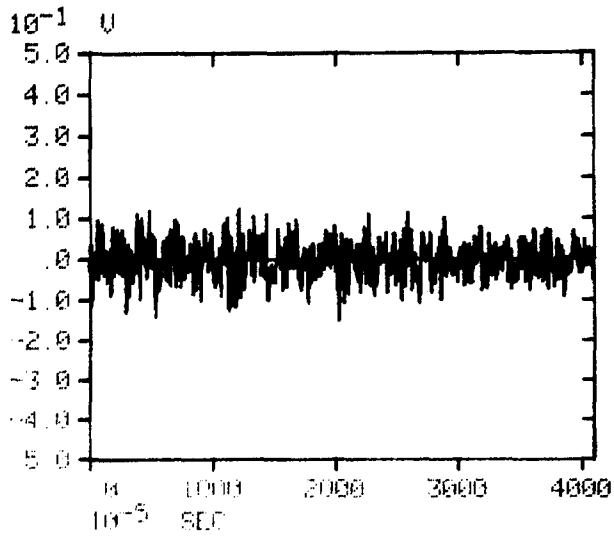

Figure 2. Sample Return Echo

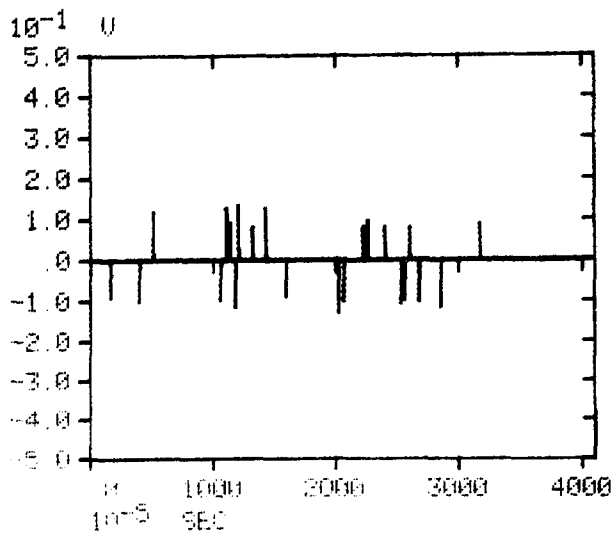

Figure 3. Detected Amplitudes and Delays

The following table gives results of the new developed estimation algorithm described in this paper for improved delays and amplitude values.

$\hat{a}$ (10^{-1} Volts)	$\Delta\tau$ (10^{-5} Sec)
- .626482	1.96
- .800409	1.13
.989757	0.80
- .851135	0.43
1.18163	0.64
.760413	0.73
-1.1728	-0.42
.967389	0.93
.771521	0.70
1.15152	0.47
- .698825	0.87
-1.0215	0.54
- .816481	0.78
.69557	0.67
.75066	1.08
.665432	1.02
- .840931	0.61
- .802457	0.79
.790138	0.37
- .929284	0.05
-1.05035	0.15
.797166	0.54

7. Conclusions

We have reported on an estimation procedure based on a linearized model of propagation of sound in layered media. The estimator assumes the availability of approximate values of the parameters sought and obtains refined values for the delays involved. Results pertaining to the application of the proposed method to field signals have been documented which show good performance of the method.

8. References

1. Robinson, E.A., "Predictive Decomposition of Seismic Traces", Geophysics, Vol. 22, No. 4, October, 1957, pp. 767-778.

2. Robinson, E.A., "Predictive Decomposition of Time Series with Applications to Seismic Exploration", Geophysics, Vol. 32, No. 3, June 1967, pp. 414-484.

3. Mendel, J.M., "White Noise Estimators for Seismic Data Processing in Oil Exploration", Proceedings Joint Automatic Control Conference JACC, 1976, p. 642-651.

4. Nahi, N.E., and Mendel, J.M., "A Time Domain Approach to Seismogram Synthesis for Layered Media", Information Processing for Oil and Gas Exploration, Volume 3, USCEE Report: 490, June 1976, Presented at the 46th Annual International SEG Meeting Houston.

5. Mendel, J.M., and Kormylo, J., "Single Channel White-Noise Estimators for Deconvolution", Geophysics, Vol. 43, No. 1, February 1978, pp. 102-124.

6. El-Hawary, F.M., and Vetter, W.J., "Estimation of Subsurface Layer Parameters by Use of a Multiple-Reflection Model for Layered Media", Proceedings of the Fourth International Conference on Port and Ocean Engineering Under Arctic Conditions (POAC 77), September 1977.

7. Deutsch, R., "Estimation Theory", Prentice-Hall, Englewood Cliffs, N.J., 1965.

8. Sage, A.P., "Optimum Systems Control", Prentice-Hall, Englewood Cliffs, N.J., 1968.

9. Vetter, W.J., "On Linear Estimates, Minimum Variance and Least-Squares Weighting Matrices", IEEE Trans-Automatic Control, Vol. Ac-16, No. 3, 1971, pp. 265-266.

10. Hutchins, R.W., McKeown, D.L., and King, L.H., "A Deep Tow High Resolution Seismic System for Continental Shelf Mapping", Geoscience Canada, Vol. 3, No. 2, May 1976, pp. 95-100.

R&D ACTIVITIES OF THE AMERICAN UNDERWATER BAND

R. E. Bailey
c/o Harold's Rogue & Jar
1814 N Street, N. W.
Washington, D. C. 20036

Abstract

The American Underwater Band, Inc., is a non-profit corporation located in Washington, D. C. Composed of four dozen part-time people, it is devoted to the development of the arts in new frontiers. Its research activities range from the discovery of underwater acoustic instruments to the discovery of new freedoms for man in the ocean and other frontiers. Projects include the R&D necessary for underwater ballet, research in human factors and R&D in marine transportation. While the projects are recreationally undertaken, the discovery potential of this organization is quite high and the potential value is enormous.

1. Introduction

The American Underwater Band, Inc., was initiated three years ago at the request of some jazz musicians. It became a non-profit corporation less than a year ago and is currently composed of four dozen individuals. Each of the individuals undertakes projects ranging from the development of underwater music and ballet (and the discovery of new musical instruments) to the invention of sophisticated hardware for applications in marine transportation. While its primary intent is the development of the arts in new frontiers, its projects often generate spin-offs of value to military and industrial endeavors. For example, there is considerable likliehood that shoes developed for underwater ballet will also have applications for precise movement in both space and underwater maneuvering.

The band organization is not structured in a formal fashion. Participation is based on a large variety of individualized motivations. Emphasis on each of the projects shifts as opportunities arise, and the individuals tend to come together when the potential of financial benefit in one or more projects becomes recognizable.

The band as an entertainment novelty has been featured in a great many forms of media over the past three years. Articles have appeared in the Washington Post, the Washington Star, the Smithsonian Magazine and National Geographic's World Magazine. It has been featured on television four times and on over a dozen radio shows both locally and nationally. In the near future, it will be featured on two network television shows and in three nationally distributed magazines.

Current sponsors for the band and its research activities include Harold's Rogue & Jar, a jazz club in downtown Washington, and the International Inn, a hotel with a year-round swimming pool where research, rehersals and concerts are undertaken. Most of the musicians come from the jazz club and there are currently an even dozen professional musicians who have performed in the band.

2. Current R&D Activities

Since the first concert featuring underwater music in August of 1974, the band organization has described itself as a research oriented group. All of its instruments have had to be discovered and engineered with little outside financial or technical assistance. Other research is being undertaken partly because of a desire to increase recreational options in the swimming pool, partly because the organization has needed products to develop income, and partly because of a planned approach to the management of discoveries. In the latter case, it would be false to say that the organization has planned out the discoveries it has made; the discoveries have been made accidentally and research in specific directions increases in accordance with the ability of the organization to market the discovery.

Despite the fact that most of the discoveries the organization has made have been applicable to interests outside the strategic scope of the band, the initial motivation for discovery and invention has been within this strategic scope. This strategic scope concerns the overall impact of a performing band on the public, and that impact is believed to be one of focusing public attention on the

water/ocean as a new frontier of almost boundless opportunities. The latter part of this intent has necessitated strategic planning. If the band merely focuses public attention on this new frontier, without specifying the ways in which the public can gain personal and social benefits, it seems unlikely that its overall impact, its financial rewards and its personal benefits will amount to anything which is significant in the lives of its participants.

The strategic plan which has been drawn up recognizes an immediate need to reward people for their activities in the environment. The rewards are initially recreational, then social and then possibly even financial. In the attempt to increase the recreational benefits, the following design goals have been specified:

1. Attract people to water environments by expanding their recognition of the activities which can be undertaken in and around them.
2. Motivate people to get into the water.
3. Motivate people to swim and dive in the water.
4. Increase the incentives for returning to the water.

" Attract " and "motivate" are two key words in these goals. Being a somewhat more flexible group than most research organizations, the band has endeavored to investigate one of the social and psychological freedoms normally disregarded by ocean technologists: the personal sensual characteristics of the environment. Not only has the environment been considered sensual for thousands of years, but it is also the only social environment where partial,and sometimes full,nudity is condoned. To motivate people to the water environment, the band is attempting to develop products which permit greater numbers of options for individuals to attract other individuals and interact with them, and which increase the personally enjoyed sensual characteristics of the environment.

Over one hundred product concepts have been conceived to fit into the design goals. They include the following range of categories

1. Fashions for the beach and water.
2. Games, sports, hobbies and accessories which motivate water entry.
3. Games, sports, hobbies and accessories which motivate swimming and diving.
4. Accessories which increase the ease with which the water can be left.
5. Services which increase the personal and social benefits which can be gained through activities around the water.

It is reasonable to describe one or two of each of these categories in terms of examples. In the fashion category, " Spray wear" allows the sunbather considerable options in terms of how much she/he exposes to attract and interact with other people. A peel-off glue is sprayed on the body and leaves, sand, plastic or cloth is then used to cover exposed parts of the body. No belt is used and the wearer feels "free" even though coverage can be more complete than is possible with most other commercially sold swimwear types.

A second example is, at first glance, laughable. " Skinny Dipper Shorts" offer wearers a form of swimwear which is both functionally useful and socially attractive. The swimwear is provided with an anchor and line and designed to permit removal and assembly into a support bouy. It is provided with symbols which are easily recognized by others. Though the product emphasizes behavior which is not socially condoned, in practice it also offers the safety advantage of providing tired swimmers with a readily available means of support.

In the category of accessories which motivate swimming and diving, the band is attempting to develop five kinds of sensual environments. These environments provide sensual experiences which are impractical to gain on land; they relate to the ability of the body to sense changes in temperature, pressure, viscosity, texture and instantaneous touch at neutral bouyancy. From one-half to all of the body surface is stimulated in these environments. The products have been given names which suggest the stimuli they provide: "Nibbler", " Tickler", "Cold Wave", etc.

In this same category, the band's participants have played underwater tennis, bowling and have devised an underwater dart game. Hobbies being investigated include underwater weaving, cooking, poetry, graphic and performing arts, in addition to underwater musical instruments, musical performances and underwater ballet.

The investments to undertake these research and development activities have been small out of necessity. The rewards have initially been recreational. For instance, having access to a pool on a year-round basis is one reward; being introduced to Scuba diving is another reward. Secondly, the rewards have included publicity; social recognition; and an identity gained as a result of being a part of an unusual endeavor. Financial rewards have not yet been gained by the organization as a collective of people. Instead, financial rewards have come to a few people who have benefitted professionally or as a result of specific discoveries and their own abilities to market those discoveries. Both the author and the band's lead musician

have benefitted by gaining all three rewards in the past years.

3. Discoveries and Spin-offs

When underwater music began four years ago, the group had to overcome several popular myths which have been developed by the public about underwater sound. The first myth was that the bubbles produced by diver exhalation would mask any musical sounds. This was disproven in less than the first week of the endeavor to play music underwater. The second myth, probably deriving from "Holywood's" visions and presentations in films, was that sound would have a great tendency to resonate underwater. The truth is that while the sound travels faster in water than in air, the water tends to dampen resonance; string instruments will not work underwater, and the aluminum bars of a glockenspiel produce a dull monotonic sound rather than providing a musical scale.

When the endeavor was initiated, it was also assumed that the world's "experts" in underwater sound (the U. S. Navy) would be able to provide the basic information necessary to construct underwater instruments. In fact, these "experts" are expert at listening to sounds currently produced by marine life and by man, but they have no idea how to produce musical tones. Now, four years after the initiation of the band's endeavor, it seems obvious as to why these "experts" have not come forward: man has discovered more than a million combinations and permutations of materials. Not only have few applications been found for the vast majority, but far fewer have ever been taken into the water - and when they have been taken into the water, their properties have been investigated and the sound they produce is considered to be of little value.

Popular myths have also been associated with the sounds that certain materials " ought to make". You can fill glass bottles with water and produce a whole range of clear tones. This "ought to work" underwater, but it doesn't. The sound is a dull "clunk ". Cymbals "ought to work", but they don't. The cracking sound of shaped metal which is bent also doesn't work.

Some of the discoveries seem to have little immediate practical value. For instance, balloons have been tried as targets for underwater dart games. But when you fill the balloons with air and weight them to stay submerged, they become more and more difficult to burst the deeper they are submerged. Unless the projectile has considerable momentum and mass, a pin will merely bounce off the balloon.

As another example, consider that the band discovered that porcelain-cover steel pots would produce a complex squeeking sound when rubbed with fingers. In an attempt to find a bow which would yeild a tone, rubber of different densities and grades was acquired. Not only was no sound produced, but the rubber in all grades seemed to be frictionless on this surface. By accident, expanded styrene was used and found to produce a very high pitched squeeking sound - almost beyond the ability of the ear to hear. Furthermore, the sound traveled beyond the air-water interface and could be clearly heard by people around the pool. This rather puzzling discovery is made more puzzling because the undertones and overtones were dampened as an underwater listener swims away from the source.

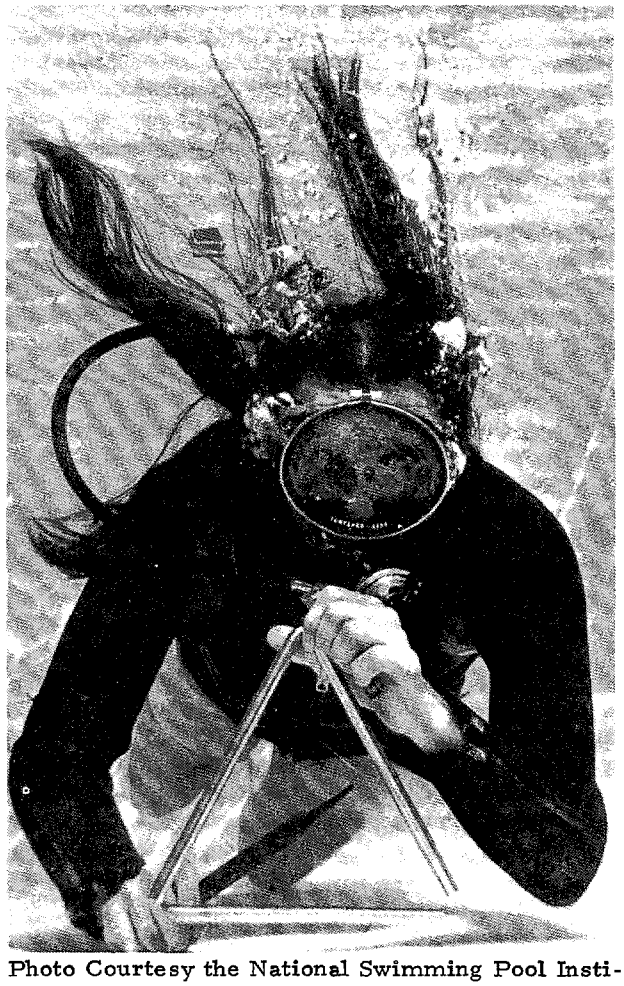

Photo Courtesy the National Swimming Pool Institute (Photo Credit, R. Black)
Terry Plumeri, a world renowned bassist who currently performs off and on for the National Symphony and for a large number of jazz clubs around the nation, is shown here as he posed for an underwater photographer in 1974. Terry later became the driving force for the formation of the American Underwater Band.

Another discovery which is puzzling relates to the ability of individuals in the water to hear the full range of tones being produced by the band when it performs; but this range is not picked up by our current hydrophones unless they are placed very close to the instruments. The result is that underwater dancers can hum along with songs being played by the musicians underwater, but the audience hears sounds which are almost monotonic. This may imply that the science and technology associated with underwater listening is very crude.

The above discoveries represent what actually amounts to several hundred individual experiments and not all the the experiments have yeilded such puzzling results. It would be inappropriate to specifically describe what these discoveries have been in this paper, because they are being marketed with the prospect of lucrative returns. However, some can be described in application terms without giving away the crucial facts.

In the fields of psychology and physiology, the band is initiating research jointly with other consulting organizations. In psychology, the research involves an investigation of several means of reducing anxiety associated with the diving environment. The anxiety derives from three kinds of stimuli: 1) a preconceived fear of the alien nature of the environment; 2) a cognitive reaction to circumstances in the environment; and 3) an instantaneous reaction to stress in the environment whether the cause of stress is recognized or not. The results of this research can be applied in training to military, industrial and sports divers. Beyond training, these results may also indicate how environments might be psychologically engineered to increase the safety of swimming and diving, which would be of interest to recreational planners and designers and the various industries concerned with water-related recreation technology.

In the physiological area, the band is initiating sensory research as a result of its endeavor to develop sensual environments. The results thus far are proprietary, but it should be obvious that the information will eventually be applicable to both military and industrial markets. The ability of the body (50% to 100%) to sense various stimuli would be of interest to apparel designers, manufacturers of bedding and furniture, sensory physiologists concerned with the handicapped, etc.

Other physiological and psychological research is either simply too proprietary or too ambiguous to be presented here.

In the field of underwater propulsion and hydrodynamics, the band has made a discovery which would seem to be applicable on a wide range to marine transportation. It would be very easy to describe this discovery here, since it is the basis for four patent applications; however, since these patent applications have not yet been submitted, the applications in very general terms will be described as they are currently known. They include:

1. Applications to in-port maneuvering of all marine vessels.
2. Applications to automatic anchoring and retrieval of anchors for all marine vessels.
3. Applications to diver transportation.
4. Applications to ASW systems.
5. Applications to underwater cargo transport.
6. Applications to underwater weapons.
7. Applications to oceanographic instruments.
8. Applications to large tanker safety systems especially associated with anchoring and propulsion.

It seems likely that if these applications prove to be worth what they are believed to be worth, the American Underwater Band will become one of the richest bands in the United States. Further basic research may indicate means of transportation in other new frontiers.

In the area of diver operations in extreme environments, research is being undertaken in several areas of interest to commercial divers because they typify environmental extremes. For instance, commercial divers often have to work in turbid waters. The band is investigating not only methods of substituting optical mediums, but also a means of movement around the work areas which decreases the possibility of making the water even more turbid than it is. In the latter case, a method of movement has been found which is also directly applicable to divers performing in the band, because their movements must be very precise, or they may destroy instrument assemblies.

4. Future R&D Directions

In late 1975, it became apparent that the band would be featured in an article in the Smithsonian Magazine. The band organization began to try to undertake several advanced research activities so that this publicity could be used to motivate others to undertake similar research activities.

One of these advanced research areas dealt with the reaction of marine life to man playing a kind of acoustic music underwater. A small survey of dolphin trainers was accomplished and it was found that 75% of those surveyed felt that the dolphin would not only like what they heard, but

that they would indicate their feelings in some specific manner. 50% felt that the dolphin might even respond by harmonizing or responding in some fashion to indicate their understanding of what man was doing underwater.

The results of this admittedly small survey bring up several questions. Dolphins have already demonstrated a liking for music played by man in air; in fact, they have selected a specific style. How would their appreciation very if they could watch man perform underwater ? If dolphins communicate emotionally, could musicians communicate with them in emotionally implied music ? Would the dolphins understand musical interpretations of love, fear, depression, etc., which we are able to interpret in our music ? If so, would they attempt to communicate back to us in similarly structured rhythms and tones ?

Photo Credit, Peter Dorfman
Phil Trupp, the American Underwater Band's Lead Musician, is shown here playing the Burrotone. Instruments are named after patrons of the band, who often finance the parts of the instrument or who have provided the band with exceptional help. In this case, an inventor by the name of Robert Burruss did the welding and assembly of four instruments, and was responsible for designing and building a workable xylophone.

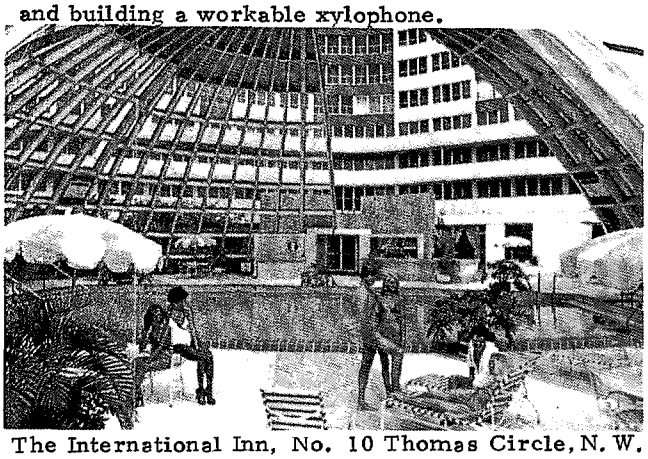

The International Inn, No. 10 Thomas Circle, N. W. is the band's year-round R&D site.

No matter what the outcome of a band-marine mammal jam session, it does seem likely that a form of music could be found which would tend to calm excited dolphins. This might be useful to dolphin trainers, and possibly even to fishermen attempting to avoid netting them. It also seems possible that comparative responses between different marine mammals might indicate intelligence on a relative scale.

Other areas of R&D relate to the response of other marine life to underwater music and underwater sound; further investigations of currently ambiguous or seemingly nebulous psychological freedoms and stresses characterized by the water environment; and as the band organization becomes larger, it is likely that a staff will be developed to direct and coordinate more advanced research into the musical and other properties of new materials in the water.

No area of water-related R&D is ridiculous if it is properly structured and if the researchers are willing to accept and interpret results in terms of real rewards - whether the reward is recreational, social or financial. It seems ridiculous to suggest that research on underwater cooking will yeild any tangible ocean technology; but if acid can be used to cook raw fish, couldn't it also be used to speed the cure time of certain epoxies?

It seems that all too often, when we think of laymen, we forget that laymen run our world. Remember that laymen include company presidents, machinists, welders, musicians and designers who in reality create everything we own. 1,000 laymen who devote $1,000 each to research - even though it may be approached from a recreational standpoint - equals a research budget of $1 million. If 10,000 laymen could be motivated by various kinds of rewards (mythical, recreational, social and financial) to spend this much money in water-related research, there would be a $10 million grass roots budget aimed at ocean technology. Now imagine what might happen if 100,000 people (10% of those owning private pools) were motivated in this direction.

As an historical example, consider that in the Aztec culture, the wheel was a toy. It was a religeous taboo to use it for any practical purpose. Of course, it is the basis of our land technology today. What taboos do we have ?

TRAFFICABILITY AND PERFORMANCE ANALYSIS FOR A DEEP OCEAN RUNNING GEAR MODULE FOR AN UNDERSEA VEHICLE

Herbert G. Herrmann

Civil Engineering Laboratory - NCBC
Port Hueneme, California

A deep ocean vehicle which maintains contact or interacts with the seafloor through a properly functioning active running gear system offers improved capabilities for search, salvage, and other work missions on the seafloor. The major technical problems involve trafficability and the maintenance of mobility while maneuvering on weak seafloor soils. An additional major consideration is the mechanical configuration of such a system as it impacts trafficability, vehicle performance, and support requirements. This paper summarizes the results of an investigation into the expected performance of a running gear module for use as an accessory to an existing unmanned deep ocean vehicle. This module is designed to provide improved vehicle performance in terms of bottom position control, work capabilities, and resistance to or reaction for larger forces. The major emphasis in this paper is placed on likely seafloor conditions to be encountered, trafficability and soft soil mobility analyses including an analysis of relevant past experience, vehicle work capabilities and support requirements and restraints imposed on the host vehicle. It is concluded that a lightweight running gear module using either continuous belt type tracks or Archimedean screws will perform satisfactorily.

INTRODUCTION

The performance of a number of deep ocean reconnaisance, salvage, and work missions undertaken by submersibles and unmanned vehicles (such as CURV's or RUWS, (see Talkington, 1978) and similar commercial vehicles) would be greatly enhanced, and some currently impossible tasks would be made feasible, by the addition of a functional powered running gear system capable of developing significant lateral forces and of resisting even larger lateral and vertical loads. Tasks as simple as positioning an instrumentation package in a cross-current or clearing cables, light debris, or sediment from a salvage site can be very difficult or impossible for a free-swimming vehicle. They are, however, quite simple for a vehicle which interacts with the seafloor. Contact with the seafloor also provides a constant basis for position reference which is very useful when operating "partially blind" in any type of current and especially in the vicinity of structures or wreckage in which the vehicle or its umbilical could become entangled.

The objective of the effort summarized here was to perform a preliminary feasibility and design study of a light-weight accessorial running gear module for use on an existing unmanned vehicle. The module would derive its power, control and mechanical support from the host vehicle and would be designed to provide an improved work capability when operating in typical deep ocean environments. This environment consists primarily of very weak cohesive soils with occasional loose granular soils and small obstacles. It was initially assumed that the components of the module would weigh less than 2,000 pounds in air and between 0 and 1,000 pounds in water and fit within a volumetric space 15 feet long by 6 feet wide by 2 feet tall. The module was to be capable of maintaining mobility in all expected environments, developing an additional drawbar pull of 500 pounds, and resisting larger loads from any direction when "parked."

BACKGROUND

A number of bottom crawling vehicles have been used on the seafloor. Table I is a representative but by no means comprehensive listing of such vehicles. Table I does not include vehicles using passive running gears such as the numerous cable and pipeline burial vehicles which typically utilize a number of sleds, nor does it include the several vehicles with active running gears designed to interact directly with a pipeline rather than the seafloor.

Most of the vehicles listed in Table I are designed for operation on stronger, more competent soils typical of nearer shore areas, and thus, apply ground pressures on the order of 3 to 12 psi. Detailed data on trafficability related performance for most vehicles are extremely limited. Such data on very weak cohesive soils (soil strengths and running gear bearing pressures of less than 1 psi) are known to exist only for the Equipment Test Chassis Track and the RUM vehicle. Both vehicles have demonstrated that mobility can be maintained and drawbar force developed reliably and predictably on these very weak soils. Figure 3 is based on an actual set of data on the RUM's performance (from Anderson et al, 1972, and from Gibson and Anderson, 1974) which is representative but shows less scatter than is typical. As implied by the results, at these very low ground pressures, the realizable drawbar is not particularly sensitive to track/ground pressure. The drawbar pull appears to be more closely related to soil strength. Reanalysis of the RUM and Equipment Test Chassis Track (Beck, 1972, and Nuttall, 1970) data suggests strongly that at moderate bearing pressures, the maximum drawbar pull will be slightly greater than the running gear's area multiplied by the soil's remolded strength at a soil depth equal to the grouser height.

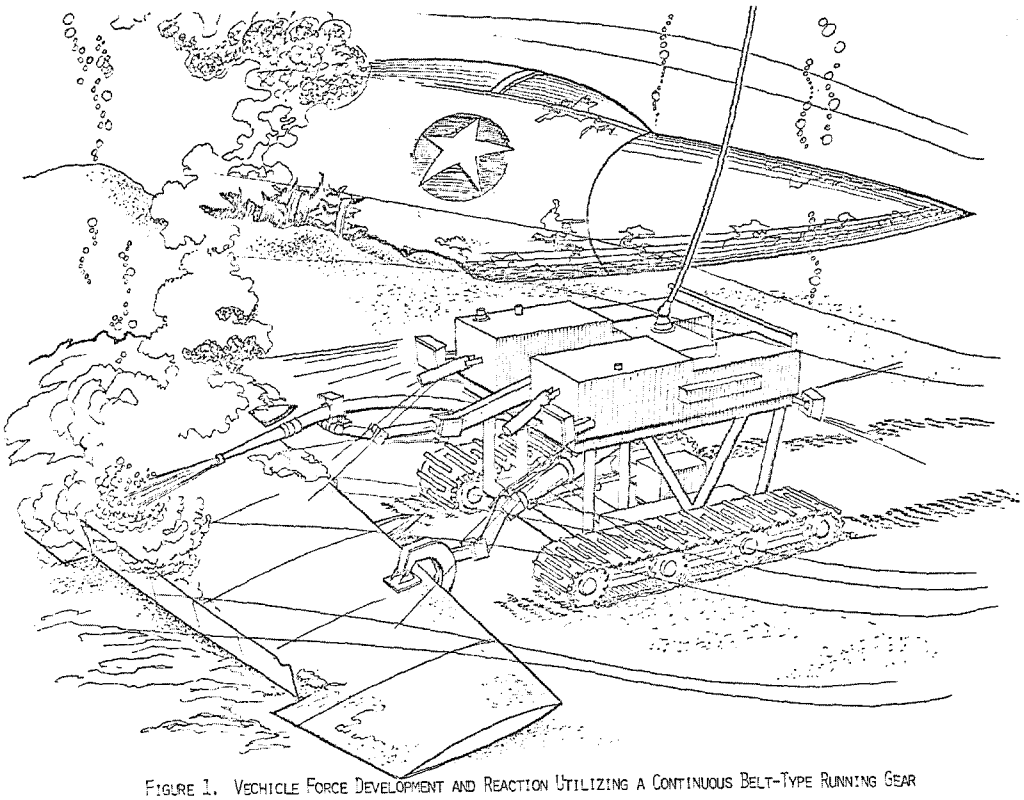

FIGURE 1. VECHICLE FORCE DEVELOPMENT AND REACTION UTILIZING A CONTINUOUS BELT-TYPE RUNNING GEAR

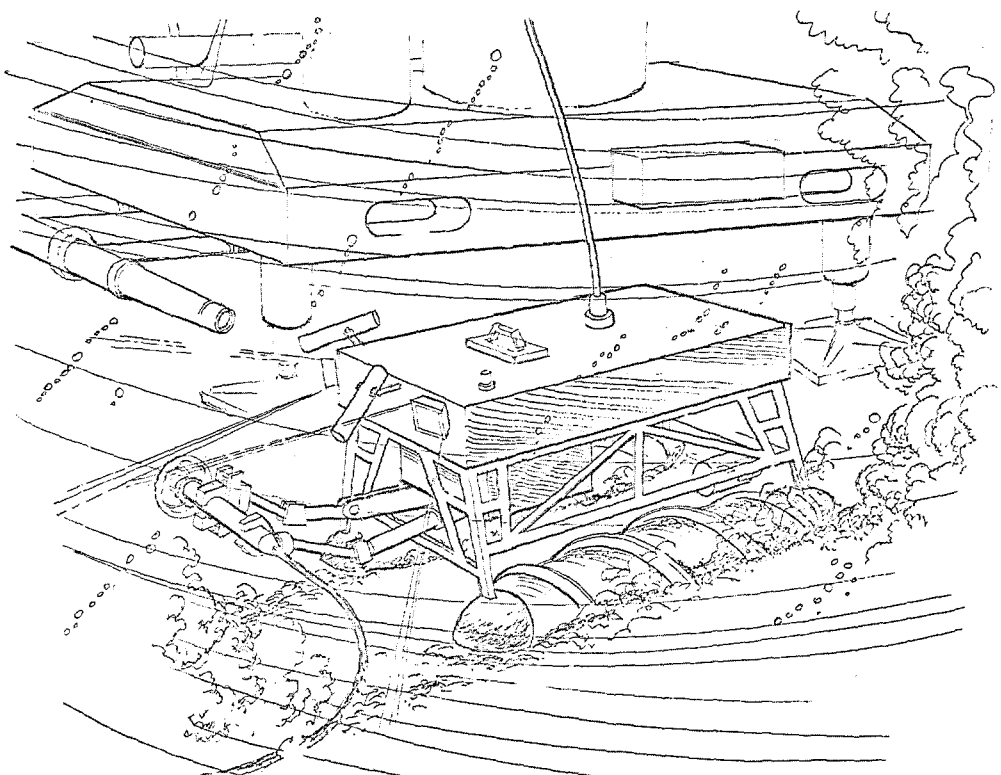

FIGURE 2. VEHICLE FORCE DEVELOPMENT AND POSITION CONTROL UTILIZING ARCHIMEDEAN SCREW

"Moderate bearing pressure" is defined as being greater than that required to embed the grousers, and less than that causing excessive sinkage and local soil failure (less than 0.25 psi and between 0.75 and 1.00 psi, respectively, for the case illustrated on Figure 3). The bearing pressure causing excessive sinkage was typically slightly greater than five times the soils remolded strength. The results of tests with RUM and the Equipment Test Chassis Track on the seafloor, and of experience being gained with vehicles operating on dredge spoil (see for example Green and Rula, 1977) demonstrate the feasibility of maintaining mobility and doing work with active running gears on extremely weak cohesive soils - vane shear strengths of less than 0.5 psi and Cone Index measurements of less than 5.

A number of types of running gear have been used on the seafloor; however, analyses by various groups and individuals (Brackett, et al (1977), Ehrlich (1978), and Turnage and Seabergh (1978) among others) have all concluded that a continuous belt type track with rigid suspension or an Archimedean Screw would be the best running gear type for the very weak cohesive soils expected. Ehrlich (1978) suggests that the Archimedean Screw would likely give the best performance but is an alternative which requires more energy (because of the friction/adhesion between the rotating pontoons and the soil) and is a newer, less refined technology. However, tests on extremely weak soil in swamp areas (Cone Index of less than 2) have shown that the Archimedean Screw is virtually impossible to immobilize. Because of its configuration, the rotor functions much as a thruster if soil strength is insufficient.

Turbidity generated by the use of a running gear is a concern. However, in situations where running gear would likely be needed (high current, zero visibility, or heavy work) any turbidity created will not likely be a problem, particularly when compared to alternate means of propulsion or station keeping. In the one comparison known to the author, the turbidities created by RUM (a tracked vehicle) and CURV III (a neutrally buoyant tethered vehicle) working at the same site in the Santa Barbara Channel were very similar in magnitude and effect.

A detailed review by Noorany (1978) of existing relevant geotechnical data suggests a typical soil profile with an extremely weak (and likely displaceable) sediment layer at the surface with an underlying sediment layer of relatively constant strength (at least for soil depths influencing running gear of the scale being considered here). The extremely weak surface layer varies on thickness from 0 to 6 inches and is totally missing at many locations in the deep ocean. Remolded soil strengths at the soil depths controlling mobility are usually in the 0.1 to 0.25 psi range or greater. Studies by Richards and Parks (1977) suggest similar values. Bearing pressures of 0.5 to 1.0 psi would typically be allowable for a number of passes although these values may have to be reduced at a work site where numerous passes or maneuvering will occur. Adhesion of these very plastic soils to running gear elements is envisioned by some as a likely problem. Experience with the RUM vehicle showed that even with a filled track (presumably due to this soil adhesion or stickiness) mobility performance was not significantly affected, Gibson (1978). Start-up or breakout forces may exceed running or operating resistance forces for some configurations by as much as 50% to 100% due to this adhesion.

Ehrlich (1978) analized the likely performance of a running gear system on these types of soils and concluded that drawbar forces of the order of 400 pounds could be realized over the range of expected environmental conditions. He suggested using either tracks or rotors (Archimedean Screws) configured as two pairs with articulation between in order to provide better maneuverability. Tracks would be of the order of 1 foot wide by 3.5 feet long. Rotors would be 1.5 feet in diameter by 3.5 feet long.

A major concern in designing such a running gear module is its effect upon the handling characteristics of the host vehicle and its support systems. In general, the size and mass of the module should be minimized in order to reduce static and dynamic line loads. In order for the running gear to function properly on the seafloor, it must exert a minimum bearing pressure which is typically derived from the vehicles net negative buoyancy. Handling of a normally neutrally buoyant vehicle in a negatively buoyant configuration will cause a number of problems. Use of variable buoyancy is one method of avoiding these problems. However, this approach is expensive in terms of cost, added mass, and mechanical complexity/reliability. A simpler approach which appears feasible at this point in the development is use of a vertical thruster to create an effective negative buoyancy when operating on the seafloor. This approach has the additional advantage of orienting this "vertical" force and the resulting bearing pressure perpendicular to the ground surface which will improve running gear performance on sloping seafloors.

The study by Hackman (1978) concluded that a running gear module would offer improved vehicle work capabilities where large forces must be resisted, accurate bottom positioning is required, bottom location must be continuously known and controllable, and where controlled movements (especially over larger distances) are needed. Typical missions requiring these capabilities include survey, excavation, salvage and recovery, construction, inspection and repair.

CONCLUSIONS

Results of the study of a running gear module for a seafloor vehicle have shown the basic feasibility and expected performance range for such a module system. The improvement in work capabilities of an existing host vehicle are significant for a number of typical work missions and the impact, especially on handling, on the host vehicle can be reduced to manageable levels. The use of a neutrally buoyant configuration with reliance on the vertical thruster to provide the required bearing pressure for satisfactory running gear performance appears quite feasible but will require further study to quantify performance levels in terms of drawbar force realizable at very low ground pressures. Additional study is also required to select

the running gear configuration.

ACKNOWLEDGMENTS

Portions of this study were supported directly by the work of Ehrlich (1978), Hackman (1978), McMahon Engineering (1978), and Noorany (1978). Their work and input along with that of Dr. Phil Valent of CEL is gratefully acknowledged. The work was sponsored by the Deep Ocean Technology Program through the Naval Facilities Engineering Command.

REFERENCES

(1) V. C. Anderson, J. R. Clinton, D. K. Gibson, and O. H. Kirsten (1972). "Instrumenting RUM for in situ Subsea Soil Surveys," in "Underwater Soil Sampling, Testing, and Construction Control," ASTM STP 501, American Society for Testing and Materials, pp. 216-231.

(2) Banzoli, V., V. Ditella, L. Dossi, and P. Gava (1976). "New Concept of Underwater Remote Controlled Tracked Vehicle for Deep Water Trenching Operations," Proceedings, Eighth Annual Offshore Technology Conference, Vol. II, Houston, TX, May, pp. 647-664.

(3) Bascom, W. (1970). "Underwater Dredge," Ocean Industry, Vol. 5, No. 8, Aug., pp. 16-18.

(4) E. Beck (1972). "Seafloor Excavation Research," Civil Engineering Laboratory Letter Report, Naval Construction Battalion Center, Port Hueneme, CA, April.

(5) E. J. Beck, T. L. Culbertson, P. J. Daly, H. A. Gaberson, and A. L. Scott (1971). "Concepts for Drilling and Excavating in and below the Ocean Bottom," Naval Civil Engineering Laboratory, Technical Report No. R725, Port Hueneme, CA, May.

(6) R. Brackett, W. Tausig, H. Herrmann, L. Tucker, and C. Ward (1976). "Nearshore Trencher: Part I - State-of-the-Art Assessment," Civil Engineering Laboratory, Technical Memorandum No. 43-77-03, Naval Construction Battalion Center, Port Hueneme, CA, October.

(7) Cordy, R. N. (1977). Personal contact with vehicle builder/owner, May - July.

(8) Ehrlich, I. R. (1978). "An Assessment of Running Gear for Seafloor Operations," CEL PO Report No. 78-M-R555 Stevens Institute of Technology, Hoboken, New Jersey, January.

(9) Gibson, D. (1978). Personal contact by H. G. Herrmann at Marine Physical Laboratory, San Diego, March.

(10) D. K. Gibson and V. C. Anderson (1974). Seafloor Soil Mechanics and Trafficability Measurements with the Tracked Vehicle 'RUM'," in Deep-Sea Sediments: Physical and Mechanical Properties, edited by A. L. Inderbitzen, Plenum Press, New York, pp. 347-366.

(11) C. E. Green and A. A. Rula (1977). "Low-ground-pressure Construction Equipment for Use in Dredge Material Containment Area Operation and Maintenance-Equipment Inventory," Army Engineer Waterways Experiment Station, Technical Report D-77-1, Vicksburg, MS, April.

(12) Hackman, D. J. (1978). "Assessment of Undersea Vehicle Work Capability Enhancement Afforded by Addition of a Running Gear System," CEL PO Report No. 78-M-R114, Battelle-Columbus Laboratories, Columbus, Ohio, February.

(13) Herrmann, H. G. (1978). Personal Communication with Mr. P. Durand of COMEX Services, May.

(14) Komatsu, Limited (1971). "Komatsu Amphibious and Underwater Bulldozers," brochure dated April 7, Tokyo, Japan, 8 pp.

(15) McMahon Engineering Services, Inc. (1978). "Analysis of Potential Missions and Identification of Host Vehicle Compatibility Constraints for the Deep Ocean Running Gear Module Concept," CEL PO Report No. 78-M-R571, San Diego, January.

(16) Noorany, I. (1978). "Geotechnical Site Classification Data for Deep Ocean Trafficability," CEL PO Report No. 78-M-R033, San Diego State University, San Diego, January.

(17) C. J. Nuttall (1970). "Test and Analysis of the Equipment Test Track," Naval Civil Engineering Laboratory Contract Report No. CR 70.017, Port Hueneme, CA, March.

(18) A. F. Richards and J. M. Parks (1977). "Geotechnical Predictor Equations for East Central North Pacific Nodule Mining Area Sediments," Proceedings, Offshore Technology Conference, Paper No. OTC 2773, Houston, TX, 2-5 May, Vol. I, pp. 377-385.

(19) Talkington, H. R. (1978). "Undersea Work Systems Research and Development," Proceedings, Tenth Annual Offshore Technology Conference, Vol. IV, Houston, May, pp. 2409-2416.

(20) Thorstensson, L. & P. Wiik (1975). "Sea Bottom Crawlers," in Proceedings of the Fourth World Congress of Underwater Activities, Vol. II, edited by J. Adolfson, Stockholm, Sweden, September.

(21) Turnage, G. W., and W. C. Seabergh (1978). "Study and Parametric Analysis of Trafficability, Running Gear, and Stability Considerations for Nearshore, Bottom-Crawling Vehicles," Technical Report (in publication), Army Engineers Waterways Experiment Station, Vicksburg, Mississippi.

(22) K. W. Wiendieck (1970). "A Preliminary Study of Seafloor Trafficability and Its Prediction," Army Engineer Waterways Experiment Station, Technical Report M-70-8, Vicksburg, MS, July.

(23) Vickers Oceanics, Limited (1977). "Sea Cat - Seabed Crawler with Dredge for Cable Burial," brochure dated April.

TABLE I, SEAFLOOR VEHICLES WITH ACTIVE RUNNING GEAR SYSTEMS

VEHICLE	FUNCTION	WEIGHT IN AIR (LBS)	RUNNING GEAR TYPE	BUILDER/OWNER	REFERENCE
COMEX Cable Plow	Diver Operated Cable Plow	45,000	Two tracks	COMEX, France	Herrmann, 1978
Crawl Cutter	Sand Dredge	100,000 (est)	Two tracks	Ocean Science & Engineering	Bascom, 1970
Equipment Test Chassis	Test Track	800	Single track	U.S. Navy	Nuttall, 1970
Hitachi JH-360	Bulldozer	70,000	Two tracks	Hitachi, Japan	Thorstensson & Wiik, 1975
Komatsu Bulldozer	Bulldozer/ Ripper	85,000	Two tracks	Komatsu, Japan	Komatsu, 1971
Navy Trencher	Diver Operated Rock Cutter/ Trencher	25,000	Two tracks	U.S. Navy	
RUM	Inspection and Some Work	27,000	Two tracks	Scripps Institute of Oceanography	Gibson & Anderson, 1974
SeaBug	Pipeline Inspection	4,500	Four wheels	UDI, Aberdeen, Scotland	Cordy, 1977
SeaCat	Cable Burial	4,000	Eight Wheels	Vickers Oceanics, Scotland	Vickers, 1977
Sumitomo Trencher	Dredge/Trencher	132,000	Two tracks	Sumitomo, Japan	Anonymous, 1974
Technomare TM-102	Dredge/Trencher	418,000	Two tracks	Technomare s.p.a., Italy	Banzoli, et al, 1976
Tramp	Inspection and Some Work	22,000	Six wheels	Winn Technology, Ltd., Ireland	Cordy, 1977

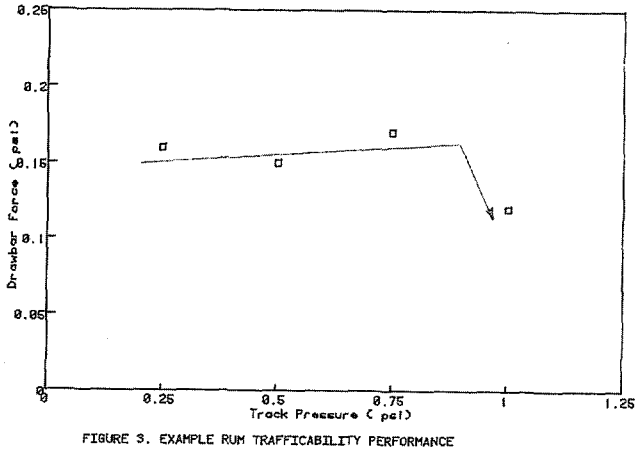

FIGURE 3. EXAMPLE RUM TRAFFICABILITY PERFORMANCE

AN AUTOMATED TIDE GAUGING NETWORK

D. C. Knudsen
Canadian Hydrographic Service
Canada Centre for Inland Waters
867 Lakeshore Road
Burlington, Ontario, Canada L7R 4A6

Abstract

A system has been developed for automatic acquisition and telemetry of tides and water levels from a network of permanent gauging stations. Called TATS, for Tidal Acquisition and Telemetry System, the new instrument consists basically of a specialized microcomputer interfaced to a water level sensor and a dial-up telephone line.

Designed as a low cost, reliable instrument for remote, unattended gauging sites, TATS operates under program control, sampling the water level as required, storing the data in memory, and transmitting the information over the telephone lines upon request. Although the data is normally accessed automatically once a day by a central computer with dial-out capability, the information is also available to anyone with a data terminal equipped with a modem or acoustic coupler. TATS can also control a teleannouncer or a dedicated landline or radio link in addition to the dial-up telephone interface.

1. Introduction

The Canadian Hydrographic Service, in addition to its surveying and charting functions, has the responsibility for monitoring tides and water levels in our navigable waterways. To this end approximately 150 permanent gauging stations have been established over the years throughout the Great Lakes, St. Lawrence Seaway, and the Atlantic and Pacific coasts. The water level records obtained from these stations serve a variety of purposes, the most important of which is to provide data from which tidal constituents can be derived by harmonic analysis. A knowledge of the tidal constituents at a given location enables accurate predictions to be made of tides years in the future. The tide tables containing these predictions are extremely useful to mariners and others, but they are obviously incapable of foreseeing storm surges and seiches, not to mention tsunamis.

However, in the last couple of decades, technological developments have made it increasingly feasible to telemeter water level information directly from a gauge to a user in real time. The practical applications of real time data, particularly for marine traffic and for tsunami and storm surge warnings have been very quickly appreciated. During the 1960's, the Tides and Water Levels Instrument Development Group installed a few telemetry gauges on an experimental basis and the response from users was so enthusiastic, the system has grown to a fully operational network of over 40 telemetry gauges in the Great Lakes and St. Lawrence River.

Three different types of telemetry system were installed during this period, and all are still in active service. The most common is the teleannouncing gauge. This provides a voice announcement of the present water level over a dial-up telephone line. A second type transmits a real time analog signal over a dedicated telephone line to drive a chart recorder at the receiving end. The third type of telemetry gauge installed during this period is not strictly speaking a real time system. A punched paper tape gauge produces a record which is fed into the paper tape reader of a telex terminal in the gauge house. Data recovery is a once-only procedure which is initiated from a telex terminal located at the Marine Environmental Data Services in Ottawa. The telex interrogated gauges are normally accessed once a day.

However, none of these systems has done much to relieve the burden of digitizing the large volume of analog strip chart records generated by the traditional recording gauges, except perhaps the few telex units which had problems of their own, particularly with regard to cost and maintenance requirements.

By late 1974 microprocessors and large capacity semiconductor memories were revolutionizing electronics, and it was apparent that it had become technologically feasible to develop a system combining fully automated routine data acquisition with the capability for real-time telemetry at a reasonable cost. The basic configuration of the new instrument, conceived in 1974 and essentially unchanged to the present, was dictated by several important considerations. One feature considered essential was an ability to continue the data acquisition process in the event of power failure or interruption of communications at the gauge house. This necessitated a battery back-up system for uninterrupted power,

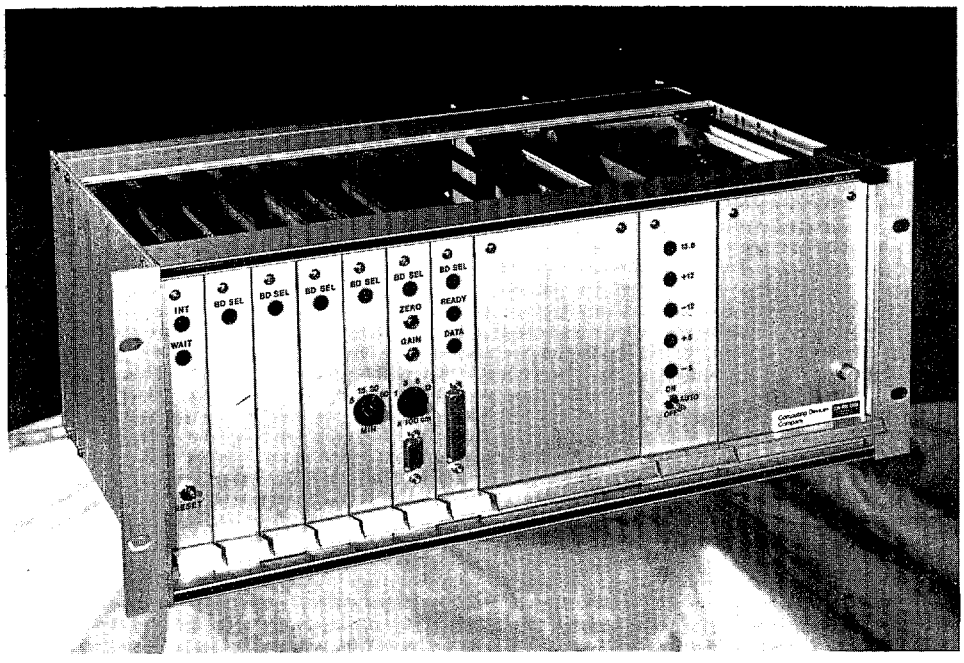

FIGURE 1. TATS PROTOTYPE

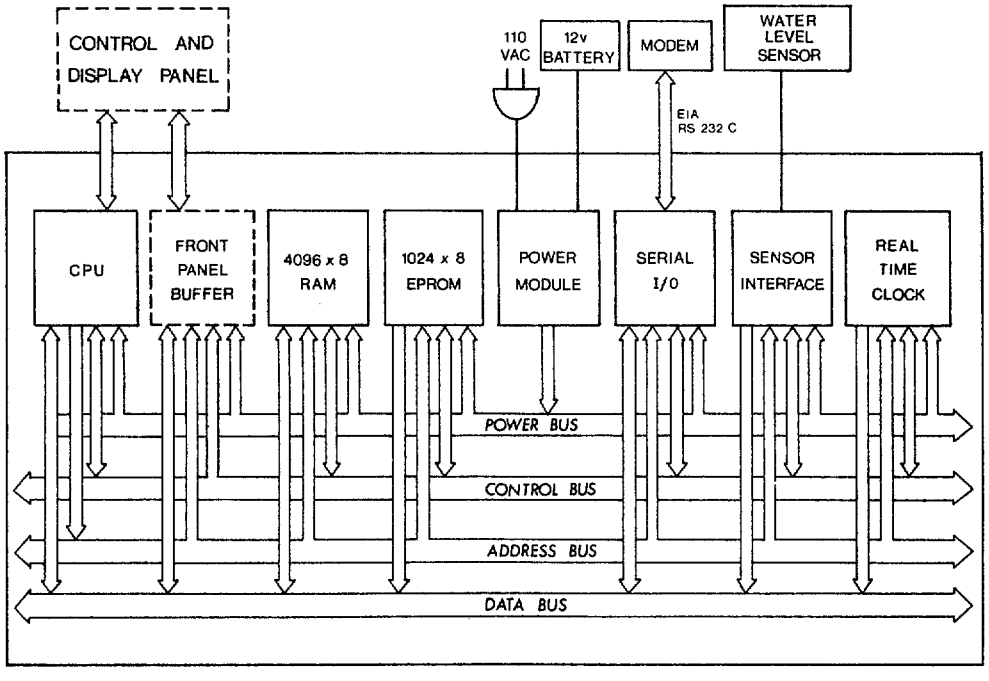

FIGURE 2. PROTOTYPE ORGANIZATION

and a local memory and clock in case of a communication failure. This requirement ruled out the possibility of a minimum telemetry system consisting only of a passive water level sensor connected to a communications channel.

A further requirement was flexibility. A telemetry system was needed which could provide real time water level information for marine traffic and tsunami warning, and at the same time, allow efficient and economical acquisition of tide data for historical purposes and for the production of tide tables.

The device which meets these requirements is, of course, the microcomputer, with memory, highly accurate crystal controlled timing, and the sort of flexibility only attainable with software. The basic system comprises a water level sensor, a microcomputer, a communications channel, and the necessary interfaces and power supplies. It is known as TATS, an acronym for Tidal Acquisition and Telemetry System.

However, the development of TATS from its conception in 1974 through a rather lengthy gestation period to its introduction in final production form in 1978, has not been entirely uneventful, despite its basically straightforward nature. In fact, TATS has gone through three distinct 'generations', partly as a result of the pace at which modern electronic technology is developing, and largely because of the familiar learning curve.

2. The Prototype

In 1974 we were enthralled, like many others, with the power and novelty of the microprocessor, and we were reluctant to design a system which used anything less than the full capabilities of the device. As a result, the original prototype shown in figure 1, was somewhat extravagant.

The prototype TATS was based on the Intel 8080. It was fully modular, as shown in figure 2, expandable up to 64K bytes of memory and had practically unlimited sensor interface possibilities. It featured a universal bus (any module could be plugged into any slot), full 8 level vectored interrupt, a hardwired real time clock module, and even a remote control and display panel with single stepping capability for debugging software in the shop. The front panel was not intended to be part of a gauge house installation.

As in the production version the normal telemetry channel was a dial-up telephone line, equipped with a standard Bell Canada low speed modem (normally operating at 300 baud, although TATS has a programmable baud rate).

The prototype TATS was installed in the summer of 1976 in a gauge house at Lauzon, which is just across the St. Lawrence River from Quebec City. The water level sensor was a float/counterweight arrangement driving a multiturn potentiometer, the output of which was digitized by an A/D converter on the sensor interface module.

3. The Second Generation

Although the prototype TATS performed admirably, it was apparent even before it was installed at Lauzon that it was needlessly complex and expensive. A second generation TATS was designed, and a total of three 'pre-production' units were constructed in our shop at the Canada Centre for Inland Waters. Although retaining the universal bus and modular construction of the prototype, the new system in its minimum configuration had only four printed circuit modules instead of seven, a simplification made possible by combining RAM and EPROM on one board, by eliminating the real time clock module in favour of an interrupt driven software clock, and by eliminating the sensor interface module altogether. It was found that many sensors, and in particular the incremental optical shaft encoder which was favoured for the majority of our applications, could be connected directly to interrupt lines on the CPU module with no further hardware interface required. In addition, the built-in line powered battery charger of the prototype was eliminated in favour of a single 12V (nominal) DC input. It was felt that a standard commercial trickle charger mounted externally with an automotive battery would be a simpler solution.

All three of these second generation TATS were installed and operated successfully in gauging stations in Lake Huron, Lake Erie, Lake Ontario, and even briefly in Viscount Melville Sound in the Canadian Arctic. A requisition was raised in early 1977 to have them manufactured in production quantities, but before the bids were in a last minute decision was made to reject them in favour of a completely new third generation TATS.

Several factors influenced this decision. The major one was the introduction at about this time of several new components, particularly the Intel 8085 microprocessor and the 8716 EPROM, which made it possible to put the entire system on one printed circuit board including the power supply, sacrificing the expandability and modularity of the earlier designs but greatly reducing the component count and the system cost, and potentially improving system reliability.

It was felt that the large number of gauging stations expected eventually to be equipped with TATS justified further development at this stage.

4. The Production System

The third generation TATS, shown in figure 3 (with the shaft encoder and sprocket) and figure 4 (the printed circuit board), is a single board microcomputer containing an Intel 8085 microprocessor, an Intel 8251 serial communications interface, an Intel 8255 programmable peripheral interface for 24 lines of general purpose parallel

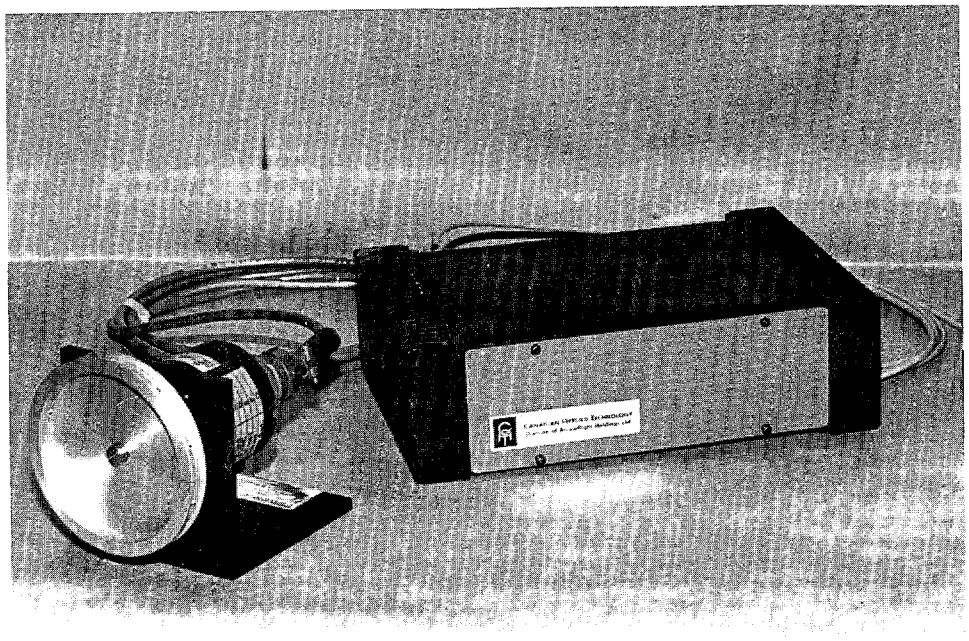

FIGURE 3. PRODUCTION VERSION WITH SHAFT ENCODER

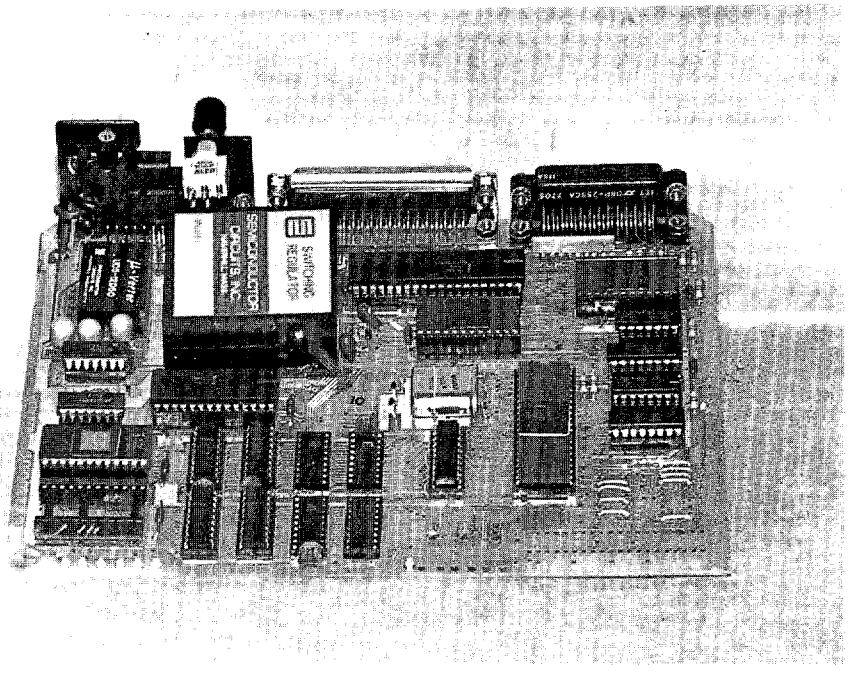

FIGURE 4. CIRCUIT BOARD OF PRODUCTION VERSION

I/O, and two Intel 8253 triple programmable counter/timers. One of the 8253's is dedicated as a programmable baud rate generator (1 counter) and as a programmable timer for the interrupt driven software real time clock (2 counters, cascaded). The frequency source in both cases is the crystal oscillator of the 8085 CPU. The other 8253 is available as an interface to sensors with a frequency or count type of output, such as incremental shaft encoders, quartz crystal pressure transducers, or transmission line water level sensors (Zwarts type), all of which have been used with TATS.

There are sockets for 4K of EPROM in 2K increments (using Intel 2716's) or 8K in 4K increments (using 2732's). Read/write memory is available in 1K increments up to 4K using industry standard 2114 4K static RAM's. This is sufficient capacity for about 1800 water level measurements with the present software.

A single switching regulator with a very wide input range for battery operation (9 to 18 volts) provides 5 volt power to all of the logic except the EIA driver which requires bipolar supplies. These are generated by a small on-board DC-DC converter which produces $\pm$ 12 volt outputs from a 5 volt input. The overall power consumption is less than 6 watts.

The prototype TATS shown in figure 1 has very few controls or displays visible. It was decided at the outset that TATS would have no hard-wired switch-selectable functions or any kind of control panel or display, because it was felt that it would be simpler and more economical if all comunications with TATS were carried out via the serial input/output interface using a standard digital data terminal.

This means that the technician who installs and services TATS will have to take a portable data terminal to the gauge house. Operations such as setting the water level sampling rate, initializing the real time clock, and adjusting the datum, will all be done with a data terminal under program control.

This intention has been compromised to some extent in the production version of TATS by the provision of sockets for 5 hexadecimal displays, driven by the 8255 PPI. These can be programmed to show the instantaneous water level or some other parameter so that a visitor to the gauge house who does not have a data terminal will at least be able to verify the accuracy of the measurement, although no real communication with the instrument is possible. This is a minor inconvenience, since it is expected that the gauge will be accessed at least once a day and a malfunction should be quickly detected.

The production version of TATS is being manufactured for the Canadian Hydrographic Service by Canadian Applied Technology, Buttonville, Ontario.

5. The Gauging Network

TATS, together with a water level sensor, a modem, and a dial-up telephone is the basic element of a network of telemetry gauges which will eventually number over 150. All of these gauging stations will be accessed automatically by a computer operated by the Marine Environmental Data Service in Ottawa. The computer has been equipped with dial-out capability, and it will be programmed to place a long distance phone call to each gauge at regular intervals, probably once a day, and to request all of the previous day's water levels. The computer can check each day's data as it comes in and if it detects any abnormality in the record it can alert MEDS personnel of possible gauge malfunction.

At present MEDS personnel are dialing the gauge houses manually and retrieving the data with a terminal equipped with digital cassette recorders; however, as the number of systems in operation increases, this task will be turned over to the computer.

Since the contents of semi-conductor memory are not destroyed when the memory is read, the same data can be accessed at different times and by different users. When a dial-up telephone line is used as the telemetry link such as in the present installations, anyone with a data terminal, and either a modem or an acoustic coupler can access the water level data. Of course, it is necessary to know the telephone number of the gauge house. This can be very convenient for a hydrographic survey party, particularly an automated survey, since the water levels from the reference station could be accessed at any time from field headquarters in computer compatible form.

The systems presently in service, communicating over dial-up telephone lines, represent the minimum TATS configuration, which is expected to be suitable for most gauge houses. However, one of the reasons for using a program controlled microcomputer instead of a hardwired system, is to obtain sufficient flexibility to handle special gauging requirements.

For example, TATS can be used equally well with radio telemetry. One such system, using Motorola PT 400's, and a special interface which utilizes the Motorola MCM 14412 modem chip, has been successfully implemented between the Canada Centre for Inland Waters and a gauge house at Port Weller, Ontario, at the downstream end of the Welland Canal.

TATS can also be used with satellite retransmission systems. An installation being planned for this fall will use a TATS connected to two Paroscientific pressure sensors, for hydrostatic and barometric pressure, and a GOES data collection platform. This system, to be installed on Vancouver Island, will be used for tsunami warning.

In a situation where real time data is required very frequently, it may be more practical to rent a dedicated telephone line or use a radio telemetry link than to make repeated long distance calls on dial-up lines. TATS is equally suitable for this application.

TATS can even be used to generate a voice announcement of the water level, to provide a teleannouncing service for users who don't have a data terminal. This can be accomplished by connecting TATS to one of a number of inexpensive voice synthesizers currently on the market.

It should be pointed out that TATS is not limited to one mode of operation at a time. Providing that the appropriate software and interfaces are available, TATS can simultaneously provide a voice announcement, drive a digital telemetry link, and watch for tsunamis.

6. Conclusions

TATS is an attempt to provide an efficient and economical answer to Canada's water level gauging requirements, both present and in the foreseeable future. State of the art digital technology has been used throughout, partly because of the reliability for which modern solid state electronics is known, but mostly to obtain the flexibility to meet a wide range of gauging requirements. An effort has been made throughout the development to keep the design as simple as possible to minimize the initial cost and also to reduce maintenance. The performance of TATS in the gauging network over the next few years should indicate to what extent these expectations have been met.

COASTAL ZONE IMPLICATIONS OF DEEP SEABED MINING

M. Karl Jugel
Marine Minerals Division
Office of Policy and Planning
National Oceanic and Atmospheric Administration
Rockville, Maryland 20852

Daniel M. Bragg
Division of Industrial Economics
Texas A&M University
College Station, Texas 77843

Abstract

While deep seabed mining for manganese nodules will take place hundreds of miles from the U.S. coasts, there are coastal zone implications brought about by the need for onshore facilities. As part of an on-going effort by the Department of Commerce's National Oceanic and Atmospheric Administration (NOAA) to develop information suitable for use in an environmental impact statement (EIS) on deep seabed mining, NOAA and Texas A&M University (TAMU) colloborated on a study to develop onshore facility location criteria for the Gulf Coast.

Application of these criteria resulted in the identification of several likely geographical areas and permits a broad assessment of what onshore facilities would mean to "host" areas.

1. Introduction

In first generation deep seabed mining systems, manganese nodules will almost certainly be brought to shore for the recovery of copper, nickel, cobalt, and in some cases manganese. This will involve the operation of nodule transport ships between the minesite and a port, unloading nodules at a marine terminal, transporting the nodules from the terminal to a processing plant, a processing plant operation, and the disposal of the remainder of the nodules after the value metals have been removed. The construction and operation of each of the facilities required will have environmental, social, and economic implications to the geographical areas where industry seeks to locate.

As early as 1972 the potential need for an environmental impact statement (EIS) on deep seabed mining was identified at a Government-industry meeting convened by the Department of Commerce's National Oceanic and Atmospheric Administration (NOAA). After preliminary research and consultation with industry, interested Federal agencies, academia, and environmental interest groups, NOAA formally began the Deep Ocean Mining Environmental Studies (DOMES) Project during 1975. The DOMES Project is designed to assess the potential environmental effects of at-sea nodule recovery operations.

During 1975 and early 1976, the Congress and others expressed the need for potential onshore, coastal zone effects of deep seabed mining to be considered as well (1, 2, 3) to complement the information being developed by the DOMES Project. Congress requested that NOAA undertake the complementary work. The result was the development of a plan for phased assessment of the potential environmental, social, and economic effects of deep seabed mining activities after nodules leave the mineship.

2. Two-Phase Approach

Most deep seabed mining technology is highly proprietary. Because of this, independent information on processing and processing-related activities suitable for use in a public document, such as an EIS, was needed. Further, it was recognized that environmental, social, and economic effects could differ significantly from one geographical area to another and that the discussion of such differences could be of importance in an EIS. Thus, NOAA formulated a plan for a two-phase assessment of the potential environmental, social, and economic effects of processing and processing-related activities.

Phase I was designed to identify the key parameters of these activities which are relevant to subsequent assessments of potential environmental, social, and economic effects. Parameters of importance included such things as land requirements, water consumption, power usage, employment, hazards from accidents, and noise. The work involved identifying which of many possible processing technologies were likely to be used commercially, estimating production levels, extensive process engineering analyses, and extensive supporting systems analyses. The work was performed under two competitively awarded contracts by Dames and Moore, assisted by the EIC Corporation and Mr. Benjamin V. Andrews III, a maritime consultant. The final reports (4) are available through the Department of Commerce's National Technical Information Service.

Phase II, which is nearing completion, was designed to develop locational criteria taking into account physical needs, economics, regulating regimes and public attitudes and then to use these to identify geographical areas which are representative of those which industry may consider. Included in each final report will also be descriptions of the environmental settings of the areas identified, but no attempt is made to rate one area against another. The West Coast study was performed for NOAA by the School of Oceanography of Oregon State University and the Gulf Coast study is being performed by the Industrial Economics Division of Texas A&M University.

NOAA has obtained assistance on the work from the deep seabed mining industry, environmental interest groups, and interested Federal agencies, such as the U.S. Bureau of Mines, the Maritime Administration, and the Environmental Protection Agency, and State governments. This assistance was used to help assure the accuracy, realism, and relevancy of the two phases.

3. Assessment of Effects

NOAA has deferred attempting to predict potential environmental, social and economic effects, both positive and negative, of onshore, coastal zone activities until further studies are performed and until preparation of an EIS must begin. However, the authors decided to make certain preliminary observations for discussion purposes. The opinions expressed are solely those of the authors.

First, despite the fact that deep seabed mining will be an entirely new industry, the onshore facilities are not very unusual industrial facilities. Second, except for disposing of the remains of nodules, after value metals are removed, the onshore operations should not make major demands on a "host" area from environmental, land-use, and social viewpoints. Third, the construction and operation of the facilities would be an economic stimulus for the "host" area and greatly increase the area's tax base. And finally, the current early interaction among Federal agencies, State and Local governments, industry and environmental interest groups will help assure the development of a viable, environmentally compatible industry.

Specifics of the potential environmental, social, and economic effects are now discussed on a component by component basis.

4. Marine Terminals

Nodules received onboard a mineship will essentially be in the form of a coarse slurry. Unless unusual transport factors, such as extremely long transportation distances are encountered, it is most logical to handle the nodules in slurry form for transportation purposes.

An example of a marine terminal designed to handle slurries is shown in Figure 1. Its primary features are a pier for tying up the nodule transport ships, one or more traveling cranes on the pier for swinging portable pumps on to the nodule transport ship, containment areas to hold nodules awaiting onshore transportation to the processing plant, and a facility for loading fuel destined for the mineship by way of returning nodule transports. It would be a dedicated facility at which 50,000-70,000 DWT ships would call every 4 to 10 days.

Figure 1

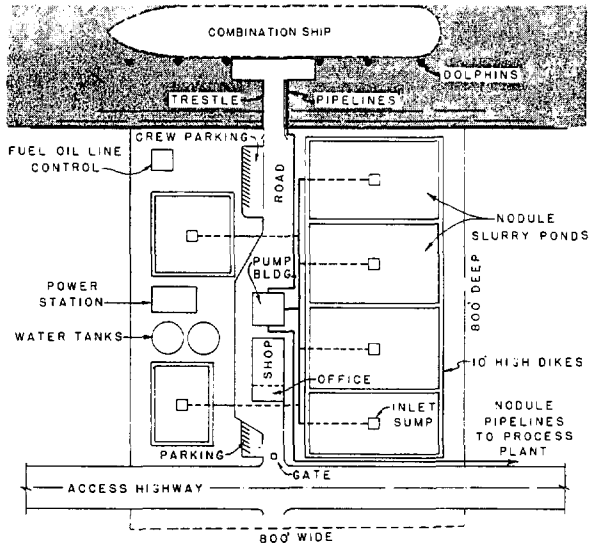

MINIMAL SLURRY TERMINAL

From a shoreline use viewpoint, the terminal would need between 600 and 900 feet of waterfront and 10 to 15 acres. Hence, this is a relatively small facility as far as commercial ports are concerned. During construction the primary environmental consideration would be from dredging the dock area to a depth of about 40 feet. New filling is carefully controlled in the States considered.

Terminal operations would not appear to raise many environmental concerns. Salt water used for re-slurrying the nodules would probably be recycled; the processing plant would de-water the slurry and return the water to the terminal for holding in the containment areas until it is needed to unload a transport. Only make-up salt water would be drawn from the harbor. The containment areas and unloading systems would be designed to prevent leakage, spills, or dusting. The amount of oil loaded on outbound nodule transports would be well below the amount for the transport to be considered a tankership.

The terminal would be a relatively innocuous facility in a commercial port. Skills typically found in a commercial port would be used, so the

30 to 50 employees would probably be drawn from the local labor market.

Other types of terminals could be considered for handling naturally dried or artificially dried nodules. These would have to consider dust control and would probably be more noisy.

5. Onshore Trasportation

If nodules are handled as a slurry for marine transportation and at the marine terminal, the most logical method to move the nodules to a processing plant is by means of a buried slurry pipeline. The pipeline has a further advantage in that it greatly facilitates the flexibility of processing plant siting because the cost of each additional mile of transportation is relatively low. In both the Gulf Coast and West Coast studies it was concluded that, depending on total system economics, the pipeline mode of transportation would permit plants to be located 25 to 50 miles inland if need be.

The most significant environmental and social effects of the pipeline would occur during the construction phase. There would be considerable excavation required in the nominally 6 acre per mile right-of-way. Pipeline routing may be difficult in some areas surrounding commercial ports. A firm will have to consider the potential disruption of both developed areas and environmentally sensitive areas in the selection of the pipeline route. Once the construction is finished, the land above can be used for other purposes as long as these uses do not interfere with access to the pipeline for maintenance. Noise created by periodic pumping stations on longer pipelines would have to be considered in determining their locations. A pipeline failure, which should be very rare, would result in the release of salt water and nodule material to the environment. The salt water released would be of more concern than the nodule material released because research indicates that nodule material is not environmentally harmful in its natural state. Potential environmental damage from a pipeline failure would probably be quite limited because of the probable difficulty a firm would have receiving approval to build a pipeline through an environmentally sensitive area in the first place.

Other means of transporting nodules would be considered if nodules are received in either naturally dried or artificially dried forms. These methods could include conveyers, either on-road or off-road trucks, and railcars. These other modes of transportation have different and in some cases, greater environmental and social considerations than a slurry pipeline.

6. Processing Plant

As illustrated in Figure 2, the processing plant can be viewed conceptually as a facility into which comes nodules, energy, reagents, and water and out of which come products, wastes, and airborne emissions. Physically, a processing plant will most likely resemble a relatively small oil refinery, except that there will probably be a storage area for coal and it would be served by a rail line to bring coal in and move products out.

PROCESSING PLANTS

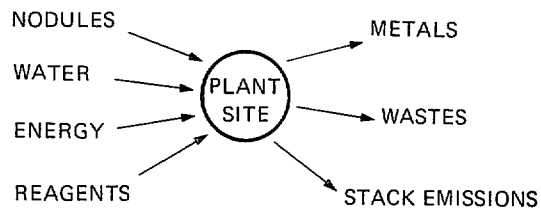

Figure 2

The total plant site is not expected to exceed 200 acres, with structures occupying about a quarter of the area. The site would be selected primarily on the basis of access to rail service and access to additional acreage for the disposal of the remains of nodules after value metals are removed and the disposal of combustion ashes. The overall requirements of a plant for acreage, services, and infrastructure would tend to preclude both industrialized urban areas and relatively undeveloped areas.

During the construction phase the environmental and social considerations would be the same as those typically associated with the multi-year construction of a major industrial facility. Perhaps the most significant effects are those associated with the influx of construction workers. The State of Hawaii's Department of Planning and Economic Development recently estimated (5) that perhaps 6,000 persons would be employed in marine terminal, pipeline, and plant construction.

Once the plant begins its three-shift per day operation, a total of 500 to 1,000 persons will be directly employed in the plant. Approximately one third of the employees are expected to be managerial and clerical, one-third skilled workers, and one-third unskilled. Depending on the existing industry in the area, an equal number of secondary and induced jobs could be created. A recent study performed by a team at the Massachusetts Institute of Technology (MIT) for NOAA (6) estimated the plant's capital cost at over $300 million and an annual plant payroll of nearly $25 million per year. In most areas the economic benefits should more than offset the demand for services and even more so if the local labor market can

provide the unskilled workers and some of the skilled workers.

Airborne emissions, water consumption, energy usage, and hazards from spills and gaseous releases were the primary environmental considerations identified for plant operations. The airborne emissions consideration arises largely from the assumption that the plants would burn coal; hooding, venting, and scrubbing were assumed to limit other emissions. Depending on the plant type, fresh water consumption would be from slightly over 2 million gallons per day to over 6 million gallons per day. This water does not necessairly have to meet drinking water standards, however. Purchased electric power needed ranges from about 24 megawatts to nearly 100 megawatts. Some of these considerations can be mitigated; for example, fuel oil could be substituted for coal, cooling water could be recycled rather than evaporated, and electric power could be generated on-site. Of particular importance in considering resource demands is trade-offs are possible. For example, a firm which finds an otherwise acceptable and economical site can make some modifications if air quality or another factor is a problem and if the cost difference does not make another site more attractive.

In processing plants the copper, nickel, and cobalt are recovered from liquid solutions. Hence, there would be relatively large volumes of liquids in a plant. Dames and Moore (4) estimated that the chances of a large scale spill would be very rare (one spill every ten million years per plant). Furthermore, segmenting the plant, to keep spillable volumes to a minimum, and diking should prevent any effects being felt off-site unless an environmentally poor site was chosen. The chance of a release of gases, such as amonnia or hydrogen sulfide, was also estimated to be very rare. While the quantities of gases stored were considered common in industrial areas (4), atmospheric transport causes potential gaseous releases to be of greater concern than liquid releases. However, plant design and site selection (e.g. avoidance of areas with poor dispersion characteristics and distances to populated areas) can be used to prevent hazards to human and animal life beyond the plant boundaries. A plant would face different natural hazards in different geographical areas (e.g. earthquakes in the West and hurricanes in the Gulf) and this would be a design consideration. Comparatively, a processing plant should be less "dangerous" than a municipal water treatment plant. Noise at the plant boundary should be no higher than that of automobile traffic on a freeway, so this should not be a major factor.

A manganese nodule processing plant is a "heavy" industrial facility, but plant design and site selection should make a plant environmentally and socially acceptable in most areas which would normally be considered for further industrial development.

7. Waste Disposal

The disposal of wastes would typically involve combining the remains of nodules after the value metals have been removed, combustion ashes, scrubber solids, and other wastes into a single, liquid waste stream. These "tailings" would be sent to containment areas where the solids would be allowed to dry by a combination of drawing off surface water ("decanting") and natural evaporation. Typical containment areas, or "tailing ponds" are illustrated in Figure 3. The use of tailings ponds may raise the greatest number of environmental and land use questions this still-to-be-born industry will face, particularly because each ton of nodules will result in roughly a ton of material to dispose of. Furthermore, several geographical areas have climate conditions which are not conducive to natural drying and stabilization. Similarly, in other geographical areas the potential effects of earthquakes would be a consideration.

Nodules and their accompanying salt water which enter the plant and the combustion ashes from coal have many constituents with poor environmental reputations depending on their chemical states. A major unresolved question is whether the processing alters their chemical states in a manner which would make them a threat to the environment using alternative disposal methods. NOAA, the Bureau of Mines, the Environmental Protection Agency and the industry are currently considering the types of research needed to answer this question.

One alternative waste disposal method to protect ground water, if necessary, is to line tailings ponds with natural or man-made material. Another, unproven, alternative would to be wash the tailings of all soluble constituents before disposal. Washed tailings could then perhaps be placed in unlined ponds, dried and used for landfilling, or returned to sea for disposal. The potential costs and difficulty of treatment are great and what "needs" to be done to tailings, if anything, cannot currently be stated. The Government-industrial research mentioned above should provide insight needed for an initial EIS. Because the industry will have to satisfy State and Federal regulatory authorities for specific processing plants, locations, and waste disposal methods, there should be ample opportunities to review the options.

8. Conclusion

The onshore, coastal zone activities which can be expected to result from deep seabed mining of manganese nodules are not particularly unusual industrial activities. However, there are environmental, social and economic implications of a type which should be addressed in an EIS on deep seabed mining.

Depending on total system economics, the majority of the onshore activities could take place some distance inland from the coast. The

Figure 3

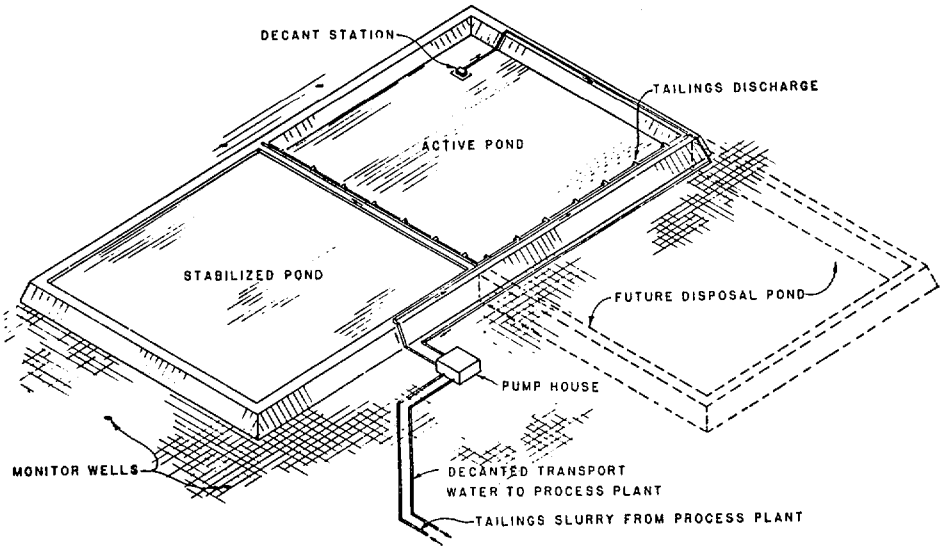

ISOMETRIC VIEW
TAILINGS DISPOSAL SCHEME

construction and operation of the facilities should be able to be accomplished in an environmentally and socially acceptable manner provided planning steps and safeguards are taken. Further research is needed to answer key questions on the disposal of the remains of nodules after the value metals have been removed; however, judgements on the need for treatment and on disposal methods should be reserved until such research is performed because of the importance of these questions to both the environment and the potential viability of the industry.

References

1. 94th Congress, State, Justice, Commerce and Judiciary Subcommittee of the Senate Appropriations Committee, "Report on the Fiscal Year 1976 Appropriation for State, Justice, Commerce and the Judiciary", 1975, Washington, D.C.

2. Marine Board, Assembly of Engineering, National Research Council, "Mining in the Outer Continental Shelf and in the Deep Ocean", 1975, National Academy of Sciences, Washington, D.C.

3. Frank, Richard A., "Deepsea Mining and the Environment", 1976, American Society of International Law, Washington, D.C.

4. Dames & Moore and EIC Corporation, "Description of Manganese Nodules Activities for Environmental Studies:
"Vol. I - Processing Systems Study"
"Vol. II - Transportation and Waste Disposal Systems"
"Vol. III - Processing Systems Technical Analyses"
1977, U.S. Department of Commerce, National Oceanic and Atmospheric Administration, Rockville, Maryland

5. Hawaii, State of, Department of Planning and Economic Development, "The Feasibility and Potential Impact of Manganese Nodule Processing in Hawaii", 1978, Honolulu, Hawaii

6. Nyhart, J. D., et al, "A Cost Model of Deep Ocean Mining and Associated Regulatory Issues," 1978, Report No. MITSG 78-4, Massachusetts Institute of Technology, Cambridge, Massachusetts

A COST MODEL FOR A FIRST GENERATION DEEP OCEAN MINING VENTURE

Professor J. D. Nyhart
Associate Professor of Management
Sloan School of Management
Department of Ocean Engineering
Massachusetts Institute of Technology
Cambridge, Massachusetts 02139

This paper reports on a study which provides a means for constructing cost estimates for a deep seabed mining operation, for simulating the projected cash flows, and for calculating the resulting economic return to the investor. By changing the assumptions and values used in the model, comparisons can be made of the impact of different policy and regulatory options on the profitability of the project. What follows is largely an adaptation of the executive summary of the initial report produced from the study project.* The project was conducted at MIT with support of the NOAA Division of Marine Minerals and the Sea Grant Program, U.S. Department of Commerce.

Fairly detailed estimates are made of the capital costs of a single hypothetical first generation ocean mining project located in the eastern central Pacific. The costs are for the major components of a five-phase mining operation cycle: prospecting, exploration, mining, transportation and processing. Operating costs are similarly estimated and aggregated. There the major components are: energy, labor, materials, fixed and miscellaneous costs. The study makes reasoned assumptions as to these characteristics for a mining operation handling three million tons of nodules a year over a 25-year commercial recovery period. Fifty percent debt was assumed, as was U.S. tax structure.

The aggregated cost estimates provide input for the financial analysis section of the model, the initial function of which is the generation of cash flow projections over the life of the project. The cash flow data form the basis for making analyses to estimate the investment returns on the operation, and for projecting the values of the annual federal, state and local tax revenues accumulated over the life of the project.

Over 75% of the cost estimates of equipment components have been developed independently of the major industry consortia. However, an industry-government-university workshop was convened in March 1977, to review the model and the first draft of the study. Many helpful suggestions were received and incorporated into the subsequent version of the model and accompanying draft, which also had the benefit of being reviewed by the workshop participants.

*Nyhart et al., "A Cost Model of Deep Ocean Mining and Associated Regulatory Issues", MITSG 78-4, March 1978

Current international and domestic legislative negotiations raise myriad policy options for the U.S. government. Most will affect the economic return to be realized from deep ocean mining and therefore the commitment of those who currently have the technological and financial resources to invest in the industry. This study provides a ready means for comparing the impact of many of the options. The model is a tool for comparison. It is not a basis for a potential investor's decision on deep ocean mining.

The model provides insight into three kinds of policy or regulatory questions.

First, a great many technical and financial determinants of the economic viability of deep ocean mining are necessarily subject to uncertainty and variation. This study permits most determinants to be changed by the program operator. Varying these estimates can provide insight into the range of technical and financial options available to the ocean miner.

The second type of questions are those concerning domestic legislation issues such as political risk coverage, comparative costs to industry for requirements of U.S. vessels, crews and processing plants, effects of different tax treatments, contribution to national income, and so on.

Third, assuming LOS negotiations will include some number of projects operated by entities other than the proposed international seabed authority or enterprise, there are numerous issues which will have impact on a mining venture's return. Among them are royalties to be paid either to the authority or to the U.S. government in anticipation of an anthority; exploration costs involved in the "banking" scheme; costs of training and technology transfer requirements; duration of "right to mine" agreements; production limits; splitting of the mining cycle into sub-cycles to be performed by different contractors; and, the time lags concomitant with the coming into force of any international agreement.

The premise of this study is that the public decision-makers involved in these issues will be beneficially informed by having available to them estimates of the financial or economic valuation of segments of the private and national interest which are based on detailed considerations of cost.

No one knows, of course, what these costs estimated in the model will prove to be. There is no deep ocean mining project in commercial production

on whose experience analysis may draw. It may even be that no one consortium has worked out all the basic problems in each of the various phases of technology described in the study. As they do, their own estimates of costs may go up.

In addition, the various major consortia and their individual corporate members have major differences among them as to the level of research and development behind or before them. They differ also as to their motivations for investing in deep ocean mining, some more interested in access to long term metals supplies, others more interested in nearer term return. Expectations as to the effectiveness of mining and processing technologies vary, as do expectations concerning the amount of debt leveraging that can be anticipated.

The analyses in the study deal with these uncertainties and differences in at least three ways. First, over one hundred analyses were made varying the values given individual parameters to examine their impact on costs or economic return. These are summarized in this paper at section D. Second, as these analyses and feedback from industry sources and others highlighted the impact of specific variables, such as ore grade, debt-equity ratios, metals prices, and totals of costs, analyses using variations of these parameters have been incorporated into ongoing studies of particular aspects of deep ocean mining such as LOS treaty terms for financial arrangements. Finally, several alternate sets of assumptions changing not one but several key parameters at a time are currently being examined in conjunction with ongoing studies.

To avoid misuse of the model, the authors also state the underlying assumptions for independent program variables and frequently define explicit bounds for them at the end of appropriate sections of appendices.

A. Cost Estimation Results. Costs are grouped into four types: research and development, prospecting and exploration, capital, and operating expenses. The values assigned to the input variables in the basic set of assumptions are identified in Chapter IV. The following table summarizes costs estimated for the basic set of assumptions, around which variations reported on below are made.

Table ES-1
Summary of Cost Estimates
(in millions of dollars)

Research & Development	50.00
Prospecting & Exploration	16.40
Capital Investment	493.05
Total Capital & Operating Expenses Prior to Commencing Commercial Recovery	559.45
Annual Operating Expenses	100.5

1. Expenses Prior to Commencing Commercial Recovery. Prospecting and exploration costs of $16.4 million are composed of four expenses: prospecting cost, exploration labor costs for the research team, the cost of conducting the mapping survey, and the cost of conducting the survey for discrete samples of nodules and soil. These prospecting and exploration costs are allocated over time and used as an input to computation of annual cash flow.

2. Capital Investment. Total capital investment in the base set of assumptions of $493 million is divided into costs allocated to three major sectors of the cost model: mining, transportation, and processing. The division of the capital investment among the sectors and sub-sectors of the ocean mining project is illustrated in Table ES-2.

Table ES-2
Allocation of Capital Costs: $493 Million
(in millions of dollars)

Mining Sector		Transport Sector		Processing Sector	
Platform	54	Sector Costs	55	Equipment	199
Pipe Handling	21			Utilities	84
Lift	9			Site	20
Power Plant	7			Buildings	20
Navigations	5			Waste Disposal	19
	96		55		342
Total Capital Costs					493

3. Operating Expenses. Estimated annual operating costs for the ocean mining project of $100.5 million are also allocated among the mining, transportation and processing sectors. The costs of each sector are further divided into the annual expenses for energy, labor, materials, fixed charges, and miscellaneous items. These costs are shown in Table ES-3.

Table ES-3
Estimated Annual Operating Costs of the Baseline Model
(in millions of dollars)

Mining Sector		Transport Sector		Processing Sector	
Energy	3.7	Energy	3.1	Energy	19.3
Labor	4.0	Labor	7.5	Labor	23.8
Materials	9.4	Materials	2.2	Materials	12.8
Fixed	3.0	Fixed	1.4	Fixed	6.8
Misc.	1.1	Misc.	0.7	Misc.	1.9
	21.1		14.9		64.5
Total Annual Operating Cost					100.5

B. Results of Economic Return Analysis. The project goes into commercial production in its sixth year. Its annual production and revenues from then through the thirtieth year are as follows:

Table ES-4
Annual Production and Revenue

	Annual Production (lbs. x 10^6)	Revenue ($ x 10^6)
Nickel	85.5	171.0
Copper	74.1	52.61
Cobalt	8.64	34.56
Manganese	0.	0.
Total Annual Revenue		258.17

The project does not report a loss for any year of commercial production. Annual cash flow turns positive in the first year of production and remains so for the life of the project.

Three measures of economic return are routinely provided in this report: Net Present Value (NPV), Internal Rate of Return (IROR), and Payback Period.

The NPV for different discount rates applied to the baseline case is shown in Table ES-5:

Table ES-5
Net Present Values for Baseline Case at Different Discount Rates
(NPV in millions of dollars)

Discount Rate	8%	10%	12%	14%	16%	18%	20%	22%	24%
NPV	349.1	230	144.6	82.4	36.4	2.1	-23.9	-43.6	-58.7

The IROR for the baseline project is 18.14%. The Payback Period is 5.4 years.

C. Effects on Costs of Changing Initial Values. Fifty-eight separate changes of individual parameters are made to test their impact on the capital and operating costs or the costs of prospecting and exploration. In most instances the changes was an upward or downward shift of 10% of initial value.

Three observations may be made.

The first concerns the use of most input variables in the cost estimation section to calculate capital and operating costs of discrete units of equipment in the 12 sub-sectors of the model. In general, a change in the value of a single variable results in changes in the capital and operating costs of one single unit, with minor changes in associated maintenance and fixed costs. These changes in costs are usually small in comparison to the total capital and operating costs of the project.

Second, there are several variables that are used throughout the model or in the processing sector and so affect costs in a number of sub-sectors. Changes in these have a larger impact on total project costs. One of these is the annual rate of ore recovery. It is a particularly critical variable since it affects the estimation of costs in all sub-sectors. A 10% reduction in the recovery rate of nodules results in a 5% decrease in capital and operating costs. The reduced recovery rate also leads to a decrease in gross revenues.

Three other variables to which the model demonstrates more than average sensitivity are indirect construction costs, contingency fees and engineering fees. These variables together comprise a factor applied to the direct costs figure in each of the sub-sectors of the processing sector. Thus each variable affects all components of processing costs, and the processing sector is the largest component of the total projects cost. A 10% change for indirect construction costs results in an increase of 2% on total capital cost. A change in the contingency fee from 15% to 20% gives an increase of 3% in project capital cost.

Finally, the group of variables associated with the lift system of the mining sector appears particularly sensitive. Changes in water depth at the mine site, in the pump submergence depth, and in the efficiency of separation of nodules from the lift discharge each results in changes of capital and operating costs of more than one million dollars. In addition, the change from an expected lifetime for the lift pipe from one year to six months results in an increase of $5.8 million in annual operating cost.

A second type of change in cost parameters concerns basic design or systems assumptions. The mining system used in the baseline model assumes that mining operations are conducted from a single mineship. The model is tested for two variations using two mineships, the first with all costs calculated from the same parameters used in the single mineship case, and the second making reasonable modifications in other costs. The results indicate significant increase in costs, an 11% increase in capital costs and a 17% increase in operating cost in the first variation. In the second, the capital cost in increased by 10%, but the operating cost is increased only by 7%.

In another analysis, distance from the port facility to the processing plant was increased from five miles to 25 miles and the distance between the processing plant and the waste disposal area was increased from 25 miles to 125 miles. These increases cause processing sector capital costs to go up from $342 to $392 million. Processing operating costs increase from $64.5 to $71.9 million.

Finally, analysis of the impact of using U.S. construction facilities and U.S. operating crews indicates a difference of approximately 7% in construction costs and as much as 6% in operating costs.

D. Effects on Economic Return of Changing Initial Values. In Chapter VI, an additional 60 analyses are made to examine the impact on the economic return estimates, of changes in the assumptions or values used in the baseline model. They comprise seven different areas:

1. Changes in revenue flowing to the project and its determinant components. Twenty-five percent increases and decreases in values are made in total revenue and price of nickel and cobalt; annual ore production is increased and decreased .5 million tons; a slow start-up with low production and high expenses is used; and the ore content of nickel and copper is reduced from 2.8% to 2%.

2. Changes in annual operating costs and its components. Twenty-five percent upward and downward shifts are made in annual operating costs, and energy, labor, materials and fixed operating costs.

3. Changes in total capital costs and its components. Twenty-five percent upward and downward changes are made in total capital costs and processing equipment, utilities, transportation, platform, pipe handling, lift system and waste system capital costs.

4. Introduction of delays. One- and two-year delays are introduced prior to the beginning of investment period, the beginning of commercial oper-

ations, and at both points combined.

5. Changes in assumptions concerning exploration and transportation costs. The daily charter rate of the research vessel is doubled and tripled; exploration is stretched out from two to 10 and to 20 years; and U.S. construction and crew costs are substituted for foreign costs.

6. Changes in assumptions concerning capital investment structure. Capital investment is allocated over four years at 5%, 15%, 45% and 35% instead of evenly over three years; 67% and no debt funding are tested; interest is payable on unpaid balance vice equal payments.

7. Changes in accounting and tax assumptions. A 6% escalation rate is introduced, capitalization vice expensing of R&D and exploration expenditures and straight line depreciation of declining balance with conversion are tested; and 22%/15% and no depletion allowances are used.

The results can be summarized in five statements of findings.

1. The largest impacts on economic return are from changing the level of revenue flowing into the project and from variables which are among the determinants of the level of revenue (market price of nickel, ore grade, production rate).

Parameters that either cut or add substantially to revenues will have a heavy direct impact on economic return. Twenty-five percent downward shifts in the level of revenues themselves lower IROR by 8.63% to 9.51%. Conversely, a comparable upward shift adds 6.31%. Twenty-five percent downward and upward shifts in the price of nickel lowers and raises IROR by 5.36% and 4.3%, respectively. Similarly, a drop in combined nickel-copper ore grade from 2.8% to 2% decreases the estimated IROR from 18.14% to 11.16%. Decreasing annual production of .5 million tons (a 16 2/3% change) reduces the IROR by more than two percentage points, while a comparable increase raises it by 1.4%. A slow start-up, with the first two years' production at 70% and 85% of projected rate, and higher than expected expenses, indicates a similar reduction in IROR.

These analyses suggest the relative sensitivity of the economic outlook to factors which are at least partially outside the control of the project's managers.

2. Twenty-five percent shifts in annual operating costs and in capital investment, two other major factors in determining cash flow (when capital investment is allocated on an annual basis), causes smaller changes in indicated economic return which, however, are large when compared to most other changes made. Shifting annual operating costs of $100.5 million a year downward and upward by 25% causes the IROR to change to 15.07% and 20.72%, respectively. Similar shifts in total capital investment, for $493 million to $616 and $370 million changes the indicated IROR to 15.01% and 21.98%.

3. Delays of two years introduced in the planned project schedule before investment and between investment and commencement of operations also cause decreases in estimated IROR to 17.01% and, more significantly, 12.95%, respectively. When these two delays are combined, the IROR decreases further to 12.28%. One-year delays cause smaller decreases. The analyses point up the impact of delay from any cause from the investor's viewpoint at the time it is considering commitment of funds, and particularly the effect of delay after those funds are invested.

4. The one other variable which indicates a relatively sizeable resulting shift in IROR is the use of debt funding. Changing the baseline assumption of 50% debt to no debt funding and to 66 2/3% debt produces IROR estimates of 15.41% and 19.53%, respectively.

5. The effects on indicated IROR of each of the other changes are, with two exceptions noted below, less than 1.1%. Many are in the neighborhood of 1/2%.

The two exceptions are the use of U.S. construction and crews, which reduces IROR to 16.26% and a 25% increase and decrease in processing equipment capital costs which lowers and raises IROR to 16.81% and 19.62%, respectively.

Thus the large majority of the variables tested for sensitivity or alternative assumptions had an impact on economic return measured in terms of one percentage point of IROR or smaller.

Three further observations should be made on these analyses. First, there may be variables to which the model may be significantly sensitive whose initial values were not changed. Second, a drop or increase of even a point of IROR implies not insignificant changes in discounted cash flows, their magnitude depending on when they occur. Third, actual experience is likely to involve several, perhaps many, changes in the values estimated in the model. It would take only a handful of small individual changes in values or assumptions, if they were all to move in one direction, to amount to a significant change in the project's economic prospects.

E. Analyses of Selected Policy Issues. Chapter VII of the study suggests in a preliminary, but illustrative way the uses in policy analysis to which the model might be put. Six policy issues are raised; most involve variables examined in Chapters V or VI.

The additional cost to the project of a policy requiring U.S. construction and crews is indicated to be $34.1 million in capital costs and $5.7 to 6.2 million per year in operating costs. This results in 1.88% drop in IROR. (Calculation of related benefits is dependent upon values external to the project.)

The effects are reviewed of policies which facilitate debt financing for the project, reduce the likelihood of delays in bringing the project into commercial production once an investment decision has been made, and grant or withhold depletion allowances. Analyses of these subjects are also reported on in Chapter VI.

The project's contribution to national income is approximated in the model by the sum of the discounted taxes paid and the discounted value of the profits distributed, using a social rate of dis-

count in both cases. For the baseline model, the cumulative discounted contribution to national income over the entire life of the project is approximately $490 million. Approximately $260 million of this sum is received through taxes and the remainder is distributed to the owners of the project.

Finally, an examination of the methodology of evaluating policy measures to provide risk coverage against premature termination of the project is begun. Calculations of the values of the guaranty payments contained in H.R. 9 and H.R. 11879 are presented. These legislative proposals are illustrative in that their provisions bracket those of H.R. 3350 which in 1978 appears to be the focus of much consideration in the House of Representatives. The effect of risk coverage provisions on the project's NPV in the event of premature termination is presented for each year in the life of the project. When weighted with a subjective statement of the likelihood of such early termination and discounted at a selected rate, these values can indicate the prospective effects of risk coverage provisions on the ocean mining project. The impacts of resale value of the project are also shown.

F. Evaluation. What emerges is a picture of deep ocean mining which from the viewpoint of a prospective industry investor could provide an economic return which might range from 15% to 22%. These figures are those generated by 25% upward and downward shifts of capital investment from the figure used in the basic set of assumptions. They encompass the results from all analyses of changes in variables made in Chapter VI, excepting delays and large fluctuations of revenues.

The choice of discount rate by the industry investor creates a second range which has to be taken into account when considering the NPV associated with the project. For example, a company using a 12% discount rate and experiencing a set of conditions producing the lower IROR of 15% would see an NPV of $80 million, while the upper rate of 22% would provide an NPV of $190 million. (The baseline set of conditions would provide an NPV of $145 million using the same discount rate.) In contrast, the industry manager using a 20% discount rate would see an NPV of -$75, -$24 and $20 million for the lower, baseline and upper sets of conditions respectively. For a corporation using a discount rate, in the middle of the earlier two, the comparable NPV figures would be -$20, $35, and $90 million, respectively.

Finally, the prospect has been noted that many technical and economic unknowns and most policy options appear likely to have comparatively minor impact taken individually, while some that do appear to have larger impacts are at least partially beyond direct control of the investor or operator. When several individual parameters are changed "unfavorably" or "favorably" in combination, their detrimental or beneficial effect may well be substantial. These findings strongly imply that the policy decision-maker must simultaneously evaluate the effects of individual policy or regulatory measures and pay attention to their combined effects on the economic prospects for deep seabed mining.